National Library of Canada
Canadian Theses Service
Ottawa, Canada
K1A 0N4

Bibliothèque nationale du Canada
Service des thèses canadiennes

NOTICE

The quality of this microform is heavily dependent upon the quality of the original thesis submitted for microfilming. Every effort has been made to ensure the highest quality of reproduction possible.

If pages are missing, contact the university which granted the degree.

Some pages may have indistinct print especially if the original pages were typed with a poor typewriter ribbon or if the university sent us an inferior photocopy.

Reproduction in full or in part of this microform is governed by the Canadian Copyright Act, R.S.C. 1970, c. C-30, and subsequent amendments.

AVIS

La qualité de cette microforme dépend grandement de la qualité de la thèse soumise au microfilmage. Nous avons tout fait pour assurer une qualité supérieure de reproduction.

S'il manque des pages, veuillez communiquer avec l'université qui a conféré le grade.

La qualité d'impression de certaines pages peut laisser à désirer, surtout si les pages originales ont été dactylographiées à l'aide d'un ruban usé ou si l'université nous a fait parvenir une photocopie de qualité inférieure.

La reproduction, même partielle, de cette microforme est soumise à la Loi canadienne sur le droit d'auteur, SRC 1970, c. C-30, et ses amendements subséquents.

NL-339 (r. 88/04) c

Canada

UNIVERSITY OF ALBERTA

NMR STUDIES OF THE INTERACTIONS BETWEEN PROTEINS IN THE THIN FILAMENT OF MUSCLE

BY

ANN PATRICIA CAMPBELL ©

A thesis submitted to the Faculty of Graduate Studies and Research in partial fulfillment of the requirements for the degree of DOCTOR OF PHILOSOPHY

DEPARTMENT OF BIOCHEMISTRY

EDMONTON, ALBERTA

SPRING, 1992

National Library
of Canada

Bibliothèque nationale
du Canada

Canadian Theses Service

Service des thèses canadiennes

Ottawa, Canada
K1A 0N4

The author has granted an irrevocable non-exclusive licence allowing the National Library of Canada to reproduce, loan, distribute or sell copies of his/her thesis by any means and in any form or format, making this thesis available to interested persons.

The author retains ownership of the copyright in his/her thesis. Neither the thesis nor substantial extracts from it may be printed or otherwise reproduced without his/her permission.

L'auteur a accordé une licence irrévocable et non exclusive permettant à la Bibliothèque nationale du Canada de reproduire, prêter, distribuer ou vendre des copies de sa thèse de quelque manière et sous quelque forme que ce soit pour mettre des exemplaires de cette thèse à la disposition des personnes intéressées.

L'auteur conserve la propriété du droit d'auteur qui protège sa thèse. Ni la thèse ni des extraits substantiels de celle-ci ne doivent être imprimés ou autrement reproduits sans son autorisation.

ISBN 0-315-73033-1

Canada

UNIVERSITY OF ALBERTA

RELEASE FORM

NAME OF AUTHOR: Ann Patricia Campbell

TITLE OF THESIS: NMR Studies of the Interactions Between Proteins in the Thin Filament of Muscle

DEGREE: Doctor of Philosophy

YEAR THIS DEGREE GRANTED: 1992

Permission is hereby granted to the University of Alberta Library to reproduce single copies of this thesis and to lend or sell such copies for private, scholarly, or scientific research purposes only.

The author reserves other publication rights and other rights in association with the copyright in the thesis, and except as hereinbefore provided neither the thesis nor any substantial portion thereof may be printed or otherwise reproduced in any material form without the author's prior written permission.

Patricia Campbell

(Student's Signature)

Ann Patricia Campbell

(Student's Permanent Address)
1107 - 11147 82nd Ave
Edmonton, Alberta
T6G 0T5

DATE: November 23, 1991

University of Alberta

Faculty of Graduate Studies and Research

The undersigned certify they have read, and recommend to the Faculty of Graduate Studies and Research for acceptance, a thesis entitled NMR Studies of the Interactions Between Proteins in the Thin Filament of Muscle

Submitted by Ann Patricia Campbell

In partial fulfillment of the requirements for the degree of Doctor of Philosophy

Brian D Sykes

Dr. Brian D. Sykes

Cyril M. Kay

Dr. Cyril M. Kay

Robert S Hodges

Dr. Robert S. Hodges

George Kotovych

Dr. George Kotovych

Walter J. Chazin

Dr. Walter Chazin

Date: November 5, 1991

Abstract

The Ca(II)-sensitive interaction between troponin C (TnC) and troponin I (TnI), two proteins in the thin filament of muscle, has been studied using nuclear magnetic resonance techniques. The conformation of the TnI inhibitory peptide, Nα-acetyl-TnI(104-115) amide, when bound to Ca(II)-saturated skeletal TnC, has been determined using the two-dimensional transferred nuclear Overhauser effect (TRNOE), a technique which allows determination of the structure of a ligand bound to a macromolecule. A theoretical evaluation of the TRNOE is presented, examining the effects of internal motions in the free and bound TnI peptide.

Two-dimensional nuclear Overhauser effect (NOE) techniques have been used to determine the identity of the residues on Ca(II)-saturated skeletal TnC which are actively involved in binding the inhibitory TnI(104-115) peptide. A model of the interaction between Ca(II)-saturated skeletal TnC and the inhibitory region of TnI is presented, based on a knowledge of the structure of the bound inhibitory region of TnI, and the residues of TnC involved at the binding interface.

Conformational changes in Ca(II)-saturated skeletal TnC induced upon the binding of the inhibitory TnI(104-115) peptide have been studied using the paramagnetic distance probe, gadolinium, as a calcium analog. The role of the flexible helical linker connecting N- and C-terminal globular domains of TnC in the binding of target proteins is discussed.

Differences in the mode of TnC-mediated relief of TnI inhibitory activity in skeletal versus cardiac systems have also been examined. The cardiac(137-148) and skeletal(104-115) TnI inhibitory peptides have identical sequences except for a single amino acid substitution of a proline at position 110 in the skeletal sequence for a threonine at position 143 in the cardiac sequence. Two-dimensional TRNOE techniques have been used to determine the conformation of the glycine-110 peptide analog, Nα-acetyl-G110-TnI(104-115) amide, bound to Ca(II)-saturated bovine cardiac TnC. The effect of the amino acid substitution at position 110 on the conformation and dynamics of the inhibitory region of TnI is discussed.

Finally, the role of amphiphilic helices in the recognition and targeting of Ca(II)-binding proteins like TnC has been examined. Two-dimensional TRNOE and NOE techniques have been used to examine and compare the structures of the inhibitory TnI(104-115) peptide and the α-helical bee venom, mastoparan, in the helix-inducing solvent TFE versus when bound to Ca(II)-saturated turkey skeletal TnC.

Acknowledgements

I would like to acknowledge some of the many individuals who have helped me with this research over the past six years. Firstly, I would like to thank my supervisor and mentor, Brian D. Sykes, who has given me the opportunity to carry out research in his laboratory, and who has given me intellectual direction and emotional support over the years. I will never forget visiting the Buddhist temples in Kyoto with him on our trip to Japan for a scientific meeting.

I would also like to thank members of the lab who have contributed to a stimulating and congenial working environment. Thanks go to Gerry McQuaid, David Corson and Don Evjen who have maintained the spectrometers and magnets. Thanks also go to the computer programming wizards in the lab; Robert Boyko and Tim Jellard. Special thanks go to Robert for writing the TRNOE and TR-IRMA computer programs.

Other members of the lab with whom I have developed good working relationships and warm friendships include Gillian Henry, Wendy Findlay, Gary Shaw, Frank Sonnichsen, David Wishart, David Hoyt, Jian-Jun Wang, Campbell McInnes, Carolyn Slupsky and Linda Golden. I would like to give my warmest appreciation to Carolyn and Linda, who have become my close friends, and especially to Carolyn who has 'toughed it out' with me in the gym and on the running track.

Other members within the department have also been supportive. In this regard, I am indebted to Jenny Van Eyk and Robert Hodges for their assistance in peptide synthesis and purification, and for their interest in collaborating with this project. I am also indebted to Mike James and Natalie Strynadka for their advice with respect to structure determination and molecular modeling. Susan Smith, our secretary, has also been a great help and a good friend over the years.

Lastly, I would like to thank my parents, Duane and Elizabeth Campbell, for their gentle love and support over the years; and I would like to thank my beautiful sister, Janet, for her sparkle and humour and comraderie. Final thanks go to my friend, Rolland Riives, for patiently taking my hand as he taught me how to dance the twelve step.

This research has been supported by the Alberta Heritage Foundation for Medical Research and the Medical Research Council of Canada in the form of studentships and research allowances.

Table of Contents

Chapter Page

I. Introduction 2
  A. The Thin Filament 3
    1. Troponin 3
      a. TnC 3
      b. TnI 4
      c. TnT 4
    2. Tropomyosin 4
    3. Actin 5
  B. The Thick Filament 5
  C. Interactions of Regulatory Proteins 6
    1. Tropomyosin-Actin 6
    2. TnT-Tropomyosin 7
    3. TnT-TnC and TnT-TnI 7
    4. TnC-TnI and TnI-Actin 9
  D. The Contractile Cycle 11
  E. Models for Muscle contraction 12
    1. Steric Blocking Model 12
    2. Allosteric 'Two-State' Model 12
    3. Expanded 'Two-State' Model 13
    4. Continuum Model 13
  F. Research Proposal 14
    1. Nuclear Magnetic Resonance Spectroscopy and Muscle Proteins 14
    2. Ca(II)-Sensitive Interaction between TnC
       and the Inhibitory Region (104-115) of TnI 18
    3. Thesis Proposal and Outline of Chapters 19
  G. References 32

II. Theoretical Evaluation of the Two-Dimensional
  Transferred Nuclear Overhauser Effect 51
  A. Introduction 52
  B. Theory 54
  C. Results 58

D. Discussion 63
E. References 72

III. Effects of Internal Motions on the Development of the Two-Dimensional Transferred Nuclear Overhauser Effect 77
A. Introduction 78
B. Theory 79
1. Chemically Equivalent Protons 81
2. Effects of Internal Motion 82
C. Results 82
D. Discussion 87
E. References 92

IV. Interaction of Troponin I and Troponin C: ^{19}F NMR Studies on the Binding of the Inhibitory Troponin I Peptide to Skeletal Troponin C 96
A. Introduction 97
B. Materials and Methods 98
1. Sample Preparation 98
a. Materials 98
b. Amino Acid Analysis 98
c. Preparation of Boc-L-p-fluorophenylalanine 99
d. Peptide Synthesis and Purification 99
e. Preparation of TnC 100
f. Preparation of Desalted, Apo TnC 101
g. Preparation of TnI Peptide NMR Samples 101
2. Nuclear Magnetic Resonance Spectroscopy 102
3. Calculation of Binding Constants 102
a. Titration of Nα-acetyl[^{19}F-phe106]TnI(104-115) amide with Apo Turkey Skeletal TnC 102
b. Titration of Nα-acetyl[^{19}F-phe106]TnI(104-115) amide with Ca(II)-Saturated Turkey Skeletal TnC 103
C. Results 104
1. Titration of Nα-acetyl[^{19}F-phe106]TnI(104-115) amide with Apo Turkey Skeletal TnC 104
2. Titration of Nα-acetyl[^{19}F-phe106]TnI(104-115) amide with Ca(II)-Saturated Turkey Skeletal TnC 104

3. Test of the Stoichiometry of Binding of Nα-acetyl[^{19}F-phe106] TnI(104-115) amide to Ca(II)-Saturated Turkey Skeletal TnC......... 105
D. Discussion.. 107
E. References.. 120

V. Interaction of Troponin I and Troponin C: Use of the Two-Dimensional Transferred Nuclear Overhauser Effect to Determine the Structure of the Inhibitory Troponin I Peptide when Bound to Skeletal Troponin C 128
A. Introduction.. 129
B. Theory.. 131
C. Materials and Methods.. 132
1. Sample Preparation.. 132
a. Materials.. 132
b. Amino Acid Analysis.. 132
c. Peptide Synthesis and Purification.. 132
d. Preparation of TnC.. 133
e. Preparation of Desalted, Apo TnC.. 133
f. Preparation of TnI Peptide ^{13}C NMR samples........................ 133
g. Preparation of TnI Peptide ^{1}H NMR samples........................ 133
2. Nuclear Magnetic Resonance Spectroscopy.............................. 134
3. Transformation of ^{1}H NMR TRNOESY Peak Intensity to Distance Restraints.. 135
4. Control Experiments to Analyze the Effects of Indirect Cross-Relaxation on the Development of the Intrapeptide TRNOEs........... 136
5. Dihedral Angle Restraints and Supplemental Distance Restraints........ 138
6. Stereospecific Assignments from ^{1}H NMR.............................. 139
7. Restrained Molecular Dynamics Calculations.............................. 140
D. Results.. 141
1. Sequential Resonance Assignments and Transferred NOEs............. 141
2. Secondary Structure.. 144
3. Distance Determination.. 144
4. Dihedral Angle Restraints.. 145
5. Supplemental Distance Restraints.. 146
6. Molecular Dynamics Calculations.. 146
E Discussion.. 148
F. References.. 176

VI. Interaction of Troponin I and Troponin C: Identification using NMR of Specific Residues in Skeletal Troponin C which are Involved in the Binding of the Inhibitory Troponin I Peptide.............................. 185
A. Introduction.. 186
B. Materials and Methods.. 188
1. Sample Preparation.. 188
a. Materials.. 188
b. Amino Acid Analysis... 188
c. Peptide Synthesis and Purification...................................... 188
d. Preparation of TnC.. 188
e. Preparation of Desalted, Apo TnC....................................... 188
f. Preparation of TnC Protein ^{1}H NMR samples....................... 188
g. Preparation of TnI Peptide-TnC Protein ^{1}H NMR samples......... 188
2. Nuclear Magnetic Resonance Spectroscopy.............................. 189
C. Results.. 189
1. Crystal Structure of Troponin C... 190
2. NMR Assignments of Troponin C.. 192
3. Interactions between TnC and the TnI Inhibitory Peptide: ^{1}H NMR Monitored Titration of Ca(II)-saturated Turkey s-TnC with the TnI Peptide.. 196
4. Interactions between TnC and the TnI Inhibitory Peptide: Identification of Specific Residues Involved in the Binding Interface... 197
D. Discussion... 200
E. References... 235

VII. Interaction of Troponin I and Troponin C: Use of Paramagnetic Lanthanides to Determine the Location of Binding of the Troponin I Peptide to Skeletal Troponin C... 243
A. Introduction.. 244
B. Theory... 247
C. Materials and Methods.. 248
1. Sample Preparation.. 248
a. Materials.. 248
b. Amino Acid Analysis... 248
c. Peptide Synthesis and Purification...................................... 249

d. Preparation of TnC.......... 249
e. Preparation of Desalted, Apo TnC.......... 249
f. Ln(III) Solutions.......... 249
g. Preparation of TnI Peptide Samples.......... 249
h. Preparation of TnC.Gd(III)$_4$ Protein Titrant.......... 249
i. Titration of TnI Peptide Sample with TnC.Gd(III)$_4$.......... 249
2. Nuclear Magnetic Resonance Spectroscopy.......... 250
D. Results.......... 250
E. Discussion.......... 252
F. References.......... 268

VIII. Interaction of Troponin I and Troponin C: Use of the Two-Dimensional Transferred Nuclear Overhauser Effect to Determine the Structure of a Glycine-110 Inhibitory Troponin I Peptide Analog when Bound to Cardiac Troponin C.......... 278
A. Introduction.......... 279
B. Theory.......... 282
C. Materials and Methods.......... 284
1. Sample Preparation.......... 284
a. Materials.......... 284
b. Amino Acid Analysis.......... 284
c. Peptide Synthesis and Purification.......... 284
d. Preparation of TnC.......... 284
e. Preparation of Desalted, Apo TnC.......... 285
f. Preparation of G110-TnI Peptide ^{1}H NMR samples.......... 285
2. Nuclear Magnetic Resonance Spectroscopy.......... 285
3. Transformation of ^{1}H NMR TRNOESY Peak Intensity to Distance Restraints.......... 285
4. Dihedral Angle Restraints and Supplemental Distance Restraints.......... 287
5. Stereospecific Assignments from ^{1}H NMR.......... 288
6. Restrained Molecular Dynamics Calculations.......... 288
D. Results.......... 290
1. Sequential Resonance Assignments and Transferred NOEs.......... 290
2. Secondary Structure.......... 292
3. Distance Determination.......... 293
4. Dihedral Angle Restraints.......... 293

5. Supplemental Distance Restraints.. 294
6. Molecular Dynamics Calculations.. 294
E. Discussion.. 296
F. References.. 322

IX. Role of Amphiphilicity in the Binding of Target Peptides to Troponin C: An NMR Comparison of the Structures of Mastoparan and the Inhibitory Troponin I Peptide in the Helix Inducing Solvent Trifluoroethanol versus when Bound to Skeletal Troponin C...................................... 333
A. Introduction.. 334
B. Theory.. 336
C. Materials and Methods... 338
1. Sample Preparation.. 338
a. Materials.. 338
b. Amino Acid Analysis... 338
c. Peptide Synthesis and Purification.................................... 338
d. Preparation of TnC.. 338
e. Preparation of Desalted, Apo TnC...................................... 338
f. Preparation of TnI Peptide ^{1}H NMR samples........................ 338
2. Nuclear Magnetic Resonance Spectroscopy.............................. 339
3. Transformation of ^{1}H NMR TRNOESY Peak Intensity to Distance Restraints.. 339
4. Dihedral Angle Restraints and Supplemental Distance Restraints....... 341
5. Stereospecific Assignments from ^{1}H NMR.............................. 341
6. Restrained Molecular Dynamics Calculations............................. 342
D. Results.. 343
1. Sequential Resonance Assignments and NOEs........................... 343
a. TnI Peptide in 50%TFE... 344
b. Mastoparan in 50%TFE... 344
c. Mastoparan in the Presence of 0.1 Molar Equivalents $TnC.Ca(II)_4$... 345
2. Secondary Structure... 347
a. TnI Peptide in 50%TFE... 347
b. Mastoparan in 50%TFE... 347
c. Mastoparan in the Presence of 0.1 Molar Equivalents $TnC.Ca(II)_4$... 348

3. Distance Determination.. 348
4. Dihedral Angle Restraints... 349
5. Molecular Dynamics Calculation.. 349
E. Discussion.. 351
F. References... 401

X. Conclusions and Future Research Directions.. 410
A. Summary... 411
B. Future Research Directions... 413
C. Transferred Iterative Relaxation Matrix Approach (TR-IRMA) from Proton-Proton Transferred NOEs: Refinement of the Structure of the Inhibitory Troponin I Peptide Bound to Troponin C........................ 415
1. Theory... 416
2. Methodology... 419
a. Calculation of a Population-Weighted Average Relaxation Matrix, $\mathbf{R}(p_B)$... 420
b. Diagonalization of the Population-Weighted Average Relaxation Matrix, $\mathbf{R}(p_B)$... 421
c. Calculation of a Mixed Matrix of Mixing Coefficients, $\mathbf{A}_{\mathbf{mix}}(\tau_m, p_B)$, with Calculated and Experimental Elements.......... 421
d. Diagonalization of the Mixed Matrix of Mixing Coefficients, $\mathbf{A}_{\mathbf{mix}}(\tau_m, p_B)$.. 422
e. Averaging over Mixing Time, τ_m.. 422
f. Averaging over Fraction Bound, p_B................................... 423
g. Conversion of $W_{ij}B_{mix}$ Matrix Elements to Bound Distance Restraints.. 423
h. Restrained Molecular Dynamics.. 423
3. Simulated Versus Experimental Results.................................... 424
D. References... 428

List of Tables, Figures and Computer Programs in Appendix

Tables in Appendix

Table IV-1 ^{19}F NMR data for the titration of N-α-acetyl[^{19}F-phe106] TnI(104-115) amide with apo turkey skeletal TnC 431

Table IV-2 ^{19}F NMR data for the titration of N-α-acetyl[^{19}F-phe106] TnI(104-115) amide with Ca(II)-saturated turkey skeletal TnC 431

Table V-1 Normalization tables for exchangeable backbone amide resonances on the TnI peptide:
  A. Amide versus exchangeable resonance 435
  B. Amide versus amide resonance 435

Table V-2 Table of TRNOE cross-peak intensities for the TnI peptide in the presence of 0.1 molar equivalents TnC.Ca(II)$_4$ 436

Table V-3 Effect of mixing time on the development of the intrapeptide TRNOE 442

Table V-4 Effect of protein concentration on the development of the intrapeptide TRNOE 448

Table V-5 Summary of distance restraints used in the MD simulations 455

Table V-6 ^{3}JαCH-NH coupling constants for the TnI peptide as a function of molar equivalents TnC.Ca(II)$_4$ 462

Table V-7 Chemical shift values for the TnI peptide backbone amide resonances as a function of temperature for
  A. 0.0 molar equivalents TnC.Ca(II)$_4$ 463
  B. 0.2 molar equivalents TnC.Ca(II)$_4$ 463
  C. 0.4 molar equivalents TnC.Ca(II)$_4$ 463

Table V-8 Temperature coefficients measured for various TnI peptide backbone amide protons versus molar equivalents TnC.Ca(II)$_4$ 464

Table V-9 GROMOS distance restraint file used in MD simulations to generate the structure of the TnI peptide bound to TnC.Ca(II)$_4$ 465

Table V-10 Chemical shift values for the TnI peptide backbone amide resonances as a function of molar equivalents TnC.Ca(II)$_4$ 475

Table V-11 Final coordinates for the structure of the TnI peptide bound to TnC generated from A. α-helical coordinates (structure 1), and B. β-strand coordinates (structure 2), following approximately 12 ps of restrained MD 476

Table V-12 Comparison of the distances between proton pairs given in the distance restraint file with those actually measured between the same proton pairs in the final structures generated from the α-helix (structure 1) and the β-strand (structure 2)................... 482

Table VII-1 T_1 measurements for various protons on the TnI peptide as a function of molar equivalents TnC.Gd(III)$_4$ to TnI peptide........ 488
Table VII-2 T_2 measurements for various protons on the TnI peptide as a function of molar equivalents TnC.Gd(III)$_4$ to TnI peptide........ 489
Table VII-3 T_1 measurements for various protons on the TnI peptide as a function of molar equivalents TnC.La(III)$_4$ to TnI peptide......... 490
Table VII-4 T_2 measurements for various protons on the TnI peptide as a function of molar equivalents TnC.La(III)$_4$ to TnI peptide......... 491
Table VII-5 Calculated values of $1/T_{1OBS\,i}{}^{Gd}$, $1/T_{2OBS\,i}{}^{Gd}$, $1/T_{1OBS\,i}{}^{La}$, $1/T_{2OBS\,i}{}^{La}$, $1/T_{1P\,i}$, $1/T_{2P\,i}$, $1/T_{1M\,i}$, $R_{max\,i}$, and $R_{min\,i}$ for various protons, i, on the TnI peptide................................. 492

Table VIII-1 Normalization tables for exchangeable backbone amide resonances on the G110-TnI peptide:
A. Amide versus exchangeable resonance................................ 495
B. Amide versus amide resonance.. 495
Table VIII-2 Table of TRNOE cross-peak intensities for the G110-TnI peptide in the presence of 0.1 molar equivalents TnC.Ca(II)$_4$................... 496
Table VIII-3 Summary of distance restraints used in the MD simulations............ 502
Table VIII-4 $^3J\alpha$CH-NH coupling constants for the G110-TnI peptide as a function of molar equivalents TnC.Ca(II)$_4$.......................... 508
Table VIII-5 Chemical shift values for the G110-TnI peptide backbone amide resonances as a function of temperature for
A. 0.0 molar equivalents TnC.Ca(II)$_4$..................................... 509
B. 0.1 molar equivalents TnC.Ca(II)$_4$..................................... 509
Table VIII-6 Temperature coefficients measured for various G110-TnI peptide backbone amide protons versus molar equivalents TnC.Ca(II)$_4$........ 510
Table VIII-7 GROMOS distance restraint file used in MD simulations to generate the structure of the G110-TnI peptide bound to TnC.Ca(II)$_4$.. 511

Table VIII-8 Chemical shift values for the G110-TnI peptide backbone amide resonances as a function of molar equivalents TnC.Ca(II)$_4$ 520

Table VIII-9 Final coordinates for the structure of the G110-TnI peptide bound to TnC generated from A. α-helical coordinates (structure 1), and B. β-strand coordinates (structure 2), following approximately 12 ps of restrained MD 521

Table VIII-10 Comparison of the distances between proton pairs given in the distance restraint file with those actually measured between the same proton pairs in the final structures generated from the α-helix (structure 1) and the β-strand (structure 2) 527

Table IX-1 Normalization tables for exchangeable backbone amide resonances on the TnI peptide in 50%TFE:
- A. Amide versus exchangeable resonance 533
- B. Amide versus amide resonance 533

Table IX-2 Normalization tables for exchangeable backbone amide resonances on mastoparan in 50%TFE:
- A. Amide versus exchangeable resonance 534
- B. Amide versus amide resonance 534

Table IX-3 Table of NOE cross-peak intensities for the TnI peptide in 50%TFE 535

Table IX-4 Table of NOE cross-peak intensities for mastoparan in 50%TFE 538

Table IX-5 Summary of distance restraints used in the MD simulations for the TnI peptide in 50%TFE 543

Table IX-6 Summary of distance restraints used in the MD simulations for mastoparan in 50%TFE 546

Table IX-7 ^{3}JαCH-NH coupling constants for the TnI peptide in 50%TFE 551

Table IX-8 ^{3}JαCH-NH coupling constants for mastoparan in 50%TFE 551

Table IX-9 GROMOS distance restraint file used in MD simulations to generate the structure of the TnI peptide in 50%TFE 552

Table IX-10 GROMOS distance restraint file used in MD simulations to generate the structure of mastoparan in 50%TFE 558

Table IX-11 Final coordinates for the structure of the TnI peptide in 50%TFE
A. α-helical coordinates (structure 1), and
B. β-strand coordinates (structure 2),
following approximately 12 ps of restrained MD 566

Table IX-12 Final coordinates for the structure of mastoparan in 50%TFE
A. α-helical coordinates (structure 1), and
B. β-strand coordinates (structure 2),
following approximately 12 ps of restrained MD........................ 572

Table IX-13 Comparison of the distances between proton pairs given in the
distance restraint file for the TnI peptide in 50%TFE
with those actually measured between the same proton pairs
in the final structures generated from the α-helix (structure 1)
and the β-strand (structure 2)... 578

Table IX-14 Comparison of the distances between proton pairs given in the
distance restraint file for mastoparan in 50%TFE
with those actually measured between the same proton pairs
in the final structures generated from the α-helix (structure 1)
and the β-strand (structure 2)... 581

Table X-1 Table of TRNOE intensities versus mixing time ($\tau_m = 75$,
150, and 500 ms) measured at 0.1 molar equivalents
TnC.Ca(II)$_4$ to TnI peptide... 586

Table X-1 Table of TRNOE intensities versus mixing time ($\tau_m = 75$,
150, and 500 ms) measured at 0.2 molar equivalents
TnC.Ca(II)$_4$ to TnI peptide... 592

Table X-3 Table of TRNOE intensities versus mixing time ($\tau_m = 75$,
150, and 500 ms) measured at 0.4 molar equivalents
TnC.Ca(II)$_4$ to TnI peptide... 600

Figures in Appendix

Figure V-1 500 MHz ^{1}H NMR spectra of the TnI peptide backbone amide resonances as a function of temperature
A. 0.0 molar equivalents TnC.Ca(II)$_4$ 432
B. 0.2 molar equivalents TnC.Ca(II)$_4$ 433
C. 0.4 molar equivalents TnC.Ca(II)$_4$ 434

Figure VIII-1 500 MHz ^{1}H NMR spectra of the G110-TnI peptide backbone amide resonances as a function of temperature
A. 0.0 molar equivalents TnC.Ca(II)$_4$ 493
B. 0.1 molar equivalents TnC.Ca(II)$_4$ 494

Computer Programs in Appendix

TRNOE: version 1 607
TRNOE: version 2 627

List of Tables Page

Table I-1 Properties of various muscle proteins.. 23
Table I-2 Sites of interaction between muscle proteins................................ 24

Table II-1 Internuclear distances of reference proton pairs in the free and bound peptide.. 65

Table V-1 Combined shifts in distance restraints from both the mixing time and protein concentration studies for a sample distance (r_{ij} = 3.5 Å).. 152
Table V-2 Chemical shifts for the assigned ^{1}H resonances of Nα-acetyl-TnI(104-115) amide in the presence of 0.1 molar equivalents TnC.Ca(II)$_4$.. 153
Table V-3 Dihedral angle values in the final structure generated from (a) α-helix (structure 1), and (b) β-strand (structure 2)................ 154

Table VI-1 Chemical shifts of assigned resonances on Ca(II)-saturated turkey s-TnC; comparison with literature values for those resonances assigned on CaM.Ca(II)$_4$ and rabbit s-TnC.Ca(II)$_4$....... 206
Table VI-2 Assignable intra- and interresidue NOEs observed in turkey s-TnC.Ca(II)$_4$ and comparison with those observed in rabbit s-TnC.Ca(II)$_4$.. 207
Table VI-3 TnI peptide-TnC protein NOEs observed in the NOESY spectrum of the 0.4 molar equivalents TnC protein to TnI peptide sample at 500 MHz in 80%H_2O/20%D_2O, and the 0.3 molar equivalents TnC protein to TnI peptide sample at 600 MHz in 100%D_2O.......... 209

Table VII-1 Range of distances calculated for various protons on the TnI peptide to the Gd(III)-filled sites on turkey s-TnC................. 260

Table VIII-1 Chemical shifts for the assigned ^{1}H resonances of Nα-acetyl-G110-TnI(104-115) amide in the presence of 0.1 molar equivalents TnC.Ca(II)$_4$.................. 303

Table VIII-2 Dihedral angle values in the final structure generated from (a) α-helix (structure 1), and (b) β-strand (structure 2)................ 304

Table IX-1 Chemical shifts for the assigned ^{1}H resonances of the TnI peptide in 50%TFE.. 356

Table IX-2 Chemical shifts for the assigned ^{1}H resonances of mastoparan in 50%TFE.. 356

Table IX-3 Chemical shifts for the assigned ^{1}H resonances of mastoparan in the presence of 0.1 molar equivalents TnC.Ca(II)$_4$................. 357

Table IX-4. Dihedral angle values in the final structure of the TnI peptide in 50%TFE generated from (a) α-helix (structure 1), and (b) β-strand (structure 2)................ 358

Table IX-5 Dihedral angle values in the final structure of mastoparan in 50%TFE generated from (a) α-helix (structure 1), and (b) β-strand (structure 2)................ 359

List of Figures

Figure I-1 A model for the molecular arrangement of the thin filament proteins.... 25

Figure I-2 X-ray crystal structure of turkey skeletal TnC.... 26

Figure I-3 X-ray crystal structure of G-actin derived from the Actin:DNAse 1 complex.... 27

Figure I-4 Schematic diagram of a myosin molecule.... 28

Figure I-5 Simplistic scheme for the biochemical and kinetic steps involved in ATP hydrolysis during muscle contraction.... 29

Figure I-6 Proposed mechanism for the generation of force by the interaction an S1 unit of a myosin filament with an actin filament.... 30

Figure I-7 Schematic diagram showing the dominant protein interactions involved in the regulation of muscle contraction.... 31

Figure II-1 TRNOE intensity versus fraction of bound peptide (p_B) for various bound correlation times ($\tau_c B$) and mixing times (τ_m).... 66

Figure II-2 r apparent calculated from TRNOE values of Figure II-1 versus fraction of bound peptide (p_B) for various bound correlation times ($\tau_c B$) and mixing times (τ_m).... 67

Figure II-3 r apparent for R112NH-R113NH proton pair versus low values of fraction of bound peptide (p_B) for various free correlation times ($\tau_c F$).... 68

Figure II-4 TRNOE intensity versus mixing time (τ_m) for various bound correlation times ($\tau_c B$) and fractions of bound peptide (p_B).... 69

Figure II-5 r apparent calculated from TRNOE values of Figure II-4 versus mixing time (τ_m) for various bound correlation times ($\tau_c B$) and fractions of bound peptide (p_B).... 70

Figure II-6 The effects of uniform internal motion in the bound peptide on the development of the TRNOE intensity and calculated distance, r apparent, for proton pair #3 (R112NH-R113NH; 2.68 Å).... 71

Figure III-1 TRNOE intensity versus mixing time (τ_m) for various free ($\tau_e F$) and bound ($\tau_e B$) internal correlation times.... 89

Figure III-2 TRNOE intensity versus mixing time (τ_m) for various fractions of bound peptide (p_B).... 90

Figure III-3 r apparent calculated from TRNOE values of Figure III-2 versus mixing time (τ_m) for various fractions of bound peptide (p_B)........... 91

Figure IV-1 ^{19}F NMR spectra of the titration of N-α-acetyl[^{19}F-phe106] TnI(104-115) amide with apo turkey skeletal TnC: Change in chemical shift of the F-phenylalanine resonance as a function of added TnC titrant... 114

Figure IV-2A ^{19}F NMR spectra of the titration of N-α-acetyl[^{19}F-phe106] TnI(104-115) amide with Ca(II)-saturated turkey skeletal TnC: Change in chemical shift of the F-phenylalanine resonance as a function of added TnC titrant 115

Figure IV-2B ^{19}F NMR spectra of the titration of N-α-acetyl[^{19}F-phe106] TnI(104-115) amide with Ca(II)-saturated turkey skeletal TnC: Change in intensity of F-phenylalanine resonance as a function of added TnC titrant.. 116

Figure IV-3 Plot of the titration of N-α-acetyl[^{19}F-phe106]TnI(104-115) amide with apo turkey skeletal TnC. The change in the chemical shift ($\Delta\delta$) of the F-phenylalanine resonance is plotted against the ratio of apo.TnC titrant to peptide ($[\text{apo.TnC}]_o$ / $[\text{TnI peptide}]_o$)........... 117

Figure IV-4 Plot of the titration of N-α-acetyl[^{19}F-phe106]TnI(104-115) amide with Ca(II)-saturated turkey skeletal TnC. The ratio of the change in intensity over observed intensity ($\Delta I/I_o$) of the F-phenylalanine resonance is plotted against the ratio of TnC titrant to peptide ($[\text{TnC.Ca}_4]_o$ / $[\text{TnI peptide}]_o$)................ 118

Figure IV-5 Contour plots showing the fit between calculated binding curves and the experimental titration data for a hypothetical two site binding of N-α-acetyl[^{19}F-phe106]TnI(104-115) amide to Ca(II)-saturated turkey skeletal TnC.................................. 119

Figure V-1 Plot of intrapeptide ^{1}H-^{1}H TRNOE intensity versus mixing time to illustrate the three types of cross-peak behaviour observed in the mixing time studies.. 155

Figure V-2 Plot of intrapeptide ^{1}H-^{1}H TRNOE intensity versus molar equivalents TnC.Ca(II)$_4$ to TnI peptide to illustrate the two types of cross-peak behaviour observed in the protein concentration studies.. 156

Figure V-3A 500 MHz ^{1}H NMR spectra of the TnI peptide in the absence and presence of 0.1 molar equivalents TnC.Ca(II)$_4$: Aliphatic upfield region of the spectrum.................................. 157
Figure V-3A 500 MHz ^{1}H NMR spectra of the TnI peptide in the absence and presence of 0.1 molar equivalents TnC.Ca(II)$_4$: Complete downfield region of the spectrum with the exchangeable guanidinium resonances of R108, R112, R113 and R115 and the aromatic F106 resonances............................. 158
Figure V-3C 500 MHz ^{1}H NMR spectra of the TnI peptide in the absence and presence of 0.1 molar equivalents TnC.Ca(II)$_4$: Expanded region of spectrum B showing backbone amide proton resonances and the C-terminal NH$_2$ group............... 159
Figure V-3D 500 MHz ^{1}H NMR spectra of the TnI peptide in the absence and presence of 0.1 molar equivalents TnC.Ca(II)$_4$: Expanded region of spectrum B showing only the backbone amide proton resonances.................................... 160
Figure V-4 Plot of the change in chemical shift of the TnI peptide backbone amide resonances as a function of molar equivalents TnC.Ca(II)$_4$........................ 161
Figure V-5 Upfield region of the DQFCOSY spectrum of the TnI peptide in the presence of 0.1 molar equivalents TnC.Ca(II)$_4$.................. 162
Figure V-6 Upfield region of the TRNOESY spectrum of the TnI peptide in the presence of 0.1 molar equivalents TnC.Ca(II)$_4$................... 163
Figure V-7 αCH-βCH region of the TRNOESY spectrum of the TnI peptide in the presence of 0.1 molar equivalents TnC.Ca(II)$_4$................... 164
Figure V-8 Downfield-βCH region of the TRNOESY spectrum of the TnI peptide in the presence of 0.1 molar equivalents TnC.Ca(II)$_4$..... 165
Figure V-9 αCH-NH region of the DQFCOSY spectrum of the TnI peptide in the presence of 0.1 molar equivalents TnC.Ca(II)$_4$................... 166
Figure V-10 αCH-NH region of the TRNOESY spectrum of the TnI peptide in the presence of 0.1 molar equivalents TnC.Ca(II)$_4$................... 167
Figure V-11 Fingerprint αCH-NH region of the NOESY spectrum of the TnI peptide superimposed upon the αCH-NH region of the TRNOESY spectrum of the same concentration TnI peptide in the presence of 0.1 molar equivalents TnC.Ca(II)$_4$................... 168

Figure V-12 Sequence of Nα-acetyl-TnI(104-115) amide together with a schematic summary of the short- and medium- range TRNOEs defining the secondary structure of the TnI peptide bound to TnC..... 169
Figure V-13 Plot of $^3J\alpha CH$-NH coupling constants versus molar equivalents $TnC.Ca(II)_4$ for various residues in the TnI peptide.................... 170
Figure V-14 Plot of δNH versus temperature for various TnI peptide backbone amide protons and molar equivalents $TnC.Ca(II)_4$.......... 171
Figure V-15 Plot of the temperature coefficients measured for various TnI peptide backbone amide protons versus molar equivalents $TnC.Ca(II)_4$ 172
Figure V-16 Stereo-diagram of the TnI peptide bound to Ca(II)-saturated TnC.... 173
Figure V-17 Photograph showing space-filling CPK model of the bound TnI peptide.. 174
Figure V-18 Superposition of the 10 MD structures taken every 0.2 ps 175

Figure VI-1 The amino acid sequence alignment of chicken s-TnC, rabbit s-TnC and rabbit CaM... 210
Figure VI-2 Stereo diagram of the hydrophobic pocket in the C-terminal domain of the crystal structure of turkey s-TnC showing selected residues in the aromatic cluster and the antiparallel β-sheet region between Ca(II) binding loops III and IV................ 211
Figure VI-3 500 MHz ^1H NMR monitored Ca(II) titration of turkey s-TnC showing slow exchange behaviour of the ring proton resonances of F102 and F151 in the C-terminal domain............................. 212
Figure VI-4 600 MHz ^1H DQFCOSY spectrum showing COSY cross-peaks for the aromatic spin systems of F102, F151, F154 and F112........ 213
Figure VI-5 600 MHz ^1H NOESY spectrum showing NOEs between the phenylalanine rings of residues F102, F151 and F154, comprising the aromatic cluster in the hydrophobic pocket of the C-terminal domain of TnC................................. 214
Figure VI-6 500 MHz ^1H NOESY spectrum showing NOEs between the δCH2 ring protons of F112 and main chain amide protons of G111 and I113 in the β-sheet region between Ca(II) binding loops III and IV................................ 215

Figure VI-7 500 MHz ^{1}H NOESY spectrum showing NOEs between the δCH2 and ξCH2 ring protons of F112 and the α-protons of F112 and I113, and between the ξCH2 ring protons of F154 and the α-protons of F112 and I149 216

Figure VI-8 500 MHz ^{1}H NOESY spectrum showing NOEs between residues in the C-terminal hydrophobic pocket and residues in the β-sheet region between Ca(II)-binding loops III and IV 217

Figure VI-9 500 MHz ^{1}H NOESY spectrum showing an NOE between the α-proton of F112 and the backbone amide proton of I113............. 218

Figure VI-10 500 MHz ^{1}H NOESY spectrum showing an NOE between the protons of I113 and the γCH3 methyl protons of I149 in the β-sheet region between Ca(II) binding loops III and IV............... 219

Figure VI-11 Lowfield region of the 500 MHz ^{1}H NMR spectrum of turkey s-TnC a. in D_2O, and b. 80%H_2O/20%D_2O.................. 220

Figure VI-12 Aromatic region of the 600 MHz ^{1}H NMR monitored titration of Ca(II)-saturated TnC with TnI peptide.................................. 221

Figure VI-13 A. Upfield region of the 600 MHz ^{1}H NMR monitored titration of Ca(II)-saturated TnC with TnI peptide; B. Upfield region of the 600 MHz ^{1}H NMR monitored titration of the Ca(II)-saturated chicken s-TnC Site III/Site IV heterodimer with TnI peptide........... 222

Figure VI-14 α-proton region of the 600 MHz ^{1}H NMR monitored titration of Ca(II)-saturated TnC with TnI peptide.................................... 223

Figure VI-15 Backbone amide region of the 600 MHz ^{1}H NMR monitored titration of Ca(II)-saturated TnC with TnI peptide...................... 224

Figure VI-16 500 MHz ^{1}H NOESY spectrum of the peptide-protein complex showing cross-peaks between I104γCH3 and I121γCH3 on TnC and various residues on the TnI peptide........................ 225

Figure VI-17 500 MHz ^{1}H NOESY spectrum of the peptide-protein complex showing cross-peaks between F154ξCH2, F154δCH2 and F102ξCH2 on TnC and F106αCH on the TnI peptide............ 226

Figure VI-18 500 MHz ^{1}H NOESY spectrum of the peptide-protein complex showing cross-peaks between aromatic ring protons on TnC and α-protons on the TnI peptide.. 227

Figure VI-19 Upfield methyl region of the 600 MHz ^{1}H NOESY spectrum of A. the TnI peptide-TnC protein complex, and B. the TnC protein alone.. 228

Figure VI-20 Upfield methyl to α-proton region of the 600 MHz ^{1}H NOESY spectrum of A. the TnI peptide-TnC protein complex, and B. the TnC protein alone 229
Figure VI-21 Upfield methyl to aromatic region of the 600 MHz ^{1}H NOESY spectrum of A. the TnI peptide-TnC protein complex, and B. the TnC protein alone 230
Figure VI-22 Aliphatic to aromatic region of the 600 MHz ^{1}H NOESY spectrum of A. the TnI peptide-TnC protein complex, and B. the TnC protein alone 231
Figure VI-23 α-proton to aromatic region of the 600 MHz ^{1}H NOESY spectrum of A. the TnI peptide-TnC protein complex, and B. the TnC protein alone 232
Figure VI-24 Backbone ribbon and fully space-filled representations of the C-terminal domain of the crystal structure of turkey s-TnC 233
Figure VI-24 Model of the TRNOE-derived structure of the TnI inhibitory peptide bound to the C-terminal domain of the crystal structure of turkey s-TnC 234

Figure VII-1A 500 MHz ^{1}H NMR monitored titration of Nα-acetyl-TnI(104-115) amide with TnC.Gd(III)$_4$: Aliphatic upfield region of the spectrum 261
Figure VII-1B 500 MHz ^{1}H NMR monitored titration of Nα-acetyl-TnI(104-115) amide with TnC.Gd(III)$_4$: Downfield region of the spectrum with the aromatic F106 resonances 262
Figure VII-1C 500 MHz ^{1}H NMR monitored titration of Nα-acetyl-TnI(104-115) amide with TnC.Gd(III)$_4$: Expanded region of spectrum B showing backbone amide proton resonances 263
Figure VII-2 500 MHz ^{1}H NMR monitored T_1 inversion recovery experiment showing backbone amide proton resonances at 0.0 molar equivalents TnC.Gd(III)$_4$ to TnI peptide 264
Figure VII-3 500 MHz ^{1}H NMR monitored T_2 Carr-Purcell-Meiboom-Gill spin-echo experiment showing backbone amide proton resonances at 0.0 molar equivalents TnC.Gd(III)$_4$ to TnI peptide 265

Figure VII-4 Increase in relaxation rates, $1/T_{1OBS}$ and $1/T_{2OBS}$, for the TnI peptide L111(δCH3)2 methyl group as a function of the molar equivalents $TnC.Ln(III)_4$ to TnI peptide 266

Figure VII-5 Plot of T_{2Pi} versus T_{1Pi} for various nuclei on the TnI peptide 267

Figure VII-6 Model of a proposed TnI peptide-induced conformational change in $TnC.Ca(II)_4$ involving the 'hinge region' in the D/E linker 267

Figure VIII-1A 500 MHz ^1H NMR spectra of the G110-TnI peptide in the absence and presence of 0.1 molar equivalents $TnC.Ca(II)_4$: Aliphatic upfield region of the spectrum 305

Figure VIII-1B 500 MHz ^1H NMR spectra of the G110-TnI peptide in the absence and presence of 0.1 molar equivalents $TnC.Ca(II)_4$: Complete downfield region of the spectrum with the exchangeable guanidinium resonances of R108, R112, R113 and R115, and the aromatic F106 resonances 306

Figure VIII-1C 500 MHz ^1H NMR spectra of the G110-TnI peptide in the absence and presence of 0.1 molar equivalents $TnC.Ca(II)_4$: Expanded region of spectrum B showing only the backbone amide proton resonances 307

Figure VIII-2 Plot of the change in chemical shift of the G110-TnI peptide backbone amide resonances as a function of molar equivalents $TnC.Ca(II)_4$ 308

Figure VIII-3 Upfield region of the DQFCOSY spectrum of the G110-TnI peptide in the presence of 0.1 molar equivalents $TnC.Ca(II)_4$ 309

Figure VIII-4 Upfield region of the TRNOESY spectrum of the G110-TnI peptide in the presence of 0.1 molar equivalents $TnC.Ca(II)_4$ 310

Figure VIII-5 αCH-βCH region of the TRNOESY spectrum of the G110-TnI peptide in the presence of 0.1 molar equivalents $TnC.Ca(II)_4$ 311

Figure VIII-6 Downfield-βCH region of the TRNOESY spectrum of the G110-TnI peptide in the presence of 0.1 molar equivalents $TnC.Ca(II)_4$ 312

Figure VIII-7 αCH-NH region of the DQFCOSY spectrum of the G110-TnI peptide in the presence of 0.1 molar equivalents $TnC.Ca(II)_4$ 313

Figure VIII-8 αCH-NH region of the TRNOESY spectrum of the G110-TnI peptide in the presence of 0.1 molar equivalents $TnC.Ca(II)_4$ 314

Figure VIII-9 Fingerprint αCH-NH region of the NOESY spectrum of the G110-TnI peptide superimposed upon the αCH-NH region of the TRNOESY spectrum of the same concentration G110-TnI peptide in the presence of 0.1 molar equivalents TnC.Ca(II)$_4$.................. 315

Figure VIII-10 Sequence of Nα-acetyl-G110-TnI(104-115) amide together with a schematic summary of the short- and medium- range TRNOEs defining the secondary structure of the G110-TnI peptide bound to TnC.. 316

Figure VIII-11 Plot of $^3J\alpha$CH-NH coupling constants versus molar equivalents TnC.Ca(II)$_4$ for various residues in the G110-TnI peptide............ 317

Figure VIII-12 Plot of δNH versus temperature for various G110-TnI peptide backbone amide protons and molar equivalents TnC.Ca(II)$_4$.......... 318

Figure VIII-13 Plot of the temperature coefficients measured for various G110-TnI peptide backbone amide protons versus molar equivalents TnC.Ca(II)$_4$.................................... 319

Figure VIII-14 Stereo-diagram of the G110-TnI peptide bound to Ca(II)-saturated TnC.. 320

Figure VIII-15 Superposition of the 10 MD structures taken every 0.2 ps........... 321

Figure IX-1A 500 MHz ^{1}H NMR spectra of the TnI peptide in H_20 and 50%TFE: Aliphatic upfield region of the spectrum..................... 360

Figure IX-1B 500 MHz ^{1}H NMR spectra of the TnI peptide in H_20 and 50%TFE: Complete downfield region of the spectrum with the exchangeable guanidinium resonances of R108, R112, R113 and R115 and the aromatic F106 resonances............................ 361

Figure IX-1C 500 MHz ^{1}H NMR spectra of the TnI peptide in H_20 and 50%TFE: Expanded region of spectrum B showing the backbone amide proton resonances and the C-terminal amide resonance......... 362

Figure IX-1D 500 MHz ^{1}H NMR spectra of the TnI peptide in H_20 and 50%TFE: Expanded region of spectrum B showing only the backbone amide proton resonances.. 363

Figure IX-2 Upfield region of the DQFCOSY spectrum of the TnI peptide in 50%TFE.. 364

Figure IX-3 Upfield region of the NOESY spectrum of the TnI peptide in 50%TFE.. 365

Figure IX-4 αCH-βCH region of the NOESY spectrum of the TnI peptide in 50%TFE 366
Figure IX-5 Downfield-βCH region of the NOESY spectrum of the TnI peptide in 50%TFE 367
Figure IX-6 αCH-NH region of the DQFCOSY spectrum of the TnI peptide in 50%TFE 368
Figure IX-7 αCH-NH region of the NOESY spectrum of the TnI peptide in 50%TFE 369
Figure IX-8 NH-NH region of the NOESY spectrum of the TnI peptide in 50%TFE showing NOEs between backbone amide protons 370
Figure IX-9A 500 MHz ^{1}H NMR spectra of mastoparan in H_20 and 50%TFE: Aliphatic upfield region of the spectrum 371
Figure IX-9B 500 MHz ^{1}H NMR spectra of mastoparan in H_20 and 50%TFE: Complete downfield region of the spectrum 372
Figure IX-9C 500 MHz ^{1}H NMR spectra of mastoparan in H_20 and 50%TFE: Expanded region of spectrum B showing only the backbone amide proton resonances 373
Figure IX-10 Upfield region of the DQFCOSY spectrum of mastoparan in 50%TFE 374
Figure IX-11 Upfield region of the NOESY spectrum of mastoparan in 50%TFE 375
Figure IX-12 αCH-βCH region of the NOESY spectrum of mastoparan in 50%TFE 376
Figure IX-13 Downfield-βCH region of the NOESY spectrum of mastoparan in 50%TFE 377
Figure IX-14 αCH-NH region of the DQFCOSY spectrum of mastoparan in 50%TFE 378
Figure IX-15 αCH-NH region of the NOESY spectrum of mastoparan in 50%TFE 379
Figure IX-16 NH-NH region of the NOESY spectrum of mastoparan in 50%TFE showing NOEs between the chemically exchanging C-terminal NH2 groups and the backbone amide of the C-terminal residue, L14 380
Figure IX-17 NH-NH region of the NOESY spectrum of mastoparan in 50%TFE showing NOEs between backbone amide protons 381

Figure IX-18A 500 MHz ^{1}H NMR spectra of mastoparan in the absence and presence of 0.1 molar equivalents TnC.Ca(II)$_4$: Aliphatic upfield region of the spectrum 382
Figure IX-18B 500 MHz ^{1}H NMR spectra of mastoparan in the absence and presence of 0.1 molar equivalents TnC.Ca(II)$_4$: Complete downfield region of the spectrum 383
Figure IX-18C 500 MHz ^{1}H NMR spectra of mastoparan in the absence and presence of 0.1 molar equivalents TnC.Ca(II)$_4$: Expanded region of spectrum B showing only the backbone amide proton resonances 384
Figure IX-19 Upfield region of the DQFCOSY spectrum of mastoparan in the presence of 0.1 molar equivalents TnC.Ca(II)$_4$ 385
Figure IX-20 Upfield region of the NOESY spectrum of mastoparan in the presence of 0.1 molar equivalents TnC.Ca(II)$_4$ 386
Figure IX-21 αCH-βCH region of the NOESY spectrum of mastoparan in the presence of 0.1 molar equivalents TnC.Ca(II)$_4$ 387
Figure IX-22 Downfield-βCH region of the NOESY spectrum of mastoparan in the presence of 0.1 molar equivalents TnC.Ca(II)$_4$ 388
Figure IX-23A αCH-NH region of the DQFCOSY spectrum of mastoparan in the presence of 0.1 molar equivalents TnC.Ca(II)$_4$: Spectrum showing L3 αCH-NH COSY cross-peak 389
Figure IX-23B αCH-NH region of the DQFCOSY spectrum of mastoparan in the presence of 0.1 molar equivalents TnC.Ca(II)$_4$: Expanded region of spectrum A 390
Figure IX-24A αCH-NH region of the NOESY spectrum of mastoparan in the presence of 0.1 molar equivalents TnC.Ca(II)$_4$: Spectrum showing L3αCH-NH and I1αCH-N2NH NOEs 391
Figure IX-24B αCH-NH region of the NOESY spectrum of mastoparan in the presence of 0.1 molar equivalents TnC.Ca(II)$_4$: Expanded region of spectrum A 392
Figure IX-25 NH-NH region of the NOESY spectrum of mastoparan in the presence of 0.1 molar equivalents TnC.Ca(II)$_4$ 393
Figure IX-26 Fingerprint αCH-NH region of the NOESY spectrum of mastoparan superimposed upon the αCH-NH region of the NOESY spectrum of the same concentration mastoparan in the presence of 0.1 molar equivalents TnC.Ca(II)$_4$ 394

Figure IX-27 Sequence of the TnI peptide together with a schematic summary of the short- and medium- range NOEs defining the secondary structure of the peptide in 50%TFE....................... 395

Figure IX-28 Sequence of mastoparan together with a schematic summary of the short- and medium- range NOEs defining the secondary structure of the peptide in 50%TFE....................... 395

Figure IX-29 Sequence of mastoparan together with a schematic summary of the short- and medium- range TRNOEs defining the secondary structure of the peptide when bound to TnC............. 396

Figure IX-30 Stereo-diagram of the TnI peptide in 50%TFE........................... 397

Figure IX-31 Stereo-diagram of mastoparan in 50%TFE............................... 398

Figure IX-32 Superposition of the 10 MD structures taken every 0.2 ps for the TnI peptide in 50%TFE... 399

Figure IX-33 Superposition of the 10 MD structures taken every 0.2 ps for mastoparan in 50%TFE.. 400

Figure X-1 Flow diagram for the transferred iterative relaxation matrix analysis (TR-IRMA) for structure determination of chemically-exchanging biomolecules from ^{1}H-^{1}H TRNOEs........................ 426

Figure X-2 Simulated TRNOE build-up curves versus experimentally measured TRNOE intensities.. 427

List of Abbreviations and Symbols

A1, A2	alkali light chains 1 and 2
Boc	*tert*-butyloxycarbonyl
CaM	calmodulin
CD	circular dichroism
2-ClZ	2-chlorobenzyloxycarbonyl
DTT	dithiothreitol
DTNB	5,5' - dithiobis (2-nitrobenzoic acid)
DEAE	diethyl-aminoethyl
DQFCOSY	two-dimensional double-quantum filtered correlation spectroscopy
DSS	disodium-2,2-dimethyl-(-2-silapentane-5-sulphonate).
EDTA	ethylenediamene tetraacetic acid
EM	energy minimization
FID	free induction decay
HLH	helix-loop-helix
HPLC	high performance liquid chromatography
IRMA	iterative relaxation matrix analysis
MD	molecular dynamics
NMR	nuclear magnetic resonance
NOE	nuclear Overhauser enhancement
NOESY	two-dimensional nuclear Overhauser enhancement spectroscopy
ppm	parts per million
ppb	parts per billion
s-CaM	skeletal calmodulin
s-TnC	skeletal troponin C
TFA	trifluoroacetic acid
TnC	troponin C
TnI	troponin I
TnT	troponin T
Tosyl	4-toluenesulfonyl
TR-IRMA	TRansferred iterative relaxation matrix analysis
TRNOE	transferred nuclear Overhauser enhancement
TRNOESY	two-dimensional transferred nuclear Overhauser enhancement spectroscopy

A, Ala	Alanine
C, Cys	Cysteine
D, Asp	Aspartate
E, Glu	Glutamate
F, Phe	Phenylalanine
G, Gly	Glycine
H, His	Histidine
I, Ile	Isoleucine
K, Lys	Lysine
L, Leu	Leucine
M, Met	Methionine
N, Asn	Asparagine
P, Pro	Proline
Q, Gln	Glutamine
R, Arg	Arginine
S, Ser	Serine
T, Thr	Threonine
V, Val	Valine
W, Trp	Tryptophan
Y, Tyr	Tyrosine

Chapter I

Introduction

Muscle contraction is initiated by nervous stimulation which causes an increase in the intracellular free Ca(II) concentration. In skeletal muscle, the rise in intracellular free Ca(II) from lower than 10^{-7} in the resting cell to about 10^{-5} M is produced by a release of Ca(II) from the sarcoplasmic reticulum. At this concentration, Ca(II) binds to the regulatory troponin complex (Tn) present in the thin filament of the myofibril. Tn consists of three different subunits; troponin C (TnC) which binds Ca(II), troponin (TnI) which binds actin and inhibits the actomyosin ATPase, and troponin T (TnT) which binds the Tn complex to tropomyosin (Greaser and Gergely, 1973). The thin filament is additionally composed of actin and tropomyosin (Tm). The actin subunits polymerize to form a double-stranded helix along which the elongated Tm molecule is polymerized head-to-tail. The two α-helical polypeptide chains of Tm, which are arranged in a coiled-coil, lie in the two grooves formed by the actin filament. One Tm spans approximately seven actin molecules and binds a single Tn complex. The three subunits of Tn are located periodically (385 Å) along the thin filament, one Tn molecule occurring one third of the distance from the carboxyl-terminal end of each Tm molecule. The molar ratio of actin:Tm:Tn in the thin filment is 7:1:1. Figure I-1 shows the molecular arrangement of the thin filament proteins, while Table I-1 lists the properties of these proteins.

The conformational changes associated with the binding of Ca(II) to the regulatory sites of the TnC subunit of Tn provide the signal for muscle contraction. The myofibril is composed of overlapping thin and thick filaments, which slide past each other during muscle contraction. The thick filament is composed primarily of myosin, which contains the ATPase activity of the myofibril required to provide the energy for the contractile force. The head of the myosin molecule forms crossbridges to the actin molecule. When the intracellular free Ca(II) concentration rises upon muscle enervation, the subsequent binding of Ca(II) to the TnC subunit of Tn leads to conformational changes not only within the TnC subunit, but also within the whole Tn complex, ultimately affecting interactions between the Tn complex and the rest of the proteins in the thin filament. These structural changes cause a stronger interaction between actin and myosin (presumably in the number of crossbridge attachments), enhanced actomyosin ATPase activity, and ultimately muscle contraction (a basic description of muscle and its regulation can be found in biochemistry textbooks such as Stryer, 1988).

A. The Thin Filament

1. Troponin

a. TnC. TnC is a highly conserved molecule among muscle types and species. Rabbit skeletal TnC is composed of 159 residues with a calculated molecular weight of 17,846 (Collins *et al.*, 1973, 1977). It is a very acidic protein owing to its high content of glutamic and aspartic acid residues. The x-ray structures of chicken (Sundaralingam *et al.*, 1985) and turkey (Herzberg and James, 1985) skeletal TnC have been solved and reveal a dumbbell-shaped molecule, approximately 75 Å long, with distinct N-terminal and C-terminal globular domains joined by a long nine-turn α-helix. Each major domain contains two Ca(II) binding sites based on the EF hand helix-loop-helix structural motif (Kretsinger and Nockolds, 1973; Collins *et al.*, 1973; Vanaman *et al.*, 1977). In skeletal TnC, the higher affinity Ca(II)/Mg(II) sites (sites III and IV) reside in the C-terminal domain and bind Ca(II) and Mg(II) with association constants of 2×10^7 and 5×10^3 M^{-1}, respectively (Potter and Gergely, 1974). The Ca(II) specific sites (sites I and II) reside in the N-terminal domain and bind Ca(II) with an association constant of $2\text{x}10^5$ M^{-1}. Figure I-2 shows the crystal structre of turkey skeletal TnC with the helices labeled A through H. The helix linking the two major domains is a composite of helices D and E.

The low affinity sites in the N-terminal domain have been implicated as the physiologically relevant triggering sites that initiate muscle contraction (Johnson *et al.*, 1979; Robertson *et al.*, 1981). At resting levels of Ca(II), only the high affinity sites of TnC are filled. After nerve stimulation and the subsequent increase in free Ca(II) concentration, the low affinity site(s) become filled. The conformational change associated with Ca(II) binding to the low affinity Ca(II) binding sites of TnC is the signal that initiates muscle contraction. The centers of the two domains are separated by about 40 Å which suggests that there are no direct interactions between them. Any conformational change due to Ca(II) binding at either site I or II could be transmitted between the two domains of TnC via the D/E linker. Kinetic studies (Grabarek *et al.*, 1986) have shown that the binding of Ca(II) to the low affinity sites perturbs the structure at C98 (part of helix E) which is located near Ca(II) binding site III and in the region where TnI inhibitory region (residues 96-116) bind.

The Ca(II) binding sites I and II were crystallized in the Ca(II)-free state and seem to be stabilized due to the interaction between the various helices comprising the Ca(II) binding sites I and II and the N-helix (residues 3-13). That there is no counterpart to the N-helix in the C-terminal domain suggests that the Ca(II) affinity for the low affinity sites may not only be a function of the residues within the Ca(II) coordinating loop, but also a function of the tertiary folding of this domain. Herzberg *et al.* (1986) predicted, based on computer modeling of the x-ray crystal structure of TnC, that residues in the C-helix would become more exposed upon Ca(II) binding to the low affinity sites.

b. TnI. Rabbit skeletal TnI is composed of 179 residues and has a calculated molecular weight of 20,864 (Wilkinson and Grand, 1975). Different isoforms of the protein exist in slow skeletal, fast skeletal and cardiac muscle, with molecular weights in the range of 20-24 kDaltons. TnI has two segments with extremely basic amino acid sequences: residues 102-135 contain 12 basic side chains and residues 5-27 contain six basic side chains. Both of these segments are significant in regulatory thin filament interactions. Two residues of isolated TnI can be phosphorylated: T11 by phosphorylase kinase and S118 by cardiac 3',5'-cyclic AMP-dependent protein kinase (Huang *et al.*, 1974; Moir *et al.*, 1977). Skeletal TnI is not phosphorylated in the whole Tn complex, and no role has yet been established for skeletal TnI phosphorylation. Functionally, TnI is the specific inhibitor of the Mg(II)-stimulated ATPase of actomyosin (Greaser and Gergely, 1973).

c. TnT. The largest of the Tn subunits, skeletal TnT has a calculated molecular weight of 30,503 and consists of 259 amino acid residues (Pearlstone and Smillie, 1976). Different isoforms of the protein exist in slow skeletal, fast skeletal and cardiac muscle, with molecular weights in the range of 31-36 kDaltons. TnT is a highly polar molecule, with a concentration of acidic side chains near its amino terminus (residues 1-39) and a predominance of basic residues near its carboxyl terminus (residues 221-259). Antibody work by Ohtsuki (1979) showed separate domains for the N- and C-terminal segments of TnT along tropomyosin in thin filaments, suggesting an elongated rod shape for TnT at least 130 Å long. Phosphorylase kinase phosphorylates three sites in TnT from rabbit fast skeletal muscle (Moir *et al.*, 1977), however no physiological role for TnT phosphorylation has been demonstrated.

2. Tropomyosin

Tropomyosin exists as a dimer of two polypeptide subunits, which associate in register in a coiled-coil fashion (Johnson and Smillie, 1975; Graceffa and Lehrer, 1980). Two types of subunits occur in skeletal muscle, α and β, with the proportions of each subunit being tissue specific (Cummins and Perry, 1973, 1974). In rabbit skeletal tropomyosin, dimers of $\alpha\alpha$ are most common. The subunits, 284 amino acid residues and 33 kDaltons each, have similar amino acid sequences (Hodges *et al.*, 1972; Sodek *et al.*, 1972). The high (>90%) helical content of the subunits allows a coiled-coil interaction between the regular nonpolar side chains and electrostatic interactions between the regular charged side chains (Hodges *et al.*, 1972). Head-to-tail overlap of tropomyosin coiled-coils in the thin filament appears to occur over eight or nine residues at the N- and C-termini of the molecule. The interaction of these residues is strengthened by hydrophobic and electrostatic interactions (Johnson and Smillie, 1975; Mak *et al.*, 1981; Mak and Smillie, 1983).

3. Actin

Actin is a highly conserved protein (Vanderkerckhove and Weber, 1978) and forms the major constituent of thin filaments. In solutions of low ionic strength, actin is a 42 kDalton monomer called G-actin because of its globular shape. As the ionic strength is increased to the physiologic level, G-actin polymerizes into a fibrous form called F-actin, which closely resembles thin filaments. In muscle, F-actin consists of two strands coiled about one another. Recently, the x-ray crystal structure of a G-actin:DNAse complex has been solved (Kabsch *et al.*, 1990; see Figure I-3). This structure illustrates that regions within the N-terminal residues 1-32 are located on the surface of the molecule. These residues have been implicated in the binding of the myosin S1 head and in the binding of TnI (Van Eyk and Hodges, 1991; Van Eyk *et al.*, 1991a).

B. The Thick Filament

The thick filament is comprised of myosin, an enzyme capable of hydrolyzing ATP. Myosin is a very large molecule (540 kDaltons) composed of two heavy chains (each 230 kDaltons) and four associated light chains (each about 20 kDaltons). The carboxy terminal regions of the two heavy chains wind around one another to form a two-stranded helical coiled-coil, while the amino terminal regions fold into two globular heads which associate with the light chains. Each globular head can bind to actin and can hydrolyze ATP. When actin binds to the myosin head, the rate of ATP hydrolysis is increased due to an increase in the rate of release of products (ADP + Pi). See Figure I-4 for a schematic diagram of a myosin molecule.

Myosin can be specifically cleaved at several sites (as indicated in Figure I-4) to yield a single-headed myosin subfragment I (SI) or a double-headed heavy meromyosin frament (HMM). The two DTNB light chains, which are not essential for ATPase activity, are destroyed during the cleavage process used to prepare S1 and HMM. The other two light chains, known as A1 (MW 21,000) and A2 (MW 16,200), are essential for ATPase activity, and remain associated with the myosin fragments. Therefore, both myosin fragments (SI and HMM) retain the ability to bind actin and hydrolyze ATP.

C. Interactions of Regulatory Proteins

1. Tropomyosin-Actin

One coiled-coil Tm molecule spans seven polymerized actin monomers, but the amino acid sequence of Tm reveals 14 quasi-equivalent repeating regions of acidic and nonpolar residues throughout the length of each chain that could serve as actin-binding sites (Parry, 1974; Stewart and MacLachlan, 1975; Stone *et al.*, 1974). Thus, in the Tm dimer there would be 28 acidic zones exposed on the surface of the molecule, arranged in 14 opposing pairs such that four sets of seven zones occur at 90° from each other (Stewart and MacLachlan, 1975). Each of these seven zones would be able to come in contact with one actin monomer. These acidic zones may interact with acidic regions on actin through Mg(II) bridges, or with positive regions on actin via salt bridges. Hydrophobic interactions between nonpolar groups may also provide additional stability (Stewart and MacLachlan, 1975). Stewart and McLachlan (1975) have proposed that one set of the seven binding sites attaches to actin in the relaxed muscle, and one set upon muscle activation, during which the Tm molecule moves one-quarter turn to interact with actin from a different angle. This model is consistent with the steric blocking mechanism of regulation. Alternatively, Philips *et al.* (1980) have suggested that Tm is continually changing connections with actin, producing a net effect of relaxation or contraction.

The head-to-tail overlap region of Tm also appears to be important in the binding of actin (Mak *et al.*, 1981). The ability of Tm to polymerize along actin greatly increases its binding affinity (Walsh and Wegner, 1980; Wegner, 1979), and Tm that is unable to polymerize owing to the removal of its C-terminal 11 residues can no longer bind to actin (Mak and Smillie, 1983). The regions of Tm and actin which are presumed to interact with each other are given in Table 1-2.

2. TnT-Tropomyosin

TnT links the Tn molecule to Tm. Regions of TnT that interact with Tm have been determined by protein fragment studies (Jackson *et al.*, 1975; Pearlstone and Smillie, 1977; Ohtsuki, 1979; Pato *et al.*, 1981; Tanokura *et al.*, 1983). These regions have been identified as residues 1-151, and 197-259. Mak and Smillie (1983) found that the removal of the C-terminal 11 residues from Tm greatly reduced the affinity of Tm for residues 1-151 of TnT. This suggests that the binding of this segment of TnT occurs at the C-terminus of Tm, perhaps extending to the N-terminus of the overlapping Tm molecule. Pearlstone and Smillie (1982) showed that Ca(II), in the presence of TnC, does not affect the binding affinity of segment 1-151 of TnT for Tm. Residues 197-259 of TnT are known to bind to TnI(105-107) and TnC (105) in a Ca(II)-sensitive manner in the presence of TnC (Pearlstone and Smillie, 1982, 1983). The TnI and TnC subunits are found near C190 of Tm, so it can be assumed that segment 197-259 of TnT binds near C190. CD studies (Pearlstone and Smillie, 1978) show a high helical content in residues 71-151 of TnT, whereas 159-227 of TnT contain a strong heptapeptide repeat similar to that in the Tm sequence (Parry, 1981), suggestive of an interaction between Tm and TnT that may be coiled-coil in nature (Mak *et al.*, 1983). The interaction of TnT with the overlap portion of Tm may stabilize the overlap region and/or have a role in the transduction of the Ca(II)-binding signal for muscle activation (Flicker *et al.*, 1982; Phillips *et al.*, 1980). The regions of TnT and Tm which are presumed to interact with each other are given in Table 1-2.

Antibody work (Ohtsuki, 1979) and EM work of rotary-shadowed molecules (Flicker *et al.*, 1982) have revealed the Tn complex as a globular mass near C190 of Tm. This region is composed primarily of TnC, TnI, and a rodlike tail (which is TnT) extending toward the C-terminus of Tm. These studies suggest at least two regions of interaction between TnT and Tm: one near C190, where TnC and TnI are found, and one along the C-terminal stretch of Tm.

3. TnT-TnC and TnT-TnI

TnT attaches Tn to Tm by its interactions with the TnC and TnI subunits. The extent of the interaction between TnT and TnC in whole Tn is uncertain, however it is known that TnT is required for Ca(II)-dependent, reversible regulation of ATPase activity, and must therefore interact either directly or indirectly with TnC.

Specific sites of TnT that interact with TnC and TnI have not been clearly identified. Residues 159-227 at the C-terminus of TnT are implicated in the binding of TnC (Ohtsuki, 1979; Pearlstone and Smillie, 1978), and lysine residues within this region of TnT show reduced reactivity with acetic anhydride when TnC and TnT are mixed (Hitchcock *et al.*, 1981). Residues 1-70 at the N-terminus of TnT have been observed to bind to TnI (Pearlstone and Smillie, 1980), but a reinvestigation showed there was no interaction between these regions at lower, more physiological ionic strength (Pearlstone and Smillie, 1983). A second region of TnT (residues 159-259), however, has been shown to interact with TnI, according to gel chromatography and CD studies (Pearlstone and Smillie, 1978, 1985). Work with peptides that overlap residues 159-259 of TnT (Pearlstone and Smillie, 1978) indicates that TnI binds at the N-terminal end of this stretch, since it binds to a peptide of residues 152-175, and that TnC binds at the C-terminal end of this region, since it binds to a peptide of residues 176-230. This conclusion is consistent with the results of lysine reactivity studies (Hitchcock *et al.*, 1981) and phosphorylation studies (Moir *et al.*, 1977) of the TnT-TnI complex. The regions of TnT which are presumed to interact with TnC and TnI are given in Table 1-2.

There may be several sites in the N-terminal region of TnC (residues 1-100) that are able to form Ca(II)-dependent interactions with TnT (Grabarek *et al.*, 1981; Weeks and Perry, 1978). Lysine reactivities in this region of TnC are reduced when TnC is complexed with TnI or TnT (Hitchcock, 1981), and TnT has been shown to cross-link to C98 of rabbit skeletal TnC alone or in a Tn complex (Tao *et al.*, 1986a, 1986b). The regions of TnC which are presumed to interact with TnT are given in Table 1-2.

Residues 57-106 of TnI contain a heptad hydrophobic repeat like that seen between residues 197-250 of TnT. This pattern is typical of a coiled-coil structure and suggestive of an interaction between these two regions on the TnI and TnT proteins (Pearlstone and Smillie, 1985). This notion is supported by Chong and Hodges (1982b) who used a photochemical cross-linker to show that C48 and C64 of TnI are very close to residues 176-230 of TnT. The same workers (Chong and Hodges, 1982c) used an iodoacetamide labeling of cysteines to show that C48 and C64 are inaccessible only in whole Tn and in a TnI-TnT complex, whereas C133 of TnI, which is presumed not to associate with TnT, is always reactive. Hitchock-DeGregori (1982) showed that several lysines in the region of residues 40-78 of TnI exhibited changed reactivity with acetic anhydride in the TnI-TnT complex. The reactivity of these lysines was sensitive to the binding of Ca(II) to TnC in whole Tn, which suggests that the interaction between TnI and TnT is Ca(II) sensitive. The regions of TnI which are presumed to interact with TnT are given in Table 1-2.

4. TnC-TnI and TnI-Actin

The Ca(II)-dependent interactions between TnC, TnI and actin are key interactions in the activation of contraction in skeletal muscle. TnI inhibits the Mg(II)-ATPase activity of actomyosin (Hartshorne and Mueller, 1968; Schaub and Perry, 1969; Greaser and Gergely, 1971; Perry *et al.*, 1972) and binds both to actin and Tm-actin (Potter and Gergely, 1974; Hitchcock, 1975). The inhibition of actomyosin ATPase is neutralized when Ca(II)-saturated TnC forms a 1:1 complex with TnI (Perry *et al.*, 1972; Weeks and Perry, 1978; Chong *et al.*, 1983). This results in potentiation of the ATPase and ultimately in muscle contraction. The region of TnI which is responsible for its inhibitory activity is the same region which is involved in a Ca(II)-sensitive 'switch' between binding to actin-Tm and binding to TnC (Van Eyk and Hodges, 1988). In the absence of Ca(II), the inhibitory region of TnI, spanned by residues 96-116, is bound to the surface of actin-Tm, inhibiting the actomyosin ATPase activity and therefore contraction. In the presence of Ca(II), this region of TnI is thought to bind to TnC (Cachia *et al.*, 1985). It has been proposed that the structural changes produced by Ca(II) binding to TnC result in the presentation of regions on the surface of TnC capable of binding TnI with high affinity (LaPorte *et al.*, 1980; Gariepy and Hodges, 1983; Cachia *et al.*, 1985).

Studies characterizing the interaction between TnC and TnI have pointed to multiple interactions between these two proteins. TnI fragment studies reported by Syska *et al.* (1976) demonstrated that two regions of the TnI protein are capable of interacting with TnC. The first of these sites spans residues 1-21, and includes the site of phosphorylation catalyzed by phosphorylase kinase (T11), whereas the second of these sites spans residues 96-116 and is adjacent to a second phosphorylation site (S117) (Moir *et al.*, 1974). Equimolar amounts of TnC completely inhibit phosphorylation at these sites (Cole and Perry, 1975). The TnI segment of residues 96-116 is of special interest because it also binds to actin and can inhibit actomyosin ATPase activity. Syska *et al.* (1976) demonstrated that a CNBr fragment of TnI (residues 96-116) mimics intact TnI in its ability to inhibit actomyosin ATPase (Syska *et al.*, 1976; Nozaki *et al.*, 1980; Talbot and Hodges, 1981a, 1981b). Talbot and Hodges (1981a), using synthetic peptides, showed that residues 104-115 of TnI comprise the minimum sequence necessary for inhibition of actomyosin ATPase activity. The synthetic peptide TnI(104-115) possesses Tm specificity (Talbot and Hodges, 1979) and TnC binding capabilities (Cachia *et al.*, 1983, 1985; Van Eyk and Hodges, 1988), which results in the release of ATPase inhibition (Cachia *et al.*, 1986). Thus, it is would appear that residues 104-115 comprise the inhibitory site of TnI and binding of this region to Ca(II)-saturated TnC leads to relief of inhibition of actomyosin ATPase, and ultimately to muscle contraction. The regions of TnI which are presumed to interact with TnC and actin are given in Table 1-2.

A number of studies employing proteolytic fragments of TnC have revealed three regions of the TnC protein capable of interacting with TnI; The C-helix (residues 50-60), the E-helix (residues 89-100) and the G-helix (residues 126-136). The six lysines of TnC which show reduced reactivity with acetic anhydride upon TnC-TnI interaction are located within these three fragments (Hitchcock, 1981). The interaction of TnI with the G-helix is not Ca(II)-dependent (Grabarek *et al.*, 1981), while the interaction with the other two regions are Ca(II)-sensitive. NMR studies and studies modifying cysteine and lysine residues (Hitchcock, 1981; Ingraham and Hodges, 1988) indicate that the residues along the D-helix become more exposed to solvent upon Ca(II) binding, potentially opening a new binding site for TnI.

There is less known about the interaction between actin and TnI. Only in the last few years has the N-terminal region of actin been implicated in the binding to TnI, in particular, TnI fragment 96-116 (Grabarek and Gergely, 1987; Levine *et al.*, 1988). The recent actin structure determined by x-ray crystallography of the G-actin:DNAse complex showed that regions within the N-terminal residues 1-32 of actin, in particular residues 1-7 and 21-28, are located on the surface of the molecule (Kabsch *et al.*, 1990; see Figure I-3). The regions of TnC and actin which are presumed to interact with TnI are given in Table I-2.

Interestingly, the same regions on actin which are presumed to interact with TnI are implicated in the acto-S1 interaction. Immunological data, crosslinking and NMR experiments have indicated that the N-terminal region of actin also contains the binding sites between actin and myosin. Crosslinking experiments have shown that the acidic residues of actin region (1-12) bound to the 20 and 50 kDalton tryptic fragments of S1 (Sutoh, 1982, 1983). NMR studies have confirmed that residues in the amino terminus of actin were perturbed during ther acto-S1 interaction (Moir and Levine, 1986; Moir *et al.*, 1987). Furthermore, antibodies specific to sequences within the N-terminal (1-28) region of actin have been produced (Mejean *et al.*, 1986, 1987; Miller *et al.*, 1987; Das Gupta *et al.*, 1990) which completely blocked the interaction of actin and S1. The regions of actin which are presumed to interact with myosin are given in Table 1-2.

D. The Contractile Cycle

The contractile force is generated by the cyclic formation and dissociation of complexes between actin and the S1 heads of myosin. The Ca(II) signal alters the acto-myosin interaction resulting in an increase in the number of crossbridge attachments between the thick and thin filament. Repeated cycles of attachment, pulling, and detachment take place during a single contraction. The crossbridges appear not to be statically attached to the thin filament but rather in a rapid equilibrium between attached and detached states such that muscle tension is a function of the sum of the number of crossbridges at any point in time (Schoenberg ***et al.***, 1984).

A generally accepted mechanism for the generation of force is shown in Figures I-5 and I-6. In resting muscle, the S1 heads of the myosin molecules are detached from the actin filament but their active sites are charged with the products of hydrolysis of ATP (ADP and Pi). These products are released very slowly and therefore the ATPase activity is very low. When muscle is stimulated, the S1 head of the myosin molecule (in which the actin-combining and enzymic sites are located) interacts with actin in some way not as yet understood and a rapid release of ADP and inorganic phosphate (Pi) ensues. This results in a rate constant for ATP hydrolysis of 10-20 s^{-1}, which is several hundred times greater than the rate of ATP hydrolysis in the resting state. At the same time, a conformational change occurs in the myosin head that forms the major part of the crossbridge, and thereby produces a change in the angle that it makes with the actin filament. The change in orientation of S1 relative to actin causes the 'power stroke' of muscle contraction: a mechanical mechanism by which the myosin head tilts from 90° to 45°. To accommodate this change in orientation and the energetic considerations involved, the actin monomer to which the head is attached is pulled forward by some 75 Å (Huxley, 1969). The dissociation of ADP and Pi from the myosin head at the end of the power stroke and the subsequent binding of ATP reverses the conformational change in S1 and leads to the very rapid release of S1 from actin. The bound ATP is hydrolyzed by the free myosin head, which resets it for the next interaction with the thin filament. Once nerve stimulation is over, Ca(II) is sequestered back into the sarcoplasmic reticulum, lowering the free Ca(II) concentration to the resting level. This reverses the interaction between the various proteins so that ATPase activity is inhibited and the muscle relaxes. (For review articles see, Leavis and Gergely, 1984, and A.S. Zot and Potter, 1987.)

E. Models for Muscle Contraction

1. Steric Blocking Model

The steric blocking model is a widely accepted yet perhaps oversimplified interpretation of the structural mechanism for regulation of skeletal muscle contraction. The model was proposed based on the three-dimensional reconstructions from electron micrographs of negatively stained actin filaments decorated with S1, and x-ray diffraction studies showing a shift in the position of Tm on the thin filament (Huxley, 1972; Haselgrove, 1972; Parry and Squire, 1973; Potter and Gergely, 1974; Wakabyashi *et al.*, 1975). This model suggests that in the absence of Ca(II), one Tm molecule (under the control of Tn) sterically blocks one F-actin unit (seven self-associated actin monomers), therefore physically blocking the interaction between actin and myosin. Upon muscle enervation, which leads to the release of Ca(II) from the sarcoplasmic reticulum and the subsequent binding of Ca(II) by the regulatory sites on the TnC subunit of Tn, Tm moves away from its blocking site and more deeply into the 'grooves' of the F-actin double helix. The Tm molecule is now in a non-blocking position, and myosin heads are able to bind actin and proceed through the ATPase-driven contraction cycle. Regulation of the position of Tm occurs via TnI. In the absence of Ca(II), TnI would be bound to actin-Tm in such a way as to block the acto-Tm interaction with myosin, while in the presence of Ca(II), the TnI-Tm-actin interaction would be broken and TnI would interact with TnC.

2. Allosteric 'Two State' Model

The allosteric model, first proposed by Eisenberg *et al.* (1980), was an attempt to link the biochemical process with the mechanical steps involved in the power stroke of muscle contraction. They presented a 'two state' model based upon the framework of allosteric models of cooperative binding for regulatory enzymes. Seven actins and one Tm or Tm-Tn complex would constitute one cooperative unit in each state. According to the 'two state' model, the regulated actin filament (actin-Tm-Tn) could exist in dynamic equilibrium between a 'weak' and a 'strong' state defined by the strength of its interaction with myosin. In order to model the mechanically significant kinetic steps in the crossbridge cycle, the two bound states were assumed to have very different mechanical properties. The initial crossbridge attachment between the actin and myosin (bound state #1) was weak (A-M-ADP-Pi). Upon phosphate release (bound state #2) there was a transition to a strongly bound state (A-M-ADP). The transition from weak to strong binding states of acto-myosin constituted the 90° to 45° movement of the myosin head, the 'power stroke'. Accordingly, Ca(II) would act as an allosteric effector to shift the equilibrium between the two states without affecting the intrinsic conformation of either state.

3. Expanded 'Two State' Model

An expansion of the allosteric 'two state' model was adapted to include the mechanism for regulation of muscle contraction (Chalovich *et al.*, 1983). The model suggested that in the presence of Ca(II), regulated actin (actin-Tm-Tn) binds S1-ATP (or S1-ADP-Pi) weakly at 90° (beginning of the crossbridge cycle), whereas regulated (actin-Tm-Tn) actin binds S1 or S1-ADP strongly at a 45° angle (at the end of the power stroke). The transition of the myosin head between 90° and 45° was assumed to occur rapidly and was associated with rapid release of Pi. As Ca(II) was removed, Tm would assume a different position of the thin filament, somehow inhibiting the rotation of S1 from the 90° state to the 45° state, and thus pushing the equilibrium toward the 'weak' form of regulated actin (actin-Tm-Tn). With actin in this 'weak' form, Pi release occurs very slowly, allowing muscle to relax. In the expanded 'two state' model, Tm does not necessarily physically block the acto-myosin interaction (as predicted by the steric blocking model) but rather blocks a kinetic transition (the release of Pi from the nucleotide active site), presumably through a conformational change in myosin and/or actin (Lehrer and Morris, 1982).

4. Continuum Model

The 'two state' model was recently modified to allow a continuum of positions on the actin filament so that under any given experimental condition of Ca(II), salt, temperature, or nucleotide bound to S1, Tm could occupy any of several condition-dependent positions rather than exist in a dynamic equilibrium between just two positions (Hill, 1983; Hill *et al.*, 1984). In the absence of Ca(II), Tm-Tn would block the myosin-binding sites on actin. In the presence of Ca(II), S1 binding to actin would shift the Tm position on actin. The position to which Tm is shifted depends on which nucleotide is bound to S1 (since the particular nucleotide may affect the angle at which S1 attaches to actin) and on the number of moles of Ca(II) bound to Tn. Therefore, the extent of blocking by Tm is determined by the degree of bend of the myosin head induced by a particular nucleotide. The extent of blocking by Tm is also determined by the conformation of the thin filament, which in turn is dictated by whether the low-affinity sites I and II on TnC are occupied by Ca(II). This suggests that there could be reciprocal interactions between S1-actin (number of crossbridge attachments) and the Ca(II) affinity of TnC.

There is some evidence from previous work to support this idea of the continuum model. Bremel and Weber (1972) demonstrated that the presence of rigor crossbridges (myosin attaches strongly to actin ion the absence of nucleotide) increases the affinity of Tn for Ca(II), suggesting an effect on crossbridge attachment on the conformation of TnC. The interaction of Tm-Tn with actin lowered the affinity of the regulatory sites of TnC (Zot *et al.*, 1983; H.G. Zot and Potter, 1987), suggesting a relationship between actin and TnC conformation. In addition, it has been proposed that cycling crossbridge interactions increase TnC affintiy for Ca(II) (Guth and Potter, 1987). Recently, by incorporating a fluorescence probe (Danz) labeled TnC into TnC-depleted muscle fibres, it was shown that there were different TnC conformations and Ca(II) affinities depending on whether the myofibril was in a weak versus strong crossbridge state (Zot and Potter, 1989). These results suggest that there is a reciprocal coupling such that conformational changes in the attachment of myosin crossbridges to actin and structural changes in TnC when Ca(II) binds can influence one another. (For a review article of the different models proposed for muscle contraction, see El-Saleh *et al.*, 1986.)

F. Research Proposal

1. Nuclear Magnetic Resonance Spectroscopy and Muscle Proteins

Nuclear Magnetic Resonance (NMR) spectroscopy is a leading technique for obtaining structural and dynamic information at the atomic level, and has been widely used to determine the structures of many proteins in solution (Wuthrich, 1986). NMR spectroscopy has been used to study the structure and dynamics of muscle proteins since the early 1960's. Through the application of direct and indirect methods using various multinuclear NMR probes, much information on the structures and kinetic features of these proteins has been derived. (For a review of NMR studies of muscle proteins up to 1984, see Ribiero *et al.*, 1984.)

^{1}H NMR studies of myosin have focussed on the flexible regions in the S1 head, since these are the regions of the molecule most likely involved in the mechanical function (Highsmith *et al.*, 1979; Highsmith and Jardetsky, 1980, 1981; Prince *et al.*, 1981; Shriver and Sykes, 1981; Sommerville *et al.*, 1990). There have also been ^{1}H NMR solution studies of Tm which have focussed on the structural dynamics and the polymerization and unfolding of the molecule (Edwards and Sykes, 1978, 1980; Brisson *et al.*, 1986; Saunders *et al.*, 1988).

There have been a comparatively larger number of ^{1}H NMR solution studies performed on actin than have been performed on myosin or Tm (Cozzone *et al.*, 1974; Nelson *et al.*, 1974; Highsmith *et al.*, 1979; Highsmith and Jardetsky, 1980; Prince *et al.*, 1981; Brauer and Sykes, 1981a, 1981b, 1982; Levine *et al.* 1988). Many of these studies have involved the interaction of actin with other proteins or co-factors. ^{1}H NMR has been used to follow the interactions between the N-terminal region of actin and TnI (Levine *et al.*, 1988), and between actin and the myosin S1 head (Highsmith and Jardetsky, 1980). ^{31}P NMR has been used to examine the ATP binding site on actin (Cozzone *et al.*, 1974; Nelson *et al.*, 1974; Brauer and Sykes, 1981a, 1981b, 1982), and ^{19}F NMR has been used to probe the myosin and Tm binding sites on actin (Barden and Phillips, 1990).

While there have been only a modest collection of NMR studies performed on myosin, Tm and actin in the literature, there have been numerous NMR studies of the Ca(II)-binding proteins in the TnC structural family. This family includes the homologous Ca(II)-binding proteins parvalbumin and calmodulin (CaM). Parvalbumin was the first Ca(II)-binding protein for which there was a solved x-ray crystal structure (Kretsinger and Nockolds, 1973); therefore it logically provided the best subject in the mid 1970's for the first series of NMR experiments performed on a Ca(II)-binding protein. ^{1}H NMR studies (Parello *et al.*, 1974; Cave *et al.*, 1976; Williams *et al.*, 1986; Padilla and Cave, 1988) and ^{13}C NMR studies (Opella *et al.*, 1974; Nelson *et al.*, 1976) have characterized the native conformation of parvalbumin. ^{1}H NMR (Birdsall *et al.*, 1979; Cave *et al.*, 1979a; Ragg *et al.*, 1986) and ^{13}C NMR (Opella *et al.*, 1974) have been used to probe the changes in the solution structure and the dynamics of parvalbumin upon the binding of metal ions; and ^{43}Ca NMR relaxation measurements (Parello *et al.*, 1978; Andersson *et al.*, 1982a; Forsen *et al.*, 1982) have given dynamical information of the Ca(II)-loaded form of the protein. Kinetic as well as competitive aspects of metal binding have been studied using direct (^{43}Ca, ^{25}Mg) (Parello *et al.*, 1978; Cave *et al.*, 1979b; Andersson *et al.*, 1981, 1982a; Forsen *et al.*, 1982) and indirect (^{23}Na, ^{113}Cd) (Grandjean *et al.*, 1977; Drakenberg *et al.*, 1978; Parello *et al.*, 1979; Cave *et al.*, 1978, 1979b, 1982; Anderson *et al.*, 1982b; Bjornson *et al.*, 1985) methods.

NMR techniques using the lanthanides as Ca(II) analogs have also been used to investigate the ion-binding properties of parvalbumins (Sowadski *et al.*, 1978; Cave *et al.*, 1979c; Lee *et al.*, 1978; Lee and Sykes, 1980a, 1980b, 1981, 1986; Corson *et al.*, 1983a, 1983b; Williams *et al.*, 1984). Lee and co-workers have used lanthanide-induced ^{1}H NMR resonance shifts and line-broadening to determine the relative compactness of the Ca(II)-

binding sites and metal-proton distances in the EF site of carp parvalbumin (Lee and Sykes, 1980a, 1980b, 1981, 1986). ^{1}H NMR (Cave *et al.*, 1979c) and ^{113}Cd NMR (Corson *et al.*, 1983a; Drakenberg *et al.*, 1985) have been used to study the stoichiometry and binding of different lanthanides and paramagnetic probes to the primary and secondary sites of the protein.

^{1}H NMR solution studies of the structure of rabbit skeletal TnC and its tryptic fragments were first reported by Levine and co-workers in 1976 (Levine *et al.*, 1986). Since then, ^{1}H NMR has been extensively used to monitor the conformational changes of TnC and its tryptic fragments upon the binding of Ca(II) or Mg(II) ions in rabbit skeletal muscle (Levine *et al.*, 1977, 1978; Seamon *et al.*, 1977; Birnbaum and Sykes, 1978; Evans *et al.*, 1980; Leavis *et al.*, 1982; Teleman *et al.*, 1983; Drabikowski *et al.*, 1985; Drakenberg *et al.*, 1987; Tsuda *et al.*, 1988, 1990), bovine cardiac muscle (Hincke *et al.*, 1981a; MacLachlan *et al.*, 1990a), and pike white muscle (McCubbin *et al.*, 1982). Kinetic as well as competitive aspects of this binding have also been studied using direct (^{25}Mg, ^{43}Ca) (Andersson *et al.*, 1981, 1982a; Forsen *et al.*, 1982) and indirect (^{23}Na, ^{113}Cd) (Forsen *et al.*, 1979; Delville *et al.*, 1980; Drakenberg *et al.*, 1987; Ellis *et al.*, 1984, 1988) NMR methods. The binding of paramagnetic lanthanides to TnC has also been studied using NMR (Lee *et al.*, 1978).

^{1}H NMR has also been used to monotor drug and peptide binding to rabbit skeletal TnC. A number of labs have studied the interaction of skeletal TnC with the whole TnI protein (Grand *et al.*, 1982; Drabikowski *et al.*, 1985) or with just the inhibitory (104-115) portion (Cachia *et al.*, 1983). The binding of trifluoperazine (TFP) (Dalgarno *et al.*, 1984; Drabikowski *et al.*, 1985) and calmidazolium (Reid *et al.*, 1990) to skeletal TnC, and the binding of bepridil to cardiac TnC (MacLachlan *et al.*, 1990b) have also been studied.

NMR studies on the solution structure of CaM followed in the early 1980's. CaM is a physiologically active protein which binds to and modulates the activity of a wide variety of enzymes and effectors. ^{1}H NMR solution studies of the structure of CaM and its tryptic fragments have been reported by numerous groups over the last ten years (Seamon, 1980; Hincke *et al.*, 1981a, 1981b; Krebs and Carafoli, 1982; Aulabagh *et al.*, 1983, 1984; Dalgarno *et al.*, 1984; Ikura *et al.*, 1983a, 1985, 1987). However, the greatest progress in the determination of the three-dimensional solution structure of CaM has come through the recent efforts of Ikura *et al.* (1990a, 1990b, 1991), who have applied the new techniques of heteronuclear triple resonance (^{1}H, ^{15}N and ^{13}C) three-dimensional NMR spectroscopy to the study of the protein.

The changes in the solution structure and the dynamics of CaM and its tryptic fragments upon binding of metal ions have been probed by ^{1}H NMR (Seamon, 1980; Ikura *et al.*, 1983b, 1984; Ikura, 1986; Klevit *et al.*, 1984; Sutoo *et al.*, 1986a, 1986b; Akiyama *et al.*, 1990); and kinetic as well as competitive aspects of this binding have also been studied using direct (^{43}Ca) (Anderson *et al.*, 1981, 1982a, 1982c; Thulin *et al.*, 1984; Teleman *et al.*, 1986) and indirect (^{23}Na, ^{113}Cd) (Delville *et al.*, 1980; Forsen *et al.*, 1980, 1982; Anderson *et al.*, 1982b, 1982c, 1985; Tsai *et al.*, 1987; Ikura *et al.*, 1989) NMR methods.

^{1}H (Krebs and Carafoli 1982; Dalgarno *et al.*, 1984; Sutoo *et al.*, 1986a; Klevit, 1987; Yazawa *et al.*, 1987; Reid *et al.*, 1990; Ohki *et al.*, 1991) and ^{113}Cd NMR (Forsen *et al.*, 1980; Thulin *et al.*, 1984; Andersson *et al.*, 1985; Linse *et al.*, 1986) have been used to monitor the binding of many drugs and inhibitors to CaM. The binding of TFP has been followed by ^{1}H NMR (Krebs and Carafoli 1982; Dalgarno *et al.*, 1984; Thulin *et al.*, 1984; Klevit, 1987), ^{43}Ca NMR (Vogel *et al.*, 1984; Shimizu *et al.*, 1988), and ^{113}Cd NMR (Forsen *et al.*, 1980). The binding of the bee venoms mastoparan and mellitin have been followed by ^{1}H NMR (Seeholzer *et al.*, 1986; Yazawa *et al.*, 1987; Ohki *et al.*, 1991) and ^{113}Cd NMR (Linse *et al.*, 1986). ^{1}H NMR has also been used to probe physiologically relevant interactions like the interaction between CaM and the (576-594)G peptide of skeletal myosin light chain kinase (sk-MLCK) (Klevit *et al.*, 1985; Klevit, 1987; Seeholzer and Wand 1989), and between CaM and a fragment of caldesmon (Yazawa *et al.*, 1987). There has been some evidence that there is communication between the two globular domains of CaM in the presence of these drugs and peptides (Linse *et al.*, 1986; Yazawa *et al.*, 1987).

While there have been many NMR studies of muscle proteins, and particularly of the Ca(II)-binding family of muscle proteins, only a few of these studies have followed the interactions of muscle proteins in the myofibril. Exceptions are the NMR studies involving the interactions between actin with TnI (Levine *et al.*, 1988), actin with myosin (Highsmith and Jardetsky, 1980; Barden and Phillips, 1990), and TnC with TnI (Grand *et al.*, 1982; Cachia *et al.*, 1983; Drabikowski *et al.*, 1985). Since the interactions between these proteins are communicated as structural rearrangements and conformational changes at the molecular level, they are particularly suited to study by solution state NMR techniques.

NMR spectroscopy has undergone a technological revolution in the last decade, evolving into a powerful method for determining structures of biological macromolecules. This rapid development has been promoted by several key advances in the field, primarily in the introduction of two- and three-dimensional NMR experiments, high field spectrometers (500 and 600 MHz), and computational algorithms for converting NMR derived distance measurements into three-dimensional structures. Armed with these new technological advances, it is now possible to examine interactions between larger proteins

(Mr > 20 kDaltons), and solve the conformations of these proteins at their template interfaces.

The Ca(II)-sensitive interactions between TnC, TnI, and actin are arguably the most important of the interactions between muscle proteins in the myofibril, since they function as the molecular 'switch' between muscle contraction and muscle relaxation. While there have been some NMR studies performed on this three-protein system, they have not determined the identity nor the three-dimensional arrangement of the residues involved at the binding interfaces. This thesis is concerned with the Ca(II)-sensitive interaction between TnC and the inhibitory region of TnI (104-115). Prior to a presentation of the thesis proposal and outline of chapter contents, a brief description of the Ca(II)-sensitive interaction between TnC and the inhibitory region of TnI in the TnC-TnI-actin system is given.

2. Ca(II)-Sensitive Interation between TnC and the Inhibitory Region (104-115) of TnI

The protein interactions involving TnC, TnI, and actin are extremely important, since they act as Ca(II)-sensitive 'switches' in regulating muscle contraction. Control of the Tm position on the actin filament resides in the fact that the TnI inhibitory region can 'flip-flop' between TnC and actin-Tm. Similarily, the N-terminal region of action (1-28) acts as a chemical switch, flip-flopping between a binding site on TnI, in particular the inhibitory region of TnI, and a binding site on S1 (Van Eyk and Hodges, 1988; Van Eyk *et al.*, 1991a). Which particular interaction dominates in the absence versus the presence of Ca(II) is dependent on the relative binding affinities of the TnI inhibitory region for TnC versus Tm-actin. Since the interactions between actin-TnI and TnI-TnC are dependent on whether Ca(II) is bound to regulatory Ca(II) binding sites I and II on TnC, the rate of ATP hydrolysis by myosin can be directly linked to Ca(II) binding to TnC.

When the regulatory Ca(II) binding sites I and II are unoccupied, the interaction between TnI and actin-Tm is dominant (see Figure I-7). Muscle relaxation is promoted due to inhibition of actomyosin ATPase activity. When the regulatory Ca(II) binding sites I and II are occupied, TnI residues 104-115 have a stronger binding affinity for TnC, presumably due to a conformational change in the TnC molecule which leads to the presentation of regions on the surface of TnC capable of binding TnI with high affinity (LaPorte *et al.*, 1980; Gariepy and Hodges, 1983; Cachia *et al.*, 1985). Thus, in the presence of saturating Ca(II), the interaction between TnI and TnC is dominant (see Figure I-7), and actin residues 1-28 cannot bind to TnI, leaving them free to interact with the myosin S1 head (Van Eyk and Hodges, 1988; Van Eyk *et al.*, 1991a). The actin-S1 interaction promotes muscle contraction, since binding of actin to the S1 head alters the conformation of the S1 head such that release of Pi occurs much more rapidly and ATPase activity is potentiated.

3. Thesis Proposal and Outline of Chapters

Using ^{1}H NMR techniques as a tool to study the Ca(II)-sensitive interaction between TnC and the inhibitory region of TnI, the following biologically important issues are addressed, the answers to which should help elucidate a fundamental regulatory step in the Ca(II)-mediated regulation of muscle contraction:

1. The conformation of the inhibitory region of skeletal TnI(104-115) when bound to skeletal Ca(II)-saturated TnC.
2. The location of binding of the inhibitory region of skeletal TnI(104-115) to Ca(II)-saturated skeletal TnC.
3. Conformational changes in Ca(II)-saturated skeletal TnC induced upon the binding of the inhibitory region of skeletal TnI(104-115); involvement of the N- and C-terminal globular domains and the role of the flexible helical linker connecting the two domains in TnC.
4. The role of amphiphilic helices in targeting Ca(II)-binding proteins like skeletal TnC; induction of 'helix-like' structure in the inhibitory region of skeletal TnI(104-115) when this region is bound to Ca(II)-saturated skeletal TnC.
5. TnC-mediated relief of TnI inhibitory activity in skeletal versus cardiac systems; comparison of the structures of the inhibitory regions of skeletal TnI(104-115) and cardiac TnI(137-148) when bound to skeletal and cardiac Ca(II)-saturated TnC, respectively.

The thesis is organized in paper format, with each individual chapter consisting of a complete set of experiments, and composed of a short introduction, a material and methods section, a results section, and a discussion section. There are ten chapters in total, and a brief outline of the contents of each chapter is given here:

Chapters II and III offer a theoretical basis for the two-dimensional intramolecular transferred nuclear Overhauser effect (TRNOE), a technique which allows determination of the structure of a ligand bound to a macromolecule. The TRNOE will be used in subsequent chapters to determine the structures of peptides bound to Ca(II)-saturated TnC, and a theoretical basis for the technique is required prior to its use experimentally. In Chapter II, a theoretical evaluation of the TRNOE is presented using a full relaxation matrix analysis first developed by Landy and Rao (1989). The effects of variables such as mixing time, fraction of bound peptide, free and bound correlation times, and other contributions to spin-lattice relaxation rates are examined in an attempt to offer practical experimental guidelines for the design of a TRNOE experiment. In Chapter III, the influence of internal motions on the development of the TRNOE is examined using the model system of the inhibitory peptide Nα-acetyl-TnI(104-115) amide bound to Ca(II)-saturated TnC. The effects of varying the effective correlation time as well as the motional order parameter for methyl group and phenyl ring rotations in the free and bound conformations of this peptide will be examined.

In Chapter IV, ^{19}F NMR spectroscopy is used to determine the association constant and the stoichiometry of binding of the TnI peptide analog Nα-acetyl[^{19}F-phe106]TnI(104-115) amide to Ca(II)-saturated turkey skeletal TnC. The extensive homology between the N- and C-terminal globular domains of TnC would lead one to suggest two possible peptide binding sites on these proteins. It is thus important to establish a stoichiometry of binding of the TnI peptide to TnC, which will then serve as a basis for the TRNOE studies presented in Chapter V.

In Chapter V, the two-dimensional intramolecular TRNOE is used to determine the structure of the inhibitory peptide Nα-acetyl-TnI(104-115) amide bound to Ca(II)-saturated skeletal TnC. The TnI peptide is extremely basic, with four arginines and two lysines (K105, K107, R108, R112, R113 and R115) within a twelve residue sequence. Alternating with these basic residues are hydrophobic ones (F106, L111 and V114). The pattern of alternating basic and hydrophobic residues is interrupted by two sequential proline residues (P109 and P110). The arrangement of the hydrophobic and basic residues in the three-dimensional structure of the bound TnI peptide will be determined, as well as the structural function of the two sequential proline residues.

In Chapter VI, two-dimensional nuclear Overhauser effect (NOE) techniques are used to determine the identity of the residues on Ca(II)-saturated turkey skeletal TnC which are actively involved in binding the inhibitory peptide Nα-acetyl-TnI(104-115) amide. Knowing the identity of these residues on TnC as well as the structure of the bound TnI peptide (determined in Chapter V) will allow a modeling of the interaction between this region of TnC and the inhibitory region of the intact TnI protein.

In Chapter VII, we use the paramagnetic lanthanide Gd(III) as a Ca(II) analog to determine the location of binding of the inhibitory peptide Nα-acetyl-TnI(104-115) amide with respect to Ca(II)-binding sites I and II in the N-terminal domain, and sites III and IV in the C-terminal domain of skeletal TnC. The unpaired electrons on the Gd(III) metal result in increased spin-lattice relaxation times of nuclei on the TnI peptide within a 20 Å radius of the metal, leading to increased spin-lattice relaxation times of the TnI peptide nuclei. This allows orientation of the TnI peptide with respect to all four metal binding sites, as it provides relative distances of the TnI peptide nuclei to the paramagnetic centers. These Gd(III)-derived distances also provide a probe for conformational changes in Ca(II)-saturated skeletal TnC induced upon the binding of the inhibitory TnI peptide. A bend in the central flexible helical linker connecting the two domains in TnC would bring the two domains together in a concerted effort to bind the TnI peptide, a conformational change which would be detected in shorter averaged distances to the paramagnetic centers.

In Chapter VIII, differences in the mode of TnC-mediated relief of TnI inhibitory activity in skeletal versus cardiac systems are examined. The cardiac(137-148) and skeletal(104-115) TnI inhibitory peptides have identical sequences except for a single amino acid substitution of a proline at position 110 in the skeletal sequence for a threonine in the cardiac sequence. The importance of the single amino acid substitution at position 110 in the TnI peptide is demonstrated by the difference in the biological action of an analog in which a glycine is substituted at position 110 of the skeletal sequence (which is equivalent to residue 143 of cardiac sequence) (Van Eyk *et al.*, 1991b). In order to examine the effect the amino acid substitution at position 110 has on the conformation and dynamics of the inhibitory region of TnI, we have used two-dimensional intramolecular TRNOE techniques to determine the structure of the glycine-110 peptide analog, Nα-acetyl-G110-TnI(104-115) amide, bound to Ca(II)-saturated bovine cardiac TnC. The question of conformational flexibility in the inhibitory TnI sequence and its effect on the differences in the mode of Ca(II) mediated relief of inhibition of actomyosin ATPase in the skeletal versus cardiac systems will be discussed.

Chapter IX examines the role of amphiphilic helices in the recognition and targeting of calcium-binding proteins like TnC. We have used two-dimensional intramolecular TRNOE and NOE techniques to examine and compare the structures of two target molecules in the helix-inducing solvent TFE, versus when bound to Ca(II)-saturated turkey skeletal TnC. The first of these target molecules is the inhibitory TnI peptide Nα-acetyl-TnI(104-115) amide, and the second of these target molecules is the bee venom mastoparan, which has a high helix forming propensity.

Chapter X is divided into two separate subchapters. The first of these subchapters is a short summary and conclusion of the work presented in this thesis. The second of these subchapters is concerned with future research projects, and proposes NMR experiments which are natural extensions of those research projects which have already been explored. One of these future research projects involves a refinement of the TRNOE-derived structure of the bound inhibitory peptide Nα-acetyl-TnI(104-115) amide, determined in Chapter V. An iterative computer method, referred to as the transferred *i*terative *r*elaxation *m*atrix *a*pproach (TR-IRMA) is proposed, adapted from the IRMA method of Boelens *et al.* (1988, 1989). The IRMA method, which uses experimental NOE data, is appropriate for the structure refinement of macromolecules in solution. The TR-IRMA method, which uses TRNOE data, is appropriate for the structure refinement of ligands undergoing chemical exchange between a free and bound environment.

Table I-1. Properties of various muscle proteins.

Protein	Mr (Daltons)	Number of Residues	Characteristic	Reference
Myosin	540,000		ATPase activity	Lowey and Cohen, 1962
S1	95,000		ATPase activity	Weeds and Taylor, 1975
HMM	365,000		ATPase activity	Weeds and Pope, 1977
Actin	42,000	375	activates ATPase	Elzinga et al., 1973
Tm	33,0009 monomer	284 monomer	binds actin and TnT	Stone et al., 1974
c-TnC	18,416	161	binds 3 Ca(II)	Van Eerd and Takahashi, 1975
s-TnC	17,846	159	binds 4 Ca(II)	Collins et al., 1977
s-TnI	20,864	178	inhibits ATPase	Wilkinson and Grand, 1975, 1978
s-TnT	30,503	259	binds Tm	Pearlstone and Smillie, 1976

Table I-2. Sites of interaction between muscle proteins.

1. Barden and Phillips, 1990.
2. Bertrand *et al.*, 1988.
3. Chong and Hodges, 1982a.
4. Grabarek *et al.*, 1981.
5. Grabarek and Gergely, 1987.
6. Hitchcock, 1981.
7. Hitchcock *et al.*, 1981.
8. Johnson and Blazyk, 1978.
9. Leavis *et al.*, 1978.
10. Levine *et al.*, 1988.
11. Mak and Smillie, 1979.
12. Moir *et al.*, 1977.
13. Mornet *et al.*, 1977.
14. Nozaki *et al.*, 1980.
15. Ohara *et al.*, 1980.
16. Ohtsuki, 1979.
17. Pato *et al.*, 1981.
18. Pearlstone and Smillie, 1978.
19. Pearlstone and Smillie, 1980.
20. Pearlstone and Smillie, 1981.
21. Pearlstone and Smillie, 1982, 1883.
22. Sutoh, 1982.
23. Sutoh, 1983.
24. Suzuki *et al.*, 1987.
25. Syska *et al.*, 1976.
26. Szilagi and Lu, 1982.
27. Talbot and Hodges, 1981a, 1981b.
28. Tanokura, 1983.
29. Tao *et al.*, 1986a, 1986b.
30. Trayer *et al.*, 1987.
31. Van Eyk and Hodges, 1988.
32. Van Eyk and Hodges, 1991.
33. Weeks and Perry, 1978.
34. Yamamoto and Sekine, 1979.

Protein	TnC	TnI	TnT	Tm	Actin	Myosin (S1)
TnC		(1-47) 25 (104-115) 14,25,27,31	(176-230) 6,12,16,18 (159-227) 7,16,18 (197-259) 21			
TnI	(50-60) 4,9 (89-100) 4,9,33 (126-136) 4		(152-175) 18,19		(1-28) 32 (1-12) 5 (1-44) 10	
TnT	(1-100) 4,6,15,29,33 (121-159) 9,15	(40-78) 7		(190-284) 3,11,17		
Tm	105 21	(104-115) 14,25,27	(71-151) 17 (159-258) 20 (197-259) 16,17,21,28		61,95 1,8 (237-335) 26	
Actin		(96-116) 10 (104-115) 27,31				A1 light chain 22,30 (702-708) 24 20 and 50 KDa junction 13,23,34
Myosin (S1)					(1-12) 22 (1-28) 31,32 (40-113) 2 (361-364) 30	

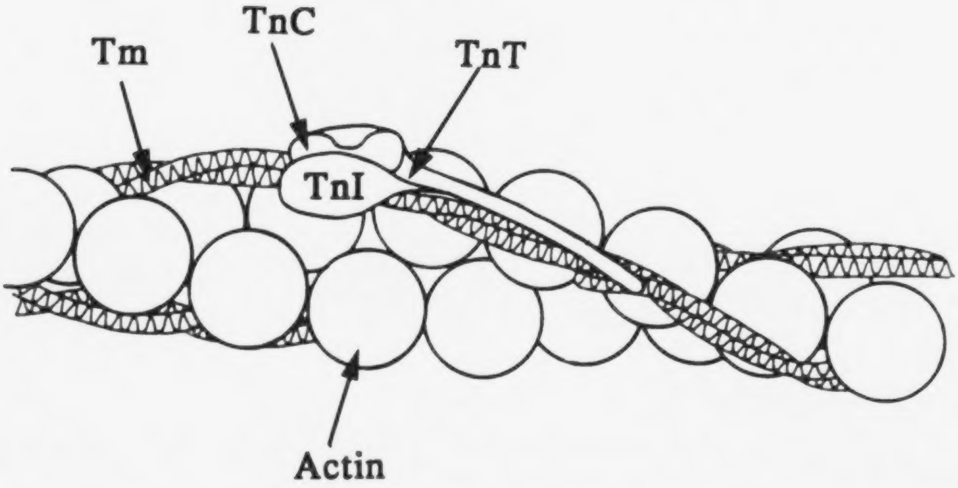

Figure I-1. A model for the molecular arrangement of the thin filament proteins. Two strands of actin molecules (open circles) form the core of the structure. Tropomyosin (Tm) molecules are illustrated as coiled-coils which lie in the grooves of the actin filament. The troponin complex (TnI, TnT, and TnC) interacts with the C-terminus of the Tm molecules. The Tn-Tm complex form the basic regulatory unit of the thin filament (Healy *et al.*, 1987).

Figure I-2. X-ray crystal structure of turkey skeletal troponin C shown as a ribbon diagram (Herzberg and James, 1985). The N-terminal domain (top) is separated from a homologous C-terminal domain (bottom) by a long α-helix. The low affinity Ca(II) specific sites I and II located in the N-terminal domain are unoccupied in the crystal form. The high affinity Ca(II)/Mg(II) sites III and IV in the C-terminal domain are filled. Helices involved in the Ca(II) binding sites are labeled A to H sequentially with the additional helix in the N-terminus of the molecule labeled as the N-helix.

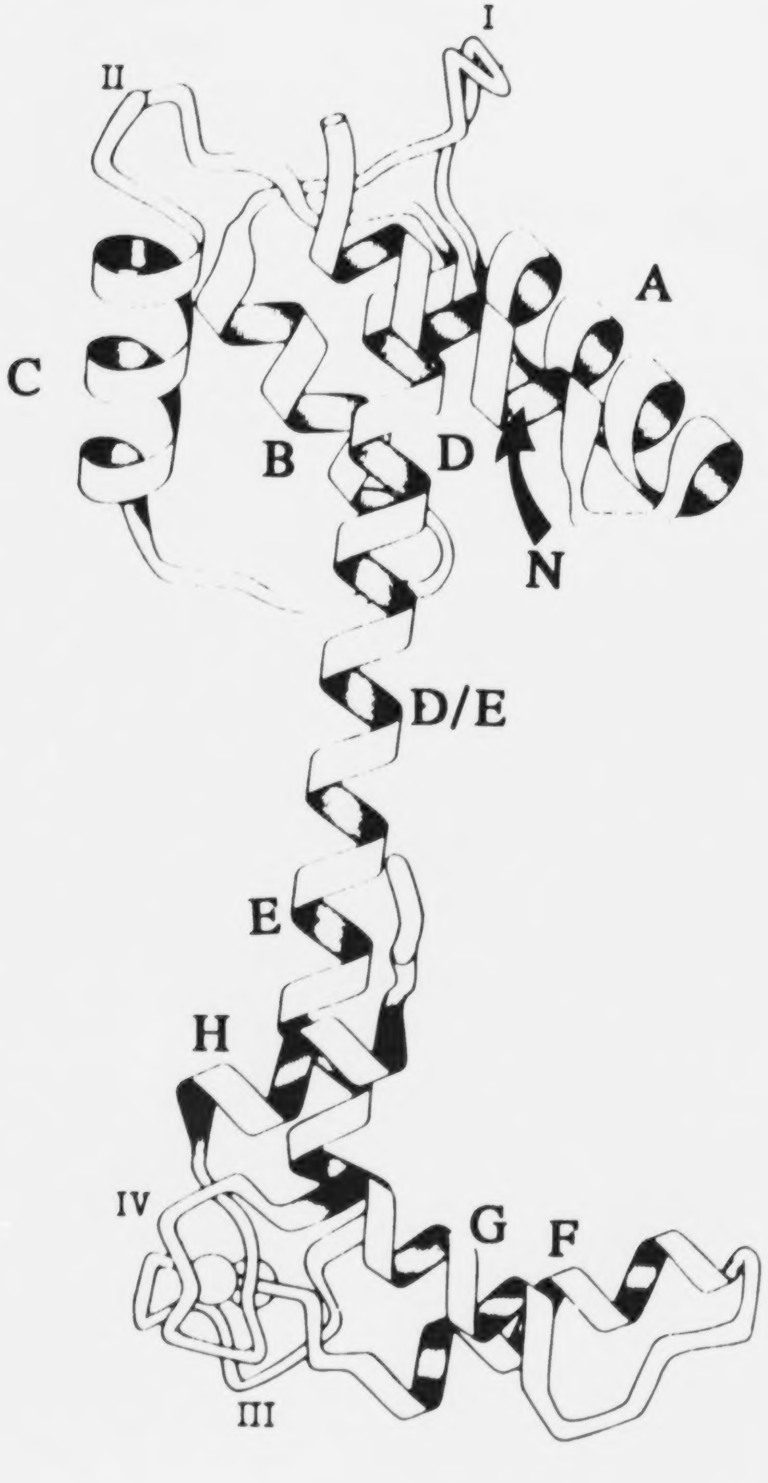
I
II
A
C
B
D
N
D/E
E
H
IV
G
F
III

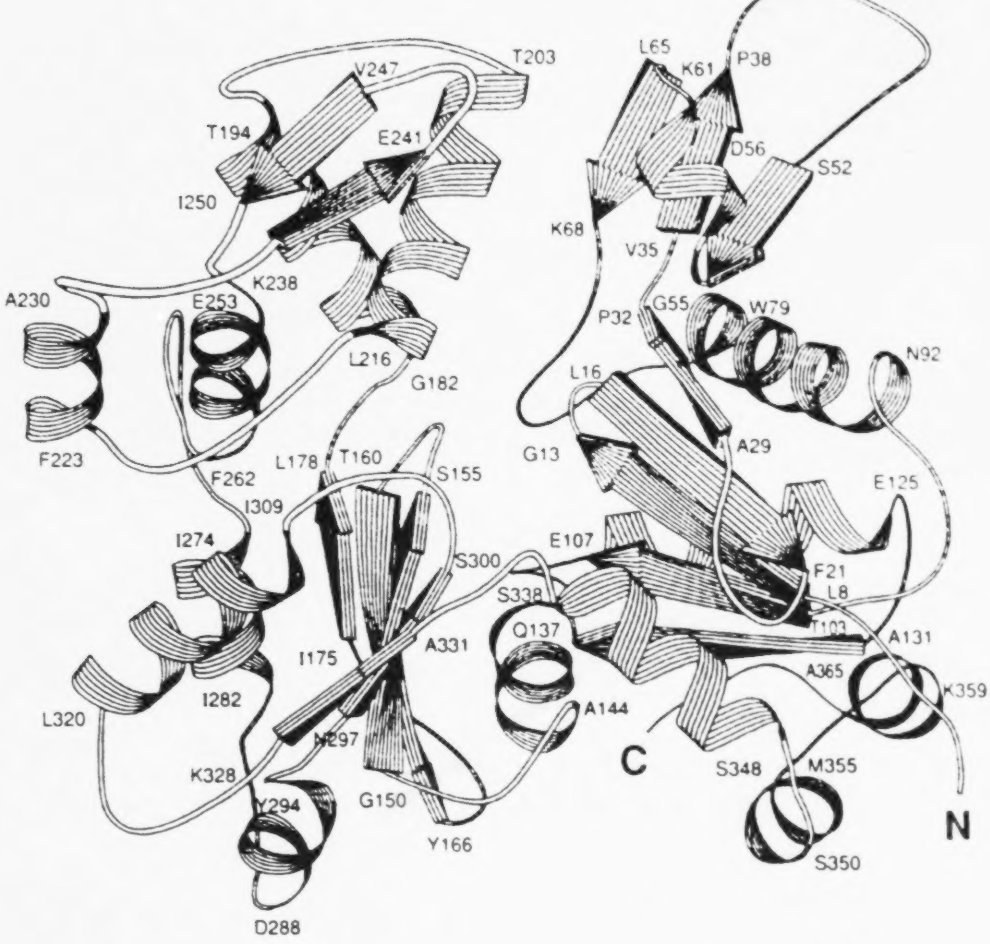
T203
V247
T194
E241
I250
L65
K61
P38
D56
S52
K68
V35
A230
K238
E253
P32
G55
W79
N92
L216
G182
L16
A29
F223
L178
T160
S155
G13
F262
I309
E125
I274
E107
S300
F21
L8
S338
T103
Q137
A331
A131
I175
A365
K359
I282
L320
A144
N297
C
S348
M355
K328
Y294
G150
Y166
N
S350
D288

Figure I-3. X-ray crystal structure of G-actin derived from the Actin:DNAse 1 complex shown as a ribbon diagram (Kabsch *et al.*, 1990). The two domains (right and left) are separated by the Ca(II) and nucleotide binding clefts. Residues are labeled periodically throughout the molecule.

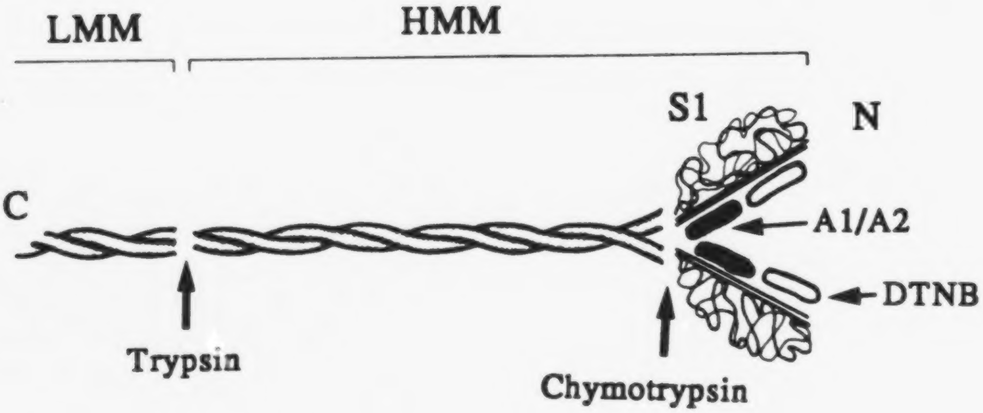
LMM
HMM
S1
N
C
A1/A2
DTNB
Trypsin
Chymotrypsin

Figure I-4. Schematic diagram of a myosin molecule. The molecule is composed of six polypeptide chains: two identical heavy chains and two pairs of light chains. S1, HMM and LMM are fragments generated by limited proteolysis at the points indicated.

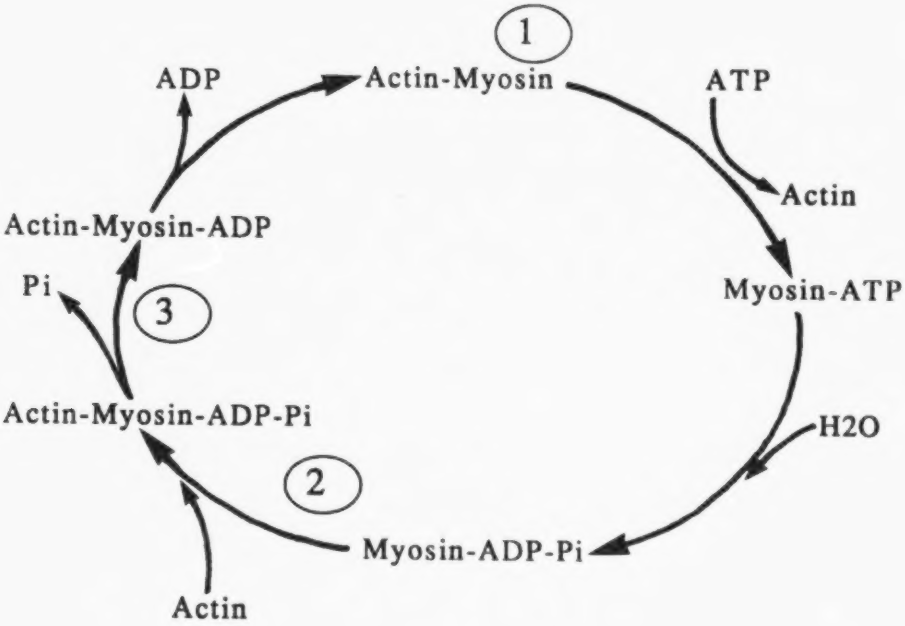
①
ADP
Actin-Myosin
ATP
Actin
Actin-Myosin-ADP
Myosin-ATP
Pi
③
Actin-Myosin-ADP-Pi
H2O
②
Myosin-ADP-Pi
Actin

Figure I-5. Simplistic scheme for the biochemical and kinetic steps involved in ATP hydrolysis during muscle contraction. (adapted from Stryer, 1988).

1. Other complexes can exist, such as myosin, myosin-ADP-Pi, myosin-ADP and actin-myosin-ATP depending on the various binding constants. However, myosin hydrolysis of ATP occurs at low rate compared to actin activated ATPase activity.

2. Crossbridge formation occurs upon actin (actin-Tm-Tn) interaction with myosin.

3. This is the step proposed to be regulated by Tn-Tm. In the absence of Ca(II), Tn-Tm blocks the release of Pi; while in the presence of Ca(II), regulated actin enhances release of Pi, producing the power stroke.

Figure I-6. Proposed mechanism for the generation of force by the interaction of an S1 unit of a myosin filament with an actin filament. In the power stroke, the thick filament moves relative to the thin filament when S1 undergoes conformational changes initiated by the release of Pi. (Stryer, 1988)

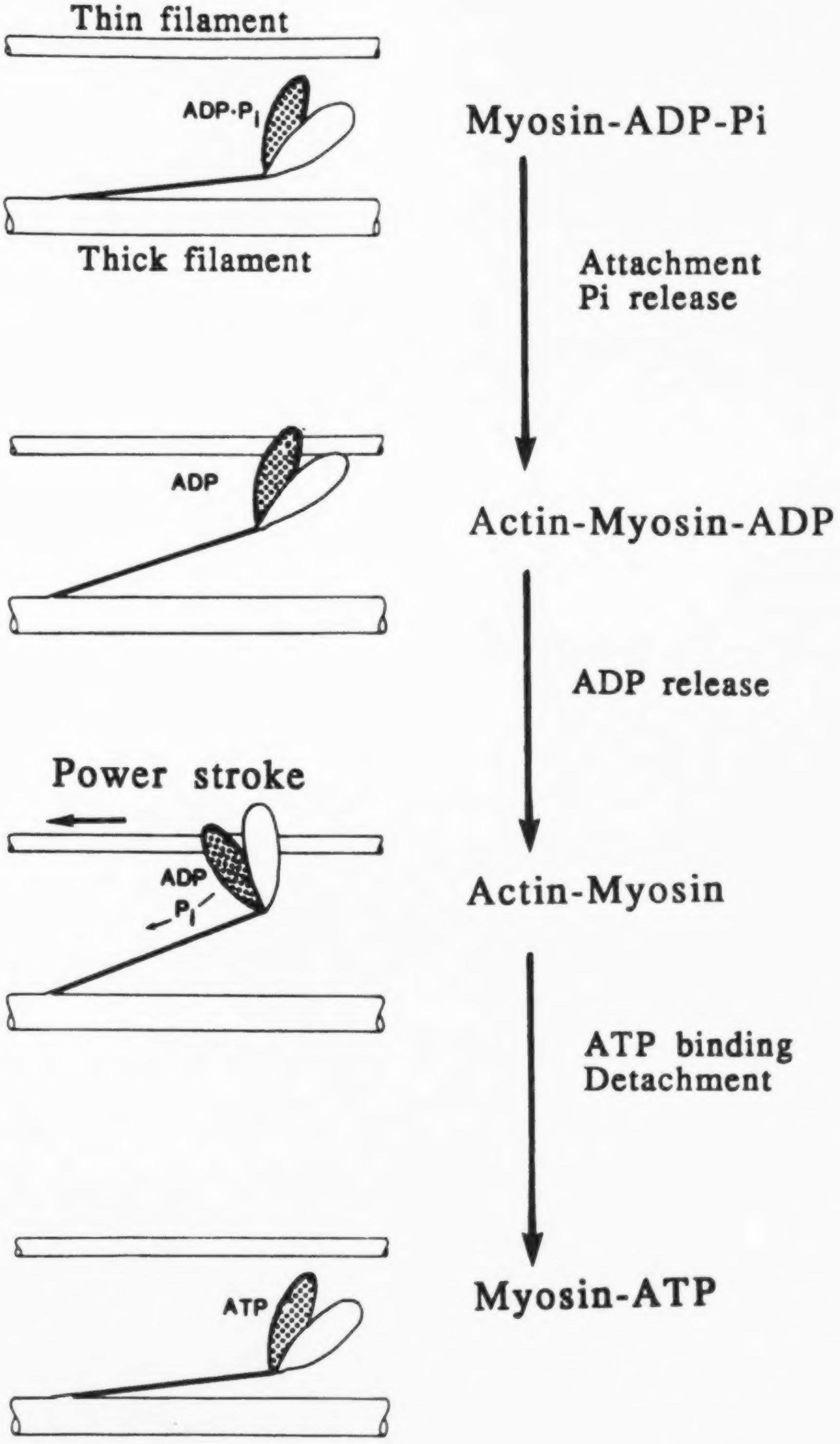
Thin filament
ADP·P$_i$
Myosin-ADP-Pi
Thick filament
Attachment
Pi release
ADP
Actin-Myosin-ADP
ADP release
Power stroke
ADP
P$_i$
Actin-Myosin
ATP binding
Detachment
ATP
Myosin-ATP

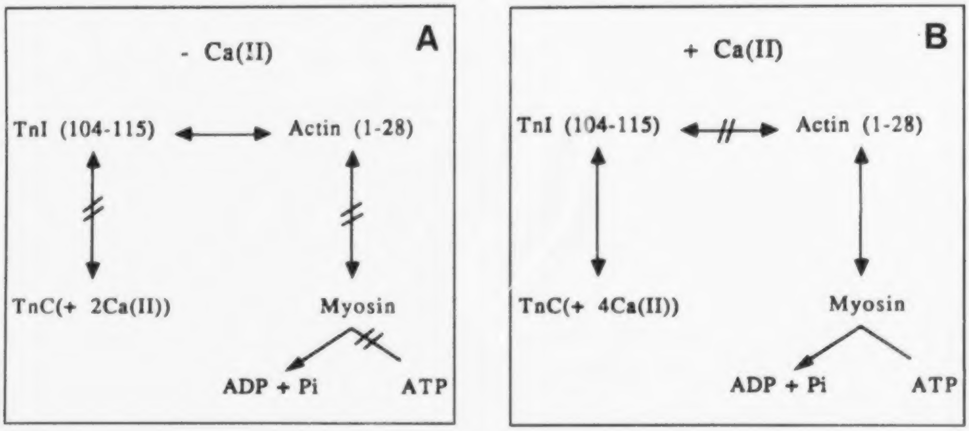
A
- Ca(II)
TnI (104-115)
Actin (1-28)
TnC(+ 2Ca(II))
Myosin
ADP + Pi
ATP
B
+ Ca(II)
TnI (104-115)
Actin (1-28)
TnC(+ 4Ca(II))
Myosin
ADP + Pi
ATP

Figure I-7. Schematic diagram showing the dominant protein interactions involved in the regulation of muscle contraction. Panel A shows the dominant interactions when the Ca(II) specific sites I and II are unoccupied and muscle is relaxed. Panel B shows the dominant interactions when the Ca(II) specific sites I and II are occupied and muscle is contracted (Van Eyk *et al.*, 1991a).

G. References

AKIYAMA, K., SUTOO, D., and REID, D.G. 1990. A ^{1}H-NMR comparison of calmodulin activation by calcium and by cadmium. Japan J. Pharmacol. **53**: 393-401.

ANDERSSON, A., DRAKENBERG, T., FORSEN, S., and THULIN, E. 1981. A ^{43}Ca and ^{25}Mg NMR study of rabbit skeletal muscle troponin C. Exchange rates and binding constants. FEBS Lett. **125**: 39-43.

ANDERSSON, A., DRAKENBERG, T., FORSEN, S., THULIN, E. and SWARD, M. 1982a. Direct observation of the calcium-43 NMR signals from Ca^{+2} ions bound to proteins. J. Am. Chem. Soc. **102**: 576-580.

ANDERSSON, A., FORSEN, S., THULIN, E. and VOGEL, H.J. 1982b. Cadmium-113 nuclear magnetic resonance studies of proteolytic fragments of calmodulin: Assignment of strong and weak cation binding sites. Biochemistry **22**: 2309-2313.

ANDERSSON, A., DRAKENBERG, T., FORSEN, S., and THULIN, E. 1982c. Characterization of the Ca^{2+} binding sites of calmodulin from bovine testis using ^{43}Ca and ^{113}Cd NMR. Eur. J. Biochem. **126**: 501-505.

ANDERSSON, A., DRAKENBERG, T., and FORSEN, S. 1985. The interaction of various drugs with calmodulin as monitored by ^{113}Cd NMR. In *Calmodulin Antagonist and Cellular Physiology* (Hidaka, H., and Hartshorne, D.J., Eds.), Chapt. 3, pp 27-44, Academic Press, New York.

AULABAUGH, A., NIEMCZURA, W.P., and GIBBONS, W.A. 1983. High field proton NMR studies of tryptic fragments of calmodulin: A comparison with the native protein. Biochem. Biophys. Res. Commun. **118**: 225-232.

AULABAUGH, A., NIEMCZURA, W.P., BLUNDELL, T.L., and GIBBONS, W.A. 1984. A study of the interactions between residues in the C-terminal half of calmodulin by one and two-dimensional NMR methods and computer modeling. Eur. J. Biochem. **143**: 409-418.

BARDEN, J.A., and PHILLIPS, L. 1990. ^{19}F NMR study of the myosin and tropomyosin binding sites on actin. Biochemistry **19**: 1348-1354.

BERTRAND, R., CHAUSSEPIED, P., KASAB, R., BOYER, M., ROUSTAN, C., and BENJAMIN, Y. 1988. Cross-linking of the skeletal myosin subfragment 1 heavy chain to the N-terminal actin segment of residues 40-113. Biochemistry **27**: 5728-5736.

BIRDSALL, W.J., LEVINE, B.A., WILLIAMS, R.J.P., DEMAILLE, J.G., HALECH, J., and PECHERE, J.F. 1979. Calcium and magnesium binding by parvalbumin - a proton magnetic resonance spectral study. Biochimie **61**: 741-750.

BIRNBAUM, E.R., and SYKES, B.D. 1978. Nuclear magnetic resonance studies of a Ca^{2+}-binding fragment of troponin C. Biochemistry **17**: 4965-4971.

BJORNSON, M.E., CORSON, D.C., and SYKES, B.D. 1985. ^{13}C and ^{113}Cd NMR studies of the chelation of metal ions by the calcium binding protein parvalbumin. J. Inorg. Biochem. **25**: 141-149.

BOELENS, R., KOENIG, T.M.G., and KAPTEIN, R. 1988. Determination of biomolecular structures from proton-proton nOes using a relaxation matrix approach. J. Mol. Struct. **173**: 299-311 .

BOELENS, R., KOENIG, T.M.G., VAN DER MAREL, G.A., VAN BOOM, J.H., and KAPTEIN, R. 1989. Iterative procedure for structure determination from proton-proton nOes using a full relaxation matrix approach. Application to a DNA octamer. J. Magn. Reson. **82**: 290-308.

BRAUER, M., and SYKES, B.D. 1981a. Phosphorus-31 nuclear magnetic resonance studies of adonosine 5'-triphosphate-calcium-G-actin complex. Biochemistry **20**: 2060-2064.

BRAUER, M., and SYKES, B.D. 1981b. Phosphorus-31 nuclear magnetic resonance studies of adonosine 5'-triphosphate bound to a nitrated derivative of G-actin. Biochemistry **20**: 6767-6775.

BRAUER, M., and SYKES, B.D. 1982. Effects of manganous ion on the phophorus-31 nuclear magnetic resonance spectrum of adonosine triphosphate bound to nitrated G-actin: proximity of divalent metal ion and nucleotide binding sites. Biochemistry **21**: 5934-5939.

BREMEL, R.D., and WEBER, A. 1972. Cooperation with actin filament in vertebrate skeletal muscle. Nature New Biology **238**: 97-101.

BRISSON, J-R., GOLOSINSKA, K., SMILLIE, L.B., and SYKES, B.D. 1986. Interaction of tropomyosin and troponin T: A proton nuclear magnetic resonance study. Biochemistry **25**: 4548-4555.

CACHIA, P.J., SYKES, B.D., and HODGES, R.S. 1983. Calcium-dependent inhibitory region of troponin. A proton magnetic resonance study on the interaction between troponin C and the synthetic peptide Nα-acetyl [F-phenylalanine106] TnI (104-115) amide. Biochemistry **22**: 4145-4152.

CACHIA, P.J., SYKES, B.D., and HODGES, R.S. 1985. Structural studies on calmodulin and troponin C. Phenothiazine, peptide, and protein interactions with calcium-induced helices. In *Calmodulin Antagonist and Cellular Physiology* (Hidaka, H., and Hartshorne, D.J., Eds.), Chapt. 5, pp 63-88, Academic Press, New York.

CACHIA, P.J., VAN EYK, J., INGRAHAM, R.H., MCCUBBIN, W.D., KAY, C.M., and HODGES, R.S. 1986. Calmodulin and troponin C. A comparative study of the interaction of mastoparan and troponin I inhibitory peptide [104-115]. Biochemistry **25**: 3553-3562.

CAVE, A., DOBSON, M., PARELLO, J., and WILLIAMS, R.J.P. 1976. Conformational mobility within the structure of muscular parvalbumins. An NMR study of the aromatic resonances of phenylalanine residues. FEBS Lett. **65**: 190-194.

CAVE, A., and LINDMAN, B. 1978. Non-equivalence of the CD and EF sites of muscular parvalbumins. A ^{113}Cd NMR study. FEBS Lett. **92**: 346-350.

CAVE, A., DAURES, M.F., PARELLO, J., SAINT-YVES, A., and SEMPERE, R. 1979a. Conformational studies on muscular parvalbumins: cooperative binding of calcium (II) to parvalbumins. Biochimie **61**: 755-765.

CAVE, A., PARELLO, J., DRAKENBERG, T., THULIN, E., and LINDMAN, B. 1979b. Mg^{+2} binding to parvalbumins studied by ^{25}Mg and ^{113}Cd spectroscopy. FEBS Lett. **100**: 148-152.

CAVE, A., PAGES, M., MOREN, P.H., and DOBSON, C.M. 1979c. NMR studies of primary and secondary sites of parvalbumins using the two paramagnetic probes Gd(III) and Mn(II). Biochimie **61**: 755-765.

CAVE, A., SAINT-YVES, A., PARELLO, J., SWARD, M., THULIN, E., and LINDMAN, B. 1982. ^{1}H and ^{113}Cd NMR studies on parvalbumin phylology and ionic interactions. Molec. Cell. Biochem. **44**: 161-172.

CHALOVICH, J.M., GREENE, L.E., and EISENBERG, E. 1983. Crosslinked myosin subfragment 1: A stable analogue of the subfragment-1-ATP complex. Proc. Natl. Acad. Sci. USA **80**: 4909-4913.

CHONG, P.C.S., and HODGES, R.S. 1982a. Photochemical cross-linking between rabbit skeletal troponin and α-tropomyosin. Attachment of the photoaffinity probe n-(4-azidobenzoyl-[2-^{3}H]glycyl)-S-(2-thiopyiridyl)-cysteine to cysteine 190 of α-tropomyosin. J. Biol. Chem. **257**: 9152-9160.

CHONG, P.C.S., and HODGES, R.S. 1982b. Proximity of sulfhydryl groups to the sites of interaction between components of the troponin C complex from rabbit skeletal muscle. J. Biol. Chem. **257**: 2549-2555.

CHONG, P.C.S., and HODGES, R.S. 1982c. Photochemical cross-linking between rabbit skeletal troponin subunits. Troponin I - Troponin T interactions. J. Biol. Chem. **257**: 11667-11672.

CHONG, P.C.S., ASSELBERGS, P.J., and HODGES, R.S. 1983. Inhibition of rabbit skeletal muscle acto-SI ATPase by troponin T. FEBS Lett. **153**: 372-376.

COLE, H.A., and PERRY, S.V. 1975. The phosphorylation of troponin I from cardiac muscle. Biochem. J. **149**: 525-533.

COLLINS, J.H., POTTER, J.D., HORN, M.J., WILSHIRE, G., and JACKMAN, N. 1973. The amino acid sequence of rabbit skeletal muscle troponin C. Gene replication and homology with calcium-binding proteins from carp and hake muscle. FEBS Lett. **36**: 268-272.

COLLINS, J.H., GREASER, M.L., POTTER, J.D., and HORN, M.J. 1977. Determination of the amino acid sequence of troponin C from rabbit skeletal muscle. J. Biol. Chem. **252**: 6356-6362.

CORSON, D.C., LEE, L., MCQUAID, G.A., and SYKES, B.D. 1983a. An optical stopped-flow and ^1H and ^{113}Cd nuclear magnetic resonance study of the kinetics and stoichiometry of the interaction of the lanthanide Yb^{+3} with carp parvalbumin. Can. J. Bioc. Cell Biol. **61**: 860-867.

CORSON, D.C., WILLIAMS, T.C., and SYKES, B.D. 1983b. Calcium binding proteins: Optical stopped-flow and proton nuclear magnetic resonance studies of the binding of the lanthanide series of metal ions to parvalbumin. Biochemistry **22**: 5882-5889.

COZZONE, P.J., NELSON, D.J., and JARDETZKY, O. 1974. Fourier transform phosphorus magnetic-resonance of ATP-calcium-G-actin complex. Biochem. Biophys. Res. Commun. **60**: 341-347.

CUMMINS, P., and PERRY, S.V. 1973. The subunits and biological activity of polymorphic forms of tropomyosin. Biochem. J. **133**: 765-777.

CUMMINS, P., and PERRY, S.V. 1974. Chemical and immunochemical characteristics of tropomyosins from striated and smooth muscle. Biochem. J. **141**: 43-49.

DALGARNO, D.C., KLEVIT, R.E., LEVINE, B.A., WILLIAMS, R.J.P., and DOBROWOLSKI, Z. 1984. ^1H NMR studies of calmodulin. Resonance assignments by use of tryptic fragments. Eur. J. Biochem. **138**: 281-289.

DALGARNO, D.C., KLEVIT, R.E., LEVINE, B.A., SCOTT, G.M.M., WILLIAMS, R.J.P., GERGELY, J., GRABAREK, Z., LEAVIS, P.C., GRAND, R.J.A., and DRABIKOWSKI, W. 1984. The nature of the trifluoperazine binding sites on calmodulin and troponin C. Biochim. Biophys. Acta **791**: 164-172.

DAS GUPTA, G., WHITE, J., CHEUNG, P., and REISLER, E. 1990. Interactions between G-actin and myosin subfragment 1: Immunochemical probing of the NH_2-terminal segment on actin. Biochemistry **29**: 8503-8508.

DELVILLE, A., GRANDJEAN, J., LASZLO, P., GERDAY, C., BRZESKA, H., and DRABIKOWSKI, W. 1980. Sodium-23 nuclear magnetic resonance as an indicator of sodium binding to troponin C and tryptic fragments, in relation to calcium content and attendant conformational changes. Eur. J. Biochem. **105**: 289-295.

DELVILLE, A., GRANDJEAN, J., LASZLO, P., GERDAY, C., BRZESKA, H., and DRABIKOWSKI, W. 1980. Sodium-23 nuclear magnetic resonance as an indicator of sodium binding to calmodulin and tryptic fragments, in relation to calcium content. Eur. J. Biochem. **109**: 515-522.

DRABIKOWSKI, W., DALGARNO, D.C., LEVINE, B.A., GERGELY, J., GRABAREK, Z., and LEAVIS, P.C. 1985. Solution conformation of the C-terminal domain of skeletal troponin C. Cation, trifluoperazine and troponin I binding effects. Eur. J. Biochem. **151**: 17-28.

DRAKENBERG, T., LINDMAN, B., M., CAVE, A., and PARELLO, J. 1978. Non-equivalence of the CD and EF sites of muscular parvalbumins. A ^{113}Cd NMR study. FEBS Lett. **92**: 346-350.

DRAKENBERG, T., SWARD, M., CAVE, A., and PARELLO, J. 1985. Metal-ion binding to parvalbumin. A ^{113}Cd NMR study of the binding of different lanthanide ions. Biochem. J. **227**: 711-717.

DRAKENBERG, T., FORSEN, S., THULIN, E., and VOGEL, H.J. 1987. The binding of Ca^{2+}, Mg^{2+} and Cd^{2+} to tryptic fragments of skeletal muscle troponin C. Cadmium-113 and proton NMR studies. J. Biol. Chem. **262**: 672-678.

EDWARDS, B.F.P., and SYKES, B.D. 1978. Assignment and characterization of the histidine resonances in the ^{1}H nuclear magnetic resonance spectra of rabbit tropomyosins. Biochemistry **17**: 684-689.

EDWARDS, B.F.P., and SYKES, B.D. 1980. Nuclear magnetic resonance evidence for the coexistence of several conformational states of rabbit cardiac and skeletal tropomyosins. Biochemistry **19**: 2577-2583.

EISENBERG, E., HILL, T.L., and CHEN, Y. Crossbridge model of muscle contraction - Quantitative analysis. 1980. Biophys. J. **29**: 195-227.

ELLIS, P.D., STRANG, P., and POTTER, J.D. 1984. Cadmium-substituted skeletal troponin C. Cadmium-113 NMR spectroscopy and metal binding investigations. J. Biol. Chem. **259**: 10348-10356.

ELLIS, P.D., MARCHETTI, P.S., STRANG, P., and POTTER, J.D. 1988. Cadmium-substituted skeletal troponin C metal binding investigations and sequence assignment of the cadmium-113 resonances. J. Biol. Chem. **263**: 10284-10288.

EL-SALEH, S.C., WARBER, K.O., and POTTER, J.D. 1986. The role of tropomyosin-troponin in the regulation of skeletal muscle contraction. J. of Mol. Cell. Motil. **7**: 287-406.

ELZINGA, M., COLLINS, J.H., KUEHL, W.M., and ADELSTEIN, R.S. 1973. Complete amino acid sequence of actin of rabbit skeletal muscle. Proc. Natl. Acad. Sci. USA **70**: 2687-2691.

EVANS, J.S., LEVINE, B.A., LEAVIS, P.C., GERGELY J., GRABAREK, Z., and DRABIKOWSKI, W. 1980. Proton magnetic resonance studies on proteolytic fragments of troponin C. Structural homology with the native molecule. Biochim. Biophys. Acta **623**: 10-28.

FLICKER, P.F., PHILLIPS, G.N., and COHEN, C. 1982. Troponin and its interactions with tropomyosin. An electron microscope study. J. Mol. Biol. **162**: 495-501.

FORSEN, S., THULIN, E., and LILJA, H. 1979. ^{113}Cd NMR in the study of calcium binding proteins: troponin C. FEBS Lett. **104**: 123-126.

FORSEN, S., THULIN, E., DRAKENBERG, T., KREBS, J., and SEAMON, K. 1980. ^{113}Cd NMR in the study of calcium binding proteins: troponin C. FEBS Lett. **104**: 123-126.

FORSEN, S., ANDERSSON, T., DRAKENBERG, T., THULIN, E., and SWARD, E. 1982. Observation of the ^{43}Ca NMR signals from Ca^{+2} ions bound to calmodulin, parvalbumin, and troponin C. Fedn. Proc. **41**: 2981-2986.

GARIEPY, J., and HODGES, R.S. 1983. Primary sequence analysis and folding behaviour of EF hands in relation to the mechanism of action of troponin C and calmodulin. FEBS Lett. **160**: 1-6.

GRACEFFA, P., and LEHRER, S.S. 1980. The excimer fluorescence of pyrene-labeled tropomyosin. A probe for conformational dynamics. J. Biol. Chem. **255**: 11296-11300.

GRABAREK, Z., DRABIKOWSKI, W., LEAVIS, P.C., ROSENFELD, S.S., and GERGELY, J. 1981. Proteolytic fragments of troponin C. Interactions with the other troponin subunits and biological activity. J. Biol. Chem. **256**: 13121-13127.

GRABAREK, Z., and GERGELY, J. 1987. Acta Biochim. Biophys. Hung. **22**: 307-316.

GRABAREK, Z., LEAVIS, P.C., and GERGELY, J. 1986. Calcium binding to the low affinity sites on troponin C induces conformational changes in the high affinity domain. A possible route of information transfer in activation of muscle contraction. J. Biol. Chem. **261**: 608-613.

GRAND, R.J.A., LEVINE, B.A., and PERRY, S.V. 1982. Proton-magnetic-resonance studies on the interaction of rabbit skeletal-muscle troponin I with troponin C and actin. Biochem J. **203**: 61-68.

GRANDJEAN, J., LASZLO, P., GERDAY, C. 1977. Sodium complexation by the calcium binding site of parvalbumin. FEBS Lett. **81**: 376-380.

GREASER, M.C., and GERGELY, J. 1971. Reconstitution of troponin activity from three protein components. J. Biol. Chem. **246**: 4226-4233.

GREASER, M.C., and GERGELY, J. 1973. Purification and properties of the components from troponin. J. Biol. Chem. **248**: 2125-2133.

GUTH, K., and POTTER, J.D. 1987. Effect of rigor and cycling cross-bridges on the structure of troponin C and on the Ca^{+2} affinity of the Ca^{+2}-specific regulatory sites in skinned rabbit psoas fibers. J. Biol. Chem. **262**: 13627-13635.

HARTSHORNE, D.J., and MUELLER, H. 1968. Fractionation of troponin into two distinct proteins. Biochem. Biophys. Res. Commun. **31**: 647-653.

HASELGROVE, J.D. 1972. X-Ray evidence for a conformational change in the actin-containing filaments of vertebrate striated muscle. Cold Spring Harbor Symp. Quant. Biol. **37**: 341-352.

HEALY, D.H., GOLOSINSKA, K., and SMILLIE, L.B. 1987. The effects of troponin I fragments T1 and T2 on the binding of nonpolymerizable tropomyosin to F-actin in the presence and absence of troponin I and troponin C. J. Biol. Chem. **262**: 9971-9978.

HERZBERG, O., and JAMES, M.N.G. 1985. Structure of the calcium regulatory muscle protein troponin C at 2.8 Å resolution. Nature **313**: 653-659.

HERZBERG, O., MOULT, J., and JAMES, M.N.G. 1986. A model for the Ca^{+2} induced conformational transition of troponin C. A trigger for muscle contraction. J. Biol. Chem. **261**: 2638-2644.

HIGHSMITH, S., AKASAKA, K., KONRAD, M., GOODY, R., HOLMES, K., WADE-JARDETSKY, N., and JARDETZKY, O. 1979. Internal motions of myosin. Biochemistry **18**: 4238-4244.

HIGHSMITH, S., and JARDETZKY, O. 1980. G-actin binding quenches internal motions in myosin subfragment-1. FEBS Lett. **121**: 55-60.

HIGHSMITH, S., and JARDETZKY, O. 1981. Internal motions of myosin 2. Biochemistry **20**: 780-783.

HILL, T.L. 1983. Two elementary models for the regulation of skeletal muscle contraction by calcium. Biophys. J. **44**: 383-396.

HILL, T.L., EISENBERG, E., and GREENE, L.E. 1984. Alternate model for cooperative equilibrium binding of myosin subfragment-1-nucleotide complex to actin-troponin-tropomyosin. Proc. Natl. Acad. Sci. USA **80**: 60-64.

HINCKE, M.T., SYKES, B.D., and KAY, C.M. 1981a. Hydrogen-1 nuclear magnetic resonance investigation of bovine cardiac troponin C. Comparison of tyrosyl assignments and calcium-induced structural changes to those of two homologous proteins, rabbit skeletal troponin C and bovine brain calmodulin. Biochemistry **20**: 3286-3294.

HINCKE, M.T., SYKES, B.D., and KAY, C.M. 1981b. Laser photochemically induced dynamic nuclear polarization proton nuclear magnetic resonance studies on three homologous calcium binding proteins: cardiac troponin C, skeletal troponin C and calmodulin. Biochemistry **20**: 4185-4193.

HITCHCOCK, S.E. 1975. Regulation of muscle contraction. Binding of troponin C involved in calcium ion-dependent interaction with troponin I. Eur. J. Biochem. **52**: 255-263.

HITCHCOCK, S.E. 1981. Study of the structure of troponin C by measuring the relative reactivities of lysines with acetic anhydride. J. Mol. Biol. **147**: 153-173.

HITCHCOCK, S.E., ZIMMERMAN, C.J., and SMALLEY, C. 1981. Study of the structure of troponin T by measuring the relative reactivities of lysines with acetic anhydride. J. Mol. Biol. **147**: 125-151.

HITCHCOCK-DEGREGORI, S.E. 1982. Study of the structure of troponin-I by measuring the relative reactivities of lysines with acetic anhydride. J. Biol. Chem. **257**: 7372-7380.

HODGES, R.S., SODEK, J., SMILLIE, L.B., and JURASEK, L. 1972. Tropomyosin: amino-acid sequence and coiled-coil structure. Cold Spring Harbor Symp. Quant. Biol. **37**: 299-310.

HUANG, T.S., BYLUND, D.B., STULL, J.T., and KREBS, E.G. 1974. The amino acid sequences of the phosphorylated sites in troponin-I from rabbit skeletal muscle. FEBS Lett. **42**: 249-256.

HUXLEY, H.E. 1969.The mechanism of muscle contraction. Science **164**: 1356-1366.

HUXLEY, H.E. 1972. Structural changes in the actin- and myosin- containing filaments during contraction. Cold Spring Harbor Symp. Quant. Biol. **37**: 361-369.

IKURA, M., HIRAOKI, T., HIKICHI, K., MIKUNI, T., YAZAWA, M., and YAGI, K. 1983a. Nuclear magnetic resonance studies on calmodulin: Spectral assignments in the calcium-free state. Biochemistry **22**: 2568-2572.

IKURA, M., HIRAOKI, T., HIKICHI, K., MIKUNI, T., YAZAWA, M., and YAGI, K. 1983b. Nuclear magnetic resonance studies on calmodulin: Calcium-induced conformational change. Biochemistry **22**: 2573-2579.

IKURA, M., HIRAOKI, T., HIKICHI, K., MINOWA, O., YAMAGUCHI, H., YAZAWA, M., and YAGI, K. 1984. Nuclear magnetic resonance studies on calmodulin: Ca^{2+}-dependent spectral change of proteolytic fragments. Biochemistry **23**: 3124-3128.

IKURA, M., MINOWA, O., and HIKICHI, K. 1985. Hydrogen bonding in the carboxyl-terminal half-fragment 78-148 of calmodulin as studied by two-dimensional nuclear magnetic resonance. Biochemistry **24**: 4264-4269.

IKURA, M. 1986. Proton nuclear magnetic resonance studies on the kinetics of tryptic fragments of calmodulin upon calcium binding. Biochim. Biophys. Acta **872**: 195-200.

IKURA, M., MINOWA, O., YAZAWA, M., YAGI, K., and HIKICHI, K. 1987. Sequence-specific assignments of downfield-shifted amide proton resonances of calmodulin. Use of two-dimensiona NMR analysis of its tryptic fragments. FEBS Lett. **219**: 17-21.

IKURA, M., HASEGAWA, N., AIMOTO, S., YAZAWA, M., YAGI, K., and HIKICHI, K. 1989. ^{113}Cd evidence for cooperative interaction between amino- and carboxyl-terminal domains of calmodulin. Biochem. Biophys. Res. Commun. **161**: 1233-1238.

IKURA, M., KAY, E., and BAX, A. 1990a. A novel approach for sequential assignment of ^{1}H, ^{13}C, and ^{15}N spectra of larger proteins: Heteronuclear triple-resonance three-dimensional NMR spectroscopy. Application to Calmodulin. Biochemistry **29**: 4659-4667.

IKURA, M., KAY, E., CLORE, M., and GRONENBORN, A.M. 1990b. Detection of nuclear Overhauser effects between degenerate amide proton resonances by heteronuclear three-dimensional nuclear magnetic resonance spectroscopy. J. Am. Chem. Soc. **112**: 9092-9022.

IKURA, M., KAY E., KRINKS, M., and BAX, A. 1991. Triple-resonance multidimensional NMR study of calmodulin complexed with the binding domain of skeletal muscle myosin light-chain kinase: Indication of a conformational change in the central helix. Biochemistry **30**: 5498-5504.

INGRAHAM, R.H., and HODGES, R.S. 1988. Effects of Ca^{+2} and subunit interaction on surface accessibility of cysteine residues in cardiac troponin. Biochemistry **27**: 5891-5898.

JACKSON, P., AMPHLETT, G.N., and PERRY, S.V. 1975. The primary structure of troponin T and the interaction with tropomyosin. Biochem. J. **151**: 85-97.

JOHNSON, J.D., and BLAZYK, J.M. 1978. Involvement of an arginine residue of actin in tropomyosin binding. Biochem. Biophys. Res. Commun. **82**: 1013-1018.

JOHNSON, J.D., CHARLTON, S.C., and POTTER, J.D. 1979. A fluorescence stopped flow analysis of Ca^{+2} exchange with troponin C. J. Biol. Chem. **254**: 3497-3502.

JOHNSON, P., and SMILLIE, L.B. 1975. Rabbit skeletal α-tropomyosin chains are in register. Biochem. Biophys. Res. Commun. **64**: 1316-1322.

KABSCH, W., MANNHERZ, H.G., SUCK, D., PAI, E.F., and HOLMES, K.C. 1990. Atomic structure of the actin:DNAseI complex. Nature **347**: 37-44.

KLEVIT, R.E., DALGARNO, D.C., LEVINE, B.A., and WILLIAMS, R.J.P. 1984. ^{1}H-NMR studies of calmodulin. The nature of the Ca^{2+}-dependent conformational change. Eur. J. of Biochem. **139**: 109-114.

KLEVIT, R.E., BLUMENTHAL, D.K., WEMMER, D.E., and KREBS, E.G. 1985. Interaction of calmodulin and a calmodulin-binding peptide from myosin light chain kinase. Major spectral changes in both occur as a result of complex formation. Biochemistry **24**: 8152-8157.

KLEVIT, R.E. 1987. Study of calmodulin-peptide interactions by NMR spectroscopy. Methods in Enzymology **139**: 197-206.

KREBS, J., and CARAFOLI, E., 1982. Influence of Ca(2+) and trifluoperazine on the structure of calmodulin. A proton nuclear magnetic resonance study. Eur. J. Biochem. **124**: 619-627.

KRETSINGER, R.H., and NOCKOLDS, C.E. 1973. Carp muscle-binding protein II. Structure determination and general description. J. Biol. Chem. **248**: 3313-3326.

LANDY, S.B., and RAO, B.D.N. 1989. Dynamical NOE in multiple-spin systems undergoing chemical exchange. J. Magn. Reson. **81**: 371-377.

LAPORTE, D.C., WIERMAN, B.M., and STORM, D.R. 1980. Calcium-induced exposure of a hydrophobic surface on calmodulin. Biochemistry **19**: 3814-3819.

LEAVIS, P.C., ROSENFELD, S.S., GERGELY, J., GRABAREK, Z., and DRABIKOWSKI, W. 1978. Proteolytic fragments of troponin C. Localization of high and low affinity Ca^{+2} binding sites and interactions with troponin I and troponin T. J. Biol. Chem. **253**: 5452-5454.

LEAVIS, P.C., EVANS, J.S., and LEVINE, B.A. 1982. Proton magnetic resonance studies on peptide fragments of troponin-C containing single calcium-binding sites. J. Inorg. Biochem **16**: 257-277.

LEAVIS, P.C., and GERGELY, J. 1984. Thin filament proteins and thin filament regulation of vertebrate muscle contraction. CRC Crit. Rev. Biochem. **16**: 235-305.

LEE, L., SYKES, B.D., and BIRNBAUM, E.R. 1978. A determination of the relative compactness of the Ca^{2+}-binding sites of a Ca^{2+}-binding fragment of troponin C and parvalbumin using lanthanide-induced ^{1}H NMR shifts. FEBS Lett. **98**: 169-172.

LEE, L., and SYKES, B.D. 1980a. Nuclear magnetic resonance determination of metal-proton distances in the EF site of carp parvalbumin using the susceptibility contribution of the line broadening of lanthanide-shifted resonances. Biochemistry **19**: 3208-3214.

LEE, L., and SYKES, B.D. 1980b. Strategies for the use of lanthanide NMR shift probes in the determination of protein structure in solution. Biophys. J. **32**: 193-210.

LEE, L., and SYKES, B.D. 1981. Proton nuclear magnetic resonance determination of the sequential Ytterbium replacement of calcium in carp parvalbumin. Biochemistry **20**: 1156-1162.

LEE, L., and SYKES, B.D. 1986. Use of lanthanide-induced nuclear magnetic resonance shifts for determination of protein structure in solution: EF calcium binding site of carp parvalbumin. Biochemistry **22**: 4366-4373.

LEHRER, S.S., and MORRIS, E.P. 1982. Dual effects of tropomyosin and troponin-tropomyosin on actomyosin subfragment-1 ATPase. J. Biol. Chem. **257**: 8073-8080.

LEVINE, B.A., MERCOLA, D., and THORNTON, J.M. 1976. Proton magnetic resonance study of troponin-C. FEBS Lett. **61**: 218-222.

LEVINE, B.A., MERCOLA, D., COFFMAN, D., and THORNTON, J.M. 1977. Calcium binding by troponin C. A proton magnetic resonance study. J. Mol. Biol. **115**: 743-760.

LEVINE, B.A., THORNTON, J.M., FERNANDES, R., KELLY, L.M., and MERCOLA, D. 1978. Comparison of the calcium- and magnesium-induced structural changes of troponin C. A proton magnetic resonance study. Biochim. Biophys. Acta **535**: 11-24.

LEVINE, B.A., MOIR, A.J.G., and PERRY, S.V. 1988. The interaction of troponin I with the N-terminal region of actin. Eur. J. Biochem. **172**: 389-397.

LINSE, S., DRAKENBERG, T., and FORSEN, S. 1986. Mastoparan binding induces a structural change affecting both the N-terminal and C-terminal domains of calmodulin: A ^{113}Cd-NMR study. FEBS Lett. **199**: 28-32.

LOWEY, S., and COHEN, C. 1962. Studies on the structure of myosin. J. Mol. Biol. **4**: 293-308.

MAK, A.S., GOLOSINSKA, K., and SMILLIE, L.B. 1981. Induction of nonpolymerizable tropomyosin binding to F-actin by troponin and its components. J. Biol. Chem. **258**: 14330-14334.

MAK, A.S., and SMILLIE, L.B. 1979. Structural interpretation of the two-site binding of troponin on the muscle thin filament. J. Mol Biol. **149**: 541-550.

MAK, A.S., and SMILLIE, L.B. 1983. Non-polymerizable tropomyosin: Preparation, some properties and F-actin binding. Biochem. Biophys. Res. Commun. **101**: 208-214.

MACLACHLAN, L.K., REID, D.G., and CARTER, N. 1990a. A proton nuclear magnetic resonance and molecular modeling study of cardiac troponin C. Calcium dependence and aromatic spectral assignments. J. Biol. Chem. **265**: 9754-9763.

MACLACHLAN, L.K., REID, D.G., MITCHELL, R.C., SALTER, C.J., and SMITH, S.J. 1990b. Binding of a calcium sensitizer, bepridil, to cardiac troponin C. A fluorescence stopped-flow kinetic, circular dichroism, and proton nuclear magnetic resonance study. J. Biol. Chem. **265**: 9764-9770.

MCCUBBIN, W.D., OIKAWA, K., SYKES, B.D., and KAY, C.M. 1982. Purification and characterization of troponin C from pike muscle: a comparative spectroscopic study with rabbit skeletal muscle troponin C. Biochemistry **21**: 5948-5956.

MEJEAN, C., BOYER, M., LABBE, J-P., DERANCOURT, J., BENJAMIN, Y., and ROUSTAN, R. 1986. Antigenic probes locate the myosin subfragment 1 interaction site on the N-terminal part of actin. Bio Sci. Rep. **6**: 493-499.

MEJEAN, C., BOYER, M., LABBE, J-P., MARLIER, L., BENJAMIN, Y., and ROUSTAN, R. 1987. Anti-actin antibodies. An immunological approach to the myosin-actin and tropomyosin-actin interfaces. Biochem J. **244**: 571-577.

MILLER, L., KALNOSKI, M., YUNOSSI, Z., BULINSKI, J.C., and REISLER, E. 1987. Antibodies directed against N-terminal residues on actin do not block acto-myosin binding. Biochemistry **26**: 6064-6070.

MOIR, A.J.G., WILKINSON, J.M., and PERRY, S.V. 1974. The phosphorylation sites of troponin I from cardiac muscle. FEBS Lett. **42**: 253-257.

MOIR, A.J.G., COLE, H.A., and PERRY, S.V. 1977. Phosphorylation sites on troponin T from white skeletal muscle and the effects of interaction with troponin C on their phosphorylation by phosphorylase kinase. Biochem. J. **161**: 371-382.

MOIR, A.J.G., and LEVINE, B. 1986. Protein cognitive sites on the surface of actin. A proton NMR study. J. Inorg. Biochem. **27**: 271-278.

MOIR, A.J.G., LEVINE, B., GOODEART, A.J., and TRAYER, J.P. 1987. Tne interaction of actin with myosin subfragment-1 and with pPDM-cross-linked S1: A ^{1}H NMR investigation. J. Muscle Res. Cell. Motil. **8**: 68-69.

MORNET, D., PANTEL, P., AUDEMORD, E., and KASAB, R. 1979. The limited tryptic cleavage of chymotryptic S-1: An approach to the characterization of the actin site in myosin heads. Biochem. Biophys. Res. Commun. **89**: 925-932.

NELSON, D.J., COZZONE, P.J., and JARDETZKY, O. 1974. ^{31}P-nuclear magnetic resonance study of ATP-G-Actin: Direct evidence for $P\beta$ and $P\gamma$ involvement in nucleotide binding. In *Molecular and Quantum Pharmacology* (Bergman, E., and Pullman, B., Eds.), pp 501-513, Reidel Publishing, Dordrecht-Holland.

NELSON, D., OPELLA, S.J., and JARDETZKY, O. 1976. ^{13}C nuclear magnetic resonance study of molecular motions and conformational transitions in muscle calcium binding parvalbumins. Biochemistry **15**: 5552-5560.

NOZAKI, S., KOBAYASHI, K., KATAYAMA, E., and MURAMATSU, I. 1980. Synthetic studies on troponin I active site preparation of a pentadecapeptide with inhibitory activity toward troponin C. Chem. Lett. **3**: 345-348.

OHKI, S-Y., TSUDA, S., JOKO, S., YAZAWA, M., YAGI, K., and HIKICHI, K. 1991. ^{1}H NMR study on amide proton exchange of calmodulin-mastoparan complex. J. Biochem. **109**: 234-237.

OHTSUKI, I. 1979. Molecular arrangement of troponin T in the thin filament. J. Biochem. **86**: 491-497.

OPELLA, S.J., NELSON, D., and JARDETZKY, O. 1974. Carbon magnetic resonance study of the conformational changes in carp muscle calcium binding parvalbumin. J. Am. Chem. Soc. **96**: 7157-7159.

PARELLO, J., CAVE, A., PUIGDOMENECH, P., MAURY, C., CAPONY, J.P., and PECHERE, J.P. 1974. Conformational studies on muscle parvalbumins. II. nuclear magnetic resonance analysis. Biochimie **56**: 61-76.

PARELLO, J., LILJA, H., CAVE, A. and LINDMAN, B. 1978. A calcium-43 NMR study of the binding of calcium to parvalbumins. FEBS Lett. **87**: 191-195.

PARELLO, J., REIMARSSON, P., THULIN, E., and LINDMAN, B. 1979. Na^+ binding to parvalbumins studied by ^{23}Na NMR. FEBS Lett. **100**: 154-156.

PADILLA, A., and CAVE, A. 1988. Two-dimensional ^{1}H nuclear magnetic resonance study of pike pI 5.0 parvalbumin (*Esox lucius*). Sequential resonance assignments and folding of the polypeptide chain J. Mol. Biol. **204**: 995-1017.

PARRY, D.A.D., and SQUIRE, J. 1973. Structural role of tropomyosin in muscle regulation: Analysis of x-ray diffraction patterns from relaxed and contracting muscles. J. Mol. Biol. **75**: 33-55.

PARRY, D.A.D., and SQUIRE, J. 1974. Structural studies on the tropomyosin/troponin complex of vertebrate skeletal muscle. Biochem. Biophys. Res. Commun. **57**: 216-224.

PARRY, D.A.D. 1981. Analysis of the amino acid sequence of a tropomyosin-binding fragment from troponin-T. J. Mol. Biol. **146**: 259-263.

PATO, M.D., MAK, A.S., and SMILLIE, L.B. 1981. Fragments of rabbit skeletal muscle α-tropomyosin. II. Binding to troponin-T. J. Biol. Chem. **256**: 602-607.

PEARLSTONE, J.R., and SMILLIE, L.B. 1976. Amino-acid sequence of tropomyosin-binding component of rabbit skeletal muscle troponin. Proc. Natl. Sci. USA **73**: 1902-1906.

PEARLSTONE, J.R., and SMILLIE, L.B. 1977. The binding site of rabbit skeletal α-tropomyosin on troponin-T. Can J. Biochem. **55**: 1032-1038.

PEARLSTONE, J.R., and SMILLIE, L.B. 1978. Troponin T fragments: Physical properties and binding to troponin C. Can J. Biochem. **56**: 521-527.

PEARLSTONE, J.R., and SMILLIE, L.B. 1980. The binding sites of rabbit skeletal troponin-I on troponin-T. Can J. Biochem. **58**: 649-654.

PEARLSTONE, J.R., and SMILLIE, L.B. 1981. Identification of a second binding region on rabbit skeletal troponin-T for α-tropomyosin. FEBS Lett. **128**: 119-122.

PEARLSTONE, J.R., and SMILLIE, L.B. 1982. Binding of troponin-T fragments to several types of tropomyosins: Sensitivity to Ca^{+2} in the presence of troponin-C. J. Biol. Chem. **257**: 10587-10592.

PEARLSTONE, J.R., and SMILLIE, L.B. 1983. Effects of troponin-I plus -C on the binding of troponin-T and its fragments to α-tropomyosin: Ca^{+2} sensitivity and cooperativity. J. Biol. Chem. **258**: 2534-2542.

PEARLSTONE, J.R., and SMILLIE, L.B. 1985. The interaction of rabbit skeletal muscle troponin-T fragments to troponin-I. Can. J. Biochem. Cell Biol. **63**: 212-218.

PERRY, S.V., COLE, H., HEAD, J.F., and WILSON, F.J. 1972. Localization and mode of action of the inhibitory protein component of the troponin complex. Cold Spring Harbor Symp. Quant. Biol. **37**: 251-262.

PHILLIPS, H.N. Jr., FILLERS, J.P., and COHEN, C. 1980. Motions of tropomyosin. Crystal as metaphor. Biophys. J. **32**: 485-500.

POTTER, J.D., and GERGELY, J. 1974. Troponin, tropomyosin and actin interactions in the Ca^{+2} regulation of muscle contraction. Biochemistry **13**: 2697-2703.

PRINCE, H.P., TRAYER, H.R., HENRY, G.D., TRAYER, I.P., DALGARNO, D.C., LEVINE, B.A., CARY, P.D., and TURNER, C. 1981. Proton nuclear magnetic-resonance spectroscopy of myosin subfragment 1 isozymes. Eur. J. Biochem. **121**: 213-219.

RAGG, E., CAVE, A., and DRAKENBERG, T. 1986. Metal ion binding to parvalbumin. A proton NMR study. Acta Chemica. Scandinavica B. **40**: 6-14.

REID, D.G., MACLACHLAN, L.K., GAJJAR, K., VOYLE, M., KING, R.J., and ENGLAND, P.J. 1990. A proton nuclear magnetic resonance and molecular modeling study of calmidazolium (R24571) binding to calmodulin and skeletal muscle troponin C. J. Biol. Chem. **265**: 9744-9753.

RIBIERO, A., PARELLO, J., and JARDETZKY, O. 1984. NMR studies of muscle proteins. Prog. Biophys. Molec. Biol. **43**: 95-160.

ROBERTSON, S.P., JOHNSON, J.D., and POTTER, J.D. 1981. The time-course of Ca^{+2} exchange with calmodulin, troponin, parvalbumin, and myosin in response to transient increases in Ca^{+2}. Biophys. J. **34**: 559-569.

SAUNDERS, C., SYKES, B.D., and SMILLIE, L.B. 1988. Comparison of the structure and dynamics of chicken gizzard and rabbit cardiac tropomyosins: ^{1}H NMR spectroscopy and measurement of amide hydrogen exchange rates. Biochemistry **27**: 7000-7008.

SCHAUB, M.C., and PERRY, S.V. 1969. The relaxing protein system of striated muscle. Biochem J. **115**: 993-1004.

SCHOENBERG, M., BRENNER, B., CHALOVICH, J.M., GREENE, L.E., and EISENBERG, E. 1984. Cross-bridge attachment in relaxed muscle. In *Contractile Mechanism in Muscle* (Polack, G.H., and Sugi, H., Eds.), pp 269-284, Plenum Publishers, N.Y.

SEAMON, K.B., HARTSHORNE, D.J., and BOTHNER-BY, A.A. 1977. Ca^{+2} and Mg^{+2} dependent conformations of troponin C as determined by ^{1}H and ^{19}F nuclear magnetic resonance. Biochemistry **16**: 4039-4046.

SEAMON, K.B. 1980. Calcium- and magnesium-dependent conformational states of calmodulin as determined by nuclear magnetic resonance. Biochemistry **19**: 207-215.

SEEHOLZER, S.H., COHN, M., PUTKEY, J.A., MEANS, A.R., and CRESI, H.L. 1986. NMR studies of a complex of deuterated calmodulin with melittin. Proc. Natl. Acad. Sci. USA **83**: 3634-3638.

SEEHOLZER, S.H., and WAND, J.A. 1989. Structural characterization of the interactions between calmodulin and skeletal muscle myosin light chain kinase: Effect of peptide(576-594)G binding on the Ca^{2+}-binding domains. Biochemistry **28**: 4011-4020.

SHIMIZU, T., and HATANO, M. 1988. ^{43}Ca nuclear magnetic resonance of Ca^{+2}-calmodulin solutions: Effects of trifluoperazine and peptides. Inorganica Chimica Acta **152**: 257-260.

SHRIVER, J.W., and SYKES, B.D. 1981. Phosphorus-31 nuclear magnetic resonance evidence for two conformations of myosin subfragment-1 nucleotide complexes. Biochemistry **20**: 2004-2012.

SODEK, J., HODGES, R.S., SMILLIE, L.B., and JUSEK, L. 1972. Amino-acid sequence of rabbit skeletal tropomyosin and its coiled-coil structure. Proc. Natl. Acad. Sci. USA **69**: 3800-3804.

SOMMERVILLE, L.E., HENRY, G.D., SYKES, B.D., and HARTSHORNE, D.J. 1990. Spin-echo ^{1}H NMR studies of differential mobility in gizzard myosin and its subfragments. Biochemistry **29**: 10855-10864.

SOWADSKI, J., CORNICK, G., and KRETSINGER, R.H. 1978. Terbium replacement of calcium in parvalbumins. J. Mol. Biol. 124: 123-132.

STEWART, M., and MACLACHLAN, A.D. 1975. Fourteen actin-binding sites on tropomyosin? Nature **257**: 331-333.

STONE, D., SODEK, J., JOHNSON, P., and SMILLIE, L.B. 1974. Tropomyosin: Correlation of amino acid sequence and structure. "Proc. IX FEBS Meeting 31" (Biro, E.N.A., Ed.), pp 125-136, Akdemia Krado, Budapest.

STRYER, L. 1988. *Biochemistry*, 3rd ed., W.H. Freeman and Company Publishers, N.Y.

SUNDARALINGAM, M., BERGSTROM, R., STRASBURG, G., RAO, S.T., GREASER, M., and WANG, B.C. 1985. Molecular structure of troponin C from chicken skeletal muscle at 3 Å resolution. Science **227**: 945-948.

SUTOH, K. 1982. Identification of myosin-binding sites on the actin sequence. Biochemistry **21**: 3654-3661.

SUTOH, K. 1983. Mapping of actin-binding sites on the heavy chain of myosin subfragment 1. Biochemistry **22**: 1579-1585.

SUTOO, D., AKIYAMA, K., FUJII, N., and MATSUSHITA, K. 1986a. ^{1}H NMR studies of calmodulin: the effect of W-7(N-(6-aminohexyl)-5-chloro-1-naphthalenesulfonamide) and Ca^{+2} on conformational changes of calmodulin. Biochim. Biophys. Acta **873**: 156-160.

SUTOO, D., AKIYAMA, K., FUJII, N., and MATSUSHITA, K. 1986b. Divalent cation dependent conformations of brain calmodulin detected by ^{1}H NMR. Japan. J. Parmacol. **40**: 169-173.

SUZUKI, R., NISHI, N., TOKURA, S., and MORITA, F. 1987. F-actin-binding synthetic heptapeptide having the amino acid sequence around the SH1 cysteinyl residue of myosin. J. Biol. Chem. **262**: 11410-11412.

SYSKA, H., WILKINSON, J.M., GRAND, R.J.A., and PERRY, S.V. 1976. The relationship between biological activity and primary structure of troponin I from white skeletal muscle of the rabbit. Biochem. J. **153**: 375-387.

SZILAGI, L., and LU, R.C. 1982. The changes of lysine reactivities of actin in complex with myosin subfragment-1, tropomyosin and troponin. Biochim. Biophys. Acta **709**: 204-211.

TALBOT, J.A., and HODGES, R.S. 1979. Synthesis and biological activity of an icosapeptide analog of the actomyosin ATPase inhibitory region of troponin I. J. Biol. Chem. **254**: 3720-3723.

TALBOT, J.A., and HODGES, R.S. 1981a. Synthetic studies on the inhibitory region of rabbit skeletal troponin I. Relationship of amino acid sequence to biological activity. J. Biol. Chem. **256**: 2798-3802.

TALBOT, H.A., and HODGES, R.S. 1981b. Comparative studies on the inhibitory region of selected species of troponin I. The use of synthetic peptide analogs to probe structure function relationships. J. Biol. Chem. **256**: 12374-12378.

TANOKURA, M., TAWADA, Y., ONO, A., and OHTSUKI, I. 1983. Chymotryptic subfragments of troponin T from rabbit skeletal muscle. Interactions with tropomyosin, troponin I and troponin C. J. Biochem. **93**: 331-337.

TAO, T., GERGELY, J., and LEAVIS, P. 1986a. Studies on the interactions between the subunits of skeletal muscle troponin using fluorescence quenching, photochemical cross-linking, and excitation energy transfer techniques. Biophys. J. **49**: 142-143.

TAO, T., SCHEINER, C., and LAMKIN, M. 1986b. Site-specific photo-cross-linking studies on interactions between troponin and tropomyosin and between subunits of troponin. Biochemistry **25**: 7633-7639.

TELEMAN, A., DRAKENBERG, T., FORSEN, S., and THULIN, E. 1983. Calcium and cadmium binding to troponin C. Evidence for cooperativity. Eur. J. Biochem. **134**: 453-457.

TELEMAN, A., DRAKENBERG, T., and FORSEN, S. 1986. Kinetics of Ca^{2+} binding to calmodulin and its tryptic fragments studied by ^{43}Ca-NMR. Biochim. Biophys. Acta **873**: 204-213.

THULIN, E., ANDERSSON, A., DRAKENBERG, T., FORSEN, S., and VOGEL, H.J. 1984. Metal ion and drug binding to proteolytic fragments of calmodulin. Proteolytic, cadmium-113, and proton nuclear magnetic resonance studies. Biochemistry **23**: 1862-1870.

TRAYER, I.P., TRAYER, H.R., and LEVINE, B.A. 1987. Evidence that the N-terminal region of A1-light chain of myosin interacts directly with the C-terminal region of actin. A proton magnetic resonance study. Eur. J. Biochem. **164**: 259-266.

TSAI, M-D., DRAKENBERG, T., THULIN, E., and FORSEN, S. 1987. Is the binding of magnesium(II) to calmodulin significant? An investigation by magnesium-25 nuclear magnetic resonance. Biochemistry **26**: 3635-3643.

TSUDA, S., HASEGAWA, Y., YOSHIDA, M., YAGI, K, and HIKICHI, K. 1988. Nuclear magnetic resonance study of rabbit skeletal troponin C: Calcium-induced conformational change. Biochemistry **27**: 4120-4126.

TSUDA, S., OGURA, K., HASEGAWA, Y., YAGI, K, and HIKICHI, K. 1990. ^{1}H NMR study of rabbit skeletal troponin C: Mg^{2+}-induced conformational change. Biochemistry **29**: 4951-4958.

VANAMAN, T.C., SHARIEL, F., and WATTERSON, D.M. 1977. Structural homology between brain modulator protein and muscle TnCs. In *Calcium-Binding Proteins and Calcium Function* (Wasserman, R.H., *et al.*, Eds.), pp 107-116, Elsevier, Amsterdam.

VANDEKECKHOVE, J., and WEBER, K. 1978. At least six different actins are expressed in a higher mammal: An analysis based on the amino acid sequence of the amino terminal tryptic peptide. J. Mol. Biol. **126**: 782-802.

VAN EERD, J-P., and TAKAHASHI, K. 1975. The determination of the complete amino acid sequence of bovine cardiac troponin C. Biochemistry **15**: 1171-1180.

VAN EYK, J.E., and HODGES, R.S. 1988. The biological importance of each amino acid residue of the troponin I inhibitory sequence 104-115 in the interaction with troponin C and tropomyosin-actin. J. Biol. Chem. **263**: 1726-1732.

VAN EYK, J.E., and HODGES, R.S. 1991. A synthetic peptide of the N-terminus of actin interacts with myosin. Biochemistry, in press.

VAN EYK, J.E., SONNICHSEN, F.D., SYKES, B.D., and HODGES, R.S. 1991a. Interaction of actin 1-28 with myosin and troponin I and the importance of these interactions to muscle regulation. In *Peptides as Probes in Muscle Research* (Ruegg, J.C., Ed.), pp 15-31, Springer-Verlag, Heidelberg.

VAN EYK, J.E., KAY, C.M., and HODGES, R.S. 1991b. A comparative study of the interactions of synthetic peptides of the skeletal and cardiac troponin I inhibitory region with skeletal and cardiac troponin C. Biochemistry, in press.

VOGEL, H.J., ANDERSSON, T., BRAUNLIN, W.H., DRAKENBERG, T., and FORSEN, S. 1984. Trifluoperazine binding to calmodulin: A shift reagent ^{43}Ca NMR study. Biochem. Biophys. Res. Commun. **122**: 1350-1356.

WAKABYASHI, T., HUXLEY, H.E., AMOS, I.A., and KING, A.J. 1975. Three dimensional image reconstruction of actin-tropomyosin complex and actin-tropomyosin-troponin T-troponin I complex. J. Mol. Biol. **93**: 477-497.

WALSH, T.P., and WEGNER, A. 1980. Effect of the state of oxidation of cysteine 190 of tropomyosin on the assembly of the actin-tropomyosin complex. Biochim. Biophys. Acta **626**: 79-87.

WEGNER, A. 1979. Equilibrium of the actin-tropomyosin interaction. J. Mol. Biol. **131**: 839-853.

WEEDS, A.G., and TAYLOR, R.S. 1975. Studies on the chymotryptic digestion of myosin - Effects of divalent cations on proteolytic susceptibility. Nature **257**: 54-56.

WEEDS, A.G., and POPE, B. 1977. Separation of subfragment-1 isozymes from rabbit skeletal muscle myosin. J. Mol. Biol. **111**: 129-157.

WEEKS, R.A, and PERRY, S.V. 1978. Characterization of a region of the primary sequence of troponin C involved in calcium ion-dependent interaction with troponin I. Biochem. J. **173**: 449-457.

WILLIAMS, T.C., CORSON, D.C., and SYKES, B.D. 1984. Calcium-binding proteins: Calcium(II)-Lanthanide(III) exchange in carp parvalbumin. J. Am. Chem. Soc. **106**: 5698-5702.

WILLIAMS, T.C., CORSON, D.C., OIKAWA, K., MCCUBBIN, W.D., KAY, C.M., and SYKES, B.D. 1986. ^{1}H NMR spectroscopic studies of calcium-binding proteins. 3. Solution conformations of rat apo-α-parvalbumin and metal-bound rat α-parvalbumin. Biochemistry **22**: 1835-1846.

WILKINSON, J.M., and GRAND, R.J.A. 1975. The amino acid sequence of troponin I from rabbit skeletal muscle. Biochem. J. **149**: 493-496.

WILKINSON, J.M., and GRAND, R.J.A. 1978. Comparison of amino acid sequence of troponin I from different striated muscles. Nature **271**: 31-35.

WUTHRICH, K. 1986. In *NMR of Proteins and Nucleic Acids*, pp 123-128, John Wiley and Sons, New York.

YAMAMOTO, K., and SEKINE, T. 1979. Interaction of myosin subfragment-1 with actin. II. Localization of the actin binding site in a fragment of subfragment-1 heavy chain. J. Biochem. **86**: 1863-1867.

YAZAWA, M., IKURA, M., HIKICHI, K., YING, L., and YAGI, K. 1987. Communication between two globular domains of calmodulin in the presence of mastoparan or caldesmon fragment. J. Biol. Chem. **262**: 10951-10954.

ZOT, H.G., IIDA, S., and POTTER, J.D. 1983. Thin filament interactions and calcium binding to troponin. Chem. Sci. **21**: 133-136.

ZOT, A.S., and POTTER, J.D. 1987. Structural aspects of troponin-tropomyosin regulation of skeletal muscle contraction. Annu. Rev. Biophys. Chem. **16**: 535-559.

ZOT, H.G., and POTTER, J.D. 1987. Calcium binding and fluorescence measurements of dansylaziridine labeled troponin C in reconstituted thin filaments. J. Muscle Res. Cell Motil. **8**: 428-436.

ZOT, A.S., and POTTER, J.D. 1989. Reciprocal coupling between troponin C and myosin crossbridge attachment. Biochemistry **28**: 6751-6756.

Chapter II

Theoretical Evaluation of the Two-Dimensional Transferred Nuclear Overhauser Effect

A. Introduction

One of the most important issues in biology is the interaction of ligands with macromolecules. Examples include the interaction of substrates with enzymes, antigens with antibodies, hormones with receptors, nucleotides with regulatory proteins, and peptides with phospholipids. Excepting those instances where the ligand has been crystallized in a complex with the macromolecule, Nuclear Magnetic Resonance spectroscopy (NMR), and specifically the intramolecular transferred nuclear Overhauser enhancement experiment (TRNOE), originally proposed by Balaram and Bothner-By (1972a, 1972b), provide the best techniques for the determination of the structure of the bound ligand. Concommittant with the rapid developments in two-dimensional NMR techniques and the use of NMR to determine the structure of proteins in solution (Wuthrich, 1986), there has been a recent emergence of interest in the TRNOE. This is evidenced by the large number of bound ligand structures that have been investigated using the TRNOE within the past five years (Ferrin and Mildvan, 1985; Banerjee *et al.*, 1985; Clore *et al.*, 1986; Glasel and Borer, 1986; Glasel, 1989; Ito *et al.*, 1987; Andersen *et al.*, 1987; Meyer *et al.*, 1988; Erhlich and Colman, 1985, 1990; Anglister *et al.*, 1989; Levy *et al.*, 1989; Milon *et al.*, 1990; Anglister and Zilber, 1990; Belivacqua *et al.*, 1990; Ni *et al.*, 1989a, 1989b, 1989c, 1990). Most of these studies have utilized two-dimensional TRNOESY methods. However, no complete theoretical evaluation of the two-dimensional TRNOESY experiment, as applied to biological systems, has been published to date.

The TRNOE is the extension of the two-dimensional nuclear Overhauser effect (NOE) to exchanging systems such as ligand-protein complexes. The intramolecular TRNOE allows the transfer of information concerning cross-relaxation between two nuclei from the bound ligand to the free ligand resonances via chemical exchange. In the unbound form, the ligand is generally characterized by short correlation times ($\tau_c < 10^{-10}$ s) and thus may be described as being either in the extreme narrowing limit ($\omega\tau_c << 1$), where the NOEs are small and positive, or at the boundary of the extreme narrowing limit ($\omega\tau_c \cong 1$), where the NOEs approach zero. When bound to the protein, the ligand is characterized by the long correlation time of the protein ($\tau_c > 10^{-8}$ s), and thus may be described as being in the spin diffusion limit ($\omega\tau_c >> 1$), where the NOEs are large and negative. In the presence of chemical exchange of the ligand between its free and bound states, negative NOEs conveying conformational information of the bound ligand are 'transferred' to the free ligand resonances where they are more easily measured because these resonances are much narrower.

In practical cases involving large proteins ($M_R > 20,000$), distances derived from measurement of two-dimensinal TRNOESY cross-peak intensities are only approximate, since cross relaxation becomes very rapid and direct cross-relaxation between two spins in the bound ligand is modified by indirect cross-relaxation with any other spins. The theoretical analysis of TRNOE experiments has been so far limited to the initial build-up rates of one-dimensional, steady-state TRNOEs and limited to two or three spins (Clore and Gronenborn, 1982, 1983). As far as the two-dimensional TRNOESY experiment is concerned, this is equivalent to an isolated spin-pair approximation which is valid only at very short mixing times (Noggle and Schirmer, 1971; Wagner and Wuthrich, 1979; Dobson *et al.*, 1982; Gronenborn and Clore, 1985).

An alternative and more rigorous approach to analyzing the TRNOE data involves the implementation of a full relaxation matrix, where a multiple spin system in the presence of chemical exchange is analyzed. The full relaxation matrix treatment of NOE data has been developed and used to refine many protein and nucleic acid structures (Keepers and James, 1984; Lefevre *et al.*, 1987; Boelens *et al.*, 1988, 1989; Borgias and James, 1988, 1989; Baleja *et al.*, 1990). Recently Landy and Rao (1989) have developed an analagous relaxation matrix procedure for the analysis of the TRNOE. They show the complications involved in calculating the NOE for exchanging systems and show how to circumvent these complication by assuming fast chemical exchange between the free and bound ligand, which is generally the situation of greatest biological interest. The larger unsymmetrical relaxation matrix is thus converted to an average relaxation matrix, which is real and symmetric and has the same dimension as the individual free and bound relaxation matrices.

The first part of this chapter describes the theory of the time-dependent intramolecular TRNOE, and examines the full relaxation matrix approach for the determination of distances in the bound ligand. The second part of this chapter uses the full relaxation matrix treatment to evaluate practical experimental considerations for determining the structure of bound ligands through the use of the TRNOE experiment. We look at the effects of variables such as mixing time, fraction of bound ligand, free and bound correlation times, and external free and bound spin-lattice relaxation rates in an attempt to offer practical experimental guidelines for the design of TRNOE experiments.

B. Theory

A description of homonuclear dipolar relaxation for a multiple spin system requires the complete set of coupled differential equations describing the evolution of longitudinal magnetizations of the individual spins. The differential equations are given by the Bloch equations (1957) and are of the form

$$dM_{zi} / d\tau_m = -W_{ii} (M_{zi} - M_{oi}) - \sum_{j\neq i} W_{ij} (M_{zj} - M_{oj}) \qquad [1]$$

where W_{ii} is given by

$$W_{ii} = (1/10) \sum_{j\neq i} \gamma^4\hbar^2 / (r_{ij})^6 \; [J_0(\omega) + 3J_1(\omega) + 6J_2(\omega)] \qquad [2]$$

and W_{ij}, the cross-relaxation rate between spins i and j, is given by

$$W_{ij} = (1/10)\, \gamma^4\hbar^2 / (r_{ij})^6 \; [6J_2(\omega) - J_0(\omega)] \qquad [3]$$

The spectral density functions take the form

$$J_n(\omega) = \tau_c /[1+(n\, \omega_0\, \tau_c)^2] \qquad [4]$$

where τ_c is the rotational correlation time of the interproton vector between i and j, identical for all interproton vectors if the spin system is tumbling isotropically in solution, τ_m is the mixing time of the TRNOESY experiment, in the case that we are considering the evolution of magnetization during the mixing time of a two-dimensional TRNOESY experiment, and ω_0 is the NMR Larmor frequency. These coupled differential equations can be written in matrix form (Solomon, 1955; Abragam, 1961; Macura and Ernst, 1980)

$$d\mathbf{M}/d\tau_m = - \mathbf{W}\bullet\mathbf{M} \qquad [5]$$

where **M** is the matrix of magnetizations and **W** is the n-dimensional relaxation matrix with diagonal elements W_{ii} and off-diagonal elements W_{ij}.
Eqn. 5 can be solved as (Bull, 1987)

$$\begin{aligned} \mathbf{M}(\tau_m) &= \exp (- \mathbf{W}\tau_m) \mathbf{M}(0) \\ &= \boldsymbol{\chi} \exp (-\boldsymbol{\lambda}\, \tau_m) \boldsymbol{\chi}^{-1}\mathbf{M}(0) \\ &= \mathbf{a}(\tau_m) \mathbf{M}(0) \end{aligned} \qquad [6]$$

where $\boldsymbol{\chi}$ is the matrix of eigenvectors of the relaxation matrix $\mathbf{W}$, $\boldsymbol{\lambda}$ is the diagonal matrix of eigenvalues, and $\mathbf{a}$ is the matrix of mixing coefficients, $a_{ij}(\tau_m)$, which are proportional to the measured TRNOESY intensities.

If the spin system undergoes chemical exchange between a free (F) and bound state (B), the coupled differential equations must be modified to include exchange terms. These equations have been derived by McConnell (1958) as modifications of the Bloch equations in the presence of chemical exchange. They have the form

$$dM_{zi}{}^{B}/d\tau_m = -W_{ii}{}^{B}\,(M_{zi}{}^{B} - M_{oi}{}^{B}) + \sum_{j\neq i} W_{ij}{}^{B}\,(M_{zi}{}^{B} - M_{oi}{}^{B}) - M_{zi}{}^{B}/\tau_B + M_{zi}{}^{F}/\tau_F \qquad [7a]$$

$$dM_{zi}{}^{F}/d\tau_m = -W_{ii}{}^{F}\,(M_{zi}{}^{F} - M_{oi}{}^{F}) + \sum_{j\neq i} W_{ij}{}^{F}\,(M_{zj}{}^{F} - M_{oj}{}^{F}) + M_{zi}{}^{B}/\tau_B - M_{zi}{}^{F}/\tau_F \qquad [7b]$$

where τ_F and τ_B are the chemical exchange lifetimes of the free and bound states, respectively. When these equations are presented in matrix form, relaxation can be described by (Landy and Rao, 1989)

$$\frac{d}{d\tau_m}\begin{bmatrix} \mathbf{m_B} \\ \mathbf{m_F} \end{bmatrix} = -\mathbf{R}\begin{bmatrix} \mathbf{m_B} \\ \mathbf{m_F} \end{bmatrix} \qquad [8]$$

where $\mathbf{m_B}$ and $\mathbf{m_F}$ are n-dimensional vectors.

To obtain the mixing coefficients $a_{ij}(\tau_m)$, $\mathbf{R}$ must be diagonalized to yield $\boldsymbol{\lambda}$, the eigenvalue matrix. But due to the lack of symmetry in matrix $\mathbf{R}$, computer methods for the diagonalization are not so readily available and the eigenvalues are not guaranteed to be real (Landy and Rao, 1989). These complications may be avoided in the regime of fast chemical exchange which results in an average relaxation matrix (Landy and Rao, 1989) which is real and symmetric. This can been seen as follows.

$\mathbf{R}$ may be separated into two parts representing exchange and relaxation (Landy and Rao, 1989) as $\mathbf{R} = \mathbf{E} + \mathcal{W}$, where $\mathbf{E}$ includes all the matrix elements involving τ_B and τ_F, and $\mathcal{W}$ is the 2n-dimensional relaxation matrix for the n-spin system in the free and bound forms.

By choice of an appropriate transformation matrix, Eqn. 8 takes the form (Landy and Rao, 1989)

$$\frac{d}{d\tau_m}\begin{bmatrix} \mathbf{m_B} + \mathbf{m_F} \\ p_B\mathbf{m_F} - p_F\mathbf{m_B} \end{bmatrix} = -\left(\begin{bmatrix} 0 & 0 \\ 0 & (\tau_B{}^{-1} + \tau_F{}^{-1})\,\mathbf{1} \end{bmatrix}\right.$$

$$\left. + \begin{bmatrix} p_B\mathbf{W_B} + p_F\mathbf{W_F} & \mathbf{W_F} - \mathbf{W_B} \\ p_Bp_F(\mathbf{W_F} - \mathbf{W_B}) & p_B\mathbf{W_F} + p_F\mathbf{W_B} \end{bmatrix}\right)\begin{bmatrix} \mathbf{m_B} + \mathbf{m_F} \\ p_B\mathbf{m_F} - p_F\mathbf{m_B} \end{bmatrix} \qquad [9]$$

where $\mathbf{W_B}$ and $\mathbf{W_F}$ are relaxation matrices for the bound and free states respectively, and p_B and p_F are the fractions of bound and free ligand. In the limit of fast chemical exchange, $\tau_B{}^{-1}$, $\tau_F{}^{-1} >> W_{ij}{}^{B}$, $W_{ij}{}^{F}$, then $m_{Bi}/m_{Fi} = p_B/p_F$ and Eqn. 9 then simplifies (Landy and Rao, 1989) to

$$\frac{d(\mathbf{m_B} + \mathbf{m_F})}{d\tau_m} \cong (\, p_B\mathbf{W_B} + p_F\mathbf{W_F}\,)\,(\, \mathbf{m_B} + \mathbf{m_F}\,) \qquad [10]$$

Thus, for fast exchange at equilibrium, the longitudinal magnetization of the spin system, summed over the exchanging species, decays as a function of the population-weighted average of the individual relaxation matrices for the bound and free states $\mathbf{R} \cong p_B\mathbf{W_B} + p_F\mathbf{W_F}$. The average relaxation matrix may then be easily diagonalized to generate the desired mixing coefficients.

If one seeks an approximate solution, one can now expand the exponential term of the solution in the form of Eqn. 6 as a Taylor series,

$$\mathbf{a}(\tau_m) = \exp(\, -\mathbf{R}\tau_m\,) = 1 - \mathbf{R}\tau_m + 0.5\,\mathbf{R}^2\tau_m{}^2 + \ldots \qquad [11]$$

At sufficiently short mixing times, the NOE cross-peak intensity is represented by the term in Eqn. 11 linear in τ_m. One may thus arrive at a linear relationship between the measured intensities $a_{ij}(\tau_m)$ and the cross-relaxation rates

$$aij(\tau_m) \cong -Rij\ \tau_m \qquad [12]$$

which for the TRNOESY in fast exchange becomes

$$aij(\tau_m) \cong -[\, p_B\, W_{ij}B + p_F\, W_{ij}F\,]\ \tau_m \qquad [13]$$

This is the result presented earlier by Clore *et al.* (Clore and Gronenborn, 1982, 1983; Gronenborn and Clore, 1985) and basically amounts to a two spin approximation. However the cross-relaxation rate between spins i and j in the bound state is so large for larger proteins that Eqn. 13 is only valid for unreasonably short values of τ_m.

To take into account possible extra relaxation pathways such as the interaction of the protons on the ligand with protons on the protein, we have added an external relaxation component in an *ad hoc* manner so that W_{ii}^F and W_{ii}^B, respectively, become $(W_{ii}^F + R_{1ext}^F)$ and $(W_{ii}^B + R_{1ext}^B)$. The result of adding an external relaxation component to the relaxation pathway of spin i is to effectively increase the spin-lattice relaxation rate of spin i by R_{1ext}.

$$\frac{1}{T_1{}^i} \equiv W_{ii} + \sum_{j \neq i} W_{ij} + R_{1ext} \equiv R_{1i} + R_{1ext} \qquad [14]$$

This also serves to keep the effects of internal motion. We show below that this has the same effect as far as the TRNOESY calculations are concerned as a more detailed approach based upon Lipari's and Szabo's model free approach (Lipari and Szabo, 1982), where internal motions in macromolecules may be specified by two independent quantities: 1. a generalized order parameter, S^2, a measure of the spatial restriction of the motion, and 2. an effective internal correlation time, τ_e, a measure of the rate of motion. The spectral density function of Eqn. 4 then becomes

$$J(\omega) = \{[S^2\tau_c / (1 + (\tau_c\omega)^2)] + [(1-S^2)\tau / (1 + (\tau\omega)^2)]\} \qquad [15]$$

where

$$1/\tau = 1/\tau_c + 1/\tau_e \qquad [16]$$

In the limits $\tau_e << \tau_c$, $(\omega\tau_c)^2 >> 1$, $(\omega\tau_e)^2 << 1$, Eqn. 15 becomes

$$J(\omega) = S^2\tau_c / (\omega\tau_c)^2 + (1 - S^2)\tau_e \qquad [17]$$

Taking the expression for the spin-lattice relaxation rate of spin i yields

$$\frac{1}{T_1{}^i} \ \alpha \ [\sum_{j \neq i} S^2\, 6\tau_c / (\tau_c\omega)^2 + (1 - S^2)\ 15\tau_c] \qquad [18]$$

Expressed in a form similar to Eqn. 14, Eqn. 18 becomes

$$\frac{1}{T_1{}^i} \ \alpha \ [S^2 R_{1i} + (1 - S^2)\ 15\tau_e] \qquad [19]$$

where R_{1i} is the relaxation rate for an isotropically reorienting macromolecule with correlation time τ_c. The extra contribution to the relaxation pathway of spin i from the internal motions increases R_{1i} by a factor of $\{S^2 + (1 - S^2)\,(15/6)\,(\tau_e/\tau_c)\,(\omega\tau_c)^2\}$.

C. Results

In this chapter, we examine the behaviour of the TRNOE using the average relaxation matrix treatment developed by Landy and Rao (1989), and adapted to a computer simulation of the TRNOE build-up curves. As a model system, we have studied the binding of a 12-residue peptide, spanning the inhibitory region of the muscle protein troponin I (TnI), to the muscle protein troponin C (TnC). The Ca(II)-mediated interaction between TnI and TnC in the thin filament of muscle tissue leads to the relief of actomyosin ATPase activity, and ultimately to muscle contraction (Leavis and Gergely, 1984; Zot and Potter, 1987). A chemically synthesized peptide analog spanning the inhibitory residues 104-115 of TnI, Nα-acetyl-TnI(104-115) amide, has been found to be the minimum sequence necessary for inhibition of actomyosin ATPase activity and is found to bind to TnC in a Ca(II)-dependent fashion with a binding constant of 10^5 M^{-1} (Cachia *et al.*, 1983; Malencik and Anderson, 1984). Thus, the interaction of this inhibitory TnI peptide with TnC is a biologically relevent system, amenable to ^1H NMR spectroscopy and TRNOE measurement. Ultimately, we would like to determine the structure of the TnI peptide when bound to TnC, and thereby gain insight into the mechanism of TnC-Ca(II)-mediated relief of inhibition of actomyosin ATPase activity.

The computer simulation (see Appendix for copy of computer program; TRNOE: version 1) takes as input the coordinates of the protons of the free and bound conformations of the TnI peptide, the correlation times of the free and bound peptide proton pairs (τ_cF, τ_cB), the external leakage relaxation rates of the free and bound peptide protons ($R_{1ext}F$, $R_{1ext}B$), the fraction of the free and bound peptide (p_F, p_B), the mixing time (τ_m), and the frequency of the experiment (ω). The coordinates for the free TnI peptide were generated from the standard Φ,Ψ angles of a β-strand ($\Phi = -118°$, $\Psi = +118°$), whereas the coordinates for the bound peptide were generated from the standard Φ,Ψ angles of an α-helix ($\Phi = -60°$, $\Psi = -40°$). This is a reasonable model to adopt since the peptide is considered to be unstructured and extended in solution, but binds to TnC with 'helix-like' structure (Campbell and Sykes, 1991; Chapter V). The proton coordinates of the TnC protein to which the TnI peptide binds were not included explicitly in the calculation, but rather as a bath of protons in which the bound TnI peptide experiences a longer correlation time and a larger external leakage relaxation rate.

In order to study the effect of internuclear separation on the development of the TRNOE between protons, four proton pairs were chosen with varying internuclear distances. Table II-1 summarizes these proton pairs and their internuclear distances in the free and bound peptide. The geminal proton pair #1, F106βCH-F106βCH', is representative of a very short internuclear distance (1.76 Å) which does not change from the free to bound TnI conformation. Although a stereospecific assignment is often possible with geminal protons of non-degenerate chemical shifts, it is not adviseable to use their measured TRNOE as a reference TRNOE when determining relative distances, as spin diffusion becomes a major problem at short distances and all calculated distances will then appear too short. A much better reference distance is offered by the vicinal proton pair #2, F106δCH-F106ξCH, on the phenylalanine ring. This internuclear distance (2.46 Å) again does not change from free to bound peptide. It has been used as the reference TRNOE to calculate distances from the computer simulated TRNOE values for the other three proton pairs in the following sections of this chapter. Proton pair #3, R112NH-R113NH is interesting in that it represents an internuclear distance diagnostic of an α-helix, but not of a β-strand, and correspondingly the internuclear distance decreases from 4.41 Å to 2.68 Å in the free versus bound peptide. Finally, proton pair #4, R112αCH-R113αCH represents a long internuclear distance, increasing only marginally from 4.74 Å to 4.86 Å in the free versus bound peptide.

The TRNOE was calculated using the following standard parameters: $\omega = 500 \times 10^6\ s^{-1}$; $R_{1ext}F = 0.00\ s^{-1}$; $R_{1ext}B = 0.50\ s^{-1}$; $\tau_cF = 0.4$ ns and $\tau_cB = 12, 25, 45, 90$ ns. Fractions bound, and mixing times, were varied to examine their effects on the development of the TRNOE. The correlation time for all protons in the free peptide was taken to be 0.4 ns, an appropriate estimate for a 12 residue peptide, whereas four different correlation times were chosen for all protons in the bound peptide, i.e., $\tau_cB = 12, 25, 45, 90$ ns. The rationale for four choices of bound correlation time is to explore the effect on the TRNOE of binding the same size ligand to different size protein complexes at different experimental temperatures. In the model, the TnI peptide binds to the TnC protein, a protein of molecular weight of 18,500 Daltons. According to a plot of experimentally determined rotational correlation times of globular proteins (Brauer and Sykes, 1987), an 18,500 Dalton protein should display a τ_c of approximately 12 ns at a temperature of 25°C. Thus, we take the first τ_c as 12 ns. However, most experimental TRNOE data would likely be acquired at a lower temperature of, say 4°C, to retard the NH exchange of the free peptide such that the αCH-NH fingerprint region can be observed. In this case, the correlation time of the protein to which the peptide binds changes according to the Stokes-Einstein equation (Boerand and Kidd, 1982)

$$\tau_c = 4/3\,\pi\, a^3\,(\eta'/kT) = V_s\,(\eta'/kT) \qquad [20]$$

where a is the radius of the protein (in cm), η' is the viscosity of the solvent (in g s^{-1} cm^{-1}), T the temperature (in °K), k = 1.3805×10^{-16} erg deg^{-1} $molecule^{-1}$ and Vs is the volume of a spherical protein ($Vs = 4/3\pi a^3$). Thus, τ_c is proportional to η'/T, so that τ_c has an appreciable temperature dependence. Pure H_20 has an η' of 0.01567 poise at 4°C, and 0.008904 poise at 25°C, so that the τ_c of a protein determined at 25°C would be almost half (0.53) that determined at 4°C. Hence, the choice of a second τ_cB of 25 ns is representative of the TnI peptide binding to TnC under experimental conditions of 4°C. We also examined the effects on the TRNOE of binding the TnI peptide to the whole troponin complex (Leavis and Gergely, 1984; Zot and Potter, 1987) (M_R = 77,500 Daltons). An inspection of τ_c experimental versus M_R (Brauer and Sykes, 1987) yields a τ_c of approximately 45 ns for a 77,500 Dalton protein at 25°C, and at an experimental temperature of 4°C, this correlation time is doubled to 90 ns. Hence, the choice of third and fourth τ_cB values of 45 and 90 ns is representative of the TnI peptide binding to the whole troponin complex under experimental conditions of 25°C and 4°C, respectively.

The first set of simulations illustrates the effect of fraction bound on the time dependence of the TRNOE, for various mixing times. The TRNOE was calculated for four values of τ_m (50, 100, 150, 200 ms), and p_B varying from 0 to 1.0. Figure II-1 shows TRNOE build-up curves as a function of fraction bound for various mixing times, interproton distances in the bound peptide and bound correlation times. The panels from left to right represent an increase in τ_m from 50 ms to 200 ms, and from top to bottom an increase in τ_cB from 12 ns to 90 ns.

The intensity of the TRNOE is essentially zero for p_B approaching zero, indicating that the contribution to the TRNOE intensity from the peptide in the free state is negligible. This is due to the fact that $(\omega\tau_cF) \cong 1$, and therefore the structure of the free peptide will contribute little to the calculated distances (we return to this point later).

It is immediately obvious from Figure II-1 that the TRNOE does not display a linear build-up in magnetization intensity as p_B is increased, for constant τ_m. The linear relationship between TRNOE intensity and p_B exists only at very small values of p_B and very short values of τ_m. For longer τ_m and larger τ_cB values, the three shorter internuclear distances (1.76, 2.46 and 2.68 Å) display a fast build-up of magnetization followed by rapid decay. This phenomenon of rapid decay is especially prevalent for proton pair #1 (1.76 Å). For τ_cB = 12 ns (Panels A, B, C, D), the TRNOE corresponding to pair #1 begins to visually diverge from linearity at $p_B > 0.3$ for τ_m = 50 ms (Panel A) but has begun to diverge from linearity at $p_B > 0.05$ for τ_m = 200 ms (Panel D). For τ_m = 50 ms (Panels A, E, I, M), the TRNOE corresponding to proton pair #1 diverges from linearity at

$p_B > 0.3$ for $\tau_cB = 12$ ns (Panel A) and has begun to diverge from linearity at $p_B > 0.05$ for $\tau_cB = 90$ ns (Panel M).

For longer τ_m and larger τ_cB, all magnetization begins to approach the same intensity, indicating that spin diffusion has spread magnetization uniformly over all protons in the peptide. Spin diffusion begins to dominate as the τ_cB increases from 12 ns to 90 ns, or as the peptide spends a proportionately longer time in the bound state (larger p_B).

Figure II-2 shows the TRNOE values of Figure II-1 translated into distances, calculated using the proton pair #2, F106δCH-F106ξCH, as the reference TRNOE and reference distance (2.46 Å). For larger values of τ_m and p_B, all distances converge to an average value of approximately 2.5 Å so that it is best to work with short τ_m and small p_B, especially when τ_cB is large. This can be a positive factor in the design of a TRNOE experiment, since an appreciable TRNOE can be observed for very low fraction of bound protein ($p_B < 0.05$), a plus if the protein is difficult to obtain in any quantity.

An appropriate question to ask is how does the conformation of the free peptide contribute to the calculated conformation of the bound peptide, given that both the free and bound relaxation matrices contribute to the final structure? Figure II-3 shows the effect of changing the correlation time of the free peptide, τ_cF, on the calculation of r apparent. At very low fraction bound, one may expect the free conformation to contribute somewhat to the final conformation due to the magnitude of fraction free, i.e., $p_F >> p_B$. We have taken the worst case scenario, where τ_cB is at its lowest value ($\tau_cB = 12$ ns). Three τ_cF values were chosen, one of 0.2 ns, corresponding to a 6 residue peptide, one of 0.4 ns, corresponding to a 12 residue peptide, and one of 0.8 ns, corresponding to a 24 residue peptide. The proton pair chosen was proton pair #3, R112NH-R113NH where $r_{ij}F = 4.41$ Å and $r_{ij}B = 2.68$ Å. According to Figure II-3, one can see at $p_B = 0.0$ that r apparent is approximately equal to 4.4 Å, the distance in the free peptide. But even at very low p_B, (p_B=0.010 or 1% bound), r apparent is already approaching the distance in the bound peptide. The curve corresponding to $\tau_cF = 0.8$ ns approaches $r_{ij}B$ the most slowly, whereas the curve corresponding to $\tau_cF = 0.2$ ns approaches $r_{ij}B$ the most quickly. The discontinuity of the $\tau_cF = 0.2$ ns curve at $p_B = 0.012$ is due to the fact that the TRNOE starts from a small positive value and passes through zero to a negative value ($\tau_cF = 0.2$ ns is in the extreme narrowing limit at $\omega = 500 \times 10^{-6}$ s^{-1}). When the TRNOE is null, r apparent approaches infinity. The other curves are continuous, owing to the fact that the TRNOE starts at a small negative number and continues to build to a larger negative number (for $\tau_cF = 0.4, 0.8$ ns, nOes are very small, but negative). Thus, one can seen that for peptides as large as 24 residues, the contribution of the free peptide conformation to the final conformation is completely obviated for $p_B \geq 0.020$. For larger peptides, one need only work at slightly higher values of fraction bound, i.e., $p_B \geq 0.050$.

The second set of simulations illustrates the effect of mixing time, τ_m, on the time dependence of TRNOE for various fractions of bound peptide, p_B. The TRNOE was calculated for four values of p_B (0.05, 0.10, 0.20, 0.40) and τ_m varying from 5 to 200 ms. Figure II-4 shows TRNOE build-up curves as a function of mixing time for various fractions bound, interproton distances in the bound peptide and bound correlation times. Figure II-5 shows the TRNOE values of Figure II-4 translated into distances, using the same reference proton pair #2. The panels from left to right represent an increase in p_B from 0.05 to 0.40, and from top to bottom an increase in τ_cB from 12 ns to 90 ns.

For longer p_B and τ_cB values, the three shorter distances again display rapid magnetization build-up and decay. For $\tau_cB = 12$ ns, (Panels A, B, C, D), the TRNOE corresponding to 1.76 Å begins to diverge from linearity at $\tau_m > 80$ ms for $p_B = 0.05$ (Panel A), but has begun to diverge from linearity for $\tau_m > 20$ ms at $p_B = 0.40$ (Panel D). For $p_B = 0.05$ (Panels A,E,I,M), the TRNOE corresponding to 1.76 Å which begins to diverge from linearity at $\tau_m > 80$ ms for $\tau_cB = 12$ ns (Panel A) has begun to diverge from linearity at $\tau_m > 20$ ms for $\tau_cB = 90$ ns (Panel M). For larger p_B and τ_cB, all magnetization begins to approach the same intensity, and distances converge to an average value of 2.5 Å as spin diffusion spreads magnetization uniformly over the bound peptide protons.

This set of simulations demonstrates how rapidly spin diffusion in larger proteins can influence the development of the TRNOE. Given that one has the ability to control at least two variables in the TRNOE experiment, τ_m and p_B, it is best to use very low p_B values but work at a reasonable τ_m which gives decent experimental signal-to-noise. This may be one of the few examples in biochemistry where less protein gives better results!

To illustrate the effects of internal motion in the bound peptide on the development of the TRNOE, we calculated the TRNOE for four values of $R_{1ext}B$ (0.50, 1.00, 2.00, 4.00 s^{-1}), and p_B varying from 0 to 1.0. For these simulation, we again chose proton pair #3, R112NH-R113NH, and translated the TRNOE values into distances using reference proton pair #2. Figure II-6A shows TRNOE build-up curves for proton pair #3 as a function of internal motion relaxation rates and fraction of bound peptide. As $R_{1ext}B$ is increased from 0.50 to 4.00 s^{-1}, the decay in the TRNOE intensity becomes more rapid. However, when these TRNOE values are translated into distances, as shown in Figure II-6B, the curves calculated for different $R_{1ext}B$ values become indistinguishable from each other. This is because we have included uniform internal motion only, where all protons in the bound peptide experience the same value of $R_{1ext}B$. Thus, although the intensity of the TRNOE between proton pair #3 is diminished by the effects of internal motion, the intensity of proton pair #2 is equally diminished, so that the calculated r apparent for pair #3 using reference pair #2 does not change as $R_{1ext}B$ is varied. If we had included a model for differential motion, such that proton pair #3 experienced an internal relaxation rate faster than that experienced by pair #2, then r apparent for pair #3 would have changed as $R_{1ext}B$ was varied. An increase in $R_{1ext}B$ for pair #3 would have been accompanied by a more rapid approach towards the averaged 'spin diffusion' value for all proton pairs in the peptide (approx. 3Å).

D. Discussion

We have examined the behaviour of the TRNOE using a relaxation matrix treatment and adapted to a computer simulation of the TRNOE build-up curves for a model system of the binding of a 12-residue peptide, spanning the inhibitory region of the muscle protein TnI, to the muscle protein TnC. It was found that the TRNOE developed from essentially zero intensity, indicating that the contribution to the TRNOE from the free peptide conformation was negligible. The contribution from the free peptide to the TRNOE-derived distance was observed only for very low fraction of bound peptide, and only when the distance between two protons in the free peptide ($r_{ij}F$) differed substantially from the distance between the same two protons in the bound peptide. The effect of the contribution of the free peptide structure to the calculated distances is contingent upon the size of the peptide. However, even for a peptide as large as 24 residues binding to a smallish protein, one need only titrate in 5% protein to have the distance calculated from the observed TRNOE correspond to the bound structure.

Uniform internal motion in the bound peptide does not affect the values of the calculated interproton distances in the bound peptide. That is, even when the peptide is not bound in a rigid conformation and undergoes rapid internal motion, the calculated distances for all proton pairs are not affected. This is because the intensities of the TRNOEs between all proton pairs are equally diminished by the effects of the uniform internal motion.

The effects of mixing time and fraction bound are essentially additive: a larger fraction bound means that the peptide spends a longer proportion of time bound where cross-relaxation between spins is more effective; a longer mixing time means that the spin magnetization of the peptide when bound to the protein has a longer opportunity to cross-relax. At larger fractions of bound peptide and at longer mixing times, a more pronounced spin diffusion effect is observed. The calculated distances for all proton pairs approach the same average values, indicating that spin-diffusion has spread magnetization uniformly over all bound peptide protons. The effects of spin diffusion become more exaggerated as the size of the template protein to which the peptide binds increases.

Although the larger correlation time of the bound peptide leads to spin diffusion (which presents a problem in the analysis of the TRNOE), it does prove to be an asset in the design of the TRNOE experiment. One need only use less protein to reduce the effects of spin diffusion. And the larger the protein, the less of it need be used to achieve a large TRNOE. For example, for a protein of $M_R \cong 80,000$ Daltons one need only bind 5% of the peptide to achieve a huge enchancement in the size of the TRNOE, as well as to achieve a linear build-up of magnetization for reasonable mixing times.

The TRNOE provides a powerful technique for the determination of bound ligand conformations. This chapter shows that the best results are obtained when very little template protein is used in the experiment and indirect cross-relaxation between bound peptide proton pairs is minimized. With the choice of an appropriate reference proton pair, an adequate starting structure may be determined from the calculated distances.

Table II-1. Internuclear distances of reference proton pairs in the free and bound peptide.

proton pair	i	j	rijF	rijB
1	F106βCH	F106βCH'	1.76 Å	1.76 Å
2	F106δCH	F106ξCH	2.46 Å	2.46 Å
3	R112NH	R113NH	4.41 Å	2.68 Å
4	R112αCH	R113αCH	4.74 Å	4.86 Å

Figure II-1. TRNOE intensity versus fraction of bound peptide (p_B) for various bound correlation times (τ_{cB}) and mixing times (τ_m). Calculations are presented for several pairs of nuclei with different internuclear separations: (□) F106βCH-F106βCH', 1.76 Å; (■) F106δCH-F106ξCH, 2.46 Å; (○) R112NH-R113NH, 2.68 Å; (●) R112αCH-R113αCH, 4.86 Å. For horizontal rows of panels (i.e. **A** → **D**) the correlation time used in the calculations is indicated to the right. For vertical columns of panels (i.e. **A**, **E**, **I**, **M**), the fraction of bound peptide used in the calculations is indicated at the top. Other parameters used in the simulation were $\omega = 500 \times 10^6\ s^{-1}$, $R_{1ext}F = 0.00\ s^{-1}$, $R_{1ext}B = 0.50\ s^{-1}$, $\tau_{cF} = 0.4$ ns.

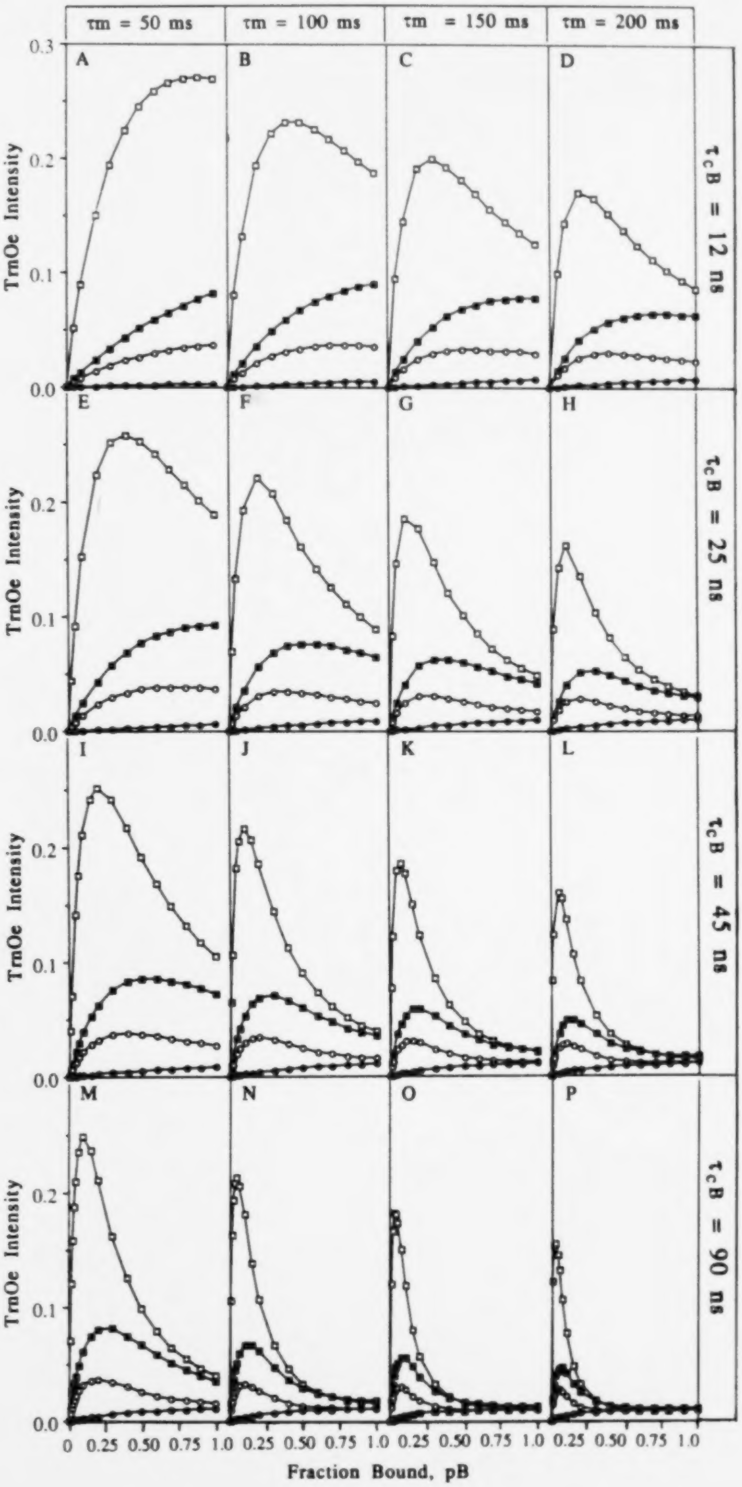
τm = 50 ms
τm = 100 ms
τm = 150 ms
τm = 200 ms
A
B
C
D
E
F
G
H
I
J
K
L
M
N
O
P
τ_cB = 12 ns
τ_cB = 25 ns
τ_cB = 45 ns
τ_cB = 90 ns
TrnOe Intensity
0.3
0.2
0.1
0.0
0 0.25 0.50 0.75 1.0
Fraction Bound, pB

Figure II-2. r apparent calculated from TRNOE values of Figure II-1 versus fraction of bound peptide (p_B) for various bound correlation times ($\tau_c B$) and mixing times (τ_m). Calculations are presented for several pairs of nuclei with different internuclear separations: (□) F106βCH-F106βCH', 1.76 Å; (○) R112NH-R113NH, 2.68 Å; (●) R112αCH-R113αCH, 4.86 Å. For horizontal rows of panels (i.e. **A** → **D**) the correlation time used in the calculations is indicated to the right. For vertical columns of panels (i.e. **A**, **E**, **I**, **M**), the fraction of bound peptide used in the calculations is indicated at the top. Distances were calculated using F106δCH-F106ξCH as the reference TRNOE intensity and reference distance, 2.46 Å.

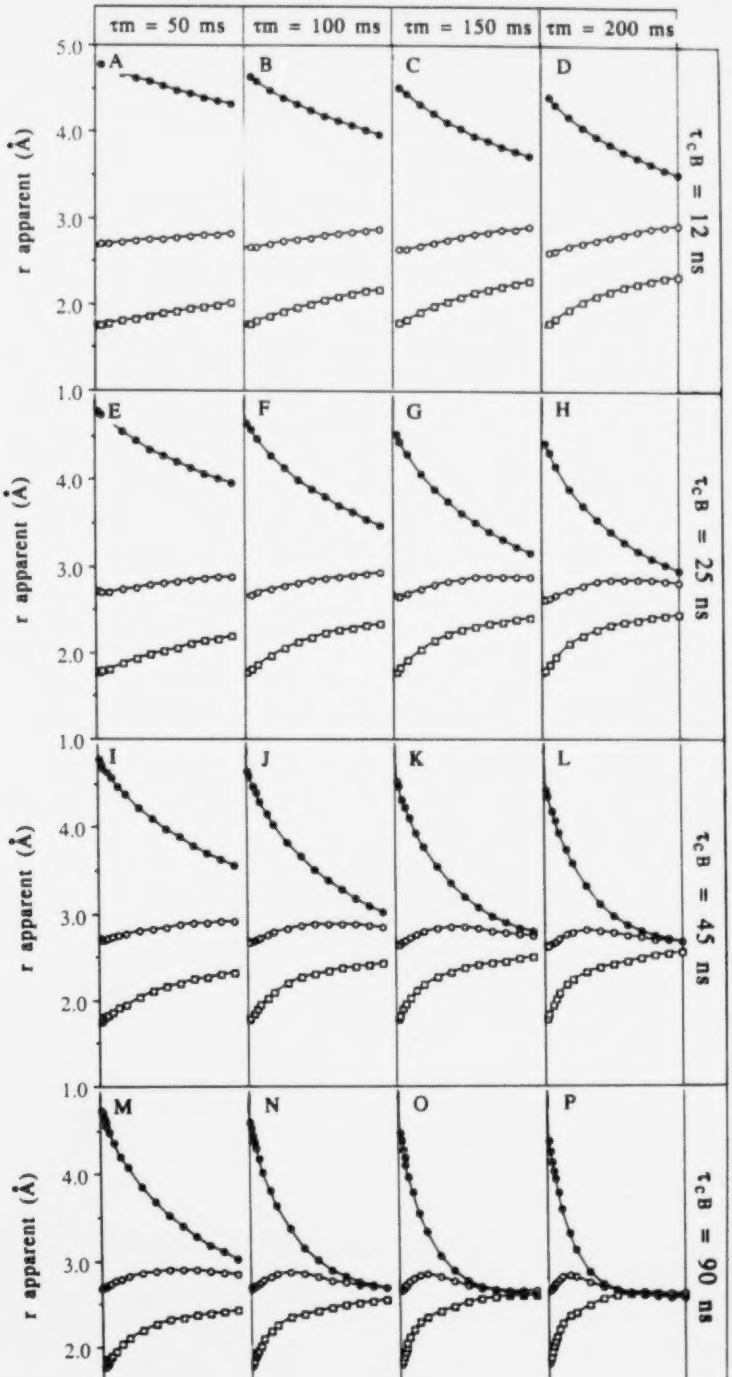
τm = 50 ms
τm = 100 ms
τm = 150 ms
τm = 200 ms
A
B
C
D
E
F
G
H
I
J
K
L
M
N
O
P
τcB = 12 ns
τcB = 25 ns
τcB = 45 ns
τcB = 90 ns
r apparent (Å)
5.0
4.0
3.0
2.0
1.0
0
0.25
0.50
0.75
1.0
Fraction Bound, pB

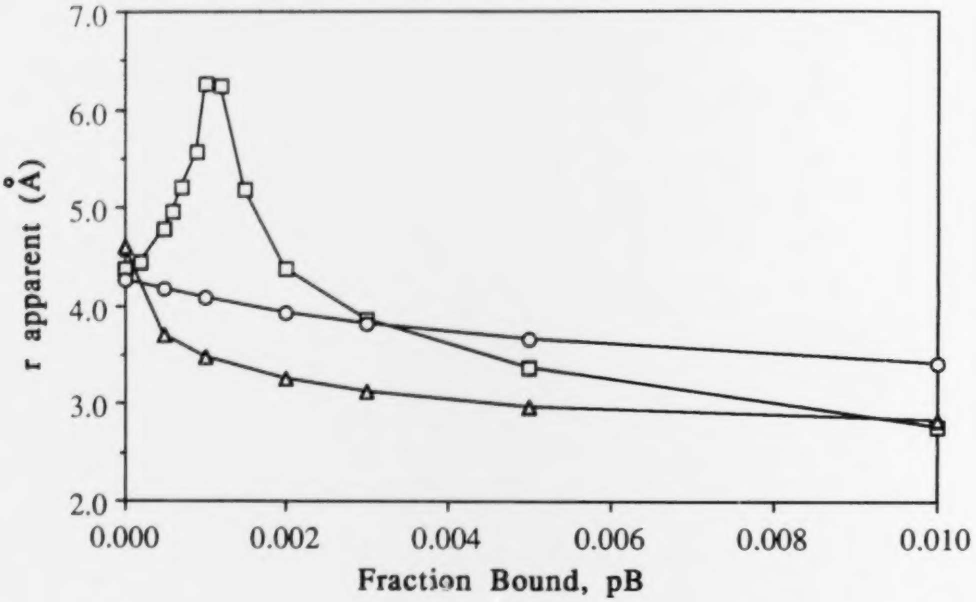

Figure II-3. r apparent for R112NH-R113NH proton pair versus low values of fraction of bound peptide (p_B) for various free correlation times (τ_cF). (□) $\tau_cF = 0.2$ ns; (△) $\tau_cF = 0.4$ ns; (○) $\tau_cF = 0.8$ ns. Other parameters used in the simulation were $\omega = 500 \times 10^6\ s^{-1}$, $R_{1ext}F = 0.00\ s^{-1}$, $R_{1ext}B = 0.50\ s^{-1}$, $\tau_cB = 12$ ns, $\tau_m = 50$ ms.

Figure II-4. TRNOE intensity versus mixing time (τ_m) for various bound correlation times (τ_cB) and fractions of bound peptide (p_B). Calculations are presented for several pairs of nuclei with different internuclear separations: (□) F106βCH-F106βCH', 1.76 Å; (■) F106δCH-F106ξCH, 2.46 Å; (○) R112NH-R113NH, 2.68 Å; (●) R112αCH-R113αCH, 4.86 Å. For horizontal rows of panels (i.e. **A** → **D**) the correlation time used in the calculations is indicated to the right. For vertical columns of panels (i.e. **A**, **E**, **I**, **M**), the mixing time used in the calculations is indicated at the top. Other parameters used in the simulation were $\omega = 500 \times 10^6$ s^{-1}, $R_{1ext}F = 0.00$ s^{-1}, $R_{1ext}B = 0.50$ s^{-1}, $\tau_cF = 0.4$ ns.

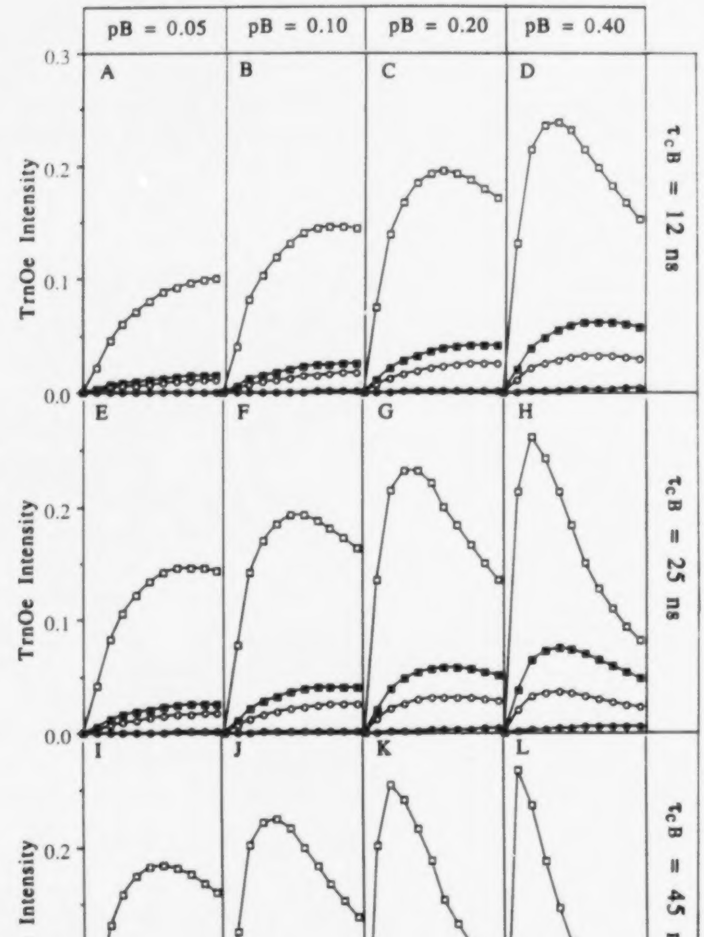
pB = 0.05
pB = 0.10
pB = 0.20
pB = 0.40
A
B
C
D
E
F
G
H
I
J
K
L
M
N
O
P
τcB = 12 ns
τcB = 25 ns
τcB = 45 ns
τcB = 90 ns
TrnOe Intensity
0.0
0.1
0.2
0.3
0
50
100
150
200
Mixing Time, τm (msec)

Figure II-5. r apparent calculated from TRNOE values of Figure II-4 versus mixing time (τ_m) for various bound correlation times (τ_cB) and fractions of bound peptide (p_B). Calculations are presented for several pairs of nuclei with different internuclear separations: (□) F106βCH-F106βCH', 1.76 Å; (○) R112NH-R113NH, 2.68 Å; (●) R112αCH-R113αCH, 4.86 Å. For horizontal rows of panels (i.e. **A** → **D**) the correlation time used in the calculations is indicated to the right. For vertical columns of panels (i.e. **A, E, I, M**), the mixing time used in the calculations is indicated at the top. Distances were calculated using F106δCH-F106ξCH as the reference TRNOE and reference distance, 2.46 Å.

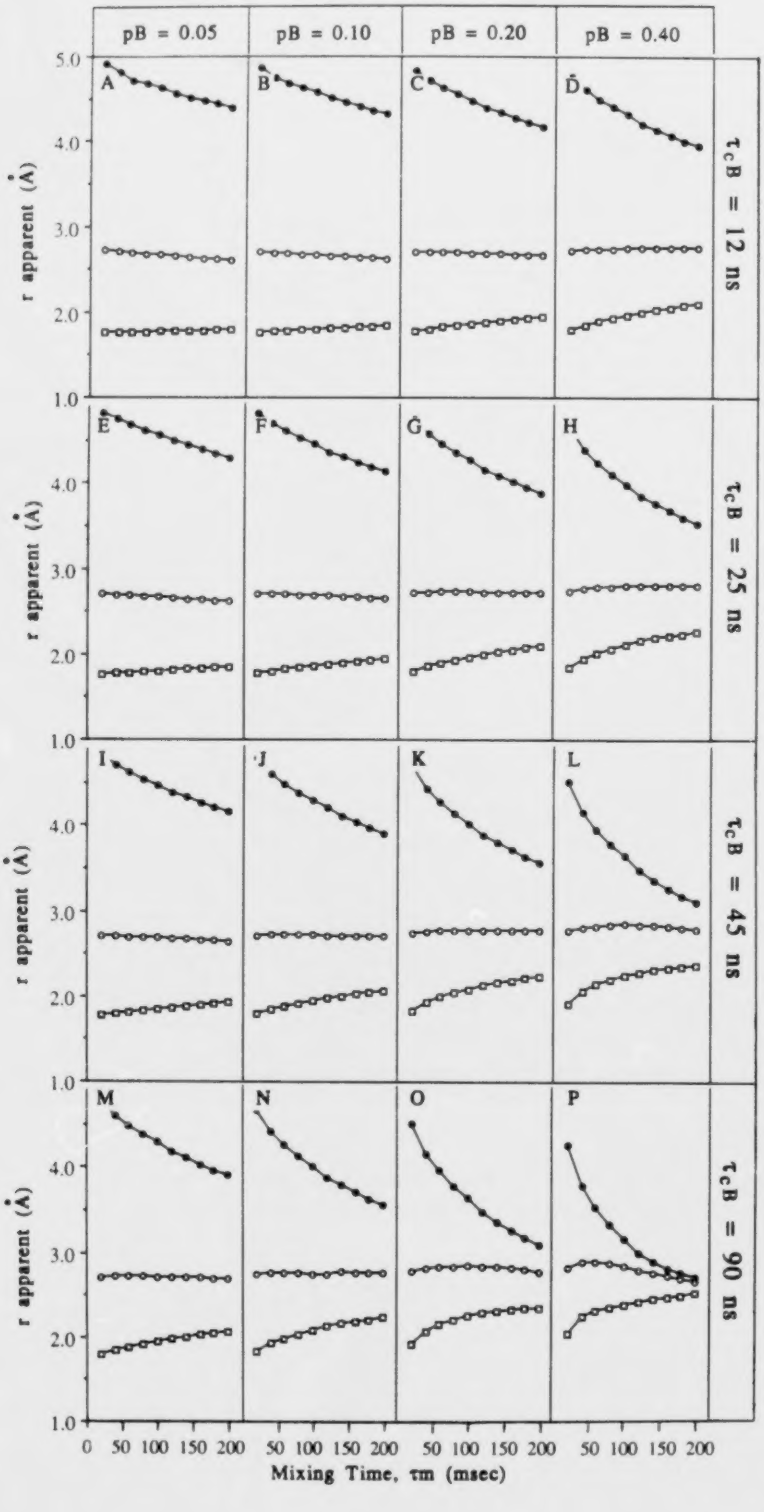
pB = 0.05
pB = 0.10
pB = 0.20
pB = 0.40
τcB = 12 ns
τcB = 25 ns
τcB = 45 ns
τcB = 90 ns
r apparent (Å)
5.0
4.0
3.0
2.0
1.0
A
B
C
D
E
F
G
H
I
J
K
L
M
N
O
P
0
50
100
150
200
Mixing Time, τm (msec)

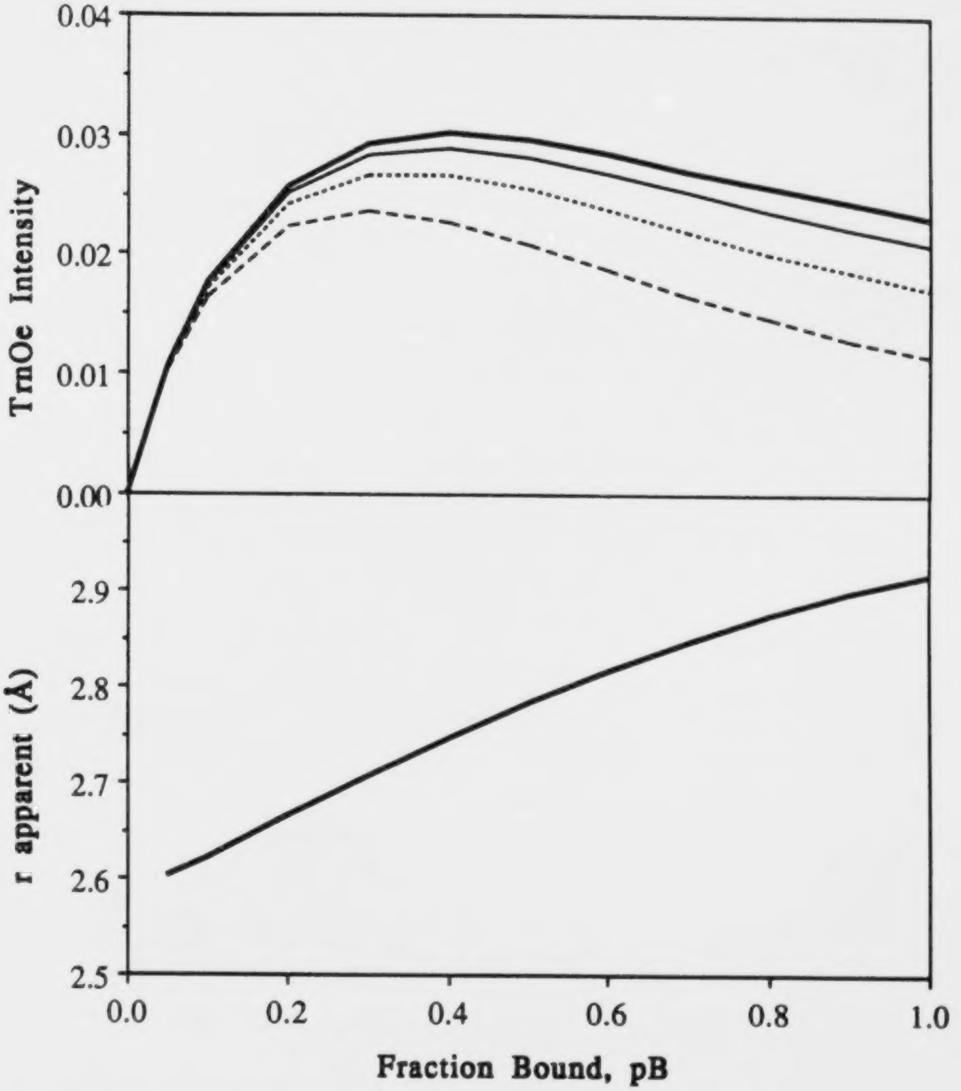

Figure II-6. The effects of uniform internal motion in the bound peptide on the development of the TRNOE intensity and calculated distance, r apparent, for proton pair #3 (R112NH-R113NH; 2.68 Å). Panel **A**: TRNOE intensity versus fraction of bound peptide (p_B) as a function of external leakage relaxation rate in the bound peptide, ($R_{1ext}B$). (**——**) $R_{1ext}B = 0.50\ s^{-1}$; (———) $R_{1ext}B = 1.00\ s^{-1}$; (·········) $R_{1ext}B = 2.00\ s^{-1}$; (-----) $R_{1ext}B = 4.00\ s^{-1}$ Panel **B**: r apparent calculated from TRNOE values of Panel A. Note that all r apparent curves calculated for the various values of $R_{1ext}B$ are indistinguishable from each other. Other parameters used in the simulation were $\omega = 500 \times 10^6\ s^{-1}$, $\tau_m = 200$ ms, $R_{1ext}F = 0.00\ s^{-1}$, $\tau_{cB} = 25$ ns, $\tau_{cF} = 0.4$ ns. Distances were calculated using F106δCH-F106ξCH as the reference TRNOE and reference distance, 2.46 Å.

E. References

ABRAGAM, A. 1961. In *The Principles of Nuclear Magnetism*, Oxford Univ. Press, London.

ANDERSEN, N.H., EATON, H.L., and NGUYEN, K.T. 1987. Small molecule conformation in the receptor-bound state by two-dimensional spin exchange experiment. Magn. Reson. in Chem. **25**: 1025-1034.

ANGLISTER, J., LEVY, R.H., and SCHERF, T. 1989. Interactions of antibody aromatic residues with a peptide of cholera toxin observed by two-dimensional transferred nuclear Overhauser effect difference spectroscopy. Biochemistry **28**: 3360-3365.

ANGLISTER, J., and ZILBER, B. 1990. Antibodies against a peptide of cholera toxin differing in cross-reactivity with the toxin differ in their specific interactions with the peptide as observed by ^{1}H NMR spectroscopy. Biochemistry **29**: 921-928.

BALARAM, P., and BOTHNER-BY, A.A. 1972a. Nuclear magnetic resonance studies of the interaction of peptides and hormones with bovine neurophysin. J. Am. Chem. Soc. **94**: 4015-4017.

BALARAM, P., and BOTHNER-BY, A.A. 1972b. Localization of tyrosine at the binding site of neurophysin II by negative nuclear Overhauser effects. J. Am. Chem. Soc. **94**: 4017-4018.

BALEJA, J.D., MOULT, J., and SYKES, B.D. 1990. Distance measurement and structure refinement with NOE data. J. Magn. Reson. **87**: 375-384.

BANERJEE, A., LEVY, H.R., LEVY, G.C., and CHAN, W.W.C. 1985. Conformations of bound nucleoside triphosphate effectors in aspartate transcarbamylase. Evidence for the London-Schmidt model by transferred nuclear Overhauser effects. Biochemistry **24**: 1593-1598.

BELIVACQUA, V.L., THOMSON, D.S., and PRESTEGARD, J.H. 1990. Conformation of methyl β-lactoside bound to ricin B-chain. Interpretation of transferred nuclear Overhauser effects facilitated by spin simulation and selective deuteration. Biochemistry **29**: 5529-5537.

BLOCH, F. 1957. Generalized theory of relaxation. Phys. Rev. **105**: 1206-1222.

BOELENS, R., KOENIG, T.M.G., and KAPTEIN, R. 1988. Determination of biomolecular structures from proton-proton NOEs using a relaxation matrix approach. J. Mol. Struct. **173**: 299-311.

BOELENS, R., KOENIG, T.M.G., VAN DER MAREL, G.A., VAN BOOM, J.H., and KAPTEIN, R. 1989. Iterative procedure for structure determination from proton-proton nOes using a full relaxation matrix approach. Application to a DNA octamer. J. Magn. Reson. **82**: 290-308.

BOERAND, R.T., and KIDD, R.G. 1982. Ann Rep. NMR Spectrosc. **13**: 320-331.

BORGIAS, B., and JAMES, T.L. 1988. COMATOSE, a method for constrained refinement of macromolecular structure based on two-dimensional nuclear Overhauser effect spectra. J. Magn. Reson. **79**: 493-512.

BORGIAS, B., and JAMES, T.L. 1989. Two-dimensional nuclear Overhauser effect: Complete relaxation matrix analysis. In *Methods in Enzymology* (N.J. Oppenheimer, and T.L. James, Eds.), Vol. **176**, Part A, pp 169-183, Academic Press Inc., New York.

BRAUER, M., and SYKES, B.D. 1987. *Phosphorus NMR in Biology* (C.T. Burt, Ed.), pp 153-184, CRC Press, Boca Raton, Florida.

BULL, T.E. 1987. Cross-correlation and 2D NOE spectra. J. Magn. Reson. **72**: 397-413.

CACHIA, P.J., SYKES, B.D., and HODGES, R.S. 1983. Calcium-dependent inhibitory region of troponin. A proton magnetic resonance study on the interaction between troponin C and the synthetic peptide Nα-acetyl [FPhe106] TnI (104-115) amide. Biochemistry **22**: 4145-4152.

CAMPBELL, A.P., and SYKES, B.D. 1991. Interaction of troponin I and troponin C: Use of the two-dimensional NMR transferred nuclear Overhauser effect to determine the structure of the inhibitory troponin I peptide when bound to skeletal troponin C. J. Mol. Biol., in press.

CLORE, G.M., and GRONENBORN, A.M. 1982. Theory and applications of the transferred nuclear Overhauser effect to the study of the conformations of small ligands bound to proteins. J. Magn. Reson. **48**: 402-417.

CLORE, G.M., and GRONENBORN, A.M. 1983. Theory of the time dependent transferred nuclear Overhauser effect. Applications to structural analysis of ligand-protein complexes in solution. J. Magn. Reson. **53**: 423-442.

CLORE, G.M., GRONENBORN, A.M., CARLSON, G., and MEYER, E.F. 1986. Stereochemistry of binding of the tetrapeptide acetyl-pro-ala-pro-tyr-NH_2 to porcine pancreatic elastase. Combined use of two-dimensional transferred nuclear Overhauser enhancement measurements, restrained molecular dynamics, x-ray crystallography and molecular modeling. J. Mol. Biol. **190**: 259-267.

DOBSON, C.M., OLEJNICZAK, E.T., POULSEN, F.M., and RATCLIFFE, R.G. 1982. Time development of proton nuclear Overhauser effects in proteins. J. Magn. Reson. **48**: 976-110.

EHRLICH, R.S., and COLMAN, R.F. 1985. ^{1}H nuclear magnetic resonance studies of the conformation and environment of nucleotides bound to pig heart NADP$^+$-dependent isocitrate dehydrogenase. Biochemistry **24**: 5378-5387.

EHRLICH, R.S., and COLMAN, R.F. 1990. Conformations of the coenzymes and the allosteric activator, ADP, bound to NAD$^+$-dependent isocitrate dehydrogenase from pig heart. Biochemistry **29**: 5179 -5187.

FERRIN, L.J., and MILDVAN, A.S. 1985. Nuclear Overhauser effect studies of the conformations and binding site environments of deoxynucleoside triphosphate substrates bound to DNA Polymerase I and its large fragment. Biochemistry **24**: 6904-6913.

GLASEL, J.A., and BORER, P.N. 1986. NMR studies of flexible opiate conformations at monoclonal antibody binding sites. I. Transferred nuclear Overhauser effects show bound conformations. Biochem. Biophys. Res. Commun. **141**: 1267-1273.

GLASEL, J.A. 1989. Nuclear magnetic resonance studies of flexible opiate conformations at monoclonal antibody binding sites. Quantitative interproton distances obtained from comparing theoretical and experimental transferred nuclear Overhauser enhancement: correlation with antibody sequence. J. Mol. Biol. **209**: 747-761.

GRONENBORN, A.M., and CLORE, G.M. 1985. Investigation of the solution structures of short nucleic acid fragments by means of nuclear Overhauser enhancement measurements. In *Progress in Nuclear Magnetic Resonance Spectroscopy* (J.W. Emsley, J. Feeney, and L.H. Sutcliffe, Eds.), Vol. **17**, pp 1-32, Pergamon Press, Oxford.

ITO, W., NISHIMURA, M.N., SAKATO, N., FUJIO, H., and ARATA, Y. 1987. A ^{1}H NMR method for the analysis of antigen-antibody interactions: Binding of a peptide fragment of lysozyme to anti-lysozyme monoclonal antibody. J. Biochem. **102**: 643-649.

KEEPERS, J.W., and JAMES, T.L. 1984. A theoretical study of distance determinations from NMR two-dimensional nuclear Overhauser effect spectra. J. Magn. Reson. **57**: 404-426.

LANDY, S.B., and RAO, B.D.N. 1989. Dynamical NOE in multiple-spin systems undergoing chemical exchange. J. Magn. Reson. **81**: 371-377.

LEAVIS, P.C., and GERGELY, J. 1984. Thin filament proteins and thin filament regulation of vertebrate muscle contraction. CRC Crit. Rev. Biochem. **16**: 235-305.

LEFEVRE, J.F., LANE, A.N., and JARDETSKY, O. 1987. Solution structure of the trp operator of *Escherichia Coli* determined by NMR. Biochemistry **26**: 5076-5090.

LEVY, H.R., ASSULIN, O., SCHERF, T., LEVITT, M., and ANGLISTER, J. 1989. Probing antibody diversity by 2D NMR. Comparison of amino acid sequences, predicted structures, and observed antibody-antigen interactions in complexes of two antipeptide antibodies. Biochemistry **28**: 7168-7175.

LIPARI, G., and SZABO, A. 1982. Model-free approach to the interpretation of nuclear magnetic resonance relaxation in macromolecules. 1. Theory and range of validity. J. Am. Chem. Soc. **104**: 4546-4559.

MACURA, S., and ERNST, R.R. 1980. Elucidation of cross-relaxation in liquids by two-dimensional NMR spectroscopy. Mol. Phys. **41**: 95-117.

MALENCIK, D.A., and ANDERSON, S.R. 1984. Peptide binding by calmodulin and its proteolytic fragments and by troponin C. Biochemistry **23**: 2420-2428.

MCCONNELL, H.M. 1958. Relaxation rates by nuclear magnetic resonance. J. Chem. Phys. **28**: 430-431.

MEYER, E.F., CLORE, G.M., GRONENBORN, A.M., and HANSEN, H.A.S. 1988. Analysis of an enzyme-substrate complex by x-ray crystallography and transferred nuclear Overhauser enhancement measurements. Porcine pancreatic elastase and a hexapeptide. Biochemistry **27**: 725-730.

MILON, A., MIYAZAWA, T., and HIGASHIJIMA, T. 1990. Transferred nuclear Overhauser effect analyses of membrane-bound enkephalin analogues by ^{1}H nuclear magnetic resonance. Correlation between activities and membrane-bound conformations. Biochemistry **29**: 65-75.

NI, F., KONISHI, Y., FRAZIER, R.B., SCHERAGA, H.A., and LORD, S.T. 1989a. High-resolution NMR studies of fibrinogen-like peptides in solution. Interaction of thrombin with residues 1-23 of the Aα chain of human fibrinogen. Biochemistry **28**: 3082-3094.

NI, F., MEINWALD, Y.C., VASQUEZ, M., and SCHERAGA, H.A. 1989b. High-resolution NMR studies of fibrinogen-like peptides in solution. Structure of a thrombin-bound peptide corresponding to residues 7-16 of the Aα chain of human fibrinogen. Biochemistry **28**: 3094-3105.

NI, F., KONISHI, Y., BULLOCK, C.D., RIVETNA, M.N., and SCHERAGA, H.A. 1989c. High-resolution NMR studies of fibrinogen-like peptides in solution. Structural basis for the bleeding disorder caused by a single mutation of Gly(12) to Val(12) in the Aα chain of human fibrinogen Rouen. Biochemistry **28**: 3106-3119.

NI, F., KONISHI, Y., and SCHERAGA, H.A. 1990. Thrombin-bound conformation of the C-terminal fragments of hirudin determined by transferred nuclear Overhauser effects. Biochemistry **29**: 4479-4489.

NOGGLE, J.H., and SCHIRMER, R.E. 1971. In *The Nuclear Overhauser Effect*, Academic Press, New York.

SOLOMON, I. 1955. Relaxation processes in a system of two spins. Phys. Rev. **99**: 559-565.

WAGNER, G., and WUTHRICH., K. 1979. Truncated driven nuclear Overhauser effect (TOE). A new technique for studies of selective ^{1}H-^{1}H Overhauser effects in the presence of spin diffusion. J. Magn. Reson. **33**: 675-680.

WUTHRICH, K. 1986. In *NMR of Proteins and Nucleic Acids* , John Wiley and Sons, New York.

ZOT, A.S., and POTTER, J.D. 1987. Structural aspects of troponin-tropomyosin regulation of skeletal muscle contraction. Annu. Rev. Biophys. Chem. **16**: 535-559.

Chapter III

Effects of Internal Motions on the Development of the Two-Dimensional Transferred Nuclear Overhauser Effect

A. Introduction

One of the most important issues in biology is the interaction of ligands with macromolecules. Examples include the interaction of substrates with enzymes, antigens with antibodies, hormones with receptors, nucleotides with regulatory proteins, and peptides with phospholipids. Excepting those instances where the ligand has been crystallized in a complex with the macromolecule, nuclear magnetic resonance spectroscopy (NMR) provides one of the best techniques for the determination of the structure of the bound ligand. Concommittant with the rapid developments in two-dimensional NMR techniques and the use of NMR to determine the structure of proteins in solution (Wuthrich, 1986), there has been a recent emergence of interest in the transferred nuclear Overhauser enhancement experiment (TRNOE) originally proposed by Balaram and Bothner-By (1972a, 1972b). This is evidenced by the large number of bound ligand structures that have been investigated using the TRNOE within the past five years (Ferrin and Mildvan, 1985; Banerjee *et al.*, 1985; Clore *et al.*, 1986; Glasel and Borer, 1986; Glasel, 1989; Ito *et al.*, 1987; Andersen *et al.*, 1987; Meyer *et al.*, 1988; Ehrlich and Colman, 1985, 1990; Anglister *et al.*, 1989; Levy *et al.*, 1989; Milon *et al.*, 1990; Anglister and Zilber, 1990; Belivacqua *et al.*, 1990; Ni *et al.*, 1989a, 1989b, 1989c, 1990).

The TRNOE is the extension of the two-dimensional nuclear Overhauser effect to exchanging systems such as ligand-protein complexes. The intramolecular TRNOE allows the transfer of information concerning cross-relaxation between two nuclei in the bound ligand to the free ligand resonances via chemical exchange. Recently Landy and Rao (1989) have developed a full relaxation matrix analysis for the TRNOE, analagous to the full relaxation matrix treatment of NOE data which has been used to refine many protein and nucleic acid structures (Keepers and James, 1984; Lefevre *et al.*, 1987; Boelens *et al.*, 1988; Borgias and James, 1988, 1989; Baleja *et al.*, 1990).

We have recently published a theoretical evaluation of the TRNOE using the full relaxation matrix approach (Campbell and Sykes, 1991a; Chapter II). We examined the effects of variables such as mixing time, fraction of bound peptide, free and bound correlation times, and other contributions to spin-lattice relaxation rates in an attempt to offer practical experimental guidelines for the design of a TRNOE experiment. These studies, however, did not fully address the question of internal motions in the free and bound peptide, and how these internal motions affect the development of the TRNOE. In this manuscript we address the influence of internal motions on the TRNOE, and issues that are introduced into the calculations such as chemically equivalent protons and the scaling of TRNOE crosspeak intensities (Yip, 1990).

B. Theory

A description of homonuclear dipolar relaxation for a multiple spin system requires the complete set of coupled differential equations describing the evolution of longitudinal magnetizations of the individual spins (Bloch, 1957). These coupled differential equations can be written in matrix form (Solomon, 1955; Abragam, 1961; Macura and Ernst, 1980)

$$d\mathbf{M}/d\tau_m = - \mathbf{W}\bullet\mathbf{M} \qquad [1]$$

where **M** is the vector of magnetizations and **W** is the n-dimensional relaxation matrix. Eqn. 1 can be solved as (Bull, 1987)

$$\begin{aligned} \mathbf{M}(\tau_m) &= \exp(-\mathbf{W}\tau_m)\,\mathbf{M}(0) \\ &= \boldsymbol{\chi}\exp(-\boldsymbol{\lambda}\,\tau_m)\,\boldsymbol{\chi}^{-1}\,\mathbf{M}(0) \qquad [2] \\ &= \mathbf{a}(\tau_m)\,\mathbf{M}(0) \end{aligned}$$

where $\boldsymbol{\chi}$ is the matrix of eigenvectors of the relaxation matrix **W**, $\boldsymbol{\lambda}$ is the diagonal matrix of eigenvalues, and **a** is the matrix of mixing coefficients which are proportional to the measured NOE intensities.

If the spin system undergoes chemical exchange between a free (F) and bound state (B), relaxation can be described by

$$\frac{d}{d\tau_m}\begin{bmatrix} \mathbf{m}_B \\ \mathbf{m}_F \end{bmatrix} = -\mathbf{R}\begin{bmatrix} \mathbf{m}_B \\ \mathbf{m}_F \end{bmatrix} \qquad [3]$$

where $\mathbf{m}_B$ and $\mathbf{m}_F$ are n-dimensional vectors; and $\mathbf{R} = \mathbf{E} + \mathbf{W}$, where **E** is the chemical exchange matrix and **W** is the 2n-dimensional relaxation matrix for the n-spin system in the free and bound forms (Landy and Rao, 1989).

To obtain the mixing coefficients $a_{ij}(\tau_m)$, **R** must be diagonalized to yield $\boldsymbol{\lambda}$, the eigenvalue matrix. But due to the lack of symmetry in matrix **R**, computer methods for the diagonalization are not so readily available and the eigenvalues are not guaranteed to be real (Landy and Rao, 1989). These complications may be avoided in the regime of fast chemical exchange. In the limit of fast chemical exchange, the longitudinal magnetization of the spin system, summed over the exchanging species, decays as a function of the population-weighted average of the individual relaxation matrices for the bound and free states (Landy and Rao, 1989)

$$\frac{d(\mathbf{m_B} + \mathbf{m_F})}{d\tau_m} \cong (p_B \mathbf{W_B} + p_F \mathbf{W_F}) (\mathbf{m_B} + \mathbf{m_F}) \qquad [4]$$

where $\mathbf{W_B}$ and $\mathbf{W_F}$ are relaxation matrices for the bound and free states, respectively, and p_B and p_F are the fractions of bound and free ligand.

Calculating the average relaxation matrix, $\mathbf{R} \cong p_B \mathbf{W_B} + p_F \mathbf{W_F}$, requires setting up individual relaxation matrices, $\mathbf{W_B}$ and $\mathbf{W_F}$. Each relaxation matrix is set up identically, in the following manner. Eqn. 1 may be then be represented as

$$\frac{d}{d\tau_m} \begin{bmatrix} m_i \\ m_j \\ \cdot \\ \cdot \\ \cdot \\ m_n \end{bmatrix} = - \begin{bmatrix} W_{ii} & W_{ji} & \cdots & W_{in} \\ W_{ji} & W_{jj} & \cdots & W_{jn} \\ & \cdot & & \\ & \cdot & & \\ & \cdot & & \\ W_{ni} & W_{nj} & \cdots & W_{nn} \end{bmatrix} \begin{bmatrix} m_i \\ m_j \\ \cdot \\ \cdot \\ \cdot \\ m_n \end{bmatrix} \qquad [5]$$

where the diagonal elements are given by

$$W_{ii} = 2(m_{oi} - 1) (\mathcal{W}_{1ii} + \mathcal{W}_{2ii}) + \sum_k m_{ok} (\mathcal{W}_{oik} + 2\mathcal{W}_{1ik} + \mathcal{W}_{2ik}) + R_{1ext} \qquad [6a]$$

and the off-diagonal elements are given by

$$W_{ij} = m_{oi} (\mathcal{W}_{2ik} - \mathcal{W}_{oik}) \qquad [6b]$$

To take into account other possible relaxation pathways we have added an external relaxation component, R_{1ext}, to the diagonal element, W_{ii}. The transition probabilities are given by (Macura and Ernst, 1980).

$$\mathcal{W}_{1ii} = 3/2\ q_{ii}\ J (\omega_i) \qquad [7a]$$

$$\mathcal{W}_{2ii} = 6\ q_{ii}\ J (2\omega_i) \qquad [7b]$$

$$\mathcal{W}_{1ij} = 3/2\ q_{ij}\ J (\omega_i) \qquad [7c]$$

$$\mathcal{W}_{oij} = q_{ij}\ J (\omega_i - \omega_j) \qquad [7d]$$

$$\mathcal{W}_{2ij} = q_{ij}\ J (\omega_i + \omega_j) \qquad [7e]$$

Here the spectral density functions take the form

$$J(\omega_i) = \tau_c / (1 + (\omega_i \tau_c)^2) \quad [8]$$

and

$$q_{ij} = 1/10\, \gamma_i^2 \gamma_j^2 \hbar^2 (r_{ij})^{-6} (\mu_o/4\pi) \quad [9]$$

where τ_c is the overall tumbling time of the peptide which modulates the interaction between spins i and j, and r_{ij} is the internuclear distance.

1. Chemically Equivalent Protons

The off-diagonal elements, W_{ij} and W_{ji}, are equivalent only if we ignore the presence of chemically equivalent groups of protons for which $m_{oi} > 1$ (such as methyl groups or aromatic rings undergoing fast internal motion). From Eqn. 6b, one can see that this results in an asymmetric relaxation matrix ($W_{ij} \neq W_{ji}$, since $m_{oi} \neq m_{oj}$) for which the eigenvalues are not guaranteed to be real. In addition, most computer algorithms for diagonalizing relaxation matrices are available for symmetric matrices only (Borgias and James, 1988, 1989). When the relaxation matrix, **W**, is real and symmetric, then the transformation matrix of orthonormal eigenvectors, $\boldsymbol{\chi}$, is a unitary matrix which has the mathematical property of having its inverse equal to its transpose ($\boldsymbol{\chi}^{-1} = \boldsymbol{\chi}^T$). Thus, Eqn. 2 simplifies to

$$\mathbf{M}(\tau_m) = \boldsymbol{\chi} \exp(-\boldsymbol{\lambda}\, \tau_m)\, \boldsymbol{\chi}^T \mathbf{M}(0) \quad [10]$$

The computer algorithm required to calculate the transpose of a matrix (as opposed to its inverse) is much simpler and computationally faster, especially as the size of the matrix increases, and thus there are computational advantages in starting with a symmetric relaxation matrix as a starting point for relaxation matrix analysis.

We considered two choices for the treatment of groups of equivalent protons: (1) the use of a single coordinate position for a pseudo proton situated geometrically in the center of the equivalent group of protons; or (2) the explicit consideration of each proton in the group. Treating each proton as an individual distinguishable proton generates a symmetric matrix ($m_{oi} = 1$). This choice is valid as long as no second order spin coupling is involved. Under these conditions, the TRNOE between a given proton and a group of equivalent protons is then the sum of the contributions from each equivalent proton in the group to the given proton. The same reasoning is involved when considering the scaling of experimental cross peak intensities when groups of equivalent protons are involved (Yip, 1990). Cross-relaxation amongst the group of equivalent protons is calculated explicitly.

2. Effects of Internal Motion

To take into account differential motion, we incorporated the order parameters S_{iF} and S_{iB} for spin i in the free and bound peptide (Baleja and Sykes, 1990), using Lipari's and Szabo's model free approach (Lipari and Szabo, 1982). In this approach, internal motions in macromolecules may be specified by two independent quantities: a generalized order parameter, S^2, and an effective internal correlation time, τ_e. The order parameter, S^2, can vary between 0 and 1. A value of one indicates that the correlation time of the interproton vector is the same as the overall tumbling time of the peptide (τ_c); a value of zero indicates complete motional freedom.

The spectral density function of Eqn. 8 then becomes

$$J(\omega_i) = [S^2\tau_c / (1 + (\omega_i\tau_c)^2)] + [(1-S^2)\tau / (1 + (\omega_i\tau)^2)] \qquad [11]$$

where

$$1/\tau = 1/\tau_c + 1/\tau_e \qquad [12]$$

C. Results

Using a model system undergoing chemical exchange, we have computer generated TRNOE build-up curves and have used these as a tool to investigate the effects of internal motion within methyl and aromatic groups. As a model system, we have chosen the binding of a 12-residue peptide, spanning the inhibitory region of the muscle protein troponin I (TnI), to the muscle protein troponin C (TnC). This system has been used in our previous calculations (Campbell and Sykes, 1991a; Chapter II), is of general biochemical interest, and is a system for which experimental data is available. We have determined the structure of the synthetic inhibitory peptide Nα-acetyl-TnI(104-115) amide bound to Ca(II)-saturated skeletal turkey TnC (Campbell and Sykes, 1989, 1991b; Chapter V) and we will take this as the bound structure. The TRNOE-derived structure of the TnI peptide bound to TnC reveals 'helix-like' structure, distorted in the center by the proline residues. The central bend in the peptide functions to bring the residues on the hydrophobic face into closer proximity with each other, thereby forming a small hydrophobic pocket, with the aromatic ring of F106 being somewhat buried by the side chains of L111 and V114. The hydrophilic, basic residues extend off the opposite face of the peptide. The coordinates for the free TnI peptide were generated from the standard Φ,Ψ angles of a β-strand ($\Phi = -118°$, $\Psi = +118°$). Explicit methyl protons were added to the free and bound TnI peptide structures using a program which places protons in an sp^3 hybridized geometry about the central carbon atom.

The computer simulation (see Appendix for copy of computer program; TRNOE: version 2) takes as input the coordinates of the protons of the free and bound conformations of the TnI peptide, the overall tumbling times of the free and bound peptide (τ_cF, τ_cB), the effective internal correlation times of the free and bound peptide (τ_eF, τ_eB), the external leakage relaxation rates of the free and bound peptide protons ($R_{1ext}F$, $R_{1ext}B$), order parameters for individual free and bound peptide protons (S_iF, S_iB), the fraction of the free and bound peptide (p_F, p_B), the mixing time (τ_m), and the frequency of the experiment (ω). The values of the parameters are as used previously ($\tau_cF = 0.4$ ns, $\tau_cB = 25$ ns, $R_{1ext}F = 1.0\ s^{-1}$, $R_{1ext}B = 2.0\ s^{-1}$) (Campbell and Sykes, 1991a; Chapter II) to facilitate comparison. The proton coordinates of the TnC protein to which the TnI peptide binds were not included explicitly in the calculation, but rather as a bath of protons in which the bound TnI peptide experiences a longer correlation time and a larger external leakage relaxation rate.

The specific TRNOEs studied were the intraresidue interaction between the αCH of V114 and the six chemically shift degenerate γCH_3 protons of the same residue, and the longer range interresidue interaction between these six γCH_3 of V114 and three chemically shift degenerate protons of F106 (two ξCH and one ςCH aromatic ring protons). If internal motions are important, they should be obvious in these interactions.

To estimate the values of S_iF and S_iB to use in these simulations, we considered the fact that for a methyl group rotating around a carbon-carbon single bond, τ_c should be decreased by a factor of $S^2 = ([3\cos^2\theta - 1]/2)^2$ (Marshall *et al.*, 1972) where θ is the angle between the i-j interproton vector and the axis of rotation (the carbon-carbon single bond). For a sp^3 hybridized methyl group, $\theta = 90°$, making $S^2 = ([3\cos^2\theta - 1]/2)^2 = 0.25$ for rotation around the methyl axis. Thus, for the methyl protons i and j of the V114 residue in the bound and free peptide, we have chosen $S_i * S_j = 0.25$, or $S_i = S_j = 0.5$. As far as aromatic rings are concerned, the geometry leads to different estimations of $S_i * S_j$ values for the different proton pairs of the ring, so we have somewhat arbitarily chosen $S_i = 0.5$ for the δ, ξ and ς aromatic protons of the F106 residue in the free and bound peptide.

Figure III-1 shows the effect of varying the effective internal correlation times for methyl groups motions in the free and bound peptide on the development of the TRNOE for the intraresidue V114αCH-(γCH$_3$)$_2$ interaction. In panel A, τ_eF is kept constant at 0.01 ns, whereas τ_eB is varied from 0.001 ns to 0.1 ns. In panel B, τ_eB is kept constant at 0.01 ns, whereas τ_eF is varied from 0.001 ns to 0.1 ns. The order parameters for individual free and bound peptide methyl protons were set at S_iF = S_iB = 0.5. One can see that changing the effective correlation time for methyl group motions has little effect on the build-up behaviour of the TRNOE (at the low fraction bound used), but a larger effect on how fast it decays. This effect is greater for internal motions in the free peptide than it is for internal motions in the bound peptide. Thus, motions in the free peptide contribute more to the overall relaxation of the exchanging system than do motions in the bound peptide, a consideration which may be easily overlooked given the emphasis on the faster cross-relaxation in the bound peptide which determines the build-up rates of the TRNOE. Looking at panel B, one can see that the less rapid the internal motion about the methyl group axis in the free peptide, the more strongly is overall relaxation affected, a function of the fact that for longer τ_e values, τ approaches the inverse of the Larmor frequency, and spin-lattice T_1 relaxation becomes more effective. We have chosen τ_eF = τ_eB = 0.01 ns for the subsequent TRNOE calculations, so that they do not depend strongly on the actual rate of the internal motion.

Figure III-2 shows the TRNOE build-up curves for the intraresidue V114αCH-(γCH$_3$)$_2$ and interresidue F106(ξCH$_2$$\varsigma$CH)-V114($\gamma$CH$_3$)$_2$ interactions calculated in the absence of methyl and ring motions in panels A and D, in the presence of methyl rotation in panels B and E, and in the presence of both methyl and ring rotation in panels C and F. One can see that the effect of internal motion is not only to dampen the buildup of the TRNOE, but to also dampen its relaxation. The build-up behaviour of the TRNOE is effectively diminished at shorter mixing times but 'spread-out' over longer mixing times. This effect is evident for the intraresidue V114αCH-(γCH$_3$)$_2$ interaction (Figures III-2A → III-2C) only for the methyl rotation, but the effects of both methyl and ring motion is evident for the interresidue F106(ξCH$_2$$\varsigma$CH)-V114($\gamma$CH$_3$)$_2$ interaction (Figures III-2D → III-2F). Examining the intraresidue V114αCH-(γCH$_3$)$_2$ interaction first we can see that Figures III-2B and III-2C are virtually identical, the only difference being that in Figure III-2B, motion was incorporated for only the methyl groups, whereas in Figure III-2C, motion was incorporated for both the methyl and the ring groups in the peptide. However, for the interresidue F106(ξCH$_2$$\varsigma$CH)-V114($\gamma$CH$_3$)$_2$ interaction, we can see that Figures III-2E and III-2F are quite different due to the incorporation of ring motion absent for Figure III-2E but present for Figure III-2F.

In Figure III-3 (A → E) the two sets of calculations presented in Figure III-2 are converted to apparent distances that would be calculated for these interactions by using a reference TRNOE calculated at the same fraction bound and mixing time; $r_{app} = r_{ref} \{[(TRNOE)_{ref} (m_{oi} \cdot m_{oj})_{obs}]/[(TRNOE)_{obs} (m_{oi} \cdot m_{oj})_{ref}]\}^{1/6}$ (Yip, 1990). As a reference proton pair we have chosen the adjacent δCH-ξCH protons on the aromatic ring of F106 for which a reference TRNOE was calculated and a reference distance of 2.46 Å (invariant of secondary peptide conformation) was measured. This reference proton pair has been used in previous calculations (Campbell and Sykes, 1991b; Chapter II). For comparison, the actual calculated distance summed and averaged over the protons involved

$$\frac{1}{r_{av}} = \left[\frac{1}{(m_{oi}+m_{oj})}\right] \Sigma i,j \left[\frac{1}{rij^6}\right]^{1/6} \qquad [13]$$

is 2.80 Å for the intraresidue V114αCH-$(\gamma CH_3)_2$ interaction, and 3.74 Å for the interresidue F106($\xi CH_2 \varsigma CH$)-V114$(\gamma CH_3)_2$ interaction. All distances were measured from the coordinates of the TnI peptide bound to TnC (Campbell and Sykes 1991b; Chapter V). The fact that the internal motion of the phenylalanine ring influences the reference TRNOE is evidenced by the change in apparent distance observed between Figures III-3B and III-3C for the intraresidue V114αCH-$(\gamma CH_3)_2$ interaction, for which the TRNOE build-up curves (Figures III-2B and III-2C) are virtually identical.

We begin first with a discussion of the effects of internal motion on the calculated distance, r_{app}, for the intraresidue V114αCH-$(\gamma CH_3)_2$ interaction (Figures III-3A → III-3C). In the absence of both methyl and ring rotation (Figure III-3A), the calculated distance r_{app} is observed to increase from approximately 2.9 Å at $\tau_m = 0$ to larger values for $\tau_m > 0$. Thus, r_{app} starts from a value close to the actual averaged distance of 2.80 Å, but continues to increase to much larger values. This occurs as a result of spin diffusion which bleeds magnetization away from the V114αCH-$(\gamma CH_3)_2$ interaction, leading to smaller TRNOE cross-peak intensities and larger calculated distances. The increase in r_{app} at longer τ_m is more pronounced for larger p_B. In the presence of methyl rotation (Figure III-3B), r_{app} is observed to decrease from approximately 3.2 Å at $\tau_m = 0$ and approach the actual calculated distance of 2.80 Å for $\tau_m > 0$. This occurs as a result of the relaxation damping effect of the internal motion which effectively diminishes the TRNOE at shorter mixing times but 'spreads-out' the TRNOE over longer mixing times. The decrease in r_{app} at longer τ_m is virtually independent of p_B as the three curves for the three values of fraction bound are almost superimposeable. In the presence of both methyl and ring rotation (Figure III-3C), r_{app} is observed to increase from approximately 2.5 Å to larger values for $\tau_m > 0$, once again increasing to values much larger than the real value of 2.80

Å. The behaviour of the r_{app} versus τ_m curves is similar to the behaviour observed in the absence of either methyl or ring motion, and is strongly dependent on p_B. The effect of incorporating motion in the reference TRNOE, F106δCH-ξCH, serves to counteract the effect of motion in the experimental TRNOE, V114αCH-(γCH3)2, essentially making it appear as if the V114 methyl group were static.

The effects of motion are manifested somewhat differently in the interresidue interaction, F106(ξCH2ςCH)-V114(γCH3)2 (Figures III-3D → III-3F). In the absence of both methyl and ring rotation (Figure III-3D), the calculated distance r_{app} is observed to decrease from approximately 4.0 Å at $\tau_m = 0$ and approach the actual calculated distance of 3.74 Å for $\tau_m > 0$. In the presence of methyl rotation (Figure III-3E), the decrease in r_{app} as a function of τ_m is more rapid. At $\tau_m = 0$, r_{app} is approximately 4.5 Å, but for $\tau_m > 0$ rapidly decreases to values much smaller than the actual calculated distance of 3.74 Å. From Figures III-3D and III-3E, it can be seen that the behaviour of the r_{app} versus τ_m curves observed in the absence of ring motion is strongly dependent on p_B. In the presence of both methyl and ring rotation (Figure III-3F), r_{app} is observed to slowly decrease from approximately 4.0 Å at $\tau_m = 0$ and approach the actual averaged distance of 3.74 Å for $\tau_m > 0$. The behaviour of the r_{app} versus τ_m curves is similar to the behaviour observed in the absence of either methyl or ring motion, but is not so strongly dependent on p_B. Incorporating ring motion affects both the reference TRNOE, F106δCH-ξCH, and the experimental TRNOE, F106(ξCH2ςCH)-V114(γCH3)2. Thus, the effect of incorporating motion in the reference TRNOE does not entirely counteract the effect of motion in the experimental TRNOE, since the magnitude of the experimental TRNOE is also affected by ring motion.

It is interesting to note the difference in the behaviour of the r_{app} versus τ_m curves for the shorter-range intraresidue V114αCH-(γCH3)2 interaction versus the longer-range interresidue F106(ξCH2ςCH)-V114(γCH3)2 interaction. In the absence of any motion, the r_{app} for the V114αCH-(γCH3)2 interaction increased with increasing τ_m (Figure III-3A), whereas the r_{app} for the F106(ξCH2ςCH)-V114(γCH3)2 interaction decreased with increasing τ_m (Figure III-3D). The incorporation of motion tends to shift the curves in the opposite direction so that the r_{app} for the V114αCH-(γCH3)2 interaction decreased slightly with increasing τ_m (Figure III-3B), and the r_{app} for the F106(ξCH2ςCH)-V114(γCH3)2 interaction remained more or less constant for increasing τ_m (Figure III-3F). Thus, the effect of incorporating internal motions when calculating apparent distances from a set of TRNOESY intensities gathered at longer τ_m and larger p_B would be to shorten intraresidue distances and lengthen interresidue distances. The incorporation of internal motions would serve to counteract the effects of spin diffusion which make shorter intraresidue distances appear longer and longer interresidue distances appear shorter.

D. Discussion

In this manuscript we have addressed the influence of internal motions on the development of the TRNOE in a ligand undergoing chemical exchange between a free and a bound state. The effect of adding internal motion within a proton pair on the ligand is to decrease the correlation time of the internuclear vector, and thus to decrease the cross-relaxation rate between the proton pair. This functions to dampen the effects of spin diffusion, especially in the bound ligand where cross-relaxation rates are much faster than in the free ligand. The build-up behaviour of the TRNOE is effectively diminished at shorter mixing times but 'spread-out' over longer mixing times. However, for small values of fraction bound, and at short mixing times where the TRNOE build-up curves are linear, the effects of internal motion (like the effects of spin diffusion) are not that noticeable, and the apparent distances approach the calculated average distances in the bound ligand. Changing the effective correlation time for methyl group motions has little effect on the build-up behaviour of the TRNOE for small values of fraction bound, but a larger effect on how fast the TRNOE decays. This effect is greater for internal motions in the free peptide than it is for internal motions in the bound peptide.

While it is clear that the incorporation of internal motion within a proton pair affects the magnitude of the observed TRNOE, and thus the apparent interproton distance, it is also clear that the incorporation of internal motion in a reference proton pair will affect the apparent interproton distances of all proton pairs which are calculated from the reference proton pair. This is because the TRNOE build-up behaviour of the reference pair is also dampened and 'spread-out' by the incorporation of internal motion. The effects of motion in the reference proton pair will generally compensate for the effects of motion in the observed proton pair. This occurs if the magnitudes of both the reference TRNOE and the observed TRNOE in the presence of internal motion are diminished with respect to their magnitudes in the absence of internal motion. However, the behaviour of the apparent distance calculated for a proton pair of interest as a function of mixing time is a complicated interplay of both the kinetics of relaxation of the proton pair of interest and of the reference proton pair, and so is not easily predicted.

It is clear that the more fully one takes into account internal motions within the molecule, the more closely do the apparent distances approximate the calculated average distances, and the smaller the dependence of the calculated apparent distance on the mixing time of the experiment or the fraction of bound protein. The apparent distances calculated for the intraresidue V114αCH-(γCH$_3$)$_2$ interaction were most accurate when a model incorporating methyl group rotation was adopted. The apparent distances calculated for the interresidue F106(ξCH$_2$$\varsigma$CH)-V114($\gamma$CH$_3$)$_2$ interaction were most accurate when a model incorporating both methyl group rotation and ring rotation was adopted. Thus, a full consideration of internal motions in a molecule does increase the accuracy of the calculated distances from the observed TRNOEs.

The issues of internal motions and equivalent protons and their effects on the development of the TRNOE have been addressed in advance of a full iterative relaxation matrix approach (Boelens *et al.*, 1989) which we will outline in Chapter X to refine the structure of the inhibitory TnI peptide bound to TnC (Campbell and Sykes, 1989, 1991b; Chapter V). The development of a *t*ransferred *i*terative *r*elaxation *m*atrix *a*pproach, which includes methods for calculating the effects internal motions, would be useful for refining the structures of bound ligands where mobile side chains are most certainly involved in the binding interface.

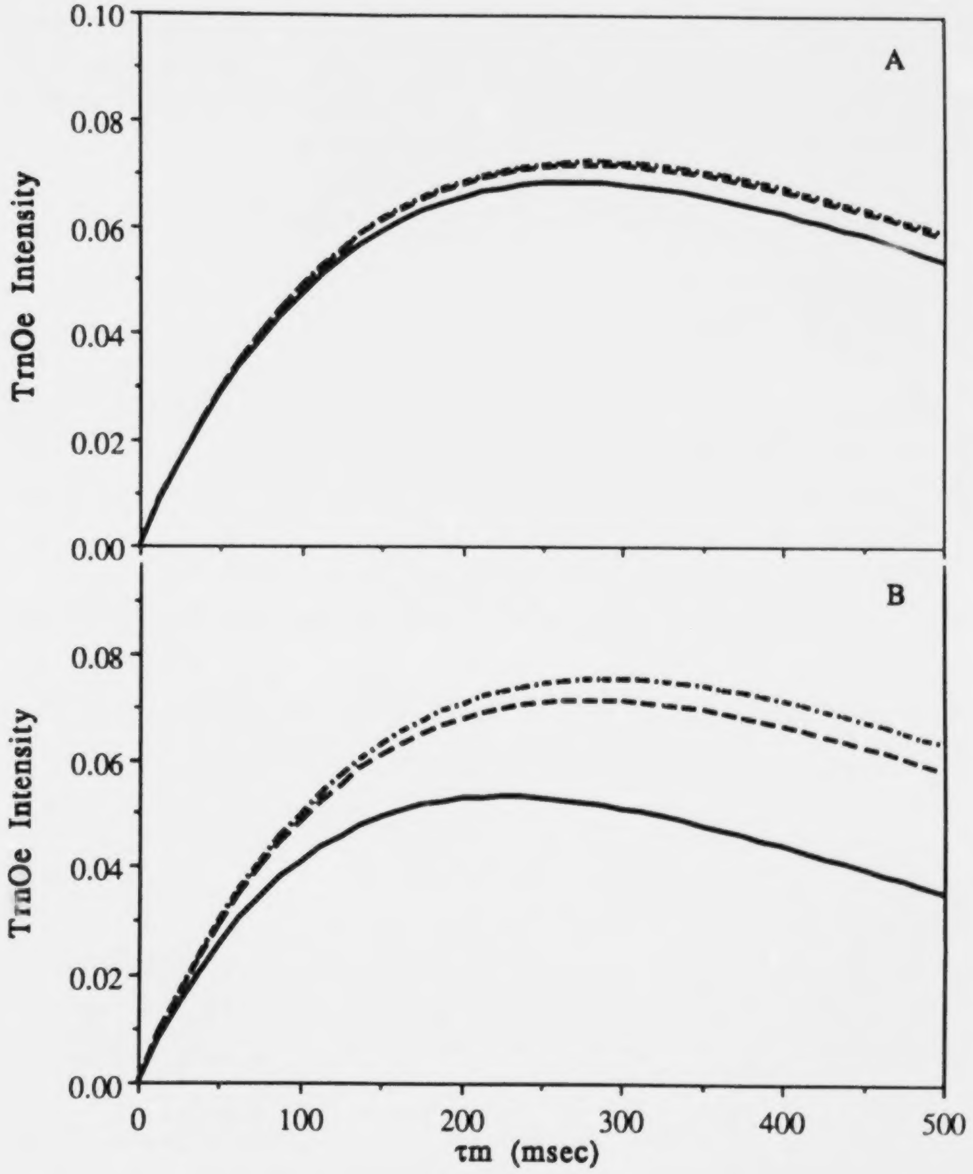

Figure III-1. TRNOE intensity versus mixing time (τ_m) for various free ($\tau_e F$) and bound ($\tau_e B$) internal correlation times. For panel **A**, $\tau_e F = 0.01$ns and $S_i F = S_i B = 0.5$ for the V114 methyl protons: (———) $\tau_e B = 0.1$ ns; (- - - - -) $\tau_e B = 0.01$ ns; (-·-·-·-·-) $\tau_e B = 0.001$ ns. For panel **B**, $\tau_e B = 0.01$ns and $S_i F = S_i B = 0.5$ for the V114 methyl protons: (———) $\tau_e F = 0.1$ ns; (- - - - -) $\tau_e F = 0.01$ ns; (-·-·-·-·-) $\tau_e F = 0.001$ ns. Other parameters used in the simulation were $\omega = 500 \times 10^6$ s^{-1}, $R_{1ext}F = 1.00$ s^{-1}, $R_{1ext}B = 2.00$ s^{-1}, $\tau_c B = 25$ ns, $\tau_c F = 0.4$ ns, p_B=0.1.

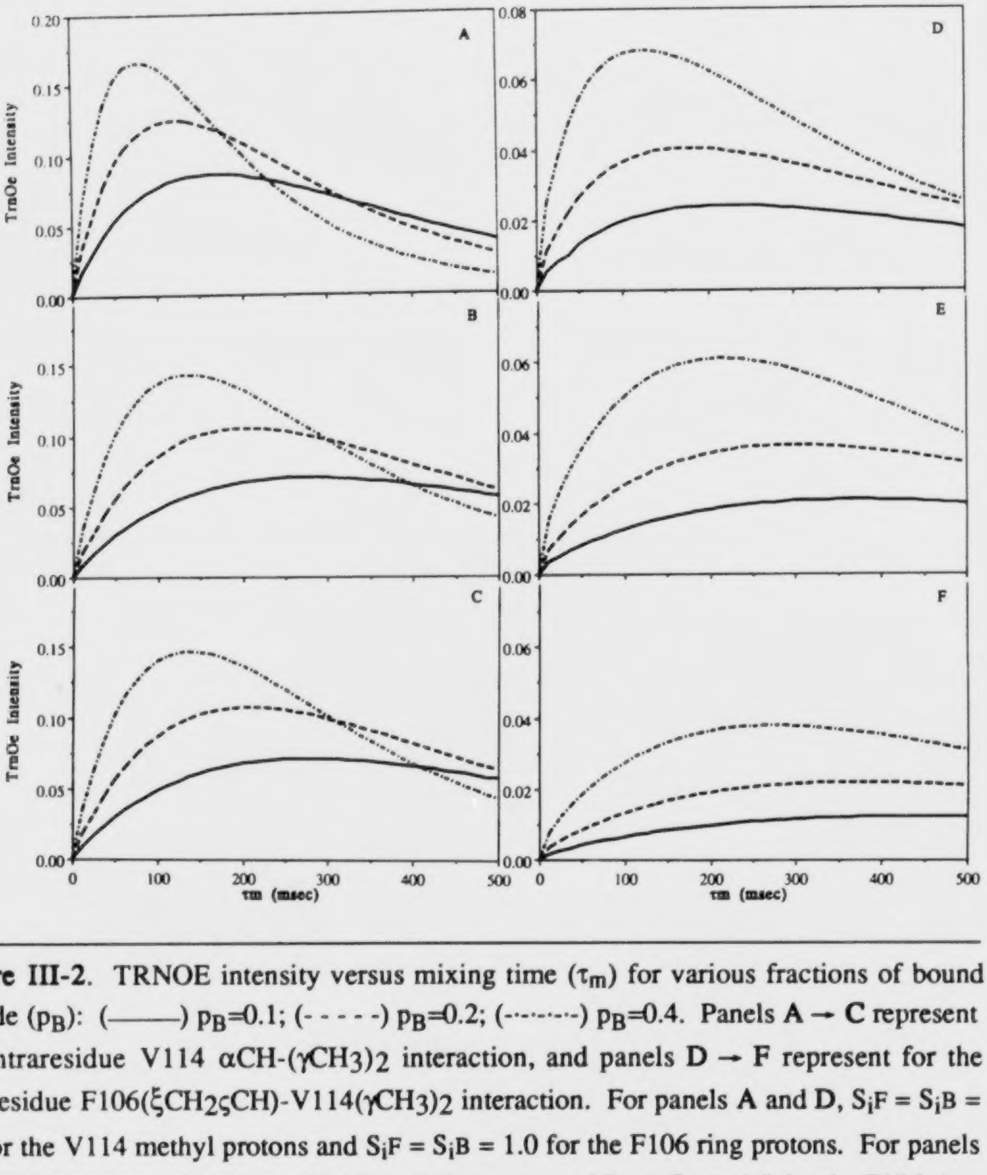

Figure III-2. TRNOE intensity versus mixing time (τ_m) for various fractions of bound peptide (p_B): (———) p_B=0.1; (- - - - -) p_B=0.2; (-·-·-·-·-) p_B=0.4. Panels **A** → **C** represent the intraresidue V114 αCH-(γCH$_3$)$_2$ interaction, and panels **D** → **F** represent for the interresidue F106(ξCH$_2\varsigma$CH)-V114(γCH$_3$)$_2$ interaction. For panels **A** and **D**, $S_iF = S_iB$ = 1.0 for the V114 methyl protons and $S_iF = S_iB$ = 1.0 for the F106 ring protons. For panels **B** and **E**, $S_iF = S_iB$ = 0.5 for the V114 methyl protons and $S_iF = S_iB$ = 1.0 for the F106 ring protons. For panels **C** and **F**, $S_iF = S_iB$ = 0.5 for the V114 methyl protons and $S_iF = S_iB$ = 0.5 for the F106 ring protons. Other parameters used in the simulation were $\omega = 500 \times 10^6$ s^{-1}, $R_{1ext}F = 1.00$ s^{-1}, $R_{1ext}B = 2.00$ s^{-1}, τ_cB = 25 ns, τ_cF = 0.4 ns, τ_eB = 0.01 ns, τ_eF = 0.01 ns.

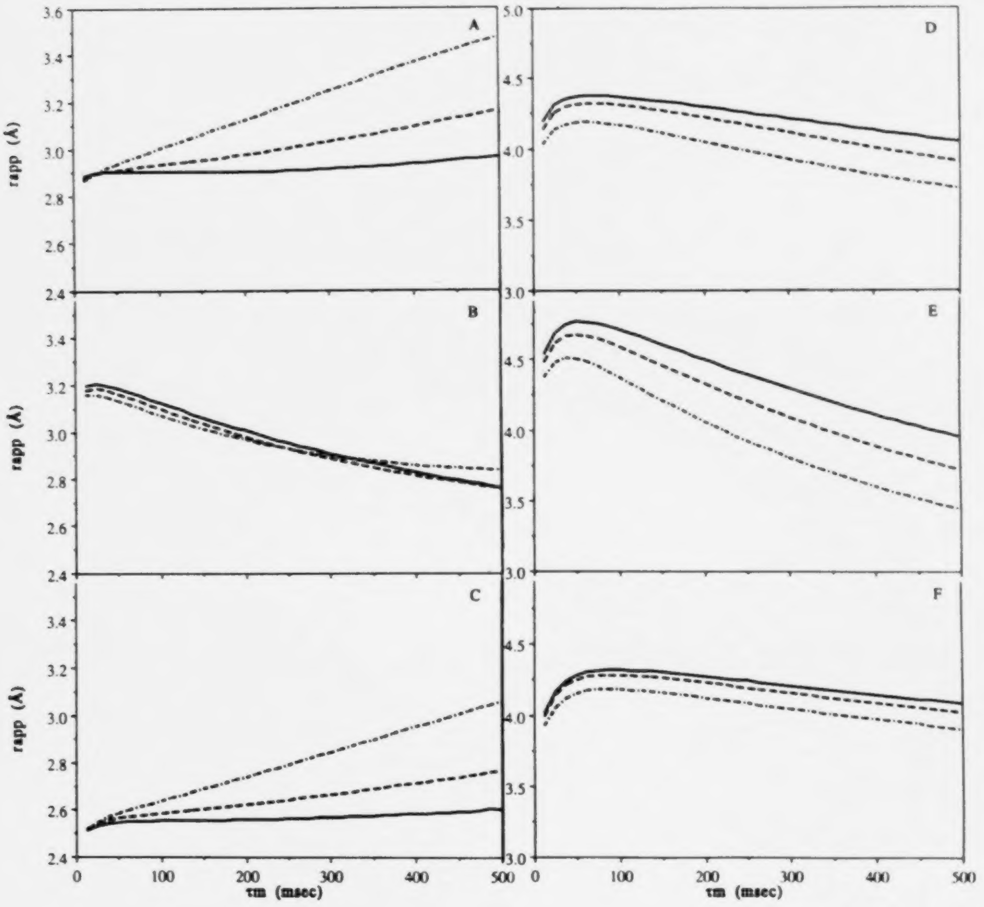

Figure III-3. r apparent calculated from TRNOE values of Figure III-2 versus mixing time (τ_m) for various fractions of bound peptide (p_B): (———) p_B=0.1; (- - - - -) p_B=0.2; (-·-·-·-·-) p_B=0.4. Distances were calculated using F106δCH-F106ξCH as the reference TRNOE intensity and reference distance, 2.48 Å. Panels **A** → **C** represent the intraresidue V114 αCH-(γCH_3)$_2$ interaction, and panels **D** → **F** represent for the interresidue F106(ξCH_2ς CH)-V114(γCH_3)$_2$ interaction. For panels **A** and **D**, $S_iF = S_iB = 1.0$ for the V114 methyl protons and $S_iF = S_iB = 1.0$ for the F106 ring protons. For panels **B** and **E**, $S_iF = S_iB = 0.5$ for the V114 methyl protons and $S_iF = S_iB = 1.0$ for the F106 ring protons. For panels **C** and **F**, $S_iF = S_iB = 0.5$ for the V114 methyl protons and $S_iF = S_iB = 0.5$ for the F106 ring protons.

E. References

ABRAGAM, A. 1961. In *The Principles of Nuclear Magnetism*, Oxford Univ. Press, London.

ANDERSEN, N.H., EATON, H.L., and NGUYEN, K.T. 1987. Small molecule conformation in the receptor-bound state by two-dimensional spin exchange experiment. Magn. Reson. in Chem. **25**: 1025-1034.

ANGLISTER, J., LEVY, R.H., and SCHERF, T. 1989. Interactions of antibody aromatic residues with a peptide of cholera toxin observed by two-dimensional transferred nuclear Overhauser effect difference spectroscopy. Biochemistry **28**: 3360-3365.

ANGLISTER, J., and ZILBER, B. 1990. Antibodies against a peptide of cholera toxin differing in cross-reactivity with the toxin differ in their specific interactions with the peptide as observed by ^{1}H NMR spectroscopy. Biochemistry **29**: 921-928.

BALARAM, P., and BOTHNER-BY, A.A. 1972a. Nuclear magnetic resonance studies of the interaction of peptides and hormones with bovine neurophysin. J. Am. Chem. Soc. **94**: 4015-4017.

BALARAM, P., and BOTHNER-BY, A.A. 1972b. Localization of tyrosine at the binding site of neurophysin II by negative nuclear Overhauser effects. J. Am. Chem. Soc. **94**: 4017-4018.

BALEJA, J.D., MOULT, J., and SYKES, B.D. 1990. Distance measurement and structure refinement with NOE data. J. Magn. Reson. **87**: 375-384.

BANERJEE, A., LEVY, H.R., LEVY, G.C., and CHAN, W.W.C. 1985. Conformations of bound nucleoside triphosphate effectors in aspartate transcarbamylase. Evidence for the London-Schmidt model by transferred nuclear Overhauser effects. Biochemistry **24**: 1593-1598.

BELIVACQUA, V.L., THOMSON, D.S., and PRESTEGARD, J.H. 1990. Conformation of methyl β-lactoside bound to ricin B-chain. Interpretation of transferred nuclear Overhauser effects facilitated by spin simulation and selective deuteration. Biochemistry **29**: 5529-5537.

BLOCH, F. 1957. Generalized theory of relaxation. Phys. Rev. **105**: 1206-1222.

BOELENS, R., KOENIG, T.M.G., and KAPTEIN, R. 1988. Determination of biomolecular structures from proton-proton NOEs using a relaxation matrix approach. J. Mol. Struct. **173**: 299-311.

BOELENS, R., KOENIG, T.M.G., VAN DER MAREL, G.A., VAN BOOM, J.H., and KAPTEIN, R. 1989. Iterative procedure for structure determination from proton-proton nOes using a full relaxation matrix approach. Application to a DNA octamer. J. Magn. Reson. **82**: 290-308.

BORGIAS, B., and JAMES, T.L. 1988. COMATOSE, a method for constrained refinement of macromolecular structure based on two-dimensional nuclear Overhauser effect spectra. J. Magn. Reson. **79**: 493-512.

BORGIAS, B., and JAMES, T.L. 1989. Two-dimensional nuclear Overhauser effect: Complete relaxation matrix analysis. In *Methods in Enzymology* (N.J. Oppenheimer, and T.L. James, Eds.), Vol. **176**, Part A, pp 169-183, Academic Press Inc., New York.

BULL, T.E. 1987. Cross-correlation and 2D NOE spectra. J. Magn. Reson. **72**: 397-413.

CAMPBELL, A.P., and SYKES, B.D. 1989. Conformation of a troponin I peptide bound to troponin C as determined by ^{1}H NMR. In *Calcium Protein Signalling: Advances in Experimental Medicine and Biology* (Hidaka, H., Ed.), Vol. **255**, pp 195-204, Plenum Press, New York.

CAMPBELL, A.P., and SYKES, B.D. 1991a. Theoretical evaluation of the two-dimensional transferred nuclear Overhauser effect. J. Magn. Reson. **93**: 77-92.

CAMPBELL, A.P., and SYKES, B.D. 1991b. Interaction of troponin I and troponin C: Use of the two-dimensional NMR transferred nuclear Overhauser effect to determine the structure of the inhibitory troponin I peptide when bound to skeletal troponin C. J. Mol. Biol., in press.

CLORE, G.M., GRONENBORN, A.M., CARLSON, G., and MEYER, E.F. 1986. Stereochemistry of binding of the tetrapeptide acetyl-pro-ala-pro-tyr-NH_2 to porcine pancreatic elastase. Combined use of two-dimensional transferred nuclear Overhauser enhancement measurements, restrained molecular dynamics, x-ray crystallography and molecular modeling. J. Mol. Biol. **190**: 259-267.

EHRLICH, R.S., and COLMAN, R.F. 1985. ^{1}H nuclear magnetic resonance studies of the conformation and environment of nucleotides bound to pig heart $NADP^+$-dependent isocitrate dehydrogenase. Biochemistry **24**: 5378-5387.

EHRLICH, R.S., and COLMAN, R.F. 1990. Conformations of the coenzymes and the allosteric activator, ADP, bound to NAD^+-dependent isocitrate dehydrogenase from pig heart. Biochemistry **29**: 5179 -5187.

FERRIN, L.J., and MILDVAN, A.S. 1985. Nuclear Overhauser effect studies of the conformations and binding site environments of deoxynucleoside triphosphate substrates bound to DNA Polymerase I and its large fragment. Biochemistry **24**: 6904-6913.

GLASEL, J.A., and BORER, P.N. 1986. NMR studies of flexible opiate conformations at monoclonal antibody binding sites. I. Transferred nuclear Overhauser effects show bound conformations. Biochem. Biophys. Res. Commun. **141**: 1267-1273.

GLASEL, J.A. 1989. Nuclear magnetic resonance studies of flexible opiate conformations at monoclonal antibody binding sites. Quantitative interproton distances obtained from comparing theoretical and experimental transferred nuclear Overhauser enhancement: correlation with antibody sequence. J. Mol. Biol. **209**: 747-761.

ITO, W., NISHIMURA, M.N., SAKATO, N., FUJIO, H., and ARATA, Y. 1987. A ^{1}H NMR method for the analysis of antigen-antibody interactions: Binding of a peptide fragment of lysozyme to anti-lysozyme monoclonal antibody. J. Biochem. **102**: 643-649.

KEEPERS, J.W., and JAMES, T.L. 1984. A theoretical study of distance determinations from NMR two-dimensional nuclear Overhauser effect spectra. J. Magn. Reson. **57**: 404-426.

LANDY, S.B., and RAO, B.D.N. 1989. Dynamical NOE in multiple-spin systems undergoing chemical exchange. J. Magn. Reson. **81**: 371-377.

LEFEVRE, J.F., LANE, A.N., and JARDETSKY, O. 1987. Solution structure of the trp operator of *Escherichia Coli* determined by NMR. Biochemistry **26**: 5076-5090.

LEVY, H.R., ASSULIN, O., SCHERF, T., LEVITT, M., and ANGLISTER, J. 1989. Probing antibody diversity by 2D NMR. Comparison of amino acid sequences, predicted structures, and observed antibody-antigen interactions in complexes of two antipeptide antibodies. Biochemistry **28**: 7168-7175.

LIPARI, G., and SZABO, A. 1982. Model-free approach to the interpretation of nuclear magnetic resonance relaxation in macromolecules. 1. Theory and range of validity. J. Am. Chem. Soc. **104**: 4546-4559.

MACURA, S., and ERNST, R.R. 1980. Elucidation of cross-relaxation in liquids by two-dimensional NMR spectroscopy. Mol. Phys. **41**: 95-117.

MARSHALL, A.G., SCHMIDT, P.G., and SYKES, B.D. 1972. Effects of internal rotation on nuclear magnetic relaxation times for macromolecules. Biochemistry **11**: 3875-3879.

MEYER, E.F., CLORE, G.M., GRONENBORN, A.M., and HANSEN, H.A.S. 1988. Analysis of an enzyme-substrate complex by x-ray crystallography and transferred nuclear Overhauser enhancement measurements. Porcine pancreatic elastase and a hexapeptide. Biochemistry **27**: 725-730.

MILON, A., MIYAZAWA, T., and HIGASHIJIMA, T. 1990. Transferred nuclear Overhauser effect analyses of membrane-bound enkephalin analogues by ^{1}H nuclear magnetic resonance. Correlation between activities and membrane-bound conformations. Biochemistry **29**: 65-75.

NI, F., KONISHI, Y., FRAZIER, R.B., SCHERAGA, H.A., and LORD, S.T. 1989a. High-resolution NMR studies of fibrinogen-like peptides in solution. Interaction of thrombin with residues 1-23 of the Aα chain of human fibrinogen. Biochemistry **28**: 3082-3094.

NI, F., MEINWALD, Y.C., VASQUEZ, M., and SCHERAGA, H.A. 1989b. High-resolution NMR studies of fibrinogen-like peptides in solution. Structure of a thrombin-bound peptide corresponding to residues 7-16 of the Aα chain of human fibrinogen. Biochemistry **28**: 3094-3105.

NI, F., KONISHI, Y., BULLOCK, C.D., RIVETNA, M.N., and SCHERAGA, H.A. 1989c. High-resolution NMR studies of fibrinogen-like peptides in solution. Structural basis for the bleeding disorder caused by a single mutation of Gly(12) to Val(12) in the Aα chain of human fibrinogen Rouen. Biochemistry **28**: 3106-3119.

NI, F., KONISHI, Y., and SCHERAGA, H.A. 1990. Thrombin-bound conformation of the C-terminal fragments of hirudin determined by transferred nuclear Overhauser effects. Biochemistry **29**: 4479-4489.

SOLOMON, I. 1955. Relaxation processes in a system of two spins. Phys. Rev. **99**: 559-565.

WUTHRICH, K. 1986. In *NMR of Proteins and Nucleic Acids* , John Wiley and Sons, New York.

YIP, P.F. 1990. Scaling NOESY cross-peaks involving methyl protons. J. Magn. Reson. **90**: 382-383.

Chapter IV

Interaction of Troponin I and Troponin C : ^{19}F NMR Studies of the Binding of the Inhibitory Troponin I Peptide to Skeletal Troponin C

A. Introduction

Contraction of vertebrate skeletal muscle is regulated by Ca(II) and requires the regulatory proteins troponin and tropomyosin (Ebashi and Endo, 1968). Troponin is a complex of three different protein subunits: troponin C (TnC) which binds Ca(II), TnI which binds actin and inhibits actomyosin ATPase, and TnT which binds to tropomyosin. The x-ray structures of chicken (Sundaralingam *et al.*, 1985) and turkey (Herzberg and James, 1985) skeletal TnC have been solved and reveal a dumbbell-shaped molecule with N-terminal and C-terminal globular domains joined by a long helical linker. Each major domain contains two Ca(II) binding sites based on the EF hand helix-loop-helix structural motif (Kretsinger and Nockolds, 1973; Collins *et al.*, 1973; Vanaman *et al.*, 1977). The higher affinity Ca(II)/Mg(II) sites (sites III and IV) reside in the C-terminal domain and bind Ca(II) and Mg(II) with association constants of 2×10^7 and 5×10^3 M^{-1}, respectively (Potter and Gergely, 1974). The Ca(II) specific sites (sites I and II) reside in the N-terminal domain and bind Ca(II) with an association constant of 2×10^5 M^{-1}. The low affinity sites in the N-terminal domain have been implicated as the physiologically relevant triggering sites (Johnson *et al.*, 1979; Robertson *et al.*, 1981).

The Ca(II)-dependent interaction between TnC and TnI is one of the key processes in the activation of contraction in skeletal muscle (for recent reviews, see Zot and Potter, 1987, and Leavis and Gergely, 1984). TnI inhibits the Mg(II)-ATPase activity of actomyosin ATPase (Hartshorne and Mueller, 1968; Schaub and Perry, 1969; Greaser and Gergely, 1971; Perry *et al.*, 1972) and binds both to actin and tropomyosin-actin (Potter and Gergely, 1974; Hitchcock, 1975). The inhibition of actomyosin ATPase is neutralized when Ca(II)-saturated TnC forms a 1:1 complex with TnI (Perry *et al.*, 1972; Weeks and Perry, 1978; Chong *et al.*, 1983; Cachia *et al.*, 1986; Van Eyk and Hodges, 1988). This results in potentiation of the ATPase and ultimately in muscle contraction.

Studies characterizing the interaction between TnC and TnI have pointed to multiple interactions between these two proteins. TnI fragment studies reported by Syska *et al.* (1976) demonstrated that two regions of the TnI protein are capable of interacting with TnC. The first of these sites spans residues 1-21, and includes the site of phosphorylation catalyzed by phosphorylase kinase (T11), whereas the second of these sites spans residues 96-116 and is adjacent to a second phosphorylation site (S117) (Moir *et al.*, 1974). Equimolar amounts of TnC completely inhibit phosphorylation at these sites (Cole and Perry, 1975). Syska *et al.* (1976) demonstrated that a CNBr fragment of TnI (residues 96-116) mimics intact TnI in its ability to inhibit actomyosin ATPase (Syska *et al.*, 1976; Nozaki *et al.*, 1980; Talbot and Hodges, 1981). Talbot and Hodges (1981), using synthetic peptides, showed that residues 104-115 of TnI comprise the minimum sequence necessary for inhibition of actomyosin ATPase activity. The synthetic peptide TnI(104-115) possesses tropomyosin specificity (Talbot and Hodges, 1979) and TnC binding capabilities (Cachia *et al.*, 1983, 1985; Van Eyk and Hodges, 1988; Van Eyk *et al.*, 1991a), which results in the release of ATPase inhibition (Cachia *et al.*, 1986; Van Eyk and Hodges, 1988). Thus, it is would appear that residues 104-115 comprise the inhibitory site of TnI and binding of this region to Ca(II)-saturated TnC leads to relief of inhibition of actomyosin ATPase, and ultimately to muscle contraction.

In this paper, we report on an ^{19}F NMR study of the interaction of the inhibitory region of TnI with turkey skeletal TnC in the presence and absence of Ca(II) using the synthetic TnI analog Nα-acetyl[^{19}F-phe106]TnI(104-115)amide. While this interaction has been studied before using ^{1}H NMR by Cachia *et al.* (1983), subsequent research by other groups has suggested multiple binding and/or multiple attachment sites on TnC for TnI or other molecules that bind to the same region of TnC (Leszyk *et al.*, 1990; Wang *et al.*, 1990; MacLachlan *et al.*, 1990; Reid *et al.*, 1990). Moroever, the determination of the x-ray structures of avian skeletal TnC (Sundaralingam *et al.*, 1985; Herzberg and James, 1985) has allowed a structural basis for the interpretation of these results. The extensive homology between the N- and C-terminal globular domains suggests two possible peptide binding sites on these proteins. In view of these findings, it is important to establish a stoichiometry of binding of the TnI peptide to TnC, which will then serve as a basis for transferred nuclear Overhauser effect studies on the conformation of the TnI peptide when bound to Ca(II)-saturated TnC.

B. Materials and Methods

1. Sample Preparation

a. Materials. All chemicals and solvents were reagent grade. Poly(styrene-*co* -1% divinylbenzene)benzhydrylamine hydrochloride resin (0.49 mmol of NH$_2$/g resin) was purchased from Bioproducts Peptide Department, Belgium. Turkey breast muscle was purchased from the local supermarket. Urea (Fisher) was purified by stirring with a mixed-bed resin (Bio-Rad AG-50 1-X8).

b. Amino Acid Analysis. The quantities of TnI peptide and TnC used were determined from amino acid analysis after hydrolysis in 100-200 µl of 6 N HCl in evacuated sealed tubes for 24 h at 110°C. The mean of the molar ratios of all accurately measurable amino acids in the acid hydrolysate was used to calculate the concentration of peptide or protein. Routine amino acid analyses were performed on a Durrum 500 amino acid analyzer. The pH values quoted are direct meter readings.

c. Preparation of Boc-L-p-fluorophenylalanine. DL-*p*-fluorophenylalanine (5 g, 27.3 mmol) was suspended in anhydrous methanol (50ml). Anhydrous HCl gas was passed through this suspension until the solid dissolved (ca. 10 min). The reaction was allowed to stand at room temperature for 8 h at which time it was evaporated to dryness and the remaining white solid dried over sodium hydroxide pellets for 8 h. This provided DL-*p*-fluorophenylalanine methyl ester hydrochloride salt (6 g, 94% yield). The product was checked by TLC (silica, 1-butanol/acetic acid/H_2O, 4:1:1 v/v/v) ($R_{f,\text{acid}}$ 0.31, $R_{f,\text{ester}}$ 0.40). Without further purification, the ester (4g, 17mmol) and triethylamine (4.0 ml) were dissolved in water (20ml). 2-[(*tert* -butoxycarbonyloxy)imino]-2-phenylacetonitrile (Boc-ON) (4.6 g, 19 mmol, 1 equiv) dissolved in *p*-dioxane (20 ml) was added to the aqueous mixture. The reaction was stirred for 18 h at room temperature, at which time it was diluted with diethyl ether (50 ml) and washed with saturated $NaHCO_3$ (3 x 10 ml) followed by water (3 x 20 ml) and saturated NaCl solution (1 x 20 ml). Drying over anhydrous $MgSO_4$ and evaporation of the solvent *in vacuo* provided Nα-Boc-DL-*p*-fluorophenylalanine methyl ester as an amber oil. This product was taken immediately and suspended in 2 mM NH_4HCO_3/0.1 N KCl buffer (150 ml) at pH 7.9 and 38° C. α-Chymotrypsin (15 mg) was added in the same buffer (2 ml), and the pH was kept constant (pH 7.9) with a pH-stat delivering 0.17 M NaOH. This reaction was stirred for 10 h at 38°C, at which point it was allowed to separate into two distinct layers. The aqueous layer was extracted with diethyl ether (4 x 25 ml) and then acidified with 5 N HCl to pH 1.8. Extraction of the acidified solution with diethyl ether (5 x 50 ml), washing the pooled organic layers with saturated NaCl solution (1 x 50 ml), and drying over anhydrous $MgSO_4$, followed by evaporation of the solvent *in vacuo* , provided a colorless oil. This oil contained a major impurity (R_f 0.83), as well as the product Boc-L-*p*-fluorophenylalanine (R_f 0.70), as judged by TLC on silica plates in isopropyl alcohol/NH_4OH/H_2O (6:3:1 v/v/v), following treatment with HCl vapour before development. The impurity was separated from the product by dissolving the oil in saturated $NaHCO_3$ solution (100 ml) and extracting with CH_2Cl_2 (3 x 25 ml). Reacidification with 5 N HCl to pH 2.0 followed by extraction with CH_2Cl_2 (3 x 20 ml), drying over anhydrous $MgSO_4$, and evaporation of the solvent *in vacuo* provided pure Boc-L-*p*-fluorophenylalanine (883 mg), which was then used for peptide synthesis.

d. Peptide Synthesis and Purification. The TnI inhibitory region analog, Nα-acetyl[^{19}F-phe106]TnI(104-115) amide, was synthesized by using the standard procedures for solid-phase synthesis (Erickson and Merrifield, 1976) on a Beckman peptide synthesizer, Model 990. The co-poly (styrene, 2% divinyl-benzene) benzhydrylamine-HCl resin was maximally substituted to 0.8 mmole of Boc-amino acid per gram of resin. All α-amino groups of the amino acids used were protected with the Boc group. The following side chain protecting groups were used: arginine(Tosyl) and lysine(2-ClZ). It has been previously shown that it is important to block the α-carbonyl and α-amino groups of synthetic peptides comprised of sequences from interior regions of proteins, especially as the peptide approaches the minimum sequence required for biological activity (Talbot and Hodges, 1981). The programs used for the deprotection, neutralization and coupling of each amino acid have been previously described (Hodges *et al.*, 1981). Amidation of the peptide COOH terminal was accomplished by coupling the C-terminal residue to the benzhydrylamine resin [0.31 mmol of Boc-arginine(Tos) and DCC/g of resin]. This resulted in a substitution level of approximately 0.29 mmol/g of amino acid resin as determined by the picrate monitoring method (Hodges and Merrifield, 1975). The N-terminal residue of the peptide was acetylated by treatment for 30 min with acetic anhydride/toluene/pyridine (1:3:3, v/v/v).

The crude TnI peptide was purified on an HPLC system comprised of a Spectra Physics SP8700 solvent delivery system, a Kratos SF7697 detector and Technical Marketing Ass. chart recorder. The peptide was purified using an analytical Pierce aquapore RP-300 column (4.6 mm I.D. x 220 mm) by employing a linear AB gradient (0.1% B per min) at 1 ml/min, where buffer A was 0.05% aqueous TFA and buffer B was 0.05% TFA in acetonitrile. The sample loads were varied between 20 and 50 mg per run. One minute fractions were collected. In order to identify the fractions containing the desired peptide, analytical runs of the various fractions were carried out using the above reversed phase column with a gradient rate of 1% B/min (Mant *et al.*, 1987; Parker *et al.*, 1987). The fractions containing the pure peptide were pooled and lyophilized.

e. Preparation of TnC. Troponin was isolated from an acetone powder of turkey breast muscle, obtained from the residue remaining after a low ionic strength extraction with a solution of 0.3 M KCl,0.15 M KH_2PO_4/K_2HPO_4 (pH 6.5),0.5 mM ATP. The powder (approx. 300 g) originating from 2 kg of breast muscle was extracted overnight at 4°C with 20 volumes of 0.6 M LiCl,50 mM Tris-HCl(pH 8.0),1 mM DTT,0.01mM $CaCl_2$ with gentle overhead stirring. The pH of the supernatant after centrifugation was slowly lowered to pH 4.6 at 4°C by addition of 2 M sodium acetate, and the precipitate of crude tropomyosin was centrifuged down. The pH of the supernatant was brought back to 7.5 by addition of a solution of saturated Tris-HCl and an ammonium sulfate fractionation carried out at 4°C. The material of interest was collected in the range of 37-65% saturation.

The protein pellet was dissolved in 10 mM NH_4HCO_3,1mM DTT, pH 8.0, and dialyzed overnight against two changes of 150 volumes of water,0.1 mM DTT at 4°C. The dialysate was then lyophilized.

Turkey troponin was resolved into its subunits by application of the lyophilized material to a DEAE-Sephacel column equilibrated with 8 M urea,50 mM Tris-HCl(pH 7.5),0.5 mM DTT,3 mM EDTA. The subunits were eluted with a linear NaCl gradient from 0 to 0.5 M at room temperature. TnI eluted first at a NaCl concentration of approximately 0.2 M, followed by TnC at 0.4 M and TnT at 0.5 M. The pooled fractions corresponding to TnC were dialyzed overnight against four changes of 150 volumes of 20 mM NH_4HCO_3 at 4°C for the removal of urea, and the dialysate again lyophilized. The crude lyophilized TnC was then redissolved in 50 mM Tris-HCl(pH 7.5),0.5 mM DTT,3mM EDTA and applied to a DEAE-Sephacel column equilibrated with the same buffer at 4°C. The protein was eluted with a linear NaCl gradient from 0.1 to 0.6 M, dialyzed against 5 mM NH_4HCO_3, and lyophilized. A final yield of approx. 400 mg of purified TnC powder was obtained, which was found to be homogeneous when examined by SDS-Page and UV spectrophotometry ($\varepsilon_{(\lambda\ 259\ nm)}$ = 0.109 O.D. units/mg/ml for turkey skeletal TnC).

f. Preparation of Desalted, Apo TnC. EDTA-free, apo TnC was prepared in the following manner. TnC was dissolved in 500 µl of 25 mM NH_4HCO_3,3 mM EDTA and applied to a Sephadex G-25 medium gel exclusion column, equilibrated with 25 mM NH_4HCO_3 at room temperature. The EDTA-free, apo TnC eluted in the void volume of the column, followed by the Ca(II)-bound EDTA. Fractions were collected in acid-washed plastic vials to prevent metal contamination. Lyophilization of the pooled TnC fractions then provided apo TnC, free of EDTA contaminants, as judged by UV spectrophotometry and ^1H NMR.

g. Preparation of TnI Peptide NMR Samples. The TnI peptide NMR samples to be used for the titration of the TnI peptide with TnC in the absence and presence of Ca(II), respectively, were prepared by dissolving the purified Nα-acetyl[^{19}F-phe106]TnI(104-115)amide synthetic peptide in 5.0 ml of 50 mM KCl,50 mM Tris-HCl(pH7.5),1 mM DTT,50% D_2O/50%H_2O to a concentration of approx. 0.20 mM. For the titrations in the presence of Ca(II), the buffer system contained 1 mM $CaCl_2$. 1 mM CF_3CO_2H was added to the TnI peptide NMR samples to act as a ^{19}F standard.

2. Nuclear Magnetic Resonance Spectroscopy

^{19}F spectra were recorded at 282.32 MHz on a Nicolet NT 300 WB NMR spectrometer equipped with a 12 mm fluorine probe. Fourier transform mode was used with quadrature detection. A simple one-pulse sequence was used, with no ^{1}H decoupling. The 90° pulse length was 30 μsec, the acquisition time was 1 sec, and the delay time between transients was 500 μsec. Separate scans were taken of the F-phenylalanine and CF_3CO_2H regions for each titration point in order to achieve adequate digital resolution in both regions. Samples were maintained at room temperature, which remained constant at 23°C. ^{19}F chemical shifts were reported relative to 1 mM CF_3CO_2H at 0.00 ppm. The sample was left to equilibrate for at least 25 min in the spectrometer prior to data collection. This was found to be the equilibration time necessary for stable chemical shift values, due to the great sensitivity of ^{19}F chemical shifts to temperature.

3. Calculation of Binding Constants

a. Titration of Nα-acetyl[^{19}F-phe106]TnI(104-115) amide with Apo Turkey Skeletal TnC. The dissociation constant for the interaction of the TnI peptide with apo TnC was determined by following the observed chemical shift of the peptide F-phenylalanine resonance as a function of added protein titrant. Assuming a 1:1 stoichiometry, the interaction of the liganding peptide with the protein is described by

$$P + L \rightleftharpoons PL \qquad [1]$$

$$K_d = [P][L]/[PL] \qquad [2]$$

where [P] is the concentration of free protein, [L] is the concentration of the free peptide and [PL] is the concentration of the peptide-protein complex given by

$$[PL] = \{(L_o + P_o + K_d) - [(L_o + P_o + K_d)^2 - 4P_oL_o]^{1/2}\} / 2 \qquad [3]$$

where L_o is the total concentration of peptide and P_o is the total concentration of the protein in the sample. If one assumes fast exchange, then the observed chemical shift of the peptide F-phenylalanine resonance at each point in the titration, δ_{obs}, is given by

$$\delta_{obs} = ([L]/L_o)\,\delta_L + ([PL]/L_o)\,\delta_{PL} \qquad [4]$$

where δ_L is the chemical shift of the free peptide and δ_{PL} is the chemical shift of the bound peptide. Substituting $[L] = L_o - [PL]$, we obtain

$$\Delta\delta = ([PL]/L_o)(\delta_{PL} - \delta_L) \qquad [5]$$

where $\Delta\delta = \delta_{obs} - \delta_L$. Thus, a non-linear least squares curve fit of a plot of $\Delta\delta$ versus P_o/L_o will provide K_d and $(\delta_{PL} - \delta_L)$ (Hull, 1975).

b. Titration of Nα-acetyl[^{19}F-phe106]TnI(104-115) amide with Ca(II)-Saturated Turkey Skeletal TnC. The dissociation constant for the interaction of the TnI peptide with Ca(II)-saturated TnC was determined by following the observed change in intensity of the peptide F-phenylalanine resonance as a function of added protein titrant. Assuming 1:1 stoichiometry and fast exchange as before, then the observed linewidth of the F-phenylalanine resonance, $\Delta\nu_{obs}$, is given by

$$\Delta\nu_{obs} = ([L]/L_o)\,\Delta\nu_L + ([PL]/L_o)\,\Delta\nu_{PL} \qquad [6]$$

where $\Delta\nu_L$ and $\Delta\nu_{PL}$ are the linewidths of the free peptide and the peptide-protein complex, respectively. T_2, the spin-spin relaxation time, is inversely proportional to $\Delta\nu$, and for Lorentzian lineshape the intensity of a signal, I, is directly proportional to T_2

$$I \propto T_2 / [1 + (\omega - \omega_o)_2 T_2{}^2] \qquad [7]$$

$$\propto T_2 \qquad \text{(on resonance; } \omega = \omega_o\text{)}$$

Thus, the inverse of the observed intensity of the F-phenylalanine resonance, I_{obs}, may be given by

$$1/I_{obs} = ([L]/L_o)(1/I_L) + ([PL]/L_o)(1/I_{PL}) \qquad [8]$$

where I_L is the intensity of the free peptide F-phenylalanine resonance and I_{PL} is the intensity of the bound peptide F-phenylalanine resonance. Eqn. 8 can be rearranged to take the form

$$\Delta I/I_{obs} = ([PL]/L_o)\{-(I_L - I_{PL})/I_{PL}\} \qquad [9]$$

where $\Delta I = I_{obs} - I_L$. Thus, a non-linear least squares curve fit of a plot of $\Delta I/I_{obs}$ versus P_o/L_o will provide K_d and $(I_L - I_{PL})/I_{PL}$ (Hull, 1975).

C. Results

1. Titration of Nα-acetyl[^{19}F-phe106]TnI(104-115) amide with Apo Turkey Skeletal TnC

Figure IV-1 shows the ^{19}F NMR spectra of the titration of the F-phe-TnI inhibitory peptide with apo TnC. The spectra have been corrected with respect to the CF_3CO_2H ^{19}F resonance at 0.0 ppm. The F-phenylalanine resonance is observed to titrate downfield upon the addition of apo TnC titrant. Changes in chemical shift ($\Delta\delta$) of the F-phenylalanine resonance as a function of increasing ratio of apo TnC titrant to peptide ($[\text{apo.TnC}]_o/[\text{TnI peptide}]_o$) are plotted in Figure IV-3. A least-squares curve fitting of this data yields a $K_d = (3.7 \pm 3.1) \times 10^{-5}$ M fitted to a 1:1 binding stoichiometry. The dissociation constant is poorly determined, but is still within an order of magnitude of the value obtained by Cachia *et al.* (1983) from a ^{1}H NMR titration of apo rabbit TnC with the same TnI peptide ($K_d = 1.4 \times 10^{-4}$ M).

2. Titration of Nα-acetyl[^{19}F-phe106]TnI(104-115) amide with Ca(II)-Saturated Turkey Skeletal TnC

Figures IV-2A and IV-2B show the ^{19}F NMR spectra of the titration of the F-phe-TnI inhibitory peptide with Ca(II)-saturated TnC. One can observe from Figure IV-2A that there are only very slight changes in the chemical shift position of the F-phenylalanine resonance as a function of added TnC titrant. Unlike the apo data, the F-phenylalanine resonance shifts very slightly upfield throughout the titration. Figure IV-2B is a different representation of the same region (-41.2 to -40.4 ppm) and demonstrates the decrease in intensity of the F-phenylalanine resonance as a function of added TnC titrant. The decrease in intensity is due to line broadening of the F-phenylalanine resonance as the peptide binds to the protein and experiences a longer correlation time. The ratio of the change in intensity over observed intensity ($\Delta I/I_{obs}$) of the F-phenylalanine resonance as a function of increasing ratio of TnC.Ca(II)$_4$ titrant to peptide ($[\text{TnC.Ca(II)}_4]_o$ / $[\text{TnI peptide}]_o$) is plotted in Figure IV-4 as the heavy black line. A non-linear least-squares curve fitting of this data yields a $K_d = (4.8 \pm 1.8) \times 10^{-5}$ M fitted to a 1:1 binding stoichiometry. The dissociation constant is better determined than in the apo case, and is of similar magnitude to the value obtained by Cachia *et al.* (1983) from a ^{1}H NMR titration of Ca(II)-saturated rabbit s-TnC with the same TnI peptide ($K_d = 1.5 \times 10^{-5}$ M). Although neither the strength of binding nor the stoichiometry of binding (1:1) appears to change appreciably between the apo and Ca(II)-saturated systems, nevertheless the binding environment on TnC to which the TnI peptide binds does appear to change, manifested in the chemical shift differences between the two titrations. The titration of the peptide to Ca(II)-saturated TnC was repeated three times, and each time revealed negligible change in the chemical shift position of the F-phenylalanine resonance.

3. Test of the Stoichiometry of Binding of Nα-acetyl[^{19}F-phe106]TnI(104-115) amide to Ca(II)-Saturated Turkey Skeletal TnC

Thus far we have assumed only one binding site on TnC for the TnI peptide. We now examine the situation where there are two hypothetical binding sites on TnC. In this case, the equation for the interaction of the liganding peptides with the protein is

$$P + L \rightleftharpoons PL + L \rightleftharpoons PL2 \qquad [10]$$

$$K_{d1} = [P][L]/[PL] \qquad [11a]$$

$$K_{d2} = [PL][L]/[PL2] \qquad [11b]$$

where [PL] and [PL2] are the concentrations of the 1:1 and 2:1 peptide-protein complexes, respectively. If one again assumes fast exchange, then Δv_{obs} is given by

$$\Delta v_{obs} = ([L]/L_o)\,\Delta v_L + ([PL]/L_o)\,\Delta v_{PL} + 2([PL2]/L_o)\,\Delta v_{PL2} \qquad [12]$$

where Δv_{PL} and Δv_{PL2} are the linewidths of the 1:1 and 2:1 peptide-protein complexes, respectively. The inverse proportionality between Δv and I allows one to express I_{obs} as

$$1/I_{obs} = ([L]/L_o)(1/I_L) + ([PL]/L_o)\{1/I_{PL} + 2([PL2]/L_o)(1/I_{PL2})\} \qquad [13]$$

where I_{PL} and I_{PL2} are the intensities of the 1:1 and 2:1 peptide-protein complexes, respectively. Substituting for $[L] = L_o - [PL] - 2[PL2]$, we obtain

$$\Delta I/I_{obs} = ([PL]/L_o)\{-(I_L - I_{PL})/I_{PL}\} + 2([PL2]/L_o)\{-(I_L - I_{PL2})/I_{PL2}\} \qquad [14]$$

where $\Delta I = I_{obs} - I_L$. This equation contains two unknown concentrations, [PL] and [PL2]; [PL2] can be described in terms of [PL] by substituting for

$$[P_o] = P + [PL] + [PL2] \qquad [15]$$

into Eqn. 11b to obtain

$$[PL2] = [PL]\,(L_o - [PL]) / (2\,[PL] + K_{d2}) \qquad [16]$$

The value of [PL] is given by the root of a cubic equation (CRC Handbook of Chemistry and Physics, 1962-1963; Williams *et al.*, 1985)

$$[PL] = 2(-A/3)^{1/2} \cos [(Ø/3) + 240°] - P_o/3 \qquad [17]$$

where

$$Ø = \arccos \{(-B/2) / [(-A^3)^{1/2} / 27]\} \qquad [18a]$$

$$A = (1/3)(3Q - P^2) \qquad [18b]$$

$$B = (1/27)(2P^3 - 9PQ + 27R) \qquad [18c]$$

$$P = (K_{d2}^2 - 4K_{d1}K_{d2} - 2L_oK_{d2}) / (K_{d2} - 4K_{d1}) \qquad [18d]$$

$$Q = (2L_oP_oK_{d2} - P_oK_{d2}^2 - K_{d1}K_{d2}^2 - L_oK_{d2}^2 - L_o^2K_{d2}) / (K_{d2} - 4K_{d1}) \qquad [18e]$$

$$R = (L_oP_oK_{d2}^2) / (K_{d2} - 4K_{d1}) \qquad [18f]$$

Thus, a plot of $\Delta I/I_{obs}$ versus P_o/L_o is a function of four parameters; K_{d1} and K_{d2} as well as $(I_L - I_{PL})/I_{PL}$ and $(I_L - I_{PL2})/I_{PL2}$.

We tested the stoichiometry of binding of the TnI peptide to Ca(II)-saturated TnC by setting $K_{d1} = 0.048$ mM, but varying K_{d2}. To test the possibility of 2:1 binding, we calculated a family of binding curves for $0.001 \text{ mM} \leq K_{d1} \leq 0.1$ mM, $K_{d2} \geq 4K_{d1}$[1] and $(I_L - I_{PL})/I_{PL} = (I_L - I_{PL2})/I_{PL2} = 0.87$. This is the value corresponding to the limiting intensity in the 1:1 fit, and is equivalent to the assumption of an equal linewidth for all bound species. We then calculated the fit between these theoretical binding curves and the experimental titration data. Figure IV-5 shows contour plots of χ versus K_{d1} and K_{d2} where χ measures the level of agreement between the theoretical curves and the experimental titration data. The contour with the lowest χ value encloses a region roughly defined by $0.056 \text{ mM} \leq K_{d1} \leq 0.071$ mM and $0.5 \text{ mM} \leq K_{d2} \leq 2.0$ mM. Thus, the experimental data points to a second site with an affinity clearly 10-20x weaker than that of the first site. It is important to note that the best fit to the experimental data obtained with a 2:1 binding stoichiometry ($\chi = 0.015$) is similar to the best fit to the experimental data obtained with a 1:1 binding stoichiometry ($\chi = 0.014$).

Figure IV-4 shows calculated titration curves assuming a two site binding model. The points and the heavy black curve show the experimental titration data best fit to a one site binding with $K_d = 0.048$ mM. The other binding curves were calculated for a two site binding keeping K_{d1} = 0.048 mM but allowing K_{d2} to vary from 2.0 mM to 0.2mM. One can see that the fit to the experimental set of points improves as K_{d2} is increased from 0.2 mM to 2.0 mM, or as the binding affinity of the TnI peptide to the hypothetical second site on TnC decreases. Thus, one may conclude that if the TnI peptide were to bind to a second site on TnC, it would do so with a 10-20x weaker affinity.

---

[1] The apparent inequivalency of the dissociation constants is a function of the statistics of binding to a second site once a first site is occupied, viz. $k_{on}2 = 2 * k_{on}1$ and $k_{off}2 = (1/2) * k_{off}1$, thus $K_{d2} = 4 K_{d1}$.

D. Discussion

From previous studies which have demonstrated that Nα-acetyl-[TnI(104-115) amide mimics the whole TnI protein by binding to actin-tropomyosin and inhibiting actomyosin ATPase activity (Talbot and Hodges, 1979, 1981), it is possible to conclude that residues 104-115 represent the inhibitory sequence of TnI and are responsible for the Ca(II)-sensitive switch that regulates ATPase activity. In the absence of Ca(II), the inhibitory region of TnI is bound to the surface of actin-tropomyosin, inhibiting the actomyosin ATPase activity and contraction (Van Eyk *et al.*, 1991b). In the presence of Ca(II), binding is thought to occur between the N-terminal region of the site III Ca(II)-binding site of TnC and residues 104-115 of TnI (Cachia *et al.*, 1985). This interaction leads to the relief of inhibition of actomyosin ATPase activity and ultimately to muscle contraction.

In an attempt to study this Ca(II)-sensitive interaction between the inhibitory region of TnI and TnC, we used ^{19}F NMR to study the binding of the synthetic peptide Nα-acetyl[^{19}F-phe106]TnI(104-115) amide to apo and Ca(II)-saturated skeletal turkey TnC. We obtained dissociation constants of $K_d = (3.7 \pm 3.1) \times 10^{-5}$ M (1:1 binding) for the apo case and $K_d = (4.8 \pm 1.8) \times 10^{-5}$ M (1:1 binding) for the Ca(II)-saturated case. While it would appear that the strength and stoichiometry of binding are not Ca(II)-sensitive, it is important to note that the dissociation constant for binding to apo TnC was not well determined and may represent weaker binding, in which case the interaction of the inhibitory TnI peptide with Ca(II)-saturated TnC may be at least two-fold stronger than its interaction with apo TnC.

We tested the possibility of 2:1 binding of the TnI peptide to Ca(II)-saturated TnC by calculating the fit of the experimental titration data to a series of theoretical binding curves in which the dissociation constants for the two hypothetical binding sites, K_{d1} and K_{d2}, were varied. We obtained the best fit for 0.056 mM $\leq K_{d1} \leq$ 0.071 mM and 0.5 mM $\leq K_{d2} \leq$ 2.0 mM. These results allow the possibility of a second site with an affinity 10-20x weaker than that of the first site.

The difference in the chemical shift behaviour of the F-phenylalanine resonance between the apo and Ca(II)-saturated experiments is indicative of a difference in the chemical environment of the bound TnI peptide in the apo versus Ca(II)-saturated cases. The TnI peptide may be binding with a different conformation or to different sites on the TnC molecule. Alternatively, the TnI peptide may bind with the same conformation and at the same site, but the structure of the TnC binding site may be different between the apo and Ca(II)-saturated forms of this molecule. This difference may be as simple as a different electrostatic potential at the binding site due to the presence of the Ca(II) ions in the Ca(II)-binding loops, or may be a complicated hydrophobic effect due to the presentation of hydrophobic patches on the surface of TnC in the Ca(II)-saturated conformation capable of binding target ligands with high affinity (Cachia *et al.*, 1985). NMR and thermodynamic studies have shown that the C-terminal domain of TnC is unordered in the apo state and becomes much more structured when two Ca(II) metals are bound to site III and IV. The N-terminal domain preserves a fair amount of structure in the apo state so does not undergo the same degree of ordering upon Ca(II) binding to sites I and II (Levine *et al.*, 1977, 1978; Tsalkova and Privalov, 1980, 1985; Yamada and Kometani, 1982; Drabikowski *et al.*, 1985).

Although the inhibitory region of TnI which interacts with TnC is well defined, there remains some argument as to which region on TnC interacts with TnI. Several studies point to an interaction of the inhibitory region of TnI with the N-terminal helix of site III in the C-terminal domain of TnC. A proteolytic fragment spanning residues 89-100 of rabbit skeletal TnC was found to be able to substitute for intact TnC in Ca(II) sensitization of the reconstituted actomyosin complex (Weeks and Perry, 1978; Grabarek *et al.*, 1981). Resonance energy transfer measurements (Tao *et al.*, 1989) found that Ca(II) binding to sites I and II of TnC in a reconstituted Tn complex led to a 5 Å decrease in the distance between the C98 region in rabbit s-TnC and the C133 region in TnI, suggesting that these two regions interact in a Ca(II)-sensitive manner. A fluorescence study (Lan *et al.*, 1989) showed that the TnI peptide is bound by the C-terminal half of CaM as well as by TR2C, with an affinity comparable to that of intact CaM or TnC. The binding affinity to the N-terminal half of CaM or to TR1C was an order of magnitude less, which suggests that the inhibitory portion of the TnI protein interacts predominantly with the C-terminal half of CaM or TnC. The TnI peptide also inhibited the tryptic hydrolysis of the midpoint of the central connecting strand of CaM and TnC, leading the authors to speculate that the TnI peptide binds TnC or CaM near the C-terminal end of the connecting strand and extending into the hydrophobic site of the C-terminal half.

Perhaps the best evidence for TnI peptide binding at the C-terminal domain of TnC comes from photocross-linking studies (Leszyk *et al.*, 1987, 1988) in which the intact TnI protein was cross-linked in the presence of Ca(II) to rabbit s-TnC specifically labeled with a maleimide group at C98 (see Figure VI-2). Upon enzymatic digestion of the heterodimers and analysis of the cross-linked peptides, the residues in TnI that appeared to be most highly cross-linked to C98 of TnC were R108, P110 and to a lesser extent R103 and K107. All of these studies point to the TnI inhibitory peptide binding near the N-terminal helix of site III in the C-terminal domain of TnC.

However, recent photo-cross linking studies by the same group of researchers using zero-length cross-links (Leszyk *et al.*, 1990) have revealed an interaction between Ca(II)-binding site II (residues 46-78) on rabbit s-TnC and the inhibitory region on the whole TnI protein, offering evidence for an interaction involving the N-terminal domain of TnC. Their results indicated that residues from the regulatory Ca(II)-binding site II (residues 46-78) formed cross-links with TnI segments spanning residues 92-167. The most highly cross-linked residues in the TnI peptide were K105 and K107. Wang *et al.* (1990) used photo-cross-linking and fluorescence studies with a recombinant TnC labeled at C57 to demonstrate that the C-helix in the N-terminal domain of TnC interacts with TnI(104-115), in confirmation of the zero-length cross-linking results (Leszyk *et al.*, 1990). As further evidence for the involvement of both domains of TnC in the binding of the TnI peptide, MacLachlan *et al.* (1990) used fluorescence stopped flow kinetics and ^{1}H NMR to demonstrate that the calcium sensitizer, bepridil, binds to the N-terminal domain of cardiac TnC with a 1:1 stoichiometry. The same research group used ^{1}H NMR and molecular modeling to study the binding of calmidazolium to TnC and concluded that binding occurs simultaneously to both the N- and C-terminal globular domains of the TnC protein (Reid *et al.*, 1990).

It is difficult to reconcile the simultaneous binding of a small ligand to both N- and C-terminal domains of TnC on the basis of the crystal structure of the protein, where the central helical linker keeps the domains widely separated. Recent solution studies of TnC and calmodulin (CaM), a structurally homologous Ca(II)-binding protein, have provided a structural framework for interpretation of the above observations. The x-ray structure of bovine brain CaM (Babu *et al.*, 1988) reveals the familiar dumbbell shaped structure, with two globular domains joined by a long helical linker. TnC and CaM bind a variety of naturally occurring extracellular peptides (Haberman and Jentsch, 1967; Malencik and Anderson, 1982, 1983a, 1983b, 1984; Compte *et al.*, 1983; Cox *et al.*, 1985), most of them positively charged amphiphilic helices. Binding typically occurs with high affinity ($K_d = 10^{-8} - 10^{-9}$ M). The N- and C- terminal globular domains of TnC and CaM have large hydrophobic patches (Babu *et al.*, 1988; Kretsinger *et al.*, 1986) flanked by regions of negative electrostatic potential, optimally designed as binding sites for basic, amphiphilic helices. On the basis of the crystal structures of TnC and CaM, it has been difficult to predict why most of the high affinity peptides bind with a 1:1 stoichiometry. The extensive homology between the N- and C-terminal domains and the extended nature of the central helical linker which keeps the domains widely separated would lead one to predict two possible, non-competitive peptide binding sites on these proteins.

Recent studies of TnC and CaM in solution suggest that the two domains are closer together than observed in the crystal structures, particularly in the Ca(II)-saturated state and/or when bound by amphiphilic peptides or target enzymes in 1:1 complexes. Byers and Kay performed hydrodynamic studies of the size and shape of bovine cardiac TnC in the presence and absence of calcium (Byers and Kay, 1982). They found that the intrinsic sedimentation coefficient ($S^0{}_{20,w}$) was increased and Stokes radius (R_S) was decreased for cardiac TnC when the protein bound calcium, indicating a conformational change to a more compact structure. Seeholzer *et al.* (1986) have investigated the structural and dynamic properties of a 1:1 deuterated CaM:melittin (Mel) complex by ^{1}H NMR. By subtracting the bound melittin spectrum ([^{2}H]CaM:Mel) from the spectrum of the nondeuterated CaM:Mel complex, they obtained spectral changes between free and complexed CaM. Perturbed resonances included resonances from both halves of the molecule. Fluorescence studies (Steiner and Norris, 1987) and proteolytic digestion studies (Caday and Steiner, 1986) have shown that melittin, which also forms a 1:1 complex with CaM, makes extensive contacts with the connecting strand and adjacent portions of the N- and C- terminal domains. Klevit *et al.* (1985) and Klevit (1987) used ^{1}H NMR to study the interaction of CaM with a skeletal muscle myosin light chain kinase (MLCK) peptide, M13(577-603). Addition of the M13 peptide to CaM in a 1:1 molar ratio caused spectral perturbations in both the N- and C-terminal domains of CaM. Ikura *et al.* (1990) used triple-resonance multidimensional NMR to study CaM complexed with the M13 peptide, and found that binding of the M13 peptide induced substantial chemical shift changes that were not localized in one particular region of the protein. The largest changes were found in the first helix of the Ca(II)-binding site I, the N-terminal portion of the central helix, and the second helix of the Ca(II)-binding site IV.

The most convincing evidence for shorter interdomain separation comes from small angle x-ray scattering studies of TnC and CaM. Small angle x-ray scattering studies of TnC (Hubbard *et al.*, 1988; Fujisawa *et al.*, 1989) indicate that the distance between the two domains decreases upon Ca(II) binding, producing a more compact structure. Small angle x-ray scattering studies of CaM.Ca(II)$_4$ complexed with the bee venom peptides melittin (Kataoka *et al.*, 1989) and mastoparan (Matsushima *et al.*, 1989; Yoshino *et al.*, 1989), and the M13 peptide (Heidorn *et al.*, 1989), indicate that the two globular domains move towards each other in a concerted effort to bind the target ligand. Kataoka *et al.* (1989) found that binding of melittin to CaM.Ca(II)$_4$ to form the 1:1 complex caused the radius of gyration, R_g, to decrease from 20.9 to 18.0 Å. Two separate groups, Matsushima *et al.* (1989) and Yoshino *et al.* (1989), found that R_g decreased by about 3 Å upon binding of both 4 mol Ca(II)/mol of protein and 1 mol mastoparan/mol of protein to form the ternary complex. Finally, Heidorn *et al.* (1989) reported an R_g for the CaM.Ca(II)$_4$:M13 equimolar complex that was 20% smaller (16 vs. 21 Å) than that of the uncomplexed CaM.Ca(II)$_4$ complex. The solvent contrast dependence of R_g for neutron scattering indicated that the peptide was located more towards the center of the complex with the CaM located more peripherally.

To test the hypothesis that the central helix of CaM could serve as a flexible tether between the two domains, mutants of CaM were created in which the two domains were constrained close to another by a specific covalent link (Persechini and Kretsinger, 1988; O'Neil and DeGrado, 1989), or were changed in distance or orientation with respect to one another by deletions in the central helix (Putkey *et al.*, 1988; Persechini *et al.*, 1989; Van Berkum *et al.*, 1990). The altered CaM molecules retained high activity towards enzyme activations, which suggests that the central helix acts as a flexible tether to allow the N- and C-terminal domains to form a single binding site capable of accomodating a wide variety of target peptides or enzymes. Strynadka and James (1990) have modelled the interaction of melittin binding to CaM where they introduced a kink in the central helix of CaM. This served to bring the two hydrophobic domains of CaM sufficiently close to bind a single melittin peptide, while maintaining reasonable stereochemistry.

Although all of the low angle x-ray scattering studies have been done on 1:1 complexes of peptide to protein, there is evidence that some peptides do bind TnC and CaM with 2:1 stoichiometry. In fact, mastoparan displays two binding sites for CaM, one with high affinity and one with lower affinity (Malencik and Anderson, 1983b, 1984; McDowell *et al.*, 1985; Linse *et al.*, 1986; Cachia *et al.*, 1986; Sanyal *et al.*, 1988). ^{113}Cd NMR studies found that two moles of mastoparan/mole of CaM broadened four ^{113}Cd NMR signals over that found in a 1:1 molar ratio, without affecting the chemical shifts (Linse *et al.*, 1986). This was interpreted as the binding of a second molecule of mastoparan with reduced affinity which does not elicit major conformational changes around the metal binding sites. Proteolytic digestion studies of CaM showed that the C-terminal fragment bound mastoparan with the same affinity as the intact protein, whereas the N-terminal fragment also bound mastoparan, but with reduced affinity (Sanyal *et al.*, 1988). The antipsychotic drug trifluoperazine (TFP) also displays one high affinity and one lower affinity binding site for CaM (Forsen *et al.*, 1980; Dalgarno *et al.*, 1984; Thulin *et al.*, 1984; Andersson *et al.*, 1985; Cachia *et al.*, 1985; Massom *et al.*, 1990). ^{113}Cd NMR studies found that two moles of TFP/mole CaM produced similar spectral changes to the four ^{113}Cd NMR signals as those observed with mastoparan binding (Forsen *et al.*, 1980; Dalgarno *et al.*, 1984; Thulin *et al.*, 1984; Andersson *et al.*, 1985). It was concluded that there were two distinct TFP binding sites, one located in the N-terminal domain and one in the C-terminal domain. The notion of two TnI peptide binding sites on TnC, one in the C-terminal domain which is at least an order of magnitude stronger than a second site in the N-terminal domain, is not inconsistent with the mastoparan and TFP results.

Strynadka and James have modeled mastoparan (1990) and TFP (1988) simultaneously binding to both the N- and C-terminal domains of CaM. Given the extended crystal structure of CaM, they reasoned that these molecules are sufficiently small that binding to one domain would not interfere with binding at the second. There is no experimental evidence that binding of TFP to CaM or TnC leads to large conformational changes in the overall dimensions of these molecules, indicative of a change in distance or orientation between the two domains. Therefore, there is no hard experimental evidence to refute their binding model of two molecules of TFP to an extended CaM.Ca(II)$_4$ structure (Strynadka and James, 1988). In addition, although the low angle x-ray scattering studies have offered compelling evidence that binding of 1 mol mastoparan to 1 mol CaM.Ca(II)$_4$ leads to a large conformational change in the CaM molecule, there have been no low angle x-ray studies of the 2:1 mastoparan:CaM.Ca(II)$_4$ ternary complex, or indeed of any 2:1 peptide:protein complexes at all. Thus, it is also possible that a 2:1 mastoparan:CaM.Ca(II)$_4$ complex, like the modelled 2:1 TFP:CaM.Ca(II)$_4$ complex, may be more extended, allowing non competitive binding of two peptide molecules to the CaM molecule. On the basis of these studies, one could imagine that binding of some target ligands to TnC or CaM in a 1:1 stoichiometry might involve the participation of both N-terminal and C-terminal domains, which essentially 'clamp down' on the target ligand to provide a single binding site. Alternatively, the binding of other (or even the same) target ligands in a 2:1 stoichiometry, could involve an extended structure, with the N- and C-terminal domains widely separated by an extended helical linker.

These solution studies of CaM and TnC serve to provide a structural framework for interpretation of the binding of the TnI inhibitory peptide to TnC. Given that the stoichiometry of binding of peptide to TnC is 1:1, it is possible to imagine a conformational change around a hinge region in the central helix of TnC which would allow the N- and C-terminal domains to form a single binding site capable of accomodating a single peptide.

This would explain the wealth of data implicating both domains in the binding of the TnI inhibitory peptide. This global conformational change in TnC.Ca(II)$_4$ when complexed to TnI could provide the trigger in a cascade of conformational changes transmitted to the thin filament proteins TnI, tropomyosin and actin, culminating in muscle contraction.

Figure IV-1. ^{19}F NMR spectra of the titration of N-α-acetyl[^{19}F-phe106]TnI(104-115) amide with apo turkey skeletal TnC: Change in chemical shift of the F-phenylalanine resonance as a function of added TnC titrant. [TnI peptide] = 0.15 mM in 50 mM KCl, 50 mM Tris-HCl (pH 7.5), 1 mM DTT and 50%D_2O/50%H_2O. Chemical shifts are corrected with respect to the CF_3CO_2H resonance at 0 ppm. [apo.TnC] / [TnI peptide] ratios used in the titration are: **a.** 0.00 **b.** 0.28 **c.** 0.56 **d.** 0.84 **e.** 1.12 **f.** 1.40 **g.** 1.69 **h.** 1.96 **i.** 2.24.

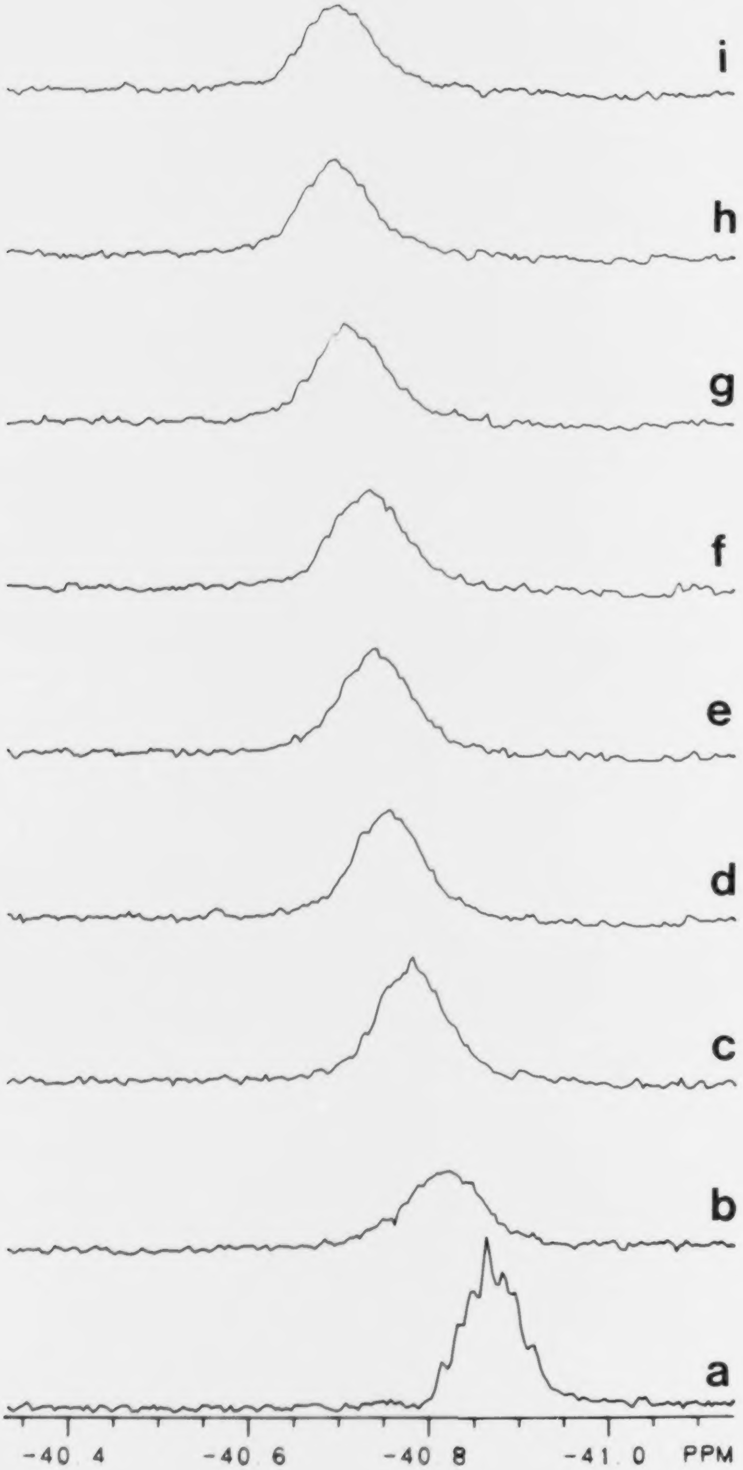

i
h
g
f
e
d
c
b
a
-40.4
-40.6
-40.8
-41.0
PPM

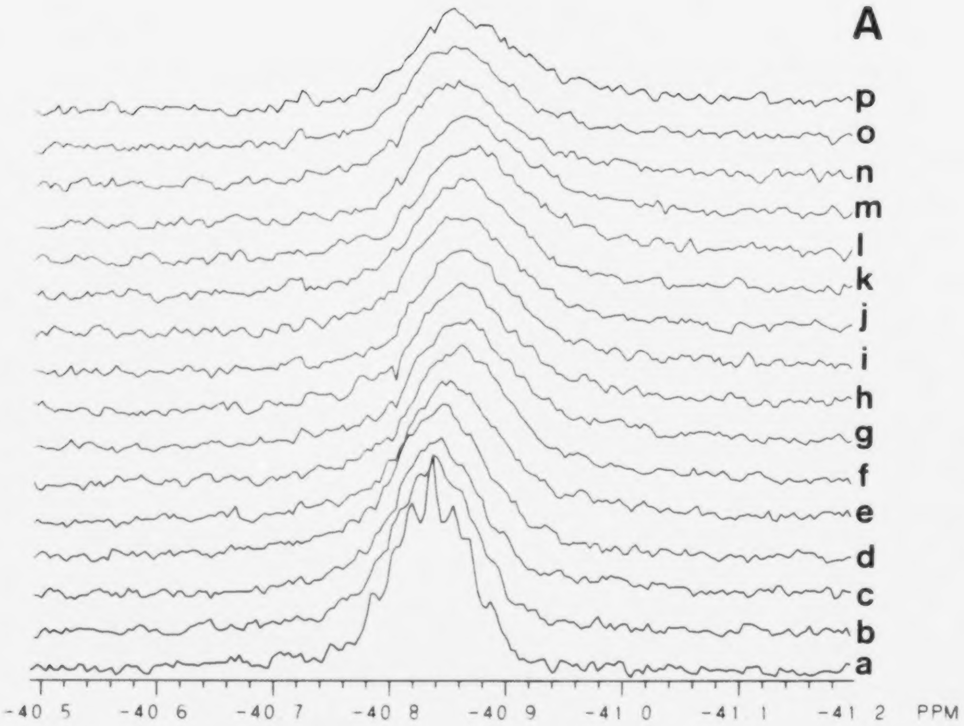

Figure IV-2A. ^{19}F NMR spectra of the titration of N-α-acetyl[^{19}F-phe106]TnI(104-115) amide with Ca(II)-saturated turkey skeletal TnC: Change in chemical shift of the F-phenylalanine resonance as a function of added TnC titrant. [TnI peptide] = 0.22 mM in 50 mM KCl, 50 mM Tris-HCl (pH 7.5), 1 mM DTT and 50%D_2O/50%H_2O. Chemical shifts are corrected with respect to the CF_3CO_2H resonance at 0 ppm. [TnC.Ca$_4$] / [TnI peptide] ratios used in the titration are: **a.** 0.00 **b.** 0.14 **c.** 0.27 **d.** 0.41 **e.** 0.54 **f.** 0.68 **g.** 0.81 **h.** 0.95 **i.** 1.08 **j.** 1.22 **k.** 1.35 **l.** 1.62 **m.** 1.89 **n.** 2.16 **o.** 2.50 **p.** 2.70.

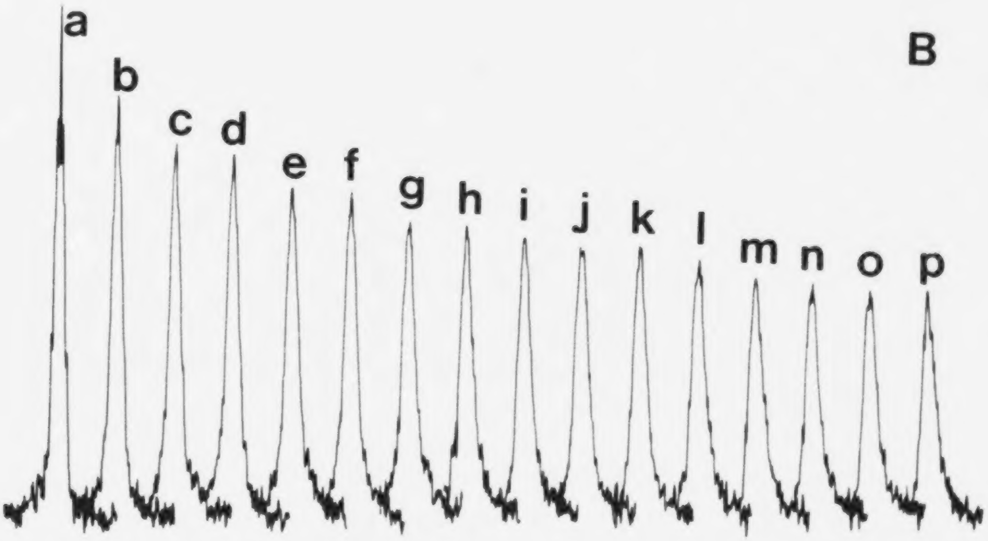

Figure IV-2B. ^{19}F NMR spectra of the titration of N-α-acetyl[^{19}F-phe106]TnI(104-115) amide with Ca(II)-saturated turkey skeletal TnC: Change in intensity of F-phenylalanine resonance as a function of added TnC titrant. [TnI peptide] = 0.22 mM in 50 mM KCl, 50 mM Tris-HCl (pH 7.5), 1 mM DTT and 50%D_2O/50%H_2O. Chemical shifts are corrected with respect to the CF_3CO_2H resonance at 0 ppm. [TnC.Ca_4] / [TnI peptide] ratios used in the titration are: **a.** 0.00 **b.** 0.14 **c.** 0.27 **d.** 0.41 **e.** 0.54 **f.** 0.68 **g.** 0.81 **h.** 0.95 **i.** 1.08 **j.** 1.22 **k.** 1.35 **l.** 1.62 **m.** 1.89 **n.** 2.16 **o.** 2.50 **p.** 2.70.

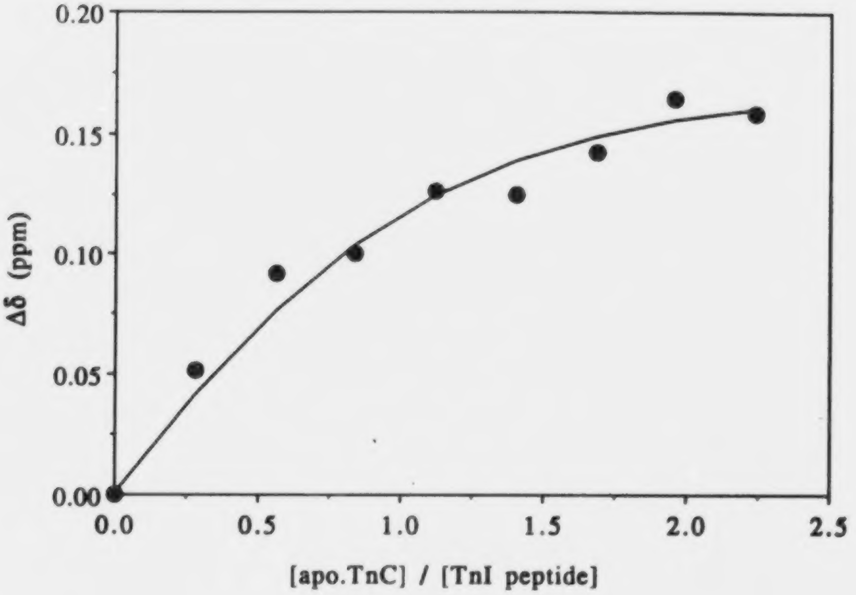

Figure IV-3. Plot of the titration of N-α-acetyl[^{19}F-phe106]TnI(104-115) amide with apo turkey skeletal TnC. The change in the chemical shift (Δδ) of the F-phenylalanine resonance is plotted against the ratio of apo.TnC titrant to peptide ($[\text{apo.TnC}]_o$ / $[\text{TnI peptide}]_o$).

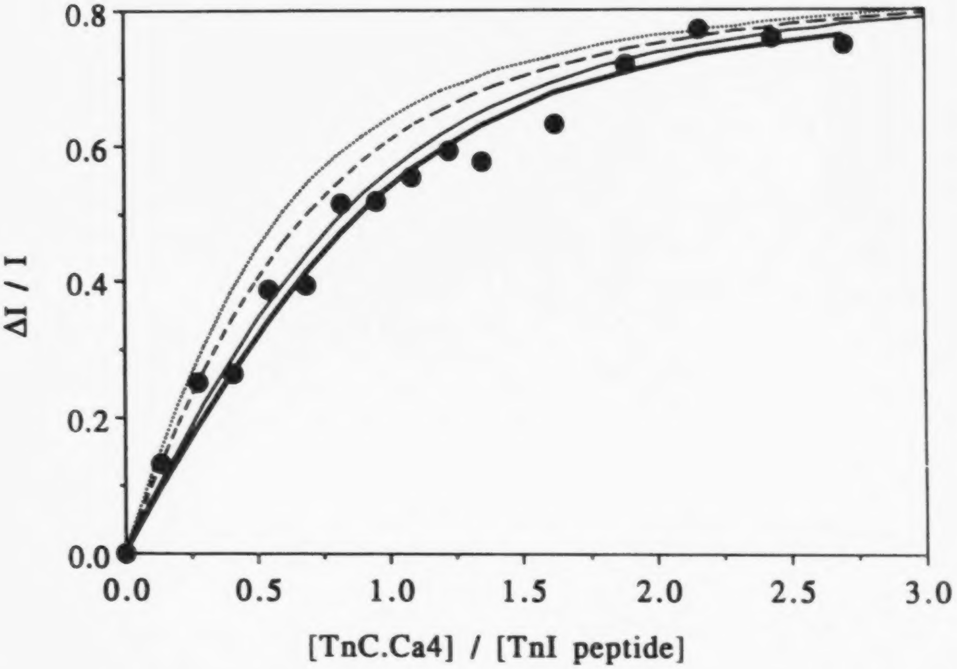

Figure IV-4. Plot of the titration of N-α-acetyl[^{19}F-phe106]TnI(104-115) amide with Ca(II)-saturated turkey skeletal TnC. The ratio of the change in intensity over observed intensity ($\Delta I/I_o$) of the F-phenylalanine resonance is plotted against the ratio of TnC titrant to peptide ($[\mathrm{TnC.Ca_4}]_o$ / $[\mathrm{TnI\ peptide}]_o$). Changes in intensity are corrected for the effects of diluting the NMR sample as the titration proceeds. The points and the heavy black curve show the experimental titration data best fit to a one site binding with K_d = 0.048 mM and maximal $(I_L - I_{PL})/I_{PL}$ = 0.87. The other binding curves were calculated assuming a two site binding with: (·······) K_{d1} = 0.048 mM, K_{d2} = 0.2 mM, $(I_L - I_{PL})/I_{PL} = (I_L - I_{PL2})/I_{PL2}$= 0.87; (- - - -) K_{d1} = 0.048 mM, K_{d2} = 0.4 mM, $(I_L - I_{PL})/I_{PL} = (I_L - I_{PL2})/I_{PL2}$= 0.87; (——) K_{d1} = 0.048 mM, K_{d2} = 2.0 mM, $(I_L - I_{PL})/I_{PL} = (I_L - I_{PL2})/I_{PL2}$= 0.87.

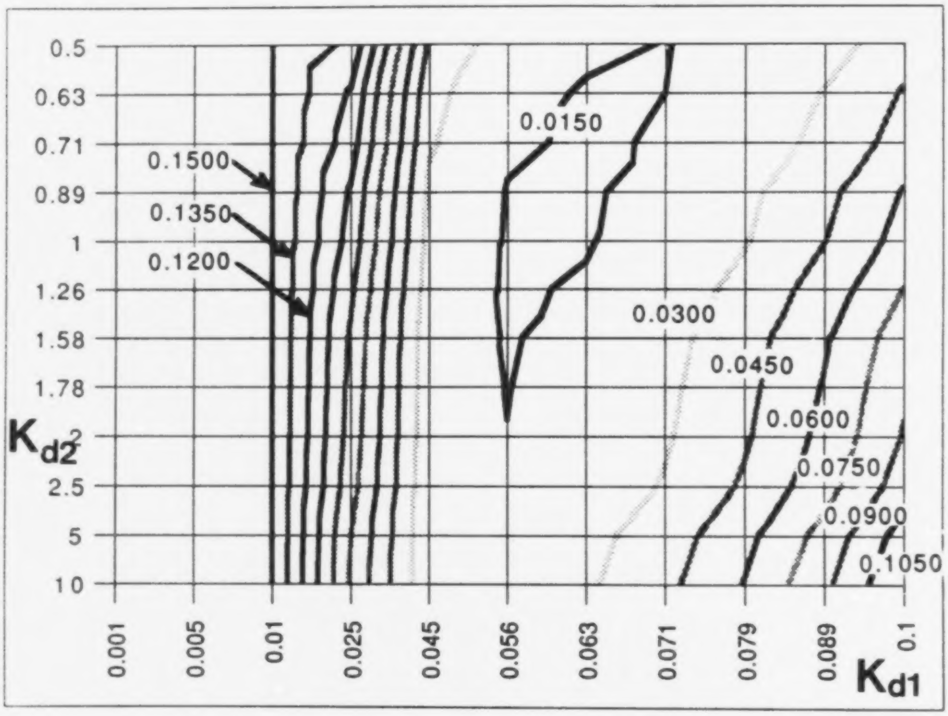

Figure IV-5. Contour plots showing the fit between calculated binding curves and the experimental titration data for a hypothetical two site binding of N-α-acetyl[^{19}F-phe106]TnI(104-115) amide to Ca(II)-saturated turkey skeletal TnC. Binding curves were calculated for 0.001 mM $\leq K_{d1} \leq 0.1$ mM, $K_{d2} \geq 4K_{d1}$ and $(I_L - I_{PL})/I_{PL} = (I_L - I_{PL2})/I_{PL2} = 0.87$. The chi value (χ) contours show the level of agreement between the calculated curves and the experimental titration data.

E. References

ANDERSSON, A., DRAKENBERG, T., and FORSEN, S. 1985. The interaction of various drugs with calmodulin as monitored by ^{113}Cd NMR. In *Calmodulin Antagonist and Cellular Physiology* (Hidaka, H., and Hartshorne, D.J., Eds.), Chapt. 3, pp 27-44, Academic Press, New York.

BABU, Y.S., BUGG, C.E., and COOK, W.J. 1988. Structure of calmodulin refined at 2.2 Å resolution. J. Mol. Biol. **204**: 191-204.

BYERS, D.M., and KAY, C.M. 1982. Hydrodynamic properties of bovine cardiac troponin C. Biochemistry **21**: 229-233.

CACHIA, P.J., GARIEPY, J., and HODGES, R.S. 1985. Structural studies on calmodulin and troponin C. Phenothiazine, peptide, and protein interactions with calcium-induced helices. In *Calmodulin Antagonist and Cellular Physiology* (Hidaka, H., and Hartshorne, D.J., Eds.), Chapt. 5, pp 63-88, Academic Press, New York.

CACHIA, P.J., SYKES, B.D., and HODGES, R.S. 1983. Calcium-dependent inhibitory region of troponin. A proton magnetic resonance study on the interaction between troponin C and the synthetic peptide Nα-acetyl [F-phenylalanine106] TnI (104-115) amide. Biochemistry **22**: 4145-4152.

CACHIA, P.J., VAN EYK, J., INGRAHAM, R.H., MCCUBBIN, W.D., KAY, C.M., and HODGES, R.S. 1986. Calmodulin and troponin C. A comparative study of the interaction of mastoparan and troponin I inhibitory peptide [104-115]. Biochemistry **25**: 3553-3562.

CADAY, C.G., and STEINER, R.F. 1986. Interaction of calmodulin with melittin. Biochem. Biophys. Res. Commun. **135**: 419-425.

CHONG, P.C.S., ASSELBERGS, P.J., and HODGES, R.S. 1983. Inhibition of rabbit skeletal muscle acto-SI ATPase by troponin T. FEBS Lett. **153**: 372-376.

COLE, H.A., and PERRY, S.V. 1975. The phosphorylation of troponin I from cardiac muscle. Biochem. J. **149**: 525-533.

COLLINS, J.H., POTTER, J.D., HORN, M.J., WILSHIRE, G., and JACKMAN, N. 1973. The amino acid sequence of rabbit skeletal muscle troponin C. Gene replication and homology with calcium-binding proteins from carp and hake muscle. FEBS Lett. **36**: 268-272.

COMPTE, M., MAULET, Y., and COX, J.A. 1983. Ca^{+2}-dependent high affinity complex formation between calmodulin and melittin. Biochem. J. **209**: 269-272.

COX, A.J., COMPTE, M., FILTON, J.E., and DEGRADO, W.F. 1985. The interaction of calmodulin with amphiphilic peptides. J. Biol. Chem. **260**: 2527-2534.

CRC Handbook of Physics and Chemistry, (1962-1963) 44th ed., pp 320, The Chemical Rubber Publishing Co., Cleveland, OH.

DALGARNO, D.C., KLEVIT, R.E., LEVINE, B.A., SCOTT, G.M.M., WILLIAMS, R.J.P., GERGELY, J., GRABAREK, Z., LEAVIS, P.C., GRAND, R.J.A., and DRABIKOWSKI, W. 1984. The nature of the trifluoperazine binding sites on calmodulin and troponin C. Biochim. Biophys. Acta **791**: 164-172.

DRABIKOWSKI, W., DALGARNO, D.C., LEVINE, B.A., GERGELY, J., GRABAREK, Z., and LEAVIS, P.C. 1985. Solution conformation of the C-terminal domain of skeletal troponin C. Cation, trifluoperazine and troponin I binding effects. Eur. J. Biochem. **151**: 17-28.

EBASHI, S., and ENDO, M. 1968. Calcium ion and muscle contraction. Prog. Biophys. Mol. Biol. **18**: 123-183.

ERICKSON, B.W., and MERRIFIELD, R.B. 1976. Solid-phase peptide synthesis. In *The Proteins*, (Neurath, H., and Hill, R.L., Eds.), Vol. **2**, pp 255-527, Academic Press, New York.

FORSEN, S., THULIN, E., DRAKENBERG, T., KREBS, J., and SEAMON, K. 1980. A ^{113}Cd NMR study of calmodulin and its interaction with calcium, magnesium and trifluoperazine. FEBS Lett. **117**: 189-194.

FUJISAWA, T., UEKI, T., and IIDA, S. 1989. Structural change of the troponin C molecule upon Ca^{+2} binding measured in solution by the x-ray scattering technique. J. Biochem. **105**: 377-383.

GRABAREK, Z., DRABIKOWSKI, W., LEAVIS, P.C., ROSENFELD, S.S., and GERGELY, J. 1981. Proteolytic fragments of troponin C. Interactions with the other troponin subunits and biological activity. J. Biol. Chem. **256**: 13121-13127.

GREASER, M.C., and GERGELY, J. 1971. Reconstitution of troponin activity from three protein components. J. Biol. Chem. **246**: 4226-4233.

HABERMAN, V.E., and JENTSCH, J. 1967. The amino acid sequence of bee venom melittin. Hoppe-Seylers Z. Physiol. Chem. **348**: 37-50.

HARTSHORNE, D.J., and MUELLER, H. 1968. Fractionation of troponin into two distinct proteins. Biochem. Biophys. Res. Commun. **31**: 647-653.

HEIDORN, D.B., SEEGER, P.A., ROKOP, S.E., BLUMENTHAL, D.K., MEANS, A.R., CRESPI, H., and TREWELLA, J. 1989. Changes in the structure of calmodulin induced by a peptide based on the calmodulin-binding domain of myosin light chain kinase. Biochemistry **28**: 6757-6764.

HERZBERG, O., and JAMES, M.N.G. 1985. Structure of the calcium regulatory muscle protein troponin C at 2.8 Å resolution. Nature **313**: 653-659.

HITCHCOCK, S.E. 1975. Regulation of muscle contraction. Binding of troponin C involved in calcium ion-dependent interaction with troponin I. Eur. J. Biochem. **52**: 255-263.

HODGES, R.S., and MERRIFIELD, R.B. 1975. Monitoring of solid phase peptide synthesis by an automated spectrophotometric picrate method. Anal. Biochem. **65**: 241-272.

HODGES, R.S., SAUND, A.K., CHONG, P.C.S., ST-PIERRE, S.A., and REID, R.E. 1981. Synthetic model for two stranded α-helical coiled-coils. Design, synthesis and characterization of an 86-residue analog of tropomyosin. J. Biol. Chem. **256**: 1214-1224.

HUBBARD, S.R., HODGSON, K.O., and DONIACH, S. 1988. Small angle x-ray scattering investigation of the solution structure of troponin-C. J. Mol. Biol. **263**: 4151-4158.

HULL, W.E. 1975. Biophysical studies of alkaline phosphatase from *Escherichia coli* using ^{19}F and ^{31}P nuclear magnetic resonance. Ph.D. Thesis, Harvard University, Cambridge, Massachusetts.

JOHNSON, J.D., CHARLTON, S.C., and POTTER, J.D. 1979. A fluorescence stopped flow analysis of Ca^{+2} exchange with troponin C. J. Biol. Chem. **254**: 3497-3502.

IKURA, M., KAY E., KRINKS, M., and BAX, A. 1990. Triple-resonance multidimensional NMR study of calmodulin complexed with the binding domain of skeletal muscle myosin light-chain kinase: Indication of a conformational change in the central helix. Biochemistry **30**: 5498-5504.

KATAOKA, M., HEAD, J.F., SEATON, B.A., and ENGELMAN, D.M. 1989. Melittin binding causes a large calcium-dependent conformational change in calmodulin. Proc. Natl. Acad. Sci. USA **86**: 6944-6948.

KLEVIT, R.E. 1987. Study of calmodulin-peptide interactions by NMR spectroscopy. Methods in Enzymology **139**: 197-206.

KLEVIT, R.E., BLUMENTHAL, D.K., WEMMER, D.E., and KREBS, E.G. 1985. Interaction of calmodulin and a calmodulin-binding peptide from myosin light chain kinase. Major spectral changes in both occur as a result of complex formation. Biochemistry **24**: 8152-8157.

KRETSINGER, R.H., and NOCKOLDS, C.E. 1973. Carp muscle-binding protein II. Structure determination and general description. J. Biol. Chem. **248**: 3313-3326.

KRETSINGER, R.H., RUDNICK, S.E., and WEISSMAN, L.J. 1986. Crystal structure of calmodulin. J. Inorg. Biochem. **28**: 289-302.

LAN, J., ALBAUGH, S., and STEINER, R.F. 1989. Interactions of troponin I and its inhibitory fragment (residues 104-115) with troponin C and calmodulin. Biochemistry **28**: 7380-7385.

LEAVIS, P.C., and GERGELY, J. 1984. Thin filament proteins and thin filament regulation of vertebrate muscle contraction. CRC Crit. Rev. Biochem. **16**: 235-305.

LESZYK, J., COLLINS, J.H., LEAVIS, P.C., and TAO, T. 1987. Cross-linking of rabbit skeletal muscle troponin with the photoactive reagent 4-maleimidobenzophenone. Identification of residues in troponin I that are close to cys-98 of troponin C. Biochemistry **26**: 7042-7047.

LESZYK, J., COLLINS, J.H., LEAVIS, P.C., and TAO, T. 1988. Cross-linking of rabbit skeletal muscle troponin subunits. Labelling of Cys-98 of troponin C with 4-maleimidobenzophenone and analysis of products formed in the binary complex with troponin T and the ternary complex with troponins I and T. Biochemistry **27**: 6983-6987.

LESZYK, J., GRABAREK, Z., GERGELY, J., and COLLINS, J.H. 1990. Characterization of zero-length cross-links between rabbit skeletal muscle troponin C and troponin I. Evidence for direct interaction between the inhibitory region of troponin I and the NH_2-terminal, regulatory domain of troponin C. Biochemistry **29**: 299-304.

LEVINE, B.A., MERCOLA, D., COFFMAN, D., and THORNTON, J.M. 1977. Calcium binding by troponin C. A proton magnetic resonance study. J. Mol. Biol. **115**: 743-760.

LEVINE, B.A., THORNTON, J.M., FERNANDES, R., KELLY, L.M., and MERCOLA, D. 1978. Comparison of the calcium- and magnesium-induced structural changes of troponin C. A proton magnetic resonance study. Biochim. Biophys. Acta **535**: 11-24.

LINSE, S., DRAKENBERG, T., and FORSEN, S. 1986. Mastoparan binding induces a structural change affecting both the N-terminal and C-terminal domains of calmodulin: A ^{113}Cd-NMR study. FEBS Lett. **199**: 28-32.

MACLACHLAN, L.K., REID, D.G., MITCHELL, R.C., SALTER, C.J., and SMITH, S.J. 1990. Binding of a calcium sensitizer, bepridil, to cardiac troponin C. A fluorescence stopped-flow kinetic, circular dichroism, and proton nuclear magnetic resonance study. J. Biol. Chem. **265**: 9764-9770.

MALENCIK, D.A., and ANDERSON, S.R. 1982. Binding of simple peptides, hormones and neurotransmitters by calmodulin. Biochemistry **21**: 3480-3486.

MALENCIK, D.A., and ANDERSON, S.R. 1983a. Binding of hormones and neuropeptides by calmodulin. Biochemistry **22**: 1995-2001.

MALENCIK, D.A., and ANDERSON, S.R. 1983b. High affinity binding of the mastoparans by calmodulin. Biochem. Biophys. Res. Commun. **114**: 50-56.

MALENCIK, D.A., and ANDERSON, S.R. 1984. Peptide binding by calmodulin and its proteolytic fragments and by troponin C. Biochemistry **23**: 2420-2428.

MANT, C.T., BURKE, T.W.L., and HODGES, R.S. 1987. Optimization of peptide separations in reversed-phase HPLC: Isocratic versus gradient elution. Chromatographia **24**: 565-572.

MASSOM, L., LEE, H., and JARRETT, H.W. 1990. Trifluoperazine binding to porcine brain calmodulin and skeletal muscle troponin C. Biochemistry **29**: 671-681.

MATSUSHIMA, N., IZUMI, Y., MATSUO, T., YOSHINO, H., UEKI, T., and MIYAKE, Y. 1989. Binding of both Ca^{+2} and mastoparan to calmodulin induces a large change in the tertiary structure. J. Biochem. **105**: 883-887.

MCDOWELL, L., SANYAL, G., and PREDERGAST, F.G. 1985. Probable role of amphiphilicity in the binding of mastoparan to calmodulin. Biochemistry **24**: 2979-1984.

MOIR, A.J.G., WILKINSON, J.M., and PERRY, S.V. 1974. The phosphorylation sites of troponin I from cardiac muscle. FEBS Lett. **42**: 253-257.

NOZAKI, S., KOBAYASHI, K., KATAYAMA, E., and MURAMATSU, I. 1980. Synthetic studies on troponin I active site preparation of a pentadecapeptide with inhibitory activity toward troponin C. Chem. Lett. **3**: 345-348.

O'NEIL, K.T., and DEGRADO, W.F. 1989. The interaction of calmodulin with fluorescent and photoreactive model peptides. Evidence for a short interdomain separation. Proteins **6**: 284-293.

PARKER, J.M.R., MANT, C.T., and HODGES, R.S. 1987. A practical approach to the preparative purification of peptides using analytical instrumentation with analytical and semipreparative columns. Chromatographia **24**: 832-838.

PERRY, S.V., COLE, H., HEAD, J.F., and WILSON, F.J. 1972. Localization and mode of action of the inhibitory protein component of the troponin complex. Cold Spring Harbor Symp. Quant. Biol. **37**: 251-262.

PERSECHINI, A., BLUMENTHAL, D.K., JARRETT, H.W., KLEE, C.B., HARDY, D.O., and KRETSINGER, R.H.1989. The effects of deletions in the central helix of calmodulin on enzyme activation and peptide binding. J. Biol. Chem. **264**: 8052-8058.

PERSECHINI, A., and KRETSINGER, R.H. 1988. The central helix of calmodulin functions as a flexible tether. J. Biol. Chem. **263**: 12175-12178.

POTTER, J.D., and GERGELY, J. 1974. Troponin, tropomyosin and actin interactions in the Ca^{+2} regulation of muscle contraction. Biochemistry **13**: 2697-2703.

PUTKEY, J.A., ONO, T., VAN BERKUM, M.F.A., and MEANS, A.R. 1988. Functional significance of the central helix of calmodulin. J. Biol. Chem. **263**: 11242-11249.

REID, D.G., MACLACHLAN, L.K., GAJJAR, K., VOYLE, M., KING, R.J., and ENGLAND, P.J. 1990. A proton nuclear magnetic resonance and molecular modeling study of calmidazolium (R24571) binding to calmodulin and skeletal muscle troponin C. J. Biol. Chem. **265**: 9744-9753.

ROBERTSON, S.P., JOHNSON, J.D., and POTTER, J.D. 1981. The time-course of Ca^{+2} exchange with calmodulin, troponin, parvalbumin, and myosin in response to transient increases in Ca^{+2}. Biophys. J. **34**: 559-569.

SANYAL, G., RICHARD, L.M., CARRAWAY, K.L. III, and PUETT, D. 1988. Binding of amphiphilic peptides to a carboxy-terminal fragment of calmodulin. Biochemistry **27**: 6229-6236.

SCHAUB, M.C., and PERRY, S.V. 1969. The relaxing protein system of striated muscle. Biochem J. **115**: 993-1004.

SEEHOLZER, S.H., COHN, M., PUTKEY, J.A., MEANS, A.R., and CRESI, H.L. 1986. NMR studies of a complex of deuterated calmodulin with melittin. Proc. Natl. Acad. Sci. USA **83**: 3634-3638.

STEINER, R.F., and NORRIS, L. 1987. Interaction of melittin with troponin C. Arch. of Biochem. and Biophys. **254**: 342-352.

STRYNADKA, N.C.J., and JAMES, M.N.G. 1990. Model for the interaction of amphiphilic helices with troponin C and calmodulin. Proteins **7**: 234-248.

STRYNADKA, N.C.J., and JAMES, M.N.G. 1988. Two trifluoperazine binding sites on calmodulin predicted from comparative molecular modeling with troponin C. Proteins **3**: 1-17.

SUNDARALINGAM, M., BERGSTROM, R., STRASBURG, G., RAO, S.T., GREASER, M., and WANG, B.C. 1985. Molecular structure of troponin C from chicken skeletal muscle at 3 Å resolution. Science **227**: 945-948.

SYSKA, H., WILKINSON, J.M., GRAND, R.J.A., and PERRY, S.V. 1976. The relationship between biological activity and primary structure of troponin I from white skeletal muscle of the rabbit. Biochem J. **153**: 375-387.

TALBOT, J.A., and HODGES, R.S. 1979. Synthesis and biological activity of an icosapeptide analog of the actomyosin ATPase inhibitory region of troponin I. J. Biol. Chem. **254**: 3720-3723.

TALBOT, J.A., and HODGES, R.S. 1981. Synthetic studies on the inhibitory region of rabbit skeletal troponin I. Relationship of amino acid sequence to biological activity. J. Biol. Chem. **256**: 2798-3802.

TAO, T., GOWELL, E., STRASBURG, G.M., GERGELY, J., and LEAVIS, P.L. 1989. Ca^{+2} dependence of the distance between Cys-98 of troponin C and Cys-133 of troponin I in the ternary troponin complex. Resonance energy transfer measurements. Biochemistry **28**: 5902-5908.

THULIN, E., ANDERSSON, A., DRAKENBERG, T., FORSEN, S., and VOGEL, H.J. 1984. Metal ion and drug binding to proteolytic fragments of calmodulin. Proteolytic, cadmium-113, and proton nuclear magnetic resonance studies. Biochemistry **23**: 1862-1870.

TSALKOVA, T.N., and PRIVALOV, P.L. 1980. Stability of troponin C. Biochim. Biophys. Acta **624**: 196-204.

TSALKOVA, T.N., and PRIVALOV, P.L. 1985. Thermodynamic study of domain organization in troponin C and calmodulin. J. Mol. Biol. **181**: 533-544.

VAN BERKUM, M.F.A., GEORGE, S.E., and MEANS, A.R. 1990. Calmodulin activation of target enzymes. Consequences of deletions in the central helix. J. Biol. Chem. **265**: 3750-3756.

VAN EYK, J.E., and HODGES, R.S. 1988. The biological importance of each amino acid residue of the troponin I inhibitory sequence 104-115 in the interaction with troponin C and tropomyosin-actin. J. Biol. Chem. **263**: 1726-1732.

VAN EYK, J.E., KAY, C.M., and HODGES, R.S. 1991a. A comparative study of the interactions of synthetic peptides of the skeletal and cardiac troponin I inhibitory region with skeletal and cardiac troponin C. Biochemistry, in press.

VAN EYK, J.E., SONNICHSEN, F.D., SYKES, B.D., and HODGES, R.S. 1991b. Interaction of actin 1-28 with myosin and troponin I and the importance of these interactions to muscle regulation. In *Peptides as Probes in Muscle Research.* (Ruegg, J.C., Ed.), pp 15-31, Springer-Verlag, Heidelberg.

VANAMAN, T.C., SHARIEL, F., and WATTERSON, D.M. 1977. Structural homology between brain modulator protein and muscle TnCs. In *Calcium-Binding Proteins and Calcium Function* (Wasserman, R.H., *et al.*, Eds.), pp 107-116, Elsevier, Amsterdam.

WANG, Z., SARKAR, S., GERGELY, J., and TAO, T. 1990. Ca^{+2}-dependent interactions between the c-helix of troponin C and troponin I. J. Biol. Chem. **265**: 4953-4957.

WEEKS, R.A., and PERRY, S.V. 1978. Characterization of a region of the primary sequence of troponin C involved in calcium ion-dependent interaction with troponin I. Biochem. J. **173**: 449-457.

WILLIAMS, T.C., SHELLING, J.G., and SYKES, B.D. 1985. NMR approaches to the characterization of the interaction of metal ions with proteins. In *Nato Advanced Study Institute on NMR in the Life Sciences*, (Bradbury, E.M., and Nicolini, C., Eds.), pp 93-103, Plenum Press, New York.

YAMADA, K., and KOMETANI, K. 1982. The changes in heat capacity and entropy of troponin C induced by calcium binding. J. Biochem. **92**: 1505-1517.

YOSHINO, H., MINARI, O., MATSUSHIMA, N., UEKI, T., MIYAKE, Y., MATSUO, T., and IZUMI, Y. 1989. Calcium-induced shape change of calmodulin with mastoparan studied by solution x-ray scattering. J. Biol. Chem. **264**: 19706-19709.

ZOT, A.S., and POTTER, J.D. 1987. Structural aspects of troponin-tropomyosin regulation of skeletal muscle contraction. Annu. Rev. Biophys. Chem. **16**: 535-559.

Chapter V

Interaction of Troponin I and Troponin C : Use of the Two-Dimensional Transferred Nuclear Overhauser Effect to Determine the Structure of the Inhibitory Troponin I Peptide When Bound to Skeletal Troponin C

A. Introduction

Contraction of vertebrate skeletal muscle is regulated by Ca(II) and requires the regulatory proteins troponin and tropomyosin (Ebashi and Endo, 1968). Troponin is a complex of three different protein subunits: Troponin C (TnC) which binds Ca(II), TnI which binds actin and inhibits actomyosin ATPase, and TnT which binds to tropomyosin. The Ca(II)-dependent interaction between TnC and TnI is one of the key processes in the activation of contraction in skeletal muscle (for recent reviews, see Zot and Potter ,1987, and Leavis and Gergely, 1984). TnI inhibits the Mg(II)-ATPase activity of actomyosin (Hartshorne and Mueller, 1968; Schaub and Perry, 1969; Greaser and Gergely, 1971; Perry *et al.*, 1972) and binds both to actin and tropomyosin-actin (Potter and Gergely, 1974; Hitchcock, 1975). The inhibition of actomyosin ATPase is neutralized when Ca(II)-saturated TnC forms a 1:1 complex with TnI (Perry *et al.*, 1972; Weeks and Perry, 1978; Chong *et al.*, 1983; Cachia *et al.*, 1986; Van Eyk and Hodges, 1988). The region of TnI which is responsible for its inhibitory activity is the same region which is involved in a Ca(II)-sensitive 'switch' between binding to actin-tropomyosin and binding to TnC. In the absence of Ca(II), the inhibitory region of TnI, spanned by residues 96-116, is bound to the surface of actin-tropomyosin, inhibiting the actomyosin ATPase activity and contraction. In the presence of Ca(II), this region of TnI is thought to bind to TnC (Cachia *et al.*, 1985). It has been proposed that the structural changes produced by Ca(II) binding to TnC result in the presentation of regions on the surface of TnC capable of binding TnI with high affinity (LaPorte *et al.*, 1980; Gariepy and Hodges, 1983; Cachia *et al.*, 1985).

Talbot and Hodges (1981) showed using synthetic peptides that residues 104-115 of TnI comprise the minimum sequence necessary for inhibition of actomyosin ATPase activity. The synthetic peptide TnI(104-115) possesses tropomyosin specificity (Talbot and Hodges, 1979) and TnC binding capability (Cachia *et al.*,1983, 1985; Van Eyk and Hodges, 1988; Van Eyk *et al.*, 1991a), which results in the release of ATPase inhibition (Cachia *et al.*, 1986; Van Eyk and Hodges, 1988). Thus, it is would appear that residues 104-115 comprise the inhibitory site of TnI and binding of this region to Ca(II)-saturated TnC leads to relief of inhibition of actomyosin ATPase, and ultimately to muscle contraction. We have recently used ^{19}F NMR to study the binding of the synthetic peptide Nα-acetyl [19FPhe106]TnI(104-115) amide to Ca(II)-saturated skeletal turkey TnC, and have obtained a dissociation constant of $K_d = 4.8 \times 10^{-5}$ M for a 1:1 binding stoichiometry (Campbell *et al.*, 1991; Chapter IV).

In the present study we use two-dimensional NMR techniques to determine the structure of the synthetic peptide Nα-acetyl-TnI(104-115) amide bound to Ca(II)-saturated turkey skeletal TnC (Campbell and Sykes, 1989). Conformational changes in the peptide induced by the formation of the TnI peptide-TnC.Ca(II)$_4$ complex were followed by the study of the transferred nuclear Overhauser effect (TRNOE). The TRNOE is the extension of the nuclear Overhauser effect (NOE), which has been widely used to determine protein structures in solution (Wuthrich, 1986), to exchanging systems such as ligand-protein complexes, and provides one of the best techniques for the determination of the structure of bound ligands (Gronenborn and Clore, 1982; Clore and Gronenborn, 1982b, 1983, 1984a, 1984b, 1984c, 1986; Levy *et al.*, 1983, 1989; Banerjee *et al.*, 1985; Ehrlich and Colman, 1985; Glasel and Borer, 1986; Andersen *et al.*, 1987; Glasel, 1989; Meyer *et al.*, 1988; Anglister *et al.*, 1989; Anglister and Zilber, 1990; Milon *et al.*, 1990; Bevilacqua *et al.*, 1990; Ni *et al.*, 1989a, 1989b, 1989c, 1990). The intramolecular TRNOE allows the transfer of information concerning cross-relaxation between two nuclei in the bound ligand to the free ligand resonances via chemical exchange. In the unbound form, the ligand is generally characterized by short correlation times ($\tau_c < 10^{-10}$ s) and thus may be described as being either in the extreme narrowing limit ($\omega\tau_c << 1$), where the NOEs are small and positive, or at the boundary of the extreme narrowing limit ($\omega\tau_c \cong 1$), where the NOEs approach zero. When bound to the protein, the ligand is characterized by the long correlation time of the protein ($\tau_c > 10^{-8}$ s), and thus may be described as being in the spin diffusion limit ($\omega\tau_c >> 1$), where the NOEs are large and negative. In the presence of chemical exchange of the ligand between its free and bound states, negative NOEs conveying conformational information of the bound ligand are 'transferred' to the free ligand resonances where they are more easily measured because these resonances are much narrower.

In the present study, the TRNOE-guided determination of the structure of the inhibitory region of TnI when complexed to whole Ca(II)-saturated TnC will allow us to understand a fundamental regulatory step in the Ca(II)-mediated regulation of muscle contraction. However, the NMR techniques developed in this chapter are not limited to the study of this particular system, but may be applied to the study of the interaction of any ligand with any target macromolecule. The TRNOE may be used to study the interaction of substrates with enzymes, antigens with antibodies, hormones with receptors, nucleotides with regulatory proteins, or peptides with phopholipids. This broad applicability makes the TRNOE one of the best techniques for the study of molecular interactions in biological systems.

B. Theory

Consider the equilibrium between the free and bound ligand

$$\mathrm{TnI(104\text{-}115) + TnC} \underset{k_{-1}}{\overset{k_1[\mathrm{TnC}]}{\rightleftharpoons}} \mathrm{TnI(104\text{-}115).TnC} \qquad [1]$$

Given fast exchange on the NMR timescale ($[4\pi^2(\delta_F-\delta_B)^2\tau_cB^2]$, $[\tau_cB/T_2B] << 1$, where τ_cB is the correlation time of the bound peptide, $|\delta_F-\delta_B|$ is the change in chemical shift upon binding, and T_2B is the spin-spin relaxation time in the bound environment), the observed chemical shifts, δ_{obs}, and linewidths, $\Delta\nu_{obs}$, are dominated by the free ligand population when $p_F >> p_B$ (where p_B is the fraction of bound ligand and p_F is the fraction of free ligand)

$$\delta_{obs} = p_F\,\delta_F + p_B\,\delta_B \qquad [2]$$

$$\Delta\nu_{obs} = p_F\,\Delta\nu_F + p_B\,\Delta\nu_B \qquad [3]$$

Conversely, the TRNOESY cross-peak intensities, a_{ij}, are dominated by the bound ligand, since the cross-relaxation rate between protons in the bound ligand is so much faster than it is in the free ligand, viz. $W_{ij}B >> W_{ij}F$

$$a_{ij}(\tau_m) \cong -\,[\,p_B\,W_{ij}B + p_F\,W_{ij}F\,]\,\tau_m \;\cong -\,[\,p_B\,W_{ij}B\,]\,\tau_m \qquad [4]$$

This is the result presented earlier by Clore *et al.* (Clore and Gronenborn, 1982a, 1983; Gronenborn and Clore, 1985) which is valid only in the limit of short τ_m. A full theoretical evaluation of the TRNOE has been presented elsewhere (Campbell and Sykes, 1991a, 1991b; Chapters II and III) based upon a full relaxation matrix approach (Landy and Rao, 1989). The $W_{ij}B$s, once obtained, yield interproton distances in the bound peptide

$$W_{ij}B \propto \langle\, 1/r_{ij}B^{\,6} \rangle \qquad [5]$$

From Eqns. 4 and 5, it can be seen that for any two pairs of bound proton resonances, $r_{ij}B$ will be simply given by Eqn. 6, using a suitable reference distance

$$r_{ij}B = \{\, (\, W_{REF} \,/\, W_{ij}B\,) \times\, r_{REF}^{\;6}\,\}^{\,1/6} \qquad [6]$$

The experimentally derived $r_{ij}B$ values may be used as distance restraints in energy minimization and molecular dynamics programs to generate a bound TnI peptide conformation.

We have used Eqns. 4-6 as a starting point for determining $r_{ij}B$ values in the bound TnI peptide. However, the generation of a correct bound peptide conformation requires an analysis of the effects of spin-diffusion experienced by the protons on the TnI peptide when it is bound to TnC. Instead of using a full relaxation matrix treatment to solve for relaxation in the multi-spin TnI peptide-TnC protein complex, we have made a variety of 'adjustments' to the $r_{ij}B$ values, guided by the full theoretical treatment. These adjustments correct for under- and over-determination of the $r_{ij}B$ values, and have been described in the materials and methods section.

C. Materials and Methods

1. Sample Preparation

a. Materials. Unless otherwise stated, all chemicals and solvents were reagent grade. Diisopropylethylamine, dichloromethane and trifluoroacetic acid were distilled prior to use. Picric acid was dissolved in dichloromethane and dried over magnesium sulfate. Acetonitrile (HPLC grade) was obtained from Fisher Scientific. Boc amino acids were purchased from Bachem Fine Chemicals (Torrance, CA, USA), Protein Research Foundation (Peptide Institute, Osaka, Japan) and Institute Armand Frappier (Quebec, Canada). Poly(styrene-*co* -1% divinylbenzene)benzhydrylamine HCl resin 200-400 mesh (≅ 0.7 meg. nitrogen/g) was purchased from Institute Armand Frappier. Turkey breast muscle was purchased from the local supermarket. Urea (Fisher) was purified by stirring with a mixed-bed resin (Bio-Rad AG-50 1-X8).

b. Amino Acid Analysis. The quantities of Nα-acetyl-TnI(104-115) amide and turkey skeletal TnC used were determined from amino acid analysis after hydrolysis in 100-200 µl of 6 N HCl in evacuated sealed tubes for 24 h at 110°C. The mean of the molar ratios of all accurately measurable amino acids in the acid hydrolysate was used to calculate the concentration of peptide or protein.

c. Peptide Synthesis and Purification. Nα-acetyl-TnI(104-115) amide was synthesized using the standard procedures for solid-phase peptide synthesis (Erickson and Merrifield, 1976) on an Applied Biosystems 430A peptide synthesizer (Foster City, California). The co-poly (styrene, 2% divinyl-benzene) benzhydrylamine-HCl resin was maximally substituted to 0.8 mmole of Boc-amino acid per gram of resin. All α-amino groups of the amino acids used were protected with the Boc group. The following side chain protecting groups were used: arginine(Tosyl) and lysine(2-ClZ). It has been previously shown that it is important to block the α-carbonyl and α-amino groups of synthetic peptides comprised of sequences from interior regions of proteins, especially as the peptide approaches the minimum sequence required for biological activity (Talbot and Hodges, 1981). The amino terminal residue of the TnI peptide was acetylated by treatment for 30 min with acetic anhydride/toluene/pyridine (1:3:3, v/v/v) and the carboxyl terminal group was amidated. The programs used for deprotection, neutralization and coupling of each amino acid, and cleavage of peptide from resin by HF have been previously described (Hodges *et al.*, 1988).

The crude TnI peptide was purified on an HPLC system comprised of a Spectra Physics SP8700 solvent delivery system, a Kratos SF7697 detector and Technical Marketing Ass. chart recorder. The peptide was purified using an analytical Pierce aquapore RP-300 column (4.6 mm I.D. X 220 mm) by employing a linear AB gradient (0.1% B per min) at 1 ml/min, where buffer A was 0.05% aqueous TFA and buffer B was 0.05% TFA in acetonitrile. The sample loads were varied between 20 and 50 mg per run. One minute fractions were collected. In order to identify the fractions containing the desired peptide, analytical runs of the various fractions were carried out using the above reversed phase column with a gradient rate of 1% B/min (Mant *et al.*, 1987; Parker *et al.*, 1987). The fractions containing the pure peptide were pooled and lyophilized.

d. Preparation of TnC. Troponin was isolated from an acetone powder of turkey breast muscle using the protocol outlined in the Materials and Methods section in Chapter IV. A final yield of approx. 400 mg of purified TnC powder was obtained, which was found to be homogenous when examined by SDS-Page and UV spectrophotometry ($\varepsilon_{(\lambda\ 259\ nm)}$ = 0.109 O.D. units/mg/ml for turkey skeletal TnC).

e. Preparation of Desalted, Apo TnC. EDTA-free, apo TnC was prepared using the protocol outlined in the Materials and Methods section in Chapter IV. The TnC protein was judged to be apo by UV spectrophotometry and ^{1}H NMR.

f. Preparation of TnI Peptide ^{13}C NMR Samples. The sample used in the ^{13}C NMR experiments was 4.5 mM Nα-acetyl-TnI(104-115) amide, dissolved in 3.0 ml 100% D_2O and at a pH of approx. 6.7. 0.75 mM dioxane was added to the sample to act as a chemical shift standard.

g. Preparation of TnI Peptide ^{1}H NMR Samples. The sample used in all ^{1}H NMR experiments was 10 mM Nα-acetyl-TnI(104-115) amide, dissolved in 650 μl of a

80%H_2O/20%D_2O solvent mixture at a pH in the range of 6.2 to 6.5 and a salt concentration of 50 mM KCl. Turkey skeletal TnC.Ca(II)$_4$ was titrated into the sample to a final concentration of approximately 1 mM TnC:4 mM $CaCl_2$ for 0.1, 2 mM TnC:8 mM $CaCl_2$ for 0.2, and 4 mM TnC:16 mM $CaCl_2$ for 0.4 molar equivalents of TnC.Ca(II)$_4$ to TnI peptide, respectively. 0.1 mM DSS was added to the sample to act as a chemical shift standard.

2. Nuclear Magnetic Resonance Spectroscopy

^{13}C NMR spectra were recorded on a Nicolet NT 300 WB NMR spectrometer at a frequency of 75.44 MHz for ^{13}C. A simple one pulse sequence was used with MLEV-16 decoupling in the ^{1}H channel. Spectral widths of 16128 Hz were used with an acquisition time of 1 s , a 90° pulse length of 28 µs, and an acquisition delay of 0.5 s.

All ^{1}H NMR spectra were obtained at 500 MHz on a Varian VXR-500 NMR spectrometer. Two-dimensional experiments were taken with 2048 data points along t_2 and with 256 t_1 increments. Spectral widths of 5000-6000 Hz and relaxation delay times of 1.6-2.3 s were employed. Streaking along t_1 was reduced by multiplying the first domain time point by a factor optimized near 0.5 (Otting *et al.*, 1986). DQFCOSY (Piatini *et al.*, 1982; Rance *et al.*, 1983) and TRNOESY data sets were acquired in the phase-sensitive method of States *et al.* (1982). The appropriate phase cycling was used for quadrature detection and to eliminate axial peaks, and in the case of TRNOESY spectra, single and multiple quantum coherences. For all data sets, the water resonance was suppressed by presaturation. The decoupler offset was set equal to the transmitter offset to prevent phase distortions around the water peak due to imperfect cancellation of the dispersive component of residual water magnetization (Hoult, 1976). Average mixing times, τ_m , of 75, 150 and 500 ms were used for the TRNOESY spectra. A random delay of ± 10 ms was incorporated to suppress zero quantum coherences. Spectra acquired at 500 ms were used for assignment purposes whereas spectra acquired at 150 ms were used for cross-peak intensity measurement, leading to structure determination. The poor signal-to-noise observed at 75 ms precluded complete cross-peak intensity measurements, however these spectra were used in mixing time studies.

3. Transformation of ^1H NMR TRNOESY Peak Intensity to Distance Restraints

^{1}H NMR TRNOESY intensities were quantified for a data set acquired at $\tau_m = 150$ ms and 0.1 molar equivalents TnC.Ca(II)$_4$ to TnI peptide. Volume integrals for each cross-peak were measured and nominally empty areas perpendicularly adjacent to each cross-peak were examined for baseline correction. The TRNOE cross-peak intensities were transformed to distance restraints using a group of stereospecifically assigned reference proton pairs which included F106NH-βCH(4.0Å), F106NH-βCH'(3.4Å), P109βCH-δCH(4.1Å), P109βCH-δCH'(3.9Å), P109βCH'-δCH(3.9Å), P109βCH'-δCH'(3.0Å), P110βCH-δCH(4.1Å), P110βCH-δCH'(3.9Å), P110βCH'-δCH(3.9Å) and P110βCH'-δCH'(3.0Å). These proton pairs were chosen because they displayed linear TRNOE build-up of magnetization for $\tau_m = 150$ ms and 0.1 molar equivalents of TnC.Ca(II)$_4$, and were well separated from overlapping cross-peaks in the TRNOESY spectrum. The reference distances for the F106 reference proton pairs corresponded to the distances found for an α-helical TnI peptide. However, these distances were not found to change more than 10% when compared to those found for the TnI peptide in a β-sheet conformation, and therefore were deemed to be independent of secondary conformation. All other reference distances involved distances between reference proton pairs in the P109 and P110 five-membered rings.

TRNOE intensities were normalized for the contribution of more than two protons to the cross-peak before they were transformed into distance restraints. We divided the TRNOE cross-peak intensities by the normalization factor $(2NaNb)/(Na+Nb)$ where *Na* was the number of protons under diagonal peak *a*, and *Nb* was the number of protons under diagonal peak *b* (Macura and Ernst, 1980; Williamson and Neuhaus, 1987). Cross-peaks connecting exchangeable proton resonances were also corrected for loss of intensity due to exchange or saturation transfer from the decoupled water peak. The exchangeable proton peak intensities were integrated in a one-dimensional spectrum obtained under the same experimental conditions as the two-dimensional spectrum (same temperature, pH, sample concentration and spectrometer settings), and the intensity of these peaks were normalized against the integrated intensity of the V114αCH peak (see Tables V-1A and V-1B in Appendix).

Table V-2 in the Appendix gives the TRNOE data set measured from the TRNOESY experiment acquired at $\tau_m = 150$ ms and 0.1 molar equivalents TnC.Ca(II)$_4$ to TnI peptide. Included in Table V-2 are the measured TRNOE intensities, the corrected and normalized TRNOE intensities, and the r_{ij}s calculated from these corrected and normalized values using the group of stereospecifically assigned reference proton pairs discussed above.

Initial error limits ($\pm\beta$) were used to set upper (r_{ij}^U) and lower (r_{ij}^L) distance bounds on the calculated distance restraints (r_{ij}), and were incorporated in the following manner: for $r_{ij} < 3.0$Å, $\beta = \pm0.2$ Å; for 3.0 Å $\leq r_{ij} < 4.0$Å, $\beta = \pm0.3$ Å; for 4.0 Å $\leq r_{ij} < 5.0$Å, $\beta = \pm0.5$ Å; and for $r_{ij} \geq 5.0$ Å, $\beta = \pm1.0$ Å. Thus, for $r_{ij} = 3.5$ Å, we set r_{ij}^U equal to 3.8 Å, and r_{ij}^L equal to 3.3 Å. Within the distance range of $r_{ij} \pm \beta$, the distance restraint term used in the MD and EM simulations contributed no energy penalty to the overall potential energy of the system.

4. Control Experiments to Analyze the Effects of Indirect Cross-Relaxation on the Development of the Intrapeptide TRNOEs

In order to analyze the effects of indirect cross-relaxation on the development of ^{1}H-^{1}H TRNOEs within the bound TnI peptide, we performed a series of control experiments. These control experiments were designed to analyze the effect of mixing time and concentration of TnC.Ca(II)$_4$ protein on the development of the TRNOEs, and to qualitatively correct for the effects of indirect cross-relaxation in a system where cross-relaxation between spins is rapid. In such a system, distances derived from measurement of TRNOESY cross-peak intensities can only be approximate, because direct cross-relaxation between two spins in the bound ligand is modified by indirect cross-relaxation with other spins. A theoretical evaluation of the TRNOE using a full relaxation matrix approach has been presented elsewhere (Campbell and Sykes, 1991a, 1991b; Chapters II and III) and has examined the effects of variables such as mixing time, fraction of bound peptide, free and bound correlation times, and other contributions to the development of the TRNOE. For the purposes of this chapter, we present only a qualitative assessment of the effects of indirect cross-relaxation, and attempt to correct for these effects in the calculation of distances from the measured TRNOEs. We also attempt to qualitatively correct for the contribution of the free peptide conformation to the calculation of the distances in the bound peptide conformation.

In order to analyze the effects of indirect cross-relaxation on the development of the intrapeptide TRNOEs, we performed a series of control experiments which included mixing time studies and protein concentration studies. For the mixing time studies, we acquired TRNOESY data sets at 0.1 molar equivalents of TnC.Ca(II)$_4$ to TnI peptide for three mixing times (τ_m = 75, 150, 500 ms) (see Table V-3 in the Appendix). For the protein concentration studies, we acquired TRNOESY data sets at τ_m = 150 ms for four concentrations of TnC.Ca(II)$_4$ (0.0, 0.1, 0.2, 0.4 molar equivalents TnC.Ca(II)$_4$ to TnI peptide) (see Table V-4 in the Appendix).

On the basis of the mixing time studies, TRNOESY cross-peaks were divided into three categories. 'A' and 'B' cross-peaks arose from direct cross-relaxation but were distinguished from each other in that the 'B' cross-peaks displayed a linear TRNOE time development up to τ_m = 150 ms, whereas 'A' cross-peaks displayed a TRNOE that had begun decreasing at τ_m = 150 ms due to the passage of magnetization along to neighbouring spins. 'C' cross-peaks arose from indirect cross-relaxation and displayed a TRNOE which developed after τ_m = 150 ms due to the acceptance of magnetization from neighbouring spins. A typical plot of TRNOE cross-peak intensity versus τ_m at 0.1 molar equivalents TnC.Ca(II)$_4$ to TnI peptide for 'A', 'B', and 'C' cross-peak types is presented in Figure V-1.

On the basis of the protein concentration studies, TRNOESY cross-peaks were also divided into two categories. 'Y' cross-peaks were not present in the absence of TnC.Ca(II)$_4$ and thus were representative of the bound TnI peptide conformation only; whereas 'X' cross-peaks were present in the absence of TnC.Ca(II)$_4$, and thus contained conformational information of the free as well as the bound state TnI peptide. A plot of TRNOE cross-peak intensity versus molar equivalents TnC.Ca(II)$_4$ to TnI peptide at τ_m = 150 ms for 'Y' and 'X' cross-peak types is presented in Figure V-2.

The results of these control experiments were incorporated into r_{ij}s as shifts towards longer or shorter distance, r_{ij}^os. With regard to the mixing time classification, a shift to a shorter distance by β Å ($r_{ij}^o = r_{ij} - \beta$)[1] compensated for spin-diffusion with 'A' type cross-peak behaviour; whereas a shift to a longer distance by β Å ($r_{ij}^o = r_{ij} + \beta$) compensated for 'C' type cross-peak behaviour. 'B' type cross-peak behaviour with linear TRNOE build-up rates required no adjustment in r_{ij}, ie. $r_{ij}^o = r_{ij}$. With regard to the TnC.Ca(II)$_4$ concentration classification, 'Y' type cross-peak behaviour required no adjustment in r_{ij}, ie. $r_{ij}^o = r_{ij}$. But for 'X' type cross-peak behaviour, a shift to a longer distance by β Å compensated for the contribution of the free peptide conformation to the overall TRNOE cross-peak intensity.

Table V-1 illustrates the combined shifts in distance restraints from both the mixing time and protein concentration studies for a sample distance, r_{ij} = 3.5 Å (β = 0.3 Å). We classified the TRNOE cross-peak behaviour into six categories, defined as AY, AX, BY, BX, CY or CX behaviour. As an example, AX behaviour is accompanied by a shift in r_{ij}

---

[1] The β used here is the same β used to set the initial error limits, so for an rij = 3.5 Å, the error limits are set as ± 0.3 Å; but if this distance is shifted to a longer distance by an additional β units, the new distance becomes (3.5 + 0.3 Å)(± 0.3 Å), or rij^o = 3.8 ± 0.3 Å.

of -β due to the A component and +β due to the X component. Thus the total shift in r_{ij} is -β +β = 0 and r_{ij}^o remains equal to r_{ij}, ie. $r_{ij}^o = r_{ij} = 3.5 \pm 0.3$ Å. CX behaviour is accompanied by a shift in r_{ij} of +β due to the C component and +β due to the X component, which makes the total shift +2β. Thus, r_{ij}^o is shifted +2β units from 3.5 Å to 4.1 Å, ie. $r_{ij}^o = r_{ij} + 2\beta = 4.1 \pm 0.5$ Å. Note that as the distance restraint is changed from 3.5 to 4.1 Å, the error limits change from 0.3 Å to 0.5 Å.

Table V-5 in the Appendix summarizes the distance restraints used in the MD simulations. Included in Table V-5 are the r_{ij}s calculated from the corrected and normalized TRNOE cross-peak intensities, the incorporated error limits (±β), the shifts in r_{ij} to r_{ij}^o from the mixing time and protein concentration behaviour of the cross-peak, and the pseudoatom adjustments in r_{ij}^U.

5. Dihedral Angle Restraints and Supplemental Distance Restraints

A curve fitting program was used to measure dihedral coupling constants in one-dimensional ^{1}H NMR spectra of the TnI peptide in the presence of 0.008, 0.016, 0.024, 0.032, 0.040, 0.048 and 0.10 molar equivalents of TnC.Ca(II)$_4$. Practically, linebroadening and spectral overlap prevented measurement of $^3J\alpha$CH-NH coupling constants for the 100% bound peptide in a 1.0 molar equivalent TnC.Ca(II)$_4$ to TnI peptide sample. Therefore, observed coupling constants were measured at low concentrations of protein and extrapolated to 100% bound peptide (see Table V-6 in the Appendix). For $^3J\alpha$CH-NH < 6.0 Hz, Φ is expected to be in the range $-85° \leq \Phi \leq -40°$ (Pardi *et al.*, 1984; Wagner *et al.*, 1987; Driscoll *et al.*, 1989). For $^3J\alpha$CH-NH > 8.0 Hz, Φ is expected to be in the range $-160° \leq \Phi \leq -80°$. All $^3J\alpha$CH-NH values in the TnI peptide were found to be less than 6.0 Hz when extrapolated to 100% bound peptide[2], therefore all Φ dihedral angles in the peptide were restrained to $-85° \leq \Phi \leq -40°$. In addition, all peptide bonds, including X-proline were restrained to $-175° \leq \omega \leq -185°$, to maintain trans configurations. We found no evidence for cis-trans X-proline peptide bond isomerization from either ^{1}H or ^{13}C NMR spectra; all X-proline peptide bonds were deemed to be trans from the pattern of ^{1}H TRNOEs and the chemical shifts of the β and γ carbons in the one-dimensional ^{13}C NMR spectra (data not shown).

---

[2] The determination of $^3J\alpha$CH-NH for 100% bound peptide is not intended to be rigorous and quantitative, therefore an error analysis was not performed. Qualitatively, the general trend of decreasing values of $^3J\alpha$CH-NH with bound peptide clearly points to small $^3J\alpha$CH-NH values for the bound peptide.

Supplementary distance restraints were obtained from intra-peptide hydrogen bonds identified by measuring temperature coefficients ($\Delta\delta/\Delta T$) of the exchangeable backbone amide protons of the TnI peptide as a function of molar equivalents of TnC.Ca(II)$_4$. The temperature dependence of amide proton resonances, in conjunction with a knowledge of secondary structure, was used to identify backbone hydrogen bonding. For a random coil peptide in H_2O, the temperature coefficients of amide proton resonances are expected to be $-6 \leq \Delta\delta/\Delta T \leq -10$ ppb; whereas for amides protected from exchange with the solvent these values are expected to decrease to $\Delta\delta/\Delta T \leq -4$ ppb (Deslauriers and Smith, 1980). Temperature coefficients were measured for 0.0, 0.1, 0.2 and 0.4 molar equivalents TnC.Ca(II)$_4$ to TnI peptide (see Figures V-1A → V-1C, Tables V-7A → V-7C and Table V-8 in the Appendix). Again, linebroadening and spectral overlap prevented measurement of $\Delta\delta/\Delta T$ for the 100% bound peptide in a 1.0 molar equivalent protein to peptide sample, therefore $\Delta\delta/\Delta T$ values were measured for relatively low concentrations of protein and extrapolated to 100% bound peptide[3].

6. Stereospecific Assignments from ^1H NMR

Stereospecific assignments of prochiral protons were available for the βCH and βCH' protons of F106, P109 and P110, and the δCH and δCH' protons of P109 and P110. Stereospecific assignments were possible for these prochiral proton pairs since they exhibited sufficiently different chemical shifts. The other prochiral protons and methyl groups on the TnI peptide were designated as pseudoatoms (Wuthrich *et al.*, 1983), and the appropriate intraresidue and long-range corrections were made on the upper bound of the distance restraints for these pseudoatoms. Unambigious stereospecific assignments may result for prochiral groups if there is a sufficiently large set of NOE, Van der Waals and covalent bond constraints as input for the structure calculation. Here, we generated a roughly determined structure using only pseudoatoms in the distance restraint file for the MD simulations, and then modified the distance restraint file to include stereospecific distance restraints consistent with the stereochemistry of this roughly determined structure. A more precisely determined structure was then generated using this modified distance restraint file as input for a second round of MD simulations. The stereospecific assignments for the phenylalanine and proline residues were in agreement with the relative strength of the $d_{\alpha\beta}$ and $d_{N\beta}$ NOE cross-peaks, and were consistent with the stereochemistry of the bound structure. The second round of MD simulations employing the stereospecific assignments are described in the following section.

---

[3] Again, the determination of $\Delta\delta/\Delta T$ for 100% bound peptide is not intended to be rigorous and quantitative, therefore an error analysis was not performed.

7. Restrained Molecular Dynamics Calculations

EM and MD calculations were carried out with the GROMOS program (de Vlieg *et al.*, 1986) and force field, which consisted of the usual terms for bonds, bond-angles, sinusoidal dihedral torsion, non-bonded interactions (Van der Waals and electrostatics), and harmonic terms to maintain proper planar or tetrahedral geometries. Two extra terms were added representing distance and dihedral restraints. The distance restraint square well potential, E_{DIS}, was defined by two functions, a biharmonic potential for $(r_{ij}{}^U - r_{ij})$ and $(r_{ij}{}^L - r_{ij}) < 5Å$, and a linear potential for $(r_{ij}{}^U - r_{ij})$ and $(r_{ij}{}^L - r_{ij}) \geq 5Å$:

$$\begin{aligned} E_{DIS} &= 0.5\, C_{DIS}\, (r_{ij}{}^U - r_{ij})^2 && \text{if } r_{ij} > r_{ij}{}^U;\ |r_{ij}{}^U - r_{ij}| < 5Å \\ &= 0.5\, C_{DIS}\, (r_{ij}{}^L - r_{ij})^2 && \text{if } r_{ij} < r_{ij}{}^L;\ |r_{ij}{}^L - r_{ij}| < 5Å \end{aligned} \qquad [7a]$$

$$\begin{aligned} E_{DIS} &= 0.5\, C_{DIS}\, (r_{ij}{}^U - r_{ij}) && \text{if } r_{ij} > r_{ij}{}^U;\ |r_{ij}{}^U - r_{ij}| \geq 5Å \\ &= 0.5\, C_{DIS}\, (r_{ij}{}^L - r_{ij}) && \text{if } r_{ij} < r_{ij}{}^L;\ |r_{ij}{}^L - r_{ij}| \geq 5Å \end{aligned} \qquad [7b]$$

where C_{DIS} was a force constant. The dihedral angle restraint, E_{DIH}, was then represented by the biharmonic potential :

$$\begin{aligned} E_{DIH} &= 0.5\, C_{DLR}\, (\Phi_k{}^U - \Phi_k)^2 && \text{if } \Phi_k > \Phi_k{}^U \\ &= 0.5\, C_{DLR}\, (\Phi_k{}^L - \Phi_k)^2 && \text{if } \Phi_k < \Phi_k{}^L \end{aligned} \qquad [8]$$

where $\Phi_k{}^U$ and $\Phi_k{}^L$ were upper and lower allowed limits of the torsion angle, Φ_k was the calculated angle, and C_{DLR} was the force constant.

Starting models were first subjected to 500 steps of conjugate gradient EM. Then the starting structures were subjected to 12 ps of MD where values of the distance restraint force constant were increased from 400 to 4000 kJ mol^{-1} nm^{-2}, and the dihedral restraint force constant from 200 to 2000 kJ mol^{-1} rad^{-2}. At 2 ps intervals, the force constants were increased and the velocities (taken from a Maxwellian distribution at 300 K) were re-initialized. During these re-initialization intervals, the structures were cooled with 500 steps of intervening EM. Newton's equations of motion were integrated with a time step of 2 fs, with all bond lengths kept rigid by the SHAKE algorithm (Ryckaert *et al.*, 1977). The molecule was weakly coupled to a temperature bath with a reference temperature of 300 K, using a coupling constant of 0.1 ps (Berendsen *et al.*, 1984). A cut-off radius of

10 Å was used for the non-bonded interactions and the non-bonded pair list was updated every 20 fs. MD runs with the highest values of C_{DIS} and C_{DLR} were continued to approximately 20 ps in total, and coordinates were then averaged over another 2 ps to give averaged MD structures which were then subjected to another 500 steps of EM to correct distortions in the structure caused by the averaging procedure.

We performed two separate MD simulations to determine the structure of Nα-acetyl-TnI(104-115) amide bound to turkey skeletal TnC.Ca(II)$_4$. The first of these simulations used a set of input coordinates derived from the standard Φ,Ψ angles of an α-helix (Φ = -60°, Ψ = -40°). The second of these simulations used a set of input coordinates derived from the standard Φ,Ψ angles of a β-strand (Φ = -118°, Ψ = +118°). The distance restraint file used as input for the MD simulations is presented in Table V-9 in the Appendix.

D. Results

1. Sequential Resonance Assignments and Transferred NOEs

Sequential assignments of the TnI peptide in the absence and presence of 0.1 molar equivalents of TnC.Ca(II)$_4$ were carried out according to the established procedures of Wuthrich *et al.* (Wuthrich *et al.*, 1982; Billeter *et al.*, 1982; Wagner *et al.*, 1982). This method relies on the observation of NOEs between the amide protons of one residue and the α-protons, β-protons and amide protons of the preceding residue ($d_{\alpha N}$, $d_{\beta N}$ *and* d_{NN}). Table V-2 shows the ^{1}H chemical shifts for the assigned resonances of the TnI peptide in the absence and presence of 0.1 molar equivalents of TnC.Ca(II)$_4$.

All DQFCOSY and NOESY spectra of the peptide in the absence and presence of protein were acquired at 5°C. The spectra were acquired at low temperature to retard the exchange of the backbone amide protons, as well as to increase the correlation time of the free peptide to produce negative intrapeptide NOEs in the absence of protein[4]. When the NOEs for the free and bound peptide are both negative, the correction for the contribution of the free peptide to the observed NOEs is much easier to accomplish.

TnC.Ca(II)$_4$ was titrated into the TnI peptide NMR sample and the shift of the ^{1}H resonances followed as a function of protein concentration. Figures V-3A → V-3D show one-dimensional spectra of the TnI peptide in the absence and the presence of 0.1 molar equivalents TnC.Ca(II)$_4$. Figure V-3A shows a portion of the aliphatic upfield region of the spectrum. Figure V-3B shows the complete downfield region of the spectrum with the exchangeable guanidinium resonances of R108, R112, R113 and R115, the aromatic F106 resonances, the C-terminal NH group, and the backbone amide resonances. Figures V-3C and V-3D show expanded regions of Figure V-3B. Figure V-3C shows the backbone amide protons and the C-terminal NH group, and Figure V-3D shows an expanded region of the backbone amide protons. One can see that the resonances of the TnI peptide experience some line broadening and change in chemical shift position, but δ_{obs} and Δv_{obs} are dominated by the free ligand population for $p_F >> p_B$ (see Eqns. 2 and 3). Figures V-4A → V-4C show plots of the change in chemical shift ($\Delta\delta$) of the peptide backbone amide proton resonances as a function of molar equivalents of TnC.Ca(II)$_4$ (see Table V-10 in the Appendix). All amides were observed to titrate downfield, but those amides observed to undergo the greatest shift during the titration belong to K105, F106, R115 and the C-terminal NH group (see Table V-2). The shifts indicate that the amides of these residues are sensing a new chemical environment in the bound peptide due either directly to interactions between the peptide and the protein, or to a new conformation of the peptide when it is bound to the protein. The shift of all resonances was observed to be in fast exchange (Campbell *et al.*, 1991; Chapter IV).

---

[4] At room temperature, the NOESY spectrum of the peptide in the absence of protein displayed weak positive cross-peaks.

Figure V-5 shows the upfield region of the DQFCOSY spectrum and Figure V-6 the upfield region of the TRNOESY spectrum of the TnI peptide in the presence of 0.1 molar equivalents TnC.Ca(II)$_4$. Figure V-7 shows the αCH-βCH region, and Figure V-8 shows the downfield-βCH region of the of the TRNOESY spectrum. An interesting cross-peak which defines the hydrophobic core of the peptide when bound to TnC is the F106δ,ξCH2ςCH-V114(γCH3)2 interaction highlighted in Figure V-8. Figure V-9 shows the αCH-NH region of the DQFCOSY spectrum, and Figure V-10 the same region in the TRNOESY spectrum.

Figure V-11 shows the αCH-NH region of the NOESY spectrum of the TnI peptide superimposed upon the αCH-NH region of the TRNOESY spectrum of the same concentration TnI peptide in the presence of 0.1 molar equivalents TnC.Ca(II)$_4$ to TnI peptide. One can see the emergence of new peptide αCH-NH cross-peaks in the presence of protein, a function of the faster cross-relaxation rate between protons in the bound peptide versus the free peptide. A NOESY spectrum of just the TnC protein in the presence of Ca(II) allowed us to dismiss the possibility of these new cross-peaks being either protein-protein or protein-peptide NOEs (data not shown). The emergence of the new set of cross-peaks in the presence of protein is due not only to the longer bound correlation time experienced by the peptide when bound to protein, but also to a new bound peptide conformation for the bound peptide. Binding to TnC.Ca(II)$_4$ induces secondary structure in the TnI peptide. The peptide NOEs present in the absence of protein are only sequential ($d_{\alpha N\,i,i+1}$), and these are not indicative of secondary structure. However, in the presence of 0.1 molar equivalents TnC.Ca(II)$_4$ to TnI peptide, the same sequential NOEs, now more aptly called TRNOEs, have grown in intensity, and longer range TRNOEs ($d_{\alpha N\,i,i+2}$, $d_{\alpha N\,i,i+3}$) are observable, indicative of defined secondary structure in the bound peptide conformation. Notice, for example, that in the absence of protein, the G104αCH2-K105NH cross-peak is extremely weak, much weaker than any of the other sequential cross-peaks in the spectrum. Whereas in the presence of protein, the G104αCH2-K105NH cross-peak has grown in intensity relative to the other cross-peaks, and a G104αCH2-F106NH has emerged (a higher vertical scale would reveal a G104αCH2-R108NH cross-peak). The emergence of new cross-peaks at the N-terminus is indicative of the development of secondary structure, whereas the increase in the relative intensity of cross-peaks at the N-terminus suggests a decreased motional freedom at the N-terminus of the bound TnI peptide. Notice also the difference in the position of the K105αCH-F106NH cross-peak in the absence and presence of protein. This is because the peptide F106NH titrates downfield with the addition of protein (see Figure V-3D and Table V-2).

The ^{13}C NMR spectra of the TnI peptide in the absence of TnC.Ca(II)$_4$ (data not presented) show the X-P109-P110-X segment of the peptide to be in an all-trans conformation. Keim *et al.* (1973) have measured ^{13}C NMR chemical shift differences between the trans and cis -G-P- configurations in the pentapeptide G-G-P-G-G. For neutral pH with dioxane as the external standard, the chemical shifts of the Cβ and Cγ carbons were given as $C\beta_{(trans)}$=30.6 ppm, $C\beta_{(cis)}$=33.1 ppm, $C\gamma_{(trans)}$=25.5 ppm, $C\gamma_{(cis)}$ 23.2 ppm. Thus, the $C\beta_{(trans)}$ carbon resonates approx. 2.5 ppm downfield of the $C\beta_{(cis)}$ carbon and the $C\gamma_{(trans)}$ carbon resonates approx. 2.3 ppm upfield of the $C\gamma_{(cis)}$ carbon. The chemical shifts measured for the TnI peptide at neutral pH and room temperature with dioxane as an external standard were approx. Cβ=30.8 ppm and Cγ=25.5 ppm for both proline residues. Furthermore, no doubling of resonances were observed for any of the residues. The presence of an all-trans peptide conformation is confirmed in the αCH-NH region of the DQFCOSY spectrum of the TnI peptide in the presence of 0.1 molar equivalents TnC.Ca(II)$_4$ (Figure V-9). This region of the spectrum displays one cross-peak for every amino acid (excluding proline which has no NH), with no indication of any cis-trans X-proline peptide bond isomerization which would cause a doubling of peaks (Dyson *et al.*, 1988).

2. Secondary Structure

A summary of the distance restraints is shown in Figure V-12. The pattern of TRNOEs describes two helical regions spanned by residues G104-R108 and R112-R115, interrupted by two central proline residues, P109-P110, which distort the helix. The sequential restraints which help define the helical regions are those between sequential backbone NH residues ($d_{NN\,i,i+1}$). These include contacts between G104NH-K105NH, K105NH-F106NH, K107NH-R108NH, L111NH-R112NH, R112NH-R113NH, R113NH-V114NH and V114NH-R115NH. A close $d_{NN\,i,i+1}$ distance of 2.8 Å is diagnostic of α-helix (Wuthrich, 1986). The distance stretches to 4.3 Å in β-strand. Another medium range restraint which helps in defining the the helical regions is the $d_{\alpha N\,i,i+3}$ close contact and this is observed for G104αCH2-K107NH, K105αCH-R108NH and R112αCH-R115NH. The medium range restraints between the F106δCH2 and ξCH2 aromatic ring protons and the P109βCH2 and γCH2 proline ring protons, and the long range restraint between the F106δCH2 and ξCH2 aromatic ring protons and the L111δCH3 and V114γCH3 methyl protons force a bend around the two central proline residues. This bend allows a closer contact between these side chains not possible if the sequence were completely α-helical. The close proximity of the F106 aromatic ring and the L111δCH3 and V114γCH3 methyl groups defines a tertiary fold and generates a hydrophobic pocket in the short 12 residue sequence of the peptide.

The sequential restraints which define an all trans R108-P109-P110-L111 peptide bond configuration are the contacts between R108αCH-P109δCH2 and P109αCH-P110δCH2. Comparison of cis and trans X-proline configurations shows that the distances between NH_i and αCH_i, $\delta CH2_{i+1}$ and αCH_{i+1} are strongly affected by cis-trans isomerization. The trans form allows close contact between αCH_i and $\delta CH2_{i+1}$ and between NH_i and $\delta CH2_{i+1}$, whereas the cis form allows close contact between αCH_i and αCH_{i+1} and between NH_i and αCH_{i+1} (Wuthrich, 1986).

3. Distance Determination

The basis for the tertiary structure computation consisted of a set of 244 interproton distance restraints comprising 94 intraresidue, 95 sequential ($|i - j| = 1$), 43 medium ($1 < |i - j| \leq 4$) and 12 long ($4 < |i - j| \leq 8$) range interresidue distances. These interproton distances were derived from pure phase absorption two-dimensional TRNOESY spectra recorded with a mixing time of 150 ms and at 0.1 molar equivalents of TnC.Ca(II)$_4$ to TnI peptide. The TRNOE intensities were normalized for the contribution of more than two protons to the cross-peak, and cross-peaks connecting exchangeable amide resonances were corrected for loss of intensity due to exchange or saturation transfer from the decoupled water peak. The normalized and corrected TRNOE cross-peak intensities were then transformed to distance restraints using a collection of reference proton pairs and error limits used to set r_{ij}^U and r_{ij}^L in order to account for systematic over- and under- determinations of r_{ij} (see experimental procedures and Table V-1).

In order to analyze the contribution of mixing time and concentration of TnC.Ca(II)$_4$ protein to the development of the intrapeptide TRNOEs, we performed a series of control experiments. The results of these mixing time and protein concentration control experiments were encorporated into r_{ij} as shifts towards a longer or shorter distance, r_{ij}^o. These shifts in r_{ij} corrected for the effects of indirect cross-relaxation at longer τ_m and higher protein concentrations (see experimental procedures and Table V-1).

When stereospecific assignments of protons were not possible, either due to dynamic effects such as rotation of the hydrogens in a methyl group or flipping of aromatic rings, or due to a degenerate chemical shift of prochiral atoms, pseudoatom representations were used (Wuthrich *et al.*, 1983). Distance restraints to such pseudoatoms were constructed from the position of the neighbouring non-hydrogen atoms by enlarging r_{ij}^U by a value calculated from the geometry of the pseudoatom (Wuthrich *et al.*, 1983).

4. Dihedral Angle Restraints

A set of Φ backbone dihedral angle restraints were derived from $^3J\alpha$CH-NH coupling constants (Pardi *et al.*, 1984) measured from a series of one-dimensional ^{1}H NMR spectra acquired for low concentrations of TnC.Ca(II)$_4$ and extrapolated to the value of $^3J\alpha$CH-NH at 100% bound peptide. A one-dimensional curve fitting program was used to more accurately measure coupling constants in a series of spectra with linewidths that increase with increasing protein concentration. Figures V-13A → V-13C show plots of $^3J\alpha$CH-NH versus molar equivalents TnC.Ca(II)$_4$ to TnI peptide for various residues in the TnI peptide. The set of dihedral angle restraints was comprised of the Φ angles for 9 residues: G104, K105, F106, K107, R108, R112, R113, V114 and R115. For $^3J\alpha$CH-NH < 6.0 Hz, Φ was restricted to the range $-85° \leq \Phi \leq -40°$, and since all measured values of $^3J\alpha$CH-NH were found to be less than 6.0 Hz when extrapolated to 100% bound peptide, all 9 Φ angles in the set of dihedral angle restraints were restricted to $-85° \leq \Phi \leq -40°$. In addition, all peptide bonds, including X-proline, were restricted to $-175° \leq \omega \leq -185°$, in order to maintain trans peptide bond configurations.

5. Supplemental Distance Restraints

Temperature coefficients ($\Delta\delta/\Delta T$) of exchangeable backbone amide protons were measured for three molar equivalents of TnC.Ca(II)$_4$ to TnI peptide (0.0, 0.2 and 0.4). Figures V-14A, V-14B and V-14C show plots of δNH versus temperature for 0.1, 0.2 and 0.4 molar equivalents of TnC.Ca(II)$_4$ to TnI peptide, respectively, and Figures V-15A and V-15B show $\Delta\delta/\Delta T$ versus molar equivalents of TnC.Ca(II)$_4$ to TnI peptide. Clearly, only the backbone amide proton of K107 displays a $\Delta\delta/\Delta T$ value of less than -4 ppb, when this value is extrapolated to 100% bound peptide. Thus, it would appear that the backbone amide proton of K107 is involved in an intrapeptide H-bond, especially since the $\Delta\delta/\Delta T$ is low (-4.7 ppb) in the absence of protein (0.0 molar equivalents), indicating that the protection of this proton from solvent is due to an intrapeptide interaction, as opposed to a peptide-protein interaction. From a knowledge of the secondary structure of the bound TnI peptide, which suggests a helical structure for residues G104-R108, we would predict an H-bond between the carbonyl group of the N-acetyl group and the backbone amide proton of K107, in accordance with the CO $_i$ - NH $_{i+4}$ H-bonding pattern in an α-helix. (We assumed α-helical structure instead of 3_{10}-helical structure, which would have involved a different H-bonding pattern; CO $_i$ - NH $_{i+3}$.) We thus included in the distance restraint file an extra distance restraint between the carbonyl oxygen of the N-acetyl group and the backbone amide proton of K107, and set the upper and lower distance limits as $r_{ij}^U = 3.2$ Å and $r_{ij}^L = 2.8$ Å, a reasonable range for an H-bond donor-acceptor pair. This supplemental distance restraint agrees with the presence of a TRNOE between the N-acetyl CH$_3$ group and the backbone amide proton of R108.

The fact that the other residues do not display protected backbone amide protons does not necessarily contradict our prediction of helical secondary structure in the bound peptide. But it does suggest that the secondary structure present in the bound peptide is probably not present in the free structure. That the backbone amide proton of K107 appears protected is probably due to residual structure in the N-terminus of the free peptide.

6. Molecular Dynamics Calculations

We performed two separate MD simulations to determine the structure of the TnI peptide bound to TnC.Ca(II)$_4$. The first simulation started from an α-helical set of input coordinates and the second simulation from a β-strand set of input coordinates (see experimental procedures for details of these simulations). The coordinates of these structures are given in Table V-11 in the Appendix and have been deposited in the

BIOMAGRES BANK for protein NMR data in Madison, Wisconsin. Table V-12 in the Appendix compares the distances between proton pairs given in the distance restraint file with those actually measured between the same proton pairs in the final structures. There are no distance violations greater than 1.7 Å for either the structure generated from the α-helix (structure 1) or the β-strand (structure 2).

Figure V-16 shows the a stereo structure of the bound TnI peptide derived from α-helical coordinates (structure 1). (Figure V-17 shows a photograph of a space-filled CPK model of the structure in Figure V-16). Following 12 ps of MD, the coordinates of 10 MD structures taken every 0.2 ps were averaged and the averaged coordinates were energy minimized to produce the final structure in the Figure V-16 (and Figure V-17)[5]. Figure V-18 shows a superposition of these 10 structures.

Table V-3 presents two sets of dihedral angle values, one set describing structure 1 and one set describing structure 2. Backbone Φ, Ψ and ω dihedral angles for all residues in the bound structures are given, as well as the side chain χ dihedral angles for the proline residues. The dihedral angles given for structure 1 agree reasonably well with the dihedral angles given for structure 2. The Φ, Ψ values describe a helical structure[6] for residues G104-R108 and L111-R115 and are in the range of $-70° \leq \Phi \leq -57°$ and $-66° \leq \Psi \leq -12°$. For P109 and P110, the Φ, Ψ angles break the helical stretch with values in the range of $-80° \leq \Phi \leq -50°$ and $154° \leq \Psi \leq 179°$ for both prolines. There are steric constraints on the conformation of the proline rings. The first proline, P109, displays a Cβ exo ring pucker in both structures (defined by $\chi^1 = 20°$, $\Phi = -80°$ for structure 1 and $\chi^1 = 22°$, $\Phi = -69°$ for structure 2); and the second proline, P110, displays a Cγ exo ring pucker in both structures (defined by $\chi^1 = -9°$, $\Phi = -78°$ for structure 1 and $\chi^1 = -27°$, $\Phi = -59°$ for structure 2). All peptide bonds in the final structures are trans. An iterative relaxation matrix analysis method for structure refinement of the bound TnI peptide structure, encorporating models for internal motion, will be presented in Chapter X.

---

[5] The inclusion of the H-bond restraint between the carbonyl oxygen of the N-acetyl CH3 group and the backbone amide proton of K107 did not bias the generation of the bound TnI peptide structure toward α-helical dihedral space. The final structures arrived at the same Φ,Ψ values reguardless of whether or not the H-bond restraint was included in the distance restraint file.

[6] α-helix is described by Φ,Ψ values of -58°,-47°; 3_{10}-helix is described by Φ,Ψ values of -76°,-5°; and Π-helix is described by Φ,Ψ values of -57°,-70° (Ghelis and Yon, 1982).

E. Discussion

TnC and the structurally homologous protein calmodulin (CaM) belong to the helix-loop-helix (HLH) Ca(II)-binding protein family (Kretsinger, 1980). The x-ray structures of avian skeletal TnC (Sundaralingam *et al.*, 1985; Herzberg and James, 1985) and CaM (Babu *et al.*, 1988) have been solved and reveal a dumbbell-shaped molecule with N-terminal and C-terminal globular domains joined by a long helical linker. Each major domain contains two HLH Ca(II) binding sites based on the EF hand motif (Kretsinger and Nockolds, 1973; Collins *et al.*, 1973; Vanaman *et al.*, 1977). The N- and C- terminal globular domains of TnC and CaM have large hydrophobic patches (Kretsinger *et al.*,1986; Babu *et al.*, 1988) flanked by regions of negative electrostatic potential, optimally designed as binding sites for basic, amphiphilic helices. There is evidence to suggest that Ca(II) binding to these proteins leads to the increased exposure of these hydrophobic surfaces which then become the sites for the interaction of target molecules (Laporte *et al.*, 1980; Gariepy and Hodges, 1983; Cachia *et al.*, 1985). Although the separate contributions of the hydrophobic and electrostatic forces to the energy of binding have not been determined, it is clear that both are involved. There is also mounting evidence to suggest that the amphiphilicity of helices on the target molecules play a crucial role in the binding interaction (Cox *et al.*, 1985; DeGrado *et al.*, 1985; McDowell *et al.*, 1985; Erickson-Viitanen *et al.*, 1987).

TnC and CaM bind a variety of naturally occurring extracellular peptides (Haberman and Jentsch, 1967; Malencik and Anderson 1982, 1983a, 1983b, 1984; Compte *et al.*, 1983; Cox *et al.*,1985), most of them positively charged amphiphilic helices. Binding typically occurs with high affinity ($K_d = 10^{-8} - 10^{-9}$ M). Solution CD and NMR studies involving β-endorphin (Malencik and Anderson, 1983a), mastoparan (Malencik and Anderson, 1983a, 1983b; McDowell *et al.*, 1985; Cachia *et al.*, 1986) and melittin (Maulet and Cox, 1983; Cox *et al.*, 1985; Seeholzer *et al.*, 1986) indicate that binding to the complementary surface of CaM leads to an increase in helix content in the peptide. Further evidence comes from the work of DeGrado and co-workers (DeGrado *et al.*, 1985; Erickson-Viitanen *et al.*, 1987) who designed amphiphilic CaM-binding peptides which bound in submicromolar dissociation constants.

The TnI peptide is extremely basic, with four arginines and two lysines (K105, K107, R108, R112, R113 and R115) within a twelve residue sequence. Alternating with these basic residues are hydrophobic ones (F106, L111 and V114). The pattern of alternating basic and hydrophobic residues is interrupted by two sequential proline residues (P109 and P110). Thus, one might expect the TnI peptide to adopt an amphiphilic helical structure, distorted in the center by the proline residues. The TRNOE-derived structure of the TnI peptide bound to TnC.Ca(II)$_4$ reveals two stretches of helical secondary structure spanned by residues G104-R108 and L111-R115, and defined by Φ,Ψ values in the range of $-70° \leq \Phi \leq -57°$ and $-66° \leq \Psi \leq -12°$. Whereas these dihedral angles roughly define α-helical secondary structure (-58°, -47°), they could also equally well define 3_{10}-helical secondary structure (-76°, -5°) or Π-helical secondary structure (-57°, -70°) (Ghelis and Yon, 1982). Therefore, it is not accurate to describe portions of the TnI peptide as being α-helical in structure, only 'helix-like', which allows for a wider range of helical secondary structure.

The helical stretches are interrupted around the two proline residues where the Φ,Ψ values are approximately -70°, -170°. The tertiary fold around the P109-P110 sequence brings the residues on the hydrophobic face of the TnI peptide into closer proximity than would otherwise be observed if the helix were straight. The ring protons of F106 are close enough to the γ-methyl protons of V114 to allow the observation of a TRNOE cross-peak between these two residues. Thus, not only does the TnI peptide have a hydrophobic face, but it also has a small hydrophobic pocket with the aromatic ring of F106 being somewhat buried by the side chains of L111 and V114. The side chains of the basic residues extend outwards on the hydrophilic face, away from this hydrophobic pocket. Although the bound conformation of the TnI peptide has a hydrophobic pocket and a hydrophilic face, strictly speaking, the tertiary fold around the two central proline residues prevents the structure as being described as an amphiphilic helix, since this implies an uninterrupted α-helical stretch of three turns or more.

One could imagine an interaction of the inhibitory TnI peptide with Ca(II)-saturated TnC which would involve contributions from both hydrophobic and electrostatic groups. The hydrophobic pocket on the TnI peptide could be positioned towards the hydrophobic pocket on the C-terminal domain of TnC, allowing ring stacking between the aromatic ring of F106 on the TnI peptide and the aromatic rings of any number of exposed phenylalanines on the Ca(II)-saturated form of TnC (F105, F151 and F154 are all exposed inside the hydrophobic pocket of TnC in the Ca(II)-bound C-terminal domain of the avian crystal structure). The side chains of L111 and V114 on the TnI peptide could interact with hydrophobic groups lining the pocket of TnC, and the long basic side chains of K105, K107, R108, R112, R113 and R115, which extend off the opposite hydrophilic face of the TnI peptide, could electrostatically interact with a number of acidic groups located around the Ca(II)-binding loops of TnC, or could hydrogen bond with the solvent, as this face of the peptide would probably not be buried by protein.

Strynadka and James (1990) have modeled the interaction of amphiphilic helices with TnC and CaM. Of particular interest is their modeled interaction of mastoparan, an α-helical amphiphilic bee venom, with the C-terminal domain of TnC. The seven hydrophobic residues on the hydrophobic face of mastoparan are modeled as interacting with such groups as I104[7], F105, I121, L122, V129, L137, M157, M158, and V161 in the hydrophobic pocket of TnC. The remaining five basic residues are modeled as either intercting with acidic groups around the Ca(II)-binding loops of TnC (E127, E133, and D136) or as extending out into the solvent.

The interaction between the inhibitory region of intact TnI and TnC is Ca(II)-sensitive. In the absence of Ca(II), the inhibitory region of TnI is bound to actin, whereas the influx of Ca(II) into the myofibril and the subsequent binding of Ca(II) to the Ca(II)-sensitive sites of TnC leads to the presentation of the hydrophobic surfaces on TnC, capable of binding the inhibitory region of TnI and sequestering this region away from actin. The actin is then free to interact with the myosin heads and muscle contraction is initiated (Van Eyk *et al.*, 1991b). We were unable to distinguish between a conformation of the TnI inhibitory peptide bound to apo TnC and one bound to Ca(II)-saturated TnC. The TRNOESY spectrum of the TnI peptide in the presence of apo TnC appeared very similar to the TRNOESY spectrum in the presence of Ca(II)-saturated TnC. This may not have been due so much to an intrinsic lack of Ca(II)-sensitivity in the TnI-TnC interaction as to the low ratio of TnC protein to TnI peptide used relative to the dissociation constant in the experiments.

The issue remains as to the location of binding of the inhibitory TnI peptide to Ca(II)-saturated TnC. Our previous work has shown that binding of the TnI peptide to Ca(II)-saturated TnC occurs with a $K_d = 4.8 \times 10^{-5}$ M using a 1:1 binding model (Campbell *et al.*, 1991; Chapter IV). Our results did not exclude the possibility of a second peptide binding site on Ca(II)-saturated TnC with an affinity 10-20x weaker than that of the first site. Thus, one could envision binding of the TnI peptide to the C-terminal domain of TnC.Ca(II)$_4$, with a much weaker interaction of a second peptide with the N-terminal domain, not unreasonable considering the extensive homology between the two domains. We will examine the location of binding for the TnI peptide to Ca(II)-saturated TnC in Chapter VI.

In conclusion, this chapter has investigated the TRNOE, an extremely useful NMR technique which is applicable to determining the structure of practially any ligand bound to any macromolecule, provided that the ligand binds specifically and with a 1:1

---

[7] This is the chicken amino acid sequence of TnC as published by Wilkinson (1976).

stoichiometry. The present study involving the TRNOE-guided determination of the structure of the inhibitory region of TnI when complexed to whole Ca(II)-saturated TnC has provided a structural framework for the details of this interaction at the molecular level, and has allowed us to probe a fundamental regulatory step in the Ca(II)-mediated regulation of muscle contraction.

Table V-1. Combined shifts in distance restraints from both the mixing time and protein concentration studies for a sample distance (r_{ij} = 3.5 Å).

TmOe cross-peak behaviour	shift in distance restraint	rijo ± β (rij = 3.5 Å)	rijU	rijL
AY	rij - β	3.2 ± 0.3 Å	3.5 Å	2.9 Å
AX	rij	3.5 ± 0.3	3.8	3.2
BY	rij	3.5 ± 0.3	3.8	3.2
BX	rij + β	3.8 ± 0.3	4.1	3.5
CY	rij + β	3.8 ± 0.3	4.1	3.5
CX	rij + 2β	4.1 ± 0.5	4.4	3.8

Table V-2. Chemical shifts for the assigned ^{1}H resonances of Nα-acetyl-TnI(104-115) amide at (a) 5°C in 50 mM KCl, pH 5.5; and at (b) 5°C with 0.1 molar equivalents TnC.Ca(II)$_4$ in 50 mM KCl, pH 6.5.

residue	NH	αCH	βCH	others
G104	(a) 8.389	(a) 3.89		(a) NAcCH3 2.06
	(b) 8.396	(b) 3.89		(b) NAcCH3 2.08
K105	(a) 8.345	(a) 4.21	(a) 1.64	(a) γCH2 1.22, δCH2 1.58, ξCH2 2.93
	(b) 8.356	(b) 4.22	(b) 1.64	(b) γCH2 1.19,1.22, δCH2 1.58, ξCH2 2.91
F106	(a) 8.269	(a) 4.63	(a) (x)2.99,(m)3.15	(a) δCH2 7.25, ξCH2ζCH 7.35
	(b) 8.294	(b) 4.62	(b) (x)2.99, (m)3.13	(b) δCH2 7.25, ξCH2ζCH 7.34
K107	(a) 8.236	(a) 4.29	(a) 1.68	(a) γCH2 1.37, δCH2 1.67, ξCH2 2.98
	(b) 8.239	(b) 4.29	(b) 1.68	(b) γCH2 1.37,1.39, δCH2 1.67, ξCH2 2.98
R108	(a) 8.453	(a) 4.56	(a) 1.72, 1.84	(a) γCH2 1.69, δCH2 3.20
	(b) 8.463	(b) 4.52	(b) 1.72, 1.84	(b) γCH2 1.69, δCH2 3.19
P109		(a) 4.68	(a) (x)1.88, (p)2.36	(a) γCH2 2.04, δCH2 (m)3.65, (m')3.85
		(b) 4.69	(b) (x)1.88, (p)2.37	(b) γCH2 2.04, δCH2 (m)3.65, (m')3.86
P110		(a) 4.42	(a) (x)1.84, (p)2.26	(a) γCH2 2.00, δCH2 (m)3.62, (m')3.77
		(b) 4.41	(b) (x)1.84, (p)2.27	(b) γCH2 2.00, δCH2 (m)3.62, (m')3.78
L111	(a) 8.420	(a) 4.26	(a) 1.64	(a) γCH 1.63, δCH3 0.88, 0.93
	(b) 8.43	(b) 4.26	(b) 1.63	(b) γCH 1.63, δCH3 0.88, 0.93
R112	(a) 8.480	(a) 4.34	(a) 1.75, 1.82	(a) γCH2 1.58, δCH2 3.20
	(b) 8.484	(b) 4.34	(b) 1.75, 1.82	(b) γCH2 1.58, δCH2 3.19
R113	(a) 8.542	(a) 4.36	(a) 1.75, 1.82	(a) γCH2 1.62, δCH2 3.20
	(b) 8.552	(b) 4.36	(b) 1.75, 1.82	(b) γCH2 1.62, δCH2 3.19
V114	(a) 8.413	(a) 4.13	(a) 2.08	(a) γCH3 0.93
	(b) 8.419	(b) 4.11	(a) 2.06	(b) γCH3 0.93
R115	(a) 8.587	(a) 4.27	(a) 1.78, 1.85	(a) γCH2 1.65, δCH2 3.20, NH 7.23, 7.72
	(b) 8.598	(b) 4.27	(b) 1.78, 1.85	(b) γCH2 1.65, δCH2 3.19, NH 7.25, 7.74

Table V-3. Dihedral angle values in the final structure generated from (a) α-helix (structure 1), and (b) β-strand (structure 2). The backbone dihedral angles are defined as $\chi1$: Cα-Cβ-Cγ-Cδ, $\chi2$: Cβ-Cγ-Cδ-N, and $\chi3$: Cγ-Cδ-N-Cα.

residue	Φ	Ψ	ω	$\chi1$	$\chi2$	$\chi3$
G104		(a) -66	(a) 178			
		(b) -62	(b) 176			
K105	(a) -57	(a) -50	(a) 172			
	(b) -63	(b) -41	(b) -175			
F106	(a) -68	(a) -43	(a) 174			
	(b) -66	(b) -41	(b) 171			
K107	(a) -70	(a) -25	(a) -177			
	(b) -71	(b) -12	(b) 177			
R108	(a) -59	(a) -38	(a) 174			
	(b) -50	(b) -44	(b) 169			
P109	(a) -80	(a) 174	(a) 174	(a) 20	(a) -34	(a) 35
	(b) -69	(b) 179	(b) 170	(b) 22	(b) -30	(b) 27
P110	(a) -78	(a) 161	(a) -170	(a) -9	(a) 0	(a) 10
	(b) -59	(b) 154	(b) -172	(b) -27	(b) 26	(b) -14
L111	(a) -59	(a) -23	(a) 172			
	(b) -63	(b) -44	(b) -178			
R112	(a) -66	(a) -43	(a) 177			
	(b) -67	(b) -14	(b) 174			
R113	(a) -69	(a) -36	(a) 171			
	(b) -68	(b) -50	(b) 172			
V114	(a) -58	(a) -43	(a) 174			
	(b) -60	(b) -60	(b) -179			
R115	(a) -65					
	(b) -70					

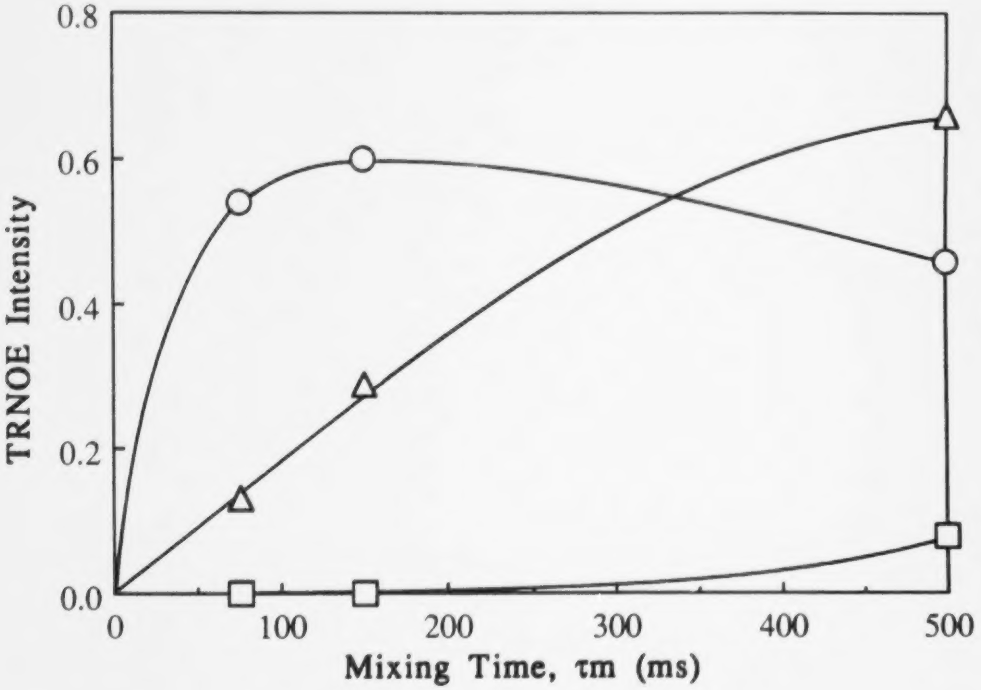

Figure V-1. Plot of intrapeptide ^{1}H-^{1}H TRNOE intensity versus mixing time to illustrate the three types of cross-peak behaviour observed in the mixing time studies @ 0.1 molar equivalents of TnC.Ca(II)$_4$. (○) F106αCH-βCH'(x), 'A' behaviour; (△) F106αCH-δCH2, 'B' behaviour; (□) F106δCH2-P109γCH2, 'C' behaviour.

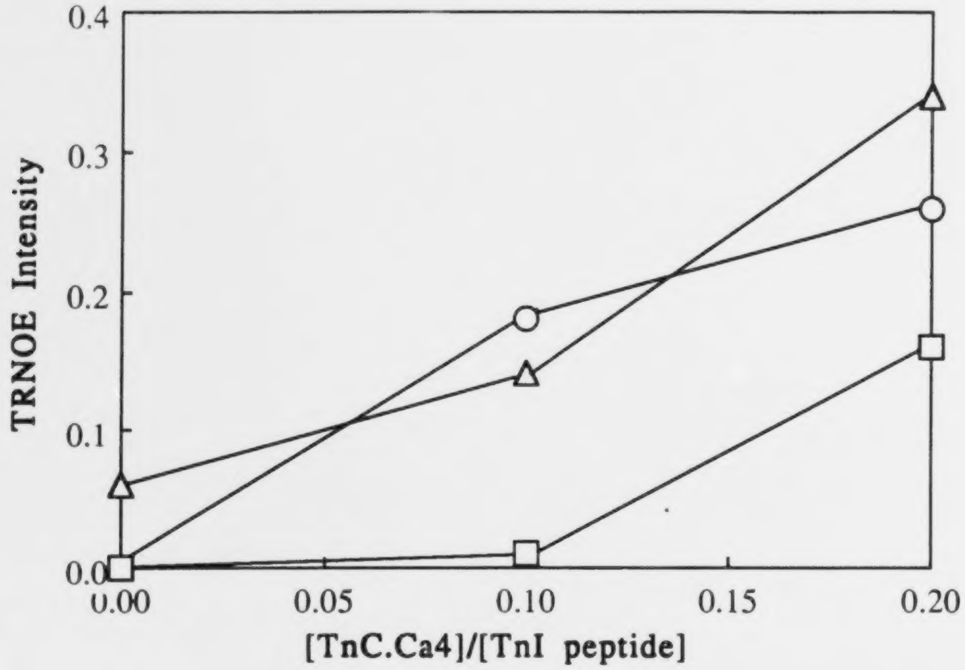

Figure V-2. Plot of intrapeptide ^{1}H-^{1}H TRNOE intensity versus molar equivalents TnC.Ca(II)$_4$ to TnI peptide to illustrate the two types of cross-peak behaviour observed in the protein concentration studies @ τ_m = 150 ms. (○) F106αCH-βCH'(x), 'Y' behaviour; (△) F106αCH-δCH2,'X' behaviour; (□) F106δCH2-P109γCH2, 'Y' behaviour.

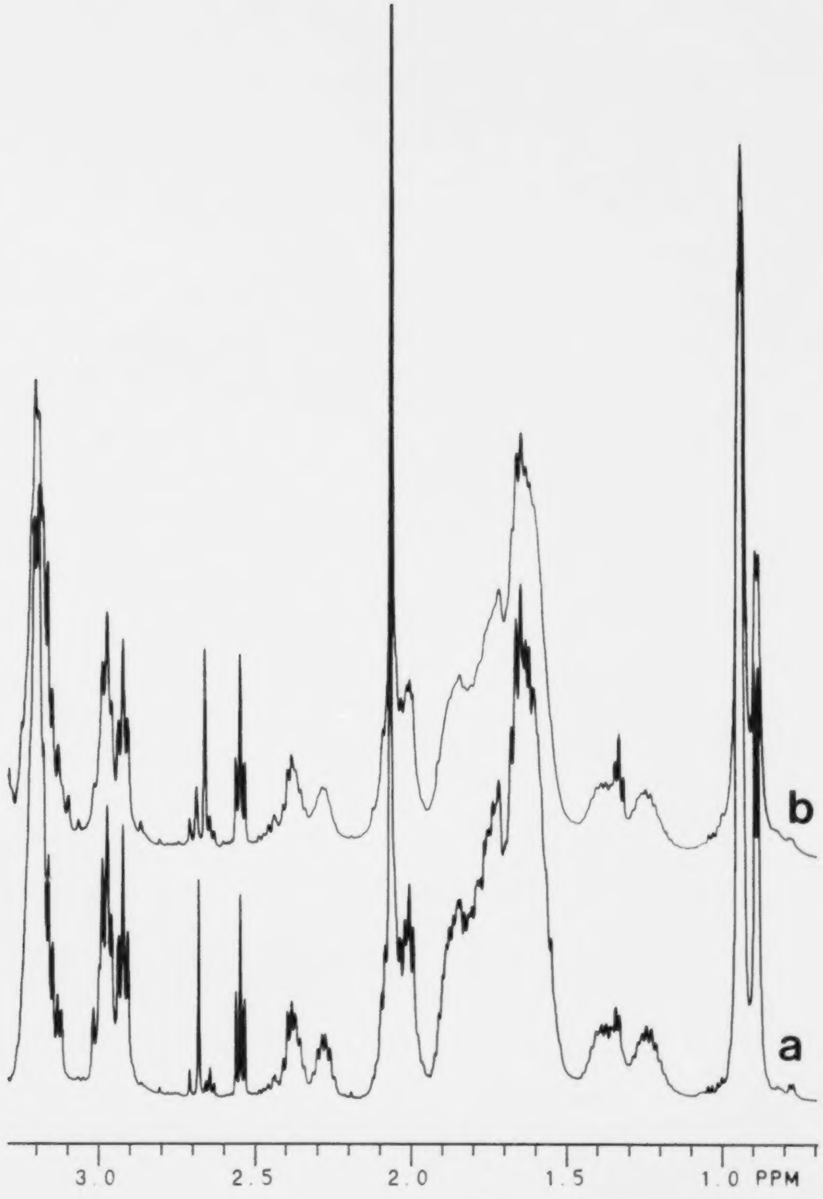

Figure V-3A. 500 MHz ^1H NMR spectra of the TnI peptide in the absence and presence of 0.1 molar equivalents TnC.Ca(II)$_4$: Aliphatic upfield region of the spectrum. **a.** 10 mM Nα-acetyl-TnI(104-115) amide, 50 mM KCl, pH 6.5, 80%H$_2$O/20%D$_2$O, 5°C; **b.** 10 mM Nα-acetyl-TnI(104-115) amide, 1 mM TnC, 4 mM CaCl$_2$, 50 mM KCl, pH 6.5, 80%H$_2$O/20%D$_2$O, 5°C.

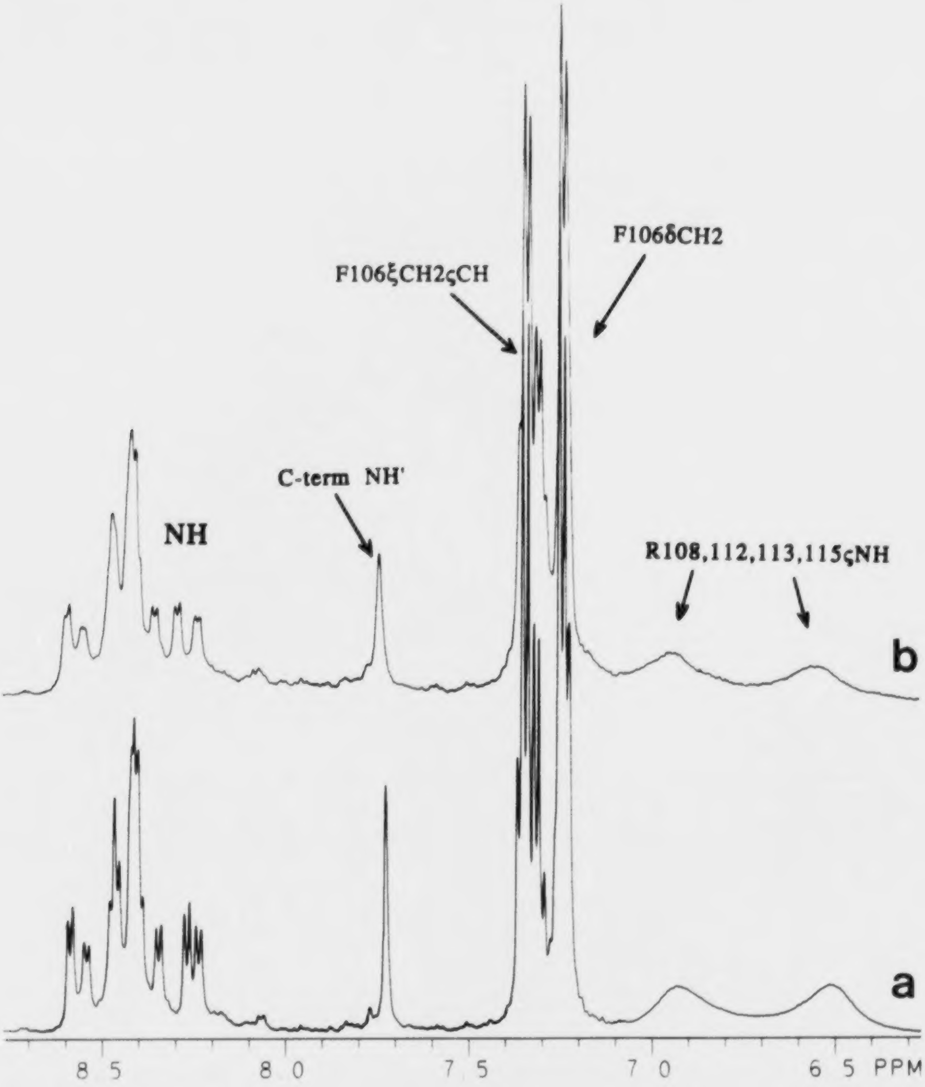

Figure V-3B. 500 MHz ^{1}H NMR spectra of the TnI peptide in the absence and presence of 0.1 molar equivalents TnC.Ca(II)$_4$: Complete downfield region of the spectrum with the exchangeable guanidinium resonances of R108, R112, R113 and R115 and the aromatic F106 resonances. **a.** 10 mM Nα-acetyl-TnI(104-115) amide, 50 mM KCl, pH 6.5, 80%H_2O/20%D_2O, 5°C; **b.** 10 mM Nα-acetyl-TnI(104-115) amide, 1 mM TnC, 4 mM $CaCl_2$, 50 mM KCl, pH 6.5, 80%H_2O/20%D_2O, 5°C.

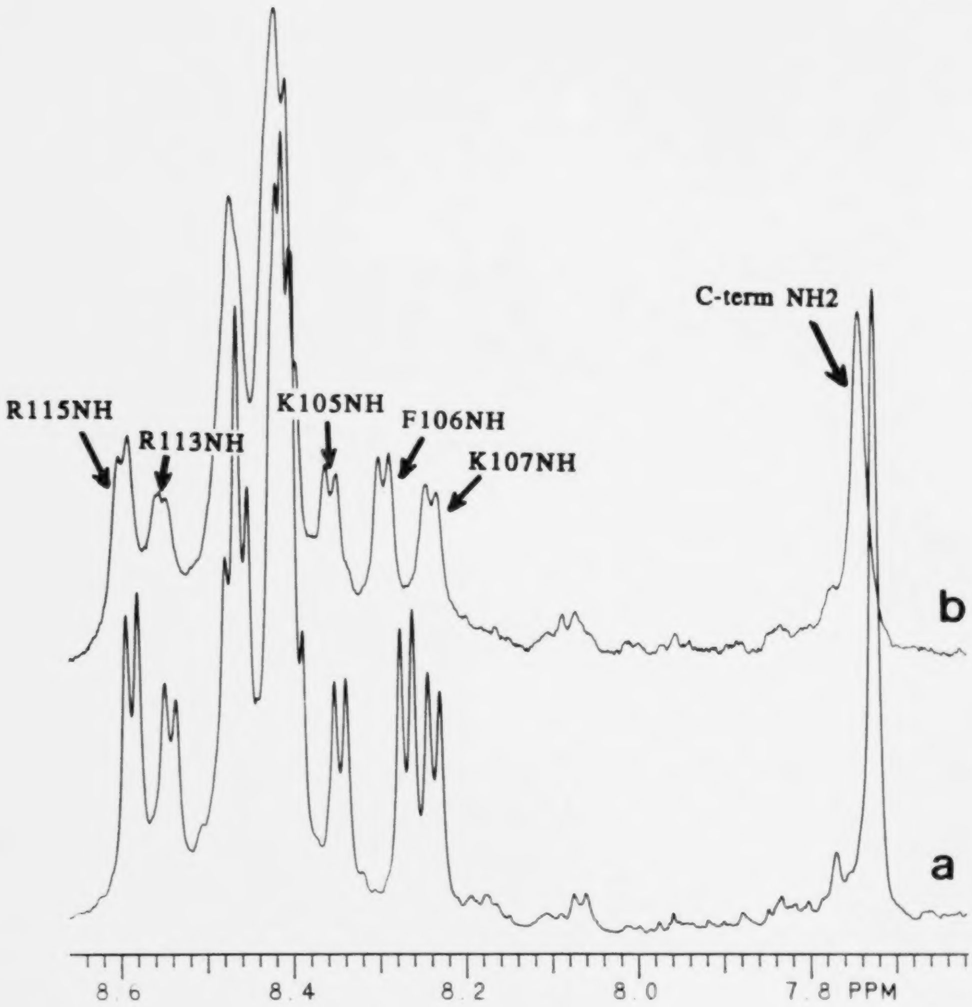

Figure V-3C. 500 MHz ^{1}H NMR spectra of the TnI peptide in the absence and presence of 0.1 molar equivalents TnC.Ca(II)$_4$: Expanded region of spectrum B showing backbone amide proton resonances and the C-terminal NH2 group. **a.** 10 mM Nα-acetyl-TnI(104-115) amide, 50 mM KCl, pH 6.5, 80%H_2O/20%D_2O, 5°C; **b.** 10 mM Nα-acetyl-TnI(104-115) amide, 1 mM TnC, 4 mM $CaCl_2$, 50 mM KCl, pH 6.5, 80%H_2O/20%D_2O, 5°C.

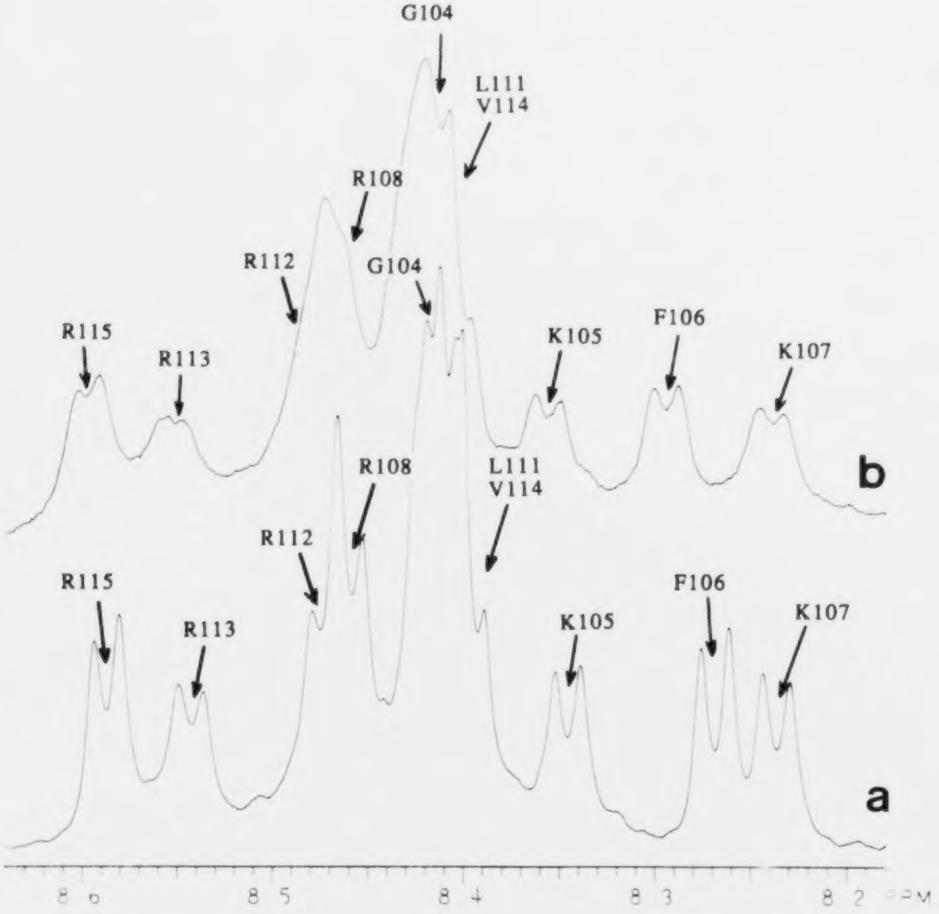

Figure V-3D. 500 MHz ^{1}H NMR spectra of the TnI peptide in the absence and presence of 0.1 molar equivalents TnC.Ca(II)$_4$: Expanded region of spectrum B showing only the backbone amide proton resonances. **a.** 10 mM Nα-acetyl-TnI(104-115) amide, 50 mM KCl, pH 6.5, 80%H$_2$O/20%D$_2$O, 5°C; **b.** 10 mM Nα-acetyl-TnI(104-115) amide, 1 mM TnC, 4 mM CaCl$_2$, 50 mM KCl, pH 6.5, 80%H$_2$O/20%D$_2$O, 5°C.

Figure V-4. Plot of the change in chemical shift of the TnI peptide backbone amide resonances as a function of molar equivalents TnC.Ca(II)$_4$.

A. (○) G104NH; (■) K105NH; (□) F106NH; (●) K107NH.
B. (■) R108NH; (○) L111NH; (●) R112NH.
C.(○) R113NH; (●) V114NH; (■) R115NH; (□) C-term NH.

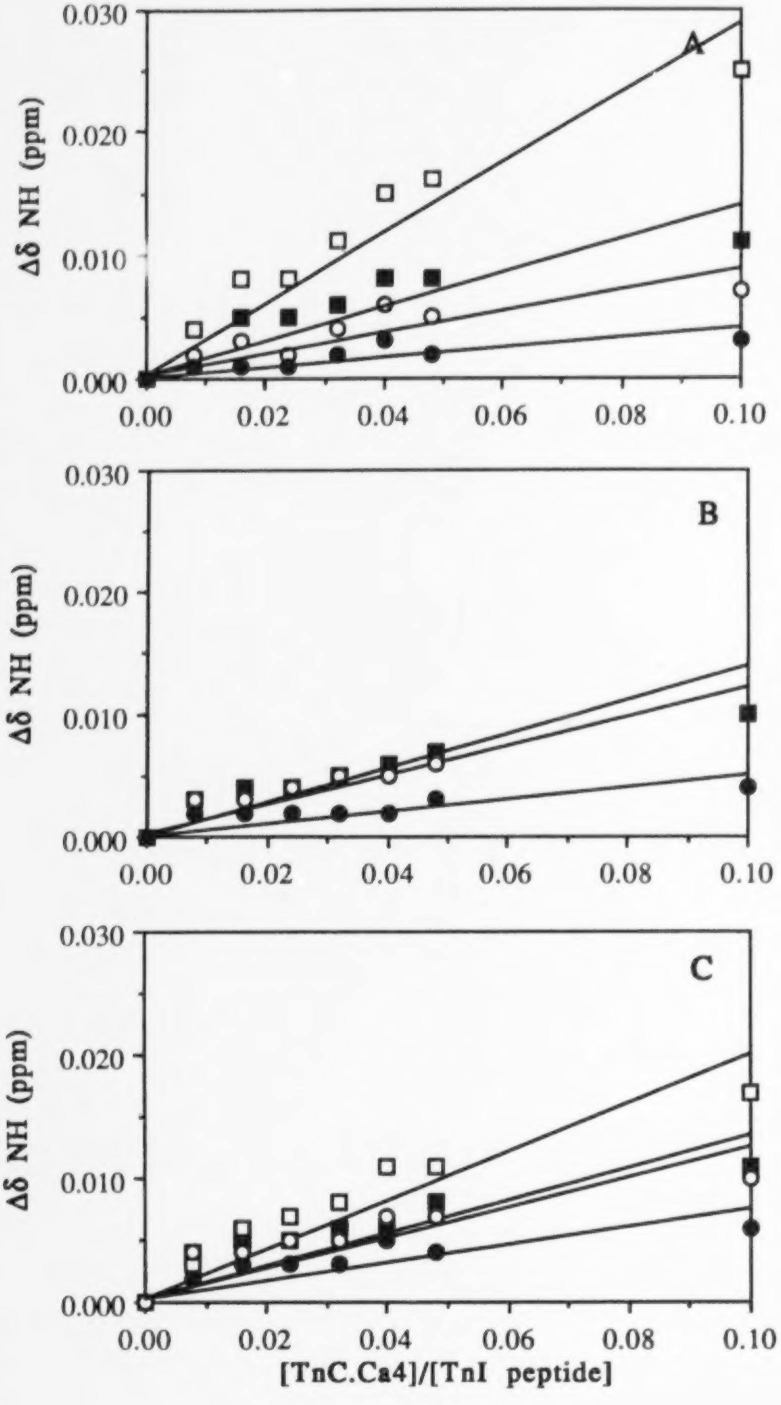
A
B
C
Δδ NH (ppm)
0.000
0.010
0.020
0.030
0.00
0.02
0.04
0.06
0.08
0.10
[TnC.Ca4]/[TnI peptide]

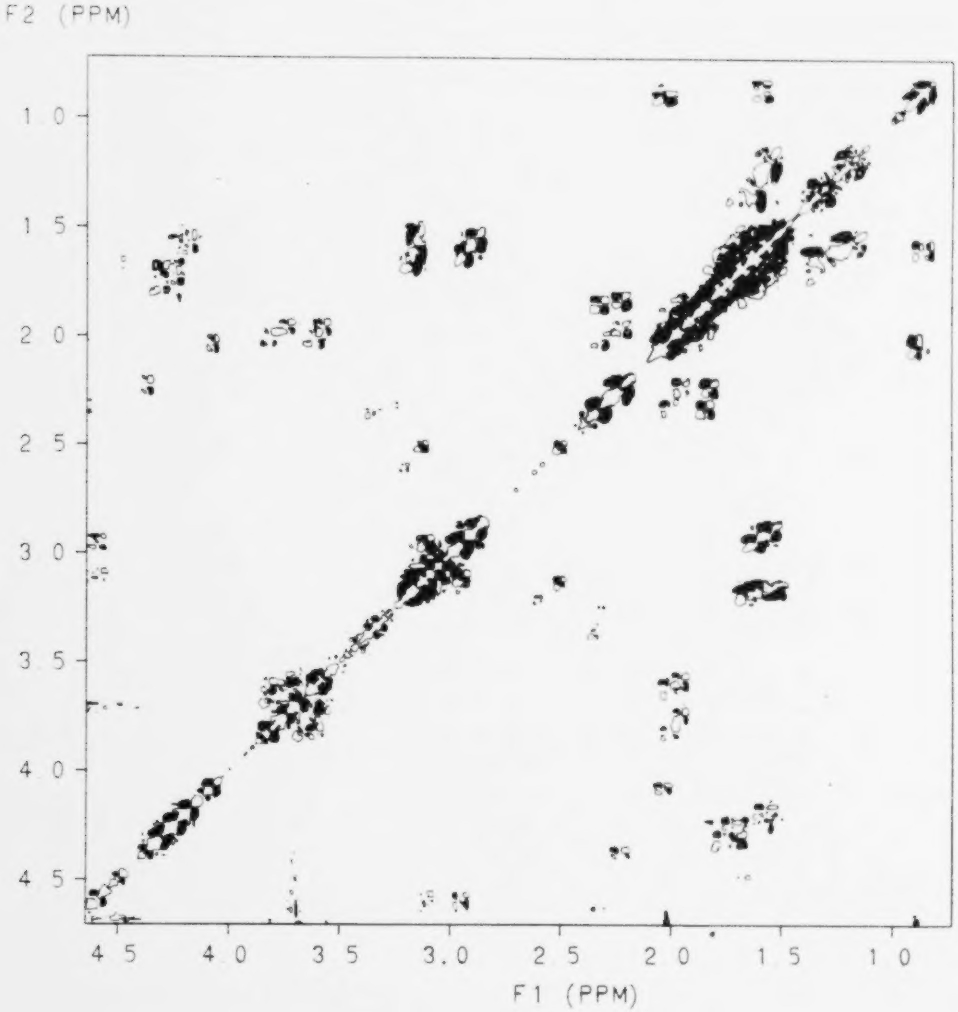

Figure V-5. Upfield region of the DQFCOSY spectrum of the TnI peptide in the presence of 0.1 molar equivalents TnC.Ca(II)$_4$. (10 mM Nα-acetyl-TnI(104-115) amide, 1 mM TnC, 4 mM CaCl$_2$, 50 mM KCl, pH 6.5, 80%H$_2$O/20%D$_2$O, 5°C)

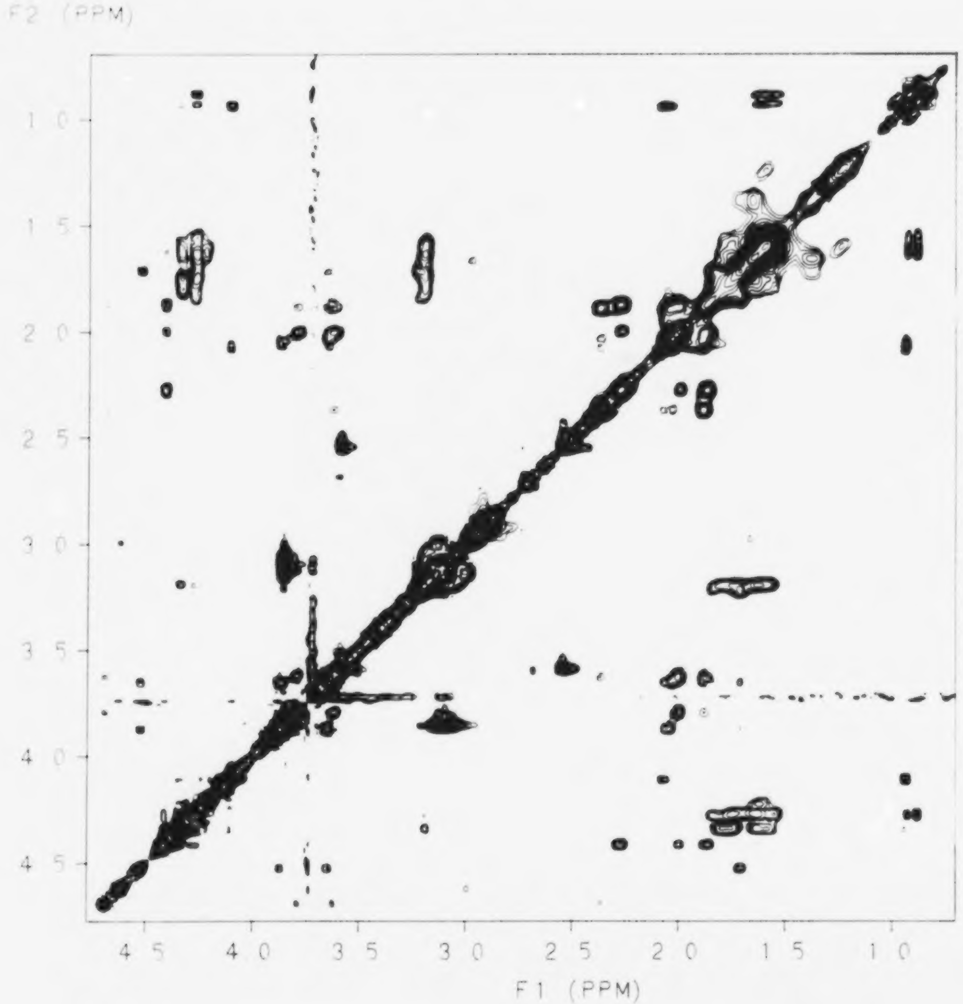

Figure V-6. Upfield region of the TRNOESY spectrum of the TnI peptide in the presence of 0.1 molar equivalents TnC.Ca(II)$_4$. (10 mM Nα-acetyl-TnI(104-115) amide, 1 mM TnC, 4 mM CaCl$_2$, 50 mM KCl, pH 6.5, 80%H$_2$O/20%D$_2$O, 5°C, τ_m = 500 ms)

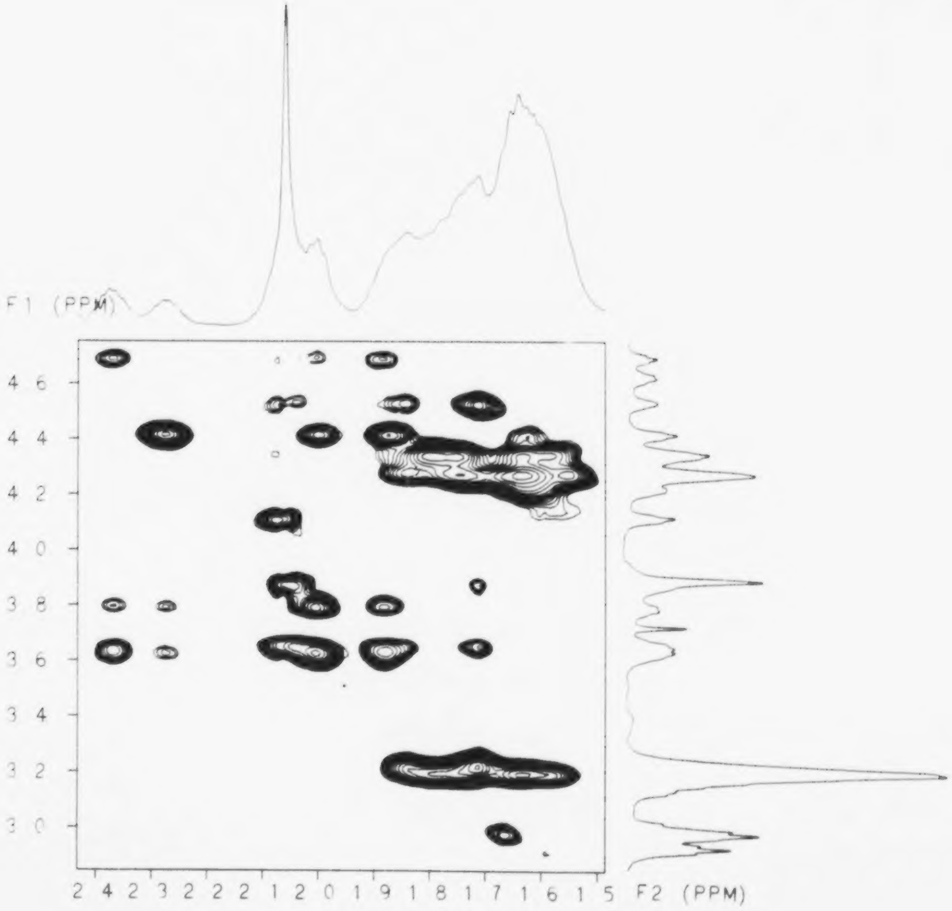

Figure V-7. αCH-βCH region of the TRNOESY spectrum of the TnI peptide in the presence of 0.1 molar equivalents TnC.Ca(II)$_4$. (10 mM Nα-acetyl-TnI(104-115) amide, 1 mM TnC, 4 mM CaCl$_2$, 50 mM KCl, pH 6.5, 80%H$_2$O/20%D$_2$O, 5°C, τ_m = 500 ms)

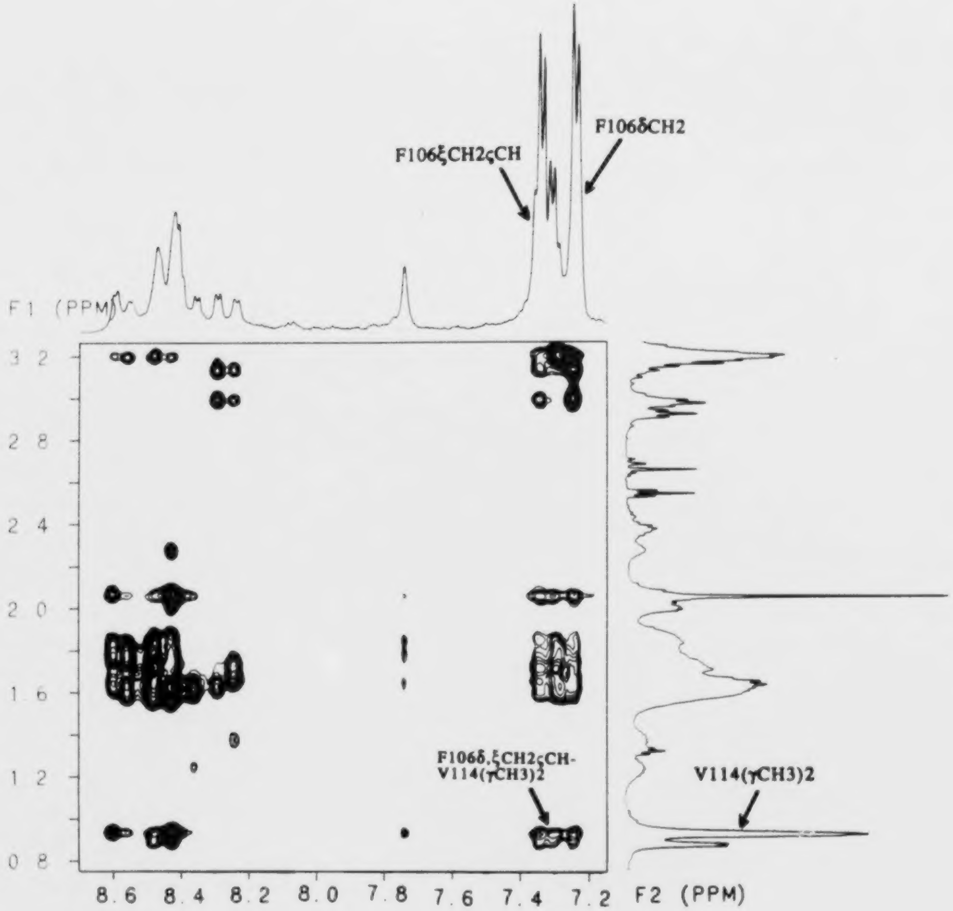

Figure V-8. Downfield-βCH region of the TRNOESY spectrum of the TnI peptide in the presence of 0.1 molar equivalents TnC.Ca(II)$_4$. (10 mM Nα-acetyl-TnI(104-115) amide, 1 mM TnC, 4 mM CaCl$_2$, 50 mM KCl, pH 6.5, 80%H$_2$O/20%D$_2$O, 5°C, τ_m = 500 ms)

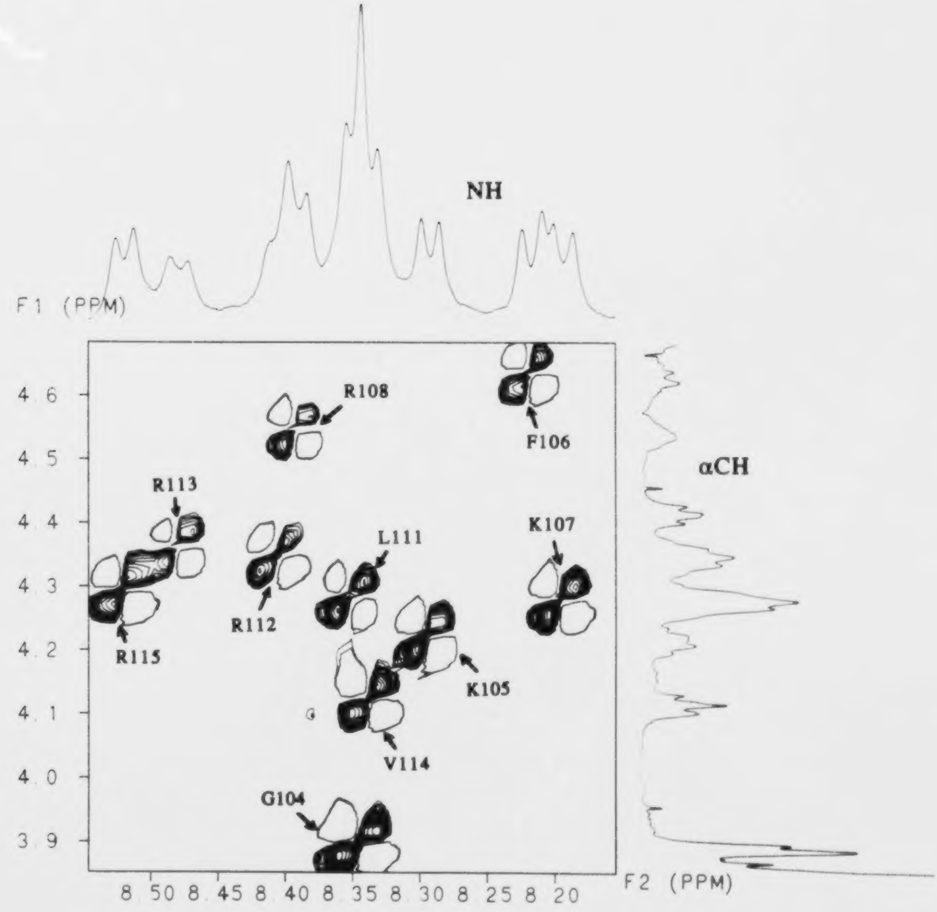

Figure V-9. αCH-NH region of the DQFCOSY spectrum of the TnI peptide in the presence of 0.1 molar equivalents TnC.Ca(II)$_4$. (10 mM Nα-acetyl-TnI(104-115) amide, 1 mM TnC, 4 mM CaCl$_2$, 50 mM KCl, pH 6.5, 80%H$_2$O/20%D$_2$O, 5°C)

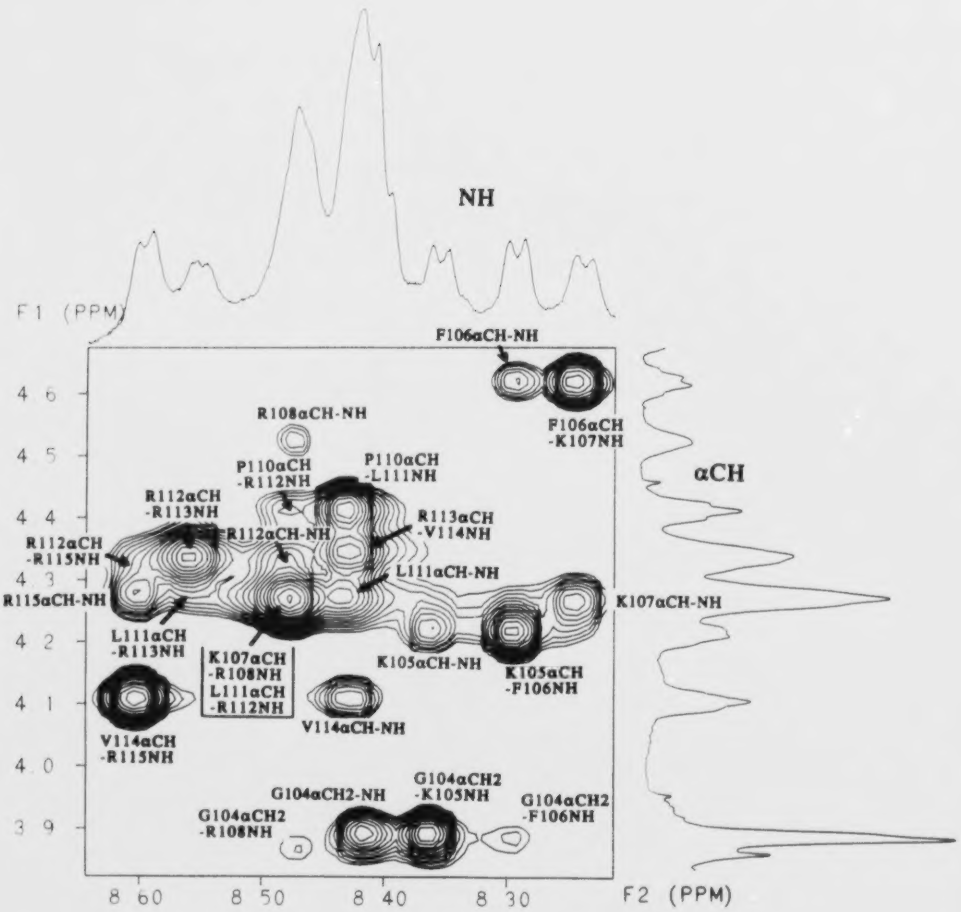

Figure V-10. αCH-NH region of the TRNOESY spectrum of the TnI peptide in the presence of 0.1 molar equivalents TnC.Ca(II)$_4$. (10 mM Nα-acetyl-TnI(104-115) amide, 1 mM TnC, 4 mM CaCl$_2$, 50 mM KCl, pH 6.5, 80%H$_2$O/20%D$_2$O, 5°C, τ_m = 500 ms)

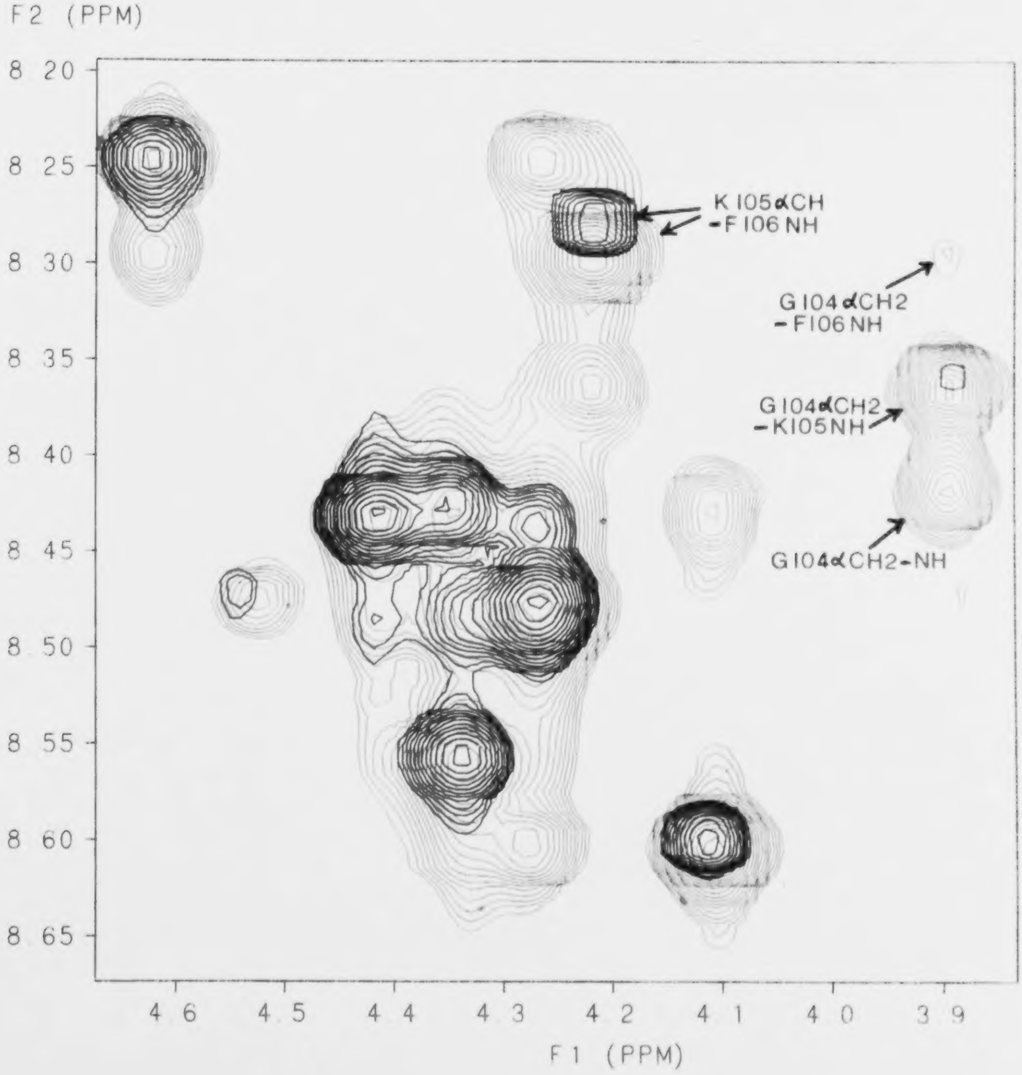

Figure V-11. Fingerprint αCH-NH region of the NOESY spectrum of the TnI peptide (shown in black contours) superimposed upon the αCH-NH region of the TRNOESY spectrum of the same concentration TnI peptide in the presence of 0.1 molar equivalents TnC.Ca(II)$_4$ (shown in red contours). Both spectra are plotted at the same vertical scale. (τ_m = 500 ms)

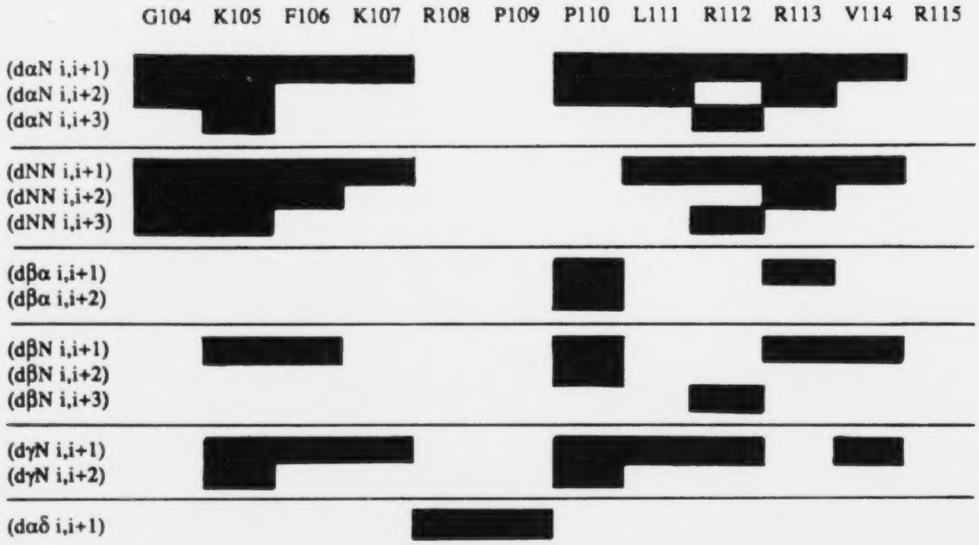

Figure V-12. Sequence of Nα-acetyl-TnI(104-115) amide together with a schematic summary of the short- and medium- range TRNOEs defining the secondary structure of the peptide bound to TnC.

Figure V-13. Plot of $^{3}J\alpha$CH-NH coupling constants versus molar equivalents TnC.Ca(II)$_4$ for various residues in the TnI peptide.

A. (●) G104NH; (○) K105NH; (■) F106NH.

B. (■) K107NH; (●) R108NH; (○) R112NH.

C. (●) R113NH; (■) V114NH; (○) R115NH.

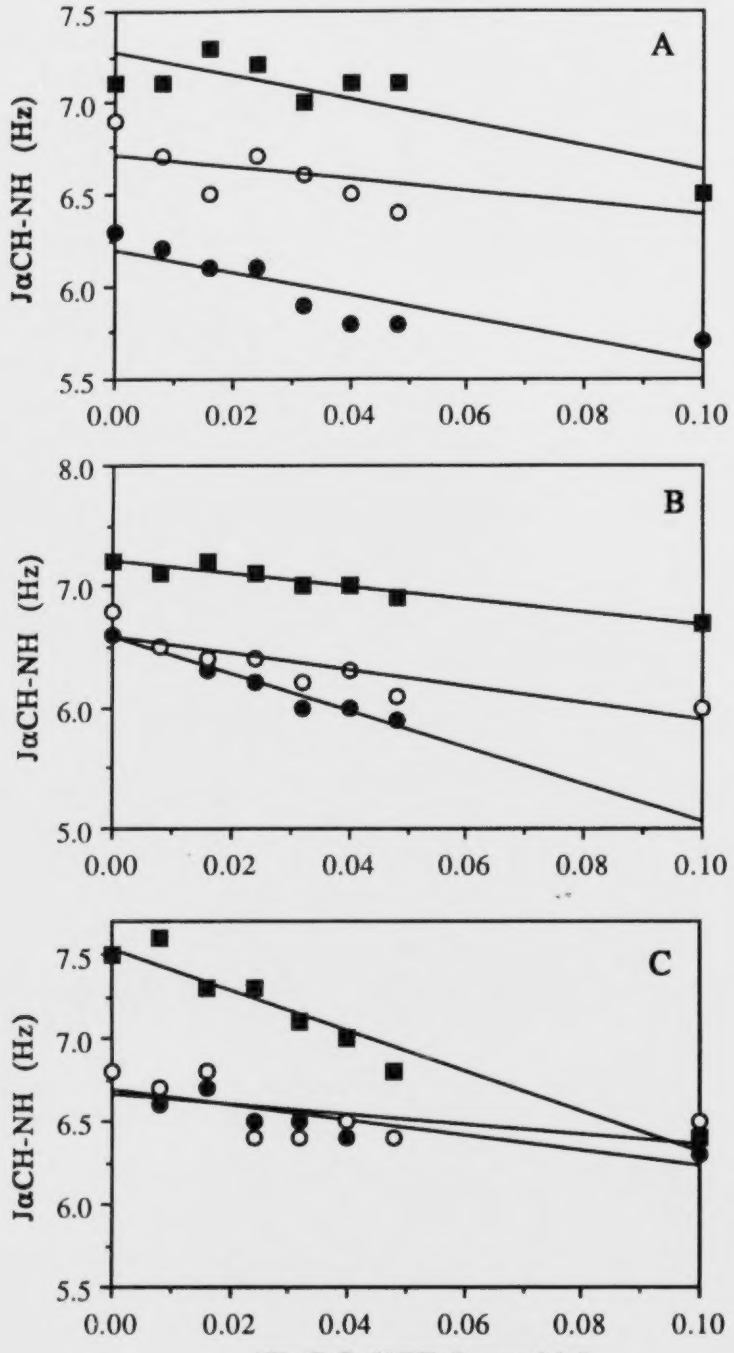
A
B
C
JαCH-NH (Hz)
7.5
7.0
6.5
6.0
5.5
8.0
5.0
0.00
0.02
0.04
0.06
0.08
0.10
[TnC.Ca4]/[TnI peptide]

Figure V-14. Plot of δNH versus temperature for **A.** 0.1 molar equivalents; **B.** 0.2 molar equivalents; and **C.** 0.4 molar equivalents.of TnC.Ca(II)$_4$ to TnI peptide.

A. (+) K105NH; (●) F106NH; (○) K107NH; (△) R108NH;
(▲) R113NH; (□) V114NH; (×) R115NH.

B. (■) G104NH; (●) F106NH; (○) K107NH; (△) R108NH;
(▲) R113NH; (□) V114NH; (×) R115NH.

C. (■) G104NH; (+) K105NH; (●) F106NH; (○) K107NH;
(△) R108NH; (▲) R113NH; (□) V114NH; (×) R115NH.

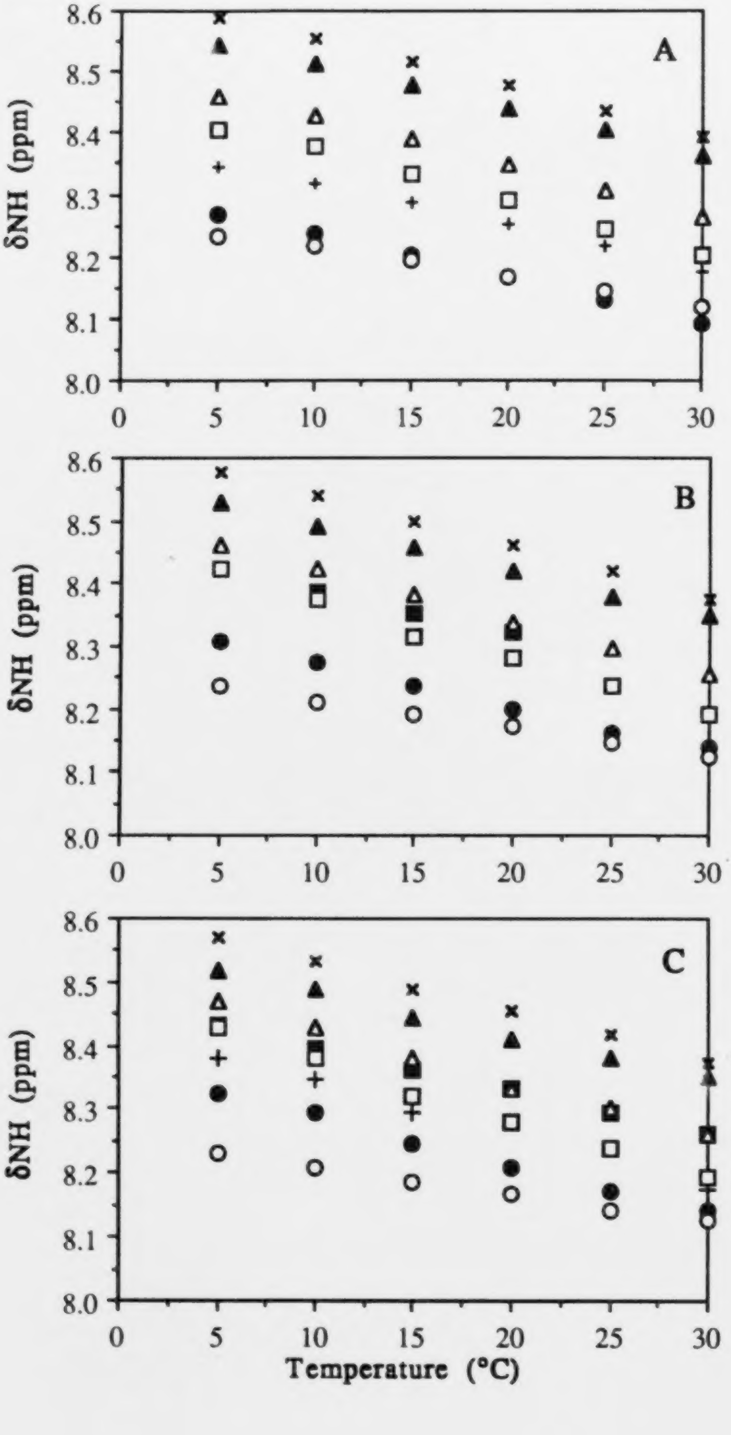A
B
C
δNH (ppm)
8.0
8.1
8.2
8.3
8.4
8.5
8.6
0
5
10
15
20
25
30
Temperature (°C)

Figure V-15. Plot of the temperature coefficients measured for various TnI peptide backbone amide protons versus molar equivalents TnC.Ca(II)$_4$.
A. (○) G104NH; (□) K105NH; (■) F106NH; (●) K107NH.
B. (■) R108NH; (●) R113NH; (□) V114NH; (○) R115NH.

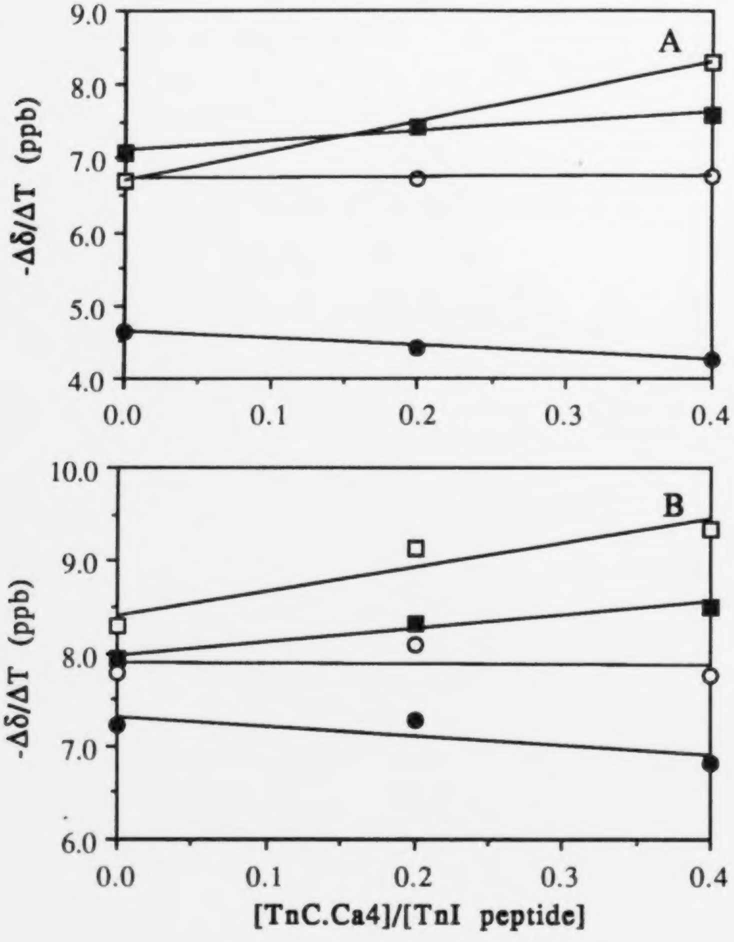
A
B
9.0
8.0
7.0
6.0
5.0
4.0
10.0
-Δδ/ΔT (ppb)
0.0
0.1
0.2
0.3
0.4
[TnC.Ca4]/[TnI peptide]

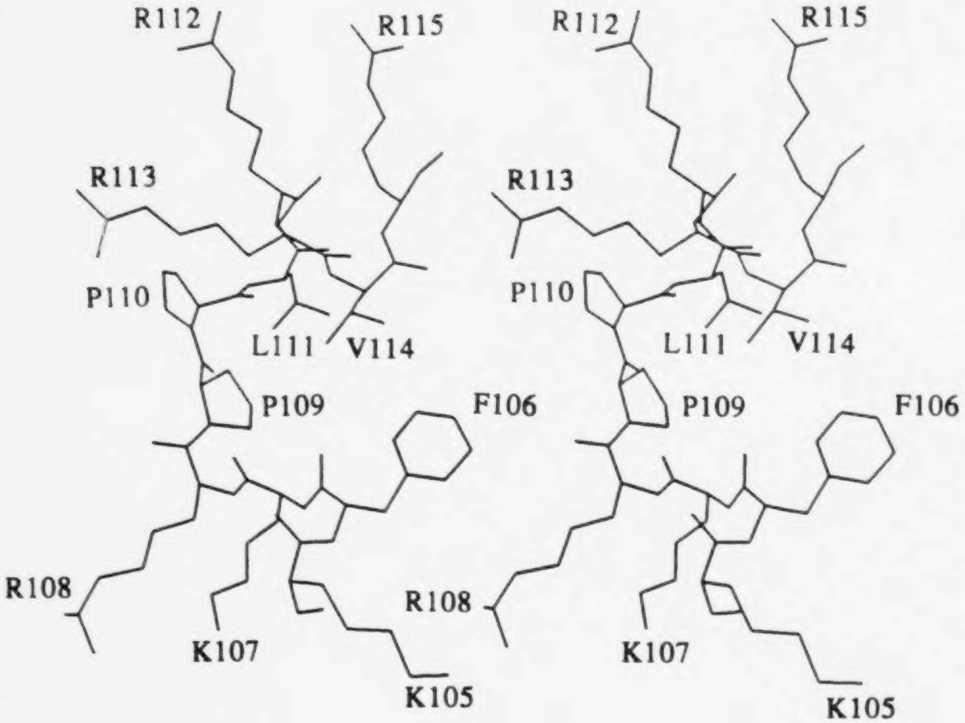
R112
R115
R113
P110
L111
V114
P109
F106
R108
K107
K105
R112
R115
R113
P110
L111
V114
P109
F106
R108
K107
K105

Figure V-16. Stereo-diagram of the TnI peptide bound to Ca(II)-saturated TnC. The final structure was generated from a set of α-helical input coordinates. Following 12 ps of MD, the coordinates of 10 MD structures taken every 0.2 ps were averaged and the averaged coordinates were energy minimized to produce the final structure in the figure.

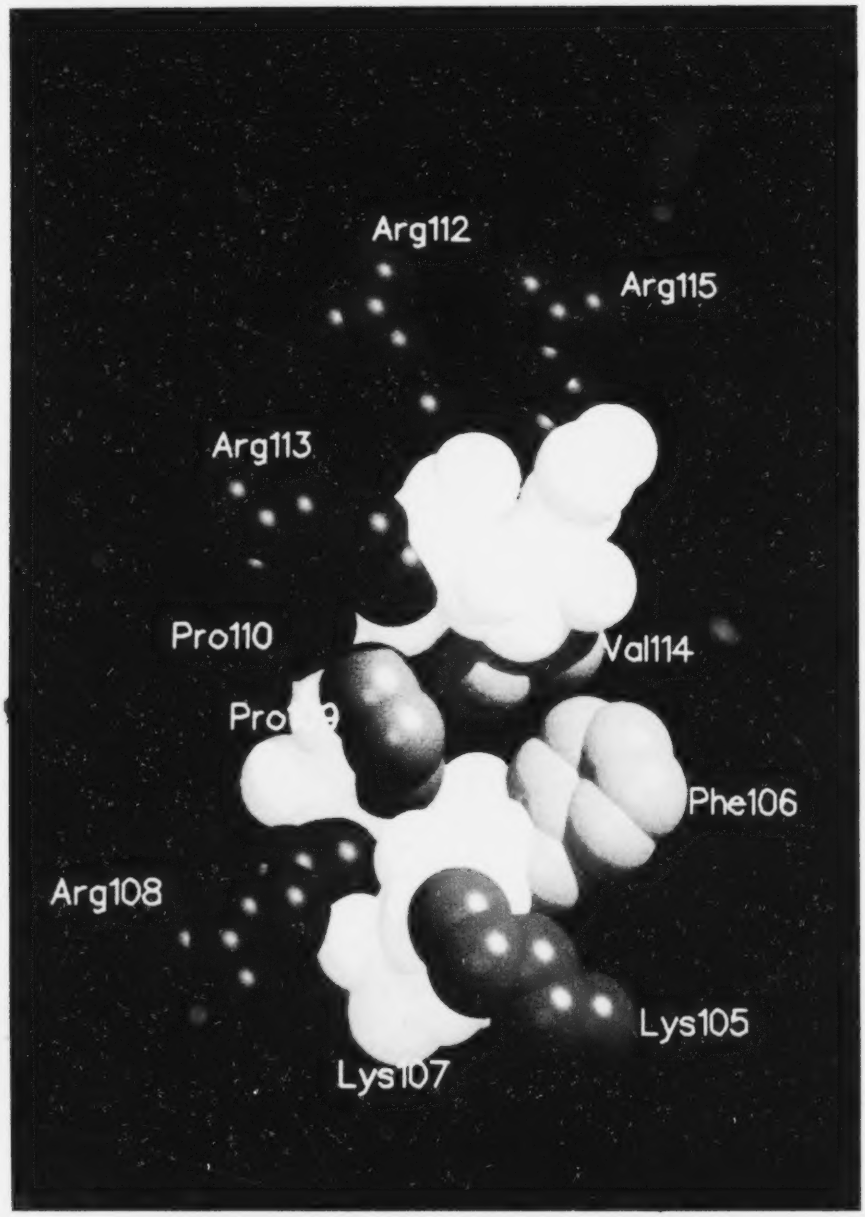
Arg112
Arg115
Arg113
Pro110
Val114
Pro 9
Phe106
Arg108
Lys105
Lys107

Figure V-17. Photograph showing space-filling CPK model of the bound TnI peptide.

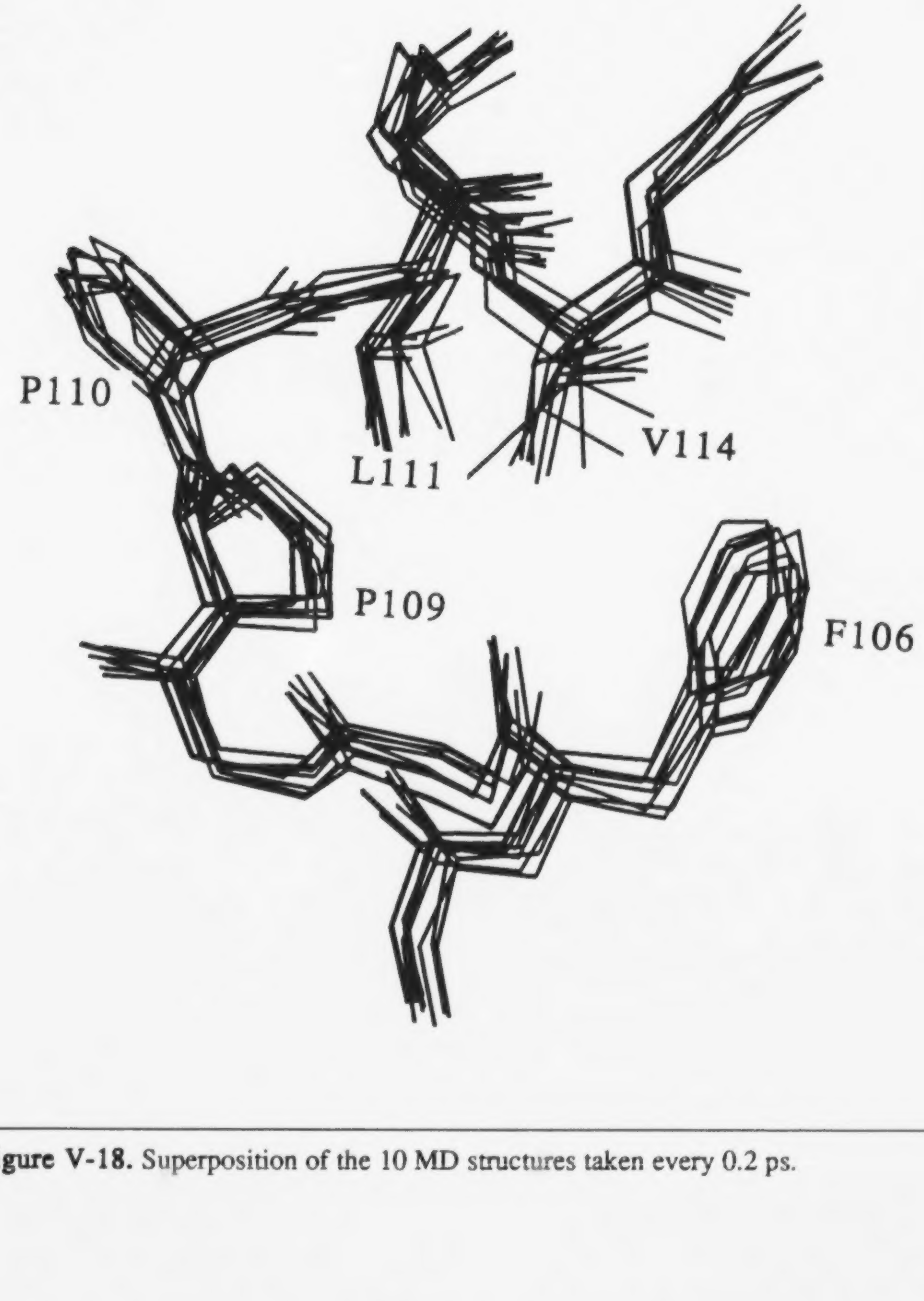
P110
L111
V114
P109
F106

Figure V-18. Superposition of the 10 MD structures taken every 0.2 ps.

F. References

ANDERSEN, N.H., EATON, H.L., and NGUYEN, K.T. 1987. Small molecule conformation in the receptor-bound state by two-dimensional spin exchange experiment. Magn. Reson. in Chem. **25**: 1025-1034.

ANGLISTER, J., LEVY, R.H., and SCHERF, T. 1989. Interactions of antibody aromatic residues with a peptide of cholera toxin observed by two-dimensional transferred nuclear Overhauser effect difference spectroscopy. Biochemistry **28**: 3360-3365.

ANGLISTER, J., and ZILBER, B. 1990. Antibodies against a peptide of cholera toxin differing in cross-reactivity with the toxin differ in their specific interactions with the peptide as observed by ^{1}H NMR spectroscopy. Biochemistry **29**: 921-928.

BABU, Y.S., BUGG, C.E., and COOK, W.J. 1988. Structure of calmodulin refined at 2.2 Å resolution. J. Mol. Biol. **204**: 191-204.

BANERJEE, A., LEVY, H.R., LEVY, G.C., and CHAN, W.W.C. 1985. Conformations of bound nucleoside triphosphate effectors in aspartate transcarbamylase. Evidence for the London-Schmidt model by transferred nuclear Overhauser effects. Biochemistry **24**: 1593-1597.

BELIVACQUA, V.L., THOMSON, D.S., and PRESTEGARD, J.H. 1990. Conformation of methyl β-lactoside bound to ricin B-chain. Interpretation of transferred nuclear Overhauser effects facilitated by spin simulation and selective deuteration. Biochemistry **29**: 5529-5537.

BERENDSEN, H.J.C., POSTMA, J.P.M., VAN GUNSTEREN, W.F., DINOLA, A., and HAAK, J.R. 1984. Molecular dynamics with coupling to an external bath. J. Chem. Phys. **81**: 3684-3690.

BILLETER, M., BRAUN, W., and WUTHRICH, K. 1982. Sequential resonance assignments in protein ^{1}H nuclear magnetic resonance spectra. Computation of sterically allowed proton-proton distances and statistical analysis of proton-proton distances in single crystal protein conformations. J. Mol. Biol. **155**: 321-346.

CACHIA, P.J., SYKES, B.D., and HODGES, R.S. 1983. Calcium-dependent inhibitory region of troponin. A proton magnetic resonance study on the interaction between troponin C and the synthetic peptide Nα-acetyl [F-phenylalanine106] TnI (104-115) amide. Biochemistry **22**: 4145-4152.

CACHIA, P.J., SYKES, B.D., and HODGES, R.S. 1985. Structural studies on calmodulin and troponin C. Phenothiazine, peptide, and protein interactions with calcium-induced helices. In *Calmodulin Antagonist and Cellular Physiology* (Hidaka, H., and Hartshorne, D.J., Eds.), Chapt. 5, pp 63-88, Academic Press, New York.

CACHIA, P.J., VAN EYK, J., INGRAHAM, R.H., MCCUBBIN, W.D., KAY, C.M., and HODGES, R.S. 1986. Calmodulin and troponin C. A comparative study of the interaction of mastoparan and troponin I inhibitory peptide [104-115]. Biochemistry **25**: 3553-3562.

CAMPBELL, A.P., and SYKES, B.D. 1989. Conformation of a troponin I peptide bound to troponin C as determined by ^{1}H NMR. In *Calcium Protein Signalling: Advances in Experimental Medicine and Biology* (Hidaka, H., Ed.), Vol. **255**, pp 195-204, Plenum Press, New York.

CAMPBELL, A.P., CACHIA, P.J., and SYKES, B.D. 1991. Interaction of troponin I and troponin C : ^{19}F NMR studies of the binding of the inhibitory troponin I peptide to turkey skeletal troponin C. Biochem. Cell Biol., in press.

CAMPBELL, A.P., and SYKES, B.D. 1991a. Theoretical evaluation of the two-dimensional transferred nuclear Overhauser effect. J. Magn. Reson. **93**: 77-92.

CAMPBELL, A.P., and SYKES, B.D. 1991b. Effects of internal motions on the development of the two-dimensional transferred nuclear Overhauser effect. J. Biomol. NMR, in press.

CHONG, P.C.S., ASSELBERGS, P.J., and HODGES, R.S. 1983. Inhibition of rabbit skeletal muscle acto S1-ATPase by troponin T. FEBS Lett. **153**: 372-376.

CLORE, G.M., and GRONENBORN, A.M. 1982a. Theory and applications of the transferred nuclear Overhauser effect to the study of the conformations of small ligands bound to proteins. J. Magn. Reson. **48**: 402-417.

CLORE, G.M., and GRONENBORN, A.M. 1983. Theory of the time dependent transferred nuclear Overhauser effect. Applications to structural analysis of ligand-protein complexes in solution. J. Magn. Reson. **53**: 423-442.

CLORE, G.M., and GRONENBORN, A.M. 1982b. Conformation of NAD$^+$ bound to yeast and horse liver alcohol dehydrogenase in solution. The use of the proton-proton transferred nuclear Overhauser enhancement. J. Mol. Biol. **157**: 155-160.

CLORE, G.M., and GRONENBORN, A.M. 1984a. Glucose-6-phosphate dehydrogenase: a transferred nuclear Overhauser enhancement study of NADP$^+$ conformations in enzyme-coenzyme binary complexes. FEBS Lett. **172**: 219-225.

CLORE, G.M., and GRONENBORN, A.M. 1984b. An unusual conformation of NAD$^+$ bound to sorbitol dehydrogenase? A time-dependent transferred nuclear Overhauser effect study. J. Mol. Biol. **172**: 559-572.

CLORE, G.M., and GRONENBORN, A.M. 1984c. Stereochemistry of ATP and GTP bound to fish haemoglobins. A transferred nuclear Overhauser enhancement, ^{31}P nuclear magnetic resonance, oxygen equilibrium and molecular modeling study. J. Mol. Biol. **178**: 731-742.

CLORE, G.M., and GRONENBORN, A.M. 1986. Stereochemistry of binding of the tetrapeptide acetyl-pro-ala-pro-tyr-NH_2 to porcine pancreatic elastase. Combined use of two-dimensional transferred nuclear Overhauser enhancement measurements, restrained molecular dynamics, x-ray crystallography and molecular modeling. J. Mol. Biol. **190**: 259-267.

COLLINS, J.H., POTTER, J.D., HORN, M.J., WILSHIRE, G., and JACKMAN, N. 1973. The amino acid sequence of rabbit skeletal muscle troponin C. Gene replication and homology with calcium-binding proteins from carp and hake muscle. FEBS Lett. **36**: 268-272.

COMPTE, M., MAULET, Y., and COX, J.A. 1983. Ca^{+2}-dependent high affinity complex formation between calmodulin and melittin. Biochem. J. **209**: 269-272.

COX, J.A., COMPTE, M., FILTON, J.E., and DEGRADO, W.F. 1985. The interaction of calmodulin with amphiphilic peptides. J. Biol. Chem. **260**: 2527-2534.

DEGRADO, W.F., PRENGERGAST, F.G., WOLFE, H.R., JR., and COX, J.A., 1985. The design, synthesis, and characterization of tight-binding inhibitors of calmodulin. J. Cell. Biochem. **29**: 83-93.

DESLAURIERS, R., and SMITH, E.C.P. 1980. The multinuclear NMR approach to peptides. Structure, conformations and dynamics. In *Biological Magnetic Resonance* (Berliner, L., and Reuben, J., Eds.), Vol. **2** , pp 243-344, Plenum Press, New York.

DE VLIEG, J., BOELENS, R., SCHEEK, R.M., KAPTEIN, R., and VAN GUNSTEREN, W.F. 1986. Restrained molecular dynamics procedures for protein tertiary structure determination from NMR data: a lac repressor headpiece structure based on information on J-coupling and from presence and absence of NOEs. Israel J. Chem. **27**: 181-188.

DRISCOLL, P.C., CLORE, M.G., BERESS, L., and GRONENBORN, A.M. 1989. Determination of the three-dimensional solution structure of the antihypertensive and antiviral protein BDS-I from the sea anemone *anemonia sulcata.* A study using nuclear magnetic resonance and hybrid distance geometry-dynamical simulated annealing. Biochemistry **28**: 2178-2187.

DYSON, J.H., RANCE, M., HOUGHTEN, R.A., LERNER, R.A., and WRIGHT, P.E. 1988. Folding of immunogenic peptide fragments of proteins in water solution. I. Sequence requirements for the formations of a reverse turn. J. Mol. Biol. **201**: 161-200.

EBASHI, S., and ENDO, M. 1968. Calcium ion and muscle contraction. Prog. Biophys. Mol. Biol. **18**: 123-183.

ERICKSON, B.W., and MERRIFIELD, R.B.1976. Solid-phase peptide synthesis. In *The Proteins*, (Neurath, H., and Hill, R.L., Eds.), Vol. **2**, pp 255-527, Academic Press, New York.

ERICKSON-VIITANEN, S., O'NEIL, K.T., and DEGRADO, W.F. 1987. Theoretical and experimental approaches to the design of calmodulin-binding peptides: A model system for studying peptide/protein interactions. In *Protein Engineering* (Oxender, D.L., and Fox, C.F., Eds.), pp 201-211, Alan R. Liss, Inc., New York.

EHRLICH, R.S., and COLMAN, R.F. 1985. ^{1}H nuclear magnetic resonance studies of the conformation and environment of nucleotides bound to pig heart NADP$^+$-dependent isocitrate dehydrogenase. Biochemistry **24**: 5378-5387.

GARIEPY, J., and HODGES, R.S. 1983. Primary sequence analysis and folding behaviour of EF hands in relation to the mechanism of action of troponin C and calmodulin. FEBS Lett. **160**: 1-6.

GHELIS, C., and YON, J. 1982. In *Protein Folding*, pp 51, Academic Press, New York.

GLASEL, J.A., and BORER, P.N. 1986. NMR studies of flexible opiate conformations at monoclonal antibody binding sites. I. Transferred nuclear Overhauser effects show bound conformations. Biochem. Biophys. Res. Commun. **141**: 1267-1273.

GLASEL, J.A. 1989. Nuclear magnetic resonance studies of flexible opiate conformations at monoclonal antibody binding sites. Quantitative interproton distances obtained from comparing theoretical and experimental transferred nuclear Overhauser enhancement: correlation with antibody sequence. J. Mol. Biol. **209**: 747-761.

GREASER, M.C., and GERGELY, J. 1971. Reconstitution of troponin activity from three protein components. J. Biol. Chem. **246**: 4226-4233.

GRONENBORN, A.M, and CLORE, G.M. 1982. Proton nuclear magnetic resonance studies on cyclic nucleotide binding to the *Escherichia coli* adenosine cyclic 3',5'- phosphate receptor protein. Biochemistry **21**: 4040-4048.

GRONENBORN, A.M, and CLORE, G.M. 1985. Investigation of the solution structures of short nucleic acid fragments by means of nuclear Overhauser enhancement measurements. In *Progress in Nuclear Magnetic Resonance Spectroscopy* (J.W. Emsley, J. Feeney, and L.H. Sutcliffe, Eds.), Vol. **17**, pp 1-32, Pergamon Press, Oxford.

HABERMAN, V.E., and JENTSCH, J. 1967. The amino acid sequence of bee venom melittin. Hoppe-Seylers Z. Physiol. Chem. **348**: 37-50.

HARTSHORNE, D.J., and MUELLER, H. 1968. Fractionation of troponin into two distinct proteins. Biochem. Biophys. Res. Commun. **31**: 647-653.

HERZBERG, O., and JAMES, M.N.G. 1985. Structure of the calcium regulatory muscle protein troponin C at 2.8 Å resolution. Nature **313**: 653-659.

HITCHCOCK, S.E. 1975. Regulation of muscle contraction. Binding of troponin C involved in calcium ion-dependent interaction with troponin I. Eur. J. Biochem. **52**: 255-263.

HODGES, R.S., SEMCHUCK, P.D., TANEJA, A.K., KAY, C.M., PARKER, J.M.R., and MANT, C.T. 1988. Protein design using model synthetic peptides. Peptide Research **1**: 19-29.

HOULT, D.I. 1976. Solvent peak saturation with single phase and quadrature Fourier transformation. J. Magn. Reson. **21**: 337-347.

KEIM, P., VIGNA, R.A., MARSHALL, R.C., and GURD, F.R.N. 1973. Carbon13 nuclear magnetic resonance of pentapeptides of glycine containing central residues of aliphatic amino acids. J. Biol. Chem. **248**: 6104-6113.

KRETSINGER, R.H., and NOCKOLDS, C.E. 1973. Carp muscle-binding protein II. Structure determination and general description. J. Biol. Chem. **248**: 3313-3326.

KRETSINGER, R.H. 1980. Structure and evolution of calcium-modified proteins. CRC Crit. Rev. Biochem. **8**: 119-174.

KRETSINGER, R.H., RUDNICK, S.E., and WEISSMAN, L.J. 1986. Crystal structure of calmodulin. J. Inorg. Biochem. **28**: 289-302.

LANDY, S.B., and RAO, B.D.N. 1989. Dynamical NOE in multiple-spin systems undergoing chemical exchange. J. Magn. Reson. **81**: 371-377.

LAPORTE, D.C., WIERMAN, B.M., and STORM, D.R. 1980. Calcium-induced exposure of a hydrophobic surface on calmodulin. Biochemistry **19**: 3814-3819.

LEAVIS, P.C., and GERGELY, J. 1984. Thin filament proteins and thin filament regulation of vertebrate muscle contraction. CRC Crit. Rev. Biochem. **16**: 235-305.

LEVY, H.R., EJCHART, A., and LEVY, G.C. 1983. Conformations of nicotinamide coenzymes bound to dehydrogenases determined by transferred nuclear Overhauser effects. Biochemistry **22**: 2792-2796.

LEVY, H.R., ASSULIN, O., SCHERF, T., LEVITT, M., and ANGLISTER, J. 1989. Probing antibody diversity by 2D NMR. Comparison of amino acid sequences, predicted structures, and observed antibody-antigen interactions in complexes of two antipeptide antibodies. Biochemistry **28**: 7168-7175.

MACURA, S., and ERNST, R.R. 1980. Elucidation of cross-relaxation in liquids by two-dimensional NMR spectroscopy. Mol. Phys. **41**: 95-117.

MALENCIK, D.A., and ANDERSON, S.R. 1982. Binding of simple peptides, hormones and neurotransmitters by calmodulin. Biochemistry **21**: 3480-3486.

MALENCIK, D.A., and ANDERSON, S.R. 1983a. Binding of hormones and neuropeptides by calmodulin. Biochemistry **22**: 1995-2001.

MALENCIK, D.A., and ANDERSON, S.R. 1983b. High affinity binding of the mastoparans by calmodulin. Biochem. Biophys. Res. Commun. **114**: 50-56.

MALENCIK, D.A., and ANDERSON, S.R. 1984. Peptide binding by calmodulin and its proteolytic fragments and by troponin C. Biochemistry **23**: 2420-2428.

MANT, C.T., BURKE, T.W.L., and HODGES, R.S. 1987. Optimization of peptide separations in reversed-phase HPLC: Isocratic versus gradient elution. Chromatographia **24**: 565-572.

MAULET, Y., and COX, J.A. 1983. Structural changes in melittin and calmodulin upon complex formation and their modulation by calcium. Biochemistry **22**: 5680-5686.

MCDOWELL, L., GUATAM, S., and PREDERGAST, F.G. 1985. Probable role of amphiphilicity in the binding of mastoparan to calmodulin. Biochemistry **24**: 2979-2984.

MEYER, E.F., CLORE, G.M., GRONENBORN, A.M., and HANSEN, H.A.S. 1988. Analysis of an enzyme-substrate complex by x-ray crystallography and transferred nuclear Overhauser enhancement measurements. Porcine pancreatic elastase and a hexapeptide. Biochemistry **27**: 725-730.

MILON, A., MIYAZAWA, T., and HIGASHIJIMA, T. 1990. Transferred nuclear Overhauser effect analyses of membrane-bound enkephalin analogues by ^{1}H nuclear magnetic resonance. Correlation between activities and membrane-bound conformations. Biochemistry **29**: 65-75.

NI, F., KONISHI, Y., FRAZIER, R.B., SCHERAGA, H.A., and LORD, S.T. 1989a. High-resolution NMR studies of fibrinogen-like peptides in solution. Interaction of thrombin with residues 1-23 of the Aα chain of human fibrinogen. Biochemistry **28**: 3082-3094.

NI, F., MEINWALD, Y.C., VASQUEZ, M., and SCHERAGA, H.A. 1989b. High-resolution NMR studies of fibrinogen-like peptides in solution. Structure of a thrombin-bound peptide corresponding to residues 7-16 of the Aα chain of human fibrinogen. Biochemistry **28**: 3094-3105.

NI, F., KONISHI, Y., BULLOCK, C.D., RIVETNA, M.N., and SCHERAGA, H.A. 1989c. High-resolution NMR studies of fibrinogen-like peptides in solution. Structural basis for the bleeding disorder caused by a single mutation of Gly(12) to Val(12) in the Aα chain of human fibrinogen Rouen. Biochemistry **28**: 3106-3119.

NI, F., KONISHI, Y., and SCHERAGA, H.A. 1990. Thrombin-bound conformation of the C-terminal fragments of hirudin determined by transferred nuclear Overhauser effects. Biochemistry **29**: 4479-4489.

OTTING, G., WIDMER, H., WAGNER, G., and WUTHRICH, K. 1986. Origin of t_1 and t_2 ridges in 2D NMR spectra and procedures for suppression. J. Magn. Reson. **66**: 187-193.

PARDI, A., BILLETER, M., and WUTHRICH, K. 1984. Calibration of the angular dependence of the amide proton-Cα proton coupling constants, $^3J_{HN\alpha}$, in a globular protein. J. Mol. Biol. **180**: 741-751.

PARKER, J.M.R., MANT, C.T., and HODGES, R.S. 1987. A practical approach to the preparative purification of peptides using analytical instrumentation with analytical and semipreparative columns. Chromatographia **24**: 832-838.

PERRY, S.V., COLE, H., HEAD, J.F., and WILSON, F.J. 1972. Localization and mode of action of the inhibitory protein component of the troponin complex. Cold Spring Harbor Symp. Quant. Biol. **37**: 251-262.

PIATINI, U., SORENSON, O.W., and ERNST, R.R. 1982. Multiple quantum filters for elucidating NMR coupling networks. J. Am. Chem. Soc. **104**: 6800-6801.

POTTER, J.D., and GERGELY, J. 1974. Troponin, tropomyosin and actin interactions in the Ca^{+2} regulation of muscle contraction. Biochemistry 13: 2697-2703.

RANCE, M., SORENSON, O.W., BODENHAUSEN, G., WAGNER, G., ERNST, R.R., and WUTHRICH, K. 1983. Improved spectral resolution in COSY ^1H NMR spectra of proteins via double quantum filtering. Biochem. Biophys. Res. Commun. **117**: 479-485.

RYCKAERT, J.P., COCCOTTI, G., and BERENDSEN, H.J.C. 1977. Numerical integration of the Cartesian equations of motion of a system with constraints: molecular dynamics of n-alkanes. J. Comput. Phys. **23**: 327-337.

SCHAUB, M.C., and PERRY, S.V. 1969. The relaxing protein system of striated muscle. Biochem. J. **115**: 993-1004.

SEEHOLZER, S.H., COHN, M., PUTKEY, J.A., MEANS, A.R., and CRESI, H.L. 1986. NMR studies of a complex of deuterated calmodulin with melittin. Proc. Natl. Acad. Sci. USA **83**: 3634-3638.

STATES, D.J., HABERKORN, R.A., and RUBEN, D.J. 1982. Two-dimensional nuclear Overhauser experiment with pure phase absorption phase in four quadrants. J. Magn. Reson. **48**: 286-292.

STRYNADKA, N.C.J., and JAMES, M.N.G. 1990. Model for the interaction of amphiphilic helices with troponin C and calmodulin. Proteins **7**: 234-248.

SUNDARALINGAM, M., BERGSTROM, R., STRASBURG, G., RAO, S.T., GREASER, M., and WANG, B.C. 1985. Molecular structure of troponin C from chicken skeletal muscle at 3 Å resolution. Science **227**: 945-948.

TALBOT, J.A., and HODGES, R.S. 1979. Synthesis and biological activity of an icosapeptide analog of the actomyosin ATPase inhibitory region of troponin I. J. Biol. Chem. **254**: 3720-3723.

TALBOT, J.A., and HODGES, R.S. 1981. Synthetic studies on the inhibitory region of rabbit skeletal troponin I. Relationship of amino acid sequence to biological activity. J. Biol. Chem. **256**: 2798-3802.

VANAMAN, T.C., SHARIEL, F., and WATTERSON, D.M. 1977. Structural homology between brain modulator protein and muscle TnCs. In *Calcium-Binding Proteins and Calcium Function* (Wasserman, R.H., *et al.*, Eds.), pp 107-116, Elsevier, Amsterdam.

VAN EYK, J.E., and HODGES, R.S. 1988. The biological importance of each amino acid residue of the troponin I inhibitory sequence 104-115 in the interaction with troponin C and tropomyosin-actin. J. Biol. Chem. **263**: 1726-1732.

VAN EYK, J.E., KAY, C.M., and HODGES, R.S. 1991a. A comparative study of the interactions of synthetic peptides of the skeletal and cardiac troponin I inhibitory region with skeletal and cardiac troponin C. Biochemistry, in press.

VAN EYK, J.E., SONNICHSEN, F.D., SYKES, B.D., and HODGES, R.S. 1991b. Interaction of actin 1-28 with myosin and troponin I and the importance of these interactions to muscle regulation. In *Peptides as Probes in Muscle Research.* (Ruegg, J.C., Ed.), pp 15-31, Springer-Verlag, Heidelberg.

WAGNER, G., BRAUN, W., HAVEL, T.E., SCHAUMANN, T., GO, N., and WUTHRICH, K. 1987. Protein structures in solution by nuclear magnetic resonance and distance geometry. The protein fold of the basic pancreatic trypsin inhibitor determined using two different algorithms, DISGEO and DISMAN. J. Mol. Biol. **196**: 611-639.

WAGNER, G., and WUTHRICH, K. 1982. Sequential resonance assignments in protein ^{1}H nuclear magnetic resonance spectra. Basic pancreatic trypsin inhibitor. J. Mol. Biol. **155**: 347-366.

WEEKS, R.A, and PERRY, S.V. 1978. Characterization of a region of the primary sequence of troponin C involved in calcium ion-dependent interaction with troponin I. Biochem. J. **173**: 449-457.

WILKINSON, J.M. 1976. The amino acid sequence of troponin from chicken skeletal muscle. FEBS Lett. **70**: 254-257.

WILLIAMSON, M.P., and NEUHAUS, D. 1987. Symmetry in NOE spectra. J. Magn. Reson. **72**: 369-375.

WUTHRICH, K., BILLETER, M., and BRAUN, W. 1983. Pseudo-structures for the 20 common amino acids for use in studies of protein conformations by measurements of intramolecular proton-proton distance constraints with nuclear magnetic resonance. J. Mol. Biol. **169**: 949-961.

WUTHRICH, K., WIDER, G., WAGNER, G., and BRAUN, W. 1982. Sequential resonance assignments as a basis for determination of spatial protein structures by high resolution proton nuclear magnetic resonance. J. Mol. Biol. **155**: 311-319.

WUTHRICH, K. 1986. In *NMR of Proteins and Nucleic Acids* , pp 123-128, John Wiley and Sons, New York.

ZOT, A.S., and POTTER, J.D. 1987. Structural aspects of troponin-tropomyosin regulation of skeletal muscle contraction. Annu. Rev. Biophys. Chem. **16**: 535-559.

Chapter VI

Interaction of Troponin I and Troponin C : Identification using NMR of Specific Residues in Skeletal Troponin C which are Involved in the Binding of an Inhibitory Troponin I Peptide.

A. Introduction

Contraction of vertebrate skeletal muscle is regulated by Ca(II) and requires the regulatory proteins troponin and tropomyosin (Ebashi and Endo, 1968). Troponin is a complex of three different protein subunits: Troponin C (TnC) which binds Ca(II), Troponin I (TnI) which binds actin and inhibits actomyosin ATPase, and Troponin T (TnT) which binds to tropomyosin. The Ca(II)-dependent interaction between TnC and TnI is one of the key processes in the activation of contraction in skeletal muscle (for recent reviews, see Zot and Potter, 1987, and Leavis and Gergely, 1984). TnI inhibits the Mg(II)-ATPase activity of acto-myosin ATPase (Hartshorne and Mueller, 1968; Schaub and Perry, 1969; Greaser and Gergely, 1971; Perry *et al.*, 1972) through interactions with both actin and tropomyosin-actin (Potter and Gergely, 1974; Hitchcock, 1975). The inhibition of actomyosin ATPase is neutralized when Ca(II)-saturated TnC forms a 1:1 complex with TnI (Perry *et al.*, 1972; Weeks and Perry, 1978; Chong *et al.*, 1983; Cachia *et al.*, 1986; Van Eyk and Hodges, 1988). This results in potentiation of the ATPase and ultimately in muscle contraction.

Talbot and Hodges (1981) showed, using synthetic peptides, that residues 104-115 of TnI comprise the minimum sequence necessary for inhibition of actomyosin ATPase activity. The synthetic peptide TnI(104-115) possesses tropomyosin specificity (Talbot and Hodges, 1979) and TnC binding capability (Cachia *et al.*, 1983, 1985; Van Eyk and Hodges, 1988; Van Eyk *et al.*, 1991), which results in the release of ATPase inhibition (Cachia *et al.*, 1986; Van Eyk and Hodges, 1988). Thus, it is would appear that residues 104-115 comprise the inhibitory site of TnI and that binding of this region to Ca(II)-saturated TnC leads to a relief of the inhibition of the actomyosin ATPase and ultimately to muscle contraction. We have recently used ^{19}F NMR to study the binding of the synthetic peptide Nα-acetyl [19FPhe106]TnI(104-115) amide to Ca(II)-saturated skeletal turkey TnC, and have obtained the following binding constants; $K_d = (3.7 \pm 3.1) \times 10^{-5}$ M for the apo protein and $K_d = (4.8 \pm 1.8) \times 10^{-5}$ M for the Ca(II)-saturated protein for a 1:1 binding stoichiometry of TnI peptide to TnC protein (Campbell *et al.*, 1991; Chapter IV). The results did not rule out the possibility of a second binding site on Ca(II)-saturated TnC with an affinity 10-20 fold weaker than that of the first.

Two-dimensional ^{1}H nuclear magnetic resonance spectroscopy has been used to determine the structure of the synthetic inhibitory peptide Nα-acetyl-TnI(104-115) amide bound to calcium-saturated s-TnC (Campbell and Sykes, 1991; Chapter V). Conformational changes in the peptide induced by the formation of the TnI peptide-TnC protein complex were followed by the study of the transferred nuclear Overhauser effect

(TRNOE), a technique which allows the structure of a ligand bound to a macromolecule to be determined. The TnI peptide is extremely basic, with four arginines and two lysines (K105, K107, R108, R112, R113 and R115) within a twelve residue sequence. Alternating with these basic residues are hydrophobic residues (F106, L111 and V114). The pattern of alternating basic and hydrophobic residues is interrupted by two sequential proline residues (P109 and P110). The TRNOE-derived structure of the TnI peptide bound to TnC.Ca(II)$_4$ reveals a helical structure, distorted in the center by the proline residues. The central bend in the peptide functions to bring the hydrophobic residues into closer proximity with each other, thereby forming a small hydrophobic pocket with the aromatic ring of F106 being somewhat buried by the side chains of L111 and V114. The hydrophilic, basic residues extend off the opposite face of the peptide.

It has been proposed that the structural changes produced by Ca(II) binding to TnC result in the presentation of hydrophobic regions on the surface of TnC capable of binding TnI with high affinity (LaPorte *et al.*, 1980; Gariepy and Hodges, 1983; Cachia *et al.*, 1985). One could thus imagine an interaction of the inhibitory TnI peptide with Ca(II)-saturated TnC which would be primarily hydrophobic in nature, but strenghtened by electrostatic forces. The hydrophobic pocket on the TnI peptide could be positioned toward the hydrophobic pocket on the C-terminal domain of TnC, allowing ring stacking between the aromatic ring of F106 on the TnI peptide and the aromatic rings of any number of exposed phenylalanines on the Ca(II)-saturated form of TnC. The side chains of L111 and V114 on the TnI peptide could interact with hydrophobic groups lining the pocket of TnC. The long basic side chains of K105, K107, R108, R112, R113 and R115, which extend off the opposite hydrophilic face of the TnI peptide, could electrostatically interact with a number of acidic groups located around the Ca(II)-binding loops of TnC, or could hydrogen bond with the solvent, since this face of the peptide would probably not be buried by protein.

In the present study we use two-dimensional NMR techniques to determine the identity of the residues on Ca(II)-saturated turkey s-TnC which are actively involved in binding the synthetic peptide Nα-acetyl-TnI(104-115) amide. Knowing the identity of these residues on TnC as well as the structure of the bound TnI peptide should allow us to undertake a modeling of the interaction between this region of TnC and the inhibitory region of the intact TnI protein. This should give us a structural framework for understanding a fundamental regulatory step in the Ca(II)-mediated regulation of muscle contraction.

B. Materials and Methods

1. Sample Preparation

a. Materials. Refer to Materials and Methods section in Chapter V.

b. Amino Acid Analysis. The quantities of Nα-acetyl-TnI(104-115) amide and turkey skeletal TnC used were determined from amino acid analysis after hydrolysis in 100-200 μl of 6 N HCl in evacuated sealed tubes for 24 h at 110°C. The mean of the molar ratios of all accurately measurable amino acids in the acid hydrolysate was used to calculate the concentration of peptide or protein.

c. Peptide Synthesis and Purification. Nα-acetyl-TnI(104-115) amide was synthesized and purified using the standard protocol outlined in the Materials and Methods section in Chapter V (Erickson and Merrifield, 1976; Talbot and Hodges, 1981; Mant *et al.*, 1987; Parker *et al.*, 1987; Hodges *et al.*, 1988).

d. Preparation of TnC. Troponin was isolated from an acetone powder of turkey breast muscle using the protocol outlined in the Materials and Methods section in Chapter IV. A final yield of approx. 400 mg of purified TnC powder was obtained, which was found to be homogenous when examined by SDS-Page and UV spectrophotometry ($\varepsilon_{(\lambda\ 259\ nm)}$ = 0.109 O.D. units/mg/ml for turkey skeletal TnC).

e. Preparation of Desalted, Apo TnC. EDTA-free, apo TnC was prepared using the protocol outlined in the Materials and Methods section in Chapter IV. The TnC protein was judged to be apo by UV spectrophotometry and ^{1}H NMR.

f. Preparation of TnC Protein ^{1}H NMR Samples. Two separate samples were used to assign resonances of the Ca(II)-saturated TnC protein. The first sample was acquired at 500 MHz in 80%H_2O/20%D_2O. This sample consisted of 3.6 mM turkey s-TnC, 16 mM $CaCl_2$, and 100 mM KCl in 650 μl of an 80%H_2O/20%D_2O solvent mixture at a pH of 6.0. The second sample, used for ^{1}H NMR spectra acquired at 600 MHz, was 2.0 mM turkey s-TnC, 12 mM $CaCl_2$, and 100 mM KCl dissolved in 650 μl of D_2O at a pD of 6.2. 0.1 mM DSS was added to each of the samples to act as a chemical shift standard. 3 mM DTT was also added to each sample to prevent oxidation of the sulfhydryls of s-TnC and thus prevent aggregation of the protein.

g. Preparation of TnI Peptide-TnC Protein ^{1}H NMR Samples. Two separate samples were used to assign TnI peptide-TnC protein NOEs. The first sample was used for ^{1}H NMR spectra acquired at 500 MHz and consisted of 9 mM Nα-acetyl-TnI(104-115) amide, 3.6 mM turkey s-TnC, 16 mM $CaCl_2$, and 100 mM KCl dissolved in 650 μl of an 80%H_2O/20%D_2O solvent mixture at a pH of 6.0. The second sample was used for ^{1}H

NMR spectra acquired at 600 MHz and consisted of 2.96 mM Nα-acetyl-TnI(104-115) amide, 0.82 mM turkey s-TnC and 5 mM $CaCl_2$, dissolved in 650 μl of D_2O at a pD of 6.1. 0.1 mM DSS was added to each sample to act as a chemical shift standard. 3 mM DTT was also added to each sample to keep the sulfhydryls of s-TnC in a reduced state and prevent aggregation of the protein.

2. Nuclear Magnetic Resonance Spectroscopy

^1H NMR spectra were obtained at 500 MHz on a Varian VXR-500 NMR spectrometer and at 600 MHz on a Varian Unity 600 NMR spectrometer. Two-dimensional experiments were taken with 2048 data points along t_2 and with 256 t_1 increments. Spectral widths of 5000-6000 Hz (for 500 MHz data) and 7500 Hz (for 600 MHz data) and relaxation delay times of 1.6-2.3 s were employed. Streaking along t_1 was reduced by multiplying the first domain time point by a factor optimized near 0.5 (Otting *et al.*, 1986). DQFCOSY (Piatini *et al.*, 1982, Rance *et al.*, 1983) and TRNOESY data sets were acquired in the phase-sensitive method of States *et al.* (1982). The appropriate phase cycling was used to achieve quadrature detection, to eliminate axial peaks, and, in the case of NOESY spectra, multiple quantum coherences. For NOESY spectra, a random delay of between -10 and +10 ms was incorporated to suppress zero quantum coherences. For all data sets, the water resonance was suppressed by presaturation. The decoupler offset was set equal to the transmitter offset to prevent phase distortions around the water peak due to imperfect cancellation of the dispersive component of residual water magnetization (Hoult, 1976). For NOESY spectra, mixing times of 150 ms and 75 ms were used to assign resonances in the Ca(II)-saturated TnC protein and to assign TnI peptide-TnC protein NOEs.

C. Results

The identification of specific residues on s-TnC which are involved in the binding of the inhibitory TnI peptide requires at least partial spectral assignments of residues in both TnC and the TnI peptide. We have previously published a complete ^1H NMR resonance assignment of the TnI inhibitory peptide (Campbell and Sykes, 1991; Chapter V), and other groups have published partial ^1H NMR resonance assignments in rabbit s-TnC (Drabikowski *et al.*, 1985; Tsuda *et al.*, 1988, 1990) and CaM (Ikura *et al.*, 1985, 1987, 1990a). To date, however, no ^1H NMR resonance assignments exist for turkey s-TnC. A partial assignment of resonances in turkey s-TnC was therefore necessary in order to establish the identity of some of the peptide-protein NOEs observed in the TnI peptide-TnC protein complex.

The partial assignment of resonances in the Ca(II)-saturated turkey s-TnC spectrum was based on a pattern of self-consistent NOEs observed in the NOESY spectrum of the Ca(II)-saturated protein, and a knowledge of the crystal structure of the avian s-TnC protein, which contains unique structural elements. The unique structural feature of TnC that proves useful in assigning the NMR spectrum of this protein is the proximity of the clusters of aromatic phenylalanine residues to residues in the β-sheet region between the Ca(II) binding loops. This results in a pattern of NOEs linking upfield ring shifted aromatic resonances in the aromatic cluster to downfield shifted α-proton and amide proton resonances in the β-sheet region. The downfield shift of the amide proton resonance is indicative of the formation of a hydrogen bond (Pardi *et al.*, 1984; Wagner *et al.*, 1983; Dalgarno *et al.*, 1983a), whereas the downfield shift of the α-proton resonances is a sign of the formation of a β-sheet structure (Dalgarno *et al.*, 1983a, b; Wishart, 1991). Thus, residues in the β-sheet region are easily identified in the NMR spectrum and provide an entry-point into the assignment of the rest of the protein, and especially into the aromatic cluster and the hydrophobic pocket.

We will begin with a discussion of the crystal structure of TnC, followed by a comparison of previously published ^{1}H NMR resonance assignments in rabbit s-TnC and CaM with our own assignments in turkey s-TnC. Armed with a partial assignment of the TnC protein, we will then proceed to the identification of specific NOEs involving resonances on the TnI peptide and resonances on the TnC protein in the TnI peptide-TnC protein complex.

1. Crystal Structure of Troponin C

The x-ray structures of chicken (Sundaralingam *et al.*, 1985) and turkey (Herzberg and James, 1985) s-TnC have been solved and reveal a dumbbell-shaped molecule with N-terminal and C-terminal globular domains joined by a long helical linker. Each major domain contains two Ca(II) binding sites based on the EF hand helix-loop-helix structural motif (Kretsinger and Nockolds, 1973; Collins *et al.*, 1973; Vanaman *et al.*, 1977) The higher affinity Ca(II)/Mg(II) sites (sites III and IV) reside in the C-terminal domain and bind Ca(II) and Mg(II) with association constants of 2×10^7 and 5×10^3 M^{-1}, respectively. The Ca(II) specific sites (sites I and II) reside in the N-terminal domain and bind Ca(II) with an association constant of 2×10^5 M^{-1} (Potter and Gergely, 1974). In the avian crystal TnC structure, only the C-terminal domain is occupied by Ca(II) ions.

Each globular domain of TnC has large hydrophobic patches (Kretsinger *et al.*, 1986; Babu *et al.*, 1988) flanked by regions of negative electrostatic potential. Figure VI-1 shows the amino acid sequence alignment of the C-terminal domains of chicken s-TnC (Wilkinson, 1976), rabbit s-TnC (Collins *et al.*, 1973) and rabbit s-CaM (Nairn *et al.*, 1984). Figure VI-2 shows the crystal structure of the C-terminal domain of turkey s-TnC. The hydrophobic patches contain aromatic clusters of four conserved phenylalanine residues in each of the TnC domains. The four phenylalanine residues comprising the N-terminal aromatic cluster are F26, F29, F75 and F78. The equivalent residues comprising the C-terminal aromatic cluster are F102, F105, F151 and F154[1]. The aromatic ring of F102 points over the rings of F148 and F151, which are partially ring stacked. F105 is more weakly associated with the hydrophobic ring cluster of F102, F151 and F154.

The Ca(II)-binding loops consist of 12 sequential residues, those at positions 1, 3, 5, 7, 9 and 12 being involved in coordination of the cation in a octahedral array. The placement of the coordinating oxygen ligands are x, y, z, -y, -x, and -z in Cartesian space, in correspondence with the positions of the residues given above. At position 9, the -z ligand is a bidentate, highly-conserved glutamic acid residue. The majority of coordinating oxygen atoms are derived from asparagine or glutamine side chains. At position 7, however, coordination comes from the main chain carbonyl oxygen atom of the residue (G34 in site I, T72 in site II, R158 in site III, and F112 in site IV). Residues 7-9 in each calcium binding loop are involved in an antiparallel β-sheet formation. The hydrophobic residue at position 8 has its side chain directed towards the interior of the domain and its main chain involved in β-sheet-type hydrogen bonding with the homologous residue in the adjacent Ca(II) binding loop. In the C-terminal domain, I113N of loop III forms a hydrogen bond to I149O of loop IV, and I149N forms a hydrogen bond to I113O. In the N-terminal domain, I37N in loop I forms a hydrogen bond to I73O of loop II and I73N forms a hydrogen bond to I37O.

---

[1] This is the amino acid numbering of chicken s-TnC as sequenced by Wilkinson *et al.* (1976). The amino acid sequences of turkey s-TnC and chicken s-TnC are identical except for: the N-terminus is unacetylated in turkey s-TnC, proline replaces alanine at position 1 in turkey s-TnC, residue 100 is asparagine in both chicken and turkey s-TnC, and residue 133 is aspartic acid in chicken s-TnC whereas it is a glutamic acid in turkey s-TnC (Golosinska *et al.*, 1991)

2. NMR Assignments of Troponin C

NMR assignments of the intact s-TnC protein (Levine *et al.*, 1977, 1978; Seamon *et al.*, 1977; Andersson *et al.*, 1982; Teleman *et al.*, 1983) have shown that when Ca(II) is progressively added to apo TnC, the higher affinity Ca(II)/Mg(II) sites (sites III and IV) are filled first and the lower affinity Ca(II) specific sites (sites I and II) second. ^{1}H and ^{113}Cd NMR studies of tryptic fragments of rabbit s-TnC have confirmed the kinetics of binding of Ca(II) to sites I - IV. Drakenberg *et al.* (1987) have shown that Ca(II) and Cd(III) bind to TR2C (89-159) in slow exchange ($k_{off} < 10\ s^{-1}$) which is consistent with the kinetics of calcium binding observed to the C-terminus of whole s-TnC. Tsuda *et al.* (1988, 1990) have made partial ^{1}H NMR assignments of the intact rabbit s-TnC protein in both its apo and Ca(II) saturated forms, and have followed the spectral changes associated with Ca(II) binding. Two resolved peaks at 6.47 ppm and 6.59 ppm, corresponding to the δCH2 protons of F99[2] and F148 respectively, were observed to emerge with addition of the first two molar equivalents of Ca(II). This observation was attributed to the slow exchange process corresponding to Ca(II) binding to the C-terminal domain. Resonances of the δCH2 protons of F72 and F23 were observed to titrate downfield from 6.46 ppm and 6.66 ppm respectively, at 2 molar equivalents of Ca(II), to 6.70 ppm and 6.74 ppm respectively, at 4 molar equivalents of Ca(II). The resonances of the aromatic protons of F23 and F72 did not change at 0 - 2 molar equivalents of Ca(II).

We have titrated turkey s-TnC with Ca(II) and have observed similar spectral changes in the ^{1}H NMR spectrum. Figure VI-3 shows the slow exchange behaviour of three resolved peaks at 6.37, 6.90 ppm, and at 6.57 ppm, which correspond to the δCH2 and ξCH2 protons of F102 and the δCH2 protons of F151, respectively. These peaks are observed to emerge with the addition of the first 2 molar equivalents of Ca(II) which bind in slow exchange to sites III and IV in the C-terminal domain. Other peaks are observed to titrate downfield upon further addition of Ca(II) in the 2 - 4 molar equivalents range. These resonances may be assigned to ring protons of phenylalanines in the N-terminal domain which experience the fast exchange binding of the third and fourth molar equivalents of Ca(II) to sites I and II. At 4 molar equivalents Ca(II), these resonances have sufficiently shifted downfield to expose F102δCH2 and F151δCH2 as the most upfield resonances in the aromatic region of the spectrum.

---

[2] Refer to Table VI-1 and Figure VI-1 for differences in amino acid numbering between rabbit s-TnC (Collins *et al.*, 1984) chicken s-TnC (Wilkinson *et al.*, 1976) and s-CaM (Nairn *et al.*, 1984).

The assignments made of the aromatic proton resonances of F102 and F151 in the Ca(II) titration are supported by the pattern of COSY and NOESY cross-peaks observed in the aromatic region of the DQFCOSY and NOESY spectra of Ca(II)-saturated turkey s-TnC. Figure IV-4 shows the 600 MHz ^{1}H DQFCOSY spectrum of TnC where COSY cross-peaks connecting the aromatic ring protons of phenylalanines F102, F112, F151 and F154 can be seen. Figure VI-5 shows the 600 MHz ^{1}H NOESY spectrum of TnC where NOEs within and between these same residues can be seen. NOEs are observed between the following aromatic ring protons: F102δCH2-F151δCH2, F102ξCH2-F151δCH2, F102δCH2-F154ξCH2, F102δCH2-F154ςCH, F102ξCH2-F154ξCH2, F102ςCH-F154δCH2, and F151δCH2-F154ξCH2. These NOEs are summarized in Table VI-2 and define the spacial proximity of the phenylalanine rings of F102, F151 and F154 in the C-terminal hydrophobic pocket of TnC. Resonance assignments of the aromatic protons of F102, F151 and F154 in the Ca(II)-saturated chicken s-TnC Site III/Site IV heterodimer by Shaw *et al.* (1991a, 1991b, and personal communications) are in agreement with the resonance assignments made here.

No NOEs were observed between the ring protons of F102, F151 and F154, and the ring protons of F112. F112 is situated in the antiparallel β-sheet region between Ca(II)-binding loops III and IV, and is not associated with the hydrophobic pocket. NOEs between the ring protons of F112 and the ring protons of the phenylalanines in the hydrophobic pocket are therefore not expected to be observed. Unfortunately, the ring proton resonances of F105 could not be located in the aromatic region of the spectrum since F105 is only loosely associated with the aromatic ring cluster in the C-terminal domain, and thus NOEs connecting the relatively isolated F105 spin system to the other phenylalanines in the cluster were not expected to be observed. Resonance assignments in the heterodimer (Shaw *et al.*, 1991a, 1991b) have placed the δCH2 and ξCH2 ring protons of F105 under the broad phenylalanine resonance at approximately 7.3 ppm where they are not easily distinguished.

Tsuda *et al.* (1988) have observed NOEs between F99, F148 and L152 in the hydrophobic pocket of the C-terminal domain of Ca(II)-saturated rabbit s-TnC similar to those we have observed between F102, F151 and F154 in the C-terminal domain of Ca(II)-saturated turkey s-TnC. Other interesting observations made by Tsuda and co-workers involved the downfield shifts of the amide proton resonances of I110 and I146, and the downfield shifts of the α-proton resonances of Y109, I110, R145 and I146. These downfield shifts imply that the amide protons of I110 and I146 form hydrogen bonds, and that the α-protons of Y109, I110, R145 and I146 are involved in a β-sheet region. According to the crystal structure of the homologous avian TnC protein, Y109 and I110 would take up positions 7 and 8 in the Ca(II) binding loop III, and R145 and I146 would take up the same positions in loop IV, placing these residues in the antiparallel β-sheet region between the two loops. The amide protons of G108 and G144 are also shifted significantly downfield in Ca(II)-saturated rabbit s-TnC, implying the presence of hydrogen bonds. In the refined crystal structures of avian s-Tnc (Herzberg and James, 1988; Satyshur *et al.*, 1988), hydrogen bonds are found between G111N and D106O$^{\delta 1}$ and between G147N and D142O$^{\delta 1}$. G108 and G144 in rabbit s-TnC are homologous to G111 and G147 in avian s-TnC.

Drabikowski *et al.* (1985) have made ^{1}H NMR assignments of the C-terminal TR2C fragment of rabbit s-TnC. Their NOE data define how the β-sheet is linked to the aromatic ring cluster. Interresidue NOE effects were observed between the different aromatic protons of F99, F102, F148 and F151, revealing the spatial proximity of these four side chains in the aromatic cluster. NOEs were also observed between the ring protons of F99 and the downfield shifted α-protons of I146 and Y109 in the β-sheet region, and between the following pairs of downfield shifted α-protons and amide protons in the β-sheet region: Y109αCH-I146NH, D111αCH-R145αCH, I146αCH-I110NH, and D147αCH-Y109αCH. In addition, there were also NOEs observed between the side chains of phenylalanines in the aromatic cluster and upfield shifted methyls. The upfield shifted methyl resonances were unassigned, but a reference to the avian crystal structure suggests that the δCH3 methyl protons of I110, I146 and L152 (homologous to I113, I149 and L155 in avian s-TnC), which are located in the hydrophobic pocket of the C-terminal domain near the aromatic cluster, may be susceptible to ring current shifts.

The crystal structure of bovine brain calmodulin (CaM) (Babu *et al.*, 1988) displays the same structural motifs as revealed in the crystal structures of avian TnC. Ikura *et al.* (1985) have made ^{1}H NMR assignments of the C-terminal TR2C(78-148) tryptic fragment of scallop CaM in the Ca(II) bound state. Downfield shifted α-proton resonances were assigned to F89, I100, S101, Q135, V136 and N137, suggesting that these residues belong in a β-sheet region of the protein. According to the crystal structure of CaM, F89, I100 and S101 take up positions 7, 8 and 9 in the Ca(II) binding loop III, and Q135, V136 and N137 take up the same positions in loop IV, placing these residues in the antiparallel β-sheet region between the two loops, and supporting the ^{1}H NMR assignments. A cross-strand NOE between amide protons of I100 and V136 was observed, providing evidence for hydrogen bonding between these two residues in the β-sheet region (I100 and V136 are homologous to the hydrogen bonded pair of residues I113 and I149 in the avian TnC structure). Upfield shifted methyl resonances were assigned to the δCH3 groups of I100, and the γCH3 groups of V136 and V142. These residues are located in the hydrophobic pocket in the homologous positions as occupied by I110, I146 and L152 in rabbit s-TnC.

Based on these resonance assignments made in the Ca(II)-saturated forms of rabbit s-TnC and CaM, we have made the resonance assignments presented in Table VI-1. The most downfield shifted α-proton resonances were assigned to F112, I113 and I149, all located within the β-sheet region. The most downfield shifted amide resonances were assigned to G111, I113 and I149, which are all involved in hydrogen bonds (I113NH to I149O, G111NH to G147O, and I149NH to I113O). We have also assigned the most upfield methyl resonances to the δCH3 methyl protons of I113 and the γCH3 methyl protons of I104 and I121 in the hydrophobic pocket. These assignments were based on assignments made of the site3/site4 heterodimer by Shaw *et al.* (1991a, 1991b, and personal communications). The aromatic ring protons of F105 could not be assigned because their chemical shift dispersion is small and they are located under the broad phenylalanine envelope which makes assignment difficult. The tentative assignment of the ring protons of F112 was based on the NOE connectivities observed between the δCH2 and ξCH2 ring protons of F112 and the main chain and side chain protons of I113 (see Figures VI-6, VI-7 and VI-8).

Table VI-2 is a comparison of the similar patterns of NOEs observed in turkey s-TnC and rabbit s-TnC (Drabikowski *et al.*, 1985). We have observed NOEs between the ξCH2 and ςCH ring protons of F102 and the αCH protons of F112 and I149 in turkey s-TnC (see Figure VI-7). This pattern was also observed in rabbit s-TnC as NOEs between the ξCH2 and ςCH ring protons of F99 and the αCH protons of Y109 and I146. We also observed NOEs between the ξCH2 ring protons of F102 and the δCH3 and γCH3 protons of I113 and I149 (see Figure VI-8). A similar pattern was observed in rabbit s-TnC as NOEs between the δCH2 and ξCH2 ring protons of F99 and unassigned methyl resonances at 0.20, 0.71 and 0.90 ppm. Due to their extreme upfield shifts, these methyl resonances could be attributed to the δCH3 and γCH3 protons of I110 and I146 in rabbit s-TnC. NOEs which were additionally observed in turkey s-TnC included NOEs between the ξCH2 ring protons of F154 and the α-protons of F112 and I149 (Figure VI-7), an NOE between the δCH2 ring protons of F151 and the δCH3 methyl protons of I113 (see Figure VI-8), a sequential NOE between the α-proton of F112 and the amide proton of I113 (see Figure VI-9), and a cross-strand NOE between the amide protons of I113 and the γCH3 methyl protons of I149 in the β-sheet region (see Figure VI-10). Figure VI-11 shows the downfield region of the 500 MHz ^{1}H NMR spectrum of turkey s-TnC in D_2O and 80%H_2O/20%D_2O with the assignments for the aromatic ring proton resonances of

F102, F112, F151 and F154, as well as with the assignments for the downfield α-proton resonances of F112, I113 and I149.

3. Interactions between TnC and the TnI Inhibitory Peptide: ^{1}H NMR Monitored Titration of Ca(II)-Saturated Turkey s-TnC with the TnI Peptide

We have used ^{1}H NMR at 600 MHz to identify several residues on turkey s-TnC which are perturbed upon binding of the inhibitory TnI peptide. A Ca(II)-saturated TnC NMR sample was titrated with TnI peptide to a final concentration of 0.3 molar equivalents TnC protein to TnI peptide, and the chemical shifts of the TnC peaks were followed as a function of peptide concentration. Figure VI-12 shows the aromatic region of the spectrum. A slight downfield shift is observed for the F102δCH2 and F154δCH2 resonances, and a marked upfield shift for the F154ςCH resonance. As well, TnI peptide F106δCH2 and F106ξCH2ςCH resonances are observed to emerge at 7.25 and 7.30 ppm with increasing peptide concentration. The shifting of the ring proton resonances of F102 and F154 on the TnC protein indicates that there may either be an interaction involving ring stacking between F102 or F154 on TnC and F106 on the TnI peptide, or there may be a slight rearrangement of the aromatic ring cluster as a consequence of peptide binding.

Figure VI-13A shows the upfield region of the titration of TnC with the TnI peptide. Marked downfield shifts for the I113δCH3 and I121γCH3 resonances and a marked upfield shift for the I104γCH3 resonance may be observed. Figure VI-13B shows the same upfield region of a 600 MHz ^{1}H NMR monitored titration of the Ca(II)-saturated chicken s-TnC Site III/Site IV heterodimer with TnI peptide (Shaw, personal communications). A comparison of Figures VI-13A and Figures VI-13B reveals the same pattern of shifts for the I113δCH3, I104γCH3 and I121γCH3 resonances. On the basis of the assignments for the γCH3 groups of I104 and I121 made in the heterodimer, we were able to make assignments for the methyl protons in the TnI peptide-TnC complex. We were also able to confirm our assignment for I113δCH3. Ambiguities in the assignments of TnI peptide-TnC protein intermolecular cross-peaks in the complex exist since, unfortunately, the γCH3 resonances of I104 and I121 coalesce at approximately 0.3 molar equivalents TnC protein to TnI peptide.

The shifting of the δ-methyl resonances of I113, a residue situated in the antiparallel β-sheet region between Ca(II)-binding loops III and IV, suggests a rearrangement of the sheet as a result of peptide binding. As I113 is mostly buried in the β-sheet region, direct contact with the TnI peptide is difficult to envision without invoking a conformational change in the TnC protein. The γCH3 groups of I104 and I121 are relatively more exposed than the δCH3 group of I113. Therefore, the shifting of these γ-methyl resonances could be a result of direct contact with the δCH3 of L111 or the γCH3 methyl groups of V114 on the TnI peptide.

Figure VI-14 shows the α-proton region of the spectrum. A downfield shift for the I113αCH resonance and marked upfield and downfield shifts for F112αCH and I149αCH, respectively, were observed. Figure VI-15 shows the backbone amide region of the spectrum in which slight downfield shifts for I113NH and I149NH can be observed. The shifting of backbone resonances for F112, I113 and I149, residues all situated within the β-sheet region, indicate a rearrangement of the sheet either due to direct contact with the TnI peptide or due to a conformational change in the protein as a result of peptide binding.

4. Interactions between TnC and the TnI Inhibitory Peptide: Identification of Specific Residues Involved in the Binding Interface

NOESY experiments of the TnI peptide-TnC protein sample were performed at 500 MHz in 80%H_2O/20%D_2O and at 600 MHz in D_2O to identify peptide-protein NOEs. The NOESY spectrum of this sample contains cross-peaks arising from three sources: (1) intramolecular TnC protein interactions, (2) intramolecular TnI peptide interactions, and (3) intermolecular TnI peptide-TnC protein interactions arising from the magnetization transfer between protein protons and bound peptide protons. The TnI peptide binds to the TnC protein in fast exchange with respect to chemical shift (Campbell *et al.*, 1991; Chapter IV) and therefore no cross-peaks arising from chemical exchange between a separate set of free and bound peptide proton resonances were observed.

To discriminate between cross-peaks arising from intramolecular versus intermolecular interactions, the NOESY spectrum of the peptide-protein complex was compared to the NOESY spectrum of the Ca(II)-saturated TnC protein alone and the NOESY spectrum of the TnI peptide alone. The NOESY spectrum of the free TnI peptide is fairly simple and has been completely assigned (Campbell and Sykes, 1991; Chapter V). The NOESY spectrum of the Ca(II)-saturated TnC protein alone is more complex, and therefore a more rigourous approach to discriminating between TnC protein intramolecular cross-peaks and TnI peptide-TnC protein intermolecular cross-peaks was needed. The approach involved taking traces through 2D NOESY spectra of TnC by itself and TnC complexed with the TnI peptide. The traces were compared and a cross-peak observed in the NOESY spectrum of TnC complexed with peptide was established as being intermolecular in origin if it was absent in the NOESY spectrum of the TnC protein alone.

We started first with a series of NOESY experiments performed at 500 MHz in 80%H_2O/20%D_2O at 30°C. Figures VI-16 through VI-19 show regions of the NOESY spectrum acquired at a mixing time of 150 ms and 0.4 molar equivalents TnC protein to TnI peptide. Accompanying 1D spectra are plotted horizontally and vertically on the top and sides of each 2D plot to facilitate interpretation. Cross-peaks enclosed in boxes were observed to appear only in the NOESY spectrum of the peptide-protein sample, and were absent in the NOESY spectrum for the TnC protein alone, as confirmed by the use of traces taken through the cross-peak in question.

Figure VI-16 shows many intermolecular cross-peaks connecting resonances of the TnI peptide to the upfield shifted methyl resonances of the TnC protein. The upfield shifted methyl resonances on the protein which could not be assigned were designated (CH3)x, (CH3)y and (CH3)z. The methyl peak at 0.42 ppm has been assigned to the nearly degenerately shifted methyl resonances of I104γCH3 and I121γCH3 on TnC. Two cross-peaks are observed involving these methyl groups to residues on the TnI peptide. These two cross-peaks connect I104γCH3 and I121γCH3 on TnC to the δCH2 group of one or all of the degenerately shifted R108, R112, R113 and R115 resonances, and to the α-protons of one or all of the degenerately shifted K107, L111 and R115 resonances on the TnI peptide. Fortunately, I104 and I121 are situated relatively close to each other on the TnC protein (see Figure VI-2), I104 being situated at the end of Helix E, just before Ca(II)-binding loop III, and I121 being situated on Helix F. These cross-peaks therefore allow an interaction between the TnI peptide and a region involving Helices E and F (with possibly Site III) on the TnC protein to be envisioned.

Figure VI-17 shows intermolecular cross-peaks between F154ξCH2, F154δCH2 and F102ξCH2 on TnC to F106αCH on the TnI peptide. These interactions are important since they suggest a close contact between F106 on the TnI peptide and F102 and F154 in the hydrophobic pocket of the C-terminal domain of TnC. Figure VI-18 shows an intermolecular cross-peak between F154ξCH2 on TnC and the degenerately shifted α-proton resonances of K107, L111 and R115 on the TnI peptide. Also visible in Figure VI-18 are intermolecular cross-peaks between F151ςCH on TnC and the degenerately shifted α-proton resonances of R112 and R113. These intermolecular cross-peaks all suggest an interaction of the TnI peptide with the aromatic ring cluster comprised of F102, F151 and F154 in the hydrophobic pocket of the C-terminal domain of TnC. Table VI-3 summarizes the intermolecular TnI peptide-TnC protein NOEs observed in the 500 MHz NOESY spectrum.

A series of NOESY experiments at 600 MHz in D_2O and 30°C were subsequently performed. Figures VI-19 through VI-23 show regions of the NOESY spectrum acquired at a mixing time of 150 ms and 0.3 molar equivalents TnC protein to TnI peptide. Panel A shows the peptide-protein sample and Panel B shows the same region of the spectrum for the TnC protein alone. Cross-peaks enclosed in boxes were observed to appear only in the NOESY spectrum of the peptide-protein sample and were absent in the NOESY spectrum for the TnC protein alone, as confirmed by the use of traces taken through the cross-peak in question.

Figures VI-19A and VI-19B show the upfield methyl region of the NOESY spectrum. An intermolecular cross-peak connecting the L111(δCH3)2 and V114(γCH3)2 methyl resonances of the TnI peptide to the upfield shifted I104γCH3 and I121γCH3 methyl resonances of the TnC protein can be observed in Panel A. Figures VI-20A and VI-20B compare the upfield methyl to α-proton region of the spectrum where many new cross-peaks may be observed. Some of these new cross-peaks (V114αCH-(γCH3)3, L111αCH-(δCH3)2 and P110αCH-L111(δCH3)2) are intra-peptide TRNOE cross-peaks. Other new cross-peaks arise from peptide-protein intermolecular interactions. These include the intermolecular cross-peaks between L111αCH on the TnI peptide and I113δCH3 on the TnC protein, and between one or all of R112αCH, R113αCH and V114αCH on the TnI peptide and I104γCH3 and I121γCH3 on the TnC protein.

Figures VI-21A and VI-21B show the upfield methyl to aromatic region of the spectrum. One can observe three new cross-peaks involving V114(γCH3)2 on the TnI peptide and F102δCH2, F151δCH2 and F154δCH2 on TnC. Figures VI-22A and VI-22B show the aliphatic to aromatic region of the spectrum for the complex in which cross-peaks involving F106δCH2 on the TnI peptide are observed. Some of these cross peaks are intrapeptide such as the long range F106δCH2-V114(γCH3)2 TRNOE cross-peak. Other cross peaks, however, are intermolecular cross-peaks connecting F106δCH2 on the TnI peptide to I113δCH3, and I104γCH3 and I121γCH3 on the TnC protein. Finally, Figures VI-23A and VI-23B show the α-proton to aromatic region of the spectrum in which a cross-peak connecting F106ξCH2 on the TnI peptide to a protein peak at 5.3 ppm, which may be F112αCH. Also visible is the intraprotein cross-peak connecting F154ξCH2-F112αCH, which may have arisen due to a conformational change in the TnC protein in the presence of bound TnI peptide.

Table VI-3 summarizes the intermolecular TnI peptide-TnC protein NOEs observed in the 600 MHz NOESY spectrum of the complex taken in D_2O. These intermolecular cross-peaks observed at 600 MHz in D_2O support and substantiate the existing set of intermolecular cross-peaks acquired at 500 MHz in $80\%H_2O/20\%D_2O$. Taken together, both sets of cross-peaks suggest an interaction of the TnI peptide with the following residues on turkey s-TnC which are all located within the hydrophobic pocket of the C-terminal domain of TnC: F102, I104, I113, I121, F151, and F154.

D. Discussion

Studies characterizing the interaction between TnC and TnI have pointed to multiple interactions between these two proteins. TnI fragment studies reported by Syska *et al.* (1976) demonstrated that two regions of the TnI protein are capable of interacting with TnC. The first region spans residues 1-21 and includes the site of phosphorylation catalyzed by phosphorylase kinase (T11). The second region spans residues 96-116 and is adjacent to a second phosphorylation site (S117) (Moir *et al.*, 1974). Equimolar amounts of TnC completely inhibit phosphorylation at these sites (Cole and Perry, 1975). Syska *et al.* (1976) demonstrated that a CNBr fragment of TnI (residues 96-116) mimics intact TnI in its ability to inhibit actomyosin ATPase (Syska *et al.*, 1976; Nozaki *et al.*, 1980; Talbot and Hodges, 1981); and Talbot and Hodges (1981) using synthetic peptides showed that residues 104-115 of TnI comprise the minimum sequence necessary for inhibition of actomyosin ATPase activity.

Although the inhibitory region of TnI which interacts with TnC is well defined, the region on TnC which interacts with the inhibitory region of TnI remains an actively researched area. We have used ^{1}H NMR to identify several residues on turkey s-TnC which interact with the inhibitory TnI peptide. The presence NOEs between residues on the TnI peptide and the ring protons of F102, F151 and F154 of turkey s-TnC point to an interaction of the inhibitory TnI peptide with the C-terminal aromatic ring cluster of this protein. The most important intermolecular NOEs in this group include those between the F106 αCH and δCH2 protons on the TnI peptide to the F102ξCH2, F154δCH2 and F154ξCH2 protons on the TnC protein. These NOEs suggest an interaction between the phenyl ring of F106 on the TnI peptide and the phenyl rings of F102 and F154 on the TnC protein. We have also observed NOEs involving L111 and V114 on the TnI peptide to I104, I121 and I113 on turkey s-TnC. The most important intermolecular NOEs in this group include those between the L111(δCH3)2 and V114(γCH3)2 protons on the TnI peptide to the I104γCH3, I121γCH3 and I113δCH3 protons on the TnC protein. These NOEs suggest an interaction between the side chains of L111 and V114 on the TnI peptide to the side chains of I113, I104 and I121 on TnC.

We have modeled the binding of the inhibitory TnI peptide with Ca(II)-saturated TnC. Figures VI-24A and VI-24B show front and side views of a backbone ribbon representation of the C-terminal domain of the crystal structure of turkey s-TnC (Herzberg and James, 1985). Residues which were identified from TnI peptide -TnC protein NOEs as being involved in the binding of the TnI inhibitory peptide are shown with their side chains in a space-filled CPK representation. These residues include the aromatic residues F102, F151 and F154, which comprise the ring cluster in the C-terminal hydrophobic pocket, and the isoleucine residues I104, I113, I121 and I149. Figures VI-24C and VI-24D show front and side views of a completely space-filled CPK representation of all side chains in the C-terminal domain of the TnC protein. These figures illustrate the comparative exposure of those residues on TnC which we believe are involved in the binding of the TnI peptide. It is clear that the aromatic rings of F102, F151 and F154 are mostly buried in the hydrophobic pocket, whereas the side chains of I113 and I149 are fairly buried in the β-sheet region between Ca(II)-binding loops III and IV. Only the side chains of I104 and I122 are exposed. This suggests that binding of the TnI peptide to TnC elicits a conformational change in the C-terminal domain of the protein allowing a greater exposure of residues in the hydrophobic pocket and β-sheet region involved in binding the peptide.

Figure VI-25 shows a model of the TRNOE-derived structure of the TnI inhibitory peptide (Campbell *et al.*, 1991; Chapter V) bound to the C-terminal domain of the crystal structure of turkey s-TnC. The backbone of the TnC protein and the TnI peptide are both shown in a ribbon representation, while the side chains of the residues involved in the binding interface are shown in a space-filled CPK representation. On the basis of peptide-protein NOEs observed between F106 on the TnI peptide and F102 and F154 on the TnC protein, we have modeled F106 as ring stacking side-to-face against F154. On the basis of the peptide-protein NOE observed between the δCH3 methyl protons of L111 on the TnI peptide and the δCH3 methyl protons of I113 on the TnC protein, we have modeled the side chain of L111 as interacting with the β-sheet region between Ca(II)-binding loops III and IV on the TnC protein, making contact with the side chains of I113 and I149 which are situated directly across the β-sheet from each other. Finally, on the basis of peptide-protein NOEs observed between the γCH3 methyl protons of V114 on the TnI peptide and the aromatic ring protons of F102, F151 and F154 on the TnC protein, we have modeled the side chain of V114 as interacting with the aromatic ring cluster, and in close proximity to F106, to which an intra-peptide TRNOE was observed (F106δCH2-V114(γCH3)2).

One assumption that has been made during the study of the interaction between the TnI peptide and the TnC protein is that the structure of TnC is constant in the presence and absence of the TnI peptide. This assumption was necessary in order to assign the peptide-protein NOEs. One cannot expect, however, that the structure of the protein is to remain the same when the TnI peptide is bound since the aromatic cluster and the hydrophobic pocket would need to become more exposed in order to interact with the peptide. A change such as this should cause changes in the chemical shift of protons which are involved in the structural change, as well as those involved in the interaction with the TnI peptide. Some of the resonance shifts of TnC could be followed as a function of TnI peptide concentration (such as the shift of the methyl groups of I104, I113 and I121), but others, which are in more crowded regions of the spectrum, could not be followed. Since many peptide resonances fall in these crowded regions of the spectrum, it is not possible at this time to unequivocally state that an NOE is observed between the peptide and the protein or just between shifted protein resonances. Therefore, it is possible that some of the peptide-protein NOEs could have been misassigned. However, given the large number of peptide-protein NOEs observed, it high improbable that all of these NOEs were misassigned, especially as they all consistently point to the TnI peptide binding near the hydrophobic pocket at the C-terminal domain of TnC.

Our findings of an interaction of the inhibitory TnI peptide with the C-terminal domain of turkey s-TnC are supported by several studies which point to an interaction of the inhibitory region of TnI with the N-terminal helix of site III in the C-terminal domain of TnC. A proteolytic fragment spanning residues 89-100 of rabbit s-TnC was found to be able to substitute for intact TnC in Ca(II) sensitization of the reconstituted actomyosin complex (Weeks and Perry, 1978; Grabarek *et al.*, 1981). Resonance energy transfer measurements (Tao *et al.*, 1989) found that Ca(II) binding to sites I and II of TnC in a reconstituted Tn complex led to a 5 Å decrease in the distance between the C98 region in rabbit s-TnC and the C133 region in TnI, suggesting that these two regions interact in a Ca(II)-sensitive manner. A fluorescence study (Lan *et al.*, 1989) showed that the TnI peptide is bound by the C-terminal half of CaM as well as by TR2C, with an affinity comparable to that of intact CaM or TnC. The binding affinity to the N-terminal half of CaM or to TR1C was an order of magnitude less, which suggests that the inhibitory portion of the TnI protein interacts predominantly with the C-terminal half of CaM or TnC. The TnI peptide also inhibited the tryptic hydrolysis of the midpoint of the central connecting strand of CaM and TnC, leading the authors to speculate that the TnI peptide binds TnC or CaM near the C-terminal end of the connecting strand and extending into the hydrophobic site of the C-terminal half.

Perhaps the best evidence for TnI peptide binding at the C-terminal domain of TnC comes from photocross-linking studies (Leszyk *et al.*, 1987, 1988) in which the intact TnI protein was cross-linked in the presence of Ca(II) to rabbit s-TnC specifically labelled with a maleimide group at C98 (see Figure VI-2). Upon enzymatic digestion of the heterodimers and analysis of the cross-linked peptides, the residues in TnI that appeared to be most highly cross-linked to C98 of TnC were R108, P110 and to a lesser extent R103 and K107. All of these studies point to the TnI inhibitory peptide binding near the N-terminal helix of site III in the C-terminal domain of TnC.

However, recent photo-cross linking studies by the same group of researchers using zero-length cross-links (Leszyk *et al.*, 1990) have revealed an interaction between Ca(II)-binding site II (residues 46-78) on rabbit s-TnC and the inhibitory region on the whole TnI protein, offering evidence for an interaction involving the N-terminal domain of TnC. Their results indicated that residues from the regulatory Ca(II)-binding site II (residues 46-78) formed cross-links with TnI segments spanning residues 92-167. The most highly cross-linked residues in the TnI peptide were K105 and K107. Wang *et al.* (1990) used photo-cross-linking and fluorescence studies with a recombinant TnC labelled at C57 to demonstrate that the C-helix in the N-terminal domain of TnC interacts with TnI(104-115), in confirmation of the zero-length cross-linking results (Leszyk *et al.*, 1990). As further evidence for the involvement of both domains of TnC in the binding of the TnI peptide, MacLachlan *et al.* (1990) used fluorescence stopped flow kinetics and ^{1}H NMR to demonstrate that the calcium sensitizer, bepridil, binds to the N-terminal domain of cardiac TnC with a 1:1 stoichiometry. The same research group used ^{1}H NMR and molecular modeling to study the binding of calmidazolium to TnC and concluded that binding occurs simultaneously to both the N- and C-terminal globular domains of the TnC protein (Reid *et al.*, 1990).

Several solution studies of CaM have also identified residues in both the C-terminal and the N-terminal domains which are involved in the binding of target molecules. Fluorescence studies (Steiner and Norris, 1987) and proteolytic digestion studies (Caday and Steiner, 1986) have shown that melittin, a bee venom, makes extensive contacts with the connecting strand and adjacent portions of the N- and C-terminal domains of CaM in the 1:1 CaM:melittin complex. Seeholzer *et al.* (1986) have investigated the structural and dynamic properties of the 1:1 deuterated CaM:melittin (Mel) complex by ^{1}H NMR. By subtracting the bound melittin spectrum ([^{2}H]CaM:Mel) from the spectrum of the nondeuterated CaM:Mel complex, they obtained spectral changes between free and complexed CaM. Perturbed resonances included F16, T26, F65, H107 and F141, implicating the involvement of both halves of the molecules.

Seeholzer and Wand (1989) also studied the 1:1 complex between CaM and the skeletal muscle MLCK peptide [skMLCK(576-594)G] by ^{1}H NMR. Upon CaM-skMLCK(576-594)G complex formation, they noticed subtle upfield and downfield shifts of residues (Y138 and Y99) in the C-terminal domain, but not in the N-terminal domain.

However, Klevit *et al.* (1985) used ^{1}H NMR to study a similar complex - the 1:1 complex of CaM with the skeletal muscle MLCK peptide, M13(577-603) - and found that addition of the M13 peptide to CaM in a 1:1 molar ratio affected resonances from residues in both halves of the molecule, specifically F16, F65, F68, F89, Y99, Y138 and F141.

Probably the most exciting piece of research to emerge involving interactions between CaM and target peptides comes from Ikura *et al.* (1991b) who used triple-resonance multidimensional NMR to study CaM complexed with M13, and found evidence for a conformational change in the central helix. ^{1}H, ^{13}C and ^{15}N Heteronuclear three- and four-dimensional NMR experiments showed that binding of the M13 peptide induced substantial chemical shift changes that were not localized in one particular region of the protein. The largest changes were found in the first helix of the Ca(II)-binding site I (E11-E14), the N-terminal portion of the central helix (M72-D78), and the second helix of the Ca(II)-binding site IV (F141-M145). No changes in secondary structure were observed for the first helix of site I or the C-terminal helix of site IV. Upon complexation with M13, a significant decrease in the amide exchange rate was observed for residues T110, L112, G113, and E114 at the end of the second helix of site III. This research supports a model for the binding of target peptides to CaM which involves both the C-terminal and the N-terminal domains, contingent on a conformational change in the central helix.

Small angle x-ray scattering studies of CaM.Ca(II)$_4$ complexed with target peptides has given evidence for the involvement of a conformational change in the central helix of CaM, bringing the two domains more closely together in a concerted effort to bind the target. Solution x-ray scattering studies of CaM complexed with the peptide M13 (577-603) (Heidorn *et al.*, 1989) reported a radius of gyration, R_g, for the CaM.Ca(II)$_4$:M13 equimolar complex that was 20% smaller (16 vs. 21 Å) than that of the uncomplexed CaM.Ca(II)$_4$ complex. The solvent contrast dependence of R_g for neutron scattering indicated that the peptide was located more towards the center of the complex with the CaM located more peripherally. Small angle x-ray scattering studies of Ca(II)-saturated CaM complexed with melittin (Kataoka *et al.*, 1989) found that binding of melittin to CaM to form the 1:1 complex caused the R_g to decrease from 20.9 to 18.0 Å; and two separate groups, Matsushima *et al.* (1989) and Yoshino *et al.* (1989), found that the R_g decreased by about 3 Å upon binding of both 4 mol Ca(II)/mol of protein and 1 mol mastoparan/mol of protein to form the ternary complex Strynadka and James (1990) have computer modeled the interaction of melittin binding to CaM where they introduced a kink in the central helix of CaM. This served to bring the two hydrophobic domains of CaM sufficiently close to bind a single melittin peptide, while maintaining reasonable stereochemistry.

These solution studies of CaM and TnC serve to provide a structural framework for interpretation of the binding of the TnI inhibitory peptide to TnC. Given that the stoichiometry of binding of peptide to TnC is 1:1, it is possible to imagine a conformational change around a hinge region in the central helix of TnC which would allow the N- and C-terminal domains to form a single binding site capable of accomodating a single peptide. The 'flexible tether' hypothesis put forward by Persechini and co-workers (Persechini and Kretsinger, 1988) proposes that the central helix acts as a flexible tether to allow the N- and C-terminal domains to form a single binding site capable of accomodating a wide variety of target peptides or enzymes. Experimental support for this hypothesis is provided by mutants of CaM in which the two domains were constrained close to another by a specific covalent link (Persechini and Kretsinger, 1988; O'Neil and DeGrado, 1989), or were changed in distance or orientation with respect to one another by deletions in the central helix (Putkey *et al.*, 1988; Persechini *et al.*, 1989; Van Berkum *et al.*, 1990). These altered CaM molecules retained high activity towards target enzymes.

In conclusion, we have investigated the residues on turkey s-TnC involved in binding the inhibitory TnI peptide. We have previously determined the structure of the TnI peptide when bound to Ca(II)-saturated TnC (Campbell and Sykes, 1991; Chapter V), and have attempted to bring together the structure and the location of binding of the TnI peptide in a model of the interaction of the inhibitory region of TnI with Ca(II)-saturated TnC. Although it is certain that the aromatic cluster in the hydrophobic pocket of the C-terminal domain of TnC is directly involved in the binding of the inhibitory TnI peptide, it is still not known whether residues in the N-terminal domain of TnC are also directly involved in the binding. Chapter VII will address the question of whether residues in the N-terminal domain of the protein are also involved, and whether binding of the TnI inhibitory peptide involves a conformational change in the central helix of TnC in order to allow a close approach of the C- and N-terminal domains in a concerted effort to provide a single binding surface for the peptide.

Table VI-1. Chemical shifts (ppm) of assigned resonances on Ca(II)-saturated turkey s-TnC at 30° C in 50 mM KCl, pH 6.0; comparison with literature values for those resonances assigned on CaM.Ca(II)$_4$ and rabbit s-TnC.Ca(II)$_4$ ((1) scallop whole CaM.Ca(II)$_4$, Ikura *et al.*, 1985; (2) Drosophila recombinant whole CaM.Ca(II)$_4$ with a Y99 to F99 substitution, Ikura *et al.*, 1990; (3) scallop TR2C.CaM.Ca(II)$_2$, Ikura *et al.*, 1987; (4) rabbit skeletal TR2C.TnC.Ca(II)$_2$, Drabikowski *et al.*, 1985 ; (5) rabbit whole s-TnC.Ca(II)$_4$, Tsuda *et al.*, 1988). Blank entries indicate that the chemical shift for the proton groups of the homologous residue were not measured or could not be assigned.

Scallop/ Drosophila CaM		Rabbit skeletal TnC		Turkey skeletal TnC	
F89δCH2		F99δCH2	6.42(4)	F102δCH2	6.37
ξCH2		ξCH2	6.96(4)	ξCH2	6.92
ςCH		ςCH		ςCH	7.16
V91γCH3		I101γCH3		I104γCH3	0.54
F92δCH2		F102δCH2	7.59(4),6.47(5)	F105δCH2	
ξCH2		ξCH2	6.95(5)	ξCH2	
ςCH		ςCH	7.25(5)	ςCH	
G98NH	10.70(1),10.65(2),10.59(3)	G108NH	10.34(5)	G111NH	10.40
Y99/F99αCH	5.20(1),5.19(3)	Y109αCH	5.29(5)	F112αCH	5.35
δCH2	6.95(1)	δCH2	6.77(4),6.76(5)	δCH2	6.89
ξCH2	7.48(1)	ξCH2	6.85(4),8.86(5)	ξCH2	7.36
I100αCH	4.93(1),4.87(3)	I110αCH	5.05(5)	I113αCH	5.25
NH	10.22(1),10.25(2),10.15(3)	NH	9.74(5)	NH	10.02
γCH3	1.02(1)	γCH3	0.92(5)	γCH3	0.91
δCH3	0.31(1)	δCH3	0.22(5)	δCH3	0.27
V108γCH3		I118γCH3		I121γCH3	0.44
V136αCH	5.29(1),5.25(3)	I146αCH	5.39(5)	I149αCH	5.35
NH	9.21(1),9.30(2),9.12(3)	NH	9.08(5)	NH	9.14
γCH3	1.34(1)	γCH3	1.31(5)	γCH3	0.91
δCH3	0.99(1)	δCH3	0.89(5)	δCH3	0.66
Y138δCH2		F148δCH2	6.54(4)	F151δCH2	6.56
ξCH2		ξCH2		ξCH2	7.18
ςCH		ςCH		ςCH	7.29
F141δCH2	6.98(1)	F151δCH2	6.59(5)	F154δCH2	6.68
ξCH2	7.18(1)	ξCH2	7.44(4),7.18(5)	ξCH2	7.09
ςCH		ςCH	7.33(5)	ςCH	7.47

Table VI-2. Assignable intra- and interresidue NOEs observed in turkey s-TnC.Ca(II)$_4$ and comparison with those observed in rabbit s-TnC.Ca(II)$_4$ ((1) Drabikowski *et al.*, 1985).

Turkey s-TnC.Ca(II)4	Rabbit s-TnC.Ca(II)4 (1)
Intraresidue	
F102 δCH2 - F102 ξCH2	F99 δCH2 - F99 ξCH2
F102 δCH2 - F102 ςCH	
F102 ξCH2 - F102 ςCH	F99 ξCH2 - F99 ςCH
F112 αCH - F112 δCH2	Y109 αCH - Y109 δCH2
F112 αCH - F112 ξCH2	Y109 αCH - Y109 ξCH2
F112 δCH2 - F112 ξCH2	Y109 δCH2 - Y109 ξCH2
I113 NH - I113 γCH3	
I149 αCH - I149 NH	I146 αCH - I146 NH
I149 NH - I149 γCH3	
F151 δCH2 - F151 ξCH2	F148 δCH2 - F148 ξCH2
F151 δCH2 - F151 ςCH	F148 δCH2 - F148 ςCH
F154 δCH2 - F154 ξCH2	F151 δCH2 - F151 ξCH2
F154 ξCH2 - F154 ςCH	F151 ξCH2 - F151 ςCH
Interresidue	
(a) nOes between residues in the aromatic ring cluster	
F102 δCH2 - F151 δCH2	F99 δCH2 - F148 δCH2
F102 ξCH2 - F151 δCH2	F99 ξCH2 - F148 δCH2
F102 δCH2 - F154 ξCH2	F99 δCH2 - F151 ξCH2
F102 δCH2 - F154ςCH	
F102 ξCH2 - F154 ξCH2	F99 ξCH2 - F151 ξCH2
F102 ςCH - F154 δCH2	
F151 δCH2 - F154 ξCH2	F148 δCH2 - F151 ξCH2
(b) nOes between residues in the aromatic ring cluster and residues in the β-sheet region	
F102 δCH2 - I113 δCH3	F99 δCH2 - CH3 (0.20ppm)
F102 ξCH2 - F112 αCH	F99 ξCH2 - Y109 αCH
F102 ξCH2 - I113 δCH3	
F102 ξCH2 - I113 γCH3	F99 ξCH2 - CH3 (0.71,0.90ppm)
F102 ξCH2 - I149 δCH3	
F102 ξCH2 - I149 γCH3	F99 ξCH2 - CH3 (0.71,0.90ppm)
F102 ξCH2 - I149 αCH	F99 ξCH2 - I146 αCH
F102 ςCH - F112 αCH	F99 ςCH - Y109 αCH

(b) (continued)

F102 ςCH - I113 NH	
F102 ςCH - I149 αCH	F99 ςCH - I146 αCH
F112 αCH - F154 ξCH2	
I113 δCH3 - F151 δCH2	
I149 αCH - F154 ξCH2	

(c) nOes between residues in the β-sheet region

G111NH - F112 δCH2	
F112 αCH - I113 NH	Y109 αCH - I110 NH
F112 δCH2 - I113 αCH	
F112 δCH2 - I113 δCH3	
F112 δCH2 - I113 γCH3	
F112 δCH2 - I113 NH	
F112 ξCH2 - I113 αCH	
I113 NH - I149 γCH3	

Table VI-3. TnI peptide-TnC protein NOEs observed in the NOESY spectrum of the 0.4 molar equivalents TnC protein to TnI peptide sample at 500 MHz in 80%H_2O/20%D_2O, and the 0.3 molar equivalents TnC protein to TnI peptide sample at 600 MHz in 100%D_2O. NOEs involving TnI peptide and TnC protein resonances which were chemically shift degenerate could not be unequivocally assigned to a single proton group on the peptide or protein.

Turkey s-TnC.Ca(II)4	N-Ac TnI (104-115) NH2
500 MHz / H2O	
I104,I121 γCH3 (0.48ppm)	L111 (δCH3)2, V114 (γCH3)2 (0.88,0.93ppm)
I104,I121 γCH3 (0.48ppm)	R108,112,113,115 δCH2 (3.20ppm)
I104,I121 γCH3 (0.48ppm)	K107,L111,R115 αCH (4.29ppm)
F102 ξCH2 (6.92ppm)	F106 αCH (4.70ppm)
F151 ςCH (7.29ppm)	R112,113 αCH (4.36ppm)
F154 δCH2 (6.68 ppm)	F106 αCH (4.70ppm)
F154 ξCH2 (7.09 ppm)	K107,L111,R115 αCH (4.29ppm)
F154 ξCH2 (7.09 ppm)	F106 αCH (4.70ppm)
600 MHz / D2O	
I104,I121 γCH3 (0.48ppm)	L111 (δCH3)2, V114 (γCH3)2 (0.88,0.93ppm)
I104,I121 γCH3 (0.48ppm)	V114 αCH (4.10ppm)
I104,I121 γCH3 (0.48ppm)	R112,113 αCH (4.36ppm)
I104,I121 γCH3 (0.48ppm)	F106 δCH2 (7.23ppm)
I113 δCH3 (0.31ppm)	L111 αCH (4.29ppm)
I113 δCH3 (0.31ppm)	F106 δCH2 (7.23ppm)
F112 αCH (5.32ppm)	F106 ξCH2 (7.30ppm)
F102 δCH2 (6.38ppm)	V114 (γCH3)2 (0.93ppm)
F151 δCH2 (6.57ppm)	V114 (γCH3)2 (0.93ppm)
F154 δCH2 (6.70ppm)	V114 (γCH3)2 (0.93ppm)

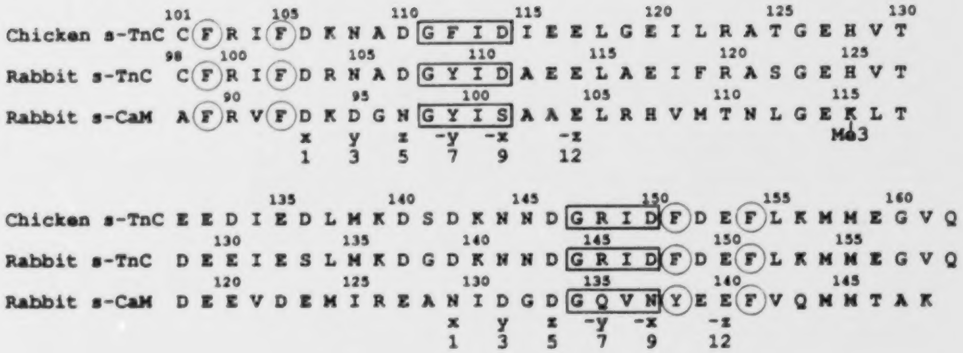
101 105 110 115 120 125 130
Chicken s-TnC C F R I F D K N A D G F I D I E E L G E I L R A T G E H V T
98 100 105 110 115 120 125
Rabbit s-TnC C F R I F D R N A D G Y I D A E E L A E I F R A S G E H V T
90 95 100 105 110 115
Rabbit s-CaM A F R V F D K D G N G Y I S A A E L R H V M T N L G E K L T
x y z -y -x -z
1 3 5 7 9 12
Me3
135 140 145 150 155 160
Chicken s-TnC E E D I E D L M K D S D K N N D G R I D F D E F L K M M E G V Q
130 135 140 145 150 155
Rabbit s-TnC D E E I E S L M K D G D K N N D G R I D F D E F L K M M E G V Q
120 125 130 135 140 145
Rabbit s-CaM D E E V D E M I R E A N I D G D G Q V N Y E E F V Q M M T A K
x y z -y -x -z
1 3 5 7 9 12

Figure VI-1. The amino acid sequence alignment of chicken s-TnC (Wilkinson, 1976), rabbit s-TnC (Collins *et al.*, 1973) and rabbit CaM (Nairn *et al.*, 1984). The amino acid numbering is indicated at the top of each sequence. Residues involved in coordinating Ca(II) are labelled as x, y, z, -y, -x and -z at positions 1, 3, 5, 7, 9 and 12, respectively. Circled residues are those comprising the aromatic cluster in the hydrophobic pocket of the C-terminal domain. Boxed residues are those involved in the antiparallel β-sheet formation between Ca(II) binding loops III and IV.

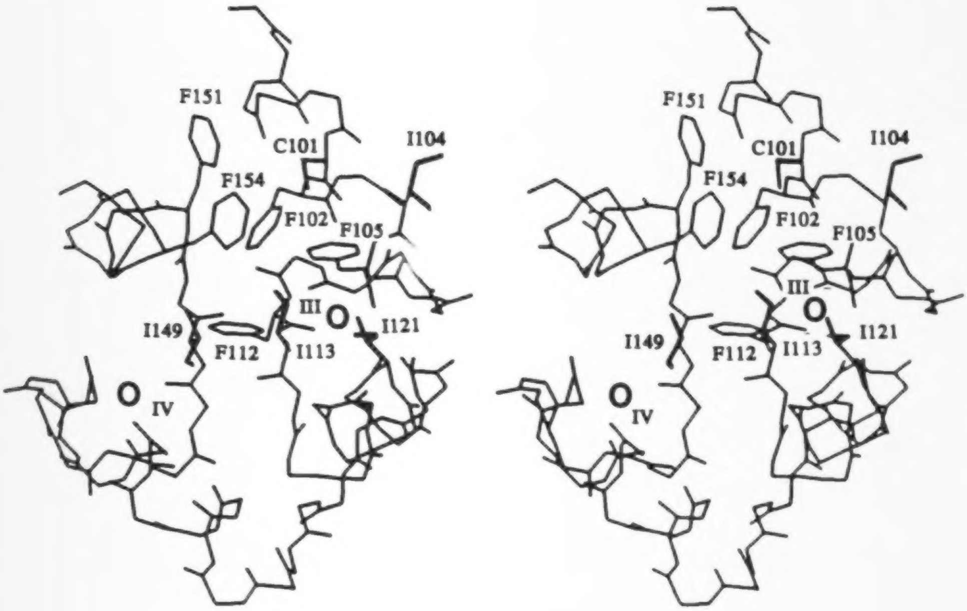
F151
C101
I104
F154
F102
F105
III
I149
F112
I113
I121
IV
F151
C101
I104
F154
F102
F105
III
I149
F112
I113
I121
IV

Figure VI-2. Stereo diagram of the hydrophobic pocket in the C-terminal domain of the crystal structure of turkey s-TnC (Herzberg and James, 1985) showing selected residues in the aromatic cluster and the antiparallel β-sheet region between Ca(II) binding loops III and IV. Ca(II) ions are shown as the open circles. Labelled residues include F102, I104, F105, I121, F151 and F154 in the hydrophobic pocket, and F112, I113 and I149 in the β-sheet region.

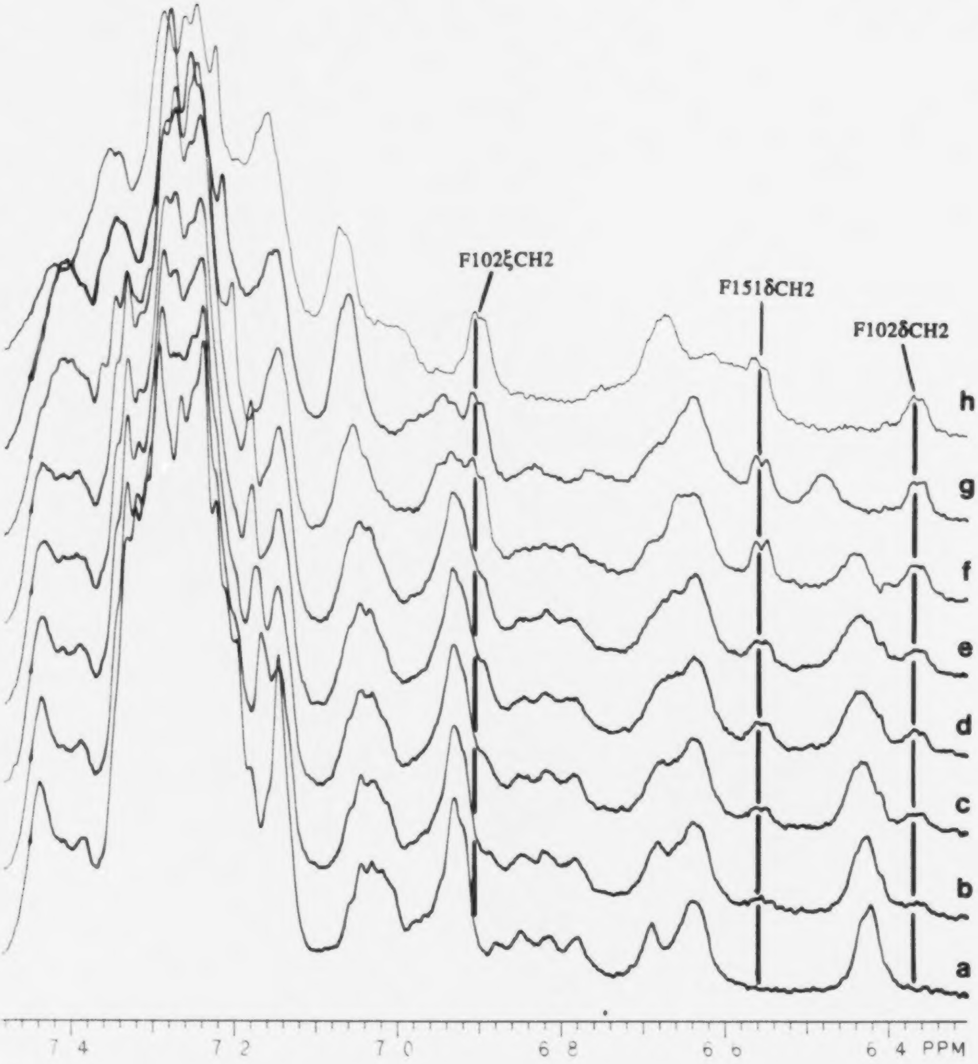

Figure VI-3. 500 MHz ^{1}H NMR monitored Ca(II) titration of turkey s-TnC showing slow exchange behaviour of the ring proton resonances of F102 and F151 in the C-terminal domain **a.** 0.0 **b.** 0.5 **c.** 1.0 **d.** 1.5 **e.** 2.0 **f.** 2.5 **g.** 3.0 **h.** 4.0 molar equivalents Ca(II) to TnC protein. (Sample was 1.1 mM turkey s-TnC, 150 mM KCl, pH 6.7, 80%H_2O/20%D_2O, 30°C.) (Titration data and figure borrowed by permission from Carolyn M. Slupsky.)

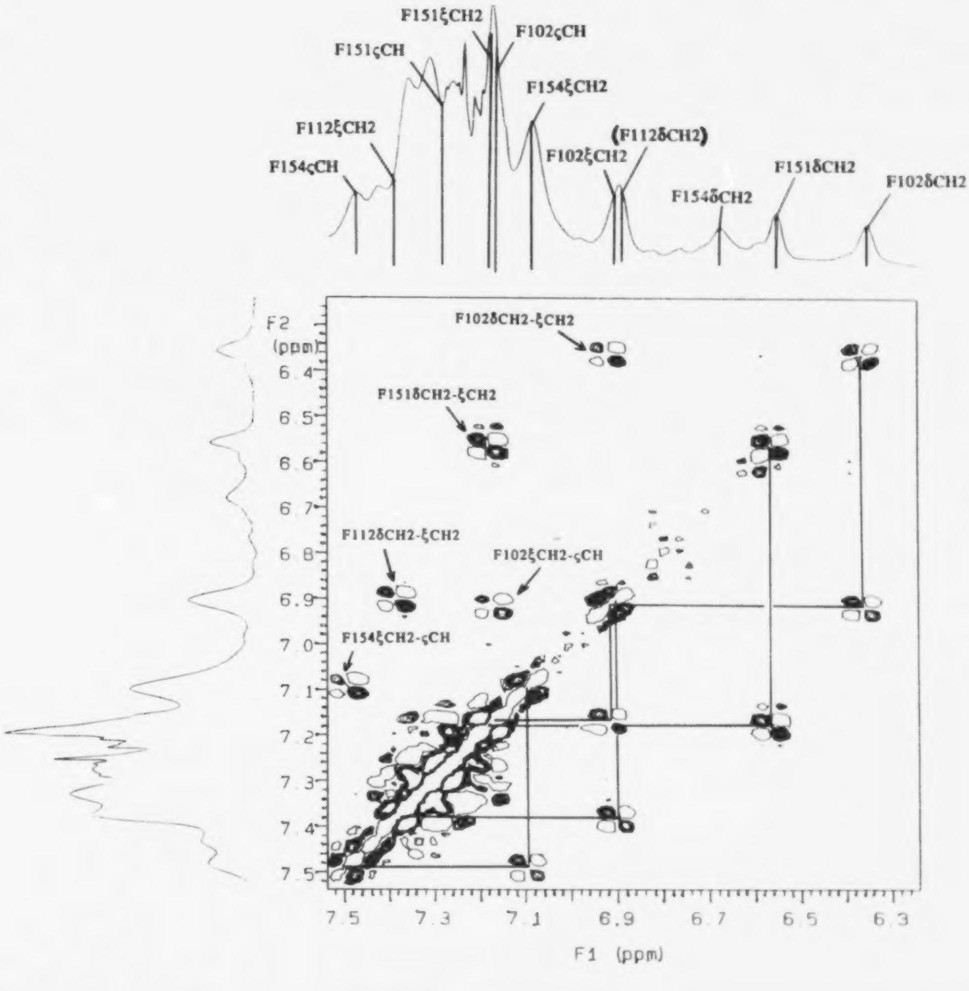

Figure VI-4. 600 MHz ^{1}H DQFCOSY spectrum showing COSY cross-peaks for the aromatic spin systems of F102, F151, F154 and F112. The brackets around F112 indicate a tentative assignment. Accompanying one-dimensional spectra are plotted with the TnC assignments shown on the horizontal axis. (Sample was 2.0 mM turkey s-TnC, 12 mM $CaCl_2$, 100 mM KCl, pD 6.2, 100%D_2O, 30°C.)

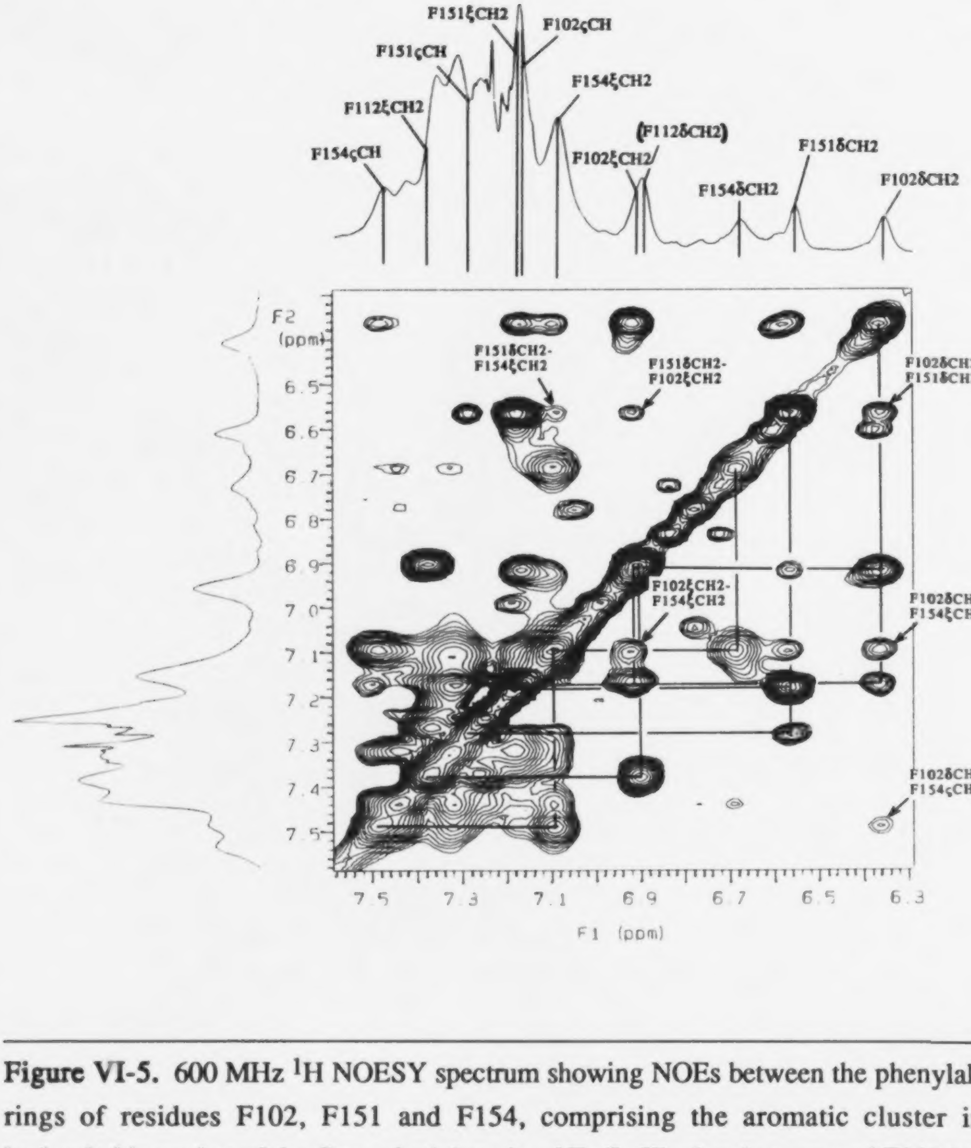

Figure VI-5. 600 MHz ^{1}H NOESY spectrum showing NOEs between the phenylalanine rings of residues F102, F151 and F154, comprising the aromatic cluster in the hydrophobic pocket of the C-terminal domain of TnC. The brackets around F112 indicate a tentative assignment. Accompanying one-dimensional spectra are plotted with the TnC assignments shown on the horizontal axis. (Sample was 2.0 mM turkey s-TnC, 12 mM $CaCl_2$, 100 mM KCl, pD 6.2, 100%D_2O, 30°C; τ_m = 150 ms.)

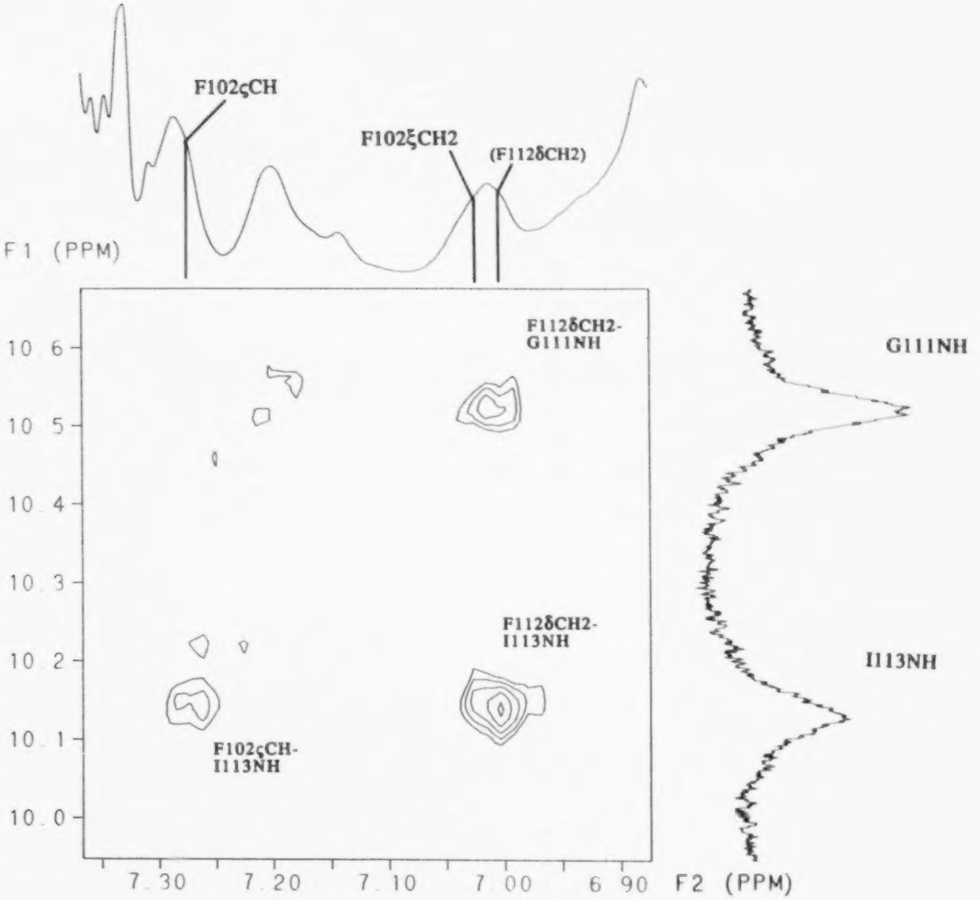

Figure VI-6. 500 MHz ^{1}H NOESY spectrum showing NOEs between the δCH2 ring protons of F112 and main chain amide protons of G111 and I113 in the β-sheet region between Ca(II) binding loops III and IV. The brackets around F112 indicate a tentative assignment. Accompanying one-dimensional spectra are plotted with the TnC assignments shown on the vertical and horizontal axes. (Sample was 3.6 mM turkey s-TnC, 16 mM $CaCl_2$, 100 mM KCl, pH 6.0, 80%H_2O/20%D_2O, 30°C; $\tau_m = 150$ ms.)

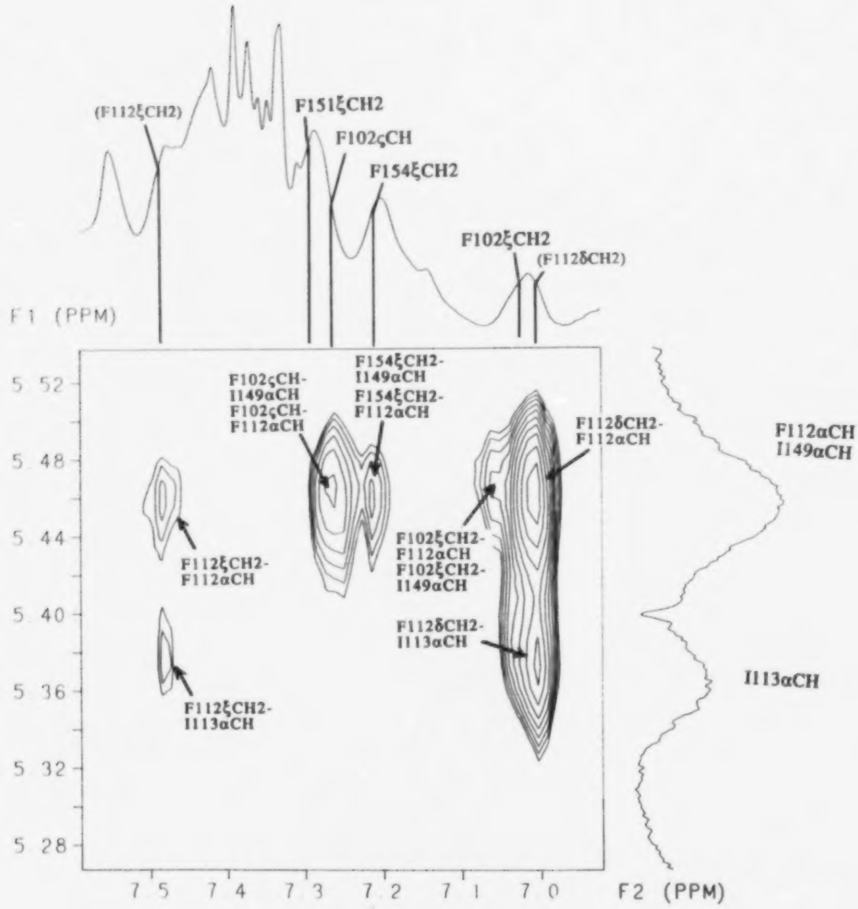

Figure VI-7. 500 MHz ^{1}H NOESY spectrum showing NOEs between the δCH2 and ξCH2 ring protons of F112 and the α-protons of F112 and I113, and between the ξCH2 ring protons of F154 and the α-protons of F112 and I149. The brackets around F112 indicate a tentative assignment. Accompanying one-dimensional spectra are plotted with the TnC assignments shown on the vertical and horizontal axes. (Sample was 3.6 mM turkey s-TnC, 16 mM $CaCl_2$, 100 mM KCl, pH 6.0, 80%H_2O/20%D_2O, 30°C; τ_m = 150 ms.)

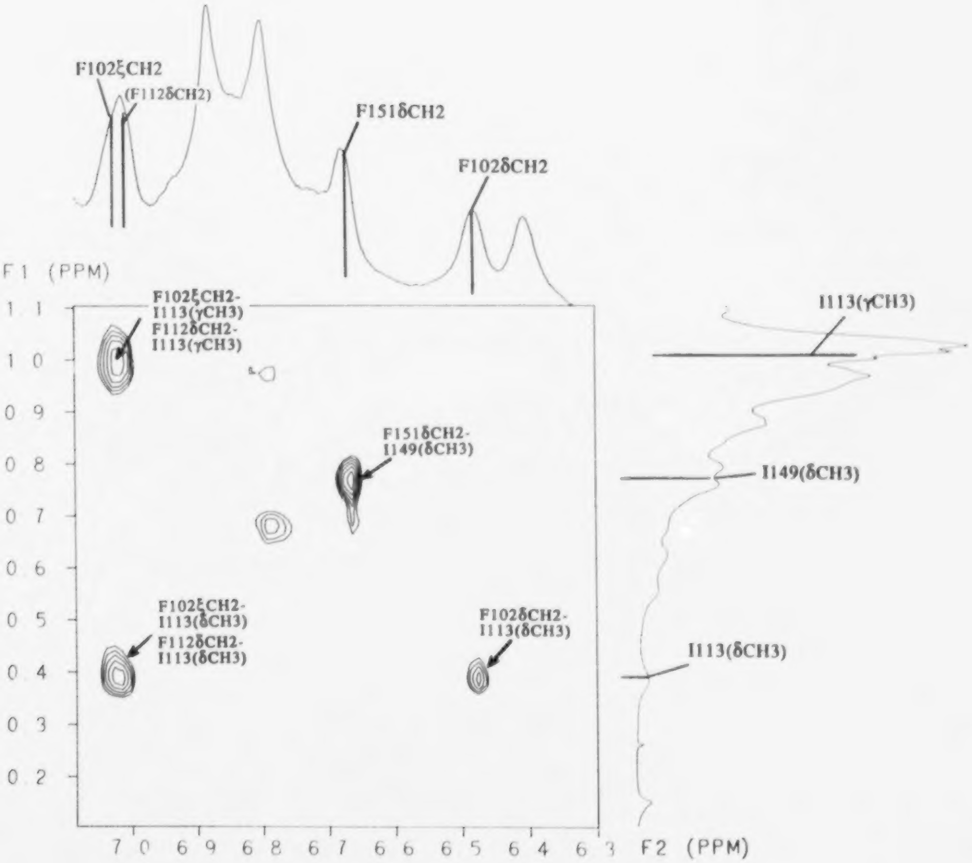

Figure VI-8. 500 MHz ^{1}H NOESY spectrum showing NOEs between residues in the C-terminal hydrophobic pocket and residues in the β-sheet region between Ca(II)-binding loops III and IV. NOEs are shown between the δCH2 and ξCH2 ring protons of F102 and δCH3 methyl protons of I113, and between the δCH2 ring protons of F151 and the δCH3 methyl protons of I149. Also shown are NOEs between the δCH2 ring protons of F112 and the δCH3 and γCH3 methyl protons of I113. The brackets around F112 indicate a tentative assignment. Accompanying one-dimensional spectra are plotted with the TnC assignments shown on the vertical and horizontal axes. (Sample was 3.6 mM turkey s-TnC, 16 mM $CaCl_2$, 100 mM KCl, pH 6.0, 80%H_2O/20%D_2O, 30°C; τ_m = 150 ms.)

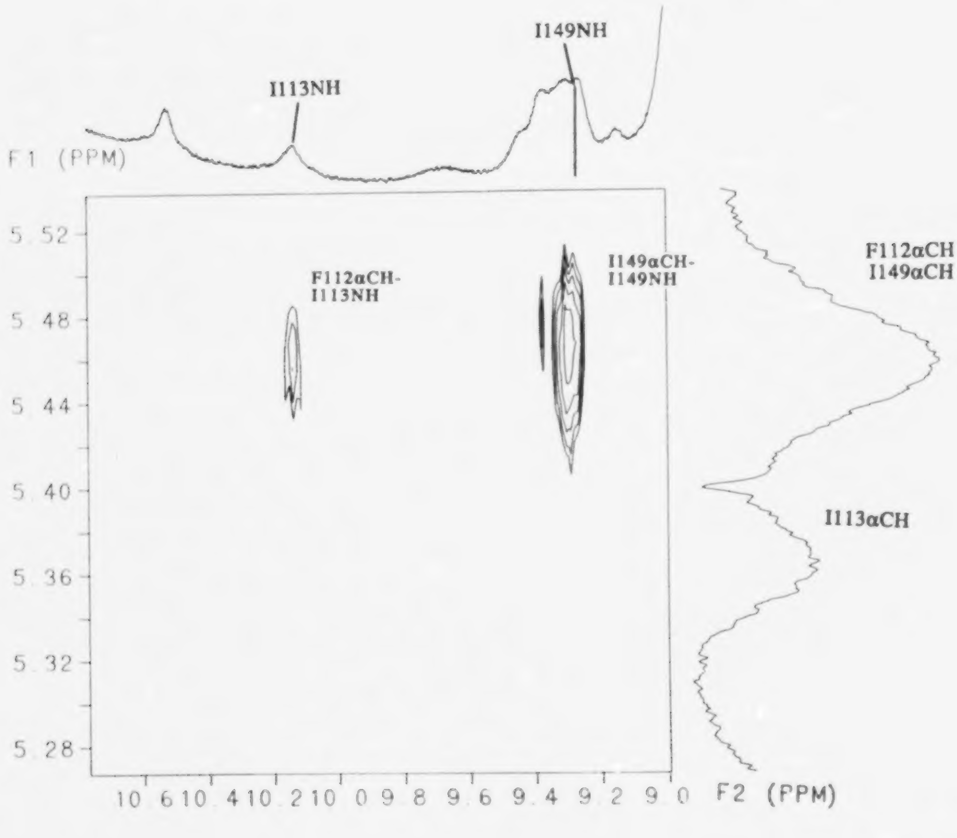

Figure VI-9. 500 MHz ^{1}H NOESY spectrum showing an NOE between the α-proton of F112 and the backbone amide proton of I113. Accompanying one-dimensional spectra are plotted with the TnC assignments shown on the vertical and horizontal axes. (Sample was 3.6 mM turkey s-TnC, 16 mM $CaCl_2$, 100 mM KCl, pH 6.0, 80%H_2O/20%D_2O, 30°C; τ_m = 150 ms.)

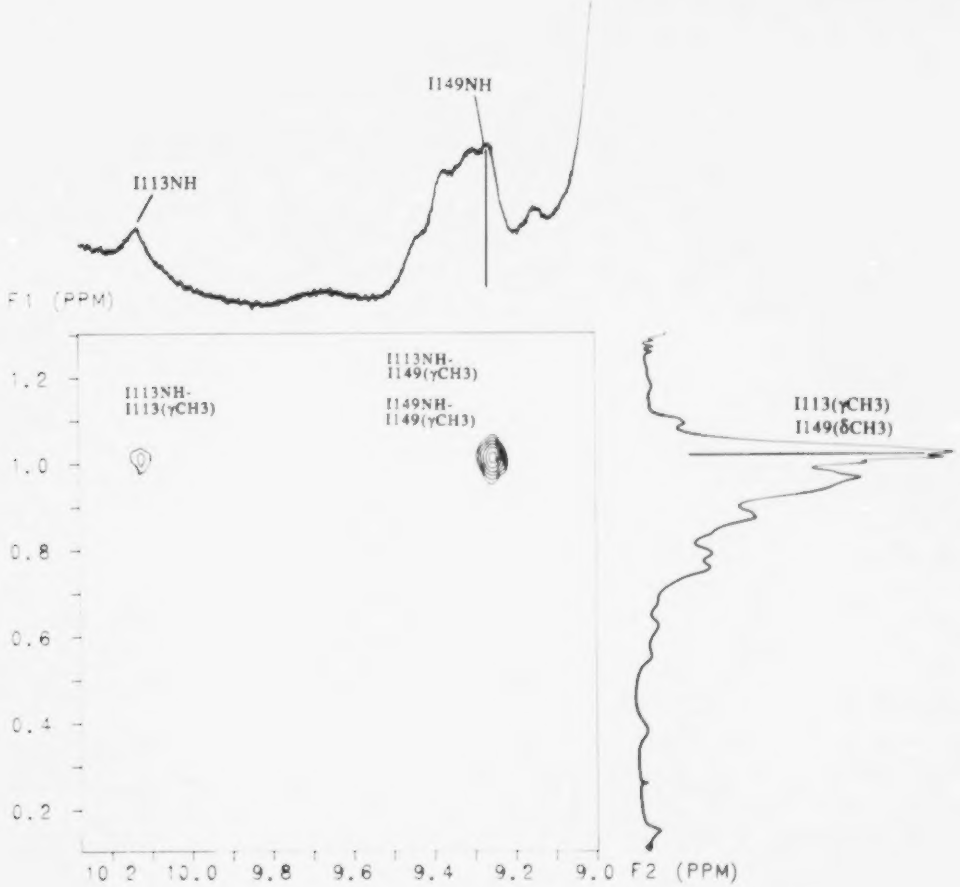

Figure VI-10. 500 MHz ^{1}H NOESY spectrum showing a cross-strand NOE between the amide protons of I113 and the γCH3 methyl protons of I149 in the β-sheet region between Ca(II) binding loops III and IV. Accompanying one-dimensional spectra are plotted with the TnC assignments shown on the vertical and horizontal axes. (Sample was 3.6 mM turkey s-TnC, 16 mM $CaCl_2$, 100 mM KCl, pH 6.0, 80%H_2O/20%D_2O, 30°C; τ_m = 150 ms.)

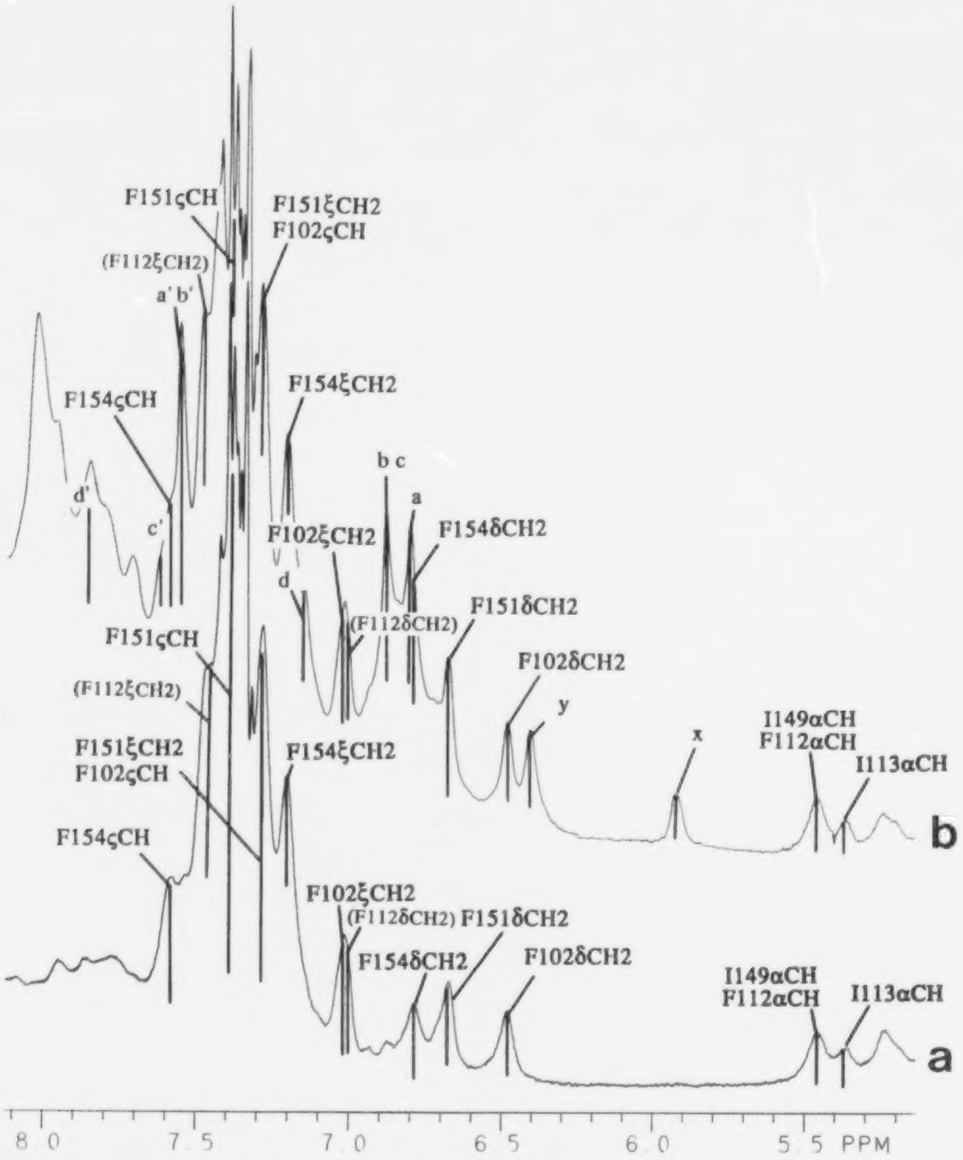

Figure VI-11. Lowfield region of the 500 MHz ^{1}H NMR spectrum of turkey s-TnC **a.** in D_2O and **b.** $80\%H_2O/20\%D_2O$. The assignments for the aromatic ring proton resonances of F102, F112, F151 and F154 are shown, as well as the assignments for the downfield α-proton resonances of F112, I113 and I149. Also shown are the exchangeable side chain amide proton pairs, a/a', b/b', c/c', d/d', and x/y which display exchange cross-peaks to each other in the NOESY spectrum of this region. The brackets around F112 indicate a tentative assignment. (Sample was 3.6 mM turkey s-TnC, 16 mM $CaCl_2$, 100 mM KCl, pH 6.0, $80\%H_2O/20\%D_2O$, 30°C.)

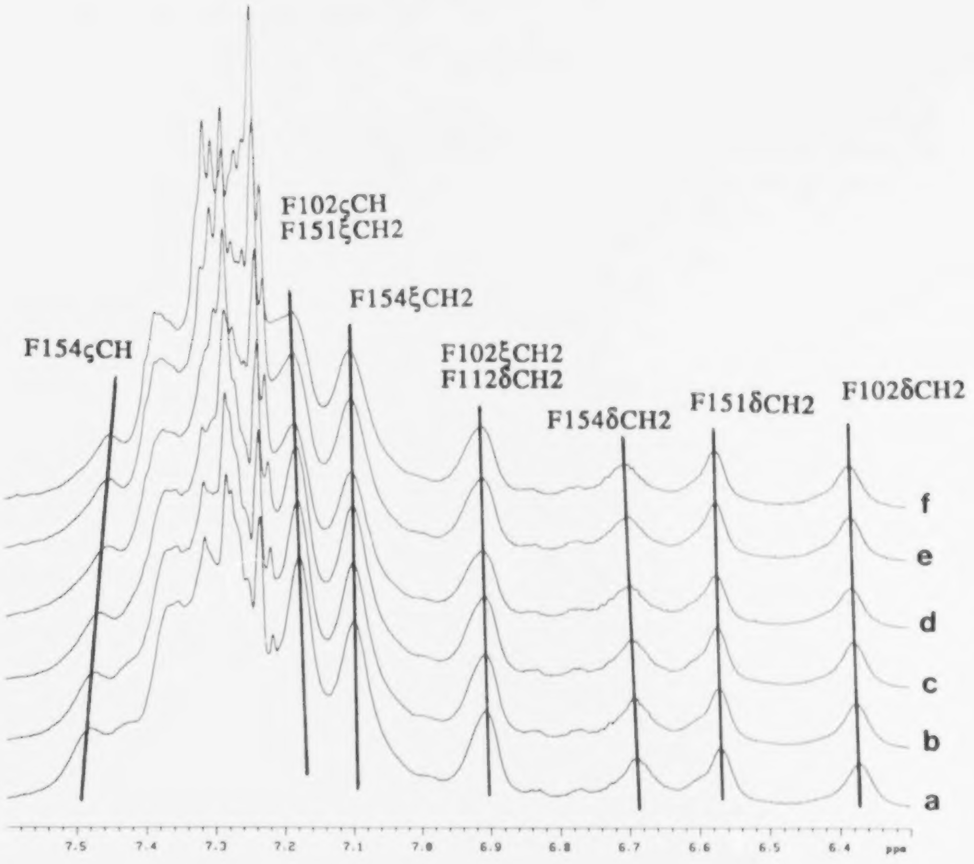

Figure VI-12. Aromatic region of the 600 MHz ^{1}H NMR monitored titration of Ca(II)-saturated TnC with TnI peptide. A slight downfield shift for F154δCH2 and a marked upfield shift for F154ςCH are observed. **a.** protein alone **b.** 1.9 **c.** 1.0 **d.** 0.5 **e.** 0.4 and **f.** 0.3 molar equivalents TnC protein to TnI peptide. (TnC protein sample was 0.9 mM turkey s-TnC, 6 mM $CaCl_2$, 100 mM KCl, pD 6.2, 100%D_2O, 30°C; panels **b.** through **f.** contained 0.45 mM, 0.88 mM, 1.74 mM, 2.15 mM and 2.96 mM TnI peptide, respectively.)

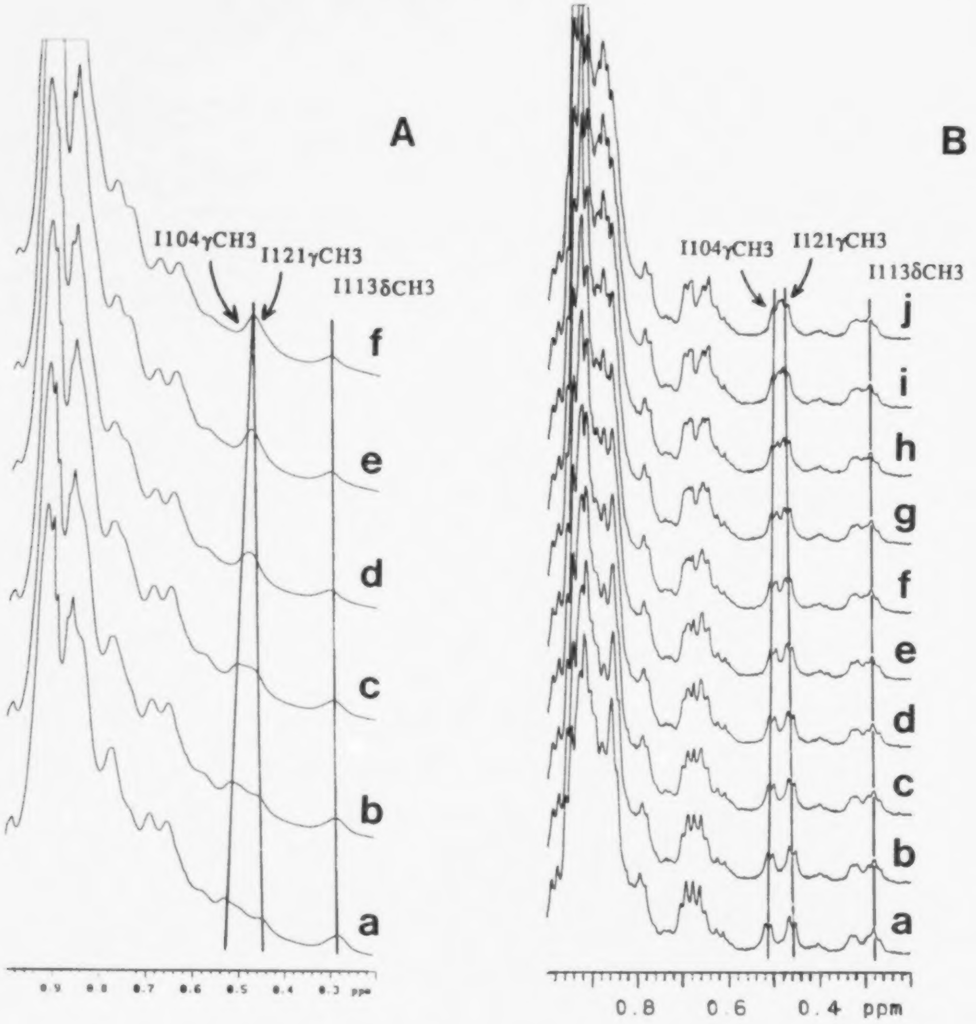

Figure VI-13. **A.**Upfield region of the 600 MHz ^{1}H NMR monitored titration of Ca(II)-saturated TnC with TnI peptide; **B.** Upfield region of the 600 MHz ^{1}H NMR monitored titration of the Ca(II)-saturated chicken s-TnC Site III/Site IV heterodimer with TnI peptide. Marked downfield shifts for I113δCH3 and I121γCH3, and a marked upfield shift for I104γCH3 are observed in both titrations. **A.** **a.** protein alone **b.** 1.9 **c.** 1.0 **d.** 0.5 **e.** 0.4 and **f.** 0.3 molar equivalents TnC protein to TnI peptide. (TnC protein sample was 0.9 mM turkey s-TnC, 6 mM $CaCl_2$, 100 mM KCl, pD 6.2, 100%D_2O, 30°C; panels b. through **f.** contained 0.45 mM, 0.88 mM, 1.74 mM, 2.15 mM and 2.96 mM TnI peptide, respectively.) **B.** **a.** protein alone **b.** 7.1 **c.** 3.6 **d.** 2.4 **e.** 1.8 **f.** 1.4 **g.** 1.2 **h.** 1.0 **i.** 0.9 and **j.** 0.8 molar equivalents TnC protein to Site III/Site IV heterodimer. (Shaw, personal communications)

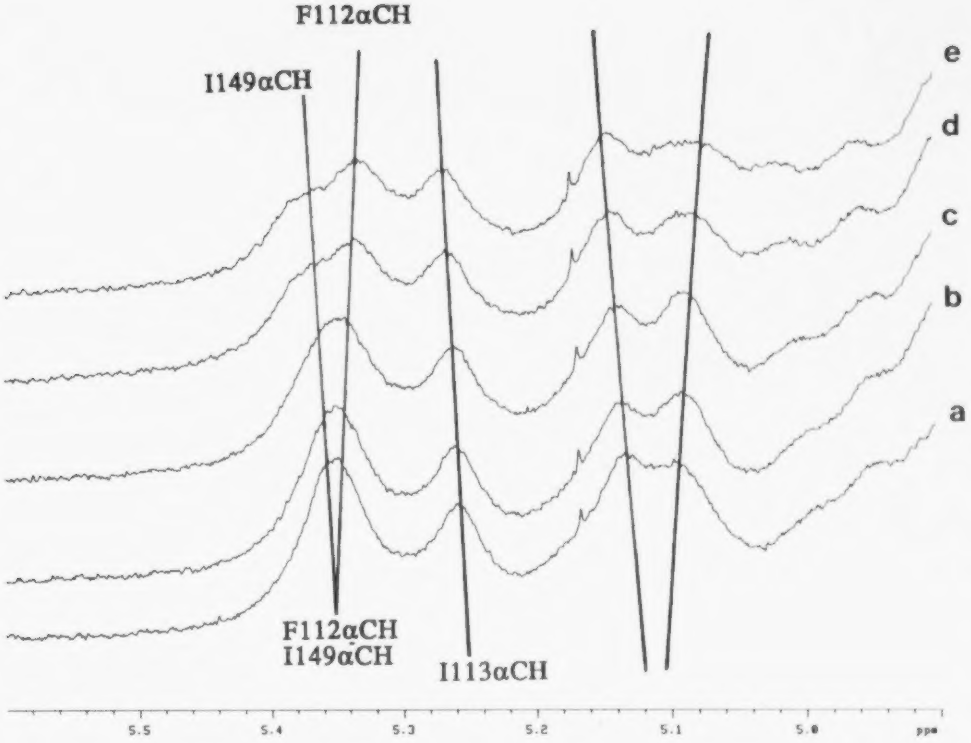

Figure VI-14. α-proton region of the 600 MHz ^{1}H NMR monitored titration of Ca(II)-saturated TnC with TnI peptide. A downfield shift for I113αCH and marked upfield and downfield shifts for F112αCH and I149αCH are observed. **a.** protein alone **b.** 1.9 **c.** 0.5 **d.** 0.4 and **e.** 0.3 molar equivalents TnC protein to TnI peptide. (TnC protein sample was 0.9 mM turkey s-TnC, 6 mM $CaCl_2$, 100 mM KCl, pD 6.2, 100%D_2O, 30°C; panels **b.** through **e.** contained 0.45 mM, 0.88 mM, 2.15 mM and 2.96 mM TnI peptide, respectively.)

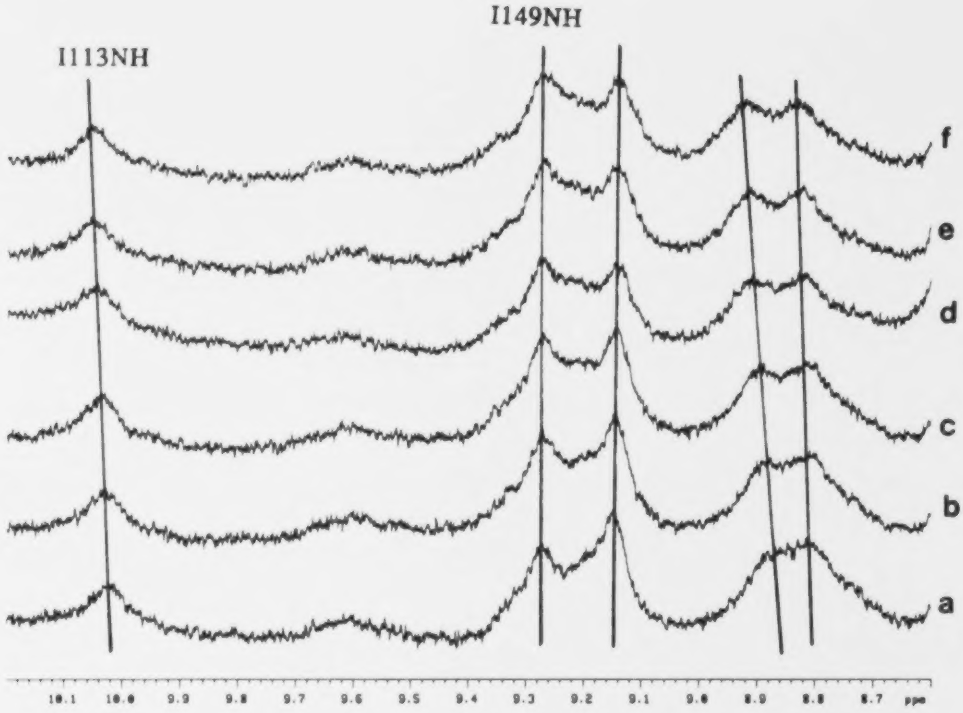

Figure VI-15. Backbone amide region of the 600 MHz ^{1}H NMR monitored titration of Ca(II)-saturated TnC with TnI peptide. Slight downfield shifts for I113NH and I149NH are observed. **a.** protein alone **b.** 1.9 **c.** 1.0 **d.** 0.5 **e.** 0.4 and **f.** 0.3 molar equivalents TnC protein to TnI peptide. (TnC protein sample was 0.9 mM turkey s-TnC, 6 mM $CaCl_2$, 100 mM KCl, pD 6.2, 100%D_2O, 30°C; panels **b.** through **f.** contained 0.45 mM, 0.88 mM, 1.74 mM, 2.15 mM and 2.96 mM TnI peptide, respectively.)

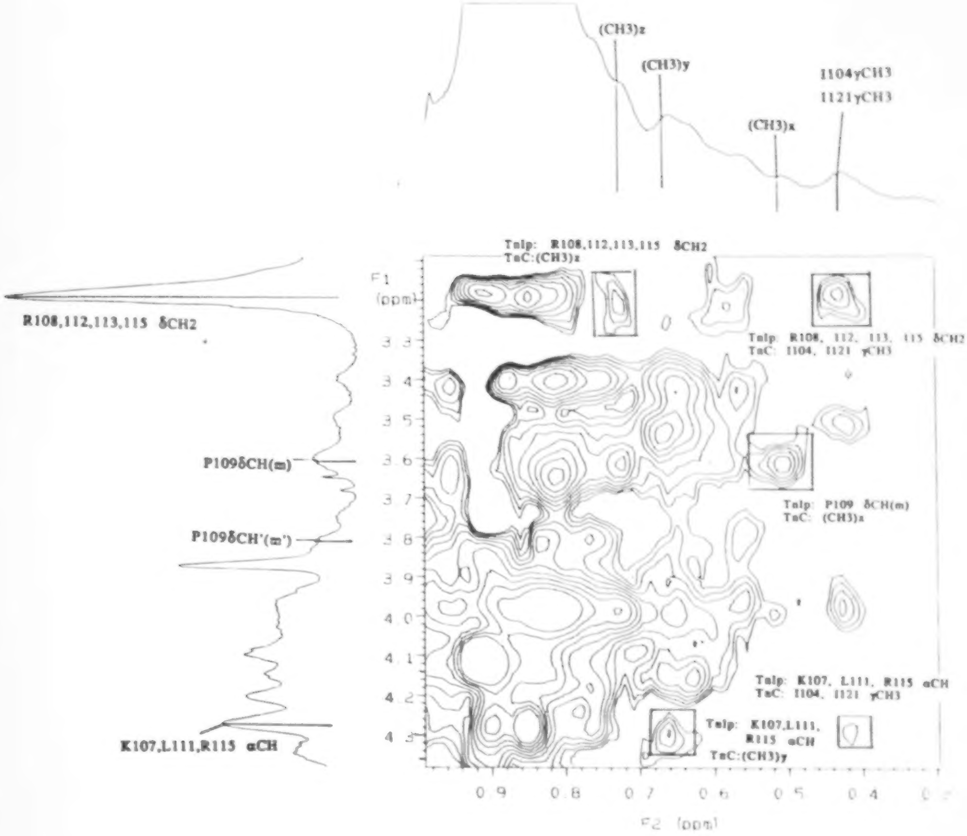

Figure VI-16. 500 MHz ^{1}H NOESY spectrum of the peptide-protein complex showing cross-peaks between I104γCH3 and I121γCH3 on TnC and various residues on the TnI peptide. Also shown are peptide-protein cross-peaks involving the unassigned, but upfield shifted methyl protons (CH3)x, (CH3)y, and (CH3)z on TnC. Accompanying one-dimensional spectra are plotted with the TnC assignments shown on the horizontal spectrum, and TnI peptide assignments shown on the vertical spectrum. (Sample was 9 mM Nα-acetyl-TnI(104-115) amide, 3.6 mM turkey s-TnC, 16 mM $CaCl_2$, 100 mM KCl, pH 6.0, 80%H_2O/20%D_2O, 30°C; $\tau_m = 150$ ms.)

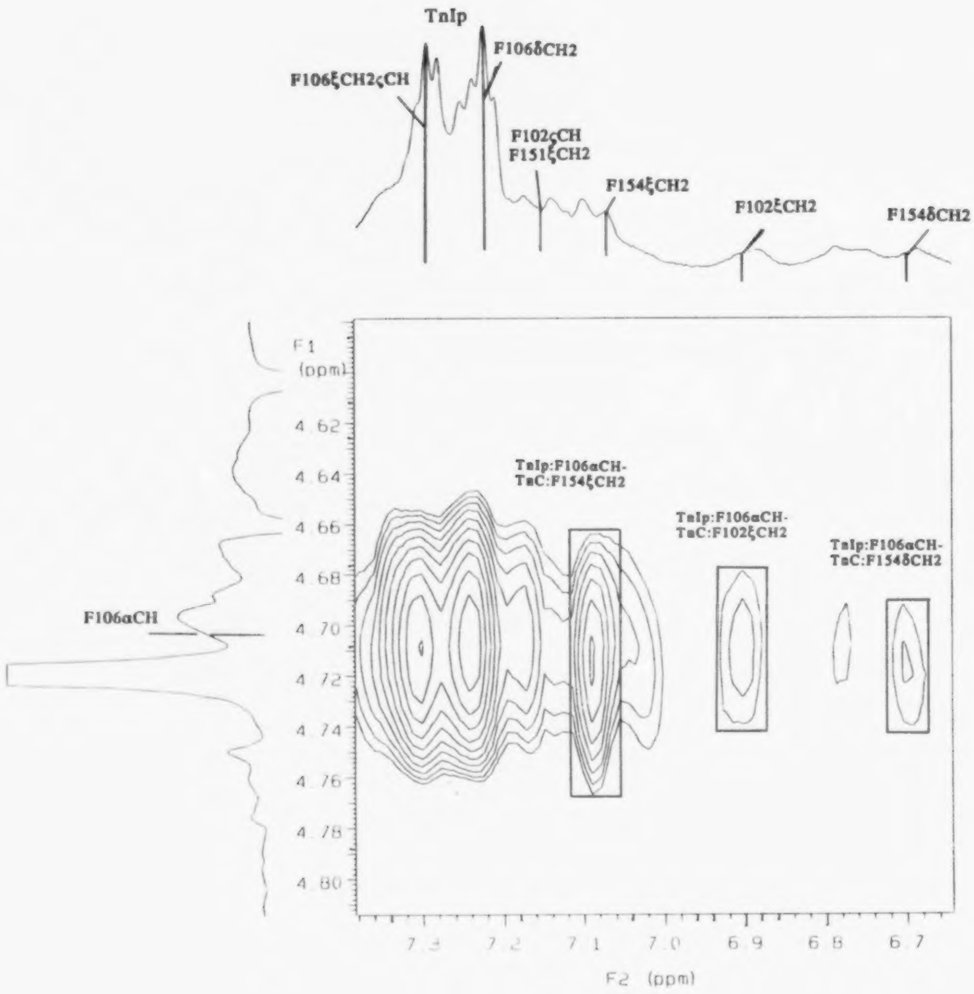

Figure VI-17. 500 MHz ^{1}H NOESY spectrum of the peptide-protein complex showing cross-peaks between F154ξCH2, F154δCH2 and F102ξCH2 on TnC and F106αCH on the TnI peptide. Accompanying one-dimensional spectra are plotted with TnC and TnI peptide assignments shown on the horizontal spectrum, and the TnI peptide F106αCH assignment shown on the vertical spectrum. (Sample was 9 mM Nα-acetyl-TnI(104-115) amide, 3.6 mM turkey s-TnC, 16 mM $CaCl_2$, 100 mM KCl, pH 6.0, 80%H_2O/20%D_2O, 30°C; $\tau_m = 150$ ms.)

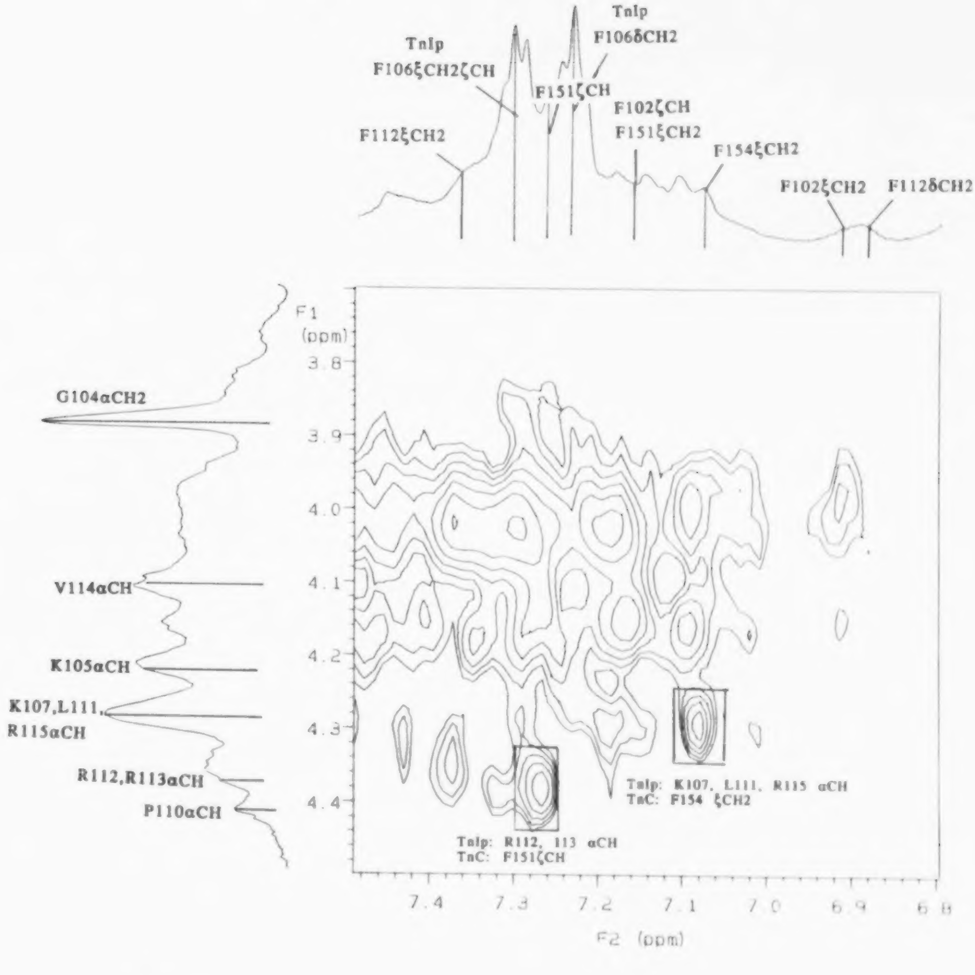

Figure VI-18. 500 MHz ^{1}H NOESY spectrum of the peptide-protein complex showing cross-peaks between aromatic ring protons on TnC and α-protons on the TnI peptide. Accompanying one-dimensional spectra are plotted with the TnC assignments shown on the horizontal spectrum, and TnI peptide assignments shown on the vertical spectrum. (Sample was 9 mM Nα-acetyl-TnI(104-115) amide, 3.6 mM turkey s-TnC, 16 mM $CaCl_2$, 100 mM KCl, pH 6.0, 80%H_2O/20%D_2O, 30°C; $\tau_m = 150$ ms.)

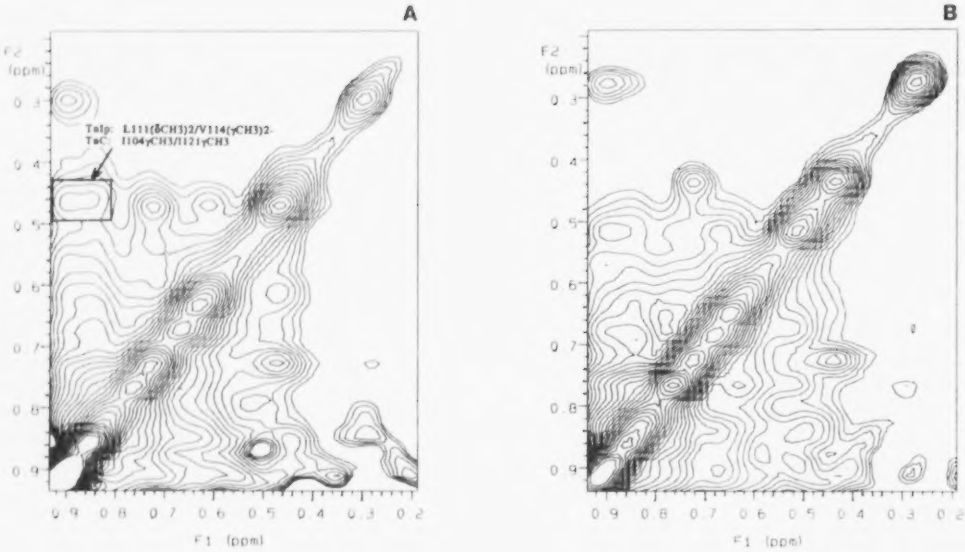

Figure VI-19. Upfield methyl region of the 600 MHz ^{1}H NOESY spectrum of **A.** TnI peptide-TnC protein complex, and **B.** TnC protein alone. Panel A shows a cross-peak connecting L111(δCH3)2 and V114(γCH3)2 on the TnI peptide to I104γCH3 and I121γCH3 on TnC. (TnI peptide-TnC protein sample was 2.96 mM Nα-acetyl-TnI(104-115) amide, 0.82 mM turkey s-TnC, 5 mM $CaCl_2$, 100 mM KCl, pD 6.1, 100%D_2O, 30°C; $\tau_m = 150$ ms.) (TnC protein sample was 2.0 mM turkey s-TnC, 12 mM $CaCl_2$, 100 mM KCl, pD 6.2, 100%D_2O, 30°C; $\tau_m = 150$ ms.)

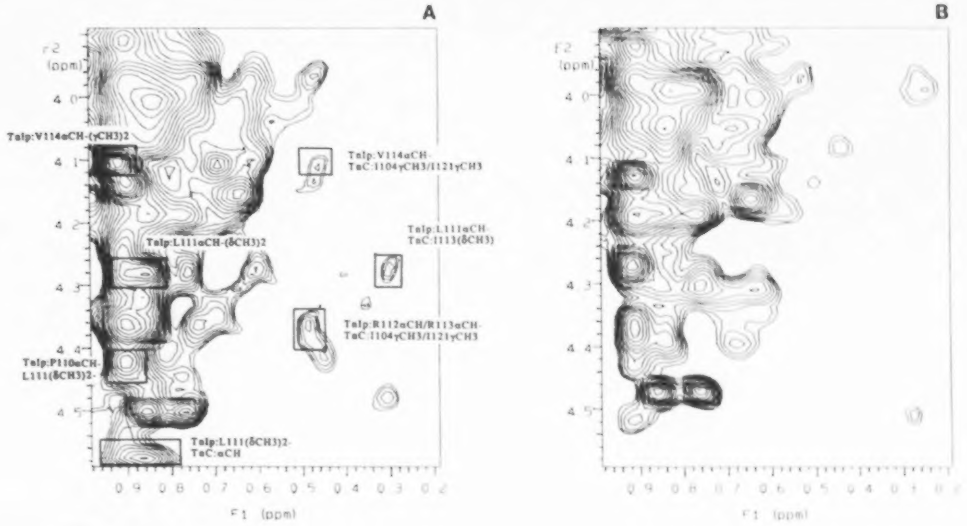

Figure VI-20. Upfield methyl to α-proton region of the 600 MHz ^{1}H NOESY spectrum of **A.** TnI peptide-TnC protein complex, and **B.** TnC protein alone. Panel A shows cross-peaks connecting L111αCH, R112αCH, R113αCH and V114αCH on the TnI peptide to I113δCH3, I104γCH3 and I121γCH3 on TnC. Intrapeptide TRNOEs are also shown which include L111αCH-(δCH3)2, P110αCH-L111(δCH3)2 and V114αCH-(γCH3)2. (TnI peptide-TnC protein sample was 2.96 mM Nα-acetyl-TnI(104-115) amide, 0.82 mM turkey s-TnC, 5 mM $CaCl_2$, 100 mM KCl, pD 6.1, 100%D_2O, 30°C; τ_m = 150 ms.) (TnC protein sample was 2.0 mM turkey s-TnC, 12 mM $CaCl_2$, 100 mM KCl, pD 6.2, 100%D_2O, 30°C; τ_m = 150 ms.)

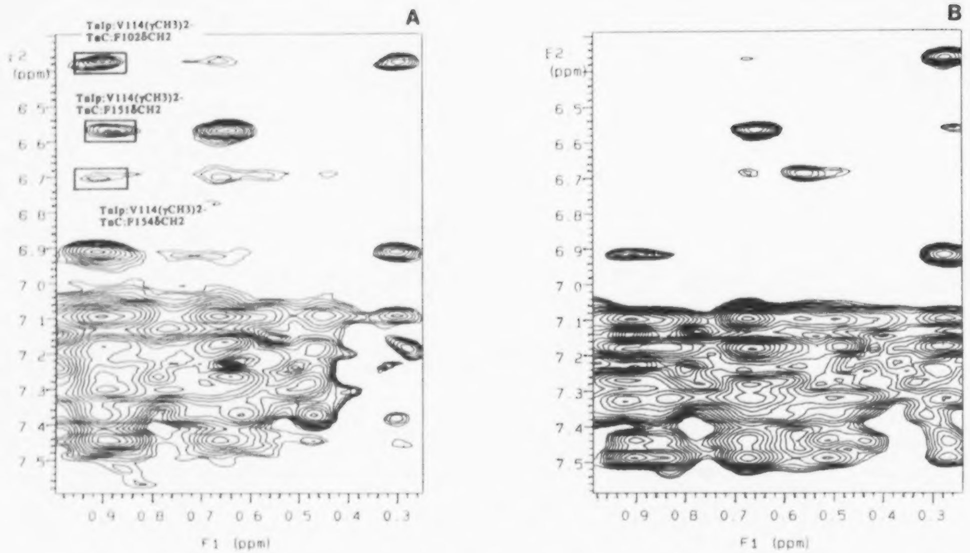

Figure VI-21. Upfield methyl to aromatic region of the 600 MHz ^{1}H NOESY spectrum of **A.** TnI peptide-TnC protein complex, and **B.** TnC protein alone. Panel A shows cross-peaks connecting V114(γCH3)2 on the TnI peptide to the aromatic ring proton resonances of F102δCH2, F151δCH2 and F154δCH2 on TnC. (TnI peptide-TnC protein sample was 2.96 mM Nα-acetyl-TnI(104-115) amide, 0.82 mM turkey s-TnC, 5 mM $CaCl_2$, 100 mM KCl, pD 6.1, 100%D_2O, 30°C; τ_m = 150 ms.) (TnC protein sample was 2.0 mM turkey s-TnC, 12 mM $CaCl_2$, 100 mM KCl, pD 6.2, 100%D_2O, 30°C; τ_m = 150 ms.)

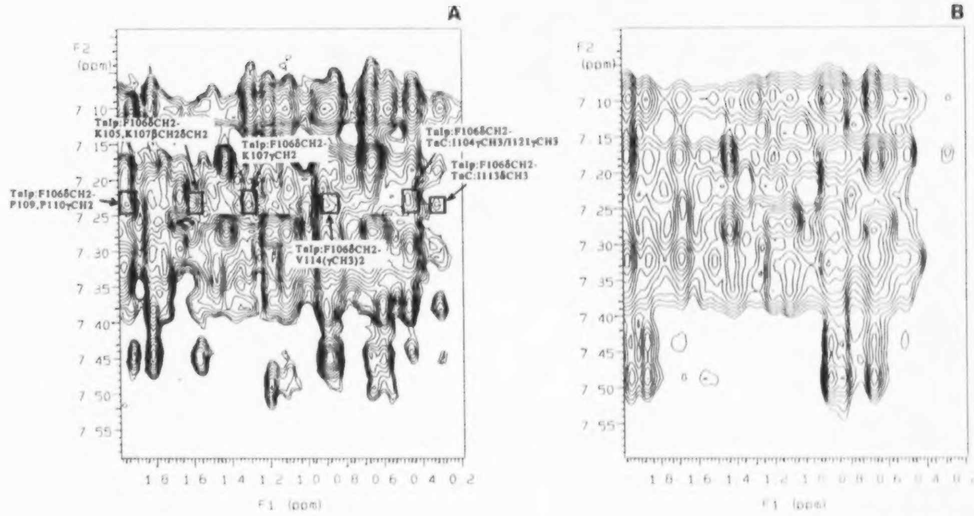

Figure VI-22. Aliphatic to aromatic region of the 600 MHz ^{1}H NOESY spectrum of **A.** TnI peptide-TnC protein complex, and **B.** TnC protein alone. Panel A shows a cross-peaks connecting F106δCH2 on the TnI peptide to I113δCH3, I104γCH3 and I121γCH3 on TnC. Intrapeptide TRNOEs are also shown, notably the long range F106δCH2-V114(γCH3)2 cross-peak. (TnI peptide-TnC protein sample was 2.96 mM Nα-acetyl-TnI(104-115) amide, 0.82 mM turkey s-TnC, 5 mM $CaCl_2$, 100 mM KCl, pD 6.1, 100%D_2O, 30°C; $\tau_m = 150$ ms.) (TnC protein sample was 2.0 mM turkey s-TnC, 12 mM $CaCl_2$, 100 mM KCl, pD 6.2, 100%D_2O, 30°C; $\tau_m = 150$ ms.)

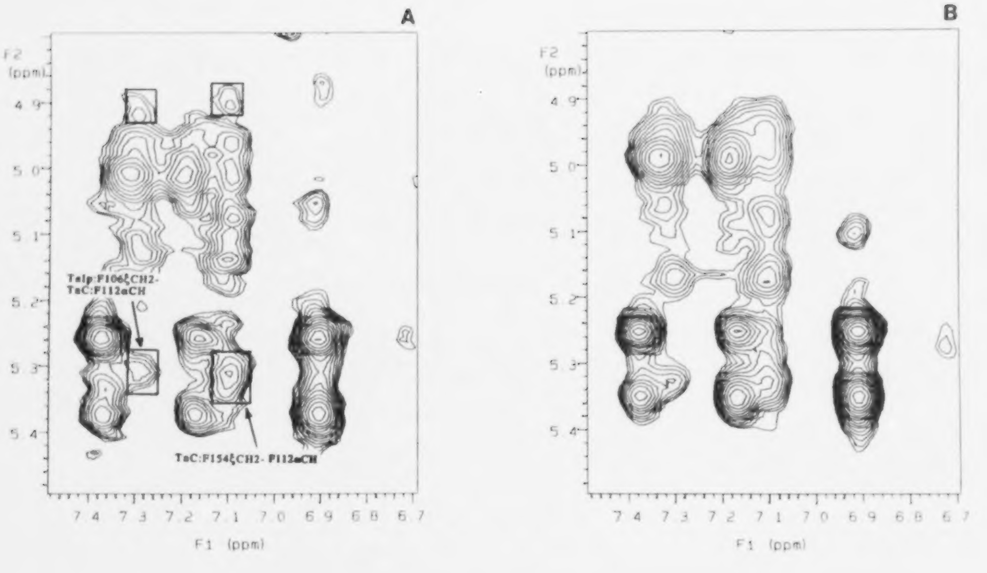

Figure VI-23. α-proton to aromatic region of the 600 MHz ^1H NOESY spectrum of A. TnI peptide-TnC protein complex, and B. TnC protein alone. Panel A shows a cross-peak connecting F106ξCH2 on the TnI peptide to a peak at 5.3 ppm which could be assigned to F112αCH on TnC (see text). Also visible in Panel A is the intraprotein cross-peak connecting F154ξCH2-F112αCH, which may have arisen due to a conformational change in the TnC protein in the presence of bound TnI peptide, or due to a chemical shift in either the F154ξCH2 or the F112αCH resonance. (TnI peptide-TnC protein sample was 2.96 mM Nα-acetyl-TnI(104-115) amide, 0.82 mM turkey s-TnC, 5 mM $CaCl_2$, 100 mM KCl, pD 6.1, 100%D_2O, 30°C; $\tau_m = 150$ ms.) (TnC protein sample was 2.0 mM turkey s-TnC, 12 mM $CaCl_2$, 100 mM KCl, pD 6.2, 100%D_2O, 30°C; $\tau_m = 150$ ms.)

Figure VI-24. Backbone ribbon (panels **A** and **B**) and fully space-filled (panels **C** and **D**) representations of the C-terminal domain of the crystal structure of turkey s-TnC (Herzberg and James, 1985). In the backbone ribbon representation, shown in panels **A** and **B**, residues involved in the binding of the TnI inhibitory peptide are shown with their side chains in a space-filled CPK representation. Phenylalanines, F102, F151, and F154 are colored in red, and isoleucines, I104, I113, I121 and I149 are colored in blue. In the fully space-filled representation, shown in panels **C** and **D**, all side chain atoms are colored in green, expect for F102, F151 and F154 which are colored in red, and I104, I113, I121 and I149 which are colored in blue. **A** and **C** represent a front view; **B** and **D** represent a side view of the molecule.

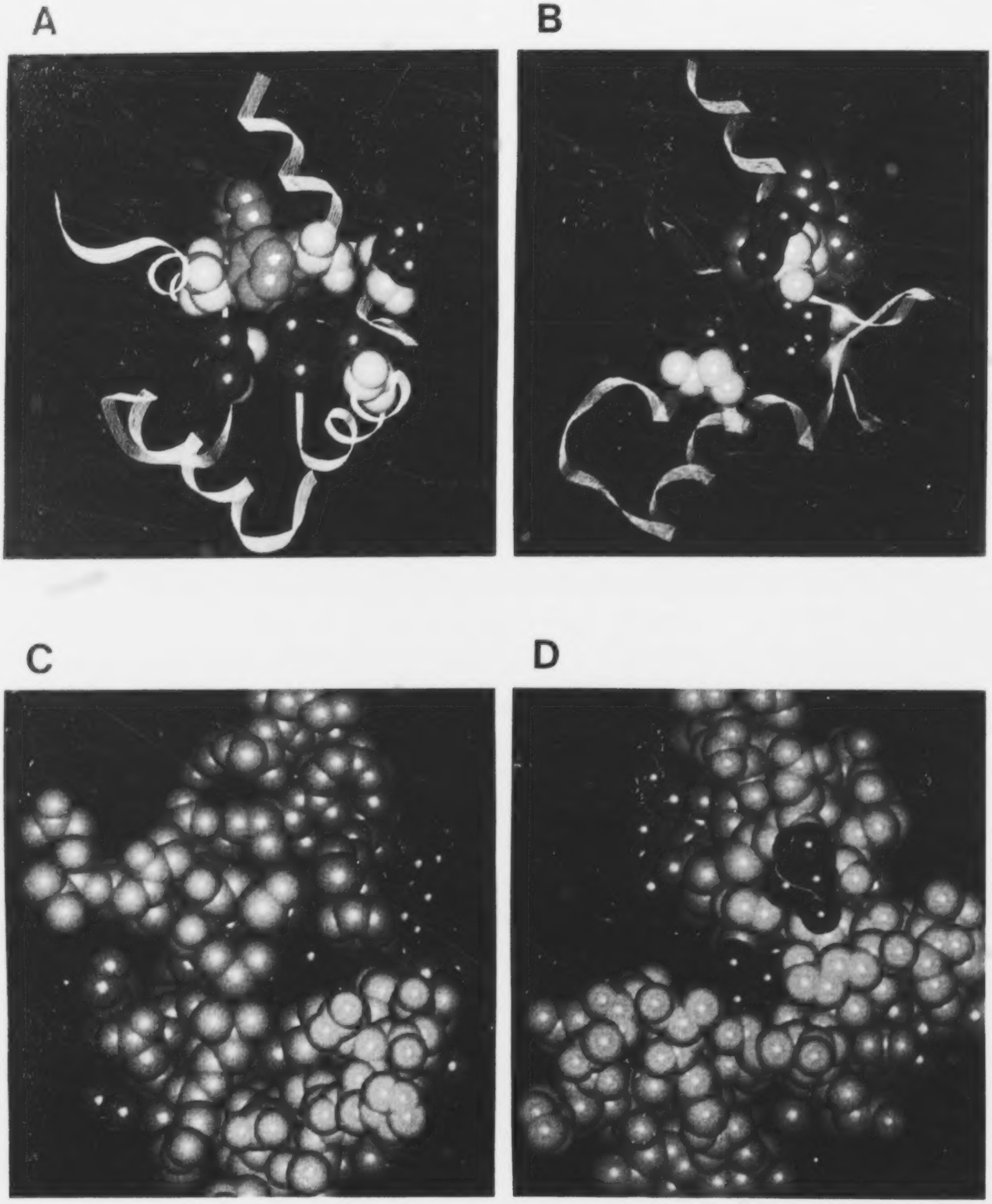
A
B
C
D

Figure VI-25. Model of the TRNOE-derived structure of the TnI inhibitory peptide (Campbell *et al.*, 1991; Chapter V) bound to the C-terminal domain of the crystal structure of turkey s-TnC (Herzberg and James, 1985). The backbone of the TnC protein and the TnI peptide are both shown in a ribbon representation, with the protein colored in yellow and the peptide colored in pink. Residues involved in the binding interface are shown with their side chains in a space-filled CPK representation. In the TnC protein, F102, F151, and F154, are colored in red, and I104, I113, I121 and I149 are colored in blue. In the TnI peptide, F106 is colored in orange, L111 is colored in light blue, and V114 is colored in purple. **A** represents a front view; **B** represents a side view of the complex.

A

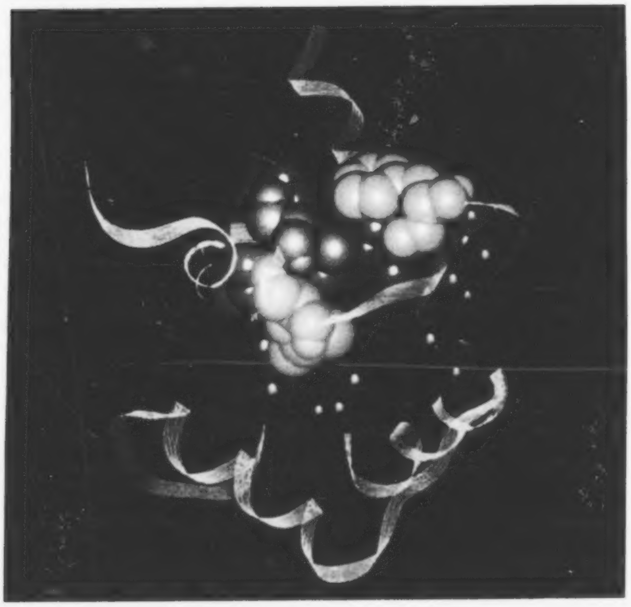

B

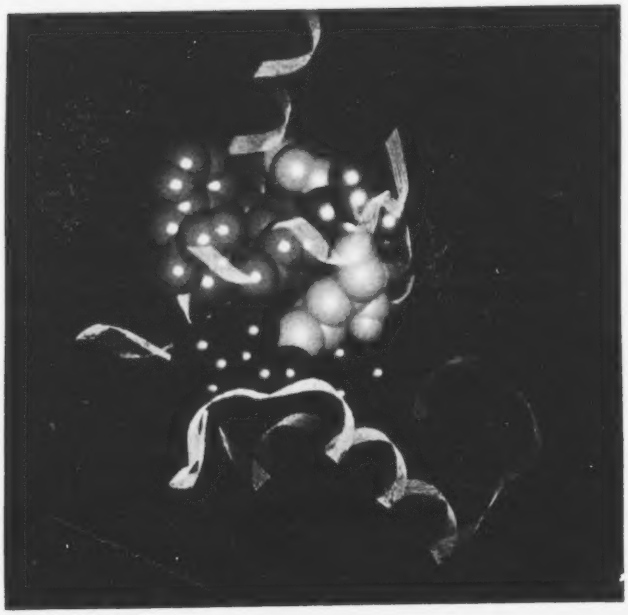

E. References

ANDERSSON, A., DRAKENBERG, T., FORSEN, S., THULIN, E. and SWARD, M. 1982. Direct observation of the ^{43}Ca NMR signals from Ca^{+2} ions bound to proteins. J. Am. Chem. Soc. **104**: 576-580.

BABU, Y.S., BUGG, C.E., and COOK, W.J. 1988. Structure of calmodulin refined at 2.2 Å resolution. J. Mol. Biol. **204**: 191-204.

CACHIA, P.J., SYKES, B.D., and HODGES, R.S. 1983. Calcium-dependent inhibitory region of troponin. A proton magnetic resonance study on the interaction between troponin C and the synthetic peptide Nα-acetyl [F-phenylalanine106] TnI (104-115) amide. Biochemistry **22**: 4145-4152.

CACHIA, P.J., SYKES, B.D., and HODGES, R.S. 1985. Structural studies on calmodulin and troponin C. Phenothiazine, peptide, and protein interactions with calcium-induced helices. In *Calmodulin Antagonist and Cellular Physiology* (Hidaka, H., and Hartshorne, D.J., Eds.), Chapt. 5, pp 63-88, Academic Press, New York.

CACHIA, P.J., VAN EYK, J., INGRAHAM, R.H., MCCUBBIN, W.D., KAY, C.M., and HODGES, R.S. 1986. Calmodulin and troponin C. A comparative study of the interaction of mastoparan and troponin I inhibitory peptide [104-115]. Biochemistry **25**: 3553-3562.

CADAY, C.G., and STEINER, R.F. 1986. Interaction of calmodulin with melittin. Biochem. Biophys. Res. Commun. **135**: 419-425.

CAMPBELL, A.P., CACHIA, P.J., and SYKES, B.D. 1991. Interaction of troponin I and troponin C : ^{19}F NMR studies of the binding of the inhibitory troponin I peptide to turkey skeletal troponin C. Biochem. Cell Biol., in press.

CAMPBELL, A.P., and SYKES, B.D. 1991. Interaction of troponin I and troponin C: Use of the two-dimensional NMR transferred nuclear Overhauser effect to determine the structure of the inhibitory troponin I peptide when bound to skeletal troponin C. J. Mol. Biol., in press.

CHONG, P.C.S., ASSELBERGS, P.J., and HODGES, R.S. 1983. Inhibition of rabbit skeletal muscle acto S1-ATPase by troponin T. FEBS Lett. **153**: 372-376.

COLE, H.A., and PERRY, S.V. 1975. The phosphorylation of troponin I from cardiac muscle. Biochem. J. **149**: 525-533.

COLLINS, J.H., POTTER, J.D., HORN, M.J., WILSHIRE, G., and JACKMAN, N. 1973. The amino acid sequence of rabbit skeletal muscle troponin C. Gene replication and homology with calcium-binding proteins from carp and hake muscle. FEBS Lett. **36**: 268-272.

DALGARNO, D.C., LEVINE, B.A., WILLIAMS, R.J.P., FULLMER, C.S., and WASSERMEN, R.H. 1983a. Proton-NMR studies of the solution conformations of vitamin-D-induced bovine intestinal calcium-binding protein. Eur. J. Biochem. **137**: 523-529.

DALGARNO, D.C., LEVINE, B.A., and WILLIAMS, R.J.P. 1983b. Structural information from NMR secondary chemical shifts of peptide α C-H protons in proteins. Biosci. Rep. **3**: 443-452.

DRABIKOWSKI, W., DALGARNO, D.C., LEVINE, B.A., GERGELY, J., GRABAREK, Z., and LEAVIS, P.C. 1985. Solution conformation of the C-terminal domain of skeletal troponin C. Cation, trifluoperazine and troponin I binding effects. Eur. J. Biochem. **151**: 17-28.

DRAKENBERG, T., FORSEN, S., THULIN, E., and VOGEL, H.J. 1987. The binding of Ca^{2+}, Mg^{2+} and Cd^{2+} to tryptic fragments of skeletal muscle troponin C. Cadmium-113 and proton NMR studies. J. Biol. Chem. **262**: 672-678.

EBASHI, S., and ENDO, M. 1968. Calcium ion and muscle contraction. Prog. Biophys. Mol. Biol. **18**: 123-183.

ERICKSON, B.W., and MERRIFIELD, R.B.1976. Solid-phase peptide synthesis. In *The Proteins*, (Neurath, H., and Hill, R.L., Eds.), Vol. **2**, pp 255-527, Academic Press, New York.

GARIEPY, J., and HODGES, R.S. 1983. Primary sequence analysis and folding behaviour of EF hands in relation to the mechanism of action of troponin C and calmodulin. FEBS Lett. **160**: 1-6.

GOLOSINSKA, K., PEARLSTONE, J.R., BORGFORD, T., OIKAWA, K., KAY, C.M., CARPENTER, M.R., and SMILLIE, L.B. 1991. Determination of and corrections to sequences of turkey and chicken troponin-C: Effects of Thr-130 to Ile mutation on Ca^{2+} affinity. J. Biol. Chem., in press.

GRABAREK, Z., DRABIKOWSKI, W., LEAVIS, P.C., ROSENFELD, S.S., and GERGELY, J. 1981. Proteolytic fragments of troponin C. Interactions with the other troponin subunits and biological activity. J. Biol. Chem. **256**: 13121-13127.

GREASER, M.C., and GERGELY, J. 1971. Reconstitution of troponin activity from three protein components. J. Biol. Chem. **246**: 4226-4233.

HARTSHORNE, D.J., and MUELLER, H. 1968. Fractionation of troponin into two distinct proteins. Biochem. Biophys. Res. Commun. **31**: 647-653.

HEIDORN, D.B., SEEGER, P.A., ROKOP, S.E., BLUMENTHAL, D.K., MEANS, A.R., CRESPI, H., and TREWELLA, J. 1989. Changes in the structure of calmodulin induced by a peptide based on the calmodulin-binding domain of myosin light chain kinase. Biochemistry **28**: 6757-6764.

HERZBERG, O., and JAMES, M.N.G. 1985. Structure of the calcium regulatory muscle protein troponin C at 2.8 Å resolution. Nature **313**: 653-659.

HERZBERG, O., and JAMES, M.N.G. 1988. Refined crystal structure of troponin C from turkey skeletal muscle at 2.0 Å resolution. J. Mol. Biol. **203**: 761-729.

HITCHCOCK, S.E. 1975. Regulation of muscle contraction. Binding of troponin C involved in calcium ion-dependent interaction with troponin I. Eur. J. Biochem. **52**: 255-263.

HODGES, R.S., SEMCHUCK, P.D., TANEJA, A.K., KAY, C.M., PARKER, J.M.R., and MANT, C.T. 1988. Protein design using model synthetic peptides. Peptide Research **1**: 19-29.

HOULT, D.I. 1976. Solvent peak saturation with single phase and quadrature Fourier transformation. J. Magn. Reson. **21**: 337-347.

IKURA, M., MINOWA, O., and HIKICHI, K. 1985. Hydrogen bonding in the carboxyl-terminal half-fragment 78-148 of calmodulin as studied by two-dimensional nuclear magnetic resonance. Biochemistry **24**: 4264-4269.

IKURA, M., MINOWA, O., YAZAWA, M., YAGI, K., and HIKICHI, K. 1987. Sequence-specific assignments of downfield-shifted amide proton resonances of calmodulin. Use of two-dimensional NMR analysis of its tryptic fragments. FEBS Lett. **219**: 17-21.

IKURA, M., KAY, E., and BAX, A. 1990a. A novel approach for sequential assignment of ^{1}H, ^{13}C, and ^{15}N spectra of larger proteins: Heteronuclear triple-resonance three-dimensional NMR spectroscopy. Application to Calmodulin. Biochemistry **29**: 4659-4667.

IKURA, M., KAY, E., KRINKS, M., and BAX, A. 1990b. Triple-resonance multidimensional NMR study of calmodulin complexed with the binding domain of skeletal muscle myosin light-chain kinase: Indication of a conformational change in the central helix. Biochemistry **30**: 5498-5504.

KATAOKA, M., HEAD, J.F., SEATON, B.A., and ENGELMAN, D.M. 1989. Melittin binding causes a large calcium-dependent conformational change in calmodulin. Proc. Natl. Acad. Sci. USA **86**: 6944-6948.

KLEVIT, R.E., BLUMENTHAL, D.K., WEMMER, D.E., and KREBS, E.G. 1985. Interaction of calmodulin and a calmodulin-binding peptide from myosin light chain kinase. Major spectral changes in both occur as a result of complex formation. Biochemistry **24**: 8152-8157.

KRETSINGER, R.H., and NOCKOLDS, C.E. 1973. Carp muscle-binding protein II. Structure determination and general description. J. Biol. Chem. **248**: 3313-3326.

KRETSINGER, R.H., RUDNICK, S.E., and WEISSMAN, L.J. 1986. Crystal structure of calmodulin. J. Inorg. Biochem. **28**: 289-302.

LAN, J., ALBAUGH, S., and STEINER, R.F. 1989. Interactions of troponin I and its inhibitory fragment (residues 104-115) with troponin C and calmodulin. Biochemistry **28**: 7380-7385.

LAPORTE, D.C., WIERMAN, B.M., and STORM, D.R. 1980. Calcium-induced exposure of a hydrophobic surface on calmodulin. Biochemistry **19**: 3814-3819.

LEAVIS, P.C., and GERGELY, J. 1984. Thin filament proteins and thin filament regulation of vertebrate muscle contraction. CRC Crit. Rev. Biochem. **16**: 235-305.

LESZYK, J., COLLINS, J.H., LEAVIS, P.C., and TAO, T. 1987. Cross-linking of rabbit skeletal muscle troponin with the photoactive reagent 4-maleimidobenzophenone. Identification of residues in troponin I that are close to cys-98 of troponin C. Biochemistry **26**: 7042-7047.

LESZYK, J., COLLINS, J.H., LEAVIS, P.C., and TAO, T. 1988. Cross-linking of rabbit skeletal muscle troponin subunits. Labelling of Cys-98 of troponin C with 4-maleimidobenzophenone and analysis of products formed in the binary complex with troponin T and the ternary complex with troponins I and T. Biochemistry **27**: 6983-6987.

LESZYK, J., GRABAREK, Z., GERGELY, J., and COLLINS, J.H. 1990. Characterization of zero-length cross-links between rabbit skeletal muscle troponin C and troponin I. Evidence for direct interaction between the inhibitory region of troponin I and the NH_2-terminal, regulatory domain of troponin C. Biochemistry **29**: 299-304.

LEVINE, B.A., MERCOLA, D., COFFMAN, D., and THORNTON, J.M. 1977. Calcium binding by troponin C. A proton magnetic resonance study. J. Mol. Biol. **115**: 743-760.

LEVINE, B.A., THORNTON, J.M., FERNANDES, R., KELLY, L.M., and MERCOLA, D. 1978. Comparison of the calcium- and magnesium-induced structural changes of troponin C. A proton magnetic resonance study. Biochim. Biophys. Acta **535**: 11-24.

MACLACHLAN, L.K., REID, D.G., MITCHELL, R.C., SALTER, C.J., and SMITH, S.J. 1990. Binding of a calcium sensitizer, bepridil, to cardiac troponin C. A fluorescence stopped-flow kinetic, circular dichroism, and proton nuclear magnetic resonance study. J. Biol. Chem. **265**: 9764-9770.

MANT, C.T., BURKE, T.W.L., and HODGES, R.S. 1987. Optimization of peptide separations in reversed-phase HPLC: Isocratic versus gradient elution. Chromatographia **24**: 565-572.

MATSUSHIMA, N., IZUMI, Y., MATSUO, T., YOSHINO, H., UEKI, T., and MIYAKE, Y. 1989. Binding of both Ca^{+2} and mastoparan to calmodulin induces a large change in the tertiary structure. J. Biochem. **105**: 883-887.

MOIR, A.J.G., WILKINSON, J.M., and PERRY, S.V. 1974. The phosphorylation sites of troponin I from cardiac muscle. FEBS Lett. **42**: 253-257.

NAIRN, A.C., GRAND, R.J.A., and PERRY, S.V. 1984. The amino acid sequence of rabbit skeletal muscle calmodulin. FEBS Lett. **167**: 215-220.

NOZAKI, S., KOBAYASHI, K., KATAYAMA, E., and MURAMATSU, I. 1980. Synthetic studies on troponin I active site preparation of a pentadecapeptide with inhibitory activity toward troponin C. Chem. Lett. **3**: 345-348.

O'NEIL, K.T., and DEGRADO, W.F. 1989. The interaction of calmodulin with fluorescent and photoreactive model peptides. Evidence for a short interdomain separation. Proteins **6**: 284-293.

OTTING, G., WIDMER, H., WAGNER, G., and WUTHRICH, K. 1986. Origin of t_1 and t_2 ridges in 2D NMR spectra and procedures for suppression. J. Magn. Reson. **66**: 187-193.

PARDI, A., BILLETER, M., and WUTHRICH, K. 1984. Calibration of the angular dependence of the amide proton-Cα proton coupling constants, ${}^3J_{HN\alpha}$, in a globular protein. J. Mol. Biol. **180**: 741-751.

PARKER, J.M.R., MANT, C.T., and HODGES, R.S. 1987. A practical approach to the preparative purification of peptides using analytical instrumentation with analytical and semipreparative columns. Chromatographia **24**: 832-838.

PERRY, S.V., COLE, H., HEAD, J.F., and WILSON, F.J. 1972. Localization and mode of action of the inhibitory protein component of the troponin complex. Cold Spring Harbor Symp. Quant. Biol. **37**: 251-262.

PERSECHINI, A., BLUMENTHAL, D.K., JARRETT, H.W., KLEE, C.B., HARDY, D.O., and KRETSINGER, R.H. 1989. The effects of deletions in the central helix of calmodulin on enzyme activation and peptide binding. J. Biol. Chem. **264**: 8052-8058.

PERSECHINI, A., and KRETSINGER, R.H. 1988. The central helix of calmodulin functions as a flexible tether. J. Biol. Chem. **263**: 12175-12178.

PIATINI, U., SORENSON, O.W., and ERNST, R.R. 1982. Multiple quantum filters for elucidating NMR coupling networks. J. Am. Chem. Soc. **104**: 6800-6801.

POTTER, J.D., and GERGELY, J. 1974. Troponin, tropomyosin and actin interactions in the Ca^{+2} regulation of muscle contraction. Biochemistry 13: 2697-2703.

PUTKEY, J.A., ONO, T., VAN BERKUM, M.F.A., and MEANS, A.R. 1988. Functional significance of the central helix of calmodulin. J. Biol. Chem. **263**: 11242-11249.

RANCE, M., SORENSON, O.W., BODENHAUSEN, G., WAGNER, G., ERNST, R.R., and WUTHRICH, K. 1983. Improved spectral resolution in COSY ^{1}H NMR spectra of proteins via double quantum filtering. Biochem. Biophys. Res. Commun. **117**: 479-485.

REID, D.G., MACLACHLAN, L.K., GAJJAR, K., VOYLE, M., KING, R.J., and ENGLAND, P.J. 1990. A proton nuclear magnetic resonance and molecular modeling study of calmidazolium (R24571) binding to calmodulin and skeletal muscle troponin C. J. Biol. Chem. **265**: 9744-9753.

SATYSHUR, K.A., RAO, S.T., PYZALSKA, D., DRENDEL, W., GREASER, M., and SUNDARALINGAM, M. 1988. Refined structure of chicken skeletal muscle troponin C in the two-calcium state at 2-Å resolution. J. Biol. Chem. **263**: 1628-1647.

SCHAUB, M.C., and PERRY, S.V. 1969. The relaxing protein system of striated muscle. Biochem J. **115**: 993-1004.

SEAMON, K.B., HARTSHORNE, D.J. and BOTHNER-BY, A.A. 1977. Ca^{+2} and Mg^{+2} dependent conformations of troponin C as determined by ^{1}H and ^{19}F nuclear magnetic resonance. Biochemistry **16**: 4039-4046.

SEEHOLZER, S.H., COHN, M., PUTKEY, J.A., MEANS, A.R., and CRESI, H.L. 1986. NMR studies of a complex of deuterated calmodulin with melittin. Proc. Natl. Acad. Sci. USA **83**: 3634-3638.

SEEHOLZER, S.H., and WAND, J.A. 1989. Structural characterization of the interactions between calmodulin and skeletal muscle myosin light chain kinase: Effect of peptide(576-594)G binding on the Ca^{2+}-binding domains. Biochemistry **28**: 4011-4020.

SHAW, G.S., HODGES, R.S., and SYKES, B.D. 1991a. Synthetic calcium-binding peptides which form heterodimeric two-site domains. In *Peptides: Chemistry and Biology* (Smith, J.A., and Rivier, J.E., Eds.), ESCOM Science Publishers, Leiden, The Netherlands, in press.

SHAW, G.S., HODGES, R.S., and SYKES, B.D. 1991b. Calcium-induced folding of troponin-C: Formation of homodimeric and heterodimeric two-site domains from synthetic peptides. In *Techniques in Protein Chemistry III* (Angelitti, R. Hogue, Ed.), Academic Press, New York, in press.

STATES, D.J., HABERKORN, R.A., and RUBEN, D.J. 1982. Two-dimensional nuclear Overhauser experiment with pure phase absorption phase in four quadrants. J. Magn. Reson. **48**: 286-292.

STEINER, R.F., and NORRIS, L. 1987. Interaction of melittin with troponin C. Arch. of Biochem. and Biophys. **254**: 342-352.

STRYNADKA, N.C.J., and JAMES, M.N.G. 1990. Model for the interaction of amphiphilic helices with troponin C and calmodulin. Proteins **7**: 234-248.

SUNDARALINGAM, M., BERGSTROM, R., STRASBURG, G., RAO, S.T., GREASER, M., and WANG, B.C. 1985. Molecular structure of troponin C from chicken skeletal muscle at 3 Å resolution. Science **227**: 945-948.

SYSKA, H., WILKINSON, J.M., GRAND, R.J.A., and PERRY, S.V. 1976. The relationship between biological activity and primary structure of troponin I from white skeletal muscle of the rabbit. Biochem. J. **153**: 375-387.

TALBOT, J.A., and HODGES, R.S. 1979. Synthesis and biological activity of an icosapeptide analog of the actomyosin ATPase inhibitory region of troponin I. J. Biol. Chem. **254**: 3720-3723.

TALBOT, J.A., and HODGES, R.S. 1981. Synthetic studies on the inhibitory region of rabbit skeletal troponin I. Relationship of amino acid sequence to biological activity. J. Biol. Chem. **256**: 2798-3802.

TAO, T., GOWELL, E., STRASBURG, G.M., GERGELY, J., and LEAVIS, P.L. 1989. Ca^{+2} dependence of the distance between Cys-98 of troponin C and Cys-133 of troponin I in the ternary troponin complex. Resonance energy transfer measurements. Biochemistry **28**: 5902-5908.

TELEMAN, O., DRAKENBERG, T., FORSEN, S., and THULIN, E. 1983. Calcium and cadmium binding to troponin C. Evidence for cooperativity. Eur. J. Biochem. **134**: 453-457.

TSUDA, S., HASEGAWA, Y., YOSHIDA, M., YAGI, K., and HIKICHI, K. 1988. Nuclear magnetic resonance study of rabbit skeletal troponin C: Calcium-induced conformational change. Biochemistry **27**: 4120-4126.

TSUDA, S., OGURA, K., HASEGAWA, Y., YAGI, K., and HIKICHI, K. 1990. ^1H NMR study of rabbit skeletal muscle troponin C: Mg^{2+} - induced conformational change. Biochemistry **29**: 4951-4958.

VANAMAN, T.C., SHARIEL, F., and WATTERSON, D.M. 1977. Structural homology between brain modulator protein and muscle TnCs. In *Calcium-Binding Proteins and Calcium Function* (Wasserman, R.H., *et al.*, Eds.), pp 107-116, Elsevier, Amsterdam.

VAN BERKUM, M.F.A., GEORGE, S.E., and MEANS, A.R. 1990. Calmodulin activation of target enzymes. Consequences of deletions in the central helix. J. Biol. Chem. **265**: 3750-3756.

VAN EYK, J.E., and HODGES, R.S. 1988. The biological importance of each amino acid residue of the troponin I inhibitory sequence 104-115 in the interaction with troponin C and tropomyosin-actin. J. Biol. Chem. **263**: 1726-1732.

VAN EYK, J.E., KAY, C.M., and HODGES, R.S. 1991. A comparative study of the interactions of synthetic peptides of the skeletal and cardiac troponin I inhibitory region with skeletal and cardiac troponin C. Biochemistry, in press

WANG, Z., SARKAR, S., GERGELY, J., and TAO, T. 1990. Ca^{+2}-dependent interactions between the c-helix of troponin C and troponin I. J. Biol. Chem. **265**: 4953-4957

WAGNER, G., PARDI, A., and WUTHRICH, K. 1983. Hydrogen bond length and ^1H NMR chemical shifts in proteins. J. Am. Chem. Soc. **105**: 5948-5949.

WEEKS, R.A, and PERRY, S.V. 1978. Characterization of a region of the primary sequence of troponin C involved in calcium ion-dependent interaction with troponin I. Biochem. J. **173**: 449-457.

WILKINSON, J.M. 1976. The amino acid sequence of troponin from chicken skeletal muscle. FEBS Lett. **70**: 254-257.

WISHART, D.S. 1991. Investigations into the denatured stated of *E. coli* thioredoxin. PhD thesis. Yale University, New Haven, Connecticut.

YOSHINO, H., MINARI, O., MATSUSHIMA, N., UEKI, T., MIYAKE, Y., MATSUO, T., and IZUMI, Y. 1989. Calcium-induced shape change of calmodulin with mastoparan studied by solution x-ray scattering. J. Biol. Chem. **264**: 19706-19709.

ZOT, A.S., and POTTER, J.D. 1987. Structural aspects of troponin-tropomyosin regulation of skeletal muscle contraction. Annu. Rev. Biophys. Chem. **16**: 535-559.

Chapter VII

Interaction of Troponin I and Troponin C : Use of Paramagnetic Lanthanides to Determine the Location of Binding of the Inhibitory Troponin I Peptide to Skeletal Troponin C.

A. Introduction

Contraction of vertebrate skeletal muscle is regulated by Ca(II) and requires the regulatory proteins troponin and tropomyosin (Ebashi and Endo, 1968). Troponin is a complex of three different protein subunits: Troponin C (TnC) which binds Ca(II), TnI which binds actin and inhibits actomyosin ATPase, and TnT which binds to tropomyosin. The Ca(II)-dependent interaction between TnC and TnI is one of the key processes in the activation of contraction in skeletal muscle (for recent reviews, see Zot and Potter, 1987, and Leavis and Gergely, 1984). TnI inhibits the Mg(II)-ATPase activity of acto-myosin ATPase (Hartshorne and Mueller, 1968; Schaub and Perry, 1969; Greaser and Gergely, 1971; Perry *et al.*, 1972) and binds both to actin and tropomyosin-actin (Potter and Gergely, 1974; Hitchcock, 1975). The inhibition of actomyosin ATPase is neutralized when Ca(II)-saturated TnC forms a 1:1 complex with TnI (Perry *et al.*, 1972; Weeks and Perry, 1978; Chong *et al.*, 1983; Cachia *et al.*, 1986; Van Eyk and Hodges, 1988). This results in potentiation of the ATPase and ultimately in muscle contraction.

The x-ray structures of chicken (Sundaralingam *et al.*, 1985a) and turkey (Herzberg and James, 1985) skeletal TnC have been solved and reveal a dumbbell-shaped molecule with N-terminal and C-terminal globular domains joined by a long helical linker. Each major domain contains two Ca(II) binding sites based on the EF hand helix-loop-helix structural motif (Kretsinger and Nockolds, 1973; Collins *et al.*, 1973; Vanaman *et al.*, 1977). The higher affinity Ca(II)/Mg(II) sites (sites III and IV) reside in the C-terminal domain and bind Ca(II) and Mg(II) with association constants of 2×10^7 and 5×10^3 M^{-1}, respectively (Potter and Gergely, 1974). The Ca(II) specific sites (sites I and II) reside in the N-terminal domain and bind Ca(II) with an association constant of 2×10^5 M^{-1}. The low affinity sites in the N-terminal domain have been implicated as the physiologically relevant triggering sites (Johnson *et al.*, 1979; Robertson *et al.*, 1981).

Studies characterizing the interaction between TnC and TnI have pointed to multiple interactions between these two proteins. TnI fragment studies reported by Syska *et al.* (1976) demonstrated that two regions of the TnI protein are capable of interacting with TnC. The first of these sites spans residues 1-21, and includes the site of phosphorylation catalyzed by phosphorylase kinase (T11), whereas the second of these sites spans residues 96-116 and is adjacent to a second phosphorylation site (S117) (Moir *et al.*, 1974). Equimolar amounts of TnC completely inhibit phosphorylation at these sites (Cole and Perry, 1975). Syska *et al.* (1976) demonstrated that a CNBr fragment of TnI (residues 96-116) mimics intact TnI in its ability to inhibit actomyosin ATPase (Syska *et al.*, 1976; Nozaki *et al.*, 1980; Talbot and Hodges, 1981). Talbot and Hodges (1981) using synthetic peptides showed that residues 104-115 of TnI comprise the minimum sequence necessary for inhibition of actomyosin ATPase activity. The synthetic peptide TnI(104-115) possesses tropomyosin specificity (Talbot and Hodges, 1979) and TnC binding capabilities (Cachia *et al.*, 1983, 1985; Van Eyk and Hodges, 1988; Van Eyk *et al.*, 1991), which results in the release of ATPase inhibition (Cachia *et al.*, 1986; Van Eyk and Hodges, 1988). Thus, it is would appear that residues 104-115 comprise the inhibitory site of TnI and binding of this region to Ca(II)-saturated TnC leads to relief of inhibition of actomyosin ATPase, and ultimately to muscle contraction.

We have recently used ^{19}F NMR to study the binding of the synthetic peptide Nα-acetyl [19FPhe106]TnI(104-115) amide to Ca(II)-saturated skeletal turkey TnC, and have obtained the following binding constants; $K_d = (3.7 \pm 3.1) \times 10^{-5}$ M for the apo case and $K_d = (4.8 \pm 1.8) \times 10^{-5}$ M for the Ca(II)-saturated case for a 1:1 binding stoichiometry of TnI peptide to TnC protein (Campbell *et al.*, 1991a; Chapter IV). The results did not rule out the possibility of a second binding site on Ca(II)-saturated TnC with an affinity 10-20 fold weaker than that of the first.

We have also used ^{1}H NMR methods to determine the structure of the inhibitory peptide Nα-acetyl-TnI(104-115) amide bound to Ca(II)-saturated s-TnC (Campbell and Sykes, 1991; Chapter V), and to identify the residues on Ca(II)-saturated s-TnC involved in binding the inhibitory peptide (Campbell *et al.*, 1991b; Chapter VI). Conformational changes in the peptide induced by the formation of the TnI peptide-TnC protein complex were followed by the study of the transferred nuclear Overhauser effect (TRNOE), a technique which allows determination of the structure of a ligand bound to a macromolecule. The structure of the bound TnI peptide reveals a helical structure, distorted around the two central proline residues. The central bend in the peptide functions to bring the hydrophobic residues into closer proximity with each other, thereby forming a small hydrophobic pocket. The hydrophilic, basic residues extend off the opposite face of the peptide. Interresidue TnI peptide-TnC protein NOEs have been assigned in the complex and have allowed identification of several residues on Ca(II)-saturated turkey skeletal TnC which interact with the TnI peptide. The presence of NOEs between residues on the TnI peptide and the ring protons of F102, F151 and F154 as well as the methyl side chains of I104, I113, I121 and I149 of turkey skeletal TnC point to an interaction of the inhibitory TnI peptide with the hydrophobic pocket and β-sheet region between Ca(II)-binding sites III and IV in the C-terminal domain of this protein. While these results have clearly implicated involvement of the C-terminal domain of TnC in the binding of the TnI peptide, there remains some question as to the involvement of the N-terminal domain.

In the present study we use the paramagnetic lanthanide Gd(III) as a Ca(II) analog to determine the location of binding of the inhibitory peptide Nα-acetyl-TnI(104-115) amide with respect to Ca(II)-binding sites I and II in the N-terminal domain, and sites III and IV in the C-terminal domain of s-TnC (Campbell *et al.*, 1990). The unpaired electrons on the Gd(III) metal result in increased spin-lattice relaxation times of nuclei on the TnI peptide within a 20 Å radius of the metal, leading to increased spin-lattice relaxation times of the TnI peptide nuclei. This allows orientation of the TnI peptide with respect to all four metal binding sites, as it provides relative distances of the TnI peptide nuclei to the paramagnetic centers.

Lanthanides have often been used as Ca(II) analogs to investigate the ion-binding properties of Ca(II) binding proteins, such as the parvalbumins (Sowadski *et al.*, 1978; Cave *et al.*, 1979; Lee *et al.*, 1978; Lee and Sykes, 1980a, 1980b, 1981, 1982, 1983, 1986; Rhee *et al.*, 1981; Corson *et al.*, 1983a, 1983b; Williams *et al.*, 1984; Drakenberg *et al.*, 1985; Henzl *et al.*, 1985), TnC (Brittain *et al.*, 1976; Lee *et al.*, 1978; Leavis *et al.*, 1980; Wang *et al.*, 1981, 1982a; Gariepy *et al.*, 1985; Marsden *et al.*, 1988, 1989), and calmodulin (CaM) (Kilhoffer *et al.*, 1980a, 1980b; Wallace *et al.*, 1982; Wang *et al.*, 1982b, 1984; Valentini and Wright, 1985; Martin *et al.*, 1986; Buccigross and Nelson, 1986; Horrocks and Tingey, 1988). (For reviews of lanthanides as probes for calcium in biological systems, see Lenkinski and Glickson, 1985, and Bertini and Luchinat, 1986. For a theoretical treatment of the use of lanthanides for solution structure determination of biomolecules by NMR, see Kemple *et al.*, 1988).

The luminescent lanthanides, Tb(III) and Eu(III), have been most useful in characterizing the metal binding properties of parvalbumin (Rhee *et al.*, 1981), TnC (Leavis *et al.*, 1980; Wang *et al.*, 1981, 1982a), and CaM (Kilhoffer *et al.*, 1980a, 1980b; Wallace *et al.*, 1982; Wang *et al.*, 1982b, 1984; Valentini and Wright, 1985; Martin *et al.*, 1986; Buccigross and Nelson, 1986; Horrocks and Tingey, 1988). Resonance energy transfer experiments with Tb(III) and Eu(III) have been used to measure distances between the Ca(II)-binding sites in carp parvalbumin (Rhee *et al.*, 1981) and rabbit s-TnC (Wang *et al.*, 1982a). Fluorescence spectroscopy and circular dichroism (CD) studies of the binding of the luminescent lanthanides Tb(III) and Eu(III) to rabbit s-TnC have shown that both lanthanides bind preferentially to the high affinity Ca(II)/Mg(II) sites (Leavis *et al.*, 1980; Wang *et al.*, 1981, 1982a). Wang *et al.* (1981) found the association constants of Tb(III) and Eu(III) to be at least an order of magnitude larger for the high and low affinity sites than the association constants measured for Ca(II) by Potter and Gergely (1974) (5.2×10^8 and 9.7×10^6 M^{-1} for Tb(III); and 4.7×10^9 and 5.3×10^7 M^{-1} for Eu(III)). The sequence of fill and relative affinity of the various lanthanide ions for the four metal-binding sites in

CaM is not so well-defined (Kilhoffer *et al.*, 1980b; Wallace *et al.*, 1982; Wang *et al.*, 1984; Buccigross and Nelson, 1986).

The paramagnetic lanthanides, Gd(III) and Yb(III), have been successfully used as distance probes for solution structure determination (Kemple *et al.*, 1988). Lee and co-workers have used the paramagnetic lanthanide Yb(III) to induce shifting and broadening of carp parvalbumin ^{1}H NMR resonances and these Yb(III)-induced spectral perturbations have been analyzed in terms of the structure of the EF site (Lee and Sykes, 1980a, 1980b, 1981, 1982, 1983). In addition, ^{1}H NMR studies using the paramagnetic lanthanide Gd(III) as a distance probe have been used to determine the structure of the Gd(III)-bound site III peptide of rabbit s-TnC (Gariepy *et al.*, 1985; Marsden *et al.*, 1989).

In this chapter, we report on the use of the ^{1}H NMR relaxation probe Gd(III) to generate metal-proton distances in the Nα-acetyl-TnI(104-115) amide - TnC.Gd(III)$_4$ complex. These distances should allow an orientation of the TnI peptide with respect to the N-terminal Gd(III)-bound sites I and II and the C-terminal Gd(III)-bound sites III and IV of TnC. The Gd(III)-derived distances to all four sites should give an idea of the proximity of the N-terminal domain to the TnI peptide, and therefore of the involvement of the N-terminal domain in the binding of the inhibitory region (104-115) of the TnI protein, an interaction which has been shown to occur at the C-terminal domain of TnC (Campbell *et al.*, 1991b; Chapter VI).

B. Theory

The relaxation times T_1 and T_2 of a nucleus *i* near a paramagnetic site are represented by the Solomon-Bloembergen (Bloembergen, 1957) equations:

$$1/T_{1Mi} = (A/r_i^{\,6})[3\tau_c/(1+(\omega\tau_c)^2)] \qquad [1a]$$

$$1/T_{2Mi} = (B/r_i^{\,6})[4\tau_c + 3\tau_c/(1+(\omega\tau_c)^2)] \qquad [1b]$$

where τ_c is the correlation time, ω is the Larmor precession frequency, r_i is the distance between the nucleus *i* and the paramagnetic ion, and A and B are quantities defined as

$$A = 2[\gamma^2\beta^2 g^2\ J(J+1)]/15 \qquad [2a]$$

$$B = [\gamma^2\beta^2 g^2\ J(J+1)]/15 \qquad [2b]$$

The quantity $[\gamma^2\beta^2g^2\ J(J+1)]/15$ has a value of $2.583 \times 10^{17}\ s^{-2}\ Å^6$ (Marinetti *et al.*, 1976), where g is the Lande g factor, J is the total angular momentum for the Gd(III) ion (7/2), β is the Bohr magneton, and γ is the gyromagnetic ratio.

If we consider a paramagnetic system in chemical exchange, the observed relaxation rates are $1/T_{1OBS}$, which have diamagnetic as well as paramagnetic contributions. If Gd(III) (4 f^7) is used in a paramagnetic system (7 unpaired electrons), La(III) (4 f^0) may be used as a suitable diamagnetic control (no unpaired electrons). Thus, for nucleus *i*, the paramagnetic contributions to the relaxation rates, $1/T_{1Pi}$ and $1/T_{2Pi}$, are given by:

$$[1/T_{1OBS}{}^{Gd} - 1/T_{1OBS}{}^{La}]^i = p_B/(T_{1Mi} + \tau_M) = 1/T_{1Pi} \qquad [3a]$$

$$[1/T_{2OBS}{}^{Gd} - 1/T_{2OBS}{}^{La}]^i = p_B/(T_{2Mi} + \tau_M) = 1/T_{2Pi} \qquad [3b]$$

where p_B is the 'fraction bound' and τ_M is the exchange lifetime of the bound state.

Calculation of distances from $1/T_{1Pi}$ and $1/T_{2Pi}$ measurements requires both a knowledge of τ_M to separate out T_{1Mi} and T_{2Mi}, and a knowledge of τ_c. Determination of τ_c and τ_M has been previously outlined by Marsden *et al.* (1989) using the following expression:

$$T_{2Pi} = T_{1Pi}(1/Á) + \tau_M(Á-1)/Á \qquad [4a]$$

$$\text{where } Á = 7/6 + (2/3)(\omega\tau_c)^2 \qquad [4b]$$

Thus, a plot of T_{2Pi} vs. T_{1Pi} for nuclei $i = 1,\ldots,n$ gives a slope of $1/Á$ and an intercept of $\tau_M(Á-1)/Á$. The slope yields τ_c from Eqn. 4b; and τ_M may be obtained from the intercept. Then r_i may be calculated from Eqn. 1a.

C. Materials and Methods

1. Sample Preparation

a. Materials. Refer to Materials and Methods section in Chapter V.

b. Amino Acid Analysis. The concentration of peptide in the Nα-acetyl-TnI(104-115) amide ^{1}H NMR sample and the concentration of protein in the TnC.Ln(III) protein titrants were determined from amino acid analysis after hydrolysis in 100-200 µl of 6 N HCl in evacuated sealed tubes for 24 h at 110°C. The mean of the molar ratios of all accurately measurable amino acids in the acid hydrolysate was used to calculate the concentration of peptide or protein.

c. Peptide Synthesis and Purification. Nα-acetyl-TnI(104-115) amide was synthesized and purified using the standard protocol outlined in the Materials and Methods section in Chapter V (Erickson and Merrifield, 1976; Talbot and Hodges, 1981; Mant *et al.*, 1987; Parker *et al.*, 1987; Hodges *et al.*, 1988).

d. Preparation of TnC. Troponin was isolated from an acetone powder of turkey breast muscle using the protocol outlined in the Materials and Methods section in Chapter IV. A final yield of approx. 400 mg of purified TnC powder was obtained, which was found to be homogenous when examined by SDS-Page and UV spectrophotometry ($\varepsilon_{(\lambda\ 259\ \mathrm{nm})}$ = 0.109 O.D. units/mg/ml for turkey skeletal TnC).

e. Preparation of Desalted, Apo TnC. EDTA-free, apo TnC was prepared using the protocol outlined in the Materials and Methods section in Chapter IV. The TnC protein was judged to be apo by UV spectrophotometry and ^{1}H NMR.

f. Ln(III) Solutions. Stock solutions of lanthanum and gadolinium were prepared with a solution of 50 mM KCl in 80%H_2O/20%D_2O, and adjusted to pH 6.74. The metal ion concentrations were determined by EDTA titration using xylenol orange as the end-point indicator (Lee and Sykes, 1980a).

g. Preparation of TnI Peptide Sample. The ^{1}H NMR sample of the TnI peptide was 5 mM Nα-acetyl-TnI(104-115) amide and 50 mM KCl, dissolved in 650 μl of a 80%H_2O/20%D_2O solvent mixture at pH 6.74.

h. Preparation of TnC.Ln(III)$_4$ Protein Titrant. The TnC.Gd(III)$_4$ titrant was prepared by dissolving apo turkey s-TnC in a 50 mM KCl, 80%H_2O/20%D_2O solvent mixture, adjusted to pH 6.74. Aliquots of the Gd(III) stock solution were added to a final molar ratio of 3.5 molar equivalents Gd(III) to TnC protein, such that all the four metal sites on the protein would be bound, but no free Gd(III) ions would be left in solution. The TnC.La(III)$_4$ titrant was prepared in a similar manner. Ratios of Ln(III) to TnC protein were determined from amino acid analysis of the apo TnC sample and EDTA titrations of the lanthanide stock solutions.

i. Titration of TnI Peptide Sample with TnC.Ln(III)$_4$. In two separate sets of experiments, TnI peptide ^{1}H NMR samples were titrated with small aliquots of TnC.Ln(III)$_4$ and TnC.Gd(III)$_4$ protein titrants. In the gadolinium set of relaxation experiments, seven such additions were made such that the molar ratios at each addition were 0.0, 0.0006, 0.0011, 0.0021, 0.0034, 0.0047, and 0.0073 molar equivalents TnC.Gd(III)$_4$ to TnI peptide. In the lanthanum set of relaxation experiments, three such additions were made such that the molar ratios at each addition were 0.0, 0.0035, 0.0072, and 0.0108 molar equivalents TnC.La(III)$_4$ to TnI peptide. At every stage in these titrations, T_1 and T_2 relaxation measurements were recorded as a function of molar equivalents TnC.Ln(III)$_4$ to TnI peptide.

2. Nuclear Magnetic Resonance Spectroscopy

All ^{1}H NMR spectra were obtained at 500 MHz on a Varian VXR-500 NMR spectrometer. For all data sets, the water resonance was suppressed by presaturation. The decoupler offset was set equal to the transmitter offset to prevent phase distortions around the water peak due to imperfect cancellation of the dispersive component of residual water magnetization (Hoult, 1976).

T_1 measurements were obtained from an inversion recovery experiment (Freeman and Hill, 1970, 1971). The pulse sequence employed was $[\ 180° - \tau - 90°(\text{FID}) - T_d\ ]_n$, where τ is the evolution period and T_d is the recovery time. T_2 measurements were obtained from a Carr-Purcell-Meiboom-Gill spin-echo experiment (Carr and Purcell, 1954; Meiboom and Gill, 1958). The pulse sequence employed was $(\ 90°_x - [\ \tau - 180°_y - \tau - \text{echo}\ ]_n$, where τ is the evolution period.

D. Results

Figures VII-1A, VII-1B and VII-1C show the ^{1}H NMR monitored titration of Nα-acetyl-TnI(104-115) amide with TnC.Gd(III)$_4$. Figure VII-1A shows the aliphatic upfield region of the spectrum, VII-1B the downfield region of the spectrum with the aromatic F106 resonances, and VII-1C the backbone amide proton resonances only. Very small amounts of TnC.Gd(III)$_4$ added to the TnI peptide lead to very large increases in the observed relaxation rates $1/T_{1OBS}^{Gd}$ and $1/T_{2OBS}^{Gd}$, according to Eqns. 1a and 1b. Since the observed linewidths are related to $1/T_2$ ($\Delta\upsilon = 1/T_2$), this is most obvious as line broadening, and is shown as a broadening of the TnI peptide resonances with increasing molar equivalents TnC.Gd(III)$_4$.

The observed spin-lattice (T_{1OBS}^{Gd}, T_{1OBS}^{La}) and spin-spin (T_{2OBS}^{Gd}, T_{2OBS}^{La}) relaxation times for individual resonances on the TnI peptide were measured at each stage of the titration with TnC.Gd(III)$_4$ and TnC.La(III)$_4$. T_{1OBS} was measured using an inversion recovery experiment (Freeman and Hill, 1970, 1971), and T_{2OBS} with a Carr-Purcell-Meiboom-Gill spin-echo experiment (Carr and Purcell, 1954; Meiboom and Gill, 1958). Figures VII-2 and VII-3 show plots of inversion recovery and spin-echo experiments, respectively, for the backbone amide resonances of the TnI peptide at 0.0 molar equivalents TnC.Gd(III)$_4$. Tables VII-1 and VII-2 in the Appendix give $T_{1OBSi}{}^{Gd}$ and $T_{2OBSi}{}^{Gd}$ for various protons, *i*, on the TnI peptide, as a function of molar equivalents TnC.Gd(III)$_4$. Tables VII-3 and VII-4 in the Appendix give $T_{1OBSi}{}^{La}$ and $T_{2OBSi}{}^{La}$ for various protons, *i*, on the TnI peptide, as a function of molar equivalents TnC.La(III)$_4$.

Figures VII-4A and VII-4B show the increase in the relaxation rates, $1/T_{1OBS}$, and $1/T_{2OBS}$, respectively, for the TnI peptide L111(δCH3)2 methyl groups as a function of molar equivalents TnC.Ln(III)$_4$. The upper line in Figure VII-4A shows a plot of $1/T_{1OBS}{}^{Gd}$ versus molar equivalents TnC.Gd(III)$_4$, and the lower line shows a plot of $1/T_{1OBS}{}^{La}$ versus molar equivalents TnC.La(III)$_4$. The upper line in Figure VII-4B shows a plot of $1/T_{2OBS}{}^{Gd}$ versus molar equivalents TnC.Gd(III)$_4$, and the lower line shows a plot of $1/T_{2OBS}{}^{La}$ versus molar equivalents TnC.La(III)$_4$. Slopes ($[1/T_{1OBS}{}^{Ln}]/p_B$, $[1/T_{2OBS}{}^{Ln}]/p_B$) are given for each line in the figures. While the slopes of the plots which correspond to the Gd(III) experiments are large and well defined, the slopes of the plots which correspond to the control La(III) experiments are virtually flat, indicating only small diamagnetic contributions to $1/T_{1OBS}{}^{Gd}$ and $1/T_{2OBS}{}^{Gd}$. The differences in the slopes measured from the plots in Figures VII-4A and VII-4B ($\{[1/T_{1OBS}{}^{Gd}]/p_B - [1/T_{1OBS}{}^{La}]/p_B\}$, and $\{[1/T_{2OBS}{}^{Gd}]/p_B - [1/T_{2OBS}{}^{La}]/p_B\}$) give the paramagnetic contribution to the spin-lattice ($1/T_{1P}$) and spin-spin ($1/T_{2P}$) relaxation rates from Eqns. 3a and 3b.

Figure VII-5 shows the plot of T_{2Pi} versus T_{1Pi} for various nuclei, *i*, on the TnI peptide. This plot yields a value for the exchange lifetime, τ_M, of the TnI peptide-TnC.Gd(III)$_4$ complex, measured from the slope {1/Á} and intercept { τ_M(Á -1)/Á }. An inspection of the graph reveals that although the intercept is readily obtained as (4.0 ± 2.0) x 10^{-4} s, the slope is very shallow and cannot be measured with any accuracy. This is due to the relationship between **Á** and τ_c described in Eqn. 4b; as the size of the complex increases, so does the correlation time, τ_c, and likewise **Á** as the square of τ_c. Thus, for small τ_c, **Á** is small, and the slope 1/**Á** is large and measurable. However, for the TnI peptide-TnC protein complex, τ_c is large, **Á** is large, and the slope 1/**Á** is small and difficult to measure. In this case, limits must be placed on the value of τ_c and **Á**. The minimum value for τ_c is obtained from inspection of Figure VII-5, from which it is clear that **Á** > 100. If **Á** > 100, Eqn. 4b limits $\tau_c > 4 \times 10^{-9}$ s. The maximum value of τ_c is equal to the rotational correlation time, τ_R. Approximating TnC as a spherical particle with molecular weight of 18,500 Daltons and at an experimental temperature of 5°C gives $\tau_R = 25 \times 10^{-9}$ s (Boerand and Kidd, 1982; Brauer and Sykes, 1987; Chapter II). Thus, with the limits of τ_c defined as 4×10^{-9} s < τ_c < 25×10^{-9} s, and $\tau_M = 4 \times 10^{-4}$ s (for small **Á**, intercept = τ_M (Á-1)/Á = τ_M), a range of distances may be calculated. Table VII-1 shows the range of distances, calculated for various protons on the TnI peptide, with R_{min} corresponding to $\tau_c = 25 \times 10^{-9}$ s and R_{max} corresponding to $\tau_c = 4 \times 10^{-9}$ s. Table VII-5 in the Appendix gives the calculated values of $1/T_{1OBSi}{}^{Gd}$, $1/T_{2OBSi}{}^{Gd}$, $1/T_{1OBSi}{}^{La}$, $1/T_{2OBSi}{}^{La}$, $1/T_{1Pi}$, $1/T_{2Pi}$, $1/T_{1Mi}$, R_{maxi} and R_{mini} for various protons, *i*, on the TnI peptide.

E. Discussion

We have used the paramagnetic lanthanide Gd(III) as a Ca(II) analog to derive a range of distances for various assigned nuclei on the TnI peptide to the Gd(III)-filled sites on TnC. Since we have used Gd(III)-saturated TnC in these experiments, we can assume that Gd(III) has occupied all four metal-binding sites in TnC, two sites (sites I and II) in the N-terminal domain, and two sites (sites III and IV) in the C-terminal domain. This means that the calculated distances, R_{max} and R_{min} (which we will represent by R_{calc}), are actually a set of averaged distances with contributions from each of the four Gd(III)-bound sites,

$$1/R_{calc} = [\ (1/R_I)^6 + (1/R_{II})^6 + (1/R_{III})^6 + (1/R_{IV})^6\ ]^{1/6} \qquad [5]$$

where R_I is the distance of a particular proton on the TnI peptide to site I, R_{II} is the distance to site II, etc. It is not possible to separate out the contributions to R_{calc} from each Gd(III)-bound site, however if one knows any one of these distances, R_I, R_{II}, R_{III}, or R_{IV}, the contribution from others can be calculated.

In Chapter VI, we assigned interresidue TnI peptide - TnC protein NOEs which allowed identification of several residues on Ca(II)-saturated s-TnC which interact with the TnI peptide. A model of this interaction was then produced on a molecular graphics system using the x-ray crystal structure of turkey s-TnC (Herzberg and James, 1985) and the TRNOE-derived structure of the TnI peptide bound to TnC (Campbell and Sykes, 1991; Chapter V) (see Figure VI-25 in Chapter VI). We assigned NOEs between residues on the TnI peptide and F102, I104, I113, I121, I149, F151, and F154, within the hydrophobic pocket in the C-terminal domain and the β-sheet region between Ca(II)-binding sites III and IV of the protein. However, the identification of these residues on TnC, implying an interaction of the TnI peptide with the C-terminal domain, does not preclude an involvement with the N-terminal domain. Both domains could be involved in the binding interface with the TnI peptide, literally 'clamping-down' on the target peptide.

The question of the involvement and/or proximity of the N-terminal domain to the C-terminal domain of TnC in the TnI peptide - TnC protein complex remains a compelling one. Using the model of the TnI peptide bound to TnC developed in Chapter VI, we can extract reasonable distances between protons on the TnI peptide to the Ca(II)-filled sites III and IV on TnC (ie. $R_{III\,i}$ and $R_{IV\,i}$ for various protons, *i*, on the TnI peptide). Using a molecular graphics system and the model developed in Chapter VI, distances were measured from selected protons on the TnI peptide to the Ca(II) ions in sites III and IV on TnC[1]. All distances to sites III and IV were found to fall within the range of 10 - 20 Å. For example, the L111(δCH3)2 methyl protons were found within a radius of 11 - 13 Å from site III, and 12 - 15 Å from site IV; the V114(γCH3)3 methyl protons were found within a radius of 14 - 18 Å from site III, and 14 - 19 Å from site IV; and the F106 ring protons were found within a radius of 14 - 17 Å from site III, and 15 - 20 Å from site IV. These distances are longer than the R_{max} and R_{min} distances calculated from the Gd(III) relaxation experiments, which were 8 Å $\leq R_{max} \leq$ 12 Å, and 5 Å $\leq R_{min} \leq$ 9 Å. Even the R_{max} distances are 2 - 8 Å shorter than the R_{III} and R_{IV} distances measured from the model!

If we take the R_{max} distances calculated from the Gd(III) experiment, and the R_{III} and R_{IV} distances measured from the model, we can calculate approximate values of R_I and R_{II} which would satisfy Eqn. 5 (we assume that the conformations of the Ca(II)-saturated and Gd(III)-saturated TnC molecules are the same). Based on Eqn. 5, we can do the following calculation for the V114(γCH3)2 methyl groups, for which, R_{max} = 10.22 Å, R_{III} = 14 Å, and R_{IV} = 14 Å;

$$1/R_{calc} = (1/10.22\ \text{Å}) = [\ (2/R_N)^6 + (1/14\ \text{Å})^6 + (1/14\ \text{Å})^6\ ]^{1/6} \qquad [6]$$

Here, $R_I = R_{II} = R_N$, ie. we have assumed that the distance of the V114(γCH3)2 methyl groups to the Gd(III) ions in sites I and II is roughly the same. Rearranging for R_N, we produce,

$$R_N = 2\ [\ (1/10.22\ \text{Å})^6 - (1/14\ \text{Å})^6 - (1/14\ \text{Å})^6\ ]^{-1/6} = 22\ \text{Å} \qquad [7]$$

Thus, the distance of the V114(γCH3)2 methyl groups to the Gd(III) ions in sites I and II is roughly 22 Å. If we repeat this calculation for the L111(δCH3)2 methyl groups, for which R_{max} = 10.34 Å, R_{III} = 11 Å, and R_{IV} = 12 Å, and for the F106 ring protons for which R_{max} = 9.64 Å, R_{III} = 14 Å, and R_{IV} = 15 Å, we calculate distances of R_N = 25 Å for the L111(δCH3)2 methyl groups, and R_N = 20 Å for the F106 ring protons. These distances are much shorter than the 40 Å distances measured between residues on the TnI peptide and Ca(II) ions in sites I and II of TnC in the model of the TnI peptide bound to TnC. This suggests that the N-terminal domain of TnC is much closer to the C-terminal domain in the peptide-protein complex than the elongated crystal structure of the protein would lead one to believe.

---

[1] The model used a pseudo-atom representation for the methyl groups of L111 and V114 and the aromatic ring protons of F106 (Wuthrich *et al.*, 1983). R_{III} and R_{IV} were measured for the pseudo-atom closest to the Ca(II) ion in site III and site IV, respectively.

Although the distance measurements in the model are rough approximations, and the Gd(III)-derived distances are inexact due to the inability to determine a definite value for τ_c, nevertheless the Gd(III)-derived distances are too short to be explained by the TnI peptide binding at the C-terminal domain of an elongated TnC molecule. If the TnI peptide binds at the C-terminal domain, near the hydrophobic pocket, then the distances to the metals in sites III and IV are too long to account for Gd(III)-derived distances in the range of 8-12 Å. This means that the N-terminal domain must also be involved in the binding of the TnI peptide, bringing the metals in sites I and II within a 20-25 Å radius of nuclei on the peptide.

Alternatively, binding of the TnI inhibitory peptide to the C-terminal domain of TnC could elicit conformational changes in this domain which would bring the Gd(III)-bound sites III and IV 2-8 Å closer to the TnI peptide nuclei. One cannot expect the structure of the TnC protein to remain unchanged when the TnI peptide binds, since the aromatic cluster and hydrophobic pocket would need to become more exposed in order to interact with the peptide. In Chapter VI (Campbell *et al.*, 1991b) the ^{1}H NMR monitored titration of Ca(II)-saturated turkey s-TnC with the TnI peptide revealed changes in the chemical shifts of TnC resonances corresponding to residues in the hydrophobic pocket of the C-terminal domain and the β-sheet region between sites III and IV. This suggests a rearrangement of the hydrophobic pocket and β-sheet region in the protein upon complexation with peptide. However, substantial chemical shifts can be induced by very subtle conformational changes, such as a change of tilt angle of a phenylalanine ring, which could cause large changes in ring currents. Therefore, although we expect subtle conformational changes in the C-terminal domain of TnC upon binding of the TnI peptide, it is not easy to envision gross changes in conformation which could account for a 2-8 Å change in proximity of the sites III and IV metal binding sites to the TnI peptide binding site upon TnI peptide - TnC protein complex formation.

The long central helix of TnC is bent about 16° at G92 in the crystal structure of chicken TnC, (Sundaralingam *et al.*, 1985a). However, it appears to be stabilized in the crystal by interhelical salt bridges between charged amino acid side chains (Sundaralingam *et al.*, 1985b). It is tempting to envision a model of the inhibitory TnI peptide binding to Ca(II)-saturated TnC in which a bend at G92 allows a closer approach of the N- and C-terminal domains in a concerted effort to bind the peptide. The hydrophobic pockets in the N- and C-terminal domains each provide half of the binding interface between which the peptide is 'sandwiched'. Figure VII-6 shows a model of a proposed TnI peptide-induced conformational change in Ca(II)-saturated TnC involving the 'hinge region' in the D/E linker. The angle, θ, describes the extent of bend at the hinge region around G92.

Many studies have examined the interaction of the inhibitory TnI peptide with Ca(II)-saturated TnC, and have given evidence of an interaction with the TnI peptide that involves both the C- and the N-terminal domains of TnC protein. Studies pointing to an interaction of the inhibitory region of TnI with the C-terminal domain, particularly the N-terminal helix of site III (Weeks and Perry, 1978; Grabarek *et al.*, 1981; Leszyk *et al.*, 1987, 1988; Tao *et al.*, 1989; Lan *et al.*, 1989; Campbell *et al.*, 1991b) have been discussed in Chapters IV and VI and will not be described here. Studies implicating both the C- and the N-terminal domains in the binding of the TnI peptide have included photo-crosslinking, fluorescence and NMR studies (Leszyk *et al.*, 1990; MacLachlan *et al.*, 1990; Wang *et al.*, 1990; Reid *et al.*, 1990). Photo-cross linking studies by Leszyk *et al.* (1990) revealed an interaction between Ca(II)-binding site II (residues 46-78) on rabbit skeletal TnC and the inhibitory region on the whole TnI protein, offering evidence for an interaction involving the N-terminal domain of TnC. Photo-cross-linking and fluorescence studies with a recombinant TnC (Wang *et al.*, 1990) demonstrated that the C-helix in the N-terminal domain of TnC interacts with TnI(104-115). MacLachlan *et al.* (1990) used fluorescence stopped flow kinetics and ^{1}H NMR to demonstrate that the calcium sensitizer, bepridil, binds to the N-terminal domain of cardiac TnC with a 1:1 stoichiometry. The same research group used ^{1}H NMR and molecular modeling to study the binding of calmidazolium to TnC and concluded that binding occurs simultaneously to both the N- and C-terminal globular domains of the TnC protein (Reid *et al.*, 1990).

Studies monitoring the binding of target drugs and inhibitors to CaM, which is structural homologous to TnC (Babu *et al.*, 1988), have also implicated residues in both the C- and the N-terminal domains. Seeholzer *et al.* (1986) investigated the structural and dynamic properties of a 1:1 deuterated CaM:melittin (Mel) complex by ^{1}H NMR. By subtracting the bound melittin spectrum ([^{2}H]CaM:Mel) from the spectrum of the nondeuterated CaM:Mel complex, they obtained spectral changes between free and complexed CaM. Perturbed resonances included F16, T26, F65, H107 and F141, implicating the involvement of both halves of the molecules. Fluorescence studies (Steiner and Norris, 1987) and proteolytic digestion studies (Caday and Steiner, 1986) have shown that melittin, which forms a 1:1 complex with CaM, makes extensive contacts with the connecting strand and adjacent portions of the N- and C-terminal domains. Klevit *et al.* (1985) and Klevit (1987) used ^{1}H NMR to study the interaction of CaM with a skeletal muscle myosin light chain kinase (MLCK) peptide, M13(577-603). Addition of the M13 peptide to CaM in a 1:1 molar ratio affected resonances from residues in both halves of the molecule, specifically F16, F65, F68, F89, Y99, Y138 and F141.

Two separate groups have offered evidence of communication between the two globular domains of CaM in the presence of target peptides (Linse *et al.*, 1986; Yazawa *et al.*, 1987). Linse *et al.* (1986) used ^{113}Cd NMR to monitor the binding of mastoparan and melittin and found that mastoparan binding induced a structural change affecting both the N- and C-terminal domains of CaM. A possible model for communication between the two lobes of CaM in the presence of melittin has been provided by Strynadka and James (1990). In this model, they introduced a kink in the central helix of CaM, serving to bring the two hydrophobic domains of CaM sufficiently close to bind a single melittin peptide, while maintaining reasonable stereochemistry.

Ikura *et al.* (1991) used triple-resonance multidimensional NMR to study CaM complexed with M13, and found evidence for a conformational change in the central helix. ^{1}H, ^{13}C and ^{15}N heteronuclear three- and four-dimensional NMR experiments showed that binding of the M13 peptide induced substantial chemical shift changes that were not localized in one particular region of the protein. The largest changes were found in the first helix of the Ca(II)-binding site I (E11-E14), the N-terminal portion of the central helix (M72-D78), and the second helix of the Ca(II)-binding site IV (F141-M145). No changes in secondary structure were observed for the first helix of site I or the C-terminal helix of site IV. Upon complexation with M13, a significant decrease in the amide exchange rate was observed for residues T110, L112, G113, and E114 at the end of the second helix of site III. These results support a model for the binding of target peptides to CaM which involves both the C-terminal and the N-terminal domains, contingent on a conformational change in the central helix.

Small angle solution x-ray scattering studies of TnC and CaM have provided the most convincing evidence for the involvement of both the N- and C-terminal domains in the binding of amphiphilic peptides or target enzymes in 1:1 complexes. Small angle x-ray scattering studies of TnC (Hubbard *et al.*, 1988; Fujisawa *et al.*, 1989) indicate that the distance between the two domains decreases upon Ca(II) binding, producing a more compact structure. Small angle x-ray scattering studies of CaM.Ca(II)$_4$ complexed with melittin (Kataoka *et al.*, 1989) and mastoparan (Matsushima *et al.*, 1989; Yoshino *et al.*, 1989), and the M13(577-603) peptide (Heidorn *et al.*, 1989), indicate that the two globular domains move towards each other in a concerted effort to bind the target ligand. Kataoka *et al.* (1989) found that binding of melittin to CaM.Ca(II)$_4$ to form the 1:1 complex caused the radius of gyration, R_g, to decrease from 20.9 to 18.0 Å, indicating that the two globular domains move towards each other in a concerted effort to bind the target ligand. Two separate groups, Matsushima *et al.* (1989) and Yoshino *et al.* (1989), found that R_g decreased by about 3 Å upon binding of both 4 mol Ca(II)/mol of protein and 1 mol mastoparan/mol of protein to form the ternary complex. Finally, Heidorn *et al.* (1989) reported an R_g for the CaM.Ca(II)$_4$:M13(577-603) equimolar complex that was 20% smaller (16 vs. 21 Å) than that of the uncomplexed CaM.Ca(II)$_4$ complex. The solvent contrast dependence of R_g for neutron scattering indicated that the peptide was located more towards the center of the complex with the CaM located more peripherally.

To test the hypothesis that the central helix of CaM could serve as a flexible tether between the two domains, mutants of CaM were created in which the two domains were constrained close to another by a specific covalent link (Persechini and Kretsinger, 1988; O'Neil and DeGrado, 1989), or were changed in distance or orientation with respect to one another by deletions in the central helix (Putkey *et al.*, 1988; Persechini *et al.*, 1989; Van Berkum *et al.*, 1990). The altered CaM molecules retained high activity towards enzyme activations, which indicated that the central helix acts as a flexible tether to allow the N- and C-terminal domains to form a single binding site capable of accomodating a wide variety of target peptides of enzymes.

Many studies have recently emerged in the literature using deletion mutants to probe the function of the connecting region between the two terminal domains of TnC and CaM. Sheng *et al.* (1991) investigated the role of the central helix of chicken s-TnC with five deletion mutants in the central D/E linker region, producing rotations in the α-helix of 20° - 160°. These mutants were assayed for their ability to regulate muscle contraction by testing their effectiveness in restoring force and Ca(II)-regulation to TnC-depleted rabbit skinned skeletal muscle fibers. They found that the change in orientation of the two Ca(II)-binding domains shifted the Ca(II)-dependence in force activation, which they proposed was related to the inability of the Ca(II)-specific domain to properly interact with its binding site on TnI, an interaction which is known to increase the affinity of TnC for Ca(II) (Potter and Gergely, 1975). Dobrowolski *et al.* (1991) also used central helix deletion mutants of chicken s-TnC to investigate the role of the D/E linker on the regulatory function of the protein, but arrived at different conclusions than did Sheng's group. They found that all mutants (except for the deletion mutant ^{88}E-D-A^{90}) were able to bind Ca(II) at the low and high affinity sites, and were able to confer Ca(II) sensitivity on regulated actomyosin

ATPase. They thus concluded that the length of the D/E linker and the orientation of the two Ca(II)-binding domains relative to each other were not crucial for regulation.

In another interesting study of the flexibility of the central helix, Yazawa *et al.* (1989) performed Ca(II)-dependent difference absorption spectroscopy, gel filtration, and trypsin digestion studies of native CaM at various ionic strengths, and found an ionic-strength-dependent decrease in ordered structure of the connecting region. They suggested that CaM may change shape depending upon the ionic strength by bending at the connecting region, fluctuating between the two extreme shapes of the bent and the dumbbell structure. Target molecules would select and fix the specific bent structure for their activation. Kataoka *et al.* (1991) used small angle x-ray scattering studies of CaM mutants with deletions in the linker region of the central helix and found that the linker region retained a predominantly α-helical conformation. They suggested that the structure of the linker region was stable enough to maintain the average orientation and separation of the lobes yet flexible enough to permit the lobes to approach each other upon binding a peptide.

These solution studies of CaM and TnC provide a structural framework for interpretation of the binding of the TnI inhibitory peptide to TnC. While it is well established that the TnI peptide binds at or near the hydrophobic pocket in the C-terminal domain in TnC, the extent of the involvement of the N-terminal domain in this binding is not known. However, evidence is beginning to emerge that the N-terminal domain is involved in the binding of the TnI inhibitory peptide, and the Gd(III)-relaxation studies presented in this chapter contribute to the weight of this evidence by suggesting that the N-terminal domain is much closer to the TnI peptide binding site at the C-terminal domain than is implied by the elongated crystal structure of the protein. It is possible to imagine a conformational change around a hinge region in the central helix of TnC which would allow the N- and C-terminal domains to form a single binding site capable of accomodating a single peptide. This would explain the wealth of data implicating both domains in the binding of the TnI inhibitory peptide. More experimentation needs to be done in this field, particularly in the area of small angle x-ray scattering solution studies of the Ca(II)-saturated TnC - inhibitory TnI peptide complex which could detect global conformational changes in the TnC molecule upon the binding of peptide. On a more subtle level, if the N-terminal domain is involved in providing the other half of the binding interface, experimental work remains to be done to determine which residues in the N-terminal domain of the protein are involved.

It is important to note that while all of these studies have characterized the interaction between TnC and the inhibitory residues(104-115) of TnI, they have not considered the interaction between TnC with the whole TnI protein. The involvement of the N-terminal domain of TnC in the binding of the inhibitory region of TnI may not be physiologically relevant when considering the binding of whole TnC to whole TnI. Studies characterizing the interaction between TnC and the whole TnI protein have pointed to multiple interactions between these two proteins. TnI fragment studies reported by Syska *et al.* (1976) demonstrated two regions of the TnI protein capable of interacting with TnC; residues 1-21, and residues 96-116. Studies employing proteolytic fragments of TnC revealed three regions of the TnC protein capable of interacting with TnI; the C-helix (residues 50-60), the E-helix (residues 89-100) and the G-helix (residues 126-136) (Grabarek *et al.*, 1981).

A model of the binding of the inhibitory region of TnI to TnC involving a bending at the hinge region of the central D/E helix may be too simplistic a picture when considering the binding of the whole TnC protein to the whole TnI protein. Nevertheless, there must be communication between the two lobes of TnC in the presence of saturating levels of Ca(II) and TnI protein since binding of Ca(II) to the low affinity sites I and II in the N-terminal domain leads to a higher affinity of the C-terminal domain of TnC for the inhibitory region of TnI. While the communication link may be the TnI protein itself, it is tempting to visualize a conformational change affecting the helical connector of the two lobes of TnC protein, especially as an exposed helix of this nature is highly unusual in protein structures, and must be designed to serve some structural purpose.

Table VII-1. Range of distances calculated for various protons on the TnI peptide to the Gd(III)-filled sites on turkey s-TnC.

Residue	Spin System	Rmin(Å)	Rmax(Å)
104	N-Acetyl CH3	7.11	9.65
104	Gly αCH2	6.76	9.16
105	Lys αCH	6.72	9.11
105	Lys γCH2	7.90	10.71
105	Lys ζCH2	6.77	9.18
106	Phe αCH	6.16	8.37
106	Phe βCH(m)	6.48	8.78
106	Phe δCH2	5.76	7.87
106	Phe ξCH2ςCH	7.11	9.64
107	Lys γCH2	7.79	10.57
108	Arg αCH	7.19	9.75
109	Pro αCH	5.66	7.67
109	Pro βCH'(p)	7.79	10.57
109	Pro γCH2	8.89	12.06
109	Pro δCH(m)	8.19	11.11
109	Pro δCH'(m')	6.76	9.16
110	Pro αCH	6.24	8.47
110	Pro βCH'(p)	7.15	9.70
110	Pro γCH2	7.51	10.19
110	Pro δCH(m)	8.19	11.11
110	Pro δCH'(m')	7.31	9.91
111	Leu (δCH3)2	7.62	10.34
114	Val αCH	7.23	9.80
114	Val (γCH3)2	7.53	10.22
115	C-term. amide NH2	7.67	10.41

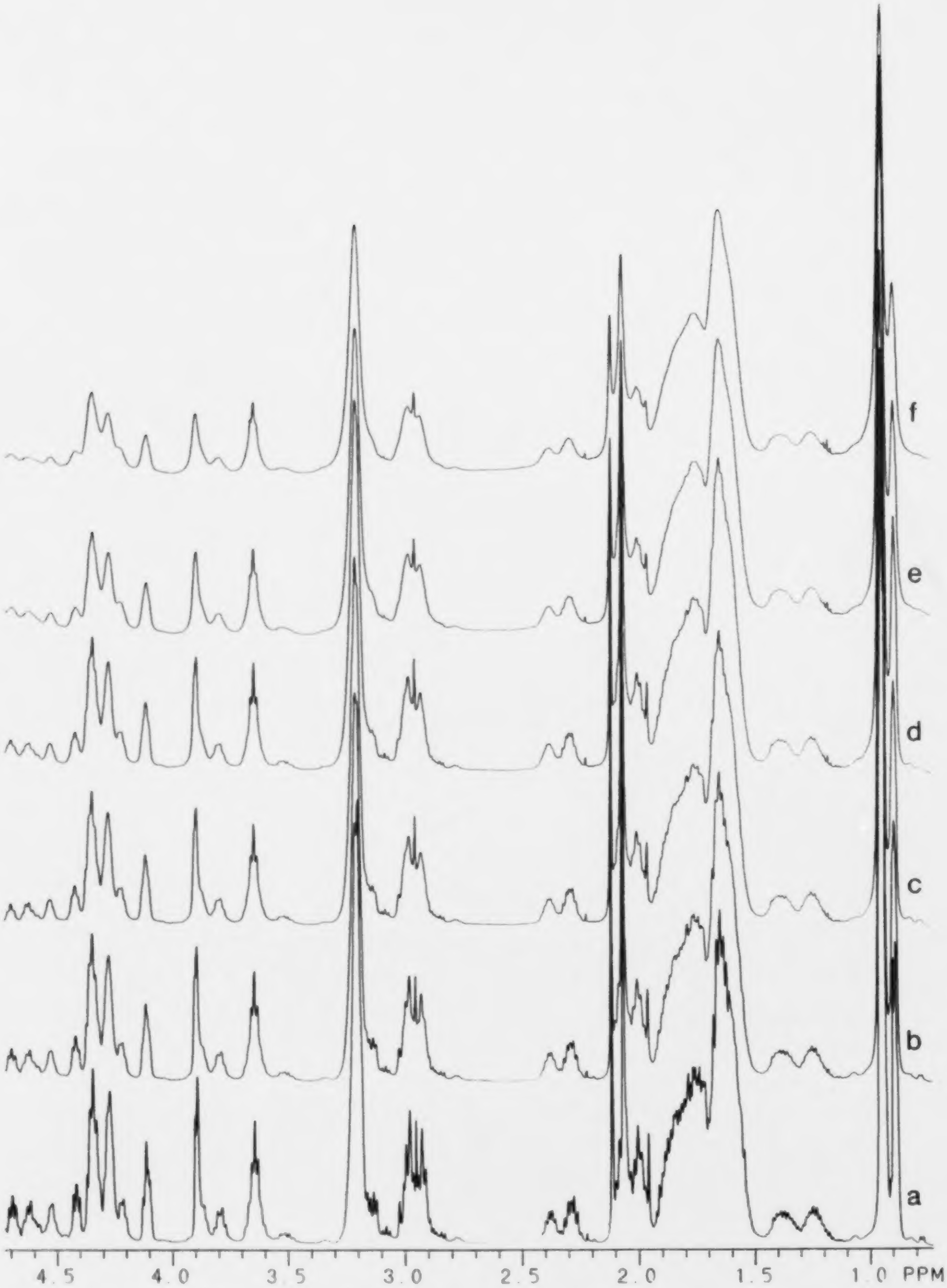

Figure VII-1A. 500 MHz ^{1}H NMR monitored titration of Nα-acetyl-TnI(104-115) amide with TnC.Gd(III)$_4$: Aliphatic upfield region of the spectrum. **a.** 0.0 **b.** 0.0006 **c.** 0.0011 **d.** 0.0021 **e.** 0.0034 **f.** 0.0047 and **g.** 0.0073 molar equivalents TnC.Gd(III)$_4$ to TnI peptide. (Sample was 5 mM Nα-acetyl-TnI(104-115) amide, 50 mM KCl, pH 6.74, 80%H_2O/20%D_2O, 5°C; panels **b.** through **g.** contained 0.0027 mM, 0.0045 mM, 0.0090 mM, 0.0144 mM, 0.0198 mM, and 0.0522 mM TnC.Gd(III)$_4$, respectively.)

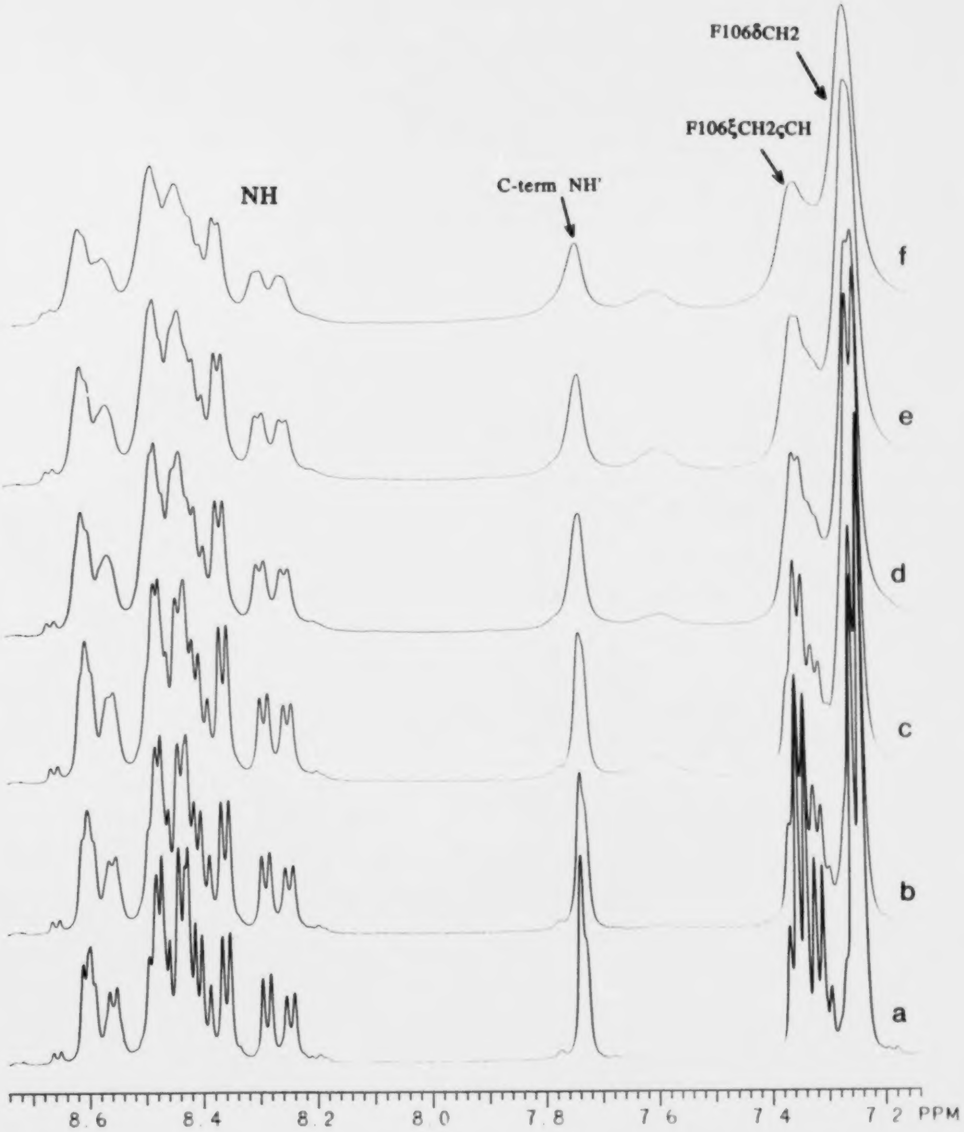

Figure VII-1B. 500 MHz ^{1}H NMR monitored titration of Nα-acetyl-TnI(104-115) amide with TnC.Gd(III)$_4$: Downfield region of the spectrum with the aromatic F106 resonances **a.** 0.0 **b.** 0.0006 **c.** 0.0011 **d.** 0.0021 **e.** 0.0034 **f.** 0.0047 and **g.** 0.0073 molar equivalents TnC.Gd(III)$_4$ to TnI peptide. (Sample was 5 mM Nα-acetyl-TnI(104-115) amide, 50 mM KCl, pH 6.74, 80%H_2O/20%D_2O, 5°C; panels **b.** through **g.** contained 0.0027 mM, 0.0045 mM, 0.0090 mM, 0.0144 mM, 0.0198 mM, and 0.0522 mM TnC.Gd(III)$_4$, respectively.)

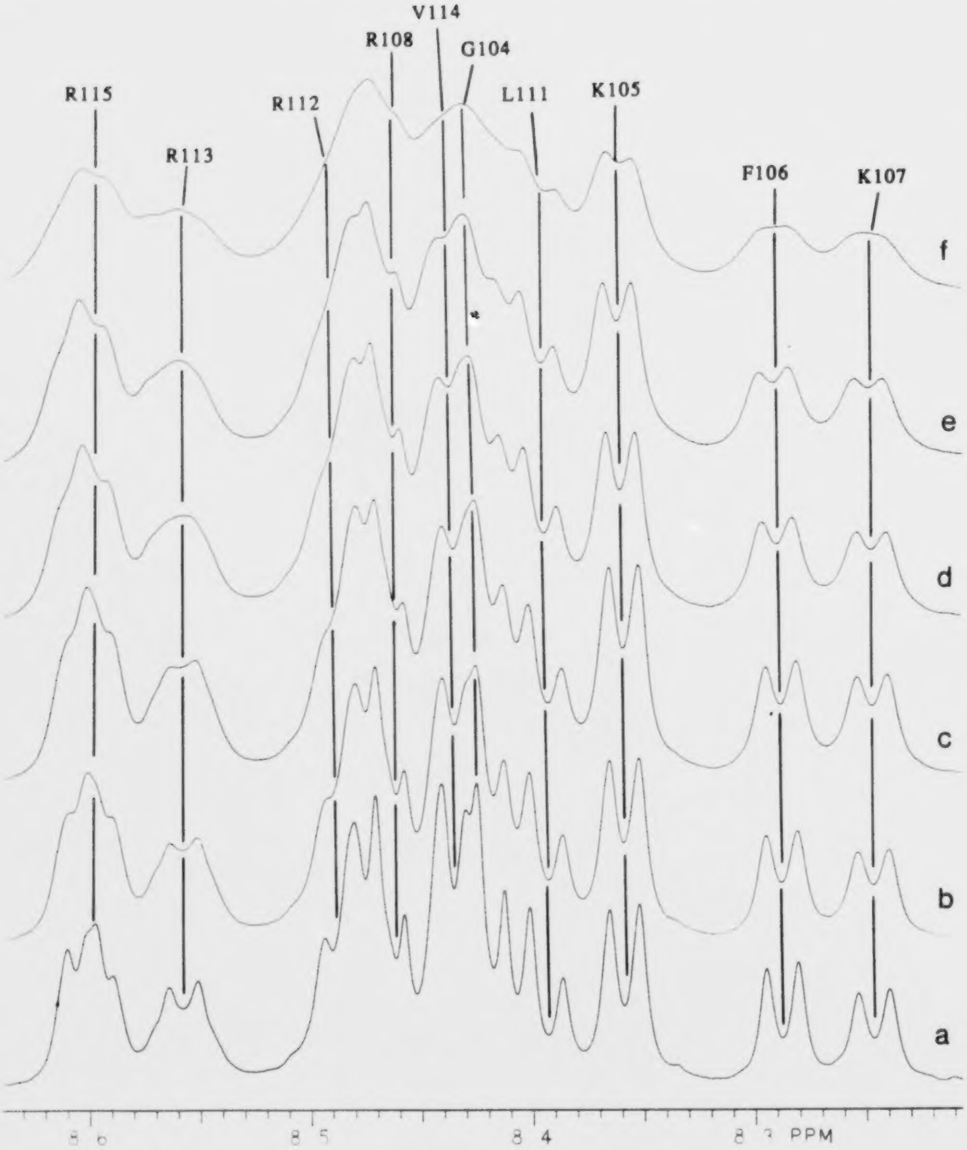

Figure VII-1C. 500 MHz ^{1}H NMR monitored titration of Nα-acetyl-TnI(104-115) amide with TnC.Gd(III)$_4$: Expanded region of spectrum B showing backbone amide proton resonances. **a.** 0.0 **b.** 0.0006 **c.** 0.0011 **d.** 0.0021 **e.** 0.0034 **f.** 0.0047 and **g.** 0.0073 molar equivalents TnC.Gd(III)$_4$ to TnI peptide. (Sample was 5 mM Nα-acetyl-TnI(104-115) amide, 50 mM KCl, pH 6.74, 80%H$_2$O/20%D$_2$O, 5°C; panels **b.** through **g.** contained 0.0027 mM, 0.0045 mM, 0.0090 mM, 0.0144 mM, 0.0198 mM, and 0.0522 mM TnC.Gd(III)$_4$, respectively.)

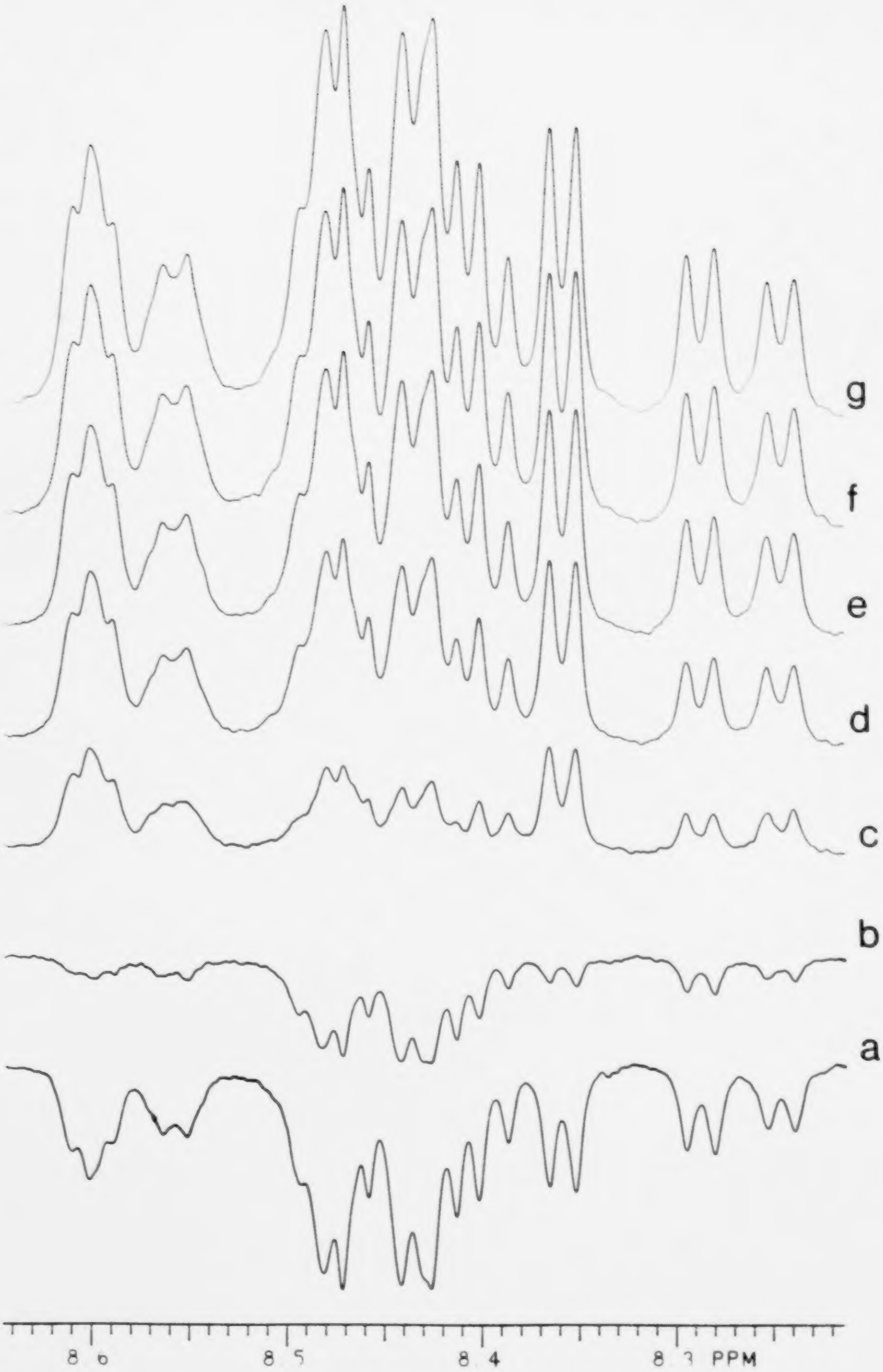

Figure VII-2. 500 MHz ^{1}H NMR monitored T_1 inversion recovery experiment ([180° - τ - 90°(FID) - T_d $]_n$; where τ is the evolution period and T_d is the recovery time) showing backbone amide proton resonances at 0.0 molar equivalents TnC.Gd(III)$_4$ to TnI peptide. **a.** τ = 0.1 s **b.** τ = 0.2 s **c.** τ = 0.4 s **d.** τ = 0.6 s **e.** τ = 0.8 s **f.** τ = 1.0 s and **g.** τ = 1.6 s.

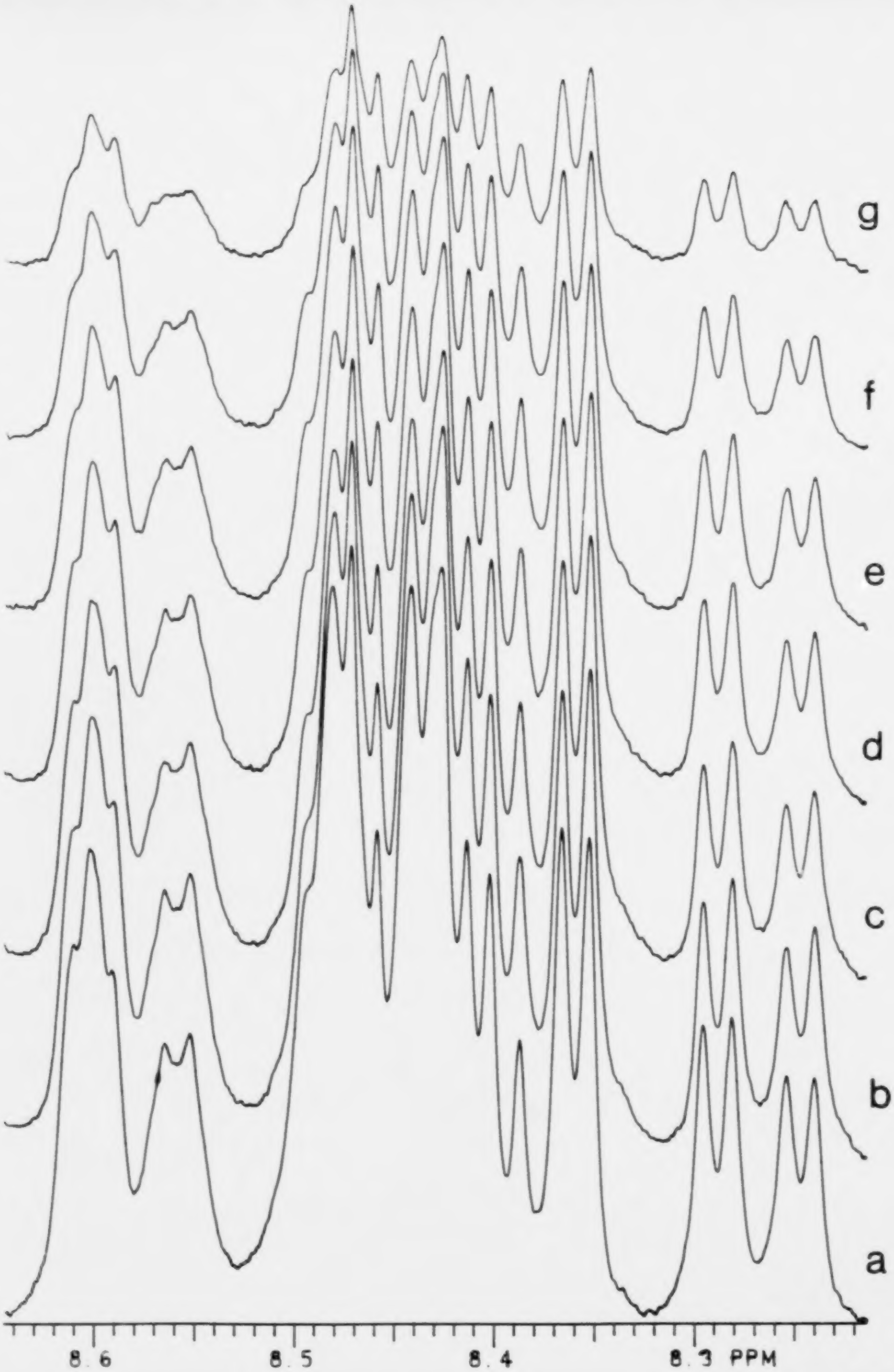

Figure VII-3. 500 MHz ^{1}H NMR monitored T_2 Carr-Purcell-Meiboom-Gill spin-echo experiment ($90°_x$ -[τ - $180°_y$ - τ - echo $]_n$; where τ is the evolution period) showing backbone amide proton resonances at 0.0 molar equivalents TnC.Gd(III)$_4$ to TnI peptide. **a.** $\tau = 0.002$ s **b.** $\tau = 0.008$ s **c.** $\tau = 0.02$ s **d.** $\tau = 0.03$ s **e.** $\tau = 0.04$ s **f.** $\tau = 0.06$ s and **g.** $\tau = 0.10$ s.

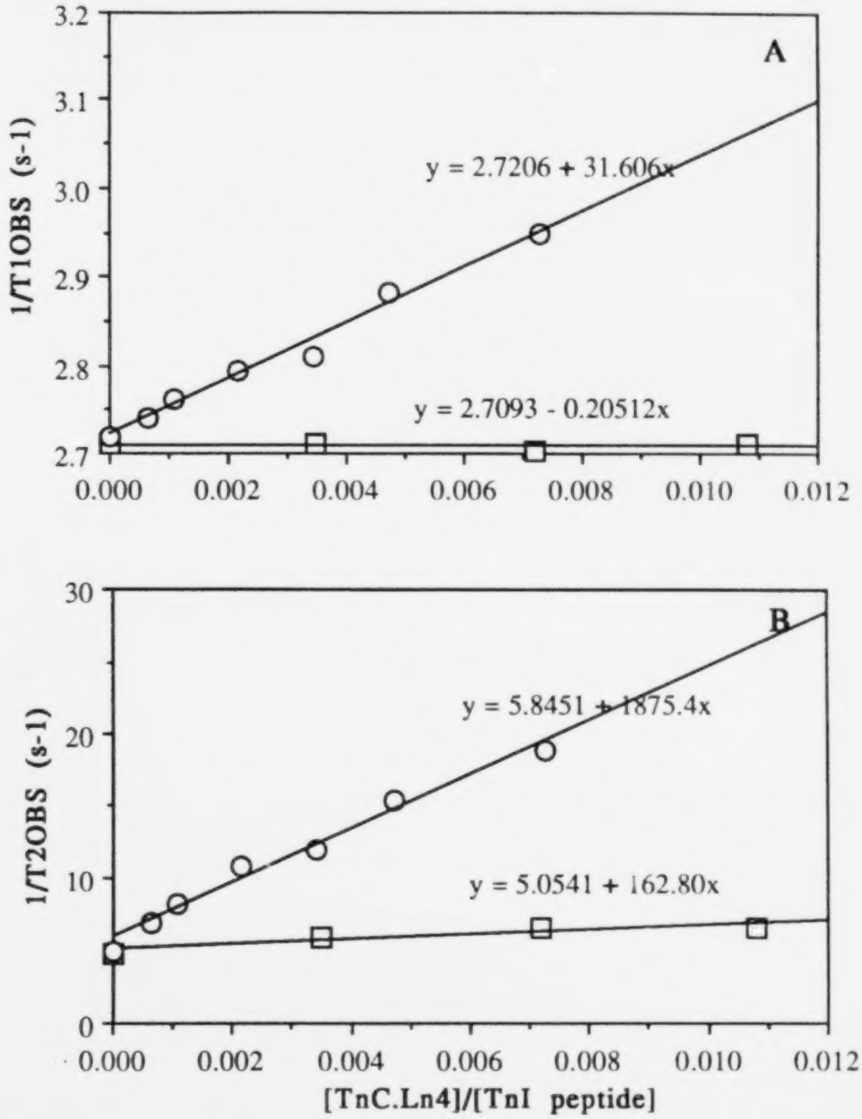

Figure VII-4. Increase in relaxation rates for the TnI peptide L111(δCH3)2 methyl group as a function of the molar equivalents TnC.Ln(III)$_4$ to TnI peptide. **A.** 1/T_{1OBS} versus [TnC.Ln(III)$_4$]/[TnI peptide]; **B.** 1/T_{2OBS} versus [TnC.Ln(III)$_4$]/[TnI peptide]. (□) La(III); (○) Gd(III).

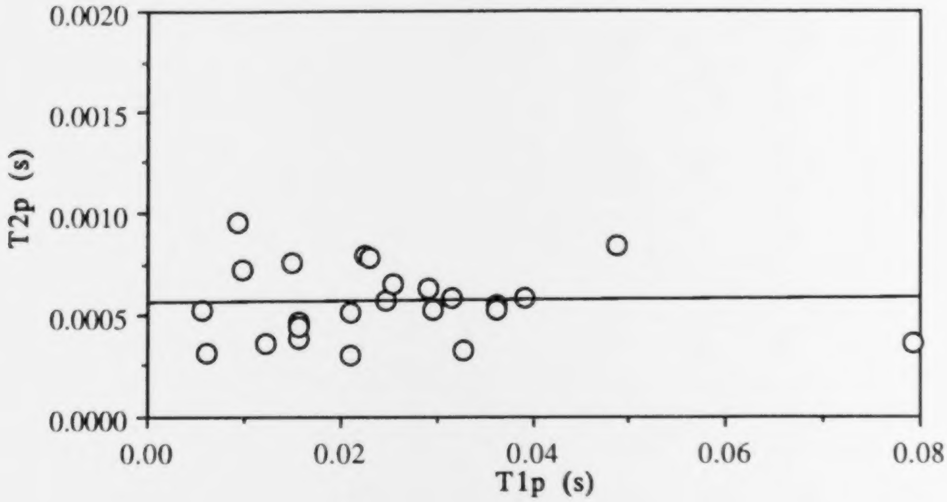

Figure VII-5. Plot of T_{2Pi} versus T_{1Pi} for various nuclei on the TnI peptide.

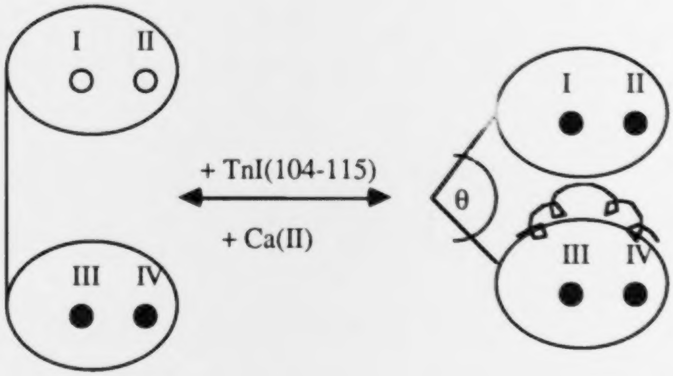
I
II
III
IV
+ TnI(104-115)
+ Ca(II)
θ
I
II
III
IV

Figure VII-6. Model of a proposed TnI peptide-induced conformational change in TnC.Ca(II)$_4$ involving the 'hinge region' in the D/E linker. The angle, θ, describes the extent of bend around G92.

F. References

BABU, Y.S., BUGG, C.E., and COOK, W.J. 1988. Structure of calmodulin refined at 2.2 Å resolution. J. Mol. Biol. **204**: 191-204.

BERTINI, I., and LUCHINAT, C. 1986. Lanthanides. In *NMR of Paramagnetic Molecules in Biological Systems.*, Chapt. 10, pp 273-295, Benjamin-Cummings.

BLOEMBERGEN, N. 1957. Proton relaxation times in paramagnetic solutions. J. Chem. Phys. **27**: 572-573.

BOERAND, R.T., and KIDD, R.G. 1982. Ann Rep. NMR Spectrosc. **13**: 320-331.

BRAUER, M., and SYKES, B.D. 1987. *Phosphorus NMR in Biology* (C.T. Burt, Ed.) pp 153-184, CRC Press, Boca Raton, Florida.

BRITTAIN, H.G., RICHARDSON, F.S., MARTIN, B.R., BURTNICK, L.D., and KAY, C.M. 1976. Circularly polarized emission of terbium(III) substituted bovine cardiac troponin-C. Biochem. Biophys. Res. Commun. **68**: 1013-1019.

BUCCIGROSS, J.M., and NELSON, D.J. 1986. EPR studies show that all lanthanides do not have the same order of binding to calmodulin. Biochem. Biophys. Res. Commun. **138**: 1243-1249.

CACHIA, P.J., SYKES, B.D., and HODGES, R.S. 1983. Calcium-dependent inhibitory region of troponin. A proton magnetic resonance study on the interaction between troponin C and the synthetic peptide Nα-acetyl [F-phenylalanine106] TnI (104-115) amide. Biochemistry **22**: 4145-4152.

CACHIA, P.J., SYKES, B.D., and HODGES, R.S. 1985. Structural studies on calmodulin and troponin C. Phenothiazine, peptide, and protein interactions with calcium-induced helices. In *Calmodulin Antagonist and Cellular Physiology* (Hidaka, H., and Hartshorne, D.J., Eds.), Chapt. 5, pp 63-88, Academic Press, New York.

CACHIA, P.J., VAN EYK, J., INGRAHAM, R.H., MCCUBBIN, W.D., KAY, C.M., and HODGES, R.S. 1986. Calmodulin and troponin C. A comparative study of the interaction of mastoparan and troponin I inhibitory peptide [104-115]. Biochemistry **25**: 3553-3562.

CADAY, C.G., and STEINER, R.F. 1986. Interaction of calmodulin with melittin. Biochem. Biophys. Res. Commun. **135**: 419-425.

CAMPBELL, A.P., MARSDEN, B.J., VAN EYK, J.V., HODGES, R.S., and SYKES, B.D. 1990. Calcium regulation of muscle contraction; NMR studies of the interaction of troponin C with calcium and troponin I. In *Frontiers of NMR in Molecular Biology. UCLA Symposia on Molecular and Cellular Biology.* (Live, D., Armitage, I., and Patel, D., Eds.), pp 99-108, John Wiley and Sons, New York.

CAMPBELL, A.P., CACHIA, P.J., and SYKES, B.D. 1991a. Interaction of troponin I and troponin C : ^{19}F NMR studies of the binding of the inhibitory troponin I peptide to turkey skeletal troponin C. Biochem. Cell Biol., in press.

CAMPBELL, A.P., and SYKES, B.D. 1991. Interaction of troponin I and troponin C: Use of the two-dimensional NMR transferred nuclear Overhauser effect to determine the structure of the inhibitory troponin I peptide when bound to skeletal troponin C. J. Mol. Biol., in press.

CAMPBELL, A.P., SLUPSKY, C.M, SHAW. G.S., and SYKES, B.D. 1991b. Interaction of troponin I and troponin C: Identification using NMR of specific residues on troponin C which are involved in the binding of an inhibitory troponin I peptide. Biochemistry, submitted.

CARR, H.Y., and PURCELL. E.M. 1954. Effects of diffusion on free precession in nuclear magnetic resonance experiments. Phys. Rev. **94**: 630-638.

CAVE, A., PAGES, M., MOREN, P.H., and DOBSON, C.M. 1979. NMR studies of primary and secondary sites of parvalbumins using the two paramagnetic probes Gd(III) and Mn(II). Biochimie **61**: 755-765.

CHONG, P.C.S., ASSELBERGS, P.J., and HODGES, R.S. 1983. Inhibition of rabbit skeletal muscle acto S1-ATPase by troponin T. FEBS Lett. **153**: 372-376.

COLE, H.A., and PERRY, S.V. 1975. The phosphorylation of troponin I from cardiac muscle. Biochem. J. **149**: 525-533.

COLLINS, J.H., POTTER, J.D., HORN, M.J., WILSHIRE, G., and JACKMAN, N. 1973. The amino acid sequence of rabbit skeletal muscle troponin C. Gene replication and homology with calcium-binding proteins from carp and hake muscle. FEBS Lett. **36**: 268-272.

CORSON, D.C., LEE, L., MCQUAID, G.A., and SYKES, B.D. 1983a. An optical stopped-flow and ^{1}H and ^{113}Cd nuclear magnetic resonance study of the kinetics and stoichiometry of the interaction of the lanthanide Yb^{+3} with carp parvalbumin. Can. J. Bioc. Cell Biol. **61**: 860-867.

CORSON, D.C., WILLIAMS, T.C., and SYKES, B.D. 1983b. Calcium binding proteins: Optical stopped-flow and proton nuclear magnetic resonance studies of the binding of the lanthanide series of metal ions to parvalbumin. Biochemistry **22**: 5882-5889.

DOBROWOLSKI, Z., XU, G-Q., and HITCHCOCK-DEGREGORI, S.E. 1991. Modified calcium-dependent regulatory function of troponin C central helix mutants. J. Biol. Chem. **266**: 5703-5710.

DRAKENBERG, T., SWARD, M., CAVE, A., and PARELLO, J. 1985. Metal-ion binding to parvalbumin. A ^{113}Cd NMR study of the binding of different lanthanide ions. Biochem. J. **227**: 711-717.

EBASHI, S., and ENDO, M. 1968. Calcium ion and muscle contraction. Prog. Biophys. Mol. Biol. **18**: 123-183.

ERICKSON, B.W., and MERRIFIELD, R.B.1976. Solid-phase peptide synthesis. In *The Proteins*, (Neurath, H., and Hill, R.L., Eds.), Vol. **2**, pp 255-527, Academic Press, New York.

FREEMAN, R., and HILL, H.D.W. 1970. Spin-lattice relaxation in high-resolution NMR spectra. J. Chem. Phys. **53**: 4103-4105.

FREEMAN, R., and HILL, H.D.W. 1971. Fourier transform study of NMR spin-lattice relaxation by "progressive saturation". J. Chem. Phys. **54**: 3367-3377.

FUJISAWA, T., UEKI, T., and IIDA, S. 1989. Strucural change of the troponin C molecule upon Ca^{+2} binding measured in solution by the x-ray scattering technique. J. Biochem. **105**: 377-383.

GARIEPY, J., KAY, L.E., KUNTZ, I.D., SYKES, B.D., and HODGES, R.S. 1985. Nuclear magnetic resonance determination of metal-proton distances in a synthetic calcium binding site of rabbit skeletal troponin C. Biochemistry **24**: 544-550.

GREASER, M.C., and GERGELY, J. 1971. Reconstitution of troponin activity from three protein components. J. Biol. Chem. **246**: 4226-4233.

GRABAREK, Z., DRABIKOWSKI, W., LEAVIS, P.C., ROSENFELD, S.S., and GERGELY, J. 1981. Proteolytic fragments of troponin C. Interactions with the other troponin subunits and biological activity. J. Biol. Chem. **256**: 13121-13127.

HARTSHORNE, D.J., and MUELLER, H. 1968. Fractionation of troponin into two distinct proteins. Biochem. Biophys. Res. Commun. **31**: 647-653.

HEIDORN, D.B., SEEGER, P.A., ROKOP, S.E., BLUMENTHAL, D.K., MEANS, A.R., CRESPI, H., and TREWELLA, J. 1989. Changes in the structure of calmodulin induced by a peptide based on the calmodulin-binding domain of myosin light chain kinase. Biochemistry **28**: 6757-6764.

HENZL, M.T., MCCUBBIN, W.D., KAY, C.M., and BIRNBAUM, E.R. 1985. Luminescence studies of lanthanide ion binding to parvalbumin. J. Biol. Chem. **260**: 8447-8455.

HERZBERG, O., and JAMES, M.N.G. 1985. Structure of the calcium regulatory muscle protein troponin C at 2.8 Å resolution. Nature **313**: 653-659.

HITCHCOCK, S.E. 1975. Regulation of muscle contraction. Binding of troponin C involved in calcium ion-dependent interaction with troponin I. Eur. J. Biochem. **52**: 255-263.

HODGES, R.S., SEMCHUCK, P.D., TANEJA, A.K., KAY, C.M., PARKER, J.M.R., and MANT, C.T. 1988. Protein design using model synthetic peptides. Peptide Research **1**: 19-29.

HORROCKS, W.D., Jr., and TINGEY, J.M. 1988. Time-resolved Europium(III) luminescence excitation spectroscopy: Characterization of calcium-binding sites of calmodulin. Biochemistry **27**: 413-419.

HOULT, D.I. 1976. Solvent peak saturation with single phase and quadrature Fourier transformation. J. Magn. Reson. **21**: 337-347.

HUBBARD, S.R., HODGSON, K.O., MARSHALL, R.C., and GURD, F.R.N. 1988. Small angle x-ray scattering investigation of the solution structure of troponin-C. J. Mol. Biol. **263**: 4151-4158.

IKURA, M., KAY, E., KRINKS, M., and BAX, A. 1991. Triple-resonance multidimensional NMR study of calmodulin complexed with the binding domain of skeletal muscle myosin light-chain kinase: Indication of a conformational change in the central helix. Biochemistry **30**: 5498-5504.

JOHNSON, J.D., CHARLTON, S.C., and POTTER, J.D. 1979. A fluorescence stopped flow analysis of Ca^{+2} exchange with troponin C. J. Biol. Chem. **254**: 3497-3502.

KATAOKA, M., HEAD, J.F., SEATON, B.A., and ENGELMAN, D.M. 1989. Melittin binding causes a large calcium-dependent conformational change in calmodulin. Proc. Natl. Acad. Sci. USA **86**: 6944-6948.

KATAOKA, M., HEAD, J.F., PERSECHINI, A., KRETSINGER, R.H., and ENGELMAN, D.M. 1991. Small-angle x-ray scattering studies of calmodulin mutants with deletions in the linker region of the central helix indicate that the linker region retains a predominantly α-helical conformation. Biochemistry **30**: 1188-1192.

KEMPLE, M.D., RAY, B.D., LIPKOWITZ, K.B., PRENDERGAST, F.G., and RAO, B.D.N. 1988. The use of lanthanides of solution structure determination of biomolecules by NMR: Evaluations of the methodology with EDTA derivatives as model systems. J. Am. Chem. Soc. **110**: 8275-8287.

KILHOFFER, M-C., DEMAILLE, J.G., and GERARD, D. 1980a Terbium as luminescent probe of calmodulin calcium-binding sites. FEBS Lett. **116**: 269-272.

KILHOFFER, M-C., GERARD, D., and DEMAILLE, J.G. 1980b Terbium binding to octopus calmodulin provides the complete sequence of ions binding. FEBS Lett. **120**: 99-103.

KLEVIT, R.E., BLUMENTHAL, D.K., WEMMER, D.E., and KREBS, E.G. 1985. Interaction of calmodulin and a calmodulin-binding peptide from myosin light chain kinase. Major spectral changes in both occur as a result of complex formation. Biochemistry **24**: 8152-8157.

KLEVIT, R.E. 1987. Study of calmodulin-peptide interactions by NMR spectroscopy. Methods in Enzymology **139**: 197-206.

KRETSINGER, R.H., and NOCKOLDS, C.E. 1973. Carp muscle-binding protein II. Structure determination and general description. J. Biol. Chem. **248**: 3313-3326.

LAN, J., ALBAUGH, S., and STEINER, R.F. 1989. Interactions of troponin I and its inhibitory fragment (residues 104-115) with troponin C and calmodulin. Biochemistry **28**: 7380-7385.

LEAVIS, P.C., NAGY, B., LEHRER, S.S., BIALKOWSKA, H., and GERGELY, J. 1980. Terbium binding to troponin C: binding stoichiometry and structural changes induced in the protein. Arch. Biochem. Biophys. **200**: 17-21.

LEAVIS, P.C., and GERGELY, J. 1984. Thin filament proteins and thin filament regulation of vertebrate muscle contraction. CRC Crit. Rev. Biochem. **16**: 235-305.

LEE, L., SYKES, B.D., and BIRNBAUM, E.R. 1978. A determination of the relative compactness of the Ca^{2+}-binding sites of a Ca^{2+}-binding fragment of troponin C and parvalbumin using lanthanide-induced ^1H NMR shifts. FEBS Lett. **98**: 169-172.

LEE, L., and SYKES, B.D. 1980a. Nuclear magnetic resonance determination of metal-proton distances in the EF site of carp parvalbumin using the susceptibility contribution of the line broadening of lanthanide-shifted resonances. Biochemistry **19**: 3208-3214.

LEE, L., and SYKES, B.D. 1980b. Strategies for the use of lanthanide NMR shift probes in the determination of protein structure in solution. Biophys. J. **32**: 193-210.

LEE, L., and SYKES, B.D. 1981. Proton nuclear magnetic resonance determination of the sequential Ytterbium replacement of calcium in carp parvalbumin. Biochemistry **20**: 1156-1162.

LEE, L., and SYKES, B.D. 1982. In *Biochemical Structure Determination by NMR*. (Bothner-By, A.A., Glickson, J., and Sykes, B.D., Eds.), pp 169-172, Marcel Dekker, New York.

LEE, L., and SYKES, B.D. 1983. Use of lanthanide-induced nuclear magnetic resonance shifts for determination of protein structure in solution: EF calcium binding site in parvalbumin. Biochemistry **22**: 4366-4373.

LEE, L., and SYKES, B.D. 1986. Use of lanthanide-induced nuclear magnetic resonance shifts for determination of protein structure in solution: EF calcium binding site of carp parvalbumin. Biochemistry **22**: 4366-4373.

LENKINSKI, R.E., and GLICKSON, J.D. 1985. Paramagnetic metal ions as nuclear magnetic resonance probes of peptide conformation in solution. In *The Peptides*, Vol. **7**, Chapt. 6, pp 301-353, Academic Press, New York.

LESZYK, J., COLLINS, J.H., LEAVIS, P.C., and TAO, T. 1987. Cross-linking of rabbit skeletal muscle troponin with the photoactive reagent 4-maleimidobenzophenone. Identification of residues in troponin I that are close to cys-98 of troponin C. Biochemistry **26**: 7042-7047.

LESZYK, J., COLLINS, J.H., LEAVIS, P.C., and TAO, T. 1988. Cross-linking of rabbit skeletal muscle troponin subunits. Labelling of Cys-98 of troponin C with 4-maleimidobenzophenone and analysis of products formed in the binary complex with troponin T and the ternary complex with troponins I and T. Biochemistry **27**: 6983-6987.

LESZYK, J., GRABAREK, Z., GERGELY, J., and COLLINS, J.H. 1990. Characterization of zero-length cross-links between rabbit skeletal muscle troponin C and troponin I. Evidence for direct interaction between the inhibitory region of troponin I and the NH_2-terminal, regulatory domain of troponin C. Biochemistry **29**: 299-304.

LINSE, S., DRAKENBERG, T., and FORSEN, S. 1986. Mastoparan binding induces a structural change affecting both the N-terminal and C-terminal domains of calmodulin: A ^{113}Cd-NMR study. FEBS Lett. **199**: 28-32.

MACLACHLAN, L.K., REID, D.G., MITCHELL, R.C., SALTER, C.J., and SMITH, S.J. 1990. Binding of a calcium sensitizer, bepridil, to cardiac troponin C. A fluorescence stopped-flow kinetic, circular dichroism, and proton nuclear magnetic resonance study. J. Biol. Chem. **265**: 9764-9770.

MANT, C.T., BURKE, T.W.L., and HODGES, R.S. 1987. Optimization of peptide separations in reversed-phase HPLC: Isocratic versus gradient elution. Chromatographia **24**: 565-572.

MARINETTI, T.D., SNYDER, G.H., and SYKES, B.D. 1976. Nuclear magnetic resonance determination of intramolecular distances in bovine pancreatic trypsin inhibitor using nitrotyrosine chelation of lanthanides. Biochemistry **15**: 4600-4607.

MARSDEN, B.J., HODGES, R.S., and SYKES, B.D. 1988. ^{1}H NMR studies of synthetic peptide analogues of calcium-binding site III of rabbit skeletal troponin-C: Effect of the lanthanum affinity of the interchange of aspartic acid and asparagine residues at the metal ion coordinating positions. Biochemistry **27**: 4198-4206.

MARSDEN, B.J., HODGES, R.S., and SYKES, B.D. 1989. A ^{1}H NMR determination of the solution conformation of a synthetic peptide analogue of calcium-binding site III of rabbit skeletal troponin C. Biochemistry **28**: 8839-8847.

MARTIN, S.R., LINSE, S., BAYLEY, P.M., and FORSEN, S. 1986. Kinetics of cadmium and terbium dissociation from calmodulin and its tryptic fragments. Eur. J. Biochem. **161**: 595-601.

MATSUSHIMA, N., IZUMI, Y., MATSUO, T., YOSHINO, H., UEKI, T., and MIYAKE, Y. 1989. Binding of both Ca^{+2} and mastoparan to calmodulin induces a large change in the tertiary structure. J. Biochem. **105**: 883-887.

MEIBOOM, S., and GILL, D. 1958. Modified spin-echo method for measuring nuclear relaxation times. Rev. Sci. Instr. **29**: 688-691.

MOIR, A.J.G., WILKINSON, J.M., and PERRY, S.V. 1974. The phosphorylation sites of troponin I from cardiac muscle. FEBS Lett. **42**: 253-257.

NOZAKI, S., KOBAYASHI, K., KATAYAMA, E., and MURAMATSU, I. 1980. Synthetic studies on troponin I active site preparation of a pentadecapeptide with inhibitory activity toward troponin C. Chem. Lett. **3**: 345-348.

O'NEIL, K.T., and DEGRADO, W.F. 1989. The interaction of calmodulin with fluorescent and photoreactive model peptides. Evidence for a short interdomain separation. Proteins **6**: 284-293.

PARKER, J.M.R., MANT, C.T., and HODGES, R.S. 1987. A practical approach to the preparative purification of peptides using analytical instrumentation with analytical and semipreparative columns. Chromatographia **24**: 832-838.

PERRY, S.V., COLE, H., HEAD, J.F., and WILSON, F.J. 1972. Localization and mode of action of the inhibitory protein component of the troponin complex. Cold Spring Harbor Symp. Quant. Biol. **37**: 251-262.

PERSECHINI, A., and KRETSINGER, R.H. 1988. The central helix of calmodulin functions as a flexible tether. J. Biol. Chem. **263**: 12175-12178.

PERSECHINI, A., BLUMENTHAL, D.K., JARRETT, H.W., KLEE, C.B., HARDY, D.O., and KRETSINGER, R.H. 1989. The effects of deletions in the central helix of calmodulin on enzyme activation and peptide binding. J. Biol. Chem. **264**: 8052-8058.

POTTER, J.D., and GERGELY, J. 1974. Troponin, tropomyosin and actin interactions in the Ca^{+2} regulation of muscle contraction. Biochemistry **13**: 2697-2703.

POTTER, J.D., and GERGELY, J. 1975. The calcium and magnesium binding sites on troponin and their role in the regulation of myofibrillar adenosine triphosphatase. J. Biol. Chem. **250**: 4628-4633.

PUTKEY, J.A., ONO, T., VAN BERKUM, M.F.A., and MEANS, A.R. 1988. Functional significance of the central helix of calmodulin. J. Biol. Chem. **263**: 11242-11249.

REID, D.G., MACLACHLAN, L.K., GAJJAR, K., VOYLE, M., KING, R.J., and ENGLAND, P.J. 1990. A proton nuclear magnetic resonance and molecular modeling study of calmidazolium (R24571) binding to calmodulin and skeletal muscle troponin C. J. Biol. Chem. **265**: 9744-9753.

RHEE, M-J., SUDNICK, D.R., ARKLE, V.K., and HORROCKS, W.D., Jr. 1981. Lanthanide ion luminescence probes. Characterization of metal ion binding sites and intermetal energy transfer distance measurements in calcium-binding proteins. 1. parvalbumin. Biochemistry **20**: 3328-3334.

ROBERTSON, S.P., JOHNSON, J.D., and POTTER, J.D. 1981. The time-course of Ca^{+2} exchange with calmodulin, troponin, parvalbumin, and myosin in response to transient increases in Ca^{+2}. Biophys. J. **34**: 559-569.

SCHAUB, M.C., and PERRY, S.V. 1969. The relaxing protein system of striated muscle. Biochem J. **115**: 993-1004.

SEEHOLZER, S.H., COHN, M., PUTKEY, J.A., MEANS, A.R., and CRESI, H.L. 1986. NMR studies of a complex of deuterated calmodulin with melittin. Proc. Natl. Acad. Sci. USA **83**: 3634-3638.

SEEHOLZER, S.H., and WAND, J.A. 1989. Structural characterization of the interactions between calmodulin and skeletal muscle myosin light chain kinase: Effect of peptide(576-594)G binding on the Ca^{2+}-binding domains. Biochemistry **28**: 4011-4020.

SHENG, Z., FRANCOIS, J-M., HITCHCOCK-DEGREGORI, S.E., and POTTER, J.D. 1991. Effects of mutations in the central helix of troponin C on its biological activity. J. Biol. Chem. **266**: 5711-5715.

SOWADSKI, J., CORNICK, G., and KRETSINGER, R.H. 1978. Terbium replacement of calcium in parvalbumins. J. Mol. Biol. **124**: 123-132.

STEINER, R.F., and NORRIS, L. 1987. Interaction of melittin with troponin C. Arch. of Biochem. and Biophys. **254**: 342-352.

STRYNADKA, N.C.J., and JAMES, M.N.G. 1990. Model for the interaction of amphiphilic helices with troponin C and calmodulin. Proteins **7**: 234-248.

SUNDARALINGAM, M., BERGSTROM, R., STRASBURG, G., RAO, S.T., GREASER, M., and WANG, B.C. 1985a. Molecular structure of troponin C from chicken skeletal muscle at 3 Å resolution. Science **227**: 945-948.

SUNDARALINGAM, M., DRENDEL, W., and GREASER, M. 1985b. Stabilization of the long central helix of troponin C by intrahelical salt bridges between charged amino acid side chains. Proc. Natl. Acad. Sci. USA **82**: 7944-7947.

SYSKA, H., WILKINSON, J.M., GRAND, R.J.A., and PERRY, S.V., 1976. The relationship between biological activity and primary structure of troponin I from white skeletal muscle of the rabbit. Biochem. J. **153**: 375-387.

TALBOT, J.A., and HODGES, R.S. 1979. Synthesis and biological activity of an icosapeptide analog of the actomyosin ATPase inhibitory region of troponin I. J. Biol. Chem. **254**: 3720-3723.

TALBOT, J.A., and HODGES, R.S. 1981. Synthetic studies on the inhibitory region of rabbit skeletal troponin I. Relationship of amino acid sequence to biological activity. J. Biol. Chem. **256**: 2798-3802.

TAO, T., GOWELL, E., STRASBURG, G.M., GERGELY, J., and LEAVIS, P.L. 1989. Ca^{+2} dependence of the distance between Cys-98 of troponin C and Cys-133 of troponin I in the ternary troponin complex. Resonance energy transfer measurements. Biochemistry **28**: 5902-5908.

VALENTINI, M.A., and WRIGHT, J.C. 1985. Site-selective laser spectroscopy of lanthanide-binding sites in calmodulin. Anal. Biochem. **150**: 47-47.

VANAMAN, T.C., SHARIEL, F., and WATTERSON, D.M. 1977. Structural homology between brain modulator protein and muscle TnCs. In *Calcium-Binding Proteins and Calcium Function* (Wasserman, R.H., *et al.*, Eds.), pp 107-116, Elsevier, Amsterdam.

VAN BERKUM, M.F.A., GEORGE, S.E., and MEANS, A.R. 1990. Calmodulin activation of target enzymes. Consequences of deletions in the central helix. J. Biol. Chem. **265**: 3750-3756.

VAN EYK, J.E., and HODGES, R.S. 1988. The biological importance of each amino acid residue of the troponin I inhibitory sequence 104-115 in the interaction with troponin C and tropomyosin-actin. J. Biol. Chem. **263**: 1726-1732.

VAN EYK, J.E., KAY, C.M., and HODGES, R.S. 1991. A comparative study of the interactions of synthetic peptides of the skeletal and cardiac troponin I inhibitory region with skeletal and cardiac troponin C. Biochemistry, in press

WALLACE, R.W., TALLANT, E.A., DOCKTER, M.E., and CHEUNG, W.Y. 1982. Calcium binding domains of calmodulin. Sequence of fill as determined with terbium luminescence. J. Biol. Chem. **257**: 1845-1854.

WANG, C-L., LEAVIS, P.C., HORROCKS, W.D. Jr., and GERGELY, J. 1981. Binding of lanthanide ions to troponin C. Biochemistry **20**: 2439-2449.

WANG, C-L., TAO, T., and GERGELY, J. 1982a. The distance between the high affinity sites of troponin-C measured by interlanthanide ion energy transfer. J. Biol. Chem. **257**: 8372-8375.

WANG, C-L., AQUARON, R.R., LEAVIS, P.C., and GERGELY, J. 1982b. Metal binding properties of calmodulin. Eur. J. Biochem. **124**: 7-12.

WANG, C-L., LEAVIS, P.C., and GERGELY, J. 1984. Kinetic studies show that Ca^{2+} and Tb^{3+} have different binding preferences toward the four Ca^{2+}-binding sites of calmodulin. Biochemistry **23**: 6410-6415.

WANG, Z., SARKAR, S., GERGELY, J., and TAO, T. 1990. Ca^{+2}-dependent interactions between the c-helix of troponin C and troponin I. J. Biol. Chem. **265**: 4953-4957

WEEKS, R.A, and PERRY, S.V. 1978. Characterization of a region of the primary sequence of troponin C involved in calcium ion-dependent interaction with troponin I. Biochem. J. **173**: 449-457.

WILLIAMS, T.C., CORSON, D.C., and SYKES, B.D. 1984. Calcium-binding proteins: Calcium(II)-Lanthanide(III) exchange in carp parvalbumin. J. Am. Chem. Soc. **106**: 5698-5702.

WUTHRICH, K., BILLETER, M., and BRAUN, W. 1983. Pseudo-structures for the 20 common amino acids for use in studies of protein conformations by measurements of intramolecular proton-proton distance constraints with nuclear magnetic resonance. J. Mol. Biol. **169**: 949-961.

YAZAWA, M., IKURA, M., HIKICHI, K., YING, L., and YAGI, K. 1987. Communication between two globular domains of calmodulin in the presence of mastoparan or caldesmon fragment. J. Biol. Chem. **262**: 10951-10954.

YAZAWA, M., MATSUZAWA, F., and YAGI, K. 1990. Inter-domain interaction and the structural flexibility of calmodulin in the connecting region of the terminal two domains. J. Biochem. **107**: 287-291.

ZOT, A.S., and POTTER, J.D. 1987. Structural aspects of troponin-tropomyosin regulation of skeletal muscle contraction. Annu. Rev. Biophys. Chem. **16**: 535-559.

Chapter VIII

Interaction of Troponin I and Troponin C : Use of the Two-Dimensional Transferred Nuclear Overhauser Effect to Determine the Structure of a Glycine-110 Inhibitory Troponin I Peptide Analog When Bound to Cardiac Troponin C

A. Introduction

Contraction of vertebrate skeletal and cardiac muscle is regulated by Ca(II) and requires the regulatory proteins troponin and tropomyosin (Ebashi and Endo, 1968). Troponin is a complex of three different protein subunits: Troponin C (TnC) which binds Ca(II), TnI which binds actin and inhibits actomyosin ATPase, and TnT which binds to tropomyosin. The Ca(II)-dependent interaction between TnC and TnI is one of the key processes in the activation of contraction in skeletal muscle (for recent reviews, see Zot and Potter, 1987, and Leavis and Gergely, 1984). TnI inhibits the Mg(II)-ATPase activity of actomyosin (Hartshorne and Mueller, 1968; Schaub and Perry, 1969; Greaser and Gergely, 1971; Perry *et al.*, 1972) and binds both to actin and tropomyosin-actin (Potter and Gergely, 1974; Hitchcock, 1975). The inhibition of actomyosin ATPase is neutralized when Ca(II)-saturated TnC forms a 1:1 complex with TnI (Perry *et al.*, 1972; Weeks and Perry, 1978; Chong *et al.*, 1983; Cachia *et al.*, 1986; Van Eyk and Hodges, 1988). The region of TnI which is responsible for its inhibitory activity is the same region which is involved in a Ca(II)-sensitive 'switch' between binding to actin-tropomyosin and binding to TnC. In the absence of Ca(II), the inhibitory region of TnI is bound to the surface of actin-tropomyosin, inhibiting the actomyosin ATPase activity and contraction. In the presence of Ca(II), this region of TnI is thought to bind to TnC (Cachia *et al.*, 1985).

TnC belongs to the helix-loop-helix (HLH) Ca(II)-binding protein family (Kretsinger, 1980). The x-ray structures of avian skeletal TnC (Sundaralingam *et al.*, 1985; Herzberg and James, 1985) have been solved and reveal a dumbbell-shaped molecule with N-terminal and C-terminal globular domains joined by a long helical linker. Each major domain contains two HLH Ca(II) binding sites based on the EF hand motif (Kretsinger and Nockolds, 1973; Collins *et al.*, 1973; Vanaman *et al.*, 1977). The N- and C-terminal globular domains of TnC and the homologous Ca(II)-binding molecule, calmodulin (CaM), have large hydrophobic patches (Kretsinger *et al.*, 1986; Babu *et al.*, 1988) flanked by regions of negative electrostatic potential, optimally designed as binding sites for basic, amphiphilic helices. There is evidence to suggest that Ca(II) binding to these proteins leads to an increased exposure of these hydrophobic surfaces which could become the sites for the interaction of target molecules (Laporte *et al.*, 1980; Gariepy and Hodges, 1983; Cachia *et al.*, 1985).

The physiological differences in the action of skeletal and cardiac muscle may be explained by differences in the amino acid sequences of skeletal and cardiac TnI and TnC, in particular at the binding interfaces between these highly conserved proteins. These differences could alter the TnC-TnI interaction and hence affect muscle regulation. Skeletal and cardiac TnC have 65% amino acid homology with the majority of substitutions occurring in the first 40 residues. Cardiac TnC has 8 amino acid differences located in Ca(II) binding site I (a result of a glycine insertion) which results in site I being nonfunctional. Hence, skeletal TnC binds four Ca(II) ions (two at the high affinity sites (III and IV) and two at the low affinity sites (I and II)), while cardiac TnC binds three Ca(II) ions (two at the high affinity sites (III and IV) and one at the single low affinity site (site II)). The high affinity sites III and IV are located in the C-terminal half of TnC and bind Ca(II) with association constants of 2 x 10^7 and 3 x 10^8 M for skeletal TnC and cardiac TnC, respectively (Potter and Gergely, 1975; Johnson and Potter, 1978; Holroyde *et al.*, 1980). Sites I and II in the N-terminal half of the molecule bind Ca(II) with association constants of 2 x 10^5 and 2 x 10^6 M for skeletal TnC and cardiac TnC, respectively. Although the low affinity sites of skeletal and cardiac TnC are the regulatory sites which trigger muscle contraction, the high affinity sites may also be involved in the regulatory process. Skeletal TnI is a more effective inhibitor of actomyosin ATPase than cardiac TnI in both cardiac and skeletal ATPase assays (Hincke *et al.*, 1977; Talbot and Hodges, 1981a). In addition, cardiac TnC is less effective than skeletal TnC at releasing the inhibition induced by either cardiac or skeletal TnI.

Talbot and Hodges (1981b) showed, using synthetic peptides, that residues 104-115 of skeletal TnI comprise the minimum sequence necessary for inhibition of actomyosin ATPase activity. The synthetic peptide TnI(104-115) possesses tropomyosin specificity (Talbot and Hodges, 1979) and TnC binding capability (Cachia *et al.*, 1983, 1985; Van Eyk and Hodges, 1988; Van Eyk *et al.*, 1991), which results in the release of ATPase inhibition (Cachia *et al.*, 1986). Thus, it is would appear that residues 104-115 comprise the inhibitory site of skeletal TnI and binding of this region to Ca(II)-saturated TnC leads to relief of inhibition of actomyosin ATPase, and ultimately to muscle contraction.

The cardiac(137-148) and skeletal(104-115) TnI inhibitory regions have identical sequences except for a single amino acid substitution of a proline at position 110 in the skeletal sequence for a threonine at position 143 in the cardiac sequence. The skeletal and cardiac TnI inhibitory peptides inhibit force development in skeletal and cardiac muscle fibres, but the cardiac peptide is less efficient, requiring a 2 to 3 fold higher concentration to reach maximum inhibition (Ruegg *et al.*, 1989).

The importance of the single amino acid substitution at position 110 in the TnI peptide is demonstrated by the difference in the biological action of an analog in which a glycine is substituted for the proline at position 110 of the skeletal TnI sequence. The G110-TnI peptide analog inhibits actomyosin ATPase activity (Van Eyk and Hodges, 1988), but is considerably less effective than the skeletal TnI peptide. Unlike the skeletal

TnI peptide, the G110-TnI peptide does not alter force development in skinned muscle fibres (Ruegg *et al.*, 1989, 1991). The difference in the action of the G110-TnI peptide compared to the skeletal TnI peptide may be attributed to the difference in the interaction of the G110-TnI peptide with TnC. Even though this analog binds to TnC almost as well as the native skeletal and cardiac peptides (Van Eyk *et al.*, 1991), the G110-TnI peptide analog has a very different effect on the Ca(II) binding affinity. The skeletal and cardiac TnI peptides alter the low affinity Ca(II) binding sites of TnC, while G110-TnI peptide analog alters the Ca(II) binding at the high affinity sites III and IV (Van Eyk *et al.*, 1991). This indicates that the biological activity of the TnI peptides is very dependent on which amino acid is present at position 110 of the skeletal sequence.

Previous studies have shown that the native skeletal TnI protein increases the Ca(II) affinity of TnC (Potter *et al.*, 1976; Wang and Cheung, 1985). It has also been shown that the skeletal TnI peptide and other TnC-binding molecules, like mastoparan and trifluoperazine (TFP), increase the Ca(II) binding affinity of skeletal TnC (Van Eyk and Hodges, 1987; Ruegg *et al.*, 1989). However, in these studies it was not possible to determine whether these TnC-binding molecules were affecting the low or high affinity sites.

Van Eyk *et al.* (1991) studied the Ca(II)-induced biphasic increases in α-helical content ($[\theta]_{222}$ measured by circular dichroism) and tyrosine fluorescence of TnC to determine the Ca(II) binding constants for the high and low affinity Ca(II) binding sites of TnC in the presence and absence of TnI peptide. They showed that both the skeletal and cardiac TnI peptides affected the low affinity sites of TnC, while the G110-TnI peptide analog affected only the high affinity sites. Although the magnitude and direction of the pCa shifts for the three peptides differed depending on whether the peptides were bound to skeletal or cardiac TnC, the skeletal and cardiac TnI peptides always altered the Ca(II) affinity of the low affinity sites while the G110-TnI peptide analog always altered the Ca(II) affinity of the high affinity sites. Thus, although the conformational change differed depending on the species of TnC, the Ca(II) binding site (low or high affinity) affected was not dependent on the TnC species, but rather on which peptide was used. Thus, the difference in primary sequence of skeletal and cardiac TnC is not as important as the sequence difference in the TnI inhibitory region, especially at position 110 in the skeletal sequence. This could be a function of the effect an amino acid substitution at this position has on the conformation adopted by the skeletal versus cardiac TnI peptide when these peptides are bound to TnC. A different bound conformation of the TnI peptide could alter the secondary structure of TnC at the binding interface, leading to a different biological response to Ca(II).

In the present chapter, we use two-dimensional NMR techniques to determine the structure of the G110-TnI peptide analog, Nα-acetyl-G110-TnI(104-115) amide, bound to Ca(II)-saturated bovine cardiac TnC. In Chapter V, we determined the structure of the skeletal TnI peptide, Nα-acetyl-TnI(104-115) amide, bound to Ca(II)-saturated skeletal troponin C (Campbell and Sykes, 1991a; Chapter V). A comparison of these two structures should reveal the effect an amino acid substitution at the central residue of the inhibitory region of TnI has on the differences in the mode of Ca(II) mediated relief of inhibition of actomyosin ATPase in the skeletal versus cardiac systems.

B. Theory

Conformational changes in the peptide induced by the formation of the G110-TnI peptide-TnC.Ca(II)$_4$ complex were followed by the study of the transferred nuclear Overhauser effect (TRNOE). The TRNOE is the extension of the NOE, which has been widely used to determine protein structures in solution (Wuthrich, 1986), and provides one of the best techniques for the determination of the structure of bound ligands (Clore and Gronenborn, 1982b, 1984a, 1984b, 1984c, 1986; Gronenborn and Clore, 1982; Levy *et al.*, 1983, 1989; Banerjee *et al.*, 1985; Ehrlich and Colman, 1985; Glasel and Borer, 1986; Andersen *et al.*, 1987; Meyer *et al.*, 1988; Anglister *et al.*, 1989; Glasel, 1989; Ni *et al.*, 1989a, 1989b, 1989c, 1990; Anglister and Zilber, 1990; Bevilacqua *et al.*, 1990; Milon *et al.*, 1990). The intramolecular TRNOE allows the transfer of information concerning cross-relaxation between two nuclei in the bound ligand to the free ligand resonances via chemical exchange. In the unbound form, the ligand is generally characterized by short correlation times ($\tau_c < 10^{-10}$ s) and thus may be described as being either in the extreme narrowing limit ($\omega\tau_c << 1$), where the NOEs are small and positive, or at the boundary of the extreme narrowing limit ($\omega\tau_c \cong 1$) where the NOEs approach zero. When bound to the protein, the ligand is characterized by the long correlation time of the protein ($\tau_c > 10^{-8}$ s), and thus may be described as being in the spin diffusion limit ($\omega\tau_c >> 1$), where the NOEs are large and negative. In the presence of chemical exchange of the ligand between its free and bound states, negative NOEs conveying conformational information of the bound ligand are 'transferred' to the free ligand resonances where they are more easily measured because these resonances are much narrower.

Consider the equilibrium between the free and bound ligand

$$\text{G110-TnI(104-115)} + \text{TnC} \underset{k_{-1}}{\overset{k_1[\text{TnC}]}{\rightleftharpoons}} \text{G110-TnI(104-115).TnC} \qquad [1]$$

Given fast exchange on the NMR timescale ($[4\pi^2(\delta_F-\delta_B)^2\tau_cB^2]$, $[\tau_cB/T_2B] << 1$, where τ_cB is the correlation time of the bound peptide, $|\delta_F-\delta_B|$ is the change in chemical shift upon binding, and T_2B is the spin-spin relaxation time in the bound environment), the observed chemical shifts, δ_{obs}, and linewidths, Δv_{obs}, are dominated by the free ligand population when $p_F >> p_B$ (where p_B is the fraction of bound ligand and p_F is the fraction of free ligand)

$$\delta_{obs} = p_F\, \delta_F + p_B\, \delta_B \qquad [2]$$

$$\Delta v_{obs} = p_F\, \Delta v_F + p_B\, \Delta v_B \qquad [3]$$

Conversely, the TRNOESY cross-peak intensities, a_{ij}, are dominated by the bound ligand, since the cross-relaxation rate between protons in the bound ligand is so much faster than it is in the free ligand, viz. $W_{ij}B >> W_{ij}F$

$$a_{ij}(\tau_m) \cong - [\, p_B\, W_{ij}B + p_F\, W_{ij}F\,]\, \tau_m \;\cong - [\, p_B\, W_{ij}B\,]\, \tau_m \qquad [4]$$

This is the result presented earlier by Clore *et al.* (Clore and Gronenborn, 1982a, 1983; Gronenborn and Clore, 1985) which is valid only in the limit of short τ_m. A full theoretical evaluation of the TRNOE has been presented elsewhere (Campbell and Sykes, 1991b; Chapter II) based upon a full relaxation matrix approach (Landy and Rao, 1989). The $W_{ij}B$s, once obtained, yield interproton distances in the bound peptide

$$W_{ij}B \propto \langle\, 1/r_{ij}B^{\,6} \rangle \qquad [5]$$

From Eqns. 4 and 5, it can be seen that for any two pairs of bound proton resonances, $r_{ij}B$ will be simply given by Eqn. 6, using a suitable reference distance

$$r_{ij}B = \{\, (\, W_{REF} / W_{ij}B\,) \times\, r_{REF}^{\;6}\, \}^{\,1/6} \qquad [6]$$

The experimentally derived $r_{ij}B$ values may be used as distance restraints in energy minimization and molecular dynamics programs to generate a bound TnI peptide conformation.

We have used Eqns. 4-6 as a starting point for determining $r_{ij}B$ values in the bound G110-TnI peptide. However, the generation of a correct bound peptide conformation requires an analysis of the effects of spin-diffusion experienced by the protons on the TnI peptide when it is bound to TnC. For the purposes of this chapter, we have neglected the effects of spin-diffusion in the generation of the G110-TnI peptide conformation when bound to cardiac TnC. In our previous determination of the structure of the skeletal TnI peptide bound to skeletal TnC, we made a variety of 'adjustments' to the $r_{ij}B$ values, in lieu of a full relaxation treatment. These adjustments corrected for under- and over-determination of the $r_{ij}B$ values. In anticipation of a full refinement of both the G110 and skeletal TnI peptide structures using a full iterative relaxation matrix analysis (Chapter X), we have opted to neglect these 'adjustments' in the determination of the bound G110-TnI peptide structure, and have chosen to use the unadjusted $r_{ij}B$ values calculated from the TRNOE intensity measurements as input for the molecular mechanics computer simulations.

C. Materials and Methods

1. Sample Preparation

a. Materials. Refer to Materials and Methods section in Chapter V.

b. Amino Acid Analysis. The quantities of Nα-acetyl-G110-TnI(104-115) amide and bovine cardiac TnC used were determined from amino acid analysis after hydrolysis in 100-200 µl of 6 N HCl in evacuated sealed tubes for 24 h at 110°C. The mean of the molar ratios of all accurately measurable amino acids in the acid hydrolysate was used to calculate the concentration of peptide or protein.

c. Peptide Synthesis and Purification. Nα-acetyl-G110-TnI(104-115) amide was synthesized and purified using the standard protocol outlined in the Materials and Methods section in Chapter V (Erickson and Merrifield, 1976; Talbot and Hodges, 1981; Mant *et al.*, 1987; Parker *et al.*, 1987; Hodges *et al.*, 1988).

d. Preparation of TnC. Troponin was isolated from an acetone powder of bovine brain tissue by the method of Strapans *et al.* (1972). A final yield of approx. 100 mg of purified TnC powder was obtained, which was found to be homogenous when examined by SDS-Page.

e. Preparation of Desalted, Apo TnC. EDTA-free, apo TnC was prepared using the protocol outlined in the Materials and Methods section in Chapter IV. The TnC protein was judged to be apo by UV spectrophotometry and ^{1}H NMR.

f. Preparation of G110-TnI Peptide ^{1}H NMR samples. The sample used in all ^{1}H NMR experiments was 7 mM Nα-acetyl-G110-TnI(104-115) amide, dissolved in 650 μl of a 80%H_20/20%D_20 solvent mixture at a pH in the range of 6.2 to 6.5 and a salt concentration of 50 mM KCl. Bovine cardiac TnC.Ca(II)$_4$ was titrated into the sample to a final concentration of approximately 0.7 mM TnC:4 mM $CaCl_2$ for 0.1 molar equivalents of TnC.Ca(II)$_4$ to G110-TnI peptide. 0.1 mM DSS was added to the sample to act as a chemical shift standard.

2. Nuclear Magnetic Resonance Spectroscopy

All ^{1}H NMR spectra were obtained at 500 MHz on a Varian VXR-500 NMR spectrometer. Two-dimensional experiments were taken with 2048 data points along t_2 and with 256 t_1 increments. Spectral widths of 5000-6000 Hz and relaxation delay times of 1.6-2.3 s were employed. Streaking along t_1 was reduced by multiplying the first domain time point by a factor optimized near 0.5 (Otting *et al.*, 1986). DQFCOSY (Piatini *et al.*, 1982; Rance *et al.*, 1983) and TRNOESY data sets were acquired in the phase-sensitive method of States *et al.* (1982). The appropriate phase cycling was used for quadrature detection and to eliminate axial peaks, and in the case of TRNOESY spectra, single and multiple quantum coherences. For all data sets, the water resonance was suppressed by presaturation. The decoupler offset was set equal to the transmitter offset to prevent phase distortions around the water peak due to imperfect cancellation of the dispersive component of residual water magnetization (Hoult, 1976). Average mixing times, τ_m, of 150 and 500 ms were used for the TRNOESY spectra. A random delay of ± 10 ms was incorporated to suppress zero quantum coherences. Spectra acquired at 500 ms were used for assignment purposes, whereas spectra acquired at 150 ms were used for cross-peak intensity measurement, leading to structure determination.

3. Transformation of ^{1}H NMR TRNOESY Peak Intensity to Distance Restraints

^{1}H NMR TRNOESY intensities were quantified for a data set acquired at τ_m = 150 ms and 0.1 molar equivalents TnC.Ca(II)$_4$ to G110-TnI peptide. Volume integrals for each cross-peak were measured and nominally empty areas perpendicularly adjacent to each cross-peak were examined for baseline correction. The TRNOE cross-peak intensities were transformed to distance restraints using a group of stereospecifically assigned reference proton pairs which included F106NH-βCH(4.0Å), F106NH-βCH'(3.4Å), P109βCH-δCH(4.1Å), P109βCH-δCH'(3.9Å), P109βCH'-δCH(3.9Å), and P109βCH'-δCH'(3.0Å). These proton pairs were chosen because they displayed linear TRNOE build-up of magnetization for τ_m = 150 ms and 0.1 molar equivalents of TnC.Ca(II)$_4$, and were well separated from overlapping cross-peaks in the TRNOESY spectrum. The reference distances for the F106 reference proton pairs corresponded to the distances found for an α-helical G110-TnI peptide. However, these distances were not found to change more than 10% when compared to those found for the G110-TnI peptide in a β-sheet conformation, and therefore were deemed to be independent of secondary conformation. All other reference distances involved distances between reference proton pairs in the P109 five-membered ring.

TRNOE intensities were normalized for the contribution of more than two protons to the cross-peak before they were transformed into distance restraints. We divided the TRNOE cross-peak intensities by the normalization factor $(2N_aN_b)/(N_a+N_b)$ where Na was the number of protons under diagonal peak *a*, and Nb was the number of protons under diagonal peak *b* (Macura and Ernst, 1980; Williamson and Neuhaus, 1987). Cross-peaks connecting exchangeable proton resonances were also corrected for loss of intensity due to exchange or saturation transfer from the decoupled water peak. The exchangeable proton peak intensities were integrated in a one-dimensional spectrum obtained under the same experimental conditions as the two-dimensional spectrum (same temperature, pH, sample concentration and spectrometer settings), and the intensity of these peaks were normalized against the integrated intensity of the V114αCH peak (see Tables VIII-1A and VIII-1B in Appendix).

Table VIII-2 in the Appendix gives the TRNOE data set measured from the TRNOESY experiment acquired at τ_m = 150 ms and 0.1 molar equivalents TnC.Ca(II)$_4$ to G110-TnI peptide. Included in Table VIII-2 are the measured TRNOE intensities, the corrected and normalized TRNOE intensities, and the r_{ij}s calculated from these corrected and normalized values using the group of stereospecifically assigned reference proton pairs discussed above.

Initial error limits (±β) were used to set upper (r_{ij}^U) and lower (r_{ij}^L) distance bounds on the calculated distance restraints (r_{ij}), and were incorporated in the following manner: for $r_{ij} < 3.0$Å, $\beta = \pm 0.2$ Å; for 3.0 Å $\leq r_{ij} < 4.0$Å, $\beta = \pm 0.3$ Å; for 4.0 Å $\leq r_{ij} <$ 5.0Å, $\beta = \pm 0.5$ Å; and for $r_{ij} \geq 5.0$ Å, $\beta = \pm 1.0$ Å. Thus, for $r_{ij} = 3.5$ Å, we set r_{ij}^U equal to 3.8 Å, and r_{ij}^L equal to 3.3 Å. Within the distance range of $r_{ij} \pm \beta$, the distance restraint term used in the MD and EM simulations contributed no energy penalty to the overall potential energy of the system. Table VIII-3 in the Appendix summarizes the distance restraints used in the MD simulations. Included in Table VIII-3 are the r_{ij}s calculated from the corrected and normalized TRNOE cross-peak intensities, the incorporated error limits (±β), and the pseudoatom adjustments in r_{ij}^U.

4. Dihedral Angle Restraints and Supplemental Distance Restraints

A curve fitting program was used to measure dihedral coupling constants in one-dimensional ^{1}H NMR spectra of the G110-TnI peptide in the presence of 0.000, 0.002, 0.040, 0.060, 0.080, and 0.10 molar equivalents of TnC.Ca(II)$_4$. Practically, linebroadening and spectral overlap prevented measurement of $^3J\alpha$CH-NH coupling constants for the 100% bound peptide in a 1.0 molar equivalent TnC.Ca(II)$_4$ to G110-TnI peptide sample. Therefore, observed coupling constants were measured at low concentrations of protein and extrapolated to 100% bound peptide (see Table VIII-4 in the Appendix). For $^3J\alpha$CH-NH < 6.0 Hz, Φ is expected to be in the range $-85° \leq \Phi \leq -40°$ (Pardi *et al.*, 1984; Wagner *et al.*, 1987; Driscoll *et al.*, 1989). For $^3J\alpha$CH-NH > 8.0 Hz, Φ is expected to be in the range $-160° \leq \Phi \leq -80°$. All $^3J\alpha$CH-NH values in the G110-TnI peptide were found to be less than 6.0 Hz when extrapolated to 100% bound peptide[1], therefore all Φ dihedral angles in the peptide were restrained to $-85° \leq \Phi \leq -40°$. In addition, all peptide bonds, including X-proline, were restrained to $-175° \leq \omega \leq -185°$ to maintain trans configurations. We found no evidence for cis-trans X-proline peptide bond isomerization from ^{1}H spectra; all X-proline peptide bonds were deemed to be trans from the pattern of ^{1}H TRNOEs.

Supplementary distance restraints were obtained from intra-peptide hydrogen bonds identified by measuring temperature coefficients ($\Delta\delta/\Delta T$) of the exchangeable backbone amide protons of the G110-TnI peptide as a function of molar equivalents of TnC.Ca(II)$_4$. The temperature dependence of amide proton resonances, in conjunction with a knowledge of secondary structure, was used to identify backbone hydrogen bonding. For a random coil peptide in H_2O, the temperature coefficients of amide proton resonances are expected to be $-6 \leq \Delta\delta/\Delta T \leq -10$ ppb, whereas for amides protected from exchange with the solvent, these values are expected to decrease to $\Delta\delta/\Delta T \leq -4$ ppb (Deslauriers and Smith, 1980). Temperature coefficients were measured for 0.0 and 0.1 molar equivalents TnC.Ca(II)$_4$ to

---

[1] The determination of $^3J\alpha$CH-NH for 100% bound peptide is not intended to be rigorous and quantitative, therefore an error analysis was not performed. Qualitatively, the general trend of decreasing values of $^3J\alpha$CH-NH with bound peptide clearly points to small $^3J\alpha$CH-NH values for the bound peptide.

G110-TnI peptide (see Figures VIII-1A and VIII-1B, Tables VIII-5A andVIII-5B and Table VIII-6 in the Appendix). Again, linebroadening and spectral overlap prevented measurement of $\Delta\delta/\Delta T$ for the 100% bound peptide in a 1.0 molar equivalent protein to peptide sample, therefore $\Delta\delta/\Delta T$ values were measured for relatively low concentrations of protein and extrapolated to 100% bound peptide[2].

5. Stereospecific Assignments from ^1H NMR

Stereospecific assignments of prochiral protons were available for the βCH and βCH' protons of F106 and P109, and the δCH and δCH' protons of P109. Stereospecific assignments were possible for these prochiral proton pairs since they exhibited sufficiently different chemical shifts. The other prochiral protons and methyl groups on the G110-TnI peptide were designated as pseudoatoms (Wuthrich *et al.*, 1983), and the appropriate intraresidue and long-range corrections were made on the upper bound of the distance restraints for these pseudoatoms. Unambigious stereospecific assignments may result for prochiral groups if there is a sufficiently large set of NOE, Van der Waals, and covalent bond constraints as input for the structure calculation. Here, we generated a roughly determined structure using only pseudoatoms in the distance restraint file for the MD simulations, and then modified the distance restraint file to include stereospecific distance restraints consistent with the stereochemistry of this roughly determined structure. A more precisely determined structure was then generated using this modified distance restraint file as input for a second round of MD simulations. The stereospecific assignments for the phenylalanine and proline residues were in agreement with the relative strength of the $d_{\alpha\beta}$ and $d_{N\beta}$ NOE cross-peaks, and were consistent with the stereochemistry of the bound structure. The second round of MD simulations employing the stereospecific assignments are described in the following section.

6. Restrained Molecular Dynamics Calculations

EM and MD calculations were carried out with the GROMOS program (de Vlieg *et al.*, 1986) and force field, which consisted of the usual terms for bonds, bond-angles, sinusoidal dihedral torsion, non-bonded interactions (Van der Waals and electrostatics), and harmonic terms to maintain proper planar or tetrahedral geometries. Two extra terms were added representing distance and dihedral restraints. The distance restraint square well potential, E_{DIS}, was defined by two functions, a biharmonic potential for $(r_{ij}^U - r_{ij})$ and $(r_{ij}^L - r_{ij}) < 5Å$, and a linear potential for $(r_{ij}^U - r_{ij})$ and $(r_{ij}^L - r_{ij}) \geq 5Å$:

---

[2] Again, the determination of $\Delta\delta/\Delta T$ for 100% bound peptide is not intended to be rigorous and quantitative, therefore an error analysis was not performed.

$$\begin{aligned} E_{DIS} &= 0.5\, C_{DIS}\, (r_{ij}^U - r_{ij})^2 && \text{if } r_{ij} > r_{ij}^U;\ |r_{ij}^U - r_{ij}| < 5Å \\ &= 0.5\, C_{DIS}\, (r_{ij}^L - r_{ij})^2 && \text{if } r_{ij} < r_{ij}^L;\ |r_{ij}^L - r_{ij}| < 5Å \end{aligned} \qquad [7a]$$

$$\begin{aligned} E_{DIS} &= 0.5\, C_{DIS}\, (r_{ij}^U - r_{ij}) && \text{if } r_{ij} > r_{ij}^U;\ |r_{ij}^U - r_{ij}| \geq 5Å \\ &= 0.5\, C_{DIS}\, (r_{ij}^L - r_{ij}) && \text{if } r_{ij} < r_{ij}^L;\ |r_{ij}^L - r_{ij}| \geq 5Å \end{aligned} \qquad [7b]$$

where C_{DIS} was a force constant. The dihedral angle restraint, E_{DIH}, was then represented by the biharmonic potential :

$$\begin{aligned} E_{DIH} &= 0.5\, C_{DLR}\, (\Phi_k^U - \Phi_k)^2 && \text{if } \Phi_k > \Phi_k^U \\ &= 0.5\, C_{DLR}\, (\Phi_k^L - \Phi_k)^2 && \text{if } \Phi_k < \Phi_k^L \end{aligned} \qquad [8]$$

where Φ_k^U and Φ_k^L were upper and lower allowed limits of the torsion angle, Φ_k was the calculated angle, and C_{DLR} was the force constant.

Starting models were first subjected to 500 steps of conjugate gradient EM. Then the starting structures were subjected to 12 ps of MD where values of the distance restraint force constant were increased from 400 to 4000 kJ mol^{-1} nm^{-2} and the dihedral restraint force constant from 200 to 2000 kJ mol^{-1} rad^{-2}. At 2 ps intervals, the force constants were increased and the velocities (taken from a Maxwellian distribution at 300 K) were re-initialized. During these re-initialization intervals, the structures were cooled with 500 steps of intervening EM. Newton's equations of motion were integrated with a time step of 2 fs, with all bond lengths kept rigid by the SHAKE algorithm (Ryckaert *et al.*, 1977). The molecule was weakly coupled to a temperature bath with a reference temperature of 300 K using a coupling constant of 0.1 ps (Berendsen *et al.*, 1984). A cut-off radius of 10 Å was used for the non-bonded interactions and the non-bonded pair list was updated every 20 fs. MD runs with the highest values of C_{DIS} and C_{DLR} were continued to approximately 20 ps in total, and coordinates were then averaged over another 2 ps to give averaged MD structures which were then subjected to another 500 steps of EM to correct distortions in the structure caused by the averaging procedure.

We performed two separate MD simulations to determine the structure of Nα-acetyl-G110-TnI(104-115) amide bound to bovine cardiac TnC.Ca(II)$_4$. The first of these simulations used a set of input coordinates derived from the standard Φ,Ψ angles of an α-helix (Φ = -60°, Ψ = -40°). The second of these simulations used a set of input coordinates derived from the standard Φ,Ψ angles of a β-strand ($\Phi = -118°$, $\Psi = +118°$). The distance restraint file used as input for the MD simulations is presented in Table VIII-7 in the Appendix.

D. Results

1. Sequential Resonance Assignments and Transferred NOEs

Sequential assignments of the G110-TnI peptide in the absence and presence of 0.1 molar equivalents of TnC.Ca(II)$_4$ were carried out according to the established procedures of Wuthrich *et al.* (Wuthrich *et al.*, 1982; Billeter *et al.*, 1982; Wagner *et al.*, 1982). This method relies on the observation of NOEs between the amide protons of one residue and the α-protons, β-protons and amide protons of the preceding residue ($d_{\alpha N}$, $d_{\beta N}$ *and* d_{NN}). Table VIII-1 shows the ^{1}H chemical shifts for the assigned resonances of the G110-TnI peptide in the absence and presence of 0.1 molar equivalents of TnC.Ca(II)$_4$.

All DQFCOSY and NOESY spectra of the peptide in the absence and presence of protein were acquired at 5°C. The spectra were acquired at low temperature to retard the exchange of the backbone amide protons, as well as to increase the correlation time of the free peptide to produce negative intrapeptide NOEs in the absence of protein[3]. When the NOEs for the free and bound peptide are both negative, the correction for the contribution of the free peptide to the observed NOEs is much easier to accomplish.

TnC.Ca(II)$_4$ was titrated into the G110-TnI peptide NMR sample and the shift of the ^{1}H resonances followed as a function of protein concentration. Figures VIII-1A →VIII-1C show one-dimensional spectra of the G110-TnI peptide in the absence and the presence of 0.1 molar equivalents TnC.Ca(II)$_4$. Figure VIII-1A shows a portion of the aliphatic upfield region of the spectrum. Figure VIII-1B shows the complete downfield region of the spectrum with the exchangeable guanidinium resonances of R108, R112, R113 and R115, the aromatic F106 resonances, the C-terminal NH group, and the backbone amide resonances. Figure VIII-1C shows an expanded region of the backbone amide protons. One can see that the resonances of the G110-TnI peptide experience some line broadening and change in chemical shift position, but δ_{obs} and $\Delta\nu_{obs}$ are dominated by the free ligand population for $p_F >> p_B$ (see Eqns. 2 and 3). Figures VIII-2A → VIII-

---

[3] At room temperature, the NOESY spectrum of the peptide in the absence of protein displayed weak positive cross-peaks.

2C show plots of the change in chemical shift ($\Delta\delta$) of the peptide backbone amide proton resonances as a function of molar equivalents of TnC.Ca(II)$_4$ (see Table VIII-8 in the Appendix). All amides were observed to titrate downfield, but those amides observed to undergo the greatest shift during the titration belong to G104, K105, F106, G110 (see Table VIII-1). The shifts indicate that the amides of these residues are sensing a new chemical environment in the bound peptide due either directly to interactions between the peptide and the protein, or to a new conformation of the peptide when it is bound to the protein. The shift of all resonances was observed to be in fast exchange (Campbell *et al.*, 1991a; Chapter IV).

Figure VIII-3 shows the upfield region of the DQFCOSY spectrum and Figure VIII-4 the upfield region of the TRNOESY spectrum of the G110-TnI peptide in the presence of 0.1 molar equivalents TnC.Ca(II)$_4$. Figure VIII-5 shows the αCH-βCH region, and Figure VIII-6 shows the downfield-βCH region of the of the TRNOESY spectrum. An interesting cross-peak which defines the hydrophobic core of the peptide when bound to TnC is the F106δ,ξCH2ςCH-V114(γCH3)2 interaction highlighted in Figure VIII-6. Figure VIII-7 shows the αCH-NH region of the DQFCOSY spectrum, and Figure VIII-8 the same region in the TRNOESY spectrum.

Figure VIII-9 shows the αCH-NH region of the NOESY spectrum of the G110-TnI peptide superimposed upon the αCH-NH region of the TRNOESY spectrum of the same concentration G110-TnI peptide in the presence of 0.1 molar equivalents TnC.Ca(II)$_4$ to G110-TnI peptide. One can see the emergence of new peptide αCH-NH cross-peaks in the presence of protein, a function of the faster cross-relaxation rate between protons in the bound peptide versus the free peptide. A NOESY spectrum of just the TnC protein in the presence of Ca(II) allowed us to dismiss the possibility of these new cross-peaks being either protein-protein or protein-peptide NOEs (data not shown). The emergence of the new set of cross-peaks in the presence of protein is due not only to the longer bound correlation time experienced by the peptide when bound to protein, but also to a new bound peptide conformation for the bound peptide. Binding to TnC.Ca(II)$_4$ induces secondary structure in the G110-TnI peptide. The peptide NOEs present in the absence of protein are only sequential ($d_{\alpha N\,i,i+1}$), and these are not indicative of secondary structure. However, in the presence of 0.1 molar equivalents TnC.Ca(II)$_4$ to G110-TnI peptide, the same sequential NOEs, now more aptly called TRNOEs, have grown in intensity, and longer range TRNOEs ($d_{\alpha N\,i,i+2}$, $d_{\alpha N\,i,i+3}$) are observable, indicative of defined secondary structure in the bound peptide conformation. Notice, for example, that in the absence of protein, the G104αCH2-K105NH cross-peak is extremely weak, much weaker than any of the other sequential cross-peaks in the spectrum. Whereas in the presence of protein, the

G104αCH2-K105NH cross-peak has grown in intensity relative to the other cross-peaks, and a new G104αCH2-F106NH cross-peak has emerged (a higher vertical scale would reveal G104αCH2-K107NH and G104αCH2-R108NH cross-peaks). The emergence of new cross-peaks at the N-terminus is indicative of the development of secondary structure, whereas the increase in the relative intensity of cross-peaks at the N-terminus suggests a decreased motional freedom at the N-terminus of the bound G110-TnI peptide. Notice also the difference in the position of the K105αCH-F106NH cross-peak in the absence and presence of protein. This is because the peptide F106NH titrates downfield with the addition of protein (see Figure VIII-1C and Table VIII-1).

2. Secondary Structure

A summary of the distance restraints is shown in Figure VIII-10. The pattern of TRNOEs describes two helical regions spanned by residues G104-R108 and R112-R115, interrupted by the central proline-glycine residues, P109-G110, which distort the helix. The sequential restraints which help define the helical regions are those between sequential backbone NH residues ($d_{NN\,i,i+1}$). These include contacts between K105NH-K107NH, K107NH-R108NH, G110NH-L111NH, R113NH-V114NH and V114NH-R115NH. A close $d_{NN\,i,i+1}$ distance of 2.8 Å is diagnostic of α-helix (Wuthrich, 1986). The distance stretches to 4.3 Å in β-strand. Another medium range restraint which helps in defining the helical regions is the $d_{\alpha N\,i,i+3}$ close contact and this is observed for G104αCH2-K107NH. The medium range restraints between the F106δCH2 and ξCH2 aromatic ring protons and the P109βCH2 and γCH2 proline ring protons, and the long range restraint between the F106δCH2 and ξCH2 aromatic ring protons and the L111δCH3 and V114γCH3 methyl protons force a bend around the two central proline residues. This bend allows a closer contact between these side chains not possible if the sequence were an uninterrupted helix. The close proximity of the F106 aromatic ring and the L111δCH3 and V114γCH3 methyl groups defines a tertiary fold and generates a hydrophobic pocket in the short 12 residue sequence of the peptide.

The sequential restraints which define an all trans R108-P109 peptide bond configuration are the contacts between R108αCH-P109δCH2. Comparison of cis and trans X-proline configurations shows that the distances between NH_i and αCH_i, $\delta CH2_{i+1}$ and αCH_{i+1} are strongly affected by cis-trans isomerization. The trans form allows close contact between αCH_i and $\delta CH2_{i+1}$ and between NH_i and $\delta CH2_{i+1}$, whereas the cis form allows close contact between αCH_i and αCH_{i+1} and between NH_i and αCH_{i+1} (Wuthrich, 1986).

3. Distance Determination

The basis for the tertiary structure computation consisted of a set of 222 interproton distance restraints comprising 87 intraresidue, 82 sequential ($|i - j| = 1$), 42 medium ($1 < |i - j| \leq 4$) and 11 long ($4 < |i - j| \leq 8$) range interresidue distances. These interproton distances were derived from pure phase absorption two-dimensional TRNOESY spectra recorded with a mixing time of 150 ms and at 0.1 molar equivalents of TnC.Ca(II)$_4$ to G110-TnI peptide. The TRNOE intensities were normalized for the contribution of more than two protons to the cross-peak, and cross-peaks connecting exchangeable amide resonances were corrected for loss of intensity due to exchange or saturation transfer from the decoupled water peak. The normalized and corrected TRNOE cross-peak intensities were then transformed to distance restraints using a collection of reference proton pairs and error limits used to set r_{ij}^U and r_{ij}^L in order to account for systematic over- and under-determinations of r_{ij} (see experimental procedures).

When stereospecific assignments of protons were not possible, either due to dynamic effects such as rotation of the hydrogens in a methyl group or flipping of aromatic rings, or due to a degenerate chemical shift of prochiral atoms, pseudoatom representations were used (Wuthrich *et al.*, 1983). Distance restraints to such pseudoatoms were constructed from the position of the neighbouring non-hydrogen atoms by enlarging r_{ij}^U by a value calculated from the geometry of the pseudoatom (Wuthrich *et al.*, 1983).

4. Dihedral Angle Restraints

A set of Φ backbone dihedral angle restraints were derived from $^3J\alpha$CH-NH coupling constants (Pardi *et al.*, 1984) measured from a series of one-dimensional ^1H NMR spectra acquired for low concentrations of TnC.Ca(II)$_4$ and extrapolated to the value of $^3J\alpha$CH-NH at 100% bound peptide. A one-dimensional curve fitting program was used to more accurately measure coupling constants in a series of spectra with linewidths that increase with increasing protein concentration. Figures VIII-11A → VIII-11C show plots of $^3J\alpha$CH-NH versus molar equivalents TnC.Ca(II)$_4$ to G110-TnI peptide for various residues in the G110-TnI peptide. The set of dihedral angle restraints was comprised of the Φ angles for 9 residues: G104, K105, F106, K107, R108, G110, L111, R112, R113, and R115. For $^3J\alpha$CH-NH < 6.0 Hz, Φ was restricted to the range $-85° \leq \Phi \leq -40°$, and since all measured values of $^3J\alpha$CH-NH were found to be less than 6.0 Hz when extrapolated to 100% bound peptide, all 9 Φ angles in the set of dihedral angle restraints were restricted to -85° ≤ Φ ≤ -40°. In addition, all peptide bonds, including X-proline, were restricted to -175° ≤ ω ≤ -185°, in order to maintain trans peptide bond configurations.

5. Supplemental Distance Restraints

Temperature coefficients ($\Delta\delta/\Delta T$) of exchangeable backbone amide protons were measured for three molar equivalents of TnC.Ca(II)$_4$ to G110-TnI peptide (0.0, 0.2 and 0.4). Figures VIII-12A → VIII-12D show plots of δNH versus temperature for 0.0 and 0.1 molar equivalents of TnC.Ca(II)$_4$ to G110-TnI peptide, and Figures VIII-13A and VIII-13B show $\Delta\delta/\Delta T$ versus molar equivalents of TnC.Ca(II)$_4$ to G110-TnI peptide. Clearly, only the backbone amide proton of K107 displays a $\Delta\delta/\Delta T$ value of less than -4 ppb, when this value is extrapolated to 100% bound peptide. Thus, it would appear that the backbone amide proton of K107 is protected by an intrapeptide interaction (as opposed to a peptide-protein interaction). From a knowledge of the secondary structure of the bound G110-TnI peptide, which suggests a helical structure for residues G104-R108, we would predict an H-bond between the carbonyl group of the N-acetyl group and the backbone amide proton of K107, in accordance with the CO_i - NH_{i+4} H-bonding pattern in an α-helix. (We assumed α-helical structure instead of 3_{10}-helical structure, which would have involved a different H-bonding pattern; $CO_{\ i}$ - $NH_{\ i+3}$.) We thus included in the distance restraint file an extra distance restraint between the carbonyl oxygen of the N-acetyl group and the backbone amide proton of K107, and set the upper and lower distance limits as $r_{ij}^U = 3.2$ Å and $r_{ij}^L = 2.8$ Å, a reasonable range for an H-bond donor-acceptor pair. This supplemental distance restraint agrees with the presence of a TRNOE between the N-acetyl CH_3 group and the backbone amide proton of R108.

The fact that the other residues do not display protected backbone amide protons does not necessarily contradict our prediction of helical secondary structure in the bound peptide. But it does suggest that the secondary structure present in the bound peptide is probably not present in the free structure. That the backbone amide proton of K107 appears protected is probably due to residual structure in the N-terminus of the free peptide in the form of the predicted intrapeptide H-bond between the N-acetyl group and K107.

6. Molecular Dynamics Calculations

We performed two separate MD simulations to determine the structure of the G110-TnI peptide bound to TnC.Ca(II)$_4$. The first simulation started from an α-helical set of input coordinates and the second simulation from a β-strand set of input coordinates (see experimental procedures for details of these simulations). The coordinates of these structures are given in Table VIII-9 in the Appendix and have been deposited in the BIOMAGRES BANK for protein NMR data in Madison, Wisconsin. Table VIII-10 in the Appendix compares the distances between proton pairs given in the distance restraint file with those actually measured between the same proton pairs in the final structures generated from the α-helix (structure 1) and the β-strand (structure 2). There are 17 distance violations for structure 1 and 16 distance violations for structure 2 which were ≥ 2.0 Å greater than the upper limit TRNOE-derived distance constraint, r_{ij}^U. This is not a large collection of distance violations given that there were a total of 222 distance constraints used to derive the final structures. Furthermore, the majority of these distance violations were for intraresidue and sequential interresidue distances, and none for long range interresidue distances.

Figure VIII-14 shows the a stereo structure of the bound G110-TnI peptide derived from α-helical coordinates (structure 1). Following 12 ps of MD, the coordinates of 10 MD structures taken every 0.2 ps were averaged and the averaged coordinates were energy minimized to produce the final structure in the figure[4]. The 10 superposed MD structures in Figure VIII-15 show that the conformation around the central residues P109-G110-L111 is poorly defined. This may be due either to an inherent flexibility around the G110 residue, or due to a paucity of TRNOE contraints for these residues, resulting in a weakly constrained region in conformational space.

Table VIII-2 presents two sets of dihedral angle values, one set describing structure 1 and one set describing structure 2. Backbone Φ, Ψ and ω dihedral angles for all residues in the bound structures are given, as well as the side chain χ dihedral angles for the proline residue. The dihedral angles given for structure 1 agree reasonably well with the dihedral angles given for structure 2, except in the central region around residues P109-G110-L111. The Ψ dihedral angle values for structure 1 were 168°, 133° and -57° for P109, G110 and L111, respectively. In structure 2, these values were -66°, 90° and -127°, respectively. Thus, it would appear that either this region of the G110-TnI peptide structure was not sufficiently defined by the TRNOE data to produce a singular conformation, or that structure 2 fell into a local energy minimum from which it was unable to escape. That this region was not sufficiently defined by the TRNOE data could be a function of local flexibility in the region around G110, in which case the G110-TnI peptide could adopt a number of conformations, even when bound to TnC. For both structures, the residues G104-R108 and L111-R115 and are in the range of $-76° \leq \Phi \leq -55°$ and $-59° \leq \Psi \leq -21°$, and describe a helical structure[5]. In structure 1, the Φ, Ψ angles break the helical stretch at P109 and G110 with values in the range of $-76° \leq \Phi \leq -55°$ and $168° \leq \Psi \leq 133°$ for both residues. In structure 2, the Φ, Ψ angles break the helical stretch one residue later at G110 and L111 with values in the range of $-76° \leq \Phi \leq -64°$ and $-127° \leq \Psi \leq 90°$ for both residues. There are steric constraints on the conformation of the proline ring of P109 which displays a $C\beta$ exo ring pucker in structure 1 defined by $\chi^1 = 15°$, $\Phi = -73°$, and a $C\gamma$ exo ring pucker in structure 2 defined by $\chi^1 = -19°$, $\Phi = -67°$. All peptide bonds in the final structures are trans.

---

[4] The inclusion of the H-bond restraint between the carbonyl oxygen of the N-acetyl CH3 group and the backbone amide proton of K107 did not bias the generation of the bound TnI peptide structure toward α-helical dihedral space. The final structures arrived at the same Φ,Ψ values reguardless of whether or not the H-bond restraint was included in the distance restraint file.

E. Discussion

The G110-TnI peptide, like the skeletal TnI peptide, is extremely basic, with four arginines and two lysines (K105, K107, R108, R112, R113 and R115) within a twelve residue sequence. Alternating with these basic residues are hydrophobic residues (F106, L111 and V114). The pattern of alternating basic and hydrophobic residues is interrupted by a proline-glycine pair (P109 and G110). The TRNOE-derived structure of the G110-TnI peptide bound to $TnC.Ca(II)_4$ reveals a helical structure, distorted in the center by this 'helix-breaking' proline-glycine sequence. The peptide is helical, except around the P109-G110 residues where the Φ,Ψ values are approximately -70°, 170° for P109 and -70°, 130° for G110. The bend around the P109-G110 sequence brings the hydrophobic residues of the G110-TnI peptide into closer proximity than would otherwise be observed if the helix were straight. The ring protons of F106 are close enough to the γ-methyl protons of V114 to allow the observation of a TRNOE cross-peak between these two residues. Thus, the G110-TnI peptide has a tertiary fold which defines a small hydrophobic pocket with the aromatic ring of F106 being somewhat buried by the side chains of L111 and V114. The side chains of the basic residues extend outwards on the hydrophilic face, away from this hydrophobic pocket.

A comparison of the conformation of the G110-TnI peptide when bound to cardiac TnC versus the conformation of the skeletal TnI peptide when bound to skeletal TnC

---

[5] α-helix is described by Φ,Ψ values of -58°,-47°; 3_{10}-helix is described by Φ,Ψ values of -76°,-5°; and Π-helix is described by Φ,Ψ values of -57°,-70° (Ghelis and Yon, 1982).

(Campbell and Sykes, 1991a; Chapter V) reveals similar but not identical structures. The structure of the bound skeletal peptide is also a distorted helix with a hydrophilic face and a hydrophobic pocket in which the side chains of F106, L111 and V114 are in close proximity. The skeletal TnI peptide is helical, except around the P109-P110 residues where the Φ,Ψ values are approximately -70°, -170° for both prolines. Although a comparison of the TRNOE-generated structures of the G110-TnI peptide and the skeletal TnI peptide reveals subtle conformational differences, the largest discernable difference between the G110-TnI peptide and the skeletal TnI peptide is obvious in the superposed MD structures for the molecular mechanics simulations. The 10 superposed structures for the skeletal TnI peptide (Campbell and Sykes, 1991a; Chapter V) are tightly constrained in conformational space, especially around the central P109-P110-L111 residues. However, the 10 superposed structures for the G110-TnI peptide analog are loosely constrained around the central P109-G110-L111 residues, either due to a paucity of TRNOE constraints for this region or due to an inherent flexibility around the G110 residue.

While it appears that the secondary structure adopted by the G110-TnI peptide analog and the skeletal TnI peptide are similar, the dynamics and flexibility of the peptides around the central position 110 are quite different, the G110-TnI peptide being much more flexible in this region than the skeletal TnI peptide. A difference in flexibility in the inhibitory region of TnI could account for the differences in biological activity observed for the skeletal versus the cardiac versus the G110-TnI peptides. The TRNOE-derived structures of the G110-TnI peptide analog and the skeletal TnI peptide show that the central sequence around P109-P110 in the skeletal peptide and P109-G110 in the analog forms a turn-like structure, such that the hydrophobic residues (F106, L111 and V114) are in close proximity. In the cardiac TnI peptide, the replacement of a proline with a threonine lowers the potential for a turn at this position by 65% (Talbot and Hodges, 1981b). The G110-TnI peptide should be more flexible than the other two TnI peptides, since glycine does not have a side chain and so can adopt a wider range of Φ and Ψ dihedral angles than proline or threonine.

Van Eyk *et al.* (1991) found that the $\theta_{220nm}/\theta_{222nm}$ ratios observed for the skeletal versus the cardiac TnI peptide in aqueous solution and TFE were not similar, indicating strongly that the conformations of the two peptides in these two solvents are different. Neither the skeletal or the cardiac peptide has a tendency to form extensive α-helical or β-sheet structure, even in the presence of 50% TFE. This may be a function of the two proline residues situated in the middle of the skeletal TnI sequence which would have a tendency to disrupt any α-helical structure. Surprisingly, the $\theta_{220nm}/\theta_{222nm}$ ratios observed in aqueous solution and TFE for cardiac versus the G110-TnI peptide were similar, but different from the $\theta_{220nm}/\theta_{222nm}$ ratios observed for the skeletal TnI peptide. It thus seems likely that the conformation and/or dynamics of the cardiac TnI peptide when bound to TnC are similar to those of the G110-TnI peptide, but different from those of the skeletal TnI peptide.

The unbound TnI peptides probably exist in aqueous solution as an ensemble of transient conformational states in dynamic equilibrium. Molecular recognition between the TnI peptide and the TnC protein would require the selection of a unique peptide conformation complementary to the three-dimensional contours of the binding surface on TnC. If the TnI peptide has a predisposition to adopt the conformation necessary for binding, the selection of the correct conformation would be statistically more favourable. The high turn potential of the P109-P110 sequence in the skeletal peptide probably predisposes the unbound peptide to adopt the 'turn conformation' necessary for binding to skeletal TnC.

In the cardiac TnI peptide, where the replacement of a proline with a threonine lowers the potential for the turn at this position, the selection of the correct 'turn conformation' for binding to TnC might be statistically less favourable. This may explain the findings that skeletal TnI is a more effective inhibitor than cardiac TnI in both cardiac and skeletal ATPase assays (Hincke *et al.*, 1977; Talbot and Hodges, 1981a; Ruegg *et al.*, 1989). In the G110-TnI peptide, where the replacement of a proline with a glycine allows greater conformational flexibility around this position, the selection of the correct 'turn conformation' for binding to TnC may also be statistically unfavourable due to the large number of conformational states available to this peptide in solution. This may in turn explain the findings that the G110-TnI peptide analog inhibits the actomyosin ATPase activity, but is considerably less effective than the skeletal TnI peptide (Van Eyk and Hodges, 1988). However, the G110-TnI peptide analog binds to a skeletal TnC or cardiac TnC affinity column (in the presence of Mg(II) or Ca(II)) almost as tightly as the native skeletal TnI peptide (Van Eyk *et al.*, 1991).

Although the skeletal, cardiac and G110-TnI peptides may adopt similar conformations when they bind to TnC, they must be affecting different residues on TnC, leading to different biological activities. The G110-TnI analog primarily affects Ca(II) binding to the high affinity sites, whereas the two native TnI peptides mainly affect Ca(II) binding to the low affinity sites. Importantly, it is the low affinity sites which are the regulatory sites for muscle contraction. This may be reflected in the fact that skeletal and cardiac TnI peptides induce equivalent inhibition of force development of skeletal and cardiac skinned muscle fibres while the G110-TnI peptide does not significantly alter force development (Ruegg *et al.*, 1991).

The suggestion that the skeletal versus the cardiac versus the G110-TnI peptides must be affecting different residues on TnC is supported by TnC-affinity chromatography of cardiac TnI analogs in which single amino acids were individually substituted with glycine. These analogs bound to skeletal and cardiac TnC affinity columns with different strengths than the corresponding skeletal glycine analogs (Van Eyk *et al.*, 1991), suggesting that residues which are important for TnC binding are different for the skeletal TnI peptide than for the cardiac TnI peptide.

In Chapter VI, we used ^{1}H NMR to identify several residues on Ca(II)-saturated s-TnC which interact with the TnI peptide in the peptide-protein complex (Campbell *et al.*, 1991b). We assigned NOEs between residues on the TnI peptide and F102, I104, I113, I121, I149, F151, and F154, within the hydrophobic pocket in the C-terminal domain and the β-sheet region between Ca(II)-binding sites III and IV of the protein. Many other studies have also identified the C-terminal domain of TnC as being the interaction site with the inhibitory region of TnI. These have included proteolytic studies (Weeks and Perry 1978; Grabarek *et al.* 1981), resonance energy transfer measurements (Tao *et al.*, 1989), fluorescence studies (Lan *et al.*, 1989), and cross-linking studies (Chong and Hodges, 1981; Leszyk *et al.*, 1987, 1988).

Given that the binding of the skeletal TnI peptide (and by analogy, the cardiac TnI peptide) to skeletal TnC occurs in the C-terminal domain, it is not clear how the bound peptide can alter the binding of Ca(II) at the low affinity sites located in the N-terminal domain of skeletal TnC. There must be communication between the two halves of the TnC molecule and/or there must be simultaneous binding of the TnI peptide to both the N- and the C-terminal domains of TnC. The N- and C-terminal domains of TnC are connected through a fusion of helices D (Ca(II) binding site II) and E (Ca(II) binding site III) (Herzberg and James, 1985; Sundaralingam *et al.*, 1985). The communication link between the N- and C-terminal domains of TnC could be this D/E linker, through which conformational changes caused by Ca(II) and/or target molecules binding at either domain could be transmitted.

Studies implicating the binding of the TnI peptide simultaneously to both the N- and the C-terminal domains of TnC have included photo-crosslinking, fluorescence and NMR studies (Leszyk *et al.*, 1990; MacLachlan *et al.*, 1990; Wang *et al.*, 1990; Reid *et al.*, 1990). Photo-cross linking studies using zero-length cross-links (Leszyk *et al.*, 1990) have revealed an interaction between Ca(II)-binding site II (residues 46-78) on rabbit skeletal TnC and TnI(104-115), offering evidence for an interaction involving the N-terminal domain of TnC, as first proposed by Grabarek *et al.* (1981). In addition, Wang *et al.* (1990) used photo-cross-linking and fluorescence studies with a recombinant TnC to demonstrate that the C-helix in the N-terminal domain of TnC interacts with TnI(104-115), in confirmation of the zero-length cross-linking results (Leszyk *et al.*, 1990). Furthermore, MacLachlan *et al.* (1990) used fluorescence stopped flow kinetics and ^{1}H NMR to demonstrate that the calcium sensitizer, bepridil, binds to the N-terminal domain of cardiac TnC with a 1:1 stoichiometry. The same research group used ^{1}H NMR and molecular modeling to study the binding of calmidazolium to TnC and concluded that binding occurs simultaneously to both the N- and C-terminal globular domains of the TnC protein (Reid *et al.*, 1990).

Several solution studies of CaM have also implicated residues in both the C-terminal and the N-terminal domains which are involved in the binding of a single target molecule. These studies include NMR studies (Klevit *et al.*, 1985; Linse *et al.*, 1986; Seeholzer *et al.*, 1986; Seeholzer and Wand, 1989; Yazawa *et al.*, 1987; Ikura *et al.*, 1991), fluorescence studies (Steiner and Norris, 1987), and proteolytic digestion studies (Caday and Steiner, 1986). Ikura *et al.* (1991) used triple-resonance multidimensional NMR to study CaM complexed with a skeletal muscle myosin light chain kinase (MLCK) peptide, M13(577-603), and found evidence for a conformational change in the central helix. Binding of the M13 peptide induced substantial chemical shift changes that were not localized in one particular region of the protein. The largest changes were found in the first helix of the Ca(II)-binding site I, the N-terminal portion of the central helix, and the second helix of the Ca(II)-binding site IV. These results support a model for the binding of target peptides to CaM which involves both the C-terminal and the N-terminal domains, contingent on a conformational change in the central helix.

Two separate groups have offered evidence of communication between the two globular domains of CaM in the presence of target peptides (Linse *et al.*, 1986; Yazawa *et al.*, 1987). Linse *et al.* (1986) used ^{113}Cd NMR to monitor the binding of mastoparan and melittin and found that mastoparan binding induced a structural change affecting both the N- and C-terminal domains of CaM. A possible model for communication between the two lobes of CaM in the presence of melittin has been provided by Strynadka and James (1990). In this model, they introduced a kink in the central helix of CaM, serving to bring the two hydrophobic domains of CaM sufficiently close to bind a single melittin peptide, while maintaining reasonable stereochemistry.

Although it is difficult to reconcile the simultaneous binding of a small ligand to both N- and C-terminal domains of TnC on the basis of the crystal structure of the protein, convincing evidence for shorter interdomain separation comes from small angle x-ray scattering studies of TnC (Hubbard *et al.*, 1988; Fujisawa *et al.*, 1989) and CaM (Kataoka *et al.*, 1989; Matsushima *et al.*, 1989; Yoshino *et al.*, 1989; Heidorn *et al.*, 1989). These studies indicate that the two globular domains move towards each other in a concerted effort to bind the target ligand, suggesting that the central helix acts as a flexible tether (Persechini and Kretsinger, 1988) in allowing the N-terminal and C-terminal domains to form a single binding site capable of accomodating a wide variety of target peptides or enzymes. The long central helix of TnC is bent about 16° at G92 in the crystal structure of chicken TnC (Sundaralingam *et al.*, 1985), therefore it is possible to envision a model of the inhibitory TnI peptide binding to Ca(II)-saturated TnC in which a bend at G92 allows a closer approach of the N- and C-terminal domains in a concerted effort to bind the peptide.

Sheng *et al.* (1991) used deletion mutants in the D/E linker of TnC to investigate the role of the central helix in regulating muscle contraction by testing their effectiveness in restoring force and Ca(II)-regulation to TnC-depleted rabbit skinned skeletal muscle fibers. These studies found that a change in orientation of the two Ca(II)-binding domains shifted the Ca(II)-dependence in force activation, which they proposed was related to the inability of the Ca(II)-specific domain to properly interact with its binding site on TnI, an interaction which is known to increase the affinity of TnC for Ca(II) (Potter and Gergely, 1975). Studies of the flexibility of the central helix in CaM (Yazawa *et al.*, 1989; Kataoka *et al.*, 1991) have suggested that the D/E linker region fluctuates between the two extreme shapes of the bent and the dumbbell structure. Target molecules would select and fix the specific bent structure for their activation.

These solution studies of CaM and TnC provide a structural framework for interpretation of the binding of the TnI inhibitory peptide to TnC. It is possible to imagine a conformational change around a hinge region (G92) in the central helix of TnC which would allow the N- and C-terminal domains to form a single binding site capable of accomodating a single peptide. The hydrophobic pockets in the N- and C-terminal domains would each provide half of the binding interface between which the peptide is 'sandwiched'. The conformational change could be the communication link between the two halves of the TnC molecule and would explain the wealth of data implicating both domains in the binding of the TnI inhibitory peptide.

Although it appears that the skeletal, cardiac and G110-TnI peptides may adopt similar conformations when they bind to TnC, they affect Ca(II) binding to different regions of the TnC molecule. The skeletal and cardiac TnI peptides affect Ca(II) binding to sites I and II in the N-terminal domain of TnC, and the G110-TnI peptide affects Ca(II) binding to sites III and IV in the C-terminal domain. Since sites I and II are the regulatory sites, only binding of the skeletal and cardiac TnI peptides to TnC induces inhibition of force development in skeletal and cardiac skinned muscle fibres, whereas the G110-TnI peptide does not significantly alter force development. Somehow, the inability of the

G110-TnI peptide to affect sites I and II must be related to the inability of this peptide to produce the required conformational change in TnC when it binds at the C-terminal domain. This conformational change could be a bending around the hinge region in the central helix of TnC which would allow the N- and C-terminal domains to form a single binding site capable of accomodating the peptide. If the conformational change which allows a close and concerted approach of the N- and C-terminal domains towards each other were the communication link between the two halves of the TnC molecule, then a peptide which fails to produce this conformational change would fail to produce the desired biological response. It is amazing that the substitution of a single proline for a glycine at position 110 of skeletal TnI should lead to such different biological responses.

Table VIII-1. Chemical shifts for the assigned ^1H resonances of Nα-acetyl-G110-TnI(104-115) amide at (a) 5°C in 50 mM KCl, pH 5.5; and at (b) 5°C with 0.1 molar equivalents $TnC.Ca(II)_4$ in 50 mM KCl, pH 6.5.

residue	NH	αCH	βCH	others
G104	(a) 8.426	(a) 3.89		(a) NAcCH3 2.06
	(b) 8.433	(b) 3.89		(b) NAcCH3 2.06
K105	(a) 8.376	(a) 4.21	(a) 1.61	(a) γCH2 1.24, δCH2 1.61, ξCH2 2.92
	(b) 8.387	(b) 4.22	(b) 1.61	(b) γCH2 1.24, δCH2 1.61, ξCH2 2.92
F106	(a) 8.292	(a) 4.62	(a) (x) 3.00, (m) 3.14	(a) δCH2 7.24, ξCH2ζCH 7.34
	(b) 8.311	(b) 4.61	(b) (x) 3.00, (m) 3.14	(b) δCH2 7.24, ξCH2ζCH 7.33
K107	(a) 8.242	(a) 4.26	(a) 1.65	(a) γCH2 1.38, δCH2 1.74, ξCH2 2.97
	(b) 8.240	(b) 4.26	(b) 1.65	(b) γCH2 1.37, δCH2 1.74, ξCH2 2.97
R108	(a) 8.480	(a) 4.53	(a) 1.72	(a) γCH2 1.85, δCH2 3.19
	(b) 8.483	(b) 4.53	(b) 1.72	(b) γCH2 1.85, δCH2 3.19
P109		(a) 4.41	(a) (x) 1.95, (p) 2.32	(a) γCH2 2.03, δCH2 (m) 3.70, (m') 3.84
		(b) 4.41	(b) (x) 1.95, (p) 2.31	(b) γCH2 2.05, δCH2 (m) 3.69, (m') 3.85
G110	(a) 8.590	(a) 3.95,3.99		
	(b) 8.597	(b) 3.92,3.98		
L111	(a) 8.224	(a) 4.33	(a) 1.59	(a) γCH 1.64, δCH3 0.87, 0.93
	(b) 8.224	(b) 4.33	(b) 1.59	(b) γCH 1.64, δCH3 0.87, 0.93
R112	(a) 8.502	(a) 4.31	(a) -	(a) γCH2 - , δCH2 3.19
	(b) 8.498	(b) 4.31	(b) -	(b) γCH2 - , δCH2 3.19
R113	(a) 8.541	(a) 4.35	(a) -	(a) γCH2 - , δCH2 3.19
	(b) 8.535	(b) 4.35	(b) -	(b) γCH2 - , δCH2 3.19
V114	(a) 8.423	(a) 4.11	(a) 2.08	(a) γCH3 0.94
	(b) 8.415	(b) 4.11	(b) 2.06	(b) γCH3 0.94
R115	(a) 8.610	(a) 4.27	(a) 1.82	(a) γCH2 - , δCH2 3.19, NH 7.23, 7.74
	(b) 8.615	(b) 4.28	(b) 1.82	(b) γCH2 - , δCH2 3.19, NH 7.23, 7.75

Table VIII-2. Dihedral angle values in the final structure generated from (a) α-helix (structure 1), and (b) β-strand (structure 2). The backbone dihedral angles are defined as χ1: Cα-Cβ-Cγ-Cδ, χ2: Cβ-Cγ-Cδ-N, and χ3: Cγ-Cδ-N-Cα.

residue	Φ	Ψ	ω	χ1	χ2	χ3
G104		(a) -50	(a) 180			
		(b) 134	(b) 174			
K105	(a) -58	(a) -59	(a) 175			
	(b) -62	(b) -51	(b) 179			
F106	(a) -71	(a) -23	(a) 175			
	(b) -66	(b) -19	(b) -178			
K107	(a) -69	(a) -49	(a) 176			
	(b) -68	(b) -40	(b) 175			
R108	(a) -63	(a) -29	(a) 171			
	(b) -57	(b) -51	(b) 170			
P109	(a) -73	(a) 168	(a) 180	(a) 15	(a) -24	(a) 24
	(b) -67	(b) -66	(b) -179	(b) -19	(b) 14	(b) -5
G110	(a) -55	(a) 133	(a) -178			
	(b) -76	(b) 90	(b) -180			
L111	(a) -55	(a) -57	(a) -179			
	(b) -64	(b) -127	(b) -176			
R112	(a) -59	(a) -21	(a) 177			
	(b) -61	(b) -21	(b) 179			
R113	(a) -58	(a) -49	(a) -180			
	(b) -55	(b) -49	(b) -174			
V114	(a) -67	(a) -33	(a) -170			
	(b) -68	(b) -31	(b) -178			
R115	(a) -60					
	(b) -67					

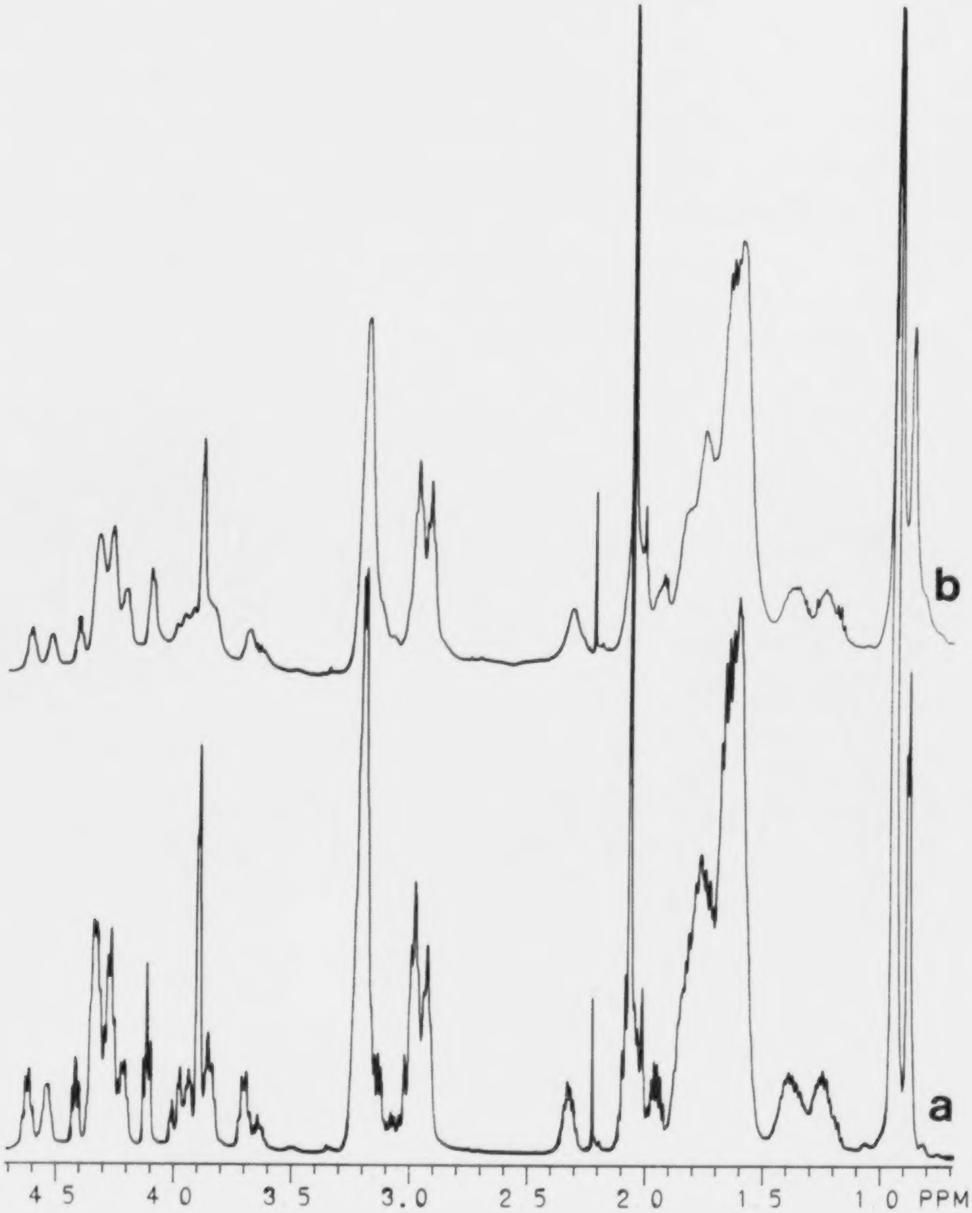

Figure VIII-1A. 500 MHz ^1H NMR spectra of the G110-TnI peptide in the absence and presence of 0.1 molar equivalents TnC.Ca(II)$_4$: Aliphatic upfield region of the spectrum. **a.** 7 mM Nα-acetyl-G110-TnI(104-115) amide, 50 mM KCl, pH 6.3, 80%H_2O/20%D_2O, 5°C; **b.** 7 mM Nα-acetyl-G110-TnI(104-115) amide, 0.7 mM TnC, 4 mM $CaCl_2$, 50 mM KCl, pH 6.3, 80%H_2O/20%D_2O, 5°C.

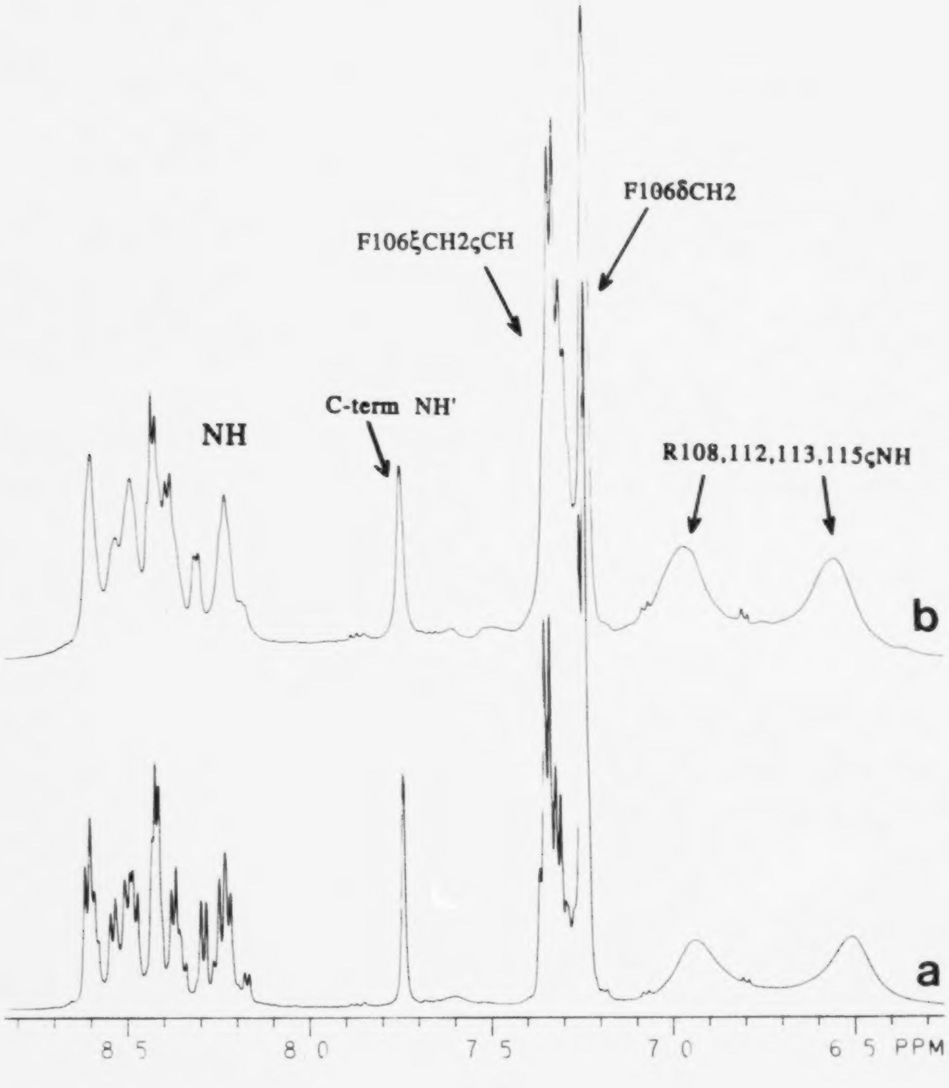

Figure VIII-1B. 500 MHz ^{1}H NMR spectra of the G110-TnI peptide in the absence and presence of 0.1 molar equivalents TnC.Ca(II)$_4$: Complete downfield region of the spectrum with the exchangeable guanidinium resonances of R108, R112, R113 and R115 and the aromatic F106 resonances. **a.** 7 mM Nα-acetyl-G110-TnI(104-115) amide, 50 mM KCl, pH 6.3, 80%H_2O/20%D_2O, 5°C; **b.** 7 mM Nα-acetyl-G110-TnI(104-115) amide, 0.7 mM TnC, 4 mM $CaCl_2$, 50 mM KCl, pH 6.3, 80%H_2O/20%D_2O, 5°C.

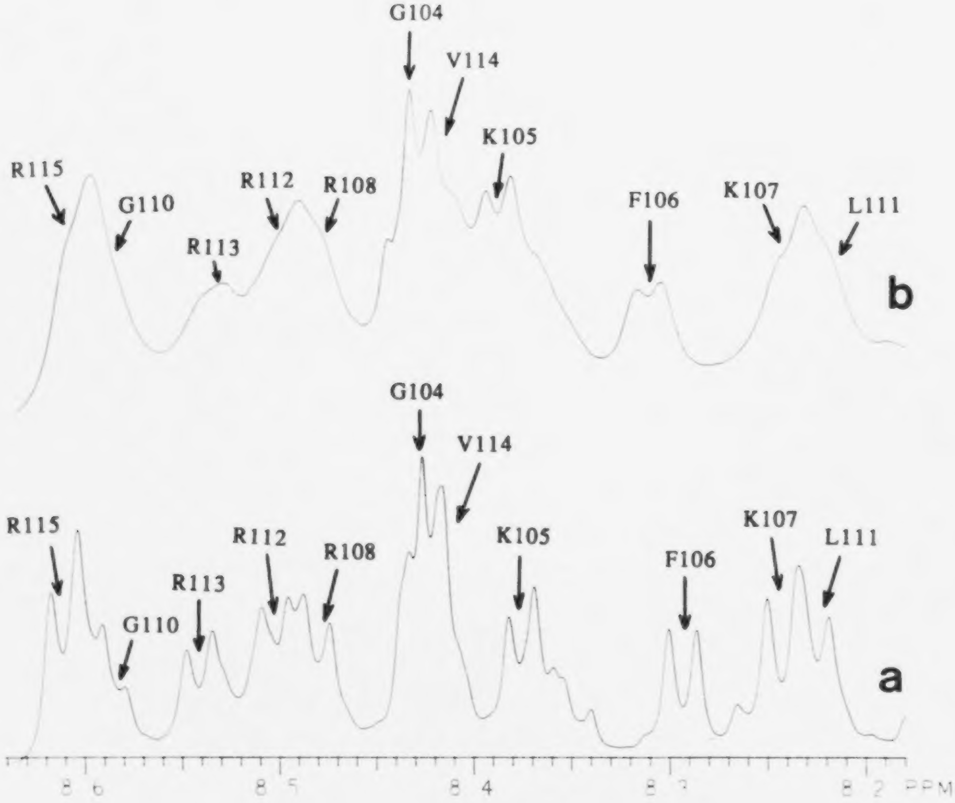

Figure VIII-1C. 500 MHz ^{1}H NMR spectra of the G110-TnI peptide in the absence and presence of 0.1 molar equivalents TnC.Ca(II)$_4$: Expanded region of spectrum B showing only the backbone amide proton resonances. **a.** 7 mM Nα-acetyl-G110-TnI(104-115) amide, 50 mM KCl, pH 6.3, 80%H_2O/20%D_2O, 5°C; **b.** 7 mM Nα-acetyl-G110-TnI(104-115) amide, 0.7 mM TnC, 4 mM $CaCl_2$, 50 mM KCl, pH 6.3, 80%H_2O/20%D_2O, 5°C.

Figure VIII-2. Plot of the change in chemical shift of the G110-TnI peptide backbone amide resonances as a function of molar equivalents $TnC.Ca(II)_4$.

A. (○) G104NH; (■) K105NH; (□) F106NH; (●) K107NH.
B. (○) R108NH; (■) G110NH; (●) L111NH.
C. (●) R112NH; (■) R113NH; (○) R115NH.

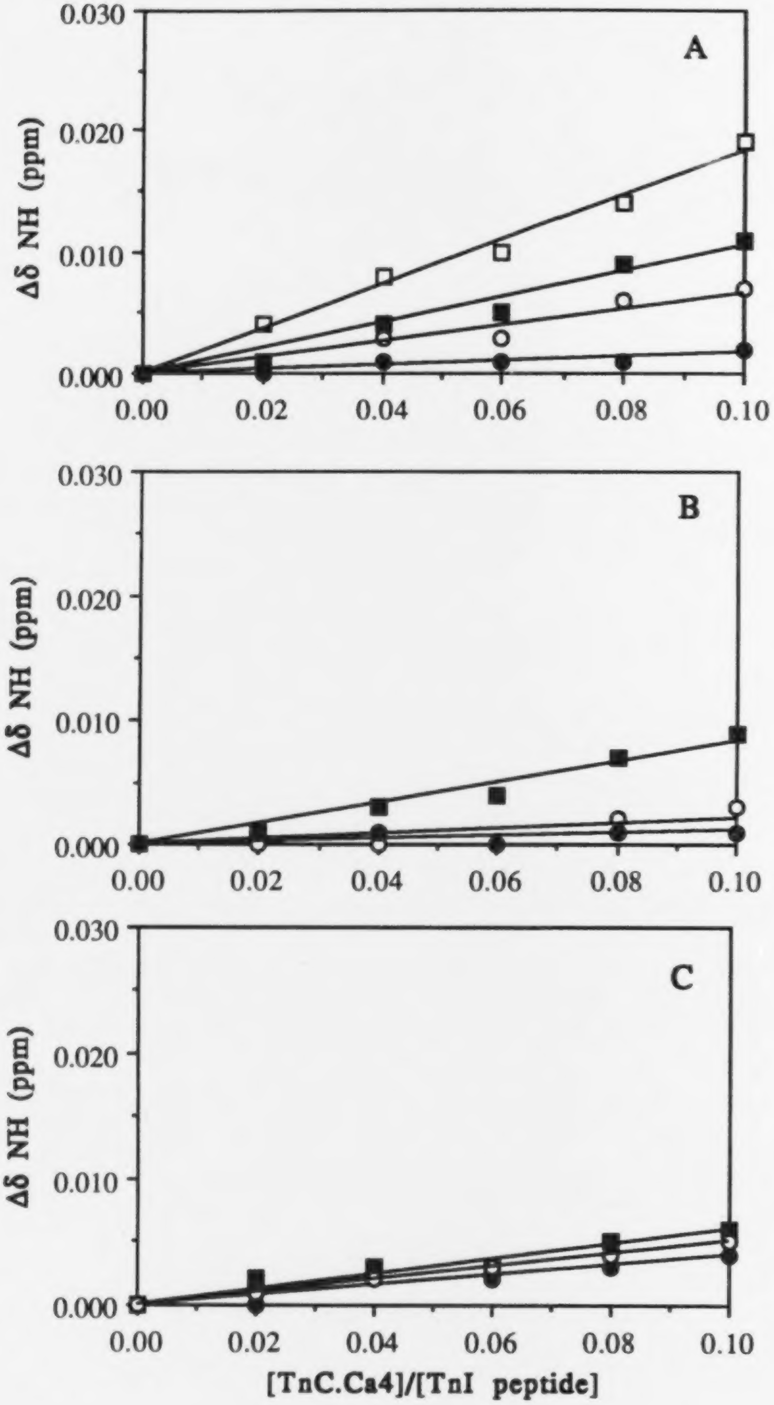
A
B
C
Δδ NH (ppm)
0.000
0.010
0.020
0.030
0.00
0.02
0.04
0.06
0.08
0.10
[TnC.Ca4]/[TnI peptide]

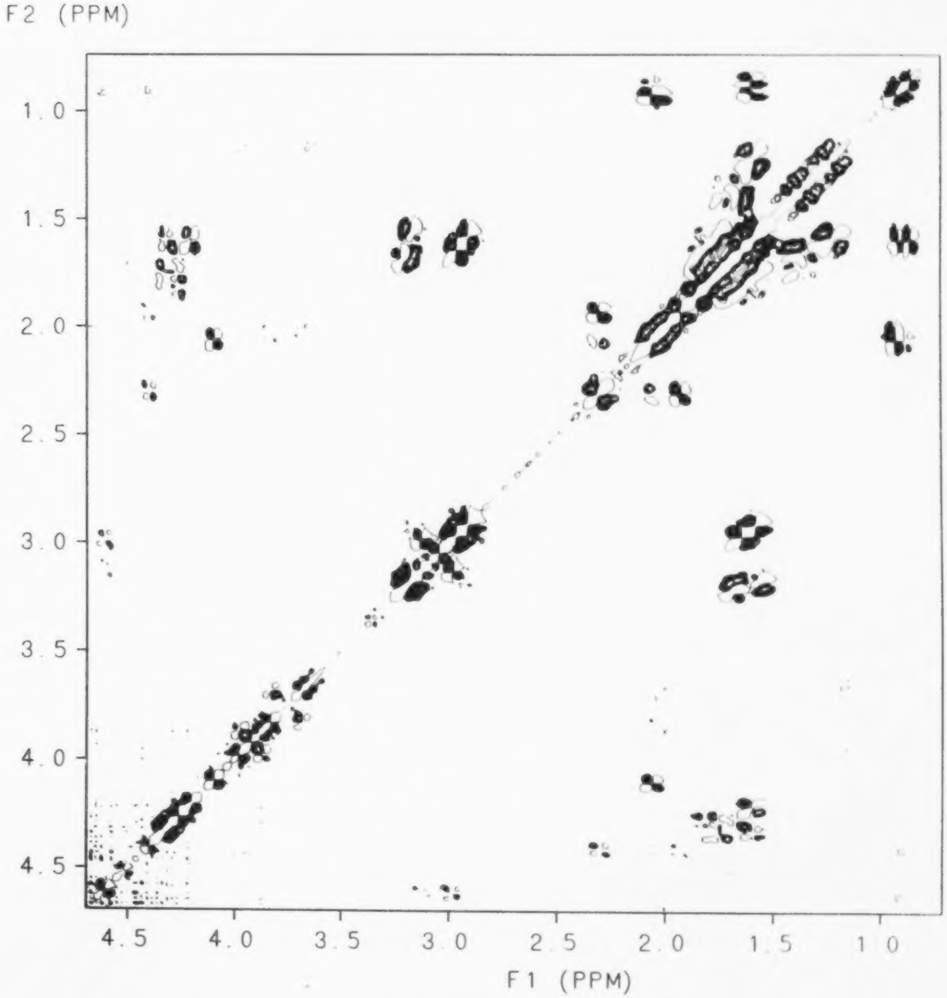

Figure VIII-3. Upfield region of the DQFCOSY spectrum of the G110-TnI peptide in the presence of 0.1 molar equivalents TnC.Ca(II)$_4$. (10 mM Nα-acetyl-G110-TnI(104-115) amide, 1 mM TnC, 4 mM CaCl$_2$, 50 mM KCl, pH 6.5, 80%H$_2$O/20%D$_2$O, 5°C)

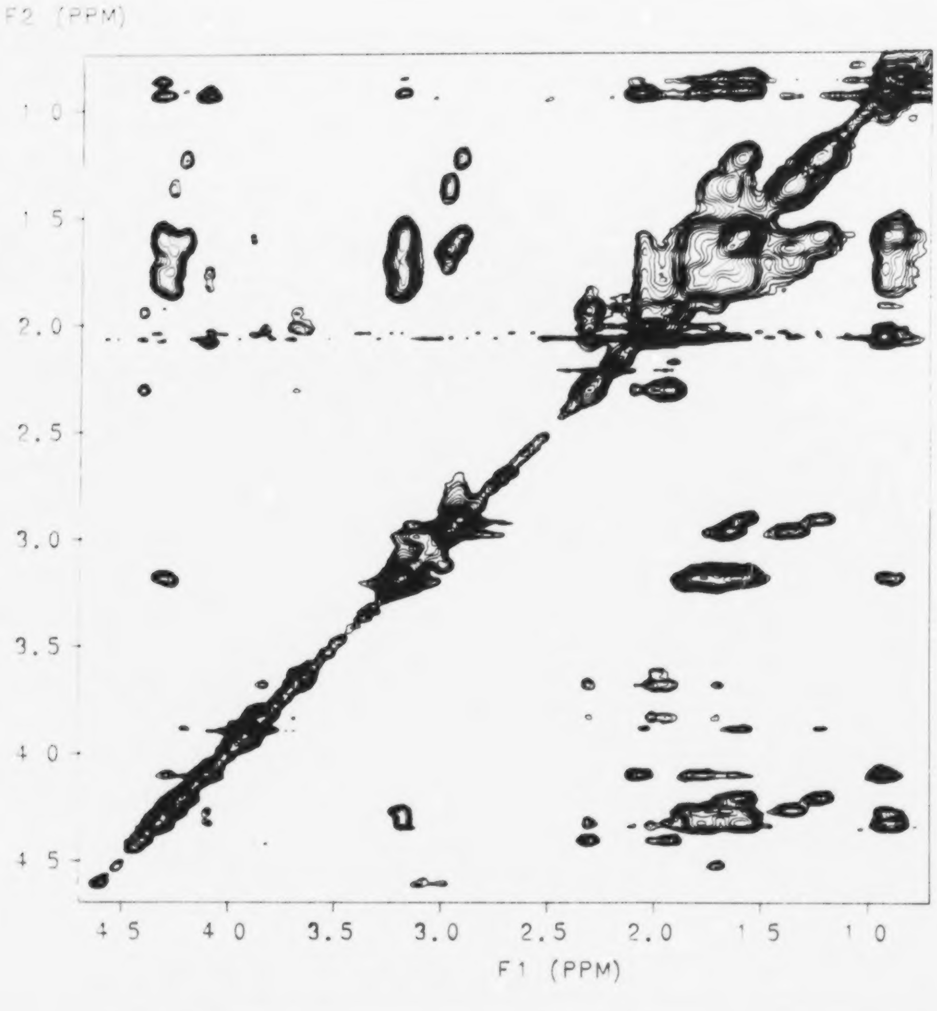

Figure VIII-4. Upfield region of the TRNOESY spectrum of the G110-TnI peptide in the presence of 0.1 molar equivalents TnC.Ca(II)$_4$. (7 mM Nα-acetyl-G110-TnI(104-115) amide, 0.7 mM TnC, 4 mM CaCl$_2$, 50 mM KCl, pH 6.3, 80%H$_2$O/20%D$_2$O, 5°C, τ_m = 500 ms)

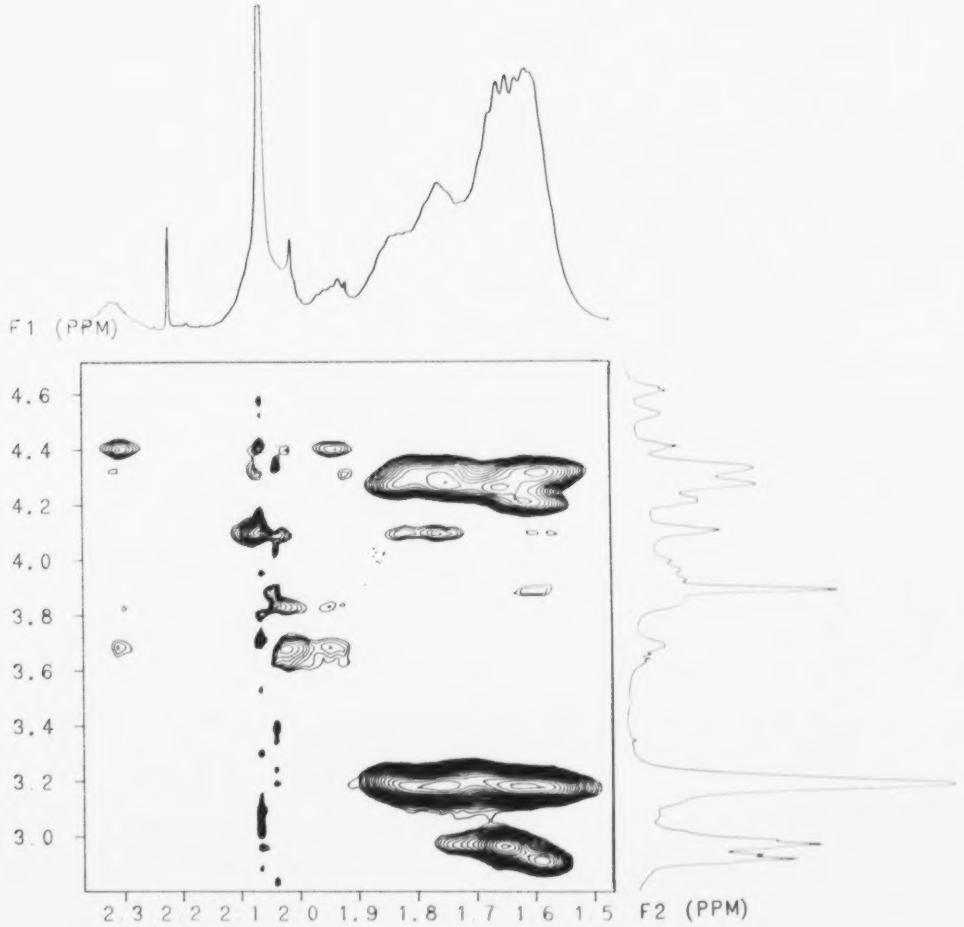

Figure VIII-5. αCH-βCH region of the TRNOESY spectrum of the G110-TnI peptide in the presence of 0.1 molar equivalents TnC.Ca(II)$_4$. (7 mM Nα-acetyl-G110-TnI(104-115) amide, 0.7 mM TnC, 4 mM CaCl$_2$, 50 mM KCl, pH 6.3, 80%H$_2$O/20%D$_2$O, 5°C, τ_m = 500 ms)

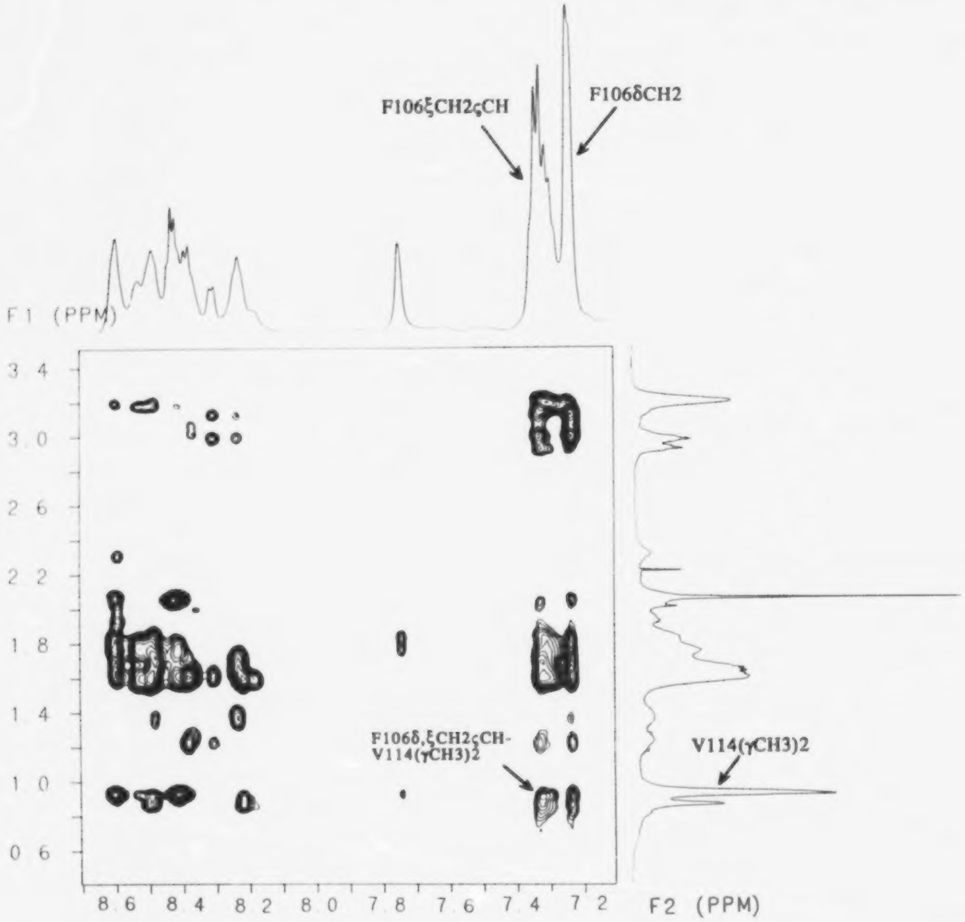

Figure VIII-6. Downfield-βCH region of the TRNOESY spectrum of the G110-TnI peptide in the presence of 0.1 molar equivalents TnC.Ca(II)$_4$. (7 mM Nα-acetyl-G110-TnI(104-115) amide, 0.7 mM TnC, 4 mM $CaCl_2$, 50 mM KCl, pH 6.3, 80%H_2O/20%D_2O, 5°C, τ_m = 500 ms)

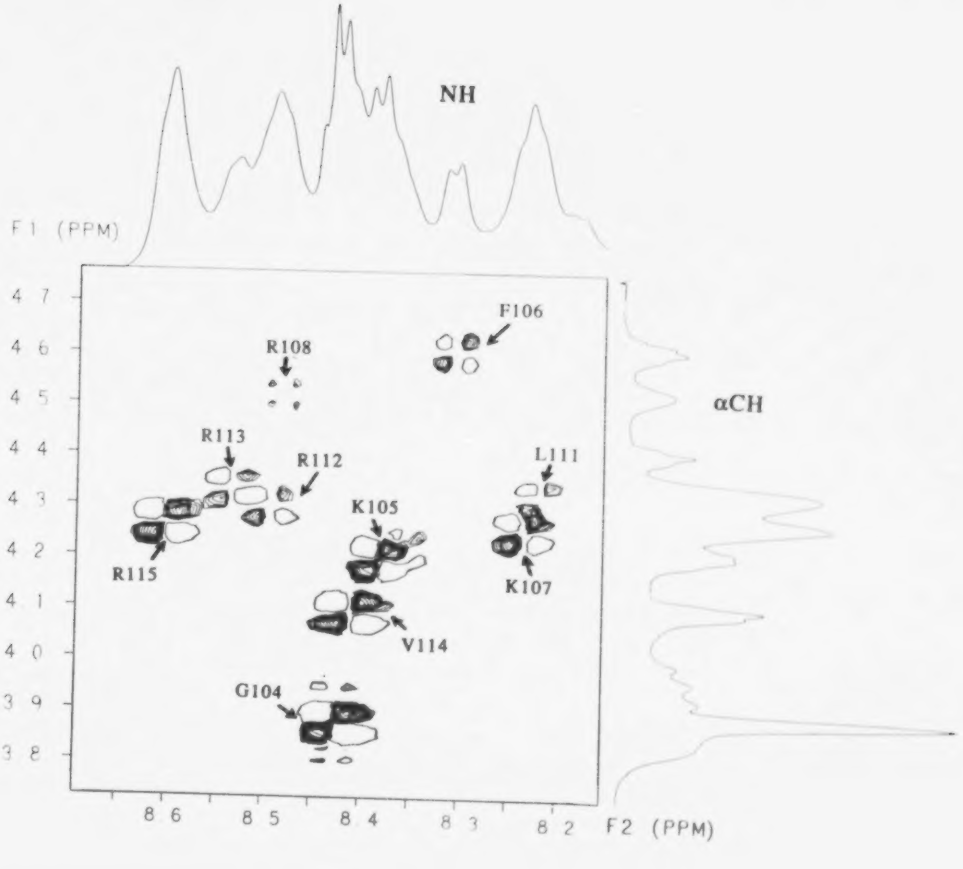

Figure VIII-7. αCH-NH region of the DQFCOSY spectrum of the G110-TnI peptide in the presence of 0.1 molar equivalents TnC.Ca(II)$_4$. (7 mM Nα-acetyl-G110-TnI(104-115) amide, 0.7 mM TnC, 4 mM $CaCl_2$, 50 mM KCl, pH 6.3, 80%H_2O/20%D_2O, 5°C)

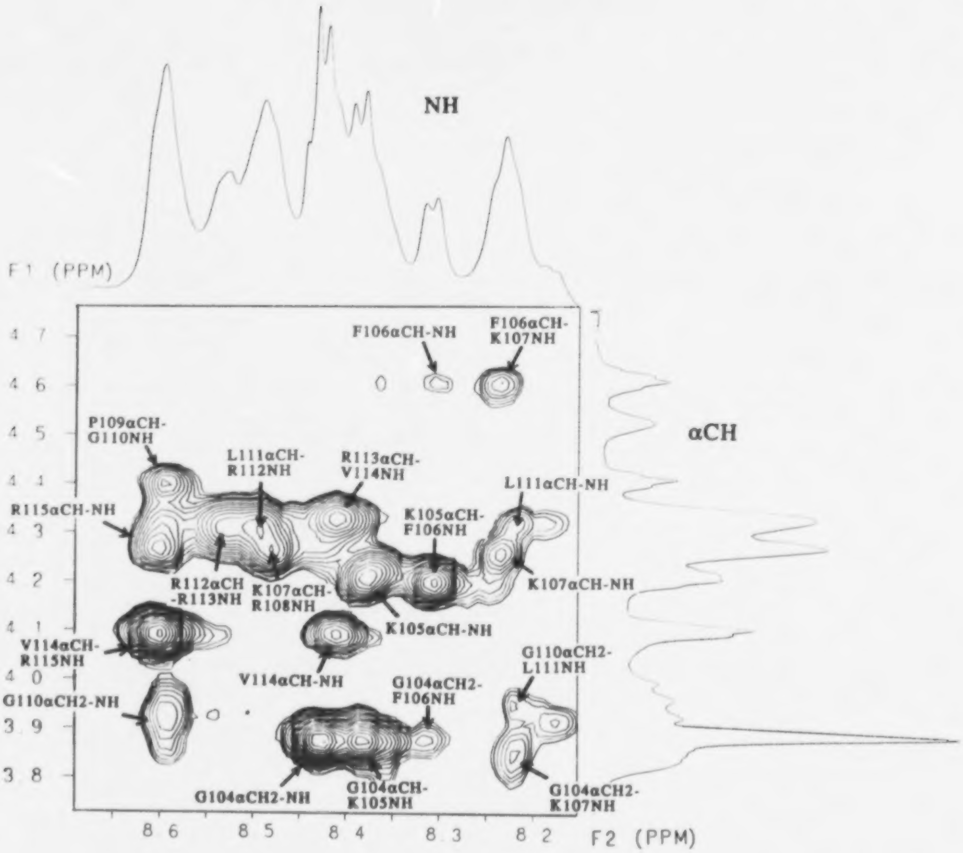

Figure VIII-8. αCH-NH region of the TRNOESY spectrum of the G110-TnI peptide in the presence of 0.1 molar equivalents TnC.Ca(II)$_4$. (7 mM Nα-acetyl-G110-TnI(104-115) amide, 0.7 mM TnC, 4 mM CaCl$_2$, 50 mM KCl, pH 6.3, 80%H$_2$O/20%D$_2$O, 5°C, τ_m = 500 ms)

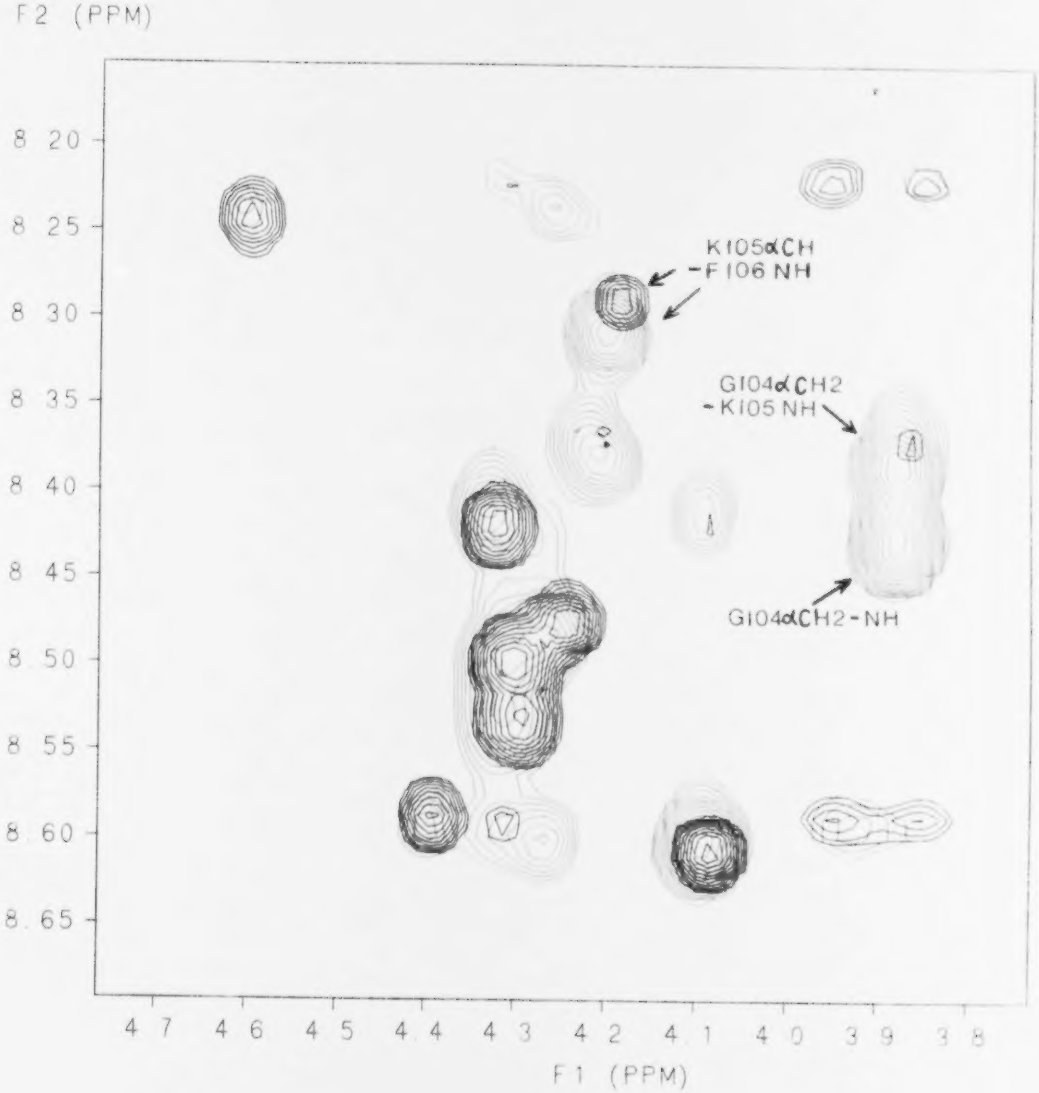

Figure VIII-9. Fingerprint αCH-NH region of the NOESY spectrum of the G110-TnI peptide (shown in black contours) superimposed upon the αCH-NH region of the TRNOESY spectrum of the same concentration G110-TnI peptide in the presence of 0.1 molar equivalents TnC.Ca(II)$_4$ (shown in red contours). Both spectra are plotted at the same vertical scale. (τ_m = 500 ms)

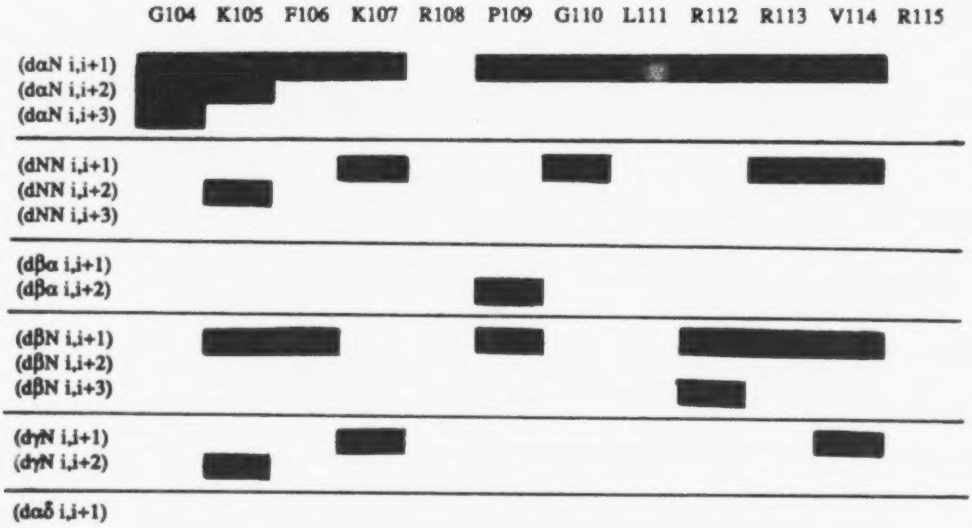

Figure VIII-10. Sequence of Nα-acetyl-G110-TnI(104-115) amide together with a schematic summary of the short- and medium- range TRNOEs defining the secondary structure of the peptide bound to TnC.

Figure VIII-11. Plot of $^{3}J\alpha$CH-NH coupling constants versus molar equivalents TnC.Ca(II)$_4$ for various residues in the G110-TnI peptide.

A. (●) G104NH; (○) K105NH; (■) F106NH; (□) K107NH.

B. (○) R108NH; (●) G110NH; (■) L111NH.

C. (○) R112NH; (●) R113NH; (□) R115NH.

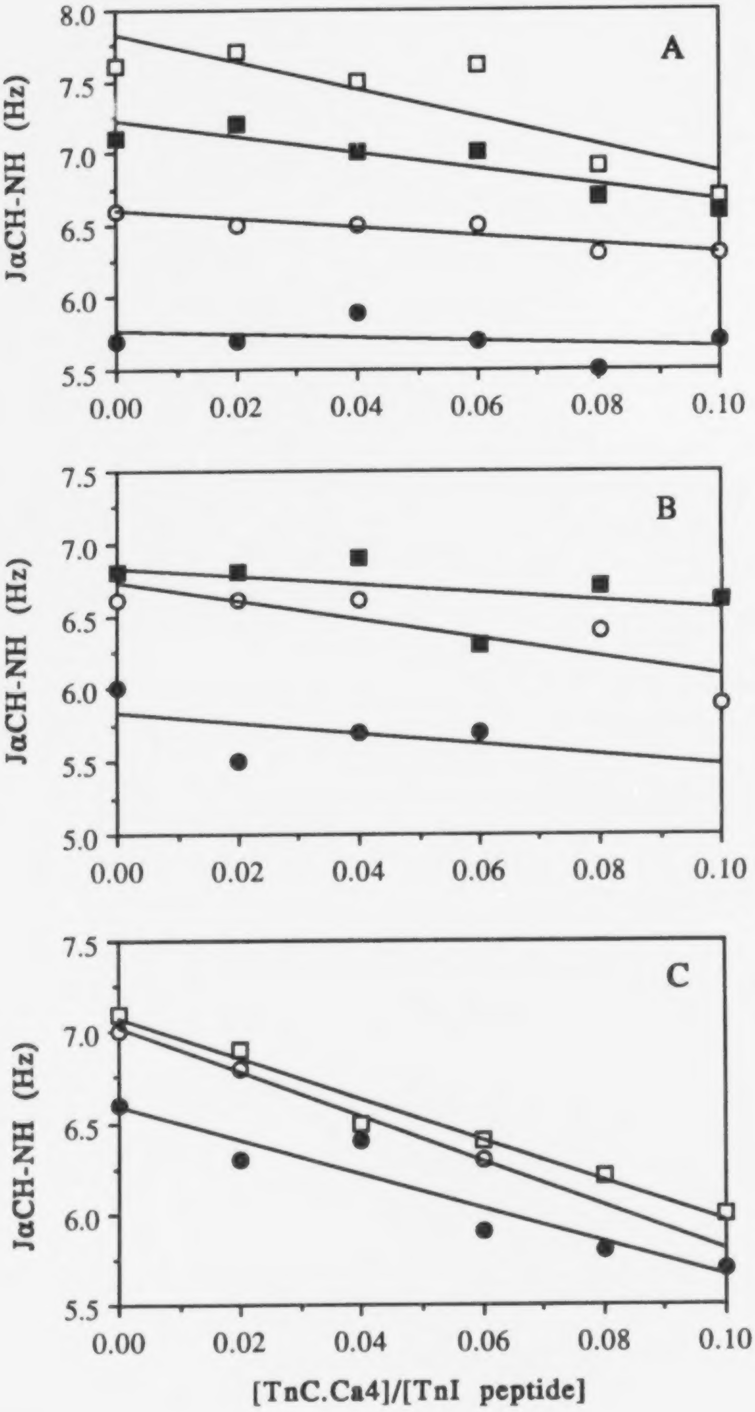
A
B
C
JαCH-NH (Hz)
8.0
7.5
7.0
6.5
6.0
5.5
5.0
0.00
0.02
0.04
0.06
0.08
0.10
[TnC.Ca4]/[TnI peptide]

Figure VIII-12. Plot of δNH versus temperature for **A, B.** 0.0 molar equivalents; and **C, D.** 0.1 molar equivalents.of TnC.Ca(II)$_4$ to G110-TnI peptide.

A. (☐) G104NH; (■) K105NH; (○) F106NH; (●) K107NH; (▲) R108NH; (△) G110NH.

B. (●) L111NH; (■) R112NH; (☐) R113NH; (○) V114NH; (▲) R115NH.

C. (☐) G104NH; (■) K105NH; (○) F106NH; (●) K107NH; (▲) R108NH; (△) G110NH.

D. (●) L111NH; (■) R112NH; (☐) R113NH; (○) V114NH; (▲) R115NH.

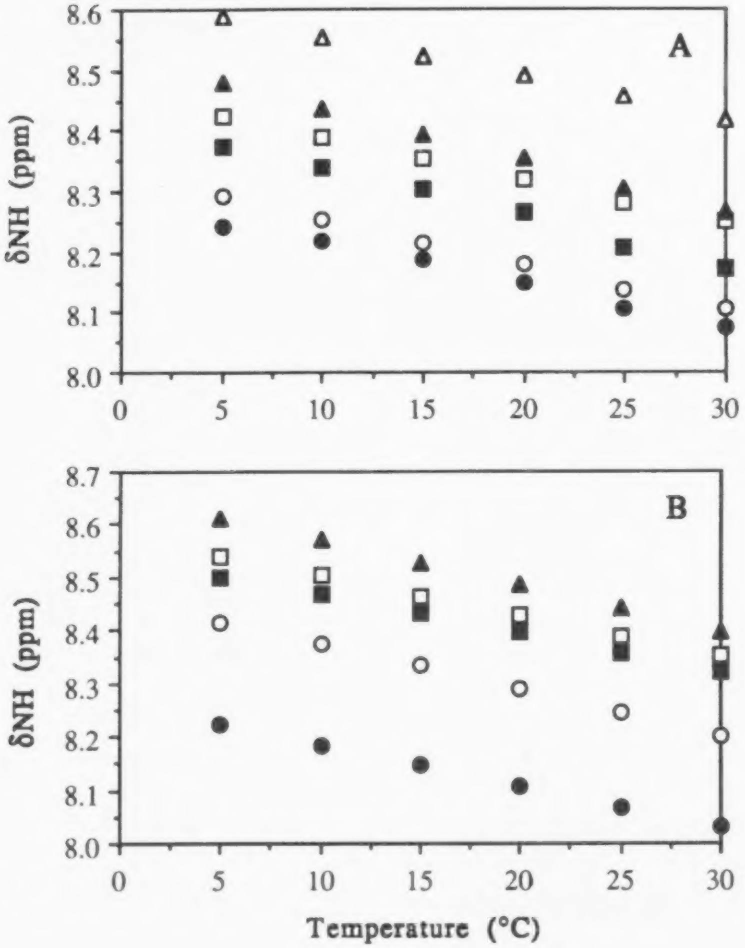
A
B
δNH (ppm)
8.0
8.1
8.2
8.3
8.4
8.5
8.6
8.7
0
5
10
15
20
25
30
Temperature (°C)

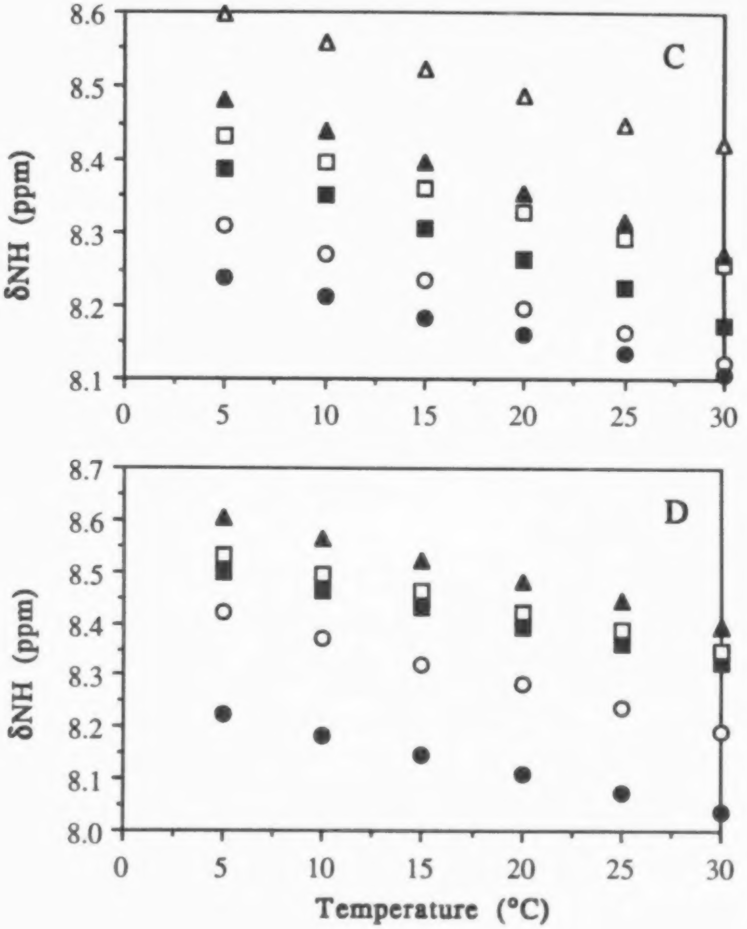
C
D
δNH (ppm)
8.6
8.5
8.4
8.3
8.2
8.1
δNH (ppm)
8.7
8.6
8.5
8.4
8.3
8.2
8.1
8.0
0
5
10
15
20
25
30
Temperature (°C)

Figure VIII-13. Plot of the temperature coefficients measured for various G110-TnI peptide backbone amide protons versus molar equivalents TnC.Ca(II)$_4$.

A. (○) G104NH; (■) K105NH; (□) F106NH; (●) K107NH; (△) R108NH.

B. (○) G110NH; (□) L111NH; (●) R112NH; (■) R113NH; (△) V114NH; (▲) R115NH.

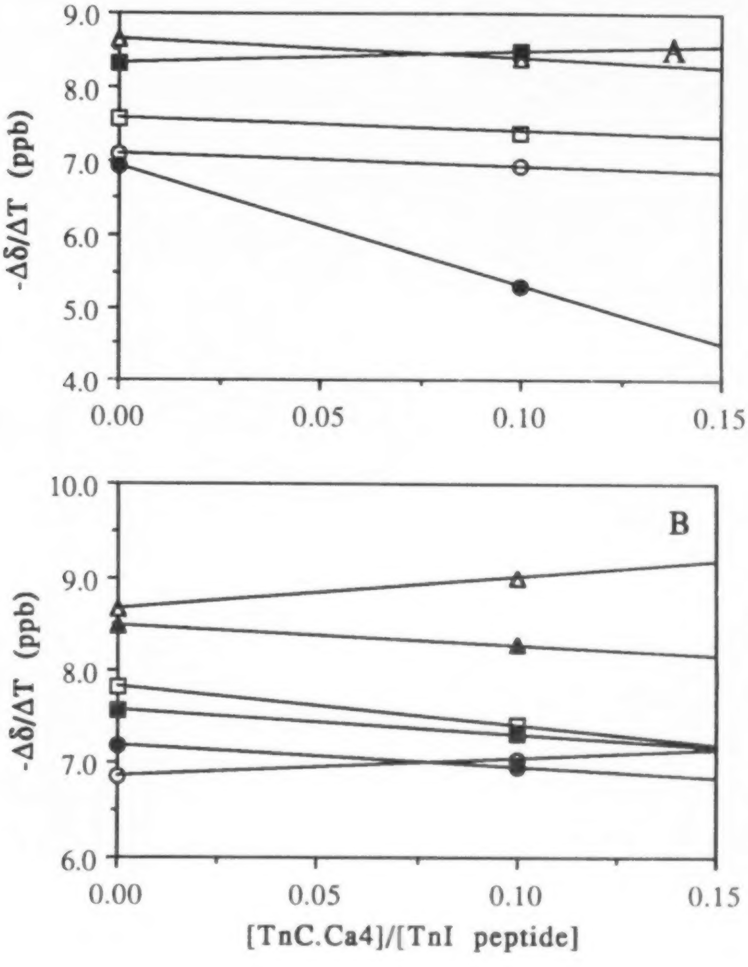
A
B
-Δδ/ΔT (ppb)
9.0
8.0
7.0
6.0
5.0
4.0
10.0
0.00
0.05
0.10
0.15
[TnC.Ca4]/[TnI peptide]

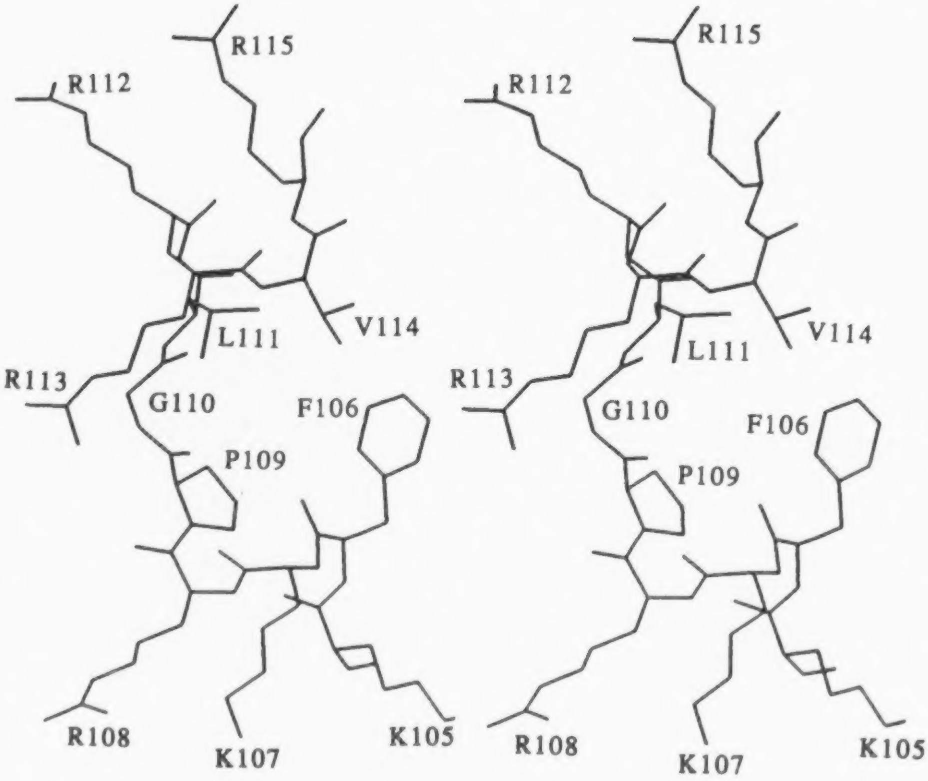
R115
R112
V114
L111
R113
G110
F106
P109
R108
K107
K105
R115
R112
L111
V114
R113
G110
F106
P109
R108
K107
K105

Figure VIII-14. Stereo-diagram of the G110-TnI peptide bound to Ca(II)-saturated TnC. The final structure was generated from a set of α-helical input coordinates. Following 12 ps of MD, the coordinates of 10 MD structures taken every 0.2 ps were averaged and the averaged coordinates were energy minimized to produce the final structure in the figure.

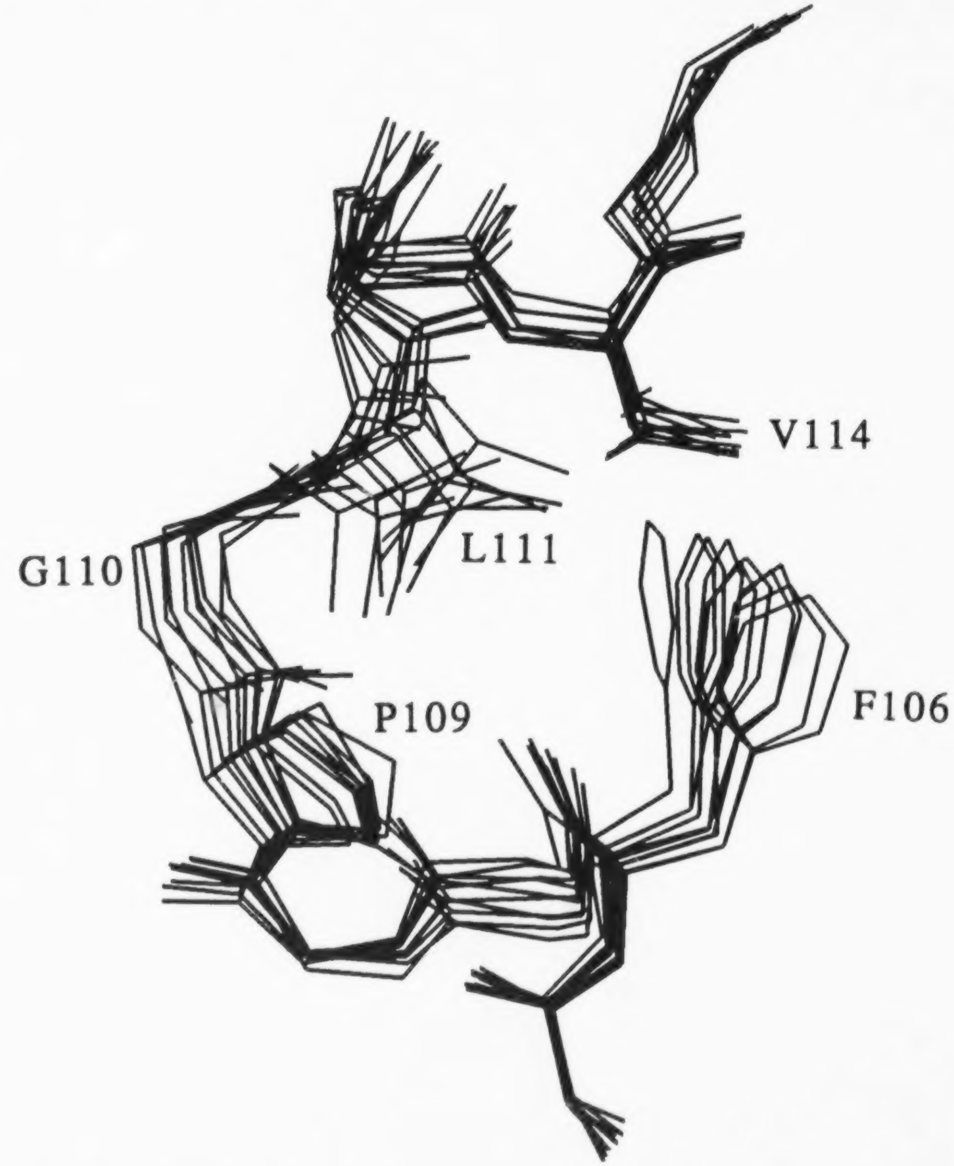
V114
L111
G110
P109
F106

Figure VIII-15. Superposition of the 10 MD structures taken every 0.2 ps.

F. References

ANDERSEN, N.H., EATON, H.L., and NGUYEN, K.T. 1987. Small molecule conformation in the receptor-bound state by two-dimensional spin exchange experiment. Magn. Reson. in Chem. **25**: 1025-1034.

ANGLISTER, J., LEVY, R.H., and SCHERF, T. 1989. Interactions of antibody aromatic residues with a peptide of cholera toxin observed by two-dimensional transferred nuclear Overhauser effect difference spectroscopy. Biochemistry **28**: 3360-3365.

ANGLISTER, J., and ZILBER, B. 1990. Antibodies against a peptide of cholera toxin differing in cross-reactivity with the toxin differ in their specific interactions with the peptide as observed by ^{1}H NMR spectroscopy. Biochemistry **29**: 921-928.

BABU, Y.S., BUGG, C.E., and COOK, W.J. 1988. Structure of calmodulin refined at 2.2 Å resolution. J. Mol. Biol. **204**: 191-204.

BANERJEE, A., LEVY, H.R., LEVY, G.C., and CHAN, W.W.C. 1985. Conformations of bound nucleoside triphosphate effectors in aspartate transcarbamylase. Evidence for the London-Schmidt model by transferred nuclear Overhauser effects. Biochemistry **24**: 1593-1597.

BELIVACQUA, V.L., THOMSON, D.S., and PRESTEGARD, J.H. 1990. Conformation of methyl β-lactoside bound to ricin B-chain. Interpretation of transferred nuclear Overhauser effects facilitated by spin simulation and selective deuteration. Biochemistry **29**: 5529-5537.

BERENDSEN, H.J.C., POSTMA, J.P.M., VAN GUNSTEREN, W.F., DINOLA, A., and HAAK, J.R. 1984. Molecular dynamics with coupling to an external bath. J. Chem. Phys. **81**: 3684-3690.

BILLETER, M., BRAUN, W., and WUTHRICH, K. 1982. Sequential resonance assignments in protein ^{1}H nuclear magnetic resonance spectra. Computation of sterically allowed proton-proton distances and statistical analysis of proton-proton distances in single crystal protein conformations. J. Mol. Biol. **155**: 321-346.

CACHIA, P.J., SYKES, B.D., and HODGES, R.S. 1983. Calcium-dependent inhibitory region of troponin. A proton magnetic resonance study on the interaction between troponin C and the synthetic peptide Nα-acetyl [F-phenylalanine106] TnI (104-115) amide. Biochemistry **22**: 4145-4152.

CACHIA, P.J., SYKES, B.D., and HODGES, R.S. 1985. Structural studies on calmodulin and troponin C. Phenothiazine, peptide, and protein interactions with calcium-induced helices. In *Calmodulin Antagonist and Cellular Physiology* (Hidaka, H., and Hartshorne, D.J., Eds.), Chapt. 5, pp 63-88, Academic Press, New York.

CACHIA, P.J., VAN EYK, J., INGRAHAM, R.H., MCCUBBIN, W.D., KAY, C.M., and HODGES, R.S. 1986. Calmodulin and troponin C. A comparative study of the interaction of mastoparan and troponin I inhibitory peptide [104-115]. Biochemistry **25**: 3553-3562.

CADAY, C.G., and STEINER, R.F. 1986. Interaction of calmodulin with melittin. Biochem. Biophys. Res. Commun. **135**: 419-425.

CAMPBELL, A.P., CACHIA, P.J., and SYKES, B.D. 1991a. Interaction of troponin I and troponin C : ^{19}F NMR studies of the binding of the inhibitory troponin I peptide to turkey skeletal troponin C. Biochem. Cell Biol., in press.

CAMPBELL, A.P., SLUPSKY, C.M., SHAW, G.S., and SYKES, B.D. 1991b. Interaction of troponin I and troponin C : Identification using NMR of specific residues on skeletal troponin C which are involved in the binding of an inhibitory troponin I peptide. Biochemistry, submitted.

CAMPBELL, A.P., and SYKES, B.D. 1991a. Interaction of troponin I and troponin C: Use of the two-dimensional NMR transferred nuclear Overhauser effect to determine the structure of the inhibitory troponin I peptide when bound to skeletal troponin C. J. Mol. Biol., in press.

CAMPBELL, A.P., and SYKES, B.D. 1991b. Theoretical evaluation of the two-dimensional transferred nuclear Overhauser effect. J. Magn. Reson. **93**: 77-92.

CHONG, P.C.S., and HODGES, R.S. 1981. Proximity of sulfhydryl groups to the sites of interaction between components of the troponin complex from rabbit skeletal muscle. J. Biol. Chem. **257**: 2549-2555.

CHONG, P.C.S., ASSELBERGS, P.J., and HODGES, R.S. 1983. Inhibition of rabbit skeletal muscle acto S1-ATPase by troponin T. FEBS Lett. **153**: 372-376.

CLORE, G.M., and GRONENBORN, A.M. 1982a. Theory and applications of the transferred nuclear Overhauser effect to the study of the conformations of small ligands bound to proteins. J. Magn. Reson. **48**: 402-417.

CLORE, G.M., and GRONENBORN, A.M. 1982b. Conformation of NAD^+ bound to yeast and horse liver alcohol dehydrogenase in solution. The use of the proton-proton transferred nuclear Overhauser enhancement. J. Mol. Biol. **157**: 155-160.

CLORE, G.M., and GRONENBORN, A.M. 1983. Theory of the time dependent transferred nuclear Overhauser effect. Applications to structural analysis of ligand-protein complexes in solution. J. Magn. Reson. **53**: 423-442.

CLORE, G.M., and GRONENBORN, A.M. 1984a. Glucose-6-phosphate dehydrogenase: a transferred nuclear Overhauser enhancement study of $NADP^+$ conformations in enzyme-coenzyme binary complexes. FEBS Lett. **172**: 219-225.

CLORE, G.M., and GRONENBORN, A.M. 1984b. An unusual conformation of NAD^+ bound to sorbitol dehydrogenase? A time-dependent transferred nuclear Overhauser effect study. J. Mol. Biol. **172**: 559-572.

CLORE, G.M., and GRONENBORN, A.M. 1984c. Stereochemistry of ATP and GTP bound to fish haemoglobins. A transferred nuclear Overhauser enhancement, ^{31}P nuclear magnetic resonance, oxygen equilibrium and molecular modeling study. J. Mol. Biol. **178**: 731-742.

CLORE, G.M., and GRONENBORN, A.M.. 1986. Stereochemistry of binding of the tetrapeptide acetyl-pro-ala-pro-tyr-NH_2 to porcine pancreatic elastase. Combined use of two-dimensional transferred nuclear Overhauser enhancement measurements, restrained molecular dynamics, x-ray crystallography and molecular modeling. J. Mol. Biol. **190**: 259-267.

COLLINS, J.H., POTTER, J.D., HORN, M.J., WILSHIRE, G., and JACKMAN, N. 1973. The amino acid sequence of rabbit skeletal muscle troponin C. Gene replication and homology with calcium-binding proteins from carp and hake muscle. FEBS Lett. **36**: 268-272.

DESLAURIERS, R., and SMITH, E.C.P. 1980. The multinuclear NMR approach to peptides. Structure, conformations and dynamics. In *Biological Magnetic Resonance* (Berliner, L., and Reuben, J., Eds.), Vol. **2**, pp 243-344, Plenum Press, New York.

DE VLIEG, J., BOELENS, R., SCHEEK, R.M., KAPTEIN, R., and VAN GUNSTEREN, W.F. 1986. Restrained molecular dynamics procedures for protein tertiary structure determination from NMR data: a lac repressor headpiece structure based on information on J-coupling and from presence and absence of NOEs. Israel J. Chem. **27**: 181-188.

DRISCOLL, P.C., CLORE, M.G., BERESS, L., and GRONENBORN, A.M. 1989. Determination of the three-dimensional solution structure of the antihypertensive and antiviral protein BDS-I from the sea anemone *anemonia sulcata*. A study using nuclear magnetic resonance and hybrid distance geometry-dynamical simulated annealing. Biochemistry **28**: 2178-2187.

EBASHI, S., and ENDO, M. 1968. Calcium ion and muscle contraction. Prog. Biophys. Mol. Biol. **18**: 123-183.

ERICKSON, B.W., and MERRIFIELD, R.B.1976. Solid-phase peptide synthesis. In *The Proteins*, (Neurath, H., and Hill, R.L., Eds.), Vol. **2**, pp 255-527, Academic Press, New York.

EHRLICH, R.S., and COLMAN, R.F. 1985. ^{1}H nuclear magnetic resonance studies of the conformation and environment of nucleotides bound to pig heart $NADP^+$-dependent isocitrate dehydrogenase. Biochemistry **24**: 5378-5387.

FUJISAWA, T., UEKI, T., and IIDA, S. 1989. Structural change of the troponin C molecule upon Ca^{+2} binding measured in solution by the x-ray scattering technique. J. Biochem. **105**: 377-383.

GARIEPY, J., and HODGES, R.S. 1983. Primary sequence analysis and folding behaviour of EF hands in relation to the mechanism of action of troponin C and calmodulin. FEBS Lett. **160**: 1-6.

GHELIS, C., and YON, J. 1982. In *Protein Folding*, pp 51, Academic Press, New York.

GLASEL, J.A., and BORER, P.N. 1986. NMR studies of flexible opiate conformations at monoclonal antibody binding sites. I. Transferred nuclear Overhauser effects show bound conformations. Biochem. Biophys. Res. Commun. **141**: 1267-1273.

GLASEL, J.A. 1989. Nuclear magnetic resonance studies of flexible opiate conformations at monoclonal antibody binding sites. Quantitative interproton distances obtained from comparing theoretical and experimental transferred nuclear Overhauser enhancement: correlation with antibody sequence. J. Mol. Biol. **209**: 747-761.

GRABAREK, Z., DRABIKOWSKI, W., LEAVIS, P.C., ROSENFELD, S.S., and GERGELY, J. 1981. Proteolytic fragments of troponin C. Interactions with the other troponin subunits and biological activity. J. Biol. Chem. **256**: 13121-13127.

GREASER, M.C., and GERGELY, J. 1971. Reconstitution of troponin activity from three protein components. J. Biol. Chem. **246**: 4226-4233.

GRONENBORN, A.M., and CLORE, G.M. 1982. Proton nuclear magnetic resonance studies on cyclic nucleotide binding to the *Escherichia coli* adenosine cyclic 3',5'- phosphate receptor protein. Biochemistry **21**: 4040-4048.

GRONENBORN, A.M., and CLORE, G.M. 1985. Investigation of the solution structures of short nucleic acid fragments by means of nuclear Overhauser enhancement measurements. In *Progress in Nuclear Magnetic Resonance Spectroscopy* (J.W. Emsley, J. Feeney, and L.H. Sutcliffe, Eds.), Vol. **17**, pp 1-32, Pergamon Press, Oxford.

HARTSHORNE, D.J., and MUELLER, H. 1968. Fractionation of troponin into two distinct proteins. Biochem. Biophys. Res. Commun. **31**: 647-653.

HEIDORN, D.B., SEEGER, P.A., ROKOP, S.E., BLUMENTHAL, D.K., MEANS, A.R., CRESPI, H., and TREWELLA, J. 1989. Changes in the structure of calmodulin induced by a peptide based on the calmodulin-binding domain of myosin light chain kinase. Biochemistry **28**: 6757-6764.

HERZBERG, O., and JAMES, M.N.G. 1985. Structure of the calcium regulatory muscle protein troponin C at 2.8 Å resolution. Nature **313**: 653-659.

HINCKE, M.T., MCCUBBIN, W.D., and KAY, C.M. 1977. A circular dichroism and biological activity study on the hybrid species formed from bovine cardiac and rabbit skeletal troponin subunits. FEBS Lett. **83**: 131-136.

HITCHCOCK, S.E. 1975. Regulation of muscle contraction. Binding of troponin C involved in calcium ion-dependent interaction with troponin I. Eur. J. Biochem. **52**: 255-263.

HODGES, R.S., SEMCHUCK, P.D., TANEJA, A.K., KAY, C.M., PARKER, J.M.R., and MANT, C.T. 1988. Protein design using model synthetic peptides. Peptide Research **1**: 19-29.

HOLROYDE, M.J., ROBERTSON, S.P., JOHNSON, J.D., SOLARNO, R.J., and POTTER, J.C. 1980. The calcium and magnesium binding sites on cardiac troponin and their role in the regulation of myofibrillar adenosine triphosphatase. J. Biol. Chem. **255**: 11688-11693.

HOULT, D.I. 1976. Solvent peak saturation with single phase and quadrature Fourier transformation. J. Magn. Reson. **21**: 337-347.

HUBBARD, S.R., HODGSON, K.O., and DONIACH, S. 1988. Small angle x-ray scattering investigation of the solution structure of troponin-C. J. Mol. Biol. **263**: 4151-4158.

KLEVIT, R.E., BLUMENTHAL, D.K., WEMMER, D.E., and KREBS, E.G. 1985. Interaction of calmodulin and a calmodulin-binding peptide from myosin light chain kinase. Major spectral changes in both occur as a result of complex formation. Biochemistry **24**: 8152-8157.

KRETSINGER, R.H., and NOCKOLDS, C.E. 1973. Carp muscle-binding protein II. Structure determination and general description. J. Biol. Chem. **248**: 3313-3326.

KRETSINGER, R.H. 1980. Structure and evolution of calcium-modified proteins. CRC Crit. Rev. Biochem. **8**: 119-174.

KRETSINGER, R.H., RUDNICK, S.E., and WEISSMAN, L.J. 1986. Crystal structure of calmodulin. J. Inorg. Biochem. **28**: 289-302.

KATAOKA, M., HEAD, J.F., SEATON, B.A., and ENGELMAN, D.M. 1989. Melittin binding causes a large calcium-dependent conformational change in calmodulin. Proc. Natl. Acad. Sci. USA **86**: 6944-6948.

LAN, J., ALBAUGH, S., and STEINER, R.F. 1989. Interactions of troponin I and its inhibitory fragment (residues 104-115) with troponin C and calmodulin. Biochemistry **28**: 7380-7385.

LANDY, S.B., and RAO, B.D.N. 1989. Dynamical NOE in multiple-spin systems undergoing chemical exchange. J. Magn. Reson. **81**: 371-377.

LAPORTE, D.C., WIERMAN, B.M., and STORM, D.R. 1980. Calcium-induced exposure of a hydrophobic surface on calmodulin. Biochemistry **19**: 3814-3819.

LEAVIS, P.C., and GERGELY, J. 1984. Thin filament proteins and thin filament regulation of vertebrate muscle contraction. CRC Crit. Rev. Biochem. **16**: 235-305.

LESZYK, J., COLLINS, J.H., LEAVIS, P.C., and TAO, T. 1987. Cross-linking of rabbit skeletal muscle troponin with the photoactive reagent 4-maleimidobenzophenone. Identification of residues in troponin I that are close to cys-98 of troponin C. Biochemistry **26**: 7042-7047.

LESZYK, J., COLLINS, J.H., LEAVIS, P.C., and TAO, T. 1988. Cross-linking of rabbit skeletal muscle troponin subunits. Labelling of Cys-98 of troponin C with 4-maleimidobenzophenone and analysis of products formed in the binary complex with troponin T and the ternary complex with troponins I and T. Biochemistry **27**: 6983-6987.

LESZYK, J., GRABAREK, Z., GERGELY, J., and COLLINS, J.H. 1990. Characterization of zero-length cross-links between rabbit skeletal muscle troponin C and troponin I. Evidence for direct interaction between the inhibitory region of troponin I and the NH_2-terminal, regulatory domain of troponin C. Biochemistry **29**: 299-304.

LEVY, H.R., EJCHART, A., and LEVY, G.C. 1983. Conformations of nicotinamide coenzymes bound to dehydrogenases determined by transferred nuclear Overhauser effects. Biochemistry **22**: 2792-2796.

LEVY, H.R., ASSULIN, O., SCHERF, T., LEVITT, M., and ANGLISTER, J. 1989. Probing antibody diversity by 2D NMR. Comparison of amino acid sequences, predicted structures, and observed antibody-antigen interactions in complexes of two antipeptide antibodies. Biochemistry **28**: 7168-7175.

LINSE, S., DRAKENBERG, T., and FORSEN, S. 1986. Mastoparan binding induces a structural change affecting both the N-terminal and C-terminal domains of calmodulin: A ^{113}Cd-NMR study. FEBS Lett. **199**: 28-32.

MACLACHLAN, L.K., REID, D.G., MITCHELL, R.C., SALTER, C.J., and SMITH, S.J. 1990. Binding of a calcium sensitizer, bepridil, to cardiac troponin C. A fluorescence stopped-flow kinetic, circular dichroism, and proton nuclear magnetic resonance study. J. Biol. Chem. **265**: 9764-9770.

MACURA, S., and ERNST, R.R. 1980. Elucidation of cross-relaxation in liquids by two-dimensional NMR spectroscopy. Mol. Phys. **41**: 95-117.

MANT, C.T., BURKE, T.W.L., and HODGES, R.S. 1987. Optimization of peptide separations in reversed-phase HPLC: Isocratic versus gradient elution. Chromatographia **24**: 565-572.

MATSUSHIMA, N., IZUMI, Y., MATSUO, T., YOSHINO, H., UEKI, T., and MIYAKE, Y. 1989. Binding of both Ca^{+2} and mastoparan to calmodulin induces a large change in the tertiary structure. J. Biochem. **105**: 883-887.

MCCUBBIN, W.D., OIKAWA, K., SYKES, B.D., and KAY, C.M. 1982. Purification and characterization of troponin C from pike muscle: a comparative spectroscopic study with rabbit skeletal muscle troponin C. Biochemistry **21**: 5948-5956.

MEYER, E.F., CLORE, G.M., GRONENBORN, A.M., and HANSEN, H.A.S. 1988. Analysis of an enzyme-substrate complex by x-ray crystallography and transferred nuclear Overhauser enhancement measurements. Porcine pancreatic elastase and a hexapeptide. Biochemistry **27**: 725-730.

MILON, A., MIYAZAWA, T., and HIGASHIJIMA, T. 1990. Transferred nuclear Overhauser effect analyses of membrane-bound enkephalin analogues by ^1H nuclear magnetic resonance. Correlation between activities and membrane-bound conformations. Biochemistry **29**: 65-75.

NI, F., KONISHI, Y., FRAZIER, R.B., SCHERAGA, H.A., and LORD, S.T. 1989a. High-resolution NMR studies of fibrinogen-like peptides in solution. Interaction of thrombin with residues 1-23 of the Aα chain of human fibrinogen. Biochemistry **28**: 3082-3094.

NI, F., MEINWALD, Y.C., VASQUEZ, M., and SCHERAGA, H.A. 1989b. High-resolution NMR studies of fibrinogen-like peptides in solution. Structure of a thrombin-bound peptide corresponding to residues 7-16 of the Aα chain of human fibrinogen. Biochemistry **28**: 3094-3105.

NI, F., KONISHI, Y., BULLOCK, C.D., RIVETNA, M.N., and SCHERAGA, H.A. 1989c. High-resolution NMR studies of fibrinogen-like peptides in solution. Structural basis for the bleeding disorder caused by a single mutation of Gly(12) to Val(12) in the Aα chain of human fibrinogen Rouen. Biochemistry **28**: 3106-3119.

NI, F., KONISHI, Y., and SCHERAGA, H.A. 1990. Thrombin-bound conformation of the C-terminal fragments of hirudin determined by transferred nuclear Overhauser effects. Biochemistry **29**: 4479-4489.

OTTING, G., WIDMER, H., WAGNER, G., and WUTHRICH, K. 1986. Origin of t_1 and t_2 ridges in 2D NMR spectra and procedures for suppression. J. Magn. Reson. **66**: 187-193.

PARDI, A., BILLETER, M., and WUTHRICH, K. 1984. Calibration of the angular dependence of the amide proton-Cα proton coupling constants, $^3J_{HN\alpha}$, in a globular protein. J. Mol. Biol. **180**: 741-751.

PARKER, J.M.R., MANT, C.T., and HODGES, R.S. 1987. A practical approach to the preparative purification of peptides using analytical instrumentation with analytical and semipreparative columns. Chromatographia **24**: 832-838.

PERRY, S.V., COLE, H., HEAD, J.F., and WILSON, F.J. 1972. Localization and mode of action of the inhibitory protein component of the troponin complex. Cold Spring Harbor Symp. Quant. Biol. **37**: 251-262.

PERSECHINI, A., and KRETSINGER, R.H. 1988. The central helix of calmodulin functions as a flexible tether. J. Biol. Chem. **263**: 12175-12178.

PIATINI, U., SORENSON, O.W., and ERNST, R.R. 1982. Multiple quantum filters for elucidating NMR coupling networks. J. Am. Chem. Soc. **104**: 6800-6801.

POTTER, J.D., and GERGELY, J. 1974. Troponin, tropomyosin and actin interactions in the Ca^{+2} regulation of muscle contraction. Biochemistry **13**: 2697-2703.

POTTER, J.D., and GERGELY, J. 1975. The calcium and magnesium binding sites on troponin and their role in the regulation of myofibrillar adenosine trophosphatase. J. Biol. Chem. **250**: 4628-4633.

POTTER, J.D., SEIDEL, J.C., LEAVIS, P., LEHRER, S.S., and GERGELY, J. 1976. Effect of Ca^{2+} binding on troponin C. Changes in spin label mobility, extrinsic fluorescence and sulfhydryl reactivity. J. Biol. Chem. **251**: 7551-7556.

RANCE, M., SORENSON, O.W., BODENHAUSEN, G., WAGNER, G., ERNST, R.R., and WUTHRICH, K. 1983. Improved spectral resolution in COSY ^1H NMR spectra of proteins via double quantum filtering. Biochem. Biophys. Res. Commun. **117**: 479-485.

REID, D.G., MACLACHLAN, L.K., GAJJAR, K., VOYLE, M., KING, R.J., and ENGLAND, P.J. 1990. A proton nuclear magnetic resonance and molecular modeling study of calmidazolium (R24571) binding to calmodulin and skeletal muscle troponin C. J. Biol. Chem. **265**: 9744-9753.

RUEGG, J.C., ZEUGNER, C., VAN EYK, J., KAY, C.M., and HODGES, R.S. 1989. Inhibition of TnI-TnC interaction and contraction of skinned muscle fibres by the synthetic peptide TnI(104-115). Pfluger Arch. **414**: 430-436.

RUEGG, J.C., ZEUGNER, C., VAN EYK, J.E., HODGES, R.S., and TRAYER, I.P. 1991. Myosin and troponin peptides affect calcium sensitivity of skinned muscle fibres. In *Peptides as Probes in Muscle Research* (Ruegg, J.C., Ed.), pp 95-109, Springer-Verlag, Heidelberg.

RYCKAERT, J.P., COCCOTTI, G., and BERENDSEN, H.J.C. 1977. Numerical integration of the Cartesian equations of motion of a system with constraints: molecular dynamics of n-alkanes. J. Comput. Phys. **23**: 327-337.

SCHAUB, M.C., and PERRY, S.V. 1969. The relaxing protein system of striated muscle. Biochem. J. **115**: 993-1004.

SEEHOLZER, S.H., COHN, M., PUTKEY, J.A., MEANS, A.R., and CRESI, H.L. 1986. NMR studies of a complex of deuterated calmodulin with melittin. Proc. Natl. Acad. Sci. USA **83**: 3634-3638.

SEEHOLZER, S.H., and WAND, J.A. 1989. Structural characterization of the interactions between calmodulin and skeletal muscle myosin light chain kinase: Effect of peptide(576-594)G binding on the Ca^{2+}-binding domains. Biochemistry **28**: 4011-4020.

STATES, D.J., HABERKORN, R.A., and RUBEN, D.J. 1982. Two-dimensional nuclear Overhauser experiment with pure phase absorption phase in four quadrants. J. Magn. Reson. **48**: 286-292.

STEINER, R.F., and NORRIS, L. 1987. Interaction of melittin with troponin C. Arch. of Biochem. and Biophys. **254**: 342-352.

STRAPANS, I., TAKAHASHI, H., RUSSELL, M.P., and WATANABE, S. 1972. Skeletal and cardiac troponins and their components. J. Biochem. (Tokyo) **72**: 723-735.

STRYNADKA, N.C.J., and JAMES, M.N.G. 1990. Model for the interaction of amphiphilic helices with troponin C and calmodulin. Proteins **7**: 234-248.

SUNDARALINGAM, M., BERGSTROM, R., STRASBURG, G., RAO, S.T., GREASER, M., and WANG, B.C. 1985. Molecular structure of troponin C from chicken skeletal muscle at 3 Å resolution. Science **227**: 945-948.

TALBOT, J.A., and HODGES, R.S. 1979. Synthesis and biological activity of an icosapeptide analog of the actomyosin ATPase inhibitory region of troponin I. J. Biol. Chem. **254**: 3720-3723.

TALBOT, J.A., and HODGES, R.S. 1981a. Comparative studies on the inhibitory region of selected species of troponin I. The use of synthetic peptide analogs to probe structure function relationships. J. Biol. Chem. **256**: 12374-12378.

TALBOT, J.A., and HODGES, R.S. 1981b. Synthetic studies on the inhibitory region of rabbit skeletal troponin I. Relationship of amino acid sequence to biological activity. J. Biol. Chem. **256**: 2798-3802.

TAO, T., GOWELL, E., STRASBURG, G.M., GERGELY, J. , and LEAVIS, P.L. 1989. Ca^{+2} dependence of the distance between Cys-98 of troponin C and Cys-133 of troponin I in the ternary troponin complex. Resonance energy transfer measurements. Biochemistry **28**: 5902-5908.

VAN EYK, J.E., and HODGES, R.S. 1987. Calmodulin and troponin C: affinity chromatographic study of divalent cation requirements for troponin I peptide (residues 104-115), mastoparan and fluphenazine binding. Biochem. Cell. Biol. **65**: 982-988.

VAN EYK, J.E., and HODGES, R.S. 1988. The biological importance of each amino acid residue of the troponin I inhibitory sequence 104-115 in the interaction with troponin C and tropomyosin-actin. J. Biol. Chem. **263**: 1726-1732.

VAN EYK, J.E., KAY, C.M., and HODGES, R.S. 1991. A comparative study of the interactions of synthetic peptides of the skeletal and cardiac TnI inhibitory region with skeletal and cardiac TnC. Biochemistry, submitted.

VANAMAN, T.C., SHARIEL, F., and WATTERSON, D.M. 1977. Structural homology between brain modulator protein and muscle TnCs. In *Calcium-Binding Proteins and Calcium Function* (Wasserman, R.H., *et al.*, Eds.), pp 107-116, Elsevier, Amsterdam.

WAGNER, G., and WUTHRICH, K. 1982. Sequential resonance assignments in protein ^1H nuclear magnetic resonance spectra. Basic pancreatic trypsin inhibitor. J. Mol. Biol. **155**: 347-366.

WAGNER, G., BRAUN, W., HAVEL, T.E., SCHAUMANN, T., GO, N., and WUTHRICH, K. 1987. Protein structures in solution by nuclear magnetic resonance and distance geometry. The protein fold of the basic pancreatic trypsin inhibitor determined using two different algorithms, DISGEO and DISMAN. J. Mol. Biol. **196**: 611-639.

WANG, C.K., and CHEUNG, H.C. 1985. Energetics of the binding of calcium and troponin I to troponin C from rabbit skeletal muscle. Biophys. J. **48**: 727-739.

WANG, Z., SARKAR, S., GERGELY, J., and TAO, T. 1990. Ca^{+2}-dependent interactions between the c-helix of troponin C and troponin I. J. Biol. Chem. **265**: 4953-4957.

WEEKS, R.A, and PERRY, S.V. 1978. Characterization of a region of the primary sequence of troponin C involved in calcium ion-dependent interaction with troponin I. Biochem. J. **173**: 449-457.

WILLIAMSON, M.P., and NEUHAUS, D. 1987. Symmetry in NOE spectra. J. Magn. Reson. **72**: 369-375.

WUTHRICH, K., WIDER, G., WAGNER, G., and BRAUN, W. 1982. Sequential resonance assignments as a basis for determination of spatial protein structures by high resolution proton nuclear magnetic resonance. J. Mol. Biol. **155**: 311-319.

WUTHRICH, K., BILLETER, M., and BRAUN, W. 1983. Pseudo-structures for the 20 common amino acids for use in studies of protein conformations by measurements of intramolecular proton-proton distance constraints with nuclear magnetic resonance. J. Mol. Biol. **169**: 949-961.

WUTHRICH, K. 1986. In *NMR of Proteins and Nucleic Acids*, pp 123-128. John Wiley and Sons, New York.

YAZAWA, M., IKURA, M., HIKICHI, K., YING, L., and YAGI, K. 1987. Communication between two globular domains of calmodulin in the presence of mastoparan or caldesmon fragment. J. Biol. Chem. **262**: 10951-10954.

YOSHINO, H., MINARI, O., MATSUSHIMA, N., UEKI, T., MIYAKE, Y., MATSUO, T., and IZUMI, Y. 1989. Calcium-induced shape change of calmodulin with mastoparan studied by solution x-ray scattering. J. Biol. Chem. **264**: 19706-19709.

ZOT, A.S., and POTTER, J.D. 1987. Structural aspects of troponin-tropomyosin regulation of skeletal muscle contraction. Annu. Rev. Biophys. Chem. **16**: 535-559.

UNIVERSITY OF ALBERTA

NMR STUDIES OF THE INTERACTIONS BETWEEN PROTEINS IN THE THIN FILAMENT OF MUSCLE

BY

ANN PATRICIA CAMPBELL ©

A thesis submitted to the Faculty of Graduate Studies and Research in partial fulfillment of the requirements for the degree of DOCTOR OF PHILOSOPHY

DEPARTMENT OF BIOCHEMISTRY

EDMONTON, ALBERTA

SPRING, 1992

Chapter Page

IX. Role of Amphiphilicity in the Binding of Target Peptides to Troponin C: An NMR Comparison of the Structures of Mastoparan and the Inhibitory Troponin I Peptide in the Helix Inducing Solvent Trifluoroethanol versus when Bound to Skeletal Troponin C.......... 333
A. Introduction.......... 334
B. Theory.......... 336
C. Materials and Methods.......... 338
  1. Sample Preparation.......... 338
    a. Materials.......... 338
    b. Amino Acid Analysis.......... 338
    c. Peptide Synthesis and Purification.......... 338
    d. Preparation of TnC.......... 338
    e. Preparation of Desalted, Apo TnC.......... 338
    f. Preparation of TnI Peptide ^{1}H NMR samples.......... 338
  2. Nuclear Magnetic Resonance Spectroscopy.......... 339
  3. Transformation of ^{1}H NMR TRNOESY Peak Intensity to Distance Restraints.......... 339
  4. Dihedral Angle Restraints and Supplemental Distance Restraints.......... 341
  5. Stereospecific Assignments from ^{1}H NMR.......... 341
  6. Restrained Molecular Dynamics Calculations.......... 342
D. Results.......... 343
  1. Sequential Resonance Assignments and NOEs.......... 343
    a. TnI Peptide in 50%TFE.......... 344
    b. Mastoparan in 50%TFE.......... 344
    c. Mastoparan in the Presence of 0.1 Molar Equivalents $TnC.Ca(II)_4$.......... 345
  2. Secondary Structure.......... 347
    a. TnI Peptide in 50%TFE.......... 347
    b. Mastoparan in 50%TFE.......... 347
    c. Mastoparan in the Presence of 0.1 Molar Equivalents $TnC.Ca(II)_4$.......... 348
  3. Distance Determination.......... 348

4. Dihedral Angle Restraints 349
5. Molecular Dynamics Calculation 349
E. Discussion 351
F. References 401

X. Conclusions and Future Research Directions 410
A. Summary 411
B. Future Research Directions 413
C. Transferred Iterative Relaxation Matrix Approach (TR-IRMA) from Proton-Proton Transferred NOEs: Refinement of the Structure of the Inhibitory Troponin I Peptide Bound to Troponin C 415
1. Theory 416
2. Methodology 419
a. Calculation of a Population-Weighted Average Relaxation Matrix, $\mathbf{R}(p_B)$ 420
b. Diagonalization of the Population-Weighted Average Relaxation Matrix, $\mathbf{R}(p_B)$ 421
c. Calculation of a Mixed Matrix of Mixing Coefficients, $\mathbf{A}_{\mathbf{mix}}(\tau_m, p_B)$, with Calculated and Experimental Elements 421
d. Diagonalization of the Mixed Matrix of Mixing Coefficients, $\mathbf{A}_{\mathbf{mix}}(\tau_m, p_B)$ 422
e. Averaging over Mixing Time, τ_m 422
f. Averaging over Fraction Bound, p_B 423
g. Conversion of $W_{ij}B_{mix}$ Matrix Elements to Bound Distance Restraints 423
h. Restrained Molecular Dynamics 423
3. Simulated Versus Experimental Results 424
D. References 428

List of Tables Page

Table IX-1 Chemical shifts for the assigned ^1H resonances of the TnI peptide in 50%TFE........ 356
Table IX-2 Chemical shifts for the assigned ^1H resonances of mastoparan in 50%TFE........ 356
Table IX-3 Chemical shifts for the assigned ^1H resonances of mastoparan in the presence of 0.1 molar equivalents $TnC.Ca(II)_4$........ 357
Table IX-4. Dihedral angle values in the final structure of the TnI peptide in 50%TFE generated from (a) α-helix (structure 1), and (b) β-strand (structure 2)........ 358
Table IX-5 Dihedral angle values in the final structure of mastoparan in 50%TFE generated from (a) α-helix (structure 1), and (b) β-strand (structure 2)........ 359

List of Figures

Figure IX-1A 500 MHz ^{1}H NMR spectra of the TnI peptide in H_20 and 50%TFE: Aliphatic upfield region of the spectrum.................... 360

Figure IX-1B 500 MHz ^{1}H NMR spectra of the TnI peptide in H_20 and 50%TFE: Complete downfield region of the spectrum with the exchangeable guanidinium resonances of R108, R112, R113 and R115 and the aromatic F106 resonances............................ 361

Figure IX-1C 500 MHz ^{1}H NMR spectra of the TnI peptide in H_20 and 50%TFE: Expanded region of spectrum B showing the backbone amide proton resonances and the C-terminal amide resonance......... 362

Figure IX-1D 500 MHz ^{1}H NMR spectra of the TnI peptide in H_20 and 50%TFE: Expanded region of spectrum B showing only the backbone amide proton resonances... 363

Figure IX-2 Upfield region of the DQFCOSY spectrum of the TnI peptide in 50%TFE.. 364

Figure IX-3 Upfield region of the NOESY spectrum of the TnI peptide in 50%TFE.. 365

Figure IX-4 αCH-βCH region of the NOESY spectrum of the TnI peptide in 50%TFE.. 366

Figure IX-5 Downfield-βCH region of the NOESY spectrum of the TnI peptide in 50%TFE.. 367

Figure IX-6 αCH-NH region of the DQFCOSY spectrum of the TnI peptide in 50%TFE.. 368

Figure IX-7 αCH-NH region of the NOESY spectrum of the TnI peptide in 50%TFE.. 369

Figure IX-8 NH-NH region of the NOESY spectrum of the TnI peptide in 50%TFE showing NOEs between backbone amide protons............ 370

Figure IX-9A 500 MHz ^{1}H NMR spectra of mastoparan in H_20 and 50%TFE: Aliphatic upfield region of the spectrum.................................. 371

Figure IX-9B 500 MHz ^{1}H NMR spectra of mastoparan in H_20 and 50%TFE: Complete downfield region of the spectrum.............................. 372

Figure IX-9C 500 MHz ^{1}H NMR spectra of mastoparan in H_20 and 50%TFE: Expanded region of spectrum B showing only the backbone amide proton resonances.............................. 373

Figure IX-10 Upfield region of the DQFCOSY spectrum of mastoparan in 50%TFE 374
Figure IX-11 Upfield region of the NOESY spectrum of mastoparan in 50%TFE 375
Figure IX-12 αCH-βCH region of the NOESY spectrum of mastoparan in 50%TFE 376
Figure IX-13 Downfield-βCH region of the NOESY spectrum of mastoparan in 50%TFE 377
Figure IX-14 αCH-NH region of the DQFCOSY spectrum of mastoparan in 50%TFE 378
Figure IX-15 αCH-NH region of the NOESY spectrum of mastoparan in 50%TFE 379
Figure IX-16 NH-NH region of the NOESY spectrum of mastoparan in 50%TFE showing NOEs between the chemically exchanging C-terminal NH2 groups and the backbone amide of the C-terminal residue, L14 380
Figure IX-17 NH-NH region of the NOESY spectrum of mastoparan in 50%TFE showing NOEs between backbone amide protons 381
Figure IX-18A 500 MHz ^{1}H NMR spectra of mastoparan in the absence and presence of 0.1 molar equivalents TnC.Ca(II)$_4$: Aliphatic upfield region of the spectrum 382
Figure IX-18B 500 MHz ^{1}H NMR spectra of mastoparan in the absence and presence of 0.1 molar equivalents TnC.Ca(II)$_4$: Complete downfield region of the spectrum 383
Figure IX-18C 500 MHz ^{1}H NMR spectra of mastoparan in the absence and presence of 0.1 molar equivalents TnC.Ca(II)$_4$: Expanded region of spectrum B showing only the backbone amide proton resonances 384
Figure IX-19 Upfield region of the DQFCOSY spectrum of mastoparan in the presence of 0.1 molar equivalents TnC.Ca(II)$_4$ 385
Figure IX-20 Upfield region of the NOESY spectrum of mastoparan in the presence of 0.1 molar equivalents TnC.Ca(II)$_4$ 386
Figure IX-21 αCH-βCH region of the NOESY spectrum of mastoparan in the presence of 0.1 molar equivalents TnC.Ca(II)$_4$ 387
Figure IX-22 Downfield-βCH region of the NOESY spectrum of mastoparan in the presence of 0.1 molar equivalents TnC.Ca(II)$_4$ 388

Figure IX-23A αCH-NH region of the DQFCOSY spectrum of mastoparan in the presence of 0.1 molar equivalents TnC.Ca(II)$_4$: Spectrum showing L3 αCH-NH COSY cross-peak 389
Figure IX-23B αCH-NH region of the DQFCOSY spectrum of mastoparan in the presence of 0.1 molar equivalents TnC.Ca(II)$_4$: Expanded region of spectrum A 390
Figure IX-24A αCH-NH region of the NOESY spectrum of mastoparan in the presence of 0.1 molar equivalents TnC.Ca(II)$_4$: Spectrum showing L3αCH-NH and I1αCH-N2NH NOEs............ 391
Figure IX-24B αCH-NH region of the NOESY spectrum of mastoparan in the presence of 0.1 molar equivalents TnC.Ca(II)$_4$: Expanded region of spectrum A 392
Figure IX-25 NH-NH region of the NOESY spectrum of mastoparan in the presence of 0.1 molar equivalents TnC.Ca(II)$_4$.................. 393
Figure IX-26 Fingerprint αCH-NH region of the NOESY spectrum of mastoparan superimposed upon the αCH-NH region of the NOESY spectrum of the same concentration mastoparan in the presence of 0.1 molar equivalents TnC.Ca(II)$_4$.................. 394
Figure IX-27 Sequence of the TnI peptide together with a schematic summary of the short- and medium- range NOEs defining the secondary structure of the peptide in 50%TFE...................... 395
Figure IX-28 Sequence of mastoparan together with a schematic summary of the short- and medium- range NOEs defining the secondary structure of the peptide in 50%TFE...................... 395
Figure IX-29 Sequence of mastoparan together with a schematic summary of the short- and medium- range TRNOEs defining the secondary structure of the peptide when bound to TnC............ 396
Figure IX-30 Stereo-diagram of the TnI peptide in 50%TFE.......................... 397
Figure IX-31 Stereo-diagram of mastoparan in 50%TFE.............................. 398
Figure IX-32 Superposition of the 10 MD structures taken every 0.2 ps for the TnI peptide in 50%TFE.. 399
Figure IX-33 Superposition of the 10 MD structures taken every 0.2 ps for mastoparan in 50%TFE.. 400

Figure X-1 Flow diagram for the transferred iterative relaxation matrix analysis (TR-IRMA) for structure determination of chemically-exchanging biomolecules from ^{1}H-^{1}H TRNOEs........................ 426

Figure X-2 Simulated TRNOE build-up curves versus experimentally measured TRNOE intensities.. 427

List of Tables, Figures and Computer Programs in Appendix

Tables in Appendix

Table IV-1 ^{19}F NMR data for the titration of N-α-acetyl[^{19}F-phe106] TnI(104-115) amide with apo turkey skeletal TnC........................ 431
Table IV-2 ^{19}F NMR data for the titration of N-α-acetyl[^{19}F-phe106] TnI(104-115) amide with Ca(II)-saturated turkey skeletal TnC........ 431

Table V-1 Normalization tables for exchangeable backbone amide resonances on the TnI peptide:
A. Amide versus exchangeable resonance................................ 435
B. Amide versus amide resonance... 435
Table V-2 Table of TRNOE cross-peak intensities for the TnI peptide in the presence of 0.1 molar equivalents TnC.Ca(II)$_4$.................. 436
Table V-3 Effect of mixing time on the development of the intrapeptide TRNOE.. 442
Table V-4 Effect of protein concentration on the development of the intrapeptide TRNOE.. 448
Table V-5 Summary of distance restraints used in the MD simulations............ 455
Table V-6 $^3J\alpha$CH-NH coupling constants for the TnI peptide as a function of molar equivalents TnC.Ca(II)$_4$.. 462
Table V-7 Chemical shift values for the TnI peptide backbone amide resonances as a function of temperature for
A. 0.0 molar equivalents TnC.Ca(II)$_4$.................................... 463
B. 0.2 molar equivalents TnC.Ca(II)$_4$.................................... 463
C. 0.4 molar equivalents TnC.Ca(II)$_4$.................................... 463
Table V-8 Temperature coefficients measured for various TnI peptide backbone amide protons versus molar equivalents TnC.Ca(II)$_4$........ 464
Table V-9 GROMOS distance restraint file used in MD simulations to generate the structure of the TnI peptide bound to TnC.Ca(II)$_4$..... 465
Table V-10 Chemical shift values for the TnI peptide backbone amide resonances as a function of molar equivalents TnC.Ca(II)$_4$............. 475
Table V-11 Final coordinates for the structure of the TnI peptide bound to TnC generated from A. α-helical coordinates (structure 1), and B. β-strand coordinates (structure 2), following approximately 12 ps of restrained MD........................ 476

Table V-12 Comparison of the distances between proton pairs given in the distance restraint file with those actually measured between the same proton pairs in the final structures generated from the α-helix (structure 1) and the β-strand (structure 2) 482

Table VII-1 T_1 measurements for various protons on the TnI peptide as a function of molar equivalents TnC.Gd(III)$_4$ to TnI peptide........ 488
Table VII-2 T_2 measurements for various protons on the TnI peptide as a function of molar equivalents TnC.Gd(III)$_4$ to TnI peptide........ 489
Table VII-3 T_1 measurements for various protons on the TnI peptide as a function of molar equivalents TnC.La(III)$_4$ to TnI peptide......... 490
Table VII-4 T_2 measurements for various protons on the TnI peptide as a function of molar equivalents TnC.La(III)$_4$ to TnI peptide......... 491
Table VII-5 Calculated values of $1/T_{1OBSi}{}^{Gd}$, $1/T_{2OBSi}{}^{Gd}$, $1/T_{1OBSi}{}^{La}$, $1/T_{2OBSi}{}^{La}$, $1/T_{1Pi}$, $1/T_{2Pi}$, $1/T_{1Mi}$, R_{maxi}, and R_{mini} for various protons, i, on the TnI peptide................................. 492

Table VIII-1 Normalization tables for exchangeable backbone amide resonances on the G110-TnI peptide:
A. Amide versus exchangeable resonance................................ 495
B. Amide versus amide resonance.. 495
Table VIII-2 Table of TRNOE cross-peak intensities for the G110-TnI peptide in the presence of 0.1 molar equivalents TnC.Ca(II)$_4$.................. 496
Table VIII-3 Summary of distance restraints used in the MD simulations............ 502
Table VIII-4 $^3J\alpha$CH-NH coupling constants for the G110-TnI peptide as a function of molar equivalents TnC.Ca(II)$_4$.......................... 508
Table VIII-5 Chemical shift values for the G110-TnI peptide backbone amide resonances as a function of temperature for
A. 0.0 molar equivalents TnC.Ca(II)$_4$..................................... 509
B. 0.1 molar equivalents TnC.Ca(II)$_4$..................................... 509
Table VIII-6 Temperature coefficients measured for various G110-TnI peptide backbone amide protons versus molar equivalents TnC.Ca(II)$_4$........ 510
Table VIII-7 GROMOS distance restraint file used in MD simulations to generate the structure of the G110-TnI peptide bound to TnC.Ca(II)$_4$.. 511

Table VIII-8 Chemical shift values for the G110-TnI peptide backbone amide resonances as a function of molar equivalents TnC.Ca(II)$_4$............. 520
Table VIII-9 Final coordinates for the structure of the G110-TnI peptide bound to TnC generated from A. α-helical coordinates (structure 1), and B. β-strand coordinates (structure 2), following approximately 12 ps of restrained MD.......................... 521
Table VIII-10 Comparison of the distances between proton pairs given in the distance restraint file with those actually measured between the same proton pairs in the final structures generated from the α-helix (structure 1) and the β-strand (structure 2).................. 527

Table IX-1 Normalization tables for exchangeable backbone amide resonances on the TnI peptide in 50%TFE:
A. Amide versus exchangeable resonance................................ 533
B. Amide versus amide resonance.. 533
Table IX-2 Normalization tables for exchangeable backbone amide resonances on mastoparan in 50%TFE:
A. Amide versus exchangeable resonance................................ 534
B. Amide versus amide resonance.. 534
Table IX-3 Table of NOE cross-peak intensities for the TnI peptide in 50%TFE.. 535
Table IX-4 Table of NOE cross-peak intensities for mastoparan in 50%TFE...... 538
Table IX-5 Summary of distance restraints used in the MD simulations for the TnI peptide in 50%TFE... 543
Table IX-6 Summary of distance restraints used in the MD simulations for mastoparan in 50%TFE.. 546
Table IX-7 $^3J\alpha CH$-NH coupling constants for the TnI peptide in 50%TFE........ 551
Table IX-8 $^3J\alpha CH$-NH coupling constants for mastoparan in 50%TFE............ 551
Table IX-9 GROMOS distance restraint file used in MD simulations to generate the structure of the TnI peptide in 50%TFE............................... 552
Table IX-10 GROMOS distance restraint file used in MD simulations to generate the structure of mastoparan in 50%TFE.................................. 558
Table IX-11 Final coordinates for the structure of the TnI peptide in 50%TFE A. α-helical coordinates (structure 1), and B. β-strand coordinates (structure 2), following approximately 12 ps of restrained MD......................... 566

Table IX-12 Final coordinates for the structure of mastoparan in 50%TFE
A. α-helical coordinates (structure 1), and
B. β-strand coordinates (structure 2),
following approximately 12 ps of restrained MD 572
Table IX-13 Comparison of the distances between proton pairs given in the distance restraint file for the TnI peptide in 50%TFE with those actually measured between the same proton pairs in the final structures generated from the α-helix (structure 1) and the β-strand (structure 2) 578
Table IX-14 Comparison of the distances between proton pairs given in the distance restraint file for mastoparan in 50%TFE with those actually measured between the same proton pairs in the final structures generated from the α-helix (structure 1) and the β-strand (structure 2) 581

Table X-1 Table of TRNOE intensities versus mixing time ($\tau_m = 75$, 150, and 500 ms) measured at 0.1 molar equivalents TnC.Ca(II)$_4$ to TnI peptide 586
Table X-1 Table of TRNOE intensities versus mixing time ($\tau_m = 75$, 150, and 500 ms) measured at 0.2 molar equivalents TnC.Ca(II)$_4$ to TnI peptide 592
Table X-3 Table of TRNOE intensities versus mixing time ($\tau_m = 75$, 150, and 500 ms) measured at 0.4 molar equivalents TnC.Ca(II)$_4$ to TnI peptide 600

Figures in Appendix

Figure V-1 500 MHz ^1H NMR spectra of the TnI peptide backbone amide resonances as a function of temperature
A. 0.0 molar equivalents $TnC.Ca(II)_4$ 432
B. 0.2 molar equivalents $TnC.Ca(II)_4$ 433
C. 0.4 molar equivalents $TnC.Ca(II)_4$ 434

Figure VIII-1 500 MHz ^1H NMR spectra of the G110-TnI peptide backbone amide resonances as a function of temperature
A. 0.0 molar equivalents $TnC.Ca(II)_4$ 493
B. 0.1 molar equivalents $TnC.Ca(II)_4$ 494

Computer Programs in Appendix

TRNOE: version 1 607
TRNOE: version 2 627

Chapter IX

Role of Amphiphilicity in the Binding of Target Peptides to Troponin C: An NMR Comparison of the Structures of Mastoparan and the Inhibitory Troponin I Peptide in the Helix Inducing Solvent Trifluoroethanol Versus Bound to Troponin C

A. Introduction

Contraction of vertebrate skeletal muscle is regulated by Ca(II) and requires the regulatory proteins troponin and tropomyosin (Ebashi and Endo, 1968). Troponin is a complex of three different protein subunits: Troponin C (TnC) which binds Ca(II), TnI which binds actin and inhibits actomyosin ATPase, and TnT which binds to tropomyosin. The Ca(II)-dependent interaction between TnC and TnI is one of the key processes in the activation of contraction in skeletal muscle (for recent reviews, see Zot and Potter, 1987, and Leavis and Gergely, 1984). TnI inhibits the Mg(II)-ATPase activity of actomyosin (Hartshorne and Mueller, 1968; Schaub and Perry, 1969; Greaser and Gergely, 1971; Perry *et al.*, 1972) and binds both to actin and tropomyosin-actin (Potter and Gergely, 1974; Hitchcock, 1975). The inhibition of actomyosin ATPase is neutralized when Ca(II)-saturated TnC forms a 1:1 complex with TnI (Perry *et al.*, 1972; Weeks and Perry, 1978; Chong *et al.*, 1983; Cachia *et al.*, 1986; Van Eyk and Hodges, 1988). The region of TnI which is responsible for its inhibitory activity is the same region which is involved in a Ca(II)-sensitive 'switch' between binding to actin-tropomyosin and binding to TnC. In the absence of Ca(II), the inhibitory region of TnI is bound to the surface of actin-tropomyosin, inhibiting the actomyosin ATPase activity and contraction. In the presence of Ca(II), this region of TnI is thought to bind to TnC (Cachia *et al.*, 1985). Talbot and Hodges (1981) showed, using synthetic peptides, that residues 104-115 of skeletal TnI comprise the minimum sequence necessary for inhibition of actomyosin ATPase activity. The synthetic peptide TnI(104-115) possesses tropomyosin specificity (Talbot and Hodges, 1979) and TnC binding capability (Cachia *et al.*, 1983, 1985; Van Eyk and Hodges, 1988; Van Eyk *et al.*, 1991), which results in the release of ATPase inhibition (Cachia *et al.*, 1986).

TnC and the homologous Ca(II)-binding protein calmodulin (CaM) belong to the HLH Ca(II)-binding protein family (Kretsinger, 1980). The x-ray structures of avian skeletal TnC (Sundaralingam *et al.*, 1985; Herzberg and James, 1985) and CaM (Babu *et al.*, 1985) have been solved and reveal a dumbbell-shaped molecule with N-terminal and C-terminal globular domains joined by a long helical linker. Each major domain contains two HLH Ca(II) binding sites based on the EF hand motif first discovered in carp parvalbumin (Kretsinger and Nockolds, 1973; Collins *et al.*, 1973; Vanaman *et al.*, 1977). TnC has two classes of Ca(II) binding sites. The higher affinity Ca(II)/Mg(II) sites are sites III and IV which are located in the C-terminal half of the molecule. These sites bind Ca(II) or Mg(II) with association constants of 2×10^7 and 5×10^3 M^{-1}, respectively. Sites I and II, in the N-terminal half of the molecule, are the Ca(II)-specific sites which bind Ca(II) with an association constant of 2 x 10^5 M^{-1} (Potter and Gergely, 1975; Johnson and Potter, 1978). CaM, in contrast, is specific for Ca(II) and contains four sites with association constants ranging from 10^5 to 10^6 M^{-1}.

The Ca(II)-bound conformations of TnC and CaM are required for high affinity binding to target molecules (Klee *et al.*, 1980; Klee *et al.*, 1982; Leavis and Gergely, 1984; Zot and Potter, 1987). There is evidence to suggest that Ca(II) binding to TnC and CaM leads to the increased exposure of hydrophobic surfaces on TnC which then become the sites for the interaction of target molecules (Walsh *et al.*, 1978; Laporte *et al.*, 1980; Tanaka *et al.*, 1980; Thiry *et al.*, 1980; Krebs and Carafoli, 1982; Prozialeck and Weiss, 1982; Gariepy and Hodges, 1983; Tanaka *et al.*, 1983; Dalgarno *et al.*, 1984; Jarrett, 1984; Cachia *et al.*, 1985; Drabikowski *et al.*, 1985; Klevit *et al.*, 1985; Guerini *et al.*, 1987; Strynadka and James, 1988). Although the details of these interactions have not been defined at the molecular level, it is clear that amphiphilic helices play a major role in target molecule binding. The N- and C- terminal globular domains of TnC and CaM have large hydrophobic patches (Kretsinger *et al.*, 1986; Babu *et al.*, 1988) flanked by regions of negative electrostatic potential, optimally designed as binding sites for basic, amphiphilic helices. Furthermore, the proposed CaM binding sites on myosin light chain kinase (Blumenthal *et al.*, 1985; Lukas *et al.*, 1986), phophofructokinase (Buschmeier *et al.*, 1987), phosphorylase b kinase (Lukas *et al.*, 1986; DeGrado *et al.*, 1987) and CaM-dependent protein kinase from brain (Lin *et al.*, 1987), all encompass short sections of each enzyme that have high amphiphilic helix forming propensities.

Many known potent inhibitors of CaM and TnC are short amphiphilic helical peptides (for a recent review see Erickson-Viitanen *et al.*, 1987). In order to understand the mechanism of binding of these various target molecules to TnC and CaM, much recent work has focused on determining the secondary structure adopted by a peptide in order to form a binding interface (Maulet and Cox, 1983; Puett *et al.*, 1983; Malencik and Anderson, 1983a; Cox *et al.*, 1985; McDowell *et al.*, 1985; Strynadka and James, 1990). Several of these studies have utilized bee or wasp venom peptides such as melittin or one of the mastoparans which are capable of forming amphiphilic α-helices upon binding to hydrophobic surfaces such as the CaM binding site (Maulet and Cox, 1983; McDowell *et al.*, 1985; Cox *et al.*, 1985; Strynadka and James, 1990).

In order to determine whether α-helical secondary structure is a prerequisite for binding to these regulatory proteins, we have used ^{1}H NMR to examine and compare the structure of two target molecules in a helix-inducing solvent versus when bound to Ca(II)-saturated TnC. The first of these target molecules which we have chosen for study is the inhibitory TnI peptide (104-115). The mechanism of binding of the TnI peptide to TnC is physiologically relevant and has been characterized by a variety of techniques which indicate that one of the sites of interaction between the peptide and the protein is the N-terminal helix of site III in the C-terminal domain of TnC (Weeks and Perry, 1978; Grabarek *et al.*, 1981; Leszyk *et al.*, 1987, 1988; Tao *et al.*, 1989; Lan *et al.*, 1989; Campbell *et al.*, 1991a). The TnI peptide binds to TnC with a dissociation constant of 4.8 x 10^{-5} M (Campbell *et al.*, 1991b; Chapter IV). The second target molecule which we have chosen for study is the bee venom peptide mastoparan. The interaction between mastoparan and TnC is not known to be physiologically relevent, however mastoparan provides a good model for the binding of amphiphilic helical target molecules to TnC and CaM since it has a high propensity to form amphiphilic α-helices, both in helix-inducing solvent and when bound to protein. Mastoparan binds to TnC with a dissociation constant of 2 x 10^{-7} M (Malencik and Anderson, 1983a, 1983b).

We have previously determined the three-dimensional structure of the TnI peptide when bound to Ca(II)-saturated TnC (Campbell and Sykes, 1991a; Chapter V) using the two-dimensional TRNOESY experiment and molecular mechanics simulations. In the present set of experiments, we determine the three-dimensional structure of the TnI peptide and the mastoparan peptide in helix-inducing solvent using the two-dimensional NOESY experiment and molecular mechanics simulations. We also use the two-dimensional TRNOESY experiment to analyze the secondary structure of mastoparan when bound to Ca(II)-saturated TnC. A comparison of the structures of these two peptides in helix-inducing solvent versus when bound to TnC should shed light on the role of amphiphilicity in the recognition of Ca(II)-binding proteins for their target molecules.

B. Theory

We have presented a more complete treatment of the theory of the TRNOE elsewhere (Campbell and Sykes, 1991b; Chapter II), however for the purposes of this paper, we will give a brief description of the experiment. In the present study, we used the TRNOE to follow the conformational changes in the mastoparan peptide induced by the formation of the mastoparan-TnC.Ca(II)$_4$ complex. The TRNOE is the extension of the NOE, which has been widely used to determine protein structures in solution (Wuthrich, 1986), to exchanging systems such as ligand-protein complexes, and provides one of the best techniques for the determination of the structure of bound ligands. The intramolecular TRNOE allows the transfer of information concerning cross-relaxation between two nuclei in the bound ligand to the free ligand resonances via chemical exchange. In the unbound form, the ligand is generally characterized by short correlation times ($\tau_c < 10^{-10}$ s) and may be described as being either in the extreme narrowing limit ($\omega\tau_c << 1$), where the NOEs are small and positive, or at the boundary of the extreme narrowing limit ($\omega\tau_c \cong 1$), where the NOEs approach zero. When bound to the protein, the ligand is characterized by the long correlation time of the protein ($\tau_c > 10^{-8}$ s), and may be described as being in the spin diffusion limit ($\omega\tau_c >> 1$), where the NOEs are large and negative. In the presence of chemical exchange of the ligand between its free and bound states, negative NOEs conveying conformational information of the bound ligand are 'transferred' to the free ligand resonances where they are more easily measured because these resonances are much narrower.

Consider the equilibrium between the free and bound ligand

$$\text{mastoparan} + \text{TnC} \underset{k_{-1}}{\overset{k_1[\text{TnC}]}{\rightleftharpoons}} \text{mastoparan.TnC} \qquad [1]$$

Given fast exchange on the NMR timescale ($[4\pi^2(\delta_F-\delta_B)^2\tau_cB^2]$, $[\tau_cB/T_2B] << 1$, where τ_cB is the correlation time of the bound peptide, $|\delta_F-\delta_B|$ is the change in chemical shift upon binding, and T_2B is the spin-spin relaxation time in the bound environment), the observed chemical shifts, δ_{obs}, and linewidths, $\Delta\nu_{obs}$, are dominated by the free ligand population when $p_F >> p_B$ (where p_B is the fraction of bound ligand and p_F is the fraction of free ligand)

$$\delta_{obs} = p_F\,\delta_F + p_B\,\delta_B \qquad [2]$$

$$\Delta\nu_{obs} = p_F\,\Delta\nu_F + p_B\,\Delta\nu_B \qquad [3]$$

Conversely, the TRNOESY cross-peak intensities, a_{ij}, are dominated by the bound ligand, since the cross-relaxation rate between protons in the bound ligand is so much faster than it is in the free ligand, viz. $W_{ij}B >> W_{ij}F$

$$a_{ij}(\tau_m) \cong -\,[\,p_B\,W_{ij}B + p_F\,W_{ij}F\,]\,\tau_m \;\cong -\,[\,p_B\,W_{ij}B\,]\,\tau_m \qquad [4]$$

The $W_{ij}B$s, once obtained, yield interproton distances in the bound peptide

$$W_{ij}B \propto \langle\, 1/r_{ij}B^{\,6} \rangle \qquad [5]$$

C. Materials and Methods

1. Sample Preparation

a. Materials. Refer to Materials and Methods section in Chapter V.

b. Amino Acid Analysis. The quantities of Nα-acetyl-TnI(104-115) amide, mastoparan and turkey skeletal TnC used were determined from amino acid analysis after hydrolysis in 100-200 μl of 6 N HCl in evacuated sealed tubes for 24 h at 110°C. The mean of the molar ratios of all accurately measurable amino acids in the acid hydrolysate was used to calculate the concentration of peptide or protein.

c. Peptide Synthesis and Purification. Nα-acetyl-TnI(104-115) amide and mastoparan were synthesized and purified using the standard protocol outlined in the Materials and Methods section in Chapter V (Erickson and Merrifield, 1976; Talbot and Hodges, 1981; Mant *et al.*, 1987; Parker *et al.*, 1987; Hodges *et al.*, 1988).

d. Preparation of TnC. Troponin was isolated from an acetone powder of turkey breast muscle using the protocol outlined in the Materials and Methods section in Chapter IV. A final yield of approx. 400 mg of purified TnC powder was obtained, which was found to be homogenous when examined by SDS-Page and UV spectrophotometry ($\varepsilon_{(\lambda\ 259\ \mathrm{nm})}$ = 0.109 O.D. units/mg/ml for turkey skeletal TnC).

e. Preparation of Desalted, Apo TnC. EDTA-free, apo TnC was prepared using the protocol outlined in the Materials and Methods section in Chapter IV. The TnC protein was judged to be apo by UV spectrophotometry and ^{1}H NMR.

f. Preparation of TnI Peptide ^{1}H NMR Samples. The TnI peptide sample used for ^{1}H NMR structure determinations in the 50%TFE solvent was 3 mM Nα-acetyl-TnI(104-115) amide, dissolved in 650 μl of a 50%TFE/50%$H_2$0 solvent mixture at pH 6.2 and a salt concentration of 50 mM KCl. The mastoparan sample used used for ^{1}H NMR structure determinations in the 50%TFE solvent was 2.5 mM mastoparan, dissolved in 650 μl of a 50%TFE/50%$H_2$0 solvent mixture at pH 6.2 and a salt concentration of 50 mM KCl. The mastoparan sample used for ^{1}H NMR structure determination in the presence of 0.1 molar equivalents Ca(II)-saturated turkey skeletal TnC was 4.0 mM mastoparan, dissolved in 650 μl of a 80%$H_2$0/20%$D_2$0 solvent mixture at pH 6.2 and a salt concentration of 50 mM KCl. Turkey skeletal TnC.Ca(II)$_4$ was titrated into the sample to a final concentration of approximately 0.4 mM TnC. 0.1 mM DSS was added to all peptide samples to act as a chemical shift standard.

2. Nuclear Magnetic Resonance Spectroscopy

All ^{1}H NMR spectra were obtained at 500 MHz on a Varian VXR-500 NMR spectrometer. Two-dimensional experiments were taken with 2048 data points along t_2 and with 256 t_1 increments. Spectral widths of 5000-6000 Hz and relaxation delay times of 1.6-2.3 s were employed. Streaking along t_1 was reduced by multiplying the first domain time point by a factor optimized near 0.5 (Otting *et al.*, 1986). DQFCOSY (Piatini *et al.*, 1982; Rance *et al.*, 1983), NOESY and TRNOESY data sets were acquired in the phase-sensitive method of States *et al.* (1982). The appropriate phase cycling was used for quadrature detection and to eliminate axial peaks, and in the case of NOESY and TRNOESY spectra, single and multiple quantum coherences. For all data sets, the water resonance was suppressed by presaturation. The decoupler offset was set equal to the transmitter offset to prevent phase distortions around the water peak due to imperfect cancellation of the dispersive component of residual water magnetization (Hoult, 1976). Average mixing times, τ_m , of 150 and 500 ms were used for the NOESY and TRNOESY spectra. A random delay of ± 10 ms was incorporated to suppress zero quantum coherences.

3. Transformation of ^{1}H NMR NOESY Peak Intensity to Distance Restraints

^{1}H NMR NOESY intensities were quantified for data sets acquired at τ_m = 150 ms for the TnI peptide in 50%TFE, and at τ_m = 500 ms for mastoparan in 50%TFE. Volume integrals for each cross-peak were measured and nominally empty areas perpendicularly adjacent to each cross-peak were examined for baseline correction. The NOE cross-peak intensities were transformed to distance restraints using a group of stereospecifically assigned reference proton pairs. For the TnI peptide in 50%TFE these included F106NH-βCH(4.0Å), F106NH-βCH'(3.4Å), F106αCH-βCH(4.5Å), F106αCH-βCH'(4.5Å), F106βCH-βCH'(1.8Å), P109βCH-βCH'(1.8Å), P109βCH-δCH(4.1Å), P109βCH-δCH'(3.9Å), P109βCH'-δCH(3.9Å), P109βCH'-δCH'(3.0Å), P109δCH-δCH'(1.8Å), P110βCH-βCH'(1.8Å), P110βCH-δCH(4.1Å), P110βCH-δCH'(3.9Å), P110βCH'-δCH(3.9Å), and P110βCH'-δCH'(3.0Å), and P110δCH-δCH'(1.8Å). The reference proton pairs used to transform NOE cross-peak intensities into distance restraints for mastoparan in 50%TFE included K4NH-αCH(3.0Å), A5NH-αCH(3.0Å), L6NH-αCH(3.0Å), A7NH-αCH(3.0Å), A8NH-αCH(3.0Å), L9NH-αCH(3.0Å), A10NH-αCH(3.0Å), L11NH-αCH(3.0Å), L12NH-αCH(3.0Å), and I13γCH-γCH'(1.76Å).

These proton pairs were chosen because they displayed linear NOE build-up of magnetization for the mixing time at which they were measured, and were well separated from overlapping cross-peaks in the NOESY spectrum. The reference distances for the F106 reference proton pairs in the TnI peptide and all NH-αCH reference proton pairs in mastoparan corresponded to the distances found for the α-helical conformations of these peptides. However, these distances were not found to change more than 10% when compared to those found for the β-sheet conformations, and therefore were deemed to be independent of secondary conformation. All other reference distances involved distances between reference proton pairs in the P109 and P110 five-membered rings of the TnI peptide, and between the γCH-γCH' geminal reference proton pairs of I13 in mastoparan.

NOE intensities were normalized for the contribution of more than two protons to the cross-peak before they were transformed into distance restraints. We divided the TRNOE cross-peak intensities by the normalization factor (2*NaNb*)/(*Na*+*Nb*) where *Na* was the number of protons under diagonal peak *a*, and *Nb* was the number of protons under diagonal peak *b* (Macura and Ernst, 1980; Williamson and Neuhaus, 1987). Cross-peaks connecting exchangeable proton resonances were also corrected for loss of intensity due to exchange or saturation transfer from the decoupled water peak. The exchangeable proton peak intensities were integrated in a one-dimensional spectrum obtained under the same experimental conditions as the two-dimensional spectrum (same temperature, pH, sample concentration and spectrometer settings), and the intensity of these peaks were normalized against the integrated intensity of the V114αCH peak for the TnI peptide and the I13αCH peak for mastoparan (see Tables IX-1A, IX-1B, IX-2A and IX-2B in the Appendix).

Tables IX-3 and IX-4 in the Appendix give the NOE data set measured from the NOESY experiment acquired at τ_m = 150 ms for the TnI peptide in 50%TFE, and τ_m = 500 ms for mastoparan in 50%TFE, respectively. Included in these tables are the measured NOE intensities, the corrected and normalized NOE intensities, and the r_{ij}s calculated from these corrected and normalized values using the group of stereospecifically assigned reference proton pairs discussed above.

Initial error limits ($\pm\beta$) were used to set upper (r_{ij}^U) and lower (r_{ij}^L) distance bounds on the calculated distance restraints (r_{ij}), and were incorporated in the following manner: for $r_{ij} < 3.0$Å, $\beta = \pm0.2$ Å; for 3.0 Å $\leq r_{ij} < 4.0$Å, $\beta = \pm0.3$ Å; for 4.0 Å $\leq r_{ij} <$ 5.0Å, $\beta = \pm0.5$ Å; and for $r_{ij} \geq 5.0$ Å, $\beta = \pm1.0$ Å. Thus, for r_{ij} = 3.5 Å, we set r_{ij}^U equal to 3.8 Å, and r_{ij}^L equal to 3.3 Å. Within the distance range of $r_{ij} \pm \beta$, the distance restraint term used in the MD and EM simulations contributed no energy penalty to the overall potential energy of the system. Tables IX-5 and IX-6 in the Appendix summarize the distance restraints used in the MD simulations for the TnI peptide and mastoparan in 50%TFE, respectively. Included in these tables are the r_{ij}s calculated from the corrected and normalized NOE cross-peak intensities, the incorporated error limits (±β), and the pseudoatom adjustments in r_{ij}^U.

4. Dihedral Angle Restraints and Supplemental Distance Restraints

A curve fitting program was used to measure dihedral coupling constants in one-dimensional ^{1}H NMR spectra of the TnI peptide and mastoparan in 50% TFE. For $^3J\alpha CH\text{-}NH < 6.0$ Hz, Φ was restricted to the range $-85° \leq \Phi \leq -40°$ (Pardi *et al.*, 1984; Wagner *et al.*, 1987; Driscoll *et al.*, 1989). For $^3J\alpha CH\text{-}NH > 8.0$ Hz, Φ was restricted to the range $-160° \leq \Phi \leq -80°$. All $^3J\alpha CH\text{-}NH$ values measured for mastoparan in 50%TFE were found to be less than 4.0 Hz, therefore all Φ dihedral angles in the peptide were restrained to $-85° \leq \Phi \leq -40°$, constraining the peptide into α-helical conformational space. However, the $^3J\alpha CH\text{-}NH$ values measured for the TnI peptide in 50%TFE ranged from 5.0 Hz to 7.3 Hz, most being in the range of $6.0 \text{ Hz} < {}^3J\alpha CH\text{-}NH < 8.0$ Hz. Therefore, it was not possible to restrain the Φ dihedral angles in the TnI peptide, as the measured $^3J\alpha CH\text{-}NH$ values did not correspond to either $-85° \leq \Phi \leq -40°$ or $-160° \leq \Phi \leq -80°$. All peptide bonds for both mastoparan and the TnI peptide, including X-proline in the TnI peptide, were restrained to $-175° \leq \omega \leq -185°$. This maintained a trans peptide bond configuration. We found no evidence for cis-trans X-proline peptide bond isomerization from ^{1}H NOESY spectra of the TnI peptide. Tables IX-7 and IX-8 in the Appendix give the $^3J\alpha CH\text{-}NH$ values for the TnI peptide and mastoparan in 50%TFE, respectively.

5. Stereospecific Assignments from ^{1}H NMR

Stereospecific assignments of prochiral protons were available for the following set of protons on the TnI peptide: F106βCH, F106βCH', P109βCH, P109βCH', P109δCH, P109δCH', P110βCH, P110βCH', P110δCH, and P110δCH'. Stereospecific assignments of prochiral protons were available for the following set of protons on mastoparan: I1γCH, I1γCH', N2βCH, N2βCH', I13γCH, and I13γCH'. Stereospecific assignments were possible for these prochiral proton pairs since they exhibited sufficiently different chemical shifts. The other prochiral protons and methyl groups on either peptide were designated as pseudoatoms (Wuthrich *et al.*, 1983), and the appropriate intraresidue and long-range corrections were made on the upper bound of the distance restraints for these pseudoatoms. Unambigious stereospecific assignments may result for prochiral groups if there is a sufficiently large set of NOE, Van der Waals, and covalent bond constraints as input for the structure calculation. Here, we generated a roughly determined structure using only pseudoatoms in the distance restraint file for the MD simulations, and then modified the distance restraint file to include stereospecific distance restraints consistent with the stereochemistry of this roughly determined structure. A more precisely determined structure was then generated using this modified distance restraint file as input for a second round of MD simulations. The stereospecific assignments for the phenylalanine and proline residues on the TnI peptide, and asparagine and isoleucine on mastoparan, were in agreement with the relative strength of the $d_{\alpha\beta}$ and $d_{N\beta}$ NOE cross-peaks, and were consistent with the stereochemistry of the bound structures. The second round of MD simulations employing the stereospecific assignments are described in the following section.

6. Restrained Molecular Dynamics Calculations

EM and MD calculations were carried out with the GROMOS program (de Vlieg *et al.*, 1986) and force field, which consisted of the usual terms for bonds, bond-angles, sinusoidal dihedral torsion, non-bonded interactions (Van der Waals and electrostatics), and harmonic terms to maintain proper planar or tetrahedral geometries. Two extra terms were added representing distance and dihedral restraints. The distance restraint square well potential, E_{DIS}, was defined by two functions, a biharmonic potential for $(r_{ij}^U - r_{ij})$ and $(r_{ij}^L - r_{ij}) < 5Å$, and a linear potential for $(r_{ij}^U - r_{ij})$ and $(r_{ij}^L - r_{ij}) \geq 5Å$:

$$\begin{array}{rll} E_{DIS} = 0.5\, C_{DIS}\, (r_{ij}^U - r_{ij})^2 & \text{if } r_{ij} > r_{ij}^U;\ |r_{ij}^U - r_{ij}| < 5Å & \\ = 0.5\, C_{DIS}\, (r_{ij}^L - r_{ij})^2 & \text{if } r_{ij} < r_{ij}^L;\ |r_{ij}^L - r_{ij}| < 5Å & [6a] \end{array}$$

$$\begin{array}{rll} E_{DIS} = 0.5\, C_{DIS}\, (r_{ij}^U - r_{ij}) & \text{if } r_{ij} > r_{ij}^U;\ |r_{ij}^U - r_{ij}| \geq 5Å & \\ = 0.5\, C_{DIS}\, (r_{ij}^L - r_{ij}) & \text{if } r_{ij} < r_{ij}^L;\ |r_{ij}^L - r_{ij}| \geq 5Å & [6b] \end{array}$$

where C_{DIS} was a force constant. The dihedral angle restraint, E_{DIH}, was then represented by the biharmonic potential :

$$\begin{array}{rll} E_{DIH} = 0.5\, C_{DLR}\, (\Phi_k^U - \Phi_k)^2 & \text{if } \Phi_k > \Phi_k^U & \\ = 0.5\, C_{DLR}\, (\Phi_k^L - \Phi_k)^2 & \text{if } \Phi_k < \Phi_k^L & [7] \end{array}$$

where Φ_k^U and Φ_k^L were upper and lower allowed limits of the torsion angle, Φ_k was the calculated angle, and C_{DLR} was the force constant.

Starting models were first subjected to 500 steps of conjugate gradient EM. Then the starting structures were subjected to 12 ps of MD where values of the distance restraint force constant were increased from 400 to 4000 kJ mol^{-1} nm^{-2} and the dihedral restraint force constant from 200 to 2000 kJ mol^{-1} rad^{-2}. At 2 ps intervals, the force constants were increased and the velocities (taken from a Maxwellian distribution at 300 K) were re-initialized. During these re-initialization intervals, the structures were cooled with 500 steps of intervening EM. Newton's equations of motion were integrated with a time step of 2 fs, with all bond lengths kept rigid by the SHAKE algorithm (Ryckaert *et al.*, 1977). The molecule was weakly coupled to a temperature bath with a reference temperature of 300 K using a coupling constant of 0.1 ps (Berendsen *et al.*, 1984). A cut-off radius of 10 Å was used for the non-bonded interactions and the non-bonded pair list was updated every 20 fs. MD runs with the highest values of C_{DIS} and C_{DLR} were continued to approximately 20 ps in total, and coordinates were then averaged over another 2 ps to give averaged MD structures which were then subjected to another 500 steps of EM to correct distortions in the structure caused by the averaging procedure.

We performed two separate MD simulations for each peptide to determine its structure in 50%TFE. The first of these simulations used a set of input coordinates derived from the standard Φ,Ψ angles of an α-helix ($\Phi = -60°$, $\Psi = -40°$). The second of these simulations used a set of input coordinates derived from the standard Φ,Ψ angles of a β-strand ($\Phi = -118°$, $\Psi = +118°$). The distance restraint file used as input for the MD simulations is presented in Tables IX-9 and IX-10 in the Appendix for the TnI peptide and mastoparan in 50%TFE, respectively.

D. Results

1. Sequential Resonance Assignments and NOEs

Sequential assignments of the TnI peptide and mastoparan in 50%TFE, and of mastoparan in the presence of 0.1 molar equivalents of $TnC.Ca(II)_4$, were carried out according to the established procedures of Wuthrich *et al.* (Wuthrich *et al.*, 1982; Billeter *et al.*, 1982; Wagner *et al.*, 1982). This method relies on the observation of NOEs between the amide protons of one residue and the α-protons, β-protons and amide protons of the preceding residue ($d_{\alpha N}$, $d_{\beta N}$ *and* d_{NN}). Tables IX-1 and IX-2 show the ^1H chemical shifts for the assigned resonances of the TnI peptide and mastoparan in 50%TFE, respectively, and Table IX-3 shows the ^{1}H chemical shifts for the assigned resonances of mastoparan in the presence of 0.1 molar equivalents of TnC.Ca(II)$_4$.

a. TnI Peptide in 50%TFE. Figures IX-1A → IX-1D show one-dimensional spectra of the TnI peptide in 50%TFE versus aqueous solution. Figure IX-1A shows the complete upfield aliphatic region of the spectrum above the water resonance. Figure IX-1B shows the complete downfield region of the spectrum with the exchangeable guanidinium resonances of R108, R112, R113 and R115, the aromatic F106 resonances, the C-terminal NH2 group, and the backbone amide resonances. Figures IX-1C and IX-1D show expanded regions of Figure IX-1B. Figure IX-1C shows the backbone amide protons and the C-terminal NH2 group, and Figure IX-1D shows an expanded region of the backbone amide protons. From Figure IX-1A one can see that there is a rearrangement of the αCH proton resonances in 50%TFE versus aqueous solvent, many of these resonances shifting upfield from their chemical shift position in aqueous solvent. A large TFE resonance is discernable at approximately 3.9 ppm. Figures IX-1B and IX-1C clearly show large upfield shifts experienced by the backbone amide proton resonances in 50%TFE versus aqueous solvent. In Figure IX-1B, a new broad resonance is observed to appear at 7.6 ppm in 50%TFE. We have assigned this resonance to the side-chain ςNH resonance of K105 and K107 from connectivity patterns in the NOESY spectrum of this sample. It would appear as if the conformation adopted by the TnI peptide in 50%TFE is such that the chemical exchange rate experienced by the side-chain ςNH groups of K105 and K107 is sufficiently slowed to allow observation of these resonances.

Figure IX-2 shows the upfield region of the DQFCOSY spectrum and Figure IX-3 the upfield region of the NOESY spectrum of the TnI peptide in 50%TFE. Figure IX-4 shows the αCH-βCH region, and Figure IX-5 the downfield-βCH region of the NOESY spectrum. Figure IX-6 shows the αCH-NH region of the DQFCOSY spectrum, and Figure IX-7 the same region in the NOESY spectrum. Figure IX-8 shows the NH-NH backbone amide region of the NOESY spectrum. The presence of an all-trans peptide conformation is confirmed in the αCH-NH region of the DQFCOSY spectrum of the TnI peptide in 50%TFE. This region of the spectrum displays one cross-peak for every amino acid (excluding proline which has no NH), with no indication of any cis-trans X-proline peptide bond isomerization which would cause a doubling of peaks (Dyson *et al.*, 1988).

b. Mastoparan in 50%TFE. Figures IX-9A → IX-9C show one-dimensional spectra of mastoparan in 50%TFE versus aqueous solution. Figure IX-9A shows the complete upfield aliphatic region of the spectrum above the water resonance. Figure IX-9B shows all exchangeable proton resonances including the backbone amide proton resonances as well as the side chain and C-terminal amide resonances, and Figure IX-9C shows an expanded region of the backbone amide protons only. From Figure IX-9A one can see that there is a rearrangement of the αCH proton resonances in 50%TFE versus aqueous solvent, many of these resonances shifting upfield from their chemical shift position in aqueous solvent. A large TFE resonance is discernable at approximately 3.9 ppm. Figures IX-9B and IX-9C clearly show large upfield shifts experienced by the backbone amide proton resonances in 50%TFE versus aqueous solvent. The backbone amide proton resonances experience a large chemical shift dispersal in 50%TFE versus aqueous solvent, which facilitates their assignment in the helix-inducing solvent. The narrow chemical shift dispersal of these same resonances in aqueous solvent precluded a complete assignment in aqueous solvent.

Figure IX-10 shows the upfield region of the DQFCOSY spectrum and Figure IX-11 the upfield region of the NOESY spectrum of the TnI peptide in 50%TFE. Figure IX-12 shows the αCH-βCH region, and Figure IX-13 the downfield-βCH region of the NOESY spectrum. Figure IX-14 shows the αCH-NH region of the DQFCOSY spectrum, and Figure IX-15 the same region in the NOESY spectrum. Figure IX-16 shows the full NH-NH region of the NOESY spectrum with NOEs from the chemically exchanging C-terminal amide protons to the backbone amide of the final residue in the sequence, L14. Figure IX-16 also shows a connectivity between a side-chain δNH of N2 and the backbone amide of the same residue. Figure IX-17 is an expanded region of Figure IX-16 and shows $d_{NN\,i,i+1}$ connectivities between the backbone amide protons, a pattern diagnostic of α-helix.

c. Mastoparan in the Presence of 0.1 Molar Equivalents TnC.Ca(II)$_4$. Figures IX-18A → IX-18C show one-dimensional spectra of mastoparan in the absence versus the presence of 0.1 molar equivalents TnC.Ca(II)$_4$ to mastoparan. Figure IX-18A shows the complete upfield aliphatic region of the spectrum above the water resonance. Figure IX-18B shows all exchangeable proton resonances including the backbone amide proton resonances as well as the side chain and C-terminal amide resonances, and Figure IX-18C shows an expanded region of the backbone amide protons only. From Figures IX-18A → IX-18C one can see that as the mastoparan peptide samples a free versus bound conformation, the resonances experience some line broadening and change in chemical shift position, but δ_{obs} and $\Delta\nu_{obs}$ are dominated by the free ligand population for $p_F >> p_B$ (Campbell and Sykes, 1991a, 1991b; Chapters II and V). The shift of all resonances was observed to be in fast exchange (Campbell *et al.*, 1991a; Chapter IV). Figures IX-18B and IX-18C clearly show a new resonance belonging to the backbone amide proton of N2, which appears in the bound spectrum of mastoparan. This is probably due to the formation of structure at the N-terminal end of the peptide as it binds to TnC.

Figure IX-19 shows the upfield region of the DQFCOSY spectrum and Figure IX-20 the upfield region of the TRNOESY spectrum of mastoparan in the presence of 0.1 molar equivalents TnC.Ca(II)$_4$. Figure IX-21 shows the αCH-βCH region, and Figure IX-22 shows the downfield-βCH region of the TRNOESY spectrum. Figure IX-23 shows the αCH-NH region of the DQFCOSY spectrum, and Figure IX-24 the same region in the TRNOESY spectrum. Figure IX-25 shows the NH-NH backbone amide region of the TRNOESY spectrum.

Figure IX-26 shows the αCH-NH region of the NOESY spectrum of mastoparan superimposed upon the αCH-NH region of the TRNOESY spectrum of the same peptide in the presence of 0.1 molar equivalents TnC.Ca(II)$_4$. One can see the emergence of new peptide αCH-NH cross-peaks in the presence of protein, a function of the faster cross-relaxation rate between protons in the bound peptide versus the free peptide. A NOESY spectrum of just the TnC protein in the presence of Ca(II) allowed us to dismiss the possibility of these new cross-peaks being either protein-protein or protein-peptide NOEs (data not shown). The emergence of the new set of cross-peaks in the presence of protein is due not only to the longer bound correlation time experienced by the peptide when bound to protein, but also to a new bound peptide conformation for the bound peptide. Binding to TnC.Ca(II)$_4$ induces secondary structure in mastoparan. The peptide NOEs present in the absence of TnC protein are much weaker in intensity than the peptide TRNOEs in the presence of TnC protein, and several new cross-peaks have emerged for resonances at the N-terminus of the peptide, although these are only intraresidue ($d_{\alpha N\,i,i}$) or sequential ($d_{\alpha N\,i,i+1}$), and therefore not diagnostic of secondary structure. In the presence of 0.1 molar equivalents TnC.Ca(II)$_4$ to mastoparan, a sequential I1αCH-N2NH cross-peak and an intraresidue L3αCH-NH cross-peak have emerged. The emergence of new cross-peaks at the N-terminus suggests the development of secondary structure, whereas the increase in the relative intensity of cross-peaks at the N-terminus suggests a decreased motional freedom at the N-terminus of the bound mastoparan peptide. The inability to discern many medium range NOEs ($d_{\alpha N\,i,i+3}$), which are diagnostic of α-helix, could paradoxically be indicative of α-helical secondary structure in the peptide. In an α-helix, the α-protons are all found to be in similar chemical environments, and therefore they all resonate at approximately the same chemical shift position. This leads to overlapping cross-peaks in the αCH-NH portion of a two-dimensional spectrum. However, from Figure IX-25 one can see three $d_{NN\,i,i+1}$ cross-peaks which are suggestive of α-helix. These are L3NH-K4NH, K4NH-A5NH, and A7NH-A8NH.

2. Secondary Structure

a. TnI Peptide in 50%TFE. A summary of the distance restraints observed for the TnI peptide in 50% TFE is shown in Figure IX-27. The pattern of NOEs is not strongly diagnostic of an α-helical conformation of the TnI peptide in 50%TFE. However, the sequential restraints which helped to define helical regions were observed between sequential backbone NH residues ($d_{NN\,i,i+1}$). These include contacts between K105NH-F106NH, K107NH-R108NH, and R113NH-V114NH. An additional close contact $d_{NN\,i,i+3}$ was observed for R112NH-R115NH. A $d_{NN\,i,i+1}$ distance of 2.8 Å is diagnostic of α-helix (Wuthrich, 1986). The distance stretches to 4.3 Å in β-strand. Another medium range restraint which helps in defining the α-helix is the $d_{\alpha N\,i,i+3}$ close contact, however no NOEs of this nature were observed for the TnI peptide in 50%TFE.

There were also no medium range restraints between the F106δCH2 and ξCH2 aromatic ring protons and the P109βCH2 and γCH2 proline ring protons, and no long range restraints between the F106δCH2 and ξCH2 aromatic ring protons and the L111δCH3 and V114γCH3 methyl protons. These medium and long range contacts were observed for the TnI peptide in the presence of 0.1 molar equivalents $TnC.Ca(II)_4$ (Campbell and Sykes, 1991a; Chapter V). These contacts defined a tertiary fold around the two central proline residues (P109, P110), which formed a small hydrophobic pocket with the F106 aromatic ring into close proximity with the L111δCH3 and V114γCH3 methyl groups. The absence of these same medium and long range NOEs suggests that the TnI peptide in 50%TFE does not bend around the central proline residues, and therefore does not have a tertiary fold or a hydrophobic pocket. Furthermore, with no great evidence of α-helical connectivities in the NOESY spectrum, the peptide probably contains little if any helical structure.

A sequential restraint which defined a trans P109-P110 peptide bond configuration was the contact between P109αCH-P110δCH2. Comparison of cis and trans X-proline configurations shows that the distances between NH_i and αCH_i, $\delta CH2_{i+1}$ and αCH_{i+1} are strongly affected by cis-trans isomerization. The trans form allows close contact between αCH_i and $\delta CH2_{i+1}$ and between NH_i and $\delta CH2_{i+1}$, whereas the cis form allows close contact between αCH_i and αCH_{i+1} and between NH_i and αCH_{i+1} (Wuthrich, 1986).

b. Mastoparan in 50%TFE. A summary of the distance restraints observed for mastoparan in 50% TFE is shown in Figure IX-28. The pattern of NOEs strongly suggests an α-helix. The ($d_{NN\,i,i+1}$) sequential restraints which helped define the α-helix included L3NH-K4NH, K4NH-A5NH, A5NH-L6NH, L6NH-A7NH, A7NH-A8NH, A8NH-L9NH, L9NH-A10NH, A10NH-K11NH, L11NH-K12NH, K12NH-I13NH, and

I13NH-L14NH. Additionally, close $d_{NN\,i,i+2}$ contacts were observed for L3NH-A5NH, K4NH-L6NH, A5NH-A7NH, A7NH-L9NH, A8NH-A10NH, L9NH-L11NH, A10NH-K12NH, L11NH-I13NH, and K12NH-L14NH, and close $d_{NN\,i,i+3}$ contacts were observed for N2NH-A5NH, and L3NH-L6NH. Medium range $d_{\alpha N\,i,i+2}$ contacts were observed for A7αCH-L9NH, K11αCH-I13NH, and K12αCH-L14NH, and medium range $d_{\alpha N\,i,i+3}$ contacts, diagnostic of α-helix, were observed for A7αCH-A10NH, A8αCH-K11NH, L9αCH-K12NH, and K11αCH-L14NH.

c. Mastoparan in the Presence of 0.1 Molar Equivalents TnC.Ca(II)$_4$. A summary of the distance restraints observed for mastoparan in the presence of 0.1 molar equivalents TnC.Ca(II)$_4$ is shown in Figure IX-29. The pattern of TRNOEs is not strongly suggestive of α-helical conformation, however several ($d_{NN\,i,i+1}$) sequential restraints were observed which included L3NH-K4NH, K4NH-A5NH, and A7NH-A8NH. There were no other connectivities observed in the TRNOESY spectrum which could be diagnostic of α-helix, or of any other secondary structure. This could have been a function of the lack of chemical shift dispersion of αCH resonances in the αCH envelope, which in itself is suggestive of α-helix, but which makes a complete assignment difficult. However, this would not explain the virtual absence of $d_{NN\,i,i+1}$ sequential NOEs in the backbone amide region of the spectrum. The absence of interresidue TRNOEs in the TRNOESY spectrum precluded a molecular mechanics simulation, as the generation of a unique conformation of mastoparan bound to TnC would have required a larger set of TRNOE-derived distance restraints.

3. Distance Determination

Interproton distances were derived from pure phase absorption two-dimensional NOESY spectra recorded with a mixing time of 150 ms for the TnI peptide in 50%TFE, and 500 ms for mastoparan in 50%TFE. Interproton distances were not measured for the TRNOESY spectrum of mastoparan in the presence of 0.1 molar equivalents TnC.Ca(II)$_4$. The NOE intensities were normalized for the contribution of more than two protons to the cross-peak, and cross-peaks connecting exchangeable amide resonances were corrected for loss of intensity due to exchange or saturation transfer from the decoupled water peak. The normalized and corrected NOE cross-peak intensities were then transformed to distance restraints using a collection of reference proton pairs and error limits used to set r_{ij}^U and r_{ij}^L in order to account for systematic over- and under- determinations of r_{ij} (see experimental procedures).

When stereospecific assignments of protons were not possible, either due to dynamic effects such as rotation of the hydrogens in a methyl group or flipping of aromatic rings, or due to a degenerate chemical shift of prochiral atoms, pseudoatom representations were used (Wuthrich *et al.*, 1983). Distance restraints to such pseudoatoms were constructed from the position of the neighbouring non-hydrogen atoms by enlarging r_{ij}^U by a value calculated from the geometry of the pseudoatom (Wuthrich *et al.*, 1983). For the TnI peptide in 50%TFE, the basis for the tertiary structure computation consisted of a set of 124 interproton distance restraints comprising 90 intraresidue, 33 sequential ($|i - j| = 1$), and 1 medium ($1 < |i - j| \leq 4$) range interresidue distances. For mastoparan in 50%TFE, the basis for the tertiary structure computation consisted of a set of 201 interproton distance restraints comprising 107 intraresidue, 55 sequential ($|i - j| = 1$), and 39 medium ($1 < |i - j| \leq 4$) range interresidue distances.

4. Dihedral Angle Restraints

A set of Φ backbone dihedral angle restraints were derived from $^3J\alpha CH\text{-}NH$ coupling constants (Pardi *et al.*, 1984) measured from one-dimensional ^1H NMR spectra. A one-dimensional curve fitting program was used to more accurately measure coupling constants. For the TnI peptide in 50%TFE, the set of dihedral angle restraints was comprised of the Φ angles for only 2 residues: G104 and R115, since these were the only two residues for which $^3J\alpha CH\text{-}NH < 6.0$ Hz. For all other residues, the coupling constant fell within the range of $6.0 \text{ Hz} < {^3J\alpha CH\text{-}NH} < 8.0$ Hz. Therefore, it was not possible to restrain these Φ dihedral angles in the TnI peptide, as the measured $^3J\alpha CH\text{-}NH$ values did not correspond to either $-85° \leq \Phi \leq -40°$ or $-160° \leq \Phi \leq -80°$. For mastoparan in 50%TFE, the set of dihedral angle restraints was comprised of the Φ angles for all 14 residues as all $^3J\alpha CH\text{-}NH$ values measured were found to be less than 4.0 Hz, and therefore all Φ dihedral angles in the peptide were restrained to $-85° \leq \Phi \leq -40°$. This constrained the peptide into α-helical conformational space. All peptide bonds for both the TnI peptide and mastoparan in 50%TFE, including X-proline in the TnI peptide, were restrained to $-175° \leq \omega \leq -185°$. This maintained a trans peptide bond configuration.

5. Molecular Dynamics Calculations

We performed two separate MD simulations for each peptide in 50%TFE to determine their structure in the helix-inducing solvent. The first simulation started from an α-helical set of input coordinates and the second simulation from a β-strand set of input coordinates (see experimental procedures for details of these simulations). The coordinates of these structures are given in Tables IX-11 and IX-12 in the Appendix for the TnI peptide and mastoparan in 50%TFE, respectively. Table IX-13 in the Appendix compares the distances between proton pairs given in the distance restraint file for the TnI peptide in 50%TFE with those actually measured between the same proton pairs in the final structure. Table IX-14 in the Appendix is the corresponding table for mastoparan in 50%TFE. From Table IX-13, one can see that for the TnI peptide in 50%TFE, there are no distance violations greater than 1.5 Å for either the structure generated from the α-helix (structure 1) or the β-strand (structure 2). From Table IX-14, one can see that for mastoparan in 50%TFE, there are no distance violations greater than 2.0 Å for the structure generated from the α-helix (structure 1), and there are no distance violations greater than 3.0 Å for the structure generated from the β-strand (structure 2).

Figures IX-30 and IX-31 show the stereo structures of the TnI peptide and mastoparan in 50%TFE, respectively, derived from α-helical coordinates (structure 1). Following 12 ps of MD, the coordinates of 10 MD structures taken every 0.2 ps were averaged and the averaged coordinates were energy minimized to produce the final structure in the figure. Figures IX-32 and IX-33 show superpositions of these 10 structures for the TnI peptide and mastoparan in 50%TFE, respectively.

Table IX-4 presents two sets of dihedral angle values describing the final structures 1 and 2 for the TnI peptide in 50% TFE. Backbone Φ, Ψ and ω dihedral angles for all residues in the bound structures are given, as well as the side chain χ dihedral angles of the proline residues. The dihedral angles given for structure 1 and structure 2 are not consistent with the values expected for an α-helix (-60°, -40°). Although the Φ angles of all residues (including P109 and P110) fall within $-72° \leq \Phi \leq -55°$, a region within helical conformation space[1], the Ψ angles for all residues take on all values within ± 180°. There is general agreement between structures 1 and 2 for the Φ angles values, however there is no strong agreement between the two structures for the Ψ angles. For example, for R108, Ψ(structure 1) = -29°, whereas Ψ(structure 2) = 126°. Thus, it would appear that there was insufficient NOE data to restrain the TnI peptide to a singular conformation, probably due to a lack of defined secondary structure for the peptide in 50%TFE. There are steric constraints on the conformation of the proline rings in that both prolines display a Cβ exo ring pucker for both structures. For P109, the dihedral angle values which define the ring pucker are $\chi^1 = 34°$, $\Phi = -41°$ for structure 1 and $\chi^1 = 16°$, $\Phi = -28°$ for structure 2. For

---

[1] α-helix is described by Φ,Ψ values of -58°,-47°; 3_{10}-helix is described by Φ,Ψ values of -76°,-5°; and Π-helix is described by Φ,Ψ values of -57°,-70° (Ghelis and Yon, 1982).

P110, the dihedral angle values which define the ring pucker are $\chi^1 = 38°$, $\Phi = -34°$ for structure 1 and $\chi^1 = 36°$, $\Phi = -33°$ for structure 2. All peptide bonds in the final structures are trans.

Table IX-5 presents two sets of dihedral angle values describing the final structures 1 and 2 for mastoparan in 50% TFE. The dihedral angles given for structure 1 and structure 2 are consistent with α-helical values, the Φ angles of all residues falling within $-86° \leq \Phi \leq -42°$, and the Ψ angles of all residues falling within $-63° \leq \Phi \leq -17°$. There is excellent agreement between the Φ, Ψ values for structures 1 and 2. Thus, it would appear that the mastoparan peptide achieved a single conformation in α-helical dihedral angle space in the molecular mechanics simulations. All peptide bonds in the final structures are trans.

E. Discussion

TnC and CaM bind a variety of naturally occurring extracellular peptides, including the opiates β-endorphin (Giedroc *et al.*, 1983) and dynorphin (Malencik and Anderson, 1984), various members of the glucagon family (Malencik and Anderson, 1982, 1983a) and a group of cytotoxic peptides, among them bee venoms melittin (Haberman and Jentsch, 1967; Compte *et al.*, 1983; Cox *et al.*, 1985) and the mastoparans (Malencik and Anderson, 1984, 1983b). Binding of these peptides to Ca(II)-saturated TnC and CaM is typically with high affinity ($K_d = 10^{-8} - 10^{-9}$ M) and has been shown to inhibit effectively the modulating activity of these two HLH proteins for their intracellular targets (Sellinger-Barnette and Weiss, 1982; Malencik and Anderson, 1982, 1983b; Compte *et al.*, 1983; Maulet and Cox, 1983; Barnette *et al.*, 1983; Giedroc *et al.*, 1983, 1985). All the inhibitory target peptides share the common characteristic of containing sequences with high propensities to form amphiphilic α-helices.

Evidence for a molecular interaction involving amphiphilic helix recognition between the target peptide and the target protein comes from the work of DeGrado and co-workers (DeGrado *et al.*, 1985; Erickson-Viitanen *et al.*, 1987) who designed amphiphilic CaM-binding peptides which bound in submicromolar dissociation constants. To test the hypothesis that CaM could recognize positively charged amphiphilic α-helical peptides independent of their precise amino acid sequence, this same group also designed a set of fluorescent analogs of a very tight binding inhibitor of CaM in which the fluorescent amino acid tryptophan was systematically moved throughout the sequence of the peptide (O'Neil *et al.*, 1990; O'Neil and DeGrado, 1990). The analogs, when complexed with CaM, displayed a periodic fluorescence decay which repeated every three or four residues, a pattern which could be explained by an α-helical structure for the bound peptide.

Solution CD and NMR studies involving β-endorphin (Malencik and Anderson, 1983a), mastoparan (Malencik and Anderson, 1983a, 1983b; McDowell *et al.*, 1985; Cachia *et al.*, 1986; Sanyal *et al.*, 1988) and melittin (Cox *et al.*, 1985; Maulet and Cox, 1983; Seeholzer *et al.*, 1986) indicated an induction of helical conformation upon complexation with the complementary surface of CaM. Sanyal *et al.* (1988) studied the binding of CaM fragments 1-77 (CaM 1-77) and 78-148 (CaM 78-148) to mastoparan X, *Polistes* mastoparan, and melittin. Difference CD spectra suggested that binding to CaM (78-148) was associated with the induction of considerable degrees of helicity in the amphiphilic peptides, which by themselves have predominantly random coil structures in aqueous solution. McDowell *et al.* (1984) showed using CD that mastoparan, mastoparan X and *Polistes* mastoparan all have a random conformation in dilute aqueous solution, but >50% helix when dissolved in 70%TFE or when the peptides are bound to CaM.

Cachia *et al.* (1986) used CD as a structure probe to examine CaM and TnC complex formation with mastoparan and the TnI inhibitory peptide (104-115). They found that complex formation between mastoparan and either CaM or TnC results in an increase in helical content, whereas the helical content of the TnI inhibitory peptide does not increase when bound to either protein. They interpreted these results as indicating that these peptides exhibit substantially different secondary structures upon binding to CaM or TnC, and that an α-helical structure was not a prerequisite for the binding of target proteins to CaM and TnC. Significantly, they found mastoparan to be 78% α-helical in 50%TFE, whereas the TnI inhibitory peptide contained no α-helix in the same solvent. The same group also examined the ability of mastoparan to regulate the acto-subfragment 1-tropomyosin ATPase and found that mastoparan and the TnI inhibitory peptide inhibited 31% and 45% of the activity, respectively.

In order to determine the role of amphiphilicity in the recognition of calcium-binding proteins for their target molecules, we have used ^{1}H NMR to examine and compare the structure of two target molecules in a helix-inducing solvent versus when bound to Ca(II)-saturated TnC. We chose the TnI inhibitory peptide (104-115) and the bee venom mastoparan as target molecules, the first since it is biologically relevant to the study of muscle contraction, and the second since it serves as a good model for amphiphilic helical peptides. The TnI peptide is extremely basic, with four arginines and two lysines (K105, K107, R108, R112, R113 and R115) within a twelve residue sequence. Alternating with these basic residues are hydrophobic ones (F106, L111 and V114). The pattern of alternating basic and hydrophobic residues is interrupted by two sequential proline residues

(P109 and P110). Mastoparan is also basic, with three lysine residues (K4, K11 and K12) within a fourteen residue sequence. With the exception of one asparagine (N2), the remainder of amino acids in the mastoparan sequence are hydrophobic, with two isoleucines (I1 and I13), four leucines (L3, L6, L9 and L14), and four alanines (A5, A6, A8 and A10). Given that the TnI peptide and mastoparan sequences contain alternating hydrophobic and hydrophilic residues, one might expect these peptides to adopt an amphiphilic helical conformation in a hydrophobic or helix-inducing environment.

In a previous study (Campbell and Sykes, 1991a; Chapter V), we used the two-dimensional TRNOESY experiment and molecular mechanics to determine the structure of the TnI peptide bound to Ca(II)-saturated skeletal TnC. The TRNOE-derived structure of the TnI peptide bound to TnC revealed a distorted helical structure with Φ,Ψ values in the α-helical range (-60°, -40°), except around the two central proline residues where the Φ,Ψ values were approximately -70°, -170°. This tertiary fold around the P109-P110 sequence functioned to bring the hydrophobic residues (F106, L111 and V114) into closer proximity with each other, thereby forming a small hydrophobic pocket. The hydrophilic, basic residues extended from the opposite face of the peptide.

Although the bound conformation of the TnI peptide has a hydrophobic pocket and a hydrophilic face, strictly speaking, the tertiary fold around the two central proline residues prevents the structure being described as an amphiphilic helix, since this implies an uninterrupted α-helical stretch of three turns or more with equal numbers of hydrophilic and hydrophobic residues on opposite faces of the helix. The inhibitory TnI peptide contains only three hydrophobes in a twelve residues sequence, an insufficient number to generate a hydrophobic face. Furthermore, these three hydrophobes are partially buried in a small hydrophobic pocket, and do not extend outward on the hydrophobic 'side' of the structure.

In the present study we used the conventional two-dimensional NOESY experiment and molecular mechanics to determine the structure of the TnI peptide in the helix-inducing solvent TFE. The NOE-derived structure of the TnI peptide in 50%TFE reveals an unstructured peptide, with little or no secondary or tertiary structure, and certainly no α-helix. The absence of tertiary structure is not surprising since a helix-inducing organic solvent like TFE would disrupt hydrophobic contacts within the TnI peptide, preventing the formation of a tertiary fold or a hydrophobic pocket. The absence of helical secondary structure is not surprising given the position of the two proline residues (P109, P110) situated in the middle of the sequence. The proline residues are 'helix-breakers' due to the limited range of dihedral angles available to them in conformational space, a function of the steric constraints on the five-membered proline ring. A twelve residue peptide with two helix-breaking residues in the center of the sequence cannot be expected to adopt an α-helical conformation, since this would involve the induction of helix over a stretch of only five residues at the N- and C-termini of the peptide. That the TnI peptide adopts 'helix-like' structure at the N- and C-terminal ends of the sequence when bound to TnC may be a function of the tertiary fold induced in the peptide by the interaction of complementary hydrophobic surfaces in the complex. The tertiary fold might maintain a proper alignment of residues in the N- and C-terminal stretches of the peptide such that they would have to adopt a 'helix-like' structure in order to interact with the complementary residues on TnC.

In the present study we also used the two-dimensional TRNOESY and NOESY experiments, coupled with molecular mechanics, to determine the structure of mastoparan bound to TnC versus in 50%TFE. When bound to TnC, mastoparan did not exhibit a high degree of α-helix or secondary structure of any nature. The absence of interresidue TRNOEs in the TRNOESY spectrum precluded a molecular mechanics simulation as the generation of a unique conformation of mastoparan bound to TnC would have required a larger set of TRNOE-derived distance restraints. The NOE-derived structure of mastoparan in 50%TFE, however, appeared to be virtually 100% α-helical, with the Φ, Ψ values for all residues in the α-helical range (-60°, -40°). Thus, although it appears that there is no strong NMR evidence to suggest that mastoparan binds to TnC as an amphiphilic helix, it certainly displays a strong tendancy to adopt α-helical structure in the unbound state, since in 50%TFE the peptide is virtually 100% α-helical.

Our structures for the TnI peptide and mastoparan in 50%TFE agree with previous CD studies (Malencik and Anderson, 1983a, 1983b; McDowell *et al.*, 1985; Cachia *et al.*, 1986; Sanyal *et al.*, 1988) which found mastoparan to be α-helical, but the TnI peptide to contain little or no α-helix in the helix-inducing solvent. However, the TRNOE-derived structure for the TnI peptide bound to TnC (Campbell and Sykes, 1991a; Chapter V), which displayed helical stretches in the N-terminal and C-terminal ends of the peptide, is not substantiated by the CD studies of Cachia *et al.* (1986) which found that the helical content of the TnI peptide did not increase when bound to either CaM or TnC.

We did not use molecular mechanics to generate a structure for mastoparan bound to Ca(II)-saturated skeletal TnC, since the quality of the TRNOE data did not allow the assignment of many interresidue NOEs. This may be partly due to a lack of chemical shift dispersion in the αCH envelope, a phenomenon in itself being suggestive of helical structure. However, the assignment of a few $d_{NN\,i,i+1}$ connectivities in the N-terminal half of mastoparan suggested the induction of some α-helix when the peptide bound to TnC. Solution CD studies of mastoparan bound to CaM (Malencik and Anderson, 1983a, 1983b; McDowell *et al.*, 1985; Cachia *et al.*, 1986; Sanyal *et al.*, 1988) and TnC (Cachia *et al.*,

1986) strongly indicate the induction of helical conformation in the peptide upon complexation with the protein. This leads us to suggest that mastoparan could indeed be α-helical when bound to TnC. However, NMR may not be the best solution technique to study the bound structure of this particular peptide as the spectrum suffers from problems of spectral overlap in the αCH region.

In this study, we have used ^{1}H NMR to investigate the role of amphiphilicity in the binding of target peptides to TnC by comparing the structures of mastoparan and the inhibitory TnI peptide (104-115) in the helix inducing solvent TFE versus when bound to Ca(II)-saturated TnC. Although we do not dispute the fact that amphiphilic helices play a role in target molecule binding, our results suggest that α-helical secondary structure is not a prerequisite for binding. The TnI peptide clearly does not bind to Ca(II)-saturated TnC as an amphiphilic helix, and displays little propensity to adopt helical structure in a helix-inducing solvent. In addition, one can not neglect the fact that when the whole TnI protein binds to TnC, it does so through at least two different regions of each molecule (Syska *et al.*, 1976; Grabarek *et al.*, 1981). There is no evidence that an individual mastoparan molecule interacts with more than one region of CaM or TnC. Consequently, we conclude that the interaction of a solitary amphiphilic helix, like mastoparan, with a single portion of a regulatory protein is not necessarily representative of a physiologically relevent interaction between natural target proteins, an interaction which may involve many regions on the proteins and may also involve the induction of tertiary as well as simple secondary structural elements.

Table IX-1. Chemical shifts for the assigned ^{1}H resonances of the TnI peptide at 5°C in 50%TFE, 50 mM KCl, pH 6.2.

residue	NH	αCH	βCH	others
G104	8.16	3.89		NAcCH3 2.07
K105	8.08	4.19	1.62	γCH2 1.22, δCH2 1.62, ξCH2 2.93
F106	7.96	4.63	(x)2.99, (m)3.22	δCH2 7.26, ξCH2ζCH 7.35
K107	8.01	4.33	1.71	γCH2 1.43, δCH2 1.83, ξCH2 2.98
R108	8.09	4.63	1.68	γCH2 1.85, δCH2 3.21
P109		4.63	(x)1.89, (p)2.34	γCH2 2.04, δCH2 (m)3.62, (m')3.83
P110		4.54	(x)2.02, (p)2.19	γCH2 2.00, δCH2 (m)3.56, (m')3.73
L111	7.97	4.26	1.64	γCH 1.67, δCH3 0.88, 0.93
R112	8.14	4.31	1.85	γCH2 1.67, δCH2 3.21
R113	8.14	4.31	1.85	γCH2 1.67, δCH2 3.21
V114	7.91	4.09	2.14	γCH3 0.96
R115	8.21	4.28	1.86	γCH2 1.66, δCH2 3.21, NH 6.98,7.42

Table IX-2. Chemical shifts for the assigned ^{1}H resonances of mastoparan at 5°C in 50%TFE, 50 mM KCl, pH 6.2.

residue	NH	αCH	βCH	others
I1	-	-	-	γCH2 (p)1.21, (t)1.51, γCH3' 0.96, δCH3 0.90
N2	-	4.79	(m)2.84, (x)3.10	CONH2 6.70, 7.66
L3	8.40	4.10	1.73	γCH 1.64, (δCH3)2 0.88, 0.92
K4	7.96	4.01	1.92	γCH2 1.50, δCH2 1.73, ξCH2 2.98
A5	7.56	4.15	1.46	
L6	7.76	4.12	1.72	γCH 1.72, (δCH3)2 0.88, 0.92
A7	8.27	4.05	1.50	
A8	7.74	4.11	1.54	
L9	8.13	4.12	1.88	γCH 1.73, (δCH3)2 0.88, 0.92
A10	8.62	3.97	1.48	
K11	7.92	3.95	1.96	γCH2 1.50, δCH2 1.73, ξCH2 2.98
K12	7.76	4.12	2.08	γCH2 1.50, δCH2 1.73, ξCH2 2.98
I13	8.34	3.82	1.87	γCH2 (p)1.19, (t)1.70, γCH3' 0.90, δCH3 0.82
L14	8.46	4.23	1.86	γCH 1.76, (δCH3)2 0.88, 0.92, NH2 6.90,7.12

Table IX-3. Chemical shifts for the assigned ^{1}H resonances of mastoparan at 5°C in the presence of 0.1 molar equivalents TnC.Ca(II)$_4$, 50 mM KCl, pH 6.3.

residue	NH	αCH	βCH	others
I1		3.85	1.94	γCH2 (p) 1.19, (ι) 1.48, γCH3' 0.98, δCH3 0.91
N2	8.87	4.85	(m) 2.82, (x) 2.94	CONH2 7.04,7.78
L3	8.69	4.20	1.70	γCH 1.70, (δCH3)2 0.88,0.94
K4	8.37	4.18	1.85	γCH2 1.50, δCH2 1.70, ξCH2 3.00
A5	8.06	4.23	1.43	
L6	8.00	4.25	1.70	γCH 1.70, (δCH3)2 0.88,0.94
A7	8.20	4.23	1.43	
A8	8.06	4.23	1.43	
L9	8.15	4.21	1.70	γCH 1.70, δ(CH3)2 0.88,0.94
A10	8.06	4.23	1.43	
K11	8.23	4.25	1.84	γCH2 1.41, δCH2 1.70, ξCH2 3.00
K12	8.08	4.22	1.82	γCH2 1.44, δCH2 1.70, ξCH2 3.00
I13	8.28	4.10	1.87	γCH2 (p) 1.21, (ι) 1.52, γCH3' 0.91, δCH3 0.86
L14	8.33	4.30	1.70	γCH 1.70, (δCH3)2 0.88,0.94, NH2 7.20,7.57

Table IX-4. Dihedral angle values in the final structure of the TnI peptide in 50% TFE generated from (a) α-helix (structure 1), and (b) β-strand (structure 2).

residue	Φ	Ψ	ω	$\chi1$	$\chi2$	$\chi3$
G104		(a) 77	(a) -178			
		(b) -34	(b) 179			
K105	(a) -65	(a) 36	(a) -174			
	(b) -51	(b) -26	(b) 180			
F106	(a) -70	(a) 11	(a) -174			
	(b) -62	(b) -40	(b) 176			
K107	(a) -69	(a) 29	(a) -176			
	(b) -70	(b) 70	(b) -174			
R108	(a) -58	(a) -29	(a) -170			
	(b) -71	(b) 126	(b) 167			
P109	(a) -61	(a) -12	(a) 172	(a) 34	(a) -41	(a) 33
	(b) -72	(b) -19	(b) 169	(b) 16	(b) -28	(b) 32
P110	(a) -55	(a) -38	(a) 177	(a) 38	(a) -34	(a) 17
	(b) -64	(b) -76	(b) 178	(b) 36	(b) -33	(b) 20
L111	(a) -70	(a) -39	(a) -173			
	(b) -66	(b) -169	(b) 173			
R112	(a) -65	(a) -72	(a) -175			
	(b) -67	(b) 159	(b) 170			
R113	(a) -69	(a) -51	(a) 178			
	(b) -66	(b) -40	(b) 170			
V114	(a) -69	(a) -180	(a) 174			
	(b) -55	(b) 110	(b) 180			
R115	(a) -67					
	(b) -55					

Table IX-5. Dihedral angle values in the final structure generated for mastoparan in 50% TFE from (a) α-helix (structure 1), and (b) β-strand (structure 2).

residue	Φ	Ψ	ω
I1		(a) 157	(a) -177
		(b) 146	(b) 178
N2	(a) -54	(a) -29	(a) 176
	(b) -76	(b) -17	(b) 179
L3	(a) -55	(a) -39	(a) 180
	(b) -63	(b) -25	(b) 175
K4	(a) -78	(a) -43	(a) 180
	(b) -70	(b) -35	(b) 174
A5	(a) -60	(a) -35	(a) 171
	(b) -67	(b) -40	(b) 171
L6	(a) -56	(a) -38	(a) 173
	(b) -57	(b) -48	(b) 176
A7	(a) -68	(a) -41	(a) 174
	(b) -65	(b) -37	(b) 174
A8	(a) -59	(a) -41	(a) 172
	(b) -56	(b) -49	(b) 176
L9	(a) -58	(a) -40	(a) 176
	(b) -56	(b) -51	(b) 178
A10	(a) -71	(a) -23	(a) 170
	(b) -58	(b) -35	(b) 171
K11	(a) -76	(a) -43	(a) 173
	(b) -85	(b) -25	(b) 170
K12	(a) -47	(a) -36	(a) 173
	(b) -57	(b) -34	(b) 175
I13	(a) -45	(a) -63	(a) -178
	(b) -42	(b) -57	(b) -180
L14	(a) -84		
	(b) -86		

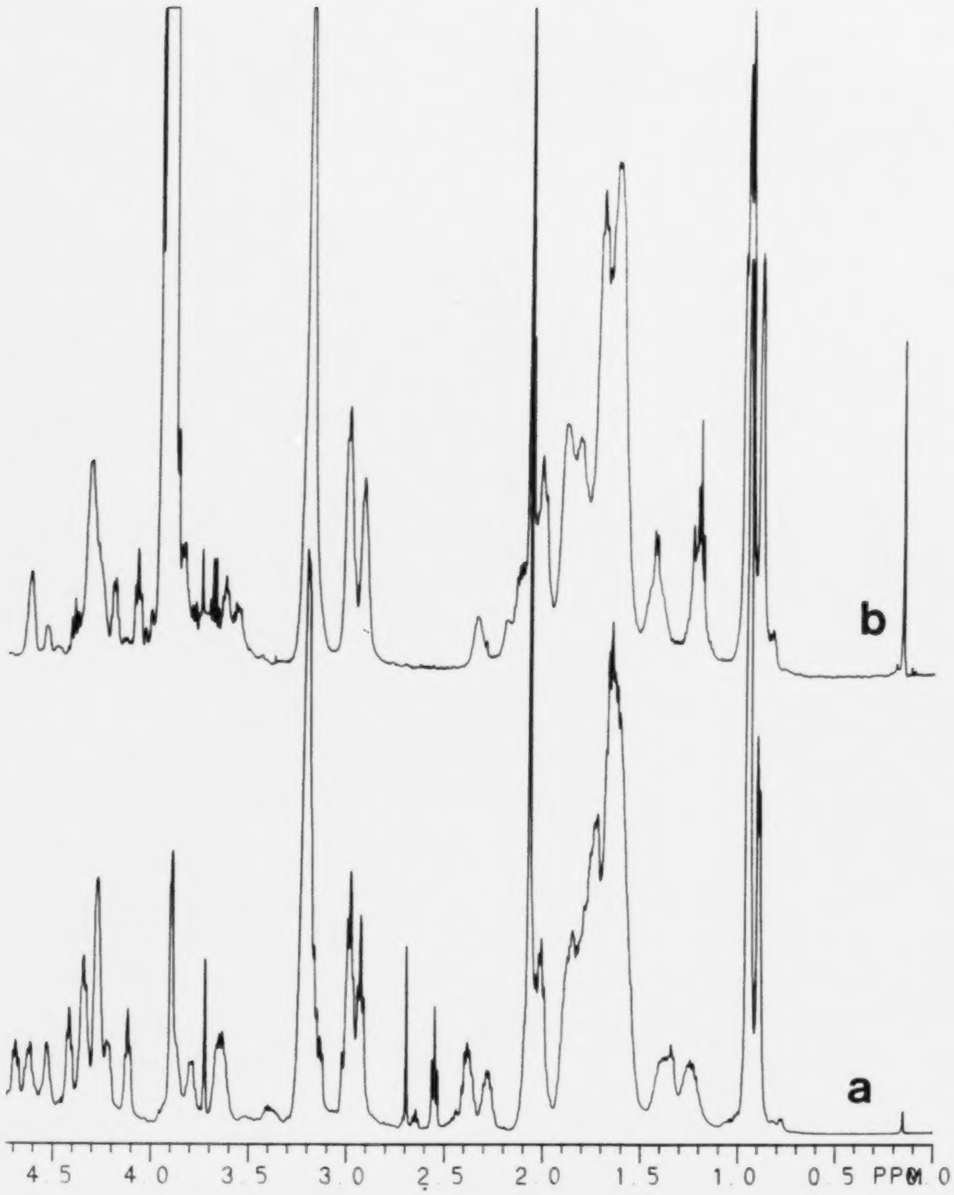

Figure IX-1A. 500 MHz ^{1}H NMR spectra of the TnI peptide in H_20 and 50%TFE: Aliphatic upfield region of the spectrum. **a.** 3 mM Nα-acetyl-TnI(104-115) amide, 50 mM KCl, pH 6.2, 80%H_2O/20%D_2O, 5°C; **b.** 3 mM Nα-acetyl-TnI(104-115) amide, 50 mM KCl, pH 6.2, 50%TFE/50%H_2O, 5°C.

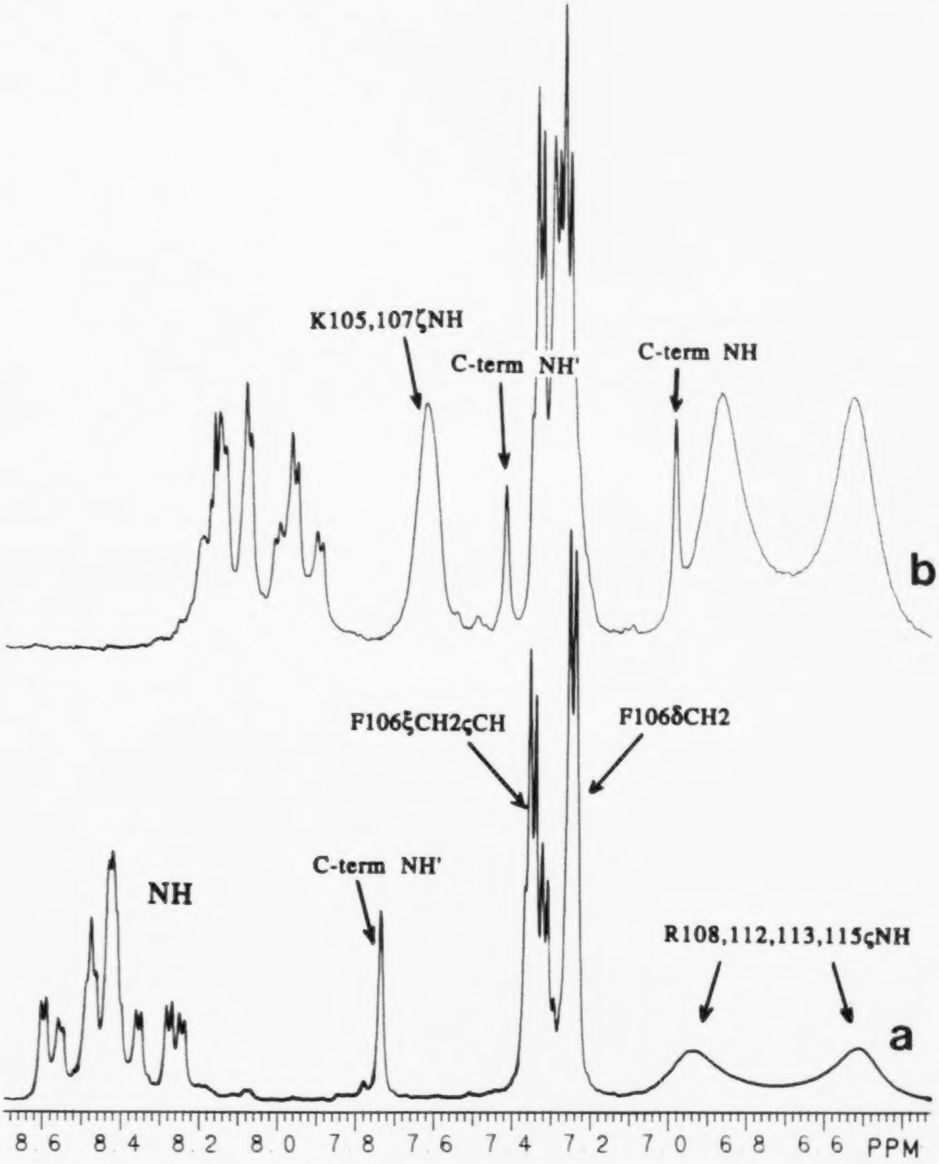

Figure IX-1B. 500 MHz ^{1}H NMR spectra of the TnI peptide in H_2O and 50%TFE: Complete downfield region of the spectrum with the exchangeable guanidinium resonances of R108, R112, R113 and R115 and the aromatic F106 resonances. **a.** 3 mM Nα-acetyl-TnI(104-115) amide, 50 mM KCl, pH 6.2, 80%H_2O/20%D_2O, 5°C; **b.** 3 mM Nα-acetyl-TnI(104-115) amide, 50 mM KCl, pH 6.2, 50%TFE/50%H_2O, 5°C.

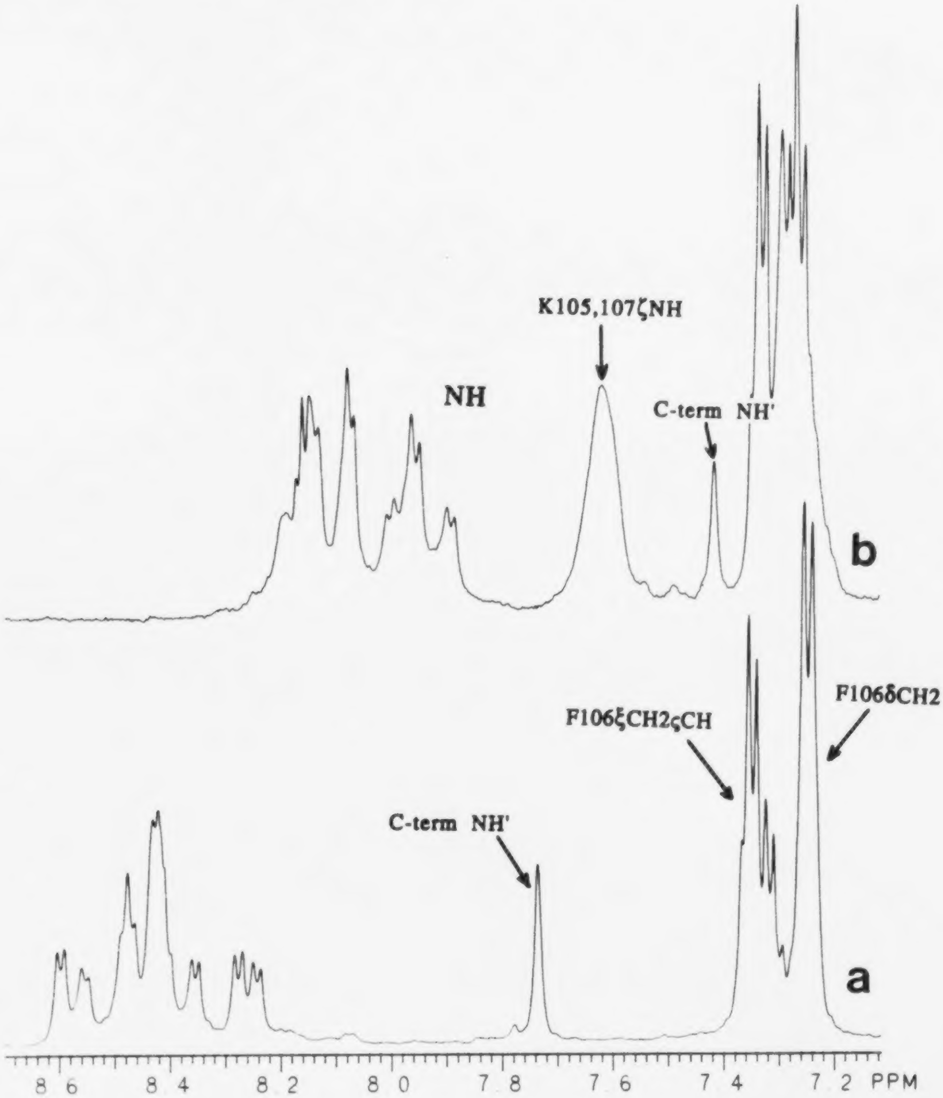

Figure IX-1C. 500 MHz ^{1}H NMR spectra of the TnI peptide in H_20 and 50%TFE: Expanded region of spectrum B showing the backbone amide proton resonances and the C-terminal amide resonance. **a.** 3 mM Nα-acetyl-TnI(104-115) amide, 50 mM KCl, pH 6.2, 80%H_2O/20%D_2O, 5°C; **b.** 3 mM Nα-acetyl-TnI(104-115) amide, 50 mM KCl, pH 6.2, 50%TFE/50%H_2O, 5°C.

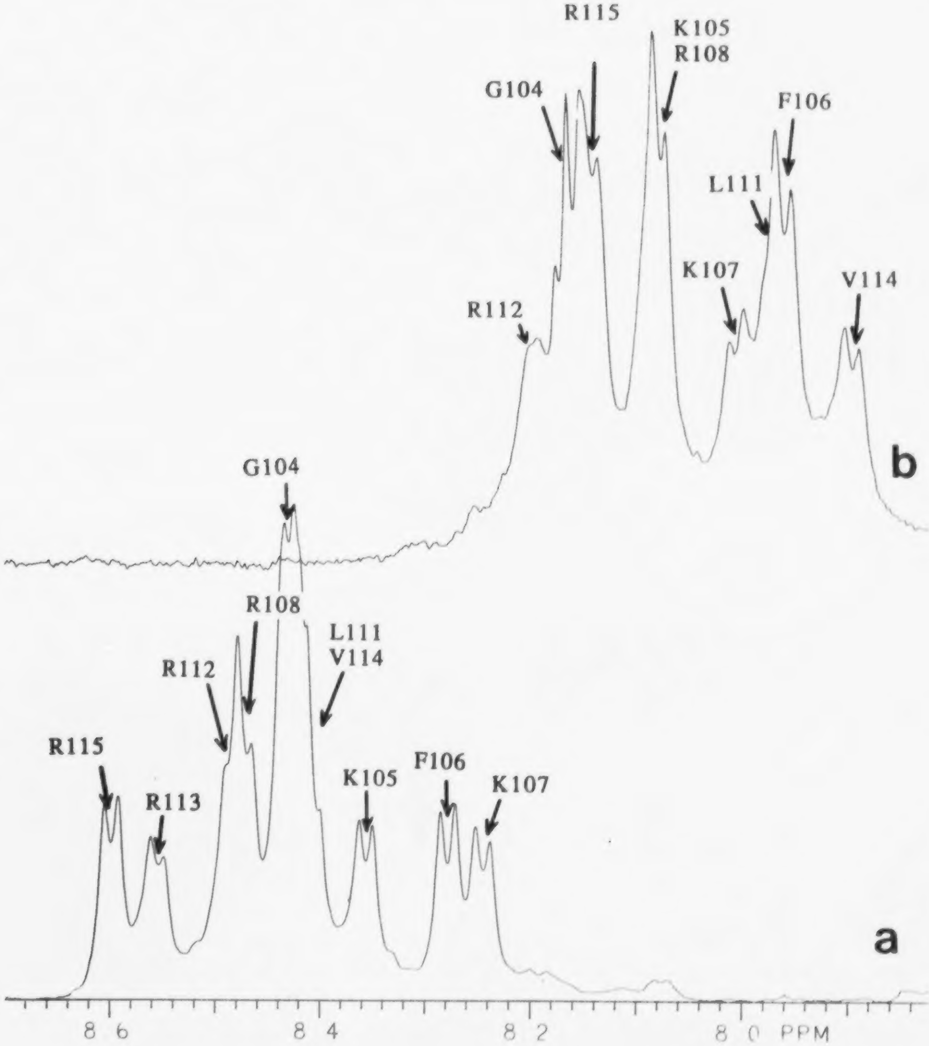

Figure IX-1D. 500 MHz ^{1}H NMR spectra of the TnI peptide in H_20 and 50%TFE: Expanded region of spectrum B showing only the backbone amide proton resonances. **a.** 3 mM Nα-acetyl-TnI(104-115) amide, 50 mM KCl, pH 6.2, 80%H_2O/20%D_2O, 5°C; **b.** 3 mM Nα-acetyl-TnI(104-115) amide, 50 mM KCl, pH 6.2, 50%TFE/50%H_2O, 5°C.

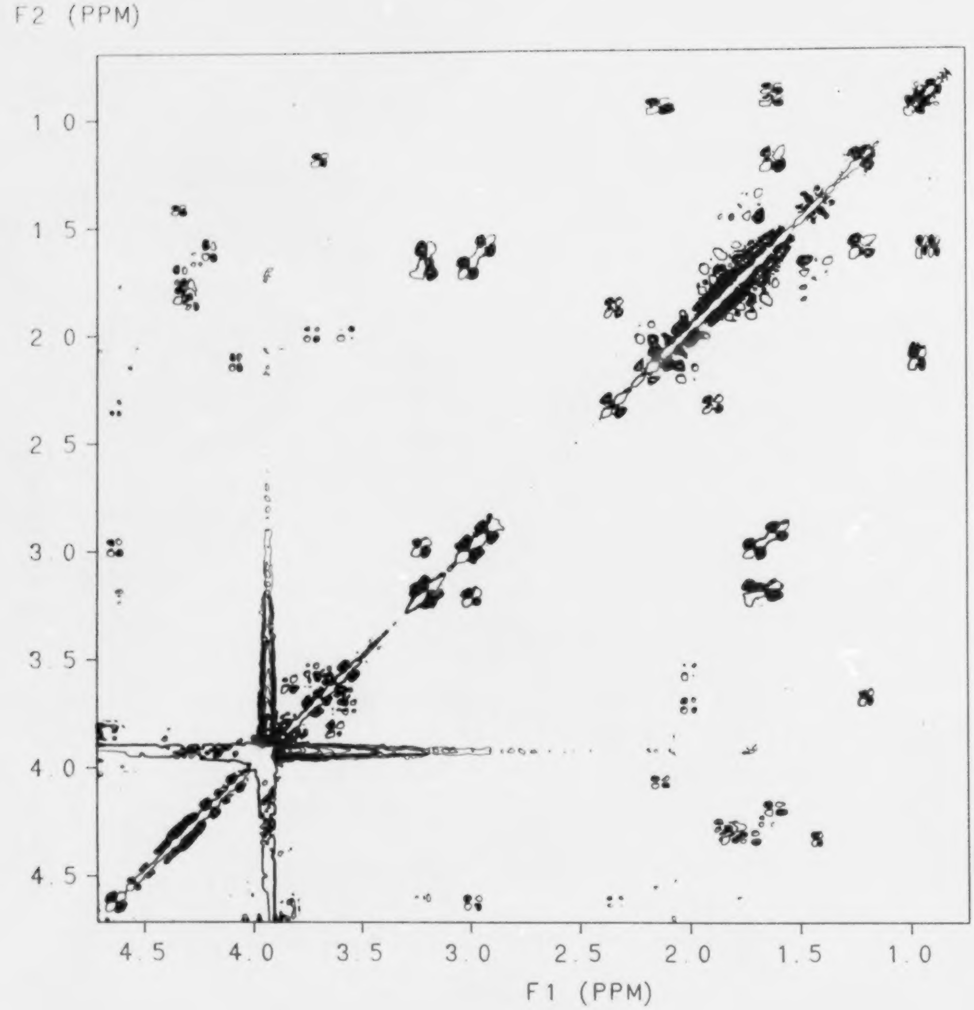

Figure IX-2. Upfield region of the DQFCOSY spectrum of the TnI peptide in 50%TFE. (3 mM Nα-acetyl-TnI(104-115) amide, 50 mM KCl, pH 6.2, 50%TFE/50%H_2O, 5°C)

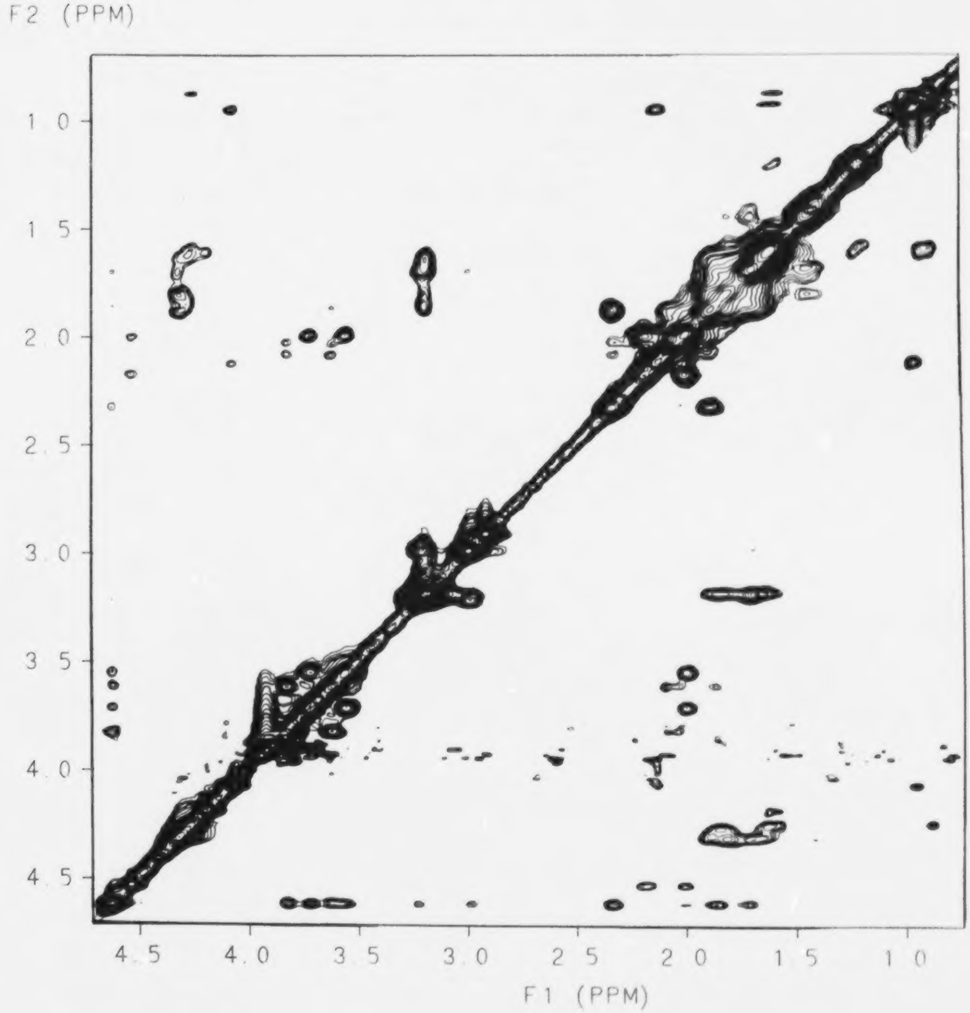

Figure IX-3. Upfield region of the NOESY spectrum of the TnI peptide in 50%TFE. (3 mM Nα-acetyl-TnI(104-115) amide, 50 mM KCl, pH 6.2, 50%TFE/50%H_2O, 5°C)

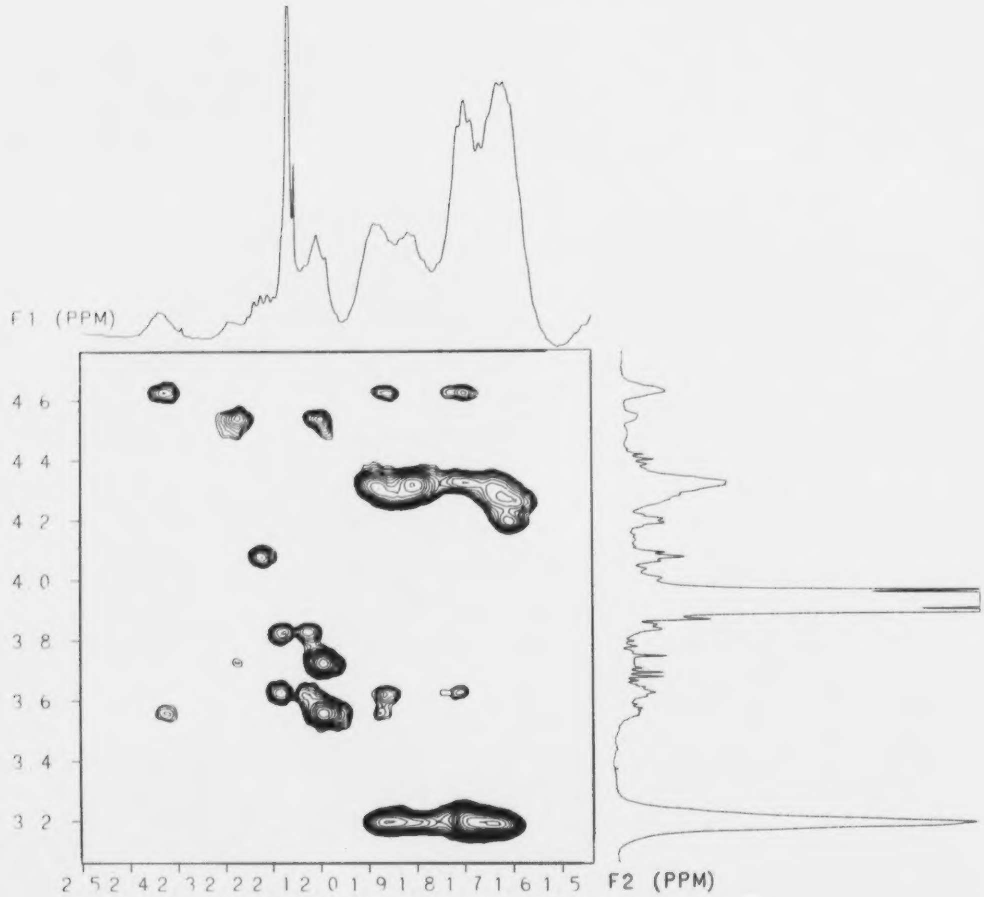

Figure IX-4. αCH-βCH region of the NOESY spectrum of the TnI peptide in 50%TFE. (3 mM Nα-acetyl-TnI(104-115) amide, 50 mM KCl, pH 6.2, 50%TFE/50%H_2O, 5°C, τ_m = 150 ms)

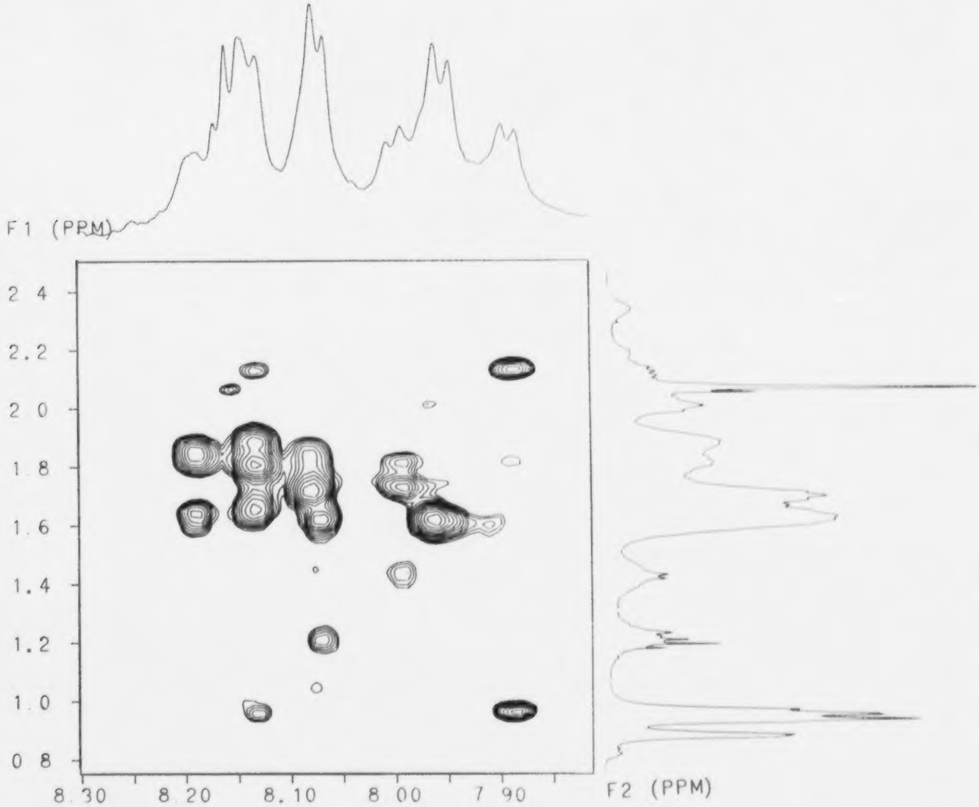

Figure IX-5. Downfield-βCH region of the NOESY spectrum of the TnI peptide in 50%TFE. (3 mM Nα-acetyl-TnI(104-115) amide, 50 mM KCl, pH 6.2, 50%TFE/50%H_2O, 5°C, τ_m = 150 ms)

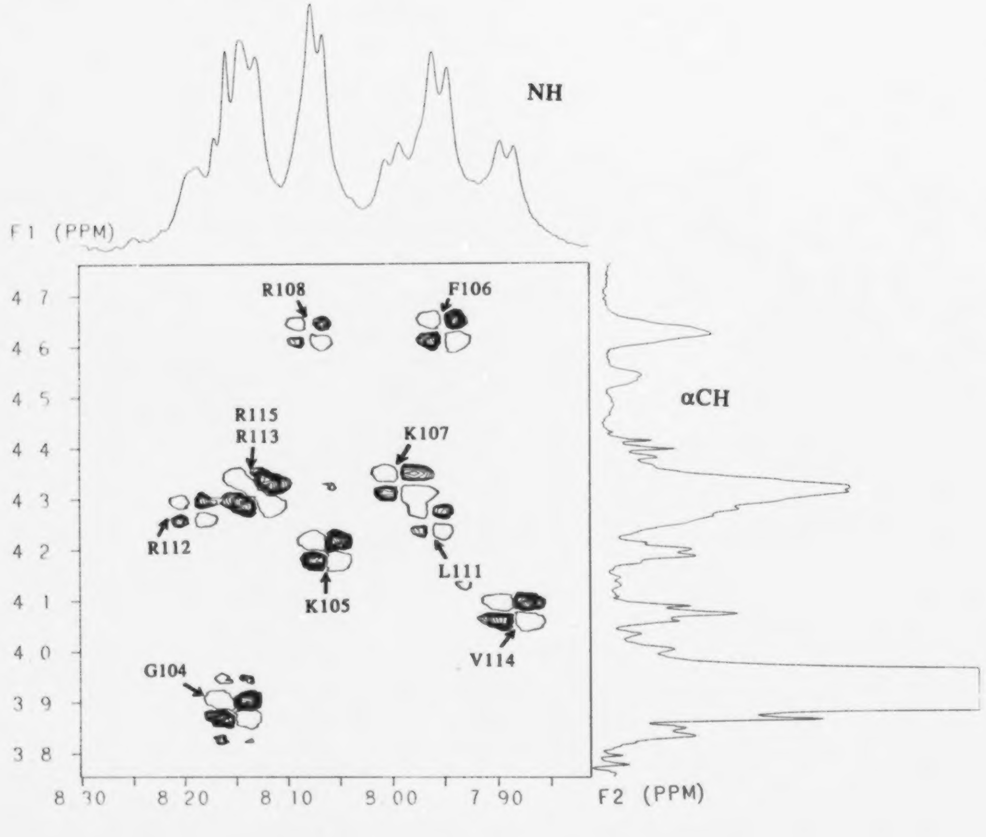

Figure IX-6. αCH-NH region of the DQFCOSY spectrum of the TnI peptide in 50%TFE. (3 mM Nα-acetyl-TnI(104-115) amide, 50 mM KCl, pH 6.2, 50%TFE/50%H_2O, 5°C)

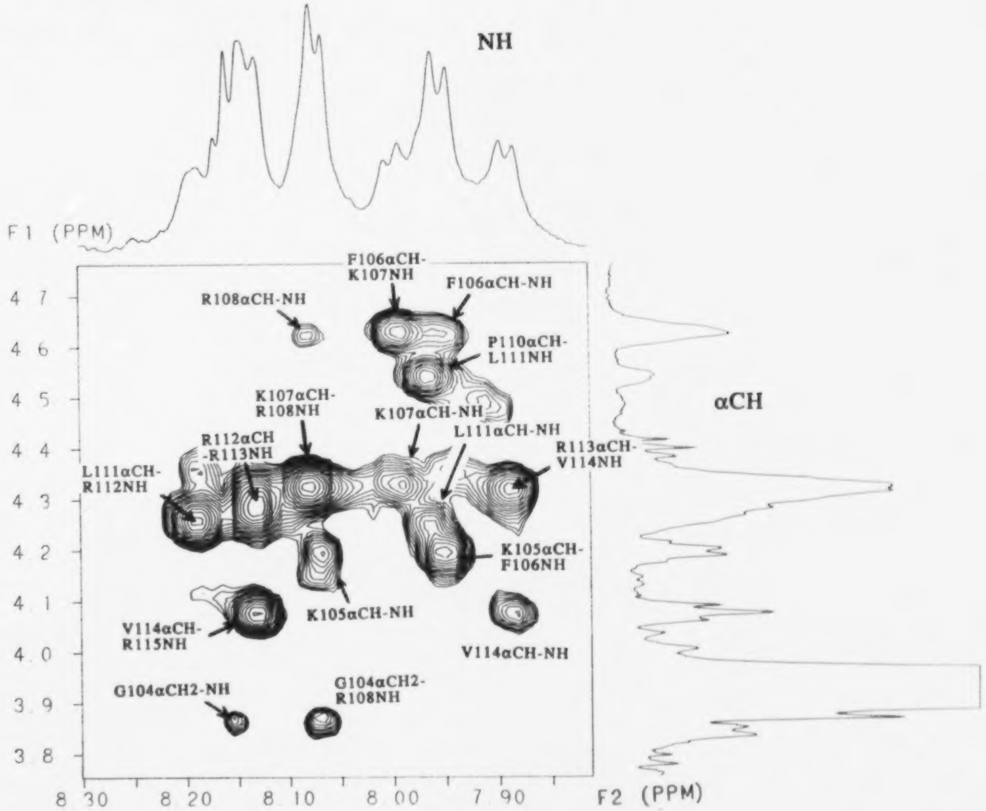

Figure IX-7. αCH-NH region of the NOESY spectrum of the TnI peptide in 50%TFE. (3 mM Nα-acetyl-TnI(104-115) amide, 50 mM KCl, pH 6.2, 50%TFE/50%H_2O, 5°C, τ_m = 150 ms)

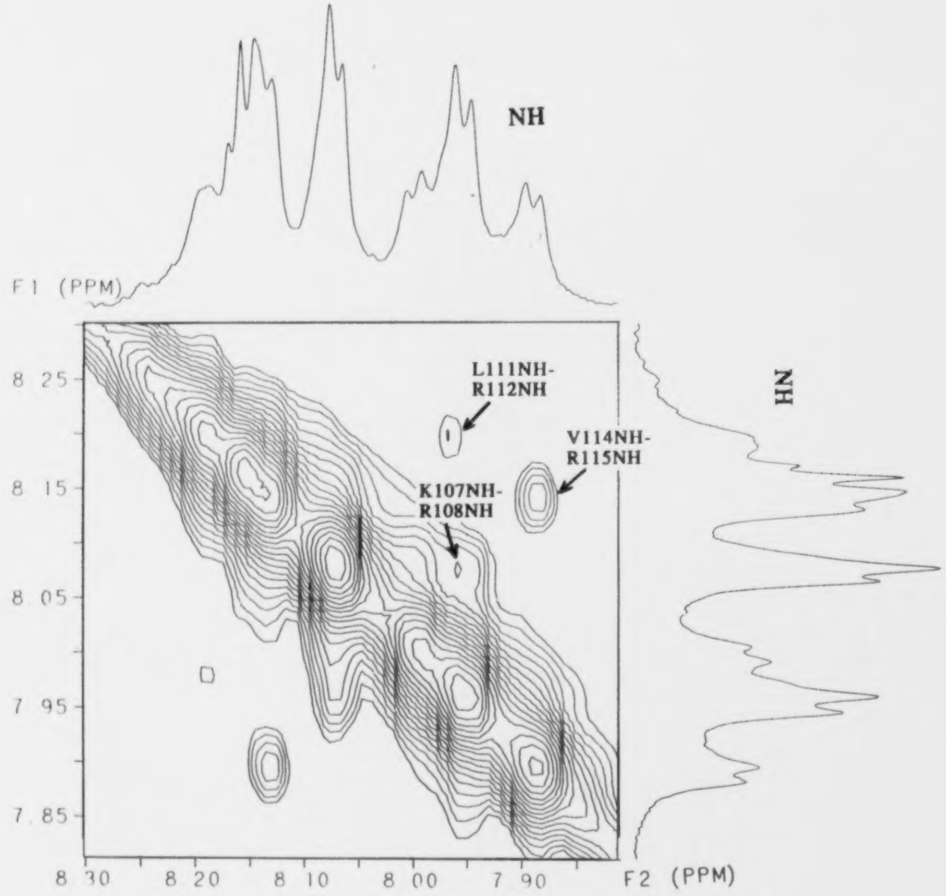

Figure IX-8. NH-NH region of the NOESY spectrum of the TnI peptide in 50%TFE showing NOEs between backbone amide protons. (3 mM Nα-acetyl-TnI(104-115) amide, 50 mM KCl, pH 6.2, 50%TFE/50%H_2O, 5°C, τ_m = 150 ms)

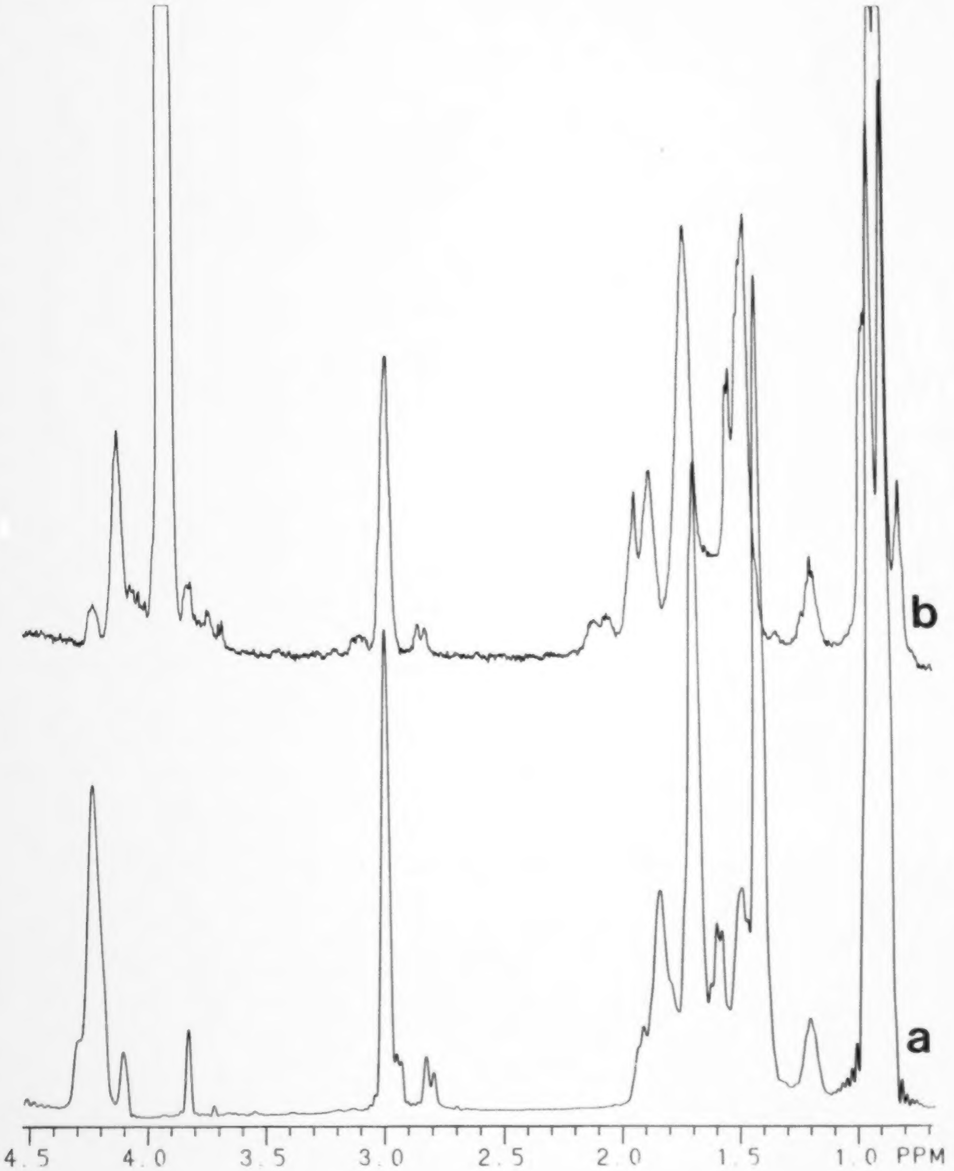

Figure IX-9A. 500 MHz ^1H NMR spectra of mastoparan in H_20 and 50%TFE: Aliphatic upfield region of the spectrum. **a.** 2.5 mM mastoparan, 50 mM KCl, pH 6.2, 80%H_20/20%D_2O, 5°C; **b.** 2.5 mM mastoparan, 50 mM KCl, pH 6.2, 50%TFE/50%H_2O, 5°C.

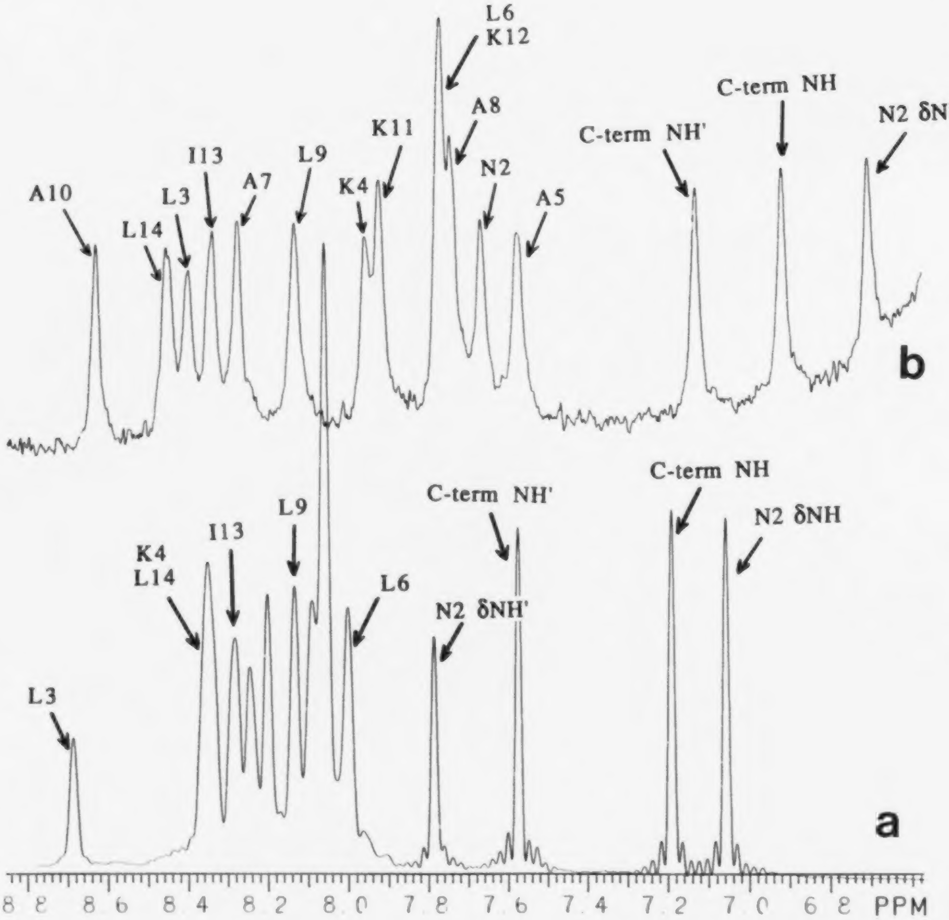

Figure IX-9B. 500 MHz ^{1}H NMR spectra of mastoparan in H_20 and 50%TFE: Complete downfield region of the spectrum. **a.** 2.5 mM mastoparan, 50 mM KCl, pH 6.2, 80%H_20/20%D_2O, 5°C; **b.** 2.5 mM mastoparan, 50 mM KCl, pH 6.2, 50%TFE/50%H_2O, 5°C.

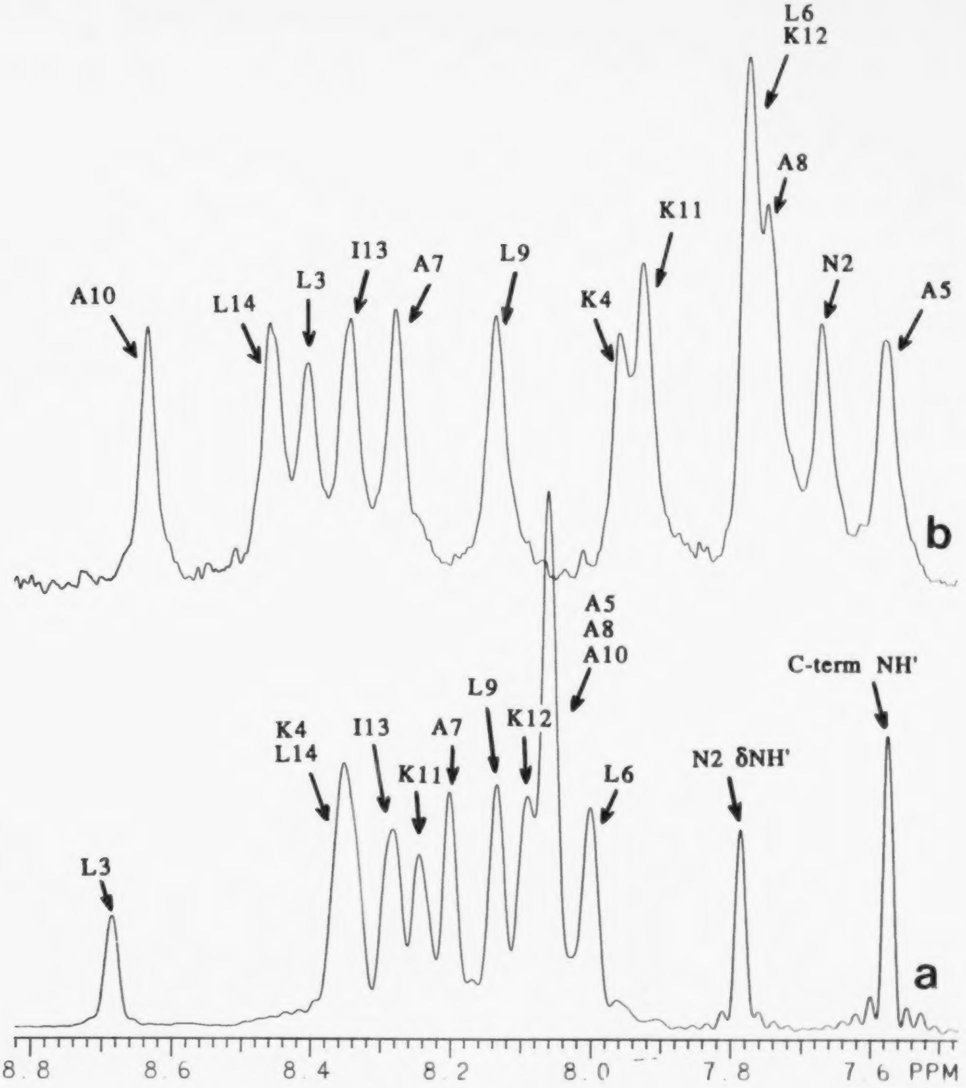

Figure IX-9C. 500 MHz ^{1}H NMR spectra of mastoparan in H_20 and 50%TFE: Expanded region of spectrum B showing only the backbone amide proton resonances. **a.** 2.5 mM mastoparan, 50 mM KCl, pH 6.2, 80%H_20/20%D_2O, 5°C; **b.** 2.5 mM mastoparan, 50 mM KCl, pH 6.2, 50%TFE/50%H_2O, 5°C.

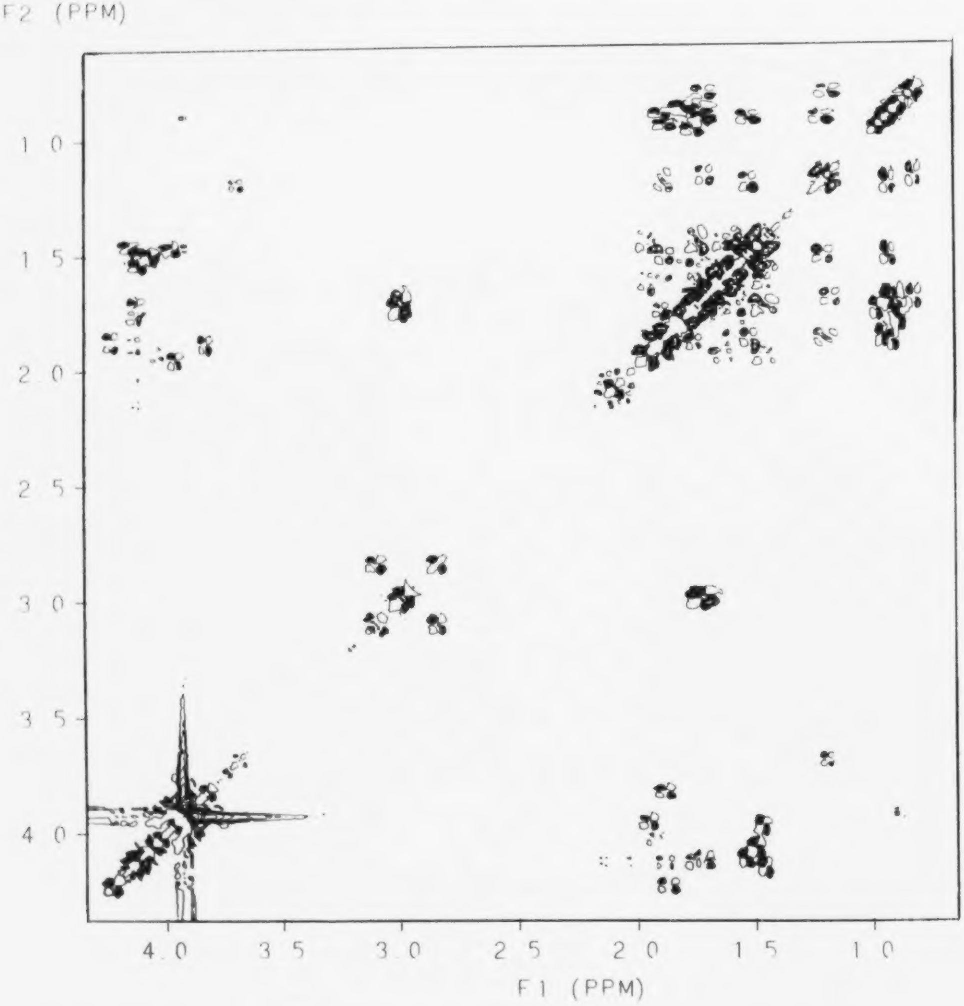

Figure IX-10. Upfield region of the DQFCOSY spectrum of mastoparan in 50%TFE. (2.5 mM mastoparan, 50 mM KCl, pH 6.2, 50%TFE/50%H_2O, 5°C)

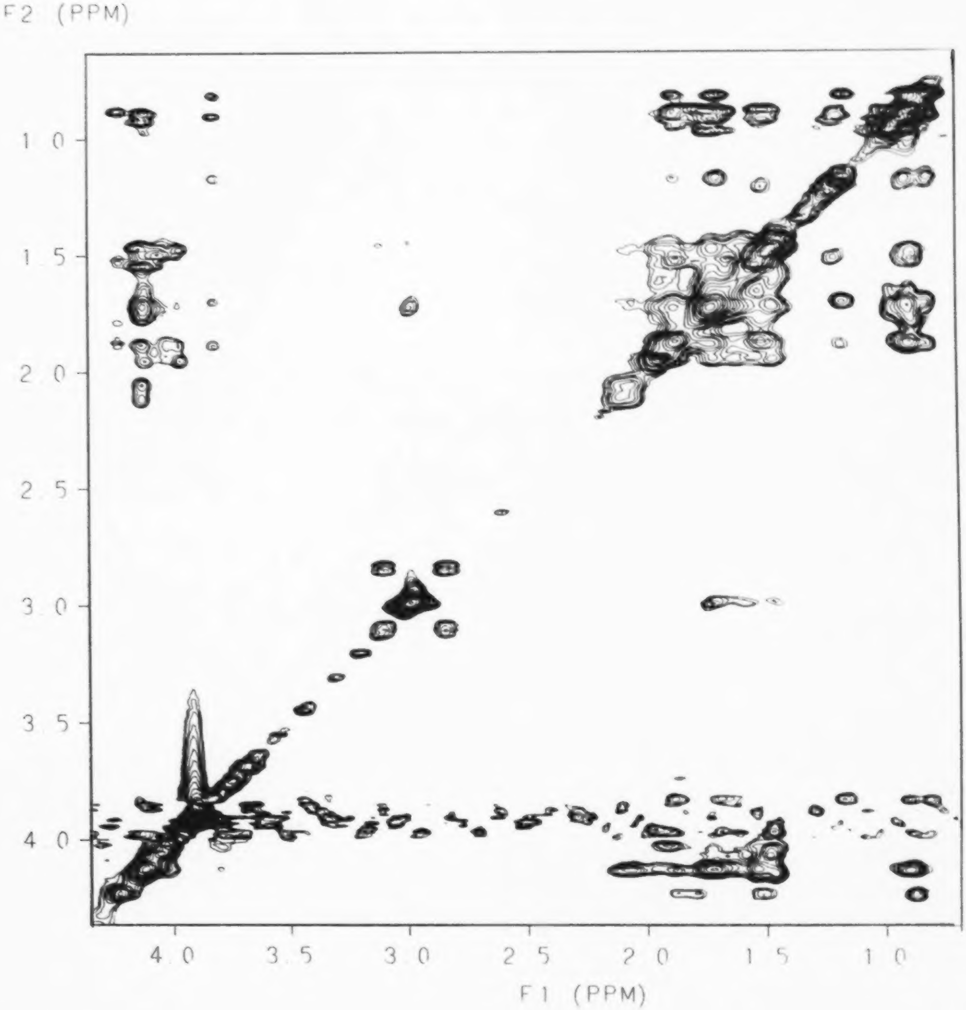

Figure IX-11. Upfield region of the NOESY spectrum of mastoparan in 50%TFE. (2.5 mM mastoparan, 50 mM KCl, pH 6.2, 50%TFE/50%H_2O, 5°C)

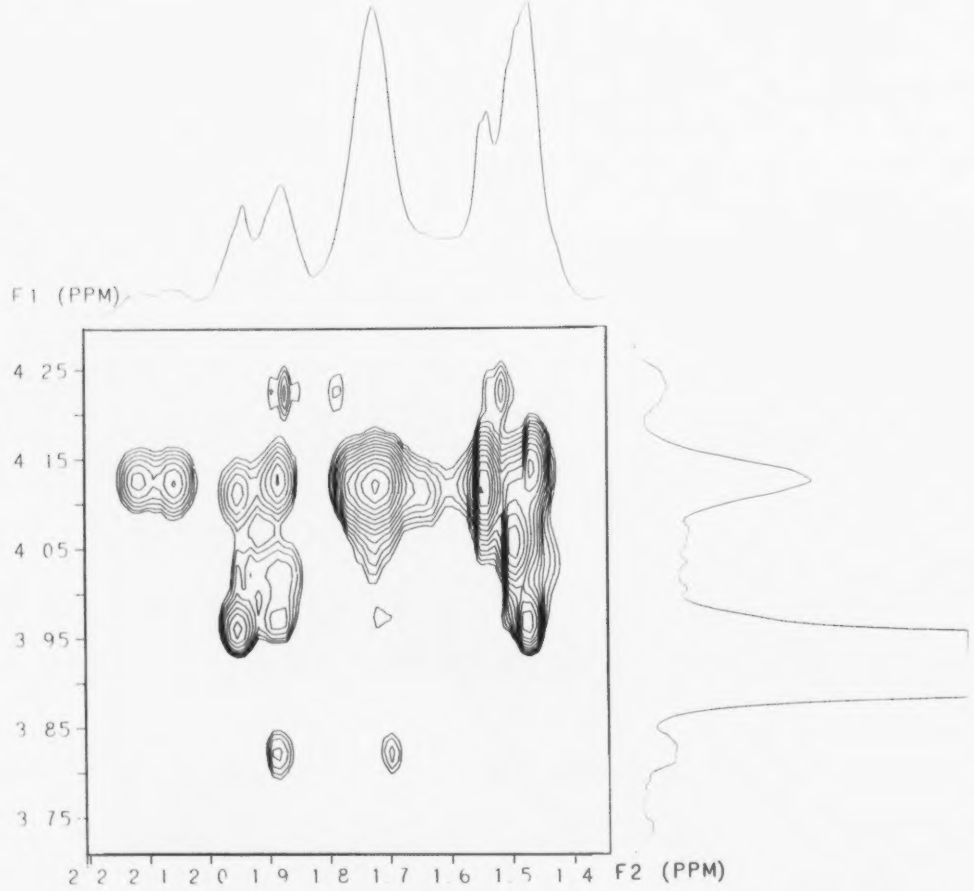

Figure IX-12. αCH-βCH region of the NOESY spectrum of mastoparan in 50%TFE. (2.5 mM mastoparan, 50 mM KCl, pH 6.2, 50%TFE/50%H_2O, 5°C, τ_m = 500 ms)

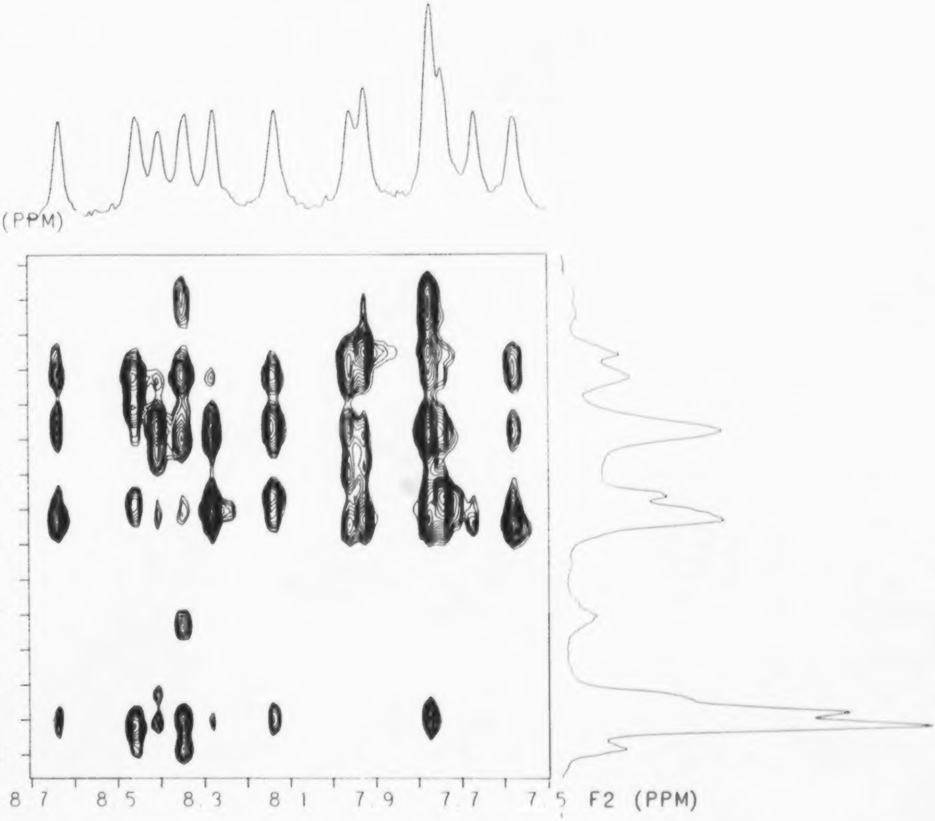

Figure IX-13. Downfield-βCH region of the NOESY spectrum of mastoparan in 50%TFE. (2.5 mM mastoparan, 50 mM KCl, pH 6.2, 50%TFE/50%H_2O, 5°C, τ_m = 500 ms)

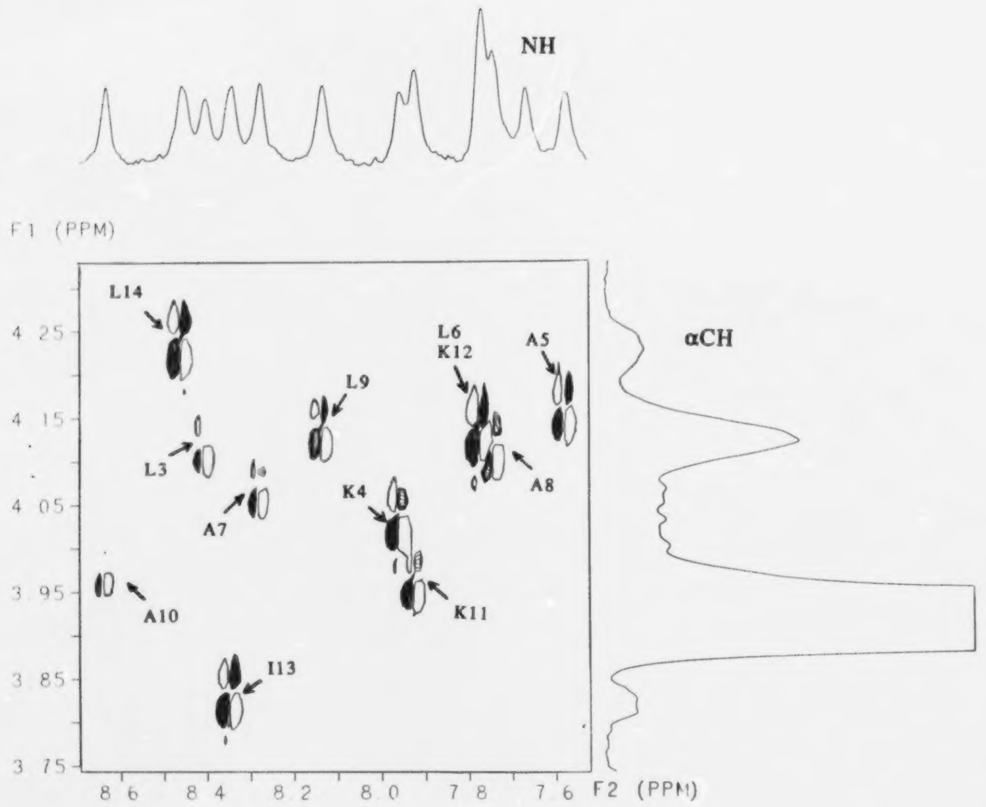

Figure IX-14. αCH-NH region of the DQFCOSY spectrum of mastoparan in 50%TFE. (2.5 mM mastoparan, 50 mM KCl, pH 6.2, 50%TFE/50%H_2O, 5°C)

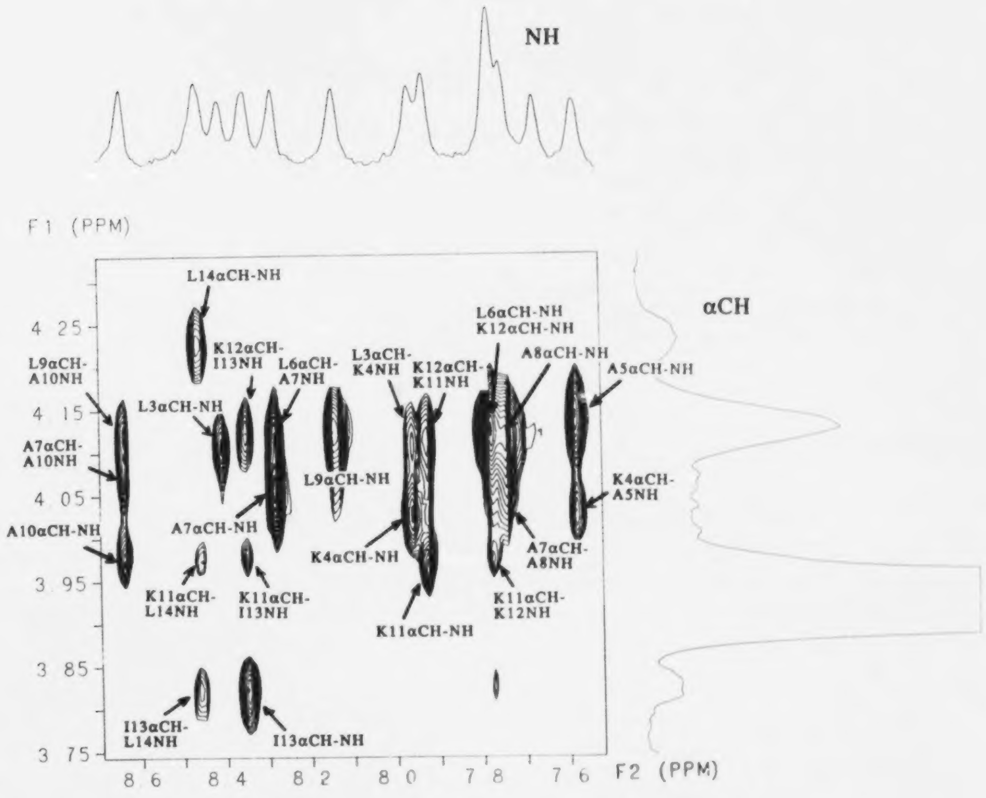

Figure IX-15. αCH-NH region of the NOESY spectrum of mastoparan in 50%TFE. (2.5 mM mastoparan, 50 mM KCl, pH 6.2, 50%TFE/50%H_2O, 5°C, τ_m = 500 ms)

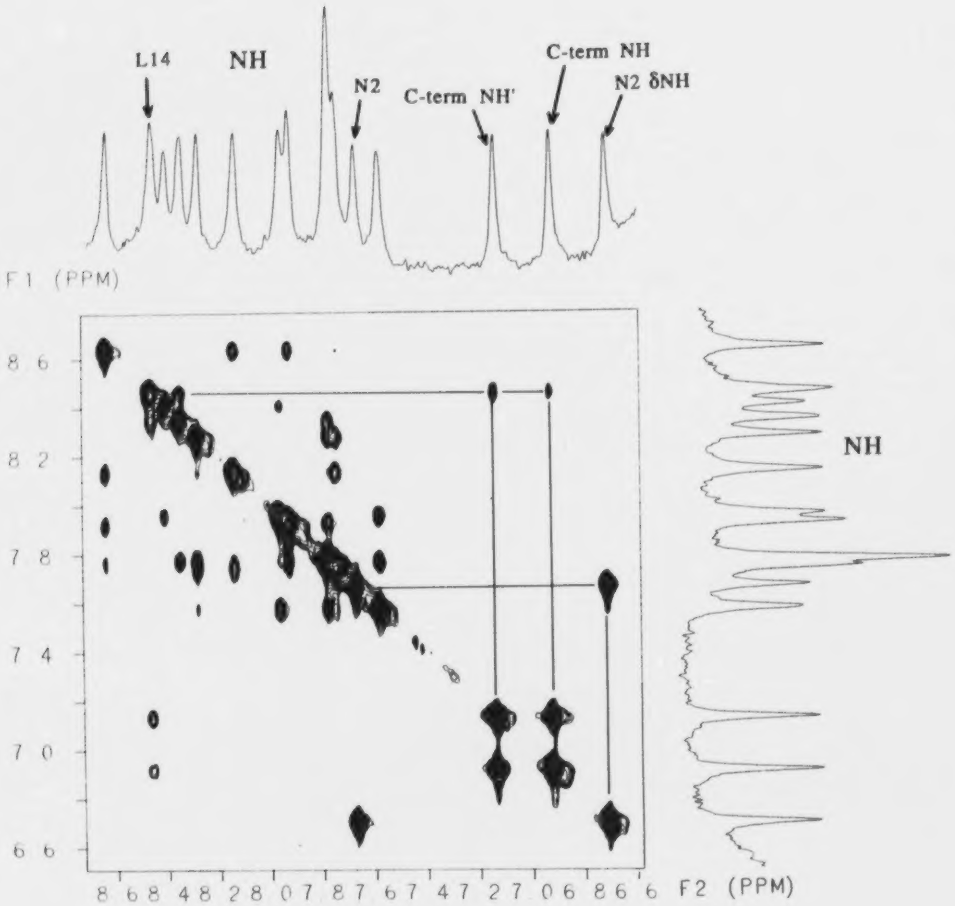

Figure IX-16. NH-NH region of the NOESY spectrum of mastoparan in 50%TFE showing NOEs between the chemically exchanging C-terminal NH2 groups and the backbone amide of the C-terminal residue, L14. Also shown is an NOE between the δNH group of N2 and its backbone amide. (2.5 mM mastoparan, 50 mM KCl, pH 6.2, 50%TFE/50%H_2O, 5°C, τ_m = 500 ms)

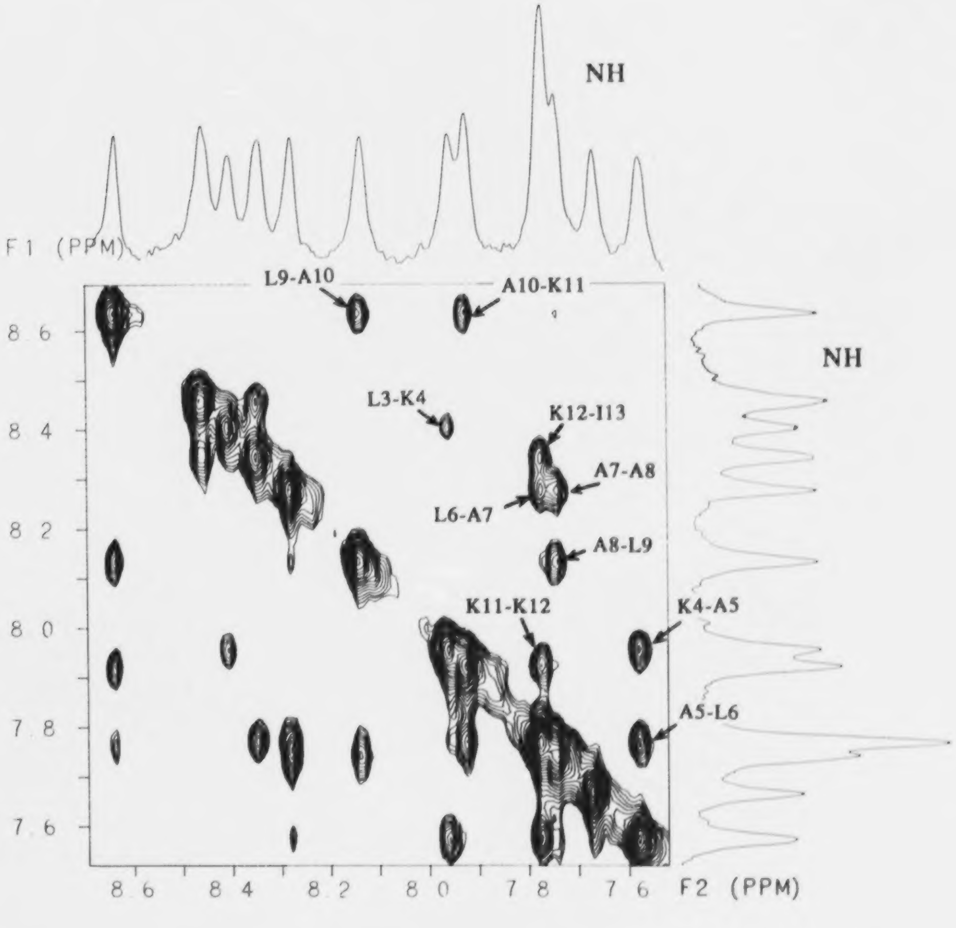

Figure IX-17. NH-NH region of the NOESY spectrum of mastoparan in 50%TFE showing NOEs between backbone amide protons. (2.5 mM mastoparan, 50 mM KCl, pH 6.2, 50%TFE/50%H_2O, 5°C, τ_m = 500 ms)

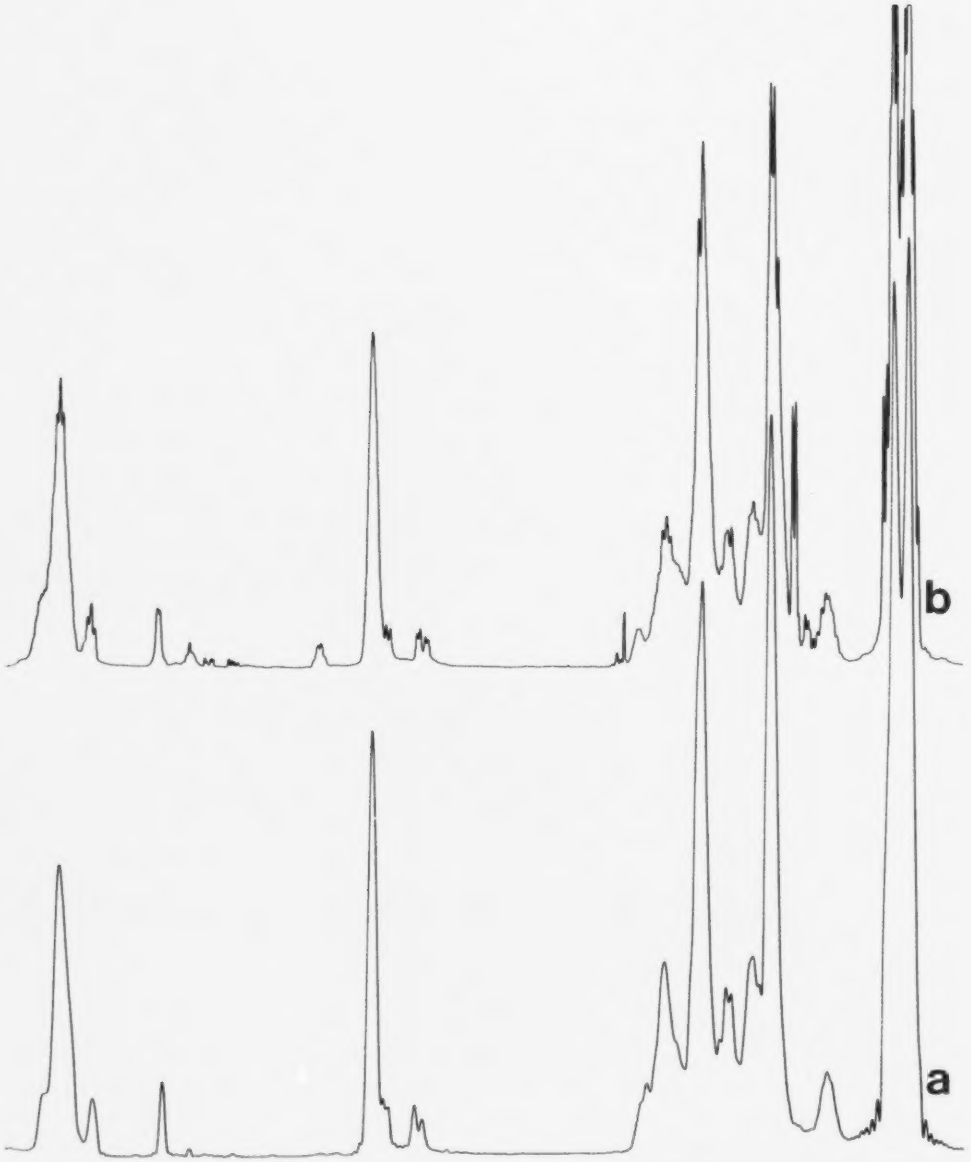

Figure IX-18A. 500 MHz ^{1}H NMR spectra of mastoparan in the absence and presence of 0.1 molar equivalents TnC.Ca(II)$_4$: Aliphatic upfield region of the spectrum. **a.** 4.0 mM mastoparan, 50 mM KCl, pH 6.3, 80%H_2O/20%D_2O, 5°C; **b.** 4.0 mM mastoparan, 0.4 mM TnC, 2 mM $CaCl_2$, 50 mM KCl, pH 6.3, 80%H_2O/20%D_2O, 5°C.

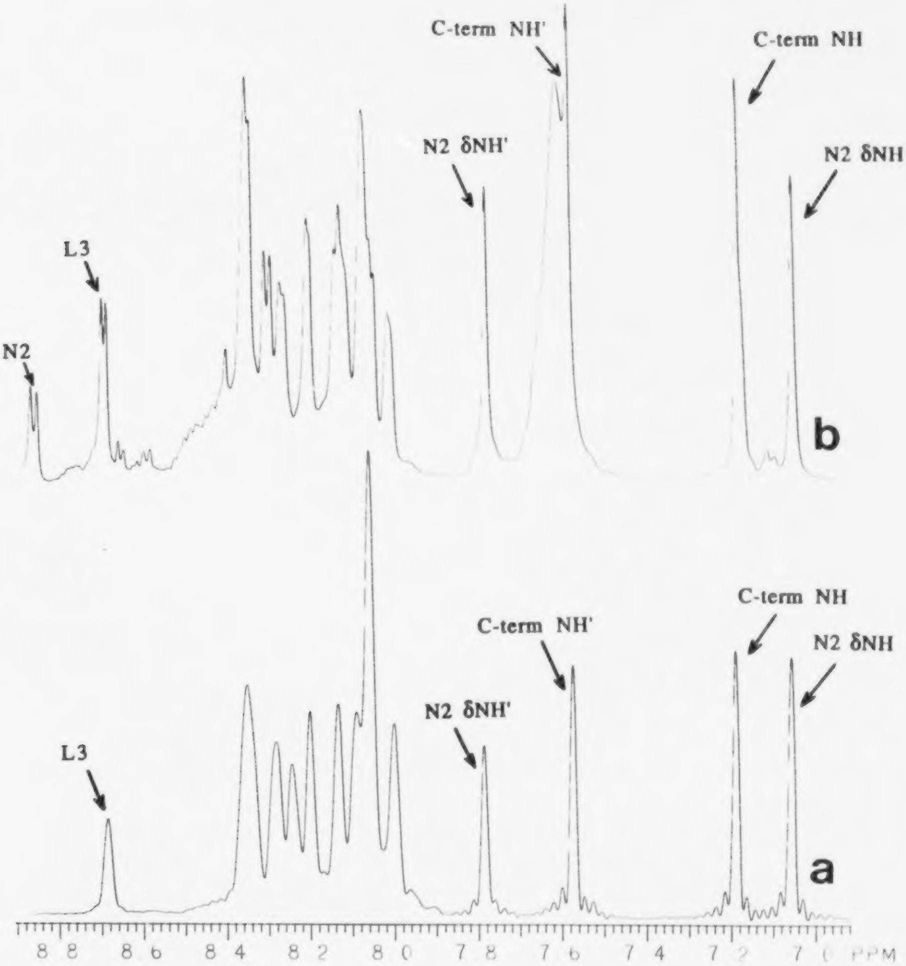

Figure IX-18B. 500 MHz ^{1}H NMR spectra of mastoparan in the absence and presence of 0.1 molar equivalents TnC.Ca(II)$_4$: Complete downfield region of the spectrum. **a.** 4.0 mM mastoparan, 50 mM KCl, pH 6.3, 80%H_2O/20%D_2O, 5°C; **b.** 4.0 mM mastoparan, 0.4 mM TnC, 2 mM $CaCl_2$, 50 mM KCl, pH 6.3, 80%H_2O/20%D_2O, 5°C.

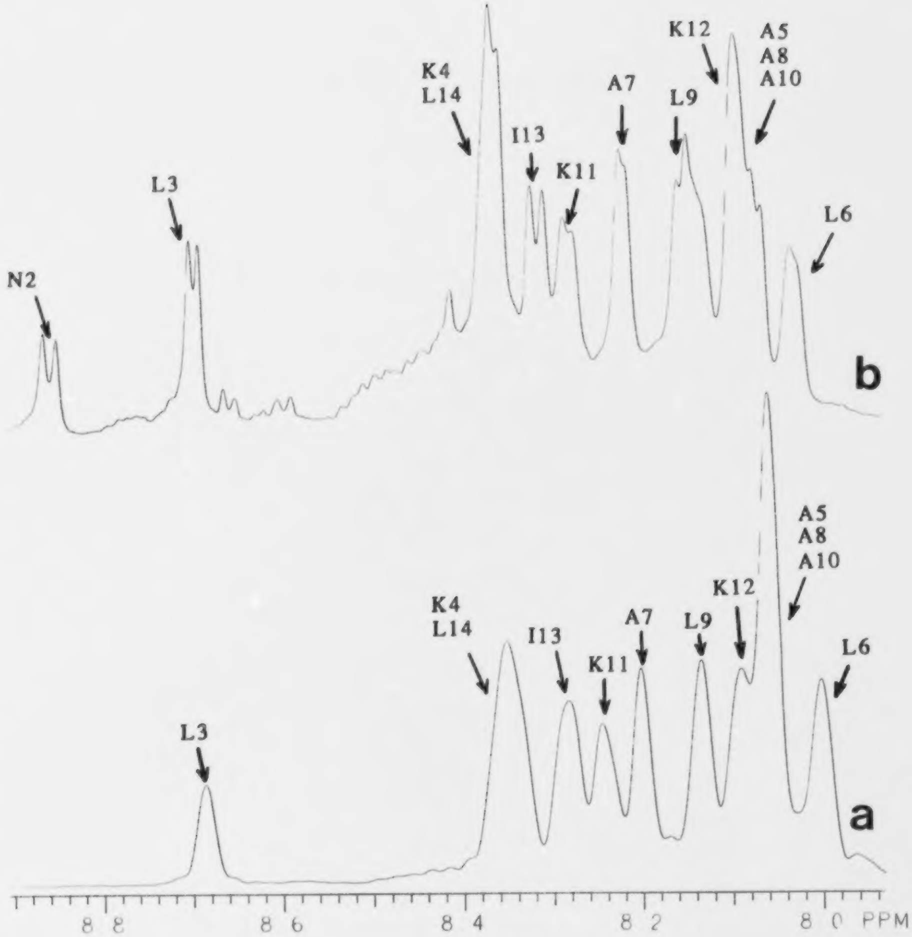

Figure IX-18C. 500 MHz ^{1}H NMR spectra of mastoparan in the absence and presence of 0.1 molar equivalents TnC.Ca(II)$_4$: Expanded region of spectrum B showing only the backbone amide proton resonances. **a.** 4.0 mM mastoparan, 50 mM KCl, pH 6.3, 80%H_2O/20%D_2O, 5°C; **b.** 4.0 mM mastoparan, 0.4 mM TnC, 2 mM $CaCl_2$, 50 mM KCl, pH 6.3, 80%H_2O/20%D_2O, 5°C.

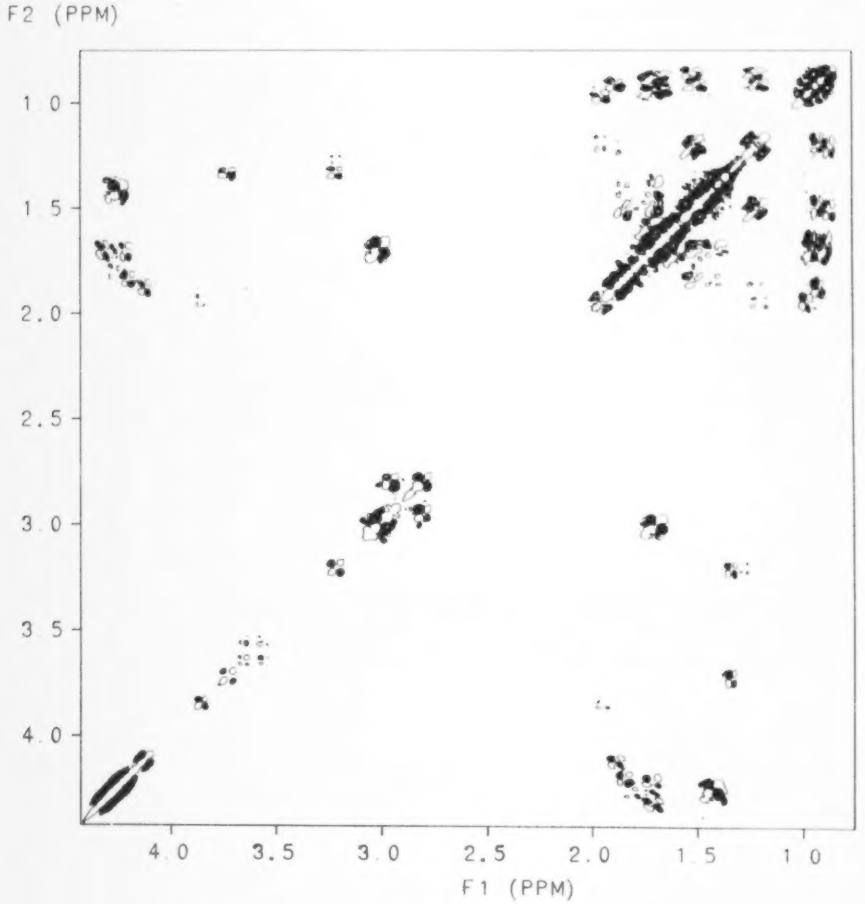

Figure IX-19. Upfield region of the DQFCOSY spectrum of mastoparan in the presence of 0.1 molar equivalents TnC.Ca(II)$_4$. (4.0 mM mastoparan, 0.4 mM TnC, 2 mM CaCl$_2$, 50 mM KCl, pH 6.3, 80%H$_2$O/20%D$_2$O, 5°C)

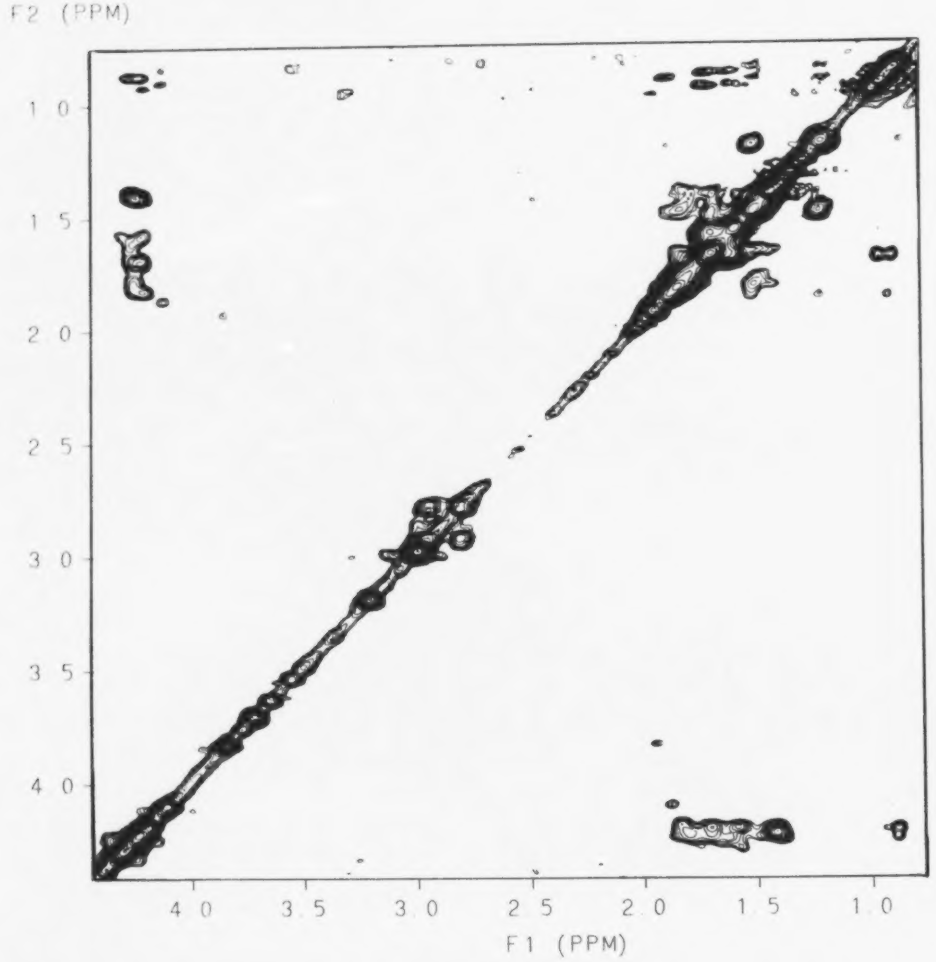

Figure IX-20. Upfield region of the NOESY spectrum of mastoparan in the presence of 0.1 molar equivalents TnC.Ca(II)$_4$. (4.0 mM mastoparan, 0.4 mM TnC, 2 mM CaCl$_2$, 50 mM KCl, pH 6.3, 80%H$_2$O/20%D$_2$O, 5°C, τ_m = 150 ms)

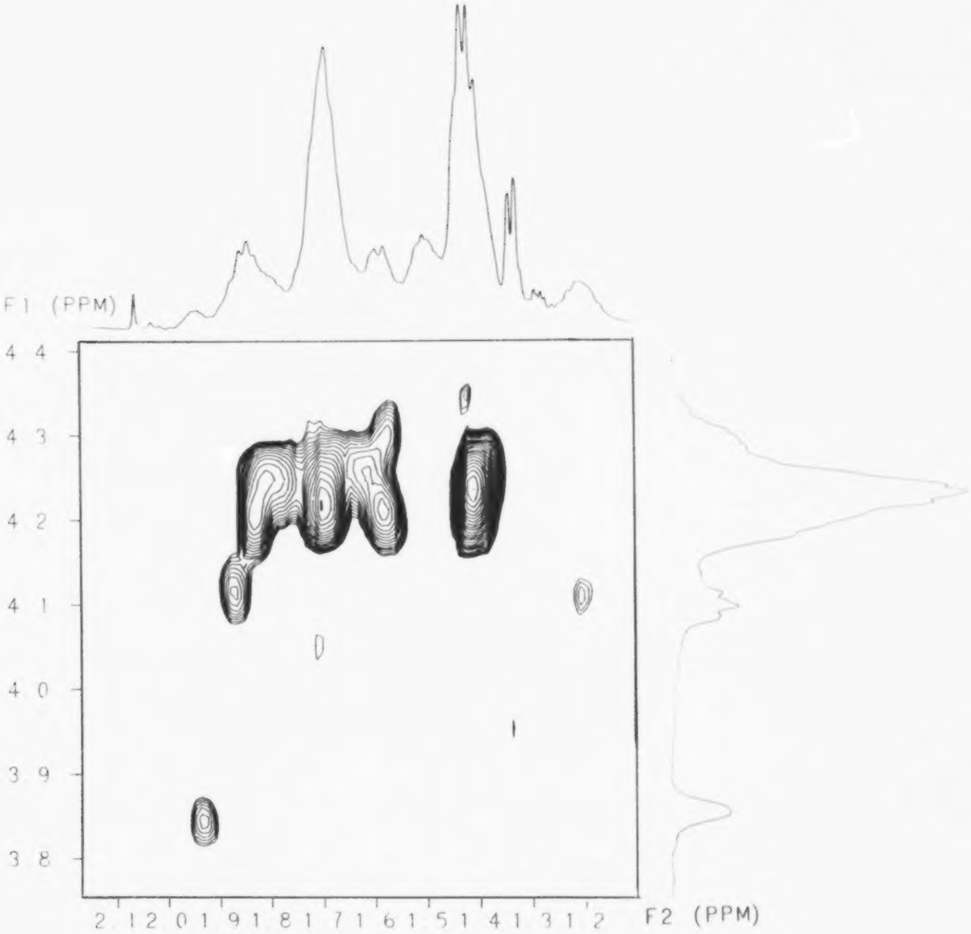

Figure IX-21. αCH-βCH region of the NOESY spectrum of mastoparan in the presence of 0.1 molar equivalents TnC.Ca(II)$_4$. (4.0 mM mastoparan, 0.4 mM TnC, 2 mM CaCl$_2$, 50 mM KCl, pH 6.3, 80%H$_2$O/20%D$_2$O, 5°C, τ_m = 150 ms)

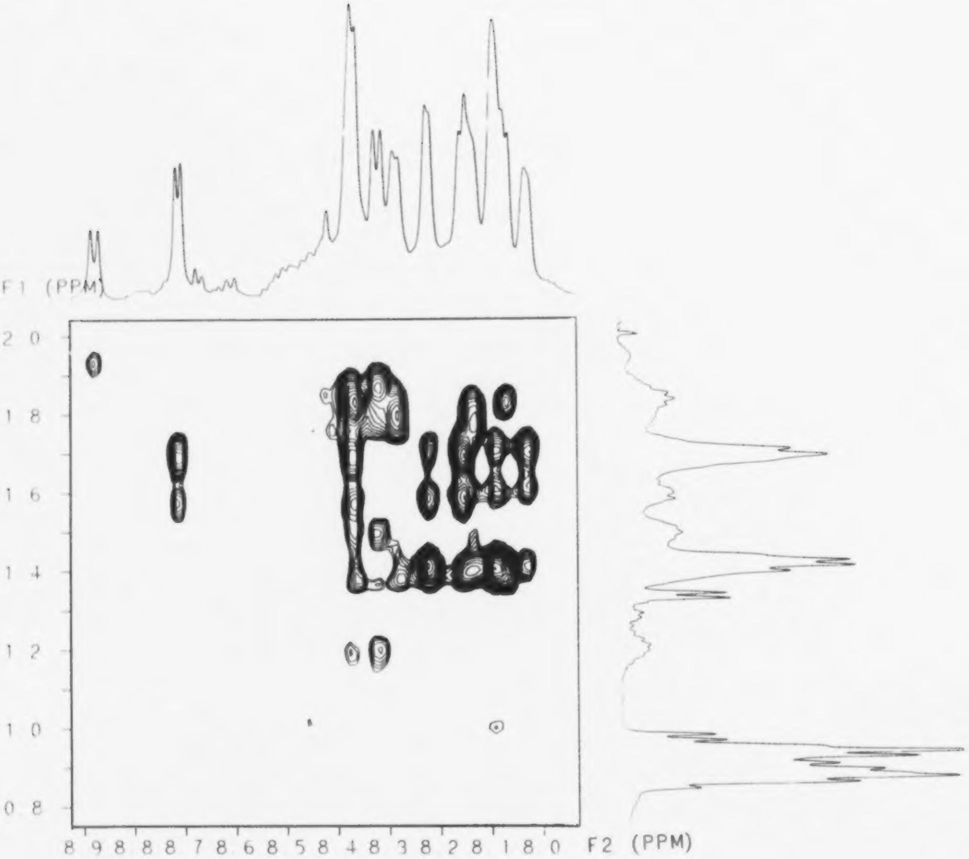

Figure IX-22. Downfield-βCH region of the NOESY spectrum of mastoparan in the presence of 0.1 molar equivalents TnC.Ca(II)$_4$. (4.0 mM mastoparan, 0.4 mM TnC, 2 mM $CaCl_2$, 50 mM KCl, pH 6.3, 80%H_2O/20%D_2O, 5°C, $\tau_m = 150$ ms)

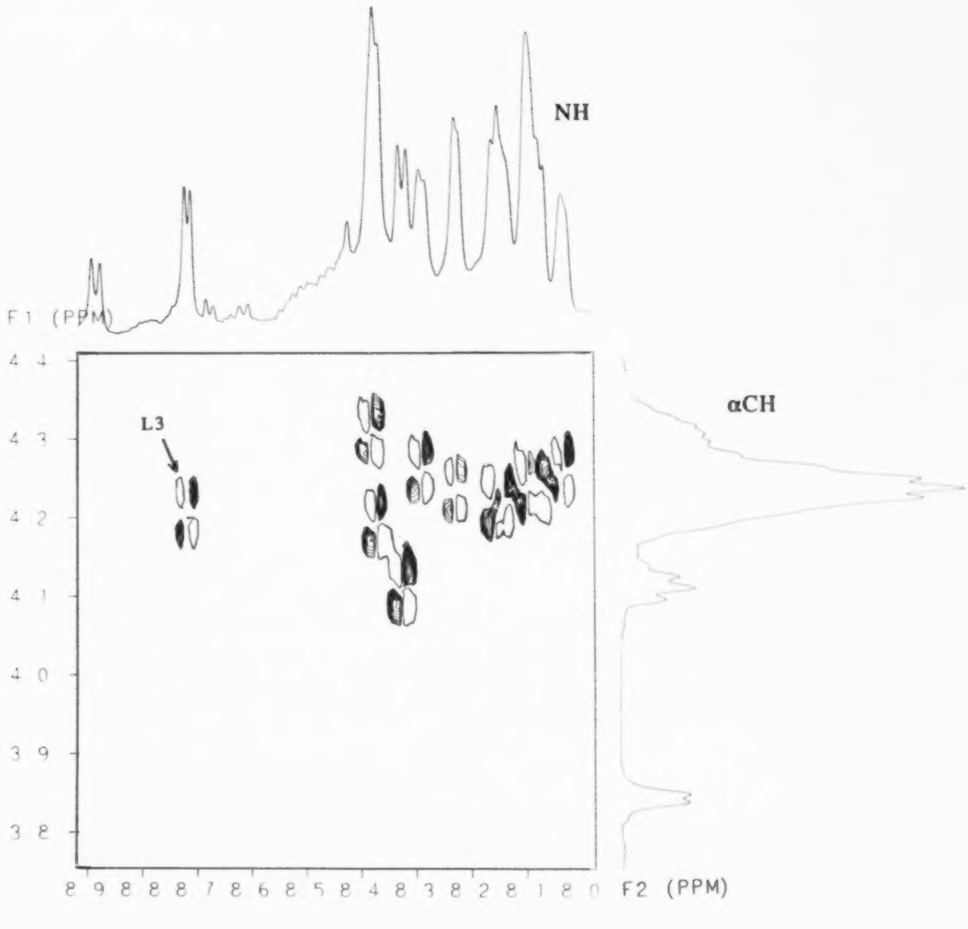

Figure IX-23A. αCH-NH region of the DQFCOSY spectrum of mastoparan in the presence of 0.1 molar equivalents TnC.Ca(II)$_4$: Spectrum showing L3αCH-NH COSY cross-peak (4.0 mM mastoparan, 0.4 mM TnC, 2 mM $CaCl_2$, 50 mM KCl, pH 6.3, 80%H_2O/20%D_2O, 5°C)

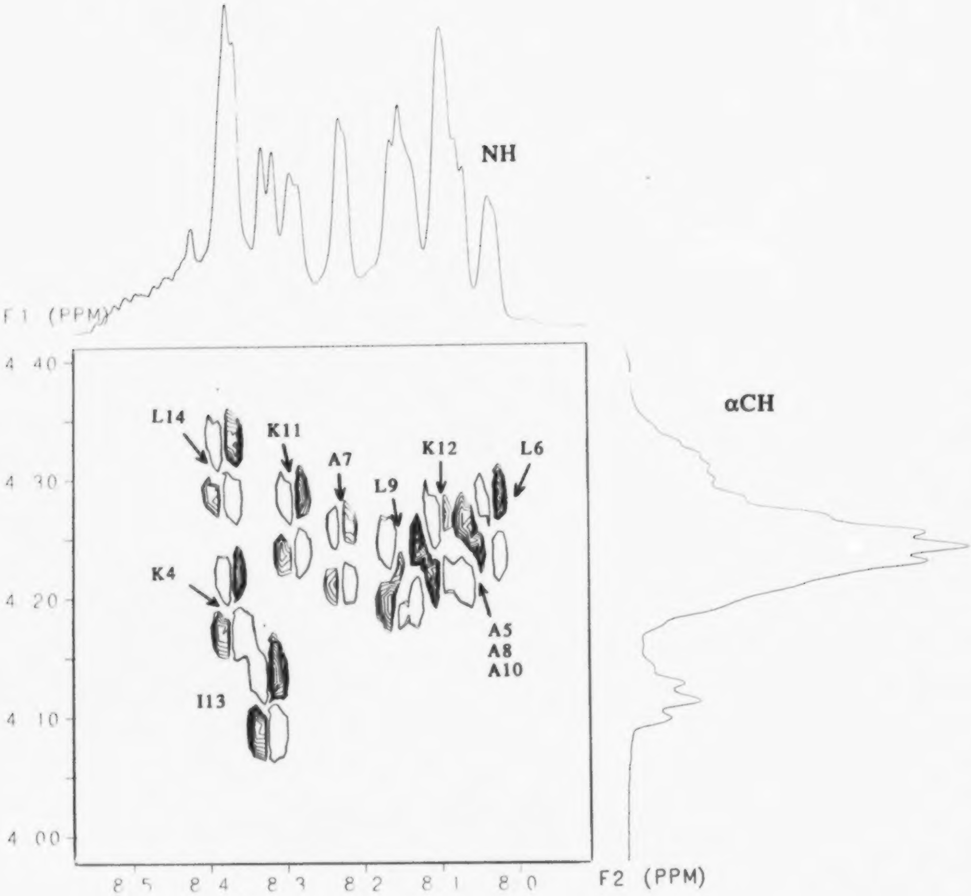

Figure IX-23B. αCH-NH region of the DQFCOSY spectrum of mastoparan in the presence of 0.1 molar equivalents TnC.Ca(II)$_4$: Expanded region of spectrum A. (4.0 mM mastoparan, 0.4 mM TnC, 2 mM CaCl$_2$, 50 mM KCl, pH 6.3, 80%H$_2$O/20%D$_2$O, 5°C)

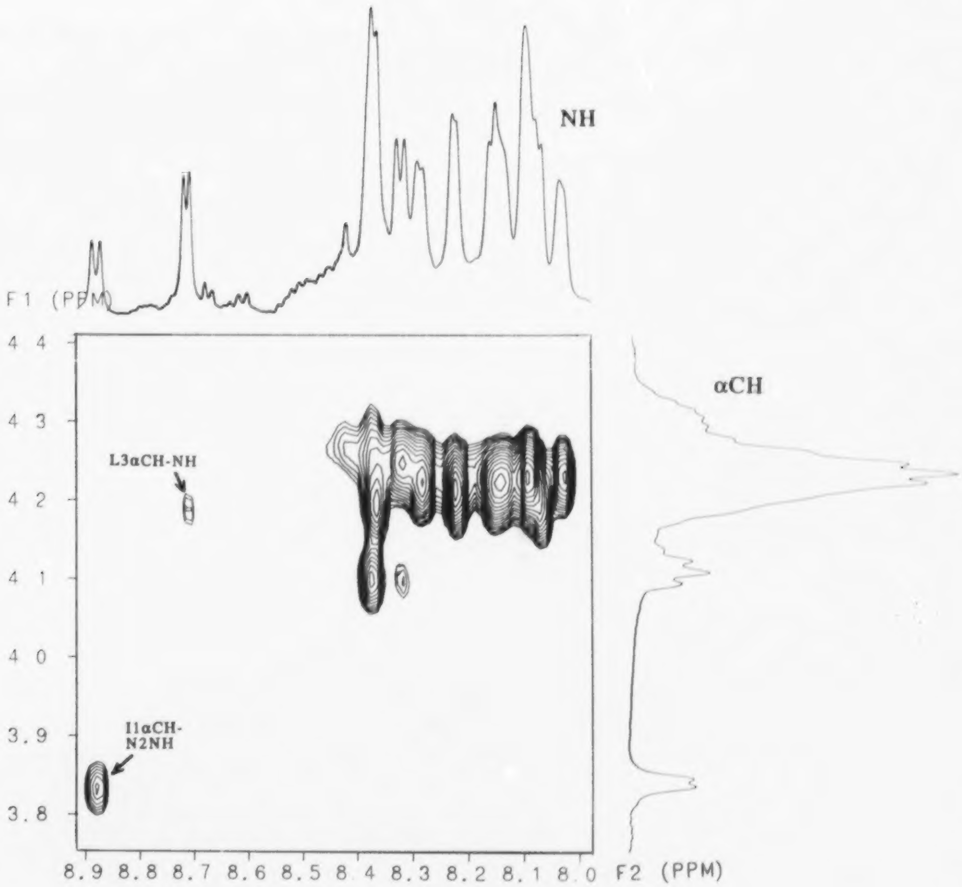

Figure IX-24A. αCH-NH region of the NOESY spectrum of mastoparan in the presence of 0.1 molar equivalents TnC.Ca(II)$_4$: Spectrum showing L3αCH-NH and I1αCH-N2NH NOEs. (4.0 mM mastoparan, 0.4 mM TnC, 2 mM CaCl$_2$, 50 mM KCl, pH 6.3, 80%H$_2$O/20%D$_2$O, 5°C, τ_m = 150 ms)

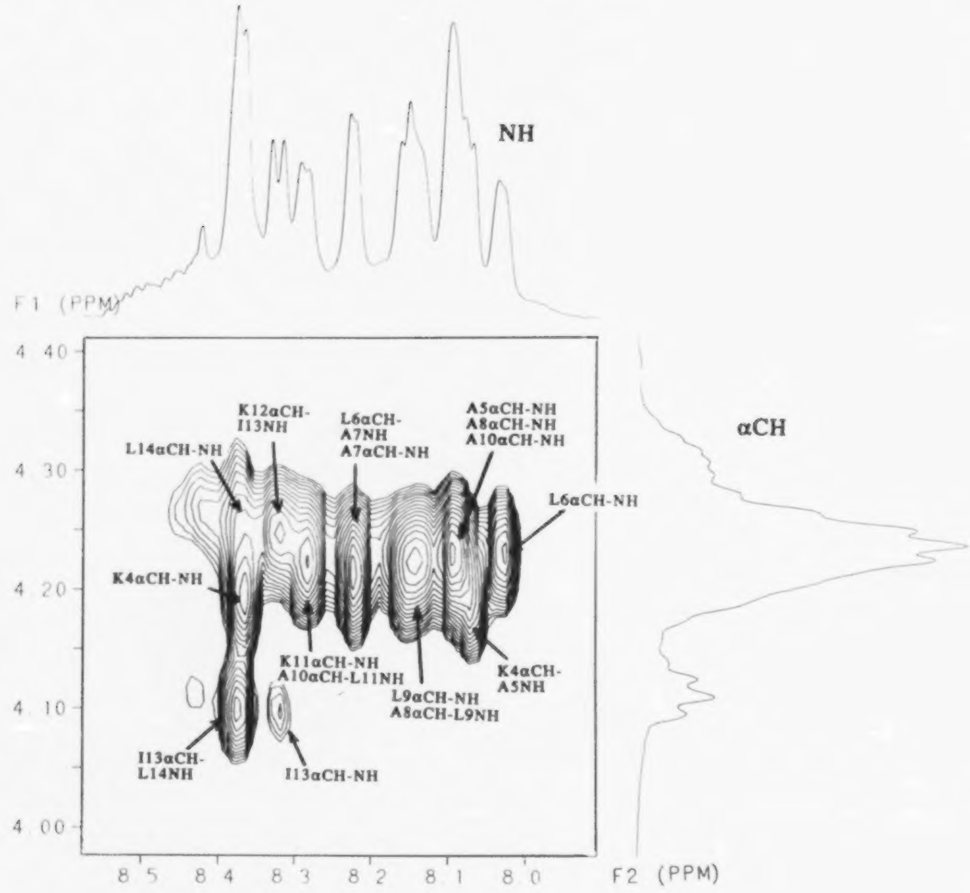

Figure IX-24B. αCH-NH region of the NOESY spectrum of mastoparan in the presence of 0.1 molar equivalents TnC.Ca(II)$_4$: Expanded region of spectrum A. (4.0 mM mastoparan, 0.4 mM TnC, 2 mM CaCl$_2$, 50 mM KCl, pH 6.3, 80%H$_2$O/20%D$_2$O, 5°C, τ_m = 150 ms)

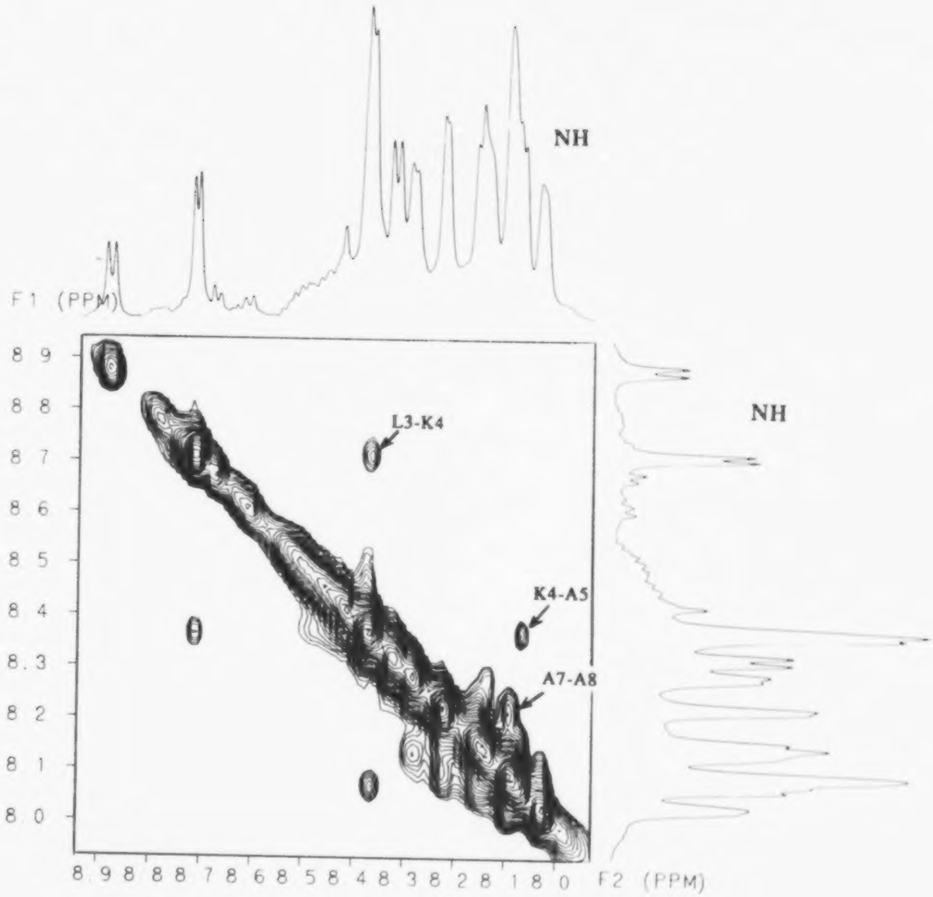

Figure IX-25. NH-NH region of the NOESY spectrum of mastoparan in the presence of 0.1 molar equivalents TnC.Ca(II)$_4$. (4.0 mM mastoparan, 0.4 mM TnC, 2 mM CaCl$_2$, 50 mM KCl, pH 6.3, 80%H$_2$O/20%D$_2$O, 5°C, τ_m = 150 ms)

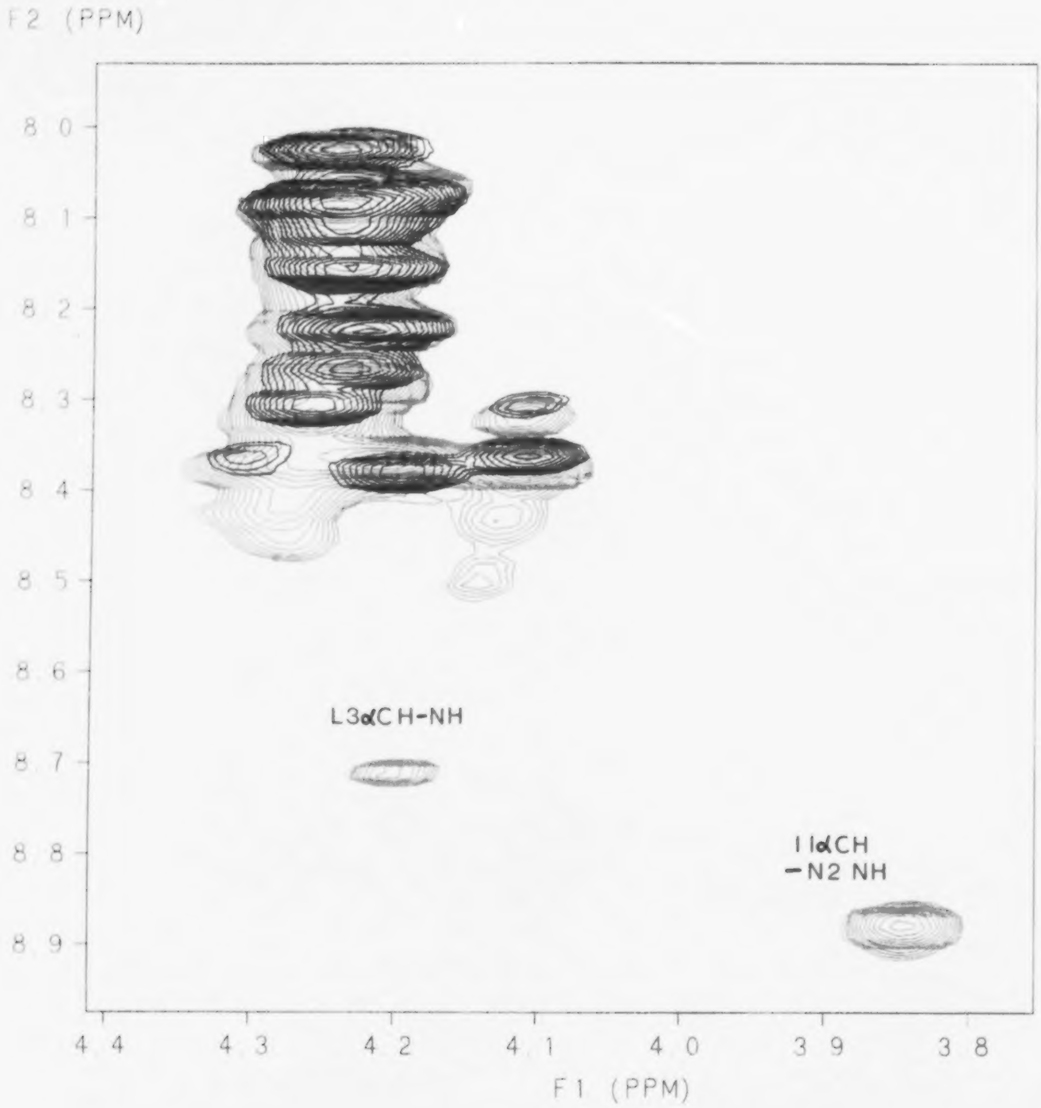

Figure IX-26. Fingerprint αCH-NH region of the NOESY spectrum of mastoparan (shown in black contours) superimposed upon the αCH-NH region of the NOESY spectrum of the same concentration mastoparan in the presence of 0.1 molar equivalents TnC.Ca(II)$_4$ (shown in red contours). Both spectra are plotted at the same vertical scale. (τ_m = 500 ms)

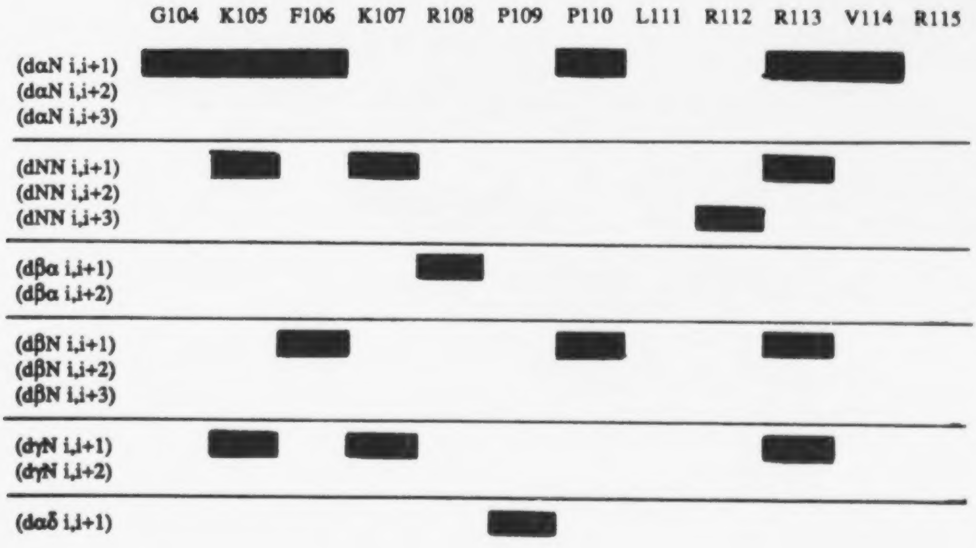

Figure IX-27. Sequence of the TnI peptide together with a schematic summary of the short- and medium- range NOEs defining the secondary structure of the peptide in 50%TFE.

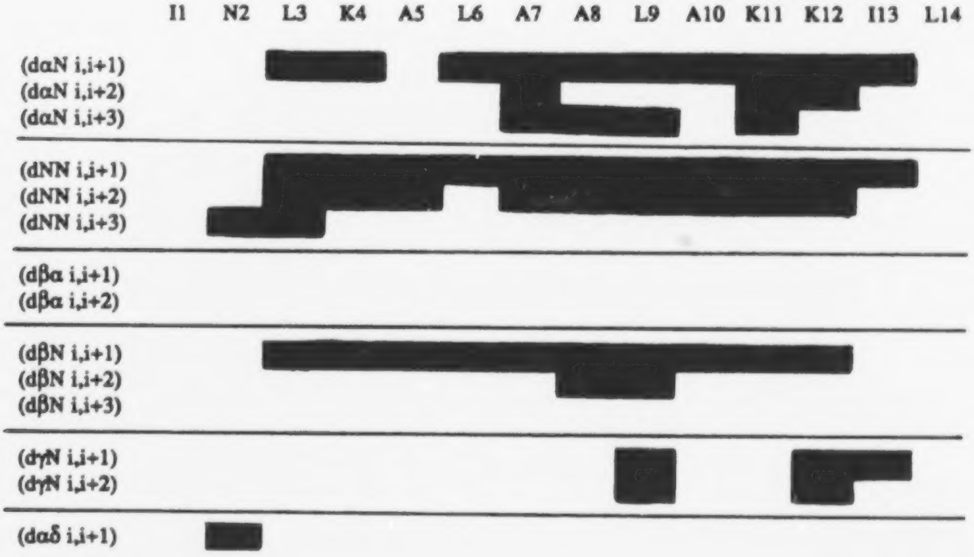

Figure IX-28. Sequence of mastoparan together with a schematic summary of the short- and medium- range NOEs defining the secondary structure of the peptide in 50%TFE.

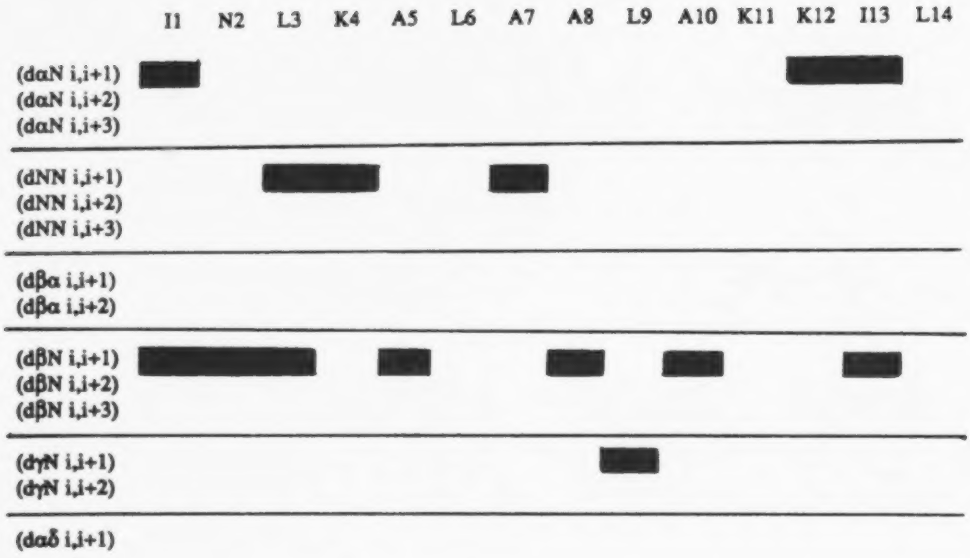

Figure IX-29. Sequence of mastoparan together with a schematic summary of the short- and medium- range TRNOEs defining the secondary structure of the peptide when bound to TnC.

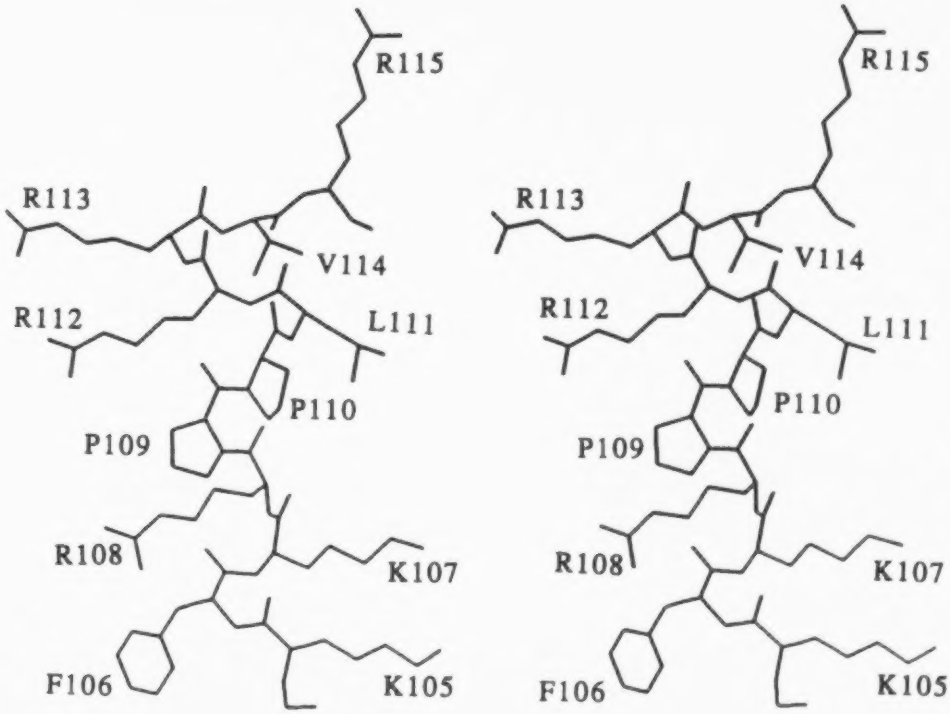
R115
R113
V114
R112
L111
P110
P109
R108
K107
F106
K105
R115
R113
V114
R112
L111
P110
P109
R108
K107
F106
K105

Figure IX-30. Stereo-diagram of the TnI peptide in 50%TFE. The final structure was generated from a set of α-helical input coordinates. Following 12 ps of MD, the coordinates of 10 MD structures taken every 0.2 ps were averaged and the averaged coordinates were energy minimized to produce the final structure in the figure.

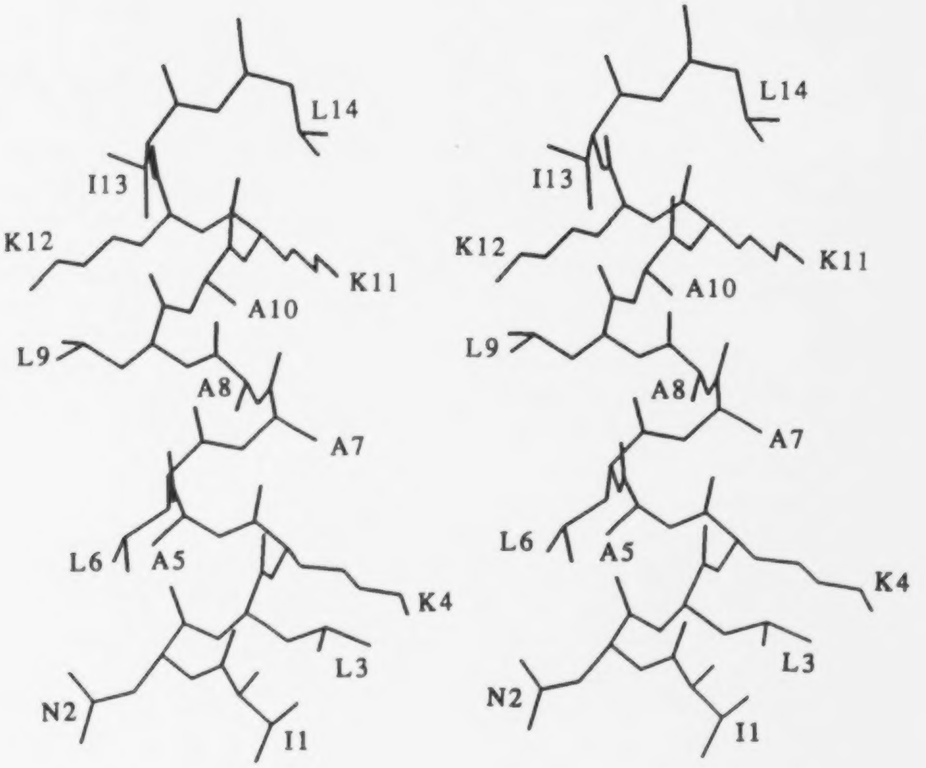
L14
I13
K12
K11
A10
L9
A8
A7
L6
A5
K4
L3
N2
I1
L14
I13
K12
K11
A10
L9
A8
A7
L6
A5
K4
L3
N2
I1

Figure IX-31. Stereo-diagram of mastoparan in 50%TFE. The final structure was generated from a set of α-helical input coordinates. Following 12 ps of MD, the coordinates of 10 MD structures taken every 0.2 ps were averaged and the averaged coordinates were energy minimized to produce the final structure in the figure.

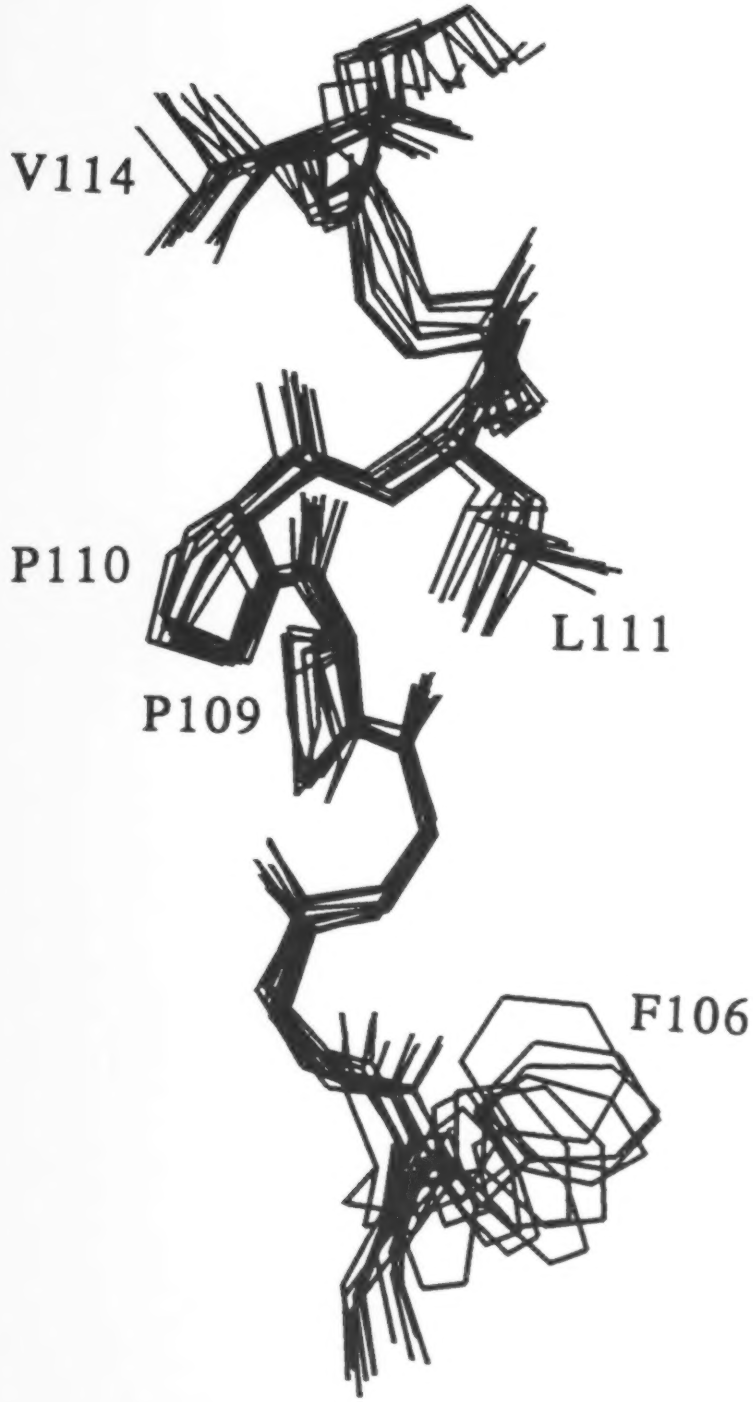
V114
P110
L111
P109
F106

Figure IX-32. Superposition of the 10 MD structures taken every 0.2 ps for the TnI peptide in 50%TFE.

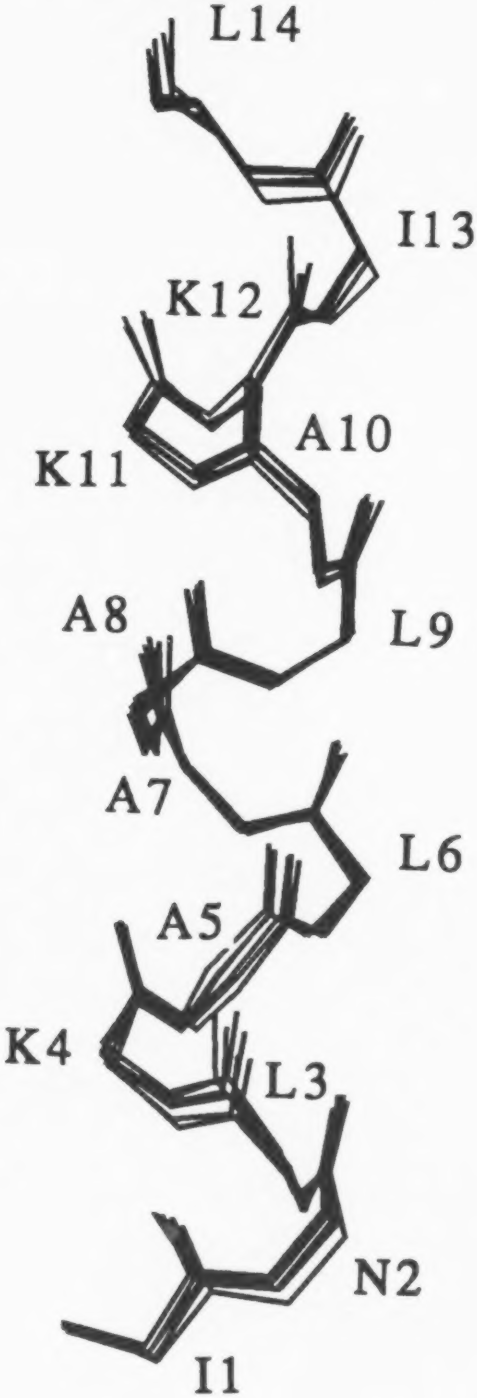
L14
I13
K12
A10
K11
A8
L9
A7
L6
A5
K4
L3
N2
I1

Figure IX-33. Superposition of the 10 MD structures taken every 0.2 ps for mastoparan in 50%TFE.

F. References

BABU, Y.S., BUGG, C.E., and COOK, W.J. 1988. Structure of calmodulin refined at 2.2 Å resolution. J. Mol. Biol. **204**: 191-204.

BARNETTE, M.S., DALY, R., and WEISS, B. 1983. Inhibition of β-endorphin and other opioid peptides with calmodulin. Biochem. Pharmacol. **32**: 2929-2933.

BERENDSEN, H.J.C., POSTMA, J.P.M., VAN GUNSTEREN, W.F., DINOLA, A., and HAAK, J.R. 1984. Molecular dynamics with coupling to an external bath. J. Chem. Phys. **81**: 3684-3690.

BILLETER, M., BRAUN, W., and WUTHRICH, K. 1982. Sequential resonance assignments in protein ^1H nuclear magnetic resonance spectra. Computation of sterically allowed proton-proton distances and statistical analysis of proton-proton distances in single crystal protein conformations. J. Mol. Biol. **155**: 321-346.

BLUMENTHAL, D.K., TAKIO, K., EDELMAN, A.N., CHARBONNEAU, H., TITANI, K., WALSH, K.A., and KREBS, E.G. 1985. Identification of the calmodulin binding domain of skeletal muscle myosin light chain kinase. Proc. Natl. Acad. Sci. USA **80**: 3187-3191.

BUSCHMEIER, B., MEYER, H.E., and MAYR, G.W. 1987. Characterization of the calmodulin binding sites of muscle phosphofructokinase and comparison with known calmodulin-binding domains. J. Biol. Chem. **262**: 9454-9462.

CACHIA, P.J., SYKES, B.D., and HODGES, R.S. 1983. Calcium-dependent inhibitory region of troponin. A proton magnetic resonance study on the interaction between troponin C and the synthetic peptide Nα-acetyl [F-phenylalanine106] TnI (104-115) amide. Biochemistry **22**: 4145-4152.

CACHIA, P.J., SYKES, B.D., and HODGES, R.S. 1985. Structural studies on calmodulin and troponin C. Phenothiazine, peptide, and protein interactions with calcium-induced helices. In *Calmodulin Antagonist and Cellular Physiology* (Hidaka, H., and Hartshorne, D.J., Eds.), Chapt. 5, pp 63-88, Academic Press, New York.

CACHIA, P.J., VAN EYK, J., INGRAHAM, R.H., MCCUBBIN, W.D., KAY, C.M., and HODGES, R.S. 1986. Calmodulin and troponin C. A comparative study of the interaction of mastoparan and troponin I inhibitory peptide [104-115]. Biochemistry **25**: 3553-3562.

CAMPBELL, A.P., and SYKES, B.D. 1991a. Interaction of troponin I and troponin C: Use of the two-dimensional NMR transferred nuclear Overhauser effect to determine the structure of the inhibitory troponin I peptide when bound to skeletal troponin C. J. Mol. Biol., in press.

CAMPBELL, A.P., and SYKES, B.D. 1991b. Theoretical evaluation of the two-dimensional transferred nuclear Overhauser effect. J. Magn. Reson. **93**: 77-92.

CAMPBELL, A.P., SLUPSKY, C.M., SHAW, G.S., and SYKES, B.D. 1991a. Interaction of troponin I and troponin C : Identification using NMR of specific residues on troponin C which are involved in the binding of an inhibitory troponin I peptide. Biochemistry, submitted.

CAMPBELL, A.P., CACHIA, P.J., and SYKES, B.D. 1991b. Interaction of troponin I and troponin C : ^{19}F NMR studies of the binding of the inhibitory troponin I peptide to turkey skeletal troponin C. Biochem. Cell Biol., in press.

CHONG, P.C.S., ASSELBERGS, P.J., and HODGES, R.S. 1983. Inhibition of rabbit skeletal muscle acto S1-ATPase by troponin T. FEBS Lett. **153**: 372-376.

COLLINS, J.H., POTTER, J.D., HORN, M.J., WILSHIRE, G., and JACKMAN, N. 1973. The amino acid sequence of rabbit skeletal muscle troponin C. Gene replication and homology with calcium-binding proteins from carp and hake muscle. FEBS Lett. **36**: 268-272.

COMPTE, M., MAULET, Y., and COX, J.A. 1983. Ca^{+2}-dependent high affinity complex formation between calmodulin and melittin. Biochem. J. **209**: 269-272.

COX, J.A., COMPTE, M., FILTON, J.E., and DEGRADO, W.F. 1985. The interaction of calmodulin with amphiphilic peptides. J. Biol. Chem. **260**: 2527-2534.

DALGARNO, D.C., KLEVIT, R.E., LEVINE, B.A., SCOTT, G.M.M., WILLIAMS, R.J.P., GERGELY, J., GRABAREK, Z., LEAVIS, P.C., GRAND, R.J.A., and DRABIKOWSKI, W. 1984. The nature of trifluoperazine binding sites on calmodulin and troponin-C. Biochim. Biophys. Acta **791**: 164-172.

DEGRADO, W.F., PRENGERGAST, F.G., WOLFE, H.R., JR., and COX, J.A., 1985. The design, synthesis, and characterization of tight-binding inhibitors of calmodulin. J. Cell. Biochem. **29**: 83-93.

DEGRADO, W.F., ERICKSON-VIITANEN, S., WOLFE, H.R., and O'NEIL, K.T. 1987. Predicted calmodulin-binding sequence in the γ-subunit of phosphorylase protein kinase. Proteins **2**: 20-33.

DE VLIEG, J., BOELENS, R., SCHEEK, R.M., KAPTEIN, R., and VAN GUNSTEREN, W.F. 1986. Restrained molecular dynamics procedures for protein tertiary structure determination from NMR data: a lac repressor headpiece structure based on information on J-coupling and from presence and absence of NOEs. Israel J. Chem. **27**: 181-188.

DRABIKOWSKI, W., DALGARNO, D.C., LEVINE, B.A., GERGELY, J., GRABAREK, Z., and LEAVIS, P.C. 1985. Solution conformation of the C-terminal domain of skeletal troponin C: Cation, trifluoperazine, and troponin I binding effects. Eur. J. Biochem. **151**: 17-28.

DRISCOLL, P.C., CLORE, M.G., BERESS, L., and GRONENBORN, A.M. 1989 Determination of the three-dimensional solution structure of the antihypertensive and antiviral protein BDS-I from the sea anemone *anemonia sulcata*. A study using nuclear magnetic resonance and hybrid distance geometry-dynamical simulated annealing. Biochemistry **28**: 2178-2187.

DYSON, J.H., RANCE, M., HOUGHTEN, R.A., LERNER, R.A., and WRIGHT, P.E. 1988. Folding of immunogenic peptide fragments of proteins in water solution. I. Sequence requirements for the formations of a reverse turn. J. Mol. Biol. **201**: 161-200.

EBASHI, S., and ENDO, M. 1968. Calcium ion and muscle contraction. Prog. Biophys. Mol. Biol. **18**: 123-183.

ERICKSON, B.W., and MERRIFIELD, R.B. 1976. Solid-phase peptide synthesis. In *The Proteins*, (Neurath, H., and Hill, R.L., Eds.), Vol. **2**, pp 255-527, Academic Press, New York.

ERICKSON-VIITANEN, S., O'NEIL, K.T., and DEGRADO, W.F. 1987. Theoretical and experimental approaches to the design of calmodulin-binding peptides: A model system for studying peptide/protein interactions. In *Protein Engineering* (Oxender, D.L., and Fox, C.F., Eds.), pp 201-211, Alan R. Liss, Inc., New York.

GARIEPY, J., and HODGES, R.S. 1983. Primary sequence analysis and folding behaviour of EF hands in relation to the mechanism of action of troponin C and calmodulin. FEBS Lett. **160**: 1-6.

GHELIS, C., and YON, J. 1982. In *Protein Folding*, pp 51, Academic Press, New York.

GIEDROC, D.R., LING, N., and PUETT, D. 1983. Identification of β-endorphin residues 19-25 as a region involved in the inhibition of calmodulin-stimulated phosphodiesterase activity. Biochemistry **22**: 5584-5591.

GIEDROC, D.R., KERAVIS, T.M., STAVOS, J.V., LING, N., WELLS, J.N., and PUETT, D. 1985. Functional properties of covalent β-endorphin peptide/calmodulin complexes. Chlorpromazine binding and phosphodiesterase activation. Biochemistry **24**: 1203-1211.

GRABAREK, Z., DRABIKOWSKI, W., LEAVIS, P.C., ROSENFELD, S.S., and GERGELY, J. 1981. Proteolytic fragments of troponin C. Interactions with the other troponin subunits and biological activity. J. Biol. Chem. **256**: 13121-13127.

GREASER, M.C., and GERGELY, J. 1971. Reconstitution of troponin activity from three protein components. J. Biol. Chem. **246**: 4226-4233.

GUERINI, D., KREBS, J., and CARAFOLI, E. 1987. Stimulation of the erythrocyte Ca^{2+}-ATPase and of bovine brain cyclic nucleotide phosphodiesterase. Eur. J. Biochem. **170**: 35-42.

HABERMAN, V.E., and JENTSCH, J. 1967. The amino acid sequence of bee venom melittin. Hoppe-Seylers Z. Physiol. Chem. **348**: 37-50.

HARTSHORNE, D.J., and MUELLER, H. 1968. Fractionation of troponin into two distinct proteins. Biochem. Biophys. Res. Commun. **31**: 647-653.

HERZBERG, O., and JAMES, M.N.G. 1985. Structure of the calcium regulatory muscle protein troponin C at 2.8 Å resolution. Nature **313**: 653-659.

HITCHCOCK, S.E. 1975. Regulation of muscle contraction. Binding of troponin C involved in calcium ion-dependent interaction with troponin I. Eur. J. Biochem. **52**: 255-263.

HODGES, R.S., SEMCHUCK, P.D., TANEJA, A.K., KAY, C.M., PARKER, J.M.R., and MANT, C.T. 1988 Protein design using model synthetic peptides. Peptide Research 1: 19-29.

HOULT, D.I. 1976. Solvent peak saturation with single phase and quadrature Fourier transformation. J. Magn. Reson. **21**: 337-347.

JARRETT, H.W. 1984. The synthesis and reaction of a specific affinity label for the hydrophobic drug-binding domains of calmodulin. J. Biol. Chem. **259**: 10136-10144.

JOHNSON, J.D., and POTTER, J.D. 1978. Detection of two classes of Ca^{+2} binding sites in troponin C with circular dichroism and tyrosine fluorescence. J. Biol. Chem. **253**: 3775-3777.

KLEVIT, R.E., BLUMENTHAL, D.K., WEMMER, D.E., and KREBS, E.G. 1985. Interaction of calmodulin and a calmodulin-binding peptide from myosin light chain kinase. Major spectral changes in both occur as a result of complex formation. Biochemistry **24**: 8152-8157.

KLEE, C.B., CROUCH, T.H., and RICHMAN, P.G. 1980. Calmodulin Annu. Rev. Biochem. **49**: 489-515.

KLEE, C.B., and VANAMAN, T.C. 1982. Calmodulin Adv. Protein Chem. **35**: 213-321.

KREBS, J., and CARAFOLI, E. 1982. Influence of Ca^{2+} and trifluoperazine on the structure of calmodulin. Eur. J. Biochem. **124**: 619-627.

KRETSINGER, R.H., and NOCKOLDS, C.E. 1973. Carp muscle-binding protein II. Structure determination and general description. J. Biol. Chem. **248**: 3313-3326.

KRETSINGER, R.H. 1980. Structure and evolution of calcium-modified proteins. CRC Crit. Rev. Biochem. **8**: 119-174.

KRETSINGER, R.H., RUDNICK, S.E., and WEISSMAN, L.J. 1986. Crystal structure of calmodulin. J. Inorg. Biochem. **28**: 289-302.

LAN, J., ALBAUGH, S., and STEINER, R.F. 1989. Interactions of troponin I and its inhibitory fragment (residues 104-115) with troponin C and calmodulin. Biochemistry **28**: 7380-7385.

LAPORTE, D.C., WIERMAN, B.M., and STORM, D.R. 1980. Calcium-induced exposure of a hydrophobic surface on calmodulin. Biochemistry **19**: 3814-3819.

LEAVIS, P.C., and GERGELY, J. 1984. Thin filament proteins and thin filament regulation of vertebrate muscle contraction. CRC Crit. Rev. Biochem. **16**: 235-305.

LESZYK, J., COLLINS, J.H., LEAVIS, P.C., and TAO, T. 1987. Cross-linking of rabbit skeletal muscle troponin with the photoactive reagent 4-maleimidobenzophenone. Identification of residues in troponin I that are close to cys-98 of troponin C. Biochemistry **26**: 7042-7047.

LESZYK, J., COLLINS, J.H., LEAVIS, P.C., and TAO, T. 1988. Cross-linking of rabbit skeletal muscle troponin subunits. Labelling of Cys-98 of troponin C with 4-maleimidobenzophenone and analysis of products formed in the binary complex with troponin T and the ternary complex with troponins I and T. Biochemistry **27**: 6983-6987.

LIN, C.R., KAPILOFF, M.S., DURGERIAN, S., TATEMOTO, K., RUSSO, A.F., HANSON, P., SCHULMAN, and ROSENFELD, M.G. 1987. Molecular cloning of a brain-specific calcium/calmodulin-dependent protein kinase. Proc. Natl. Acad. Sci. USA **84**: 5962-5968.

LUKAS, T.J., BURGESS, W.H., PREDERGAST, F.G., LAU, W., and WATTERSON, D.M. 1986. Calmodulin binding domains: Characterization of a phosphorylation and calmodulin binding site from myosin light chain kinse. Biochemistry **25**: 1458-1464.

MACURA, S., and ERNST, R.R. 1980. Elucidation of cross-relaxation in liquids by two-dimensional NMR spectroscopy. Mol. Phys. **41**: 95-117.

MALENCIK, D.A., and ANDERSON, S.R. 1982. Binding of simple peptides, hormones and neurotransmitters by calmodulin. Biochemistry **21**: 3480-3486.

MALENCIK, D.A., and ANDERSON, S.R. 1983a. Binding of hormones and neuropeptides by calmodulin. Biochemistry **22**: 1995-2001.

MALENCIK, D.A., and ANDERSON, S.R. 1983b. High affinity binding of the mastoparans by calmodulin. Biochem. Biophys. Res. Commun. **114**: 50-56.

MALENCIK, D.A., and ANDERSON, S.R. 1984. Peptide binding by calmodulin and its proteolytic fragments and by troponin C. Biochemistry **23**: 2420-2428.

MANT, C.T., BURKE, T.W.L., and HODGES, R.S. 1987. Optimization of peptide separations in reversed-phase HPLC: Isocratic versus gradient elution. Chromatographia **24**: 565-572.

MAULET, Y., and COX, J.A. 1983. Structural changes in melittin and calmodulin upon complex formation and their modulation by calcium. Biochemistry **22**: 5680-5686.

MCDOWELL, L., GUATAM, S., and PREDERGAST, F.G. 1985. Probable role of amphiphilicity in the binding of mastoparan to calmodulin. Biochemistry **24**: 2979-2984.

O'NEIL, K.T., WOLFE, H.R., JR, ERICKSON-VIITANEN, and DEGRADO, W.F. 1990. Fluorescence properties of calmodulin-binding peptides reflect alpha-helical periodicity. Science **236**: 1454-1456.

O'NEIL, K.T., and DEGRADO, W.F. 1990. How calmodulin binds its targets: sequence independent recognition of amphiphilic α-helices. Trends in Biol. Sci. **15**: 59-64.

OTTING, G., WIDMER, H., WAGNER, G., and WUTHRICH, K. 1986. Origin of t_1 and t_2 ridges in 2D NMR spectra and procedures for suppression. J. Magn. Reson. **66**: 187-193.

PARDI, A., BILLETER, M., and WUTHRICH, K. 1984. Calibration of the angular dependence of the amide proton-Cα proton coupling constants, $^3J_{HN\alpha}$, in a globular protein. J. Mol. Biol. **180**: 741-751.

PARKER, J.M.R., MANT, C.T., and HODGES, R.S. 1987. A practical approach to the preparative purification of peptides using analytical instrumentation with analytical and semipreparative columns. Chromatographia **24**: 832-838.

PERRY, S.V., COLE, H., HEAD, J.F., and WILSON, F.J. 1972. Localization and mode of action of the inhibitory protein component of the troponin complex. Cold Spring Harbor Symp. Quant. Biol. **37**: 251-262.

PIATINI, U., SORENSON, O.W., and ERNST, R.R. 1982. Multiple quantum filters for elucidating NMR coupling networks. J. Am. Chem. Soc. **104**: 6800-6801.

POTTER, J.D., and GERGELY, J. 1974. Troponin, tropomyosin and actin interactions in the Ca^{+2} regulation of muscle contraction. Biochemistry **13**: 2697-2703.

POTTER, J.D., and GERGELY, J. 1975. The calcium and magnesium binding sites on troponin and their role in the regulation of myofibrillar adenosine triphosphatase. J. Biol. Chem. **250**: 4628-4633.

PROZIALECK, W.C., and WEISS, B. 1982. Inhibition of calmodulin by phenothiazines and related drugs: Structure-activity relationships. J. Pharmacol. Exp. Ther. **222**: 509-514.

PUETT, D., GIEDROC, D.P., TOLLEFSON, S., and LING, N. 1983. Peptides (N.Y.) **4**: 191-194.

RANCE, M., SORENSON, O.W., BODENHAUSEN, G., WAGNER, G., ERNST, R.R., and WUTHRICH, K. 1983. Improved spectral resolution in COSY ^{1}H NMR spectra of proteins via double quantum filtering. Biochem. Biophys. Res. Commun. **117**: 479-485.

RYCKAERT, J.P., COCCOTTI, G., and BERENDSEN, H.J.C. 1977. Numerical integration of the Cartesian equations of motion of a system with constraints: molecular dynamics of n-alkanes. J. Comput. Phys. **23**: 327-337.

SANYAL, G., RICHARD, L.M., CARRAWAY, K.L., and PUETT, D. 1988. Binding of amphiphilic peptides to a carboxy-terminal tryptic fragment of calmodulin. Biochemistry **27**: 6229-6236.

SCHAUB, M.C., and PERRY, S.V. 1969. The relaxing protein system of striated muscle. Biochem. J. **115**: 993-1004.

SEEHOLZER, S.H., COHN, M., PUTKEY, J.A., MEANS, A.R., and CRESI, H.L. 1986. NMR studies of a complex of deuterated calmodulin with melittin. Proc. Natl. Acad. Sci. USA **83**: 3634-3638.

SELLINGER-BARNETTE, M., and WEISS, B. 1982. Interaction of β-endorphin and other opioid peptides with calmodulin. Mol. Pharmacol. **21**: 86-91.

STATES, D.J., HABERKORN, R.A., and RUBEN, D.J. 1982. Two-dimensional nuclear Overhauser experiment with pure phase absorption phase in four quadrants. J. Magn. Reson. **48**: 286-292.

STRYNADKA, N.C.J., and JAMES, M.N.G. 1988. Two trifluoperazine-binding sites on calmodulin predicted from comparative molecular modeling with troponin-C. Proteins **3**: 1-17.

STRYNADKA, N.C.J., and JAMES, M.N.G. 1990. Model for the interaction of amphiphilic helices with troponin C and calmodulin. Proteins **7**: 234-248.

SUNDARALINGAM, M., BERGSTROM, R., STRASBURG, G., RAO, S.T., GREASER, M., and WANG, B.C. 1985. Molecular structure of troponin C from chicken skeletal muscle at 3 Å resolution. Science **227**: 945-948.

SYSKA, H., WILKINSON, J.M., GRAND, R.J.A., and PERRY, S.V. 1976. The relationship between biological activity and primary structure of troponin I from white skeletal muscle of the rabbit. Biochem. J. **153**: 375-389.

TALBOT, J.A., and HODGES, R.S. 1979. Synthesis and biological activity of an icosapeptide analog of the actomyosin ATPase inhibitory region of troponin I. J. Biol. Chem. **254**: 3720-3723.

TALBOT, J.A., and HODGES, R.S. 1981. Synthetic studies on the inhibitory region of rabbit skeletal troponin I. Relationship of amino acid sequence to biological activity. J. Biol. Chem. **256**: 2798-3802.

TANAKA, T., and HIDAKA, H. 1980. Hydrophobic regions function in calmodulin-enzyme interactions. J. Biol. Chem. **255**: 11078-11080.

TANAKA, T., OHMURA, T., and HIDAKA, H. 1983. Calmodulin antagonists binding sites on calmodulin. Pharmacology **26**: 249-257.

TAO, T., GOWELL, E., STRASBURG, G.M., GERGELY, J., and LEAVIS, P.L. 1989. Ca^{+2} dependence of the distance between Cys-98 of troponin C and Cys-133 of troponin I in the ternary troponin complex. Resonance energy transfer measurements. Biochemistry **28**: 5902-5908.

THIRY, P., VANDERMEERS, A., VEDERMEERS-PIRET, M.C., RATHE, J., and CHRISTOPHE, J. 1980. The activation of brain adenylate cyclase and brain cyclic-nucleotide phosphodiesterase by seven calmodulin derivatives. Eur. J. Biochem. **103**: 409-414.

VANAMAN, T.C., SHARIEL, F., and WATTERSON, D.M. 1977. Structural homology between brain modulator protein and muscle TnCs. In *Calcium-Binding Proteins and Calcium Function* (Wasserman, R.H., *et al.*, Eds.), pp 107-116, Elsevier, Amsterdam.

VAN EYK, J.E., and HODGES, R.S. 1988. The biological importance of each amino acid residue of the troponin I inhibitory sequence 104-115 in the interaction with troponin C and tropomyosin-actin. J. Biol. Chem. **263**: 1726-1732.

VAN EYK, J.E., KAY, C.M., and HODGES, R.S. 1991. A comparative study of the interactions of synthetic peptides of the skeletal and cardiac troponin I inhibitory region with skeletal and cardiac troponin C. Biochemistry, in press.

WAGNER, G., BRAUN, W., HAVEL, T.E., SCHAUMANN, T., GO, N., and WUTHRICH, K. 1987. Protein structures in solution by nuclear magnetic resonance and distance geometry. The protein fold of the basic pancreatic trypsin inhibitor determined using two different algorithms, DISGEO and DISMAN. J. Mol. Biol. **196**: 611-639.

WAGNER, G., and WUTHRICH, K. 1982. Sequential resonance assignments in protein ^1H nuclear magnetic resonance spectra. Basic pancreatic trypsin inhibitor. J. Mol. Biol. **155**: 347-366.

WALSH, M., STEVENS, F.C., OIKAWA, K., and KAY, C.M. 1978. Chemical modification studies on the Ca^{2+}-dependent protein modulator: The role of methionine residues in the activation of cyclic nucleotide phosphodiesterase. Biochemistry **17**: 3924-3930.

WEEKS, R.A, and PERRY, S.V. 1978. Characterization of a region of the primary sequence of troponin C involved in calcium ion-dependent interaction with troponin I. Biochem. J. **173**: 449-457.

WILLIAMSON, M.P., and NEUHAUS, D. 1987. Symmetry in NOE spectra. J. Magn. Reson. **72**: 369-375.

WUTHRICH, K., BILLETER, M., and BRAUN, W. 1983. Pseudo-structures for the 20 common amino acids for use in studies of protein conformations by measurements of intramolecular proton-proton distance constraints with nuclear magnetic resonance. J. Mol. Biol. **169**: 949-961.

WUTHRICH, K., WIDER, G., WAGNER, G., and BRAUN, W. 1982. Sequential resonance assignments as a basis for determination of spatial protein structures by high resolution proton nuclear magnetic resonance. J. Mol. Biol. **155**: 311-319.

WUTHRICH, K. 1986. In *NMR of Proteins and Nucleic Acids* , pp 123-128, John Wiley and Sons, New York.

ZOT, A.S., and POTTER, J.D. 1987. Structural aspects of troponin-tropomyosin regulation of skeletal muscle contraction. Annu. Rev. Biophys. Chem. **16**: 535-559.

Chapter X

Conclusions and Future Research Directions

A. Summary

This thesis has used ^{1}H NMR techniques as a tool to study the Ca(II)-sensitive interaction between TnC and the inhibitory region of TnI in an effort to elucidate a fundamental regulatory step in the Ca(II)-mediated regulation of muscle contraction.

Chapters II and III offered a theoretical basis for the two-dimensional intramolecular transferred nuclear Overhauser effect (TRNOE), a technique which allows determination of the structure of a ligand bound to a macromolecule. In Chapter II, a theoretical evaluation of the TRNOE was presented using a full relaxation matrix analysis first developed by Landy and Rao (1989) (Campbell and Sykes, 1991a). In Chapter III, the influence of internal motions on the development of the TRNOE was examined using the model system of the inhibitory skeletal TnI peptide Nα-acetyl-TnI(104-115) amide bound to Ca(II)-saturated TnC (Campbell and Sykes, 1991b).

In Chapter IV, ^{19}F NMR spectroscopy was used to determine the dissociation constant and the stoichiometry of binding of the skeletal TnI peptide analog Nα-acetyl[^{19}F-phe106]TnI(104-115)amide to Ca(II)-saturated turkey skeletal TnC. A dissociation constant of $K_d = 4.8 \times 10^{-5}$ M for a 1:1 binding stoichiometry (Campbell *et al.*, 1991a) was obtained. The results did not rule out the possibility of a second binding site on Ca(II)-saturated TnC with an affinity 10-20 fold weaker than that of the first.

In Chapter V, the two-dimensional intramolecular TRNOE was used to determine the conformation of the inhibitory skeletal TnI peptide, Nα-acetyl-TnI(104-115) amide, bound to Ca(II)-saturated skeletal TnC (Campbell and Sykes, 1991c). The structure of the bound TnI peptide revealed a distorted helix with a tertiary fold around the P109-P110 sequence. The central bend in the peptide functioned to bring the hydrophobic residues (F106, L111 and V114) into closer proximity with each other, thereby forming a small hydrophobic pocket capable of interacting with a hydrophobic patch on TnC.

In Chapter VI, two-dimensional nuclear Overhauser effect (NOE) techniques were used to determine the identity of the residues on Ca(II)-saturated turkey skeletal TnC which are actively involved in binding the inhibitory peptide Nα-acetyl-TnI(104-115) amide (Campbell *et al.*, 1991b). TnI peptide-TnC protein NOEs were found between residues on the TnI peptide and F102, I104, I113, I121, I149, F151 and F154 on turkey skeletal TnC. This pointed to an interaction of the inhibitory TnI peptide with the hydrophobic pocket and β-sheet region between Ca(II)-binding sites III and IV in the C-terminal domain of the TnC protein. A model for the interaction of the inhibitory TnI peptide with the C-terminal domain of TnC was presented.

In Chapter VII, the paramagnetic lanthanide Gd(III) was used as a Ca(II) analog to determine the location of binding of the inhibitory peptide Nα-acetyl-TnI(104-115) amide with respect to Ca(II)-binding sites I and II in the N-terminal domain, and sites III and IV in the C-terminal domain of skeletal TnC. The N-terminal domain was found to be within a 20-25 Å radius of nuclei on the peptide, suggesting involvement of both the N- and C-terminal globular domains in the binding of the TnI peptide. These results support a model for a TnI peptide-induced conformational change in the flexible central helix of the TnC molecule, allowing a closer approach of the N- and C-terminal domains in a concerted effort to bind the target peptide.

In Chapter VIII, differences in the mode of TnC-mediated relief of TnI inhibitory activity in skeletal versus cardiac systems was examined. The cardiac(137-148) and skeletal(104-115) TnI inhibitory peptides have identical sequences except for a single amino acid substitution of a proline at position 110 in the skeletal sequence for a threonine in the cardiac sequence. In order to examine the effect of an amino acid substitution at position 110 on the conformation and dynamics of the inhibitory region of TnI, we used two-dimensional intramolecular TRNOE techniques to determine the structure of a glycine-110 peptide analog, Nα-acetyl-G110-TnI(104-115) amide, bound to Ca(II)-saturated bovine cardiac TnC. The effect of conformational flexibility in the inhibitory TnI sequence on differences in the mode of the Ca(II) mediated relief of inhibition of actomyosin ATPase in the skeletal versus cardiac systems was discussed.

In Chapter IX, the role of amphiphilic helices in targeting Ca(II)-binding proteins like skeletal TnC was examined. Two-dimensional intramolecular TRNOE and NOE techniques were used to examine and compare the structures of the inhibitory TnI peptide and the bee venom mastoparan in the helix-inducing solvent TFE, versus when bound to Ca(II)-saturated turkey skeletal TnC. The NMR evidence suggested that whereas mastoparan bound to TnC as an amphiphilic helix, the TnI peptide bound to TnC as a 'helix-like' structure, distorted by a tertiary fold in the sequence around the two central proline residues. Furthermore, whereas mastoparan adopted α-helical conformation in TFE, the TnI peptide showed no evidence for formation of α-helix in the helix-inducing solvent. We concluded that α-helical structure was not a prerequisite for the binding of target proteins to CaM and TnC. In the case of the interaction between the inhibitory TnI peptide and TnC, binding seems to be contingent on a proper alignment of hydrophobic residues on the TnI peptide, which is itself dependent on the formation of the tertiary fold around the two central proline residues in the TnI peptide sequence.

B. Future Research Directions

NMR spectroscopy of muscle proteins in the 1970's and 1980's was mostly confined to one-dimensional experiments of single protein components in the thin or thick filament. Interactions between muscle proteins were difficult to follow due to the complications involved in obtaining adequate spectral resolution for even small proteins ($M_R \leq 20$ kDaltons), let alone binary or ternary complexes. However, the study of muscle protein biochemistry using NMR spectroscopy has undergone great progress in the past few years. This is partly due to recent advances in the field which have included the introduction of two- and three-dimensional NMR experiments, high field spectrometers (500 and 600 MHz), and computational algorithms for converting NMR derived restraints into three-dimensional structures.

This thesis has utilized some of these new NMR techniques to study the Ca(II)-sensitive interaction between TnI and TnC in the thin filament of muscle. Particularly useful have been high-field (500 and 600 MHz) homonuclear two-dimensional experiments, the transferred nuclear Overhauser experiment (TRNOE), and molecular mechanics simulations. These techniques have allowed the determination of the three-dimensional structure of the TnI inhibitory peptide(104-115) when bound to Ca(II)-saturated TnC, and the identification of residues on TnC which are involved at the interface between the two proteins. A full refinement of the structure of the bound inhibitory peptide is in progress using an iterative relaxation matrix analysis, adapted for the TRNOE experiment. This refinement strategy will be outlined later in the chapter.

Central to these methods have been the use of synthetic peptide analogs made possible through the development of solid-state peptide synthetic techniques. Synthetic peptides spanning the region of interest in the TnI protein have greatly simplified the study of the interaction between TnC and TnI, as they have circumvented the spectral overlap problem associated with the NMR spectrum of two non-identical proteins interacting in solution.

Although homonuclear two-dimensional NMR experiments performed at high field are powerful tools for structure elucidation, complete assignment of the ^1H NMR spectra of proteins larger than approximately 15 kDaltons is still difficult using these methods alone. Fortunately, several recent advances in the field of molecular biology have allowed sufficiently detailed assignment to be made for proteins as large as 30 kDaltons, such that three-dimensional structure determination is now possible. Thanks to molecular biology, isotope labeling of proteins with ^2H, ^{13}C and ^{15}N has provided a powerful method for editing the complex overlapped spectra of large proteins. Extending the NMR experiment into a third dimension has also provided a means of avoiding overlap of cross peaks in two-dimensional NMR spectra.

At the laboratory of Ad Bax at the National Institute of Health, three-dimensional heteronuclear experiments have allowed the complete assignment of backbone and side chain nuclei leading to the determination of the three-dimensional structure of the Ca(II)-binding protein calmodulin (CaM) (Ikura *et al.*, 1990a, 1990b). In addition, Bax and co-workers have studied the interaction of isotopically-labeled CaM with the binding domain of skeletal muscle myosin light-chain kinase (Ikura *et al.*, 1991). The future of NMR spectroscopy as applied to the study of muscle proteins lies in these new heteronuclear multidimensional techniques. In the laboratory of Brian Sykes at the University of Alberta, work is underway to determine the structure of the cloned and isotopically-labelled TnC protein in its apo and Ca(II)-bound states. Other research projects in the laboratory include the determination of the structure of the N-terminal region of actin bound to the troponin complex, a project which could be expanded to include a study of the interaction between whole TnI and actin, and whole TnI and TnC. It is possible that by the end of the decade, the solution structures of all of the components of muscle could be available, including the structural mechanisms for the Ca(II)-sensitive interactions amongst them.

C. Transferred Iterative Relaxation Matrix Approach (TR-IRMA) from Proton-Proton Transferred NOEs: Refinement of the Structure of the Inhibitory Troponin I Peptide Bound to Troponin C

In Chapter II we presented a theoretical evaluation of the TRNOE, based on the relaxation matrix approach developed by Landy and Rao (1989), where we examined the effects of variables such as mixing time, fraction of bound peptide, free and bound correlation times, and other contributions to spin-lattice relaxation rates (Campbell and Sykes, 1991a). In Chapter III we examined the question of internal motions in the free and bound peptide, and how these internal motions affected the development of the TRNOE (Campbell and Sykes, 1991b). Now we present an iterative procedure for structure determination of chemically exchanging ligands from ^{1}H-^{1}H TRNOEs, in which spin diffusion is fully taken into account.

In practical cases involving large proteins (M_R > 20,000), distances derived from measurement of two-dimensional TRNOESY cross-peak intensities are only approximate, since cross relaxation becomes very rapid and direct cross-relaxation between two spins in the bound ligand is modified by indirect cross-relaxation with any other spins. The theoretical analysis of TRNOE experiments has been so far limited to the initial build-up rates of one-dimensional, steady-state TRNOEs and limited to two or three spins (Clore and Gronenborn, 1982, 1983). As far as the two-dimensional TRNOESY experiment is concerned, this is equivalent to an isolated spin-pair approximation which is valid only at very short mixing times (Noggle and Schirmer, 1971; Wagner and Wuthrich, 1979; Dobson *et al.*, 1982; Gronenborn and Clore, 1985).

An alternative and more rigorous approach to analyzing the TRNOE data involves the implementation of a full relaxation matrix, where a multiple spin system in the presence of chemical exchange is analyzed. The full relaxation matrix treatment of NOE data has been developed and used to refine many protein and nucleic acid structures (Keepers and James, 1984; Lefevre *et al.*, 1987; Boelens *et al.*, 1988; Borgias and James, 1988, 1989; Baleja *et al.*, 1990). However, to date, no complete relaxation matrix treatment of TRNOE data, which would take into account the effects of indirect magnetization transfer between spins, has been used to refine these bound ligand structures.

Here we propose an iterative relaxation matrix analysis for ligands binding to macromolecules, adapted from the *i*terative *r*elaxation *m*atrix *a*pproach (IRMA) of Boelens *et al.* (1988, 1989). We will refer to our procedure as the *t*ransferred *i*terative *r*elaxation *m*atrix *a*pproach (TR-IRMA), with the important distinction that our procedure is appropriate for the special case of multispin systems undergoing relaxation and chemical exchange, whereas the IRMA procedure is appropriate for multispin systems undergoing relaxation only. We will present the theory and methodology for the refinement of the structure of the bound inhibitory TnI(104-115) peptide, the structure for which was determined in Chapter V using two-dimensional TRNOESY experiments (Campbell and Sykes, 1991c).

Since work is still currently underway in the laboratory involving the writing and implementation of the computer program, a refined structure will not be presented here. However, in the near future we anticipate a fully refined structure of the TnI peptide bound to Ca(II)-saturated TnC, with models encorporated for internal motions in the free and bound peptide. We have measured TRNOE intensities at three molar ratios TnC protein to TnI peptide (0.1, 0.2, and 0.4 molar equivalents TnC.Ca(II)$_4$ to TnI peptide), and at three mixing times (τ_m = 75, 150 and 500 ms)[1]. Tables of these measured and normalized[2] TRNOE intensities for the various protein concentrations and mixing times are found in Tables X-1, X-2 and X-3 in the Appendix.

1. Theory

We have already presented a theoretical treatment of the two-dimensional TRNOESY experiment, incorporating models for internal motion, in Chapters II and III. However, in the interests of completeness, we present the theory again, especially as the following equations form the basis for the refinement calculations in the TR-IRMA computer program.

A description of homonuclear dipolar relaxation for a multiple spin system requires the complete set of coupled differential equations describing the evolution of longitudinal magnetizations of the individual spins (Bloch, 1957). These coupled differential equations can be written in matrix form (Solomon, 1955; Abragam, 1961; Macura and Ernst, 1980)

$$d\mathbf{M}/d\tau_m = -\,\mathbf{W}\bullet\mathbf{M} \qquad [1]$$

where **M** is the vector of magnetizations and **W** is the n-dimensional relaxation matrix. Eqn. 1 can be solved as (Bull, 1987)

---

[1] See the Materials and Methods section of Chapter V for details of peptide and protein sample preparation, and ^{1}H NMR spectral parameters used for acquisition of these data sets.

[2] The measured TRNOE intensities were normalized for the contribution of more than two protons to the cross-peak using the procedure outlined in the Materials and Methods section in Chapter V.

$$\begin{aligned} \mathbf{M}(\tau_m) &= \exp(-\mathbf{W}\tau_m)\,\mathbf{M}(0) \\ &= \boldsymbol{\chi}\exp(-\boldsymbol{\lambda}\,\tau_m)\,\boldsymbol{\chi}^{-1}\,\mathbf{M}(0) \\ &= \mathbf{a}(\tau_m)\,\mathbf{M}(0) \end{aligned} \qquad [2]$$

where $\boldsymbol{\chi}$ is the matrix of eigenvectors of the relaxation matrix $\mathbf{W}$, $\boldsymbol{\lambda}$ is the diagonal matrix of eigenvalues, and $\mathbf{a}$ is the matrix of mixing coefficients which are proportional to the measured NOE intensities.

If the spin system undergoes chemical exchange between a free (F) and bound state (B), relaxation can be described by

$$\frac{d}{d\tau_m}\begin{bmatrix} \mathbf{m}_B \\ \mathbf{m}_F \end{bmatrix} = -\mathbf{R}\begin{bmatrix} \mathbf{m}_B \\ \mathbf{m}_F \end{bmatrix} \qquad [3]$$

where $\mathbf{m}_B$ and $\mathbf{m}_F$ are n-dimensional vectors, $\mathbf{R} = \mathbf{E} + \mathbf{W}$, where E is the chemical exchange matrix, and $\mathbf{W}$ is the 2n-dimensional relaxation matrix for the n-spin system in the free and bound forms (Landy and Rao, 1989).

To obtain the mixing coefficients $a_{ij}(\tau_m)$, $\mathbf{R}$ must be diagonalized to yield $\boldsymbol{\lambda}$, the eigenvalue matrix. But due to the lack of symmetry in matrix $\mathbf{R}$, computer methods for the diagonalization are not so readily available and the eigenvalues are not guaranteed to be real (Landy and Rao, 1989). These complications may be avoided in the regime of fast chemical exchange. In the limit of fast chemical exchange, the longitudinal magnetization of the spin system, summed over the exchanging species, decays as a function of the population-weighted average of the individual relaxation matrices for the bound and free states (Landy and Rao, 1989)

$$\frac{d(\mathbf{m}_B + \mathbf{m}_F)}{d\tau_m} \cong (\, p_B\mathbf{W}_B + p_F\mathbf{W}_F\,)\,(\,\mathbf{m}_B + \mathbf{m}_F\,) \qquad [4]$$

where $\mathbf{W}_B$ and $\mathbf{W}_F$ are relaxation matrices for the bound and free states respectively, and p_B and p_F are the fractions of bound and free ligand.

Calculating the average relaxation matrix, $\mathbf{R} \cong p_B\mathbf{W}_B + p_F\mathbf{W}_F$, requires setting up individual relaxation matrices, $\mathbf{W}_B$ and $\mathbf{W}_F$. Each relaxation matrix is set up identically, in the following manner. Eqn. 1 may be then be represented as

$$\frac{d}{d\tau_m}\begin{bmatrix} m_i \\ m_j \\ \cdot \\ \cdot \\ \cdot \\ m_n \end{bmatrix} = -\begin{bmatrix} W_{ii} & W_{ji} & \ldots & W_{in} \\ W_{ji} & W_{jj} & \ldots & W_{jn} \\ & & \cdot & \\ & & \cdot & \\ & & \cdot & \\ W_{ni} & W_{nj} & \ldots & W_{nn} \end{bmatrix}\begin{bmatrix} m_i \\ m_j \\ \cdot \\ \cdot \\ \cdot \\ m_n \end{bmatrix} \qquad [5]$$

where the diagonal elements are given by

$$W_{ii} = 2(m_{oi} - 1)\,(\,\mathcal{W}_{1ii} + \mathcal{W}_{2ii}\,) \;+\; \sum_{k} m_{ok}\,(\,\mathcal{W}_{oik} + 2\mathcal{W}_{1ik} + \mathcal{W}_{2ik}\,) \;+ R_{1ext} \qquad [6a]$$

and the off-diagonal elements are given by

$$W_{ij} = m_{oi}\,(\,\mathcal{W}_{2ik} - \mathcal{W}_{oik}\,) \qquad [6b]$$

To take into account other possible relaxation pathways, we have added an external relaxation component, R_{1ext}, to the diagonal element, W_{ii}. The transition probabilities are given by (Macura and Ernst, 1980).

$$\mathcal{W}_{1ii} = 3/2\; q_{ii}\; J(\,\omega_i\,) \qquad [7a]$$

$$\mathcal{W}_{2ii} = 6\; q_{ii}\; J\,(\,2\omega_i\,) \qquad [7b]$$

$$\mathcal{W}_{1ij} = 3/2\; q_{ij}\; J\,(\,\omega_i\,) \qquad [7c]$$

$$\mathcal{W}_{oij} = q_{ij}\; J\,(\,\omega_i - \omega_j\,) \qquad [7d]$$

$$\mathcal{W}_{2ij} = q_{ij}\; J\,(\,\omega_i + \omega_j\,) \qquad [7e]$$

Here the spectral density functions take the form

$$J\,(\,\omega_i\,) = \tau_c \,/\, (\,1 + (\,\omega_i\tau_c\,)^2\,) \qquad [8]$$

and

$$q_{ij} = 1/10\; \gamma_i^2\, \gamma_j^2\, h^2\, (r_{ij})^{-6}\, (\mu_o/4\pi) \qquad [9]$$

where τ_c is the overall tumbling time of the peptide which modulates the interaction between spins i and j, and r_{ij} is the internuclear distance.

The off-diagonal elements, W_{ij} and W_{ji}, are equivalent only if we ignore the presence of chemically equivalent groups of protons for which $m_{oi} > 1$, such as a methyl groups or aromatic rings in the presence of fast internal motion. This results in an asymmetric relaxation matrix for which the eigenvalues are not guaranteed to be real. When the relaxation matrix, **W**, is real and symmetric, then the transformation matrix of othonormal eigenvectors, $\boldsymbol{\chi}$, is a unitary matrix which has the mathematical property of having its inverse equal to its transpose ($\boldsymbol{\chi}^{-1} = \boldsymbol{\chi}^T$). Thus, Eqn. 2 simplifies to

$$\mathbf{M}(\tau_m) = \boldsymbol{\chi} \exp(-\boldsymbol{\lambda}\, \tau_m)\, \boldsymbol{\chi}^T \mathbf{M}(0) \qquad [10]$$

Each proton in a chemically equivalent group was treated as an individual distinguishable proton, generating a symmetric matrix ($m_{oi} = 1$). This choice is valid as long as no second order spin coupling is involved. Under these conditions, the TRNOE between a given proton and a group of equivalent protons is then the sum of the contributions from each equivalent proton in the group to the given proton. The same reasoning is involved when considering the scaling of experimental cross peak intensities when groups of equivalent protons are involved (Yip, 1990). Cross relaxation amongst the group of equivalent protons is calculated explicitly.

To take into account differential motion, we incorporated the order parameters S_iF and S_iB for spin i in the free and bound peptide (Baleja *et al.*, 1990), using Lipari's and Szabo's model free approach (Lipari and Szabo, 1982). In this approach, internal motions in macromolecules may be specified by two independent quantities: a generalized order parameter, S^2 and an effective internal correlation time τ_e. The order parameter, S^2, can vary between 0 and 1. A value of one indicates that the correlation time of the interproton vector is the same as the overall tumbling time of the peptide (τ_c); a value of zero indicates complete motional freedom.

The spectral density function of Eqn. 8 then becomes

$$J(\omega_i) = [S^2\tau_c / (1 + (\omega_i\tau_c)^2)] + [(1-S^2)\tau / (1 + (\omega_i\tau)^2)] \qquad [11]$$

where

$$1/\tau = 1/\tau_c + 1/\tau_e \qquad [12]$$

2. Methodology

The computer program, TR-IRMA, takes as input the coordinates of the protons of the free and bound conformations of the TnI peptide ($(x_i,y_i,z_i)_F$, $(x_i,y_i,z_i)_B$), the overall tumbling times of the free and bound peptide (τ_cF, τ_cB), the effective internal correlation times of the free and bound peptide (τ_eF, τ_eB), the external leakage relaxation rates of the free and bound peptide protons ($R_{1ext}F$, $R_{1ext}B$), order parameters for individual free and bound peptide protons (S_iF, S_iB), the fraction of the free and bound peptide (p_F, p_B), the mixing time (τ_m), and the frequency of the experiment (ω).

A flow diagram for TR-IRMA is shown in Figure X-1. The procedure starts with initial structural models for the bound and free conformations. The starting coordinates for the bound TnI peptide, $(x_i,y_i,z_i)_B$, are taken from the TRNOE-determined structure of the synthetic peptide Nα-acetyl-TnI(104-115) amide bound to Ca(II)-saturated turkey skeletal TnC (Campbell and Sykes, 1991b; Chapter V). The coordinates for the free TnI peptide, $(x_i,y_i,z_i)_F$, are generated from the standard Φ,Ψ angles of a β-strand (ϕ=-118°, ψ=+118°). This is a reasonable model to adopt since the peptide is considered to be unstructured and extended in solution. Explicit methyl protons are added to the free and bound TnI peptide structures using a program which places protons in an sp^3 hybridized geometry about the central carbon atom.

a. Calculation of a Population-Weighted Average Relaxation Matrix, $\mathbf{R}(p_B)$.

The free and bound relaxation matrices, $\mathbf{W_F}$ and $\mathbf{W_B}$, are calculated from the free and bound coordinates ($(x_i,y_i,z_i)_F$, $(x_i,y_i,z_i)_B$), the free and bound overall tumbling times (τ_cF, τ_cB), the free and bound external leakage relaxation rates ($R_{1ext}F$, $R_{1ext}B$), and the frequency of the experiment (ω). Calculation of the diagonal and off-diagonal elements of the relaxation matrices, W_{ii} and W_{ij}, requires calculation of the spectral density functions, followed by calculation of the transition probabilities. When internal motions are incorporated for individual protons, the spectral density functions are modified to include the effects of decreasing the order parameter, and of adding an effective internal correlation time, according to Eqns. 11 and 12.

To model the effects of internal motion in the bound TnI peptide, we decrease the S_iF and S_iB order parameters for the protons of the L111δCH3 and V114γCH3 methyl groups, and for the δCH2, ξCH2 and ςCH protons of the F106 aromatic ring (see Chapter III). We consider the fact that for a methyl group rotating around a carbon-carbon single bond, τ_c should be decreased by a factor of $S^2 = ([3\cos^2\theta - 1]/2)^2$ (Marshall et al., 1972) where θ is the angle between the i-j interproton vector and the axis of rotation (the carbon-carbon single bond). For an sp^3 hybridized methyl group, $\theta = 90°$, making $S^2 = ([3\cos^2\theta - 1]/2)^2 = 0.25$ for rotation around the methyl axis. Thus, for the methyl protons i and j of the L111δCH3 and V114γCH3 groups in the bound and free peptide, we choose $S_i * S_j = 0.25$, or $S_i = S_j = 0.5$. As far as aromatic rings are concerned, the geometry leads to different estimations of $S_i * S_j$ values for the different proton pairs of the ring, so we somewhat arbitarily choose $S_i = 0.5$ for the δCH, ξCH and ςCH aromatic protons of the F106 residue in the free and bound peptide.

Once the free and bound relaxation matrices are calculated, a population-weighted average relaxation matrix is calculated from the fraction of the free and bound peptide (p_F, p_B)

$$\mathbf{R}(p_B) = p_B\mathbf{W_B} + p_F\mathbf{W_F}. \qquad [13]$$

b. Diagonalization of the Population-Weighted Average Relaxation Matrix, $\mathbf{R}(p_B)$.

The population-weighted average relaxation matrix, $\mathbf{R}(p_B)$, is then diagonalized to yield the eigenvalue matrix, $\boldsymbol{\lambda}(p_B)$, from which a matrix of mixing coefficients, $\mathbf{A_{calc}}(\tau_m,p_B)$, is calculated.

$$\mathbf{A_{calc}}(\tau_m,p_B) = \boldsymbol{\chi} \exp(-\boldsymbol{\lambda}\,\tau_m)^{\,T} \qquad [14]$$

Since the population-weighted relaxation matrix, $\mathbf{R}(p_B)$, is a function of p_B, the matrix of mixing coefficients, $\mathbf{A_{calc}}(\tau_{m,}\, p_B)$, is now a function of both p_B and τ_m. We collected nine sets of two-dimensional TRNOESY data at three mixing times (τ_m = 75, 150 and 500 ms) and three separate values of fraction bound (p_B = 0.1, 0.2 and 0.4); therefore we are required to calculate nine matrices of mixing coefficients, corresponding to each of these data sets.

c. Calculation of a Mixed Matrix of Mixing Coefficients, $\mathbf{A_{mix}}(\tau_m,p_B)$,with Calculated and Experimental Elements.

When experimental TRNOEs are available for the off-diagonal elements of $\mathbf{A_{calc}}(\tau_m,p_B)$, then these elements are replaced by the measured ones.

$$\mathbf{A_{mix}}(\tau_m,p_B) = S * \mathbf{A_{exp}}(\tau_m,p_B) + \mathbf{A_{calc}}(\tau_m,p_B) \qquad [15]$$

A scaling factor, S, is used to multiply the experimental TRNOEs, and is calculated from a collection of well resolved calibration cross-peaks, $a_{ijexp}(\tau_m,p_B)$, measured from the two-dimensional TRNOESY data sets.

$$S = \frac{\Sigma\,(a_{ijcalc}(\tau_m,p_B) * a_{ijexp}(\tau_m,p_B))^2}{\Sigma\,(a_{ijexp}(\tau_m,p_B))^2} \qquad [16]$$

At this stage in the TR-IRMA cycle, an 'R' factor is calculated. The R factor is a measure of root mean square differences in the measured and scaled calibration cross-peaks,

$S^* a_{ij\mathrm{exp}}(\tau_m, p_B)$, versus the calculated mixing coefficients, $a_{ij\mathrm{calc}}(\tau_m, p_B)$, for the same proton pairs. With each iteration, the refinement of the bound peptide structure is judged on the basis of a decrease in the value of 'R' towards a lower limiting value.

$$R = \frac{\Sigma\, |a_{ij\mathrm{calc}}(\tau_m, p_B) - S^* a_{ij\mathrm{exp}}(\tau_m, p_B)|^2}{\Sigma\, (a_{ij\mathrm{exp}}(\tau_m, p_B))^2} \qquad [17]$$

d. Diagonalization of the Mixed Matrix of Mixing Coefficients, $\mathbf{A_{mix}}(\tau_m, p_B)$.

The mixed matrix of mixing coefficients, $\mathbf{A_{mix}}(\tau_m, p_B)$, is then back-diagonalized to yield the eigenvalue matrix, $\mathbf{D_{mix}}(\tau_m, p_B)$, from which a relaxation matrix is calculated in which the cross-relaxation elements now include the effects of spin diffusion.

$$\mathbf{R_{mix}}(p_B) = -\,U\, \frac{\ln(\mathbf{D_{mix}}(\tau_m, p_B))}{\tau_m}\, U^T \qquad [18]$$

e. Averaging over Mixing Time, τ_m.

In the case of a time series with several mixing times, the relaxation matrix elements, $R_{ij\,\mathrm{mix}}(p_B)$, can be averaged with a weighting function (based on mixing time or NOE intensity) (Boelens *et al.*, 1988, 1989). Here we simply average over all mixing times without the use of a weighting function.

$$R_{ij\mathrm{mix}}(p_B) = \sum_{\tau_m} \frac{R_{ij\mathrm{mix}}(p_B)}{n} \qquad [19]$$

We started with nine bound relaxation matrices, $\mathbf{R_{mix}}(p_B)$, corresponding to the three mixing times and the three values of fraction bound for which the two-dimensional TRNOESY data sets were acquired. After averaging over mixing time we are left with only three bound relaxation matrices, one for each fraction bound.

After we average over mixing time for each value of fraction bound, we subtract out the elements of the free relaxation matrix from the averaged relaxation matrix, leaving only the elements of the bound relaxation matrix.

$$\mathbf{W_{Bmix}} = \frac{\mathbf{R_{mix}}(p_B) - p_F \mathbf{W_{Fmix}}}{p_B} \qquad [20]$$

f. Averaging over Fraction Bound, p_B.

In the case of a protein concentration series, the bound relaxation matrix elements, $W_{ij}B_{mix}$, can also be averaged. Here we simply average over all values of fraction bound, again without the use of a weighting function.

$$W_{ij}B_{mix} = \sum_{p_B} \frac{W_{ij}B_{mix}}{n} \tag{21}$$

Averaging over three relaxation matrices, corresponding to the three values of fraction bound, leaves a single bound relaxation matrix, $\mathbf{W_{Bmix}}$, which contains contributions from all nine two-dimensional TRNOESY data sets.

g. Conversion of $W_{ij}B_{mix}$ Matrix Elements to Bound Distance Restraints.

The distance restraints are calculated as

$$r_{ij} = r_o \left[\frac{W_{ijo}B_{mix}}{W_{ij}B_{mix}}\right]^{1/6} \tag{22}$$

where r_o is the calibration distance, and $W_{ijo}B_{mix}$ is the calibration cross-relaxation element in the bound relaxation matrix. Correction terms, $\pm\beta$, are added or subtracted from the distance restraints in the following manner to yield upper and lower distance bounds, r_{ij}^U and r_{ij}^L, respectively.

$$\text{for } 1.0\ \text{Å} \leq r_{ij} < 2.0\ \text{Å},\ \beta = \pm\, 0.1\ \text{Å} \tag{23a}$$
$$\text{for } 2.0\ \text{Å} \leq r_{ij} < 3.0\ \text{Å},\ \beta = \pm\, 0.2\ \text{Å} \tag{23b}$$
$$\text{for } 3.0\ \text{Å} \leq r_{ij} < 5.0\ \text{Å},\ \beta = \pm\, 0.3\ \text{Å} \tag{23c}$$
$$\text{for } 4.0\ \text{Å} \leq r_{ij} < 6.0\ \text{Å},\ \beta = \pm\, 0.5\ \text{Å} \tag{23d}$$
$$\text{for } r_{ij} \geq 5.0\ \text{Å},\ \beta = \pm\, 0.1\ \text{Å} \tag{23e}$$

h. Restrained Molecular Dynamics.

The restrained molecular dynamics calculations on the bound TnI peptide are performed with a molecular mechanics program and force field consisting of the usual terms for bonds, bond-angles, sinusoidal dihedral torsion, non-bonded interactions (Van der Waals and electrostatics), and harmonic terms to maintain proper planar or tetrahedral geometries (see Chapters V, VIII and IX). Two extra terms are added representing distance and dihedral restraints. The distance restraint square well potential, E_{DIS}, is defined by two functions, a biharmonic potential for $(r_{ij}^U - r_{ij})$ and $(r_{ij}^L - r_{ij}) < 5$Å, and a linear potential for $(r_{ij}^U - r_{ij})$ and $(r_{ij}^L - r_{ij}) \geq 5$Å:

$$E_{DIS} = 0.5\ C_{DIS}\ (r_{ij}^U - r_{ij})^2 \qquad \text{if } r_{ij} > r_{ij}^U;\ |r_{ij}^U - r_{ij}| < 5Å$$
$$= 0.5\ C_{DIS}\ (r_{ij}^L - r_{ij})^2 \qquad \text{if } r_{ij} < r_{ij}^L;\ |r_{ij}^L - r_{ij}| < 5Å \qquad [24a]$$

$$E_{DIS} = 0.5\ C_{DIS}\ (r_{ij}^U - r_{ij}) \qquad \text{if } r_{ij} > r_{ij}^U;\ |r_{ij}^U - r_{ij}| \geq 5Å$$
$$= 0.5\ C_{DIS}\ (r_{ij}^L - r_{ij}) \qquad \text{if } r_{ij} < r_{ij}^L;\ |r_{ij}^L - r_{ij}| \geq 5Å \qquad [24b]$$

where C_{DIS} is a force constant. The dihedral angle restraint, E_{DIH}, is then represented by the biharmonic potential :

$$E_{DIH} = 0.5\ C_{DLR}\ (\Phi_k^U - \Phi_k)^2 \qquad \text{if } \Phi_k > \Phi_k^U$$
$$= 0.5\ C_{DLR}\ (\Phi_k^L - \Phi_k)^2 \qquad \text{if } \Phi_k < \Phi_k^L \qquad [25]$$

where Φ_k^U and Φ_k^L are upper and lower allowed limits of the torsion angle, Φ_k is the calculated angle, and C_{DLR} is the force constant.

3. Simulated Versus Experimental Results

The TRNOE intensities for three sample proton pairs (F106βCH(m)-βCH'(x), P109αCH-βCH(x), and V114αCH-(γCH3)2) were calculated as a function of τ_m for three values of p_B (p_B = 0.1, 0.2, 0.4) using the following standard parameters: $\omega = 500 \times 10^6$ s^{-1}, $\tau_c F = 0.4$ ns, $\tau_c B = 25$ ns, $\tau_e F = 0.01$ ns, $\tau_e B = 0.01$ ns, $R_{1ext}F = 1.0\ s^{-1}$, $R_{1ext}B = 2.0\ s^{-1}$, $S_iF = S_iB = 0.5$ for the V114 methyl protons, and $S_iF = S_iB = 0.5$ for the F106 ring protons.

The TRNOE intensities for these three sample proton pairs (measured for p_B = 0.1, 0.2, 0.4, and τ_m = 75, 150, 500 ms) were multiplied by a scaling factor, S = 0.0067, in order to bring the magnitude of the measured value more closely in line with the magnitude of the simulated value. The scaling factor was calculated using Eqn. 16 and a set of 15 calibration proton pairs for which TRNOE intensities had been measured (also for p_B = 0.1, 0.2, 0.4, and τ_m = 75, 150, 500 ms). The set of calibration proton pairs consisted of: F106βCH(m)-βCH'(x), F106βCH(m)-δCH2, F106βCH'(x)-δCH2, P110αCH-βCH(x), P110αCH-βCH'(p), P110αCH-γCH2, P110βCH(x)-βCH'(p), P110βCH(x)-δCH(m), P110βCH(x)-δCH'(m'), P110βCH'(p)-δCH(m), P110βCH'(p)-δCH'(m'), P110γCH2-δCH(m), P110γCH2-δCH'(m'), L111αCH-βCH2, L111αCH-(δCH3)2, V114αCH-βCH, V114αCH-(γCH3)2.

Figure X-2 shows a plot of the simulated TRNOE build-up curves versus the experimentally measured TRNOE intensities for F106βCH(m)-βCH'(x), P109αCH-

βCH(x), and V114αCH-(γCH3)2. The simulated TRNOE build-up curves are represented by the solid black lines, whereas the measured TRNOE intensities are represented by the symbols. It is obvious that although the agreement between the measured and simulated TRNOE intensities for F106βCH(m)-βCH'(x) (Panel A) and P109αCH-βCH(x) (Panel B) is reasonable, the agreement between the measured and simulated values for V114αCH-(γCH3)2 (Panel C) is poor. The measured values are two orders of magnitude larger than the simulated values for the V114αCH-(γCH3)2 proton pair, and it appears as if the effects of spin diffusion in the simulated TRNOE build-up curves are much stronger than observed in the experimentally measured data. An R factor was calculated using Eqn. 17 for the chosen simulation parameters and using the set of calibration TRNOEs listed above, and yielded a value of $R = 0.80$. This suggests that the structure is far from being perfectly 'refined'. However, it is likely that several rounds of iterative refinement using the TR-IRMA program, and adjusting the values for τ_cF, τ_cB, τ_eF, τ_eB, R_{1ext}F, R_{1ext}B, S_iF, and S_iB with each iteration, should obtain an improved structural model for the bound TnI peptide, incorporating the effects of spin-diffusion and internal motions.

Figure X-1. Flow diagram for the transferred iterative relaxation matrix analysis (TR-IRMA) for structure determination of chemically-exchanging biomolecules from ^1H-^1H TRNOEs. Details of the procedure are discussed in the text.

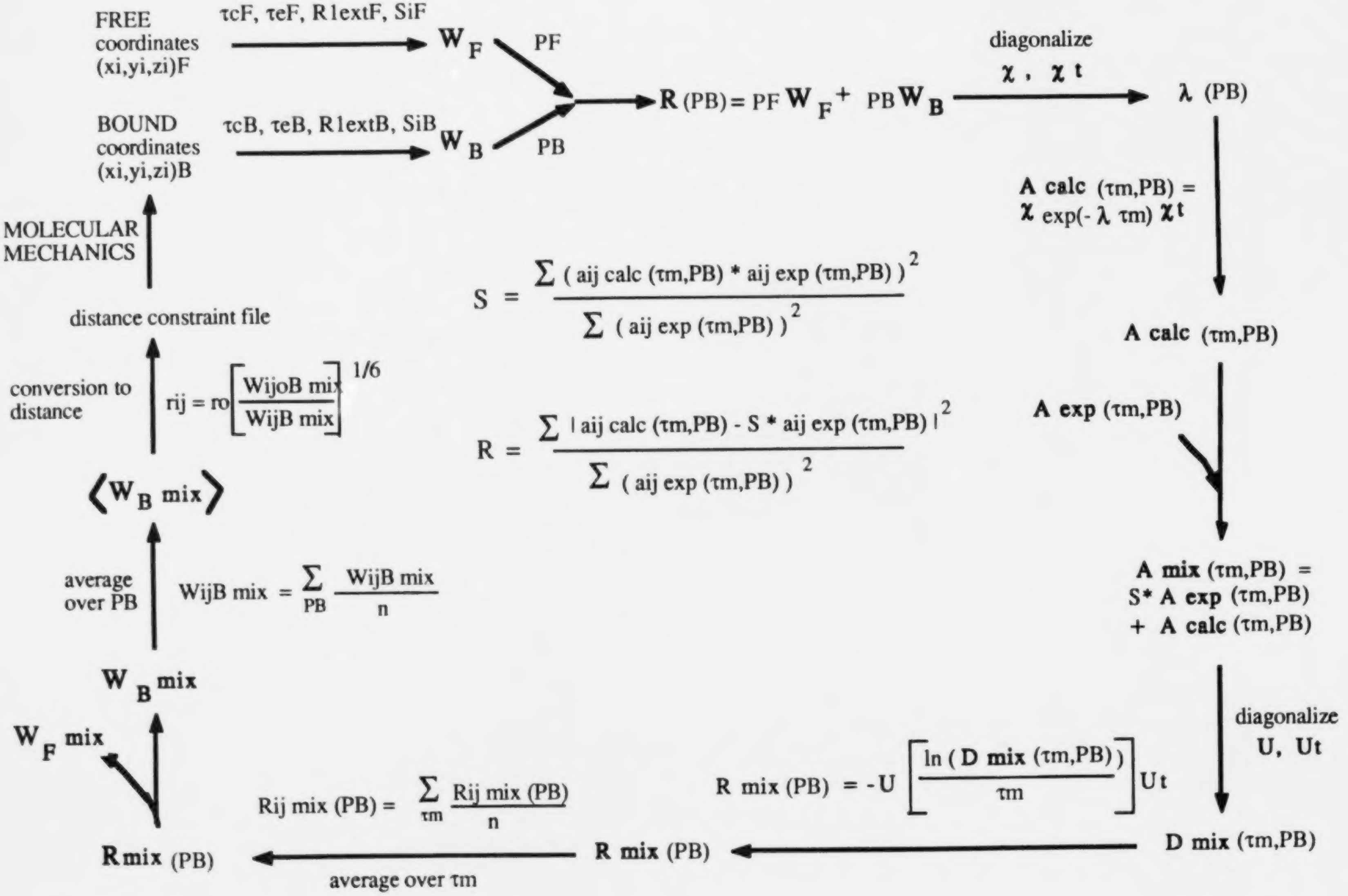
FREE coordinates (xi,yi,zi)F
τcF, τeF, R1extF, SiF
W_F
PF
BOUND coordinates (xi,yi,zi)B
τcB, τeB, R1extB, SiB
W_B
PB
$R(PB) = PF\,W_F + PB\,W_B$
diagonalize
χ, χt
λ (PB)
A calc (τm,PB) = χ exp(- λ τm) χt
A calc (τm,PB)
A exp (τm,PB)
A mix (τm,PB) = S* A exp (τm,PB) + A calc (τm,PB)
diagonalize
U, Ut
D mix (τm,PB)
$R\ mix\ (PB) = -U \left[\frac{\ln(D\ mix\ (\tau m,PB))}{\tau m} \right] Ut$
R mix (PB)
average over τm
$Rij\ mix\ (PB) = \sum_{\tau m} \frac{Rij\ mix\ (PB)}{n}$
Rmix (PB)
W_F mix
W_B mix
average over PB
$WijB\ mix = \sum_{PB} \frac{WijB\ mix}{n}$
$\langle W_B\ mix \rangle$
conversion to distance
$rij = ro \left[\frac{WijoB\ mix}{WijB\ mix} \right]^{1/6}$
distance constraint file
MOLECULAR MECHANICS
$S = \frac{\sum (aij\ calc\ (\tau m,PB) * aij\ exp\ (\tau m,PB))^2}{\sum (aij\ exp\ (\tau m,PB))^2}$
$R = \frac{\sum | aij\ calc\ (\tau m,PB) - S * aij\ exp\ (\tau m,PB) |^2}{\sum (aij\ exp\ (\tau m,PB))^2}$

Figure X-2. Simulated TRNOE build-up curves versus experimentally measured TRNOE intensities for the following intraresidue proton pairs: A. F106βCH(m)-βCH'(x), B. P109αCH-βCH(x), and C. V114αCH-(γCH3)2. The parameters used in the simulation were $\omega = 500 \times 10^6\ s^{-1}$, $p_B = 0.1, 0.2, 0.4$, $\tau_cF = 0.4$ ns, $\tau_cB = 25$ ns, $\tau_eF = 0.01$ ns, $\tau_eB = 0.01$ ns, $R_{1ext}F = 1.0\ s^{-1}$, $R_{1ext}B = 2.0\ s^{-1}$, $S_iF = S_iB = 0.5$ for the V114 methyl protons, and $S_iF = S_iB = 0.5$ for the F106 ring protons. The measured TRNOE intensities were multiplied by a scaling factor $S = 0.0067$. The simulated TRNOE build-up curves are represented by the solid black lines, whereas the measured TRNOE intensities are represented by the symbols: (●) $p_B = 0.0$, (○) $p_B = 0.1$, (□) $p_B = 0.2$, (△) $p_B = 0.4$.

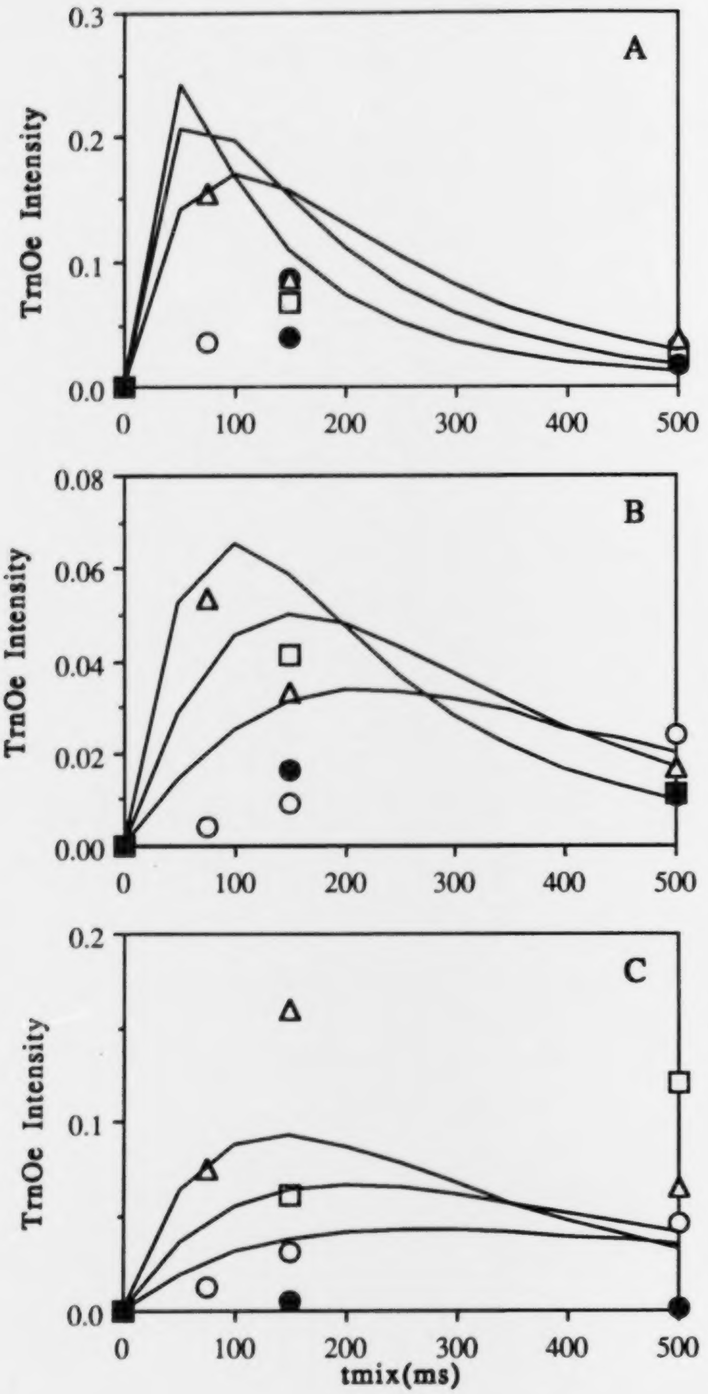
A
TrnOe Intensity
0.0
0.1
0.2
0.3
0
100
200
300
400
500
B
TrnOe Intensity
0.00
0.02
0.04
0.06
0.08
0
100
200
300
400
500
C
TrnOe Intensity
0.0
0.1
0.2
0
100
200
300
400
500
tmix(ms)

D. References

ABRAGAM, A. 1961. In *The Principles of Nuclear Magnetism*, Oxford Univ. Press, London.

BALEJA, J.D., MOULT, J., and SYKES, B.D. 1990. Distance measurement and structure refinement with NOE data. J. Magn. Reson. **87**: 375-384.

BLOCH, F. 1957. Generalized theory of relaxation. Phys. Rev. **105**: 1206-1222.

BOELENS, R., KOENIG, T.M.G., and KAPTEIN, R. 1988. Determination of biomolecular structures from proton-proton nOes using a relaxation matrix approach. J. Mol. Struct. **173**: 299-311.

BOELENS, R., KOENIG, T.M.G., VAN DER MAREL, G.A., VAN BOOM, J.H., and KAPTEIN, R. 1989. Iterative procedure for structure determination from proton-proton nOes using a full relaxation matrix approach. Application to a DNA octamer. J. Magn. Reson. **82**: 290-308.

BORGIAS, B., and JAMES, T.L. 1988. COMATOSE, a method for constrained refinement of macromolecular structure based on two-dimensional nuclear Overhauser effect spectra. J. Magn. Reson. **79**: 493-512.

BORGIAS, B., and JAMES, T.L. 1989. Two-dimensional nuclear Overhauser effect: Complete relaxation matrix analysis. In *Methods in Enzymology* (N.J. Oppenheimer, and T.L. James, Eds.), Vol. **176**, Part A, pp 169-183, Academic Press Inc., New York.

BULL, T.E. 1987. Cross-correlation and 2D NOE spectra. J. Magn. Reson. **72**: 397-413.

CAMPBELL, A.P., and SYKES, B.D. 1991a. Theoretical evaluation of the two-dimensional transferred nuclear Overhauser effect. J. Magn. Reson. **93**: 77-92.

CAMPBELL, A.P., and SYKES, B.D. 1991b. Effects of internal motions on the development of the two-dimensional transferred nuclear Overhauser effect. J. Biomol. NMR, in press.

CAMPBELL, A.P., and SYKES, B.D. 1991c. Interaction of troponin I and troponin C: Use of the two-dimensional NMR transferred nuclear Overhauser effect to determine the structure of the inhibitory troponin I peptide when bound to skeletal troponin C. J. Mol. Biol., in press.

CAMPBELL, A.P., CACHIA, P.J., and SYKES, B.D. 1991a. Interaction of troponin I and troponin C : ^{19}F NMR studies of the binding of the inhibitory troponin I peptide to turkey skeletal troponin C. Biochem. Cell Biol., in press.

CAMPBELL, A.P., SLUPSKY, C.M., SHAW, G.S., and SYKES, B.D. 1991b. Interaction of troponin I and troponin C : Identification using NMR of specific residues in troponin C which are involved in the binding of an inhibitory troponin I peptide. Biochemistry, submitted.

CLORE, G.M., and GRONENBORN, A.M. 1982. Theory and applications of the transferred nuclear Overhauser effect to the study of the conformations of small ligands bound to proteins. J. Magn. Reson. **48**: 402-417.

CLORE, G.M., and GRONENBORN, A.M. 1983. Theory of the time dependent transferred nuclear Overhauser effect. Applications to structural analysis of ligand-protein complexes in solution. J. Magn. Reson. **53**: 423-442.

DOBSON, C.M., OLEJNICZAK, E.T., POULSEN, F.M., and RATCLIFFE, R.G. 1982. Time development of proton nuclear Overhauser effects in proteins. J. Magn. Reson. **48**: 976-110.

GRONENBORN, A.M., and CLORE, G.M. 1985. Investigation of the solution structures of short nucleic acid fragments by means of nuclear Overhauser enhancement measurements. In *Progress in Nuclear Magnetic Resonance Spectroscopy* (J.W. Emsley, J. Feeney, and L.H. Sutcliffe, Eds.), Vol. **17**, pp 1-32, Pergamon Press, Oxford.

IKURA, M., KAY, E., and BAX, A. 1990a. A novel approach for sequential assignment of ^{1}H, ^{13}C, and ^{15}N spectra of larger proteins: Heteronuclear triple-resonance three-dimensional NMR spectroscopy. Application to Calmodulin. Biochemistry **29**: 4659-4667.

IKURA, M., KAY, E., CLORE, M., and GRONENBORN, A.M. 1990b. Detection of nuclear Overhauser effects between degenerate amide proton resonances by heteronuclear three-dimensional nuclear magnetic resonance spectroscopy. J. Am. Chem. Soc. **112**: 9092-9022.

IKURA, M., KAY, L.E., KRINKS, M., and BAX, A. 1991. Triple-resonance multidimensional NMR study of calmodulin complexed with the binding domain of skeletal muscle myosin light-chain kinase: Indication of a conformational change in the central helix. Biochemistry **30**: 5498-5504.

KEEPERS, J.W., and JAMES, T.L. 1984. A theoretical study of distance determinations from NMR two-dimensional nuclear Overhauser effect spectra. J. Magn. Reson. **57**: 404-426.

LANDY, S.B., and RAO, B.D.N. 1989. Dynamical NOE in multiple-spin systems undergoing chemical exchange. J. Magn. Reson. **81**: 371-377.

LEFEVRE, J.F., LANE, A.N., and JARDETSKY, O. 1987. Solution structure of the trp operator of *Escherichia Coli* determined by NMR. Biochemistry **26**: 5076-5090.

LIPARI, G., and SZABO, A. 1982. Model-free approach to the interpretation of nuclear magnetic resonance relaxation in macromolecules. 1. Theory and range of validity. J. Am. Chem. Soc. **104**: 4546-4559.

MACURA, S., and ERNST, R.R. 1980. Elucidation of cross-relaxation in liquids by two-dimensional NMR spectroscopy. Mol. Phys. **41**: 95-117.

MARSHALL, A.G., SCHMIDT, P.G., and SYKES, B.D. Effects of internal rotation on nuclear magnetic relaxation times for macromolecules. 1972. Biochemistry **11**: 3875-3879.

NOGGLE, J.H., and SCHIRMER, R.E. 1971. In *The Nuclear Overhauser Effect*, Academic Press, New York.

SOLOMON, I. 1955. Relaxation processes in a system of two spins. Phys. Rev. **99**: 559-565.

WAGNER, G., and WUTHRICH, K. 1979. Truncated driven nuclear Overhauser effect (TOE). A new technique for studies of selective ^{1}H-^{1}H Overhauser effects in the presence of spin diffusion. J. Magn. Reson. **33**: 675-680.

WUTHRICH, K. 1986. In *NMR of Proteins and Nucleic Acids* , John Wiley and Sons, New York.

YIP, P.F. 1990. Scaling NOESY cross-peaks involving methyl protons. J. Magn. Reson. **90**: 382-383.

Table IV-1. ^{19}F NMR data for the titration of N-α-acetyl[^{19}F-phe106]TnI(104-115) amide with apo turkey skeletal TnC.

[TnC.apo]/ [TnI peptide]	Δδ (ppm)
0.00	0.000
0.28	0.052
0.56	0.092
0.84	0.100
1.12	0.126
1.40	0.250
1.69	0.142
1.96	0.164
2.24	0.158

Table IV-2. ^{19}F NMR data for the titration of N-α-acetyl[^{19}F-phe106]TnI(104-115) amide with Ca(II)-saturated turkey skeletal TnC.

[TnC.Ca4]/ [TnI peptide]	ΔI/IOBS
0.00	0.000
0.14	0.134
0.27	0.254
0.41	0.266
0.54	0.390
0.68	0.394
0.81	0.514
0.95	0.519
1.08	0.555
1.22	0.593
1.35	0.578
1.62	0.632
1.89	0.718
2.16	0.770
2.50	0.758
2.70	0.747

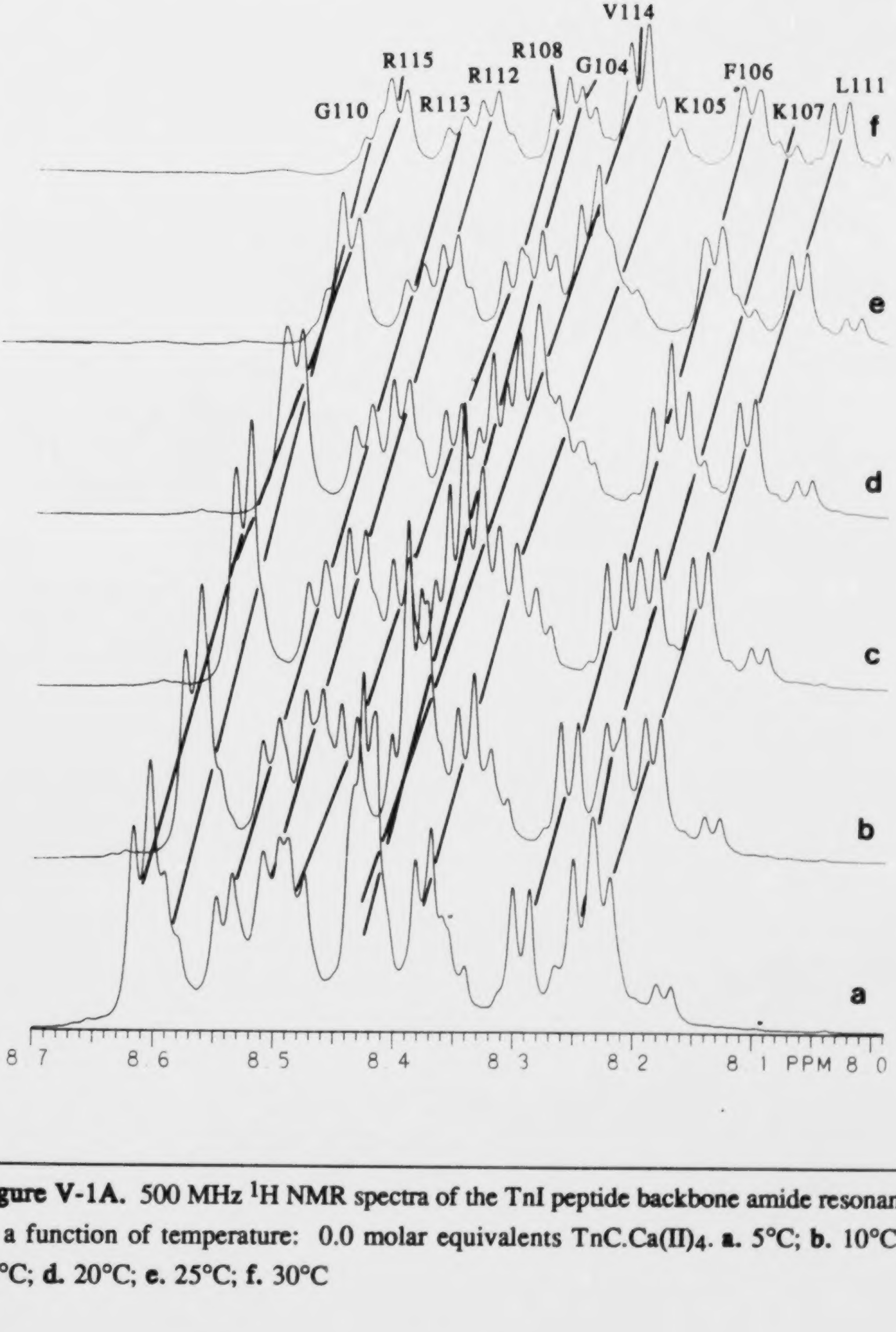

Figure V-1A. 500 MHz ^{1}H NMR spectra of the TnI peptide backbone amide resonances as a function of temperature: 0.0 molar equivalents TnC.Ca(II)$_4$. **a.** 5°C; **b.** 10°C; **c.** 15°C; **d.** 20°C; **e.** 25°C; **f.** 30°C

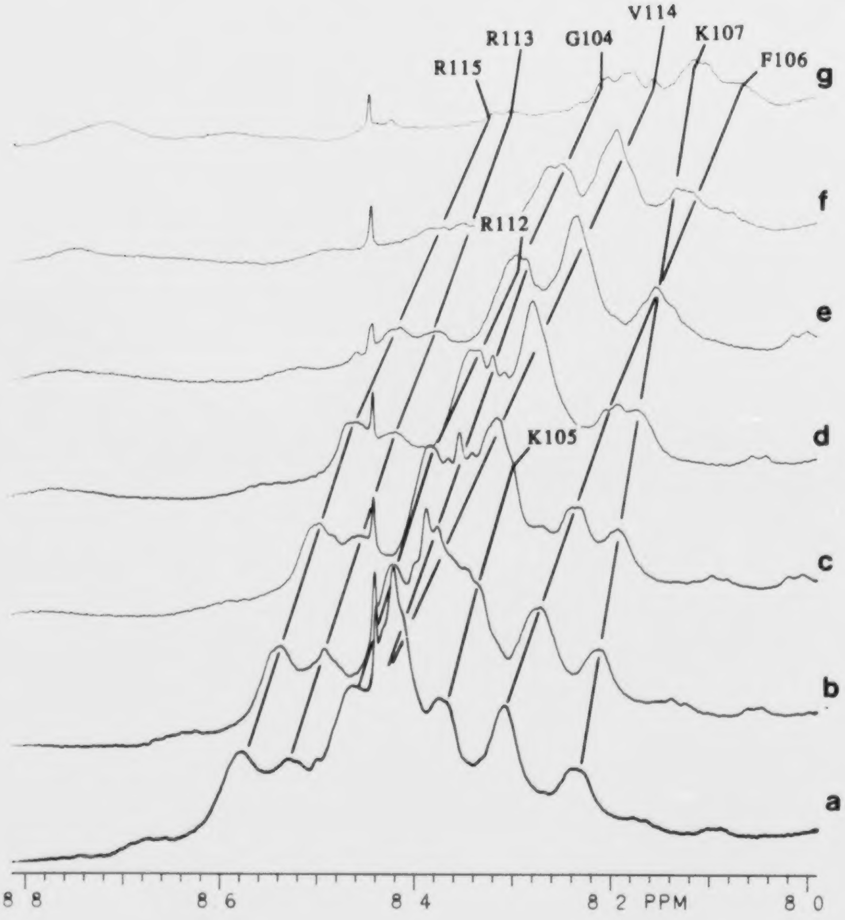

Figure V-1B. 500 MHz ^{1}H NMR spectra of the TnI peptide backbone amide resonances as a function of temperature: 0.2 molar equivalents TnC.Ca(II)$_4$. **a.** 5°C; **b.** 10°C; **c.** 15°C; **d.** 20°C; **e.** 25°C; **f.** 30°C

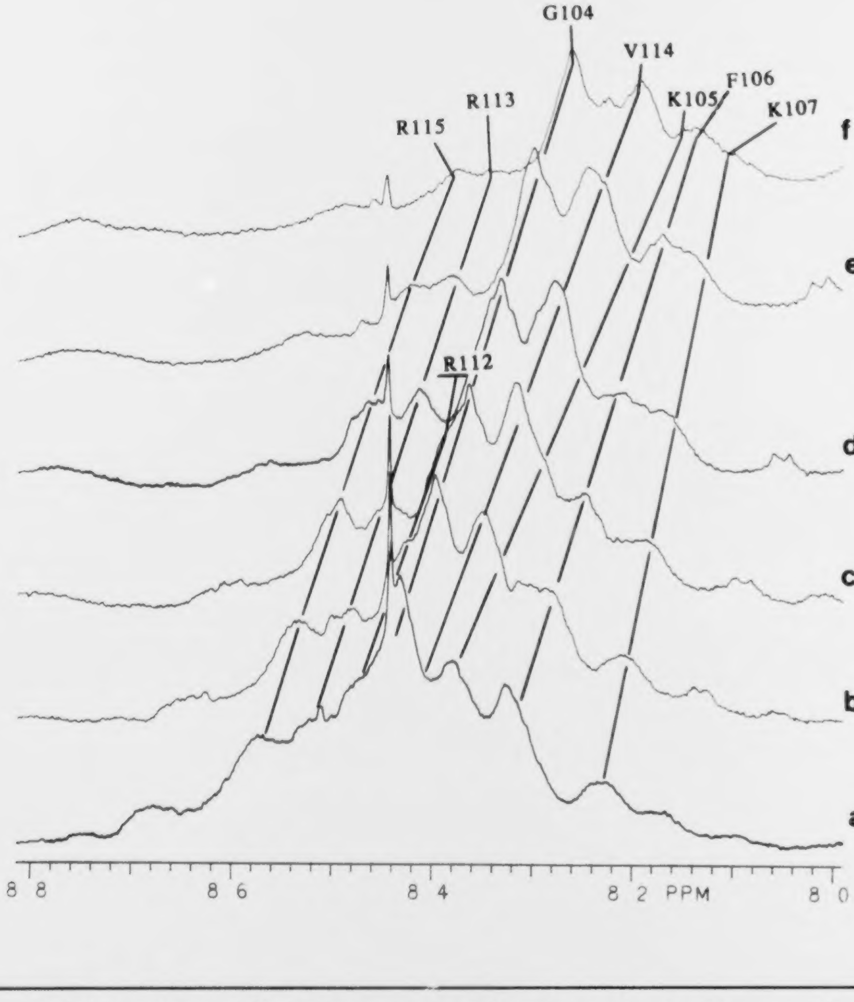

Figure V-1C. 500 MHz ^{1}H NMR spectra of the TnI peptide backbone amide resonances as a function of temperature: 0.4 molar equivalents TnC.Ca(II)$_4$. **a.** 5°C; **b.** 10°C; **c.** 15°C; **d.** 20°C; **e.** 25°C; **f.** 30°C

Table V-1. Normalization tables for exchangeable backbone amide resonances on the TnI peptide. **A.** Amide versus nonexchangeable resonance; **B.** Amide versus amide resonance. The intensities (*Na*) of the exchangeable proton peaks were integrated in a one-dimensional spectrum, and the intensity of these peaks were normalized against the integrated intensity of the V114αCH peak. The normalization factor (2*NaNb*)/(*Na*+*Nb*) was then calculated for variable values of *Nb*.

	Na	Nb=1	Nb=2	Nb=3
G104	0.53	0.70	0.84	0.90
K105	0.53	0.70	0.84	0.90
F106	0.42	0.60	0.70	0.74
K107	0.50	0.66	0.80	0.86
R108	0.28	0.44	0.50	0.51
L111	0.53	0.70	0.84	0.90
R112	0.42	0.60	0.70	0.74
R113	0.40	0.58	0.66	0.70
V114	0.53	0.70	0.84	0.90
R115	0.50	0.66	0.80	0.86

	Na	G104	K105	F106	K107	R108	L111	R112	R113	V114	R115
G104	0.53	-	0.54	0.46	0.52	0.36	0.54	0.46	0.46	0.54	0.52
K105	0.53	0.54	-	0.46	0.52	0.36	0.54	0.46	0.46	0.54	0.52
F106	0.42	0.46	0.46	-	0.46	0.34	0.46	0.42	0.40	0.46	0.46
K107	0.50	0.52	0.52	0.46	-	0.36	0.52	0.46	0.44	0.52	0.50
R108	0.28	0.36	0.36	0.34	0.36	-	0.36	0.34	0.32	0.36	0.36
L111	0.53	0.54	0.54	0.46	0.52	0.36	-	0.46	0.46	0.54	0.52
R112	0.42	0.46	0.46	0.42	0.46	0.34	0.46	-	0.40	0.46	0.46
R113	0.40	0.46	0.46	0.40	0.44	0.32	0.46	0.40	-	0.46	0.44
V114	0.53	0.54	0.54	0.46	0.52	0.36	0.54	0.46	0.46	-	0.52
R115	0.50	0.52	0.52	0.46	0.50	0.36	0.52	0.46	0.44	0.52	-

Table V-2. Table of TRNOE cross-peak intensities for the TnI peptide in the presence of 0.1 molar equivalents TnC.Ca(II)$_4$. Included in the table are the measured TRNOE intensities, the corrected and normalized TRNOE intensities, and the r$_{ij}$s calculated from these corrected and normalized values.

spin system	TRNOE measured	TRNOE normalized	rij calculated (Å)
K105αCH-βCH2	2.000	1.515	3.3
K105αCH-γCH2	0.970	0.735	3.8
K105βCH2-γCH2	1.080	0.540	4.0
K105γCH2-δCH2	1.080	0.540	4.0
K105δCH2-ξCH2	1.500	0.750	3.7
K105βCH2-NH	1.520	0.600	3.9
K105γCH2-ξCH2	2.000	1.000	3.6
K105γCH2-NH	0.325	0.464	4.1
F106αCH-βCH(m)	0.917	0.917	3.6
F106αCH-βCH'(x)	3.380	3.380	2.8
F106αCH-δCH2	0.694	0.526	4.0
F106βCH(m)-βCH'(x)	6.480	6.480	2.5
F106βCH'(x)-NH	0.523	0.872	3.6
F106βCH(m)-NH	1.210	2.017	3.1
F106βCH2-δCH2	1.260	0.630	3.9
F106NH-δCH2	0.391	0.559	3.9
K107αCH-βCH2	2.070	1.568	3.3
K107αCH-γCH2	1.380	1.045	3.5
K107βCH2-γCH2	4.480	2.240	3.1
K107γCH2-NH	0.789	0.986	3.6
K107δCH2-γCH2	6.250	3.310	2.9
K107δCH2-ξCH2	1.950	0.975	3.6
K107δCH2-NH	1.710	-	5.0
K107γCH2-ξCH2	2.420	1.210	3.4
K107γCH2-NH	0.325	0.492	4.0
R108αCH-βCH2	1.290	0.977	3.6
R108αCH-γCH2	0.666	0.505	4.0
R108βCH2-NH	0.374	7.480	2.5
R108δCH2-NH	0.377	0.754	3.7
P109αCH-βCH(x)	0.323	0.323	4.4
P109αCH-βCH'(p)	0.896	0.896	3.6
P109αCH-γCH2	0.174	0.132	5.1
P109βCH(x)-βCH'(p)	11.300	11.300	2.3
P109βCH(x)-δCH'(m')	1.700	1.700	3.2
P109βCH(x)-δCH(m)	0.748	0.748	3.7

P109βCH(x)-γCH2	10.000	7.650	2.4
P109βCH'(p)-δCH(m)	1.780	1.780	3.2
P109βCH'(p)-δCH'(m')	1.240	1.240	3.4
P109βCH'(p)-γCH2	6.910	5.230	2.6
P109γCH2-δCH2	2.100	1.591	3.3
P109δCH(m)-δCH'(m')	5.190	5.190	2.6
P110αCH-βCH(x)	1.690	1.690	3.2
P110αCH-βCH'(p)	3.240	3.240	2.9
P110αCH-γCH2	0.741	0.561	3.9
P110βCH(x)-βCH'(p)	12.800	12.800	2.2
P110βCH(x)-δCH'(m')	1.700	1.700	3.2
P110βCH(x)-δCH(m)	0.967	0.967	3.6
P110βCH(x)-γCH2	10.000	7.652	2.4
P110βCH'(p)-δCH(m)	1.330	1.330	3.4
P110βCH'(p)-δCH'(m')	0.741	0.741	3.7
P110βCH'(p)-γCH2	5.280	4.000	2.8
P110γCH2-δCH2	2.980	2.258	3.1
P110δCH(m)-δCH'(m')	4.870	4.870	2.7
L111αCH-βCH2	3.000	2.273	3.1
L111αCH-(δCH3)2	2.210	0.372	4.3
L111βCH2-(δCH3)2	1.930	0.643	3.8
L111γCH-(δCH3)2	2.180	1.275	3.4
L111βCH2-NH	2.530	3.012	2.9
L111(δCH3)2-NH	2.210	1.510	3.3
R112αCH-βCH2	1.490	1.129	3.5
R112αCH-δCH2	0.620	0.470	4.1
R112βCH2-NH	2.530	3.614	2.8
R112δCH2-NH	0.377	0.539	4.0
R113αCH-βCH2	3.110	2.356	3.0
R113αCH-δCH2	0.620	0.470	4.1
R113βCH2-NH	3.260	4.939	2.6
R113δCH2-NH	0.377	0.571	3.9
V114αCH-βCH	1.020	1.500	3.3
V114αCH-(γCH3)2	2.290	1.330	3.4
V114βCH-(γCH3)2	7.640	4.468	2.7
V114βCH-NH	1.120	1.600	3.3
V114(γCH3)2-NH	1.190	1.222	3.4
R115αCH-βCH2	1.320	1.200	3.4
R115αCH-δCH2	0.639	0.484	4.1
R115βCH2-NH	1.280	1.600	3.3

N-Acetyl CH3-G104αCH2	1.390	0.579	3.9
N-Acetyl CH3-G104NH	1.120	1.244	3.4
N-Acetyl CH3-K105NH	0.441	0.490	4.0
N-Acetyl CH3-R108NH	0.420	0.823	3.7
G104NH-K105γCH2	0.207	0.206	4.7

G104NH-K107γCH2	0.145	0.207	4.7
K105βCH2-F106NH	0.615	0.879	3.6
K105γCH2-F106NH	0.196	0.327	4.4
K105γCH2-K107NH	0.142	0.215	4.7
K105γCH2-R108NH	0.166	0.368	4.3
K105δCH2-F106NH	0.328	0.469	4.1
K105NH-K107γCH2	0.105	0.150	5.0
F106γCH2-K107NH	0.812	1.231	3.4
F106δCH2-K107NH	0.200	0.250	4.6
F106NH-K107γCH2	0.220	0.314	4.4
K107γCH2-R108NH	0.146	0.292	4.4
K107NH-R108δCH2	0.168	0.210	4.7
R108αCH-P109γCH2	0.310	0.235	4.6
R108αCH-P109δCH(m)	3.570	3.570	3.1
R108αCH-P109δCH'(m')	2.040	2.040	2.8
R108NH-P109βCH2	0.066	0.151	5.0
R108NH-P109γCH2	0.180	0.360	4.3
P109αCH-P110δCH(m)	1.700	1.700	3.1
P109αCH-P110δCH'(m')	2.070	2.070	3.2
P109αCH-P110βCH(x)	0.167	0.167	4.9
P110αCH-R112βCH2	0.151	0.114	5.3
P110βCH(x)-L111NH	1.760	2.522	3.0
P110βCH(x)-R112αCH	0.520	0.520	4.0
P110βCH'(p)-L111αCH	0.924	0.924	3.6
P110βCH'(p)-L111NH	1.670	2.390	3.0
P110βCH'(p)-R112αCH	0.033	0.033	6.5
P110βCH2-R112NH	1.050	1.500	3.3
P110γCH2-L111αCH	0.726	0.550	4.0
P110γCH2-L111NH	0.380	0.452	4.1
P110γCH2-R112αCH	0.250	0.189	4.8
P110γCH2-R112NH	0.070	0.100	5.4
L111(δCH3)2-R112αCH	0.230	0.135	5.1
L111(δCH3)2-R112NH	0.944	0.969	3.6
L111NH-R112δCH2	0.140	0.167	4.9
R112βCH2-R113NH	0.810	1.227	3.4
R112βCH2-R115NH	0.959	1.013	3.5
R112βCH2-Cterm NH	0.373	0.283	4.5
R112βCH2-Cterm NH'	0.373	0.283	4.5
R112δCH2-R113NH	0.100	0.151	5.0
R112NH-R113δCH2	0.100	0.143	5.1
R112NH-V114βCH	0.402	0.670	3.8
R113αCH-V114βCH	0.150	0.150	5.0
R113αCH-V114(γCH3)2	0.379	0.221	4.7
R113βCH2-V114αCH	0.296	0.224	4.7
R113βCH2-V114NH	0.420	0.500	4.0
R113δCH2-V114NH	0.140	0.167	4.9

R113NH-V114(γCH3)2	0.316	0.369	4.3
V114αCH-R115βCH2	0.296	0.224	4.7
V114βCH-R115NH	0.771	1.168	3.4
V114(γCH3)2-R115NH	0.699	0.757	3.7
V114(γCH3)2-Cterm NH	0.241	0.199	4.8
V114(γCH3)2-Cterm NH'	0.241	0.199	4.8
V114NH-R115βCH2	1.190	1.417	3.3
V114NH-R115δCH2	0.140	0.167	4.9
R115αCH-Cterm NH	1.300	1.240	3.4
R115αCH-Cterm NH'	1.300	1.240	3.4
R115βCH2-Cterm NH	0.367	0.278	4.5
R115βCH2-Cterm NH'	0.367	0.278	4.5

F106δCH2-K105βCH2	0.210	0.105	5.4
F106δCH2-K105γCH2	0.297	0.199	4.8
F106δCH2-K107βCH2	0.230	0.155	5.0
F106δCH2-K107γCH2	0.266	0.133	5.1
F106δCH2-K107ξCH2	0.700	0.350	4.3
F106δCH2-R108δCH2	5.090	2.545	3.0
F106δCH2-P109βCH(x)	0.065	0.045	6.3
F106δCH2-P109γCH2	0.130	0.071	5.8
F106δCH2-L111βCH2	0.170	0.129	5.2
F106δCH2-L111(δCH3)2	0.968	0.323	4.4
F106δCH2-V114βCH	0.494	0.374	4.2
F106δCH2-V114(γCH3)2	0.543	0.181	4.9
F106ξCH2-K105βCH2	0.996	0.415	4.2
F106ξCH2-K105γCH2	0.325	0.135	5.1
F106ξCH2-K107βCH2	1.280	0.533	4.0
F106ξCH2-K107γCH2	0.318	0.135	5.1
F106ξCH2-R108βCH2	0.040	0.017	7.5
F106ξCH2-P109βCH(x)	0.040	0.027	6.9
F106ξCH2-P109βCH'(p)	0.140	0.093	5.5
F106ξCH2-P109γCH2	0.350	0.135	5.1
F106ξCH2-L111(δCH3)2	0.532	0.133	5.1
F106ξCH2-V114βCH	0.658	0.437	4.1
F106ξCH2-V114(γCH3)2	1.040	0.260	4.5
F106ςCH-K105βCH2	-	0.415	4.2
F106ςCH-K105γCH2	-	0.135	5.1
F106ςCH-K107βCH2	-	0.533	4.0
F106ςCH-K107γCH2	-	0.135	5.1
F106ςCH-R108βCH2	-	0.017	7.5
F106ςCH-P109βCH(x)	-	0.027	6.9
F106ςCH-P109βCH'(p)	-	0.093	5.5
F106ςCH-P109γCH2	-	0.135	5.1
F106ςCH-L111(δCH3)2	-	0.133	5.1
F106ςCH-V114βCH	-	0.437	4.1

F106ςCH-V114(γCH3)2	-	0.260	4.5
R108βCH2-P109δCH(m)	1.030	0.780	3.7
R108βCH2-P109δCH(m')	0.616	0.467	4.1
P109δCH(m)-V114βCH	0.020	0.020	6.9
P109δCH'(m')-V114βCH	0.100	0.100	5.4
P110βCH(x)-L111βCH2	1.280	0.750	3.7
P110γCH2-L111(δCH3)2	1.060	0.353	4.3
L111(δCH3)2-R112δCH2	0.129	0.033	6.6
R112βCH2-V114(γCH3)2	1.440	0.480	4.1
R113δCH2-V114(γCH2)3	0.054	0.018	7.4
V114(γCH3)2-R115βCH2	1.440	0.300	4.4
V114(γCH3)2-R115δCH2	0.050	0.017	7.5
P109βCH'(p)-P110δCH(m)	2.370	2.370	3.0
P109βCH'(p)-P110δCH'(m')	3.300	3.300	2.8
P110βCH'(p)-P109δCH(m)	0.080	0.080	5.5
P110βCH(x)-P109δCH'(m')	0.144	0.144	5.0
P110γCH2-P109δCH(m)	0.182	0.138	5.0
P110γCH2-P109δCH(m')	0.207	0.157	5.0
K105αCH-F106αCH	0.260	0.260	4.5
F106αCH-K107αCH	0.535	0.535	4.0
F106αCH-R108αCH	0.021	0.021	7.0
K107αCH-F108αCH	0.100	0.100	5.4
R108αCH-P109αCH	0.380	0.380	4.2
R108αCH-P110αCH	0.060	0.060	5.9
P110αCH-L111αCH	0.300	0.300	4.4
R113αCH-V114αCH	0.270	0.270	4.5
V114αCH-R115αCH	0.590	0.590	3.9
G104NH-K105NH	5.510	10.200	2.3
G104NH-F106NH	2.250	4.889	2.7
G104NH-K107NH	0.389	0.748	3.7
K105NH-F106NH	1.980	4.304	2.7
K105NH-K107NH	0.470	0.915	3.6
K105NH-R108NH	0.130	0.361	4.3
F106NH-K107NH	3.240	7.043	2.5
F106NH-R108NH	0.329	0.329	4.3
K107NH-R108NH	0.957	2.655	3.0
L111NH-R112NH	4.450	4.450	2.7
R112NH-R113NH	1.840	4.600	2.7
R112NH-R115NH	0.551	1.198	3.4
R113NH-V114NH	0.978	2.126	3.1
R113NH-R115NH	2.030	5.977	2.6
V114NH-R115NH	0.694	1.335	3.4

R115NH-Cterm NH	0.060	0.075	5.7
R115NH-Cterm NH'	0.060	0.075	5.7
G104αCH2-NH	0.605	0.720	3.8
G104αCH2-K105NH	1.090	1.298	3.4
G104αCH2-F106NH	0.175	0.250	4.6
G104αCH2-R108NH	0.159	0.318	4.4
K105αCH-NH	0.498	0.711	3.8
K105αCH-F106NH	1.410	2.350	3.0
K105αCH-K107NH	0.238	0.361	4.3
K105αCH-R108NH	0.160	0.363	4.3
F106αCH-NH	0.427	0.712	3.8
F106αCH-K107NH	1.620	2.700	3.0
K107αCH-NH	0.808	1.224	3.4
K107αCH-R108NH	0.554	1.260	3.4
R108αCH-NH	0.363	0.825	3.7
P110αCH-L111NH	3.230	3.230	2.9
P110αCH-R112NH	0.327	0.545	4.0
L111αCH-NH	2.360	2.360	3.0
L111αCH-R112NH	0.696	1.160	3.5
L111αCH-R113NH	0.672	1.159	3.5
R112αCH-NH	1.180	1.961	3.1
R112αCH-R113NH	1.780	3.068	2.9
R112αCH-R115NH	0.345	0.523	4.0
R113αCH-NH	1.780	3.069	2.9
R113αCH-V114NH	3.150	4.500	2.7
R113αCH-R115NH	0.345	0.523	4.0
V114αCH-NH	0.860	1.229	3.4
V114αCH-R113NH	0.100	0.172	2.7
V114αCH-R115NH	2.750	4.167	2.7
R115αCH-NH	0.886	1.342	3.4

Table V-3. Effect of mixing time on the development of the intrapeptide TRNOE. Table showing TRNOE intensities versus mixing time measured from TRNOESY data sets acquired at 0.1 molar equivalents of TnC.Ca(II)$_4$ to TnI peptide and three separate mixing times (τ_m = 75, 150, 500 ms).

spin system	TRNOE		
tmix (ms)	500	150	75
K105αCH-βCH2δCH2	2.03	0.73	0.25
K105αCH-γCH2	1.07	0.76	-
K105βCH2δCH2-γCH2	1.19	0.32	0.05
K105βCH2δCH2-NH	1.11	0.83	0.27
K105γCH2-ξCH2	0.33	0.10	-
K105γCH2-NH	0.07	0.03	-
F106αCH-βCH(m)	0.33	0.18	0.06
F106αCH-βCH'(x)	0.46	0.60	0.54
F106αCH-δCH2	0.66	0.29	0.13
F106βCH(m)-βCH'(x)	2.42	6.48	2.73
F106βCH(m)-NH	0.36	0.37	0.20
F106βCH(m)-δCH2	1.39	0.89	0.43
F106βCH(m)-ξCH2ςCH	0.16	-	-
F106βCH'(x)-NH	0.47	0.53	0.33
F106βCH'(x)-δCH2	1.43	1.10	0.51
F106βCH'(x)-ξCH2ςCH	0.47	0.09	0.05
F106NH-δCH2	0.21	0.09	0.15
K107αCH-βCH2δCH2	2.00	1.00	0.50
K107αCH-γCH2	0.97	0.47	0.36
K107βCH2-γCH2	1.62	1.03	0.79
K107βCH2-NH	0.44	0.48	0.09
K107δCH2-γCH2	2.47	1.91	2.47
K107δCH2-NH	0.41	0.49	0.04
K107γCH2-ξCH2	0.95	0.44	0.18
K107γCH2-NH	0.19	0.14	0.27
R108αCH-βCH2	1.02	0.31	0.41
R108αCH-γCH2	0.87	0.23	0.24
R108αCH-δCH2	0.13	-	-
R108βCH2γCH2-δCH2	5.00	3.70	1.80
R108βCH2γCH2-NH	2.46	3.39	2.02
R108δCH2-δNH	0.44	0.37	0.21
R108δCH2-NH	0.11	-	-
P109αCH-βCH(x)	0.98	0.13	-

P109αCH-βCH'(p)	0.19	0.47	0.28
P109αCH-γCH2	1.69	0.31	-
P109βCH(x)-βCH'(p)	6.67	6.16	4.39
P109βCH(x)-δCH(m)	1.25	0.44	0.21
P109βCH(x)-δCH'(m')	0.77	0.09	-
P109βCH(x)-γCH2	4.18	4.36	5.30
P109βCH'(p)-δCH(m)	0.70	0.67	-
P109βCH'(p)-δCH'(m')	0.18	0.02	-
P109βCH'(p)-γCH2	3.26	3.17	1.73
P109γCH2-δCH(m)	2.43	1.82	0.48
P109γCH2-δCH'(m')	2.11	1.43	0.57
P109δCH(m)-δCH'(m')	1.46	5.19	4.62
P110αCH-βCH(x)	1.81	0.70	0.32
P110αCH-βCH'(p)	1.77	1.82	0.90
P110αCH-γCH2	1.29	0.55	0.47
P110βCH(x)-βCH'(p)	6.67	8.41	5.68
P110βCH(x)-δCH(m)	1.25	1.47	0.95
P110βCH(x)-δCH'(m')	0.96	0.42	0.09
P110βCH(x)-γCH2	4.18	4.36	5.30
P110βCH'(p)-δCH(m)	6.61	0.10	-
P110βCH'(p)-δCH'(m')	0.40	0.16	0.03
P110βCH'(p)-γCH2	4.13	4.47	1.96
P110γCH2-δCH(m)	2.43	1.47	1.19
P110γCH2-δCH'(m')	2.62	2.08	1.63
P110δCH(m)-δCH'(m')	1.57	4.87	3.86
L111αCH-βCH2	4.80	1.60	0.77
L111αCH-(δCH3)2	2.26	1.23	0.58
L111βCH2-(δCH3)2	4.75	3.85	1.65
L111γCH-(δCH3)2	7.19	5.30	0.50
L111βCH2-NH	2.62	2.21	1.25
L111(δCH3)2-NH	0.54	0.30	0.10
R112αCH-βCH2γCH2	5.05	3.07	1.66
R112αCH-δCH2	0.67	0.57	-
R112βCH2γCH2-δCH2	5.60	3.70	1.80
R112βCH2γCH2-NH	1.95	1.80	0.88
R112δCH2-δNH	0.44	0.37	0.21
R112δCH2-NH	0.11	-	-
R113αCH-βCH2γCH2	6.62	4.58	3.16
R113αCH-δCH2	0.67	0.57	-
R113βCH2γCH2-δCH2	5.00	3.70	1.80
R113βCH2γCH2-NH	1.49	1.80	1.17
R113δCH2-δNH	0.44	0.37	0.21
R113δCH2-NH	0.16	-	-

V114αCH-βCH	1.78	1.22	0.55
V114αCH-(γCH3)2	3.53	2.39	0.95
V114βCH-(γCH3)2	7.19	5.14	2.25
V114βCH-NH	1.39	1.32	0.70
V114(γCH3)2-NH	1.20	0.60	0.20
R115αCH-βCH2γCH2	5.00	2.94	2.00
R115αCH-δCH2	0.80	0.30	-
R115βCH2γCH2-δCH2	5.00	3.70	1.80
R115βCH2γCH2-NH	1.01	1.07	0.72
R115δCH2-δNH	0.44	0.37	0.21
C-term NH-NH'	2.50	3.87	2.79
G104NH-K105γCH2	-	-	0.11
K105βCH2-F106NH	0.38	0.08	-
K105γCH2-F106NH	0.02	-	-
K105γCH2-R108NH	-	-	0.61
F106βCH(m)-K107NH	0.21	0.14	-
F106βCH'(x)-K107NH	0.28	0.22	-
F106δCH2-K107NH	0.20	0.02	-
K107γCH2-R108NH	0.16	0.14	-
R108αCH-P109γCH2	0.72	0.31	-
R108αCH-P109δCH(m)	0.98	0.91	0.79
R108αCH-P109δCH'(m')	0.84	1.28	0.71
R108NH-P109βCH(x)	0.33	0.35	0.30
R108NH-P109βCH'(p)	0.20	0.12	-
R108NH-P109γCH2	0.23	0.18	-
R108NH-P109δCH(m)	0.14	-	-
P109αCH-P110δCH(m)	0.87	0.51	0.73
P109αCH-P110δCH'(m')	1.05	0.78	0.66
P110αCH-R112βCH2	1.07	0.14	-
P110βCH(x)-L111NH	0.65	0.43	0.31
P110βCH(x)-R112αCH	0.92	0.52	-
P110βCH'(p)-L111αCH	0.23	0.15	-
P110βCH'(p)-L111NH	0.55	0.47	0.27
P110βCH'(p)-R112αCH	0.98	0.51	0.33
P110βCH'(p)-R112NH	0.20	0.11	-
P110γCH2-L111αCH	0.72	-	-
P110γCH2-L111NH	0.30	0.19	-
P110γCH2-R112αCH	0.73	0.25	-
P110γCH2-R112NH	0.23	0.07	-
L111(δCH3)2-R112αCH	1.37	0.23	-
L111(δCH3)2-R112NH	0.37	-	-
R112βCH2-R113NH	0.92	0.55	0.13

R112βCH2-R115NH	0.41	0.33	0.10
R112βCH2-Cterm NH'	0.03	-	-
R113αCH-V114βCH	0.46	0.15	-
R113βCH2-V114αCH	0.75	0.13	-
R113βCH2-V114NH	0.53	0.42	0.58
R113δCH2-V114NH	0.12	-	-
R113NH-V114(γCH3)2	0.17	-	-
V114αCH-Cterm NH	0.21	-	-
V114αCH-Cterm NH'	0.12	-	-
V114βCH-R115NH	0.33	0.28	0.11
V114(γCH3)2-R115NH	0.62	0.16	0.04
V114NH-R115βCH2γCH2	0.53	0.42	0.58
R115αCH-Cterm NH	0.45	0.32	-
R115αCH-Cterm NH'	0.93	0.78	0.52
R115βCH2γCH2-Cterm NH	0.42	0.09	0.04
R115βCH2γCH2-Cterm NH'	0.27	0.16	0.04
F106δCH2-K105βCH2	0.26	0.21	0.07
F106δCH2-K105γCH2	0.05	0.05	-
F106δCH2-K107βCH2	0.24	0.23	0.09
F106δCH2-R108βCH2	0.24	-	-
F106δCH2-P109βCH(x)	0.10	0.07	-
F106δCH2-P109βCH'(p)	0.14	-	-
F106δCH2-P109γCH2	0.16	0.13	-
F106δCH2-L111βCH2	0.26	0.17	-
F106δCH2-L111(δCH3)2	0.25	-	-
F106δCH2-V114(γCH3)2	0.38	-	-
F106ξCH2ςCH-K105βCH2	0.12	-	-
F106ξCH2ςCH-K105γCH2	0.07	-	-
F106ξCH2ςCH-K107βCH2	0.25	-	-
F106ξCH2ςCH-R108βCH2	0.25	0.04	0.03
F106ξCH2ςCH-R108γCH2	0.32	0.11	0.06
F106ξCH2ςCH-P109βCH(x)	0.12	0.04	-
F106ξCH2ςCH-P109βCH'(p)	0.30	0.14	-
F106ξCH2ςCH-P109γCH2	0.12	0.35	-
F106ξCH2ςCH-L111βCH2	0.12	-	-
F106ξCH2ςCH-L111(δCH3)2	0.41	-	-
F106ξCH2ςCH-V114(γCH3)2	0.41	1.04	-
K107ξCH2-R108δCH2	0.55	-	1.18
R108βCH2-P109δCH(m)	0.83	0.49	0.07
R108βCH2-P109δCH'(m')	0.57	0.13	-
P109δCH'(m')-V114βCH	1.04	0.52	-

P110βCH(x)-L111(δCH3)2	0.46	0.35	-
P110γCH2-L111(δCH3)2	1.32	1.06	-
L111(δCH3)2-R112δCH2	0.28	-	-
R112βCH2-V114(γCH3)2	1.79	1.44	-
V114(γCH3)2-R115βCH2	1.79	1.44	-
P109βCH'(p)-P110δCH(m)	0.19	0.38	-
P109βCH'(p)-P110δCH'(m')	0.31	0.29	0.27
P109γCH2-P110δCH(m)	0.48	-	-
P109γCH2-P110δCH'(m')	0.17	-	-
P110βCH(x)-P109δCH'(m')	0.27	0.31	0.06
P110βCH'(p)-P109δCH(m)	0.15	0.21	-
P110βCH'(p)-P109δCH'(m')	0.10	-	-
P110γCH2-P109δCH(m)	0.71	0.81	0.37
P110γCH2-P109δCH'(m')	0.53	0.30	0.51
K105αCH-F106αCH	0.15	0.26	-
K105αCH-V114αCH	0.42	0.37	-
F106αCH-K107αCH	0.08	0.11	-
F106αCH-R108αCH	-	0.16	0.46
F106αCH-P109αCH	0.05	-	-
K107αCH-R108αCH	0.12	0.10	0.54
R108αCH-P109αCH	0.06	0.02	-
R108αCH-P110αCH	0.05	0.06	0.51
P109αCH-P110αCH	0.02	-	-
P110αCH-L111αCH	0.27	0.30	0.76
R113αCH-V114αCH	0.37	0.27	0.25
V114αCH-R115αCH	0.61	0.59	1.46
G104NH-K105NH	0.34	-	-
K105NH-F106NH	0.32	0.61	-
K105NH-K107NH	0.09	0.23	-
K105NH-R112NH	0.33	1.00	-
F106NH-K107NH	0.19	0.32	-
K107NH-R108NH	0.08	0.08	-
R112NH-R113NH	0.30	1.65	-
R112NH-R115NH	0.07	-	-
R113NH-V114NH	0.15	0.50	-
V114NH-R115NH	0.12	0.27	-
R115NH-Cterm NH'	0.08	0.06	0.11
G104αCH2-NH	0.76	0.36	0.27
G104αCH2-K105NH	0.78	0.67	0.40

G104αCH2-F106NH	0.10	0.03	0.07
G104αCH2-R108NH	0.08	-	-
K105αCH-NH	0.46	0.33	0.20
K105αCH-F106NH	1.02	1.01	0.56
K105αCH-R108NH	0.21	0.17	0.14
F106αCH-NH	0.23	0.19	0.16
F106αCH-K107NH	0.70	0.87	0.59
K107αCH-NH	0.52	0.52	0.27
K107αCH-R108NH	1.32	2.05	1.25
R108αCH-NH	0.21	0.22	0.08
P110αCH-L111NH	1.02	1.72	1.29
P110αCH-R112NH	0.21	0.19	0.07
L111αCH-NH	1.25	0.78	0.84
L111αCH-R112NH	1.32	2.05	1.25
R112αCH-NH	1.81	1.78	1.33
R112αCH-R113NH	0.91	1.26	0.87
R112αCH-R115NH	0.35	0.16	-
R113αCH-NH	0.91	1.26	0.87
R113αCH-V114NH	1.81	2.25	1.46
V114αCH-NH	0.21	0.28	0.34
V114αCH-R113NH	0.46	0.10	0.14
V114αCH-R115NH	2.39	2.54	1.72
R115αCH-NH	0.40	0.78	0.34

Table V-4. Effect of protein concentration on the development of the intrapeptide TRNOE. Table showing TRNOE intensities versus protein concentration measured from TRNOESY data sets acquired at τ_m = 150 ms and four separate protein concentrations (0.0, 0.1, 0.2, 0.4 molar equivalents TnC.Ca(II)$_4$ to TnI peptide).

	TRNOE							
M.E. TnC.Ca4	0.00	0.00	0.10	0.10	0.20	0.20	0.40	0.40
spin system	meas	corr	meas	corr	meas	corr	meas	corr
K105αCH-βCH2δCH2	1.19	2.38	2.00	4.00	7.52	24.21	4.23	14.09
K105αCH-γCH2	0.00	0.00	0.97	1.94	1.42	4.57	1.08	3.60
K105βCH2δCH2-γCH2	0.87	1.74	2.16	4.32	4.19	13.49	4.21	14.02
K105δCH2-ξCH2	0.00	0.00	1.50	3.00	2.46	7.92	3.91	13.02
K105βCH2δCH2-NH	0.37	0.74	1.52	3.04	2.66	8.57	2.16	7.20
K105γCH2-ξCH2	0.00	0.00	2.00	4.00	0.91	2.93	1.21	4.03
K105γCH2-NH	0.00	0.00	0.49	0.98	1.02	3.28	0.88	2.93
F106αCH-βCH(m)	0.00	0.00	3.38	6.76	1.40	4.51	0.41	1.37
F106αCH-βCH'(x)	0.00	0.00	0.92	1.84	0.80	2.58	0.20	0.67
F106αCH-δCH2	0.28	0.56	0.69	1.38	1.06	3.41	0.43	1.43
F106αCH-ξCH2ςCH	0.00	0.00	0.00	0.00	0.08	0.26	-	-
F106βCH(m)-βCH'(x)	3.21	6.42	9.59	19.18	-	-	1.97	6.57
F106βCH(m)-NH	0.11	0.22	0.52	1.04	1.36	4.38	0.45	1.50
F106βCH(m)-δCH2	1.41	2.82	1.26	2.52	2.54	8.18	1.61	5.37
F106βCH(m)-ξCH2ςCH	0.14	0.28	0.13	0.26	1.29	4.15	1.11	3.70
F106βCH'(x)-NH	0.28	0.56	1.21	2.42	1.15	3.70	0.45	1.50
F106βCH'(x)-δCH2	0.67	1.34	1.26	2.52	3.63	11.69	1.73	5.77
F106βCH'(x)-δCH2	-	-	-	-	-	-	1.18	3.93
F106NH-ξCH2ςCH	0.00	0.00	0.39	0.78	0.62	2.00	0.23	0.77
F106NH-ξCH2ςCH	0.00	0.00	0.00	0.00	0.21	0.68	0.11	0.37
K107αCH-βCH2δCH2	1.83	3.66	2.99	5.98	6.40	20.60	2.24	7.47
K107αCH-γCH2	0.00	0.00	1.38	2.76	2.56	8.24	1.45	4.83
K107βCH2-γCH2	1.29	2.58	4.48	8.96	7.20	23.10	3.75	12.50
K107βCH2-NH	0.49	0.98	2.50	5.00	3.10	9.99	1.61	5.37
K107δCH2-γCH2	1.29	2.58	6.25	12.50	7.20	23.10	3.75	12.50
K107δCH2-ξCH2	3.58	7.16	10.73	21.46	12.30	39.60	6.98	23.27
K107δCH2-NH	0.00	0.00	1.71	3.42	-	-	-	-
K107γCH2-ξCH2	0.00	0.00	2.42	4.84	3.36	10.80	2.07	6.90
K107γCH2-NH	0.00	0.00	0.57	1.14	1.13	3.64	0.85	2.83
K107ξCH2-NH	0.00	0.00	0.21	0.42	-	-	0.27	0.90
R108αCH-βCH2	2.52	5.04	1.29	2.58	1.40	4.51	0.69	2.30
R108αCH-γCH2	0.69	1.28	0.67	1.34	1.01	3.25	-	-
R108βCH2γCH2-δCH2	2.54	5.08	5.80	11.60	1.35	4.35	2.34	7.80
R108βCHγCH2-NH	1.48	2.96	5.62	11.24	5.56	17.90	1.08	3.60

R108δCH2-δNH	0.00	0.00	3.50	7.00	2.50	8.05	-	-
R108δCH2-NH	0.10	0.20	0.38	0.76	0.30	0.97	0.40	1.33
P109αCH-βCH(x)	0.22	0.44	0.32	0.64	0.27	0.87	-	-
P109αCH-βCH'(p)	0.51	1.02	0.90	1.80	0.32	1.03	-	-
P109αCH-γCH2	0.00	0.00	0.17	0.34	0.27	0.87	-	-
P109βCH(x)-βCH'(p)	5.70	11.40	11.30	22.60	4.30	13.80	2.97	9.90
P109βCH(x)-δCH(m)	0.87	1.74	1.70	3.40	1.51	4.86	0.70	2.33
P109βCH(x)-δCH'(m')	0.00	0.00	0.75	1.50	1.94	6.25	0.46	1.53
P109βCH(x)-γCH2	4.55	9.10	10.10	20.20	8.86	28.52	-	-
P109βCH'(p)-δCH(m)	0.00	0.00	1.78	3.56	1.46	4.70	0.32	1.07
P109βCH'(p)-δCH'(m')	0.00	0.00	1.24	2.48	1.78	5.73	0.84	2.80
P109βCH'(p)-γCH2	1.21	2.42	6.91	13.82	5.95	19.16	3.54	11.80
P109γCH2-δCH(m)	2.14	4.28	1.48	2.96	2.12	6.82	0.65	2.17
P109γCH2-δCH'(m')	2.44	4.88	2.10	4.20	2.75	8.86	-	-
P109δCH(m)-δCH'(m')	8.92	17.84	7.61	15.22	-	-	0.56	1.87
P110αCH-βCH(x)	1.33	2.66	1.69	3.38	2.26	7.28	0.75	2.50
P110αCH-βCH'(p)	2.52	5.04	3.24	6.48	2.39	7.70	1.10	3.67
P110αCH-γCH2	0.49	0.98	0.74	1.48	1.08	3.47	1.03	3.43
P110βCH(x)-βCH'(p)	7.17	14.34	12.80	25.60	7.25	23.34	6.01	20.03
P110βCH(x)-δCH(m)	1.72	3.44	1.70	3.40	1.51	4.86	0.70	2.33
P110βCH(x)-δCH'(m')	0.72	1.44	0.97	1.94	1.14	3.67	0.46	1.53
P110βCH(x)-γCH2	4.37	8.74	10.10	20.20	8.54	27.56	9.17	30.57
P110βCH'(p)-δCH(m)	1.36	2.72	1.33	2.66	0.80	2.58	0.32	1.07
P110βCH'(p)-δCH'(m')	0.78	1.56	0.74	1.48	0.93	2.99	0.84	2.80
P110βCH'(p)-γCH2	0.60	1.20	5.28	10.56	5.29	17.03	7.15	23.67
P110γCH2-δCH(m)	3.29	6.58	1.48	2.96	2.12	6.83	0.65	2.17
P110γCH2-δCH'(m')	3.46	6.92	2.98	5.96	1.96	6.31	1.13	4.33
P110δCH(m)-δCH'(m')	8.80	17.60	9.63	19.26	-	-	0.47	1.57
L111αCH-βCH2γCH	1.83	3.66	4.21	8.42	6.40	20.60	2.24	7.47
L111αCH-(δCH3)2	1.17	2.34	2.08	4.16	6.10	19.64	3.43	11.43
L111βCH2-(δCH3)2	0.84	1.68	2.53	5.06	0.94	3.02	-	-
L111γCH-(δCH3)2	0.84	1.68	2.18	4.36	5.70	18.35	19.10	63.67
L111βCH2γCH-NH	2.20	4.40	4.04	8.08	3.81	12.26	2.28	9.33
L111(δCH3)2-NH	0.24	0.48	1.06	2.12	1.60	5.15	0.81	2.70
R112αCH-βCH2γCH2	1.62	3.24	2.55	5.10	5.80	18.68	2.11	7.03
R112αCH-δCH2	0.00	0.00	0.62	1.24	0.70	2.25	0.50	1.67
R112βCH2γCH2-δCH2	2.54	5.08	5.80	11.60	1.35	4.35	2.34	7.80
R112βCH2γCH2-NH	0.71	1.42	4.04	8.08	2.26	7.28	1.08	3.60
R112δCH2-δNH	0.00	0.00	3.50	7.00	2.50	8.05	-	-
R112δCH2-NH	0.10	0.20	0.38	0.76	0.30	0.97	0.40	1.33
R113αCH-βCH2γCH2	1.62	3.24	5.65	11.30	5.80	18.68	2.11	7.03
R113αCH-δCH2	0.00	0.00	0.62	1.24	0.70	2.25	0.50	1.67
R113βCH2γCH2-δCH2	2.54	5.08	5.80	11.60	1.35	4.35	2.34	7.80
R113βCH2γCH2-NH	0.64	1.28	3.26	6.52	3.55	11.40	1.19	3.98
R113δCH2-δNH	0.00	0.00	3.50	7.00	2.50	8.05	-	-
R113δCH2-NH	0.10	0.20	0.38	0.76	0.27	0.87	0.40	1.33

V114αCH-βCH	0.86	1.72	1.02	2.04	4.44	14.30	2.02	6.73
V114αCH-(γCH3)2	0.33	0.66	2.29	4.58	7.20	23.10	-	-
V114βCH-(γCH3)2	1.98	3.96	7.64	15.28	12.40	39.93	12.00	40.00
V114βCH-NH	0.42	0.84	1.12	2.24	1.02	3.28	0.57	1.90
V114(γCH3)2-NH	0.24	0.48	1.19	2.38	1.60	5.15	0.81	2.70
R115αCH-βCH2γCH2	1.83	3.66	3.41	6.82	6.40	20.60	2.24	7.47
R115αCH-δCH2	0.00	0.00	0.64	1.28	1.26	4.06	0.50	1.67
R115βCH2γCH2-δCH2	2.54	5.08	5.80	11.60	1.35	4.35	2.34	7.80
R115βCH2γCH2-NH	0.20	0.40	1.58	3.16	12.40	39.93	0.89	2.97
R115δCH2-δNH	0.00	0.00	3.50	7.00	2.50	8.05	-	-
R115δCH2-NH	0.10	0.20	0.38	0.76	0.35	1.13	0.40	1.33
C-term NH-NH'	1.47	2.94	4.39	8.79	4.21	13.56	2.04	6.80
N-Acetyl CH3-G104αCH2	0.00	0.00	1.39	2.78	3.27	10.53	1.43	4.77
N-Acetyl CH3-G104NH	0.42	0.84	1.12	2.24	1.02	3.28	0.56	1.87
N-Acetyl CH3-K105NH	0.00	0.00	0.44	0.88	1.00	3.22	0.86	2.87
N-Acetyl CH3-R108αCH	0.00	0.00	0.21	0.42	0.77	2.48	-	-
G104NH-K105γCH2	0.00	0.00	0.32	0.64	-	-	-	-
G104NH-K107γCH2	0.00	0.00	0.27	0.54	-	-	0.30	1.00
K105αCH-F106δCH2	0.00	0.00	0.00	0.00	0.14	0.45	-	-
K105βCH2δCH2 -F106NH	0.36	0.72	0.95	1.90	2.29	7.37	1.97	6.57
K105γCH2-F106NH	0.00	0.00	0.20	0.40	0.46	1.48	0.56	1.87
K105γCH2-K107NH	0.00	0.00	0.14	0.28	0.32	1.03	-	-
K105γCH2-R108NH	0.00	0.00	0.16	0.32	-	-	-	-
K105NH-F106δCH2	0.00	0.00	0.00	0.00	0.17	0.55	-	-
K105NH-K107γCH2	0.00	0.00	0.20	0.40	0.71	2.28	0.27	0.90
K105NH-V114(γCH3)2	0.00	0.00	0.31	0.62	1.50	4.83	1.35	4.50
F106βCH(m)-K107NH	0.00	0.00	0.21	0.42	0.96	3.09	-	-
F106βCH'(x)-K107NH	0.00	0.00	0.21	0.42	0.89	2.87	-	-
F106δCH2-K107αCH	0.00	0.00	0.00	0.00	0.14	0.45	-	-
F106δCH2-K107NH	0.00	0.00	0.20	0.40	0.51	1.64	-	-
F106δCH2-R108NH	0.00	0.00	0.00	0.00	0.13	0.42	0.16	-
F106ξCH2ςCH-R108αCH	0.00	0.00	0.00	0.00	0.29	0.93	-	-
F106NH-K107γCH2	0.00	0.00	0.22	0.44	0.57	1.83	0.24	0.80
K107βCH2γCH2 -R108αCH	0.00	0.00	0.00	0.00	1.10	3.54	-	-
K107γCH2-R108NH	0.00	0.00	0.30	0.60	0.62	2.00	0.25	0.83
K107NH-R108δCH2	0.00	0.00	0.35	0.70	0.15	0.48	-	-
R108αCH-P109δCH(m)	1.81	3.62	2.04	4.08	1.58	5.09	-	-
R108αCH-P109δCH'(m')	2.04	4.08	3.57	7.14	1.00	3.22	0.42	1.40
R108αCH-V114βCH	0.00	0.00	0.21	0.42	0.77	2.48	-	-
R108NH-P109βCH(x)	0.60	1.20	0.69	1.38	0.47	1.51	0.56	1.87
P109αCH-P110δCH(m)	0.69	1.38	2.07	4.14	0.93	2.99	-	-
P109αCH-P110δCH'(m')	0.71	1.42	1.70	3.40	0.56	1.80	-	-
P109αCH-R112βCH2	0.00	0.00	0.37	0.74	-	-	-	-

P109αCH-V114βCH	0.00	0.00	0.11	0.22	0.55	1.77	-	-
P109αCH-P110βCH(x)	0.00	0.00	0.61	1.22	-	-	-	-
P110αCH-L111βCH2γCH	0.00	0.00	0.00	0.00	0.53	1.71	1.68	5.60
P110αCH-R112βCH2	0.00	0.00	0.15	0.30	0.53	1.71	-	-
P110βCH(x)-L111NH	0.80	1.60	0.79	1.58	0.90	2.90	0.73	2.43
P110βCH'(p)-L111αCH	0.00	0.00	0.92	1.84	-	-	0.81	2.70
P110βCH'(p)-L111NH	0.83	1.66	0.75	1.50	1.05	3.38	0.47	1.57
P110βCH'(p)-R112NH	0.00	0.00	0.10	0.20	-	-	-	-
P110γCH2-L111αCH	0.00	0.00	0.73	1.46	0.97	3.12	1.14	3.80
P110γCH2-L111NH	0.21	0.42	0.38	0.76	0.54	1.74	-	-
L111(δCH3)2-R112NH	0.18	0.36	0.94	1.86	1.77	5.70	1.06	3.53
L111NH-R112δCH2	0.00	0.00	0.14	0.28	0.27	0.87	-	-
R112βCH2-R113NH	0.32	0.64	1.46	2.92	1.50	4.83	-	-
R112βCH2-R115NH	0.00	0.00	1.35	2.70	1.33	4.28	0.61	2.03
R112βCH2γCH2-Cterm NH'	0.00	0.00	0.58	1.16	1.84	5.92	0.81	2.70
R112δCH2-R113NH	0.00	0.00	0.10	0.20	0.18	0.58	-	-
R112NH-R113δCH2	0.00	0.00	0.10	0.20	0.30	0.97	-	-
R112NH-V114βCH	0.00	0.00	0.40	0.80	0.39	1.26	-	-
R113αCH-V114(γCH3)2	0.00	0.00	0.38	0.76	0.89	2.87	1.33	4.43
R113βCH2γCH2-V114αCH	0.00	0.00	0.30	0.60	1.58	5.09	3.06	10.20
R113δCH2-V114NH	0.00	0.00	0.14	0.28	0.18	0.58	-	-
R113NH-V114(γCH3)2	0.10	0.20	0.32	0.64	0.87	2.80	0.66	2.20
V114αCH-R115βCH2γCH2	0.00	0.00	0.30	0.60	1.58	5.09	-	-
V114αCH-Cterm NH	0.00	0.00	0.00	0.00	0.23	0.74	-	-
V114βCH-R115NH	0.00	0.00	0.77	1.54	1.00	3.22	0.49	1.63
V114(γCH3)2-R115NH	0.21	0.42	0.70	1.40	1.80	5.80	1.06	3.53
V114(γCH3)2-Cterm NH	0.00	0.00	0.34	0.68	1.28	4.12	1.11	3.70
V114NH-R115βCH2γCH2	0.16	0.32	1.63	3.26	-	-	-	-
V114NH-R115δCH2	0.00	0.00	0.14	0.28	0.18	0.58	-	-
R115αCH-Cterm NH	0.00	0.00	1.24	2.48	2.07	6.67	1.09	3.63
R115αCH-Cterm NH'	0.00	0.00	0.51	1.04	1.42	4.57	0.83	2.77
R115βCH2γCH2-Cterm NH	0.00	0.00	0.62	1.24	2.27	7.30	1.26	4.20
F106δCH2-K105γCH2	0.00	0.00	0.40	0.80	1.30	4.19	0.48	1.60
F106δCH2-K107βCH2δCH2	0.00	0.00	0.35	0.70	6.23	20.06	3.43	11.40
F106δCH2-K107γCH2	0.00	0.00	0.27	0.54	1.81	5.82	0.33	1.10
F106δCH2-K107ξCH2	0.00	0.00	0.70	1.40	-	-	-	-
F106δCH2-R108δCH2	0.00	0.00	5.09	10.18	-	-	-	-
F106δCH2-P109βCH'(p)	0.00	0.00	0.00	0.00	0.50	1.61	0.73	2.43

F106δCH2-P109γCH2	0.00	0.00	0.07	0.14	0.48	1.55	0.39	1.30
F106δCH2-P110βCH'(p)	0.00	0.00	0.00	0.00	0.50	1.61	0.29	0.97
F106δCH2-P110γCH2	0.00	0.00	0.07	0.14	0.48	1.55	0.73	2.43
F106δCH2-L111(δCH3)2	0.00	0.00	0.97	1.94	1.80	5.80	0.39	1.30
F106δCH2-V114βCH	0.00	0.00	0.49	0.98	1.13	3.63	0.29	0.97
F106δCH2-V114(γCH3)2	0.00	0.00	0.54	1.08	1.80	5.80	1.95	6.50
F106ξCH2ςCH -K105βCH2	0.00	0.00	1.00	2.00	4.71	15.17	0.58	1.93
F106ξCH2ςCH -K105γCH2	0.00	0.00	0.33	0.66	1.17	3.76	1.95	6.50
F106ξCH2ςCH -K107βCH2	0.00	0.00	1.28	2.56	4.71	15.17	1.56	5.20
F106ξCH2ςCH -K107γCH2	0.00	0.00	0.32	0.64	1.57	5.06	0.35	1.17
F106ξCH2ςCH -R108βCH2	0.00	0.00	-	-	5.83	18.77	1.56	5.20
F106ξCH2ςCH -P109βCH(x)	0.00	0.00	0.00	0.00	1.15	3.70	0.29	0.97
F106ξCH2ςCH -P109βCH'(p)	0.00	0.00	0.00	0.00	0.53	1.71	-	-
F106ξCH2ςCH -P109γCH2	0.00	0.00	0.18	0.36	0.49	1.58	0.55	1.83
F106ξCH2ςCH -P110βCH(x)	0.00	0.00	0.00	0.00	1.15	3.70	0.36	1.20
F106ξCH2ςCH -P110βCH'(p)	0.00	0.00	0.00	0.00	0.53	1.71	0.27	0.90
F106ξCH2ςCH -P110γCH2	0.00	0.00	0.18	0.36	0.49	1.58	0.55	1.83
F106ξCH2ςCH -L111(δCH3)2	0.00	0.00	0.53	1.06	1.75	5.63	0.36	1.20
F106ξCH2ςCH -V114βCH	0.00	0.00	0.66	1.32	1.23	3.96	0.27	0.90
F106ξCH2ςCH -V114(γCH3)2	0.00	0.00	1.04	2.08	1.75	5.63	1.30	4.30
R108βCH2-P109δCH(m)	0.51	1.02	1.03	2.06	1.74	5.60	0.97	3.23
R108βCH2- P109δCH'(m')	0.00	0.00	0.62	1.24	1.13	3.63	0.91	3.03
P109δCH(m)-V114βCH	0.00	0.00	3.41	6.82	1.35	4.35	-	-
P109δCH'(m')-V114βCH	0.00	0.00	1.69	3.38	-	-	-	-
L111(δCH3)2 -P110βCH(x)	0.00	0.00	0.00	0.00	4.60	14.81	4.08	13.60
L111(δCH3)2 -R112βCH2γCH2	0.00	0.00	0.00	0.00	8.15	26.24	-	-
L111(δCH3)2-R112δCH2	0.00	0.00	0.13	0.26	1.66	5.35	-	-

R113βCH2γCH2 -V114(γCH3)2	0.00	0.00	0.00	0.00	4.07	13.11	-	-
R113δCH2-V114(γCH2)3	0.00	0.00	0.05	0.10	0.83	2.67	1.20	4.00
V114(γCH3)2 -R115βCH2γCH2	0.00	0.00	0.00	0.00	4.07	13.11	-	-
V114(γCH3)2-R115δCH2	0.00	0.00	0.05	0.10	0.83	2.67	1.20	4.00
P109βCH'(p) -P110δCH(m)	0.96	1.92	1.78	3.56	1.42	4.57	-	-
P109βCH'(p) -P110δCH'(m')	0.90	1.80	0.63	1.26	1.00	3.22	-	-
K107αCH-F108αCH	1.27	2.54	1.50	3.00	-	-	-	-
R108αCH-P110αCH	-	-	1.10	2.20	-	-	-	-
P110αCH-L111αCH	0.92	1.84	1.59	3.18	0.88	2.83	-	-
P110αCH-R112αCH	-	-	2.33	4.66	-	-	-	-
R113αCH-V114αCH	2.23	4.46	2.50	5.00	0.89	2.87	-	-
V114αCH-R115αCH	2.17	4.34	2.50	5.00	1.18	3.80	0.71	2.37
G104NH-K105NH	0.88	1.76	5.51	11.02	-	-	-	-
G104NH-F106NH	0.00	0.00	0.74	1.48	1.36	4.37	-	-
G104NH-K107NH	0.00	0.00	0.39	0.78	0.66	2.13	-	-
K105NH-F106NH	0.14	0.28	1.98	3.96	0.96	3.09	-	-
K105NH-K107NH	0.00	0.00	0.47	0.94	1.12	3.61	-	-
K105NH-R108NH	0.00	0.00	0.73	1.46	-	-	-	-
F106NH-K107NH	0.24	0.48	3.24	6.48	1.86	5.99	0.49	1.63
F106NH-R108NH	0.00	0.00	0.33	0.66	0.20	3.42	0.50	1.67
K107NH-R108NH	0.11	0.22	0.45	0.90	0.90	2.90	0.32	1.07
L111NH-R112NH	-	-	4.45	8.90	-	-	-	-
R112NH-R113NH	0.21	0.42	1.84	3.68	2.46	7.92	-	-
R112NH-R115NH	0.09	0.18	0.55	1.10	0.78	2.51	0.48	1.60
R113NH-V114NH	0.21	0.42	0.98	1.96	0.81	2.61	-	-
R113NH-R115NH	0.00	0.00	2.63	5.26	-	-	-	-
V114NH-R115NH	0.19	0.38	0.69	1.38	0.93	2.99	-	-
R115NH-Cterm NH2	0.00	0.00	0.14	0.28	0.25	0.81	-	-
G104αCH2-NH	0.00	0.00	0.61	1.22	1.76	5.68	1.39	4.63
G104αCH2-K105NH	0.20	0.40	1.09	2.18	2.07	6.69	1.01	3.67
G104αCH2-F106NH	0.00	0.00	0.18	0.36	0.55	1.78	0.24	0.80
G104αCH2-R108NH	0.00	0.00	0.16	0.32	0.13	0.42	0.21	0.70
K105αCH-NH	0.06	0.12	0.50	1.00	0.86	2.76	0.72	2.40
K105αCH-F106NH	0.59	1.18	1.41	2.82	2.21	7.13	0.95	3.17
K105αCH-K107NH	0.00	0.00	0.24	0.48	0.60	1.93	-	-
K105αCH-R108NH	0.00	0.00	0.16	0.32	0.39	1.26	-	-
F106αCH-NH	0.00	0.00	0.43	0.86	0.55	1.78	0.19	0.63
F106αCH-K107NH	1.31	2.62	1.62	3.24	0.41	1.31	0.21	0.70

K107αCH-NH	0.18	0.36	0.81	1.62	1.06	4.56	0.35	1.17
K107αCH-R108NH	2.24	4.48	3.15	6.30	2.20	7.11	0.46	1.53
R108αCH-NH	0.30	0.60	0.36	0.72	0.31	0.42	-	-
P110αCH-L111NH	2.60	5.20	3.23	6.46	1.64	5.30	0.24	0.80
P110αCH-R112NH	0.00	0.00	0.33	0.66	0.42	1.35	-	-
L111αCH-NH	1.13	2.26	2.36	4.72	1.79	5.78	0.27	0.90
L111αCH-R112NH	2.24	4.48	3.15	6.30	2.20	7.11	0.46	1.53
L111αCH-R113NH	0.00	0.00	0.67	1.34	0.58	1.87	-	-
R112αCH-NH	0.52	1.04	1.18	2.36	1.00	3.23	0.32	1.07
R112αCH-R113NH	1.14	2.28	1.78	3.56	1.23	3.97	0.51	1.70
R113αCH-NH	0.00	0.00	0.35	0.70	1.23	3.97	0.51	1.70
R113αCH-V114NH	1.14	2.28	1.78	3.56	2.35	7.59	0.27	0.90
R113αCH-R115NH	2.32	4.64	3.15	6.30	3.06	9.88	0.14	0.47
V114αCH-NH	0.00	0.00	0.35	0.70	1.59	5.14	0.32	1.07
V114αCH-R113NH	0.20	0.40	0.86	1.92	0.63	2.02	-	-
V114αCH-R115NH	1.15	2.30	2.75	4.50	2.84	9.17	0.64	2.13
R115αCH-NH	0.11	0.22	0.89	1.78	0.70	2.26	0.42	1.40

Table V-5. Summary of distance restraints used in the MD simulations. Included in the table are the calculated r_{ij}s from the corrected and normalized TRNOE cross-peak intensities, the incorporated error limits (±β), the shifts in r_{ij} to r_{ij}^{o} from the mixing time and protein concentration behaviour of the cross-peak, and the pseudoatom adjustments in r_{ij}^{U}.

spin system	rij ± β (Å)	crosspeak behaviour	rij° ± β (Å)	Ψ-atom correction (Å)	rijU (Å)	rijL (Å)
K105αCH-βCH2	3.3±0.3	BY	3.3±0.3		3.6	3.0
K105αCH-γCH2	3.8±0.3	CY(+β)	4.1±0.5	0.6	5.6	3.6
K105βCH2-γCH2	4.0±0.5	BY	4.0±0.5		4.5	3.5
K105γCH2-δCH2	4.0±0.5	BY	4.0±0.5		4.5	3.5
K105δCH2-ξCH2	3.7±0.3	BY	3.7±0.3		4.0	3.4
K105βCH2-NH	3.9±0.3	BY	3.9±0.3	0.6	4.8	3.6
K105γCH2-ξCH2	3.6±0.3	BY	3.6±0.3		3.9	3.3
K105γCH2-NH	4.1±0.5	CY(+β)	4.6±0.5	1.0	6.1	4.1
F106αCH-βCH(m)	3.6±0.3	AY(-β)	3.3±0.3		3.6	3.0
F106αCH-βCH'(x)	2.8±0.2	BY	2.8±0.2		3.0	2.6
F106αCH-δCH2	4.0±0.5	BX(+β)	4.5±0.5	2.0	7.0	4.0
F106βCH(m)-βCH'(x)	2.5±0.2	AY(-β)	2.3±0.2		2.5	2.1
F106βCH'(x)-NH	3.6±0.3	BY	3.6±0.3		3.9	3.3
F106βCH(m)-NH	3.1±0.3	BY	3.1±0.3		3.4	2.8
F106βCH2-δCH2	3.9±0.3	BY	3.9±0.3		4.2	3.6
F106NH-δCH2	3.9±0.3	BY	3.9±0.3	2.4	6.6	3.6
K107αCH-βCH2	3.3±0.3	BY	3.3±0.3		3.6	3.0
K107αCH-γCH2	3.5±0.3	BY	3.5±0.3	0.6	4.4	3.2
K107βCH2-γCH2	3.1±0.3	BY	3.1±0.3		3.4	2.8
K107βCH2-NH	3.6±0.3	BY	3.6±0.3	0.6	4.5	3.3
K107δCH2-γCH2	2.9±0.2	AY(-β)	2.7±0.2		2.9	2.5
K107δCH2-ξCH2	3.6±0.3	BY	3.6±0.3		3.9	3.3
K107δCH2-NH	5.0±1.0	BY	5.0±1.0		6.0	4.0
K107γCH2-ξCH2	3.4±0.3	BY	3.4±0.3		3.7	3.1
K107γCH2-NH	4.0±0.5	BY	4.0±0.5	1.0	5.5	3.5
R108αCH-βCH2	3.6±0.3	BX(+β)	3.9±0.3		4.2	3.6
R108αCH-γCH2	4.0±0.5	BX(+β)	4.5±0.5	0.6	5.6	4.0
R108αCH-δCH2	4.1±0.5	CY(+β)	4.6±0.5	1.0	6.1	4.1
R108γCH2-δCH2	3.5±0.3	BY	3.5±0.3		3.8	3.2
R108βCH2-NH	2.5±0.2	BY	2.5±0.2	0.6	3.3	2.3
R108δCH2-NH	3.7±0.3	CY(+β)	4.0±0.5		4.5	3.5
P109αCH-βCH(x)	4.4±0.5	BX(+β)	4.9±0.5		5.4	4.4
P109αCH-βCH'(p)	3.6±0.3	BX(+β)	3.9±0.3		4.2	3.6

P109αCH-γCH2	5.1±1.0	BY	5.1±1.0		6.1	4.1
P109βCH(x)-βCH'(p)	2.3±0.2	BY	2.3±0.2		2.5	2.1
P109βCH(x)-δCH'(m')	3.2±0.3	BX(+β)	3.5±0.3		3.8	3.2
P109βCH(x)-δCH(m)	3.7±0.3	CY(+β)	4.0±0.5		4.5	3.5
P109βCH(x)-γCH2	2.4±0.2	AY(-β)	2.2±0.2		2.4	2.0
P109βCH'(p)-δCH(m)	3.2±0.3	CY(+β)	3.5±0.3		3.8	3.2
P109βCH'(p) -δCH'(m')	3.4±0.3	CY(+β)	3.7±0.3		4.0	3.4
P109βCH'(p)-γCH2	2.6±0.2	AY(-β)	2.4±0.2		2.6	2.2
P109γCH2-δCH2	3.3±0.3	BY	3.3±0.3		3.6	3.0
P109δCH(m)-δCH'(m')	2.6±0.2	AY(-β)	2.4±0.2		2.6	2.2
P110αCH-βCH(x)	3.2±0.3	BY	3.2±0.3		3.5	2.9
P110αCH-βCH'(p)	2.9±0.2	BY	2.9±0.2		3.1	2.7
P110αCH-γCH2	3.9±0.3	BX(+β)	4.2±0.5		4.7	3.7
P110βCH(x)-βCH'(p)	2.2±0.2	BY	2.2±0.2		2.4	2.0
P110βCH(x)-δCH(m)	3.2±0.3	BX(+β)	3.5±0.3		3.8	3.2
P110βCH(x)-δCH'(m')	3.6±0.3	BX(+β)	3.9±0.3		4.2	3.6
P110βCH(x)-γCH2	2.4±0.2	AY(-β)	2.2±0.2		2.4	2.0
P110βCH'(p)-δCH(m)	3.4±0.3	CX(+2β)	4.0±0.5		4.5	3.5
P110βCH'(p) -δCH'(m')	3.7±0.3	CX(+2β)	4.3±0.5		4.9	3.7
P110βCH'(p)-γCH2	2.8±0.2	AY(-β)	2.6±0.2		2.8	2.4
P110γCH2-δCH2	3.1±0.3	BY	3.1±0.3		3.4	2.7
P110δCH(m)-δCH'(m')	2.7±0.2	AY(-β)	2.5±0.2		2.7	2.3
L111αCH-βCH2	3.1±0.3	BY	3.1±0.3		3.4	2.8
L111αCH-(δCH3)2	4.3±0.5	BY	4.3±0.5	1.7	6.5	3.8
L111βCH2-(δCH3)2	3.8±0.3	BY	3.8±0.3		4.1	3.5
L111γCH-(δCH3)2	3.4±0.3	BY	3.4±0.3		3.7	3.1
L111βCH2-NH	2.9±0.2	BY	2.9±0.2	0.6	3.7	2.7
L111(δCH3)2-NH	3.3±0.3	BY	3.3±0.3		3.6	3.0
R112αCH-βCH2	3.5±0.3	BY	3.5±0.3		3.8	3.2
R112αCH-δCH2	4.1±0.5	CY(+β)	4.6±0.5		5.1	4.1
R112γCH2-δCH2	2.7±0.2	BY	2.7±0.2		2.9	2.5
R112βCH2-NH	2.8±0.2	BY	2.8±0.2	0.6	3.6	2.6
R112δCH2-NH	4.0±0.5	CY(+β)	4.5±0.5		5.0	4.0
R113αCH-βCH2	3.0±0.3	BY	3.0±0.3		3.3	2.7
R113αCH-δCH2	4.1±0.5	CY(+β)	4.6±0.5	1.0	6.1	4.1
R113γCH2-δCH2	2.7±0.2	BY	2.7±0.2		2.9	2.5
R113βCH2-NH	2.6±0.2	BY	2.6±0.2	0.6	3.4	2.4
R113δCH2-NH	3.9±0.3	CY(+β)	4.2±0.5		4.5	3.9
V114αCH-βCH	3.3±0.3	BY	3.3±0.3		3.6	3.0
V114αCH-(γCH3)2	3.4±0.3	BY	3.4±0.3	0.6	4.3	3.1
V114βCH-(γCH3)2	2.7±0.2	BY	2.7±0.2		2.9	2.5
V114βCH-NH	3.3±0.3	BY	3.3±0.3		3.6	3.0
V114(γCH3)2-NH	3.4±0.3	BY	3.4±0.3	1.7	5.4	3.1
R115αCH-βCH2	3.4±0.3	BY	3.4±0.3		3.7	3.1

R115αCH-δCH2	4.1±0.5	CY(+β)	4.6±0.5	1.0	6.1	4.1
R115γCH2-δCH2	2.7±0.2	BY	2.7±0.2		2.9	2.5
R115βCH2-NH	3.3±0.3	BY	3.3±0.3	0.6	4.2	3.0
R115δCH2-NH	5.0±1.0	BY	5.0±1.0		6.0	4.0
C-term NH-NH'	1.8±0.2	AY(-β)	1.6±0.2		1.8	1.4
N-Acetyl CH3 -G104αCH2	3.9±0.3	BY	3.9±0.3		4.2	3.6
N-Acetyl CH3 -G104NH	3.4±0.3	BX(+β)	3.7±0.3		4.0	3.4
N-Acetyl CH3 -K105NH	4.0±0.5	BY	4.0±0.5		4.5	3.5
N-Acetyl CH3 -R108NH	3.7±0.3	BY	3.7±0.3		4.0	3.4
G104NH-K105γCH2	4.7±0.5	AY(-β)	4.2±0.5	1.0	5.7	3.7
G104NH-K107γCH2	4.7±0.5	BY	4.7±0.5	1.0	6.2	4.2
K105βCH2-F106NH	3.6±0.3	CX(+2β)	4.2±0.5	1.0	5.7	3.7
K105γCH2-F106NH	4.4±0.5	CY(+β)	4.9±0.5	1.0	6.4	4.4
K105γCH2-K107NH	4.7±0.5	BY	4.7±0.5	1.0	6.2	4.2
K105γCH2-R108NH	4.3±0.5	AY(-β)	3.8±0.3	1.0	5.1	3.5
K105δCH2-F106NH	4.1±0.5	BY	4.1±0.5	1.0	5.6	3.6
K105NH-K107γCH2	5.0±1.0	BY	5.0±1.0	1.0	7.0	4.0
F106βCH2-K107NH	3.4±0.3	CY(+β)	3.7±0.3	1.0	5.0	3.4
F106δCH-K107NH	4.6±0.5	CY(+β)	5.1±1.0	2.4	8.5	4.1
F106NH-K107γCH2	4.4±0.5	BY	4.4±0.5	1.0	5.9	3.9
K107γCH2-R108NH	4.4±0.5	CY(+β)	4.9±0.5	1.0	6.4	4.4
K107NH-R108δCH2	4.7±0.5	BY	4.7±0.5	1.0	6.2	4.2
R108αCH-P109γCH2	4.6±0.5	CY(+β)	5.1±1.0	1.0	7.1	4.1
R108αCH -P109δCH(m)	3.1±0.3	BY	3.1±0.3		3.4	2.8
R108αCH -P109δCH'(m')	2.8±0.2	BY	2.8±0.2		3.0	2.6
R108NH-P109βCH2	5.0±1.0	BY	5.0±1.0	1.0	7.0	4.0
R108NH-P109γCH2	4.3±0.5	CY(+β)	4.8±0.5	1.0	6.3	4.3
P109αCH -P109δCH(m)	3.1±0.3	BY	3.1±0.3		3.4	2.8
P109αCH -P109δCH'(m')	3.2±0.3	BY	3.2±0.3		3.5	2.9
P109αCH-P110βCH2	4.9±0.5	BY	4.9±0.5	1.0	6.4	4.4
P110αCH-R112βCH2	5.3±1.0	CY(+β)	6.3±1.0	1.0	8.3	5.3
P110βCH(x)-L111NH	3.0±0.3	BX(+β)	3.3±0.3		3.6	3.0
P110βCH(x)-R112αCH	4.0±0.5	CY(+β)	4.5±0.5		5.0	4.0
P110βCH2-L111αCH	3.6±0.3	CY(+β)	3.9±0.3	1.0	5.2	3.6
P110βCH'(p)-L111NH	3.0±0.3	BX(+β)	3.3±0.3		3.6	3.0

P110βCH'(p) -R112αCH	6.5±1.0	BY	6.5±1.0		7.5	5.5
P110βCH2-R112NH	3.3±0.3	CY(+β)	3.6±0.3	1.0	4.9	3.3
P110γCH2-L111αCH	4.0±0.5	CY(+β)	4.5±0.5	1.0	6.0	4.0
P110γCH2-L111NH	4.1±0.5	CX(+2β)	5.1±1.0	1.0	7.1	4.1
P110γCH2-R112αCH	4.8±0.5	CY(+β)	5.3±1.0	1.0	6.8	4.8
P110γCH2-R112NH	5.4±1.0	CY(+β)	6.4±1.0	1.0	8.4	5.4
L111(δCH3)2 -R112αCH	5.1±1.0	CY(+β)	6.1±1.0	2.4	9.5	5.1
L111(δCH3)2-R112NH	3.6±0.3	CY(+β)	3.9±0.3	2.4	6.6	3.6
L111NH-R112δCH2	4.9±0.5	BY	4.9±0.5	1.0	6.4	4.4
R112βCH2-R113NH	3.4±0.3	BX(+β)	3.7±0.3	1.0	5.0	3.4
R112βCH2-R115NH	3.5±0.3	BY	3.5±0.3	1.0	4.8	3.2
R112βCH2-Cterm NH	4.5±0.5	CY(+β)	5.0±1.0	1.0	6.5	4.5
R112βCH2-Cterm NH'	4.5±0.5	CY(+β)	5.0±1.0	1.0	6.5	4.5
R112δCH2-R113NH	5.0±1.0	CY(+β)	6.0±1.0	1.0	7.0	4.0
R112NH-R113δCH2	5.1±1.0	BY	5.1±1.0	1.0	7.1	4.1
R112NH-V114βCH	3.8±0.3	BY	3.8±0.3		4.1	3.5
R113αCH-V114βCH	5.0±1.0	CY(+β)	6.0±1.0		7.0	5.0
R113αCH -V114(γCH3)2	4.7±0.5	BY	4.7±0.5	2.4	7.6	4.2
R113βCH2-V114αCH	4.7±0.5	CY(+β)	5.2±1.0	1.0	7.2	4.2
R113βCH2-V114NH	4.0±0.5	AY(-β)	3.5±0.3	1.0	4.8	3.2
R113δCH2-V114NH	4.9±0.5	CY(+β)	5.4±1.0	1.0	6.9	4.9
R113NH- V114(γCH3)2	4.3±0.5	CX(+2β)	5.3±1.0	2.4	8.7	4.3
V114αCH-R115βCH2	4.7±0.5	BY	4.7±0.5	1.0	6.2	4.2
V114βCH-R115NH	3.4±0.3	BY	3.4±0.3		3.7	3.1
V114(γCH3)2 -R115NH	3.7±0.3	BX(+β)	4.0±0.5	3.4	7.9	3.5
V114(γCH3)2 -Cterm NH	4.8±0.5	BY	4.8±0.5	2.4	7.7	4.3
V114(γCH3)2 -Cterm NH'	4.8±0.5	BY	4.8±0.5	2.4	7.7	4.3
V114NH-R115βCH2	3.3±0.3	AY(-β)	3.0±0.3	1.0	4.3	2.7
V114NH-R115δCH2	4.9±0.5	BY	4.9±0.5	1.0	6.4	4.4
R115αCH-Cterm NH	3.4±0.3	CY(+β)	3.7±0.3		4.0	3.4
R115αCH-Cterm NH'	3.4±0.3	BY	3.4±0.3		3.7	3.1
R115βCH2-Cterm NH	4.5±0.5	BY	4.5±0.5		5.0	4.0
R115βCH2-Cterm NH'	4.5±0.5	BY	4.5±0.5		5.0	4.0

F106δCH2-K105βCH2	5.4±1.0	BY	5.4±1.0	3.4	9.8	4.4
F106δCH2-K105γCH2	4.8±0.5	CY(+β)	5.3±1.0	3.4	9.7	4.3
F106δCH2-K107βCH2	5.0±1.0	BY	5.0±1.0	3.4	9.4	4.0
F106δCH2-K107γCH2	5.1±1.0	BY	5.1±1.0	3.4	9.5	4.1

F106δCH2-K107ξCH2	4.3±0.5	BY	4.3±0.5	3.4	8.2	3.8
F106δCH2-R108δCH2	3.0±0.3	CY(+β)	3.3±0.3	3.4	7.0	3.0
F106δCH2-P109βCH(x)	6.3±1.0	BY	6.3±1.0	2.4	9.7	5.3
F106δCH2-P109γCH2	5.8±1.0	CY(+β)	6.8±1.0	3.4	11.2	5.8
F106δCH2-L111βCH2	5.2±1.0	CY(+β)	6.2±1.0	3.4	9.6	5.2
F106δCH2-L111(δCH3)2	4.4±0.5	CY(+β)	4.9±0.5	4.8	10.2	4.4
F106δCH2-V114βCH	4.2±0.5	BY	4.2±0.5	2.4	7.1	3.7
F106δCH2-V114(γCH3)2	4.9±0.5	CY(+β)	5.4±1.0	4.8	11.2	4.9
F106ξCH2-K105βCH2	4.2±0.5	CY(+β)	4.7±0.5	3.4	8.6	4.2
F106ξCH2-K105γCH2	5.1±1.0	CY(+β)	6.1±1.0	3.4	10.5	5.1
F106ξCH2-K107βCH2	4.0±0.5	CY(+β)	4.5±0.5	3.4	8.4	4.0
F106ξCH2-K107γCH2	5.1±1.0	BY	5.1±1.0	3.4	9.5	4.1
F106ξCH2-R108βCH2	7.5±1.0	BY	7.5±1.0	3.4	11.9	6.5
F106ξCH2-P109βCH(x)	6.9±1.0	CY(+β)	7.9±1.0	2.4	11.3	6.9
F106ξCH2-P109βCH'(p)	5.5±1.0	CY(+β)	6.5±1.0	2.4	9.9	5.5
F106ξCH2-P109γCH2	5.1±1.0	CY(+β)	6.1±1.0	3.4	10.5	5.1
F106ξCH2-L111(δCH3)2	5.1±1.0	CY(+β)	6.1±1.0	4.8	11.9	5.1
F106ξCH2-V114βCH	4.1±0.5	BY	4.1±0.5	2.4	7.0	3.6
F106ξCH2-V114(γCH3)2	4.5±0.5	BY	4.5±0.5	4.8	9.8	4.0
F106ζCH-K105βCH2	4.2±0.5	CY(+β)	4.7±0.5	3.0	8.2	4.2
F106ζCH-K105γCH2	5.1±1.0	CY(+β)	6.1±1.0	3.0	10.1	5.1
F106ζCH-K107βCH2	4.0±0.5	CY(+β)	4.5±0.5	3.0	8.0	4.0
F106ζCH-K107γCH2	5.1±1.0	BY	5.1±1.0	3.0	9.1	4.1
F106ζCH-R108βCH2	7.5±1.0	BY	7.5±1.0	3.0	11.5	6.5
F106ζCH-P109βCH(x)	6.9±1.0	CY(+β)	7.9±1.0	2.0	10.9	6.9
F106ζCH-P109βCH'(p)	5.5±1.0	CY(+β)	6.5±1.0	2.0	9.5	5.5
F106ζCH-P109γCH2	5.1±1.0	CY(+β)	6.1±1.0	3.0	9.1	5.1
F106ζCH-L111(δCH3)2	5.1±1.0	CY(+β)	6.1±1.0	4.4	11.5	5.1
F106ζCH-V114βCH	4.1±0.5	BY	4.1±0.5	2.0	6.6	3.6
F106ζCH-V114(γCH3)2	4.5±0.5	BY	4.5±0.5	4.4	9.4	4.0
R108βCH2-P109δCH(m)	3.7±0.3	CX(+2β)	4.2±0.5	1.0	5.7	3.7
R108βCH2-P109δCH(m')	4.1±0.5	CY(+β)	4.6±0.5	1.0	6.1	4.1

P109δCH(m) -V114βCH	6.9±1.0	BY	6.9±1.0		7.9	5.9
P109δCH'(m') -V114βCH	5.4±1.0	BY	5.4±1.0		6.4	4.4
P110βCH(x) -L111βCH2	3.7±0.3	CY(+β)	4.0±0.5	1.0	5.5	3.5
P110γCH2 -L111(δCH3)2	4.3±0.5	CY(+β)	4.8±0.5	3.4	8.7	4.3
L111(δCH3)2 -R112δCH2	6.6±1.0	CY(+β)	7.6±1.0	3.4	12.0	6.6
R112βCH2 -V114(γCH2)3	4.1±0.5	CY(+β)	4.6±0.5	3.4	8.5	4.1
R113δCH2 -V114(γCH2)3	7.4±1.0	BY	7.4±1.0	3.4	11.8	6.4
V114(γCH3)2 -R115βCH2	4.4±0.5	CY(+β)	4.9±0.5	3.4	7.8	4.4
V114(γCH3)2 -R115δCH2	7.5±1.0	BY	7.5±1.0	3.4	10.9	6.5
P109βCH'(p) -P110δCH(m)	3.0±0.3	BX(+β)	3.3±0.3		3.6	3.0
P109βCH'(p) -P110δCH'(m')	2.8±0.2	BX(+β)	3.0±0.3		3.3	2.7
P110βCH'(p) -P109δCH(m)	5.5±1.0	BX(+β)	6.5±1.0		7.5	5.5
P110βCH(x) -P109δCH'(m')	5.0±1.0	BX(+β)	6.0±1.0		7.0	5.0
P110γCH -P109δCH(m)	5.0±1.0	CY(+β)	6.0±1.0	1.0	8.0	5.0
P110γCH -P109δCH(m')	5.0±1.0	CY(+β)	6.0±1.0	1.0	8.0	5.0
K105αCH-F106αCH	4.5±0.5	BY	4.5±0.5		5.0	4.0
F106αCH-K107αCH	4.0±0.5	CY(+β)	4.5±0.5		5.0	4.0
F106αCH-R108αCH	7.0±1.0	AY(-β)	6.0±1.0		7.0	5.0
K107αCH-F108αCH	5.4±1.0	AX	5.4±1.0		6.4	4.4
R108αCH-P109αCH	4.2±0.5	CY(+β)	4.7±0.5		5.2	4.2
R108αCH-P110αCH	5.9±1.0	AY(-β)	4.9±0.5		5.4	4.4
P110αCH-L111αCH	4.4±0.5	AX	4.4±0.5		4.9	3.9
R113αCH-V114αCH	4.5±0.5	BX(+β)	5.0±1.0		6.0	4.0
V114αCH-R115αCH	3.9±0.3	AX	3.9±0.3		4.2	3.6
G104NH-K105NH	2.3±0.2	CY(+β)	2.5±0.2		2.7	2.3
G104NH-F106NH	2.7±0.2	BY	2.7±0.2		2.9	2.5
G104NH-K107NH	3.7±0.3	BY	3.7±0.3		4.0	3.4

K105NH-F106NH	2.7±0.2	CY(+β)	2.9±0.2		3.1	2.7
K105NH-K107NH	3.6±0.3	CY(+β)	3.9±0.3		4.2	3.6
K105NH-R108NH	4.3±0.5	BY	4.3±0.5		4.8	3.8
F106NH-K107NH	2.5±0.2	CY(+β)	2.7±0.2		2.9	2.5
F106NH-R108NH	4.3±0.5	BY	4.3±0.5		4.8	3.8
K107NH-R108NH	3.0±0.3	CY(+β)	3.3±0.3		3.6	3.0
L111NH-R112NH	2.7±0.2	BY	2.7±0.2		2.9	2.5
R112NH-R113NH	2.7±0.2	CY(+β)	2.9±0.2		3.1	2.7
R112NH-R115NH	3.4±0.3	BY	3.4±0.3		3.7	3.1
R113NH-V114NH	3.1±0.3	CY(+β)	3.4±0.3		3.7	3.1
R113NH-R115NH	2.6±0.2	BY	2.6±0.2		2.8	2.4
V114NH-R115NH	3.4±0.3	CY(+β)	3.7±0.3		4.0	3.4
R115NH-Cterm NH	5.7±1.0	BY	5.7±1.0		6.7	4.7
R115NH-Cterm NH'	5.7±1.0	BY	5.7±1.0		6.7	4.7

G104αCH2-NH	3.8±0.3	BY	3.8±0.3		4.1	3.5
G104αCH2-K105NH	3.4±0.3	BY	3.4±0.3	1.0	4.7	3.1
G104αCH2-F106NH	4.6±0.5	BY	4.6±0.5	1.0	6.1	4.1
G104αCH2-R108NH	4.4±0.5	CY(+β)	4.9±0.5	1.0	6.4	4.4
K105αCH-NH	3.8±0.3	BY	3.8±0.3		4.1	3.5
K105αCH-F106NH	3.0±0.3	BY	3.0±0.3		3.3	2.7
K105αCH-K107NH	4.3±0.5	BY	4.3±0.5		4.8	3.8
K105αCH-R108NH	4.3±0.5	BY	4.3±0.5		4.8	3.8
F106αCH-NH	3.8±0.3	BY	3.8±0.3		4.1	3.5
F106αCH-K107NH	3.0±0.3	BX(+β)	3.3±0.3		3.6	3.0
K107αCH-NH	3.4±0.3	BY	3.4±0.3		3.7	3.1
K107αCH-R108NH	3.4±0.3	BY	3.4±0.3		3.7	3.1
R108αCH-NH	3.7±0.3	BX(+β)	4.0±0.5		4.5	3.5
P110αCH-L111NH	2.9±0.2	BY	2.9±0.2		3.1	2.7
P110αCH-R112NH	4.0±0.5	BY	4.0±0.5		4.5	3.5
L111αCH-NH	3.0±0.3	BY	3.0±0.3		3.3	2.7
L111αCH-R112NH	3.5±0.3	BY	3.5±0.3		3.8	3.2
L111αCH-R113NH	3.5±0.3	BY	3.5±0.3		3.8	3.2
R112αCH-NH	3.1±0.3	BX(+β)	3.4±0.3		3.7	3.1
R112αCH-R113NH	2.9±0.2	BX(+β)	3.1±0.3		3.4	2.8
R112αCH-R115NH	4.0±0.5	BY	4.0±0.5		4.5	3.5
R113αCH-NH	2.9±0.2	BY	2.9±0.2		3.1	2.7
R113αCH-V114NH	2.7±0.2	BY	2.7±0.2		2.9	2.5
R113αCH-R115NH	4.0±0.5	BY	4.0±0.5		4.5	3.5
V114αCH-NH	3.4±0.3	BY	3.4±0.3		3.7	3.1
V114αCH-R113NH	2.7±0.2	BY	2.7±0.2		2.9	2.5
V114αCH-R115NH	2.7±0.2	BY	2.7±0.2		2.9	2.5
R115αCH-NH	3.4±0.3	BY	3.4±0.3		3.7	3.1

Table V-6. ^{3}JαCH-NH coupling constants for the TnI peptide as a function of molar equivalents TnC.Ca(II)$_4$.

TNC/TNIp	0.000	0.008	0.016	0.024	0.032	0.040	0.048	0.100
JαCH-NH	(Hz)							
G104	6.3	6.2	6.1	6.1	5.9	5.8	5.8	5.7
K105	6.9	6.7	6.5	6.7	6.6	6.5	6.4	6.5
F106	7.1	7.1	7.3	7.2	7.0	7.1	7.1	6.5
K107	7.2	7.1	7.2	7.1	7.0	7.0	6.9	6.7
R108	6.6	6.5	6.3	6.2	6.0	6.0	5.9	6.0
R112	6.8	6.5	6.4	6.4	6.2	6.3	6.1	6.0
R113	6.8	6.6	6.7	6.5	6.5	6.4	6.4	6.3
V114	7.5	7.6	7.3	7.3	7.1	7.0	6.8	6.4
R115	6.8	6.7	6.8	6.4	6.4	6.5	6.4	6.5

Table V-7. Chemical shift values for the TnI peptide backbone amide resonances as a function of temperature for **A.** 0.0 molar equivalents TnC.Ca(II)$_4$. **B.** 0.2 molar equivalents TnC.Ca(II)$_4$. **C.** 0.4 molar equivalents TnC.Ca(II)$_4$.

A.	temperature	5 °C	10 °C	15 °C	20 °C	25 °C	30 °C
	K105 (ppm)	8.343	8.318	8.286	8.252	8.218	8.176
	F106	8.267	8.237	8.201	8.168	8.129	8.091
	K107	8.232	8.219	8.195	8.168	8.147	8.118
	R108	8.458	8.427	8.388	8.347	8.305	8.262
	L111	8.416	8.377	8.350	8.311	8.267	8.225
	R112	8.473	8.445	8.407	8.369	8.330	8.292
	R113	8.543	8.514	8.379	8.441	8.404	8.364
	V114	8.406	8.377	8.333	8.290	8.246	8.203
	R115	8.587	8.556	8.517	8.477	8.437	8.394

B.	temperature	5 °C	10 °C	15 °C	20 °C	25 °C	30 °C
	G104 (ppm)	8.422	8.387	8.353	8.321	8.235	8.155
	K105	8.372	8.339				
	F106	8.307	8.275	8.238	8.198	8.160	8.125
	K107	8.236	8.212	8.193	8.173	8.145	8.105
	R108	8.463	8.422	8.384	8.339	8.296	8.194
	L111	8.422	8.375	8.314	8.280	8.235	8.155
	R112	8.463	8.422	8.384	8.339	8.296	8.194
	R113	8.528	8.490	8.457	8.420	8.380	8.241
	V114	8.422	8.375	8.314	8.280	8.235	8.155
	R115	8.579	8.539	8.499	8.462	8.419	8.304

C.	temperature	5 °C	10 °C	15 °C	20 °C	25 °C	30 °C
	G104 (ppm)	8.431	8.395	8.362	8.330	8.296	8.260
	K105	8.380	8.347	8.295			8.175
	F106	8.324	8.294	8.246	8.209	8.170	8.140
	K107	8.231	8.209	8.186	8.169	8.143	8.125
	R108	8.470	8.429	8.381	8.330	8.300	8.260
	L111	8.430	8.380	8.320	8.280	8.240	8.195
	R112	8.470	8.429	8.381	8.330	8.300	8.260
	R113	8.517	8.488	8.442	8.410	8.379	8.350
	V114	8.430	8.380	8.320	8.280	8.240	8.185
	R115	8.570	8.532	8.490	8.455	8.418	8.374

Table V-8. Temperature coefficients measured for various TnI peptide backbone amide protons versus molar equivalents TnC.Ca(II)$_4$.

TNC/TNIp	0.0	0.2	0.4
Δδ/ΔT,G104 (ppb)		6.74	6.77
Δδ/ΔT,K105	6.68		8.31
Δδ/ΔT,F106	7.07	7.42	7.59
Δδ/ΔT,K107	4.65	4.42	4.26
Δδ/ΔT,R108	7.93	8.33	8.50
Δδ/ΔT,R113	7.22	7.27	6.82
Δδ/ΔT,V114	8.29	9.14	9.34
Δδ/ΔT,R115	7.78	8.10	7.75

Table V-9. GROMOS distance restraint file used in MD simulations to generate the structure of the TnI peptide bound to TnC.Ca(II)$_4$.

```
TnI peptide, 0.1 M.E. skeletal TnC.Ca4, tm=150ms
500
   1     2                    5       5                         0    0.40
   1     2                    5       5                         0   -0.34
   1     2                    5       6     4     7             3    0.42
   1     2                    5       6     4     7             3   -0.36
   1     2                    5      10                         0    0.45
   1     2                    5      10                         0   -0.35
   1     2                    5      48                         0    0.40
   1     2                    5      48                         0   -0.34
   5                          0       6     4     7             3    0.41
   5                          0       6     4     7             3   -0.35
   5                          0      10                         0    0.27
   5                          0      10                         0   -0.23
   5                          0      13    12    14             3    0.57
   5                          0      13    12    14             3   -0.37
   5                          0      23                         0    0.29
   5                          0      23                         0   -0.25
   5                          0      35                         0    0.40
   5                          0      35                         0   -0.34
   5                          0      38    37    39             3    0.62
   5                          0      38    37    39             3   -0.42
   6     4     7              3      10                         0    0.47
   6     4     7              3      10                         0   -0.31
   6     4     7              3      23                         0    0.61
   6     4     7              3      23                         0   -0.41
   6     4     7              3      48                         0    0.64
   6     4     7              3      48                         0   -0.44
  10                          0      11     9    12    20       1    0.41
  10                          0      11     9    12    20       1   -0.35
  10                          0      12    11    13             3    0.48
  10                          0      12    11    13             3   -0.36
  10                          0      13    12    14             3    0.61
  10                          0      13    12    14             3   -0.41
  10                          0      23                         0    0.31
  10                          0      23                         0   -0.27
  10                          0      35                         0    0.42
  10                          0      35                         0   -0.36
  10                          0      38    37    39             3    0.70
  10                          0      38    37    39             3   -0.40
  10                          0      48                         0    0.48
  10                          0      48                         0   -0.38
  11     9    12    20        1      12    11    13             3    0.36
  11     9    12    20        1      12    11    13             3   -0.30
  11     9    12    20        1      13    12    14             3    0.56
  11     9    12    20        1      13    12    14             3   -0.36
  11     9    12    20        1      23                         0    0.33
  11     9    12    20        1      23                         0   -0.27
  11     9    12    20        1      24    22    25    32       1    0.50
  11     9    12    20        1      24    22    25    32       1   -0.40
  11     9    12    20        1      35                         0    0.48
  11     9    12    20        1      35                         0   -0.38
  11     9    12    20        1      48                         0    0.48
  11     9    12    20        1      48                         0   -0.38
  12    11    13              3      13    12    14             3    0.45
  12    11    13              3      13    12    14             3   -0.35
  12    11    13              3      23                         0    0.57
  12    11    13              3      23                         0   -0.37
  12    11    13              3      26                         0    0.98
  12    11    13              3      26                         0   -0.44
```

12	11	13		3	31				0	0.66
12	11	13		3	31				0	-0.42
12	11	13		3	31	29	30		2	0.82
12	11	13		3	31	29	30		2	-0.42
13	12	14		3	14	13	15		3	0.45
13	12	14		3	14	13	15		3	-0.35
13	12	14		3	15	14	16		3	0.39
13	12	14		3	15	14	16		3	-0.33
13	12	14		3	23				0	0.64
13	12	14		3	23				0	-0.44
13	12	14		3	26				0	0.97
13	12	14		3	26				0	-0.43
13	12	14		3	31				0	1.05
13	12	14		3	31				0	-0.51
13	12	14		3	31	29	30		2	1.01
13	12	14		3	31	29	30		2	-0.51
13	12	14		3	35				0	0.62
13	12	14		3	35				0	-0.42
13	12	14		3	48				0	0.51
13	12	14		3	48				0	-0.35
14	13	15		3	15	14	16		3	0.40
14	13	15		3	15	14	16		3	-0.34
14	13	15		3	23				0	0.56
14	13	15		3	23				0	-0.36
23				0	24	22	25	32	1	0.41
23				0	24	22	25	32	1	-0.35
23				0	25	26	24		4	0.34
23				0	25	26	24		4	-0.28
23				0	25	24	26		4	0.39
23				0	25	24	26		4	-0.33
23				0	26				0	0.66
23				0	26				0	-0.36
23				0	35				0	0.29
23				0	35				0	-0.25
23				0	38	37	39		3	0.59
23				0	38	37	39		3	-0.39
23				0	48				0	0.48
23				0	48				0	-0.38
24	22	25	32	1	25	26	24		4	0.36
24	22	25	32	1	25	26	24		4	-0.30
24	22	25	32	1	25	24	26		4	0.30
24	22	25	32	1	25	24	26		4	-0.26
24	22	25	32	1	26				0	0.70
24	22	25	32	1	26				0	-0.40
24	22	25	32	1	35				0	0.36
24	22	25	32	1	35				0	-0.30
24	22	25	32	1	36	34	37	45	1	0.50
24	22	25	32	1	36	34	37	45	1	-0.40
24	22	25	32	1	49	47	50	62	1	0.70
24	22	25	32	1	49	47	50	62	1	-0.50
25	26	24		4	25	24	26		4	0.25
25	26	24		4	25	24	26		4	-0.21
25	24	26		3	26				0	0.42
25	24	26		3	26				0	-0.36
25	24	26		3	35				0	0.50
25	24	26		3	35				0	-0.34
26				0	35				0	0.85
26				0	35				0	-0.41
26				0	37	36	38		3	0.94
26				0	37	36	38		3	-0.40

26			0	38	37	39		3	0.95
26			0	38	37	39		3	-0.41
26			0	40	39	41		3	0.82
26			0	40	39	41		3	-0.38
26			0	52	51	53		3	0.70
26			0	52	51	53		3	-0.30
26			0	67	66	68		3	1.12
26			0	67	66	68		3	-0.58
26			0	66	67	65		4	0.97
26			0	66	67	65		4	-0.53
26			0	81	82	80		3	0.96
26			0	81	82	80		3	-0.52
26			0	82	83	84		6	1.02
26			0	82	83	84		6	-0.44
26			0	124	123	125	126	1	0.71
26			0	124	123	125	126	1	-0.37
26			0	124	125	126		6	1.12
26			0	124	125	126		6	-0.49
31			0	37	36	38		3	0.84
31			0	37	36	38		3	-0.40
31			0	38	37	39		3	0.95
31			0	38	37	39		3	-0.41
31			0	50	49	51		3	1.19
31			0	50	49	51		3	-0.65
31			0	67	66	68		3	1.05
31			0	67	66	68		3	-0.51
31			0	66	67	65		4	1.13
31			0	66	67	65		4	-0.69
31			0	66	65	67		4	0.99
31			0	66	65	67		4	-0.55
31			0	82	83	84		6	1.19
31			0	82	83	84		6	-0.51
31			0	124	123	125	126	1	0.70
31			0	124	123	125	126	1	-0.36
31			0	124	125	126		6	0.98
31			0	124	125	126		6	-0.40
31	29	30	2	37	36	38		3	0.80
31	29	30	2	37	36	38		3	-0.40
31	29	30	2	38	37	39		3	0.91
31	29	30	2	38	37	39		3	-0.41
31	29	30	2	50	49	51		3	1.15
31	29	30	2	50	49	51		3	-0.65
31	29	30	2	67	66	68		3	0.95
31	29	30	2	67	66	68		3	-0.51
31	29	30	2	66	67	65		4	1.09
31	29	30	2	66	67	65		4	-0.69
31	29	30	2	66	65	67		4	0.95
31	29	30	2	66	65	67		4	-0.55
31	29	30	2	82	83	85		6	1.15
31	29	30	2	82	83	85		6	-0.51
31	29	30	2	124	123	125	126	1	0.66
31	29	30	2	124	123	125	126	1	-0.36
31	29	30	2	124	125	126		6	0.94
31	29	30	2	124	125	126		6	-0.40
35			0	36	34	37	45	1	0.37
35			0	36	34	37	45	1	-0.31
35			0	37	36	38		3	0.45
35			0	37	36	38		3	-0.30
35			0	38	37	39		3	0.55
35			0	38	37	39		3	-0.35

35				0	39	38	40		3	0.60
35				0	39	38	40		3	-0.40
35				0	48				0	0.36
35				0	48				0	-0.30
35				0	52	51	53		3	0.62
35				0	52	51	53		3	-0.42
36	34	37	45	1	37	36	38		3	0.36
36	34	37	45	1	37	36	38		3	-0.30
36	34	37	45	1	38	37	39		3	0.44
36	34	37	45	1	38	37	39		3	-0.32
36	34	37	45	1	48				0	0.37
36	34	37	45	1	48				0	-0.31
36	34	37	45	1	49	47	50	62	1	0.64
36	34	37	45	1	49	47	50	62	1	-0.44
37	36	38		3	38	37	39		3	0.34
37	36	38		3	38	37	39		3	-0.28
38	37	39		3	39	38	40		3	0.29
38	37	39		3	39	38	40		3	-0.25
38	37	39		3	40	39	41		3	0.37
38	37	39		3	40	39	41		3	-0.31
38	37	39		3	48				0	0.64
38	37	39		3	48				0	-0.44
39	38	40		3	40	39	41		3	0.39
39	38	40		3	40	39	41		3	-0.33
48				0	49	47	50	62	1	0.45
48				0	49	47	50	62	1	-0.35
48				0	50	49	51		3	0.33
48				0	50	49	51		3	-0.23
48				0	52	51	53		3	0.45
48				0	52	51	53		3	-0.35
48				0	66	65	67		3	0.70
48				0	66	65	67		3	-0.40
48				0	67	66	68		3	0.63
48				0	67	66	68		3	-0.43
49	47	50	62	1	50	49	51		3	0.42
49	47	50	62	1	50	49	51		3	-0.36
49	47	50	62	1	51	50	52		3	0.56
49	47	50	62	1	51	50	52		3	-0.40
49	47	50	62	1	52	51	53		3	0.61
49	47	50	62	1	52	51	53		3	-0.41
49	47	50	62	1	65	64	66	69	1	0.52
49	47	50	62	1	65	64	66	69	1	-0.42
49	47	50	62	1	68	64	67		4	0.30
49	47	50	62	1	68	64	67		4	-0.26
49	47	50	62	1	68	67	64		4	0.34
49	47	50	62	1	68	67	64		4	-0.28
49	47	50	62	1	67	66	68		3	0.71
49	47	50	62	1	67	66	68		3	-0.41
49	47	50	62	1	72	71	73	76	1	0.59
49	47	50	62	1	72	71	73	76	1	-0.39
50	49	51		3	68	64	67		4	0.61
50	49	51		3	68	64	67		4	-0.41
50	49	51		3	68	67	64		4	0.57
50	49	51		3	68	67	64		4	-0.37
51	50	52		3	52	51	53		3	0.38
51	50	52		3	52	51	53		3	-0.32
65	64	66	69	1	66	67	65		4	0.54
65	64	66	69	1	66	67	65		4	-0.44
65	64	66	69	1	66	65	67		4	0.42
65	64	66	69	1	66	65	67		4	-0.36

65	64	66	69	1	67	66	68		3	0.61
65	64	66	69	1	67	66	68		3	-0.41
65	64	66	69	1	75	71	74		4	0.35
65	64	66	69	1	75	71	74		4	-0.29
65	64	66	69	1	75	74	71		4	0.34
65	64	66	69	1	75	74	71		4	-0.28
65	64	66	69	1	73	72	74		3	0.64
65	64	66	69	1	73	72	74		3	-0.44
66	67	65		4	66	65	67		4	0.25
66	67	65		4	66	65	67		4	-0.21
66	67	65		4	67	66	68		3	0.24
66	67	65		4	67	66	68		3	-0.20
66	67	65		4	68	64	67		4	0.38
66	67	65		4	68	64	67		4	-0.32
66	67	65		4	68	67	64		4	0.45
66	67	65		4	68	67	64		4	-0.35
66	65	67		4	67	66	68		3	0.26
66	65	67		4	67	66	68		3	-0.22
66	65	67		4	68	64	67		4	0.40
66	65	67		4	68	64	67		4	-0.34
66	65	67		4	68	67	64		4	0.38
66	65	67		4	68	67	64		4	-0.32
66	65	67		4	75	71	74		4	0.33
66	65	67		4	75	71	74		4	-0.27
66	65	67		4	75	74	71		4	0.36
66	65	67		4	75	74	71		4	-0.30
67	66	68		3	68	67	64		3	0.36
67	66	68		3	68	67	64		3	-0.30
68	64	67		4	68	67	64		4	0.26
68	64	67		4	68	67	64		4	-0.22
68	64	67		4	73	74	72		4	0.70
68	64	67		4	73	74	72		4	-0.50
68	64	67		4	74	73	75		3	0.80
68	64	67		4	74	73	75		3	-0.50
68	67	64		4	73	72	74		4	0.75
68	67	64		4	73	72	74		4	-0.55
68	67	64		4	74	73	75		3	0.80
68	67	64		4	74	73	75		3	-0.50
68	64	67		4	124	123	125	126	1	0.64
68	64	67		4	124	123	125	126	1	-0.44
68	67	64		4	124	123	125	126	1	0.79
68	67	64		4	124	123	125	126	1	-0.59
72	71	73	76	1	73	74	72		4	0.35
72	71	73	76	1	73	74	72		4	-0.29
72	71	73	76	1	73	72	74		4	0.31
72	71	73	76	1	73	72	74		4	-0.27
72	71	73	76	1	74	73	75		3	0.47
72	71	73	76	1	74	73	75		3	-0.37
72	71	73	76	1	79				0	0.31
72	71	73	76	1	79				0	-0.27
72	71	73	76	1	80	78	81	85	1	0.49
72	71	73	76	1	80	78	81	85	1	-0.39
72	71	73	76	1	88				0	0.45
72	71	73	76	1	88				0	-0.35
72	71	73	76	1	90	89	91		3	0.83
72	71	73	76	1	90	89	91		3	-0.53
73	74	72		4	73	72	74		4	0.24
73	74	72		4	73	72	74		4	-0.20
73	74	72		4	74	73	75		3	0.24
73	74	72		4	74	73	75		3	-0.20

73	74	72		4	75	71	74		4	0.42
73	74	72		4	75	71	74		4	-0.36
73	74	72		4	75	74	71		4	0.38
73	74	72		4	75	74	71		4	-0.32
73	74	72		4	79				0	0.36
73	74	72		4	79				0	-0.30
73	74	72		4	81	80	82		6	0.55
73	74	72		4	81	80	82		6	-0.35
73	74	72		4	89	87	90	102	1	0.50
73	74	72		4	89	87	90	102	1	-0.40
73	72	74		4	74	73	75		3	0.28
73	72	74		4	74	73	75		3	-0.24
73	72	74		4	75	71	74		4	0.49
73	72	74		4	75	71	74		4	-0.37
73	72	74		4	75	74	71		4	0.45
73	72	74		4	75	74	71		4	-0.35
73	72	74		4	79				0	0.36
73	72	74		4	79				0	-0.30
73	72	74		3	80	78	81	85	1	0.52
73	72	74		3	80	78	81	85	1	-0.36
73	72	74		3	88				0	0.49
73	72	74		3	88				0	-0.33
73	72	74		4	89	87	90	102	1	0.75
73	72	74		4	89	87	90	102	1	-0.55
74	73	75		3	75	74	71		3	0.34
74	73	75		3	75	74	71		3	-0.27
74	73	75		3	79				0	0.71
74	73	75		3	79				0	-0.41
74	73	75		3	80	78	81	85	1	0.60
74	73	75		3	80	78	81	85	1	-0.40
74	73	75		3	82	83	84		6	0.87
74	73	75		3	82	83	84		6	-0.43
74	73	75		3	88				0	0.84
74	73	75		3	88				0	-0.54
74	73	75		3	89	87	90	102	1	0.68
74	73	75		3	89	87	90	102	1	-0.48
75	71	74		4	75	74	71		4	0.27
75	71	74		4	75	74	71		4	-0.23
79				0	80	78	81	85	1	0.33
79				0	80	78	81	85	1	-0.27
79				0	81	80	82		3	0.37
79				0	81	80	82		3	-0.27
79				0	82	83	84		6	0.36
79				0	82	83	84		6	-0.30
79				0	88				0	0.29
79				0	88				0	-0.25
79				0	92	91	93		3	0.64
79				0	92	91	93		3	-0.44
80	78	81	85	1	81	80	82		3	0.34
80	78	81	85	1	81	80	82		3	-0.28
80	78	81	85	1	82	83	84		6	0.65
80	78	81	85	1	82	83	84		6	-0.38
80	78	81	85	1	88				0	0.38
80	78	81	85	1	88				0	-0.32
80	78	81	85	1	105				0	0.38
80	78	81	85	1	105				0	-0.32
81	80	82		3	82	83	84		6	0.41
81	80	82		3	82	83	84		6	-0.35
82	81	83	84	1	82	83	84		6	0.37
82	81	83	84	1	82	83	84		6	-0.31

82	83	84		6	88				0	0.66
82	83	84		6	88				0	-0.36
82	83	84		6	89	87	90	102	1	0.95
82	83	84		6	89	87	90	102	1	-0.51
82	83	84		6	92	91	93		3	1.20
82	83	84		6	92	91	93		3	-0.66
88				0	89	87	90	102	1	0.37
88				0	89	87	90	102	1	-0.31
88				0	90	89	91		3	0.36
88				0	90	89	91		3	-0.26
88				0	92	91	93		3	0.50
88				0	92	91	93		3	-0.40
88				0	105				0	0.31
88				0	105				0	-0.27
88				0	109	108	110		3	0.71
88				0	109	108	110		3	-0.41
88				0	124	123	125	126	1	0.41
88				0	124	123	125	126	1	-0.35
88				0	130				0	0.37
88				0	130				0	-0.31
89	87	90	102	1	90	89	91		3	0.38
89	87	90	102	1	90	89	91		3	-0.32
89	87	90	102	1	92	91	93		3	0.51
89	87	90	102	1	92	91	93		3	-0.41
89	87	90	102	1	105				0	0.34
89	87	90	102	1	105				0	-0.28
89	87	90	102	1	130				0	0.45
89	87	90	102	1	130				0	-0.35
90	89	91		3	105				0	0.50
90	89	91		3	105				0	-0.34
90	89	91		3	124	125	126		6	0.85
90	89	91		3	124	125	126		6	-0.41
90	89	91		3	130				0	0.48
90	89	91		3	130				0	-0.32
90	89	91		3	147				0	0.65
90	89	91		3	147				0	-0.45
90	89	91		3	148				0	0.65
90	89	91		3	148				0	-0.45
91	90	92		3	92	91	93		3	0.29
91	90	92		3	92	91	93		3	-0.25
92	91	93		3	105				0	0.70
92	91	93		3	105				0	-0.40
105				0	106	104	107	119	1	0.31
105				0	106	104	107	119	1	-0.27
105				0	107	106	108		3	0.34
105				0	107	106	108		3	-0.24
105				0	109	108	110		3	0.45
105				0	109	108	110		3	-0.39
105				0	122				0	0.37
105				0	122				0	-0.31
105				0	123	121	124	127	1	0.29
105				0	123	121	124	127	1	-0.25
105				0	124	125	126		6	0.87
105				0	124	125	126		6	-0.43
105				0	130				0	0.28
105				0	130				0	-0.24
106	104	107	119	1	107	106	108		3	0.33
106	104	107	119	1	107	106	108		3	-0.27
106	104	107	119	1	109	108	110		3	0.61
106	104	107	119	1	109	108	110		3	-0.41

106	104	107	119	1	122				0	0.29
106	104	107	119	1	122				0	-0.25
106	104	107	119	1	123	121	124	127	1	0.60
106	104	107	119	1	123	121	124	127	1	-0.40
106	104	107	119	1	124	123	125	126	1	0.70
106	104	107	119	1	124	123	125	126	1	-0.50
106	104	107	119	1	124	125	126		6	0.76
106	104	107	119	1	124	125	126		6	-0.42
106	104	107	119	1	130				0	0.45
106	104	107	119	1	130				0	-0.35
107	106	108		3	122				0	0.48
107	106	108		3	122				0	-0.32
107	106	108		3	123	121	124	127	1	0.72
107	106	108		3	123	121	124	127	1	-0.42
108	107	109		3	109	108	110		3	0.29
108	107	109		3	109	108	110		3	-0.25
109	108	110		3	122				0	0.69
109	108	110		3	122				0	-0.49
109	108	110		3	124	125	126		6	1.18
109	108	110		3	124	125	126		6	-0.64
122				0	123	121	124	127	1	0.37
122				0	123	121	124	127	1	-0.31
122				0	124	123	125	126	1	0.36
122				0	124	123	125	126	1	-0.30
122				0	124	125	126		6	0.54
122				0	124	125	126		6	-0.31
122				0	130				0	0.40
122				0	130				0	-0.34
122				0	132	131	133		3	0.43
122				0	132	131	133		3	-0.27
122				0	134	133	135		3	0.64
122				0	134	133	135		3	-0.44
123	121	124	127	1	124	123	125	126	1	0.36
123	121	124	127	1	124	123	125	126	1	-0.30
123	121	124	127	1	124	125	126		6	0.43
123	121	124	127	1	124	125	126		6	-0.31
123	121	124	127	1	130				0	0.29
123	121	124	127	1	130				0	-0.25
123	121	124	127	1	131	129	132	144	1	0.42
123	121	124	127	1	131	129	132	144	1	-0.36
123	121	124	127	1	132	131	133		3	0.62
123	121	124	127	1	132	131	133		3	-0.42
124	123	125	126	1	124	125	126		6	0.29
124	123	125	126	1	124	125	126		6	-0.25
124	123	125	126	1	130				0	0.37
124	123	125	126	1	130				0	-0.31
124	125	126		6	130				0	0.79
124	125	126		6	130				0	-0.35
124	125	126		6	132	131	133		3	0.78
124	125	126		6	132	131	133		3	-0.44
124	125	126		6	134	133	135		3	1.09
124	125	126		6	134	133	135		3	-0.65
124	125	126		6	147				0	0.77
124	125	126		6	147				0	-0.43
124	125	126		6	148				0	0.77
124	125	126		6	148				0	-0.43
130				0	131	129	132	144	1	0.37
130				0	131	129	132	144	1	-0.31
130				0	132	131	133		3	0.42
130				0	132	131	133		3	-0.30

130				0	134	133	135	3	0.60
130				0	134	133	135	3	-0.40
130				0	147			0	0.67
130				0	147			0	-0.47
130				0	148			0	0.67
130				0	148			0	-0.47
131	129	132	144	1	132	131	133	3	0.37
131	129	132	144	1	132	131	133	3	-0.31
131	129	132	144	1	134	133	135	3	0.61
131	129	132	144	1	134	133	135	3	-0.41
131	129	132	144	1	147			0	0.40
131	129	132	144	1	147			0	-0.34
131	129	132	144	1	148			0	0.37
131	129	132	144	1	148			0	-0.31
132	131	133		3	147			0	0.50
132	131	133		3	147			0	-0.40
132	131	133		3	148			0	0.50
132	131	133		3	148			0	-0.40
133	132	134		3	134	133	135	3	0.29
133	132	134		3	134	133	135	3	-0.25
147				0	148			0	0.18
147				0	148			0	-0.14

Table V-10. Chemical shift values for the TnI peptide backbone amide resonances as a function of molar equivalents $TnC.Ca(II)_4$.

TNC/TNIp (ppm)	0.000	0.008	0.016	0.024	0.032	0.040	0.048	0.100
δG104NH	8.389	8.391	8.392	8.391	8.393	8.395	8.394	8.396
δK105NH	8.345	8.349	8.350	8.350	8.351	8.353	8.353	8.356
δF106NH	8.269	8.273	8.277	8.277	8.280	8.284	8.285	8.294
δK107NH	8.236	8.237	8.237	8.237	8.238	8.239	8.238	8.239
δR108NH	8.453	8.456	8.457	8.457	8.458	8.459	8.460	8.463
δL111NH	8.420	8.423	8.423	8.424	8.425	8.425	8.426	
δR112NH	8.480	8.482	8.482	8.482	8.482	8.482	8.483	8.484
δR113NH	8.542	8.546	8.546	8.547	8.547	8.549	8.549	8.552
δV114NH	8.413	8.415	8.416	8.416	8.416	8.418	8.417	8.419
δR115NH	8.587	8.591	8.592	8.592	8.593	8.593	8.595	8.598
δC-term NH	7.725	7.728	7.731	7.732	7.733	7.736	7.736	7.742
ΔδG104NH	0.000	0.002	0.003	0.002	0.004	0.006	0.005	0.007
ΔδK105NH	0.000	0.004	0.005	0.005	0.006	0.008	0.008	0.011
ΔδF106NH	0.000	0.004	0.008	0.008	0.011	0.015	0.016	0.025
ΔδK107NH	0.000	0.001	0.001	0.001	0.002	0.003	0.002	0.003
ΔδR108NH	0.000	0.003	0.004	0.004	0.005	0.006	0.007	0.010
ΔδL111NH	0.000	0.003	0.003	0.004	0.005	0.005	0.006	
ΔδR112NH	0.000	0.002	0.002	0.002	0.002	0.002	0.003	0.004
ΔδR113NH	0.000	0.004	0.004	0.005	0.005	0.007	0.007	0.010
ΔδV114NH	0.000	0.002	0.003	0.003	0.003	0.005	0.004	0.006
ΔδR115NH	0.000	0.004	0.005	0.005	0.006	0.006	0.008	0.011
ΔδC-term NH	0.000	0.003	0.006	0.007	0.008	0.011	0.011	0.017

Table V-11. Final coordinates for the structure of the TnI peptide bound to TnC generated from **A.** α-helical coordinates (structure 1), and **B.** β-strand coordinates (structure 2), following approximately 12 ps of restrained MD.

```
AVE.COORDS 10-15PS   TnI peptide, 0.1 M.E. skeletal TnC Ca4, tm=150ms, starting with alfa-helical coordinates
 148
   1GLY    ACC   1   0.429  -0.718  -0.122  0.0337  0.0120 -0.0013  0.0617  0.0039 -0.0128  0.0273
   1GLY      C   2   0.365  -0.815  -0.025  0.0211  0.0099  0.0140  0.0386 -0.0045 -0.0153  0.0147
   1GLY      O   3   0.370  -0.804   0.096  0.0325  0.0349  0.0206  0.0475 -0.0078 -0.0187  0.0151
   1GLY      N   4   0.296  -0.912  -0.081  0.0271  0.0182  0.0109  0.0432 -0.0006 -0.0241  0.0198
   1GLY      H   5   0.311  -0.863  -0.002  0.0259  0.0101  0.0112  0.0449 -0.0035 -0.0242  0.0227
   1GLY     CA   6   0.160  -0.943  -0.123  0.0141  0.0230  0.0052  0.0136 -0.0010 -0.0079  0.0058
   1GLY      C   7   0.071  -0.838  -0.057  0.0105  0.0188 -0.0007  0.0079  0.0063 -0.0028  0.0049
   1GLY      O   8   0.014  -0.749  -0.117  0.0177  0.0173  0.0024  0.0106 -0.0005 -0.0015  0.0251
   2LYSH     N   9   0.065  -0.845   0.075  0.0115  0.0232 -0.0006  0.0066  0.0049 -0.0033  0.0045
   2LYSH     H  10   0.113  -0.915   0.116  0.0273  0.0586  0.0130  0.0158 -0.0059 -0.0046  0.0075
   2LYSH    CA  11  -0.009  -0.753   0.162  0.0116  0.0206 -0.0089  0.0058  0.0117 -0.0055  0.0083
   2LYSH    CB  12   0.013  -0.776   0.311  0.0169  0.0352 -0.0134  0.0071  0.0108 -0.0026  0.0084
   2LYSH    CG  13  -0.098  -0.707   0.389  0.0203  0.0318 -0.0168  0.0200  0.0123 -0.0078  0.0093
   2LYSH    CD  14  -0.151  -0.797   0.493  0.0709  0.0919 -0.0157  0.0518  0.0655  0.0107  0.0690
   2LYSH    CE  15  -0.248  -0.738   0.589  0.0366  0.0402 -0.0315  0.0533  0.0171 -0.0096  0.0164
   2LYSH    NZ  16  -0.368  -0.693   0.532  0.0494  0.0270 -0.0144  0.0591  0.0266 -0.0013  0.0621
   2LYSH   HZ1  17  -0.365  -0.662   0.502  0.2802  0.1475  0.1617  0.5162 -0.0283 -0.0617  0.1770
   2LYSH   HZ2  18  -0.411  -0.714   0.501  0.1995  0.0220 -0.0577  0.2405 -0.0185  0.1395  0.3360
   2LYSH   HZ3  19  -0.405  -0.671   0.553  0.2503  0.1703  0.0353  0.1648 -0.1320  0.0420  0.4159
   2LYSH     C  20   0.038  -0.611   0.139  0.0110  0.0146 -0.0104  0.0080  0.0045 -0.0010  0.0104
   2LYSH     O  21  -0.040  -0.523   0.111  0.0328  0.0174 -0.0118  0.0181 -0.0133  0.0179  0.0630
   3PHE      N  22   0.170  -0.595   0.143  0.0111  0.0140 -0.0061  0.0104  0.0075  0.0017  0.0089
   3PHE      H  23   0.228  -0.670   0.148  0.0161  0.0167 -0.0017  0.0143  0.0096 -0.0100  0.0172
   3PHE     CA  24   0.226  -0.460   0.139  0.0116  0.0083 -0.0068  0.0126  0.0008  0.0083  0.0141
   3PHE     CB  25   0.374  -0.467   0.176  0.0187  0.0086 -0.0042  0.0222  0.0021  0.0132  0.0252
   3PHE     CG  26   0.424  -0.328   0.212  0.0262  0.0175 -0.0158  0.0251 -0.0134  0.0278  0.0360
   3PHE    CD1  27   0.530  -0.278   0.139  0.0403  0.0143 -0.0134  0.0414 -0.0126  0.0508  0.0651
   3PHE    CD2  28   0.361  -0.254   0.311  0.0316  0.0428 -0.0251  0.0179 -0.0202  0.0144  0.0342
   3PHE    CE1  29   0.574  -0.150   0.169  0.0551  0.0239 -0.0304  0.0475 -0.0339  0.0617  0.0940
   3PHE    CE2  30   0.404  -0.125   0.340  0.0497  0.0756 -0.0361  0.0233 -0.0350  0.0142  0.0501
   3PHE     CZ  31   0.510  -0.076   0.266  0.0593  0.0599 -0.0412  0.0332 -0.0512  0.0403  0.0850
   3PHE      C  32   0.205  -0.388   0.006  0.0223  0.0206 -0.0162  0.0257 -0.0073  0.0167  0.0204
   3PHE      O  33   0.179  -0.270   0.006  0.0477  0.0887 -0.0265  0.0193 -0.0310  0.0199  0.0351
   4LYSH     N  34   0.225  -0.460  -0.104  0.0196  0.0060 -0.0045  0.0336  0.0014  0.0198  0.0193
   4LYSH     H  35   0.251  -0.551  -0.104  0.0244  0.0137  0.0118  0.0428  0.0099  0.0196  0.0167
   4LYSH    CA  36   0.194  -0.402  -0.235  0.0256  0.0101 -0.0086  0.0408 -0.0081  0.0252  0.0260
   4LYSH    CB  37   0.243  -0.479  -0.355  0.0352  0.0066  0.0104  0.0786  0.0075  0.0360  0.0205
   4LYSH    CG  38   0.390  -0.482  -0.380  0.1215  0.0056  0.0209  0.3318  0.0062  0.0871  0.0270
   4LYSH    CD  39   0.449  -0.395  -0.467  0.0881  0.0560 -0.0538  0.1277  0.0537 -0.0432  0.0807
   4LYSH    CE  40   0.588  -0.414  -0.502  0.1599  0.0562 -0.0927  0.2977  0.0694 -0.1339  0.1258
   4LYSH    NZ  41   0.638  -0.328  -0.587  0.2199  0.1998 -0.1359  0.1535  0.2368 -0.1556  0.3063
   4LYSH   HZ1  42   0.679  -0.298  -0.588  0.3933  0.1927 -0.1260  0.0923  0.2037 -0.1435  0.8949
   4LYSH   HZ2  43   0.659  -0.339  -0.625  0.6175  0.8448 -0.2039  0.5054  0.6371 -0.1649  0.5022
   4LYSH   HZ3  44   0.620  -0.276  -0.607  0.3105  0.2066 -0.1477  0.3130  0.2089 -0.0222  0.4119
   4LYSH     C  45   0.046  -0.381  -0.264  0.0160  0.0107 -0.0059  0.0150 -0.0069  0.0128  0.0224
   4LYSH     O  46   0.015  -0.299  -0.348  0.0240  0.0251 -0.0021  0.0238 -0.0061  0.0174  0.0230
   5ARG      N  47  -0.039  -0.458  -0.199  0.0123  0.0040 -0.0012  0.0077 -0.0055  0.0094  0.0253
   5ARG      H  48  -0.006  -0.517  -0.132  0.0210  0.0049  0.0057  0.0213  0.0014  0.0220  0.0370
   5ARG     CA  49  -0.184  -0.459  -0.217  0.0119  0.0043  0.0016  0.0008 -0.0070 -0.0028  0.0307
   5ARG     CB  50  -0.234  -0.580  -0.138  0.0202  0.0057 -0.0001  0.0025 -0.0013  0.0013  0.0525
   5ARG     CG  51  -0.355  -0.581  -0.049  0.0493  0.0169  0.0159  0.0403  0.0243  0.0338  0.0907
   5ARG     CD  52  -0.326  -0.611   0.094  0.0301  0.0192 -0.0035  0.0168  0.0195 -0.0251  0.0544
   5ARG     NE  53  -0.432  -0.569   0.186  0.0561  0.0481 -0.0111  0.0075  0.0663 -0.0156  0.1127
   5ARG     HE  54  -0.518  -0.596   0.174  0.1155  0.0596 -0.0336  0.0489  0.0666  0.0050  0.2379
   5ARG     CZ  55  -0.420  -0.488   0.289  0.0781  0.1320 -0.0073  0.0024  0.1135 -0.0074  0.1001
   5ARG    NH1  56  -0.521  -0.466   0.369  0.1321  0.1975  0.0507  0.0255  0.1821  0.0458  0.1733
   5ARG   HH11  57  -0.601  -0.512   0.356  0.1640  0.1403  0.0524  0.0770  0.1866  0.0824  0.2747
   5ARG   HH12  58  -0.512  -0.404   0.437  0.1885  0.3574  0.0748  0.0378  0.2407  0.0401  0.1703
```

University of Alberta

5ARG	NH2	59	-0.311	-0.419	0.315	0.1054	0.2212	-0.0622	0.0270	0.1100	-0.0359	0.0679
5ARG	HH21	60	-0.236	-0.430	0.259	0.1063	0.1800	-0.0957	0.0789	0.0773	-0.0488	0.0600
5ARG	HH22	61	-0.306	-0.357	0.385	0.1596	0.3698	-0.0777	0.0310	0.1406	-0.0436	0.0778
5ARG	C	62	-0.267	-0.333	-0.195	0.0117	0.0107	0.0044	0.0022	-0.0083	-0.0039	0.0223
5ARG	O	63	-0.362	-0.317	-0.271	0.0219	0.0178	0.0179	0.0196	-0.0155	-0.0182	0.0284
6PRO	N	64	-0.242	-0.245	-0.098	0.0095	0.0118	0.0006	0.0013	-0.0059	0.0007	0.0153
6PRO	CA	65	-0.316	-0.120	-0.089	0.0095	0.0147	0.0003	0.0009	-0.0001	-0.0021	0.0130
6PRO	CB	66	-0.299	-0.068	0.054	0.0208	0.0440	-0.0057	0.0081	0.0078	-0.0018	0.0104
6PRO	CG	67	-0.210	-0.170	0.123	0.0233	0.0443	-0.0131	0.0181	0.0006	0.0081	0.0076
6PRO	CD	68	-0.142	-0.243	0.008	0.0145	0.0211	-0.0074	0.0100	-0.0088	0.0085	0.0125
6PRO	C	69	-0.260	-0.018	-0.188	0.0115	0.0226	0.0015	0.0041	0.0019	-0.0020	0.0078
6PRO	O	70	-0.157	-0.046	-0.247	0.0230	0.0345	0.0088	0.0109	0.0158	0.0018	0.0235
7PRO	N	71	-0.314	0.101	-0.210	0.0140	0.0254	0.0029	0.0063	0.0026	0.0006	0.0102
7PRO	CA	72	-0.239	0.192	-0.298	0.0145	0.0253	0.0078	0.0098	0.0037	0.0044	0.0083
7PRO	CB	73	-0.342	0.295	-0.343	0.0197	0.0229	0.0053	0.0095	0.0008	0.0082	0.0269
7PRO	CG	74	-0.458	0.276	-0.250	0.0513	0.0356	0.0150	0.0271	0.0275	0.0393	0.0911
7PRO	CD	75	-0.442	0.153	-0.164	0.0251	0.0304	0.0058	0.0101	0.0142	0.0073	0.0347
7PRO	C	76	-0.123	0.254	-0.222	0.0120	0.0198	0.0105	0.0114	0.0070	0.0019	0.0049
7PRO	O	77	-0.124	0.258	-0.101	0.0284	0.0375	-0.0157	0.0411	0.0110	-0.0030	0.0065
8LEU	N	78	-0.028	0.304	-0.300	0.0142	0.0210	0.0120	0.0145	0.0099	0.0033	0.0070
8LEU	H	79	-0.057	0.314	-0.390	0.0196	0.0249	0.0072	0.0272	0.0085	0.0019	0.0066
8LEU	CA	80	0.104	0.350	-0.253	0.0143	0.0202	0.0124	0.0137	0.0094	0.0064	0.0091
8LEU	CB	81	0.188	0.386	-0.375	0.0181	0.0247	0.0168	0.0165	0.0135	0.0114	0.0132
8LEU	CG	82	0.175	0.293	-0.494	0.0264	0.0449	0.0225	0.0225	0.0158	0.0102	0.0119
8LEU	CD1	83	0.208	0.147	-0.474	0.0572	0.1282	0.0400	0.0253	0.0249	0.0072	0.0182
8LEU	CD2	84	0.275	0.339	-0.597	0.0488	0.0701	0.0316	0.0523	0.0348	0.0198	0.0240
8LEU	C	85	0.109	0.461	-0.148	0.0132	0.0106	0.0112	0.0179	0.0028	0.0040	0.0113
8LEU	O	86	0.202	0.477	-0.070	0.0203	0.0122	0.0141	0.0300	-0.0031	0.0078	0.0187
9ARG	N	87	0.001	0.537	-0.143	0.0094	0.0076	0.0074	0.0138	-0.0003	-0.0005	0.0068
9ARG	H	88	-0.067	0.527	-0.209	0.0142	0.0087	0.0094	0.0208	-0.0025	-0.0065	0.0132
9ARG	CA	89	-0.020	0.638	-0.038	0.0076	0.0037	0.0024	0.0134	-0.0032	-0.0007	0.0059
9ARG	CB	90	-0.149	0.717	-0.051	0.0184	0.0136	0.0169	0.0333	-0.0019	0.0019	0.0082
9ARG	CG	91	-0.184	0.743	-0.194	0.0556	0.0400	0.0594	0.1160	-0.0055	-0.0034	0.0108
9ARG	CD	92	-0.317	0.806	-0.215	0.0211	0.0218	0.0193	0.0326	-0.0041	0.0032	0.0090
9ARG	NE	93	-0.427	0.729	-0.169	0.0336	0.0234	-0.0072	0.0718	-0.0030	-0.0074	0.0056
9ARG	HE	94	-0.440	0.740	-0.080	0.0872	0.0163	-0.0419	0.2365	0.0073	-0.0312	0.0087
9ARG	CZ	95	-0.508	0.654	-0.240	0.0625	0.0876	-0.0409	0.0805	-0.0291	0.0101	0.0193
9ARG	NH1	96	-0.605	0.594	-0.183	0.1776	0.1597	-0.1957	0.3229	-0.0466	0.0412	0.0503
9ARG	HH11	97	-0.610	0.603	-0.095	0.3008	0.2783	-0.3711	0.5649	-0.0338	0.0632	0.0593
9ARG	HH12	98	-0.668	0.543	-0.225	0.2340	0.2202	-0.2386	0.3881	-0.0759	0.0330	0.0939
9ARG	NH2	99	-0.504	0.636	-0.367	0.0743	0.1820	-0.0168	0.0160	-0.0593	0.0058	0.0249
9ARG	HH21	100	-0.446	0.681	-0.414	0.1217	0.2407	-0.0308	0.1066	-0.0538	0.0165	0.0179
9ARG	HH22	101	-0.561	0.580	-0.408	0.1368	0.2893	-0.0589	0.0277	-0.1250	0.0167	0.0935
9ARG	C	102	-0.037	0.574	0.100	0.0078	0.0022	-0.0026	0.0142	-0.0007	-0.0008	0.0069
9ARG	O	103	0.013	0.632	0.195	0.0117	0.0120	-0.0120	0.0195	-0.0006	0.0027	0.0037
10ARG	N	104	-0.115	0.467	0.103	0.0081	0.0017	0.0001	0.0102	-0.0008	-0.0043	0.0126
10ARG	H	105	-0.153	0.427	0.025	0.0077	0.0041	0.0013	0.0061	-0.0006	-0.0052	0.0130
10ARG	CA	106	-0.140	0.387	0.223	0.0125	0.0065	0.0038	0.0194	0.0032	-0.0022	0.0115
10ARG	CB	107	-0.251	0.285	0.202	0.0138	0.0102	0.0040	0.0087	0.0082	0.0031	0.0225
10ARG	CG	108	-0.383	0.350	0.200	0.0566	0.0168	0.0224	0.0529	0.0042	0.0034	0.1003
10ARG	CD	109	-0.495	0.298	0.164	0.1099	0.0091	0.0213	0.2523	-0.0012	-0.0911	0.0683
10ARG	NE	110	-0.621	0.362	0.190	0.0575	0.0120	-0.0077	0.0892	0.0185	-0.0382	0.0712
10ARG	HE	111	-0.616	0.446	0.168	0.0888	0.0610	-0.0320	0.1451	0.0279	-0.0052	0.0603
10ARG	CZ	112	-0.723	0.310	0.236	0.1179	0.0475	0.0067	0.0037	0.0856	0.0137	0.3024
10ARG	NH1	113	-0.826	0.378	0.270	0.1649	0.0802	0.0328	0.0529	0.1538	0.0605	0.3616
10ARG	HH11	114	-0.833	0.465	0.262	0.1527	0.1068	0.0702	0.0614	0.1379	0.0666	0.2899
10ARG	HH12	115	-0.899	0.338	0.300	0.3295	0.1635	0.0348	0.1355	0.3094	0.0968	0.6896
10ARG	NH2	116	-0.728	0.188	0.254	0.3002	0.2205	0.0001	0.0081	0.1569	0.0444	0.6722
10ARG	HH21	117	-0.656	0.138	0.237	0.3606	0.3043	0.0994	0.0511	0.1299	0.0007	0.7263
10ARG	HH22	118	-0.799	0.155	0.285	0.5190	0.4096	-0.1465	0.1128	0.2840	0.1419	1.0346

```
   10ARG      C  119  -0.016   0.310   0.266  0.0207  0.0081  0.0051  0.0369  0.0065  0.0183  0.0172
   10ARG      O  120   0.019   0.295   0.381  0.0375  0.0194  0.0136  0.0733  0.0037  0.0269  0.0198
   11VAL      N  121   0.050   0.270   0.158  0.0182  0.0078  0.0031  0.0263  0.0074  0.0160  0.0204
   11VAL      H  122   0.010   0.280   0.072  0.0174  0.0071  0.0032  0.0219  0.0020  0.0047  0.0231
   11VAL     CA  123   0.184   0.210   0.161  0.0227  0.0102  0.0071  0.0328  0.0064  0.0255  0.0249
   11VAL     CB  124   0.224   0.175   0.018  0.0203  0.0077  0.0100  0.0195  0.0111  0.0172  0.0338
   11VAL    CG1  125   0.131   0.066  -0.031  0.0343  0.0250  0.0017  0.0204  0.0170  0.0089  0.0576
   11VAL    CG2  126   0.370   0.137   0.011  0.0426  0.0138  0.0255  0.0612  0.0142  0.0251  0.0529
   11VAL      C  127   0.283   0.305   0.228  0.0246  0.0100  0.0040  0.0526  0.0019  0.0221  0.0113
   11VAL      O  128   0.365   0.266   0.309  0.0378  0.0281  0.0087  0.0664 -0.0083  0.0260  0.0188
   12ARG      N  129   0.271   0.432   0.193  0.0212  0.0031  0.0006  0.0510 -0.0003  0.0170  0.0094
   12ARG      H  130   0.215   0.458   0.120  0.0220  0.0063  0.0019  0.0485 -0.0031  0.0149  0.0111
   12ARG     CA  131   0.347   0.540   0.256  0.0279  0.0075 -0.0089  0.0680 -0.0039  0.0148  0.0082
   12ARG     CB  132   0.319   0.664   0.172  0.0237  0.0131 -0.0146  0.0523  0.0000  0.0064  0.0058
   12ARG     CG  133   0.439   0.752   0.150  0.0360  0.0292 -0.0317  0.0543  0.0081 -0.0246  0.0245
   12ARG     CD  134   0.437   0.783   0.002  0.0297  0.0343 -0.0102  0.0251  0.0271 -0.0076  0.0297
   12ARG     NE  135   0.333   0.880  -0.029  0.0456  0.0815  0.0114  0.0155  0.0515  0.0020  0.0399
   12ARG     HE  136   0.280   0.908   0.044  0.0690  0.0931  0.0201  0.0677  0.0565 -0.0096  0.0462
   12ARG     CZ  137   0.308   0.935  -0.146  0.0708  0.1450  0.0443  0.0149  0.0798  0.0254  0.0525
   12ARG    NH1  138   0.205   1.018  -0.161  0.0935  0.1898  0.0821  0.0416  0.0871  0.0396  0.0491
   12ARG   HH11  139   0.145   1.039  -0.093  0.1107  0.2201  0.0984  0.0559  0.0996  0.0424  0.0560
   12ARG   HH12  140   0.195   1.055  -0.243  0.1406  0.2575  0.1537  0.0988  0.1175  0.0651  0.0654
   12ARG    NH2  141   0.380   0.909  -0.255  0.0762  0.1574  0.0390  0.0178  0.0853  0.0238  0.0533
   12ARG   HH21  142   0.458   0.859  -0.247  0.0746  0.1290  0.0310  0.0341  0.0703  0.0008  0.0606
   12ARG   HH22  143   0.362   0.935  -0.340  0.1215  0.2297  0.0773  0.0669  0.1024  0.0458  0.0678
   12ARG      C  144   0.321   0.568   0.404  0.0362  0.0088 -0.0200  0.0930 -0.0020  0.0127  0.0069
   12ARG      O  145   0.397   0.637   0.468  0.0667  0.0265 -0.0599  0.1675 -0.0038  0.0088  0.0062
   12ARG      N  146   0.217   0.525   0.468  0.0450  0.0177 -0.0249  0.1041  0.0035  0.0156  0.0133
   12ARG     H1  147   0.162   0.457   0.442  0.0705  0.0442 -0.0436  0.1086  0.0137  0.0154  0.0588
   12ARG     H2  148   0.195   0.569   0.548  0.0736  0.0210 -0.0149  0.1870  0.0071 -0.0017  0.0127
AVE.COORDS 10-15PS    TnI peptide, 0.1 M.E. skeletal TnC.Ca4, tm=150ms, starting with beta-strand coordinates
  148
    1GLY    ACC    1  -0.181  -0.646   0.058  0.1501  0.1519  0.0742  0.0412 -0.1920 -0.0896  0.2572
    1GLY      C    2  -0.188  -0.740   0.176  0.1458  0.0977  0.0351  0.0160 -0.1767 -0.0658  0.3237
    1GLY      O    3  -0.091  -0.804   0.216  0.1358  0.0930  0.0321  0.0141 -0.1656 -0.0596  0.3004
    1GLY      N    4  -0.303  -0.748   0.240  0.1753  0.0706  0.0174  0.0139 -0.1722 -0.0435  0.4416
    1GLY      H    5  -0.209  -0.754   0.248  0.1582  0.0716  0.0366  0.0273 -0.1601 -0.0797  0.3758
    1GLY     CA    6  -0.377  -0.668   0.336  0.1830  0.0255  0.0012  0.0110 -0.1066 -0.0234  0.5125
    1GLY      C    7  -0.275  -0.582   0.409  0.1306  0.0046  0.0016  0.0088 -0.0346 -0.0334  0.3784
    1GLY      O    8  -0.269  -0.460   0.400  0.1306  0.0032  0.0034  0.0082 -0.0206 -0.0364  0.3804
   2LYSH      N    9  -0.184  -0.650   0.477  0.1036  0.0027 -0.0028  0.0078  0.0011 -0.0209  0.3005
   2LYSH      H   10  -0.197  -0.744   0.483  0.1079  0.0207 -0.0085  0.0096 -0.0063 -0.0190  0.2933
   2LYSH     CA   11  -0.069  -0.596   0.549  0.0657  0.0116 -0.0086  0.0128  0.0383 -0.0177  0.1727
   2LYSH     CB   12   0.023  -0.696   0.617  0.0506  0.0382 -0.0086  0.0235  0.0547 -0.0072  0.0903
   2LYSH     CG   13   0.067  -0.637   0.749  0.0764  0.1472 -0.0235  0.0238  0.0856 -0.0068  0.0584
   2LYSH     CD   14  -0.047  -0.631   0.848  0.1492  0.2620 -0.0469  0.0380  0.1878 -0.0337  0.1475
   2LYSH     CE   15  -0.009  -0.586   0.984  0.2116  0.4341 -0.1484  0.0767  0.2218 -0.0743  0.1239
   2LYSH     NZ   16  -0.129  -0.602   1.061  0.3114  0.5854 -0.1693  0.0620  0.3912 -0.1093  0.2867
   2LYSH    HZ1   17  -0.113  -0.567   1.139  0.4605  0.8294 -0.3884  0.2368  0.4814 -0.2192  0.3153
   2LYSH    HZ2   18  -0.188  -0.560   1.018  0.4102  0.5944 -0.0464  0.0367  0.5403 -0.0827  0.5994
   2LYSH    HZ3   19  -0.145  -0.687   1.080  0.2706  0.5935 -0.1760  0.0680  0.2566 -0.0650  0.1505
   2LYSH      C   20   0.024  -0.527   0.453  0.0316  0.0029 -0.0008  0.0087 -0.0100 -0.0129  0.0831
   2LYSH      O   21   0.070  -0.416   0.478  0.0235  0.0065  0.0026  0.0046 -0.0031 -0.0114  0.0594
    3PHE      N   22   0.047  -0.584   0.336  0.0375  0.0226  0.0043  0.0118 -0.0370 -0.0201  0.0781
    3PHE      H   23  -0.007  -0.661   0.317  0.0537  0.0389  0.0004  0.0139 -0.0539 -0.0204  0.1082
    3PHE     CA   24   0.146  -0.523   0.247  0.0305  0.0453  0.0192  0.0164 -0.0348 -0.0190  0.0298
    3PHE     CB   25   0.168  -0.603   0.120  0.0592  0.1192  0.0491  0.0258 -0.0595 -0.0276  0.0326
    3PHE     CG   26   0.278  -0.541   0.038  0.0863  0.2237  0.0751  0.0302  0.0038 -0.0011  0.0051
    3PHE    CD1   27   0.404  -0.542   0.090  0.0781  0.1536  0.0634  0.0364  0.0781  0.0380  0.0442
    3PHE    CD2   28   0.236  -0.479  -0.077  0.1455  0.3890  0.1149  0.0378 -0.0254 -0.0104  0.0096
```

University of Alberta

```
3PHE     CE1   29   0.497  -0.467   0.022  0.1426  0.2243  0.0962  0.0571  0.1702  0.0885  0.1463
3PHE     CE2   30   0.329  -0.406  -0.145  0.1983  0.5185  0.1592  0.0540  0.0942  0.0308  0.0225
3PHE      CZ   31   0.455  -0.403  -0.092  0.1955  0.4025  0.1519  0.0686  0.2055  0.0870  0.1155
3PHE       C   32   0.088  -0.387   0.205  0.0411  0.0701  0.0268  0.0182 -0.0454 -0.0234  0.0350
3PHE       O   33   0.162  -0.289   0.197  0.0359  0.0632  0.0289  0.0232 -0.0243 -0.0186  0.0215
4LYSH      N   34  -0.041  -0.379   0.177  0.0563  0.0786  0.0333  0.0193 -0.0722 -0.0347  0.0710
4LYSH      H   35  -0.093  -0.459   0.179  0.0680  0.0877  0.0310  0.0172 -0.0877 -0.0348  0.0990
4LYSH     CA   36  -0.111  -0.252   0.154  0.0687  0.1014  0.0417  0.0222 -0.0873 -0.0400  0.0825
4LYSH     CB   37  -0.242  -0.284   0.084  0.1150  0.1370  0.0592  0.0386 -0.1490 -0.0671  0.1694
4LYSH     CG   38  -0.234  -0.306  -0.066  0.1621  0.2107  0.1289  0.0895 -0.1966 -0.1233  0.1860
4LYSH     CD   39  -0.361  -0.313  -0.133  0.1113  0.1345 -0.0154  0.0772 -0.1273  0.0182  0.1222
4LYSH     CE   40  -0.353  -0.323  -0.283  0.1067  0.1215  0.0218  0.0640 -0.1171 -0.0326  0.1345
4LYSH     NZ   41  -0.329  -0.204  -0.332  0.1293  0.1034 -0.0716  0.1424  0.0724 -0.0982  0.1421
4LYSH    HZ1   42  -0.260  -0.176  -0.292  0.2438  0.1154 -0.1681  0.4885  0.0497 -0.1535  0.1275
4LYSH    HZ2   43  -0.317  -0.199  -0.425  0.1377  0.1119 -0.0571  0.1459  0.0954 -0.0915  0.1553
4LYSH    HZ3   44  -0.392  -0.154  -0.303  0.2079  0.3421 -0.0790  0.0915  0.2077 -0.0684  0.1902
4LYSH      C   45  -0.137  -0.157   0.270  0.0584  0.0536  0.0324  0.0249 -0.0671 -0.0458  0.0967
4LYSH      O   46  -0.211  -0.061   0.257  0.1046  0.1047  0.0659  0.0470 -0.1195 -0.0811  0.1622
5ARG       N   47  -0.073  -0.183   0.381  0.0254  0.0090  0.0063  0.0098 -0.0146 -0.0215  0.0573
5ARG       H   48  -0.020  -0.263   0.377  0.0253  0.0114  0.0082  0.0108 -0.0158 -0.0222  0.0537
5ARG      CA   49  -0.084  -0.096   0.497  0.0168  0.0122  0.0017  0.0026  0.0167  0.0005  0.0357
5ARG      CB   50   0.008  -0.148   0.605  0.0262  0.0454  0.0198  0.0149  0.0262  0.0117  0.0184
5ARG      CG   51   0.155  -0.159   0.574  0.0174  0.0320 -0.0038  0.0104  0.0051  0.0055  0.0099
5ARG      CD   52   0.236  -0.249   0.665  0.0195  0.0436  0.0080  0.0085  0.0052 -0.0022  0.0065
5ARG      NE   53   0.341  -0.312   0.587  0.0149  0.0133 -0.0106  0.0220  0.0017 -0.0073  0.0093
5ARG      HE   54   0.307  -0.342   0.512  0.0876  0.0110 -0.0046  0.1943  0.0050 -0.0916  0.0574
5ARG      CZ   55   0.467  -0.323   0.612  0.0208  0.0255  0.0092  0.0054 -0.0251 -0.0121  0.0315
5ARG     NH1   56   0.553  -0.389   0.535  0.0165  0.0122 -0.0051  0.0096 -0.0082  0.0014  0.0277
5ARG    HH11   57   0.521  -0.435   0.465  0.0400  0.0116 -0.0140  0.0749  0.0116 -0.0305  0.0336
5ARG    HH12   58   0.645  -0.388   0.549  0.0410  0.0145  0.0055  0.0241 -0.0235 -0.0184  0.0844
5ARG     NH2   59   0.510  -0.287   0.712  0.1517  0.0852  0.0977  0.1553 -0.1121 -0.1789  0.2146
5ARG    HH21   60   0.451  -0.213   0.762  0.2017  0.1200  0.1179  0.2002 -0.1201 -0.2302  0.2851
5ARG    HH22   61   0.595  -0.281   0.732  0.3063  0.1407  0.1980  0.3752 -0.1992 -0.3749  0.4031
5ARG       C   62  -0.062   0.053   0.478  0.0067  0.0148 -0.0021  0.0036  0.0006 -0.0005  0.0017
5ARG       O   63  -0.146   0.121   0.535  0.0139  0.0188  0.0108  0.0110 -0.0065  0.0001  0.0119
6PRO       N   64   0.034   0.111   0.407  0.0092  0.0153 -0.0074  0.0061 -0.0030  0.0025  0.0061
6PRO      CA   65   0.038   0.252   0.372  0.0217  0.0119 -0.0107  0.0121 -0.0179  0.0196  0.0412
6PRO      CB   66   0.171   0.280   0.304  0.0465  0.0107 -0.0172  0.0384 -0.0147  0.0474  0.0904
6PRO      CG   67   0.253   0.155   0.312  0.0360  0.0187 -0.0125  0.0378  0.0075  0.0116  0.0515
6PRO      CD   68   0.149   0.050   0.340  0.0170  0.0205 -0.0038  0.0191  0.0059  0.0070  0.0114
6PRO       C   69  -0.075   0.277   0.272  0.0315  0.0143 -0.0153  0.0369 -0.0184  0.0344  0.0434
6PRO       O   70  -0.148   0.187   0.237  0.0696  0.0618 -0.0624  0.0791 -0.0571  0.0624  0.0679
7PRO       N   71  -0.107   0.393   0.217  0.0289  0.0058  0.0040  0.0475  0.0022  0.0370  0.0334
7PRO      CA   72  -0.203   0.402   0.107  0.0429  0.0097  0.0073  0.0828 -0.0002  0.0470  0.0362
7PRO      CB   73  -0.211   0.546   0.059  0.0492  0.0467  0.0463  0.0811  0.0129  0.0334  0.0198
7PRO      CG   74  -0.097   0.610   0.133  0.0405  0.0731  0.0359  0.0278  0.0243  0.0216  0.0205
7PRO      CD   75  -0.064   0.527   0.255  0.0298  0.0217  0.0217  0.0346  0.0210  0.0322  0.0332
7PRO       C   76  -0.152   0.317  -0.009  0.0385  0.0138  0.0026  0.0482 -0.0117  0.0366  0.0535
7PRO       O   77  -0.032   0.302  -0.024  0.0457  0.0140  0.0133  0.0539 -0.0153  0.0128  0.0692
8LEU       N   78  -0.244   0.270  -0.093  0.0399  0.0146 -0.0014  0.0336 -0.0165  0.0361  0.0715
8LEU       H   79  -0.331   0.306  -0.079  0.0455  0.0124  0.0016  0.0580 -0.0114  0.0466  0.0662
8LEU      CA   80  -0.208   0.174  -0.198  0.0494  0.0219  0.0013  0.0109 -0.0317  0.0150  0.1154
8LEU      CB   81  -0.325   0.130  -0.285  0.0683  0.0346 -0.0073  0.0117 -0.0501  0.0082  0.1585
8LEU      CG   82  -0.460   0.145  -0.218  0.0965  0.0160 -0.0017  0.0137 -0.0421 -0.0194  0.2599
8LEU     CD1   83  -0.482   0.048  -0.111  0.1077  0.0497  0.0422  0.0909  0.0145  0.0077  0.1824
8LEU     CD2   84  -0.570   0.123  -0.313  0.1747  0.0366 -0.0422  0.1157 -0.0839  0.0406  0.3718
8LEU       C   85  -0.109   0.235  -0.295  0.0382  0.0115  0.0093  0.0237 -0.0258 -0.0181  0.0794
8LEU       O   86  -0.017   0.165  -0.333  0.0487  0.0293  0.0285  0.0495 -0.0376 -0.0376  0.0671
9ARG       N   87  -0.134   0.359  -0.335  0.0290  0.0032 -0.0004  0.0231 -0.0058 -0.0127  0.0608
9ARG       H   88  -0.212   0.397  -0.295  0.0348  0.0047 -0.0028  0.0220  0.0047 -0.0052  0.0777
```

University of Alberta

9ARG	CA	89	-0.063	0.444	-0.430	0.0241	0.0037	0.0022	0.0310	-0.0030	-0.0228	0.0376
9ARG	CB	90	-0.139	0.573	-0.457	0.0282	0.0128	-0.0095	0.0142	0.0116	-0.0156	0.0576
9ARG	CG	91	-0.258	0.535	-0.540	0.0617	0.0059	-0.0015	0.0064	-0.0215	-0.0106	0.1728
9ARG	CD	92	-0.377	0.626	-0.558	0.0803	0.0024	0.0006	0.0142	0.0009	0.0183	0.2244
9ARG	NE	93	-0.464	0.556	-0.651	0.1483	0.0224	0.0011	0.0086	-0.0675	-0.0189	0.4139
9ARG	HE	94	-0.451	0.571	-0.736	0.1815	0.0431	-0.0037	0.1194	-0.0224	-0.1932	0.3821
9ARG	CZ	95	-0.556	0.476	-0.628	0.3252	0.0993	-0.0759	0.0633	-0.2680	0.2182	0.8128
9ARG	NH1	96	-0.631	0.428	-0.724	0.4420	0.1839	-0.0455	0.0186	-0.4219	0.1004	1.1235
9ARG	HH11	97	-0.628	0.450	-0.809	0.4294	0.2000	0.0423	0.0675	-0.3635	-0.1775	1.0205
9ARG	HH12	98	-0.691	0.369	-0.699	0.6507	0.3125	-0.1626	0.0919	-0.6570	0.3291	1.5476
9ARG	NH2	99	-0.580	0.440	-0.514	0.5851	0.1920	-0.2911	0.4865	-0.4252	0.7167	1.0768
9ARG	HH21	100	-0.526	0.476	-0.450	0.5479	0.1521	-0.2900	0.6877	-0.3161	0.7260	0.8039
9ARG	HH22	101	-0.645	0.382	-0.503	0.8834	0.3547	-0.4918	0.7655	-0.6978	1.0675	1.5301
9ARG	C	102	0.077	0.488	-0.388	0.0276	0.0067	-0.0065	0.0550	0.0006	-0.0263	0.0212
9ARG	O	103	0.154	0.543	-0.464	0.0377	0.0082	-0.0156	0.0868	0.0026	-0.0267	0.0182
10ARG	N	104	0.108	0.470	-0.260	0.0259	0.0114	-0.0140	0.0470	0.0054	-0.0240	0.0193
10ARG	H	105	0.050	0.427	-0.198	0.0296	0.0195	-0.0137	0.0474	0.0099	-0.0250	0.0218
10ARG	CA	106	0.242	0.496	-0.209	0.0306	0.0207	-0.0313	0.0664	0.0011	-0.0071	0.0048
10ARG	CB	107	0.235	0.488	-0.057	0.0381	0.0407	-0.0393	0.0684	0.0053	-0.0094	0.0051
10ARG	CG	108	0.351	0.532	0.018	0.0724	0.0491	0.0317	0.1272	-0.0306	-0.0629	0.0410
10ARG	CD	109	0.301	0.601	0.137	0.0516	0.0615	0.0469	0.0528	-0.0360	-0.0404	0.0406
10ARG	NE	110	0.254	0.731	0.111	0.0987	0.0149	0.0132	0.0318	-0.0403	-0.0228	0.2495
10ARG	HE	111	0.258	0.760	0.024	0.1359	0.0309	0.0007	0.0760	-0.0611	0.0796	0.3007
10ARG	CZ	112	0.202	0.812	0.197	0.1978	0.0134	-0.0025	0.0609	0.0003	-0.1472	0.5192
10ARG	NH1	113	0.160	0.930	0.164	0.3289	0.0138	-0.0045	0.0395	-0.0024	-0.1081	0.9333
10ARG	HH11	114	0.158	0.961	0.077	0.3794	0.0187	-0.0166	0.0694	-0.0340	0.0449	1.0500
10ARG	HH12	115	0.127	0.989	0.226	0.4486	0.0593	0.0023	0.0791	0.0046	-0.2606	1.2074
10ARG	NH2	116	0.187	0.783	0.322	0.2473	0.0668	-0.0614	0.2108	0.0676	-0.3001	0.4641
10ARG	HH21	117	0.216	0.701	0.353	0.2066	0.0758	-0.0578	0.2741	0.0373	-0.2423	0.2698
10ARG	HH22	118	0.151	0.841	0.383	0.3913	0.1405	-0.1217	0.3365	0.1299	-0.4669	0.6970
10ARG	C	119	0.332	0.390	-0.271	0.0364	0.0067	-0.0158	0.0983	0.0003	-0.0033	0.0043
10ARG	O	120	0.438	0.411	-0.325	0.0692	0.0134	-0.0092	0.1664	0.0110	0.0303	0.0280
11VAL	N	121	0.276	0.271	-0.252	0.0290	0.0051	0.0058	0.0731	-0.0041	-0.0197	0.0089
11VAL	H	122	0.203	0.255	-0.194	0.0266	0.0051	-0.0021	0.0430	0.0032	-0.0261	0.0316
11VAL	CA	123	0.327	0.149	-0.313	0.0493	0.0285	0.0467	0.1043	-0.0175	-0.0264	0.0152
11VAL	CB	124	0.241	0.034	-0.264	0.0509	0.0677	0.0515	0.0607	-0.0335	-0.0319	0.0242
11VAL	CG1	125	0.258	0.012	-0.114	0.0482	0.0467	0.0450	0.0775	-0.0214	-0.0338	0.0203
11VAL	CG2	126	0.280	-0.092	-0.336	0.1087	0.2272	0.1025	0.0806	-0.0229	-0.0296	0.0182
11VAL	C	127	0.320	0.170	-0.464	0.0565	0.0460	0.0676	0.1073	-0.0184	-0.0215	0.0164
11VAL	O	128	0.422	0.167	-0.531	0.0719	0.0587	0.0847	0.1348	-0.0069	-0.0015	0.0222
12ARG	N	129	0.197	0.192	-0.507	0.0496	0.0504	0.0604	0.0754	-0.0300	-0.0358	0.0229
12ARG	H	130	0.128	0.197	-0.441	0.0413	0.0406	0.0447	0.0534	-0.0318	-0.0354	0.0300
12ARG	CA	131	0.157	0.213	-0.647	0.0703	0.0832	0.0885	0.1030	-0.0399	-0.0441	0.0248
12ARG	CB	132	0.006	0.194	-0.646	0.0745	0.0928	0.0636	0.0754	-0.0695	-0.0514	0.0554
12ARG	CG	133	-0.033	0.053	-0.630	0.1856	0.1902	0.0533	0.0656	-0.2095	-0.0854	0.3009
12ARG	CD	134	-0.126	-0.006	-0.682	0.0803	0.0223	-0.0039	0.1552	-0.0110	-0.0207	0.0634
12ARG	NE	135	-0.138	-0.147	-0.652	0.0710	0.0287	-0.0152	0.1341	0.0116	-0.0653	0.0503
12ARG	HE	136	-0.175	-0.152	-0.571	0.0709	0.0977	0.0290	0.0717	0.0067	-0.0329	0.0433
12ARG	CZ	137	-0.106	-0.248	-0.723	0.1240	0.1062	-0.1243	0.1616	0.1006	-0.1162	0.1041
12ARG	NH1	138	-0.119	-0.370	-0.675	0.1522	0.1299	-0.1042	0.1404	0.1429	-0.1262	0.1863
12ARG	HH11	139	-0.155	-0.387	-0.594	0.1312	0.1095	-0.0093	0.1279	0.0843	-0.0771	0.1563
12ARG	HH12	140	-0.091	-0.438	-0.725	0.2679	0.3281	-0.1965	0.1573	0.2879	-0.1763	0.3184
12ARG	NH2	141	-0.070	-0.232	-0.845	0.2482	0.3653	-0.2737	0.2445	0.2063	-0.1518	0.1347
12ARG	HH21	142	-0.074	-0.151	-0.887	0.2625	0.3732	-0.2888	0.3261	0.1492	-0.1004	0.0881
12ARG	HH22	143	-0.041	-0.299	-0.893	0.4209	0.7477	-0.3632	0.2699	0.3894	-0.2119	0.2449
12ARG	C	144	0.198	0.342	-0.716	0.0713	0.0707	0.0960	0.1383	-0.0129	-0.0164	0.0048
12ARG	O	145	0.118	0.421	-0.764	0.0691	0.0739	0.0902	0.1164	-0.0262	-0.0288	0.0171
12ARG	N	146	0.324	0.373	-0.718	0.1121	0.0548	0.1067	0.2486	0.0166	0.0601	0.0329
12ARG	H1	147	0.393	0.323	-0.676	0.1348	0.0644	0.1219	0.2861	0.0138	0.0714	0.0540
12ARG	H2	148	0.342	0.455	-0.760	0.1474	0.0462	0.0827	0.3188	0.0206	0.1310	0.0773

University of Alberta

Table V-12. Comparison of the distances between proton pairs given in the TRNOE-derived distance restraint file (rijU, rijL) with those actually measured between the same proton pairs in the final structures generated from the α-helix (rijα) and the β-strand (rijβ).

spin system	rijα(Å)	rijβ(Å)	rijU(Å)	rijL(Å)
K105αCH-βCH2	2.57	2.61	3.6	3.0
K105αCH-βCH2	2.71	2.88	5.6	3.6
K105βCH2-γCH2	2.36	2.24	4.5	3.5
K105γCH2-δCH2	2.31	2.36	4.5	3.5
K105δCH2-ξCH2	2.18	2.35	4.0	3.4
K105βCH2-NH	2.50	2.61	4.8	3.6
K105γCH2-ξCH2	3.03	2.61	3.9	3.3
K105γCH2-NH	4.38	4.40	6.1	4.1
F106αCH-βCH(m)	2.48	2.38	3.6	3.0
F106αCH-βCH'(x)	2.90	2.88	3.0	2.6
F106αCH-δCH2	2.63	2.65	7.0	4.0
F106βCH(m)-βCH'(x)	1.63	1.63	2.5	2.1
F106βCH'(x)-NH	2.65	2.73	3.9	3.3
F106βCH(m)-NH	2.38	2.67	3.4	2.8
F106βCH2-δCH2	1.91	1.89	4.2	3.6
F106NH-δCH2	3.99	4.16	6.6	3.6
K107αCH-βCH2	2.62	2.63	3.6	3.0
K107αCH-βCH2	2.93	2.66	4.4	3.2
K107βCH2-γCH2	2.23	2.36	3.4	2.8
K107βCH2-NH	2.93	2.71	4.5	3.3
K107δCH2-γCH2	2.14	2.25	2.9	2.5
K107δCH2-ξCH2	2.31	2.29	3.9	3.3
K107δCH2-NH	4.63	4.49	6.0	4.0
K107γCH2-ξCH2	2.43	2.88	3.7	3.1
K107γCH2-NH	3.07	3.25	5.5	3.5
R108αCH-βCH2	2.41	2.27	4.2	3.6
R108αCH-γCH2	3.45	3.61	5.6	4.0
R108αCH-δCH2	4.70	4.82	6.1	4.1
R108γCH2-δCH2	2.32	2.35	3.8	3.2
R108βCH2-NH	2.29	2.97	3.3	2.3
R108δCH2-NH	3.84	4.24	4.5	3.5
P109αCH-βCH(x)	2.79	2.78	5.4	4.4
P109αCH-βCH'(p)	2.27	2.23	4.2	3.6
P109αCH-γCH2	3.60	3.56	6.1	4.1
P109βCH(x)-βCH'(p)	1.63	1.63	2.5	2.1
P109βCH(x)-δCH'(m')	3.01	3.02	3.8	3.2
P109βCH(x)-δCH(m)	3.85	3.79	4.5	3.5

P109βCH(x)-γCH2	2.43	2.40	2.4	2.0
P109βCH'(p)-δCH(m)	3.91	3.80	3.8	3.2
P109βCH'(p)-δCH'(m')	3.74	3.73	4.0	3.4
P109βCH'(p)-γCH2	2.32	2.29	2.6	2.2
P109γCH2-δCH2	2.26	2.22	3.6	3.0
P109δCH(m)-δCH'(m')	1.63	1.63	2.6	2.2
P110αCH-βCH(x)	2.70	2.74	3.5	2.9
P110αCH-βCH'(p)	2.27	2.25	3.1	2.7
P110αCH-γCH2	3.71	3.64	4.7	3.7
P110βCH(x)-βCH'(p)	1.63	1.63	2.4	2.0
P110βCH(x)-δCH(m)	3.97	3.85	3.8	3.2
P110βCH(x)-δCH'(m')	3.67	3.92	4.2	3.6
P110βCH(x)-γCH2	2.29	2.29	2.4	2.0
P110βCH'(p)-δCH(m)	3.52	3.13	4.5	3.5
P110βCH'(p)-δCH'(m')	3.91	3.88	4.9	3.7
P110βCH'(p)-γCH2	2.34	2.41	2.8	2.4
P110γCH2-δCH2	2.21	2.23	3.4	2.7
P110δCH(m)-δCH'(m')	1.63	1.63	2.7	2.3
L111αCH-βCH2	2.52	2.44	3.4	2.8
L111αCH-(δCH3)2	3.60	3.75	6.5	3.8
L111βCH2-(δCH3)2	2.59	2.58	4.1	3.5
L111γCH-(δCH3)2	1.86	1.84	3.7	3.1
L111βCH2-NH	3.04	3.26	3.7	2.7
L111(δCH3)2-NH	3.53	3.39	3.6	3.0
R112αCH-βCH2	2.50	2.63	3.8	3.2
R112αCH-δCH2	4.61	4.43	5.1	4.1
R112γCH2-δCH2	2.18	2.35	2.9	2.5
R112βCH2-NH	3.12	2.84	3.6	2.6
R112δCH2-NH	4.21	4.08	5.0	4.0
R113αCH-βCH2	2.59	2.53	3.3	2.7
R113αCH-δCH2	4.14	4.25	6.1	4.1
R113γCH2-δCH2	2.01	2.22	2.9	2.5
R113βCH2-NH	2.77	2.23	3.4	2.4
R113δCH2-NH	3.97	4.86	4.5	3.9
V114αCH-βCH	2.91	2.86	3.6	3.0
V114αCH-(γCH3)2	2.51	2.47	4.3	3.1
V114βCH-(γCH3)2	1.81	1.84	2.9	2.5
V114βCH-NH	2.36	2.25	3.6	3.0
V114(γCH3)2-NH	3.32	3.20	5.4	3.1
R115αCH-βCH2	2.65	2.63	3.7	3.1
R115αCH-δCH2	3.88	3.87	6.1	4.1
R115γCH2-δCH2	2.28	1.93	2.9	2.5
R115βCH2-NH	2.27	2.68	4.2	3.0
R115δCH2-NH	4.27	4.32	6.0	4.0
C-term NH-NH'	1.58	1.65	1.8	1.4

N-Acetyl CH3-G104αCH2	4.16	4.05	4.2	3.6
N-Acetyl CH3-G104NH	2.55	2.53	4.0	3.4
N-Acetyl CH3-K105NH	4.73	4.67	4.5	3.5
N-Acetyl CH3-R108NH	4.84	5.25	4.0	3.4
G104NH-K105γCH2	6.11	6.24	5.7	3.7
G104NH-K107γCH2	5.06	5.61	6.2	4.2
K105βCH2-F106NH	2.87	2.96	5.7	3.7
K105γCH2-F106NH	4.17	4.63	6.4	4.4
K105γCH2-K107NH	6.17	6.40	6.2	4.2
K105γCH2-R108NH	5.42	5.42	5.1	3.5
K105δCH2-F106NH	5.35	5.27	5.6	3.6
K105NH-K107γCH2	6.94	7.23	7.0	4.0
F106βCH2-K107NH	3.22	3.09	5.0	3.4
F106δCH-K107NH	4.24	4.05	8.5	4.1
F106NH-K107γCH2	5.61	5.70	5.9	3.9
K107γCH2-R108NH	4.86	5.03	6.4	4.4
K107NH-R108δCH2	5.78	6.62	6.2	4.2
R108αCH-P109γCH2	5.72	5.92	7.1	4.1
R108αCH-P109δCH(m)	3.80	3.96	3.4	2.8
R108αCH-P109δCH'(m')	4.20	4.15	3.0	2.6
R108NH-P109βCH2	6.25	6.35	7.0	4.0
R108NH-P109γCH2	5.00	5.33	6.3	4.3
P109αCH-P110δCH(m)	2.57	3.13	3.4	2.8
P109αCH-P110δCH'(m')	3.19	2.85	3.5	2.9
P109αCH-P110βCH2	5.51	5.77	6.4	4.4
P110αCH-R112βCH2	6.97	6.56	8.3	5.3
P110βCH(x)-L111NH	2.65	2.83	3.6	3.0
P110βCH(x)-R112αCH	5.56	5.18	5.0	4.0
P110βCH2-L111αCH	5.14	5.07	5.2	3.6
P110βCH'(p)-L111NH	3.19	3.27	3.6	3.0
P110βCH'(p)-R112αCH	7.13	6.71	7.5	5.5
P110βCH2-R112NH	3.77	3.63	4.9	3.3
P110γCH2-L111αCH	6.44	6.27	6.0	4.0
P110γCH2-L111NH	4.68	4.80	7.1	4.1
P110γCH2-R112αCH	7.10	6.84	6.8	4.8
P110γCH2-R112NH	4.88	5.08	8.4	5.4
L111(δCH3)2-R112αCH	6.99	6.45	9.5	5.1
L111(δCH3)2-R112NH	5.46	4.68	6.6	3.6
L111NH-R112δCH2	6.25	5.90	6.4	4.4
R112βCH2-R113NH	3.11	3.59	5.0	3.4
R112βCH2-R115NH	5.00	4.98	4.8	3.2
R112βCH2-Cterm NH	6.30	6.45	6.5	4.5
R112βCH2-Cterm NH'	6.90	5.92	6.5	4.5
R112δCH2-R113NH	5.34	6.06	7.0	4.0
R112NH-R113δCH2	6.13	7.28	7.1	4.1
R112NH-V114βCH	4.26	4.94	4.1	3.5

R113αCH-V114βCH	5.46	5.49	7.0	5.0
R113αCH-V114(γCH3)2	6.46	6.43	7.6	4.2
R113βCH2-V114αCH	4.37	4.85	7.2	4.2
R113βCH2-V114NH	2.87	2.71	4.8	3.2
R113δCH2-V114NH	5.04	5.12	6.9	4.9
R113NH-V114(γCH3)2	5.40	5.33	8.7	4.3
V114αCH-R115βCH2	5.61	5.92	6.2	4.2
V114βCH-R115NH	2.61	2.12	3.7	3.1
V114(γCH3)2-R115NH	4.05	3.69	7.9	3.5
V114(γCH3)2-Cterm NH	6.03	6.07	7.7	4.3
V114(γCH3)2-Cterm NH'	7.51	7.49	7.7	4.3
V114NH-R115βCH2	4.79	5.15	4.3	2.7
V114NH-R115δCH2	6.75	6.74	6.4	4.4
R115αCH-Cterm NH	3.40	2.56	4.0	3.4
R115αCH-Cterm NH'	3.88	3.41	3.7	3.1
R115βCH2-Cterm NH	3.80	4.35	5.0	4.0
R115βCH2-Cterm NH'	4.18	4.47	5.0	4.0
F106δCH2-K105βCH2	6.15	6.42	9.8	4.4
F106δCH2-K105γCH2	6.54	7.43	9.7	4.3
F106δCH2-K107βCH2	6.65	6.28	9.4	4.0
F106δCH2-K107γCH2	5.98	5.34	9.5	4.1
F106δCH2-K107ξCH2	7.33	7.50	8.2	3.8
F106δCH2-R108δCH2	7.33	7.41	7.0	3.0
F106δCH2-P109βCH(x)	7.80	8.71	9.7	5.3
F106δCH2-P109γCH2	6.46	7.41	11.2	5.8
F106δCH2-L111βCH2	9.82	9.60	9.6	5.2
F106δCH2-L111(δCH3)2	9.57	10.52	10.2	4.4
F106δCH2-V114βCH	6.69	6.91	7.1	3.7
F106δCH2-V114(γCH3)2	4.97	5.47	11.2	4.9
F106ξCH2-K105βCH2	8.62	8.75	8.6	4.2
F106ξCH2-K105γCH2	8.60	9.41	10.5	5.1
F106ξCH2-K107βCH2	8.42	7.83	8.4	4.0
F106ξCH2-K107γCH2	7.67	6.47	9.5	4.1
F106ξCH2-R108βCH2	9.92	9.15	11.9	6.5
F106ξCH2-P109βCH(x)	8.00	8.25	11.3	6.9
F106ξCH2-P109βCH'(p)	9.13	9.09	9.9	5.5
F106ξCH2-P109γCH2	7.26	6.96	10.5	5.1
F106ξCH2-L111(δCH3)2	9.03	11.09	11.9	5.1
F106ξCH2-V114βCH	5.40	5.86	7.0	3.6
F106ξCH2-V114(γCH3)2	4.10	4.10	9.8	4.0
F106ζCH-K105βCH2	9.57	9.68	8.2	4.2
F106ζCH-K105γCH2	9.45	10.24	10.1	5.1
F106ζCH-K107βCH2	9.17	8.56	8.0	4.0
F106ζCH-K107γCH2	8.41	7.10	9.1	4.1
F106ζCH-R108βCH2	10.75	9.79	11.5	6.5

F106ζCH-P109βCH(x)	8.30	8.27	10.9	6.9
F106ζCH-P109βCH'(p)	9.51	9.11	9.5	5.5
F106ζCH-P109γCH2	7.78	7.02	9.1	5.1
F106ζCH-L111(δCH3)2	8.19	10.07	11.5	5.1
F106ζCH-V114βCH	5.19	5.72	6.6	3.6
F106ζCH-V114(γCH3)2	4.19	3.91	9.4	4.0
R108βCH2-P109δCH(m)	3.53	3.56	5.7	3.7
R108βCH2-P109δCH(m')	4.74	4.57	6.1	4.1
P109δCH(m)-V114βCH	6.82	6.88	7.9	5.9
P109δCH'(m')-V114βCH	5.26	5.41	6.4	4.4
P110βCH(x)-L111βCH2	4.40	4.34	5.5	3.5
P110γCH2-L111(δCH3)2	8.14	8.19	8.7	4.3
L111(δCH3)2-R112δCH2	9.01	7.02	12.0	6.6
R112βCH2-V114(γCH3)2	7.89	8.22	8.5	4.1
R113δCH2-V114(γCH2)3	7.81	7.54	11.8	6.4
V114(γCH3)2-R115βCH2	6.20	6.08	7.8	4.4
V114(γCH3)2-R115δCH2	7.14	6.67	10.9	6.5
P109βCH'(p)-P110δCH(m)	3.42	3.91	3.6	3.0
P109βCH'(p)-P110δCH'(m')	2.95	2.64	3.3	2.7
P110βCH'(p)-P109δCH(m)	8.15	8.40	7.5	5.5
P110βCH(x)-P109δCH'(m')	7.04	6.94	7.0	5.0
P110γCH2-P109δCH(m)	8.05	7.79	8.0	5.0
P110γCH2-P109δCH(m')	7.09	6.90	8.0	5.0
K105αCH-F106αCH	4.62	4.72	5.0	4.0
F106αCH-K107αCH	4.44	4.65	5.0	4.0
F106αCH-R108αCH	6.42	6.26	7.0	5.0
K107αCH-F108αCH	4.72	4.51	6.4	4.4
R108αCH-P109αCH	4.41	4.65	5.2	4.2
R108αCH-P110αCH	6.11	6.15	5.9	3.9
P110αCH-L111αCH	3.99	4.13	4.9	3.9
R113αCH-V114αCH	4.84	4.82	6.0	4.0
V114αCH-R115αCH	4.64	4.66	4.2	3.6
G104NH-K105NH	2.36	2.36	2.7	2.3
G104NH-F106NH	2.58	2.33	2.9	2.5
G104NH-K107NH	3.34	3.24	4.0	3.4
K105NH-F106NH	2.73	2.66	3.1	2.7
K105NH-K107NH	4.47	4.29	4.2	3.6
K105NH-R108NH	4.84	5.23	4.8	3.8
F106NH-K107NH	2.80	2.59	2.9	2.5
F106NH-R108NH	3.96	4.03	4.8	3.8
K107NH-R108NH	2.61	2.88	3.6	3.0
L111NH-R112NH	2.80	2.63	2.9	2.5

R112NH-R113NH	2.69	2.81	3.1	2.7
R112NH-R115NH	4.39	4.21	3.7	3.1
R113NH-V114NH	2.24	2.30	3.7	3.1
R113NH-R115NH	3.81	3.44	2.8	2.4
V114NH-R115NH	2.76	2.65	4.0	3.4
R115NH-Cterm NH	3.26	3.76	6.7	4.7
R115NH-Cterm NH'	4.43	4.63	6.7	4.7
G104αCH2-NH	2.59	2.59	4.1	3.5
G104αCH2-K105NH	2.85	2.85	4.7	3.1
G104αCH2-F106NH	4.48	4.28	6.1	4.1
G104αCH2-R108NH	4.94	5.82	6.4	4.4
K105αCH-NH	2.61	2.58	4.1	3.5
K105αCH-F106NH	3.47	3.41	3.3	2.7
K105αCH-K107NH	4.82	4.45	4.8	3.8
K105αCH-R108NH	3.82	3.78	4.8	3.8
F106αCH-NH	2.74	2.78	4.1	3.5
F106αCH-K107NH	3.51	3.51	3.6	3.0
K107αCH-NH	2.62	2.73	3.7	3.1
K107αCH-R108NH	3.33	2.84	3.7	3.1
R108αCH-NH	2.59	2.67	4.5	3.5
P110αCH-L111NH	2.22	2.33	3.1	2.7
P110αCH-R112NH	4.38	4.44	4.5	3.5
L111αCH-NH	2.74	2.70	3.3	2.7
L111αCH-R112NH	3.28	3.37	3.8	3.2
L111αCH-R113NH	4.01	4.00	3.8	3.2
R112αCH-NH	2.64	2.63	3.7	3.1
R112αCH-R113NH	3.51	3.31	3.4	2.8
R112αCH-R115NH	3.29	2.71	4.5	3.5
R113αCH-NH	2.68	2.78	3.1	2.7
R113αCH-V114NH	3.31	3.42	2.9	2.5
R113αCH-R115NH	4.18	4.65	4.5	3.5
V114αCH-NH	2.71	2.68	3.7	3.1
V114αCH-R113NH	4.88	4.83	2.9	2.5
V114αCH-R115NH	3.47	3.38	2.9	2.5
R115αCH-NH	2.69	2.77	3.7	3.1

Table VII-1. $T_{1\mathrm{OBS}i}$ measurements for various protons, *i*, on the TnI peptide as a function of molar equivalents TnC.Gd(III)$_4$ to TnI peptide.

	T1OBS(s)	T1OBS(s)	T1OBS(s)	T1OBS(s)	T1OBS(s)	T1OBS(s)	T1OBS(s)
[TnC.Gd4]/[TnI peptide]	0.0000	0.0006	0.0011	0.0021	0.0034	0.0047	0.0073
N-Ac CH3	0.958±0.033	0.849±0.005	0.830±0.004	0.795±0.004	0.775±0.008	0.736±0.008	0.693±0.011
G104αCH2	0.488±0.012	0.463±0.008	0.448±0.009	0.446±0.008	0.427±0.010	0.413±0.009	0.382±0.009
K105αCH	0.668±0.040	0.650±0.020	0.635±0.005	0.612±0.012	0.573±0.012	0.542±0.021	0.463±0.018
K105γCH2	0.337±0.010	0.331±0.010	0.327±0.005	0.324±0.010	0.320±0.005	0.317±0.011	0.316±0.012
K105ξCH2	0.494±0.009	0.473±0.006	0.463±0.002	0.456±0.007	0.435±0.010	0.426±0.009	0.396±0.007
F106αCH	0.533±0.016	0.499±0.023	0.484±0.009	0.447±0.009	0.418±0.024	0.401±0.009	
F106βCH(m)	0.427±0.006	0.423±0.006	0.414±0.013	0.397±0.004	0.386±0.012	0.353±0.004	0.332±0.013
F106δCH2	0.904±0.014	0.864±0.007	0.664±0.016	0.526±0.008	0.519±0.012	0.499±0.033	0.435±0.008
F106ξCH2ςCH	1.333±0.015	1.244±0.039	1.197±0.038	1.108±0.016	1.015±0.019	0.949±0.021	0.885±0.016
K107γCH2	0.347±0.008	0.344±0.007	0.341±0.009	0.337±0.011	0.033±0.007	0.326±0.013	0.325±0.012
R108αCH	0.509±0.010	0.500±0.009	0.487±0.009	0.479±0.006	0.467±0.016	0.453±0.014	
P109αCH	0.507±0.019	0.495±0.028	0.482±0.026	0.434±0.010	0.371±0.019	0.350±0.017	
P109βCH'(p)	0.509±0.008	0.500±0.008	0.490±0.008	0.479±0.002	0.475±0.008	0.453±0.009	0.445±0.004
P109γCH2	0.621±0.012	0.618±0.005	0.614±0.010	0.610±0.008	0.602±0.012	0.580±0.009	0.577±0.012
P109δCH(m)	0.533±0.004	0.519±0.005	0.511±0.005	0.504±0.004	0.500±0.008	0.493±0.006	0.473±0.004
P109δCH'(m')	0.487±0.010	0.475±0.004	0.468±0.013	0.456±0.007	0.440±0.015	0.434±0.010	0.387±0.011
P110αCH	0.739±0.011	0.723±0.009	0.687±0.014	0.623±0.014	0.568±0.015	0.539±0.019	0.452±0.017
P110βCH'(p)	0.548±0.013	0.537±0.010	0.522±0.014	0.506±0.006	0.496±0.012	0.485±0.009	0.466±0.014
P110γCH2	0.622±0.009	0.593±0.004	0.585±0.009	0.576±0.006	0.564±0.010	0.544±0.020	0.532±0.016
P110δCH(m)	0.533±0.004	0.519±0.005	0.511±0.005	0.504±0.004	0.500±0.008	0.493±0.006	0.473±0.004
P110δCH'(m')	0.514±0.004	0.510±0.010	0.472±0.019	0.469±0.006	0.461±0.024	0.438±0.006	0.405±0.014
L111(δCH3)2	0.368±0.008	0.365±0.009	0.362±0.010	0.358±0.007	0.356±0.010	0.347±0.006	0.339±0.013
V114αCH	0.674±0.010	0.652±0.010	0.629±0.012	0.610±0.005	0.586±0.009	0.567±0.013	0.529±0.014
V114(γCH3)2	0.356±0.009	0.353±0.008	0.349±0.009	0.346±0.008	0.340±0.009	0.337±0.009	0.325±0.012
C-term NH	0.518±0.017	0.504±0.011	0.487±0.013	0.473±0.001	0.456±0.005	0.437±0.009	0.428±0.010

Table VII-2. T_{2OBSi} measurements for various protons, *i*, on the TnI peptide as a function of molar equivalents TnC.Gd(III)$_4$ to TnI peptide.

	T2OBS(s)	T2OBS(s)	T2OBS(s)	T2OBS(s)	T2OBS(s)	T2OBS(s)	T2OBS(s)
[TnC.Gd4]/[TnI peptide]	0.0000	0.0006	0.0011	0.0021	0.0034	0.0047	0.0073
N-Ac CH3	0.414±0.048	0.201±0.018	0.172±0.017	0.111±0.009	0.100±0.006	0.081±0.002	0.056±0.002
G104αCH2	0.140±0.009	0.110±0.010	0.093±0.010	0.075±0.005	0.065±0.004	0.053±0.003	0.041±0.002
K105αCH	0.140±0.010	0.111±0.009	0.104±0.011	0.088±0.012	0.083±0.003	0.060±0.002	0.053±0.001
K105γCH2	0.157±0.010	0.123±0.009	0.108±0.007	0.090±0.005	0.072±0.003	0.062±0.002	0.051±0.002
K105ξCH2	0.156±0.010	0.112±0.004	0.094±0.003	0.072±0.005	0.063±0.001	0.053±0.001	0.043±0.001
F106αCH	0.128±0.027	0.112±0.002	0.091±0.010	0.081±0.027	0.070±0.010	0.062±0.002	0.055±0.006
F106βCH(m)	0.103±0.012	0.079±0.004	0.073±0.002	0.055±0.001	0.047±0.001	0.042±0.002	0.031±0.001
F106δCH2	0.353±0.016	0.159±0.003	0.117±0.002	0.075±0.003	0.064±0.001	0.050±0.003	0.036±0.001
F106ξCH2ςCH	0.392±0.010	0.177±0.001	0.121±0.003	0.083±0.002	0.070±0.002	0.047±0.001	0.037±0.001
K107γCH2	0.139±0.011	0.107±0.009	0.096±0.003	0.080±0.002	0.071±0.003	0.050±0.004	0.045±0.002
R108αCH	0.091±0.011	0.082±0.009	0.069±0.010	0.059±0.002	0.054±0.003	0.047±0.003	0.041±0.001
P109αCH	0.152±0.016	0.085±0.014	0.081±0.011	0.074±0.003	0.064±0.002	0.052±0.001	0.043±0.004
P109βCH'(p)	0.119±0.004	0.091±0.006	0.079±0.003	0.063±0.002	0.059±0.004	0.045±0.003	0.040±0.003
P109γCH2	0.126±0.009	0.086±0.009	0.078±0.009	0.068±0.006	0.050±0.006	0.044±0.004	
P109δCH(m)	0.128±0.003	0.122±0.008	0.114±0.007	0.094±0.006	0.077±0.003	0.064±0.002	0.060±0.001
P109δCH'(m')	0.073±0.009	0.061±0.001	0.054±0.001	0.043±0.003	0.039±0.001	0.035±0.001	
P110αCH	0.125±0.019	0.109±0.007	0.094±0.006	0.074±0.003	0.071±0.001	0.056±0.002	0.048±0.003
P110βCH'(p)	0.144±0.011	0.112±0.007	0.102±0.005	0.088±0.003	0.076±0.006	0.056±0.003	0.055±0.003
P110γCH2	0.119±0.009	0.106±0.006	0.098±0.003	0.078±0.004	0.073±0.001	0.062±0.003	0.048±0.001
P110δCH(m)	0.128±0.003	0.122±0.008	0.114±0.007	0.094±0.006	0.077±0.003	0.064±0.002	0.060±0.001
P110δCH'(m')	0.065±0.006	0.058±0.001	0.052±0.002	0.046±0.001	0.041±0.002	0.039±0.001	0.031±0.002
L111(δCH3)2	0.203±0.004	0.145±0.007	0.122±0.006	0.093±0.003	0.083±0.003	0.065±0.004	0.053±0.002
V114αCH	0.140±0.016	0.099±0.013	0.090±0.010	0.077±0.015	0.068±0.002	0.060±0.003	0.058±0.003
V114(γCH3)2	0.183±0.012	0.136±0.008	0.125±0.014	0.090±0.003	0.077±0.003	0.064±0.002	0.051±0.002
C-term NH	0.203±0.014	0.119±0.007	0.100±0.006	0.068±0.005	0.054±0.002	0.045±0.001	0.034±0.001

Table VII-3. T_{1OBSi} measurements for various protons, *i*, on the TnI peptide as a function of molar equivalents TnC.La(III)$_4$ to TnI peptide.

	T1OBS(s)	T1OBS(s)	T1OBS(s)	T1OBS(s)
[TnC.La4]/[TnI peptide]	0.0000	0.0035	0.0072	0.0108
N-Ac CH3	0.918±0.006	0.918±0.006	0.935±0.009	0.929±0.004
G104αCH2	0.490±0.007	0.489±0.009	0.485±0.008	0.473±0.012
K105αCH	0.699±0.011	0.653±0.005	0.632±0.009	0.596±0.021
K105γCH2	0.337±0.007	0.332±0.006	0.337±0.007	0.337±0.007
K105ξCH2	0.480±0.006	0.478±0.007	0.478±0.008	0.477±0.007
F106αCH	0.552±0.009	0.536±0.012	0.507±0.025	
F106βCH(m)	0.419±0.005	0.410±0.007	0.398±0.004	0.394±0.012
F106δCH2	0.843±0.019	0.885±0.034	0.920±0.029	0.926±0.028
F106ξCH2ςCH	1.298±0.011	1.247±0.010	1.224±0.015	1.208±0.015
K107γCH2	0.345±0.009	0.343±0.007	0.344±0.007	0.345±0.008
R108αCH	0.500±0.013	0.492±0.012	0.496±0.015	0.484±0.013
P109αCH	0.505±0.020	0.497±0.010	0.455±0.015	0.443±0.017
P109βCH'(p)	0.510±0.012	0.496±0.006	0.497±0.015	0.476±0.008
P109γCH2	0.628±0.017	0.617±0.009	0.602±0.010	0.605±0.007
P109δCH(m)	0.492±0.007	0.484±0.007	0.482±0.007	0.477±0.006
P109δCH'(m')	0.496±0.012	0.490±0.013	0.495±0.020	0.485±0.016
P110αCH	0.734±0.013	0.693±0.020	0.703±0.006	0.635±0.051
P110βCH'(p)	0.531±0.006	0.534±0.008	0.522±0.009	0.523±0.007
P110γCH2	0.605±0.008	0.600±0.006	0.607±0.012	0.607±0.010
P110δCH(m)	0.492±0.007	0.484±0.007	0.482±0.007	0.477±0.006
P110δCH'(m')	0.501±0.015	0.495±0.012	0.496±0.015	0.493±0.011
L111(δCH3)2	0.369±0.006	0.369±0.006	0.370±0.009	0.369±0.008
V114αCH	0.691±0.017	0.669±0.014	0.653±0.011	0.640±0.005
V114(γCH3)2	0.357±0.007	0.354±0.007	0.356±0.008	0.354±0.008
C-term NH	0.338±0.004	0.309±0.006	0.300±0.012	0.308±0.010

Table VII-4. T_{2OBSi} measurements for various protons, *i*, on the TnI peptide as a function of molar equivalents TnC.La(III)$_4$ to TnI peptide.

	T2OBS(s)	T2OBS(s)	T2OBS(s)	T2OBS(s)
[TnC.La4]/[TnI peptide]	0.0000	0.0035	0.0072	0.0108
N-Ac CH3	0.419±0.008	0.382±0.007	0.375±0.040	0.360±0.040
G104αCH2	0.166±0.006	0.155±0.014	0.136±0.008	0.131±0.010
K105αCH	0.236±0.017	0.186±0.020	0.135±0.009	0.144±0.011
K105γCH2	0.162±0.005	0.141±0.014	0.132±0.010	0.137±0.010
K105ξCH2	0.158±0.013	0.148±0.010	0.150±0.005	0.162±0.004
F106αCH	0.220±0.025	0.199±0.012	0.157±0.038	0.116±0.007
F106βCH(m)	0.103±0.004	0.098±0.001	0.093±0.010	0.084±0.005
F106δCH2	0.297±0.013	0.299±0.009	0.268±0.009	0.255±0.004
F106ξCH2ςCH	0.352±0.023	0.313±0.015	0.292±0.010	0.281±0.016
K107γCH2	0.147±0.006	0.138±0.014	0.107±0.008	0.106±0.007
R108αCH	0.123±0.011	0.121±0.009	0.079±0.005	0.074±0.015
P109αCH	0.227±0.032	0.165±0.020	0.105±0.017	0.218±0.023
P109βCH'(p)	0.119±0.006	0.102±0.009	0.095±0.005	0.081±0.004
P109γCH2	0.188±0.016	0.109±0.010	0.090±0.018	0.092±0.016
P109δCH(m)	0.131±0.004	0.121±0.009	0.103±0.010	0.108±0.009
P109δCH'(m')	0.063±0.006	0.054±0.004	0.053±0.004	0.045±0.004
P110αCH	0.186±0.007	0.155±0.017	0.135±0.008	0.103±0.006
P110βCH'(p)	0.137±0.005	0.131±0.006	0.122±0.006	0.118±0.006
P110γCH2	0.119±0.002	0.110±0.008	0.106±0.004	0.107±0.006
P110δCH(m)	0.131±0.004	0.121±0.009	0.103±0.010	0.108±0.009
P110δCH'(m')	0.065±0.002	0.055±0.006	0.053±0.004	0.049±0.005
L111(δCH3)2	0.210±0.006	0.170±0.014	0.152±0.010	0.154±0.008
V114αCH	0.189±0.007	0.193±0.018	0.153±0.006	0.188±0.006
V114(γCH3)2	0.177±0.007	0.170±0.010	0.159±0.007	0.146±0.004
C-term NH	0.156±0.003	0.123±0.004	0.108±0.003	0.109±0.003

Table VII-5. Calculated values of $1/T_{1OBSi}^{Gd}$, $1/T_{2OBSi}^{Gd}$, $1/T_{1OBSi}^{La}$, $1/T_{2OBSi}^{La}$, $1/T_{1Pi}$, $1/T_{2Pi}$, $1/T_{1Mi}$, R_{maxi} and R_{mini} for various protons, *i*, on the TnI peptide.

	1/T1OBSGd	1/T2OBSGd	1/T1OBSLa	1/T2OBSLa	1/T1p	1/T2p	1/T1M	Rmin (Å)	Rmax (Å)
N-Ac CH3	47.5	1979	0.0	34	47.5	1945	48.4	7.11	9.65
G104αCH2	70.9	2311	6.6	159	64.3	2152	66.0	6.76	9.16
K105αCH	88.5	1606	21.9	281	66.6	1325	68.4	6.72	9.11
K105γCH2	25.6	1812	0.0	107	25.6	1705	25.9	7.90	10.71
K105ξCH2	64.0	2246	0.4	0	63.6	2246	65.3	6.77	9.18
F106αCH	131.2	1425	22.3	376	108.9	1049	113.9	6.16	8.37
F106βCH(m)	96.9	2979	14.6	198	82.3	2781	85.1	6.48	8.78
F106δCH2	160.8	3289	0.0	57	160.8	3232	171.9	5.76	7.87
F106ξCH2ςCH	52.9	3329	5.2	66	47.7	3263	48.6	7.11	9.64
K107γCH2	28.4	2109	0.7	278	27.7	1831	28.0	7.79	10.57
R108αCH	49.5	1841	4.9	571	44.6	1270	45.4	7.19	9.75
P109αCH	206.0	2033	28.2	111	177.8	1922	191.4	5.66	7.67
P109βCH'(p)	39.2	2264	11.5	347	27.7	1917	28.0	7.79	10.57
P109γCH2	18.7	3026	6.1	253	12.6	2773	12.7	8.89	12.06
P109δCH(m)	26.0	1365	5.5	175	20.5	1190	20.7	8.19	11.11
P109δCH'(m')	67.5	3141	3.2	536	64.3	2605	66.0	6.76	9.16
P110αCH	118.7	1777	17.0	387	101.7	1390	106.0	6.24	8.47
P110βCH'(p)	43.0	1653	3.6	113	39.4	1540	46.9	7.15	9.70
P110γCH2	34.4	1673	0.0	88	34.4	1585	34.9	7.51	10.19
P110δCH(m)	26.0	1365	5.5	175	20.5	1190	20.7	8.19	11.11
P110δCH'(m')	43.0	2202	2.5	435	40.5	1767	41.2	7.31	9.91
L111(δCH3)2	31.6	1875	0.0	163	31.6	1712	32.0	7.62	10.34
V114αCH	53.9	1321	10.6	40	43.3	1281	44.1	7.23	9.80
V114(γCH3)2	35.4	1928	1.5	111	33.9	1917	34.4	7.53	10.22
C-term NH	57.0	3294	26.5	260	30.5	3034	30.8	7.67	10.41

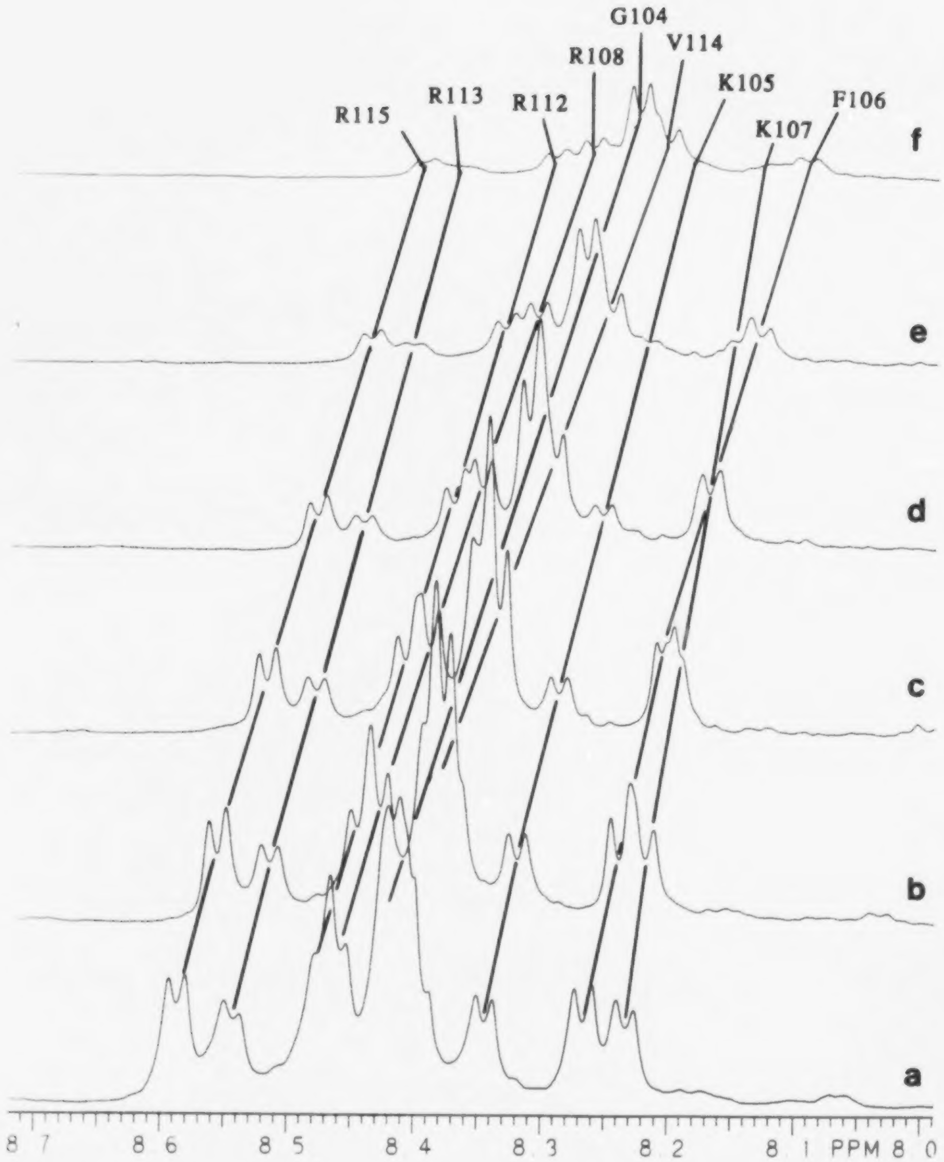

Figure VIII-1A. 500 MHz ^{1}H NMR spectra of the G110-TnI peptide backbone amide resonances as a function of temperature: 0.0 molar equivalents TnC.Ca(II)$_4$. **a.** 5°C; **b.** 10°C; **c.** 15°C; **d.** 20°C; **e.** 25°C; **f.** 30°C

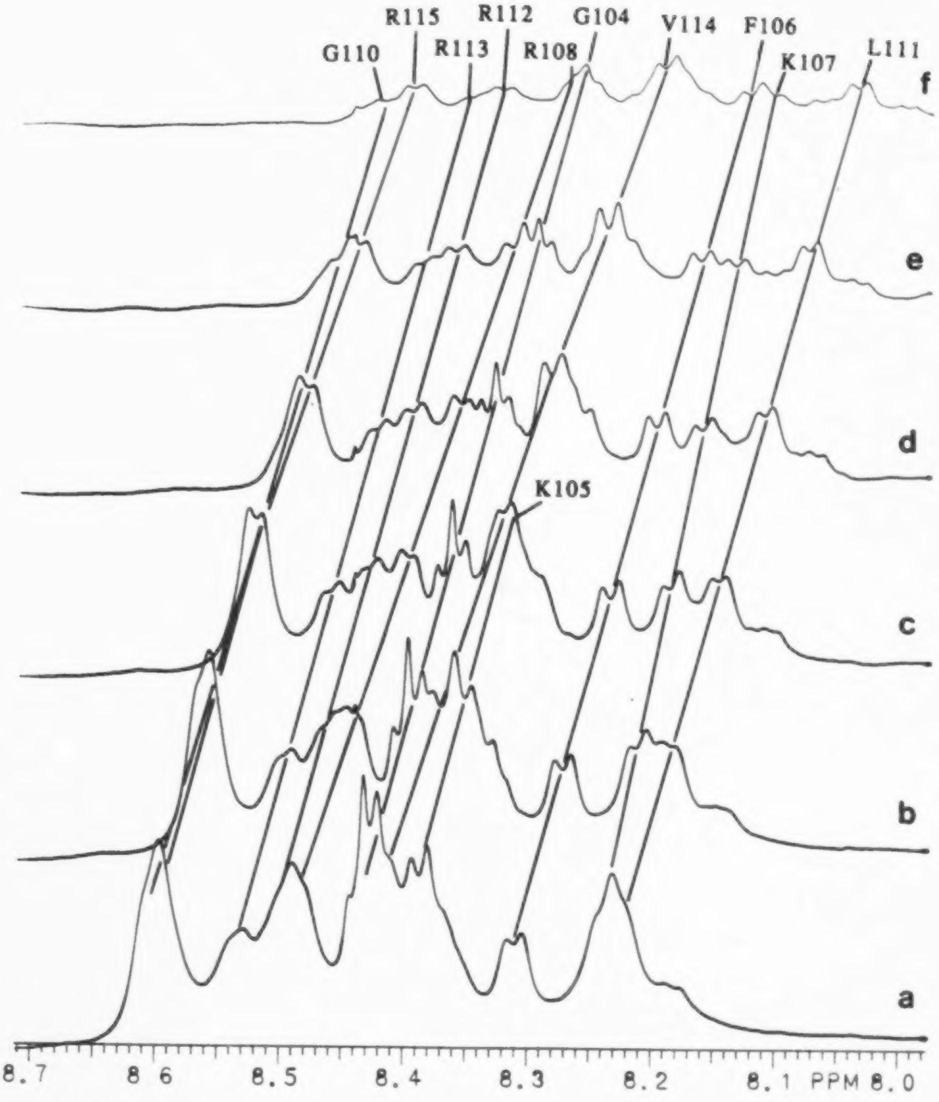

Figure VIII-1B. 500 MHz ^{1}H NMR spectra of the G110-TnI peptide backbone amide resonances as a function of temperature: 0.1 molar equivalents TnC.Ca(II)$_4$. **a.** 5°C; **b.** 10°C; **c.** 15°C; **d.** 20°C; **e.** 25°C; **f.** 30°C

Table VIII-1. Normalization tables for exchangeable backbone amide resonances on the G110-TnI peptide. **A.** Amide versus nonexchangeable resonance; **B.** Amide versus amide resonance. The intensities (*Na*) of the exchangeable proton peaks were integrated in a one-dimensional spectrum, and the intensity of these peaks were normalized against the integrated intensity of the V114αCH peak. The normalization factor (2*NaNb*)/(*Na*+*Nb*) was then calculated for variable values of *Nb*.

A.	Na	Nb=1	Nb=2	Nb=3
G104	0.75	0.86	1.09	1.20
K105	1.00	1.00	1.32	1.50
F106	0.84	0.91	1.18	1.31
K107	0.92	0.96	1.26	1.41
R108	1.00	1.00	1.32	1.50
G110	1.00	1.00	1.32	1.50
L111	0.92	0.96	1.26	1.41
R112	1.00	1.00	1.32	1.50
R113	1.00	1.00	1.32	1.50
V114	1.00	1.00	1.32	1.50
R115	1.00	1.00	1.32	1.50

B.	Na	G104	K105	F106	K107	R108	G110	L111	R112	R113	V114	R115
G104	0.75	-	0.86	0.79	0.83	0.86	0.86	0.83	0.86	0.86	0.86	0.86
K105	1.00	0.86	-	0.91	0.96	1.00	1.00	0.96	1.00	1.00	1.00	1.00
F106	0.84	0.79	0.91	-	0.88	0.91	0.91	0.88	0.91	0.91	0.91	0.91
K107	0.92	0.83	0.96	0.88	-	0.96	0.96	0.92	0.96	0.96	0.96	0.96
R108	1.00	0.86	1.00	0.91	0.96	-	1.00	0.96	1.00	1.00	1.00	1.00
G110	1.00	0.86	1.00	0.91	0.96	1.00	-	0.96	1.00	1.00	1.00	1.00
L111	0.92	0.83	0.96	0.88	0.92	0.96	0.96	-	0.96	0.96	0.96	0.96
R112	1.00	0.86	1.00	0.91	0.96	1.00	1.00	0.96	-	1.00	1.00	1.00
R113	1.00	0.86	1.00	0.91	0.96	1.00	1.00	0.96	1.00	-	1.00	1.00
V114	1.00	0.86	1.00	0.91	0.96	1.00	1.00	0.96	1.00	1.00	-	1.00
R115	1.00	0.86	1.00	0.91	0.96	1.00	1.00	0.96	1.00	1.00	1.00	-

Table VIII-2. Table of TRNOE cross-peak intensities for the G110-TnI peptide in the presence of 0.1 molar equivalents TnC.Ca(II)$_4$. Included in the table are the measured TRNOE intensities, the corrected and normalized TRNOE intensities, and the r_{ij}s calculated from these corrected and normalized values.

spin system	TRNOE measured	TRNOE normalized	rij calculated (Å)
K105αCH-βCH2	4.280	3.242	2.4
K105αCH-γCH2	1.210	0.917	3.1
K105βCH2-γCH2	3.670	1.835	2.7
K105γCH2-δCH2	3.670	1.835	2.7
K105δCH2-ξCH2	2.850	1.425	2.8
K105βCH2-NH	3.400	2.575	2.5
K105γCH2-ξCH2	1.330	0.665	3.2
K105γCH2-NH	1.230	0.932	3.0
F106αCH-βCH(m)	0.343	0.343	3.7
F106αCH-βCH'(x)	0.462	0.462	3.5
F106αCH-δCH2	0.308	0.233	3.9
F106αCH-ξCH2	0.055	0.037	5.5
F106αCH-ςCH2	-	0.037	5.5
F106βCH(m)-βCH'(x)	1.180	1.180	2.9
F106βCH'(x)-NH	0.582	0.640	3.3
F106βCH(m)-NH	0.471	0.518	3.4
F106βCH(m)-δCH2	2.460	1.864	2.7
F106βCH(m)-ξCH2	0.984	0.656	3.2
F106βCH(m)-ςCH	-	0.656	3.2
F106βCH'(p)-δCH2	2.810	2.129	2.6
F106βCH'(p)-ξCH2	1.000	0.667	3.2
F106βCH'(p)-ςCH	-	0.667	3.2
F106NH-δCH2	0.696	0.590	3.3
F106NH-ξCH2	0.284	0.217	4.0
F106NH-ςCH	-	0.217	4.0
K107αCH-βCH2	5.000	3.788	2.4
K107αCH-γCH2	1.240	0.939	3.0
K107βCH2-γCH2	11.000	5.500	2.2
K107βCH2-NH	2.100	1.667	2.7
K107δCH2-γCH2	4.070	2.035	2.6
K107δCH2-ξCH2	4.960	2.480	2.5
K107γCH2-ξCH2	2.240	1.120	2.9
K107γCH2-NH	1.090	0.865	3.1
R108αCH-βCH2	0.891	0.675	3.2
R108αCH-γCH2	0.263	0.199	4.0

R108βCH2-NH	3.220	2.439	2.6
R108γCH2-δCH2	3.550	1.775	2.7
R108δCH2-NH	0.611	0.463	3.5
P109αCH-βCH(x)	0.729	0.729	3.2
P109αCH-βCH'(p)	0.796	0.796	3.1
P109αCH-γCH2	0.560	0.424	3.5
P109βCH(x)-βCH'(p)	3.560	3.560	2.4
P109βCH(x)-δCH'(m')	0.438	0.438	3.5
P109βCH(x)-δCH(m)	0.454	0.454	3.5
P109βCH'(p)-δCH(m)	0.368	0.368	3.6
P109βCH'(p)-δCH'(m')	0.220	0.220	4.0
P109βCH'(p)-γCH2	2.990	2.265	2.6
P109γCH2-δCH(m)	1.050	0.795	3.1
P109γCH2-δCH'(m')	0.834	0.632	3.3
P109δCH(m)-δCH'(m')	0.457	0.457	3.5
L111αCH-βCH2	4.330	3.280	2.4
L111αCH-(δCH3)2	3.880	2.269	2.6
L111βCH2-(δCH3)2	10.300	3.433	2.4
L111γCH-(δCH3)2	10.300	6.023	2.2
L111βCH2-NH	1.900	1.508	2.8
L111(δCH3)2-NH	1.200	0.750	3.2
R112αCH-βCH2	2.290	1.735	2.7
R112αCH-δCH2	0.743	0.563	3.3
R112γCH2-δCH2	3.550	1.775	2.7
R112βCH2-NH	3.650	2.765	2.5
R112δCH2-NH	0.289	0.219	4.0
R113αCH-βCH2	2.290	1.735	2.7
R113αCH-δCH2	0.743	0.563	3.3
R113γCH2-δCH2	3.550	1.775	2.7
R113βCH2-NH	3.650	2.765	2.5
R113δCH2-NH	0.289	0.219	4.0
V114αCH-βCH	1.970	1.970	2.7
V114αCH-(γCH3)2	5.190	3.036	2.5
V114βCH-(γCH3)2	11.200	6.550	2.1
V114βCH-NH	1.780	1.780	2.7
V114(γCH3)2-NH	2.900	1.692	2.7
R115αCH-βCH2	3.890	2.947	2.5
R115αCH-δCH2	0.743	0.563	3.3
R115γCH2-δCH2	3.550	1.775	2.7
R115βCH2-NH	2.230	1.689	2.7
R115δCH2-NH	0.461	0.349	3.6
C-term NH-NH'	2.460	2.460	2.5
N-Acetyl CH3-G104αCH2	0.585	0.244	3.9
N-Acetyl CH3-G104NH	1.780	1.483	2.8
G104αCH2-K105βCH2	1.210	0.605	3.3

G104αCH2-K105γCH2	0.360	0.180	4.1
G104αCH2-F106δCH2	0.078	0.039	5.4
G104αCH2-F106ξCH2	0.085	0.035	5.5
G104αCH2-F106ςCH	-	0.035	5.5
G104αCH2-K107γCH2	0.112	0.056	5.1
G104NH-K107γCH2	0.235	0.216	4.0
K105αCH-F106βCH(x)	0.248	0.248	3.9
K105αCH-F106βCH'(p)	0.229	0.229	3.9
K105βCH2-F106NH	1.520	1.288	2.9
K105γCH2-F106NH	0.359	0.304	3.7
K105γCH2-K107NH	0.092	0.073	4.9
K105NH-F106δCH2	0.403	0.305	3.7
K105NH-F106ξCH2	0.208	0.139	4.3
K105NH-F106ςCH	-	0.139	4.3
K105NH-K107γCH2	0.284	0.215	4.0
F106αCH-R108βCH2	0.617	0.467	3.5
F106βCH(x)-K107NH	0.459	0.478	3.4
F106βCH'(p)-K107NH	0.423	0.441	3.4
F106βCH(x)-K107αCH	0.205	0.205	4.0
F106δCH2-K107NH	0.613	0.487	3.4
F106ξCH2-K107NH	0.262	0.186	4.1
F106ςCH2-K107NH	-	0.186	4.1
F106δCH2-R108NH	0.236	0.179	4.1
F106ξCH2-R108NH	0.182	0.121	4.4
F106ςCH2-R108NH	-	0.121	4.4
F106NH-K107γCH2	0.209	0.177	4.1
F106NH-V114(γCH3)2	0.250	0.170	4.2
K107γCH2-R108NH	0.544	0.412	3.5
G110αCH2-L111βCH2	0.387	0.293	3.8
G110αCH2-L111(δCH3)2	0.801	0.468	3.5
P109βCH(x)-G110NH	0.437	0.437	3.5
P109βCH'(p)-G110NH	0.380	0.380	3.6
P109βCH(x)-L111αCH	0.419	0.419	3.5
P109βCH'(p)-L111αCH	0.374	0.374	3.6
P109γCH2-L111αCH	0.941	0.713	3.2
L111(δCH3)2-R112NH	1.230	0.719	3.2
R112βCH2-R113NH	1.110	0.841	3.1
R112βCH2-R115NH	0.945	0.716	3.2
R112βCH2-Cterm NH	0.437	0.331	3.7
R112βCH2-Cterm NH'	-	0.331	3.7
R113βCH2-V114αCH	1.425	0.109	3.0
R113βCH2-V114NH	0.885	0.670	3.2
R113βCH2-R115NH	0.945	0.716	3.2
R113δCH2-V114αCH	0.144	0.109	4.5
R113δCH2-V114NH	0.227	0.172	4.1
R113NH-V114(γCH3)2	0.529	0.309	3.7

V114αCH-R115βCH2	1.425	1.080	3.0
V114αCH-R115δCH2	0.144	0.109	4.5
V114αCH-Cterm NH	0.068	0.068	4.9
V114αCH-Cterm NH'	-	0.068	4.9
V114βCH-R115NH	1.360	1.030	3.0
V114βCH-Cterm NH	0.805	0.610	3.3
V114βCH-Cterm NH'	-	0.610	3.3
V114(γCH3)2-R115αCH	1.370	0.810	3.1
V114(γCH3)2-R115NH	1.780	1.041	3.0
V114(γCH3)2-Cterm NH	0.402	0.235	3.9
V114(γCH3)2-Cterm NH'	-	0.235	3.9
V114NH-R115βCH2	0.885	0.670	3.2
V114NH-R115δCH2	0.227	0.172	4.1
R115αCH-Cterm NH	0.706	0.706	3.2
R115αCH-Cterm NH'	0.891	0.891	3.1
R115βCH2-Cterm NH	0.925	0.701	3.2
R115βCH2-Cterm NH'	-	0.701	3.2

F106δCH2-K105βCH2	0.828	0.414	3.5
F106δCH2-K105δCH2	0.828	0.414	3.5
F106δCH2-K107βCH2	0.828	0.414	3.5
F106δCH2-K107γCH2	0.828	0.414	3.5
F106δCH2-R108βCH2	0.828	0.414	3.5
F106δCH2-P109βCH(x)	0.207	0.156	4.2
F106δCH2-P109βCH'(p)	0.133	0.100	4.6
F106δCH2-P109γCH2	0.402	0.201	4.0
F106δCH2-V114βCH	0.402	0.305	3.7
F106δCH2-V114(γCH3)2	1.650	0.550	3.4
F106ξCH2-K105βCH2	2.280	0.950	3.0
F106ξCH2-K105γCH2	0.911	0.413	3.5
F106ξCH2-K105δCH2	2.280	0.950	3.0
F106ξCH2-K105ξCH2	0.507	0.211	4.0
F106ξCH2-R108βCH2	2.280	0.950	3.0
F106ξCH2-P109βCH(x)	0.298	0.199	4.0
F106ξCH2-P109βCH'(p)	0.248	0.165	4.2
F106ξCH2-P109γCH2	0.395	0.165	4.2
F106ξCH2-V114βCH	0.395	0.263	3.8
F106ξCH2-V114(γCH3)2	2.390	0.598	3.3
F106ςCH-K105βCH2	-	0.950	3.0
F106ςCH-K105γCH2	-	0.413	3.5
F106ςCH-K105δCH2	-	0.950	3.0
F106ςCH-K105ξCH2	-	0.211	4.0
F106ςCH-R108βCH2	-	0.950	3.0
F106ςCH-P109βCH(x)	-	0.199	4.0
F106ςCH-P109βCH'(p)	-	0.165	4.2
F106ςCH-P109γCH2	-	0.165	4.2

F106ςCH-V114βCH	-	0.263	3.8
F106ςCH-V114(γCH3)2	-	0.598	3.3

F106βCH(m)-V114(γCH3)2	0.464	0.271	3.8
F106βCH'(p)-V114(γCH3)2	0.543	0.318	3.7
R108βCH2-P109δCH(m)	0.644	0.488	3.3
R108βCH2-P109δCH(m')	0.651	0.554	3.4
P109βCH(x)-V114(γCH3)2	1.100	0.643	3.3
P109δCH'(m')-V114(γCH3)2	0.362	0.212	4.0
L111(δCH3)2-R112βCH2	2.250	0.750	3.2
L111(δCH3)2-R112δCH2	0.543	0.181	4.1
R113βCH2-V114(γCH3)2	2.250	0.750	3.2
R113δCH2-V114βCH	0.176	0.133	4.3
R113δCH2-V114(γCH2)3	0.543	0.181	4.1
V114βCH-R115δCH2	0.176	0.133	4.3
V114(γCH3)2-R115βCH2	2.250	0.750	3.2
V114(γCH3)2-R115δCH2	0.543	0.181	4.1

G104αCH2-K105αCH	0.180	0.090	4.7
G110αCH2-L111αCH	0.252	0.148	4.3
R113αCH-V114αCH	0.146	0.146	4.3
V114αCH-R115αCH	0.187	0.187	4.1

K105NH-K107NH	0.339	0.353	3.6
K107NH-R108NH	0.476	0.500	3.4
G110NH-L111NH	0.205	0.214	4.0
R113NH-V114NH	0.337	0.337	3.7
V114NH-R115NH	0.341	0.341	3.7
R115NH-Cterm NH	0.171	0.171	4.1
R115NH-Cterm NH'	0.191	0.191	4.1

G104αCH2-NH	1.390	1.275	2.9
G104αCH2-K105NH	1.440	1.091	3.0
G104αCH2-F106NH	0.286	0.242	3.9
G104αCH2-K107NH	0.224	0.178	4.1
G104αCH2-R108NH	0.132	0.100	4.6
K105αCH-NH	0.826	0.826	3.1
K105αCH-F106NH	0.704	0.773	3.1
K105αCH-K107NH	0.142	0.148	4.3
F106αCH-NH	0.065	0.071	4.9
F106αCH-K105NH	0.053	0.053	5.1
F106αCH-K107NH	0.178	0.185	4.1
K107αCH-NH	0.278	0.290	3.8
K107αCH-G104NH	0.237	0.276	3.8
K107αCH-R108NH	0.485	0.485	3.4
P109αCH-G110NH	0.244	0.244	3.9

G110αCH2-NH	0.667	0.505	3.4
G110αCH2-L111NH	0.368	0.383	3.6
L111αCH-NH	0.142	0.148	4.3
L111αCH-R112NH	0.793	0.793	3.1
R112αCH-NH	0.793	0.793	3.1
R112αCH-R113NH	0.650	0.650	3.3
R113αCH-NH	0.650	0.650	3.3
R113αCH-V114NH	0.765	0.765	3.2
V114αCH-NH	0.439	0.439	3.5
V114αCH-R113NH	0.279	0.279	3.8
V114αCH-R115NH	1.540	1.540	2.8
R115αCH-NH	0.544	0.544	3.4

Table VIII-3. Summary of distance restraints used in the MD simulations. Included in the table are the calculated r_{ij}s from the corrected and normalized TRNOE cross-peak intensities, the incorporated error limits (±β), and the pseudoatom adjustments in r_{ij}^{U}.

spin system	rij ± β (Å)	Ψ-atom correction (Å)	rijU (Å)	rijL (Å)
K105αCH-βCH2	2.4±0.2		2.6	2.2
K105αCH-γCH2	3.1±0.3	0.6	4.0	2.8
K105βCH2-γCH2	2.7±0.2		2.9	2.5
K105γCH2-δCH2	2.7±0.2		2.9	2.5
K105δCH2-ξCH2	2.8±0.2		3.0	2.6
K105βCH2-NH	2.5±0.2	0.6	3.3	2.3
K105γCH2-ξCH2	3.2±0.3		3.5	2.9
K105γCH2-NH	3.0±0.3	1.0	4.3	2.7
F106αCH-βCH(m)	3.7±0.3		4.0	3.4
F106αCH-βCH'(x)	3.5±0.3		3.8	3.2
F106αCH-δCH2	3.9±0.3	2.0	6.2	3.6
F106αCH-ξCH2	5.5±1.0	2.0	8.5	4.5
F106αCH-ςCH2	5.5±1.0	2.0	8.5	4.5
F106βCH(m)-βCH'(x)	2.9±0.2		3.1	2.7
F106βCH'(x)-NH	3.3±0.3		3.6	3.0
F106βCH(m)-NH	3.4±0.3		3.7	3.1
F106βCH(m)-δCH2	2.7±0.2		2.9	2.5
F106βCH(m)-ξCH2	3.2±0.3		3.5	2.9
F106βCH(m)-ςCH	3.2±0.3		3.5	2.9
F106βCH'(x)-δCH2	2.6±0.2		2.8	2.4
F106βCH'(x)-ξCH2	3.2±0.3		3.5	2.9
F106βCH'(x)-ςCH	3.2±0.3		3.5	2.9
F106NH-δCH2	3.3±0.3	2.4	6.0	3.0
F106NH-ξCH2	4.0±0.5	2.4	6.9	3.5
F106NH-ςCH	4.0±0.5	1.0	5.5	3.5
K107αCH-βCH2	2.4±0.2		2.6	2.2
K107αCH-γCH2	3.0±0.3	0.6	3.9	2.7
K107βCH2-γCH2	2.2±0.2		2.4	2.0
K107βCH2-NH	2.7±0.2	0.6	3.5	2.5
K107δCH2-γCH2	2.6±0.2		2.8	2.4
K107δCH2-ξCH2	2.5±0.2		2.7	2.3
K107γCH2-ξCH2	2.9±0.2		3.1	2.7
K107γCH2-NH	3.1±0.3	1.0	4.4	2.8
R108αCH-βCH2	3.2±0.3		3.5	2.9
R108αCH-γCH2	4.0±0.5	0.6	5.1	3.5
R108βCH2-NH	2.6±0.2	0.6	3.4	2.4

R108γCH2-δCH2	2.7±0.2		2.9	2.5
R108δCH2-NH	3.5±0.3		3.8	3.2
P109αCH-βCH(x)	3.2±0.3		3.5	2.9
P109αCH-βCH'(p)	3.1±0.3		3.4	2.8
P109αCH-γCH2	3.5±0.3		3.8	3.2
P109βCH(x)-βCH'(p)	2.4±0.2		2.6	2.2
P109βCH(x)-δCH'(m')	3.5±0.3		3.8	3.2
P109βCH(x)-δCH(m)	3.5±0.3		3.8	3.2
P109βCH'(p)-δCH(m)	3.6±0.3		3.9	3.3
P109βCH'(p)-δCH'(m')	4.0±0.5		4.5	3.5
P109βCH'(p)-γCH2	2.6±0.2		2.8	2.4
P109γCH2-δCH(m)	3.1±0.3		3.4	2.8
P109γCH2-δCH'(m')	3.3±0.3		3.6	3.0
P109δCH(m)-δCH'(m')	3.5±0.3		3.8	3.2
L111αCH-βCH2	2.4±0.2		2.6	2.2
L111αCH-(δCH3)2	2.6±0.2	1.7	4.5	2.4
L111βCH2-(δCH3)2	2.4±0.2		2.6	2.2
L111γCH-(δCH3)2	2.2±0.2		2.4	2.0
L111βCH2-NH	2.8±0.2	0.6	3.6	2.6
L111(δCH3)2-NH	3.2±0.3		3.5	2.9
R112αCH-βCH2	2.7±0.2		2.9	2.5
R112αCH-δCH2	3.3±0.3	1.0	4.6	3.0
R112γCH2-δCH2	2.7±0.2		2.9	2.5
R112βCH2-NH	2.5±0.2	0.6	3.3	2.3
R112δCH2-NH	4.0±0.5		4.5	3.5
R113αCH-βCH2	2.7±0.2		2.9	2.5
R113αCH-δCH2	3.3±0.3	1.0	4.6	3.0
R113γCH2-δCH2	2.7±0.2		2.9	2.5
R113βCH2-NH	2.5±0.2	0.6	3.3	2.3
R113δCH2-NH	4.0±0.5		4.5	3.5
V114αCH-βCH	2.7±0.2		2.9	2.5
V114αCH-(γCH3)2	2.5±0.2	0.6	3.3	2.3
V114βCH-(γCH3)2	2.1±0.2		2.3	1.9
V114βCH-NH	2.7±0.2		2.9	2.5
V114(γCH3)2-NH	2.7±0.2	1.7	4.6	2.5
R115αCH-βCH2	2.5±0.2		2.7	2.3
R115αCH-δCH2	3.3±0.3	1.0	4.6	3.0
R115γCH2-δCH2	2.7±0.2		2.9	2.5
R115βCH2-NH	2.7±0.2	0.6	3.5	2.5
R115δCH2-NH	3.6±0.3		3.9	3.3
C-term NH-NH'	2.5±0.2		2.7	2.3
N-Acetyl CH3-G104αCH2	3.9±0.3		4.2	3.6
N-Acetyl CH3-G104NH	2.8±0.2		3.0	2.6
G104αCH2-K105βCH2	3.3±0.3	2.0	5.6	3.0
G104αCH2-K105γCH2	4.1±0.5	2.0	6.6	3.6

G104αCH2-F106δCH2	5.4±1.0	3.4	9.8	4.4
G104αCH2-F106ξCH2	5.5±1.0	3.4	9.9	4.5
G104αCH2-F106ςCH	5.5±1.0	3.0	9.5	4.5
G104αCH2-K107γCH2	5.1±1.0	2.0	8.1	4.1
G104NH-K107γCH2	4.0±0.5	1.0	5.5	3.5
K105αCH-F106βCH(m)	3.9±0.3		4.2	3.6
K105αCH-F106βCH'(x)	3.9±0.3		4.2	3.6
K105βCH2-F106NH	2.9±0.2	1.0	4.1	2.7
K105γCH2-F106NH	3.7±0.3	1.0	5.0	3.4
K105γCH2-K107NH	4.9±0.5	1.0	6.4	4.4
K105NH-F106δCH2	3.7±0.3	2.4	6.4	3.4
K105NH-F106ξCH2	4.3±0.5	2.4	7.2	3.8
K105NH-F106ςCH	4.3±0.5	2.0	6.8	3.8
K105NH-K107γCH2	4.0±0.5	1.0	5.5	3.5
F106αCH-R108βCH2	3.5±0.3	1.0	4.8	3.2
F106βCH(m)-K107NH	3.4±0.3		3.7	3.1
F106βCH'(x)-K107NH	3.4±0.3		3.7	3.1
F106βCH(m)-K107αCH	4.0±0.5		4.5	3.5
F106δCH2-K107NH	3.4±0.3	2.4	6.1	3.1
F106ξCH2-K107NH	4.1±0.5	2.4	7.0	3.6
F106ςCH2-K107NH	4.1±0.5	2.0	6.6	3.6
F106δCH2-R108NH	4.1±0.5	2.4	7.0	3.6
F106ξCH2-R108NH	4.4±0.5	2.4	7.3	3.9
F106ςCH2-R108NH	4.4±0.5	2.0	6.9	3.9
F106NH-K107γCH2	4.1±0.5	1.0	5.6	3.6
F106NH-V114(γCH3)2	4.2±0.5	2.4	7.1	3.7
K107γCH2-R108NH	3.5±0.3	1.0	4.8	3.2
G110αCH2-L111βCH2	3.8±0.3	2.0	6.1	3.5
G110αCH2-L111(δCH3)2	3.5±0.3	3.4	7.2	3.2
P109βCH(x)-G110NH	3.5±0.3		3.8	3.2
P109βCH'(p)-G110NH	3.6±0.3		3.9	3.3
P109βCH(x)-L111αCH	3.5±0.3		3.8	3.2
P109βCH'(p)-L111αCH	3.6±0.3		3.9	3.3
P109γCH2-L111αCH	3.2±0.3	1.0	4.5	2.9
L111(δCH3)2-R112NH	3.2±0.3	2.4	5.9	2.9
R112βCH2-R113NH	3.1±0.3	1.0	4.4	2.8
R112βCH2-R115NH	3.2±0.3	1.0	4.5	2.9
R112βCH2-Cterm NH	3.7±0.3	1.0	5.0	3.4
R112βCH2-Cterm NH'	3.7±0.3	1.0	5.0	3.4
R113βCH2-V114αCH	3.0±0.3	1.0	4.3	2.7
R113βCH2-V114NH	3.2±0.3	1.0	4.5	2.9
R113βCH2-R115NH	3.2±0.3	1.0	4.5	2.9
R113δCH2-V114αCH	4.5±0.5	1.0	6.0	4.0
R113δCH2-V114NH	4.1±0.5	1.0	5.6	3.6
R113NH-V114(γCH3)2	3.7±0.3	2.4	6.4	3.4
V114αCH-R115βCH2	3.0±0.3	1.0	4.3	2.7

V114αCH-R115δCH2	4.5±0.5	1.0	6.0	4.0
V114αCH-Cterm NH	4.9±0.5		5.4	4.4
V114αCH-Cterm NH'	4.9±0.5		5.4	4.4
V114βCH-R115NH	3.0±0.3		3.3	2.7
V114βCH-Cterm NH	3.3±0.3		3.6	3.0
V114βCH-Cterm NH'	3.3±0.3		3.6	3.0
V114(γCH3)2-R115αCH	3.1±0.3	2.4	5.8	2.8
V114(γCH3)2-R115NH	3.0±0.3	2.4	5.7	2.7
V114(γCH3)2-Cterm NH	3.9±0.3	2.4	6.6	3.6
V114(γCH3)2-Cterm NH'	3.9±0.3	2.4	6.6	3.6
V114NH-R115βCH2	3.2±0.3	1.0	4.5	2.9
V114NH-R115δCH2	4.1±0.5	1.0	5.6	3.6
R115αCH-Cterm NH	3.2±0.3		3.5	2.9
R115αCH-Cterm NH'	3.1±0.3		3.4	2.8
R115βCH2-Cterm NH	3.2±0.3		3.5	2.9
R115βCH2-Cterm NH'	3.2±0.3		3.5	2.9
F106δCH2-K105βCH2	3.5±0.3	3.4	7.2	3.2
F106δCH2-K105δCH2	3.5±0.3	3.4	7.2	3.2
F106δCH2-K107βCH2	3.5±0.3	3.4	7.2	3.2
F106δCH2-K107γCH2	3.5±0.3	3.4	7.2	3.2
F106δCH2-R108βCH2	3.5±0.3	3.4	7.2	3.2
F106δCH2-P109βCH(x)	4.2±0.5	2.4	7.1	3.7
F106δCH2-P109βCH'(p)	4.6±0.5	2.4	7.5	4.1
F106δCH2-P109γCH2	4.0±0.5	3.4	7.9	3.5
F106δCH2-V114βCH	3.7±0.3	2.4	6.4	3.4
F106δCH2-V114(γCH3)2	3.4±0.3	4.8	8.5	3.1
F106ξCH2-K105βCH2	3.0±0.3	3.4	6.7	2.7
F106ξCH2-K105γCH2	3.5±0.3	3.4	7.2	3.2
F106ξCH2-K105δCH2	3.0±0.3	3.4	6.7	2.7
F106ξCH2-K105ξCH2	4.0±0.5	3.4	7.9	3.5
F106ξCH2-R108βCH2	3.0±0.3	3.4	6.7	2.7
F106ξCH2-P109βCH(x)	4.0±0.5	2.4	6.9	3.5
F106ξCH2-P109βCH'(p)	4.2±0.5	2.4	7.1	3.7
F106ξCH2-P109γCH2	4.2±0.5	3.4	8.1	3.7
F106ξCH2-V114βCH	3.8±0.3	2.4	6.5	3.5
F106ξCH2-V114(γCH3)2	3.3±0.3	4.8	8.4	3.0
F106ςCH-K105βCH2	3.0±0.3	3.0	6.3	2.7
F106ςCH-K105γCH2	3.5±0.3	3.0	6.8	3.2
F106ςCH-K105δCH2	3.0±0.3	3.0	6.3	2.7
F106ςCH-K105ξCH2	4.0±0.5	3.0	7.5	3.5
F106ςCH-R108βCH2	3.0±0.3	3.0	6.3	2.7
F106ςCH-P109βCH(x)	4.0±0.5	2.0	6.5	3.5
F106ςCH-P109βCH'(p)	4.2±0.5	2.0	6.7	3.7
F106ςCH-P109γCH2	4.2±0.5	3.0	7.7	3.7
F106ςCH-V114βCH	3.8±0.3	2.0	6.1	3.5

F106ςCH-V114(γCH3)2	3.3±0.3	4.4	8.0	3.0
F106βCH(m)-V114(γCH3)2	3.8±0.3	2.4	6.5	3.5
F106βCH'(p)-V114(γCH3)2	3.7±0.3	2.4	6.4	3.4
R108βCH2-P109δCH(m)	3.3±0.3	1.0	4.6	3.0
R108βCH2-P109δCH(m')	3.4±0.3	1.0	4.7	3.1
P109βCH(x)-V114(γCH3)2	3.3±0.3	2.4	6.0	3.0
P109δCH'(m')-V114(γCH3)2	4.0±0.5	2.4	6.9	3.5
L111(δCH3)2-R112βCH2	3.2±0.3	3.4	6.9	2.9
L111(δCH3)2-R112δCH2	4.1±0.5	3.4	8.0	3.6
R113βCH2-V114(γCH3)2	3.2±0.3	3.4	6.9	2.9
R113δCH2-V114βCH	4.3±0.5	1.0	5.8	3.8
R113δCH2-V114(γCH2)3	4.1±0.5	3.4	8.0	3.6
V114βCH-R115δCH2	4.3±0.5	1.0	5.8	3.8
V114(γCH3)2-R115βCH2	3.2±0.3	3.4	6.9	2.9
V114(γCH3)2-R115δCH2	4.1±0.5	3.4	8.0	3.6
G104αCH2-K105αCH	4.7±0.5	1.0	6.2	4.2
G110αCH2-L111αCH	4.3±0.5	1.0	5.8	3.8
R113αCH-V114αCH	4.3±0.5		4.8	3.8
V114αCH-R115αCH	4.1±0.5		4.6	3.6
K105NH-K107NH	3.6±0.3		3.9	3.3
K107NH-R108NH	3.4±0.3		3.7	3.1
G110NH-L111NH	4.0±0.5		4.5	3.5
R113NH-V114NH	3.7±0.3		4.0	3.4
V114NH-R115NH	3.7±0.3		4.0	3.4
R115NH-Cterm NH	4.1±0.5		4.6	3.6
R115NH-Cterm NH'	4.1±0.5		4.6	3.6
G104αCH2-NH	2.9±0.2		3.1	2.7
G104αCH2-K105NH	3.0±0.3	1.0	4.3	2.7
G104αCH2-F106NH	3.9±0.3	1.0	5.2	3.6
G104αCH2-K107NH	4.1±0.5	1.0	5.6	3.6
G104αCH2-R108NH	4.6±0.5	1.0	6.1	4.1
K105αCH-NH	3.1±0.3		3.4	2.8
K105αCH-F106NH	3.1±0.3		3.4	2.8
K105αCH-K107NH	4.3±0.5		4.8	3.8
F106αCH-NH	4.9±0.5		5.4	4.4
F106αCH-K105NH	5.1±1.0		6.1	4.1
F106αCH-K107NH	4.1±0.5		4.6	3.6
K107αCH-NH	3.8±0.3		4.1	3.5
K107αCH-G104NH	3.8±0.3		4.1	3.5
K107αCH-R108NH	3.4±0.3		3.7	3.1
P109αCH-G110NH	3.9±0.3		4.2	3.6
G110αCH2-NH	3.4±0.3		3.7	3.1

G110αCH2-L111NH	3.6±0.3	1.0	4.9	3.3
L111αCH-NH	4.3±0.5		4.8	3.8
L111αCH-R112NH	3.1±0.3		3.4	2.8
R112αCH-NH	3.1±0.3		3.4	2.8
R112αCH-R113NH	3.3±0.3		3.6	3.0
R113αCH-NH	3.3±0.3		3.6	3.0
R113αCH-V114NH	3.2±0.3		3.5	2.9
V114αCH-NH	3.5±0.3		3.8	3.2
V114αCH-R113NH	3.8±0.3		4.1	3.5
V114αCH-R115NH	2.8±0.2		3.0	2.6
R115αCH-NH	3.4±0.3		3.7	3.1

Table VIII-4. ${}^{3}J\alpha$CH-NH coupling constants for the G110-TnI peptide as a function of molar equivalents TnC.Ca(II)$_4$.

TNC/TNIp	0.000	0.002	0.040	0.060	0.080	0.100
JαCH-NH	(Hz)					
G104	5.7	5.7	5.9	5.7	5.5	5.7
K105	6.6	6.5	6.5	6.5	6.3	6.3
F106	7.1	7.2	7.0	7.0	6.7	6.6
K107	7.6	7.7	7.5	7.6	6.9	6.7
R108	6.6	6.6	6.6	6.3	6.4	5.9
G110	6.0	5.5	5.7	5.7		
L111	6.8	6.8	6.9	6.3	6.7	6.6
R112	7.0	6.8	6.5	6.3		
R113	6.6	6.3	6.4	5.9	5.8	5.7
V114	7.8	7.5				
R115	7.1	6.9	6.5	6.4	6.2	6.0

Table VIII-5. Chemical shift values for the G110-TnI peptide backbone amide resonances as a function of temperature for **A.** 0.0 molar equivalents TnC.Ca(II)$_4$. **B.** 0.1 molar equivalents TnC.Ca(II)$_4$.

A. temperature	5 °C	10 °C	15 °C	20 °C	25 °C	30 °C
G104 (ppm)	8.425	8.388	8.355	8.320	8.280	8.248
K105	8.375	8.340	8.305	8.264	8.208	8.171
F106	8.293	8.254	8.216	8.180	8.136	8.106
K107	8.243	8.217	8.188	8.147	8.107	8.074
R108	8.480	8.436	8.394	8.353	8.304	8.265
G110	8.590	8.555	8.521	8.491	8.456	8.415
L111	8.225	8.184	8.145	8.107	8.065	8.030
R112	8.501	8.466	8.433	8.396	8.356	8.323
R113	8.540	8.502	8.464	8.428	8.386	8.352
V114	8.416	8.373	8.335	8.291	8.243	8.200
R115	8.610	8.569	8.526	8.484	8.440	8.399

B. temperature	5 °C	10 °C	15 °C	20 °C	25 °C	30 °C
G104 (ppm)	8.432	8.398	8.362	8.329	8.294	8.258
K105	8.387	8.352	8.308	8.265	8.227	8.174
F106	8.310	8.271	8.234	8.198	8.163	8.123
K107	9.239	8.212	8.184	8.160	8.134	8.105
R108	8.481	8.440	8.398	8.356	8.315	8.271
G110	8.597	8.558	8.521	8.487	8.447	8.424
L111	8.222	8.185	8.147	8.111	8.075	8.036
R112	8.498	8.463	8.429	8.394	8.361	8.323
R113	8.532	8.496	8.460	8.423	8.387	8.349
V114	8.421	8.370	8.320	8.283	8.238	8.193
R115	8.602	8.564	8.521	8.480	8.442	8.394

Table VIII-6. Temperature coefficients measured for various G110-TnI peptide backbone amide protons versus molar equivalents TnC.Ca(II)$_4$.

TNC/TNIp	0.0	0.1
$\Delta\delta/\Delta T$,G104 (ppb)	7.11	6.94
$\Delta\delta/\Delta T$,K105	8.33	8.47
$\Delta\delta/\Delta T$,F106	7.57	7.40
$\Delta\delta/\Delta T$,K107	6.95	5.30
$\Delta\delta/\Delta T$,R108	8.64	8.38
$\Delta\delta/\Delta T$,G110	6.87	7.04
$\Delta\delta/\Delta T$,L111	7.83	7.41
$\Delta\delta/\Delta T$,R112	7.18	6.95
$\Delta\delta/\Delta T$,R113	7.57	7.31
$\Delta\delta/\Delta T$,V114	8.65	8.99
$\Delta\delta/\Delta T$,R115	8.48	8.27

Table VIII-7. GROMOS distance restraint file used in MD simulations to generate the structure of the G110-TnI peptide bound to TnC.Ca(II)$_4$.

```
Gly110-TnI peptide, 0.1 M.E. cardiac TnC.Ca4, tm=150ms (version 1)
 458
   1     2                   5         5                       0    0.30
   1     2                   5         5                       0   -0.26
   1     2                   5         6     4     7           3    0.42
   1     2                   5         6     4     7           3   -0.36
   5                         0         6     4     7           3    0.31
   5                         0         6     4     7           3   -0.27
   6     4     7             3        11     9    12    20     1    0.62
   6     4     7             3        11     9    12    20     1   -0.42
   6     4     7             3        13    12    14           3    0.66
   6     4     7             3        13    12    14           3   -0.36
   6     4     7             3        12    11    13           3    0.56
   6     4     7             3        12    11    13           3   -0.30
   6     4     7             3        26                       0    0.98
   6     4     7             3        26                       0   -0.44
   6     4     7             3        31                       0    0.95
   6     4     7             3        31                       0   -0.45
   6     4     7             3        31    29    30           2    0.95
   6     4     7             3        31    29    30           2   -0.45
   6     4     7             3        38    37    39           3    0.81
   6     4     7             3        38    37    39           3   -0.41
   5                         0        36    34    37    45     1    0.41
   5                         0        36    34    37    45     1   -0.35
   5                         0        38    37    39           3    0.55
   5                         0        38    37    39           3   -0.35
   6     4     7             3        10                       0    0.43
   6     4     7             3        10                       0   -0.27
   6     4     7             3        23                       0    0.52
   6     4     7             3        23                       0   -0.36
   6     4     7             3        35                       0    0.56
   6     4     7             3        35                       0   -0.36
   6     4     7             3        48                       0    0.61
   6     4     7             3        48                       0   -0.41
  10                         0        11     9    12    20     1    0.34
  10                         0        11     9    12    20     1   -0.28
  10                         0        12    11    13           3    0.33
  10                         0        12    11    13           3   -0.23
  10                         0        13    12    14           3    0.43
  10                         0        13    12    14           3   -0.27
  10                         0        24    22    25    32     1    0.61
  10                         0        24    22    25    32     1   -0.41
  10                         0        35                       0    0.39
  10                         0        35                       0   -0.33
  10                         0        38    37    39           3    0.55
  10                         0        38    37    39           3   -0.35
  11     9    12    20       1        12    11    13           3    0.26
  11     9    12    20       1        12    11    13           3   -0.22
  11     9    12    20       1        13    12    14           3    0.40
  11     9    12    20       1        13    12    14           3   -0.28
  11     9    12    20       1        23                       0    0.34
  11     9    12    20       1        23                       0   -0.28
  11     9    12    20       1        35                       0    0.48
  11     9    12    20       1        35                       0   -0.38
  11     9    12    20       1        25    26    24           4    0.42
  11     9    12    20       1        25    26    24           4   -0.36
  11     9    12    20       1        25    24    26           4    0.42
  11     9    12    20       1        25    24    26           4   -0.36
  12    11    13             3        13    12    14           3    0.29
  12    11    13             3        13    12    14           3   -0.25
```

12	11	13		3	23				0	0.41
12	11	13		3	23				0	-0.27
15	14	16		3	31				0	0.79
15	14	16		3	31				0	-0.35
15	14	16		3	31	29	30		2	0.75
15	14	16		3	31	29	30		2	-0.35
13	12	14		3	14	13	15		3	0.29
13	12	14		3	14	13	15		3	-0.25
13	12	14		3	15	14	16		3	0.35
13	12	14		3	15	14	16		3	-0.29
13	12	14		3	23				0	0.50
13	12	14		3	23				0	-0.34
10				0	26				0	0.64
10				0	26				0	-0.34
10				0	31				0	0.72
10				0	31				0	-0.38
10				0	31	29	30		2	0.68
10				0	31	29	30		2	-0.38
13	12	14		3	35				0	0.64
13	12	14		3	35				0	-0.44
14	13	15		3	15	14	16		3	0.30
14	13	15		3	15	14	16		3	-0.26
23				0	24	22	25	32	1	0.54
23				0	24	22	25	32	1	-0.44
23				0	25	26	24		4	0.36
23				0	25	26	24		4	-0.30
23				0	25	24	26		4	0.37
23				0	25	24	26		4	-0.31
23				0	26				0	0.60
23				0	26				0	-0.30
23				0	31				0	0.69
23				0	31				0	-0.35
23				0	31	29	30		2	0.55
23				0	31	29	30		2	-0.35
23				0	38	37	39		3	0.56
23				0	38	37	39		3	-0.36
23				0	122	123	124		6	0.71
23				0	122	123	124		6	-0.37
24	22	25	32	1	25	26	24		4	0.40
24	22	25	32	1	25	26	24		4	-0.34
24	22	25	32	1	25	24	26		4	0.38
24	22	25	32	1	25	24	26		4	-0.32
24	22	25	32	1	26				0	0.62
24	22	25	32	1	26				0	-0.36
24	22	25	32	1	31				0	0.85
24	22	25	32	1	31				0	-0.45
24	22	25	32	1	31	29	30		2	0.85
24	22	25	32	1	31	29	30		2	-0.45
24	22	25	32	1	35				0	0.46
24	22	25	32	1	35				0	-0.36
24	22	25	32	1	50	49	51		3	0.48
24	22	25	32	1	50	49	51		3	-0.32
25	26	24		4	25	24	26		4	0.31
25	26	24		4	25	24	26		4	-0.27
25	26	24		4	26				0	0.29
25	26	24		4	26				0	-0.25
25	26	24		4	31				0	0.35
25	26	24		4	31				0	-0.29
25	26	24		4	31	29	30		2	0.35
25	26	24		4	31	29	30		2	-0.29

25	24	26	4	26				0	0.28
25	24	26	4	26				0	-0.24
25	24	26	4	31				0	0.35
25	24	26	4	31				0	-0.29
25	24	26	4	31	29	30		2	0.35
25	24	26	4	31	29	30		2	-0.29
25	26	24	4	35				0	0.37
25	26	24	4	35				0	-0.31
25	24	26	4	35				0	0.37
25	24	26	4	35				0	-0.31
25	26	24	4	36	34	37	45	1	0.45
25	26	24	4	36	34	37	45	1	-0.35
25	26	24	4	122	123	124		6	0.65
25	26	24	4	122	123	124		6	-0.35
25	24	26	4	122	123	124		6	0.64
25	24	26	4	122	123	124		6	-0.34
26			0	35				0	0.61
26			0	35				0	-0.31
31			0	35				0	0.70
31			0	35				0	-0.36
31	29		2	35				0	0.66
31	29		2	35				0	-0.36
26			0	48				0	0.70
26			0	48				0	-0.36
31			0	48				0	0.73
31			0	48				0	-0.39
31	29	30	2	48				0	0.69
31	29	30	2	48				0	-0.39
26			0	12	11	13		3	0.72
26			0	12	11	13		3	-0.32
26			0	14	13	15		3	0.72
26			0	14	13	15		3	-0.32
26			0	37	36	38		3	0.72
26			0	37	36	38		3	-0.32
26			0	38	37	39		3	0.72
26			0	38	37	39		3	-0.32
26			0	50	49	51		3	0.72
26			0	50	49	51		3	-0.32
26			0	67	66	68		3	0.79
26			0	67	66	68		3	-0.35
26			0	66	67	65		4	0.71
26			0	66	67	65		4	-0.37
26			0	66	65	67		4	0.75
26			0	66	65	67		4	-0.41
26			0	122	121	123	124	1	0.64
26			0	122	121	123	124	1	-0.34
26			0	122	123	124		6	0.85
26			0	122	123	124		6	-0.31
31			0	12	11	13		3	0.67
31			0	12	11	13		3	-0.27
31			0	13	12	14		3	0.72
31			0	13	12	14		3	-0.32
31			0	14	13	15		3	0.67
31			0	14	13	15		3	-0.27
31			0	50	49	51		3	0.67
31			0	50	49	51		3	-0.27
31			0	67	66	68		3	0.81
31			0	67	66	68		3	-0.37
31			0	66	67	65		4	0.69
31			0	66	67	65		4	-0.35

31				0	66	65	67		4	0.71
31				0	66	65	67		4	-0.37
31				0	122	121	123	124	1	0.65
31				0	122	121	123	124	1	-0.35
31				0	122	123	124		6	0.84
31				0	122	123	124		6	-0.30
31	29	30		2	12	11	13		3	0.63
31	29	30		2	12	11	13		3	-0.27
31	29	30		2	13	12	14		3	0.68
31	29	30		2	13	12	14		3	-0.32
31	29	30		2	14	13	15		3	0.63
31	29	30		2	14	13	15		3	-0.27
31	29	30		2	50	49	51		3	0.63
31	29	30		2	50	49	51		3	-0.27
31	29	30		2	67	66	68		3	0.77
31	29	30		2	67	66	68		3	-0.37
31	29	30		2	66	67	65		4	0.65
31	29	30		2	66	67	65		4	-0.35
31	29	30		2	66	65	67		4	0.67
31	29	30		2	66	65	67		4	-0.37
31	29	30		2	122	121	123	124	1	0.61
31	29	30		2	122	121	123	124	1	-0.35
31	29	30		2	122	123	124		6	0.80
31	29	30		2	122	123	124		6	-0.30
35				0	36	34	37	45	1	0.41
35				0	36	34	37	45	1	-0.35
35				0	37	36	38		3	0.35
35				0	37	36	38		3	-0.25
35				0	38	37	39		3	0.44
35				0	38	37	39		3	-0.28
35				0	48				0	0.37
35				0	48				0	-0.31
36	34	37	35	1	37	36	38		3	0.26
36	34	37	35	1	37	36	38		3	-0.22
36	34	37	35	1	38	37	39		3	0.39
36	34	37	35	1	38	37	39		3	-0.27
36	34	37	35	1	48				0	0.37
36	34	37	35	1	48				0	-0.31
37	36	38		3	38	37	39		3	0.24
37	36	38		3	38	37	39		3	-0.20
38	37	39		3	39	38	40		3	0.28
38	37	39		3	39	38	40		3	-0.24
38	37	39		3	40	39	41		3	0.31
38	37	39		3	40	39	41		3	-0.27
38	37	39		3	48				0	0.48
38	37	39		3	48				0	-0.32
39	38	40		3	40	39	41		3	0.27
39	38	40		3	40	39	41		3	-0.23
48				0	50	49	51		3	0.34
48				0	50	49	51		3	-0.24
48				0	52	51	53		3	0.38
48				0	52	51	53		3	-0.32
49	47	50	62	1	50	49	51		3	0.35
49	47	50	62	1	50	49	51		3	-0.29
49	47	50	62	1	51	50	52		3	0.51
49	47	50	62	1	51	50	52		3	-0.35
50	49	51		3	51	50	52		3	0.29
50	49	51		3	51	50	52		3	-0.25
50	49	51		3	68	64	67		4	0.46
50	49	51		3	68	64	67		4	-0.30

50	49	51		3	68	67	64		4	0.47
50	49	51		3	68	67	64		4	-0.31
51	50	52		3	52	51	53		3	0.29
51	50	52		3	52	51	53		3	-0.25
65	64	66	69	1	66	67	65		4	0.35
65	64	66	69	1	66	67	65		4	-0.29
65	64	66	69	1	66	65	67		4	0.34
65	64	66	69	1	66	65	67		4	-0.28
65	64	66	69	1	67	66	68		3	0.38
65	64	66	69	1	67	66	68		3	-0.32
65	64	66	69	1	72				0	0.42
65	64	66	69	1	72				0	-0.36
66	67	65		4	66	65	67		4	0.26
66	67	65		4	66	65	67		4	-0.22
66	67	65		4	68	64	67		4	0.38
66	67	65		4	68	64	67		4	-0.32
66	67	65		4	68	67	64		4	0.38
66	67	65		4	68	67	64		4	-0.32
66	65	67		4	67	66	68		3	0.28
66	65	67		4	67	66	68		3	-0.24
66	65	67		4	68	64	67		4	0.45
66	65	67		4	68	64	67		4	-0.35
66	65	67		4	68	67	64		4	0.39
66	65	67		4	68	67	64		4	-0.33
67	66	68		3	68	64	67		4	0.36
67	66	68		3	68	64	67		4	-0.30
67	66	68		3	68	67	64		4	0.34
67	66	68		3	68	67	64		4	-0.28
68	64	67		4	68	67	64		4	0.38
68	64	67		4	68	67	64		4	-0.32
66	67	65		4	122	123	124		6	0.60
66	67	65		4	122	123	124		6	-0.30
68	64	67		4	122	123	124		6	0.69
68	64	67		4	122	123	124		6	-0.35
72				0	73	71	74		3	0.37
72				0	73	71	74		3	-0.31
73	71	74		3	77				0	0.49
73	71	74		3	77				0	-0.33
73	71	74		3	78	76	79	83	1	0.58
73	71	74		3	78	76	79	83	1	-0.38
72				0	77				0	0.45
72				0	77				0	-0.35
73	71	74		3	79	78	80		3	0.61
73	71	74		3	79	78	80		3	-0.35
73	71	74		3	80	81	82		6	0.72
73	71	74		3	80	81	82		6	-0.32
66	67	65		4	72				0	0.38
66	67	65		4	72				0	-0.32
66	67	65		4	78	76	79	83	1	0.38
66	67	65		4	78	76	79	83	1	-0.32
66	65	67		4	72				0	0.39
66	65	67		4	72				0	-0.33
66	65	67		4	78	76	79	83	1	0.39
66	65	67		4	78	76	79	83	1	-0.33
67	66	68		3	78	76	79	83	1	0.45
67	66	68		3	78	76	79	83	1	-0.29
77				0	78	76	79	83	1	0.48
77				0	78	76	79	83	1	-0.38
77				0	79	78	80		3	0.36
77				0	79	78	80		3	-0.26

77				0	80	81	82		6	0.35
77				0	80	81	82		6	-0.29
78	76	79	83	1	79	78	80		3	0.26
78	76	79	83	1	79	78	80		3	-0.22
78	76	79	83	1	80	81	82		6	0.45
78	76	79	83	1	80	81	82		6	-0.24
78	76	79	83	1	86				0	0.34
78	76	79	83	1	86				0	-0.28
79	78	80		3	80	81	82		6	0.26
79	78	80		3	80	81	82		6	-0.22
80	79	81	82	1	80	81	82		6	0.24
80	79	81	82	1	80	81	82		6	-0.20
80	81	82		6	86				0	0.59
80	81	82		6	86				0	-0.29
80	81	82		6	88	87	89		3	0.69
80	81	82		6	88	87	89		3	-0.29
80	81	82		6	90	89	91		3	0.80
80	81	82		6	90	89	91		3	-0.36
86				0	87	85	88	100	1	0.34
86				0	87	85	88	100	1	-0.28
86				0	88	87	89		3	0.33
86				0	88	87	89		3	-0.23
86				0	90	89	91		3	0.45
86				0	90	89	91		3	-0.35
87	85	88	100	1	88	87	89		3	0.29
87	85	88	100	1	88	87	89		3	-0.25
87	85	88	100	1	90	89	91		3	0.46
87	85	88	100	1	90	89	91		3	-0.30
87	85	88	100	1	103				0	0.36
87	85	88	100	1	103				0	-0.30
88	87	89		3	89	88	90		3	0.29
88	87	89		3	89	88	90		3	-0.25
88	87	89		3	103				0	0.44
88	87	89		3	103				0	-0.28
88	87	89		3	128				0	0.45
88	87	89		3	128				0	-0.29
88	87	89		3	145				0	0.50
88	87	89		3	145				0	-0.34
88	87	89		3	146				0	0.50
88	87	89		3	146				0	-0.34
89	88	90		3	90	89	91		3	0.29
89	88	90		3	90	89	91		3	-0.25
103				0	104	102	105	117	1	0.36
103				0	104	102	105	117	1	-0.30
103				0	105	104	106		3	0.33
103				0	105	104	106		3	-0.23
103				0	107	106	108		3	0.45
103				0	107	106	108		3	-0.35
103				0	120				0	0.40
103				0	120				0	-0.34
103				0	121	119	122	125	1	0.41
103				0	121	119	122	125	1	-0.35
103				0	122	123	124		6	0.64
103				0	122	123	124		6	-0.34
104	102	105	117	1	105	104	106		3	0.29
104	102	105	117	1	105	104	106		3	-0.25
104	102	105	117	1	107	106	108		3	0.46
104	102	105	117	1	107	106	108		3	-0.30
104	102	105	117	1	120				0	0.35
104	102	105	117	1	120				0	-0.29

104	102	105	117	1	121	119	122	125	1	0.48
104	102	105	117	1	121	119	122	125	1	-0.38
105	104	106		3	106	105	107		3	0.29
105	104	106		3	106	105	107		3	-0.25
105	104	106		3	128				0	0.45
105	104	106		3	128				0	-0.29
107	106	108		3	121	119	122	125	1	0.60
107	106	108		3	121	119	122	125	1	-0.40
107	106	108		3	122	121	123	124	1	0.58
107	106	108		3	122	121	123	124	1	-0.38
105	104	106		3	122	123	124		6	0.69
105	104	106		3	122	123	124		6	-0.29
105	104	106		3	121	119	122	125	1	0.43
105	104	106		3	121	119	122	125	1	-0.27
105	104	106		3	120				0	0.45
105	104	106		3	120				0	-0.29
106	105	107		3	107	106	108		3	0.29
106	105	107		3	107	106	108		3	-0.25
107	106	108		3	120				0	0.56
107	106	108		3	120				0	-0.36
107	106	108		3	122	123	124		6	0.80
107	106	108		3	122	123	124		6	-0.36
120				0	121	119	122	125	1	0.38
120				0	121	119	122	125	1	-0.32
120				0	122	121	123	124	1	0.29
120				0	122	121	123	124	1	-0.25
120				0	122	123	124		6	0.46
120				0	122	123	124		6	-0.25
120				0	128				0	0.40
120				0	128				0	-0.34
120				0	130	129	131		3	0.45
120				0	130	129	131		3	-0.29
120				0	132	131	133		3	0.56
120				0	132	131	133		3	-0.36
121	119	122	125	1	122	121	123	124	1	0.29
121	119	122	125	1	122	121	123	124	1	-0.25
121	119	122	125	1	122	123	124		6	0.33
121	119	122	125	1	122	123	124		6	-0.23
121	119	122	125	1	128				0	0.30
121	119	122	125	1	128				0	-0.26
121	119	122	125	1	129	127	130	142	1	0.46
121	119	122	125	1	129	127	130	142	1	-0.36
121	119	122	125	1	130	129	131		3	0.43
121	119	122	125	1	130	129	131		3	-0.27
121	119	122	125	1	132	131	133		3	0.60
121	119	122	125	1	132	131	133		3	-0.40
121	119	122	125	1	145				0	0.54
121	119	122	125	1	145				0	-0.44
121	119	122	125	1	146				0	0.54
121	119	122	125	1	146				0	-0.44
122	121	123	124	1	122	123	124		6	0.23
122	121	123	124	1	122	123	124		6	-0.19
122	121	123	124	1	128				0	0.33
122	121	123	124	1	128				0	-0.27
122	121	123	124	1	132	131	133		3	0.58
122	121	123	124	1	132	131	133		3	-0.38
122	121	123	124	1	145				0	0.36
122	121	123	124	1	145				0	-0.30
122	121	123	124	1	146				0	0.36
122	121	123	124	1	146				0	-0.30

```
122  123  124        6     128                       0   0.57
122  123  124        6     128                       0  -0.27
122  123  124        6     129  127  130  142        1   0.58
122  123  124        6     129  127  130  142        1  -0.28
122  123  124        6     130  129  131             3   0.69
122  123  124        6     130  129  131             3  -0.29
122  123  124        6     132  131  133             3   0.80
122  123  124        6     132  131  133             3  -0.36
122  123  124        6     145                       0   0.66
122  123  124        6     145                       0  -0.36
122  123  124        6     146                       0   0.66
122  123  124        6     146                       0  -0.36
128                  0     129  127  130  142        1   0.37
128                  0     129  127  130  142        1  -0.31
128                  0     130  129  131             3   0.35
128                  0     130  129  131             3  -0.25
128                  0     132  131  133             3   0.39
128                  0     132  131  133             3  -0.33
128                  0     145                       0   0.46
128                  0     145                       0  -0.36
128                  0     146                       0   0.46
128                  0     146                       0  -0.36
129  127  130  142   1     130  129  131             3   0.27
129  127  130  142   1     130  129  131             3  -0.23
129  127  130  142   1     132  131  133             3   0.46
129  127  130  142   1     132  131  133             3  -0.30
129  127  130  142   1     145                       0   0.35
129  127  130  142   1     145                       0  -0.29
129  127  130  142   1     146                       0   0.34
129  127  130  142   1     146                       0  -0.28
130  129  131        3     131  130  132             3   0.29
130  129  131        3     131  130  132             3  -0.25
130  129  131        3     145                       0   0.35
130  129  131        3     145                       0  -0.29
130  129  131        3     146                       0   0.35
130  129  131        3     146                       0  -0.29
131  130  132        3     132  131  133             3   0.29
131  130  132        3     132  131  133             3  -0.25
145                  0     146                       0   0.27
145                  0     146                       0  -0.23
```

Table VIII-8. Chemical shift values for the G110-TnI peptide backbone amide resonances as a function of molar equivalents TnC.Ca(II)$_4$.

TNC/TNIp (ppm)	0.000	0.020	0.040	0.060	0.080	0.010
δG104NH	8.426	8.426	8.429	8.429	8.432	8.433
δK105NH	8.376	8.377	8.380	8.381	8.385	8.387
δF106NH	8.292	8.296	8.300	8.302	8.306	8.311
δK107NH	8.242	8.242	8.241	8.241	8.241	8.240
δR108NH	8.480	8.480	8.480	8.480	8.482	8.483
δG110NH	8.590	8.591	8.593	8.594	8.597	8.599
δL111NH	8.224	8.223	8.223	8.224	8.223	8.223
δR112NH	8.502	8.502	8.500	8.500	8.499	8.498
δR113NH	8.541	8.539	8.538	8.538	8.536	8.535
δV114NH	8.423	8.422	8.423		8.416	8.415
δR115NH	8.610	8.609	8.608	8.607	8.606	8.605
ΔδG104NH	0.000	0.000	0.003	0.003	0.006	0.007
ΔδK105NH	0.000	0.001	0.004	0.005	0.009	0.011
ΔδF106NH	0.000	0.004	0.008	0.010	0.014	0.019
ΔδK107NH	0.000	0.000	0.001	0.001	0.001	0.002
ΔδR108NH	0.000	0.000	0.000	0.000	0.002	0.003
ΔδG110NH	0.000	0.001	0.003	0.004	0.007	0.009
ΔδL111NH	0.000	0.001	0.001	0.000	0.001	0.001
ΔδR112NH	0.000	0.000	0.002	0.002	0.003	0.004
ΔδR113NH	0.000	0.002	0.003	0.003	0.005	0.006
ΔδV114NH	0.000	0.001	0.000		0.007	0.008
ΔδR115NH	0.000	0.001	0.002	0.003	0.004	0.005

Table VIII-9. Final coordinates for the structure of the G110-TnI peptide bound to TnC generated from **A.** α-helical coordinates (structure 1), and **B.** β-strand coordinates (structure 2), following approximately 12 ps of restrained MD.

```
AVE.COORDS 10-15PS   G110-TnI peptide, 0.1 M E. cardiac TnC.Ca4, tm=150ms, starting with alfa-helical coordinates
 146
   1GLY     ACC    1   0.430  -0.569   0.738  0.1245  0.0185  0.0119  0.2812 -0.0345 -0.0253  0.0739
   1GLY       C    2   0.343  -0.548   0.619  0.0747  0.0194  0.0453  0.1274 -0.0378 -0.0897  0.0772
   1GLY       O    3   0.356  -0.448   0.550  0.0745  0.0252  0.0517  0.1325 -0.0374 -0.0881  0.0657
   1GLY       N    4   0.257  -0.645   0.605  0.0859  0.0598  0.0557  0.0558 -0.0907 -0.0845  0.1421
   1GLY       H    5   0.300  -0.570   0.575  0.0812  0.0216  0.0365  0.0972 -0.0473 -0.0841  0.1248
   1GLY      CA    6   0.113  -0.651   0.620  0.0480  0.0674  0.0233  0.0105 -0.0602 -0.0238  0.0661
   1GLY       C    7   0.029  -0.524   0.622  0.0234  0.0282  0.0043  0.0023 -0.0303 -0.0051  0.0399
   1GLY       O    8  -0.071  -0.506   0.553  0.0280  0.0376  0.0040  0.0033 -0.0377 -0.0015  0.0430
   2LYSH      N    9   0.074  -0.433   0.707  0.0154  0.0142  0.0030  0.0025 -0.0188 -0.0038  0.0294
   2LYSH      H   10   0.149  -0.454   0.762  0.0296  0.0265  0.0146  0.0129 -0.0342 -0.0178  0.0494
   2LYSH     CA   11   0.018  -0.301   0.733  0.0065  0.0019  0.0009  0.0033  0.0022  0.0048  0.0141
   2LYSH     CB   12   0.101  -0.246   0.847  0.0102  0.0167  0.0004  0.0091  0.0067 -0.0013  0.0047
   2LYSH     CG   13   0.040  -0.125   0.916  0.0251  0.0469  0.0093  0.0147  0.0047 -0.0091  0.0138
   2LYSH     CD   14   0.110  -0.094   1.046  0.0538  0.0822  0.0168  0.0553 -0.0102 -0.0310  0.0239
   2LYSH     CE   15   0.070  -0.086   1.129  0.4269  0.0891  0.2233  1.1211 -0.0509 -0.1476  0.0706
   2LYSH     NZ   16   0.128  -0.065   1.260  0.4069  0.0805  0.2773  1.0729 -0.0430 -0.1736  0.0672
   2LYSH    HZ1   17   0.127  -0.085   1.294  0.8700  0.3445  0.3383  2.0528 -0.2184 -0.3673  0.2126
   2LYSH    HZ2   18   0.167  -0.064   1.273  0.4646  0.1027 -0.1787  1.2387 -0.0390  0.0297  0.0523
   2LYSH    HZ3   19   0.128  -0.040   1.298  0.5346  0.5006  0.6423  0.9470 -0.2091 -0.3252  0.1563
   2LYSH      C   20   0.010  -0.216   0.607  0.0028  0.0018 -0.0007  0.0014  0.0023 -0.0023  0.0052
   2LYSH      O   21  -0.098  -0.169   0.573  0.0063  0.0078  0.0042  0.0057 -0.0013 -0.0019  0.0054
   3PHE       N   22   0.122  -0.190   0.541  0.0085  0.0049 -0.0073  0.0132  0.0051 -0.0091  0.0074
   3PHE       H   23   0.205  -0.221   0.577  0.0181  0.0023 -0.0058  0.0364  0.0014 -0.0128  0.0156
   3PHE      CA   24   0.144  -0.121   0.414  0.0195  0.0218 -0.0263  0.0328  0.0074 -0.0098  0.0040
   3PHE      CB   25   0.290  -0.080   0.414  0.0430  0.0323 -0.0499  0.0808  0.0205 -0.0300  0.0160
   3PHE      CG   26   0.346  -0.013   0.539  0.0274  0.0205 -0.0248  0.0524  0.0133 -0.0192  0.0095
   3PHE     CD1   27   0.452  -0.076   0.600  0.0394  0.0293 -0.0156  0.0700  0.0004 -0.0265  0.0187
   3PHE     CD2   28   0.285   0.103   0.581  0.0275  0.0241 -0.0284  0.0491  0.0066 -0.0177  0.0093
   3PHE     CE1   29   0.497  -0.011   0.714  0.0442  0.0351 -0.0202  0.0803 -0.0043 -0.0238  0.0173
   3PHE     CE2   30   0.326   0.169   0.695  0.0333  0.0395 -0.0418  0.0528  0.0085 -0.0153  0.0075
   3PHE      CZ   31   0.434   0.105   0.755  0.0337  0.0332 -0.0417  0.0634  0.0066 -0.0129  0.0047
   3PHE       C   32   0.101  -0.189   0.284  0.0327  0.0241 -0.0361  0.0637  0.0114 -0.0234  0.0103
   3PHE       O   33   0.077  -0.118   0.187  0.0511  0.0755 -0.0656  0.0718  0.0158 -0.0151  0.0060
   4LYSH      N   34   0.093  -0.320   0.296  0.0320  0.0058 -0.0150  0.0589  0.0091 -0.0399  0.0314
   4LYSH      H   35   0.118  -0.358   0.379  0.0318  0.0060 -0.0014  0.0392 -0.0034 -0.0355  0.0501
   4LYSH     CA   36   0.045  -0.412   0.192  0.0446  0.0064 -0.0169  0.0788  0.0134 -0.0598  0.0485
   4LYSH     CB   37   0.074  -0.556   0.227  0.0777  0.0436  0.0208  0.0790  0.0005 -0.0864  0.1105
   4LYSH     CG   38   0.218  -0.601   0.213  0.1084  0.0559  0.0588  0.1709 -0.0244 -0.1222  0.0984
   4LYSH     CD   39   0.257  -0.622   0.068  0.1091  0.0251  0.0588  0.2030 -0.0386 -0.1401  0.0991
   4LYSH     CE   40   0.197  -0.743   0.000  0.1493  0.0251  0.0360  0.2547 -0.0236 -0.2037  0.1681
   4LYSH     NZ   41   0.239  -0.760  -0.137  0.1881  0.0172 -0.0117  0.3467  0.0103 -0.2626  0.2005
   4LYSH    HZ1   42   0.199  -0.700  -0.182  0.2577  0.1619 -0.1051  0.3903  0.1024 -0.2577  0.2210
   4LYSH    HZ2   43   0.322  -0.751  -0.148  0.3257  0.0353  0.0344  0.7002 -0.0046 -0.3855  0.2418
   4LYSH    HZ3   44   0.210  -0.836  -0.169  0.1404  0.0710 -0.0074  0.2148 -0.0018 -0.1657  0.1356
   4LYSH      C   45  -0.104  -0.398   0.165  0.0288  0.0084 -0.0178  0.0533  0.0101 -0.0319  0.0247
   4LYSH      O   46  -0.158  -0.391   0.059  0.0756  0.0302 -0.0344  0.1816  0.0139 -0.0333  0.0149
   5ARG       N   47  -0.180  -0.399   0.272  0.0085  0.0014 -0.0005  0.0077  0.0007 -0.0089  0.0163
   5ARG       H   48  -0.144  -0.413   0.357  0.0205  0.0054  0.0095  0.0304 -0.0047  0.0006  0.0255
   5ARG      CA   49  -0.325  -0.378   0.269  0.0028  0.0020  0.0010  0.0022 -0.0008 -0.0010  0.0041
   5ARG      CB   50  -0.384  -0.407   0.406  0.0069  0.0065 -0.0055  0.0089  0.0014 -0.0010  0.0052
   5ARG      CG   51  -0.500  -0.504   0.403  0.0314  0.0269 -0.0313  0.0409  0.0015  0.0041  0.0262
   5ARG      CD   52  -0.482  -0.637   0.385  0.1246  0.1146 -0.0658  0.0459  0.0068 -0.0438  0.2133
   5ARG      NE   53  -0.591  -0.725   0.401  0.0811  0.1489 -0.0976  0.0655 -0.0135  0.0035  0.0289
   5ARG      HE   54  -0.644  -0.712   0.479  0.0982  0.2020 -0.1162  0.0782 -0.0024 -0.0100  0.0146
   5ARG      CZ   55  -0.622  -0.825   0.320  0.0947  0.1779 -0.1304  0.1046 -0.0007  0.0008  0.0016
   5ARG     NH1   56  -0.732  -0.891   0.340  0.1843  0.2705 -0.2453  0.2349  0.0611 -0.0725  0.0476
   5ARG    HH11   57  -0.798  -0.865   0.401  0.2352  0.2829 -0.3065  0.3393  0.1068 -0.1130  0.0835
   5ARG    HH12   58  -0.743  -0.968   0.289  0.2510  0.3487 -0.2877  0.2821  0.0740 -0.1214  0.1221
```

University of Alberta

University of Alberta

5ARG	NH2	59	-0.550	-0.856	0.214	0.0752	0.1571	-0.0747	0.0635	-0.0202	0.0127	0.0051
5ARG	HH21	60	-0.491	-0.790	0.184	0.0558	0.0978	-0.0265	0.0406	-0.0104	0.0270	0.0290
5ARG	HH22	61	-0.550	-0.939	0.171	0.1168	0.2387	-0.1030	0.0931	-0.0236	-0.0154	0.0188
5ARG	C	62	-0.391	-0.249	0.222	0.0104	0.0161	0.0023	0.0039	-0.0123	-0.0008	0.0111
5ARG	O	63	-0.499	-0.256	0.165	0.0197	0.0249	0.0034	0.0082	-0.0246	-0.0053	0.0261
6PRO	N	64	-0.330	-0.133	0.235	0.0197	0.0367	-0.0065	0.0081	-0.0219	0.0064	0.0144
6PRO	CA	65	-0.382	-0.010	0.174	0.0521	0.0927	-0.0123	0.0123	-0.0653	0.0155	0.0512
6PRO	CB	66	-0.308	0.105	0.242	0.0458	0.0918	-0.0144	0.0088	-0.0486	0.0145	0.0367
6PRO	CG	67	-0.215	0.044	0.344	0.0373	0.0683	-0.0140	0.0046	-0.0429	0.0122	0.0391
6PRO	CD	68	-0.208	-0.103	0.309	0.0140	0.0235	-0.0111	0.0074	-0.0083	0.0048	0.0110
6PRO	C	69	-0.360	-0.014	0.024	0.0908	0.2040	-0.0536	0.0269	-0.0866	0.0284	0.0416
6PRO	O	70	-0.295	-0.097	-0.028	0.1540	0.4253	-0.0101	0.0184	-0.0794	-0.0007	0.0182
7GLY	N	71	-0.419	0.074	-0.052	0.1015	0.1515	-0.0701	0.0794	-0.0932	0.0685	0.0736
7GLY	H	72	-0.476	0.139	-0.012	0.1192	0.1480	-0.0402	0.1119	-0.0940	0.0859	0.0977
7GLY	CA	73	-0.409	0.086	-0.197	0.1267	0.1515	-0.1139	0.1518	-0.0974	0.0985	0.0769
7GLY	C	74	-0.265	0.097	-0.238	0.0773	0.1501	-0.0426	0.0301	-0.0781	0.0312	0.0516
7GLY	O	75	-0.189	0.172	-0.184	0.0532	0.0932	-0.0164	0.0286	-0.0330	-0.0040	0.0378
8LEU	N	76	-0.229	0.019	-0.337	0.1197	0.2902	-0.0137	0.0075	-0.1292	0.0072	0.0615
8LEU	H	77	-0.297	-0.034	-0.372	0.1749	0.4021	-0.0934	0.0479	-0.1561	0.0254	0.0749
8LEU	CA	78	-0.096	0.009	-0.392	0.1429	0.3240	0.1209	0.0554	-0.1217	-0.0456	0.0493
8LEU	CB	79	-0.096	-0.080	-0.514	0.2190	0.5561	0.1428	0.0435	-0.1449	-0.0464	0.0573
8LEU	CG	80	-0.141	-0.217	-0.478	0.3441	0.8959	0.1184	0.0229	-0.2962	-0.0326	0.1136
8LEU	CD1	81	-0.054	-0.303	-0.523	0.5538	0.6706	0.2435	0.1054	-0.7375	-0.2905	0.8855
8LEU	CD2	82	-0.261	-0.260	-0.534	0.2547	0.6376	0.0268	0.0621	0.1273	0.0387	0.0642
8LEU	C	83	-0.039	0.141	-0.436	0.0977	0.1416	0.1117	0.1058	-0.0770	-0.0650	0.0458
8LEU	O	84	0.063	0.184	-0.389	0.1701	0.2202	0.1388	0.1373	-0.1784	-0.1205	0.1528
9ARG	N	85	-0.107	0.205	-0.520	0.0435	0.0126	0.0212	0.1144	0.0020	-0.0011	0.0037
9ARG	H	86	-0.185	0.168	-0.556	0.0471	0.0149	-0.0046	0.0867	-0.0031	0.0496	0.0397
9ARG	CA	87	-0.057	0.330	-0.567	0.0924	0.0506	-0.1007	0.2196	0.0035	-0.0007	0.0072
9ARG	CB	88	-0.140	0.380	-0.669	0.2700	0.3880	-0.3232	0.2917	-0.1921	0.1579	0.1304
9ARG	CG	89	-0.170	0.336	-0.778	0.6931	0.5013	-0.6469	1.4417	-0.1546	0.4096	0.1363
9ARG	CD	90	-0.062	0.277	-0.853	0.8877	0.5991	-0.9685	2.0271	0.0525	-0.0060	0.0370
9ARG	NE	91	-0.012	0.181	-0.809	0.9232	0.7541	-1.0669	1.5779	0.5642	-0.8137	0.4374
9ARG	HE	92	-0.008	0.184	-0.749	1.0931	1.7131	-1.1119	0.8914	1.0261	-0.7114	0.6748
9ARG	CZ	93	0.030	0.089	-0.842	1.2797	0.2610	-0.7229	2.3761	0.4688	-1.6595	1.2020
9ARG	NH1	94	0.070	0.013	-0.782	1.6976	0.6407	-0.8604	1.7430	1.0495	-2.1380	2.7091
9ARG	HH11	95	0.070	0.026	-0.713	1.8526	1.3607	-1.0152	1.0667	1.8385	-1.7288	3.1303
9ARG	HH12	96	0.102	-0.059	-0.804	2.1500	0.4854	-0.6249	2.2961	0.7258	-2.8531	3.6684
9ARG	NH2	97	0.030	0.064	-0.933	1.7768	0.0539	0.2469	4.0851	-0.1943	-2.0099	1.1914
9ARG	HH21	98	-0.010	0.118	-0.972	1.9389	0.2059	0.8585	4.6811	-0.2887	-1.6122	0.9296
9ARG	HH22	99	0.070	-0.005	-0.963	2.2343	0.2214	0.7035	4.8481	-0.5208	-2.6241	1.6333
9ARG	C	100	-0.028	0.445	-0.473	0.0606	0.0257	-0.0483	0.1254	-0.0108	0.0405	0.0306
9ARG	O	101	0.042	0.538	-0.506	0.0929	0.0602	-0.0680	0.1503	0.0045	0.0572	0.0683
10ARG	N	102	-0.089	0.438	-0.358	0.0283	0.0059	-0.0115	0.0454	-0.0125	0.0325	0.0335
10ARG	H	103	-0.148	0.366	-0.343	0.0216	0.0110	-0.0128	0.0395	-0.0018	0.0090	0.0144
10ARG	CA	104	-0.063	0.539	-0.257	0.0416	0.0078	-0.0027	0.0076	-0.0216	0.0187	0.1096
10ARG	CB	105	-0.141	0.508	-0.130	0.0436	0.0108	0.0047	0.0165	-0.0072	-0.0271	0.1034
10ARG	CG	106	-0.286	0.536	-0.156	0.0809	0.0156	0.0221	0.1010	-0.0181	-0.0365	0.1261
10ARG	CD	107	-0.363	0.452	-0.065	0.1106	0.0232	-0.0292	0.2337	0.0097	-0.0684	0.0748
10ARG	NE	108	-0.478	0.517	-0.033	0.2553	0.0727	0.1480	0.6662	-0.0150	-0.0350	0.0271
10ARG	HE	109	-0.489	0.597	-0.002	0.4250	0.1792	0.2884	0.9505	-0.0853	-0.2603	0.1454
10ARG	CZ	110	-0.590	0.475	-0.033	0.3835	0.0678	0.1700	0.9122	0.0646	0.3878	0.1704
10ARG	NH1	111	-0.695	0.550	-0.019	0.5281	0.1548	0.3559	1.2707	0.1073	0.4105	0.1587
10ARG	HH11	112	-0.693	0.628	-0.021	0.5683	0.2333	0.4570	1.2661	-0.0161	0.0617	0.2055
10ARG	HH12	113	-0.770	0.519	-0.010	0.7441	0.1818	0.4149	1.5630	0.2317	0.8291	0.4877
10ARG	NH2	114	-0.605	0.360	-0.043	0.6011	0.0567	0.0598	0.8937	0.0396	0.8544	0.8528
10ARG	HH21	115	-0.531	0.307	-0.053	0.6609	0.0814	0.0213	0.7220	-0.0036	0.8935	1.1793
10ARG	HH22	116	-0.689	0.329	-0.048	0.8105	0.0760	0.0628	0.9918	0.0336	1.0906	1.3635
10ARG	C	117	0.085	0.546	-0.221	0.0397	0.0088	-0.0043	0.0032	-0.0217	0.0088	0.1072
10ARG	O	118	0.141	0.653	-0.206	0.0654	0.0208	-0.0097	0.0065	-0.0381	0.0101	0.1688

University of Alberta

```
    11VAL       N  119  0.136   0.426  -0.195  0.0333  0.0075 -0.0015  0.0039 -0.0171  0.0048  0.0886
    11VAL       H  120  0.086   0.345  -0.205  0.0363  0.0092 -0.0015  0.0035 -0.0175  0.0044  0.0963
    11VAL      CA  121  0.276   0.408  -0.157  0.0269  0.0043 -0.0011  0.0061 -0.0080  0.0047  0.0703
    11VAL      CB  122  0.296   0.267  -0.101  0.0316  0.0045  0.0006  0.0086 -0.0093  0.0103  0.0815
    11VAL     CG1  123  0.428   0.269  -0.031  0.0270  0.0245 -0.0108  0.0234 -0.0139  0.0051  0.0332
    11VAL     CG2  124  0.287   0.153  -0.196  0.0731  0.1005 -0.0010  0.0097 -0.0890  0.0018  0.1090
    11VAL       C  125  0.372   0.441  -0.270  0.0264  0.0185  0.0029  0.0083 -0.0111  0.0071  0.0525
    11VAL       O  126  0.481   0.485  -0.240  0.0449  0.0272 -0.0199  0.0578 -0.0272  0.0412  0.0497
    12ARG       N  127  0.341   0.419  -0.397  0.0349  0.0325  0.0065  0.0111 -0.0048 -0.0207  0.0612
    12ARG       H  128  0.252   0.396  -0.421  0.0391  0.0355  0.0006  0.0285 -0.0036 -0.0312  0.0532
    12ARG      CA  129  0.434   0.429  -0.510  0.0337  0.0297  0.0081  0.0089 -0.0061 -0.0142  0.0627
    12ARG      CB  130  0.362   0.372  -0.630  0.0647  0.0422 -0.0010  0.0614  0.0173 -0.0702  0.0906
    12ARG      CG  131  0.249   0.441  -0.703  0.0916  0.0563  0.0003  0.1687 -0.0021 -0.0842  0.0498
    12ARG      CD  132  0.280   0.570  -0.774  0.1060  0.0885  0.0354  0.2186 -0.0062 -0.0358  0.0109
    12ARG      NE  133  0.346   0.538  -0.900  0.1270  0.1044  0.1056  0.2718 -0.0118 -0.0192  0.0046
    12ARG      HE  134  0.304   0.464  -0.940  0.1473  0.1588  0.0915  0.2712  0.0002 -0.0280  0.0120
    12ARG      CZ  135  0.447   0.603  -0.955  0.1524  0.0773  0.1268  0.3736 -0.0043  0.0104  0.0063
    12ARG     NH1  136  0.460   0.593  -1.085  0.2312  0.0682  0.1358  0.6127  0.0036 -0.0204  0.0127
    12ARG    HH11  137  0.400   0.557  -1.143  0.3041  0.1307  0.1201  0.7396  0.0067 -0.0488  0.0419
    12ARG    HH12  138  0.541   0.619  -1.119  0.2830  0.0241  0.0825  0.8047 -0.0042 -0.0770  0.0203
    12ARG     NH2  139  0.537   0.674  -0.889  0.1314  0.0765  0.1056  0.2984  0.0100  0.0617  0.0192
    12ARG    HH21  140  0.520   0.686  -0.798  0.1313  0.0969  0.0621  0.2782  0.0042  0.0577  0.0188
    12ARG    HH22  141  0.612   0.713  -0.930  0.1471  0.1089  0.1318  0.2768  0.0455  0.0909  0.0556
    12ARG       C  142  0.494   0.567  -0.525  0.0339  0.0659  0.0050  0.0053 -0.0334  0.0013  0.0306
    12ARG       O  143  0.605   0.585  -0.572  0.0511  0.0749 -0.0134  0.0330 -0.0376  0.0303  0.0456
    12ARG       N  144  0.447   0.684  -0.495  0.0689  0.1759  0.0359  0.0122 -0.0353 -0.0107  0.0187
    12ARG      H1  145  0.504   0.754  -0.521  0.1025  0.2887  0.0248  0.0113  0.0013  0.0003  0.0075
    12ARG      H2  146  0.368   0.714  -0.452  0.0866  0.2014  0.0568  0.0197 -0.0145 -0.0070  0.0389
AVE.COORDS 10-15PS    G110-TnI peptide, 0.1 M.E. cardiac TnC.Ca4, tm=150ms, starting with beta-strand coordinates
 146
     1GLY     ACC    1 -0.293  -0.126   0.686  0.3011  0.0849  0.2239  0.6534 -0.1144 -0.2927  0.1651
     1GLY       C    2 -0.363  -0.023   0.611  0.1720  0.0088  0.0029  0.3636 -0.0107 -0.2180  0.1436
     1GLY       O    3 -0.335   0.090   0.589  0.2508  0.0586 -0.1177  0.3939  0.0632 -0.3037  0.3000
     1GLY       N    4 -0.476  -0.063   0.566  0.0673  0.0069  0.0103  0.1446 -0.0142 -0.0655  0.0503
     1GLY       H    5 -0.413   0.004   0.574  0.1113  0.0203 -0.0510  0.2422  0.0215 -0.1227  0.0714
     1GLY      CA    6 -0.529  -0.083   0.432  0.0398  0.0103 -0.0049  0.0654 -0.0100 -0.0399  0.0437
     1GLY       C    7 -0.503  -0.226   0.385  0.0354  0.0089 -0.0076  0.0627 -0.0048 -0.0351  0.0348
     1GLY       O    8 -0.393  -0.278   0.396  0.0586  0.0113  0.0045  0.1056 -0.0122 -0.0674  0.0587
    2LYSH       N    9 -0.609  -0.282   0.330  0.0151  0.0058 -0.0042  0.0254 -0.0031 -0.0103  0.0142
    2LYSH       H   10 -0.691  -0.236   0.329  0.0188  0.0107  0.0045  0.0309 -0.0046 -0.0129  0.0147
    2LYSH      CA   11 -0.602  -0.414   0.267  0.0110  0.0081  0.0013  0.0158  0.0054  0.0030  0.0090
    2LYSH      CB   12 -0.739  -0.457   0.219  0.0150  0.0108 -0.0063  0.0083  0.0137 -0.0088  0.0260
    2LYSH      CG   13 -0.850  -0.466   0.318  0.0339  0.0069 -0.0010  0.0814  0.0055 -0.0020  0.0133
    2LYSH      CD   14 -0.975  -0.520   0.269  0.1417  0.0149 -0.0444  0.4007  0.0050 -0.0382  0.0096
    2LYSH      CE   15 -1.086  -0.509   0.368  0.2534  0.0183 -0.0822  0.7104  0.0151 -0.1010  0.0315
    2LYSH      NZ   16 -1.182  -0.559   0.329  0.7434  0.0920 -0.2154  2.0490  0.0370 -0.3323  0.0893
    2LYSH     HZ1   17 -1.156  -0.628   0.314  0.9997  0.2893 -0.6506  2.4494  0.1572 -0.6431  0.2605
    2LYSH     HZ2   18 -1.242  -0.557   0.398  0.7869  0.0848 -0.2019  2.1151  0.0571 -0.3792  0.1608
    2LYSH     HZ3   19 -1.198  -0.533   0.256  1.0562  0.1841  0.0814  2.9351  0.0265 -0.1295  0.0495
    2LYSH       C   20 -0.503  -0.403   0.150  0.0099  0.0063 -0.0018  0.0119  0.0061  0.0022  0.0115
    2LYSH       O   21 -0.401  -0.469   0.140  0.0109  0.0112  0.0000  0.0044  0.0092  0.0034  0.0170
     3PHE       N   22 -0.534  -0.301   0.072  0.0097  0.0043 -0.0018  0.0074  0.0052  0.0002  0.0173
     3PHE       H   23 -0.609  -0.246   0.093  0.0188  0.0111  0.0046  0.0134  0.0139  0.0079  0.0320
     3PHE      CA   24 -0.464  -0.256  -0.049  0.0143  0.0122  0.0081  0.0080  0.0102  0.0064  0.0227
     3PHE      CB   25 -0.546  -0.149  -0.118  0.0290  0.0297  0.0202  0.0199  0.0159  0.0184  0.0375
     3PHE      CG   26 -0.691  -0.185  -0.150  0.0252  0.0281  0.0260  0.0254  0.0143  0.0111  0.0221
     3PHE     CD1   27 -0.716  -0.269  -0.232  0.1146  0.0423 -0.0615  0.1859  0.0550 -0.1011  0.1157
     3PHE     CD2   28 -0.780  -0.123  -0.101  0.2012  0.0303  0.0989  0.5071 -0.0210 -0.1243  0.0661
     3PHE     CE1   29 -0.845  -0.298  -0.276  0.1187  0.0460 -0.0654  0.1942  0.0524 -0.1082  0.1157
     3PHE     CE2   30 -0.911  -0.154  -0.137  0.2103  0.0311  0.0962  0.5279 -0.0252 -0.1162  0.0719
```

University of Alberta

```
3PHE      CZ   31  -0.931  -0.236  -0.223  0.0328  0.0290  0.0259  0.0430  0.0087  0.0173  0.0264
3PHE       C   32  -0.323  -0.202  -0.023  0.0206  0.0118  0.0038  0.0045  0.0181  0.0089  0.0453
3PHE       O   33  -0.251  -0.190  -0.120  0.0310  0.0176  0.0060  0.0208  0.0241  0.0217  0.0547
4LYSH      N   34  -0.294  -0.166   0.100  0.0311  0.0082 -0.0061  0.0130  0.0108 -0.0266  0.0721
4LYSH      H   35  -0.354  -0.182   0.172  0.0354  0.0088 -0.0078  0.0443  0.0054 -0.0432  0.0530
4LYSH     CA   36  -0.165  -0.108   0.139  0.0565  0.0146 -0.0180  0.0425  0.0165 -0.0605  0.1124
4LYSH     CB   37  -0.176  -0.058   0.283  0.0780  0.0265 -0.0315  0.0773  0.0262 -0.0927  0.1301
4LYSH     CG   38  -0.199   0.089   0.287  0.1610  0.1378 -0.0767  0.0565  0.1649 -0.1216  0.2889
4LYSH     CD   39  -0.081   0.157   0.322  0.2622  0.4225 -0.3153  0.2487  0.1596 -0.1411  0.1155
4LYSH     CE   40  -0.011   0.253   0.265  0.1327  0.0973 -0.0210  0.0423  0.0815  0.0344  0.2585
4LYSH     NZ   41   0.069   0.241   0.219  0.1706  0.1872 -0.0333  0.2270  0.0772 -0.0609  0.0977
4LYSH    HZ1   42   0.081   0.268   0.226  0.4529  0.2122 -0.0212  0.7325  0.0480 -0.2201  0.4140
4LYSH    HZ2   43   0.081   0.217   0.203  0.4631  0.3041  0.2755  0.6749  0.1380 -0.0157  0.4104
4LYSH    HZ3   44   0.094   0.230   0.199  0.4619  0.8405 -0.2999  0.3186  0.2444 -0.1583  0.2264
4LYSH      C   45  -0.057  -0.215   0.126  0.0429  0.0155 -0.0144  0.0436  0.0094 -0.0454  0.0695
4LYSH      O   46   0.053  -0.182   0.083  0.0352  0.0172 -0.0052  0.0241  0.0120 -0.0284  0.0643
5ARG       N   47  -0.092  -0.336   0.166  0.0326  0.0059 -0.0078  0.0557 -0.0008 -0.0257  0.0362
5ARG       H   48  -0.177  -0.354   0.207  0.0314  0.0049 -0.0023  0.0539 -0.0013 -0.0203  0.0353
5ARG      CA   49  -0.003  -0.450   0.150  0.0272  0.0023 -0.0020  0.0613 -0.0034 -0.0037  0.0181
5ARG      CB   50  -0.064  -0.578   0.205  0.0405  0.0058  0.0121  0.0825  0.0047  0.0399  0.0333
5ARG      CG   51  -0.096  -0.573   0.352  0.0795  0.0351  0.0310  0.1596  0.0328  0.0469  0.0437
5ARG      CD   52  -0.138  -0.708   0.396  0.1211  0.1030  0.1043  0.1558  0.0895  0.1196  0.1043
5ARG      NE   53  -0.087  -0.728   0.527  0.2177  0.2774  0.2581  0.3089  0.1245  0.1259  0.0667
5ARG      HE   54  -0.054  -0.678   0.576  0.3351  0.1678  0.0906  0.7366  0.0373  0.2018  0.1007
5ARG      CZ   55  -0.081  -0.819   0.589  0.4870  1.2188  0.5098  0.2287  0.0620  0.0275  0.0135
5ARG     NH1   56  -0.033  -0.829   0.710  0.6058  1.3993  0.6185  0.4074  0.0240  0.0195  0.0109
5ARG    HH11   57  -0.004  -0.785   0.760  0.4813  0.6987  0.4211  0.7032  0.1102  0.0474  0.0419
5ARG    HH12   58  -0.031  -0.882   0.747  1.1059  2.9023  0.7828  0.3438 -0.2970 -0.0277  0.0715
5ARG     NH2   59  -0.119  -0.902   0.535  1.0238  2.8728  0.5084  0.1146 -0.1579 -0.0521  0.0841
5ARG    HH21   60  -0.138  -0.897   0.445  1.0045  2.7398  0.4982  0.1864 -0.1407 -0.0877  0.0874
5ARG    HH22   61  -0.127  -0.961   0.586  1.5439  4.4036  0.2575  0.0407 -0.4624 -0.0516  0.1875
5ARG       C   62   0.036  -0.470   0.004  0.0110  0.0027 -0.0027  0.0101 -0.0013  0.0029  0.0203
5ARG       O   63   0.155  -0.486  -0.020  0.0153  0.0030  0.0015  0.0091 -0.0015  0.0055  0.0337
6PRO       N   64  -0.050  -0.477  -0.096  0.0100  0.0042  0.0004  0.0047 -0.0023  0.0067  0.0211
6PRO      CA   65   0.003  -0.474  -0.232  0.0257  0.0185  0.0188  0.0373 -0.0023  0.0094  0.0211
6PRO      CB   66  -0.114  -0.517  -0.321  0.0306  0.0271  0.0275  0.0404 -0.0064 -0.0117  0.0243
6PRO      CG   67  -0.241  -0.506  -0.240  0.0165  0.0129  0.0079  0.0090 -0.0122 -0.0079  0.0277
6PRO      CD   68  -0.194  -0.503  -0.095  0.0136  0.0038  0.0009  0.0146 -0.0030  0.0004  0.0225
6PRO       C   69   0.066  -0.342  -0.272  0.0338  0.0253  0.0227  0.0519  0.0104  0.0309  0.0242
6PRO       O   70   0.186  -0.344  -0.290  0.0681  0.0327  0.0398  0.0913  0.0377  0.0812  0.0802
7GLY       N   71  -0.015  -0.238  -0.280  0.0310  0.0178  0.0085  0.0353  0.0024  0.0319  0.0399
7GLY       H   72  -0.106  -0.244  -0.259  0.0444  0.0194  0.0134  0.0239  0.0091  0.0193  0.0900
7GLY      CA   73   0.022  -0.102  -0.318  0.0449  0.0311 -0.0059  0.0470 -0.0138  0.0479  0.0566
7GLY       C   74   0.094  -0.039  -0.200  0.0492  0.0174 -0.0243  0.0597 -0.0246  0.0627  0.0706
7GLY       O   75   0.035   0.017  -0.109  0.0507  0.0146 -0.0277  0.0757 -0.0246  0.0652  0.0618
8LEU       N   76   0.225  -0.062  -0.207  0.0393  0.0198 -0.0198  0.0335 -0.0251  0.0407  0.0647
8LEU       H   77   0.262  -0.113  -0.277  0.0508  0.0318 -0.0080  0.0159 -0.0433  0.0092  0.1047
8LEU      CA   78   0.321  -0.015  -0.108  0.0483  0.0145 -0.0293  0.0918 -0.0139  0.0466  0.0387
8LEU      CB   79   0.453  -0.081  -0.136  0.0613  0.0307 -0.0135  0.0370 -0.0470  0.0312  0.1161
8LEU      CG   80   0.442  -0.224  -0.141  0.2084  0.0899 -0.0077  0.0383 -0.1676  0.0338  0.4971
8LEU     CD1   81   0.425  -0.276  -0.012  0.4516  0.2664 -0.0855  0.2355 -0.2124  0.4086  0.8529
8LEU     CD2   82   0.565  -0.283  -0.198  0.2782  0.1325  0.0758  0.0869 -0.2372 -0.1356  0.6151
8LEU       C   83   0.332   0.133  -0.099  0.0438  0.0168 -0.0067  0.0970 -0.0008 -0.0297  0.0175
8LEU       O   84   0.231   0.199  -0.082  0.0709  0.0354  0.0157  0.1333  0.0122 -0.0456  0.0440
9ARG       N   85   0.449   0.189  -0.109  0.0598  0.0160 -0.0106  0.0640 -0.0080 -0.0661  0.0994
9ARG       H   86   0.520   0.129  -0.132  0.0671  0.0188 -0.0188  0.0473  0.0091 -0.0578  0.1352
9ARG      CA   87   0.477   0.330  -0.095  0.1132  0.0177  0.0177  0.0615 -0.0562 -0.1124  0.2604
9ARG      CB   88   0.622   0.354  -0.111  0.2167  0.0114  0.0074  0.0174 -0.0692 -0.0750  0.6214
9ARG      CG   89   0.708   0.266  -0.032  0.2821  0.0872  0.1172  0.1745 -0.1961 -0.2586  0.5846
9ARG      CD   90   0.836   0.259  -0.027  0.5595  0.0639  0.0103  0.0997 -0.2243  0.2011  1.5148
```

9ARG	NE	91	0.897	0.190	-0.069	0.3738	0.0458	0.1103	0.6408	0.0908	0.4885	0.4347
9ARG	HE	92	0.853	0.178	-0.126	0.6273	0.1425	0.2747	1.4850	0.0530	0.4878	0.2543
9ARG	CZ	93	1.010	0.143	-0.034	0.3616	0.0752	[illegible]	0.7539	0.1163	0.3969	0.2558
9ARG	NH1	94	1.047	0.067	-0.078	0.6798	0.3048	0.5532	1.6732	-0.1021	-0.1808	0.0613
9ARG	HH11	95	0.994	0.038	-0.130	0.9537	0.4564	0.7261	2.1386	-0.3279	-0.5913	0.2660
9ARG	HH12	96	1.128	0.038	-0.057	0.8990	0.4418	0.7424	2.0169	-0.2564	-0.4228	0.2383
9ARG	NH2	97	1.093	0.172	0.045	0.4036	0.0381	0.0442	0.3281	0.0595	0.4741	0.8447
9ARG	HH21	98	1.074	0.235	0.077	0.6579	0.0260	-0.0323	0.1569	-0.0869	0.4810	1.7907
9ARG	HH22	99	1.171	0.130	0.063	0.3863	0.0823	0.0702	0.3562	0.0152	0.3792	0.7205
9ARG	C	100	0.409	0.423	-0.194	0.0831	0.0023	0.0017	0.0678	-0.0061	-0.1044	0.1792
9ARG	O	101	0.401	0.539	-0.158	0.0736	0.0120	0.0102	0.0634	-0.0189	-0.0908	0.1455
10ARG	N	102	0.366	0.373	-0.308	0.0752	0.0155	-0.0188	0.0693	0.0364	-0.0926	0.1407
10ARG	H	103	0.374	0.282	-0.335	0.0826	0.0373	-0.0154	0.0701	0.0316	-0.0945	0.1403
10ARG	CA	104	0.297	0.454	-0.409	0.0789	0.0266	-0.0222	0.0960	0.0475	-0.0833	0.1140
10ARG	CB	105	0.256	0.361	-0.522	0.1311	0.0811	-0.0753	0.1867	0.0889	-0.1311	0.1254
10ARG	CG	106	0.368	0.312	-0.595	0.2407	0.0783	-0.1303	0.3093	0.1356	-0.3137	0.3346
10ARG	CD	107	0.362	0.281	-0.730	0.2494	0.3814	-0.1094	0.0767	0.3194	-0.1163	0.2900
10ARG	NE	108	0.302	0.186	-0.754	0.0879	0.1661	0.0772	0.0754	-0.0323	-0.0168	0.0222
10ARG	HE	109	0.243	0.198	-0.754	0.3741	0.3581	0.3153	0.3962	-0.3241	-0.2661	0.3679
10ARG	CZ	110	0.318	0.078	-0.779	0.1122	0.2731	-0.0235	0.0350	0.0403	-0.0097	0.0286
10ARG	NH1	111	0.255	0.007	-0.791	0.5042	0.6387	-0.2609	0.3711	0.3306	-0.4179	0.5029
10ARG	HH11	112	0.196	0.028	-0.783	0.8433	0.4235	-0.2750	1.1600	0.1041	-1.0016	0.9463
10ARG	HH12	113	0.278	-0.066	-0.807	0.7877	1.3344	-0.3197	0.2431	0.8617	-0.3589	0.7857
10ARG	NH2	114	0.392	0.032	-0.790	0.4079	0.6502	0.1951	0.0948	-0.2360	-0.0704	0.4787
10ARG	HH21	115	0.430	0.079	-0.785	0.7641	0.4906	0.3089	0.2958	-0.5620	-0.5021	1.5057
10ARG	HH22	116	0.412	-0.043	-0.805	0.7107	1.4328	0.4530	0.1958	-0.2115	-0.0176	0.5037
10ARG	C	117	0.176	0.523	-0.348	0.0548	0.0151	-0.0171	0.0781	0.0298	-0.0547	0.0713
10ARG	O	118	0.162	0.640	-0.377	0.0900	0.0352	-0.0119	0.0650	0.0696	-0.0587	0.1699
11VAL	N	119	0.099	0.441	-0.280	0.0370	0.0039	-0.0011	0.0833	0.0022	-0.0347	0.0238
11VAL	H	120	0.130	0.352	-0.266	0.0409	0.0035	0.0149	0.0944	-0.0054	-0.0412	0.0248
11VAL	CA	121	-0.031	0.464	-0.217	0.0258	0.0028	0.0087	0.0643	-0.0010	0.0002	0.0102
11VAL	CB	122	-0.089	0.330	-0.179	0.0424	0.0146	0.0155	0.0795	0.0005	0.0443	0.0330
11VAL	CG1	123	-0.138	0.274	-0.307	0.1031	0.1129	-0.0902	0.1300	-0.0734	0.0858	0.0663
11VAL	CG2	124	-0.212	0.341	-0.099	0.1061	0.0712	0.0420	0.0635	0.0926	0.0978	0.1837
11VAL	C	125	-0.019	0.559	-0.099	0.0503	0.0252	0.0405	0.1037	-0.0027	-0.0262	0.0219
11VAL	O	126	-0.115	0.630	-0.078	0.0687	0.0259	0.0454	0.1209	0.0069	-0.0202	0.0593
12ARG	N	127	0.089	0.566	-0.024	0.0683	0.0562	0.0701	0.1073	-0.0309	-0.0584	0.0414
12ARG	H	128	0.167	0.513	-0.039	0.0886	0.0618	0.0832	0.1302	-0.0567	-0.0942	0.0738
12ARG	CA	129	0.100	0.653	0.092	0.1109	0.1257	0.1201	0.1386	-0.0676	-0.0869	0.0683
12ARG	CB	130	0.224	0.620	0.174	0.1383	0.1790	0.1272	0.1181	-0.1205	-0.0968	0.1177
12ARG	CG	131	0.348	0.693	0.131	0.1347	0.1976	0.1064	0.0711	-0.1457	-0.0640	0.1356
12ARG	CD	132	0.465	0.623	0.189	0.1141	0.1673	0.1242	0.1070	-0.0832	-0.0555	0.0680
12ARG	NE	133	0.574	0.706	0.147	0.1410	0.1180	0.1700	0.2802	-0.0086	-0.0058	0.0248
12ARG	HE	134	0.593	0.742	0.070	0.2102	0.3794	0.2192	0.2261	0.0255	0.0065	0.0252
12ARG	CZ	135	0.655	0.755	0.217	0.3049	0.0347	-0.0108	0.8213	-0.0290	0.1387	0.0588
12ARG	NH1	136	0.748	0.826	0.164	0.4867	0.0619	-0.0976	1.2722	-0.0486	0.3300	0.1261
12ARG	HH11	137	0.762	0.847	0.083	0.4409	0.0668	0.1421	1.1019	0.0481	0.3420	0.1541
12ARG	HH12	138	0.800	0.858	0.213	0.8178	0.3083	-0.5835	1.9505	-0.1884	0.5167	0.1945
12ARG	NH2	139	0.643	0.738	0.338	0.5195	0.2078	-0.3621	1.2307	-0.1278	0.2359	0.1199
12ARG	HH21	140	0.589	0.673	0.369	0.4396	0.1854	-0.2500	0.9624	-0.1412	0.2426	0.1710
12ARG	HH22	141	0.689	0.785	0.389	0.8553	0.5698	-0.8737	1.8298	-0.2474	0.3898	0.1664
12ARG	C	142	0.099	0.799	0.051	0.1294	0.1343	0.1218	0.1151	-0.1130	-0.1093	0.1388
12ARG	O	143	0.032	0.874	0.117	0.1952	0.1946	0.1701	0.1850	-0.1441	-0.1778	0.2059
12ARG	N	144	0.155	0.870	-0.045	0.1309	0.1139	0.0912	0.0873	-0.1322	-0.0898	0.1914
12ARG	H1	145	0.228	0.855	-0.100	0.1236	0.0601	0.0380	0.0500	-0.1041	-0.0284	0.2606
12ARG	H2	146	0.119	0.956	-0.060	0.1753	0.1921	0.1232	0.0964	-0.1965	-0.1182	0.2375

University of Alberta

Table VIII-10. Comparison of the distances between proton pairs given in the TRNOE-derived distance restraint file (rijU, rijL) with those actually measured between the same proton pairs in the final structures generated from the α-helix (rijα) and the β-strand (rijβ).

spin system	rijα(Å)	rijβ(Å)	rijU(Å)	rijL(Å)
K105αCH-βCH2	2.54	2.47	2.6	2.2
K105αCH-γCH2	2.62	2.77	4.0	2.8
K105βCH2-γCH2	2.36	2.31	2.9	2.5
K105γCH2-δCH2	2.40	2.27	2.9	2.5
K105δCH2-ξCH2	2.38	2.40	3.0	2.6
K105βCH2-NH	2.11	2.92	3.3	2.3
K105γCH2-ξCH2	2.57	2.54	3.5	2.9
K105γCH2-NH	4.13	2.67	4.3	2.7
F106αCH-βCH(m)	2.90	2.89	4.0	3.4
F106αCH-βCH'(x)	2.38	2.38	3.8	3.2
F106αCH-δCH2	2.95	2.84	6.2	3.6
F106αCH-ξCH2	5.13	5.00	8.5	4.5
F106αCH-ςCH2	6.06	5.94	8.5	4.5
F106βCH(m)-βCH'(x)	1.63	1.63	3.1	2.7
F106βCH'(x)-NH	2.34	2.42	3.6	3.0
F106βCH(m)-NH	3.30	3.38	3.7	3.1
F106βCH(m)-δCH2	2.06	2.07	2.9	2.5
F106βCH(m)-ξCH2	4.55	4.45	3.5	2.9
F106βCH(m)-ςCH	5.53	5.42	3.5	2.9
F106βCH'(x)-δCH2	2.06	2.07	2.8	2.4
F106βCH'(x)-ξCH2	4.54	4.45	3.5	2.9
F106βCH'(x)-ςCH	5.52	5.42	3.5	2.9
F106NH-δCH2	2.54	2.64	6.0	3.0
F106NH-ξCH2	4.36	4.51	6.9	3.5
F106NH-ςCH	5.24	5.41	5.5	3.5
K107αCH-βCH2	2.32	2.49	2.6	2.2
K107αCH-γCH2	3.55	3.19	3.9	2.7
K107βCH2-γCH2	2.22	2.28	2.4	2.0
K107βCH2-NH	2.83	2.58	3.5	2.5
K107δCH2-γCH2	2.22	2.17	2.8	2.4
K107δCH2-ξCH2	2.35	2.06	2.7	2.3
K107γCH2-ξCH2	3.04	3.03	3.1	2.7
K107γCH2-NH	3.10	3.33	4.4	2.8
R108αCH-βCH2	2.68	2.52	3.5	2.9
R108αCH-γCH2	3.07	2.69	5.1	3.5
R108βCH2-NH	2.43	2.92	3.4	2.4

R108γCH2-δCH2	2.23	2.34	2.9	2.5
R108δCH2-NH	3.75	4.24	3.8	3.2
P109αCH-βCH(x)	2.76	2.71	3.5	2.9
P109αCH-βCH'(p)	2.23	2.28	3.4	2.8
P109αCH-γCH2	3.62	3.78	3.8	3.2
P109βCH(x)-βCH'(p)	1.63	1.63	2.6	2.2
P109βCH(x)-δCH'(m')	3.16	3.77	3.8	3.2
P109βCH(x)-δCH(m)	3.87	3.86	3.8	3.2
P109βCH'(p)-δCH(m)	3.81	3.82	3.9	3.3
P109βCH'(p)-δCH'(m')	3.80	3.21	4.5	3.5
P109βCH'(p)-γCH2	2.31	2.40	2.8	2.4
P109γCH2-δCH(m)	2.31	2.34	3.4	2.8
P109γCH2-δCH'(m')	2.44	2.42	3.6	3.0
P109δCH(m)-δCH'(m')	1.63	1.63	3.8	3.2
L111αCH-βCH2	2.57	2.52	2.6	2.2
L111αCH-(δCH3)2	3.74	3.46	4.5	2.4
L111βCH2-(δCH3)2	2.51	3.12	2.6	2.2
L111γCH-(δCH3)2	1.82	2.46	2.4	2.0
L111βCH2-NH	2.93	2.82	3.6	2.6
L111(δCH3)2-NH	3.44	3.56	3.5	2.9
R112αCH-βCH2	2.49	2.52	2.9	2.5
R112αCH-δCH2	3.11	4.35	4.6	3.0
R112γCH2-δCH2	2.24	2.30	2.9	2.5
R112βCH2-NH	2.85	2.93	3.3	2.3
R112δCH2-NH	3.97	4.12	4.5	3.5
R113αCH-βCH2	2.59	2.56	2.9	2.5
R113αCH-δCH2	4.26	3.99	4.6	3.0
R113γCH2-δCH2	2.36	2.23	2.9	2.5
R113βCH2-NH	2.92	2.66	3.3	2.3
R113δCH2-NH	3.62	2.72	4.5	3.5
V114αCH-βCH	2.46	2.18	2.9	2.5
V114αCH-(γCH3)2	2.93	3.28	3.3	2.3
V114βCH-(γCH3)2	1.80	1.88	2.3	1.9
V114βCH-NH	2.34	2.87	2.9	2.5
V114(γCH3)2-NH	3.37	2.40	4.6	2.5
R115αCH-βCH2	2.15	2.24	2.7	2.3
R115αCH-δCH2	4.39	4.59	4.6	3.0
R115γCH2-δCH2	2.23	2.35	2.9	2.5
R115βCH2-NH	2.72	2.72	3.5	2.5
R115δCH2-NH	4.05	4.02	3.9	3.3
C-term NH-NH'	1.58	1.54	2.7	2.3
N-Acetyl CH3-G104αCH2	4.07	4.24	4.2	3.6
N-Acetyl CH3-G104NH	2.41	2.42	3.0	2.6
G104αCH2-K105βCH2	4.99	5.27	5.6	3.0
G104αCH2-K105γCH2	6.73	5.01	6.6	3.6

G104αCH2-F106δCH2	7.42	5.87	9.8	4.4
G104αCH2-F106ξCH2	8.88	7.55	9.9	4.5
G104αCH2-F106ςCH	9.56	8.33	9.5	4.5
G104αCH2-K107γCH2	4.14	3.68	8.1	4.1
G104NH-K107γCH2	3.23	3.58	5.5	3.5
K105αCH-F106βCH(m)	5.75	5.71	4.2	3.6
K105αCH-F106βCH'(x)	6.39	6.49	4.2	3.6
K105βCH2-F106NH	2.95	2.73	4.1	2.7
K105γCH2-F106NH	4.01	4.19	5.0	3.4
K105γCH2-K107NH	5.92	5.94	6.4	4.4
K105NH-F106δCH2	5.32	4.82	6.4	3.4
K105NH-F106ξCH2	6.27	6.02	7.2	3.8
K105NH-F106ςCH	6.86	6.71	6.8	3.8
K105NH-K107γCH2	5.38	5.68	5.5	3.5
F106αCH-R108βCH2	5.60	5.52	4.8	3.2
F106βCH(m)-K107NH	2.99	3.21	3.7	3.1
F106βCH'(x)-K107NH	3.90	4.07	3.7	3.1
F106βCH(m)-K107αCH	4.39	4.27	4.5	3.5
F106δCH2-K107NH	4.43	4.66	6.1	3.1
F106ξCH2-K107NH	6.75	7.01	7.0	3.6
F106ςCH2-K107NH	7.62	7.93	6.6	3.6
F106δCH2-R108NH	6.58	6.48	7.0	3.6
F106ξCH2-R108NH	8.72	8.76	7.3	3.9
F106ςCH2-R108NH	9.61	9.70	6.9	3.9
F106NH-K107γCH2	5.05	5.43	5.6	3.6
F106NH-V114(γCH3)2	8.27	7.54	7.1	3.7
K107γCH2-R108NH	4.54	4.81	4.8	3.2
G110αCH2-L111βCH2	5.24	5.42	6.1	3.5
G110αCH2-L111(δCH3)2	5.76	6.09	7.2	3.2
P109βCH(x)-G110NH	2.90	2.57	3.8	3.2
P109βCH'(p)-G110NH	3.18	3.79	3.9	3.3
P109βCH(x)-L111αCH	5.65	6.95	3.8	3.2
P109βCH'(p)-L111αCH	7.14	7.65	3.9	3.3
P109γCH2-L111αCH	7.24	7.80	4.5	2.9
L111(δCH3)2-R112NH	4.69	4.25	5.9	2.9
R112βCH2-R113NH	3.29	3.48	4.4	2.8
R112βCH2-R115NH	4.87	5.02	4.5	2.9
R112βCH2-Cterm NH	7.60	6.22	5.0	3.4
R112βCH2-Cterm NH'	6.43	7.73	5.0	3.4
R113βCH2-V114αCH	4.13	4.20	4.3	2.7
R113βCH2-V114NH	2.80	2.80	4.5	2.9
R113βCH2-R115NH	5.12	5.26	4.5	2.9
R113δCH2-V114αCH	6.49	7.13	6.0	4.0
R113δCH2-V114NH	4.68	5.72	5.6	3.6
R113NH-V114(γCH3)2	5.94	5.78	6.4	3.4
V114αCH-R115βCH2	5.91	5.97	4.3	2.7

V114αCH-R115δCH2	6.87	7.55	6.0	4.0
V114αCH-Cterm NH	5.58	5.06	5.4	4.4
V114αCH-Cterm NH'	4.43	5.43	5.4	4.4
V114βCH-R115NH	4.10	3.15	3.3	2.7
V114βCH-Cterm NH	7.55	6.30	3.6	3.0
V114βCH-Cterm NH'	6.41	6.97	3.6	3.0
V114(γCH3)2-R115αCH	4.39	5.27	5.8	2.8
V114(γCH3)2-R115NH	3.84	4.46	5.7	2.7
V114(γCH3)2-Cterm NH	7.01	7.00	6.6	3.6
V114(γCH3)2-Cterm NH'	6.17	7.36	6.6	3.6
V114NH-R115βCH2	5.33	5.44	4.5	2.9
V114NH-R115δCH2	6.44	6.33	5.6	3.6
R115αCH-Cterm NH	3.81	3.92	3.5	2.9
R115αCH-Cterm NH'	3.73	3.96	3.4	2.8
R115βCH2-Cterm NH	4.69	4.19	3.5	2.9
R115βCH2-Cterm NH'	4.41	4.77	3.5	2.9
F106δCH2-K105βCH2	4.56	4.28	7.2	3.2
F106δCH2-K105δCH2	5.65	5.88	7.2	3.2
F106δCH2-K107βCH2	7.21	7.13	7.2	3.2
F106δCH2-K107γCH2	6.66	6.84	7.2	3.2
F106δCH2-R108βCH2	8.05	8.23	7.2	3.2
F106δCH2-P109βCH(x)	7.23	6.81	7.1	3.7
F106δCH2-P109βCH'(p)	7.82	7.55	7.5	4.1
F106δCH2-P109γCH2	5.61	5.20	7.9	3.5
F106δCH2-V114βCH	6.47	8.14	6.4	3.4
F106δCH2-V114(γCH3)2	6.89	7.03	8.5	3.1
F106ξCH2-K105βCH2	4.81	4.87	6.7	2.7
F106ξCH2-K105δCH2	5.02	6.39	6.7	2.7
F106ξCH2-K105ξCH2	4.55	5.38	7.9	3.5
F106ξCH2-R108βCH2	9.83	10.21	6.7	2.7
F106ξCH2-P109βCH(x)	9.02	8.59	6.9	3.5
F106ξCH2-P109βCH'(p)	9.35	9.20	7.1	3.7
F106ξCH2-P109γCH2	7.23	6.91	8.1	3.7
F106ξCH2-V114βCH	8.36	10.49	6.5	3.5
F106ξCH2-V114(γCH3)2	8.79	9.17	8.4	3.0
F106ςCH-K105βCH2	5.26	5.44	6.3	2.7
F106ςCH-K105δCH2	5.36	6.79	6.3	2.7
F106ςCH-K105ξCH2	4.49	5.53	7.5	3.5
F106ςCH-R108βCH2	10.61	11.06	6.3	2.7
F106ςCH-P109βCH(x)	9.83	9.39	6.5	3.5
F106ςCH-P109βCH'(p)	10.07	9.95	6.7	3.7
F106ςCH-P109γCH2	8.02	7.71	7.7	3.7
F106ςCH-V114βCH	9.19	11.42	6.1	3.5
F106ςCH-V114(γCH3)2	9.61	10.05	8.0	3.0

F106βCH(m)-V114(γCH3)2	6.28	5.37	6.5	3.5
F106βCH'(x)-V114(γCH3)2	5.07	5.31	6.4	3.4
R108βCH2-P109δCH(m)	4.06	3.35	4.6	3.0
R108βCH2-P109δCH(m')	2.82	2.64	4.7	3.1
P109βCH(x)-V114(γCH3)2	6.95	7.88	6.0	3.0
P109δCH'(m')-V114(γCH3)2	7.00	7.53	6.9	3.5
L111(δCH3)2-R112βCH2	7.40	7.04	6.9	2.9
L111(δCH3)2-R112δCH2	7.04	6.98	8.0	3.6
R113βCH2-V114(γCH3)2	5.76	5.13	6.9	2.9
R113δCH2-V114βCH	5.90	7.65	5.8	3.8
V114βCH-R115δCH2	8.10	6.70	5.8	3.8
V114(γCH3)2-R115βCH2	5.47	6.55	6.9	2.9
V114(γCH3)2-R115δCH2	7.76	8.29	8.0	3.6
G104αCH2-K105αCH	4.51	4.45	6.2	4.2
G110αCH2-L111αCH	4.35	4.47	5.8	3.8
R113αCH-V114αCH	4.67	4.78	4.8	3.8
V114αCH-R115αCH	4.75	4.61	4.6	3.6
K105NH-K107NH	3.96	3.76	3.9	3.3
K107NH-R108NH	2.69	2.49	3.7	3.1
G110NH-L111NH	4.38	3.91	4.5	3.5
R113NH-V114NH	2.72	2.63	4.0	3.4
V114NH-R115NH	2.77	2.81	4.0	3.4
R115NH-Cterm NH	4.49	3.53	4.6	3.6
R115NH-Cterm NH'	3.40	4.46	4.6	3.6
G104αCH2-NH	2.54	2.28	3.1	2.7
G104αCH2-K105NH	2.91	2.48	4.3	2.7
G104αCH2-F106NH	4.98	3.75	5.2	3.6
G104αCH2-K107NH	4.25	3.37	5.6	3.6
G104αCH2-R108NH	4.59	5.29	6.1	4.1
K105αCH-NH	2.70	2.72	3.4	2.8
K105αCH-F106NH	3.48	3.39	3.4	2.8
K105αCH-K107NH	4.32	4.04	4.8	3.8
F106αCH-NH	2.70	2.66	5.4	4.4
F106αCH-K105NH	5.40	5.04	6.1	4.1
F106αCH-K107NH	3.18	3.34	4.6	3.6
K107αCH-NH	2.70	2.75	4.1	3.5
K107αCH-G104NH	5.39	5.66	4.1	3.5
K107αCH-R108NH	2.95	3.06	3.7	3.1
P109αCH-G110NH	2.45	3.48	4.2	3.6
G110αCH2-NH	2.28	2.31	3.7	3.1
G110αCH2-L111NH	2.43	2.70	4.9	3.3
L111αCH-NH	2.60	2.69	4.8	3.8
L111αCH-R112NH	3.41	3.12	3.4	2.8

R112αCH-NH	2.55	2.65	3.4	2.8
R112αCH-R113NH	3.21	3.45	3.6	3.0
R113αCH-NH	2.80	2.66	3.6	3.0
R113αCH-V114NH	3.45	3.37	3.5	2.9
V114αCH-NH	2.73	2.71	3.8	3.2
V114αCH-R113NH	5.23	5.20	4.1	3.5
V114αCH-R115NH	3.47	3.56	3.0	2.6
R115αCH-NH	2.74	2.67	3.7	3.1

Table IX-1. Normalization tables for exchangeable backbone amide resonances on the TnI peptide in 50%TFE. **A.** Amide versus nonexchangeable resonance; **B.** Amide versus amide resonance. The intensities (*Na*) of the exchangeable proton peaks were integrated in a one-dimensional spectrum, and the intensity of these peaks were normalized against the integrated intensity of the V114αCH peak. The normalization factor (2*NaNb*)/(*Na*+*Nb*) was then calculated for variable values of *Nb*.

A.	Na	Nb=1	Nb=2	Nb=3
G104	1.42	1.17	1.66	1.93
K105	1.11	1.05	1.43	1.62
F106	1.25	1.11	1.54	1.76
K107	0.77	0.87	1.12	1.23
R108	1.25	1.11	1.54	1.76
L111	1.42	1.17	1.66	1.93
R112	1.00	1.00	1.33	1.50
R113	1.00	1.00	1.33	1.50
V114	0.91	0.95	1.25	1.40
R115	0.91	0.95	1.25	1.40

B.	Na	G104	K105	F106	K107	R108	L111	R112	R113	V114	R115
G104	1.42	-	1.24	1.32	1.00	1.32	1.42	1.18	1.18	1.10	1.10
K105	1.11	1.24	-	1.18	0.90	1.18	1.24	1.06	1.06	1.00	1.00
F106	1.25	1.32	1.18	-	0.96	1.26	1.32	1.12	1.12	1.06	1.06
K107	0.77	1.00	0.90	0.96	-	0.96	1.00	0.88	0.88	0.84	0.84
R108	1.25	1.32	1.18	1.26	0.96	-	1.32	1.12	1.12	1.06	1.06
L111	1.42	1.42	1.24	1.32	1.00	1.32	-	1.18	1.18	1.10	1.10
R112	1.00	1.18	1.06	1.12	0.88	1.12	1.18	-	1.00	0.96	0.96
R113	1.00	1.18	1.06	1.12	0.88	1.12	1.18	1.00	-	0.96	0.96
V114	0.91	1.10	1.00	1.06	0.84	1.06	1.10	0.96	0.96	-	0.92
R115	0.91	1.10	1.00	1.06	0.84	1.06	1.10	0.96	0.96	0.92	-

Table IX-2. Normalization tables for exchangeable backbone amide resonances on mastoparan in 50%TFE. **A.** Amide versus nonexchangeable resonance; **B.** Amide versus amide resonance. The intensities (*Na*) of the exchangeable proton peaks were integrated in a one-dimensional spectrum, and the intensity of these peaks were normalized against the integrated intensity of the I13 αCH peak. The normalization factor (2*NaNb*)/(*Na*+*Nb*) was then calculated for variable values of *Nb*.

A.	Na	Nb=1	Nb=2	Nb=3
I1	-	-	-	-
N2	0.79	0.88	1.14	1.25
L3	0.48	0.64	0.78	0.82
K4	0.69	0.82	1.02	1.12
A5	0.88	0.94	1.22	1.36
L6	0.71	0.84	1.04	1.15
A7	0.76	0.86	1.10	1.22
A8	0.98	0.98	1.32	1.48
L9	0.90	0.94	1.24	1.38
A10	0.71	0.84	1.04	1.15
L11	1.12	1.06	1.44	1.63
L12	0.71	0.84	1.04	1.15
I13	0.83	0.90	1.18	1.30
L14	0.88	0.94	1.22	1.36
N2 CONH2	0.40	0.80	1.00	1.10
L14 C-tm NH	0.46	0.92	1.20	1.34

B.	Na	N2	L3	K4	A5	L6	A7	A8	L9	A10	L11	L12	I13	L14
I1	-	-	-	-	-	-	-	-	-	-	-	-	-	-
N2	0.79	-	0.60	0.78	0.84	0.74	0.78	0.88	0.84	0.74	0.92	0.74	0.80	0.84
L3	0.48	0.60	-	0.56	0.62	0.58	0.58	0.64	0.62	0.58	0.66	0.58	0.60	0.62
K4	0.69	0.78	0.56	-	0.76	0.70	0.72	0.80	0.78	0.70	0.86	0.70	0.76	0.76
A5	0.88	0.84	0.62	0.76	-	0.78	0.82	0.92	0.88	0.78	0.98	0.78	0.82	0.88
L6	0.71	0.74	0.58	0.70	0.78	-	0.74	0.82	0.80	0.72	0.86	0.72	0.76	0.78
A7	0.76	0.78	0.58	0.72	0.82	0.74	-	0.78	0.82	0.74	0.92	0.74	0.80	0.82
A8	0.98	0.88	0.64	0.80	0.92	0.82	0.78	-	0.94	0.82	1.04	0.82	0.90	0.92
L9	0.90	0.84	0.62	0.78	0.88	0.80	0.82	0.94	-	0.80	1.00	0.80	0.86	0.88
A10	0.71	0.74	0.58	0.70	0.78	0.72	0.74	0.82	0.80	-	0.86	0.72	0.76	0.78
L11	1.12	0.92	0.66	0.86	0.98	0.86	0.92	1.04	1.00	0.86	-	0.86	0.96	0.98
L12	0.71	0.74	0.58	0.70	0.78	0.72	0.74	0.82	0.80	0.72	0.86	-	0.76	0.78
I13	0.83	0.80	0.60	0.76	0.82	0.76	0.80	0.90	0.86	0.76	0.96	0.76	-	0.82
L14	0.88	0.84	0.62	0.76	0.88	0.78	0.82	0.92	0.88	0.78	0.98	0.78	0.82	-

Table IX-3. Table of NOE cross-peak intensities for the TnI peptide in 50%TFE. Included in the table are the measured NOE intensities, the corrected and normalized NOE intensities, and the r_{ij}s calculated from these corrected and normalized values.

spin system	NOE measured	NOE normalized	rij calculated (Å)
K105αCH-βCH2	0.483	0.364	3.5
K105αCH-γCH2	0.091	0.069	4.8
K105βCH2-γCH2	0.830	0.312	3.6
K105βCH2-NH	0.640	0.448	3.4
K105γCH2-δCH2	-	0.312	3.6
K105γCH2-NH	0.212	0.148	4.2
F106αCH-βCH(m)	0.321	0.321	3.6
F106αCH-βCH'(x)	0.292	0.292	3.7
F106αCH-δCH2	0.077	0.058	4.9
F106βCH(m)-βCH'(x)	4.210	4.210	2.3
F106βCH(m)-NH	0.151	0.136	4.2
F106βCH(m)-δCH2	0.350	0.265	3.7
F106βCH'(x)-NH	0.290	0.261	3.8
F106βCH'(x)-δCH2	0.344	0.265	3.7
F106NH-δCH2	0.144	0.094	4.5
K107αCH-βCH2	0.807	0.611	3.2
K107αCH-γCH2	0.199	0.151	4.2
K107βCH2-γCH2	0.799	0.400	3.5
K107βCH2-NH	0.382	0.341	3.6
K107γCH2-δCH2	1.570	0.785	3.1
K107γCH2-NH	0.172	0.154	4.1
K107δCH2-NH	0.273	0.241	3.8
R108αCH-δCH2	0.070	0.053	5.0
R108βCH2-δCH2	0.840	0.042	5.2
R108βCH2-NH	0.733	0.476	3.4
R108γCH2-δCH2	-	0.250	3.8
R108γCH2-NH	0.458	0.297	3.7
R108δCH2-NH	0.050	0.032	5.5
P109αCH-βCH'(x)	0.605	0.605	3.2
P109αCH-βCH(p)	0.586	0.586	3.2
P109αCH-δCH(m)	0.414	0.414	3.5
P109αCH-δCH'(m')	0.541	0.541	3.3
P109βCH'(x)-βCH(p)	2.010	2.010	2.6
P109βCH'(x)-δCH(m)	0.420	0.420	3.4
P109βCH'(x)-δCH'(m')	0.266	0.266	3.7
P109βCH'(x)-γCH2	0.350	0.265	3.7

P109βCH(p)-δCH(m)	0.022	0.022	5.9
P109βCH(p)-δCH'(m')	0.080	0.080	4.7
P109βCH(p)-γCH2	0.251	0.190	4.0
P109γCH2-δCH(m)	0.582	0.340	3.6
P109γCH2-δCH'(m')	0.578	0.340	3.6
P109δCH(m)-δCH'(m')	1.690	1.690	2.7
P110αCH-βCH'(x)	0.319	0.320	3.6
P110αCH-βCH(p)	0.380	0.380	3.5
P110βCH'(x)-βCH(p)	3.370	3.370	2.4
P110βCH'(x)-δCH(m)	0.918	0.918	3.0
P110βCH'(x)-δCH'(m')	0.815	0.815	3.0
P110βCH(p)-δCH(m)	0.058	0.058	4.9
P110βCH(p)-δCH'(m')	0.073	0.073	4.7
P110δCH(m)-δCH'(m')	1.970	1.970	2.6
L111αCH-βCH2	0.995	0.758	3.1
L111αCH-(δCH3)2	0.220	0.129	4.3
L111γCH-(δCH3)2	1.340	0.528	3.3
L111βCH2-NH	1.050	0.597	3.2
L111(δCH3)2-NH	0.257	0.133	4.2
R112αCH-δCH2	0.070	0.053	5.0
R112βCH2-δCH2	0.500	0.250	3.8
R112βCH2-NH	0.600	0.450	3.4
R112γCH2-δCH2	0.840	0.420	3.4
R112γCH2-NH	0.350	0.265	3.7
R112δCH2-NH	0.024	0.017	6.2
R113αCH-δCH2	0.070	0.053	5.0
R113βCH2-δCH2	0.500	0.250	3.8
R113βCH2-NH	0.600	0.450	3.4
R113γCH2-δCH2	0.840	0.420	3.4
R113γCH2-NH	0.350	0.265	3.7
R113δCH2-NH	0.020	0.170	4.1
V114αCH-βCH	0.278	0.278	3.7
V114αCH-(γCH3)2	0.284	0.166	4.1
V114βCH-(γCH3)2	0.853	0.499	3.3
V114βCH-NH	0.279	0.294	3.7
V114(γCH3)2-NH	0.359	0.227	3.9
R115αCH-βCH2	0.612	0.407	3.5
R115αCH-δCH2	0.104	0.079	4.7
R115βCH2-δCH2	0.500	0.130	4.3
R115βCH2-NH	0.548	0.438	3.4
R115γCH2-δCH2	0.840	0.420	3.4
R115γCH2-NH	0.483	0.386	3.5
R115δCH2-NH	0.030	0.024	5.8
C-term NH-NH'	1.690	1.690	2.7
N-Ac CH3-G104 NH	0.143	0.074	4.7

F106βCH2-K107NH	0.104	0.067	4.8
K105γCH2-F106NH	0.100	0.064	4.9
K107γCH2-R108NH	0.100	0.088	4.6
R108βCH2-P109αCH	0.527	0.399	3.5
P109αCH-P110βCH'(x)	0.291	0.291	3.7
P109αCH-P110δCH(m)	0.390	0.390	3.5
P109αCH-P110δCH'(m')	0.439	0.439	3.4
P110βCH'(x)-L111NH	0.164	0.140	4.2
P110βCH(p)-L111NH	0.074	0.063	4.9
L111(δCH3)2-R112NH	0.160	0.107	4.4
R113βCH2-V114NH	0.284	0.227	3.9
R113γCH2-V114NH	0.402	0.322	3.6
R113NH-V114βCH	0.127	0.130	4.3
R113NH-V114(γCH3)2	0.160	0.093	4.5
F106βCH'(x)-K107δCH2	0.196	0.148	4.2
R108βCH2-P109δCH(m)	0.230	0.174	4.0
P109βCH'(x)-P110δCH(m)	0.168	0.168	4.1
P109βCH'(x)-P110δCH(m')	0.050	0.050	5.1
P109βCH(p)-P110δCH(m)	0.121	0.121	4.3
P109βCH(p)-P110δCH'(m')	0.088	0.088	4.6
K105NH-F106NH	0.382	0.324	3.6
K107NH-R108NH	0.477	0.497	3.3
R112NH-Cterm NH2	0.070	0.070	4.8
R113NH-V114NH	0.533	0.558	3.3
G104αCH2-NH	0.233	0.196	4.0
G104αCH2-K105NH	0.462	0.438	3.4
K105αCH-NH	0.169	0.161	4.1
K105αCH-F106NH	0.325	0.292	3.7
F106αCH-NH	0.121	0.108	4.4
F106αCH-K107NH	0.221	0.254	3.8
F106NH-K107αCH	0.255	0.293	3.7
K107αCH-NH	0.366	0.421	3.4
K107αCH-R108NH	0.951	0.856	3.0
R108αCH-NH	0.045	0.040	5.3
P110αCH-L111NH	0.313	0.268	3.8
L111αCH-NH	0.167	0.143	4.2
R112αCH-NH	0.435	0.435	3.4
R113αCH-NH	0.435	0.435	3.4
R113αCH-V114NH	0.492	0.518	3.3
V114αCH-NH	0.149	0.157	4.1
V114αCH-R115NH	0.402	0.423	3.4
R115αCH-NH	0.765	0.805	3.1

Table IX-4. Table of NOE cross-peak intensities for mastoparan in 50%TFE. Included in the table are the measured NOE intensities, the corrected and normalized NOE intensities, and the r_{ij}s calculated from these corrected and normalized values.

---

spin system	NOE measured	NOE normalized	rij calculated (Å)
I1βCH-(γCH3')	1.46	0.97	2.3
I1βCH-γCH'(p)	2.29	2.29	1.9
I1γCH'(p)-γCH(t)	0.96	0.96	2.3
I1γCH'(p)-(γCH3')	1.11	0.74	2.4
I1γCH'(p)-(δCH3)	1.11	0.74	2.4
N2βCH'(m)-βCH(x)	0.91	0.91	2.3
N2CONH2	1.11	1.52	2.1
N2CONH2-βCH'(m)	0.28	0.24	2.9
N2CONH2-βCH(x)	0.27	0.24	2.9
L3NH-αCH	0.19	0.30	2.8
L3NH-βCH2	0.48	0.62	2.5
L3NH-γCH	0.18	0.28	2.9
L3NH-(δCH3)2	0.17	0.19	3.1
L3αCH-βCH2	1.80	1.36	2.1
L3αCH-(δCH3)2	0.40	0.23	3.0
L3βCH2-(δCH3)2	-	0.50	2.6
L3γCH-(δCH3)2	1.50	0.29	2.8
K4NH-αCH	0.26	0.32	2.8
K4NH-βCH2	0.57	0.56	2.5
K4NH-γCH2	0.26	0.26	2.9
K4αCH-βCH2	0.63	0.48	2.6
K4βCH2-γCH2	1.08	0.54	2.5
K4βCH2-δCH2	0.57	0.29	2.8
K4γCH2-ξCH2	0.13	0.07	3.7
K4δCH2-ξCH2	0.19	0.10	3.5
K4γCH2-δCH2	1.20	0.60	2.5
A5NH-αCH	0.37	0.39	2.7
A5NH-βCH3	0.55	0.40	2.7
A5αCH-βCH3	0.96	0.64	2.5
L6NH-αCH	0.36	0.43	3.6
L6NH-βCH2	0.75	0.72	2.4
L6NH-γCH	0.30	0.36	2.7
L6NH-(δCH3)2	0.49	0.39	2.7
L6αCH-βCH2	1.80	1.36	2.1
L6αCH-(δCH3)2	0.40	0.23	3.0
L6βCH2-(δCH3)2	2.00	0.50	2.6

L6γCH-(δCH3)2	-	0.29	2.8
A7NH-αCH	0.37	0.43	2.6
A7NH-βCH3	0.77	0.63	2.5
A7αCH-βCH3	1.45	0.97	2.3
A8NH-αCH	1.21	1.23	2.2
A8NH-βCH3	0.77	0.52	2.6
A8αCH-βCH3	1.34	0.89	2.3
L9NH-αCH	0.51	0.54	2.5
L9NH-βCH2	0.38	0.31	2.8
L9NH-γCH	0.59	0.63	4.5
L9NH-(δCH3)2	0.24	0.15	4.5
L9αCH-βCH2	0.85	0.64	3.5
L9αCH-(δCH3)2	0.40	0.23	3.0
L9βCH2-(δCH3)2	2.00	0.50	2.6
L9γCH-(δCH3)2	-	0.29	2.8
A10NH-αCH	0.28	0.33	2.8
A10NH-βCH3	0.47	0.41	2.7
A10αCH-βCH3	1.03	0.69	2.4
K11NH-αCH	0.44	0.42	2.7
K11NH-βCH2	0.77	0.53	2.5
K11NH-γCH2	0.32	0.22	3.0
K11αCH-βCH2	1.39	1.05	2.2
K11βCH2-γCH2	1.05	0.53	2.5
K11βCH2-δCH2	0.85	0.43	2.6
K11γCH2-ξCH2	0.13	0.07	3.7
K11δCH2-ξCH2	0.19	0.10	3.5
K11γCH2-δCH2	1.20	0.60	2.5
K12NH-αCH	0.36	0.43	2.6
K12NH-βCH2	0.60	0.58	2.5
K12NH-γCH2	0.26	0.25	2.9
K12αCH-βCH2	1.01	0.77	2.4
K12βCH2-γCH2	1.08	0.54	2.5
K12βCH2-δCH2	0.57	0.29	2.8
K12γCH2-ξCH2	0.13	0.07	3.7
K12δCH2-ξCH2	0.19	0.10	3.5
K12γCH2-δCH2	1.20	0.60	2.5
I13NH-αCH	0.27	0.30	2.8
I13NH-βCH	0.50	0.56	2.5
I13NH-γCH'(p)	0.54	0.60	2.5
I13NH-γCH(t)	0.18	0.19	3.1
I13NH-(γCH3')	0.36	0.28	2.9
I13NH-(δCH3)	0.17	0.13	3.3
I13αCH-βCH	0.28	0.28	2.9
I13αCH-γCH'(p)	0.19	0.19	3.1
I13αCH-γCH(t)	0.26	0.26	2.9
I13αCH-(γCH3')	0.25	0.17	3.1

I13αCH-(δCH3)	0.21	0.14	3.2
I13βCH-(γCH3')	1.46	0.97	2.3
I13βCH-(δCH3)	0.58	0.39	2.7
I13βCH-γCH'(p)	2.87	2.87	1.9
I13βCH-γCH(t)	0.44	0.44	2.6
I13γCH'(p)-γCH(t)	0.98	0.98	2.3
I13γCH'(p)-(δCH3)	1.36	0.91	2.3
I13γCH(t)-(γCH3')	0.78	0.52	2.6
I13γCH(t)-(δCH3)	0.75	0.50	2.6
L14NH-αCH	0.17	0.18	3.1
L14NH-βCH2	0.58	0.48	2.6
L14NH-γCH	0.37	0.33	2.8
L14NH-(δCH3)2	0.49	0.32	2.8
L14αCH-βCH2	0.43	0.33	2.8
L14αCH-(δCH3)2	0.32	0.19	3.1
L14βCH2-(δCH3)2	2.00	0.50	2.6
L14γCH-(δCH3)2	-	0.29	2.8
L14 Cterm NH2	1.50	1.74	2.0
I1(δCH3)-L3NH	0.11	0.13	3.3
L3(δCH3)2-K4NH	0.07	0.06	3.8
L6(δCH3)2-A5NH	0.08	0.05	3.9
L6(δCH3)2-A7NH	0.14	0.10	3.5
L9(δCH3)2-A10NH	0.21	0.17	3.1
I13(γCH3')-K11NH	0.05	0.04	4.1
A5βCH3-N2CONH	0.20	0.16	3.2
A5βCH3-N2CONH'	0.20	0.16	3.2
K11αCH-L14 Cterm NH	0.11	0.09	3.5
K11αCH-L14 Cterm NH'	0.11	0.09	3.5
K12αCH-L14 Cterm NH	0.05	0.05	3.9
K12αCH-L14 Cterm NH'	0.05	0.05	3.9
K12γCH-L14 Cterm NH	0.20	0.17	3.1
K12γCH-L14 Cterm NH'	0.20	0.17	3.1
I13αCH-L14 Cterm NH	0.03	0.03	4.3
I13αCH-L14 Cterm NH'	0.03	0.03	4.3
L14αCH-L14 Cterm NH	0.07	0.08	3.6
L14αCH-L14 Cterm NH'	0.07	0.08	3.6
L14βCH2-L14 Cterm NH	0.41	0.34	2.8
L14βCH2-L14 Cterm NH'	0.41	0.34	2.8
L14(δCH3)2-L14 Cterm NH	0.18	0.11	3.4
L14(δCH3)2-L14 Cterm NH'	0.18	0.11	3.4
N2βCH2-A5βCH3	0.12	0.08	3.6
N2αCH-L3βCH2	0.34	0.26	2.9

N2αCH-L3(δCH3)2	0.61	0.36	2.7
N2αCH-K4βCH2	0.15	0.11	3.4
N2αCH-A5βCH3	0.32	0.21	3.0
K11αCH-I13(γCH3')	0.15	0.10	3.7
K11αCH-I13(δCH3)	0.02	0.01	6.3
K12γCH2-L14αCH	0.30	0.23	3.0
K4γCH2-L3NH	0.14	0.22	3.0
L3βCH2-K4NH	0.29	0.28	2.9
A5βCH3-K4NH	0.26	0.23	3.0
K4βCH2-A5NH	0.35	0.29	2.8
L6βCH2-A5NH	0.23	0.19	3.1
A8βCH3-A5NH	0.16	0.12	3.3
A5βCH3-L6NH	0.41	0.36	2.7
L6βCH2-A7NH	0.51	0.46	2.6
A7βCH3-A8NH	0.51	0.34	2.8
A8βCH3-L9NH	0.37	0.27	2.9
A10βCH3-L9NH	0.06	0.04	4.0
A8βCH3-A10NH	0.07	0.06	3.8
L9βCH2-A10NH	0.27	0.26	2.9
L9γCH-A10NH	0.03	0.04	4.0
L9βCH2-K11NH	0.06	0.04	4.0
L9γCH-K11NH	0.22	0.21	5.0
K11βCH2-A10NH	0.61	0.58	2.5
K11γCH2-A10NH	0.23	0.22	3.0
A10βCH3-K11NH	0.46	0.28	2.9
K11βCH2-K12NH	0.37	0.36	2.7
I13βCH-K12NH	0.22	0.26	2.9
K12βCH2-I13NH	0.22	0.19	3.1
K12γCH2-I13NH	0.21	0.17	3.1
I13γCH'(p)-L14NH	0.13	0.14	3.2
K12γCH2-K14NH	0.30	0.22	3.0
I13γCH(t)-K12NH	0.02	0.02	4.6
I13γCH(t)-L14NH	0.03	0.03	4.3
L3αCH-K4NH	0.08	0.10	3.5
K4αCH-A5NH	0.13	0.14	3.2
L6αCH-A7NH	0.10	0.12	3.3
A7αCH-L6NH	0.17	0.20	3.0
A7αCH-A8NH	0.08	0.10	3.5
A7αCH-L9NH	0.04	0.04	4.0
A7αCH-A10NH	0.10	0.11	3.4
A8αCH-A7NH	0.10	0.12	3.3
A8αCH-L9NH	0.12	0.13	3.3
A8αCH-K11NH	0.12	0.11	3.4
L9αCH-A10NH	0.15	0.26	3.2

L9αCH-K12NH	0.09	0.11	3.4
A10αCH-K11NH	0.14	0.13	3.3
K11αCH-K12NH	0.19	0.23	3.0
K11αCH-I13NH	0.04	0.04	4.0
K11αCH-L14NH	0.17	0.18	3.1
K12αCH-K11NH	0.21	0.20	3.0
K12αCH-I13NH	0.18	0.20	3.0
K12αCH-L14NH	0.03	0.03	4.3
I13αCH-K12NH	0.07	0.08	3.6
I13αCH-L14NH	0.12	0.13	3.3
L3NH-K4NH	0.15	0.27	2.9
L3NH-L6NH	0.03	0.05	3.9
L3NH-A5NH	0.03	0.05	3.9
K4NH-L6NH	0.12	0.17	3.1
K4NH-A5NH	0.29	0.38	2.7
A5NH-L6NH	0.28	0.36	2.7
A5NH-A7NH	0.06	0.07	3.7
L6NH-A7NH	0.21	0.28	2.9
A7NH-A8NH	0.31	0.38	2.7
A7NH-L9NH	0.04	0.05	3.9
A8NH-L9NH	0.26	0.28	2.9
A8NH-A10NH	0.05	0.06	3.8
L9NH-A10NH	0.21	0.25	2.9
L9NH-K11NH	0.03	0.03	4.3
A10NH-K11NH	0.18	0.21	3.0
A10NH-K12NH	0.04	0.05	3.9
K11NH-K12NH	0.27	0.31	2.8
K11NH-I13NH	0.04	0.04	4.1
K12NH-I13NH	0.24	0.32	2.8
K12NH-L14NH	0.03	0.04	4.1
I13NH-L14NH	0.21	0.24	2.9
I13NH-L14 Cterm NH	0.11	0.24	3.3
L14NH-L14 Cterm NH	0.11	0.24	2.9

Table IX-5. Summary of distance restraints used in the MD simulations for the TnI peptide in 50%TFE. Included in the table are the calculated r_{ij}s from the corrected and normalized NOE cross-peak intensities, the incorporated error limits (±β), and the pseudoatom adjustments in r_{ij}^{U}.

spin system	rij ± β (Å)	Ψ-atom correction (Å)	rijU (Å)	rijL (Å)
K105αCH-βCH2	3.5±0.3		3.8	3.2
K105αCH-γCH2	4.8±0.5	0.6	5.9	4.3
K105βCH2-γCH2	3.6±0.3		3.9	3.3
K105βCH2-NH	3.4±0.3	0.6	4.3	3.1
K105γCH2-δCH2	3.6±0.3		3.9	3.3
K105γCH2-NH	4.2±0.5	1.0	5.7	3.7
F106αCH-βCH(m)	3.6±0.3		3.9	3.3
F106αCH-βCH'(x)	3.7±0.3		4.0	3.4
F106αCH-δCH2	4.9±0.5	2.0	7.4	4.4
F106βCH(m)-βCH'(x)	2.3±0.2		2.5	2.1
F106βCH(m)-NH	4.2±0.5		4.7	3.7
F106βCH(m)-δCH2	3.7±0.3		4.0	3.4
F106βCH'(x)-NH	3.8±0.3		4.1	3.5
F106βCH'(x)-δCH2	3.7±0.3		4.0	3.4
F106NH-δCH2	4.5±0.5	2.4	7.4	4.0
K107αCH-βCH2	3.2±0.3		3.5	2.9
K107αCH-γCH2	4.2±0.5	0.6	5.3	3.7
K107βCH2-γCH2	3.5±0.3		3.8	3.2
K107βCH2-NH	3.6±0.3	0.6	4.5	3.3
K107γCH2-δCH2	3.1±0.3		3.4	2.8
K107γCH2-NH	4.1±0.5	1.0	5.6	3.6
K107δCH2-NH	3.8±0.3		4.1	3.5
R108αCH-δCH2	5.0±1.0	1.0	7.0	4.0
R108βCH2-δCH2	5.2±1.0		6.2	4.2
R108βCH2-NH	3.4±0.3	0.6	4.3	3.1
R108γCH2-δCH2	3.8±0.3		4.1	3.5
R108γCH2-NH	3.7±0.3	1.0	5.0	3.4
R108δCH2-NH	5.5±1.0		6.5	4.5
P109αCH-βCH'(x)	3.2±0.3		3.5	2.9
P109αCH-βCH(p)	3.2±0.3		3.5	2.9
P109αCH-δCH(m)	3.5±0.3		3.8	3.2
P109αCH-δCH'(m')	3.3±0.3		3.6	3.0
P109βCH'(x)-βCH(p)	2.6±0.2		2.8	2.4
P109βCH'(x)-δCH(m)	3.4±0.3		3.7	3.1
P109βCH'(x)-δCH'(m')	3.7±0.3		4.0	3.4

P109βCH'(x)-γCH2	3.7±0.3		4.0	3.4
P109βCH(p)-δCH(m)	5.9±1.0		6.9	4.9
P109βCH(p)-δCH'(m')	4.7±0.5		5.3	4.3
P109βCH(p)-γCH2	4.0±0.5		4.5	3.5
P109γCH2-δCH(m)	3.6±0.3		3.9	3.3
P109γCH2-δCH'(m')	3.6±0.3		3.9	3.3
P109δCH(m)-δCH'(m')	2.7±0.2		2.9	2.5
P110aCH-βCH'(x)	3.6±0.3		3.9	3.3
P110αCH-βCH(p)	3.5±0.3		3.8	3.2
P110βCH'(x)-βCH(p)	2.4±0.2		2.6	2.2
P110βCH'(x)-δCH(m)	3.0±0.3		3.3	2.7
P110βCH'(x)-δCH'(m')	3.0±0.3		3.3	2.7
P110βCH(p)-δCH(m)	4.9±0.5		5.4	4.4
P110βCH(p)-δCH'(m')	4.7±0.5		5.2	4.2
P110δCH(m)-δCH'(m')	2.6±0.2		2.8	2.4
L111αCH-βCH2	3.1±0.3		3.4	2.8
L111αCH-(δCH3)2	4.3±0.5	1.7	6.5	3.8
L111γCH-(δCH3)2	3.3±0.3		3.6	3.0
L111βCH2-NH	3.2±0.3	0.6	4.1	2.9
L111(δCH3)2-NH	4.2±0.5		4.7	3.7
R112αCH-δCH2	5.0±1.0	1.0	7.0	4.0
R112βCH2-δCH2	3.8±0.3		4.1	3.5
R112βCH2-NH	3.4±0.3	0.6	4.3	3.1
R112γCH2-δCH2	3.4±0.3		3.7	3.1
R112γCH2-NH	3.7±0.3	1.0	5.0	3.4
R112δCH2-NH	6.2±1.0		7.2	5.2
R113αCH-δCH2	5.0±1.0	1.0	7.0	4.0
R113βCH2-δCH2	3.8±0.3		4.1	3.5
R113βCH2-NH	3.4±0.3	0.6	4.3	3.1
R113γCH2-δCH2	3.4±0.3		3.7	3.1
R113γCH2-NH	3.7±0.3	1.0	5.0	3.4
R113δCH2-NH	4.1±0.5		4.6	3.6
V114αCH-βCH	3.7±0.3		4.0	3.4
V114αCH-(γCH3)2	4.1±0.5	0.6	5.2	3.6
V114βCH-(γCH3)2	3.3±0.3		3.6	3.0
V114βCH-NH	3.7±0.3		4.0	3.4
V114(γCH3)2-NH	3.9±0.3	1.7	5.9	3.6
R115αCH-βCH2	3.5±0.3	0.6	4.4	3.2
R115αCH-δCH2	4.7±0.5	1.0	6.2	4.2
R115βCH2-δCH2	4.3±0.5		4.8	3.8
R115βCH2-NH	3.4±0.3	0.6	4.3	3.1
R115γCH2-δCH2	3.4±0.3		3.7	3.1
R115γCH2-NH	3.5±0.3	1.0	4.8	3.2
R115δCH2-NH	5.8±1.0		6.8	4.8
C-term NH-NH'	2.7±0.2		2.9	2.5

N-Ac CH3-G104 NH	4.7±0.5		5.2	4.2
F106βCH2-K107NH	4.8±0.5	1.0	6.3	4.3
K105γCH2-F106NH	4.9±0.5	1.0	6.4	4.4
K107γCH2-R108NH	4.6±0.5	1.0	6.1	4.1
R108βCH2-P109αCH	3.5±0.3	1.0	4.8	3.2
P109αCH-P110βCH'(x)	3.7±0.3		4.0	3.4
P109αCH-P110δCH(m)	3.5±0.3		3.8	3.2
P109αCH-P110δCH'(m')	3.4±0.3		3.7	3.1
P110βCH'(x)-L111NH	4.2±0.5		4.7	3.7
P110βCH(p)-L111NH	4.9±0.5		5.4	4.4
L111(δCH3)2-R112NH	4.4±0.5	2.4	7.3	3.9
R113βCH2-V114NH	3.9±0.3	1.0	5.2	3.6
R113γCH2-V114NH	3.6±0.3	1.0	4.9	3.3
R113NH-V114βCH	4.3±0.5		4.8	3.8
R113NH-V114(γCH3)2	4.5±0.5	2.4	7.4	4.0

F106βCH'(x)-K107δCH2	4.2±0.5	1.0	5.7	3.7
R108βCH2-P109δCH(m)	4.0±0.5	1.0	5.5	3.5
P109βCH'(x)-P110δCH(m)	4.1±0.5		4.6	3.6
P109βCH'(x)-P110δCH(m')	5.1±1.0		6.1	4.1
P109βCH(p)-P110δCH(m)	4.3±0.5		4.8	3.8
P109βCH(p)-P110δCH'(m')	4.6±0.5		5.1	4.1

K105NH-F106NH	3.6±0.3		3.9	3.3
K107NH-R108NH	3.3±0.3		3.6	3.0
R112NH-Cterm NH2	4.8±0.5		5.3	4.3
R113NH-V114NH	3.3±0.3		3.6	3.0

G104αCH2-NH	4.0±0.5		4.5	3.5
G104αCH2-K105NH	3.4±0.3	1.0	3.8	3.1
K105αCH-NH	4.1±0.5		4.6	3.6
K105αCH-F106NH	3.7±0.3		4.0	3.4
F106αCH-NH	4.4±0.5		4.9	3.9
F106αCH-K107NH	3.8±0.3		4.1	3.5
F106NH-K107αCH	3.7±0.3		4.0	3.4
K107αCH-NH	3.4±0.3		3.7	3.1
K107αCH-R108NH	3.0±0.3		3.3	2.7
R108αCH-NH	5.3±1.0		6.3	4.3
P110αCH-L111NH	3.8±0.3		4.1	3.5
L111αCH-NH	4.2±0.5		4.7	3.7
R112αCH-NH	3.4±0.3		3.7	3.1
R113αCH-NH	3.4±0.3		3.7	3.1
R113αCH-V114NH	3.3±0.3		3.6	3.0
V114αCH-NH	4.1±0.5		4.6	3.6
V114αCH-R113NH	3.3±0.3		3.6	3.0
V114αCH-R115NH	3.4±0.3		3.7	3.1

R115αCH-NH	3.1±0.3		3.4	2.8

Table IX-6. Summary of distance restraints used in the MD simulations for mastoparan in 50%TFE. Included in the table are the calculated r_{ij}s from the corrected and normalized NOE cross-peak intensities, the incorporated error limits (±β), and the pseudoatom adjustments in r_{ij}^{U}.

spin system	rij±β (Å)	Ψ-atom correction (Å)	rijU (Å)	rijL (Å)
I1βCH-(γCH3')	2.3±0.2		2.5 Å	2.1 Å
I1βCH-γCH'(p)	1.9±0.1		2.0	1.8
I1γCH'(p)-γCH(t)	2.3±0.2		2.5	2.1
I1γCH'(p)-(γCH3')	2.4±0.2		2.6	2.2
I1γCH'(p)-(δCH3)	2.4±0.2		2.6	2.2
N2βCH'(m)-βCH(x)	2.3±0.2		2.5	2.1
N2CONH2	2.1±0.2		2.3	1.9
N2CONH2-βCH'(m)	2.9±0.2		3.1	2.7
N2CONH2-βCH(x)	2.9±0.2		3.1	2.7
L3NH-αCH	2.8±0.2		3.0	2.6
L3NH-βCH2	2.5±0.2	0.6	3.3	2.3
L3NH-γCH	2.9±0.2		3.1	2.7
L3NH-(δCH3)2	3.1±0.3		3.4	2.8
L3αCH-βCH2	2.1±0.2		2.3	1.9
L3αCH-(δCH3)2	3.0±0.3	1.7	5.0	2.7
L3βCH2-(δCH3)2	2.6±0.2		2.8	2.4
L3γCH-(δCH3)2	2.8±0.2		3.0	2.6
K4NH-αCH	2.8±0.2		3.0	2.6
K4NH-βCH2	2.5±0.2	0.6	3.3	2.3
K4NH-γCH2	2.9±0.2	1.0	4.1	2.7
K4αCH-βCH2	2.6±0.2		2.8	2.4
K4βCH2-γCH2	2.5±0.2		2.7	2.3
K4βCH2-δCH2	2.8±0.2		3.0	2.6
K4γCH2-ξCH2	3.7±0.3		4.0	3.4
K4δCH2-ξCH2	3.5±0.3		3.8	3.2
K4γCH2-δCH2	2.5±0.2		2.7	2.3
A5NH-αCH	2.7±0.2		2.9	2.5
A5NH-βCH3	2.7±0.2	0.6	3.5	2.5
A5αCH-βCH3	2.5±0.2		2.7	2.3
L6NH-αCH	3.6±0.3		3.9	3.3
L6NH-βCH2	2.4±0.2	0.6	3.2	2.2

L6NH-γCH	2.7±0.2		2.9	2.5
L6NH-(δCH3)2	2.7±0.2		2.9	2.5
L6αCH-βCH2	2.1±0.2		2.3	1.9
L6αCH-(δCH3)2	3.0±0.3	1.7	5.0	2.7
L6βCH2-(δCH3)2	2.6±0.2		2.8	2.2
L6γCH-(δCH3)2	2.8±0.2		3.0	2.6
A7NH-αCH	2.6±0.2		2.8	2.4
A7NH-βCH3	2.5±0.2	0.6	3.3	2.3
A7αCH-βCH3	2.3±0.2		2.5	2.1
A8NH-αCH	2.2±0.2		2.4	2.0
A8NH-βCH3	2.6±0.2	0.6	3.4	2.4
A8αCH-βCH3	2.3±0.2		2.5	2.1
L9NH-αCH	2.5±0.2		2.7	2.3
L9NH-βCH2	2.8±0.2	0.6	3.6	2.6
L9NH-γCH	4.5±0.5		5.0	4.0
L9NH-(δCH3)2	4.5±0.5		5.0	4.0
L9αCH-βCH2	3.5±0.3		3.8	3.2
L9αCH-(δCH3)2	3.0±0.3	1.7	5.0	2.7
L9βCH2-(δCH3)2	2.6±0.2		2.8	2.4
L9γCH-(δCH3)2	2.8±0.2		3.0	2.6
A10NH-αCH	2.8±0.2		3.0	2.6
A10NH-βCH3	2.7±0.2	0.6	3.5	2.5
A10αCH-βCH3	2.4±0.2		2.6	2.2
K11NH-αCH	2.7±0.2		2.9	2.5
K11NH-βCH2	2.5±0.2		2.7	2.3
K11NH-γCH2	3.0±0.3		3.3	2.7
K11αCH-βCH2	2.2±0.2		2.4	2.0
K11βCH2-γCH2	2.5±0.2		2.7	2.3
K11βCH2-δCH2	2.6±0.2		2.8	2.4
K11γCH2-ξCH2	3.7±0.3		4.0	3.4
K11δCH2-ξCH2	3.5±0.3		3.8	3.2
K11γCH2-δCH2	2.5±0.2		2.7	2.3
K12NH-αCH	2.6±0.2		2.8	2.4
K12NH-βCH2	2.5±0.2	0.6	3.3	2.3
K12NH-γCH2	2.9±0.2	1.0	4.1	2.7
K12αCH-βCH2	2.4±0.2		2.6	2.2
K12βCH2-γCH2	2.5±0.2		2.7	2.3
K12βCH2-δCH2	2.8±0.2		3.0	2.6
K12γCH2-ξCH2	3.7±0.3		4.0	3.4
K12δCH2-ξCH2	3.5±0.3		3.8	3.2
K12γCH2-δCH2	2.5±0.2		2.7	2.3
I13NH-αCH	2.8±0.2		3.0	2.6
I13NH-βCH	2.5±0.2		2.7	2.3
I13NH-γCH'(p)	2.5±0.2		2.7	2.3
I13NH-γCH(t)	3.1±0.3		3.4	2.8
I13NH-(γCH3')	2.9±0.2	1.0	4.1	2.7

I13NH-(δCH3)	3.3±0.3		3.6	3.0
I13αCH-βCH	2.9±0.2		3.1	2.7
I13αCH-γCH'(p)	3.1±0.3		3.4	2.8
I13αCH-γCH(t)	2.9±0.2		3.1	2.7
I13αCH-(γCH3')	3.1±0.3	0.6	4.0	2.8
I13αCH-(δCH3)	3.2±0.3	1.0	4.5	2.9
I13βCH-(γCH3')	2.3±0.2		2.5	2.1
I13βCH-(δCH3)	2.7±0.2		2.9	2.5
I13βCH-γCH'(p)	1.9±0.1		2.0	1.8
I13βCH-γCH(t)	2.6±0.2		2.8	2.4
I13γCH'(p)-γCH(t)	2.3±0.2		2.5	2.1
I13γCH'(p)-(δCH3)	2.3±0.2		2.5	2.1
I13γCH(t)-(γCH3')	2.6±0.2		2.8	2.4
I13γCH(t)-(δCH3)	2.6±0.2		2.8	2.4
L14NH-αCH	3.1±0.3		3.4	2.8
L14NH-βCH2	2.6±0.2	0.6	3.4	2.4
L14NH-γCH	2.8±0.2		3.0	2.6
L14NH-(δCH3)2	2.8±0.2		3.0	2.6
L14αCH-βCH2	2.8±0.2		3.0	2.6
L14αCH-(δCH3)2	3.1±0.3	1.7	5.1	2.8
L14βCH2-(δCH3)2	2.6±0.2		2.8	2.4
L14γCH-(δCH3)2	2.8±0.2		3.0	2.6
L14 Cterm NH2	2.0±0.2		2.2	1.8
I1(δCH3)-L3NH	3.3±0.3	1.0	4.6	3.0
L3(δCH3)2-K4NH	3.8±0.3	2.4	6.5	3.5
L6(δCH3)2-A5NH	3.9±0.3	2.4	6.6	3.6
L6(δCH3)2-A7NH	3.5±0.3	2.4	6.2	3.2
L9(δCH3)2-A10NH	3.1±0.3	2.4	5.8	2.8
I13(γCH3')-K11NH	4.1±0.5	1.0	5.6	3.6
A5βCH3-N2CONH	3.2±0.3	1.0	4.5	2.9
A5βCH3-N2CONH'	3.2±0.3	1.0	4.5	2.9
K11αCH-L14 Cterm NH	3.5±0.3		3.8	3.2
K11αCH-L14 Cterm NH'	3.5±0.3		3.8	3.2
K12αCH-L14 Cterm NH	3.9±0.3		4.2	3.6
K12αCH-L14 Cterm NH'	3.9±0.3		4.2	3.6
K12γCH-L14 Cterm NH	3.1±0.3	1.0	4.4	2.8
K12γCH-L14 Cterm NH'	3.1±0.3	1.0	4.4	2.8
I13αCH-L14 Cterm NH	4.3±0.5		4.8	3.8
I13αCH-L14 Cterm NH'	4.3±0.5		4.8	3.8
L14αCH-L14 Cterm NH	3.6±0.3		3.9	3.3
L14αCH-L14 Cterm NH'	3.6±0.3		3.9	3.3
L14βCH2-L14 Cterm NH	2.8±0.2		3.0	2.6
L14βCH2-L14 Cterm NH'	2.8±0.2		3.0	2.6
L14(δCH3)2-L14 Cterm NH	3.4±0.3		3.7	3.1

L14(δCH3)2-L14 Cterm NH'	3.4±0.3		3.7	3.1
N2βCH2-A5βCH3	3.6±0.3	2.0	5.9	3.3
N2αCH-L3βCH2	2.9±0.2	1.0	4.1	2.7
N2αCH-L3(δCH3)2	2.7±0.2	2.4	5.3	2.5
N2αCH-K4βCH2	3.4±0.3	1.0	4.7	3.1
N2αCH-A5βCH3	3.0±0.3	1.0	4.3	2.7
K11αCH-I13(γCH3')	3.7±0.3	1.0	4.0	3.4
K11αCH-I13(δCH3)	6.3±1.0	1.0	8.3	5.3
K12γCH2-L14αCH	3.0±0.3	1.0	4.3	2.7
K4γCH2-L3NH	3.0±0.3	1.0	4.3	2.7
L3βCH2-K4NH	2.9±0.2	1.0	4.1	2.7
A5βCH3-K4NH	3.0±0.3	1.0	4.3	2.7
K4βCH2-A5NH	2.8±0.2	1.0	4.0	2.6
L6βCH2-A5NH	3.1±0.3	1.0	4.4	2.8
A8βCH3-A5NH	3.3±0.3	1.0	4.6	3.0
A5βCH3-L6NH	2.7±0.2	1.0	3.9	2.5
L6βCH2-A7NH	2.6±0.2	1.0	3.8	2.4
A7βCH3-A8NH	2.8±0.2	1.0	4.0	2.6
A8βCH3-L9NH	2.9±0.2	1.0	4.1	2.7
A10βCH3-L9NH	4.0±0.5	1.0	5.5	3.5
A8βCH3-A10NH	3.8±0.3	1.0	5.1	3.5
L9βCH2-A10NH	2.9±0.2	1.0	4.1	2.7
L9γCH-A10NH	4.0±0.5		4.5	3.5
L9βCH2-K11NH	4.0±0.5	1.0	5.5	3.5
L9γCH-K11NH	5.0±1.0		6.0	4.0
K11βCH2-A10NH	2.5±0.2	1.0	3.7	2.3
K11γCH2-A10NH	3.0±0.3	1.0	4.3	2.7
A10βCH3-K11NH	2.9±0.2	1.0	4.1	2.7
K11βCH2-K12NH	2.7±0.2	1.0	3.9	2.5
I13βCH-K12NH	2.9±0.2		3.1	2.7
K12βCH2-I13NH	3.1±0.3	1.0	4.4	2.8
K12γCH2-I13NH	3.1±0.3	1.0	4.4	2.8
I13γCH'(p)-L14NH	3.2±0.3		3.5	2.9
K12γCH2-K14NH	3.0±0.3	1.0	4.3	2.7
I13γCH(t)-K12NH	4.6±0.5		5.1	4.1
I13γCH(t)-L14NH	4.3±0.5		4.9	3.9
L3αCH-K4NH	3.5±0.3		3.8	3.2
K4αCH-A5NH	3.2±0.3		3.5	2.9
L6αCH-A7NH	3.3±0.3		3.6	3.0
A7αCH-L6NH	3.0±0.3		3.3	2.7
A7αCH-A8NH	3.5±0.3		3.8	3.2
A7αCH-L9NH	4.0±0.5		4.5	3.5

A7αCH-A10NH	3.4±0.3	3.7	3.1
A8αCH-A7NH	3.3±0.3	3.6	3.0
A8αCH-L9NH	3.3±0.3	3.6	3.0
A8αCH-K11NH	3.4±0.3	3.7	3.1
L9αCH-A10NH	3.2±0.3	3.5	2.9
L9αCH-K12NH	3.4±0.3	3.7	3.1
A10αCH-K11NH	3.3±0.3	3.6	3.0
K11αCH-K12NH	3.0±0.3	3.3	2.7
K11αCH-I13NH	4.0±0.5	4.5	3.5
K11αCH-L14NH	3.1±0.3	3.4	2.8
K12αCH-K11NH	3.0±0.3	3.3	2.7
K12αCH-I13NH	3.0±0.3	3.3	2.7
K12αCH-L14NH	4.3±0.5	4.8	3.8
I13αCH-K12NH	3.6±0.3	3.9	3.3
I13αCH-L14NH	3.3±0.3	3.6	3.0
L3NH-K4NH	2.9±0.2	3.1	2.7
L3NH-L6NH	3.9±0.3	4.2	3.6
L3NH-A5NH	3.9±0.3	4.2	3.6
K4NH-L6NH	3.1±0.3	3.4	2.8
K4NH-A5NH	2.7±0.2	2.9	2.5
A5NH-L6NH	2.7±0.2	2.9	2.5
A5NH-A7NH	3.7±0.3	4.0	3.4
L6NH-A7NH	2.9±0.2	3.1	2.7
A7NH-A8NH	2.7±0.2	2.9	2.5
A7NH-L9NH	3.9±0.3	4.2	3.6
A8NH-L9NH	2.9±0.2	3.1	2.7
A8NH-A10NH	3.8±0.3	4.1	3.5
L9NH-A10NH	2.9±0.2	3.1	2.7
L9NH-K11NH	4.3±0.5	4.8	3.8
A10NH-K11NH	3.0±0.3	3.3	2.7
A10NH-K12NH	3.9±0.3	4.2	3.6
K11NH-K12NH	2.8±0.2	3.0	2.6
K11NH-I13NH	4.1±0.5	4.6	3.6
K12NH-I13NH	2.8±0.2	3.0	2.6
K12NH-L14NH	4.1±0.5	4.6	3.6
I13NH-L14NH	2.9±0.2	3.1	2.7
I13NH-L14 Cterm NH	3.3±0.3	3.6	3.0
L14NH-L14 Cterm NH	2.9±0.2	3.1	2.7

Table IX-7. $^3J\alpha CH$-NH coupling constants for the TnI peptide in 50%TFE.

	JαCH-NH (Hz)
G104	5.8
K105	6.6
F106	6.6
K107	7.3
R108	6.3
L111	6.3
R112	6.4
R113	6.4
V114	7.2
R115	5.0

Table IX-8. $^3J\alpha CH$-NH coupling constants for mastoparan in 50%TFE.

	JαCH-NH (Hz)
I1	< 4.0
N2	< 4.0
L3	< 4.0
K4	< 4.0
A5	< 4.0
L6	< 4.0
A7	< 4.0
A8	< 4.0
L9	< 4.0
A10	< 4.0
L11	< 4.0
L12	< 4.0
I13	< 4.0
L14	< 4.0

Table IX-9. GROMOS distance restraint file used in MD simulations to generate the structure of the TnI peptide in 50%TFE.

```
TnI peptide, 50% TFE, tm=150ms
 250
   1    2                  5        5                       0    0.52
   1    2                  5        5                       0   -0.42
   5                       0        6    4    7             3    0.45
   5                       0        6    4    7             3   -0.35
   6    4    7             3       10                       0    0.47
   6    4    7             3       10                       0   -0.31
  10                       0       11    9   12   20        1    0.46
  10                       0       11    9   12   20        1   -0.36
  10                       0       12   11   13             3    0.43
  10                       0       12   11   13             3   -0.31
  10                       0       13   12   14             3    0.57
  10                       0       13   12   14             3   -0.37
  10                       0       23                       0    0.39
  10                       0       23                       0   -0.33
  11    9   12   20        1       12   11   13             3    0.38
  11    9   12   20        1       12   11   13             3   -0.32
  11    9   12   20        1       13   12   14             3    0.59
  11    9   12   20        1       13   12   14             3   -0.43
  11    9   12   20        1       23                       0    0.40
  11    9   12   20        1       23                       0   -0.34
  12   11   13             3       13   12   14             3    0.39
  12   11   13             3       13   12   14             3   -0.33
  13   12   14             3       14   13   15             3    0.39
  13   12   14             3       14   13   15             3   -0.33
  13   12   14             3       23                       0    0.64
  13   12   14             3       23                       0   -0.44
  23                       0       24   22   25   32        1    0.49
  23                       0       24   22   25   32        1   -0.39
  23                       0       25   26   24             4    0.47
  23                       0       25   26   24             4   -0.37
  23                       0       25   24   26             4    0.41
  23                       0       25   24   26             4   -0.35
  23                       0       26                       0    0.74
  23                       0       26                       0   -0.40
  23                       0       36   34   37   45        1    0.40
  23                       0       36   34   37   45        1   -0.34
  24   22   25   32        1       25   26   24             4    0.39
  24   22   25   32        1       25   26   24             4   -0.33
  24   22   25   32        1       25   24   26             4    0.40
  24   22   25   32        1       25   24   26             4   -0.34
  24   22   25   32        1       26                       0    0.74
  24   22   25   32        1       26                       0   -0.44
  24   22   25   32        1       35                       0    0.41
  24   22   25   32        1       35                       0   -0.35
  25   26   24             4       25   24   26             4    0.25
  25   26   24             4       25   24   26             4   -0.21
  25   24   26             3       26                       0    0.40
  25   24   26             3       26                       0   -0.34
  25   24   26             3       35                       0    0.63
  25   24   26             3       35                       0   -0.43
  25   26   24             4       39   38   40             3    0.57
  25   26   24             4       39   38   40             3   -0.37
  35                       0       36   34   37   45        1    0.37
  35                       0       36   34   37   45        1   -0.31
  35                       0       37   36   38             3    0.45
  35                       0       37   36   38             3   -0.33
  35                       0       38   37   39             3    0.56
  35                       0       38   37   39             3   -0.36
```

35				0	39	38	40		3	0.41
35				0	39	38	40		3	-0.35
35				0	48				0	0.36
35				0	48				0	-0.30
36	34	37	45	1	37	36	38		3	0.35
36	34	37	45	1	37	36	38		3	-0.29
36	34	37	45	1	38	37	39		3	0.53
36	34	37	45	1	38	37	39		3	-0.37
36	34	37	45	1	48				0	0.33
36	34	37	45	1	48				0	-0.27
37	36	38		3	38	37	39		3	0.38
37	36	38		3	38	37	39		3	-0.32
38	37	39		3	39	38	40		3	0.34
38	37	39		3	39	38	40		3	-0.28
38	37	39		3	48				0	0.61
38	37	39		3	48				0	-0.41
48				0	49	47	50	62	1	0.63
48				0	49	47	50	62	1	-0.43
48				0	50	49	51		3	0.43
48				0	50	49	51		3	-0.31
48				0	51	49	52		3	0.50
48				0	51	49	52		3	-0.34
48				0	52	51	53		3	0.65
48				0	52	51	53		3	-0.45
49	47	50	62	1	52	51	53		3	0.70
49	47	50	62	1	52	51	53		3	-0.40
50	49	51		3	52	51	53		3	0.62
50	49	51		3	52	51	53		3	-0.42
50	49	51		3	65	64	66	69	1	0.48
50	49	51		3	65	64	66	69	1	-0.32
50	49	51		3	68	67	64		4	0.55
50	49	51		3	68	67	64		4	-0.35
51	50	52		3	52	51	53		3	0.41
51	50	52		3	52	51	53		3	-0.35
65	64	66	69	1	66	67	65		4	0.35
65	64	66	69	1	66	67	65		4	-0.29
65	64	66	69	1	66	65	67		4	0.35
65	64	66	69	1	66	65	67		4	-0.29
65	64	66	69	1	68	64	67		4	0.36
65	64	66	69	1	68	64	67		4	-0.30
65	64	66	69	1	68	67	64		4	0.38
65	64	66	69	1	68	67	64		4	-0.32
65	64	66	69	1	75	71	74		4	0.37
65	64	66	69	1	75	71	74		4	-0.31
65	64	66	69	1	75	74	71		4	0.38
65	64	66	69	1	75	74	71		4	-0.32
65	64	66	69	1	73	74	72		4	0.40
65	64	66	69	1	73	74	72		4	-0.34
66	67	65		4	66	65	67		4	0.28
66	67	65		4	66	65	67		4	-0.24
66	67	65		4	67	66	68		3	0.40
66	67	65		4	67	66	68		3	-0.34
66	67	65		4	68	64	67		4	0.40
66	67	65		4	68	64	67		4	-0.34
66	67	65		4	68	67	64		4	0.37
66	67	65		4	68	67	64		4	-0.31
66	67	65		4	75	71	74		4	0.61
66	67	65		4	75	71	74		4	-0.41
66	67	65		4	75	74	71		4	0.46
66	67	65		4	75	74	71		4	-0.36

66	65	67		4	67	66	68		3	0.45
66	65	67		4	67	66	68		3	-0.35
66	65	67		4	68	64	67		4	0.53
66	65	67		4	68	64	67		4	-0.43
66	65	67		4	68	67	64		4	0.69
66	65	67		4	68	67	64		4	-0.49
66	65	67		4	75	71	74		4	0.51
66	65	67		4	75	71	74		4	-0.41
66	65	67		4	75	74	71		4	0.48
66	65	67		4	75	74	71		4	-0.38
67	66	68		3	68	67	64		3	0.39
67	66	68		3	68	67	64		3	-0.33
68	64	67		4	68	67	64		4	0.29
68	64	67		4	68	67	64		4	-0.25
72	71	73	76	1	73	74	72		4	0.39
72	71	73	76	1	73	74	72		4	-0.33
72	71	73	76	1	73	72	74		4	0.38
72	71	73	76	1	73	72	74		4	-0.32
72	71	73	76	1	79				0	0.41
72	71	73	76	1	79				0	-0.35
73	74	72		4	73	72	74		4	0.26
73	74	72		4	73	72	74		4	-0.22
73	74	72		4	75	71	74		4	0.33
73	74	72		4	75	71	74		4	-0.27
73	74	72		4	75	74	71		4	0.33
73	74	72		4	75	74	71		4	-0.27
73	74	72		4	79				0	0.47
73	74	72		4	79				0	-0.37
73	72	74		4	75	71	74		4	0.52
73	72	74		4	75	71	74		4	-0.42
73	72	74		4	75	74	71		4	0.54
73	72	74		4	75	74	71		4	-0.44
73	72	74		4	79				0	0.54
73	72	74		4	79				0	-0.44
75	71	74		4	75	74	71		4	0.28
75	71	74		4	75	74	71		4	-0.24
79				0	80	78	81	85	1	0.47
79				0	80	78	81	85	1	-0.37
79				0	81	80	82		3	0.35
79				0	81	80	82		3	-0.29
79				0	82	81	83	84	1	0.35
79				0	82	81	83	84	1	-0.29
79				0	82	83	84		6	0.65
79				0	82	83	84		6	-0.37
80	78	81	85	1	81	80	82		3	0.34
80	78	81	85	1	81	80	82		3	-0.28
80	78	81	85	1	82	83	84		6	0.48
80	78	81	85	1	82	83	84		6	-0.38
82	81	83	84	1	82	83	84		6	0.36
82	81	83	84	1	82	83	84		6	-0.30
82	83	84		6	88				0	0.73
82	83	84		6	88				0	-0.39
88				0	89	87	90	102	1	0.37
88				0	89	87	90	102	1	-0.31
88				0	90	89	91		3	0.43
88				0	90	89	91		3	-0.31
88				0	91	90	92		3	0.50
88				0	91	90	92		3	-0.34
88				0	92	91	93		3	0.72
88				0	92	91	93		3	-0.52

88				0	147				0	0.53
88				0	147				0	-0.43
88				0	148				0	0.53
88				0	148				0	-0.43
89	87	90	102	1	92	91	93		3	0.70
89	87	90	102	1	92	91	93		3	-0.40
90	89	91		3	92	91	93		3	0.41
90	89	91		3	92	91	93		3	-0.35
91	90	92		3	92	91	93		3	0.37
91	90	92		3	92	91	93		3	-0.31
105				0	106	104	107	119	1	0.37
105				0	106	104	107	119	1	-0.31
105				0	107	106	108		3	0.43
105				0	107	106	108		3	-0.31
105				0	108	107	109		3	0.50
105				0	108	107	109		3	-0.34
105				0	109	108	110		3	0.46
105				0	109	108	110		3	-0.36
105				0	122				0	0.36
105				0	122				0	-0.30
105				0	123	121	124	127	1	0.36
105				0	123	121	124	127	1	-0.30
105				0	124	123	125	126	1	0.48
105				0	124	123	125	126	1	-0.38
105				0	124	125	126		6	0.74
105				0	124	125	126		6	-0.40
106	104	107	119	1	109	108	110		3	0.70
106	104	107	119	1	109	108	110		3	-0.40
106	104	107	119	1	122				0	0.36
106	104	107	119	1	122				0	-0.30
107	106	108		3	109	108	110		3	0.41
107	106	108		3	109	108	110		3	-0.35
107	106	108		3	122				0	0.52
107	106	108		3	122				0	-0.36
108	107	109		3	109	108	110		3	0.37
108	107	109		3	109	108	110		3	-0.31
108	107	109		3	122				0	0.49
108	107	109		3	122				0	-0.33
122				0	123	121	124	127	1	0.46
122				0	123	121	124	127	1	-0.36
122				0	124	123	125	126	1	0.40
122				0	124	123	125	126	1	-0.34
122				0	124	125	126		6	0.59
122				0	124	125	126		6	-0.36
123	121	124	127	1	124	123	125	126	1	0.40
123	121	124	127	1	124	123	125	126	1	-0.34
123	121	124	127	1	124	125	126		6	0.52
123	121	124	127	1	124	125	126		6	-0.36
123	121	124	127	1	130				0	0.37
123	121	124	127	1	130				0	-0.31
124	123	125	126	1	124	125	126		6	0.36
124	123	125	126	1	124	125	126		6	-0.30
130				0	131	129	132	144	1	0.34
130				0	131	129	132	144	1	-0.28
130				0	132	131	133		3	0.43
130				0	132	131	133		3	-0.31
130				0	133	132	134		3	0.48
130				0	133	132	134		3	-0.32
130				0	134	133	135		3	0.68
130				0	134	133	135		3	-0.48

131	129	132	144	1	132	131	133	3	0.38
131	129	132	144	1	132	131	133	3	-0.32
131	129	132	144	1	133	132	134	3	0.44
131	129	132	144	1	133	132	134	3	-0.32
131	129	132	144	1	134	133	135	3	0.62
131	129	132	144	1	134	133	135	3	-0.42
132	131	133		3	134	133	135	3	0.48
132	131	133		3	134	133	135	3	-0.38
133	132	134		3	134	133	135	3	0.37
133	132	134		3	134	133	135	3	-0.31
147				0	148			0	0.29
147				0	148			0	-0.25

Table IX-10. GROMOS distance restraint file used in MD simulations to generate the structure of mastoparan in 50%TFE.

```
mastoparan, 50%TFE, tm=500msec
 398
     6     5     7     8     1           8     6                       5    0.25
     6     5     7     8     1           8     6                       5   -0.21
     6     5     7     8     1           7     9     6                 4    0.20
     6     5     7     8     1           7     9     6                 4   -0.18
     7     6     9           4           7     9     6                 4    0.25
     7     6     9           4           7     9     6                 4   -0.21
     7     9     6           4           8     6                       5    0.26
     7     9     6           4           8     6                       5   -0.22
     7     9     6           4           9     7                       5    0.26
     7     9     6           4           9     7                       5   -0.22
     9     7                 5          24                             0    0.46
     9     7                 5          24                             0   -0.30
    15    14    16           4          15    16    14                 4    0.25
    15    14    16           4          15    16    14                 4   -0.21
    15    14    16           3          19                             0    0.31
    15    14    16           3          19                             0   -0.27
    15    14    16           3          20                             0    0.31
    15    14    16           3          20                             0   -0.27
    19                       0          20                             0    0.23
    19                       0          20                             0   -0.19
    14    12    15    21     1          27    28    29                 6    0.53
    14    12    15    21     1          27    28    29                 6   -0.25
    14    12    15    21     1          26    25    27                 3    0.41
    14    12    15    21     1          26    25    27                 3   -0.27
    14    12    15    21     1          35    34    36                 3    0.47
    14    12    15    21     1          35    34    36                 3   -0.31
    14    12    15    21     1          48    47                       5    0.43
    14    12    15    21     1          48    47                       5   -0.27
    15    14    16           3          48    47                       5    0.59
    15    14    16           3          48    47                       5   -0.33
    19                       0          46                             0    0.75
    19                       0          46                             0   -0.31
    20                       0          46                             0    0.78
    20                       0          46                             0   -0.31
    19                       0          48    47                       5    0.45
    19                       0          48    47                       5   -0.29
    20                       0          48    47                       5    0.45
    20                       0          48    47                       5   -0.29
    24                       0          25    23    26    30           1    0.30
    24                       0          25    23    26    30           1   -0.26
    24                       0          26    25    27                 3    0.33
    24                       0          26    25    27                 3   -0.23
    24                       0          27    26    28    29           1    0.31
    24                       0          27    26    28    29           1   -0.27
    24                       0          27    28    29                 6    0.34
    24                       0          27    28    29                 6   -0.28
    25    23    26    30     1          26    25    27                 3    0.23
    25    23    26    30     1          26    25    27                 3   -0.19
    25    23    26    30     1          27    28    29                 6    0.50
    25    23    26    30     1          27    28    29                 6   -0.27
    26    25    27           3          27    28    29                 6    0.28
    26    25    27           3          27    28    29                 6   -0.24
    27    26    28    29     1          27    28    29                 6    0.30
    27    26    28    29     1          27    28    29                 6   -0.26
    24                       0          33                             0    0.31
    24                       0          33                             0   -0.27
    24                       0          36    35    37                 3    0.43
    24                       0          36    35    37                 3   -0.27
```

24				0	46				0	0.42
24				0	46				0	-0.36
24				0	52				0	0.42
24				0	52				0	-0.36
25	23	26	30	1	33				0	0.38
25	23	26	30	1	33				0	-0.32
26	25	27		3	33				0	0.41
26	25	27		3	33				0	-0.27
27	28	29		6	33				0	0.65
27	28	29		6	33				0	-0.35
33				0	34	32	35	43	1	0.30
33				0	34	32	35	43	1	-0.26
33				0	35	34	36		3	0.33
33				0	35	34	36		3	-0.23
33				0	36	35	37		3	0.41
33				0	36	35	37		3	-0.27
34	32	35	43	1	35	34	36		3	0.28
34	32	35	43	1	35	34	36		3	-0.24
35	34	36		3	36	35	37		3	0.27
35	34	36		3	36	35	37		3	-0.23
35	34	36		3	37	36	38		3	0.30
35	34	36		3	37	36	38		3	-0.26
36	35	37		3	37	36	38		3	0.27
36	35	37		3	37	36	38		3	-0.23
36	35	37		3	38	37	39		3	0.40
36	35	37		3	38	37	39		3	-0.34
37	36	38		3	38	37	39		3	0.38
37	36	38		3	38	37	39		3	-0.32
33				0	52				0	0.34
33				0	52				0	-0.28
33				0	46				0	0.29
33				0	46				0	-0.25
33				0	48	47			5	0.43
33				0	48	47			5	-0.27
34	32	35	43	1	46				0	0.35
34	32	35	43	1	46				0	-0.29
35	34	36		3	46				0	0.40
35	34	36		3	46				0	-0.26
46				0	47	45	48	49	1	0.29
46				0	47	45	48	49	1	-0.25
46				0	48	47			5	0.35
46				0	48	47			5	-0.25
47	45	48	49	1	48	47			5	0.27
47	45	48	49	1	48	47			5	-0.23
46				0	52				0	0.29
46				0	52				0	-0.25
46				0	61				0	0.40
46				0	61				0	-0.34
46				0	54	53	55		3	0.44
46				0	54	53	55		3	-0.28
46				0	55	56	57		6	0.66
46				0	55	56	57		6	-0.36
46				0	69	68			5	0.48
46				0	69	68			5	-0.30
48	47			5	52				0	0.39
48	47			5	52				0	-0.25
52				0	53	51	54	58	1	0.28
52				0	53	51	54	58	1	-0.24
52				0	54	53	55		3	0.32
52				0	54	53	55		3	-0.22

52				0	55	54	56	57	1	0.29
52				0	55	54	56	57	1	-0.25
52				0	55	56	57		6	0.29
52				0	55	56	57		6	-0.25
53	51	54	58	1	54	53	55		3	0.23
53	51	54	58	1	54	53	55		3	-0.19
53	51	54	58	1	55	56	57		6	0.50
53	51	54	58	1	55	56	57		6	-0.27
54	53	55		3	55	56	57		6	0.28
54	53	55		3	55	56	57		6	-0.24
55	54	56	57	1	55	56	57		6	0.30
55	54	56	57	1	55	56	57		6	-0.26
52				0	61				0	0.31
52				0	61				0	-0.27
52				0	62	60	63	64	1	0.33
52				0	62	60	63	64	1	-0.27
53	51	54	58	1	61				0	0.36
53	51	54	58	1	61				0	-0.30
54	53	55		3	61				0	0.38
54	53	55		3	61				0	-0.24
55	56	57		6	61				0	0.62
55	56	57		6	61				0	-0.32
61				0	62	60	63	64	1	0.28
61				0	62	60	63	64	1	-0.24
61				0	63	62			5	0.33
61				0	63	62			5	-0.23
62	60	63	64	1	63	62			5	0.25
62	60	63	64	1	63	62			5	-0.21
61				0	67				0	0.29
61				0	67				0	-0.25
61				0	68	66	69	70	1	0.53
61				0	68	66	69	70	1	-0.30
61				0	73				0	0.42
61				0	73				0	-0.36
62	60	63	64	1	67				0	0.38
62	60	63	64	1	67				0	-0.32
62	60	63	64	1	73				0	0.45
62	60	63	64	1	73				0	-0.35
62	60	63	64	1	82				0	0.37
62	60	63	64	1	82				0	-0.31
63	62			5	67				0	0.40
63	62			5	67				0	-0.26
67				0	68	66	69	70	1	0.24
67				0	68	66	69	70	1	-0.20
67				0	69	68			5	0.34
67				0	69	68			5	-0.24
68	66	69	70	1	69	68			5	0.25
68	66	69	70	1	69	68			5	-0.21
67				0	73				0	0.31
67				0	73				0	-0.27
67				0	82				0	0.41
67				0	82				0	-0.35
69	68			5	73				0	0.41
69	68			5	73				0	-0.27
69	68			5	82				0	0.55
69	68			5	82				0	-0.35
73				0	74	72	75	79	1	0.27
73				0	74	72	75	79	1	-0.23
73				0	75	74	76		3	0.36
73				0	75	74	76		3	-0.26

73				0	76	75	77	78	1	0.50
73				0	76	75	77	78	1	-0.40
73				0	76	77	78		6	0.50
73				0	76	77	78		6	-0.40
74	72	75	79	1	75	74	76		3	0.27
74	72	75	79	1	75	74	76		3	-0.23
74	72	75	79	1	76	77	78		6	0.50
74	72	75	79	1	76	77	78		6	-0.27
75	74	76		3	76	77	78		6	0.28
75	74	76		3	76	77	78		6	-0.24
76	75	77	78	1	76	77	78		6	0.30
76	75	77	78	1	76	77	78		6	-0.26
73				0	82				0	0.31
73				0	82				0	-0.27
73				0	84	83			5	0.55
73				0	84	83			5	-0.35
73				0	88				0	0.48
73				0	88				0	-0.38
74	72	75	79	1	82				0	0.35
74	72	75	79	1	82				0	-0.29
75	74	76		3	82				0	0.41
75	74	76		3	82				0	-0.27
75	74	76		3	88				0	0.55
75	74	76		3	88				0	-0.35
76	75	77	78	1	82				0	0.45
76	75	77	78	1	82				0	-0.35
76	75	77	78	1	88				0	0.60
76	75	77	78	1	88				0	-0.40
76	77	78		6	82				0	0.58
76	77	78		6	82				0	-0.28
82				0	83	81	84	85	1	0.30
82				0	83	81	84	85	1	-0.26
82				0	84	83			5	0.35
82				0	84	83			5	-0.25
83	81	84	85	1	84	83			5	0.26
83	81	84	85	1	84	83			5	-0.22
82				0	88				0	0.33
82				0	88				0	-0.27
82				0	101				0	0.42
82				0	101				0	-0.36
88				0	89	87	90	98	1	0.29
88				0	89	87	90	98	1	-0.25
88				0	90	89	91		3	0.37
88				0	90	89	91		3	-0.23
88				0	91	90	92		3	0.43
88				0	91	90	92		3	-0.27
89	87	90	98	1	90	89	91		3	0.24
89	87	90	98	1	90	89	91		3	-0.20
90	89	91		3	91	90	92		3	0.27
90	89	91		3	91	90	92		3	-0.23
90	89	91		3	92	91	93		3	0.28
90	89	91		3	92	91	93		3	-0.24
91	90	92		3	92	91	93		3	0.27
91	90	92		3	92	91	93		3	-0.23
91	90	92		3	93	92	94		3	0.40
91	90	92		3	93	92	94		3	-0.34
92	91	93		3	93	92	94		3	0.38
92	91	93		3	93	92	94		3	-0.32
88				0	84	83			5	0.41
88				0	84	83			5	-0.27

88				0	101				0	0.30
88				0	101				0	-0.26
88				0	102	100	103	111	1	0.33
88				0	102	100	103	111	1	-0.27
88				0	114				0	0.46
88				0	114				0	-0.36
88				0	118	116			5	0.56
88				0	118	116			5	-0.36
89	87	90	98	1	101				0	0.33
89	87	90	98	1	101				0	-0.27
89	87	90	98	1	114				0	0.45
89	87	90	98	1	114				0	-0.35
89	87	90	98	1	118	116			5	0.40
89	87	90	98	1	118	116			5	-0.34
89	87	90	98	1	119	117			5	0.83
89	87	90	98	1	119	117			5	-0.53
89	87	90	98	1	123				0	0.34
89	87	90	98	1	123				0	-0.28
89	87	90	98	1	132				0	0.38
89	87	90	98	1	132				0	-0.32
89	87	90	98	1	133				0	0.38
89	87	90	98	1	133				0	-0.32
89	88	91		3	101				0	0.39
89	88	91		3	101				0	-0.25
101				0	102	100	103	111	1	0.28
101				0	102	100	103	111	1	-0.24
101				0	103	102	104		3	0.33
101				0	103	102	104		3	-0.23
101				0	104	103	105		3	0.41
101				0	104	103	105		3	-0.27
102	100	103	111	1	103	102	104		3	0.26
102	100	103	111	1	103	102	104		3	-0.22
103	102	104		3	104	103	105		3	0.27
103	102	104		3	104	103	105		3	-0.23
103	102	104		3	105	104	106		3	0.30
103	102	104		3	105	104	106		3	-0.26
104	103	105		3	105	104	106		3	0.27
104	103	105		3	105	104	106		3	-0.23
104	103	105		3	106	105	107		3	0.40
104	103	105		3	106	105	107		3	-0.34
105	104	106		3	106	105	107		3	0.38
105	104	106		3	106	105	107		3	-0.32
101				0	114				0	0.30
101				0	114				0	-0.26
101				0	115	113	116	120	1	0.39
101				0	115	113	116	120	1	-0.33
101				0	116	115	117	118	1	0.31
101				0	116	115	117	118	1	-0.27
101				0	117	116	119		4	0.51
101				0	117	116	119		4	-0.41
101				0	123				0	0.46
101				0	123				0	-0.36
102	100	103	111	1	114				0	0.33
102	100	103	111	1	114				0	-0.27
102	100	103	111	1	123				0	0.48
102	100	103	111	1	123				0	-0.38
102	100	103	111	1	132				0	0.42
102	100	103	111	1	132				0	-0.36
102	100	103	111	1	133				0	0.42
102	100	103	111	1	133				0	-0.36

103	102	104		3	114				0	0.44
103	102	104		3	114				0	-0.28
104	103	105		3	114				0	0.44
104	103	105		3	114				0	-0.28
104	103	105		3	123				0	0.43
104	103	105		3	123				0	-0.27
104	103	105		3	124	122	125	129	1	0.43
104	103	105		3	124	122	125	129	1	-0.27
104	103	105		3	132				0	0.44
104	103	105		3	132				0	-0.28
104	103	105		3	133				0	0.44
104	103	105		3	133				0	-0.28
114				0	115	113	116	120	1	0.30
114				0	115	113	116	120	1	-0.26
114				0	116	115	117	118	1	0.27
114				0	116	115	117	118	1	-0.23
114				0	117	116	119		4	0.34
114				0	117	116	119		4	-0.28
114				0	117	119	116		4	0.27
114				0	117	119	116		4	-0.23
114				0	118	116			5	0.41
114				0	118	116			5	-0.27
114				0	119	117			5	0.35
114				0	119	117			5	-0.29
115	113	116	120	1	116	115	117	118	1	0.31
115	113	116	120	1	116	115	117	118	1	-0.27
115	113	116	120	1	117	116	119		4	0.31
115	113	116	120	1	117	116	119		4	-0.27
115	113	116	120	1	117	119	116		4	0.34
115	113	116	120	1	117	119	116		4	-0.28
115	113	116	120	1	118	116			5	0.40
115	113	116	120	1	118	116			5	-0.28
115	113	116	120	1	119	117			5	0.45
115	113	116	120	1	119	117			5	-0.29
116	115	117	118	1	117	116	119		4	0.28
116	115	117	118	1	117	116	119		4	-0.24
116	115	117	118	1	117	119	116		4	0.20
116	115	117	118	1	117	119	116		4	-0.18
116	115	117	118	1	118	116			5	0.25
116	115	117	118	1	118	116			5	-0.21
116	115	117	118	1	119	117			5	0.29
116	115	117	118	1	119	117			5	-0.25
117	116	119		4	117	119	116		4	0.25
117	116	119		4	117	119	116		4	-0.21
117	116	119		4	118	116			5	0.28
117	116	119		4	118	116			5	-0.24
117	116	119		4	119	117			5	0.28
117	116	119		4	119	117			5	-0.24
117	119	116		4	119	117			5	0.25
117	119	116		4	119	117			5	-0.21
114				0	123				0	0.31
114				0	123				0	-0.27
114				0	132				0	0.36
114				0	132				0	-0.30
114				0	133				0	0.36
114				0	133				0	-0.30
115	113	116	120	1	123				0	0.36
115	113	116	120	1	123				0	-0.30
115	113	116	120	1	132				0	0.48
115	113	116	120	1	132				0	-0.38

115	113	116	120	1	133				0	0.48
115	113	116	120	1	133				0	-0.38
117	116	119		4	123				0	0.49
117	116	119		4	123				0	-0.39
117	119	116		4	123				0	0.35
117	119	116		4	123				0	-0.29
123				0	124	122	125	129	1	0.34
123				0	124	122	125	129	1	-0.28
123				0	125	124	126		3	0.34
123				0	125	124	126		3	-0.24
123				0	126	125	127	128	1	0.30
123				0	126	125	127	128	1	-0.26
123				0	126	127	128		6	0.30
123				0	126	127	128		6	-0.26
124	122	125	129	1	125	124	126		3	0.30
124	122	125	129	1	125	124	126		3	-0.26
124	122	125	129	1	126	127	128		6	0.51
124	122	125	129	1	126	127	128		6	-0.28
125	124	126		3	126	127	128		6	0.28
125	124	126		3	126	127	128		6	-0.24
126	125	127	128	1	126	127	128		6	0.30
126	125	127	128	1	126	127	128		6	-0.26
132				0	133				0	0.22
132				0	133				0	-0.18
123				0	133				0	0.31
123				0	133				0	-0.27
123				0	133				0	0.31
123				0	133				0	-0.27
124	122	125	129	1	132				0	0.39
124	122	125	129	1	132				0	-0.33
124	122	125	129	1	133				0	0.39
124	122	125	129	1	133				0	-0.33
125	124	126		3	132				0	0.30
125	124	126		3	132				0	-0.26
125	124	126		3	133				0	0.30
125	124	126		3	133				0	-0.26
126	127	128		6	132				0	0.37
126	127	128		6	132				0	-0.31
126	127	128		6	133				0	0.37
126	127	128		6	133				0	-0.31

Table IX-11. Final coordinates for the structure of the TnI peptide in 50%TFE **A.** α-helical coordinates (structure 1), and **B.** β-strand coordinates (structure 2), following approximately 12 ps of restrained MD.

```
AVE COORDS 10-15PS   TnI peptide, 50% TFE, tm=150ms, starting with alfa-helical coordinates
 148
   1GLY     ACC    1   0.160  -1.441  -0.247  0.2987  0.7794 -0.1992  0.0837  0.1386 -0.0378  0.0329
   1GLY       C    2   0.287  -1.402  -0.181  0.1878  0.4992 -0.0117  0.0027  0.1700 -0.0043  0.0614
   1GLY       O    3   0.305  -1.415  -0.062  0.1528  0.3826  0.0299  0.0150  0.1455  0.0109  0.0608
   1GLY       N    4   0.379  -1.338  -0.249  0.1845  0.4336  0.0632  0.0134  0.1973  0.0343  0.1063
   1GLY       H    5   0.374  -1.367  -0.161  0.1556  0.3680  0.0425  0.0104  0.1708  0.0212  0.0884
   1GLY      CA    6   0.439  -1.209  -0.280  0.1691  0.3117  0.0900  0.0308  0.2229  0.0628  0.1649
   1GLY       C    7   0.349  -1.099  -0.231  0.0972  0.1642  0.0260  0.0065  0.1374  0.0228  0.1209
   1GLY       O    8   0.283  -1.045  -0.314  0.0752  0.0686 -0.0348  0.0246  0.0832 -0.0390  0.1323
  2LYSH       N    9   0.348  -1.072  -0.102  0.1159  0.1984  0.0821  0.0477  0.1371  0.0538  0.1016
  2LYSH       H   10   0.404  -1.119  -0.044  0.1777  0.2817  0.1778  0.1379  0.1694  0.1048  0.1136
  2LYSH      CA   11   0.265  -0.972  -0.035  0.0794  0.1334  0.0568  0.0426  0.0862  0.0305  0.0622
  2LYSH      CB   12   0.278  -1.005   0.112  0.1342  0.2003  0.1497  0.1275  0.1182  0.0820  0.0750
  2LYSH      CG   13   0.408  -0.960   0.172  0.1692  0.2232  0.2329  0.2651  0.0370  0.0272  0.0192
  2LYSH      CD   14   0.527  -1.044   0.133  0.2240  0.2779  0.2854  0.3198  0.1141  0.1020  0.0744
  2LYSH      CE   15   0.636  -0.964   0.063  0.2023  0.2595  0.2421  0.2818  0.0770  0.0449  0.0655
  2LYSH      NZ   16   0.678  -0.852   0.131  0.2114  0.1808  0.2580  0.4227 -0.0174 -0.0485  0.0308
  2LYSH     HZ1   17   0.648  -0.811   0.160  0.4722  0.8678  0.3530  0.3431  0.1148 -0.0431  0.2057
  2LYSH     HZ2   18   0.707  -0.855   0.169  0.5284  0.2388  0.3604  1.0271 -0.2390 -0.5047  0.3193
  2LYSH     HZ3   19   0.702  -0.812   0.110  0.1952  0.1468 -0.0533  0.2687 -0.1024  0.0595  0.1701
  2LYSH       C   20   0.287  -0.827  -0.068  0.0322  0.0547  0.0286  0.0369  0.0066 -0.0039  0.0052
  2LYSH       O   21   0.275  -0.737   0.014  0.0637  0.1280  0.0579  0.0568 -0.0016 -0.0133  0.0065
  3PHE        N   22   0.318  -0.804  -0.191  0.0098  0.0087  0.0019  0.0129  0.0011 -0.0076  0.0076
  3PHE        H   23   0.307  -0.880  -0.245  0.0187  0.0347  0.0014  0.0121 -0.0042 -0.0070  0.0094
  3PHE       CA   24   0.354  -0.670  -0.234  0.0310  0.0349 -0.0004  0.0130  0.0361 -0.0095  0.0451
  3PHE       CB   25   0.422  -0.679  -0.367  0.0988  0.1777  0.0256  0.0230  0.1223  0.0090  0.0958
  3PHE       CG   26   0.518  -0.786  -0.415  0.1171  0.1693 -0.0087  0.0045  0.1680 -0.0057  0.1775
  3PHE      CD1   27   0.484  -0.879  -0.508  0.1231  0.2228  0.0230  0.0136  0.1275 -0.0020  0.1329
  3PHE      CD2   28   0.642  -0.793  -0.364  0.2000  0.1272 -0.0683  0.0595  0.2258 -0.1091  0.4133
  3PHE      CE1   29   0.570  -0.975  -0.552  0.1615  0.2218 -0.0004  0.0214  0.1613 -0.0496  0.2412
  3PHE      CE2   30   0.731  -0.888  -0.406  0.2751  0.1076 -0.0885  0.1197  0.2378 -0.2122  0.5980
  3PHE       CZ   31   0.694  -0.978  -0.501  0.2369  0.1663 -0.0563  0.0715  0.2281 -0.1514  0.4730
  3PHE        C   32   0.246  -0.563  -0.238  0.0237  0.0498  0.0028  0.0057  0.0261  0.0000  0.0157
  3PHE        O   33   0.262  -0.454  -0.290  0.0646  0.1443  0.0113  0.0067  0.0748  0.0049  0.0427
  4LYSH       N   34   0.137  -0.601  -0.181  0.0110  0.0135  0.0018  0.0032 -0.0117  0.0016  0.0163
  4LYSH       H   35   0.154  -0.680  -0.132  0.0183  0.0141  0.0055  0.0065 -0.0016  0.0098  0.0343
  4LYSH      CA   36   0.013  -0.528  -0.180  0.0493  0.0204  0.0064  0.0039 -0.0472 -0.0180  0.1236
  4LYSH      CB   37  -0.093  -0.621  -0.138  0.1540  0.0069 -0.0059  0.0222  0.0016 -0.0451  0.4329
  4LYSH      CG   38  -0.126  -0.748  -0.212  0.2374  0.0595 -0.0016  0.0281 -0.1549 -0.0594  0.6245
  4LYSH      CD   39  -0.085  -0.748  -0.353  0.2899  0.2216  0.0883  0.0870 -0.3142 -0.2008  0.5611
  4LYSH      CE   40  -0.047  -0.859  -0.378  0.7788  1.4090  0.5945  0.3544 -0.8749 -0.3821  0.5731
  4LYSH      NZ   41  -0.018  -0.836  -0.483  1.4793  2.9608  1.6532  1.2112 -0.8311 -0.4157  0.2661
  4LYSH     HZ1   42  -0.041  -0.782  -0.525  1.6793  3.5650  1.6304  1.0471 -1.1082 -0.3952  0.4259
  4LYSH     HZ2   43   0.011  -0.823  -0.500  1.4496  2.2316  1.6646  1.9066 -0.2244 -0.1660  0.2105
  4LYSH     HZ3   44  -0.030  -0.906  -0.479  2.0431  4.5108  1.9507  1.2707 -1.0500 -0.3705  0.3479
  4LYSH       C   45   0.004  -0.399  -0.100  0.0318  0.0050  0.0005  0.0036 -0.0125 -0.0046  0.0869
  4LYSH       O   46  -0.100  -0.355  -0.052  0.0337  0.0037 -0.0002  0.0199 -0.0025  0.0184  0.0775
  5ARG        N   47   0.116  -0.329  -0.085  0.0228  0.0037  0.0018  0.0023 -0.0063 -0.0106  0.0626
  5ARG        H   48   0.183  -0.371  -0.137  0.0315  0.0098  0.0089  0.0161 -0.0132 -0.0297  0.0685
  5ARG       CA   49   0.136  -0.207  -0.006  0.0105  0.0035  0.0004  0.0007  0.0025  0.0009  0.0274
  5ARG       CB   50   0.286  -0.186  -0.013  0.0148  0.0036 -0.0034  0.0221  0.0043 -0.0127  0.0188
  5ARG       CG   51   0.365  -0.276   0.082  0.0207  0.0049  0.0043  0.0171 -0.0105 -0.0222  0.0400
  5ARG       CD   52   0.361  -0.249   0.231  0.0229  0.0135  0.0082  0.0187 -0.0156 -0.0117  0.0364
  5ARG       NE   53   0.315  -0.116   0.266  0.0184  0.0190 -0.0044  0.0148 -0.0004 -0.0120  0.0214
  5ARG       HE   54   0.234  -0.131   0.311  0.0230  0.0202  0.0094  0.0309 -0.0014 -0.0018  0.0180
  5ARG       CZ   55   0.379  -0.001   0.257  0.0462  0.0562 -0.0344  0.0342  0.0247 -0.0321  0.0482
  5ARG      NH1   56   0.328   0.115   0.297  0.0588  0.1210 -0.0360  0.0243  0.0358 -0.0208  0.0309
  5ARG     HH11   57   0.242   0.109   0.335  0.0493  0.1092 -0.0009  0.0193  0.0096 -0.0111  0.0194
  5ARG     HH12   58   0.376   0.196   0.285  0.0919  0.1893 -0.0653  0.0340  0.0673 -0.0369  0.0523
```

University of Alberta

University of Alberta

```
 5ARG    NH2   59   0.498  -0.001   0.202  0.0920  0.0655 -0.0736  0.1019  0.0586 -0.0935  0.1088
 5ARG   HH21   60   0.544  -0.078   0.171  0.1127  0.0392 -0.0609  0.1380  0.0609 -0.1322  0.1609
 5ARG   HH22   61   0.546   0.080   0.187  0.1166  0.1030 -0.1103  0.1312  0.0849 -0.1058  0.1157
 5ARG      C   62   0.056  -0.080  -0.029  0.0025  0.0029 -0.0005  0.0012  0.0015  0.0012  0.0033
 5ARG      O   63   0.041  -0.018   0.076  0.0042  0.0061  0.0011  0.0022 -0.0027 -0.0005  0.0044
 6PRO      N   64   0.004  -0.043  -0.145  0.0087  0.0162 -0.0041  0.0081 -0.0004  0.0031  0.0019
 6PRO     CA   65  -0.053   0.091  -0.161  0.0189  0.0255 -0.0036  0.0104 -0.0151  0.0121  0.0208
 6PRO     CB   66  -0.076   0.108  -0.310  0.0553  0.0988 -0.0272  0.0362 -0.0420  0.0299  0.0310
 6PRO     CG   67   0.002  -0.008  -0.369  0.0757  0.1629 -0.0339  0.0582  0.0087  0.0132  0.0062
 6PRO     CD   68  -0.011  -0.119  -0.269  0.0274  0.0511 -0.0140  0.0288  0.0025 -0.0043  0.0024
 6PRO      C   69  -0.170   0.151  -0.085  0.0252  0.0140  0.0011  0.0058 -0.0197  0.0048  0.0559
 6PRO      O   70  -0.188   0.271  -0.094  0.0452  0.0151 -0.0022  0.0061 -0.0131  0.0111  0.1144
 7PRO      N   71  -0.251   0.079  -0.008  0.0229  0.0066  0.0033  0.0043 -0.0123 -0.0058  0.0577
 7PRO     CA   72  -0.354   0.132   0.081  0.0389  0.0033  0.0039  0.0108 -0.0034 -0.0233  0.1026
 7PRO     CB   73  -0.417   0.012   0.151  0.0414  0.0093 -0.0095  0.0246  0.0249 -0.0407  0.0902
 7PRO     CG   74  -0.402  -0.100   0.050  0.0176  0.0016  0.0024  0.0090 -0.0048 -0.0135  0.0422
 7PRO     CD   75  -0.265  -0.067  -0.007  0.0124  0.0043  0.0013  0.0049 -0.0061 -0.0061  0.0282
 7PRO      C   76  -0.299   0.233   0.181  0.0362  0.0088 -0.0016  0.0096  0.0124 -0.0225  0.0903
 7PRO      O   77  -0.369   0.328   0.214  0.0541  0.0088  0.0024  0.0226  0.0069 -0.0434  0.1308
 8LEU      N   78  -0.179   0.212   0.234  0.0244  0.0132 -0.0074  0.0077  0.0157 -0.0164  0.0522
 8LEU      H   79  -0.120   0.139   0.217  0.0253  0.0168 -0.0058  0.0064  0.0121 -0.0161  0.0526
 8LEU     CA   80  -0.115   0.307   0.326  0.0210  0.0147 -0.0053  0.0048  0.0168 -0.0128  0.0435
 8LEU     CB   81  -0.002   0.234   0.396  0.0163  0.0321 -0.0034  0.0018  0.0202 -0.0012  0.0149
 8LEU     CG   82  -0.029   0.120   0.492  0.0347  0.0821 -0.0304  0.0141  0.0125 -0.0020  0.0079
 8LEU    CD1   83   0.080   0.106   0.598  0.0547  0.1253 -0.0314  0.0341 -0.0045  0.0020  0.0048
 8LEU    CD2   84  -0.025  -0.008   0.411  0.0338  0.0739 -0.0146  0.0055 -0.0146  0.0005  0.0220
 8LEU      C   85  -0.067   0.441   0.272  0.0132  0.0106  0.0033  0.0044  0.0024 -0.0064  0.0246
 8LEU      O   86  -0.081   0.549   0.328  0.0257  0.0546  0.0138  0.0049 -0.0056 -0.0035  0.0176
 9ARG      N   87  -0.013   0.429   0.153  0.0225  0.0089 -0.0037  0.0184  0.0142 -0.0168  0.0401
 9ARG      H   88  -0.029   0.342   0.120  0.0415  0.0403 -0.0265  0.0275  0.0462 -0.0299  0.0568
 9ARG     CA   89   0.058   0.521   0.064  0.0211  0.0089 -0.0030  0.0146  0.0058 -0.0117  0.0399
 9ARG     CB   90   0.116   0.436  -0.045  0.0543  0.0564 -0.0159  0.0206  0.0642 -0.0167  0.0858
 9ARG     CG   91   0.247   0.375  -0.008  0.1035  0.0696  0.0257  0.0266  0.1051  0.0191  0.2143
 9ARG     CD   92   0.321   0.313  -0.122  0.1989  0.2111  0.0222  0.0099  0.2660  0.0156  0.3758
 9ARG     NE   93   0.323   0.179  -0.134  0.0323  0.0057  0.0049  0.0113  0.0130  0.0150  0.0799
 9ARG     HE   94   0.318   0.133  -0.054  0.0296  0.0283 -0.0146  0.0310  0.0239 -0.0214  0.0296
 9ARG     CZ   95   0.330   0.125  -0.239  0.0969  0.1579 -0.1169  0.0970 -0.0546  0.0512  0.0357
 9ARG    NH1   96   0.352   0.006  -0.237  0.2095  0.4505 -0.1442  0.0864  0.1937 -0.0469  0.0915
 9ARG   HH11   97   0.369  -0.038  -0.163  0.2047  0.3473  0.0322  0.0529  0.2636  0.0289  0.2139
 9ARG   HH12   98   0.352  -0.040  -0.307  0.4688  0.9493 -0.4195  0.2592  0.4036 -0.1579  0.1980
 9ARG    NH2   99   0.320   0.182  -0.348  0.3091  0.3510 -0.3669  0.4179 -0.2135  0.2323  0.1586
 9ARG   HH21  100   0.330   0.269  -0.354  0.3405  0.2015 -0.2497  0.4323 -0.2608  0.3810  0.3878
 9ARG   HH22  101   0.304   0.133  -0.414  0.5711  0.8060 -0.7626  0.7881 -0.2338  0.2546  0.1191
 9ARG      C  102  -0.021   0.637   0.010  0.0173  0.0032 -0.0015  0.0438  0.0002 -0.0005  0.0049
 9ARG      O  103  -0.001   0.748   0.047  0.0365  0.0149 -0.0171  0.0321 -0.0256  0.0310  0.0625
10ARG      N  104  -0.110   0.608  -0.081  0.0502  0.0132  0.0279  0.1071 -0.0156 -0.0490  0.0303
10ARG      H  105  -0.139   0.521  -0.096  0.0905  0.0287  0.0467  0.1183 -0.0512 -0.1136  0.1246
10ARG     CA  106  -0.184   0.713  -0.149  0.0803  0.0227  0.0635  0.2126  0.0020  0.0010  0.0057
10ARG     CB  107  -0.251   0.647  -0.262  0.2130  0.0604  0.1662  0.5354 -0.0467 -0.1388  0.0431
10ARG     CG  108  -0.353   0.732  -0.328  0.2124  0.0086  0.0662  0.6132  0.0083  0.0749  0.0154
10ARG     CD  109  -0.496   0.689  -0.338  0.2072  0.0190  0.0966  0.5589  0.0044 -0.0196  0.0437
10ARG     NE  110  -0.586   0.782  -0.282  0.2777  0.0030  0.0385  0.6944 -0.0165 -0.2732  0.1356
10ARG     HE  111  -0.532   0.851  -0.277  0.4143  0.0188 -0.0041  0.7797  0.0049 -0.5479  0.4446
10ARG     CZ  112  -0.712   0.762  -0.249  0.2608  0.0097  0.0769  0.7143 -0.0200 -0.1953  0.0584
10ARG    NH1  113  -0.779   0.856  -0.193  0.3801  0.0135 -0.0068  0.8368  0.0139 -0.4741  0.2899
10ARG   HH11  114  -0.735   0.929  -0.176  0.5804  0.0384 -0.1202  0.9877  0.0976 -0.8125  0.7151
10ARG   HH12  115  -0.868   0.851  -0.166  0.3573  0.0235  0.0452  0.8219  0.0104 -0.3738  0.2265
10ARG    NH2  116  -0.768   0.650  -0.261  0.2404  0.0539  0.1652  0.6477  0.0300  0.0942  0.0194
10ARG   HH21  117  -0.716   0.583  -0.293  0.2831  0.1034  0.2111  0.6043  0.1111  0.2684  0.1414
10ARG   HH22  118  -0.857   0.633  -0.236  0.2522  0.0624  0.1668  0.6478  0.0399  0.1095  0.0463
```

```
   10ARG      C  119  -0.279   0.782  -0.056  0.0241  0.0033  0.0085  0.0609  0.0029  0.0143  0.0081
   10ARG      O  120  -0.287   0.901  -0.047  0.0485  0.0159 -0.0094  0.0534 -0.0052  0.0589  0.0761
   11VAL      N  121  -0.355   0.699   0.008  0.0151  0.0063  0.0019  0.0108  0.0019 -0.0141  0.0283
   11VAL      H  122  -0.357   0.606  -0.003  0.0408  0.0056  0.0052  0.0144 -0.0067 -0.0340  0.1022
   11VAL     CA  123  -0.448   0.754   0.105  0.0232  0.0293  0.0137  0.0096  0.0245  0.0158  0.0306
   11VAL     CB  124  -0.549   0.658   0.163  0.0706  0.0446  0.0266  0.0281  0.0674  0.0577  0.1392
   11VAL    CG1  125  -0.571   0.539   0.075  0.1200  0.0228  0.0021  0.0045  0.0425  0.0019  0.3326
   11VAL    CG2  126  -0.683   0.726   0.183  0.0584  0.0362  0.0281  0.0473  0.0497  0.0541  0.0916
   11VAL      C  127  -0.376   0.809   0.224  0.0513  0.0660  0.0696  0.0854  0.0080  0.0076  0.0024
   11VAL      O  128  -0.255   0.804   0.227  0.1015  0.0720  0.1146  0.2020 -0.0137 -0.0375  0.0304
   12ARG      N  129  -0.449   0.862   0.321  0.0589  0.0739  0.0831  0.1013  0.0072  0.0089  0.0014
   12ARG      H  130  -0.541   0.878   0.312  0.0478  0.0670  0.0583  0.0611  0.0123  0.0096  0.0154
   12ARG     CA  131  -0.391   0.906   0.446  0.1203  0.0860  0.1492  0.2691 -0.0149 -0.0262  0.0057
   12ARG     CB  132  -0.504   0.977   0.519  0.0984  0.0863  0.1255  0.2026  0.0053  0.0012  0.0064
   12ARG     CG  133  -0.534   1.119   0.484  0.0546  0.0085  0.0187  0.1404 -0.0042 -0.0440  0.0149
   12ARG     CD  134  -0.440   1.217   0.539  0.1566  0.0118 -0.0379  0.3295  0.0275 -0.1912  0.1285
   12ARG     NE  135  -0.305   1.189   0.492  0.1716  0.0081 -0.0072  0.4293  0.0100 -0.1585  0.0775
   12ARG     HE  136  -0.255   1.126   0.528  0.2542  0.0430  0.1116  0.6866  0.0225  0.0059  0.0330
   12ARG     CZ  137  -0.238   1.242   0.395  0.1653  0.0269 -0.0773  0.2592  0.0676 -0.2295  0.2098
   12ARG    NH1  138  -0.118   1.203   0.366  0.1801  0.0064 -0.0407  0.3927  0.0201 -0.2207  0.1411
   12ARG   HH11  139  -0.073   1.155   0.408  0.3222  0.0547  0.1191  0.8125 -0.0537 -0.1179  0.0994
   12ARG   HH12  140  -0.073   1.217   0.296  0.2145  0.0810 -0.1310  0.2401  0.1473 -0.2726  0.3225
   12ARG    NH2  141  -0.284   1.326   0.322  0.2742  0.1656 -0.0868  0.0605  0.3083 -0.1744  0.5965
   12ARG   HH21  142  -0.375   1.336   0.320  0.3191  0.2144 -0.0144  0.0130  0.3902 -0.0288  0.7297
   12ARG   HH22  143  -0.230   1.378   0.270  0.4029  0.2652 -0.1148  0.0866  0.4585 -0.1673  0.8569
   12ARG      C  144  -0.336   0.794   0.529  0.2267  0.2391  0.3178  0.4378  0.0087  0.0152  0.0033
   12ARG      O  145  -0.377   0.778   0.635  0.4147  0.5376  0.5900  0.6761  0.1020  0.1168  0.0306
   12ARG      N  146  -0.244   0.711   0.490  0.2022  0.1642  0.2569  0.4137 -0.0530 -0.0754  0.0288
   12ARG     H1  147  -0.215   0.714   0.407  0.1970  0.0707  0.1738  0.4632 -0.0393 -0.1177  0.0570
   12ARG     H2  148  -0.210   0.648   0.547  0.2739  0.2958  0.3531  0.4564 -0.1094 -0.1028  0.0696
TnI peptide, 50% TFE, tm=150ms, starting with beta-strand coordinates
  148
    1GLY    ACC    1  -0.909  -1.045   0.589 -1.0529 -0.1860 -0.3654
    1GLY      C    2  -0.866  -1.177   0.526  0.1013  0.3277 -0.4348
    1GLY      O    3  -0.905  -1.287   0.565  0.5106  0.1910 -0.2269
    1GLY      N    4  -0.784  -1.163   0.421  0.9178  0.5759  0.1714
    1GLY      H    5  -0.809  -1.246   0.463 -0.3560  1.9407  2.3656
    1GLY     CA    6  -0.650  -1.149   0.364  0.6568 -0.0976 -0.4503
    1GLY      C    7  -0.628  -1.023   0.279  0.6168  0.1044 -0.2346
    1GLY      O    8  -0.524  -0.958   0.284  0.2841  0.5931 -0.4410
    2LYSH     N    9  -0.733  -0.980   0.208  0.4353 -0.0155 -0.0216
    2LYSH     H   10  -0.811  -1.036   0.207  0.3356 -0.0960 -4.5289
    2LYSH    CA   11  -0.743  -0.864   0.120  0.3009 -0.1408 -0.1572
    2LYSH    CB   12  -0.888  -0.878   0.074  0.0190 -0.9513  1.0011
    2LYSH    CG   13  -0.998  -0.808   0.155  0.3497  0.6946  0.1342
    2LYSH    CD   14  -1.017  -0.869   0.294 -0.0097  0.2697 -0.1650
    2LYSH    CE   15  -1.150  -0.818   0.349  0.0765  0.1115  0.0822
    2LYSH    NZ   16  -1.159  -0.862   0.489 -0.0460  0.1929  0.1002
    2LYSH   HZ1   17  -1.244  -0.833   0.524  0.9486  1.6507  1.4825
    2LYSH   HZ2   18  -1.160  -0.956   0.504 -5.5009 -0.5609 -2.7518
    2LYSH   HZ3   19  -1.094  -0.808   0.535  1.9820  0.2019 -2.5801
    2LYSH     C   20  -0.701  -0.722   0.161 -0.3078  0.0566 -0.2134
    2LYSH     O   21  -0.663  -0.639   0.078 -0.5887  0.7341  0.3218
    3PHE      N   22  -0.704  -0.694   0.291  0.1066 -0.6232 -0.0445
    3PHE      H   23  -0.707  -0.773   0.346  3.8555 -3.9754 -3.9331
    3PHE     CA   24  -0.667  -0.564   0.349 -0.8546 -0.5367  0.4657
    3PHE     CB   25  -0.707  -0.557   0.496 -1.3337 -0.7946  0.3124
    3PHE     CG   26  -0.633  -0.648   0.595  0.1332 -0.1140 -0.1439
    3PHE    CD1   27  -0.691  -0.774   0.607 -0.8996  0.4420  0.5496
    3PHE    CD2   28  -0.530  -0.608   0.679  0.1679 -0.6509  0.0235
```

University of Alberta

3PHE	CE1	29	-0.650	-0.871	0.698	0.4888	-0.8148	-1.2540
3PHE	CE2	30	-0.485	-0.700	0.773	0.2649	-0.5135	0.1480
3PHE	CZ	31	-0.550	-0.823	0.781	-1.3638	0.3294	0.3991
3PHE	C	32	-0.523	-0.514	0.330	-0.9888	-0.0382	0.3221
3PHE	O	33	-0.500	-0.398	0.299	-0.1389	-0.3456	-0.2594
4LYSH	N	34	-0.432	-0.610	0.341	-0.2247	0.7274	0.1697
4LYSH	H	35	-0.456	-0.699	0.368	0.9824	0.7593	1.3173
4LYSH	CA	36	-0.286	-0.604	0.321	-0.2601	0.6743	-0.2370
4LYSH	CB	37	-0.220	-0.726	0.385	-0.0762	0.4365	-0.8705
4LYSH	CG	38	-0.122	-0.669	0.488	-0.4971	-0.0237	-0.1900
4LYSH	CD	39	-0.187	-0.566	0.580	0.2517	0.3771	-0.0648
4LYSH	CE	40	-0.109	-0.434	0.589	-0.4429	0.6622	0.4439
4LYSH	NZ	41	-0.123	-0.368	0.458	-0.5055	0.4934	0.2828
4LYSH	HZ1	42	-0.094	-0.437	0.398	3.9676	2.5153	-0.1761
4LYSH	HZ2	43	-0.215	-0.343	0.444	-1.4381	-3.4062	-1.5736
4LYSH	HZ3	44	-0.062	-0.295	0.449	-5.7633	5.9150	2.0337
4LYSH	C	45	-0.236	-0.585	0.177	0.5624	0.1909	0.0100
4LYSH	O	46	-0.182	-0.679	0.118	1.0977	0.4732	0.0515
5ARG	N	47	-0.263	-0.464	0.130	0.7225	0.4060	0.4814
5ARG	H	48	-0.300	-0.405	0.196	0.9006	-1.2700	2.1358
5ARG	CA	49	-0.241	-0.415	-0.007	-0.1959	0.3607	0.2799
5ARG	CB	50	-0.309	-0.279	-0.029	-0.4785	0.1247	-0.1418
5ARG	CG	51	-0.460	-0.293	-0.011	-0.6608	0.2030	-1.0031
5ARG	CD	52	-0.533	-0.169	0.040	0.2849	-0.0400	0.9749
5ARG	NE	53	-0.579	-0.092	-0.077	0.4267	-0.4706	0.6533
5ARG	HE	54	-0.659	-0.123	-0.120	0.1896	-2.2457	2.2695
5ARG	CZ	55	-0.513	0.014	-0.125	0.1394	-0.6191	-0.0216
5ARG	NH1	56	-0.545	0.077	-0.240	-0.3203	0.7216	0.7497
5ARG	HH11	57	-0.614	0.046	-0.299	0.6053	-2.7876	1.2204
5ARG	HH12	58	-0.499	0.158	-0.260	0.4667	-0.0942	-1.0271
5ARG	NH2	59	-0.408	0.069	-0.064	-0.1227	0.3844	-0.4813
5ARG	HH21	60	-0.370	0.022	0.011	-0.8255	0.6842	0.0763
5ARG	HH22	61	-0.372	0.155	-0.087	1.1895	-0.0481	-0.1410
5ARG	C	62	-0.097	-0.392	-0.052	-0.1235	-0.1134	0.1807
5ARG	O	63	-0.024	-0.328	0.023	-0.5764	0.3896	0.2043
6PRO	N	64	-0.062	-0.455	-0.164	0.0320	-0.6386	0.5058
6PRO	CA	65	0.065	-0.410	-0.224	-0.1451	0.5642	0.9652
6PRO	CB	66	0.107	-0.533	-0.305	-0.3075	0.1913	1.4999
6PRO	CG	67	-0.003	-0.639	-0.292	0.2455	-0.5937	-0.0139
6PRO	CD	68	-0.126	-0.565	-0.238	0.3031	-0.3380	-0.1819
6PRO	C	69	0.089	-0.277	-0.296	0.4833	-0.0123	0.0134
6PRO	O	70	0.202	-0.232	-0.312	0.4965	-0.4067	-0.8658
7PRO	N	71	-0.015	-0.208	-0.341	0.2471	-0.0227	0.3802
7PRO	CA	72	-0.009	-0.069	-0.390	0.3541	-0.2895	-0.3096
7PRO	CB	73	-0.152	-0.041	-0.435	0.5550	-0.2713	-0.9556
7PRO	CG	74	-0.220	-0.172	-0.473	0.8530	-0.5453	-0.6022
7PRO	CD	75	-0.152	-0.258	-0.366	0.2814	0.0120	0.1608
7PRO	C	76	0.031	0.021	-0.274	0.2889	-0.3629	-0.2233
7PRO	O	77	-0.051	0.094	-0.218	0.4140	-0.2623	-0.1607
8LEU	N	78	0.156	0.027	-0.229	0.2994	0.3531	-0.2881
8LEU	H	79	0.227	-0.021	-0.273	0.7003	0.4048	0.3865
8LEU	CA	80	0.194	0.117	-0.119	0.6167	0.2563	-0.3127
8LEU	CB	81	0.340	0.098	-0.077	0.6790	0.9505	-0.1832
8LEU	CG	82	0.389	-0.014	0.014	0.2330	0.4804	-0.4844
8LEU	CD1	83	0.297	-0.016	0.136	-0.3778	0.0571	-1.0353
8LEU	CD2	84	0.534	-0.001	0.062	0.0810	-0.3057	0.2929
8LEU	C	85	0.175	0.258	-0.176	-0.3020	0.0407	-0.4502
8LEU	O	86	0.116	0.280	-0.282	0.4464	0.3364	-0.8627
9ARG	N	87	0.222	0.362	-0.107	0.4154	-0.2971	-0.4158
9ARG	H	88	0.258	0.349	-0.019	1.7595	-1.2234	-1.0772

University of Alberta

```
  9ARG     CA   89   0.220    0.496   -0.166  -0.0887  -0.1908  -0.1981
  9ARG     CB   90   0.264    0.614   -0.079  -0.1816  -0.2956   0.0126
  9ARG     CG   91   0.187    0.659    0.046   0.6534  -0.1371   0.4770
  9ARG     CD   92   0.056    0.734    0.028   0.1267  -1.0058   0.6656
  9ARG     NE   93  -0.033    0.646   -0.048  -0.8803   0.2209   0.3248
  9ARG     HE   94  -0.015    0.651   -0.143  -2.0405  -0.0767   0.0525
  9ARG     CZ   95  -0.133    0.570    0.000   0.3677  -0.9735   1.0717
  9ARG    NH1   96  -0.192    0.492   -0.092  -0.0056   0.2557   0.1629
  9ARG   HH11   97  -0.163    0.488   -0.183   0.5840   0.3955   0.3470
  9ARG   HH12   98  -0.267    0.435   -0.073   0.9947  -1.2541  -0.0710
  9ARG    NH2   99  -0.193    0.585    0.119  -0.8727  -0.2177   0.3509
  9ARG   HH21  100  -0.176    0.657    0.180  -3.7672   1.0935  -0.2215
  9ARG   HH22  101  -0.252    0.513    0.141   0.4857  -0.9969   1.5141
  9ARG      C  102   0.319    0.495   -0.283  -0.2027  -0.0455  -0.2637
  9ARG      O  103   0.416    0.420   -0.285  -0.0469   0.1467   0.3619
 10ARG      N  104   0.316    0.582   -0.384  -0.4840  -0.0004  -0.1758
 10ARG      H  105   0.242    0.640   -0.400   1.4081   2.0359  -2.5342
 10ARG     CA  106   0.423    0.596   -0.485  -0.1852   0.5798   0.1799
 10ARG     CB  107   0.380    0.691   -0.596  -0.1766   0.8372   0.3505
 10ARG     CG  108   0.479    0.714   -0.710  -0.4011   0.0339   0.0216
 10ARG     CD  109   0.518    0.861   -0.725  -0.0587  -0.1235  -0.6737
 10ARG     NE  110   0.625    0.898   -0.631  -0.6354  -0.6251   0.1653
 10ARG     HE  111   0.686    0.835   -0.593  -1.0901  -0.2978   1.4587
 10ARG     CZ  112   0.642    1.025   -0.590   0.3597  -0.5407  -0.5541
 10ARG    NH1  113   0.736    1.056   -0.501  -0.1267  -1.3199   0.2734
 10ARG   HH11  114   0.793    0.996   -0.453  -1.1438  -0.9202   2.0678
 10ARG   HH12  115   0.741    1.152   -0.496  -2.1412  -1.0698  -1.5571
 10ARG    NH2  116   0.566    1.127   -0.632   0.7019   0.0265   0.1202
 10ARG   HH21  117   0.501    1.120   -0.702  -3.5466   0.0923   3.5803
 10ARG   HH22  118   0.569    1.212   -0.587   1.2594   0.7231  -1.1438
 10ARG      C  119   0.541    0.649   -0.403   0.1478   0.5986  -0.3063
 10ARG      O  120   0.656    0.607   -0.413  -0.2110  -0.4400   0.0883
 11VAL      N  121   0.506    0.739   -0.312   0.4237  -0.1052   0.4379
 11VAL      H  122   0.413    0.760   -0.315  -0.4944  -3.1313   2.2473
 11VAL     CA  123   0.589    0.795   -0.203   0.0510   0.3085   0.5078
 11VAL     CB  124   0.498    0.885   -0.120  -0.5881  -0.0532   0.2016
 11VAL    CG1  125   0.429    0.996   -0.200  -0.0326   0.0986  -0.0682
 11VAL    CG2  126   0.589    0.959   -0.022  -0.9418   0.2360   0.3166
 11VAL      C  127   0.643    0.677   -0.123  -0.2839  -0.0938   0.0705
 11VAL      O  128   0.570    0.599   -0.063  -0.5682   0.5279   0.4650
 12ARG      N  129   0.774    0.653   -0.134  -0.2857  -0.2292   0.0072
 12ARG      H  130   0.822    0.709   -0.195  -0.5231   0.5722   0.5048
 12ARG     CA  131   0.852    0.547   -0.068  -0.1132   0.0075   0.1216
 12ARG     CB  132   1.000    0.565   -0.102  -0.4555   0.1505  -1.3019
 12ARG     CG  133   1.071    0.429   -0.096  -0.0147   0.4770   0.2487
 12ARG     CD  134   1.210    0.440   -0.032   0.0892  -0.6959   0.1042
 12ARG     NE  135   1.231    0.535    0.078  -0.0049   0.1570  -0.5191
 12ARG     HE  136   1.152    0.574    0.117  -0.8465  -0.5014  -1.6070
 12ARG     CZ  137   1.354    0.572    0.114   0.3018  -0.6898  -0.6778
 12ARG    NH1  138   1.371    0.681    0.191   0.9142  -0.7183  -0.8127
 12ARG   HH11  139   1.301    0.723    0.241   1.1708   0.5924  -1.5012
 12ARG   HH12  140   1.456    0.724    0.192   0.5828  -0.1070   0.6346
 12ARG    NH2  141   1.461    0.495    0.090   0.7031  -0.4764   0.2417
 12ARG   HH21  142   1.447    0.422    0.029  -3.6438  -0.6212   1.1275
 12ARG   HH22  143   1.545    0.510    0.135   1.6354  -2.7732  -0.6621
 12ARG      C  144   0.838    0.548    0.084  -0.2169   0.2858   0.1807
 12ARG      O  145   0.920    0.601    0.159   0.6124   0.1898  -0.6805
 12ARG      N  146   0.738    0.480    0.139   0.0024   0.8070   1.1729
 12ARG     H1  147   0.679    0.435    0.078  -0.6376   1.4902   1.2783
 12ARG     H2  148   0.740    0.476    0.235   1.0332  -1.0514   1.1397
```

University of Alberta

Table IX-12. Final coordinates for the structure of mastoparan in 50%TFE **A.** α-helical coordinates (structure 1), and **B.** β-strand coordinates (structure 2), following approximately 12 ps of restrained MD.

```
AVE COORDS 10-15PS   mastoparan, 50% TFE, tm=500ms, starting with alfa-helical coordinates
 133
   1ILE     H1    1  -0.463  -0.861   0.019  0.1279  0.0754  0.0936  0.2472  0.0593  0.0701  0.0610
   1ILE     H2    2  -0.465  -0.854  -0.022  0.1154  0.0428  0.0341  0.1613  0.0448 -0.0481  0.1422
   1ILE      N    3  -0.450  -0.922  -0.007  0.0063  0.0091 -0.0041  0.0045 -0.0062  0.0017  0.0053
   1ILE      H    4  -0.457  -0.839  -0.019  0.0606  0.0189  0.0127  0.0624  0.0408  0.0336  0.1004
   1ILE     CA    5  -0.317  -0.980  -0.029  0.0115  0.0040 -0.0045  0.0058 -0.0097  0.0113  0.0246
   1ILE     CB    6  -0.327  -1.062  -0.157  0.0145  0.0011 -0.0002  0.0005 -0.0028 -0.0033  0.0420
   1ILE    CG1    7  -0.207  -1.157  -0.163  0.0345  0.0041  0.0021  0.0019  0.0066  0.0017  0.0973
   1ILE    CG2    8  -0.330  -0.975  -0.281  0.0126  0.0060 -0.0004  0.0126  0.0036 -0.0139  0.0194
   1ILE     CD    9  -0.210  -1.266  -0.057  0.0499  0.0261  0.0049  0.0040  0.0068  0.0114  0.1196
   1ILE      C   10  -0.216  -0.867  -0.032  0.0109  0.0083 -0.0092  0.0107 -0.0102  0.0115  0.0137
   1ILE      O   11  -0.255  -0.754  -0.057  0.0086  0.0166 -0.0095  0.0057 -0.0019  0.0005  0.0037
   2ASN      N   12  -0.090  -0.897  -0.005  0.0286  0.0115 -0.0130  0.0151 -0.0258  0.0292  0.0592
   2ASN      H   13  -0.065  -0.987   0.009  0.0600  0.0130 -0.0148  0.0170 -0.0438  0.0493  0.1498
   2ASN     CA   14   0.020  -0.800   0.004  0.0240  0.0108 -0.0129  0.0156 -0.0222  0.0265  0.0455
   2ASN     CB   15   0.147  -0.878   0.033  0.0629  0.0164 -0.0155  0.0155 -0.0506  0.0480  0.1569
   2ASN     CG   16   0.175  -0.992  -0.063  0.0925  0.0043 -0.0007  0.0006 -0.0318  0.0066  0.2728
   2ASN    OD1   17   0.111  -1.097  -0.063  0.1240  0.0063 -0.0014  0.0011 -0.0343  0.0023  0.3648
   2ASN    ND2   18   0.274  -0.972  -0.148  0.1064  0.0019  0.0007  0.0032 -0.0055 -0.0312  0.3140
   2ASN   HD21   19   0.319  -0.889  -0.149  0.0748  0.0054 -0.0013  0.0033 -0.0078 -0.0208  0.2155
   2ASN   HD22   20   0.298  -1.041  -0.208  0.1540  0.0097 -0.0064  0.0179  0.0279 -0.0854  0.4345
   2ASN      C   21   0.039  -0.709  -0.116  0.0055  0.0015 -0.0003  0.0004 -0.0044  0.0011  0.0147
   2ASN      O   22   0.081  -0.594  -0.102  0.0023  0.0037 -0.0017  0.0012 -0.0022  0.0014  0.0021
   3LEU      N   23   0.002  -0.760  -0.232  0.0119  0.0011 -0.0031  0.0141  0.0043 -0.0166  0.0204
   3LEU      H   24  -0.030  -0.850  -0.239  0.0213  0.0025 -0.0028  0.0152  0.0046 -0.0262  0.0461
   3LEU     CA   25   0.002  -0.689  -0.360  0.0263  0.0125 -0.0275  0.0627  0.0065 -0.0146  0.0036
   3LEU     CB   26  -0.059  -0.778  -0.467  0.0485  0.0202 -0.0456  0.1125  0.0131 -0.0356  0.0128
   3LEU     CG   27   0.033  -0.890  -0.511  0.0851  0.0242 -0.0554  0.1619  0.0361 -0.1057  0.0691
   3LEU    CD1   28  -0.016  -0.942  -0.644  0.1499  0.0470 -0.1164  0.3161  0.0598 -0.1651  0.0867
   3LEU    CD2   29   0.031  -1.006  -0.414  0.0979  0.0303 -0.0295  0.0841  0.0523 -0.1202  0.1794
   3LEU      C   30  -0.078  -0.561  -0.351  0.0280  0.0130 -0.0220  0.0548 -0.0126  0.0293  0.0161
   3LEU      O   31  -0.041  -0.457  -0.404  0.0517  0.0325 -0.0422  0.0813 -0.0293  0.0577  0.0413
   4LYSH     N   32  -0.188  -0.571  -0.279  0.0248  0.0039 -0.0114  0.0384 -0.0105  0.0310  0.0320
   4LYSH     H   33  -0.206  -0.655  -0.238  0.0148  0.0019  0.0005  0.0241  0.0034  0.0151  0.0183
   4LYSH    CA   34  -0.287  -0.467  -0.250  0.0388  0.0114 -0.0114  0.0146 -0.0300  0.0313  0.0904
   4LYSH    CB   35  -0.417  -0.533  -0.207  0.0370  0.0013  0.0008  0.0022 -0.0087 -0.0038  0.1075
   4LYSH    CG   36  -0.478  -0.633  -0.306  0.0311  0.0034 -0.0026  0.0070 -0.0168  0.0125  0.0828
   4LYSH    CD   37  -0.615  -0.679  -0.261  0.0558  0.0029 -0.0009  0.0021  0.0002  0.0056  0.1623
   4LYSH    CE   38  -0.723  -0.600  -0.305  0.0688  0.0067  0.0283  0.1833 -0.0086 -0.0453  0.0163
   4LYSH    NZ   39  -0.737  -0.490  -0.234  0.0894  0.0407  0.0478  0.0613  0.0718  0.0914  0.1661
   4LYSH   HZ1   40  -0.671  -0.500  -0.274  0.1288  0.0361  0.0160  0.1273  0.0709 -0.0085  0.2228
   4LYSH   HZ2   41  -0.804  -0.440  -0.255  0.2443  0.0738  0.1437  0.2890  0.1575  0.3157  0.3702
   4LYSH   HZ3   42  -0.709  -0.476  -0.154  0.1269  0.2025  0.0640  0.0304  0.1359  0.0216  0.1479
   4LYSH     C   43  -0.231  -0.377  -0.140  0.0342  0.0010 -0.0008  0.0028 -0.0055  0.0122  0.0987
   4LYSH     O   44  -0.244  -0.256  -0.144  0.0594  0.0021 -0.0021  0.0027 -0.0148  0.0150  0.1734
   5ALA      N   45  -0.172  -0.440  -0.041  0.0169  0.0059 -0.0028  0.0025  0.0148 -0.0072  0.0422
   5ALA      H   46  -0.163  -0.535  -0.038  0.0142  0.0132 -0.0042  0.0025  0.0169 -0.0055  0.0268
   5ALA     CA   47  -0.111  -0.373   0.074  0.0271  0.0250 -0.0196  0.0162  0.0312 -0.0243  0.0403
   5ALA     CB   48  -0.056  -0.477   0.171  0.0330  0.0623 -0.0420  0.0291  0.0213 -0.0140  0.0075
   5ALA      C   49   0.001  -0.278   0.033  0.0207  0.0160 -0.0111  0.0079  0.0244 -0.0170  0.0383
   5ALA      O   50   0.019  -0.174   0.096  0.0361  0.0187 -0.0173  0.0193  0.0340 -0.0366  0.0701
   6LEU      N   51   0.072  -0.317  -0.072  0.0109  0.0087 -0.0021  0.0010  0.0136 -0.0035  0.0230
   6LEU      H   52   0.065  -0.405  -0.106  0.0070  0.0041 -0.0008  0.0005  0.0046 -0.0015  0.0162
   6LEU     CA   53   0.172  -0.234  -0.142  0.0099  0.0035  0.0013  0.0015  0.0089  0.0036  0.0248
   6LEU     CB   54   0.226  -0.318  -0.258  0.0119  0.0092  0.0095  0.0114  0.0109  0.0110  0.0153
   6LEU     CG   55   0.322  -0.426  -0.208  0.0049  0.0065  0.0039  0.0035  0.0050  0.0030  0.0047
   6LEU    CD1   56   0.458  -0.366  -0.173  0.0046  0.0076  0.0044  0.0027  0.0036  0.0019  0.0033
   6LEU    CD2   57   0.335  -0.531  -0.317  0.0089  0.0059  0.0039  0.0138  0.0044 -0.0029  0.0071
   6LEU      C   58   0.115  -0.102  -0.193  0.0118  0.0004  0.0006  0.0013  0.0024  0.0022  0.0337
```

University of Alberta

```
 6LEU     O    59   0.181   0.001  -0.187  0.0209  0.0047 -0.0031  0.0041 -0.0153  0.0115  0.0539
 7ALA     N    60  -0.008  -0.102  -0.242  0.0121  0.0014 -0.0009  0.0026  0.0026 -0.0072  0.0321
 7ALA     H    61  -0.058  -0.183  -0.254  0.0197  0.0058 -0.0042  0.0049  0.0058 -0.0098  0.0484
 7ALA    CA    62  -0.077   0.021  -0.280  0.0129  0.0010  0.0015  0.0051 -0.0048 -0.0118  0.0327
 7ALA    CB    63  -0.206  -0.013  -0.354  0.0135  0.0004  0.0005  0.0129 -0.0015 -0.0176  0.0271
 7ALA     C    64  -0.111   0.108  -0.159  0.0147  0.0062  0.0058  0.0066 -0.0131 -0.0143  0.0314
 7ALA     O    65  -0.100   0.230  -0.165  0.0224  0.0368  0.0118  0.0065 -0.0148 -0.0114  0.0239
 8ALA     N    66  -0.155   0.045  -0.051  0.0169  0.0041  0.0016  0.0093 -0.0022 -0.0183  0.0372
 8ALA     H    67  -0.172  -0.049  -0.052  0.0238  0.0178 -0.0047  0.0106  0.0116 -0.0209  0.0429
 8ALA    CA    68  -0.181   0.110   0.078  0.0192  0.0033  0.0038  0.0148 -0.0070 -0.0241  0.0395
 8ALA    CB    69  -0.231   0.008   0.178  0.0279  0.0120 -0.0087  0.0207  0.0139 -0.0317  0.0509
 8ALA     C    70  -0.055   0.177   0.133  0.0145  0.0062  0.0042  0.0031 -0.0134 -0.0098  0.0342
 8ALA     O    71  -0.060   0.287   0.186  0.0138  0.0072  0.0045  0.0032 -0.0138 -0.0094  0.0310
 9LEU     N    72   0.060   0.110   0.119  0.0140  0.0038  0.0017  0.0014 -0.0098 -0.0043  0.0369
 9LEU     H    73   0.060   0.021   0.084  0.0135  0.0050  0.0022  0.0021 -0.0089 -0.0040  0.0332
 9LEU    CA    74   0.191   0.167   0.151  0.0150  0.0027  0.0021  0.0017 -0.0078 -0.0065  0.0406
 9LEU    CB    75   0.299   0.062   0.121  0.0096  0.0008  0.0010  0.0020 -0.0016  0.0021  0.0261
 9LEU    CG    76   0.443   0.104   0.145  0.0326  0.0023 -0.0005  0.0027 -0.0067 -0.0077  0.0926
 9LEU   CD1    77   0.533  -0.001   0.083  0.0564  0.0045  0.0096  0.0241 -0.0189 -0.0334  0.1406
 9LEU   CD2    78   0.479   0.109   0.293  0.0424  0.0193  0.0046  0.0025 -0.0414 -0.0131  0.1054
 9LEU     C    79   0.219   0.294   0.072  0.0156  0.0065  0.0022  0.0030 -0.0152 -0.0052  0.0372
 9LEU     O    80   0.269   0.391   0.130  0.0192  0.0174 -0.0011  0.0028 -0.0232 -0.0009  0.0373
10ALA     N    81   0.182   0.298  -0.056  0.0171  0.0055  0.0045  0.0091 -0.0140 -0.0096  0.0367
10ALA     H    82   0.143   0.221  -0.097  0.0201  0.0071  0.0063  0.0099 -0.0169 -0.0127  0.0432
10ALA    CA    83   0.197   0.419  -0.138  0.0160  0.0047  0.0059  0.0139 -0.0110 -0.0089  0.0293
10ALA    CB    84   0.178   0.380  -0.285  0.0217  0.0037  0.0095  0.0286 -0.0058 -0.0187  0.0329
10ALA     C    85   0.101   0.532  -0.101  0.0113  0.0065  0.0050  0.0112 -0.0096 -0.0056  0.0161
10ALA     O    86   0.125   0.648  -0.135  0.0111  0.0115  0.0070  0.0136 -0.0024 -0.0032  0.0080
11LYSH    N    87  -0.010   0.496  -0.039  0.0134  0.0036  0.0033  0.0097 -0.0096 -0.0076  0.0270
11LYSH    H    88  -0.030   0.402  -0.034  0.0186  0.0019  0.0020  0.0099 -0.0076 -0.0094  0.0439
11LYSH   CA    89  -0.109   0.584   0.025  0.0095  0.0042  0.0022  0.0057 -0.0086 -0.0032  0.0186
11LYSH   CB    90  -0.238   0.503   0.039  0.0107  0.0063  0.0009  0.0016 -0.0097 -0.0042  0.0241
11LYSH   CG    91  -0.345   0.570   0.123  0.0150  0.0075 -0.0096  0.0152  0.0076 -0.0038  0.0222
11LYSH   CD    92  -0.418   0.471   0.211  0.0387  0.0429 -0.0493  0.0658 -0.0072  0.0051  0.0073
11LYSH   CE    93  -0.342   0.429   0.335  0.0643  0.1208 -0.0625  0.0548 -0.0370  0.0077  0.0173
11LYSH   NZ    94  -0.416   0.326   0.403  0.1174  0.2449 -0.1348  0.0764 -0.0435  0.0175  0.0309
11LYSH  HZ1    95  -0.496   0.358   0.436  0.1358  0.2556 -0.1713  0.1267  0.0418 -0.0242  0.0251
11LYSH  HZ2    96  -0.435   0.251   0.349  0.1297  0.2491 -0.1235  0.0731 -0.0660  0.0108  0.0670
11LYSH  HZ3    97  -0.362   0.308   0.477  0.1810  0.3910 -0.1765  0.0849 -0.1055  0.0537  0.0671
11LYSH    C    98  -0.065   0.641   0.160  0.0097  0.0052  0.0015  0.0057 -0.0081 -0.0029  0.0184
11LYSH    O    99  -0.091   0.756   0.192  0.0206  0.0218  0.0077  0.0083 -0.0247 -0.0072  0.0317
12LYSH    N   100  -0.005   0.554   0.240  0.0063  0.0013 -0.0006  0.0027  0.0025  0.0022  0.0150
12LYSH    H   101  -0.003   0.462   0.215  0.0101  0.0045 -0.0002  0.0020  0.0037  0.0031  0.0240
12LYSH   CA   102   0.061   0.581   0.368  0.0080  0.0020  0.0044  0.0141  0.0033  0.0102  0.0080
12LYSH   CB   103   0.130   0.452   0.408  0.0168  0.0011  0.0013  0.0169  0.0009  0.0220  0.0325
12LYSH   CG   104   0.228   0.463   0.523  0.0304  0.0074  0.0117  0.0653  0.0012  0.0308  0.0187
12LYSH   CD   105   0.285   0.328   0.562  0.0724  0.0059  0.0210  0.1114  0.0211  0.1047  0.0999
12LYSH   CE   106   0.418   0.330   0.635  0.0511  0.0154  0.0270  0.0807  0.0247  0.0672  0.0572
12LYSH   NZ   107   0.398   0.391   0.766  0.0680  0.0156  0.0429  0.1535  0.0231  0.0671  0.0347
12LYSH  HZ1   108   0.347   0.330   0.813  0.1017  0.0452  0.0682  0.1816  0.0512  0.1138  0.0782
12LYSH  HZ2   109   0.483   0.407   0.804  0.0923  0.0124  0.0480  0.2228  0.0170  0.0596  0.0418
12LYSH  HZ3   110   0.345   0.468   0.756  0.0613  0.0233  0.0382  0.1301  0.0200  0.0486  0.0304
12LYSH    C   111   0.156   0.701   0.361  0.0045  0.0021  0.0033  0.0097 -0.0014 -0.0039  0.0018
12LYSH    O   112   0.168   0.778   0.454  0.0240  0.0068  0.0017  0.0418 -0.0016 -0.0310  0.0233
13ILE     N   113   0.218   0.708   0.244  0.0024  0.0026 -0.0023  0.0028 -0.0006 -0.0002  0.0017
13ILE     H   114   0.207   0.634   0.186  0.0085  0.0083 -0.0074  0.0114  0.0047 -0.0077  0.0058
13ILE    CA   115   0.306   0.810   0.188  0.0166  0.0065 -0.0114  0.0205 -0.0110  0.0188  0.0227
13ILE    CB   116   0.317   0.765   0.044  0.0345  0.0123 -0.0269  0.0822 -0.0067  0.0248  0.0088
13ILE   CG1   117   0.417   0.651   0.038  0.0322  0.0174 -0.0330  0.0670  0.0113 -0.0170  0.0122
13ILE   CG2   118   0.351   0.876  -0.052  0.1026  0.0242 -0.0544  0.2076 -0.0268  0.1198  0.0759
```

University of Alberta

```
   13ILE     CD  119   0.552   0.668   0.104  0.0346  0.0190 -0.0232  0.0339 -0.0076 -0.0028  0.0509
   13ILE      C  120   0.252   0.949   0.212  0.0445  0.0119 -0.0116  0.0149 -0.0347  0.0309  0.1067
   13ILE      O  121   0.311   1.029   0.282  0.0662  0.0104 -0.0024  0.0075 -0.0425  0.0040  0.1806
   14LEU      N  122   0.135   0.974   0.154  0.0537  0.0138 -0.0176  0.0237 -0.0400  0.0494  0.1236
   14LEU      H  123   0.087   0.906   0.109  0.0342  0.0062 -0.0137  0.0312 -0.0192  0.0438  0.0651
   14LEU     CA  124   0.068   1.103   0.162  0.1108  0.0228 -0.0200  0.0219 -0.0802  0.0680  0.2879
   14LEU     CB  125  -0.033   1.129   0.052  0.1217  0.0148 -0.0330  0.0763 -0.0589  0.1377  0.2740
   14LEU     CG  126  -0.132   1.019   0.023  0.0513  0.0030 -0.0078  0.0426 -0.0118  0.0673  0.1082
   14LEU    CD1  127  -0.081   0.935  -0.091  0.0749  0.0346  0.0527  0.1077  0.0385  0.0880  0.0823
   14LEU    CD2  128  -0.266   1.079  -0.012  0.0358  0.0048 -0.0057  0.0330 -0.0168  0.0164  0.0695
   14LEU      C  129  -0.012   1.110   0.291  0.1165  0.0363  0.0160  0.0117 -0.1028 -0.0393  0.3017
   14LEU      O  130  -0.013   1.206   0.365  0.1964  0.0477  0.0399  0.0358 -0.1465 -0.1189  0.5057
   14LEU      N  131  -0.087   1.006   0.308  0.0541  0.0359  0.0267  0.0285 -0.0579 -0.0442  0.0977
   14LEU     H1  132  -0.074   0.927   0.262  0.0166  0.0228  0.0090  0.0104 -0.0185 -0.0058  0.0167
   14LEU     H2  133  -0.159   1.016   0.367  0.0908  0.0552  0.0725  0.1241 -0.0710 -0.1002  0.0932
AVE.COORDS 10-15PS   mastoparan, 50% TFA, tm=500ms, starting with beta-strand coordinates
 133
    1ILE     H1    1   0.292  -1.096  -0.100  0.0172  0.0133 -0.0091  0.0157 -0.0142  0.0181  0.0226
    1ILE     H2    2   0.324  -1.186  -0.014  0.0762  0.0231 -0.0065  0.0418 -0.0193 -0.0715  0.1638
    1ILE      N    3   0.365  -1.134  -0.057  0.0011  0.0017  0.0015  0.0014  0.0005  0.0005  0.0003
    1ILE      H    4   0.277  -1.099  -0.062  0.0092  0.0038  0.0078  0.0181 -0.0028 -0.0084  0.0057
    1ILE     CA    5   0.463  -1.040  -0.001  0.0029  0.0074  0.0014  0.0005 -0.0022 -0.0004  0.0007
    1ILE     CB    6   0.551  -0.996  -0.118  0.0023  0.0011  0.0017  0.0028 -0.0018 -0.0027  0.0029
    1ILE    CG1    7   0.681  -0.942  -0.058  0.0074  0.0015  0.0038  0.0107 -0.0035 -0.0103  0.0100
    1ILE    CG2    8   0.487  -0.886  -0.203  0.0040  0.0033 -0.0015  0.0054  0.0019  0.0026  0.0035
    1ILE     CD    9   0.779  -1.054  -0.024  0.0080  0.0015  0.0043  0.0121 -0.0036 -0.0102  0.0105
    1ILE      C   10   0.384  -0.928   0.066  0.0018  0.0046 -0.0008  0.0007  0.0004 -0.0002  0.0001
    1ILE      O   11   0.278  -0.888   0.018  0.0029  0.0042 -0.0002  0.0032 -0.0009 -0.0017  0.0012
    2ASN      N   12   0.442  -0.877   0.175  0.0014  0.0040 -0.0008  0.0001  0.0005 -0.0001  0.0001
    2ASN      H   13   0.526  -0.911   0.205  0.0044  0.0103  0.0020  0.0004 -0.0049 -0.0010  0.0025
    2ASN     CA   14   0.380  -0.766   0.248  0.0015  0.0012 -0.0010  0.0020  0.0004 -0.0015  0.0013
    2ASN     CB   15   0.435  -0.762   0.391  0.0009  0.0012  0.0001  0.0006  0.0011  0.0002  0.0010
    2ASN     CG   16   0.316  -0.758   0.486  0.0052  0.0008  0.0000  0.0131  0.0011  0.0003  0.0017
    2ASN    OD1   17   0.267  -0.863   0.527  0.0088  0.0016 -0.0009  0.0177  0.0016  0.0089  0.0071
    2ASN    ND2   18   0.270  -0.637   0.516  0.0116  0.0019  0.0066  0.0245 -0.0024 -0.0114  0.0085
    2ASN   HD21   19   0.298  -0.555   0.476  0.0120  0.0048  0.0106  0.0233 -0.0054 -0.0124  0.0078
    2ASN   HD22   20   0.200  -0.636   0.581  0.0161  0.0025 -0.0037  0.0215  0.0066 -0.0202  0.0244
    2ASN      C   21   0.388  -0.624   0.191  0.0012  0.0007  0.0007  0.0018 -0.0005 -0.0014  0.0012
    2ASN      O   22   0.315  -0.533   0.225  0.0046  0.0084  0.0058  0.0048  0.0018  0.0010  0.0005
    3LEU      N   23   0.481  -0.608   0.097  0.0018  0.0002  0.0003  0.0017  0.0006 -0.0008  0.0035
    3LEU      H   24   0.537  -0.681   0.069  0.0031  0.0013  0.0012  0.0025  0.0023  0.0005  0.0055
    3LEU     CA   25   0.504  -0.481   0.028  0.0021  0.0009  0.0008  0.0008 -0.0005 -0.0008  0.0046
    3LEU     CB   26   0.630  -0.499  -0.056  0.0025  0.0003  0.0000  0.0002  0.0005  0.0011  0.0070
    3LEU     CG   27   0.754  -0.483   0.031  0.0083  0.0019 -0.0027  0.0066 -0.0042  0.0104  0.0164
    3LEU    CD1   28   0.871  -0.442  -0.059  0.0098  0.0017 -0.0030  0.0087 -0.0034  0.0125  0.0189
    3LEU    CD2   29   0.792  -0.614   0.101  0.0147  0.0012  0.0018  0.0133  0.0026  0.0199  0.0297
    3LEU      C   30   0.387  -0.429  -0.056  0.0017  0.0005  0.0005  0.0005  0.0000 -0.0003  0.0041
    3LEU      O   31   0.373  -0.307  -0.063  0.0063  0.0026  0.0008  0.0002 -0.0046 -0.0013  0.0159
   4LYSH      N   32   0.303  -0.523  -0.099  0.0019  0.0001  0.0001  0.0002  0.0005  0.0011  0.0055
   4LYSH      H   33   0.317  -0.617  -0.089  0.0047  0.0001 -0.0002  0.0004 -0.0012  0.0024  0.0135
   4LYSH     CA   34   0.180  -0.491  -0.171  0.0012  0.0003  0.0000  0.0005  0.0009  0.0002  0.0029
   4LYSH     CB   35   0.116  -0.616  -0.232  0.0019  0.0024 -0.0010  0.0016  0.0019 -0.0004  0.0015
   4LYSH     CG   36   0.217  -0.690  -0.319  0.0014  0.0020  0.0008  0.0010  0.0009  0.0011  0.0012
   4LYSH     CD   37   0.142  -0.791  -0.405  0.0036  0.0058 -0.0025  0.0019  0.0034 -0.0005  0.0030
   4LYSH     CE   38   0.236  -0.868  -0.499  0.0097  0.0080 -0.0013  0.0162  0.0035 -0.0080  0.0050
   4LYSH     NZ   39   0.296  -0.783  -0.600  0.0233  0.0061 -0.0120  0.0601  0.0047 -0.0080  0.0036
   4LYSH    HZ1   40   0.376  -0.804  -0.633  0.0889  0.0455  0.0791  0.2067  0.0254  0.0402  0.0145
   4LYSH    HZ2   41   0.228  -0.805  -0.655  0.0090  0.0197  0.0030  0.0009  0.0011  0.0018  0.0064
   4LYSH    HZ3   42   0.363  -0.797  -0.548  0.0162  0.0050 -0.0063  0.0198  0.0094 -0.0204  0.0239
   4LYSH      C   43   0.077  -0.425  -0.080  0.0016  0.0025 -0.0007  0.0002  0.0012 -0.0006  0.0019
```

University of Alberta

University of Alberta

4LYSH	O	44	0.001	-0.336	-0.113	0.0073	0.0190	0.0058	0.0024	0.0008	0.0007	0.0004
5ALA	N	45	0.077	-0.471	0.045	0.0016	0.0006	-0.0007	0.0013	-0.0001	0.0013	0.0029
5ALA	H	46	0.131	-0.544	0.074	0.0064	0.0001	0.0009	0.0068	0.0006	0.0073	0.0124
5ALA	CA	47	-0.003	-0.413	0.153	0.0024	0.0040	-0.0026	0.0024	0.0007	0.0003	0.0009
5ALA	CB	48	0.007	-0.501	0.277	0.0064	0.0145	-0.0060	0.0035	-0.0001	0.0011	0.0011
5ALA	C	49	0.044	-0.271	0.186	0.0032	0.0068	-0.0028	0.0020	0.0006	0.0005	0.0008
5ALA	O	50	-0.037	-0.180	0.201	0.0068	0.0103	-0.0029	0.0011	0.0047	0.0002	0.0090
6LEU	N	51	0.176	-0.252	0.185	0.0038	0.0064	-0.0036	0.0038	-0.0027	0.0020	0.0013
6LEU	H	52	0.237	-0.325	0.176	0.0048	0.0049	-0.0029	0.0046	-0.0042	0.0043	0.0048
6LEU	CA	53	0.240	-0.121	0.195	0.0053	0.0101	-0.0050	0.0043	-0.0039	0.0020	0.0015
6LEU	CB	54	0.391	-0.142	0.191	0.0063	0.0092	-0.0051	0.0031	-0.0078	0.0043	0.0066
6LEU	CG	55	0.448	-0.209	0.315	0.0095	0.0139	-0.0076	0.0048	-0.0113	0.0067	0.0097
6LEU	CD1	56	0.443	-0.114	0.435	0.0104	0.0107	-0.0050	0.0103	-0.0105	0.0047	0.0102
6LEU	CD2	57	0.594	-0.247	0.287	0.0107	0.0128	-0.0082	0.0058	-0.0119	0.0087	0.0135
6LEU	C	58	0.193	-0.025	0.086	0.0026	0.0065	-0.0011	0.0003	0.0001	-0.0003	0.0009
6LEU	O	59	0.162	0.090	0.118	0.0060	0.0101	-0.0026	0.0008	0.0059	-0.0021	0.0072
7ALA	N	60	0.193	-0.075	-0.037	0.0013	0.0030	0.0010	0.0006	-0.0010	-0.0001	0.0005
7ALA	H	61	0.227	-0.163	-0.054	0.0012	0.0016	-0.0007	0.0003	0.0013	-0.0005	0.0017
7ALA	CA	62	0.144	-0.002	-0.154	0.0055	0.0028	0.0028	0.0099	0.0005	0.0057	0.0039
7ALA	CB	63	0.176	-0.082	-0.281	0.0124	0.0011	0.0050	0.0357	-0.0001	0.0023	0.0005
7ALA	C	64	-0.005	0.028	-0.149	0.0068	0.0036	0.0033	0.0076	0.0036	0.0084	0.0093
7ALA	O	65	-0.046	0.135	-0.193	0.0163	0.0042	0.0046	0.0122	0.0085	0.0198	0.0325
8ALA	N	66	-0.087	-0.062	-0.096	0.0034	0.0048	0.0021	0.0031	0.0017	0.0026	0.0022
8ALA	H	67	-0.057	-0.150	-0.073	0.0038	0.0079	0.0023	0.0024	-0.0029	-0.0009	0.0011
8ALA	CA	68	-0.231	-0.039	-0.073	0.0029	0.0053	0.0012	0.0007	0.0031	0.0013	0.0026
8ALA	CB	69	-0.292	-0.163	-0.005	0.0024	0.0042	0.0017	0.0007	0.0031	0.0013	0.0025
8ALA	C	70	-0.254	0.085	0.014	0.0039	0.0062	-0.0003	0.0001	0.0038	0.0004	0.0054
8ALA	O	71	-0.336	0.171	-0.018	0.0062	0.0051	-0.0003	0.0003	0.0021	-0.0018	0.0131
9LEU	N	72	-0.181	0.090	0.124	0.0042	0.0077	0.0018	0.0015	0.0046	0.0018	0.0032
9LEU	H	73	-0.124	0.016	0.146	0.0098	0.0203	0.0102	0.0068	0.0064	0.0038	0.0022
9LEU	CA	74	-0.176	0.200	0.222	0.0015	0.0001	-0.0001	0.0040	0.0000	0.0012	0.0004
9LEU	CB	75	-0.076	0.160	0.330	0.0054	0.0022	-0.0036	0.0093	-0.0028	0.0064	0.0046
9LEU	CG	76	-0.090	0.242	0.457	0.0100	0.0076	-0.0032	0.0210	-0.0033	0.0021	0.0014
9LEU	CD1	77	0.001	0.360	0.456	0.0493	0.1311	-0.0402	0.0158	-0.0057	0.0033	0.0009
9LEU	CD2	78	-0.062	0.156	0.577	0.0246	0.0262	-0.0116	0.0458	-0.0057	0.0081	0.0020
9LEU	C	79	-0.138	0.330	0.150	0.0017	0.0001	-0.0001	0.0042	0.0000	0.0018	0.0008
9LEU	O	80	-0.212	0.429	0.161	0.0036	0.0017	0.0037	0.0086	0.0007	0.0018	0.0004
10ALA	N	81	-0.031	0.326	0.073	0.0020	0.0006	0.0003	0.0039	0.0006	0.0021	0.0014
10ALA	H	82	0.019	0.244	0.067	0.0031	0.0021	0.0009	0.0039	0.0020	0.0031	0.0033
10ALA	CA	83	0.023	0.435	-0.009	0.0009	0.0005	0.0006	0.0017	0.0005	0.0006	0.0005
10ALA	CB	84	0.148	0.387	-0.084	0.0012	0.0009	0.0012	0.0017	0.0006	0.0008	0.0010
10ALA	C	85	-0.075	0.491	-0.113	0.0011	0.0016	0.0008	0.0018	0.0002	0.0003	0.0001
10ALA	O	86	-0.074	0.609	-0.147	0.0019	0.0038	0.0022	0.0017	0.0001	0.0002	0.0000
11LYSH	N	87	-0.160	0.406	-0.170	0.0012	0.0011	0.0003	0.0022	0.0006	0.0006	0.0004
11LYSH	H	88	-0.150	0.311	-0.158	0.0015	0.0007	0.0001	0.0025	0.0003	0.0018	0.0014
11LYSH	CA	89	-0.271	0.448	-0.256	0.0006	0.0010	0.0001	0.0004	0.0005	0.0003	0.0004
11LYSH	CB	90	-0.297	0.336	-0.357	0.0021	0.0008	-0.0006	0.0011	-0.0005	-0.0013	0.0045
11LYSH	CG	91	-0.191	0.344	-0.466	0.0058	0.0129	-0.0013	0.0017	0.0040	-0.0021	0.0030
11LYSH	CD	92	-0.211	0.254	-0.587	0.0127	0.0269	0.0099	0.0050	-0.0080	-0.0052	0.0062
11LYSH	CE	93	-0.195	0.104	-0.567	0.0032	0.0035	0.0013	0.0026	-0.0005	-0.0029	0.0034
11LYSH	NZ	94	-0.325	0.043	-0.574	0.0344	0.0003	0.0006	0.0079	0.0045	-0.0078	0.0950
11LYSH	HZ1	95	-0.373	0.083	-0.502	0.0523	0.0231	0.0040	0.0088	0.0528	0.0030	0.1251
11LYSH	HZ2	96	-0.371	0.058	-0.655	0.0607	0.0099	0.0064	0.0115	-0.0393	-0.0190	0.1608
11LYSH	HZ3	97	-0.312	-0.050	-0.556	0.0328	0.0034	-0.0041	0.0065	0.0116	-0.0049	0.0886
11LYSH	C	98	-0.401	0.488	-0.188	0.0011	0.0011	0.0010	0.0014	0.0008	0.0011	0.0009
11LYSH	O	99	-0.477	0.568	-0.243	0.0050	0.0043	0.0047	0.0065	0.0024	0.0046	0.0042
12LYSH	N	100	-0.425	0.436	-0.067	0.0002	0.0002	-0.0002	0.0002	0.0000	0.0001	0.0001
12LYSH	H	101	-0.372	0.364	-0.033	0.0006	0.0003	0.0006	0.0012	-0.0002	-0.0002	0.0003
12LYSH	CA	102	-0.532	0.474	0.026	0.0004	0.0001	-0.0002	0.0009	0.0001	0.0001	0.0002
12LYSH	CB	103	-0.520	0.384	0.148	0.0018	0.0009	0.0010	0.0028	0.0012	0.0019	0.0017

```
12LYSH    CG  104  -0.619   0.413   0.259  0.0026  0.0048  0.0001  0.0005  0.0033 -0.0002  0.0023
12LYSH    CD  105  -0.558   0.511   0.358  0.0060  0.0117  0.0072  0.0052 -0.0035 -0.0019  0.0011
12LYSH    CE  106  -0.468   0.448   0.462  0.0339  0.0556  0.0300  0.0209 -0.0261 -0.0063  0.0252
12LYSH    NZ  107  -0.406   0.544   0.552  0.0292  0.0362  0.0358  0.0467 -0.0124 -0.0097  0.0048
12LYSH   HZ1  108  -0.479   0.577   0.595  0.0391  0.0192  0.0210  0.0908  0.0114  0.0180  0.0072
12LYSH   HZ2  109  -0.345   0.509   0.613  0.0683  0.1377  0.0560  0.0402 -0.0586 -0.0178  0.0270
12LYSH   HZ3  110  -0.368   0.608   0.500  0.0490  0.0147  0.0182  0.0956 -0.0215 -0.0462  0.0367
12LYSH     C  111  -0.525   0.623   0.060  0.0010  0.0017 -0.0005  0.0011  0.0003 -0.0005  0.0002
12LYSH     O  112  -0.627   0.688   0.078  0.0019  0.0019  0.0005  0.0017 -0.0003  0.0017  0.0020
13ILE      N  113  -0.399   0.668   0.064  0.0018  0.0027 -0.0018  0.0016  0.0011 -0.0012  0.0011
13ILE      H  114  -0.328   0.603   0.054  0.0016  0.0027 -0.0019  0.0014  0.0008 -0.0004  0.0008
13ILE     CA  115  -0.349   0.804   0.082  0.0043  0.0067 -0.0044  0.0031  0.0038 -0.0030  0.0030
13ILE     CB  116  -0.205   0.797   0.034  0.0022  0.0036 -0.0017  0.0010 -0.0025  0.0014  0.0021
13ILE    CG1  117  -0.120   0.727   0.139  0.0138  0.0215 -0.0106  0.0054 -0.0177  0.0087  0.0146
13ILE    CG2  118  -0.143   0.931  -0.005  0.0070  0.0047 -0.0002  0.0024  0.0029  0.0053  0.0139
13ILE     CD  119  -0.123   0.773   0.283  0.0377  0.0974 -0.0165  0.0035 -0.0326  0.0046  0.0121
13ILE      C  120  -0.436   0.900  -0.001  0.0047  0.0080 -0.0028  0.0030  0.0049 -0.0025  0.0033
13ILE      O  121  -0.496   0.995   0.051  0.0075  0.0127  0.0022  0.0064  0.0035 -0.0032  0.0033
14LEU      N  122  -0.445   0.874  -0.131  0.0032  0.0015 -0.0025  0.0043  0.0023 -0.0038  0.0037
14LEU      H  123  -0.398   0.797  -0.164  0.0053  0.0015 -0.0031  0.0065  0.0032 -0.0071  0.0079
14LEU     CA  124  -0.522   0.952  -0.228  0.0039  0.0002 -0.0004  0.0018  0.0008 -0.0042  0.0096
14LEU     CB  125  -0.468   0.939  -0.370  0.0073  0.0102  0.0092  0.0090 -0.0028 -0.0014  0.0026
14LEU     CG  126  -0.428   0.800  -0.418  0.0056  0.0009  0.0011  0.0092 -0.0017 -0.0074  0.0068
14LEU    CD1  127  -0.277   0.782  -0.400  0.0060  0.0006  0.0006  0.0018 -0.0012 -0.0051  0.0156
14LEU    CD2  128  -0.468   0.788  -0.565  0.0139  0.0149 -0.0044  0.0190 -0.0042 -0.0096  0.0078
14LEU      C  129  -0.666   0.904  -0.230  0.0117  0.0006 -0.0006  0.0019 -0.0020 -0.0036  0.0325
14LEU      O  130  -0.761   0.980  -0.218  0.0348  0.0010 -0.0011  0.0013 -0.0007 -0.0011  0.1022
14LEU      N  131  -0.668   0.774  -0.256  0.0031  0.0008 -0.0003  0.0010 -0.0023  0.0015  0.0075
14LEU     H1  132  -0.587   0.728  -0.235  0.0077  0.0018 -0.0013  0.0023 -0.0054  0.0057  0.0189
14LEU     H2  133  -0.747   0.736  -0.293  0.0006  0.0002  0.0002  0.0010  0.0003  0.0000  0.0007
```

University of Alberta

Table IX-13. Comparison of the distances between proton pairs given in the NOE-derived distance restraint file (rijU, rijL) for the TnI peptide in 50%TFE with those actually measured between the same proton pairs in the final structures generated from the α-helix (rijα) and the β-strand (rijβ).

---

spin system	rijα(Å)	rijβ(Å)	rijU(Å)	rijL(Å)
K105αCH-βCH2	2.29		3.8	3.2
K105αCH-γCH2	3.74	3.85	5.9	4.3
K105βCH2-γCH2	2.21	2.22	3.9	3.3
K105NH-βCH2	2.65	2.38	4.3	3.1
K105γCH2-δCH2	2.30	2.38	3.9	3.3
K105NH-γCH2	3.24	3.56	5.7	3.7
F106αCH-βCH(m)	2.28	2.40	3.9	3.3
F106αCH-βCH'(x)	2.84	2.38	4.0	3.4
F106αCH-δCH2	3.11	3.48	7.4	4.4
F106βCH(m)-βCH'(x)	1.63	1.63	2.5	2.1
F106NH-βCH(m)	3.56	3.59	4.7	3.7
F106βCH2-δCH2	1.85	1.90	4.0	3.4
F106NH-βCH'(x)	2.78	2.66	4.1	3.5
F106NH-δCH2	2.87	2.88	7.4	4.0
K107αCH-βCH2	2.50	2.65	3.5	2.9
K107αCH-γCH2	3.46	2.85	5.3	3.7
K107βCH2-γCH2	2.12	2.24	3.8	3.2
K107NH-βCH2	2.89	2.41	4.5	3.3
K107γCH2-δCH2	2.34	2.33	3.4	2.8
K107NH-γCH2	3.32	4.09	5.6	3.6
K107NH-δCH2	3.56	3.48	4.1	3.5
R108αCH-δCH2	3.44	4.55	7.0	4.0
R108βCH2-δCH2	3.55	3.04	6.2	4.2
R108NH-βCH2	2.72	2.96	4.3	3.1
R108γCH2-δCH2	2.14	2.29	4.1	3.5
R108NH-γCH2	3.20	3.31	5.0	3.4
R108NH-δCH2	4.60	3.63	6.5	4.5
P109αCH-βCH(x)	2.95	2.87	3.5	2.9
P109αCH-βCH'(p)	2.44	2.39	3.5	2.9
P109αCH-δCH(m)	3.65	3.76	3.8	3.2
P109αCH-δCH'(m')	3.70	3.85	3.6	3.0
P109βCH(x)-βCH'(p)	1.63	1.63	2.8	2.4
P109βCH(x)-δCH(m)	2.81	3.16	3.7	3.1
P109βCH(x)-δCH'(m')	3.76	3.91	4.0	3.4
P109βCH(x)-γCH2	2.48	2.41	4.0	3.4

P109βCH'(p)-δCH(m)	4.01	4.28	6.9	4.9
P109βCH'(p)-δCH'(m')	3.71	3.07	5.3	4.3
P109βCH'(p)-γCH2	2.30	2.33	4.5	3.5
P109γCH2-δCH2	2.25	2.27	3.9	3.3
P109δCH(m)-δCH'(m')	1.63	1.63	2.9	2.5
P110αCH-βCH(x)	2.90	2.86	3.9	3.3
P110αCH-βCH'(p)	2.30	2.28	3.8	3.2
P110βCH(x)-βCH'(p)	1.63	1.63	2.6	2.2
P110βCH(x)-δCH(m)	2.73	2.68	3.3	2.7
P110βCH(x)-δCH'(m')	3.66	3.62	3.3	2.7
P110βCH'(p)-δCH(m)	3.96	3.91	5.4	4.4
P110βCH'(p)-δCH'(m')	3.69	3.64	5.2	4.2
P110δCH(m)-δCH'(m')	1.63	1.63	2.8	2.4
L111αCH-βCH2	2.57	2.52	3.4	2.8
L111αCH-(δCH3)2	3.94	3.40	6.5	3.8
L111γCH-(δCH3)2	1.87	1.84	3.6	3.0
L111NH-βCH2	2.66	2.81	4.1	2.9
L111NH-(δCH3)2	3.45	4.35	4.7	3.7
R112αCH-δCH2	4.24	3.72	7.0	4.0
R112βCH2-δCH2	2.81	3.36	4.1	3.5
R112NH-βCH2	2.61	3.08	4.3	3.1
R112γCH2-δCH2	2.27	2.22	3.7	3.1
R112NH-γCH2	3.07	3.25	5.0	3.4
R112NH-δCH2	4.73	4.92	7.2	5.2
R113αCH-δCH2	4.55	4.55	7.0	4.0
R113βCH2-δCH2	2.93	2.98	4.1	3.5
R113NH-βCH2	2.20	2.27	4.3	3.1
R113γCH2-δCH2	2.29	2.28	3.7	3.1
R113NH-γCH2	4.15	4.31	5.0	3.4
R113NH-δCH2	4.76	5.12	4.6	3.6
V114αCH-βCH	2.82	2.86	4.0	3.4
V114αCH-(γCH3)2	2.57	2.47	5.2	3.6
V114βCH-(γCH3)2	1.84	1.87	3.6	3.0
V114NH-βCH	2.97	2.45	4.0	3.4
V114NH-(γCH3)2	3.13	3.24	5.9	3.6
R115αCH-βCH2	2.61	2.62	4.4	3.2
R115αCH-δCH2	3.18	4.48	6.2	4.2
R115βCH2-δCH2	3.21	3.16	4.8	3.8
R115NH-βCH2	2.58	2.38	4.3	3.1
R115γCH2-δCH2	2.15	2.19	3.7	3.1
R115NH-γCH2	2.95	4.07	4.8	3.2
R115NH-δCH2	4.72	5.47	6.8	4.8
C-term NH-NH'	1.55	1.73	2.9	2.5
N-Ac CH3-G104 NH	2.75	2.90	5.2	4.2
F106βCH2-K107NH	3.76	3.72	6.3	4.3

K105γCH2-F106NH	4.65	3.85	6.4	4.4
K107γCH2-R108NH	5.42	4.69	6.1	4.1
R108βCH2-P109αCH	4.15	4.38	4.8	3.2
P109αCH-P110βCH(x)	5.41	5.43	4.0	3.4
P109αCH-P110δCH(m)	3.67	3.71	3.8	3.2
P109αCH-P110δCH'(m')	3.63	3.66	3.7	3.1
P110βCH(x)-L111NH	2.90	4.39	4.7	3.7
P110βCH'(p)-L111NH	4.11	4.50	5.4	4.4
L111(δCH3)2-R112NH	4.97	4.15	7.3	3.9
R113βCH2-V114NH	3.00	2.96	5.2	3.6
R113γCH2-V114NH	3.90	4.46	4.9	3.3
R113NH-V114βCH	5.19	4.14	4.8	3.8
R113NH-V114(γCH3)2	5.60	5.29	7.4	4.0
F106βCH'(x)-K107δCH2	4.34	4.78	5.7	3.7
R108βCH2-P109δCH(m)	3.42	4.27	5.5	3.5
P109βCH(x)-P110δCH(m)	3.19	3.07	4.6	3.6
P109βCH(x)-P110δCH(m')	4.36	4.28	6.1	4.1
P109βCH'(p)-P110δCH(m)	4.40	4.22	4.8	3.8
P109βCH'(p)-P110δCH'(m')	5.18	5.07	5.1	4.1
K105NH-F106NH	3.27	3.15	3.9	3.3
K107NH-R108NH	3.10	3.75	3.6	3.0
R112NH-Cterm NH	5.05	4.41	5.3	4.3
R112NH-Cterm NH'	5.56	5.59	5.3	4.3
R113NH-V114NH	2.52	2.26	3.6	3.0
G104αCH2-NH	2.48	2.25	4.5	3.5
G104αCH2-K105NH	2.89	3.03	3.8	3.1
K105αCH-NH	2.71	2.65	4.6	3.6
K105αCH-F106NH	2.42	3.11	4.0	3.4
F106αCH-NH	2.75	2.75	4.9	3.9
F106αCH-K107NH	2.65	3.39	4.1	3.5
F106NH-K107αCH	4.87	5.12	4.0	3.4
K107αCH-NH	2.74	2.64	3.7	3.1
K107αCH-R108NH	2.59	2.10	3.3	2.7
R108αCH-NH	2.76	2.68	6.3	4.3
P110αCH-L111NH	3.59	2.57	4.1	3.5
L111αCH-NH	2.67	2.77	4.7	3.7
R112αCH-NH	2.74	2.67	3.7	3.1
R113αCH-NH	2.78	2.74	3.7	3.1
R113αCH-V114NH	3.45	3.32	3.6	3.0
V114αCH-NH	2.61	2.79	4.6	3.6
V114αCH-R113NH	4.87	5.00	3.6	3.0
V114αCH-R115NH	2.74	2.14	3.7	3.1
R115αCH-NH	2.69	2.64	3.4	2.8

Table IX-14. Comparison of the distances between proton pairs given in the NOE-derived distance restraint file (rijU, rijL) for mastoparan in 50%TFE with those actually measured between the same proton pairs in the final structures generated from the α-helix (rijα) and the β-strand (rijβ).

spin system	rijα(Å)	rijβ(Å)	rijU(Å)	rijL(Å)
I1βCH-(γCH3')	2.34	2.36	2.5	2.1
I1βCH-γCH'(p)	2.46	2.56	2.0	1.8
I1γCH'(p)-γCH(t)	1.63	1.63	2.5	2.1
I1γCH'(p)-(γCH3')	2.81	2.70	2.6	2.2
I1γCH'(p)-(δCH3)	2.36	2.38	2.6	2.2
N2βCH'(m)-βCH(x)	1.63	1.63	2.5	2.1
N2CONH2	1.64	1.65	2.3	1.9
N2CONH2-βCH'(m)	2.65	2.91	3.1	2.7
N2CONH2-βCH(x)	3.54	3.62	3.1	2.7
L3NH-αCH	2.64	2.71	3.0	2.6
L3NH-βCH2	2.75	2.66	3.3	2.3
L3NH-γCH	3.18	3.33	3.1	2.7
L3NH-(δCH3)2	3.27	3.45	3.4	2.8
L3αCH-βCH2	2.57	2.62	2.3	1.9
L3αCH-(δCH3)2	3.70	3.64	5.0	2.7
L3βCH2-(δCH3)2	2.52	2.54	2.8	2.4
L3γCH-(δCH3)2	1.85	1.85	3.0	2.6
K4NH-αCH	2.77	2.65	3.0	2.6
K4NH-βCH2	2.83	2.89	3.3	2.3
K4NH-γCH2	2.73	2.42	4.1	2.7
K4αCH-βCH2	2.48	2.54	2.8	2.4
K4βCH2-γCH2	2.37	2.38	2.7	2.3
K4βCH2-δCH2	2.84	2.45	3.0	2.6
K4γCH2-ξCH2	3.09	3.02	4.0	3.4
K4δCH2-ξCH2	2.12	2.26	3.8	3.2
K4γCH2-δCH2	2.27	2.38	2.7	2.3
A5NH-αCH	2.66	2.68	2.9	2.5
A5NH-βCH3	2.61	2.61	3.5	2.5
A5αCH-βCH3	2.40	2.40	2.7	2.3
L6NH-αCH	2.65	2.67	3.9	3.3
L6NH-βCH2	2.71	2.75	3.2	2.2
L6NH-γCH	2.31	2.26	2.9	2.5
L6NH-(δCH3)2	3.83	3.85	2.9	2.5
L6αCH-βCH2	2.60	2.56	2.3	1.9
L6αCH-(δCH3)2	3.49	3.46	5.0	2.7
L6βCH2-(δCH3)2	2.56	2.54	2.8	2.2

L6γCH-(δCH3)2	1.83	1.85	3.0	2.6
A7NH-αCH	2.70	2.69	2.8	2.4
A7NH-βCH3	2.66	2.66	3.3	2.3
A7αCH-βCH3	2.42	2.43	2.5	2.1
A8NH-αCH	2.66	2.65	2.4	2.0
A8NH-βCH3	2.64	2.65	3.4	2.4
A8αCH-βCH3	2.39	2.42	2.5	2.1
L9NH-αCH	2.68	2.70	2.7	2.3
L9NH-βCH2	2.27	2.23	3.6	2.6
L9NH-γCH	4.32	4.15	5.0	4.0
L9NH-(δCH3)2	4.71	4.70	5.0	4.0
L9αCH-βCH2	2.52	2.55	3.8	3.2
L9αCH-(δCH3)2	3.64	3.70	5.0	2.7
L9βCH2-(δCH3)2	2.52	2.54	2.8	2.4
L9γCH-(δCH3)2	1.86	1.82	3.0	2.6
A10NH-αCH	2.74	2.63	3.0	2.6
A10NH-βCH3	2.68	2.64	3.5	2.5
A10αCH-βCH3	2.44	2.45	2.6	2.2
K11NH-αCH	2.76	2.76	2.9	2.5
K11NH-βCH2	2.27	2.73	2.7	2.3
K11NH-γCH2	4.26	3.11	3.3	2.7
K11αCH-βCH2	2.52	2.64	2.4	2.0
K11βCH2-γCH2	2.33	2.37	2.7	2.3
K11βCH2-δCH2	2.90	3.08	2.8	2.4
K11γCH2-ξCH2	2.99	3.20	4.0	3.4
K11δCH2-ξCH2	2.37	2.31	3.8	3.2
K11γCH2-δCH2	2.23	2.20	2.7	2.3
K12NH-αCH	2.64	2.67	2.8	2.4
K12NH-βCH2	2.15	2.16	3.3	2.3
K12NH-γCH2	4.17	4.22	4.1	2.7
K12αCH-βCH2	2.47	2.50	2.6	2.2
K12βCH2-γCH2	2.35	2.26	2.7	2.3
K12βCH2-δCH2	2.50	3.17	3.0	2.6
K12γCH2-ξCH2	3.11	2.26	4.0	3.4
K12δCH2-ξCH2	2.23	2.36	3.8	3.2
K12γCH2-δCH2	2.35	2.26	2.7	2.3
I13NH-αCH	2.66	2.63	3.0	2.6
I13NH-βCH	2.01	2.13	2.7	2.3
I13NH-γCH'(p)	2.07	2.01	2.7	2.3
I13NH-γCH(t)	3.34	3.35	3.4	2.8
I13NH-(γCH3')	4.02	4.14	4.1	2.7
I13NH-(δCH3)	3.83	3.77	3.6	3.0
I13αCH-βCH	2.88	2.86	3.1	2.7
I13αCH-γCH'(p)	2.88	2.92	3.4	2.8
I13αCH-γCH(t)	3.46	3.50	3.1	2.7
I13αCH-(γCH3')	3.19	3.20	4.0	2.8

I13αCH-(δCH3)	2.61	2.73	4.5	2.9
I13βCH-(γCH3')	2.29	2.33	2.5	2.1
I13βCH-(δCH3)	3.75	3.77	2.9	2.5
I13βCH-γCH'(p)	2.29	2.29	2.0	1.8
I13βCH-γCH(t)	2.42	2.43	2.8	2.4
I13γCH'(p)-γCH(t)	1.63	1.63	2.5	2.1
I13γCH'(p)-(δCH3)	2.34	2.34	2.5	2.1
I13γCH(t)-(γCH3')	2.79	2.77	2.8	2.4
I13γCH(t)-(δCH3)	2.34	2.34	2.8	2.4
L14NH-αCH	2.71	2.77	3.4	2.8
L14NH-βCH2	3.10	3.12	3.4	2.4
L14NH-γCH	2.36	2.26	3.0	2.6
L14NH-(δCH3)2	3.39	3.37	3.0	2.6
L14αCH-βCH2	2.22	2.23	3.0	2.6
L14αCH-(δCH3)2	4.30	4.31	5.1	2.8
L14βCH2-(δCH3)2	2.48	2.47	2.8	2.4
L14γCH-(δCH3)2	1.84	1.84	3.0	2.6
L14 Cterm NH2	1.62	1.70	2.2	1.8
I1(δCH3)-L3NH	5.18	4.84	4.6	3.0
L3(δCH3)2-K4NH	4.93	5.46	6.5	3.5
L6(δCH3)2-A5NH	6.22	6.22	6.6	3.6
L6(δCH3)2-A7NH	5.45	5.24	6.2	3.2
L9(δCH3)2-A10NH	5.07	4.66	5.8	2.8
I13(γCH3')-K11NH	6.33	6.65	5.6	3.6
A5βCH3-N2CONH	6.32	3.38	4.5	2.9
A5βCH3-N2CONH'	7.55	3.56	4.5	2.9
K11αCH-L14 Cterm NH	4.00	4.05	3.8	3.2
K11αCH-L14 Cterm NH'	5.36	5.49	3.8	3.2
K12αCH-L14 Cterm NH	3.70	3.47	4.2	3.6
K12αCH-L14 Cterm NH'	4.42	4.10	4.2	3.6
K12γCH-L14 Cterm NH	5.95	6.08	4.4	2.8
K12γCH-L14 Cterm NH'	6.69	6.59	4.4	2.8
I13αCH-L14 Cterm NH	4.84	4.86	4.8	3.8
I13αCH-L14 Cterm NH'	6.05	6.21	4.8	3.8
L14αCH-L14 Cterm NH	3.42	3.29	3.9	3.3
L14αCH-L14 Cterm NH'	4.00	4.00	3.9	3.3
L14βCH2-L14 Cterm NH	3.50	3.32	3.0	2.6
L14βCH2-L14 Cterm NH'	4.01	3.94	3.0	2.6
L14(δCH3)2-L14 Cterm NH	3.58	3.52	3.7	3.1
L14(δCH3)2-L14 Cterm NH'	4.38	4.41	3.7	3.1
N2βCH2-A5βCH3	4.45	5.48	5.9	3.3
N2αCH-L3βCH2	5.77	5.68	4.1	2.7

N2αCH-L3(δCH3)2	6.61	6.56	5.3	2.5
N2αCH-K4βCH2	5.40	5.37	4.7	3.1
N2αCH-A5βCH3	2.67	3.93	4.3	2.7
K11αCH-I13(γCH3')	5.35	5.23	4.0	3.4
K11αCH-I13(δCH3)	7.17	6.69	8.3	5.3
K12γCH2-L14αCH	7.70	8.16	4.3	2.7

K4γCH2-L3NH	4.81	4.69	4.3	2.7
L3βCH2-K4NH	2.92	3.32	4.1	2.7
A5βCH3-K4NH	4.85	5.09	4.3	2.7
K4βCH2-A5NH	3.03	3.18	4.0	2.6
L6βCH2-A5NH	5.17	5.16	4.4	2.8
A8βCH3-A5NH	5.78	5.66	4.6	3.0
A5βCH3-L6NH	3.31	3.28	3.9	2.5
L6βCH2-A7NH	3.04	2.83	3.8	2.4
A7βCH3-A8NH	3.25	3.40	4.0	2.6
A8βCH3-L9NH	3.25	3.06	4.1	2.7
A10βCH3-L9NH	5.45	5.29	5.5	3.5
A8βCH3-A10NH	5.40	5.45	5.1	3.5
L9βCH2-A10NH	3.23	2.91	4.1	2.7
L9γCH-A10NH	3.72	4.46	4.5	3.5
L9βCH2-K11NH	5.21	5.31	5.5	3.5
L9γCH-K11NH	5.45	6.22	6.0	4.0
K11βCH2-A10NH	4.12	4.08	3.7	2.3
K11γCH2-A10NH	5.32	5.10	4.3	2.7
A10βCH3-K11NH	3.50	3.37	4.1	2.7
K11βCH2-K12NH	2.69	2.48	3.9	2.5
I13βCH-K12NH	4.10	4.15	3.1	2.7
K12βCH2-I13NH	3.16	3.18	4.4	2.8
K12γCH2-I13NH	3.84	4.55	4.4	2.8
I13γCH'(p)-L14NH	4.41	4.27	3.5	2.9
K12γCH2-K14NH	6.10	6.50	4.3	2.7
I13γCH(t)-K12NH	5.43	5.27	5.1	4.1
I13γCH(t)-L14NH	4.73	4.66	4.9	3.9

L3αCH-K4NH	3.35	3.42	3.8	3.2
K4αCH-A5NH	3.49	3.46	3.5	2.9
L6αCH-A7NH	3.51	3.46	3.6	3.0
A7αCH-L6NH	5.34	5.26	3.3	2.7
A7αCH-A8NH	3.49	3.52	3.8	3.2
A7αCH-L9NH	4.32	4.39	4.5	3.5
A7αCH-A10NH	3.25	3.20	3.7	3.1
A8αCH-A7NH	5.17	5.29	3.6	3.0
A8αCH-L9NH	3.50	3.45	3.6	3.0
A8αCH-K11NH	3.28	3.56	3.7	3.1
L9αCH-A10NH	3.49	3.48	3.5	2.9

L9αCH-K12NH	3.33	3.49	3.7	3.1
A10αCH-K11NH	3.34	3.49	3.6	3.0
K11αCH-K12NH	3.41	3.40	3.3	2.7
K11αCH-I13NH	3.95	3.68	4.5	3.5
K11αCH-L14NH	3.49	3.36	3.4	2.8
K12αCH-K11NH	5.12	5.13	3.3	2.7
K12αCH-I13NH	3.31	3.34	3.3	2.7
K12αCH-L14NH	4.53	4.30	4.8	3.8
I13αCH-K12NH	5.33	5.15	3.9	3.3
I13αCH-L14NH	3.44	3.46	3.6	3.0
L3NH-K4NH	2.63	2.79	3.1	2.7
L3NH-L6NH	4.74	4.78	4.2	3.6
L3NH-A5NH	3.97	4.29	4.2	3.6
K4NH-L6NH	3.92	4.03	3.4	2.8
K4NH-A5NH	2.37	2.58	2.9	2.5
A5NH-L6NH	2.71	2.64	2.9	2.5
A5NH-A7NH	4.26	4.13	4.0	3.4
L6NH-A7NH	2.94	2.82	3.1	2.7
A7NH-A8NH	2.68	2.85	2.9	2.5
A7NH-L9NH	4.12	4.42	4.2	3.6
A8NH-L9NH	2.78	2.83	3.1	2.7
A8NH-A10NH	4.17	4.25	4.1	3.5
L9NH-A10NH	2.82	2.81	3.1	2.7
L9NH-K11NH	4.09	4.24	4.8	3.8
A10NH-K11NH	2.58	2.90	3.3	2.7
A10NH-K12NH	4.20	4.22	4.2	3.6
K11NH-K12NH	2.58	2.60	3.0	2.6
K11NH-I13NH	3.98	4.02	4.6	3.6
K12NH-I13NH	2.73	2.58	3.0	2.6
K12NH-L14NH	4.65	4.53	4.6	3.6
I13NH-L14NH	3.07	3.00	3.1	2.7
I13NH-L14 Cterm NH	4.13	4.08	3.6	3.0
I13NH-L14 Cterm NH	5.59	5.60	3.6	3.0
L14NH-L14 Cterm NH	3.73	3.77	3.1	2.7
L14NH-L14 Cterm NH	3.73	3.77	3.1	2.7

Table X-1. Table of TRNOE intensities versus mixing time (τm = 75, 150, and 500 ms) measured at 0.1 molar equivalents TnC.Ca(II)$_4$ to TnI peptide.

spin system	measured intensities			normalized intensities		
tmix (ms)	500	150	75	500	150	75
K105αCH-βCH2	4.06	1.46	0.50	2.03	0.73	0.25
K105αCH-γCH2	2.14	1.52	-	1.07	0.76	-
K105βCH2-γCH2	2.38	0.64	0.10	0.30	0.08	0.03
K105γCH2-δCH2	2.38	0.64	0.10	0.30	0.08	0.03
K105βCH2-NH	2.22	1.66	0.54	1.11	0.83	0.27
K105γCH2-ξCH2	0.66	0.20	-	0.17	0.05	-
K105γCH2-NH	0.14	0.06	-	0.07	0.03	-
F106αCH-βCH(m)	0.66	0.36	0.12	0.66	0.36	0.12
F106αCH-βCH'(x)	0.92	1.20	1.08	0.92	1.20	1.08
F106αCH-δCH2	1.32	0.58	0.26	0.66	0.29	0.13
F106βCH(m)-βCH'(x)	4.84	12.96	5.46	4.84	12.96	5.46
F106βCH(m)-NH	0.72	0.74	0.40	0.72	0.74	0.40
F106βCH(m)-δCH2	2.78	1.78	0.86	1.39	0.89	0.43
F106βCH(m)-ξCH2	0.32	-	-	0.11	-	-
F106βCH(m)-ςCH	0.32	-	-	0.11	-	-
F106βCH'(x)-NH	0.94	1.06	0.66	0.94	1.06	0.66
F106βCH'(x)-δCH2	2.86	2.20	1.02	1.43	1.10	0.51
F106βCH'(x)-ξCH2	0.94	0.18	0.10	0.31	0.06	0.03
F106βCH'(x)-ςCH	0.94	0.18	0.10	0.31	0.06	0.03
F106NH-δCH2	0.42	0.18	0.30	0.21	0.09	0.15
K107αCH-βCH2	4.00	2.00	1.00	2.00	1.00	0.50
K107αCH-γCH2	1.94	0.94	0.72	0.97	0.47	0.36
K107βCH2-γCH2	3.24	2.06	1.58	0.81	0.52	0.40
K107βCH2-NH	0.88	0.96	0.18	0.44	0.48	0.09
K107δCH2-γCH2	4.94	3.82	4.94	1.24	0.96	1.24
K107δCH2-NH	0.82	0.98	0.08	0.41	0.49	0.04
K107γCH2-ξCH2	1.90	0.88	0.36	0.48	0.22	0.09
K107γCH2-NH	0.38	0.28	0.54	0.19	0.14	0.27
R108αCH-βCH2	2.04	0.62	0.82	1.02	0.31	0.41
R108αCH-γCH2	1.74	0.46	0.48	0.87	0.23	0.24
R108αCH-δCH2	0.26	-	-	0.13	-	-
R108βCH2-γCH2	10.00	7.40	3.60	1.25	0.93	0.45
R108γCH2-δCH2	10.00	7.40	3.60	1.25	0.93	0.45
R108βCH2-NH	4.92	6.78	4.04	2.46	3.39	2.02
R108δCH2-NH	0.22	-	-	0.11	-	-

P109αCH-βCH(x)	1.96	0.26	-	1.96	0.26	-
P109αCH-βCH'(p)	0.38	0.94	0.56	0.38	0.94	0.56
P109αCH-γCH2	3.38	0.62	-	1.69	0.31	-
P109βCH(x)-βCH'(p)	13.34	12.32	8.78	13.34	12.32	8.78
P109βCH(x)-δCH(m)	2.50	0.88	0.42	2.50	0.88	0.42
P109βCH(x)-δCH'(m')	1.54	0.18	-	1.54	0.18	-
P109βCH(x)-γCH2	8.36	8.72	10.60	4.18	4.36	5.30
P109βCH'(p)-δCH(m)	1.40	1.34	-	1.50	1.34	-
P109βCH'(p)-δCH'(m')	0.36	0.04	-	0.36	0.04	-
P109βCH'(p)-γCH2	6.52	6.34	3.46	3.26	3.17	1.73
P109γCH2-δCH(m)	4.86	3.64	0.96	2.43	1.82	0.48
P109γCH2-δCH'(m')	4.22	2.86	1.14	2.11	1.43	0.57
P109δCH(m)-δCH'(m')	2.92	10.38	9.24	2.92	10.38	9.24
P110αCH-βCH(x)	3.62	1.40	0.64	3.62	1.40	0.64
P110αCH-βCH'(p)	3.54	3.64	1.80	3.54	3.64	1.80
P110αCH-γCH2	2.58	1.10	0.94	1.29	0.55	0.47
P110βCH(x)-βCH'(p)	13.34	16.82	11.36	13.34	16.82	11.36
P110βCH(x)-δCH(m)	2.50	2.94	1.90	2.50	2.94	1.90
P110βCH(x)-δCH'(m')	1.92	0.84	0.18	1.92	0.84	0.18
P110βCH(x)-γCH2	8.36	8.72	10.60	4.18	4.36	5.30
P110βCH'(p)-δCH(m)	13.22	0.20	-	13.22	0.20	-
P110βCH'(p)-δCH'(m')	1.10	0.32	0.06	1.10	0.32	0.06
P110βCH'(p)-γCH2	8.26	8.94	3.92	4.13	4.47	1.96
P110γCH2-δCH(m)	4.86	2.94	2.38	2.43	1.47	1.19
P110γCH2-δCH'(m')	5.24	4.16	3.26	2.62	2.08	1.63
P110δCH(m)-δCH'(m')	3.14	9.74	7.72	3.14	9.74	7.72
L111αCH-βCH2	9.60	3.20	1.54	4.80	1.60	0.77
L111αCH-(δCH3)2	4.52	2.46	1.16	0.75	0.41	0.19
L111βCH2-(δCH3)2	9.50	7.70	3.30	0.79	0.64	0.28
L111γCH-(δCH3)2	14.38	10.60	1.00	2.40	1.77	0.17
L111βCH2-NH	5.24	4.42	2.50	2.62	2.21	1.25
L111(δCH3)2-NH	1.08	0.60	0.20	0.18	0.10	0.03
R112αCH-βCH2	10.10	6.14	3.32	5.05	3.07	1.66
R112αCH-δCH2	1.34	1.14	-	0.67	0.57	-
R112βCH2-γCH2	11.20	7.40	3.60	1.40	0.93	0.45
R112γCH2-δCH2	11.20	7.40	3.60	1.40	0.93	0.45
R112βCH2-NH	3.90	3.60	1.76	1.95	1.80	0.88
R112δCH2-NH	0.22	-	-	0.11	-	-
R113αCH-βCH2	13.24	9.16	6.32	6.62	4.58	3.16
R113αCH-δCH2	1.34	1.14	-	0.67	0.57	-
R113βCH2-γCH2	10.00	7.40	3.60	1.25	0.93	0.45
R113γCH2-δCH2	10.00	7.40	3.60	1.25	0.93	0.45
R113βCH2-NH	2.98	3.60	2.34	1.49	1.80	1.17

R113δCH2-NH	0.32	-	-	0.16	-	-
V114αCH-βCH	3.56	2.44	1.10	3.56	2.44	1.10
V114αCH-(γCH3)2	7.06	4.78	1.90	1.18	0.80	0.32
V114βCH-(γCH3)2	14.38	10.28	4.50	2.40	1.71	0.75
V114βCH-NH	2.78	2.64	1.40	2.78	2.64	1.40
V114(γCH3)2-NH	2.40	1.20	0.40	0.40	0.20	0.07
R115αCH-βCH2	10.00	5.88	4.00	5.00	2.94	2.00
R115αCH-δCH2	1.60	0.60	-	0.80	0.30	-
R115βCH2-γCH2	10.00	7.40	3.60	1.25	0.93	0.45
R115γCH2-δCH2	10.00	7.40	3.60	1.25	0.93	0.45
R115βCH2-NH	2.02	2.14	1.44	1.01	1.07	0.72
C-term NH-NH'	5.00	7.74	5.58	5.00	7.74	5.58

G104NH-K105γCH2	-	-	0.22	-	-	0.11
K105βCH2-F106NH	0.76	0.16	-	0.38	0.08	-
K105γCH2-F106NH	0.04	-	-	0.02	-	-
K105γCH2-R108NH	-	-	1.22	-	-	0.61
F106βCH(m)-K107NH	0.42	0.28	-	0.42	0.28	-
F106βCH'(x)-K107NH	0.56	0.44	-	0.56	0.44	-
F106δCH2-K107NH	0.40	0.04	-	0.20	0.02	-
K107γCH2-R108NH	0.32	0.28	-	0.17	0.14	-
R108αCH-P109γCH2	1.44	0.62	-	0.72	0.31	-
R108αCH-P109δCH(m)	1.96	1.82	1.58	1.96	1.82	1.58
R108αCH-P109δCH'(m')	1.68	2.56	1.42	1.68	2.56	1.42
R108NH-P109βCH(x)	0.66	0.70	0.60	0.66	0.70	0.60
R108NH-P109βCH'(p)	0.40	0.24	-	0.40	0.24	-
R108NH-P109γCH2	0.46	0.36	-	0.23	0.18	-
R108NH-P109δCH(m)	0.28	-	-	0.28	-	-
P109αCH-P110δCH(m)	1.74	1.02	1.46	1.74	1.02	1.46
P109αCH-P110δCH'(m')	2.10	1.56	1.32	2.10	1.56	1.32
P110αCH-R112βCH2	2.14	0.28	-	1.07	0.14	-
P110βCH(x)-L111NH	1.30	0.86	0.62	1.30	0.86	0.62
P110βCH(x)-R112αCH	1.84	1.04	-	1.84	1.04	-
P110βCH'(p)-L111αCH	0.46	0.30	-	0.46	0.30	-
P110βCH'(p)-L111NH	1.10	0.94	0.54	1.10	0.94	0.54
P110βCH'(p)-R112αCH	1.96	1.02	0.66	1.96	1.02	0.66
P110βCH'(p)-R112NH	0.40	0.22	-	0.40	0.22	-
P110γCH2-L111αCH	1.44	-	-	0.72	-	-
P110γCH2-L111NH	0.60	0.38	-	0.30	0.19	-
P110γCH2-R112αCH	1.46	0.50	-	0.73	0.25	-
P110γCH2-R112NH	0.46	0.14	-	0.23	0.07	-
L111(δCH3)2-R112αCH	2.74	0.46	-	0.46	0.08	-
L111(δCH3)2-R112NH	0.74	-	-	0.12	-	-

R112βCH2-R113NH	1.84	1.10	0.26	0.92	0.55	0.13
R112βCH2-R115NH	0.82	0.66	0.20	0.41	0.33	0.10
R112βCH2-Cterm NH'	0.06	-	-	0.03	-	-
R113αCH-V114βCH	0.92	0.30	-	0.92	0.30	-
R113βCH2-V114αCH	1.50	0.26	-	0.75	0.13	-
R113βCH2-V114NH	1.06	0.84	1.16	0.53	0.42	0.58
R113δCH2-V114NH	0.24	-	-	0.12	-	-
R113NH-V114(γCH3)2	0.34	-	-	0.06	-	-
V114αCH-Cterm NH	0.42	-	-	0.42	-	-
V114αCH-Cterm NH'	0.24	-	-	0.24	-	-
V114βCH-R115NH	0.66	0.56	0.22	0.66	0.56	0.22
V114(γCH3)2-R115NH	1.24	0.32	0.08	0.21	0.05	0.01
V114NH-R115βCH2	1.06	0.84	1.16	0.53	0.42	0.29
R115αCH-Cterm NH	0.90	0.64	-	0.90	0.64	-
R115αCH-Cterm NH'	1.86	1.56	1.04	1.86	1.56	1.04
R115βCH2-Cterm NH	0.84	0.18	0.08	0.42	0.09	0.04
R115βCH2-Cterm NH'	0.54	0.32	0.08	0.27	0.16	0.04

F106δCH2-K105βCH2	0.52	0.42	0.14	0.13	0.11	0.04
F106δCH2-K105γCH2	0.10	0.10	-	0.03	0.03	-
F106δCH2-K107βCH2	0.48	0.46	0.18	0.12	0.12	0.05
F106δCH2-R108βCH2	0.48	-	-	0.12	-	-
F106δCH2-P109βCH(x)	0.20	0.14	-	0.10	0.07	-
F106δCH2-P109βCH'(p)	0.28	-	-	0.14	-	-
F106δCH2-P109γCH2	0.32	0.26	-	0.08	0.07	-
F106δCH2-L111βCH2	0.52	0.34	-	0.13	0.09	-
F106δCH2-L111(δCH3)2	0.50	-	-	0.04	-	-
F106δCH2-V114(γCH3)2	0.76	-	-	0.07	-	-
F106ξCH2-K105βCH2	0.24	-	-	0.04	-	-
F106ξCH2-K105γCH2	0.14	-	-	0.02	-	-
F106ξCH2-K107βCH2	0.50	-	-	0.08	-	-
F106ξCH2-R108βCH2	0.50	0.08	0.06	0.08	0.01	0.01
F106ξCH2-R108γCH2	0.64	0.22	0.12	0.11	0.04	0.02
F106ξCH2-P109βCH(x)	0.24	0.08	-	0.08	0.03	-
F106ξCH2-P109βCH'(p)	0.60	0.28	-	0.20	0.09	-
F106ξCH2-P109γCH2	0.24	0.70	-	0.04	0.12	-
F106ξCH2-L111βCH2	0.24	-	-	0.04	-	-
F106ξCH2-L111(δCH3)2	0.82	-	-	0.05	-	-
F106ξCH2-V114(γCH3)2	0.82	2.08	-	0.05	0.12	-
F106ςCH-K105βCH2	0.24	-	-	0.04	-	-
F106ςCH-K105γCH2	0.14	-	-	0.02	-	-
F106ςCH-K107βCH2	0.50	-	-	0.08	-	-
F106ςCH-R108βCH2	0.50	0.08	0.06	0.08	0.01	0.01

F106ςCH-R108γCH2	0.64	0.22	0.12	0.11	0.04	0.02
F106ςCH-P109βCH(x)	0.24	0.08	-	0.08	0.03	-
F106ςCH-P109βCH'(p)	0.60	0.28	-	0.20	0.09	-
F106ςCH-P109γCH2	0.24	0.70	-	0.04	0.12	-
F106ςCH-L111βCH2	0.24	-	-	0.04	-	-
F106ςCH-L111(δCH3)2	0.82	-	-	0.05	-	-
F106ςCH-V114(γCH3)2	0.82	2.08	-	0.05	0.12	-
K107ξCH2-R108δCH2	1.10	-	2.36	0.28	-	0.59
R108βCH2-P109δCH(m)	1.66	0.98	0.14	0.83	0.49	0.07
R108βCH2-P109δCH'(m')	1.14	0.26	-	0.57	0.13	-
P109δCH'(m')-V114βCH	2.08	1.04	-	2.08	1.04	-
P110βCH(x)-L111(δCH3)2	0.92	0.70	-	0.15	0.12	-
P110γCH2-L111(δCH3)2	2.64	2.12	-	0.22	0.18	-
L111(δCH3)2-R112δCH2	0.56	-	-	0.05	-	-
R112βCH2-V114(γCH3)2	3.58	2.88	-	0.30	0.24	-
V114(γCH3)2-R115βCH2	3.58	2.88	-	0.30	0.24	-
P109βCH'(p)-P110δCH(m)	0.38	0.76	-	0.38	0.76	-
P109βCH'(p)-P110δCH'(m')	0.62	0.58	0.54	0.62	0.58	0.54
P109γCH2-P110δCH(m)	0.96	-	-	0.48	-	-
P109γCH2-P110δCH'(m')	0.34	-	-	0.17	-	-
P110βCH(x)-P109δCH'(m')	0.54	0.62	0.12	0.54	0.62	0.12
P110βCH'(p)-P109δCH(m)	0.30	0.42	-	0.30	0.42	-
P110βCH'(p)-P109δCH'(m')	0.20	-	-	0.20	-	-
P110γCH2-P109δCH(m)	1.42	1.62	0.74	0.71	0.81	0.37
P110γCH2-P109δCH'(m')	1.06	0.60	1.02	0.53	0.30	0.51
K105αCH-F106αCH	0.30	0.52	-	0.30	0.52	-
K105αCH-V114αCH	0.84	0.74	-	0.84	0.74	-
F106αCH-K107αCH	0.16	0.22	-	0.16	0.22	-
F106αCH-R108αCH	-	0.32	0.92	-	0.32	0.92
F106αCH-P109αCH	0.10	-	-	0.10	-	-
K107αCH-R108αCH	0.24	0.20	1.08	0.24	0.20	1.08
R108αCH-P109αCH	0.12	0.04	-	0.12	0.04	-
R108αCH-P110αCH	0.10	0.12	1.02	0.10	0.12	1.02
P109αCH-P110αCH	0.04	-	-	0.04	-	-
P110αCH-L111αCH	0.54	0.60	1.52	0.54	0.60	1.52
R113αCH-V114αCH	0.74	0.54	0.50	0.74	0.54	0.50
V114αCH-R115αCH	1.22	1.18	2.92	1.22	1.18	2.92
G104NH-K105NH	0.68	-	-	0.68	-	-
K105NH-F106NH	0.64	1.22	-	0.64	1.22	-

K105NH-K107NH	0.18	0.46	-	0.18	0.46	-
K105NH-R112NH	0.66	2.00	-	0.66	2.00	-
F106NH-K107NH	0.38	0.64	-	0.38	0.64	-
K107NH-R108NH	0.16	0.16	-	0.16	0.16	-
R112NH-R113NH	0.60	3.30	-	0.60	3.30	-
R112NH-R115NH	0.14	-	-	0.14	-	-
R113NH-V114NH	0.30	1.00	-	0.30	1.00	-
V114NH-R115NH	0.24	0.54	-	0.24	0.54	-
R115NH-Cterm NH'	0.16	0.12	0.22	0.16	0.12	0.22
G104αCH2-NH	1.52	0.72	0.54	0.76	0.36	0.27
G104αCH2-K105NH	1.56	1.34	0.80	0.78	0.67	0.40
G104αCH2-F106NH	0.20	0.06	0.14	0.10	0.03	0.07
G104αCH2-R108NH	0.16	-	-	0.08	-	-
K105αCH-NH	0.92	0.66	0.40	0.92	0.66	0.40
K105αCH-F106NH	2.04	2.02	1.12	2.04	2.02	1.12
K105αCH-R108NH	0.42	0.34	0.28	0.42	0.34	0.28
F106αCH-NH	0.46	0.38	0.32	0.46	0.38	0.32
F106αCH-K107NH	1.40	1.74	1.18	1.40	1.74	1.18
K107αCH-NH	1.04	1.04	0.54	1.04	1.04	0.54
K107αCH-R108NH	2.64	4.10	2.50	2.64	4.10	2.50
R108αCH-NH	0.42	0.44	0.16	0.42	0.44	0.16
P110αCH-L111NH	2.04	3.44	2.58	2.04	3.44	2.58
P110αCH-R112NH	0.42	0.38	0.14	0.42	0.38	0.14
L111αCH-NH	2.50	1.56	1.68	2.50	1.56	1.68
L111αCH-R112NH	2.64	4.10	2.50	2.64	4.10	2.50
R112αCH-NH	3.62	3.56	2.66	3.62	3.56	2.66
R112αCH-R113NH	1.82	2.52	1.74	1.82	2.52	1.74
R112αCH-R115NH	0.70	0.32	-	0.70	0.32	-
R113αCH-NH	1.82	2.52	1.74	1.82	2.52	1.74
R113αCH-V114NH	3.62	4.50	2.92	3.62	4.50	2.92
V114αCH-NH	0.42	0.56	0.68	0.42	0.56	0.68
V114αCH-R113NH	0.92	0.20	0.28	0.92	0.20	0.28
V114αCH-R115NH	4.78	5.08	3.44	4.78	5.08	3.44
R115αCH-NH	0.80	1.56	0.68	0.80	1.56	0.68

Table X-2. Table of TRNOE intensities versus mixing time (τm = 150 and 500 ms) measured at 0.2 molar equivalents TnC.Ca(II)$_4$ to TnI peptide.

spin system	measured intensities		normalized intensities	
tmix (ms)	500	150	500	150
K105αCH-βCH2	8.96	14.53	4.48	7.26
K105αCH-γCH2	5.28	6.08	2.64	3.04
K105αCH-ξCH2	1.38	-	0.69	-
K105βCH2-γCH2	21.66	33.28	2.71	4.16
K105δCH2-γCH2	21.66	33.28	2.71	4.16
K105δCH2-ξCH2	9.89	8.54	4.95	2.14
K105βCH2-NH	3.87	8.61	1.94	4.31
K105γCH2-ξCH2	4.74	4.16	1.19	1.04
K105γCH2-NH	1.54	2.18	0.77	1.09
K105ξCH2-NH	0.42	-	0.21	-
F106αCH-βCH(m)	1.09	2.43	1.09	2.43
F106αCH-βCH'(x)	2.78	3.33	2.78	3.33
F106αCH-δCH2	0.93	2.05	0.47	1.03
F106αCH-ξCH2	0.77	0.45	0.26	0.15
F106αCH-ςCH	0.77	0.45	0.26	0.15
F106βCH(m)-βCH'(x)	3.68	10.18	3.68	10.18
F106βCH(m)-δCH2	3.94	6.43	1.97	3.22
F106βCH(m)-ξCH2	3.23	3.74	1.08	1.25
F106βCH(m)-ςCH	3.23	3.74	1.08	1.25
F106βCH'(x)-δCH2	4.16	6.53	2.08	3.27
F106βCH'(x)-ξCH2	3.55	-	1.18	-
F106βCH'(x)-ςCH	3.55	-	1.18	-
F106βCH(m)-NH	0.77	2.66	0.77	2.66
F106βCH'(x)-NH	0.70	2.21	0.70	2.21
F106NH-δCH2	1.70	1.82	0.85	0.91
F106NH-ξCH2	0.90	0.90	0.30	0.30
F106NH-ςCH	0.90	0.90	0.30	0.30
K107αCH-βCH2	7.74	14.08	3.87	7.04
K107αCH-γCH2	3.97	7.30	1.99	3.65
K107αCH-ξCH2	1.41	1.60	0.70	0.80
K107βCH2-γCH2	29.82	55.04	3.73	6.88
K107δCH2-γCH2	29.82	55.04	3.73	6.88
K107δCH2-ξCH2	12.93	18.62	3.23	9.31
K107βCH2-NH	3.01	7.84	1.50	3.92

K107γCH2-ξCH2	5.06	8.06	1.27	2.01
K107γCH2-NH	1.38	2.27	0.69	1.14
K107ξCH2-NH	0.29	-	0.15	-
R108αCH-βCH2	4.45	8.35	2.23	4.18
R108αCH-δCH2	1.82	2.72	0.91	1.36
R108βCH2-γCH2	10.88	19.84	1.36	2.48
R108γCH2-δCH2	10.88	19.84	1.36	2.48
R108βCH2-NH	2.69	8.86	1.35	4.43
R108δCH2-NH	0.80	1.31	0.40	0.66
P109αCH-βCH(x)	-	2.66	-	2.66
P109αCH-βCH'(p)	-	1.54	-	1.54
P109αCH-γCH2	-	2.59	-	1.30
P109βCH(x)-βCH'(p)	4.29	18.85	4.29	18.85
P109βCH(x)-δCH(m)	1.47	4.58	1.47	4.58
P109βCH(x)-δCH'(m')	0.83	3.94	0.83	3.94
P109βCH(x)-γCH2	10.18	12.51	5.09	6.26
P109βCH'(p)-δCH(m)	0.35	2.11	0.35	2.11
P109βCH'(p)-δCH'(m')	0.32	2.72	0.32	2.72
P109βCH'(p)-γCH2	11.74	13.98	5.87	6.99
P109γCH2-δCH(m)	1.60	7.20	0.80	3.60
P109γCH2-δCH'(m')	1.15	3.55	0.58	1.78
P109δCH(m)-δCH'(m')	1.60	4.77	1.60	4.77
P110αCH-βCH(x)	1.66	6.18	1.66	6.18
P110αCH-βCH'(p)	1.09	5.57	1.09	5.57
P110αCH-γCH2	2.27	5.57	1.14	2.79
P110βCH(x)-βCH'(p)	9.44	13.12	9.44	13.12
P110βCH(x)-δCH(m)	1.47	4.58	1.47	4.58
P110βCH(x)-δCH'(m')	0.83	4.00	0.83	4.00
P110βCH(x)-γCH2	10.18	12.51	5.09	6.25
P110βCH'(p)-δCH(m)	0.35	1.50	0.35	1.50
P110βCH'(p)-δCH'(m')	0.32	2.85	0.32	2.85
P110βCH'(p)-γCH2	5.31	21.54	2.66	10.77
P110γCH2-δCH(m)	1.60	7.20	0.80	3.60
P110γCH2-δCH'(m')	1.15	6.85	0.58	3.43
P110δCH(m)-δCH'(m')	1.60	4.22	1.60	4.22
L111αCH-βCH2	7.74	14.08	3.87	7.04
L111αCH-(δCH3)2	7.65	15.01	0.64	2.50
L111βCH2-(δCH3)2	28.13	44.80	3.52	2.49
L111γCH-(δCH3)2	28.13	44.80	3.52	2.49
L111βCH2-NH	4.96	8.80	2.48	4.40
L111(δCH3)2-NH	2.40	4.00	0.40	0.67
R112αCH-βCH2	5.82	13.95	2.91	6.98
R112αCH-δCH2	1.82	2.72	0.91	1.36

R112βCH2-δCH2	10.88	19.84	1.36	2.48
R112γCH2-δCH2	10.88	19.84	1.36	2.48
R112βCH2-NH	2.69	7.26	1.35	3.36
R112δCH2-NH	0.80	1.31	0.40	0.66
R113αCH-βCH2	5.82	13.95	2.91	6.98
R113αCH-δCH2	1.82	2.72	0.91	1.36
R113βCH2-δCH2	10.88	19.84	1.36	2.48
R113γCH2-δCH2	10.88	19.84	1.36	2.48
R113βCH2-NH	1.86	5.18	0.93	2.59
R113δCH2-NH	0.80	1.31	0.40	0.66
V114αCH-βCH	3.10	8.70	3.10	8.70
V114αCH-(γCH3)2	9.18	18.14	1.53	3.02
V114βCH-(γCH3)2	15.62	26.75	2.60	4.46
V114βCH-NH	2.82	3.81	2.82	3.81
V114(γCH3)2-NH	2.40	4.00	0.40	0.67
R115αCH-βCH2	7.74	14.08	3.87	7.04
R115αCH-δCH2	1.82	2.72	0.91	1.36
R115βCH2-δCH2	10.88	19.84	1.36	2.48
R115γCH2-δCH2	10.88	19.84	1.36	2.48
R115βCH2-NH	1.82	5.41	0.91	2.70
R115δCH2-NH	0.80	1.31	0.40	0.66
C-term NH-NH'	1.47	9.86	1.47	9.86

NAcCH3-G104αCH2	3.55	3.55	0.59	0.59
NAcCH3-G104NH	2.82	3.81	0.94	1.27
NAcCH3-K105NH	1.41	2.69	0.47	0.90
G104NH-K105γCH2	0.80	-	0.40	-
G104NH-K107γCH2	0.93	-	0.47	-
G104αCH2-F106δCH2	0.93	0.54	0.23	0.14
G104αCH2-F106ξCH2	0.90	0.80	0.15	0.13
G104αCH2-F106ςCH	0.90	0.80	0.15	0.13
G104αCH2-K105γCH2	1.44	-	0.36	-
G104αCH2-K105βCH2	8.19	3.26	1.03	0.41
G104αCH2-K105δCH2	8.19	3.26	1.03	0.41
K105NH-F106δCH2	-	0.70	-	-
K105NH-F106βCH(m)	-	0.45	-	-
K105NH-K107γCH2	0.80	1.15	0.40	0.57
K105NH-L111(δCH3)2	1.92	2.53	0.16	0.21
K105NH-V114(γCH3)2	1.92	2.53	0.16	0.21
K105αCH-F106δCH2	1.12	-	0.66	-
K105αCH-F106βCH2(mx)	2.94	-	1.47	-
K105αCH-K107γCH2	2.98	-	1.46	-
K105βCH2-F106NH	3.17	4.64	1.59	2.32

K105γCH2-F106NH	1.02	1.31	0.51	0.65
K105γCH2-K107αCH	2.11	-	1.06	-
F106NH-K107γCH2	0.90	1.18	0.45	0.59
F106NH-P109βCH(x)	0.64	-	0.64	-
F106NH-P109γCH2	0.86	1.06	0.43	0.27
F106NH-V114βCH	0.86	1.06	0.86	0.53
F106NH-L111(δCH3)2	2.05	1.44	0.17	0.12
F106NH-V114(γCH3)2	2.05	1.44	0.17	0.12
F106αCH-R108βCH2	4.42	-	2.21	-
F106βCH(m)-K107NH	0.29	1.66	0.29	1.66
F106βCH(m)-V114αCH	0.74	0.86	0.74	0.86
F106βCH'(x)-K107NH	0.29	1.38	0.29	1.38
F106βCH'(x)-V114αCH	0.99	1.06	0.99	1.06
F106δCH2-K107αCH	1.12	-	0.56	-
F106δCH2-K107NH	0.86	1.50	0.43	0.75
F106δCH2-R108NH	1.89	0.42	0.95	0.21
F106δCH2-V114αCH	0.38	0.64	0.19	0.32
F106ξCH2-K107NH	0.42	0.99	0.14	0.33
F106ξCH2-R108NH	1.44	0.38	0.48	0.13
F106ξCH2-V114αCH	0.83	1.15	0.31	0.38
F106ςCH-K107NH	0.42	0.99	0.14	0.33
F106ςCH-R108NH	1.44	0.38	0.48	0.13
F106ςCH-V114αCH	0.83	1.15	0.31	0.38
K107NH-R108βCH2	0.80	-	0.40	-
K107NH-V114βCH	0.58	-	0.58	-
K107NH-L111(δCH3)2	1.47	1.09	0.13	0.09
K107NH-V114(γCH3)2	1.47	1.09	0.13	0.09
K107γCH2-R108NH	1.18	1.82	0.59	0.91
K107ξCH2-R108NH	0.29	0.45	0.15	0.23
R108NH-P109βCH(x)	1.15	3.01	1.15	3.01
R108NH-P109βCH'(p)	0.51	0.83	0.51	0.83
R108NH-P109γCH2	1.22	1.57	0.61	0.79
R108αCH-P109γCH2	0.99	2.98	0.45	1.49
R108αCH-P109δCH(m)	0.35	1.60	0.35	1.60
R108αCH-P109δCH'(m')	1.50	2.66	1.50	2.66
P109αCH-P110δCH(m)	-	0.90	-	0.90
P109αCH-P110δCH'(m')	0.99	1.31	0.99	1.31
P109βCH(x)-V114αCH	3.04	4.03	3.04	4.03
P109βCH'(p)-V114αCH	2.37	6.46	2.37	6.46
P110αCH-L111(δCH3)2	2.91	3.46	0.49	0.58
P110αCH-L111βCH2	1.70	4.99	0.85	2.50
P110βCH(x)-L111αCH	3.10	3.01	3.10	3.01
P110βCH(x)-L111NH	2.43	3.36	2.43	3.36

P110βCH'(p)-L111αCH	1.41	1.14	1.41	1.14
P110βCH'(p)-L111NH	0.93	2.27	0.93	2.27
P110γCH2-L111αCH	4.45	4.19	2.23	2.08
P110γCH2-R112NH	2.14	-	1.07	-
L111(δCH3)2-R112NH	2.02	4.48	0.34	0.75
R112αCH-L111(δCH3)2	2.08	3.04	0.35	0.51
R112βCH2-R113NH	1.89	5.18	0.95	2.59
R112βCH2-R115NH	1.82	3.90	0.91	1.95
R112βCH2-Cterm NH	1.70	2.37	0.85	1.19
R113NH-V114βCH	0.96	1.28	0.96	1.28
R113NH-V114(γCH3)2	1.76	2.14	0.29	0.36
R113αCH-V114βCH	-	3.14	-	3.14
R113αCH-V114(γCH3)2	2.08	3.04	0.35	0.51
R113βCH2-V114αCH	4.70	4.99	2.35	2.49
V114αCH-R115βCH2	4.70	4.99	2.35	2.49
V114αCH-R113δCH2	1.50	-	0.38	-
V114αCH-R115δCH2	1.50	-	0.38	-
V114αCH-CtermNH	0.58	1.02	0.58	1.02
V114βCH-R115NH	1.28	2.11	1.28	2.11
V114βCH-Cterm NH	0.74	-	0.37	-
V114(γCH3)2-R115NH	2.30	4.10	0.46	0.68
V114(γCH3)2-Cterm NH	2.75	1.95	0.49	0.33
R115NH-Cterm NH	0.26	-	0.26	-
R115αCH-Cterm NH	1.06	3.71	1.06	3.71
R115αCH-Cterm NH'	1.31	3.30	1.31	3.30
R115βCH2-Cterm NH	1.50	3.55	0.75	1.78
R115δCH2-Cterm NH	0.51	0.70	0.26	0.35
F106δCH2-K105βCH2	9.44	10.53	1.18	1.32
F106δCH2-K107βCH2	9.44	10.53	1.18	1.32
F106δCH2-K105γCH2	1.79	3.07	0.45	0.77
F106δCH2-K107γCH2	2.08	3.42	0.52	1.71
F106δCH2-P109βCH(x)	3.62	5.66	0.91	1.42
F106δCH2-P110βCH(x)	3.62	5.66	0.91	1.42
F106δCH2-P109βCH'(p)	1.92	2.78	0.48	0.70
F106δCH2-P110βCH'(p)	1.92	2.78	0.48	0.70
F106δCH2-P109γCH2	1.54	4.13	0.13	0.34
F106δCH2-P110γCH2	1.54	4.13	0.13	0.34
F106δCH2-V114βCH	1.54	4.13	0.26	0.69
F106δCH2-L111(δCH3)2	3.01	3.39	0.13	0.14
F106δCH2-V114(γCH3)2	3.01	3.39	0.13	0.14
F106ξCH2-K105βCH2	8.67	13.06	0.72	1.09
F106ξCH2-K107βCH2	8.67	13.06	0.72	1.09

F106ξCH2-K105γCH2	1.34	2.85	0.22	0.48
F106ξCH2-K107γCH2	1.60	3.58	0.27	0.60
F106ξCH2-P109βCH(x)	3.39	5.22	0.57	0.87
F106ξCH2-P110βCH(x)	3.39	5.22	0.57	0.87
F106ξCH2-P109βCH'(p)	2.02	3.20	0.34	0.53
F106ξCH2-P110βCH'(p)	2.02	3.20	0.34	0.53
F106ξCH2-P109γCH2	2.94	4.67	0.16	0.26
F106ξCH2-P110γCH2	2.94	4.67	0.16	0.26
F106ξCH2-V114βCH	2.94	4.67	0.33	0.52
F106ξCH2-L111(δCH3)2	6.14	6.59	0.17	0.18
F106ξCH2-V114(γCH3)2	6.14	6.59	0.17	0.18
F106ςCH-K105βCH2	8.67	13.06	0.72	1.09
F106ςCH-K107βCH2	8.67	13.06	0.72	1.09
F106ςCH-K105γCH2	1.34	2.85	0.22	0.48
F106ςCH-K107γCH2	1.60	3.58	0.27	0.60
F106ςCH-P109βCH(x)	3.39	5.22	0.57	0.87
F106ςCH-P110βCH(x)	3.39	5.22	0.57	0.87
F106ςCH-P109βCH'(p)	2.02	3.20	0.34	0.53
F106ςCH-P110βCH'(p)	2.02	3.20	0.34	0.53
F106ςCH-P109γCH2	2.94	4.67	0.16	0.26
F106ςCH-P110γCH2	2.94	4.67	0.16	0.26
F106ςCH-V114βCH	2.94	4.67	0.33	0.52
F106ςCH-L111(δCH3)2	6.14	6.59	0.17	0.18
F106ςCH-V114(γCH3)2	6.14	6.59	0.17	0.18
K105γCH2-K107ξCH2	1.38	-	0.35	-
K105ξCH2-K107γCH2	2.24	-	0.56	-
K105ξCH2-V114(γCH3)2	2.05	-	0.17	-
F106βCH(m)-P109βCH(x)	6.46	-	3.23	-
F106βCH(m)-P110βCH(x)	6.46	-	3.23	-
F106βCH(m)-P109γCH2	6.46	2.20	1.62	0.55
F106βCH(m)-P110γCH2	6.46	2.20	1.62	0.55
F106βCH(m)-V114αCH	0.74	0.86	0.74	0.86
F106βCH(m)-V114βCH	2.30	2.02	2.30	2.02
F106βCH(m)-L111(δCH3)2	2.94	0.90	0.25	0.08
F106βCH(m)-V114(γCH3)2	2.94	0.90	0.25	0.08
F106βCH'(x)-K105γCH2	4.99	-	1.25	-
F106βCH'(x)-K107γCH2	4.99	-	1.25	-
F106βCH'(x)-P109βCH'(p)	0.80	-	0.40	-
F106βCH'(x)-P110βCH'(p)	0.80	-	0.40	-
F106βCH'(x)-P109γCH2	-	2.59	-	0.65
F106βCH'(x)-P110γCH2	-	2.59	-	0.65

F106βCH'(x)-V114αCH	0.99	1.06	0.99	1.06
F106βCH'(x)-V114βCH	5.57	2.59	5.57	2.59
R108βCH2-P109δCH(m)	4.80	4.29	2.40	2.15
R108βCH2-P109δCH'(m')	2.94	5.89	1.47	2.95
P109βCH'(p)-P110δCH'(m')	-	2.69	-	2.69
P109δCH(m)-L111(δCH3)2	2.56	-	0.21	-
P109δCH(m)-V114(γCH3)2	2.56	-	0.21	-
P109δCH'(m')-L111(δCH3)2	1.95	2.98	0.16	0.25
P109δCH'(m')-V114(γCH3)2	1.95	2.98	0.16	0.25
P110βCH(x)-L111(δCH3)2	11.90	10.66	1.98	1.78
P110βCH'(p)-L111βCH2	10.34	13.63	5.17	6.82
P110βCH'(p)-L111(δCH3)2	9.09	8.96	1.52	0.75
P110γCH2-L111βCH2	19.90	39.68	4.98	9.92
P110γCH2-L111(δCH3)2	10.72	10.34	0.89	0.86
L111(δCH3)2-R112βCH2	6.91	10.56	0.58	0.88
L111(δCH3)2-R112δCH2	2.66	-	0.22	-
R113δCH2-V114(γCH3)2	5.38	7.97	0.22	0.33
R115δCH2-V114(γCH3)2	5.38	7.97	0.22	0.33
R113βCH2-V114(γCH3)2	6.92	10.59	0.58	0.89
V114(γCH3)2-R115βCH2	6.92	10.59	0.58	0.89
G104αCH2-K105αCH	-	1.09	-	0.55
F106αCH-K107αCH	0.45	0.74	0.45	0.74
K107αCH-R108αCH	0.26	0.86	0.26	0.86
R108αCH-P110αCH	0.51	-	0.51	-
P110αCH-L111αCH	0.38	1.66	0.38	1.66
R112αCH-R115αCH	0.48	-	0.48	-
R113αCH-V114αCH	1.31	1.25	1.31	1.25
V114αCH-R115αCH	1.82	3.20	1.82	3.20
F106NH-K107NH	0.64	3.42	0.64	3.42
F106NH-R108NH	1.18	0.90	1.18	0.90
K107NH-R108NH	0.58	0.90	0.58	0.90
R112NH-R113NH	0.42	-	0.42	-
R112NH-R115NH	0.35	2.59	0.35	2.59
V114NH-R115NH	0.67	1.50	0.67	1.50
R115NH-C term NH	2.62	0.74	2.62	0.74

G104αCH2-NH	3.97	5.66	1.98	2.83
G104αCH2-K105NH	2.27	4.86	1.14	2.43
G104αCH2-F106NH	0.70	0.61	0.35	0.31
G104αCH2-R108NH	0.51	-	0.26	-
K105αCH-NH	1.76	2.59	1.76	2.59
K105αCH-F106NH	1.66	4.48	1.66	4.48
F106αCH-NH	0.26	0.96	0.26	0.96
F106αCH-K107NH	0.22	2.24	0.22	2.24
F106αCH-R108NH	1.25	-	1.25	-
K107αCH-NH	0.70	2.24	0.70	2.24
K107αCH-R108NH	2.14	3.42	2.14	3.42
R108αCH-NH	-	0.45	-	0.45
P110αCH-L111NH	0.42	2.18	0.42	2.18
P110αCH-R112NH	-	1.06	-	1.06
L111αCH-NH	1.25	2.78	1.25	2.78
L111αCH-R112NH	1.25	3.42	1.25	3.42
L111αCH-R113NH	0.80	1.82	0.80	1.82
R112αCH-NH	1.28	2.24	1.28	2.24
R112αCH-R113NH	1.18	4.54	1.18	4.54
R112αCH-R115NH	0.61	1.47	0.61	1.47
R113αCH-NH	1.18	14.53	1.18	14.53
R113αCH-V114NH	0.77	3.30	0.77	3.30
V114αCH-NH	1.18	1.86	1.18	1.86
V114αCH-F106NH	0.58	-	0.58	-
V114αCH-R115NH	0.80	4.74	0.80	4.74
R115αCH-NH	1.54	2.43	1.54	2.43

Table X-3. Table of TRNOE intensities versus mixing time (τm = 75, 150, and 500 ms) measured at 0.4 molar equivalents TnC.Ca(II)$_4$ to TnI peptide.

spin system	measured intensities			normalized intensities		
tmix (ms)	500	150	75	500	150	75
K105αCH-βCH2	7.66	27.92	11.42	1.92	13.96	5.71
K105αCH-γCH2	7.66	7.13	3.56	1.92	3.57	1.78
K105αCH-ξCH2	2.11	3.37	-	1.06	1.69	-
K105βCH2-γCH2	23.83	27.79	24.82	2.98	3.47	3.10
K105δCH2-γCH2	23.83	27.79	24.82	2.98	3.47	3.10
K105δCH2-ξCH2	15.25	25.81	1.65	3.81	6.45	0.41
K105βCH2-NH	4.75	14.36	-	2.38	7.13	-
K105γCH2-ξCH2	6.07	7.99	-	1.52	2.00	-
K105γCH2-NH	1.45	5.81	-	0.73	2.91	-
K105ξCH2-NH	0.79	-	-	0.39	-	-
F106αCH-βCH(m)	5.35	1.32	2.24	5.35	1.32	2.24
F106αCH-βCH'(x)	5.35	2.71	3.43	5.35	2.71	3.43
F106αCH-δCH2	0.86	2.84	-	0.43	1.42	-
F106αCH-ξCH2	0.73	-	-	0.24	-	-
F106αCH-ςCH	0.73	-	-	0.24	-	-
F106βCH(m)-βCH'(x)	5.68	13.00	23.10	5.68	13.00	23.10
F106βCH(m)-δCH2	3.63	10.63	2.38	1.82	5.32	1.19
F106βCH(m)-ξCH2	3.10	7.33	-	1.03	2.44	-
F106βCH(m)-ςCH	3.10	7.33	-	1.03	2.44	-
F106βCH(m)-NH	2.31	5.87	-	1.16	2.94	-
F106βCH'(x)-NH	2.31	5.87	-	1.16	2.94	-
F106βCH'(x)-δCH2	3.56	11.42	2.90	1.78	5.71	1.45
F106βCH'(x)-ξCH2	3.10	7.79	-	1.03	2.60	-
F106βCH'(x)-ςCH	3.10	7.79	-	1.03	2.60	-
F106NH-δCH2	1.39	1.52	-	0.70	0.76	-
F106NH-ξCH2	1.06	0.73	-	0.35	0.12	-
F106NH-ςCH	1.06	0.73	-	0.35	0.12	-
K107αCH-βCH2	7.06	14.78	5.54	3.53	7.39	2.77
K107αCH-γCH2	7.26	9.57	4.42	3.63	4.79	2.21
K107αCH-ξCH2	4.03	2.51	-	2.02	1.26	-
K107βCH2-γCH2	25.01	49.57	55.84	3.13	6.20	6.98
K107δCH2-γCH2	25.01	49.57	55.84	3.13	6.20	6.98
K107δCH2-ξCH2	14.45	46.07	9.24	3.61	11.52	2.31
K107βCH2-NH	3.70	10.63	-	1.85	5.32	-

K107γCH2-ξCH2	7.66	13.66	-	1.92	6.83	-
K107γCH2-NH	1.12	5.61	-	0.56	2.81	-
K107ξCH2-NH	0.92	1.78	-	0.46	0.89	-
R108αCH-βCH2	-	4.55	3.23	-	2.28	1.62
R108αCH-δCH2	2.64	3.30	-	1.32	1.65	-
R108βCH2-δCH2	2.90	15.44	-	1.45	3.86	-
R108γCH2-δCH2	4.36	15.44	-	1.09	3.86	-
R108βCH-NH	2.51	7.13	-	1.26	3.57	-
R108δCH2-NH	1.32	2.64	-	0.66	1.32	-
P109βCH(x)-βCH'(p)	6.27	19.60	29.57	6.27	19.60	29.57
P109βCH(x)-δCH(m)	1.25	4.62	2.71	1.25	4.62	2.71
P109βCH(x)-δCH'(m')	0.86	3.04	6.07	0.86	3.04	6.07
P109βCH'(p)-δCH(m)	0.20	2.11	0.99	0.20	2.11	0.99
P109βCH'(p)-δCH'(m')	0.33	5.54	3.43	0.33	5.54	3.43
P109βCH'(p)-γCH2	6.93	23.36	54.25	3.47	11.68	27.13
P109γCH2-δCH(m)	1.78	4.29	1.52	0.89	2.15	0.76
P109γCH2-δCH'(m')	1.52	-	-	0.76	-	-
P109δCH(m)-δCH'(m')	0.13	3.70	4.75	0.13	3.70	4.75
P110αCH-βCH(x)	2.51	4.95	8.05	2.51	4.95	8.05
P110αCH-βCH'(p)	2.05	7.26	8.38	2.05	7.26	8.38
P110αCH-γCH2	3.10	6.80	5.54	1.55	3.40	2.77
P110βCH(x)-βCH'(p)	17.95	39.67	39.27	17.95	39.67	39.27
P110βCH(x)-δCH(m)	1.25	4.62	2.71	1.25	4.62	2.71
P110βCH(x)-δCH'(m')	0.86	3.04	6.07	0.86	3.04	6.07
P110βCH(x)-γCH2	21.58	60.52	-	10.79	30.26	-
P110βCH'(p)-δCH(m)	0.20	2.11	0.99	0.20	2.11	0.99
P110βCH'(p)-δCH'(m')	0.33	5.54	3.43	0.33	5.54	3.43
P110βCH'(p)-γCH2	23.10	47.19	-	11.05	23.60	-
P110γCH2-δCH(m)	1.78	4.29	1.52	0.89	2.15	0.76
P110γCH2-δCH'(m')	1.52	7.46	6.80	0.76	3.73	3.40
P110δCH(m)-δCH'(m')	0.13	3.10	3.63	0.13	3.10	3.63
L111αCH-βCH2	7.06	14.78	5.54	3.53	7.39	2.77
L111αCH-(δCH3)2	10.56	22.64	6.67	1.76	3.77	1.11
L111βCH2-(δCH3)2	31.75	126.06	40.33	1.32	5.25	1.68
L111γCH-(δCH3)2	31.75	126.06	40.33	2.65	10.51	3.36
L111βCH2-NH	5.15	15.05	-	2.58	7.53	-
L111(δCH3)2-NH	1.91	5.35	-	0.32	0.89	-
R112αCH-βCH2	5.08	13.93	5.35	2.54	6.97	2.68
R112αCH-δCH2	2.64	3.30	-	1.32	1.65	-
R112βCH2-δCH2	2.90	15.44	-	0.72	3.86	-
R112γCH2-δCH2	4.36	15.44	-	1.09	3.86	-
R112βCH2-NH	2.51	7.13	-	1.76	3.57	-
R112δCH2-NH	1.32	2.64	-	0.66	1.32	-

R113αCH-βCH2	5.08	13.93	5.35	2.54	6.97	2.68
R113αCH-δCH2	2.64	3.30	-	1.32	1.65	-
R113βCH2-δCH2	2.90	15.44	-	0.72	3.86	-
R113γCH2-δCH2	4.36	15.44	-	1.09	3.86	-
R113βCH2-NH	4.88	7.85	-	2.44	3.93	-
R113δCH2-NH	1.32	2.64	-	0.66	1.32	-
V114αCH-βCH	3.43	13.33	14.26	3.43	13.33	14.26
V114αCH-(γCH3)2	9.77	24.02	11.29	1.63	2.00	1.88
V114βCH-(γCH3)2	31.02	79.20	49.10	5.18	13.20	8.18
V114βCH-NH	3.63	3.76	-	3.63	3.76	2.68
V114(γCH3)2-NH	1.91	5.35	-	0.32	0.89	-
R115αCH-βCH2	6.40	14.78	11.48	3.20	7.39	5.74
R115αCH-δCH2	2.64	3.30	-	1.32	1.65	-
R115βCH2-δCH2	2.90	15.44	-	0.72	3.86	-
R115γCH2-δCH2	4.36	15.44	-	1.09	3.86	-
R115βCH2-NH	4.36	5.87	-	2.18	2.94	-
R115δCH2-NH	1.32	2.64	-	0.66	1.32	-
C-term NH-NH'	2.24	13.46	-	2.24	13.46	-
NAcCH3-G104αCH2	7.52	9.44	-	1.25	1.57	-
NAcCH3-G104NH	3.63	3.70	2.51	1.21	1.23	0.84
NAcCH3-K105NH	2.18	5.68	-	0.73	1.89	-
G104NH-K105γCH2	0.92	-	-	0.56	-	
G104NH-K107γCH2	0.92	1.98	-	0.46	0.99	-
G104αCH2-F106δCH2	0.99	-	-	0.25	-	-
G104αCH2-F106ξCH2	0.99	-	-	0.17	-	-
G104αCH2-F106ςCH	0.99	-	-	0.17	-	-
K105βCH2-F106NH	4.22	6.50	-	2.11	3.75	-
K105γCH2-F106NH	0.66	3.70	-	0.33	1.85	-
K105NH-K107γCH2	0.73	1.78	-	0.37	0.89	-
K105NH-L111(δCH3)2	3.30	8.91	-	0.28	0.74	-
K105NH-V114(γCH3)2	3.30	8.91	-	0.28	0.74	-
F106αCH-R108βCH2	-	2.38	-	-	1.19	-
F106NH-K107γCH2	0.53	1.58	-	0.27	0.79	-
F106NH-P109βCH(x)	-	3.43	-	-	3.43	-
F106NH-P109βCH'(p)	-	2.31	-	-	2.31	-
F106NH-P109γCH2	-	4.49	-	-	1.13	-
F106NH-V114βCH	-	4.49	-	-	2.25	-
F106NH-L111(δCH3)2	3.56	5.48	-	0.30	0.46	-
F106NH-V114(γCH3)2	3.56	5.48	-	0.30	0.46	-
K107γCH2-R108NH	1.12	1.65	-	0.56	0.83	-
K107ξCH2-R108NH	0.66	-	-	0.33	-	-
F106δCH2-K107NH	0.86	1.65	-	0.43	0.83	-

F106ξCH2-K107NH	0.86	0.92	-	0.29	0.31	-
F106ςCH-K107NH	0.86	0.92	-	0.29	0.31	-
R108αCH-P109βCH(x)	-	2.31	-	-	2.31	-
R108αCH-P109βCH'(p)	-	3.30	-	-	3.30	-
R108αCH-P109γCH2	-	2.31	-	-	1.66	-
R108αCH-P109δCH(m)	-	-	1.32	-	-	1.32
R108αCH-P109δCH'(m')	-	2.77	4.03	-	2.77	4.03
F106δCH2-R108NH	0.92	1.06	-	0.46	0.53	-
F106ξCH2-R108NH	0.79	0.99	-	0.26	0.33	-
F106ςCH-R108NH	0.79	0.99	-	0.26	0.33	-
F106δCH2-V114αCH	0.66	-	-	0.33	-	-
F106ξCH2-V114αCH	0.59	-	-	0.20	-	-
F106ςCH-V114αCH	0.59	-	-	0.20	-	-
R108NH-P109βCH(x)	2.24	3.70	-	2.24	3.70	-
R108NH-P109βCH'(p)	1.12	2.11	-	1.12	2.11	-
R108NH-P109γCH2	2.64	4.03	-	1.32	2.02	-
P109αCH-P110δCH(m)	-	-	0.86	-	-	0.86
P109αCH-P110δCH'(m')	-	-	1.12	-	-	1.12
P109βCH(x)-V114αCH	-	5.08	-	-	5.08	-
P109βCH'(p)-V114αCH	-	8.32	-	-	8.32	-
P110αCH-L111(δCH3)2	4.62	7.85	5.54	0.77	1.31	0.92
P110αCH-L111βCH2	-	11.09	-	-	5.55	-
P110βCH(x)-L111αCH	-	7.66	-	-	7.66	-
P110βCH(x)-L111NH	1.58	4.82	-	1.58	4.82	-
P110βCH'(p)-L111αCH	4.16	5.35	-	4.16	5.35	-
P110βCH'(p)-L111NH	1.98	3.10	-	1.98	3.10	-
P110γCH2-L111αCH	6.73	7.52	-	3.37	3.76	-
P110γCH2-L111NH	1.85	-	-	0.93	-	-
L111(δCH3)2-R112NH	2.77	7.00	-	0.46	1.17	-
R112βCH2-R115NH	-	4.03	-	-	2.02	-
R112βCH2-Cterm NH	-	5.35	-	-	2.68	-
R113αCH-V114(γCH3)2	7.52	8.78	6.86	1.25	1.46	1.14
R113βCH2-V114αCH	3.37	20.20	-	1.69	10.10	-
R113NH-V114βCH	1.78	3.50	-	1.78	3.50	-
R113NH-V114(γCH3)2	2.31	4.36	-	0.39	0.73	-
V114αCH-R113δCH2	-	3.43	-	-	0.86	-
V114αCH-R115δCH2	-	3.43	-	-	0.86	-
V114(γCH3)2-Cterm NH	3.83	7.33	-	0.64	1.22	-
V114βCH-R115NH	1.52	3.23	-	1.52	3.23	-
V114(γCH3)2-R115NH	2.31	7.00	-	0.39	1.17	-
R115αCH-Cterm NH	0.86	5.48	-	0.86	5.48	-
R115αCH-Cterm NH'	2.24	7.19	-	2.24	7.19	-
R115βCH2-Cterm NH	-	8.32	-	-	4.16	-

R115δCH2-Cterm NH	1.25	-	-	0.63	-	-
F106δCH2-K105βCH2	12.80	22.64	-	1.60	2.83	-
F106δCH2-K107βCH2	12.80	22.64	-	1.60	2.83	-
F106δCH2-K105γCH2	3.04	3.17	-	0.76	3.47	-
F106δCH2-K107γCH2	2.56	2.18	-	0.64	0.55	-
F106δCH2-P109βCH(x)	5.15	9.64	-	1.29	2.41	-
F106δCH2-P110βCH(x)	5.15	9.64	-	1.29	2.41	-
F106δCH2-P109βCH'(p)	4.62	5.15	-	1.16	1.29	-
F106δCH2-P110βCH'(p)	4.62	5.15	-	1.16	1.29	-
F106δCH2-P109γCH2	1.72	3.83	-	0.22	0.48	-
F106δCH2-P110γCH2	1.72	3.83	-	0.22	0.48	-
F106δCH2-V114βCH	3.17	3.83	-	1.59	1.92	-
F106δCH2-L111(δCH3)2	9.04	25.67	6.93	0.75	1.07	0.29
F106δCH2-V114(γCH3)2	9.04	25.67	6.93	0.75	1.07	0.29
F106ξCH2-K105βCH2	11.09	20.66	-	0.92	1.72	-
F106ξCH2-K107βCH2	11.09	20.66	-	0.92	1.72	-
F106ξCH2-K105γCH2	2.71	2.31	-	0.45	0.39	-
F106ξCH2-K107γCH2	2.05	1.91	-	0.34	0.32	-
F106ξCH2-P109βCH(x)	4.75	7.26	-	0.79	1.21	-
F106ξCH2-P110βCH(x)	4.75	7.26	-	0.79	1.21	-
F106ξCH2-P109βCH'(p)	4.29	4.82	-	0.72	0.80	-
F106ξCH2-P110βCH'(p)	4.29	4.82	-	0.72	0.80	-
F106ξCH2-P109γCH2	1.65	3.63	-	0.14	0.31	-
F106ξCH2-P110γCH2	1.65	3.63	-	0.14	0.31	-
F106ξCH2-V114βCH	3.43	3.63	-	1.14	1.21	-
F106ξCH2-L111(δCH3)2	7.00	17.09	10.10	0.19	0.47	0.28
F106ξCH2-V114(γCH3)2	1.06	17.09	10.10	0.19	0.47	0.28
F106ςCH-K105βCH2	11.09	20.66	-	0.92	1.72	-
F106ςCH-K107βCH2	11.09	20.66	-	0.92	1.72	-
F106ςCH-K105γCH2	2.71	2.31	-	0.45	0.39	-
F106ςCH-K107γCH2	2.05	1.91	-	0.34	0.32	-
F106ςCH-P109βCH(x)	4.75	7.26	-	0.79	1.21	-
F106ςCH-P110βCH(x)	4.75	7.26	-	0.79	1.21	-
F106ςCH-P109βCH'(p)	4.29	4.82	-	0.72	0.80	-
F106ςCH-P110βCH'(p)	4.29	4.82	-	0.72	0.80	-
F106ςCH-P109γCH2	1.65	3.63	-	0.14	0.31	-
F106ςCH-P110γCH2	1.65	3.63	-	0.14	0.31	-
F106ςCH-V114βCH	3.43	3.63	-	1.14	1.21	-
F106ςCH-L111(δCH3)2	7.00	17.09	10.10	0.19	0.47	0.28
F106ςCH-V114(γCH3)2	1.06	17.09	10.10	0.19	0.47	0.28
K105ξCH2-V114(γCH3)2	-	3.63	-	-	0.30	-

F106βCH(m)-K107αCH	-	2.97	-	-	2.97	-
F106βCH(m)-P109βCH(x)	-	3.50	-	-	1.75	-
F106βCH(m)-P110βCH(x)	-	3.50	-	-	1.75	-
F106βCH(m)-P109βCH'(p)	-	4.42	-	-	2.21	-
F106βCH(m)-P110βCH'(p)	-	4.42	-	-	2.21	-
F106βCH(m)-P109γCH2	3.96	3.63	-	1.98	1.82	-
F106βCH(m)-P110γCH2	-	2.51	-	-	1.26	-
F106βCH(m)-V114αCH	-	3.63	-	-	3.63	-
F106βCH(m)-V114βCH	3.96	2.71	-	3.96	2.71	-
F106βCH(m)-L111(δCH3)2	-	6.86	-	-	0.57	-
F106βCH(m)-V114(γCH3)2	-	6.86	-	-	0.57	-
F106βCH'(x)-P109βCH'(p)	-	4.75	-	-	2.38	-
F106βCH'(x)-P110βCH'(p)	-	4.75	-	-	2.38	-
F106βCH'(x)-P109γCH2	3.96	4.16	-	1.98	2.08	-
F106βCH'(x)-P110γCH2	-	4.88	-	-	2.44	-
F106βCH'(x)-V114βCH	3.96	2.90	-	3.96	2.90	-
R108βCH2-P109δCH(m)	-	6.40	-	-	3.20	-
R108βCH2-P109δCH'(m')	7.99	6.01	-	4.00	3.01	-
P109δCH(m)-L111(δCH3)2	-	5.74	5.08	-	0.48	0.42
P109δCH(m)-V114(γCH3)2	-	5.74	5.08	-	0.48	0.42
P109δCH'(m')-L111(δCH3)2	3.37	6.01	7.26	0.28	0.50	0.61
P109δCH'(m')-V114(γCH3)2	3.37	6.01	7.26	0.28	0.50	0.61
P110βCH'(p)-L111(δCH3)2	16.37	26.93	-	2.73	4.49	-
P110δCH(m)-L111(δCH3)2	-	-	4.42	-	-	0.74
P110δCH'(m')-L111(δCH3)2	-	-	8.25	-	-	1.38
P110γCH2-L111(δCH3)2	19.87	44.42	36.37	1.66	3.70	3.03
R113δCH2-V114(γCH3)2	16.57	15.91	-	1.38	0.67	-
R115δCH2-V114(γCH3)2	16.57	15.91	-	1.38	0.67	-
G104αCH2-K105αCH	15.71	2.84	-	7.86	1.42	-
R112αCH-R115αCH	-	3.30	-	-	3.30	-
V114αCH-R115αCH	-	4.69	-	-	4.69	-
F106NH-K107NH	-	3.23	-	-	3.23	-
F106NH-R108NH	0.33	3.30	-	0.33	3.30	-
K107NH-R108NH	0.20	2.11	-	0.20	2.11	-
F106NH-R115NH	0.66	-	-	0.66	-	-

K107NH-R115NH	0.33	-	-	0.33	-	-
R112NH-R115NH	0.26	3.17	-	0.26	3.17	-
V114NH-R115NH	0.53	-	-	0.53	-	-
G104αCH2-NH	2.90	9.17	1.32	1.45	4.59	0.66
G104αCH2-K105NH	1.85	6.67	1.39	0.93	3.34	0.70
G104αCH2-F106NH	0.73	1.58	-	0.37	0.79	-
G104αCH2-R108NH	0.46	1.39	-	0.23	0.70	-
K105αCH-NH	2.38	4.75	1.45	2.38	4.75	1.45
K105αCH-F106NH	1.72	6.27	1.85	1.72	6.27	1.85
K105αCH-R108NH	1.19	-	-	1.19	-	-
F106αCH-NH	-	1.25	0.33	-	1.25	0.33
F106αCH-K107NH	-	1.39	7.39	-	1.39	7.39
K107αCH-NH	0.59	2.31	1.32	0.59	2.31	1.32
K107αCH-R108NH	1.12	3.04	0.92	1.12	3.04	0.92
R108αCH-NH	-	-	0.59	-	-	0.59
P110αCH-L111NH	0.33	1.58	-	0.33	1.58	-
L111αCH-NH	1.39	1.78	0.66	1.39	1.78	0.66
L111αCH-R112NH	1.12	3.04	0.92	1.12	3.04	0.92
R112αCH-NH	0.40	2.11	-	0.40	2.11	-
R112αCH-R113NH	1.25	3.37	0.92	1.25	3.37	0.92
R112αCH-R115NH	0.40	0.92	-	0.40	0.92	-
R113αCH-NH	1.25	3.37	0.92	1.25	3.37	0.92
R113αCH-V114NH	0.59	1.78	0.66	0.59	1.78	0.66
V114αCH-NH	-	2.11	-	-	2.11	-
V114αCH-F106NH	0.99	0.99	-	0.99	0.99	-
V114αCH-R115NH	1.12	4.22	-	1.12	4.22	-
R115αCH-NH	1.39	2.77	1.19	1.39	2.77	1.19

TRNOE: version 1

```
#
# Makefile for Trnoesy program
#
CFLAGS = -c -O
DFLAGS = -c -g
OBJECTS = calc.o plot.o eigen.o minv.o
LIBES = -lm -lsuntool -lsunwindow -lpixrect
#
trnoesy:  main.h $(OBJECTS)
	cc -O $(OBJECTS) $(LIBES) -o trnoesy

calc.o:  main.h calc.c
	cc $(CFLAGS) calc.c

eigen.o:  main.h eigen.c
	cc $(CFLAGS) eigen.c

minv.o:  main.h minv.c
	cc $(CFLAGS) minv.c

plot.o:  main.h plot.c
	cc $(CFLAGS) plot.c

trnoecoords:  trnoecoords.c
	nice cc -o trnoecoords trnoecoords.c
```

```
/*
 Header file for trnoesy program. Sept 18 1989.
*/
#include <stdio.h>
#include <string.h>
#include <math.h>
#include <suntool/sunview.h>
#include <suntool/panel.h>
#include <suntool/textsw.h>
#include <suntool/canvas.h>

/* define all of our various color constants */
/* background = 0,  foreground = 15 */
#define WHITE     1
#define LTYELLOW   2
#define DKYELLOW   3
#define PINK    4
#define RED     5
#define DKRED    6
#define LTGREEN   7
#define GREEN    8
#define TURQUOISE   9
#define LTBLUE    10
#define BLUE    11
#define DKBLUE    12
#define PURPLE    13
#define BLACK    14

#define MAXPROTNUM    121      /* number of Protons + 1 */
#define MAXPROTSQU    14401    /* MAXPROTNUM*MAXPROTNUM + 1*/
#define MAXPROTTRI          7261     /* (MAXPROTNUM * MAXPROTNUM+1)/2 + 1*,
#define MAX_LENGTH   256
#define MAX_TAUPOINTS  100

#define color_xor(aColor) ((PIX_SRC ^ PIX_DST) | PIX_COLOR(aColor))
```

```
#define color_src(aColor) (PIX_SRC | PIX_COLOR(aColor))
#define color_or(aColor) ((PIX_SRC | PIX_DST) | PIX_COLOR(aColor))

/* program variables */

FILE    *fopen();
FILE    *echofp;        /* echo input file */
FILE        *tabfp;        /* stores numeric results */
FILE        *cntlfp;        /* trnoesy control file */

Frame   base_frame;       /* graphics data structures */
Pixwin  *pw;
Canvas  plot_canvas;

int   tr_x, tr_y;      /* origin of graphics window */
int   tr_width, tr_height;         /* size of that window */
int   x_origin, y_origin;          /* location of axis origin */
int   x_len, y_len;                /* length of axis in pixels */
int   dhLab;                       /* labeling offset */

double  yPixel_ratio;     /* for converting nums to pixels */
double  xPixel_ratio;
int   tauIncNum;      /* number of points to plot */
double  xMin, yMin, xMax, yMax;    /* min/max values for plotting */

char   protonLabel[MAXPROTNUM][10]; /* names for the protons */
char   tablesFname[MAX_LENGTH];  /* filename for numeric results */
char   line[MAX_LENGTH];     /* generic character string */
char   *rc;          /* used by fgets */

double  pi;
double  qConstant;

double  fRelaxMatrix[MAXPROTNUM][MAXPROTNUM];
double  bRelaxMatrix[MAXPROTNUM][MAXPROTNUM];
double  relaxMatrix[MAXPROTNUM][MAXPROTNUM];
double  upperTriangle[MAXPROTTRI];
double  result[MAXPROTSQU];
double  vectors[MAXPROTNUM][MAXPROTNUM];
double  vectorsInverse[MAXPROTNUM][MAXPROTNUM];
double  diagonalRelax[MAXPROTNUM];
double  distance[MAXPROTNUM][MAXPROTNUM];
double  tauMix[MAX_TAUPOINTS];

double  w0[MAXPROTNUM][MAXPROTNUM];
double  w1[MAXPROTNUM][MAXPROTNUM];
double  w2[MAXPROTNUM][MAXPROTNUM];
double  spectralDensity[3];

double  x[MAXPROTNUM];      /* holds proton coordinates */
double  y[MAXPROTNUM];
double  z[MAXPROTNUM];

int   numberProtons;     /* number of protons in datafile */
double  dMaxNoe;        /* distance Max nOe*/
double  dMinNoe;        /* distance Min nOe */
double  fb;         /* bound/free ratio */
double      tauDisplay;       /* mix time for tables */
int   protId;        /* current fixed proton */
int   doEigFlag;       /* recalc eigenvalues */
```

```
extern Notify_error notify_dispatch(); /* external routines used */

/*
Purpose: This program calculates TrNOESY cross peak intensities
    on the basis of a full matrix analysis under the
    assumption of fast exchange.

    Maximum number of protons can also be altered via the
    constants MAXPROTNUM, MAXPROTSQU, MAXPROTTRI in the
    file "trnoesy.h".

Usage:   trnoesy

    Note: The program assumes a control file called "trnoesy.cntl"
    exists. The user should get a copy of the example file and
    modify it appropriately (it is documented). The control file
    is where all input or locations for input are read.


Input File Format:

        Title:   TrNoesy - BDS - Aug. 30
    28        # of Protons
   #          Label           X[I]       Y[I]       Z[I]
   1          D51NH           9.80       24.12      21.38
            (etc)


Author:  Robert Boyko (translated from Basic on HP to C on sun)
Date:  Sept 18, 1989
Place:  Brian Sykes Lab
    Dept. of Biochemistry
    University of Alberta

*/

#include "main.h"    /* include header file */


/*****************************************************************/
init()
{
 double gamma1, hBar;
 char filename[MAX_LENGTH];
 char *ctime();
 long timeofday, *tloc[8];

 pi = 3.14159;
 gamma1 = 4255.0 * (2*pi);
 hBar = 6.62e-27 / (2*pi);
 qConstant = 0.1 * gamma1*gamma1*gamma1*gamma1 * hBar*hBar;
 doEigFlag = TRUE;

 fprintf(stdout, "\n\n");
 fprintf(stdout, "***** TrNoesy - version 1.1  May 8/90 *****\n");
 timeofday = time(tloc);
 fprintf(stdout, "***** Date:  %s\n\n", ctime(tloc));
 fprintf(stdout, "Enter Trnoesy control file: ");
 rc = fgets(line, MAX_LENGTH, stdin);
 sscanf(line, "%s", filename);
 fprintf(stdout, "Trnoesy control file = %s\n", filename);
 cntlfp = fopen(filename, "r");
 if (cntlfp == NULL) {
  fprintf(stderr," Cannot open trnoesy control file...\n");
  exit(1);
 }

 rc = fgets(line, MAX_LENGTH, cntlfp);
 sscanf(line, "%s", filename);
 fprintf(stdout, "Echo input file = %s\n", filename);
 echofp = fopen(filename, "w");
 if (echofp == NULL) {
  fprintf(stderr," Cannot open input echo file...\n");
  exit(1);
 }

 rc = fgets(line, MAX_LENGTH, cntlfp);
 sscanf(line, "%s", tablesFname);
 fprintf(stdout, "Tabular results file = %s\n", tablesFname);
 tabfp = fopen(tablesFname, "w");
 if (tabfp == NULL) {
  fprintf(stderr," Cannot open tabular results file...\n");
  exit(1);
 }
} /* init */


/*************************************************************/
/* define plotting screen
*/
init_graphics()
{
 base_frame = window_create (NULL, FRAME,
            WIN_X, tr_x,
            WIN_Y, tr_y,
            WIN_WIDTH, tr_width,
            WIN_HEIGHT, tr_height,
            FRAME_LABEL,
   " << Trnoesy   Version 1.0   09/18/89 >>",
            0);
 plot_canvas = window_create (base_frame, CANVAS,
             tr_x, tr_y, 0);
 pw = canvas_pixwin (plot_canvas);
 set_canvas_colors (pw);
} /*init_graphics */


/*************************************************************/
/* get resonance frequency and return result in "omega"
*/
getResFreq(omega)
double *omega;
{
 double tmp;
 rc = fgets(line, MAX_LENGTH, cntlfp);
 sscanf(line, "%F", &tmp);
 fprintf(stdout, "Resonance frequency = %f\n", tmp);
 *omega = 2.0 * pi * tmp * 1000000.0;
} /* getResFreq */


/*************************************************************/
/* get those parameters associated with either free or bound structure.
** "fstr" is either 'free' or 'bound'.
** Returns the value of tauc and external relaxation rate.
*/
getParms(fstr, tauc, ext)
char  *fstr;
double *tauc, *ext;
{
 int i;
 FILE  *fp;
 char filename[MAX_LENGTH];

 /* open coordinate file */
 rc = fgets(line, MAX_LENGTH, cntlfp);
 sscanf(line, "%s", filename);
 fprintf(stdout, "\nData file = %s\n", filename);
 fp = fopen(filename, "r");
 if (fp == NULL) {
  fprintf(stderr," Cannot read data file...\n");
  exit(1);
 }

 /* read contents of coordinate file */
 fgets(line, MAX_LENGTH, fp);   /* read title line */
 fscanf(fp, "%d\n", &numberProtons);
 fprintf(stdout, "Number of Protons = %d\n", numberProtons);
 if (numberProtons >= MAXPROTNUM) {
  fprintf(stderr," Error, Maximum number of protons = %d\n",MAXPROTNUM);
  exit(1);
 }
 fgets(line, MAX_LENGTH, fp);   /* read comment header line */
 for (i=1; i<=numberProtons; i++) {
  fscanf(fp, "%s%F%F%F", protonLabel[i], &x[i], &y[i], &z[i]);
  fprintf(echofp,"%s %f %f %f\n", protonLabel[i], x[i], y[i], z[i]);
 }

 /* read input correlation time */
 rc = fgets(line, MAX_LENGTH, cntlfp);
 sscanf(line, "%F",  tauc);
 fprintf(stdout, "Correlation time of '%s' molecule(ns) = %f\n", fstr, *ta
 *tauc = *tauc * 1.0e-09;

 /* read input external relaxation rate */
 rc = fgets(line, MAX_LENGTH, cntlfp);
 sscanf(line, "%F",  ext);
 fprintf(stdout, "Contribution to relaxation Rate = %f\n", *ext);
} /* getParms */


/*************************************************************/
getGraphData()
{
 register int j;
 int   tauMixFlag;
 rc = fgets(line, MAX_LENGTH, cntlfp);
 sscanf(line, "%d%d\n", &tr_x, &tr_y);
 fprintf(stdout, "\nLocation of graphics window: %d %d\n", tr_x, tr_y);

 rc = fgets(line, MAX_LENGTH, cntlfp);
 sscanf(line, "%d%d\n", &tr_width, &tr_height);
 fprintf(stdout, "Graphics window width in pixels: %d\n", tr_width);
 fprintf(stdout, "Graphics window height in pixels: %d\n", tr_height);

 x_origin = 80;
 y_origin = tr_height - 90;
 x_len = tr_width - x_origin - 120;
 y_len = y_origin - 70;
 dhLab = 50;

 yMin = 0.0;
 rc = fgets(line, MAX_LENGTH, cntlfp);
 sscanf(line, "%F\n", &yMax);
 fprintf(stdout, "\nMaximum value for n0e = %5.2f\n", yMax);

 xMin = 0.0;
 rc = fgets(line, MAX_LENGTH, cntlfp);
 sscanf(line, "%F\n", &xMax);
 fprintf(stdout, "Maximum value for tau mix = %5.2f\n", xMax);

 yPixel_ratio = y_len / (yMax - yMin);
 xPixel_ratio = x_len / (xMax - xMin);

 rc = fgets(line, MAX_LENGTH, cntlfp);
 sscanf(line, "%d\n", &tauMixFlag);
 fprintf(stdout, "tau mix Flag = %5d\n", tauMixFlag);

 rc = fgets(line, MAX_LENGTH, cntlfp);
 sscanf(line, "%d\n", &tauIncNum);
 fprintf(stdout, "Number of increments for tau mix = %d\n", tauIncNum);

 if (tauIncNum >= MAX_TAUPOINTS) {
  fprintf(stderr," Error, Maximum number of increments = %d\n",MAX_TAUPO
  exit(1);
 }

 if (tauMixFlag == 0) {
  for (j=0; j<=tauIncNum; j++)
   tauMix[j] = (xMax * j) / (double) tauIncNum;
 }
 else {
  tauMix[0] = 0.00;
  for (j=1; j<=tauIncNum; j++) {
   rc = fgets(line, MAX_LENGTH, cntlfp);
   sscanf(line, "%F\n", &tauMix[j]);
  }
 }

} /* getGraphData */


/**************************************************************/
getCalcData()
{
 rc = fgets(line, MAX_LENGTH, cntlfp);
```

```
  sscanf(line, "%F\n", &dMinNoe);
  fprintf(stdout, "\nMin nOe Distance cutoff (ang) = %6.2f\n", dMinNoe);
  dMinNoe = dMinNoe * 1.0e-08;

  rc = fgets(line, MAX_LENGTH, cntlfp);
  sscanf(line, "%F\n", &dMaxNoe);
  fprintf(stdout, "Max nOe Distance cutoff (ang) = %6.2f\n", dMaxNoe);
  dMaxNoe = dMaxNoe * 1.0e-08;

  rc = fgets(line, MAX_LENGTH, cntlfp);
  sscanf(line, "%F\n", &fb);
  fprintf(stdout, "Starting %% of bound to free = %6.2f\n", fb);
  fb = fb / 100.0;

  rc = fgets(line, MAX_LENGTH, cntlfp);
  sscanf(line, "%d\n", &protId);
  fprintf(stdout, "Proton ID for choosing nOe's = %d\n", protId);
 } /* getCalcData */


 /*************************************************************/
 calcSpecDens(omega, tauc)
 double omega, tauc;
 {
  spectralDensity[0] = tauc;
  spectralDensity[1] = tauc / (1 + (omega*tauc) * (omega*tauc));
  spectralDensity[2] = tauc / (1 + (2*omega*tauc) * (2*omega*tauc));
 } /* calcSpecDens */


 /*************************************************************/
 /*  Determine distance matrix
 */
 setDistances()
 {
  register int  i, j;
  register double xd, yd, zd;
  for (i=1; i<=numberProtons; i++) {
   for (j=1; j<=numberProtons; j++) {
    if (i == j)
     distance[i][j] = 0.0;
    else {
     xd = x[i] - x[j];
     yd = y[i] - y[j];
     zd = z[i] - z[j];
     distance[i][j] = sqrt(xd*xd + yd*yd + zd*zd) * 1.0e-08;
    }
   }
  }
 }  /* setDistances */


 /*************************************************************/
 setWMat()
 {
  register int  i, j;
  register double d6;
  for (i=1; i<=numberProtons; i++) {
   for (j=1; j<=numberProtons; j++) {
    if (i != j) {
```

```
    d6 = pow(distance[i][j], 6.0);
    w0[i][j] = (qConstant*spectralDensity[0]) / d6;
    w1[i][j] = (1.5 * qConstant*spectralDensity[1]) / d6;
    w2[i][j] = (6.0 * qConstant*spectralDensity[2]) / d6;
   }
  }
 }
} /* setWMat */


/**************************************************************/
/* Sets either the free or bound relaxation matrix
*/
setRelaxMat(rMat, ext)
register double rMat[MAXPROTNUM][MAXPROTNUM];
register double ext;
{
 register int i, j, k;
 for (i=1; i<=numberProtons; i++) {
  for (j=1; j<=numberProtons; j++) {
   rMat[i][j] = 0;
  }
 }
 for (i=1; i<=numberProtons; i++) {
  for (j=1; j<=numberProtons; j++) {
   if (i == j) {
    for (k=1; k<=numberProtons; k++) {
     if (k != i)
      rMat[i][i]= rMat[i][i]+(w0[i][k]+2*w1[i][k]+w2[i][k]);
    }
    rMat[i][i] = rMat[i][i] + ext;
   }
   else {
    rMat[i][j] = w2[i][j] - w0[i][j];
   }
  }
 }
} /* setRelaxMat */


/**************************************************************/
/* Get data required to run this program
*/
getData()
{
 double omega, tauc, extFree, extBound;

 getResFreq(&omega);
 getParms("free", &tauc, &extFree);
 calcSpecDens(omega, tauc);
 setDistances();
 setWMat();
 setRelaxMat(fRelaxMatrix, extFree);

 getParms("bound", &tauc, &extBound);
 calcSpecDens(omega, tauc);
 setDistances();
 setWMat();
 setRelaxMat(bRelaxMatrix, extBound);
 getGraphData();
 getCalcData();
} /* getData */


/**************************************************************/
/* erase the screen and draw only the axis, ticmarks, and labels
*/
do_graphics()
{
 char s[50];

 /* make window visible and empty */
 window_set(base_frame, WIN_SHOW, TRUE, 0);
 pw_rop(pw, 0, 0, tr_width, tr_height, PIX_CLR, pw, 0, 0);

 /* draw axis */
 draw_axis(BLACK);
 y_tics(5, RED);
 x_tics(6, RED);

 /* draw labels and title of plot */
 sprintf(s, "Proton: %s   bound = %%%-6.2f", protonLabel[protId], fb*100)
 draw_title(s, BLACK);
 draw_xLabel("tau Mix", BLACK);
 draw_yLabel("nOe", BLACK);

 /* tell notifier to show all this stuff on the screen */
 notify_dispatch();
} /* dographics */


/**************************************************************/
/* Computes crosspeak info given a fixed proton and fixed
** bound/free ratio.
*/
do_crosspeaks()
{
 register double  crosspeak;
 register int  j, m, t;
 register int  x1, y1, x2, y2, xc, yc;
 int       yPos;
 double     cMax;

 fprintf(stdout, "\n\n");
 fprintf(stdout, "ProtonLabel      Crosspeak          Rij          Mix\n");

 yPos = y_origin - (y_len / 2);
 for (j=1; j<=numberProtons; j++) {
  if ((distance[protId][j] <= dMaxNoe) &&
   (distance[protId][j] >= dMinNoe) && (j != protId)) {
   cMax = -HUGE;
   x1 = x_origin - xMin * xPixel_ratio;
   y1 = y_origin - yMin * yPixel_ratio;

   for (t=0; t<=tauIncNum; t++) {
    crosspeak = 0;
    for (m=1; m<=numberProtons; m++)
     crosspeak = crosspeak + vectors[protId][m] *
      exp(-diagonalRelax[m]*tauMix[t]) * vectorsInverse[m][j];
     x2 = x_origin + (tauMix[t] - xMin) * xPixel_ratio;
     y2 = y_origin - (crosspeak - yMin) * yPixel_ratio;
     pw_vector(pw, x1, y1, x2, y2, color_src(BLUE), 1);
     x1 = x2;
     y1 = y2;
     if (crosspeak > cMax) {
      cMax = crosspeak;
      xc = x1;
      yc = y1;
     }
    }
    pw_text(pw, x_origin+x_len+dhLab, yPos,
        color_or(BLACK), 0, protonLabel[j]);
    pw_vector(pw, xc, yc, x_origin+x_len+dhLab-3, yPos-7,
        color_src(GREEN), 1);  /* draw label line */
    notify_dispatch();      /* show new graph line */
    yPos = yPos + 14;       /* proton label offset */

    crosspeak = 0;
    for (m=1; m<=numberProtons; m++)
     crosspeak = crosspeak + vectors[protId][m] *
      exp(-diagonalRelax[m]*tauDisplay) * vectorsInverse[m][j];
    fprintf(stdout, " %10s %#14.5f %#11.2f %#11.2f\n",
     protonLabel[j], crosspeak, distance[protId][j]*1.0e08, tauDisplay);
   }
  }
} /* do_crosspeaks */


/*****************************************************************/
/* save crosspeak data into tabular results file
*/
save_tables()
{
 register double  crosspeak;
 register int    j, m, t;
 double    dist;

 fprintf(tabfp, "\n\n");
 fprintf(tabfp, "Proton: %s   Bound to free: %%%-6.2f\n\n",
      protonLabel[protId], fb*100);
 fprintf(tabfp, "ProtonLabel    Crosspeak           Rij           Mix\n");

 for (j=1; j<=numberProtons; j++) {
  dist = distance[protId][j];
  if ((dist <= dMaxNoe) && (dist >= dMinNoe) && (j != protId)) {
   for (t=0; t<=tauIncNum; t++) {
    crosspeak = 0;
    for (m=1; m<=numberProtons; m++)
     crosspeak = crosspeak + vectors[protId][m] *
      exp(-diagonalRelax[m]*tauMix[t]) * vectorsInverse[m][j];
    fprintf(tabfp, " %10s %#12.5f %#12.2f %#12.2f\n",
     protonLabel[j], crosspeak, dist*1.0e08, tauMix[t]);
   }
  }
 }
} /* save_tables */


/*****************************************************************/
```

```
/* dumps the plot canvas to a rasterfile
*/
save_plot(fname)
char  *fname;
{
 FILE *fp;
 colormap_t *colormap = NULL;
 int type = RT_STANDARD;
 int copy_flag = TRUE;
 struct pixrect *screen, *pp;

 fp = fopen(fname, "w");
 if (fp == NULL) {
  fprintf(stderr," Cannot open file for saving plot...\n");
  return(1);
 }
 screen = pr_open("/dev/fb");
 pp = pr_region(screen, tr_x, tr_y, tr_width, tr_height);
 pr_dump(pp, fp, colormap, type, copy_flag);
 pr_close(screen);
 fclose(fp);

 fprintf(stdout, "Plot file saved in %s\n", fname);
} /* save_plot */


/****************************************************************/
/* Processes user queries to the program
*/
do_user()
{
 char fName[60];
 int select, pdh;

 do {
  fprintf(stdout, "\n");
  fprintf(stdout, " 1) Save Plot\n");
  fprintf(stdout, " 2) Save crosspeak numbers\n");
  fprintf(stdout, " 3) Change fixed proton (current ID is %d)\n", protId)
  fprintf(stdout, " 4) Change bound/free percentage (currently %6.2f%%)\n
  fprintf(stdout, " 5) Change displayed tauMix\n");
  fprintf(stdout, " 6) Change Max nOe\n");
  fprintf(stdout, " 7) Change distance cutoffs\n");
  fprintf(stdout, " 8) Execute\n");
  fprintf(stdout, " 9) Quit\n");
  fscanf(stdin, "%d", &select);

  if (select == 1) {
   fprintf(stdout, " Enter filename for saving plot: \n");
   fscanf(stdin, "%59s", fName);
   fprintf(stdout, "File name is:  %s\n", fName);
   save_plot(fName);
  }
   else if (select == 2) {
   fprintf(stdout, "Results appended to:  %s\n", tablesFname);
   save_tables();
  }
   else if (select == 3) {
   fprintf(stdout, "Enter ID number of new proton:\n");
   fscanf(stdin, "%d", &pdh);
   if ((pdh <= numberProtons) && (pdh >= 1)) {
    fprintf(stdout, "Label of new proton:  %s\n", protonLabel[pdh]);
    fprintf(stdout, "ID number of new proton:  %d\n", pdh);
    protId = pdh;
    fprintf(stdout,"\n");
   }
   else
    fprintf(stdout, "Illegal proton Id!\n");
  }
   else if (select == 4) {
   fprintf(stdout, "Enter new bound/free percentage:\n");
   fscanf(stdin, "%F", &fb);
   fprintf(stdout, "Bound/free percentage is now:  %6.2f%%\n", fb);
   fb = fb / 100.0;
   doEigFlag = TRUE;
   fprintf(stdout,"\n");
  }
  else if (select == 5) {
   fprintf(stdout, "Enter tau Mix value for displaying crosspeak tables
   fscanf(stdin, "%F", &tauDisplay);
   fprintf(stdout, "Tau mix value to display is:  %-6.2f\n", tauDisplay
   fprintf(stdout,"\n");
  }
   else if (select == 6) {
   fprintf(stdout, "Enter new Maximum value for nOe:\n");
   fscanf(stdin, "%f", &yMax);
   fprintf(stdout, "nOe maximum is now:  %5.2f\n", yMax);
   yPixel_ratio = y_len / (yMax - yMin);
   fprintf(stdout,"\n");
  }
   else if (select == 7) {
   fprintf(stdout, "Enter new nOe minimum distance cutoff (ang):\n");
   fscanf(stdin, "%F", &dMinNoe);
   fprintf(stdout, "Min nOe distance cutoff is:  %6.2f\n", dMinNoe);
   dMinNoe = dMinNoe * 1.0e-08;
   fprintf(stdout,"\n");
   fprintf(stdout, "Enter new nOe maximum distance cutoff (ang):\n");
   fscanf(stdin, "%F", &dMaxNoe);
   fprintf(stdout, "Max nOe distance cutoff is:  %6.2f\n", dMaxNoe);
   dMaxNoe = dMaxNoe * 1.0e-08;
   fprintf(stdout,"\n");
  }
  else if (select == 8) {
   return(0);
  }
  else if (select == 9) {
   close(tabfp);
   close(echofp);
   return(1);
  }
  else
   select = 0;
 } while (select < 8);
} /* do_user */

/*************************************************************/
/* Main calculation loop
*/
calc()
{
 register int  i, j, k;

 for (i=1; i<=numberProtons; i++)
  for (j=1; j<=numberProtons; j++)
   relaxMatrix[i][j] = (1-fb)*fRelaxMatrix[i][j]+fb*bRelaxMatrix[i][j];
 k = 1;
 for (i=1; i<=numberProtons; i++)
  for (j=1; j<=i; j++) {
   upperTriangle[k] = relaxMatrix[i][j];
   k = k + 1;
  }

 eigen(upperTriangle, result, numberProtons); /* eigenvectors */
 doEigFlag = FALSE;

 k = 1;
 for (i=1; i<=numberProtons; i++)
  for (j=1; j<=numberProtons; j++) {
   vectors[j][i] = result[k];
   k = k + 1;
  }

 minv(vectors, numberProtons, vectorsInverse); /* matrix inverse */

 j = 0;
 for (i=1; i<=numberProtons; i++) {
  j += i;
  diagonalRelax[i] = upperTriangle[j];
 }
} /* calc */

/************************************************************/
/* Main events handler.
*/
do_events()
{
 int    quitFlag;
 quitFlag = 0;
 while (!quitFlag) {   /* keep looping until user decides to quit */
  if (doEigFlag)    /* user has changed "fb" */
   calc();
  do_graphics();    /* sets up screen for plotting */
  do_crosspeaks();   /* does crosspeak calc + plotting */
  quitFlag = do_user(); /* what does the user want to do with it */
 }
} /* do_events */

/************************************************************/
/* main program
*/
main()
{
 init();
 getData();
 init_graphics();
 do_events();
}

#include "main.h"
```

```
eigen(aMat, rv, n)
register double *aMat;
double *rv;
int     n;
/*
  Purpose: Computes eigenvectors of a symmetric matrix.
           AMAT is an uppertriangular matrix in array form.
           RV will contain the eigenvector matrix (array form).
           N is the dimension of AMAT
*/
{
 register int i, m, l, il, im, iq;
 register double tmp1, tmp2, cosx, sinx;
 register double *rilr, *rimr;
 int   lq, mq, ll, lm, mm, ind;
 double  x, y, sqrt2;
 double aMatll, aMatlm, aMatmm;
 double  sincs, cosx2, sinx2, thr, anorm, anrmx, range;
 int  loopFlag;

/***** Generate identity matrix *****/
 range = 1.0e-06;           /* accuracy of results */
 sqrt2 = sqrt(2.0);
 iq = -n;
 for (l=1; l<=n; l++) {
  iq = iq + n;
  for (i=1; i<=n; i++) {
   m = iq + i;
   rv[m] = 0.0;
   if (i == l)
    rv[m] = 1.0;
  }
 }

/***** Compute initial and final norms (aNorm and anrmx) *****/
 anorm = 0.0;
 m = 0;
 for (l=1; l<=n; l++) {
  m = m + l;
  iq = m + l;
  for (i=l+1; i<=n; i++) {
   anorm = anorm + aMat[iq] * aMat[iq];
   iq += i;
  }
 }
 if (anorm <= 0)
  return(0);
 anorm = sqrt2 * sqrt(anorm);
 anrmx = anorm * range / (double)n;

/***** Initialize indicators and compute threshold, thr *****/
 ind = 0;
 thr = anorm;
 thr = thr / (double)n;
 l = 1;
 m = 2;
 mq = 1;
 lq = 0;
 lm = 2;
 loopFlag = 1;
```

```
/***** Loop until we have attained solution *****/
 do {
  if (fabs(aMat[lm]) >= thr) {
   ind = 1;
   ll = l + lq;
   mm = m + mq;
   aMatll = aMat[ll];
   aMatlm = aMat[lm];
   aMatmm = aMat[mm];
   tmp1 = 0.5 * (aMatll - aMatmm);
   tmp2 = -aMatlm / sqrt(aMatlm * aMatlm + tmp1*tmp1);
   if (tmp1 < 0)
    tmp2 = -tmp2;

/***** Compute sin and cos *****/
   sinx = tmp2 / sqrt(2.0 * (1.0 + sqrt(1.0 - tmp2*tmp2)));
   sinx2 = sinx * sinx;
   cosx = sqrt(1.0 - sinx2);
   cosx2 = cosx * cosx;
   sincs = sinx * cosx;

/***** Rotate L and M columns *****/
   rilr = &rv[n * (l-1) + 1];
   rimr = &rv[n * (m-1) + 1];
   iq = 0;
   for (i=1; i<=n; i++) {
    if ((i != l) && (i != m)) {
     if (i < m)
      im = i + mq;
     else
      im = m + iq;
     if (i < l)
      il = i + lq;
     else
      il = l + iq;
     tmp1 = aMat[il];
     tmp2 = aMat[im];
     aMat[il] = tmp1 * cosx - tmp2 * sinx;
     aMat[im] = tmp1 * sinx + tmp2 * cosx;
    }
    tmp1 = *rilr;
    tmp2 = *rimr;
    *rilr++ = tmp1 * cosx - tmp2 * sinx;
    *rimr++ = tmp1 * sinx + tmp2 * cosx;
    iq += i;
   }
   tmp1 = 2.0 * aMatlm * sincs;
   aMat[lm] = (aMatll-aMatmm)*sincs + aMatlm*(cosx2-sinx2);
   aMat[ll] = aMatll * cosx2 + aMatmm * sinx2 - tmp1;
   aMat[mm] = aMatll * sinx2 + aMatmm * cosx2 + tmp1;
  }

/***** Tests for completion *****/
/***** Test for M = last column *****/
  if (m != n) {
   mq += m;
   m++;
   lm = l + mq;
  }
  else {
/***** Test for L = second from last column *****/
   if (l != (n-1)) {
    lq += 1;
    l++;
    m = l + 1;
    mq = lq + 1;
    lm = l + mq;
   }
   else {
    if (ind == 1) {
     ind = 0;
     l = 1;
     m = 2;
    }
    else {
/***** Compare threshold with final norm *****/
     if (thr > anrmx) {
      thr = thr / (double)n;
      l = 1;
      m = 2;
     }
     else
      loopFlag = 0;
    }
    mq = 1;
    lq = 0;
    lm = 2;
   }
  }
 } while (loopFlag);
} /* eigen */

#include "main.h"

/*************************************************************/
minv(aMat, size, zMat)
register double aMat[MAXPROTNUM][MAXPROTNUM];
register double zMat[MAXPROTNUM][MAXPROTNUM];
register int size;
/*
 Purpose: Finds the inverse of the square matrix "aMat" and
    returns the result in "zMat". "aMat" will not be
    changed but the local variable "mMat" will eventually
    be set to the identity matrix when the inverse
    is found.
*/
{
 register int k, j, i;
 register double *zptr, *mptr;
 register double *zp, *mp;
 register double tmp;
 register double mMat[MAXPROTNUM][MAXPROTNUM];

 for (i=1; i<=size; i++) {
  for (k=1; k<=size; k++) {
   mMat[i][k] = aMat[i][k];
   if (i == k)
    zMat[i][k] = 1;
   else
```

```
     zMat[i][k] = 0;
    }
   }
   for (i=1; i<=size; i++) {
    tmp = mMat[i][i];
    zptr = &zMat[i][1];
    mptr = &mMat[i][1];
    for (k=1; k<=size; k++) {
     *zptr++ = *zptr / tmp;
     *mptr++ = *mptr / tmp;
    }
    for (j=1; j<=size; j++) {
     if (i != j) {
      zptr = &zMat[j][1];
      zp = &zMat[i][1];
      mptr = &mMat[j][1];
      mp = &mMat[i][1];
      tmp = mMat[j][i];
      for (k=1; k<=size; k++) {
       *zptr++ = *zptr - *zp++ * tmp;
       *mptr++ = *mptr - *mp++ * tmp;
      }
     }
    }
   }
  }
/*
 File:  plot.c
 Purpose: Contains all functions with regards to drawing on
    the plot canvas.
*/

#define CHARWIDTH   6
#define CHARHEIGHT  16
#define CMS_SIZE    16

#include "main.h"

unsigned char redColor[CMS_SIZE] =
  { 255,255,255,255,255,255,100,210, 10, 10,210, 10,  0,200,0,0};
unsigned char greenColor[CMS_SIZE] =
 { 255,255,255,255,210, 10,  0,255,255,255,210, 10,  0,  0,0,0};
unsigned char blueColor[CMS_SIZE] =
 { 255,255,180,  0,210, 10,  0,210, 10,255,255,255,100,200,0,0};


/************************************************************/
set_canvas_colors(pw)
Pixwin  *pw;
{

/* Set background color to white for now anyways */
 redColor[0] = 0xFF;
 greenColor[0] = 0xFF;
 blueColor[0] = 0xFF;

/* Set the colormap, tells machine what colors we have */
 pw_setcmsname (pw, "showcolor");
 pw_putcolormap (pw, 0, CMS_SIZE, redColor, greenColor, blueColor);
/*
```

```
 pw_reversevideo (pw, 0, 15);
*/
}

/***************************************************************/
draw_axis (aColor)
{
 pw_vector (pw, x_origin, y_origin-y_len-5, x_origin, y_origin, color_xc
 pw_vector (pw, x_origin, y_origin, x_origin+x_len+5, y_origin, color_xc
}

/***************************************************************/
draw_title (title, aColor)
char *title;
int   aColor;
{
 int xPos, yPos;
 xPos = ((x_origin + x_len) / 2) - (0.5 * strlen(title)*CHARWIDTH);
 yPos = y_origin - y_len - 20;
 pw_text (pw, xPos, yPos, color_xor(aColor), 0, title);
}

/***************************************************************/
draw_xLabel (xLabel, xColor)
char   *xLabel;
int  xColor;
{
 int xLabPos;
 xLabPos = (x_origin + (x_len / 2)) - (0.5 * strlen(xLabel)*CHARWIDTH);
 pw_text (pw, xLabPos, y_origin+40, color_xor(xColor), 0, xLabel);
}

/***************************************************************/
draw_yLabel (yLabel, yColor)
char  *yLabel;
int   yColor;
{
 int i, len, xLabPos, yLabPos;
 len = strlen (yLabel);
 xLabPos = x_origin - 70;
 yLabPos = (y_origin - (y_len / 2)) - (0.5 * len * CHARHEIGHT);
 for (i=0; i<len; i++) {
  yLabPos = yLabPos + CHARHEIGHT;
  pw_char (pw, xLabPos, yLabPos, color_xor(yColor), 0, yLabel[i]);
 }
}

/***************************************************************/
x_tics (sections, aColor)
int  sections, aColor;     /* number of tics, tic-color */
{
 int  i, y1, y2, x0, xValLab;
 int xtic_top, xtic_bot;
 double xInc, xVal, xValInc;
 char *sVal;

 sVal = (char *) malloc (60);
 xVal = xMin;
 xInc = 1.0 * x_len / (double)sections;
 xValInc = (xMax - xMin) / (double)sections;
 xtic_top = y_origin - 5;
 xtic_bot = y_origin + 5;
 for (i=1; i<=sections; i++) {
  x0 = x_origin + rint(xInc * i);
  pw_vector (pw, x0, xtic_top, x0, xtic_bot, color_xor(aColor), 1);
  xVal = xMin + xValInc * i;
  sprintf (sVal, "%.4g", xVal);
  xValLab = x0 - (0.5 * strlen(sVal)*CHARWIDTH);
  pw_text (pw, xValLab, y_origin+20, color_xor(aColor), 0, sVal);
 }
 free (sVal);
}

/**************************************************************/
y_tics (sections, aColor)
int  sections, aColor;     /* number of tics, tic-color */
{
 int  i, y0, xValLab;
 int ytic_left, ytic_right;
 double yInc, yVal, yValInc;
 char *sVal;

 sVal = (char *) malloc (60);
 y0 = y_origin;
 yVal = yMin;
 yInc = y_len / (double)sections;
 yValInc = (yMax - yMin) / (double)sections;
 ytic_left = x_origin - 5;
 ytic_right = x_origin + 5;
 for (i=1; i<=sections; i++) {
  y0 = y_origin - rint(yInc * i);
  pw_vector (pw, ytic_left, y0, ytic_right, y0, color_xor(aColor), 1);
  yVal = yMin + yValInc * i;
  sprintf (sVal, "%.4g", yVal);
  xValLab = x_origin - 20 - (strlen(sVal)*CHARWIDTH);
  pw_text (pw, xValLab, y0, color_xor(aColor), 0, sVal);
 }
 free (sVal);
}
```

TRNOE: version 2

```
#
# Makefile for Trnoesy program
#
CFLAGS = -c -O
DFLAGS = -c -g
OBJECTS = sunview.o cntl.o setup.o minv.o eigen.o calc.o main.o
LIBES = -lm -lsuntool -lsunwindow -lpixrect
#
trnoesy: trnoesy.h $(OBJECTS)
   cc -O $(OBJECTS) $(LIBES)  -o trnoesy

main.o:  trnoesy.h main.c
   cc $(CFLAGS) main.c

calc.o:  trnoesy.h calc.c
   cc $(CFLAGS) calc.c

eigen.o: trnoesy.h eigen.c
   cc $(CFLAGS) eigen.c

minv.o:  trnoesy.h minv.c
   cc $(CFLAGS) minv.c

setup.o: trnoesy.h setup.c
   cc $(CFLAGS) setup.c

cntl.o:  trnoesy.h cntl.c
   cc $(CFLAGS) cntl.c

sunview.o: trnoesy.h sunview.c
   cc $(CFLAGS) sunview.c
```

```
/*
 Header file for trnoesy program. Mar 20 1990.
*/
#include <stdio.h>
#include <string.h>
#include <math.h>

#define MININT             (1 << 32 - 1)
#define MAXINT             (~MININT)
#define FALSE              0
#define TRUE               1

/* define all of our various color constants */
/* background = 0,  foreground = 15 */
#define WHITE    1
#define LTYELLOW   2
#define DKYELLOW   3
#define PINK    4
#define RED     5
#define DKRED    6
#define LTGREEN    7
#define GREEN    8
#define TURQUOISE   9
#define LTBLUE    10
#define BLUE    11
#define DKBLUE    12
#define PURPLE    13
#define BLACK    14
```

```
#define MAXPROTNUM   131       /* number of Protons + 1 */
#define MAXPROTSQU   16901     /* MAXPROTNUM*MAXPROTNUM + 1*/
#define MAXPROTTRI            8647     /* (MAXPROTNUM * MAXPROTNUM+1)/2 + 1
#define MAX_LENGTH   256
#define MAX_TAUPOINTS  100

#define color_xor(aColor) ((PIX_SRC ^ PIX_DST) | PIX_COLOR(aColor))
#define color_src(aColor) (PIX_SRC | PIX_COLOR(aColor))
#define color_or(aColor) ((PIX_SRC | PIX_DST) | PIX_COLOR(aColor))

/* program variables */

FILE   *fopen();
FILE   *echofp;     /* echo input file */
FILE        *tabfp;      /* stores numeric results */
FILE        *cntlfp;     /* trnoesy control file */
FILE  *crickfp;     /* cricket graph results */

int   tr_x, tr_y;     /* origin of graphics window */
int   tr_width, tr_height;        /* size of that window */
int   x_origin, y_origin;         /* location of axis origin */
int   x_len, y_len;               /* length of axis in pixels */
int   dhLab;                      /* labeling offset */

double  yPixel_ratio;    /* for converting nums to pixels */
double  xPixel_ratio;
int   tauIncNum;     /* number of points to plot */
double  xMin, yMin, xMax, yMax;     /* min/max values for plotting */

char  protonLabel[MAXPROTNUM][10]; /* names for the protons */
char  tablesFname[MAX_LENGTH];  /* fname for numeric results */
char  cricketFname[MAX_LENGTH];  /* fname for cricket graph */
char  line[MAX_LENGTH];    /* generic character string */
char  *rc;       /* used by fgets */

double  pi;
double  qConstant;

double  fRelaxMatrix[MAXPROTNUM][MAXPROTNUM];
double  bRelaxMatrix[MAXPROTNUM][MAXPROTNUM];
double  relaxMatrix[MAXPROTNUM][MAXPROTNUM];
double  upperTriangle[MAXPROTTRI];
double  result[MAXPROTSQU];
double  tMat[MAXPROTNUM][MAXPROTNUM];
double  tMatInv[MAXPROTNUM][MAXPROTNUM];
double  diagonalRelax[MAXPROTNUM];
double  distance[MAXPROTNUM][MAXPROTNUM];
double  tauMix[MAX_TAUPOINTS];
double  crosspeakTable[MAX_TAUPOINTS][100];

double  w0[MAXPROTNUM][MAXPROTNUM];
double  w1[MAXPROTNUM][MAXPROTNUM];
double  w2[MAXPROTNUM][MAXPROTNUM];
double  spectralDensity[MAXPROTNUM][MAXPROTNUM][3];

double  x[MAXPROTNUM];    /* holds proton coordinates */
double  y[MAXPROTNUM];
double  z[MAXPROTNUM];
double  s[MAXPROTNUM];    /* S value for bound protons */
double  r1int[MAXPROTNUM];    /* r1 internal for bound protons */
```

```
int   m0[MAXPROTNUM];     /* diagonal elements initial
           magnetization matrix*/
int   gn[MAXPROTNUM];     /*  group number */

int   numberProtons;     /* number of protons in datafile */
double  dMaxNoe;      /* distance Max nOe*/
double  dMinNoe;      /* distance Min nOe */
double  fb;       /* bound/free ratio */
double      tauDisplay;      /* mix time for tables */
int   protId;       /* fixed proton #1 */
int   protId2;      /* fixed proton #2 */
int   doEigFlag;      /* recalc eigenvalues */
int   graphFlag;      /* display graphics? */
int   saveTableNum;

/*
 file: main.c
 contains main driver routines for the trnoesy program.
*/

#include "trnoesy.h"    /* include header file */

static char  fName[255];


/**************************************************************/
/* main program
*/
main()
{
 long timeofday, *tloc[8];
 char *ctime();

 fprintf(stdout, "\n\n");
 fprintf(stdout, "***** trnoesy - version 2.1   May 27/91 *****\n");
 timeofday = time(tloc);
 fprintf(stdout, "***** Date:  %s\n\n", ctime(tloc));

 cntl();     /* read control file: see cntl.c */
 setup();   /* init data structures: see setup.c */

 if (graphFlag)
  init_graphics();

 do_events();

} /* main */


/**************************************************************/
/* Main events handler.
*/
do_events()
{
 int    quitFlag;

 quitFlag = FALSE;
 while (!quitFlag) {  /* Keep looping until user decides to quit */

  if (doEigFlag)  /* user has changed "fb" */
```

```
   do_calc();

   if (graphFlag)
    do_graphics(); /* sets up screen for plotting */

   if (protId2 == 0)
    f1_crosspeaks(stdout, FALSE); /* do crosspk calc (1 fixed) */
  else
    f2_crosspeaks(stdout, FALSE); /* do crosspk calc (2 fixed) */

  quitFlag = do_user(); /* get user queries from keyboard */

 }

} /* do_events */


/***************************************************************/
/* Processes user queries to the program
*/
do_user()
{
 int select;

 do {
  print_menu();
  fscanf(stdin, "%d", &select);

  switch (select) {
   case 1:   do_save_plot(); break;
   case 2:   do_save_crosspeak(); break;
   case 3:   do_cricket_graph(); break;
   case 4:   do_fix_prot1(); break;
   case 5:   do_fix_prot2(); break;
   case 6:   do_fb(); break;
   case 7:   do_tauMix(); break;
   case 8:   do_noe(); break;
   case 9:   do_distance(); break;
   case 10:  return(0);
   case 11:  return(1);
   default:  select = 0;
  }
 } while (select < 9);

} /* do_user */


/***************************************************************/
/* print menu options.
*/
print_menu()
{

 fprintf(stdout, "\n");
 fprintf(stdout, " 1) Save Plot\n");
 fprintf(stdout, " 2) Save crosspeak numbers\n");
 fprintf(stdout, " 3) Cricket Graph Dump \n");
 fprintf(stdout, " 4) One fixed proton (Proton 1 is %d)\n", protId);
 fprintf(stdout, " 5) Two fixed protons (Proton 2 is %d)\n", protId2);
 fprintf(stdout, " 6) Change bound/free percent (currently %6.2f%%)\n",
    fb*100);
 fprintf(stdout, " 7) Change displayed tauMix\n");
 fprintf(stdout, " 8) Change Max nOe\n");
 fprintf(stdout, " 9) Change distance cutoffs\n");
 fprintf(stdout, "10) Execute\n");
 fprintf(stdout, "11) Quit\n");

} /* print_menu */


/**************************************************************/
/* save plots to a file.
*/
do_save_plot()
{

 fprintf(stdout, " Enter filename for saving plot: \n");
 fscanf(stdin, "%59s", fName);
 fprintf(stdout, "File name is:  %s\n", fName);
 save_plot(fName);

} /* do_save_plot */


/**************************************************************/
/* save crosspeaks into tab delimited format.
*/
do_cricket_graph()
{
 register int t, i;

 fprintf(stdout, "Results written to:  %s\n", cricketFname);
 fprintf(crickfp, "\n");
 fprintf(crickfp, "mix(ms)\n");
 for (t=0; t<=tauIncNum; t++) {
  fprintf(crickfp, "%4d\t", (int)(tauMix[t] * 1000));
  for (i=0; i<saveTableNum; i++) {
   fprintf(crickfp, "%8.5f\t", crosspeakTable[t][i]);
  }
  fprintf(crickfp, "\n");
 }
 fflush(crickfp);

} /* do_cricket_graph */


/**************************************************************/
/* save crosspeak info to a file.
*/
do_save_crosspeak()
{

 fprintf(stdout, "Results appended to:  %s\n", tablesFname);
 fprintf(tabfp, "\n\n");
 fprintf(tabfp, "Proton: %s   Bound to free: %%%-6.2f",
      protonLabel[protId], fb*100);

 if (protId2 == 0)
  f1_crosspeaks(tabfp, TRUE);  /* do crosspeak calc (1 fixed) */
 else
```

```
  f2_crosspeaks(tabfp, TRUE);  /* do crosspeak calc (2 fixed) */
 } /* do_save_crosspeak */


/*************************************************************/
/* user wishes to change the proton id.
*/
do_fix_prot1()
{
 int pdh;

 fprintf(stdout, "Enter ID number of fixed proton:\n");
 fscanf(stdin, "%d", &pdh);
 if ((pdh <= numberProtons) && (pdh >= 1)) {
  fprintf(stdout, "Label of fixed proton:  %s\n", protonLabel[pdh]);
  fprintf(stdout, "ID number of fixed proton:  %d\n", pdh);
  protId = pdh;
  protId2 = 0;
  fprintf(stdout,"\n");
 }
 else
  fprintf(stdout, "Illegal proton Id!\n");

} /* do_fix_prot1 */


/*************************************************************/
/* select proton pairs to analyze.
*/
do_fix_prot2()
{
 int pdh1, pdh2;

 fprintf(stdout, "Enter ID numbers of proton pair:\n");
 fscanf(stdin, "%d %d", &pdh1, &pdh2);
 if (((pdh1 <= numberProtons) && (pdh1 >= 1)) &&
    ((pdh2 <= numberProtons) && (pdh2 >= 1))) {
  fprintf(stdout, "Label of proton 1:  %s\n", protonLabel[pdh1]);
  fprintf(stdout, "Label of proton 2:  %s\n", protonLabel[pdh2]);
  fprintf(stdout, "ID number of fixed proton 1:  %d\n", pdh1);
  fprintf(stdout, "ID number of fixed proton 2:  %d\n", pdh2);
  protId = pdh1;
  protId2 = pdh2;
  fprintf(stdout,"\n");
 }
 else
  fprintf(stdout, "Illegal proton Id!\n");

} /* do_fix_prot2 */


/*************************************************************/
/* change free/bund percentage.
*/
do_fb()
{

 fprintf(stdout, "Enter new bound/free percentage:\n");
 fscanf(stdin, "%F", &fb);
 fprintf(stdout, "Bound/free percentage is now:  %6.2f%%\n", fb);
 fb = fb / 100.0;
 doEigFlag = TRUE;
 fprintf(stdout,"\n");

} /* do_fb */


/**************************************************************/
/* change tauMix.
*/
do_tauMix()
{

 fprintf(stdout, "Enter tauMix for displaying crosspeak tables:\n");
 fscanf(stdin, "%F", &tauDisplay);
 fprintf(stdout, "Tau mix value to display is:  %-6.2f\n", tauDisplay);
 fprintf(stdout,"\n");

} /* do_tauMix */


/**************************************************************/
/* change max Noe.
*/
do_noe()
{

 fprintf(stdout, "Enter new Maximum value for nOe:\n");
 fscanf(stdin, "%f", &yMax);
 fprintf(stdout, "nOe maximum is now:  %5.2f\n", yMax);
 yPixel_ratio = y_len / (yMax - yMin);
 fprintf(stdout,"\n");

} /* do_noe */


/**************************************************************/
/* change max Noe.
*/
do_distance()
{

 fprintf(stdout, "Enter new nOe minimum distance cutoff (ang):\n");
 fscanf(stdin, "%F", &dMinNoe);
 fprintf(stdout, "Min nOe distance cutoff is:  %6.2f\n", dMinNoe);
 dMinNoe = dMinNoe * 1.0e-08;
 fprintf(stdout,"\n");
 fprintf(stdout, "Enter new nOe maximum distance cutoff (ang):\n");
 fscanf(stdin, "%F", &dMaxNoe);
 fprintf(stdout, "Max nOe distance cutoff is:  %6.2f\n", dMaxNoe);
 dMaxNoe = dMaxNoe * 1.0e-08;
 fprintf(stdout,"\n");

} /* do_distance */

/*
 file: calc.c
 contains calculation routines for trnoesy.
*/
```

```
#include "trnoesy.h"     /* include header file */

double find_crosspeak();


/***************************************************************/
/* Main calculation loop
*/
do_calc()
{
 register int  i, j, k;

 for (i=1; i<=numberProtons; i++) {
  for (j=1; j<=numberProtons; j++) {
   relaxMatrix[i][j] = (1-fb) * fRelaxMatrix[i][j] +
    fb * bRelaxMatrix[i][j];
  }
 }
 k = 1;
 for (i=1; i<=numberProtons; i++) {
  for (j=1; j<=i; j++) {
   upperTriangle[k] = relaxMatrix[i][j];
   k = k + 1;
  }
 }

 eigen(upperTriangle, result, numberProtons); /* eigenvectors */
 doEigFlag = FALSE;

 k = 1;
 for (i=1; i<=numberProtons; i++) {
  for (j=1; j<=numberProtons; j++) {
   tMat[j][i] = result[k];
   k = k + 1;
  }
 }

 minv(tMat, numberProtons, tMatInv);    /* matrix inverse */

 j = 0;
 for (i=1; i<=numberProtons; i++) {
  j += i;
  diagonalRelax[i] = upperTriangle[j];
 }

} /* do_calc */


/***************************************************************/
/* Computes crosspeak info given 1 fixed proton and fixed
** bound/free ratio.
*/
f1_crosspeaks(outfp, saveFlag)
FILE *outfp;
int saveFlag;
{
 register int   i, t, gNum, cpFound;
 double    dist, crosspeak;
 int      mark[MAXPROTNUM];
 fprintf(outfp,"\nProtonLabel    Crosspeak          Rij             Mix\n;
 cpFound = 0;
 for (i=0; i<MAXPROTNUM; i++)
  mark[i] = FALSE;

 for (i=1; i<=numberProtons; i++) {
  gNum = gn[i];
  dist = distance[protId][i];
  if ((dist <= dMaxNoe) &&
    (dist >= dMinNoe) &&
    (i != protId) &&
    ((gNum == 0) || (gNum != gn[protId])) &&
    (mark[gNum] == FALSE)) {

   if (saveFlag == TRUE) {
    for (t=0; t<=tauIncNum; t++) {
     crosspeak = find_crosspeak(protId, i, tauMix[t]);
     crosspeakTable[t][saveTableNum] = crosspeak;
     fprintf(outfp, " %10s %#12.5f %#12.2f %#12.2f\n",
      protonLabel[i], crosspeak, dist*1.0e08, tauMix[t]);
    }
    if (saveTableNum < 99)
     saveTableNum++;
   }

   else {
    if (graphFlag == TRUE)
     crosspeaks_graphics(cpFound, i);
    crosspeak = find_crosspeak(protId, i, tauDisplay);
    fprintf(outfp, " %10s %#12.5f %#12.2f %#12.2f\n",
     protonLabel[i], crosspeak, dist*1.0e08, tauDisplay);
   }

   cpFound++;
   if (gNum > 0)
    mark[gNum] = TRUE;
  }
 }
 fprintf(outfp, "     ***** End of table *****\n");
 fflush(outfp);

} /* f1_crosspeaks */


/****************************************************************/
/* Computes crosspeak info given 2 fixed protons and fixed
** bound/free ratio.
*/
f2_crosspeaks(outfp, saveFlag)
FILE *outfp;
int saveFlag;
{
 register int   t;
 double    dist, crosspeak;

 fprintf(outfp, "\nProtonLabel    Crosspeak          Rij             Mix\n");

 dist = distance[protId][protId2];
 if (saveFlag == TRUE) {
  for (t=0; t<=tauIncNum; t++) {
   crosspeak = find_crosspeak(protId, protId2, tauMix[t]);
   crosspeakTable[t][saveTableNum] = crosspeak;
   fprintf(outfp, " %10s %#12.5f %#12.2f %#12.2f\n",
    protonLabel[protId2], crosspeak, dist*1.0e08, tauMix[t]);
  }
  saveTableNum++;
 }

 else {
  if (graphFlag == TRUE)
   crosspeaks_graphics(0, protId2);
  crosspeak = find_crosspeak(protId, protId2, tauDisplay);
  fprintf(outfp, " %10s %#12.5f %#12.2f %#12.2f\n",
   protonLabel[protId2], crosspeak, dist*1.0e08, tauDisplay);
 }

 fprintf(outfp, "      ***** End of table *****\n");
 fflush(outfp);

} /* f2_crosspeaks */


/*****************************************************************/
/* find the value of one crosspeak.
*/
double find_crosspeak(id1, id2, tauMix)
int id1, id2;     /* id numbers for protons */
double tauMix;    /* tau Mix value */
{
 register int  j, k, m, gNum1, gNum2;
 double    peak;

 peak = 0.0;
 gNum1 = gn[id1];
 gNum2 = gn[id2];

 if ((gNum1 == 0) && (gNum2 == 0)) {
  for (j=1; j<=numberProtons; j++) {
   peak += tMat[id1][j] * exp(-diagonalRelax[j]*tauMix) *
        tMatInv[j][id2];
  }
 }

 else if ((gNum1 != 0) && (gNum2 == 0)) {
  for (k=1; k<=numberProtons; k++) { /* find all protons */
   if (gNum1 == gn[k]) {
    for (j=1; j<=numberProtons; j++) {
     peak += tMat[k][j] * exp(-diagonalRelax[j]*tauMix) *
        tMatInv[j][id2];
    }
   }
  }
 }

 else if ((gNum1 == 0) && (gNum2 != 0)) {
  for (k=1; k<=numberProtons; k++) { /* find all protons */
   if (gNum2 == gn[k]) {
    for (j=1; j<=numberProtons; j++) {
     peak += tMat[id1][j] * exp(-diagonalRelax[j]*tauMix) *
```

```
         tMatInv[j][k];
      }
     }
    }
   }

   else {
    for (m=1; m<=numberProtons; m++) { /* find all protons */
     if (gNum1 == gn[m]) {
      for (k=1; k<=numberProtons; k++) { /* find all protons */
       if (gNum2 == gn[k]) {
        for (j=1; j<=numberProtons; j++) {
         peak += tMat[m][j] * exp(-diagonalRelax[j] *
           tauMix) * tMatInv[j][k];
        }
       }
      }
     }
    }
   }

   return(peak);

  } /* find_crosspeak */

  /*
   file: eigen.c
   Purpose: Computes eigenvectors of a symmetric matrix.
              AMAT is an uppertriangular matrix in array form.
              RV will contain the eigenvector matrix (array form).
              N is the dimension of AMAT
  */

  #include "trnoesy.h"

  eigen(aMat, rv, n)
  register double *aMat;
  double *rv;
  int    n;
  {
   register int i, m, l, il, im, iq;
   register double tmp1, tmp2, cosx, sinx;
   register double *rilr, *rimr;
   int  lq, mq, ll, lm, mm, ind;
   double  x, y, sqrt2;
   double aMatll, aMatlm, aMatmm;
   double  sincs, cosx2, sinx2, thr, anorm, anrmx, range;
   int  loopFlag;

  /***** Generate identity matrix *****/
   range = 1.0e-06;       /* accuracy of results */
   sqrt2 = sqrt(2.0);
   iq = -n;
   for (l=1; l<=n; l++) {
    iq = iq + n;
    for (i=1; i<=n; i++) {
     m = iq + i;
     rv[m] = 0.0;
     if (i == l)
      rv[m] = 1.0;
  }
 }

/***** Compute initial and final norms (aNorm and anrmx) *****/
 anorm = 0.0;
 m = 0;
 for (l=1; l<=n; l++) {
  m = m + 1;
  iq = m + 1;
  for (i=l+1; i<=n; i++) {
   anorm = anorm + aMat[iq] * aMat[iq];
   iq += i;
  }
 }
 if (anorm <= 0)
  return(0);
 anorm = sqrt2 * sqrt(anorm);
 anrmx = anorm * range / (double)n;

/***** Initialize indicators and compute threshold, thr *****/
 ind = 0;
 thr = anorm;
 thr = thr / (double)n;
 l = 1;
 m = 2;
 mq = 1;
 lq = 0;
 lm = 2;
 loopFlag = 1;

/***** Loop until we have attained solution *****/
 do {
  if (fabs(aMat[lm]) >= thr) {
   ind = 1;
   ll = l + lq;
   mm = m + mq;
   aMatll = aMat[ll];
   aMatlm = aMat[lm];
   aMatmm = aMat[mm];
   tmp1 = 0.5 * (aMatll - aMatmm);
   tmp2 = -aMatlm / sqrt(aMatlm * aMatlm + tmp1*tmp1);
   if (tmp1 < 0)
    tmp2 = -tmp2;

/***** Compute sin and cos *****/
   sinx = tmp2 / sqrt(2.0 * (1.0 + sqrt(1.0 - tmp2*tmp2)));
   sinx2 = sinx * sinx;
   cosx = sqrt(1.0 - sinx2);
   cosx2 = cosx * cosx;
   sincs = sinx * cosx;

/***** Rotate L and M columns *****/
   rilr = &rv[n * (l-1) + 1];
   rimr = &rv[n * (m-1) + 1];
   iq = 0;
   for (i=1; i<=n; i++) {
    if ((i != l) && (i != m)) {
     if (i < m)
      im = i + mq;
     else
```

```
      im = m + iq;
     if (i < l)
      il = i + lq;
     else
      il = l + iq;
     tmp1 = aMat[il];
     tmp2 = aMat[im];
     aMat[il] = tmp1 * cosx - tmp2 * sinx;
     aMat[im] = tmp1 * sinx + tmp2 * cosx;
    }
    tmp1 = *rilr;
    tmp2 = *rimr;
    *rilr++ = tmp1 * cosx - tmp2 * sinx;
    *rimr++ = tmp1 * sinx + tmp2 * cosx;
    iq += i;
   }
   tmp1 = 2.0 * aMatlm * sincs;
   aMat[lm] = (aMatll-aMatmm)*sincs + aMatlm*(cosx2-sinx2);
   aMat[ll] = aMatll * cosx2 + aMatmm * sinx2 - tmp1;
   aMat[mm] = aMatll * sinx2 + aMatmm * cosx2 + tmp1;
  }

/***** Tests for completion *****/
/***** Test for M = last column *****/
  if (m != n) {
   mq += m;
   m++;
   lm = l + mq;
  }
  else {
/***** Test for L = second from last column *****/
   if (l != (n-1)) {
    lq += l;
    l++;
    m = l + 1;
    mq = lq + l;
    lm = l + mq;
   }
   else {
    if (ind == 1) {
     ind = 0;
     l = 1;
     m = 2;
    }
    else {
/***** Compare threshold with final norm *****/
     if (thr > anrmx) {
      thr = thr / (double)n;
      l = 1;
      m = 2;
     }
     else
      loopFlag = 0;
    }
    mq = 1;
    lq = 0;
    lm = 2;
   }
  }
 } while (loopFlag);
} /* eigen */

/*
 file: minv.c
 Purpose:  Finds the inverse of the square matrix "aMat" and
    returns the result in "zMat". "aMat" will not be
    changed but the local variable "mMat" will eventually
    be set to the identity matrix when the inverse
    is found.
*/

#include "trnoesy.h"

double mMat[MAXPROTNUM][MAXPROTNUM];


/****************************************************************/
minv(aMat, size, zMat)
register double aMat[MAXPROTNUM][MAXPROTNUM];
register double zMat[MAXPROTNUM][MAXPROTNUM];
register int size;
{
 register int k, j, i;
 register double *zptr, *mptr;
 register double *zp, *mp;
 register double tmp;

 for (i=1; i<=size; i++) {
  for (k=1; k<=size; k++) {
   mMat[i][k] = aMat[i][k];
   if (i == k)
    zMat[i][k] = 1;
   else
    zMat[i][k] = 0;
  }
 }
 for (i=1; i<=size; i++) {
  tmp = mMat[i][i];
  zptr = &zMat[i][1];
  mptr = &mMat[i][1];
  for (k=1; k<=size; k++) {
   *zptr++ = *zptr / tmp;
   *mptr++ = *mptr / tmp;
  }
  for (j=1; j<=size; j++) {
   if (i != j) {
    zptr = &zMat[j][1];
    zp = &zMat[i][1];
    mptr = &mMat[j][1];
    mp = &mMat[i][1];
    tmp = mMat[j][i];
    for (k=1; k<=size; k++) {
     *zptr++ = *zptr - *zp++ * tmp;
     *mptr++ = *mptr - *mp++ * tmp;
    }
   }
  }
 }
```

```
} /* minv */

/*
 file: setup.c
 contains initial calculation routines for trnoesy.
*/

#include "trnoesy.h"    /* include header file */


/***************************************************************/
/* Get data required to run this program
*/
setup()
{
 double omega, tauc, taucInt, extFree, extBound;

 getResFreq(&omega);
 getParms("free", &tauc, &taucInt, &extFree);
 calcSpecDens(spectralDensity, omega, tauc, taucInt);
 setDistances();
 setWMat();
 setRelaxMat(fRelaxMatrix, extFree);

 getParms("bound", &tauc, &taucInt, &extBound);
 calcSpecDens(spectralDensity, omega, tauc, taucInt);
 setDistances();
 setWMat();
 setRelaxMat(bRelaxMatrix, extBound);

 getGraphData();
 getCalcData();

} /* setup */


/***************************************************************/
/* calculate spectral density matrix
*/
calcSpecDens(sd, omega, tauc, taucInt)
double sd[MAXPROTNUM][MAXPROTNUM][3];
double omega, tauc, taucInt;
{
 register int  i, j;
 double    tau, sij;

 for (i=1; i<=numberProtons; i++) {
  for (j=1; j<=numberProtons; j++) {
   if (i != j) {

    tau = 1 / ((1 / tauc) + (1 / taucInt));
    sij = s[i] * s[j];

    sd[i][j][0] = (sij*tauc) + (1-sij)*tau;
    sd[i][j][1] = ((sij*tauc) / (1 + omega*tauc*omega*tauc)) +
     (((1-sij) * tau) / (1 + omega*tau*omega*tau));
    sd[i][j][2] = ((sij*tauc) / (1 + 4*omega*tauc*omega*tauc)) +
     (((1-sij) * tau) / (1 + 4*omega*tau*omega*tau));

   }
  }
 }

} /* calcSpecDens */


/************************************************************/
/* calculate spectral density matrix
*/
calcSpecDensOld(omega, tauc)
double omega, tauc;
{
 register int  i, j;
 double    tau_ij;

 for (i=1; i<=numberProtons; i++) {
  for (j=1; j<=numberProtons; j++) {
   if (i != j) {
    tau_ij = s[i] * s[j] * tauc;
    spectralDensity[i][j][0] = tau_ij;
    spectralDensity[i][j][1] = tau_ij / (1 + (omega*tau_ij) *
            (omega*tau_ij));
    spectralDensity[i][j][2] = tau_ij / (1 + (2*omega*tau_ij) *
            (2*omega*tau_ij));
   }
  }
 }

} /* calcSpecDensOld */


/************************************************************/
/*  Determine distance matrix
*/
setDistances()
{
 register int i, j;
 double   xd, yd, zd;

 for (i=1; i<=numberProtons; i++) {
  for (j=1; j<=numberProtons; j++) {
   if (i == j)
    distance[i][j] = 0.0;
   else {
    xd = x[i] - x[j];
    yd = y[i] - y[j];
    zd = z[i] - z[j];
    distance[i][j] = sqrt(xd*xd + yd*yd + zd*zd) * 1.0e-08;
   }
  }
 }

}  /* setDistances */


/************************************************************/
/* needed to calculate relaxation matrix
*/
setWMat()
{
 register int i, j;
 double   d6;

 for (i=1; i<=numberProtons; i++) {
  for (j=1; j<=numberProtons; j++) {
   if (i != j) {
    d6 = pow(distance[i][j], 6.0);
    w0[i][j] = (qConstant*spectralDensity[i][j][0]) / d6;
    w1[i][j] = (1.5 * qConstant*spectralDensity[i][j][1]) / d6;
    w2[i][j] = (6.0 * qConstant*spectralDensity[i][j][2]) / d6;
   }
  }
 }

} /* setWMat */


/*****************************************************************/
/* obtains either the free or bound relaxation matrix
*/
setRelaxMat(rMat, ext)
register double rMat[MAXPROTNUM][MAXPROTNUM];
register double ext;
{
 register int i, j, k;

 for (i=1; i<=numberProtons; i++) {
  for (j=1; j<=numberProtons; j++) {
   rMat[i][j] = 0;
  }
 }

 for (i=1; i<=numberProtons; i++) {
  for (j=1; j<=numberProtons; j++) {
   if (i == j) {
    for (k=1; k<=numberProtons; k++) {
     if (k != i)
      rMat[i][i] += (w0[i][k] + 2*w1[i][k] + w2[i][k]);
    }
    rMat[i][i] += ext + r1int[i];
   }
   else
    rMat[i][j] = (w2[i][j] - w0[i][j]);
  }
 }

} /* setRelaxMat */

/*
 file: cntl.c
 routines for initializing and reading program variables.
*/

#include "trnoesy.h"    /* include header file */


/*****************************************************************/
/* Initialize variables and get control file.
*/
cntl()
```

```
{
 double gamma1, hBar;
 char filename[MAX_LENGTH];

 pi = 3.14159;
 gamma1 = 4255.0 * (2*pi);
 hBar = 6.62e-27 / (2*pi);
 qConstant = 0.1 * gamma1*gamma1*gamma1*gamma1 * hBar*hBar;
 doEigFlag = TRUE;
 protId2 = 0;
 saveTableNum = 0;

 fprintf(stdout, "Enter Trnoesy control file: ");
 rc = fgets(line, MAX_LENGTH, stdin);
 sscanf(line, "%s", filename);
 fprintf(stdout, "Trnoesy control file = %s\n", filename);
 cntlfp = fopen(filename, "r");
 if (cntlfp == NULL) {
  fprintf(stderr," Cannot open trnoesy control file...\n");
  exit(1);
 }

 fgets(line, MAX_LENGTH, cntlfp);   /* read comment line */
 rc = fgets(line, MAX_LENGTH, cntlfp);
 sscanf(line, "%s", filename);
 fprintf(stdout, "Echo input file = %s\n", filename);
 echofp = fopen(filename, "w");
 if (echofp == NULL) {
  fprintf(stderr," Cannot open input echo file...\n");
  exit(1);
 }

 rc = fgets(line, MAX_LENGTH, cntlfp);
 sscanf(line, "%s", tablesFname);
 fprintf(stdout, "Tabular results file = %s\n", tablesFname);
 tabfp = fopen(tablesFname, "w");
 if (tabfp == NULL) {
  fprintf(stderr," Cannot open tabular results file...\n");
  exit(1);
 }

 rc = fgets(line, MAX_LENGTH, cntlfp);
 sscanf(line, "%s", cricketFname);
 fprintf(stdout, "Cricket Graph results file = %s\n", cricketFname);
 crickfp = fopen(cricketFname, "w");
 if (crickfp == NULL) {
  fprintf(stderr," Cannot open cricket graph results file...\n");
  exit(1);
 }

} /* cntl */


/***************************************************************/
/* get resonance frequency and return result in "omega"
*/
getResFreq(omega)
double *omega;
{
 double tmp;
 rc = fgets(line, MAX_LENGTH, cntlfp);
 sscanf(line, "%F", &tmp);
 fprintf(stdout, "Resonance frequency = %f\n", tmp);
 *omega = 2.0 * pi * tmp * 1000000.0;

} /* getResFreq */


/***********************************************************/
/* get those parameters associated with either free or bound structure.
** "fstr" is either 'free' or 'bound'.
** Returns the value of tauc and external relaxation rate.
*/
getParms(fstr, tauc, taucInt, ext)
char  *fstr;
double *tauc, *taucInt, *ext;
{
 int i, sNum;
 FILE  *fp;
 char filename[MAX_LENGTH], tStr[40];

/* open coordinate file */
 rc = fgets(line, MAX_LENGTH, cntlfp);
 sscanf(line, "%s", filename);
 fprintf(stdout, "\nData file = %s\n", filename);
 fp = fopen(filename, "r");
 if (fp == NULL) {
  fprintf(stderr," Cannot read data file...\n");
  exit(1);
 }

/* read contents of coordinate file */
 fgets(line, MAX_LENGTH, fp);   /* read title line */
 fscanf(fp, "%d\n", &numberProtons);
 fprintf(stdout, "Number of Protons = %d\n", numberProtons);
 if (numberProtons >= MAXPROTNUM) {
  fprintf(stderr," Error, Max number of protons = %d\n", MAXPROTNUM);
  exit(1);
 }
 fgets(line, MAX_LENGTH, fp);   /* read comment header line */

/* read each line in the coordinate file */
 for (i=1; i<=numberProtons; i++) {
  fscanf(fp, "%s%F%F%F%d%F%F%d", protonLabel[i], &x[i], &y[i], &z[i],
     &m0[i], &r1int[i], &s[i], &gn[i]);
  fprintf(echofp,"%s %f %f %f %d %f %f %d\n", protonLabel[i],
     x[i], y[i], z[i], m0[i], r1int[i], s[i], gn[i]);
 }
 fflush(echofp);

/* read input correlation time */
 rc = fgets(line, MAX_LENGTH, cntlfp);
 sscanf(line, "%F",  tauc);
 fprintf(stdout, "Correlation time of '%s' molecule(ns) = %f\n",
  fstr, *tauc);
 *tauc = *tauc * 1.0e-09;

/* read internal correlation time */
 rc = fgets(line, MAX_LENGTH, cntlfp);
 sscanf(line, "%F",  taucInt);
 fprintf(stdout, "Internal correlation time of '%s' molecule(ns) = %f\n",
  fstr, *taucInt);
 *taucInt = *taucInt * 1.0e-09;

/* read input external relaxation rate */
 rc = fgets(line, MAX_LENGTH, cntlfp);
 sscanf(line, "%F",  ext);
 fprintf(stdout, "Contribution to relaxation Rate = %f\n", *ext);

} /* getParms */


/***********************************************************/
/* obtain variables for drawing graphs on the screen
*/
getGraphData()
{
 register int j;
 int   tauMixFlag;

 rc = fgets(line, MAX_LENGTH, cntlfp);
 sscanf(line, "%d\n", &graphFlag);
 fprintf(stdout, "\nGraphics flag (0=off, 1=on): %d\n", graphFlag);

 rc = fgets(line, MAX_LENGTH, cntlfp);
 sscanf(line, "%d%d\n", &tr_x, &tr_y);
 fprintf(stdout, "\nLocation of graphics window: %d %d\n", tr_x, tr_y);

 rc = fgets(line, MAX_LENGTH, cntlfp);
 sscanf(line, "%d%d\n", &tr_width, &tr_height);
 fprintf(stdout, "Graphics window width in pixels: %d\n", tr_width);
 fprintf(stdout, "Graphics window height in pixels: %d\n", tr_height);

 x_origin = 80;
 y_origin = tr_height - 90;
 x_len = tr_width - x_origin - 120;
 y_len = y_origin - 70;
 dhLab = 50;

 yMin = 0.0;
 rc = fgets(line, MAX_LENGTH, cntlfp);
 sscanf(line, "%F\n", &yMax);
 fprintf(stdout, "\nMaximum value for nOe = %5.2f\n", yMax);

 xMin = 0.0;
 rc = fgets(line, MAX_LENGTH, cntlfp);
 sscanf(line, "%F\n", &xMax);
 fprintf(stdout, "Maximum value for tau mix = %5.2f\n", xMax);

 yPixel_ratio = y_len / (yMax - yMin);
 xPixel_ratio = x_len / (xMax - xMin);

 rc = fgets(line, MAX_LENGTH, cntlfp);
 sscanf(line, "%d\n", &tauMixFlag);
 fprintf(stdout, "tau mix Flag = %5d\n", tauMixFlag);

 rc = fgets(line, MAX_LENGTH, cntlfp);
 sscanf(line, "%d\n", &tauIncNum);
 fprintf(stdout, "Number of increments for tau mix = %d\n", tauIncNum);
 if (tauIncNum >= MAX_TAUPOINTS) {
  fprintf(stderr," Error, Maximum number of increments = %d\n",
    MAX_TAUPOINTS);
  exit(1);
 }

 if (tauMixFlag == 0) {
  for (j=0; j<=tauIncNum; j++)
   tauMix[j] = (xMax * j) / (double) tauIncNum;
 }

 else {
  tauMix[0] = 0.00;
  for (j=1; j<=tauIncNum; j++) {
   rc = fgets(line, MAX_LENGTH, cntlfp);
   sscanf(line, "%F\n", &tauMix[j]);
  }
 }

} /* getGraphData */


/*****************************************************************/
/* calculation variables
*/
getCalcData()
{

 rc = fgets(line, MAX_LENGTH, cntlfp);
 sscanf(line, "%F\n", &dMinNoe);
 fprintf(stdout, "\nMin nOe Distance cutoff (ang) = %6.2f\n", dMinNoe);
 dMinNoe = dMinNoe * 1.0e-08;

 rc = fgets(line, MAX_LENGTH, cntlfp);
 sscanf(line, "%F\n", &dMaxNoe);
 fprintf(stdout, "Max nOe Distance cutoff (ang) = %6.2f\n", dMaxNoe);
 dMaxNoe = dMaxNoe * 1.0e-08;

 rc = fgets(line, MAX_LENGTH, cntlfp);
 sscanf(line, "%F\n", &fb);
 fprintf(stdout, "Starting %% of bound to free = %6.2f\n", fb);
 fb = fb / 100.0;

 rc = fgets(line, MAX_LENGTH, cntlfp);
 sscanf(line, "%d\n", &protId);
 fprintf(stdout, "Proton ID for choosing nOe's = %d\n", protId);

} /* getCalcData */

/*
 file: sunview.c
 contains all routines that require sunview routines for trnoesy.
*/

#include <suntool/sunview.h>
#include <suntool/panel.h>
#include <suntool/textsw.h>
#include <suntool/canvas.h>
```

```
#define CHARWIDTH  6
#define CHARHEIGHT  16
#define CMS_SIZE  16

#include "trnoesy.h"    /* include header file */

unsigned char redColor[CMS_SIZE] =
 { 255,255,255,255,255,255,100,210, 10, 10,210, 10,  0,200,0,0};

unsigned char greenColor[CMS_SIZE] =
 { 255,255,255,255,210, 10,  0,255,255,255,210, 10,  0,  0,0,0};

unsigned char blueColor[CMS_SIZE] =
 { 255,255,180,  0,210, 10,  0,210, 10,255,255,255,100,200,0,0};


Frame base_frame;
Pixwin *pw;
Canvas plot_canvas;

extern Notify_error notify_dispatch();  /* external routines used */
extern double find_crosspeak();


/**************************************************************/
/* define plotting screen
*/
init_graphics()
{

 base_frame = window_create (NULL, FRAME,
        WIN_X, tr_x,
        WIN_Y, tr_y,
        WIN_WIDTH, tr_width,
        WIN_HEIGHT, tr_height,
        FRAME_LABEL,
   "        << trnoesy graphics >>",
        0);

 plot_canvas = window_create (base_frame, CANVAS, tr_x, tr_y, 0);
 pw = canvas_pixwin (plot_canvas);
 set_canvas_colors (pw);

} /*init_graphics */


/**************************************************************/
/* erase the screen and draw only the axis, ticmarks, and labels
*/
do_graphics()
{
 char sVal[50];

/* make window visible and empty */
 window_set(base_frame, WIN_SHOW, TRUE, 0);
 pw_rop(pw, 0, 0, tr_width, tr_height, PIX_CLR, pw, 0, 0);

/* draw axis */
 draw_axis(BLACK);
 y_tics(5, RED);
 x_tics(6, RED);

/* draw labels and title of plot */
 sprintf(sVal, "Proton: %s   bound = %%%-6.2f",
  protonLabel[protId], fb*100);
 draw_title(sVal, BLACK);
 draw_xLabel("tau Mix", BLACK);
 draw_yLabel("nOe", BLACK);

/* tell notifier to show all this stuff on the screen */
 notify_dispatch();

} /* do_graphics */


/************************************************************/
/* do crosspeak graphics.
*/
crosspeaks_graphics(count, id)
int count, id;
{
 register int  t, yPos, x1, y1, x2, y2, xc, yc;
 double    cMax, crosspeak;

 cMax = MININT;
 x1 = x_origin - xMin * xPixel_ratio;
 y1 = y_origin - yMin * yPixel_ratio;

 for (t=0; t<=tauIncNum; t++) {
  crosspeak = find_crosspeak(protId, id, tauMix[t], id);
  x2 = x_origin + (tauMix[t] - xMin) * xPixel_ratio;
  y2 = y_origin - (crosspeak - yMin) * yPixel_ratio;
  pw_vector(pw, x1, y1, x2, y2, color_src(BLUE), 1);
  x1 = x2;
  y1 = y2;
  if (crosspeak > cMax) {
   cMax = crosspeak;
   xc = x1;
   yc = y1;
  }
 }

 yPos = y_origin - (y_len / 2) + count * 14; /* proton label offset */
 pw_text(pw, x_origin+x_len+dhLab, yPos,
  color_or(BLACK), 0, protonLabel[id]);
 pw_vector(pw, xc, yc, x_origin+x_len+dhLab-3, yPos-7,
  color_src(GREEN), 1);  /* draw label line */

 notify_dispatch();     /* show new graph line */

} /* crosspeaks_graphics */


/**************************************************************/
/* dumps the plot canvas to a rasterfile
*/
save_plot(fname)
char  *fname;
{
 FILE *fp;
```

```
  colormap_t *colormap = NULL;
  int type = RT_STANDARD;
  int copy_flag = TRUE;
  struct pixrect *screen, *pp;

  fp = fopen(fname, "w");
  if (fp == NULL) {
   fprintf(stderr," Cannot open file for saving plot...\n");
   return(1);
  }
 screen = pr_open("/dev/fb");
 pp = pr_region(screen, tr_x, tr_y, tr_width, tr_height);
 pr_dump(pp, fp, colormap, type, copy_flag);
 pr_close(screen);
 fclose(fp);

 fprintf(stdout, "Plot file saved in %s\n", fname);

} /* save_plot */


/*****************************************************************/
set_canvas_colors(pw)
Pixwin  *pw;
{

/* Set background color to white for now anyways */
 redColor[0] = 0xFF;
 greenColor[0] = 0xFF;
 blueColor[0] = 0xFF;

/* Set the colormap, tells machine what colors we have */
 pw_setcmsname (pw, "showcolor");
 pw_putcolormap (pw, 0, CMS_SIZE, redColor, greenColor, blueColor);

} /* set_canvas_colors */


/*****************************************************************/
draw_axis (aColor)
{

 pw_vector (pw, x_origin, y_origin-y_len-5, x_origin, y_origin,
   color_xor(aColor), 1);
 pw_vector (pw, x_origin, y_origin, x_origin+x_len+5, y_origin,
   color_xor(aColor), 1);

} /* draw_axis */


/*****************************************************************/
draw_title (title, aColor)
char *title;
int   aColor;
{
 int xPos, yPos;

 xPos = ((x_origin + x_len) / 2) - (0.5 * strlen(title)*CHARWIDTH);
 yPos = y_origin - y_len - 20;
 pw_text (pw, xPos, yPos, color_xor(aColor), 0, title);
```

```
} /* draw_title */


/************************************************************/
draw_xLabel (xLabel, xColor)
char   *xLabel;
int  xColor;
{
 int xLabPos;

 xLabPos = (x_origin + (x_len / 2)) - (0.5 * strlen(xLabel)*CHARWIDTH);
 pw_text (pw, xLabPos, y_origin+40, color_xor(xColor), 0, xLabel);

} /* draw_xLabel */


/************************************************************/
draw_yLabel (yLabel, yColor)
char  *yLabel;
int   yColor;
{
 register int i, len, xLabPos, yLabPos;

 len = strlen (yLabel);
 xLabPos = x_origin - 70;
 yLabPos = (y_origin - (y_len / 2)) - (0.5 * len * CHARHEIGHT);

 for (i=0; i<len; i++) {
  yLabPos = yLabPos + CHARHEIGHT;
  pw_char (pw, xLabPos, yLabPos, color_xor(yColor), 0, yLabel[i]);
 }

} /* draw_yLabel */


/************************************************************/
x_tics (sections, aColor)
int  sections, aColor;     /* number of tics, tic-color */
{
 register int  i, x0, xValLab;
 register int  xtic_top, xtic_bot;
 double   xInc, xVal, xValInc;
 char   sVal[60];

 xVal = xMin;
 xInc = x_len / (double)sections;
 xValInc = (xMax - xMin) / (double)sections;
 xtic_top = y_origin - 5;
 xtic_bot = y_origin + 5;

 for (i=1; i<=sections; i++) {
  x0 = x_origin + rint(xInc * i);
  pw_vector (pw, x0, xtic_top, x0, xtic_bot, color_xor(aColor), 1);
  xVal = xMin + xValInc * i;
  sprintf (sVal, "%.4g", xVal);
  xValLab = x0 - (0.5 * strlen(sVal)*CHARWIDTH);
  pw_text (pw, xValLab, y_origin+20, color_xor(aColor), 0, sVal);
 }
```

```
} /* x_tics */


/***************************************************************/
y_tics (sections, aColor)
int  sections, aColor;     /* number of tics, tic-color */
{
 register int  i, y0, xValLab;
 register int  ytic_left, ytic_right;
 double   yInc, yVal, yValInc;
 char   sVal[60];

 yVal = yMin;
 yInc = y_len / (double)sections;
 yValInc = (yMax - yMin) / (double)sections;
 ytic_left = x_origin - 5;
 ytic_right = x_origin + 5;

 for (i=1; i<=sections; i++) {
  y0 = y_origin - rint(yInc * i);
  pw_vector (pw, ytic_left, y0, ytic_right, y0, color_xor(aColor), 1);
  yVal = yMin + yValInc * i;
  sprintf (sVal, "%.4g", yVal);
  xValLab = x_origin - 20 - (strlen(sVal)*CHARWIDTH);
  pw_text (pw, xValLab, y0, color_xor(aColor), 0, sVal);
 }

} /* y_tics */
```